

*Carnegie  
Institution*

OF WASHINGTON

*Year Book 69*

*1969-1970*







Director's Office








# *Carnegie Institution*

*OF WASHINGTON*

## *Year Book 69*

*1969-1970*






Library of Congress Catalog Card Number 3-16716  
Port City Press, Baltimore, Maryland



# *Contents*

	<i>page</i>
Officers and Staff	v
Report of the President	1
Reports of Departments and Special Studies	69
Hale Observatories	71
Geophysical Laboratory	131
Department of Terrestrial Magnetism	363
Committee on Image Tubes for Telescopes	553
Department of Embryology	557
Department of Plant Biology	617
Genetics Research Unit	715
Bibliography	723
Administrative Reports	725
Report of the Executive Committee	727
Report of Auditors	729
Abstract of Minutes of the Seventy-Second Meeting of the Board of Trustees	743
Articles of Incorporation	745
By-Laws of the Institution	749
Index	755





Digitized by the Internet Archive  
in 2012 with funding from  
LYRASIS Members and Sloan Foundation

# *President and Trustees*

## PRESIDENT

Caryl P. Haskins

## BOARD OF TRUSTEES

James N. White  
*Chairman*

Garrison Norton  
*Vice-Chairman*

William McC. Martin, Jr.  
*Secretary*

Sir Eric Ashby  
Amory H. Bradford  
Vannevar Bush  
Michael Ference, Jr.  
Carl J. Gilbert  
William T. Golden  
Crawford H. Greenewalt  
Caryl P. Haskins  
Alfred L. Loomis  
Robert A. Lovett  
William McC. Martin, Jr.  
Keith S. McHugh  
Henry S. Morgan  
William I. Myers  
Garrison Norton  
Robert M. Pennoyer  
Richard S. Perkins  
William M. Roth  
William W. Rubey  
Frank Stanton  
Charles P. Taft  
Charles H. Townes  
Juan T. Trippe  
James N. White



## *Trustees (continued)*

### AUDITING COMMITTEE

Keith S. McHugh, *Chairman*  
Alfred L. Loomis  
Juan T. Trippe

### EXECUTIVE COMMITTEE

Garrison Norton, *Chairman*  
Michael Ference, Jr.  
Crawford H. Greenewalt  
Caryl P. Haskins  
William McC. Martin, Jr.  
Keith S. McHugh  
Henry S. Morgan  
William I. Myers  
Richard S. Perkins  
Frank Stanton  
James N. White

### RETIREMENT COMMITTEE

Frank Stanton, *Chairman*  
Amory H. Bradford  
Richard S. Perkins  
William M. Roth

### COMMITTEE ON ASTRONOMY

Crawford H. Greenewalt, *Chairman*  
Amory H. Bradford  
William McC. Martin, Jr.

### FINANCE COMMITTEE

Richard S. Perkins, *Chairman*  
Crawford H. Greenewalt  
Alfred L. Loomis  
Keith S. McHugh  
Henry S. Morgan  
Robert M. Pennoyer

### COMMITTEE ON BIOLOGICAL SCIENCES

William I. Myers, *Chairman*  
William T. Golden  
Charles P. Taft

### NOMINATING COMMITTEE

Henry S. Morgan, *Chairman*  
Garrison Norton  
Charles H. Townes  
James N. White

### COMMITTEE ON TERRESTRIAL SCIENCES

Juan T. Trippe, *Chairman*  
Richard S. Perkins  
Charles H. Townes

# Staff

## HALE OBSERVATORIES

*813 Santa Barbara Street  
Pasadena, California 91106*

Horace W. Babcock, *Director*  
J. Beverley Oke, *Associate Director*  
Halton C. Arp  
Edwin W. Dennison  
Jesse L. Greenstein  
James E. Gunn  
Robert F. Howard  
Jerome Kristian  
Robert B. Leighton  
Guido Münch  
George W. Preston III  
Bruce H. Rule  
Allan R. Sandage  
Wallace L. W. Sargent  
Leonard T. Searle  
Maarten Schmidt  
Arthur H. Vaughan, Jr.  
Olin C. Wilson  
Harold Zirin

## GEOPHYSICAL LABORATORY

*2801 Upton Street, N.W.  
Washington, D.C. 20008*

Philip H. Abelson, *Director*  
Peter M. Bell  
Francis R. Boyd, Jr.  
Felix Chayes  
Gordon L. Davis  
Gabrielle Donnay  
Joseph L. England  
Larry W. Finger  
P. Edgar Hare  
Thomas C. Hoering  
Thomas E. Krogh  
Gunnar Kullerud  
Donald H. Lindsley  
J. Frank Schairer  
Hatten S. Yoder, Jr.

## DEPARTMENT OF

## TERRESTRIAL MAGNETISM

*5241 Broad Branch Road, N.W.  
Washington, D.C. 20015*

Ellis T. Bolton, *Director*  
L. Thomas Aldrich, *Associate  
Director*  
Merle A. Tuve, *Distinguished  
Service Member*  
Roy J. Britten  
Louis Brown  
Dean B. Cowie  
W. Kent Ford, Jr.  
Stanley R. Hart  
Bill H. Hoyer  
David E. James  
David E. Kohne  
Richard B. Roberts  
Vera C. Rubin  
I. Selwyn Sacks  
Kenneth C. Turner



## *Staff (continued)*

### DEPARTMENT OF PLANT BIOLOGY

*Stanford, California 94305*

C. Stacy French, *Director*  
Olle Björkman  
Jeanette S. Brown  
David C. Fork  
William M. Hiesey, *Emeritus*  
Malcolm A. Nobs

### DEPARTMENT OF EMBRYOLOGY

*115 West University Parkway  
Baltimore, Maryland 21210*

James D. Ebert, *Director*  
Bent G. Böving  
Donald D. Brown  
Igor B. Dawid  
Robert L. DeHaan  
Douglas M. Fambrough  
Elizabeth M. Ramsey  
Ronald H. Reeder

### GENETICS RESEARCH UNIT

*Cold Spring Harbor  
New York 11724*

Alfred D. Hershey, *Director*  
Barbara McClintock, *Distinguished  
Service Member*  
Elizabeth Burgi

*Cytogenetics Laboratory  
Ann Arbor, Michigan*

Helen Gay

## *Staff (continued)*

### OFFICE OF ADMINISTRATION

*1530 P Street, N.W., Washington, D.C. 20005*

Caryl P. Haskins	<i>President</i>
Edward A. Ackerman	<i>Executive Officer</i>
James W. Boise	<i>Bursar; Secretary-Treasurer, Retirement Trust; Executive Secretary to the Finance Committee</i>
Marjorie H. Walburn	<i>Assistant to the President</i>
Sheila A. McGough	<i>Editor</i>
Kenneth R. Henard	<i>Assistant Bursar; Assistant Treasurer, Retirement Trust</i>
Pamela W. Thomas *	<i>Associate Editor</i>
Joseph M. S. Haraburda	<i>Assistant to the Bursar</i>
A. Gerald Thompson	<i>Information Officer</i>

---

Marshall Hornblower	<i>Counsel</i>
Montgomery S. Bradley	<i>Administrative Associate</i>

### STAFF MEMBER IN SPECIAL SUBJECT AREA

Tatiana Proskouriakoff

### RESEARCH ASSOCIATE AT LARGE

Harry E. D. Pollock

\* Resigned June 22, 1970.



# Former Presidents and Trustees

## PRESIDENTS

Daniel Coit Gilman, 1902-1904

Robert Simpson Woodward, 1904-1920

John Campbell Merriam, 1921-1938;

*President Emeritus 1939-1945*

Vannevar Bush, 1939-1955

## TRUSTEES

Alexander Agassiz	1904-05	Seth Low	1902-16
George J. Baldwin	1925-27	Wayne MacVeagh	1902-07
Thomas Barbour	1934-46	Andrew W. Mellon	1924-37
James F. Bell	1935-61	Margaret Carnegie Miller	1955-67
John S. Billings	1902-13	Roswell Miller	1933-55
Robert Woods Bliss	1936-62	Darius O. Mills	1902-09
Lindsay Bradford	1940-58	S. Weir Mitchell	1902-14
Omar N. Bradley	1948-69	Andrew J. Montague	1907-35
Robert S. Brookings	1910-29	William W. Morrow	1902-29
John L. Cadwalader	1903-14	Seeley G. Mudd	1940-68
William W. Campbell	1929-38	William Church Osborn	1927-34
John J. Carty	1916-32	James Parmelee	1917-31
Whitefoord R. Cole	1925-34	Wm. Barclay Parsons	1907-32
Frederic A. Delano	1927-49	Stewart Paton	1916-42
Cleveland H. Dodge	1903-23	George W. Pepper	1914-19
William E. Dodge	1902-03	John J. Pershing	1930-43
Charles P. Fenner	1914-24	Henning W. Prentis, Jr.	1942-59
Homer L. Ferguson	1927-52	Henry S. Pritchett	1906-36
Simon Flexner	1910-14	Gordon S. Rentschler	1946-48
W. Cameron Forbes	1920-55	David Rockefeller	1952-56
James Forrestal	1948-49	Elihu Root	1902-37
William N. Frew	1902-15	Elihu Root, Jr.	1937-67
Lyman J. Gage	1902-12	Julius Rosenwald	1929-31
Walter S. Gifford	1931-66	Martin A. Ryerson	1908-28
Cass Gilbert	1924-34	Henry R. Shepley	1937-62
Frederick H. Gillett	1924-35	Theobald Smith	1914-34
Daniel C. Gilman	1902-08	John C. Spooner	1902-07
John Hay	1902-05	William Benson Storey	1924-39
Barklie McKee Henry	1949-66	Richard P. Strong	1934-48
Myron T. Herrick	1915-29	William H. Taft	1906-15
Abram S. Hewitt	1902-03	William S. Thayer	1929-32
Henry L. Higginson	1902-19	James W. Wadsworth	1932-52
Ethan A. Hitchcock	1902-09	Charles D. Walcott	1902-27
Henry Hitchcock	1902	Frederic C. Walcott	1931-48
Herbert Hoover	1920-49	Henry P. Walcott	1910-24
William Wirt Howe	1903-09	Lewis H. Weed	1935-52
Charles L. Hutchinson	1902-04	William H. Welch	1906-34
Walter A. Jessup	1938-44	Andrew D. White	1902-03
Frank B. Jewett	1933-49	Edward D. White	1902-03
Samuel P. Langley	1904-06	Henry White	1913-27
Ernest O. Lawrence	1944-58	George W. Wickersham	1909-36
Charles A. Lindbergh	1934-39	Robert E. Wilson	1953-64
William Lindsay	1902-09	Robert S. Woodward	1905-24
Henry Cabot Lodge	1914-24	Carroll D. Wright	1902-08

Under the original charter, from the date of organization until April 28, 1904, the following were *ex officio* members of the Board of Trustees: the President of the United States, the President of the Senate, the Speaker of the House of Representatives, the Secretary of the Smithsonian Institution, and the President of the National Academy of Sciences.

*Report* OF  
*THE President*



*You never enjoy the world aright, till the sea itself floweth in your veins, till you are clothed with the heavens, and crowned with the stars: and perceive yourself to be the sole heir of the whole world, and more than so, because men who are in it who are every one sole heirs as well as you . . .*

*The world is a mirror of infinite beauty, yet no man sees it. It is a region of Light and Peace, did not men disquiet it.*

THOMAS TRAHERNE

*To be unafraid and yet to be free implies an assurance that order is not opposed to freedom or even external to it but is an element of it—a thing without which freedom itself is not and cannot be. It is towards this concept that mankind appears to be struggling.*

CHARLES MORGAN—*Reflections in a Mirror*

*And lastly there is the internationalism of science: it is the one remaining force of cohesion between peoples who may be at war on every other issue. Whether the man who upsets my scientific theories is my countryman or my enemy is immaterial: the theories are upset all the same. Perhaps, then, it is through reflection on the ethical and moral implications of science and technology, that is to say the influences of these studies on humanism, that a country may make its greatest contribution to civilisation.*

SIR ERIC ASHBY

THE BEGINNING OF EACH NEW DECADE in the life of science provides for America, as for the world, a special vantage point from which to view afresh, and ponder anew, its discoveries and its direction and their significance for the human condition, present and future. From the vantage point of 1970, challenges to the scientific way are more than usually critical. For, though science's own vision of its work and mission must and surely will remain steady over the years ahead, in a time of such newly enlarged consciousness of social obligation as we feel today, and in a time of such heightened awareness of the essential fragility of our physical world, the view of science held generally in the society that supports it, and the consequent expectations from it and demands upon it, could change in subtle and sometimes dangerous ways.

Upon the breadth and depth and verity of the picture of science and its work held by society at large and upon its continued acceptance over the years to come, much of the future stature and effectiveness of the scientific mode itself, and with them much of the spiritual and cultural integrity as well as the material progress of the nation, will inevitably depend. For it has always been true that a nation achieves continuing greatness, and continues to produce great men, in accord with its own ideas of greatness, and in the areas where it recognizes, encourages, rewards, and honors greatness. So the challenges ahead for science, not only in a

substantive, but in a social, sense, may indeed be more novel, more subtle, and more demanding than they have ever been.

The veritable revolution in comprehension of our universe and of our own relations to it that we have recently experienced are not, of course, at all new in human history. They are as old as the world of Aristarchus of Samos or of Copernicus and Galileo; as recent as that of Darwin and of the revolution in physics during the early years of the twentieth century. Each revolution prefaced new vision, a widened intellectual scope, for the generations that followed. But such major conceptual transformations never come easily. The greater the gap between old and new, the more difficult and traumatic they are and the more reluctantly they are accepted. One recalls the seventeen centuries that elapsed before the notion of Aristarchus that the earth, instead of being the center of the universe, was in fact a satellite of the sun gained any firm and general foothold in man's intellectual tradition, spurred by the work of Copernicus and the publication of *De revolutionibus orbium coelestium*. One recalls the elements of hostility in the initial reception of the *Origin of Species*, and that it was nearly a century before there was full and general acceptance of the new ideas it expounded. One is reminded of the forty-five years of virtual oblivion that greeted the critical paper of Mendel, even though it was published not nearly so obscurely as has often been supposed. One remembers the relatively long struggle that followed the development of the new physics before it, too, offered a fresh basis for human understanding. Hostility, resistance, and with them, often enough, a poignant sense of diminution of man's own place and significance in the universe of his imagining have been the common accompaniments of great conceptual change throughout the history of science. But it is notable too that those negations, so natural and so altogether human, have also, in the end, revealed a subtle and apparently paradoxical obverse, an obverse ultimately of profound significance for human growth. Over and over again we have seen that the final acceptance of a new stage of human understanding about the natural world—an acceptance which at first appeared to sanction an intolerable demeaning of man's stature and accordingly was resented and long resisted—has instead fostered a new order of human sensitivity and appreciative capacity; has signaled, indeed, a new and salutary humility before the wonder and the glory of the unfolding universe. And with that humility has characteristically come a renewed sense of the integrity of the partnership of man and his environment, a sense of a deep and fundamental unity with nature. That may well be one ultimate fruit of the dynamic advances of the last decades. We can properly anticipate its ripening over the years to come.

But there may be one important aspect in which the experience of the last two decades has differed significantly from all that went before. In none of the earlier great periods—not even during the revolution of physical concepts in the early years of this century—did means exist to communicate the new findings almost instantaneously and universally. Nor, in the earlier periods, did there exist a potential audience of anywhere nearly comparable numbers: an audience sensitized to information of this kind, eager to hear and ponder it, but at the same time, because of the nature of its particular training and experience, frequently lacking a basic appreciation of the wider framework of scientific knowledge, of the organic fabric that made the great discoveries possible. In the absence of that rather sophisticated kind of appreciation, each new advance must



appear episodic, detached from its logical context, and so, inevitably, deeply unpredictable. A series of novel advances, even if in the same field and actually logically related, can easily be interpreted as a succession of unconnected events, replete with power for change, replete with power to disorganize the known, ruthless and in a real sense capricious in their impact. When the apprehensions that such misconceptions naturally engender are reinforced by other related anxieties of our age, real understanding and support of science by the society can be genuinely threatened. One of the most important, as well as one of the most subtle and difficult, of all the demands ahead may be to bridge the gaps of such misunderstanding.

There can be little doubt that the swiftness and the scope of scientific advance over the last two decades, the degree to which it has enlarged horizons and has added to the richness and the beauty and the inspiration of the very quality of life, have in themselves created a strong impression of discontinuity, of quantum leaps of experience and intellect. How striking it is, for instance, to reflect that only a decade has passed since the discovery of the first quasi-stellar radio source, which was optically identified at the Hale Observatories by Sandage and Matthews. It was three years later that Schmidt solved the puzzle of the peculiar spectra, setting a new and almost incomprehensibly enlarged distance-scale, of the order, perhaps, of 9 to 10 billion light-years for the universe. It is but three years since the measurement of the order of redshift shown by the quasar Parkes 0237-23 established yet a new upper figure for the shift, and so for the implications that it may carry for the dimensions of the universe, and even this has currently been exceeded. Only a decade ago the very designation *quasar*, now so nearly a household word around the globe, was yet to be coined. It is only three years, too, since Anthony Hewish and his colleagues at Cambridge University detected that new class of stars, the pulsars, which still present so many theoretical puzzles to the astronomer. Another name, now so widely familiar to an interested public, did not exist even a half-decade ago.

Again, it comes as something of a surprise to recall that the very term DNA, and the revolution in our vision of the nature of life epitomized in the concept and the knowledge that genetic information is indeed coded, were largely unknown, except among those professionally concerned with that area of research, less than two decades ago. Yet that frame of reference is now so widely taken for granted that it seems always to have formed the basis for our thinking about the nature of life. And, in the context of the deep and continuous stream of scientific thought that flows beneath its apparent discontinuities, it is worth recalling that the year 1969 marked the hundredth anniversary of the discovery of DNA by Friedrich Miescher, which he named *nuclein*.

It is only a few years since the idea that the basic principles of the genetic code are the same for all living creatures, from bacterium to advanced plant to fish to reptile to bird and mammal and man, became widely accepted and familiar. It is a still shorter time since one reasonable deduction from this knowledge—the view that all contemporary life may be related in evolution at a deeper level than we had hitherto considered—has become familiar to men and women everywhere who think about the nature of life and its origins, or who are specifically concerned about man's own position in the natural world. The vision that such lines of thought suggest has surely affected our view of organic nature and of our-

selves more deeply than any single scientific event since the work of Darwin. And yet it is almost of today.

It is hardly a decade since man's history on earth was widely thought to encompass at most a little more than a million years; when Neanderthal man, dwelling in Europe 75 thousand years ago, was generally regarded as a primitive, remote ancestor. Today we no longer marvel at the thought that creatures definitely manlike in their structure and probably in their general habits, creatures almost certainly of man's immediate ancestry, were widely distributed in the Old World some 15 million years ago. The concept, at once humbling and inspiring, that the shaping of modern man has required 15 million years or more—a concept hardly considered a decade ago—now seems altogether familiar.

It is much less than ten years since we achieved what seems, at last, to be a really clear picture of the structure of the very surface of the earth on which we dwell. Indeed, only about three years have passed since a comprehensive model was at last generally accepted—the model of an outer zone divided into a series of plates, segments of a sphere, each rigid in itself but mobile with respect to its neighbors, created at oceanic ridges and, in turn, buckled downward at oceanic trenches. Only since the refinement of that model and its recent confirmation in a variety of ways—by its satisfactory accounting for and predicting of the fault plane solutions of earthquakes; by the consistency it lends to the patterns of distribution of worldwide volcanism; by the picture that it offers of the mechanisms and character of continental drift—have we really attained a clear understanding even of the outer layers of our planet.

Again, in a framework where the shock of discovery and the impression of discontinuity that it creates have been particularly keenly and universally felt, it was only ten years ago that we embarked on that immense adventure in the infinitesimally thin shell of outer space that lies between us and the moon; the adventure that was to culminate in our first physical contact with our satellite. At the beginning of that adventure, though the moon had been under searching observation by astronomers for a half-century and more and we actually knew a great deal about it, we still had no firsthand or widely held appreciation of the actual depth of its inhospitality. Throughout the decade there was lively speculation that the moon might harbor, or might have harbored, life in some form, further knowledge of which, of course, could be of the utmost fascination and importance. There were, naturally, opinions to the contrary, based on strong though indirect inference. Yet it was only after the moon had actually been explored that men everywhere were ready, reluctantly, to accept the view that, so far as we can at present determine, life remains a unique property of our own planet at least within the solar system. As the certainty of the lifelessness of the moon finally struck home, and as the image of its frigid inhospitality was confirmed over and over again by the amazing photographs that the astronauts secured, there emerged among men and women generally a new appreciation of their own celestial island. The crowning impact, with little doubt, came with the publication of the photographs of planet earth taken from the moon. Those views of the variegated, beautifully colored, lonely globe whirling in space may have had a more powerful influence in impressing upon men and women everywhere both a greater respect for the planet on which they are so utterly dependent and which in turn is so completely in their keeping, and a deeper feeling for the order of its fragility. That, surely, has been an evolution of vision alone sufficient to distinguish the decade just closed from all its predecessors.



Given the cumulative impact of all these revolutionary changes in our percepts of our universe, of our planet, of the life upon it, and of ourselves against this wide and turbulent panorama that so recently was so unfamiliar, what wonder that we are so heavily burdened today with a feeling of profound unrelatedness, with a sense of catastrophic detachment in the currents of our time from all that has gone before? What wonder that we are often tempted to believe that we exist in a lonely and sometimes frightening intellectual isolation?

What wonder, perhaps, that the current popular image of science has become so fragmented? There are those who still see in the scientific mode what has guided its greatest practitioners through more than three centuries. They can still view the scientific way as perhaps the most powerful liberator of the mind and spirit that man has known in his long searching after knowledge and confidence; as one of the most important factors reinforcing the sanctity and the security of the individual; as the medium through which new vistas of the extent and overwhelming glory of man's universe can be brought home in visions ever more compelling to expand the spirit. Yet there are others, of the highest moral and intellectual stature, who feel that science brings to society a philosophy of purposelessness, a view that man reacts automatically to his environment rather than responding creatively to it, and that the chief method of science is a destructive analysis.

It is important both for the genuineness and effectiveness of the relationships of science to society, and for the welfare of science itself, that varied and divergent estimates of its strengths and vulnerabilities and its proper social functions be continually made and explored. Yet there is a real danger that contrasting views so radically opposed and polarized as some of the more extreme that are current today can, over the long run, only be seriously damaging to science. They are all too likely to prove equally damaging in other vital sectors of our national life as well. And so it becomes extraordinarily important that a sober and accurate understanding of the real nature and tasks and constraints of science, a real appreciation of the modes in which it works and of the values underlying them, should be conveyed as widely as possible in the society. To further that, indeed, may well be one of the most important tasks of the coming decade, in the interest alike of science and of the society that it serves. One of the important elements in this task will be the dissipation of that powerful illusion of discontinuity, of sudden and catastrophic change, that the very triumphs of science in the last decade have so frequently fostered.

That notion of sharp discontinuity is of course a myth, across the whole scientific front. The year 1970, for instance, marks the 497th anniversary of the birth of Nicolaus Copernicus, the 406th of Galileo Galilei, the 399th of Johannes Kepler. Through all those centuries the integrity and continuity of that thin, clear stream of astronomical exploration have been maintained. Even particular lines of investigation that contributed directly to the current triumphs of cosmology found their inception almost half a century ago in Hubble's concept of an expanding universe, and in the early measurements of the redshifts of the spectra of faint, far-distant objects in the heavens, in the hands of Humason and Minkowski and the company of their colleagues. And in our own day the first—and so far the only—optical pulsar known, discovered two years ago in the Crab Nebula, proved in fact to be a celestial object that Walter Baade and Rudolf Minkowski, at the Mount Wilson and Palomar Observatories, had espe-



cially noted twenty-seven years before and predicted would be found to have special properties as a remnant of the supernova itself.

Again, as we look back at the events surrounding the publication of the *Origin of Species*, it is all too easy to regard that great advance of understanding as a major discontinuity in the scientific stream, as a titanic revolution of man's thought, taken in isolation and without precedent. At this distance it is all too easy to ignore the scientific matrix from which it sprang: the matrix which, in vague and unformulated intuition, had engaged Erasmus Darwin in his *Zoonomia* more than half a century before the publication of the *Origin*; the matrix from which sprang the independent formulation of evolutionary theory by Alfred Russel Wallace at Ternate; the matrix from which the obscure Edward Blyth was able to correctly outline a theory of evolution in a paper actually preceding the publications of Darwin—though, ironically, his inferences from that theory were precisely wrong, supporting conclusions the very opposite of Darwin's own.

As multifarious threads of scientific investigation in every field link the dramatic findings of today intimately with those of the past in a close-woven fabric, so that fabric, unbroken, extends into the future. Nowhere can this be more vividly illustrated than among discoveries of the year just past.

The tide of investigation of the quasars continues unabated, participated in, now, by a larger number of astronomers. This year, once again, a new value has been set for the redshift of a quasi-stellar object. A quasar identified a year ago with the radio source 4C 05.34 has been found to show a redshift value of  $z=2.877$ , remarkably higher than the highest figure previously well confirmed, of  $z=2.358$  for the object designated 4C 25.05. This evidence for values notably greater than  $z=2$  is particularly dramatic.

The great questions of the basic nature of the quasars, of how their extraordinary redshifts and presumed immense astronomical distances are to be related to their apparently small dimensions and hence necessarily tremendous luminosities, even the fundamental question of precisely what the gigantic redshifts mean, remain the enigmas that they have been ever since quasars were first reported. The challenge for the next decade is immense.

The challenge of the pulsars, too, remains as great, with many of the mysteries surrounding them still unresolved, though new and suggestive data have recently been accumulated and stimulating new finds have characterized the current year. The basic view of pulsars as spinning neutron stars seems satisfactory as a general theory of their nature, but a host of puzzles remains. Indeed, the precise mechanism by which the pulsars emit their finely timed and extraordinarily regular bursts of radio, optical, and X-ray energy remains one of the great challenges to astronomical research in the 1970's. An intriguing enigma was added during the year just past by evidence that pulsar NP 0532, the pulsar associated with the Crab Nebula, emits bursts of gamma radiation, with a periodicity of 33 milliseconds corresponding to that of the pulsar itself. Yet another question has been raised by the observation that in pulsars the fluctuations of pulse height may be periodic. That phenomenon was first observed in pulsar CP 1919, and has since been detected in others. A pronounced modulation recently observed in CP 0834 may not be readily explicable by current theories of pulsar constitution.

Activity has been intense along the broadest fronts of cosmology during the year just past, and promises to continue so throughout the decade. Questions are

being asked about possible convergences, at the level of evolution and dynamics, between quasars and galaxies, and new experimental models of quasars are being devised. The mysteries surrounding the production of bursts of X-ray energy from "X-ray stars" still remain, and there do not seem, as yet, to be acceptable models to account for them. But recent studies of the fine structure of optical flares in Sco X-1, one of the few X-ray stars so far identified with a visible object, may hold the promise of new theoretical approaches to the question.

Since his earliest concern with the universe man has reflected upon its origin, and has pondered whether in time as in space it had a finite beginning and will have a finite end. In recent decades, such thinking has crystallized around two quite different concepts: the "steady state" picture, with its assumption that matter throughout the universe is in continuous equilibrium between creation and destruction, and the theory of the "big bang," taking its roots in the picture of an expanding universe and postulating that, at a given point in time, all matter was gathered into an extremely dense mass, which exploded, perhaps some 10 billions of years ago, to form the expanding universe in which we dwell. Throughout the last decade a variety of evidence has accumulated, which points to the second view.

Thus through multifarious channels, of which these are but a representative few, the life-stream of cosmology, the constant and ever advancing search for knowledge and understanding of our universe, flows undiminished into the new decade, extending the uninterrupted quest that has captivated the spirit of man since the days of Copernicus.

The march of investigation of man's nearer world: his search for a fuller understanding of his immediate physical and organic environments, of the fellow-inhabitants of his planet, and ultimately of himself, shows the same undiminished vigor, the same continuity with its past and its prospective future, the same kinds of gains in perception and in power. During the year just past, it has been distinguished by several dramatic milestones. A major landmark on the long investigative trail of the structure and functioning of DNA was the culmination, during 1970, of seventeen years of planning and research directed toward the laboratory assembly of a gene from wholly synthetic building blocks. Following a strategy outlined in detail when he shared the Nobel award for his part in deciphering the genetic code, Har Gobind Khorana this year announced a successful assembly of the seventy-seven bases that make up a gene which specifies the formation of the transfer-RNA of alanine in yeast. The way that goal was achieved offers a dramatic and illuminating illustration of the deep-laid continuity so characteristic of every major line of research.

In 1965 at Cornell University, Robert Holley succeeded for the first time in elucidating the structure of a natural nucleic acid. It was this same transfer-RNA, serving as an adapter to put alanine into its proper sequence. Once known, that structure could be made to provide information from which the structure of the gene coding for it could be inferred, using the rules for base-pairing earlier formulated by Watson and Crick. Thus both the basic theory and the design of a strategy for demonstrating it were fairly straightforward. But practical execution of the strategy was both difficult and subtle. For it is by no means experimentally feasible to assemble the required bases in an appropriate linear order simply by adding them one at a time in the correct sequence. The success-



ful procedure, made practicable, among other things, by the discovery in 1967 of a "DNA-joining enzyme," involved linking segments of chemically synthesized DNA, each consisting of several bases, in such a fashion that each fragment left an "overhang," a "sticky loose end" serving to attach and align the next piece of DNA.

An extraordinary goal has been attained in the artificial synthesis and assembly of a biological molecule central in directing a vital life process. Will it "work" in the cell, proving that it is truly functionally equivalent to the natural gene coding for the particular transfer-RNA? That remains to be seen.

Other notable accomplishments in molecular biology have marked the year, each rooted quite as firmly in work of earlier decades and each significant for the future. Late in 1969 at Harvard, for example, the isolation of the *lac* operon from the genome of *Escherichia coli* was announced. This operon includes three genes which code for enzymes involved in the metabolism of lactose by the cell, together with a series of "switches" controlling the operation. At about the same time, Dorothy Hodgkin and her group at Oxford were able to announce the resolution of the precise configuration of the insulin molecule—the first protein hormone to be so resolved. This extraordinarily difficult accomplishment climaxed seven years of work, and rested on related investigations dating back to 1935. The contributions of the new knowledge to a fuller understanding of diabetes during the coming decade may well prove of major significance to medicine.

On yet another front, work in many laboratories all over the world is leading to ever more precise genetic mapping of RNA bacteriophages, and of the modes of transcription of the information carried in their genomes. In the summer of 1970 a significant and rather striking discovery was reported, which took its roots in earlier work of H. M. Temin. It was found that in certain RNA viruses associated with the genesis of some animal tumors, notably the Rous sarcoma virus and the Rausch mouse leukemia virus, RNA can actually act as a template to direct the synthesis of DNA. This represented a precise reversal of the conventional and much more usual sequence of flow of genetic information from DNA to RNA to protein. Nevertheless, it is a pattern that was envisioned as a real possibility early in the decade of the 1950's by Francis Crick in his "Central Dogma" of molecular biology. For some time there have been suggestive hints in this direction. It is known, for instance, that inhibitors of DNA synthesis can protect some animal cells from infection by certain RNA viruses. A suggestion, detailed in the current *Year Book*, that the RNA of Rous sarcoma virus interacts with the initiating site for host cellular DNA synthesis was reported from the Department of Embryology of the Carnegie Institution. It now appears that a specific enzyme in those RNA viruses indeed catalyzes the building of host-cell DNA upon the viral RNA. The precise mechanism of this building is not yet certainly established. But it appears possible that an intermediate RNA-DNA hybrid strand is formed which may then change to duplex DNA by displacement of the RNA strand—a DNA now carrying some of the information of the viral RNA. Such a DNA duplex strand could presumably replicate thereafter in the ordinary manner. Whatever the process may be, the fact that in certain organisms the usual direction of flow of genetic information from DNA to RNA may be reversed adds another interesting variant to the panoply of molecular genetics.

While these novel findings were being made at the molecular level of the gene and of the RNA, work at other biological levels was progressing too, quite as novel and surely carrying quite as significant long-range implications. One note-



worthy approach involved the first successful attempt to model the function of a cellular organelle. The lysosomes are intracellular saclike structures which store lysozyme, a powerful digestive enzyme. They can release the enzyme, at appropriate times, to combat bacteria threatening the organisms containing them. Accurate timing of the release is of great practical importance, for lysozyme at large within a cell can itself be fatal to it. Such functional features were successfully represented in the model, which in the coming decade should aid materially in understanding the lysosome and its action. Equally or more important, the work may stimulate and help to inform other attempts to model more complex and even more significant organelles of the cell, for instance, the mitochondria. Modeling of this kind cannot fail to advance our understanding of biological action at a level of organization intermediate between that of the critical biological molecules, which are the focus of so much current research, and that of the entire cell.

At the level of the structure and function of the chromosomes, the year has seen remarkable technical achievements. Some have considerable implications for medicine. All are of significance in genetics research.

The fact that most cells of nearly all higher organisms are diploid has long placed real restrictions on their genetic study—restrictions that do not constrain investigators in bacterial genetics. The virtual impossibility of obtaining pure lines of many multicellular organisms of genetic interest, lines that are truly and reliably homozygous for all the characters studied, has long posed serious obstacles to quantitative investigations of heredity in such plants and animals. The dream of a geneticist working with cultures of cells of higher organisms would be to have available a line containing only one set of chromosomes per cell. That goal has now been reached. By removing the maternal nuclei from frog ova which had already been penetrated by sperm cells, and inducing the operated eggs to develop thereafter, Jerome Freed and Lisolette Mezger-Freed, working at the Institute for Cancer Research in Philadelphia, have been able to establish two lines of haploid cells that survived some fifty subcultures without either becoming diploid or being overgrown by alien diploid cells. Such cell lines of vertebrates, once stabilized, should provide tools of great potential usefulness.

Several years ago, Yoshio Okada of the University of Osaka in Japan first clearly demonstrated the possibility of fusing cells from very different organisms by the intervention of a virus, a possibility brilliantly exploited by Mary Weiss, Henry Harris, and Hayden Coon. Most dramatic was the fusion of mouse cells with human tissue cells that had been transformed with sarcoma virus 40. Such "hybrid" cells contained chromosome sets of both parents. During subsequent cell divisions the human chromosomes were preferentially eliminated. This preferential loss permitted direct study of characteristics associated with the human chromosomes, and also of the action of the virus itself.

A similar effort, though using very different techniques and with results so far confined to fusing the cytoplasm of plant cells, is now being pursued at the University of Nottingham. The method in this delicate operation has been to extract the contents of the plant cells from their containing coats and to fuse the two cytoplasm by special manipulation. Nuclear fusion, analogous to that obtained with the mouse and human cells, does not seem yet to have been achieved. But the reliable production of fused cells including two nuclei containing sets of chromosomes from different plant species may offer a significant approach to the "hybridization" of crop plants that cannot be crossed by conventional methods.

And such crops include some of the most critical food staples of man, including barley, oats, and corn.

Similar experiments with protozoa are under way, at the State University of New York at Buffalo. Methods have been perfected to separate cell coat, cytoplasm, and nucleus in individuals from differing strains of *Amoeba proteus*, and to recombine them by injecting empty cell coats with cytoplasm, and then, in a delicate micromanipulation, reinjecting the appropriate nucleus. Viable clones of amoebae made up of such mixtures seem to have been achieved. A new tool may be in the making for the critical investigation of various major components of one protozoan cell functioning in the environment of another.

Ninety-nine years ago Sir Edwin Ray Lankester wrote: "The chemical differences of various species and genera of animals and plants are certainly as significant for deciphering their origins as the differences of form. If we could define clearly the differences in molecular constitution and functioning of different kinds of organisms, we should be able to perceive the evolutionary patterns of development more readily than from morphological considerations." A century later that prophecy is being vividly realized in many contexts where the approaches of the study of evolution intersect those of molecular biology. One of the most exciting, with its greatest insights almost certainly still ahead, has been built around techniques of base-pair matching in the DNAs and RNAs of organisms at various phyletic levels, carried forward in several laboratories but pioneered particularly actively and fruitfully at the Carnegie Institution of Washington over recent decades. The convergence of genetic, phylogenetic, paleontological, and evolutionary concepts, meeting on this common ground, has permitted conjecture, perhaps more suggestive and pertinent than ever before, of the orders of geological time involved in the occurrence and establishment of those molecular base modifications in the DNA that clearly provide the raw materials for organic evolution. The concept and the dramatic demonstrations of replicated segments of DNA in the chromosomes of a wide variety of higher organisms—replications, in the extreme, of the order of a million copies—raise searching questions in many areas of molecular genetics and developmental biology, but perhaps nowhere more suggestively than in the study of evolutionary mechanisms. Already it becomes easier to understand how certain apparently difficult biochemical evolutionary "bottlenecks" that some many-celled organisms have clearly passed—barriers, for example, like the transition from the single type of hemoglobin in the blood of the lamprey to the multiple molecular species in the blood of higher vertebrates—were negotiated. Many repeated units of the DNA, "free" to mutate while nonmutating congeners can continue to code for the original, unmodified elements, would appear to be essential to the survival of the organism at the point where that particular chapter of change begins. Investigations contrasting the degree of evolutionary divergence between families of repeated DNA sequences unique to particular members of biological groups obviously related yet long reproductively isolated, such as various rodents, with that in families more broadly shared among such groups—and so probably already present before the members had evolved to reproductively isolated species—have long been carried forward in the Department of Terrestrial Magnetism of the Carnegie Institution. Studies motivated by a similar philosophy are being undertaken at another biochemical level, comparing the amino acid sequences in par-



ticular homologous proteins of different species of plant or animal with a view to correlating similarities and differences with phylogenetic relationships deduced from more conventional evidence. An interesting example of work of this kind involves the conjugated protein cytochrome C, biologically crucial since it forms an essential part of the respiratory chain that functions in the terminal phase of the oxidative metabolism of carbohydrates in animal nutrition, yet "flexible" in the sense that several primary molecular structures could be consistent with that vital function, and particularly informative to work with since amino acid sequences have been deduced in some thirty species.

But the most sweeping evolutionary questions at the level of biochemical genetics are still unanswered. How the genetic code first appeared and then evolved, and, earlier even than that, how life itself originated on earth remain for the future to resolve, though dim and narrow pencils of illumination already play over them. The fact that in all organisms living today the processes both of replication of the DNA and of the effective translation of its code require highly precise enzymes, and that, at the same time, the molecular structures of those same enzymes are precisely specified by the DNA itself, poses a remarkable evolutionary mystery. How can a particular strand of DNA, dependent for its replication on a highly specific enzyme, have possibly evolved the code to direct the information of that same enzyme, given the obvious condition that the evolutionary survival of the organism containing it must have depended on the success of such replication? This question, of course, raises another. Did the code and the means of translating it appear simultaneously in evolution? It seems almost incredible that any such coincidence could have occurred, given the extraordinary complexities of both sides and the requirement that they be coordinated accurately for survival. By a pre-Darwinian (or a skeptic of evolution after Darwin) this puzzle would surely have been interpreted as the most powerful sort of evidence for special creation. In our day another, but still far from demonstrated (or possibly demonstrable), view seems the only logical one: the view that a primitive and generalized mode of replication of genetic material arose in evolution either before the existence of these critical enzymes or coordinately with proteins which gradually took on crude and generalized enzyme-like functions. Such a tentative hypothesis at least emphasizes once again how far even the most primitive of contemporary single cells have evolved at the most critical biochemical levels—how far, indeed, the exquisite adjustments of such an evolution must have proceeded before anything that in our world we would even recognize as life was possible. By the same token, evidence of that stage in the emergence of life clearly disappeared from our planet long ago, snuffed out by billions of generations of more complex organisms which still must have been far more primitive than anything we now know. So we are left with a real gap in our understanding. New and testable insights into this problem would rank with the greatest of all our advances in evolutionary theory. Indeed, they might well provide innovations for all biological thinking as pioneering and stimulating and important as was the concept of the gene itself in the biology of its day.

At the level of the most fundamental of all questions about evolution—how the particular molecules from which living systems were initially built became available on earth in the first place, and how remote their own origin may have been in time and place—research and thinking of the last years have shed suggestive light. It now seems clear that a number of molecules, including water, ammonia, hydrogen cyanide, cyanogen, formaldehyde, perhaps methane, all or



severally may have been critically related to the origin of life. It has been well known for some years now that when such substances react in the laboratory in the presence of suitable electrical or radiant energy and appropriate simple catalysts, their products include a high proportion of molecules that are of critical significance as constituents in both the nucleic acids and the proteins of contemporary life. As in the evolution of DNA and its processes of coding and of replication, all evidence of these very early stages must have been permanently lost over the vast stretch of time that biochemically more modern life has occupied the planet and preempted all its niches.

There are reasons for supposing that these first steps of life must indeed have been taken at a very remote period of earth history, when our planet was still relatively young—perhaps 3 to 4 billion years ago. Thus a special biological interest as well as an intense interest in the broader contexts of the evolution of our galaxy and our solar system attaches to the continuing discoveries of species of molecules in outer space which a decade ago were surely not expected there, accomplished through the searching probes of radio astronomy. Two years ago Charles H. Townes, with his colleagues at the University of California, detected the signature of ammonia in the radio spectrum of a cloud lying in the direction of Sagittarius, near the center of the Milky Way and perhaps 30 thousand light-years from the earth. This was the first time that a molecule of such complexity had been identified in interstellar space. Work of this character has continued, with striking new findings. Last year free formaldehyde was detected in interstellar space—a most unexpected finding, since it had been thought too fragile to endure the bombardment of radiation and particles to which it would be expected to have been exposed.

Recently, evidences of the hydroxyl radical have been reported from the same space “clouds” as those offering refuge to formaldehyde. The signature of molecular hydrogen in outer space has also been reported recently, and early this year evidence of carbon monoxide was found in interstellar space. And in 1970 Dr. David Buhl and Dr. Lewis E. Snyder reported an emission signal from hydrogen cyanide. Less than half a century ago, interstellar space was widely believed to be a complete vacuum. It is striking to reflect, now, that such molecules as these do indeed exist there. It is interesting to recall, too, that hydrogen cyanide is a prominent constituent of those gaseous mixtures which, when illuminated with ultraviolet light in the laboratory, have been found to evolve significant yields of amino acids, the building blocks of the proteins.

The greatest advances in our understanding of all these novel elements in the picture of the evolution of life must lie ahead. But there will surely be other and equally exciting intellectual challenges, too. Perhaps the greatest for the decade of the seventies will lie at the frontier of research in the structure and mechanism and functioning of nerve and brain. It is not a new frontier, for scientists have worked along it, breaching it at points, for full two generations. But the subtlety and complexity of the problems are so great that effective attack on them has had in many cases to wait for the development of more delicate and penetrating tools, physical and theoretical, than we have ever had before. Now some of those physical and intellectual tools are becoming available, in the shape of more powerful scanning electron microscopes; more efficient stains to trace the detailed topology of nerve nets; microelectrodes of improved individual design

grouped into more complex arrays, permitting finer resolution of patterns of nerve impulses than ever before; adaptation of special techniques of cell culture to achieve the proliferation of single nerve cells on artificial media and the maintenance and study of nerve nets in the laboratory; new techniques of behavioral observation and analysis; a growing knowledge of drug action at a molecular level; and the adaptation of computer techniques to analysis of the extraordinarily involved and elaborate sets of signals that nerve-muscle complexes generate in any animal above the level of a jellyfish or a sea anemone. But, most important of all, the subject is now attracting a large number of investigators of the very first rank, entering it *de novo*, or transferring from distinguished research careers in other fields in the firm belief that for the remainder of the century this will be the area, above all others, to challenge their talents and that moreover it may well develop into the most significant of all research frontiers in furthering human welfare in the most individual and fundamental sense.

Like many areas of inquiry that will engage us most vitally during the remainder of the century, this is no single discipline. Rather it is a meeting ground of many: neuroanatomy, neurophysiology, neurochemistry, statistical biology, experimental psychology, ethology, and a variety of others. Obviously, the attack must continue to be mounted, as it has been in the past, from many apparently disparate directions: from the aspects of growth and the mechanisms of message transmission at the level of the individual neuron; of embryogenesis and the early embryonic growth of nerve tissues, especially comparatively among various organisms; at the level of multiple innervation of organs; at the supremely difficult level of brain and behavior, to name but a few. All these arenas, of course, have been explored, in one facet or another, over the past fifty years or more. What we may now well expect, however, are insights of continually greater depth and generality. Newer areas will surely be approached along avenues that shed increasing light beyond the subjects of immediate investigation. One such suggestive research salient involves analysis of the suppressive effects of specific chemicals, including the antibiotic puromycin, upon the expression of memory in the mouse, and of equally highly specific effects of certain other compounds in restoring that expression, being carried forward currently at the Carnegie Institution of Washington and the University of Pennsylvania. It is of special interest, too, that work elsewhere in the Institution has shown that actinomycin D, puromycin, and cycloheximide, the first of which blocks RNA synthesis, the second and third the synthesis of protein, all inhibit the development of a high concentration of receptors in innervated muscle fibers away from the neuromuscular junction, fibers that normally develop rapidly when isolated rat muscle is maintained in organ culture. All three of these substances have figured prominently in memory research. Both these programs are described in detail in the current *Year Book*.

As we enter the decade of the seventies, it is crystal clear that in America, as over the world, the tide of scientific research has never flowed more vigorously. Never in history has it been so many-branched, so subtle, so penetrating in its vision of ourselves and of our world. Never, surely, has it pointed to more exciting new frontiers than today, or offered so many intellectual opportunities. More than ever there is profound pertinence in the moving observation of John Wheeler, in his address before the International Atomic Energy Commission in Vienna in 1968 entitled *Marie Sklodowska-Curie as Copernicus of the World of the Small*: "Today, thanks not least to these great investigators, we see in our mind's eye



each decade of the distance scale alive with its own special activities, from the expansion of the universe at  $10^{28}$  centimeters to the growth of a crystal at  $10^{-1}$  centimeter, and from the collapse of a white dwarf star at  $10^8$  centimeters to the form factor of the protein at  $10^{-16}$  centimeter."

The impressive continuity of the flow of science from the past to the present and on into the future—precisely in an age when doubts about that continuity are so often expressed—embraces, of course, far more than substance. It involves as well a continuity of intellectual tradition: a continuity of that priceless drive to satisfy the curiosity of the investigator and to slake the thirst for knowledge of those who follow his work; and, above all, a continuity of growth in the individual stature of men and women who pioneer on scientific frontiers. But these continuities are also of the utmost importance for our whole society, extending far beyond the relative handful actively caught up in them, and this for many and different reasons. History is eloquent that it is through *and only through* the unrelenting thirst for knowledge, and the constant striving to satisfy curiosity that accompanies it, that all the truly great advances in our understanding of the world have come. It is a fair inference that the gaining of further major insights about our world and ourselves will depend in large measure on how well we understand this dedication and support it in the future. That is a point demanding special emphasis today, when we may be tempted to carelessly extrapolate pragmatic approaches beyond their proper domain into areas where they no longer serve us well.

The lives of Newton and Darwin, of Mendel and Faraday, find their counterparts among a legion of further investigators, widely or little known, who have served world civilization from their time to ours. Albert Einstein once wrote, in the setting of an earlier day: "... [scientific] endeavors are based on the belief that existence should have a completely harmonious structure. Today we have less ground than ever before for allowing ourselves to be forced away from this wonderful belief." It is clear today that this profound observation is more deeply pertinent to our society than it has ever been. For at the very time when the river of science is flowing most abundantly, when its steady returns in the form of new knowledge and new insights have never been more vigorous, when its future potential has never seemed greater, the tangible threats to its welfare are indeed of an order that we have not experienced for a long time.

The fabric of unease with science that exists today is spun of far too many threads too intricately interwoven to permit any comprehensive description, or indeed to allow full comprehension of its nature at present. Quite possibly, complete understanding is inherently impossible now; perhaps the situation can be seen whole only by future historians of science. But it is surely possible to distinguish certain of its elements and to examine them critically. It will be important to attempt this with vigor and persistence during the coming decade.

Some of the most obvious and indeed striking elements may also be among the more intractable. The rapid evolution of the society itself over the past decade; the almost cataclysmic shifts of priorities in patterns of commitment and demand within large segments of the body politic; decline of faith in older approaches; fears about the possibly unfamiliar shape of a future political world; with a host of related concerns as broad and yet as inchoate, fuel a climate of anxiety which includes science in its ambient. Added to all this, there is evidence



in places of a sheer intellectual weariness, a reaction of some to the cumulative circumstance of many years of extraordinarily vigorous intellectual growth, and with it high intellectual demands—the reaction that so often in history has more severely affected those who inherit an atmosphere of stress than those who have been directly caught up in the experience of it. Peter Medawar has recently pointed out some striking similarities of our own time to the first half of the seventeenth century in England. That epoch, like this, was not characterized by any strongly marked systems of belief. Rather, like our own, it was an uneasy time, plagued by the sense of emptiness so characteristic when one set of doctrines is widely felt to have been outgrown, but another more adequate and satisfying has not yet been conceived. In our time, indeed, we may have come full circle. For it was at the end of that uncertain, vacuous period, in the second half of the seventeenth century, that the new climate of rationalism—the atmosphere in which science itself was to root so vigorously—appeared and prospered and spread to create a new theater for the emotions and the energies of men. The central feature of that doctrine, of course, was its reliance on the power of reason, and, in consequence, its elevation of the processes of reason to the very apex of the goals and values of society. That was a novel, and a heady, and an extraordinarily viable doctrine. The culture suddenly exposed to it swept forward as on a tide. But though the vast momentum that it generated was to endure into our own age, the sheer force of its novelty was gradually diluted by growing familiarity. And as this happened, a subtle but important transformation of attitude took place that surely has important implications for our own time. As Medawar has presciently noted, the seventeenth-century idea of the *necessity* of reason slowly crystallized to an eighteenth-century view of the *sufficiency* of reason. It was Thomas Henry Huxley who remarked that it is the fate of a new scientific concept to begin as heresy and end as orthodoxy, and that transformation is not restricted to the ideas of science. A progressively orthodox reliance on the sufficiency of reason to solve all of man's relationships with the world, a reliance that increasingly characterized the latter half of the nineteenth century and the first half of the twentieth, may have laid the ground in some measure for the considerable loss of faith in reason itself that threatens our own age. Extreme views typically invoke opposite reactions. As Medawar has also noted, we live in an age more than touched by the damaging philosophy that reason itself not only is not *sufficient* for us; it is no longer *necessary* for us. That curious inversion can exert a considerable adverse influence, not only on science, but on all rational thinking.

Another current hazard for the philosophy of the scientific way may become more evident, and also more comprehensible, when viewed against the opening years of the seventeenth century. The dissatisfactions of that period clearly made it appear, to those who were living through it, a time of retrogression and decay, a time of both intellectual and material wandering, when philosophical rootlessness presaged a long eclipse of the human mind and spirit. A similar kind of dismay is surely with us today. As with any other generalized malaise, we seek avidly to identify its objects concretely and specifically. In our age the social effects of technology, whatever they may be, are specific targets of such unease: the obvious—and real—foci for depths and intensities of anxiety which they may often justify, but for which they are in fact only partly responsible. Indeed, the all-too-brief span of general concern about any specific problem, so widely evident and so deplored today, is precisely what would be expected in a time of deeper

and less focused unease. And in an age when there is often a failure to distinguish the considerable and important differences between the nature of technology and of science, science too tends to share the spotlight in this anxiety-ridden disenchantment.

No ages of human history ever precisely repeat the courses of earlier ones. Comparisons are likely to miss the specific features that later history will show to have had key significance. Nonetheless, if the comparison between our times and the early years of the seventeenth century carries any validity at all, it may also bring hope. For when the change came, when the spiritual and intellectual world touched new and firmer ground in the second half of that century, the burst of creative energy released was, of course, immense. This was not the period when the idea of science *originated*. The concept itself was in fact far older. But it was indeed the period when science found congenial soil, and so took firm root and flourished. Its stimulants were the revival of optimism and belief, the climate of hope for the future. It may not be unrealistic to anticipate that we shall emerge from our present doubt and uncertainty, however long it may take us to do so and however difficult the building of a new philosophical base may be, in a similar burst of revived hope and creativity.

In a nearer and more detailed view, however, there are other and more practical threads in the fabric of unease that to so considerable a degree envelops science at the beginning of this decade. Prominent among them are drastically reduced prospects of public support over at least the near future—a reduction inevitably involving grave risks to spirit and vitality and effectiveness within science itself, and outwardly to understanding and esteem and so effective moral support in the society at large. And the whole situation is now compounded by the widespread current pressures for immediate scientific “relevance.” This last demand, of course, is by no means novel. The history of science in the United States, as elsewhere in the world, has comprehended repeated shifts in the priorities publicly accorded to “pure” versus “applied” science, ranging along the whole spectrum between them. The relative values popularly assigned to the extremes of the spectrum have periodically been reversed. That is normal and desirable. For, although long experience makes it quite clear that the greatest gains in man’s mastering as well as his understanding of his world have characteristically been achieved through advances in “pure” science taken in the most literal sense, the maturing of those discoveries has characteristically been the great contribution of the applied field. Any sharp distinction between these two aspects of science is unrealistic and can be damaging. Ideally they should form constituent parts of a well-balanced whole, the investigators in each sector distinguishable neither by initial training nor basic motivation nor intrinsic ability. Any pronounced and prolonged weighting of value between them in either direction is bound to be harmful. If it occurs, vigorous rectification is vital to the best interests of a nation, as Great Britain today is attempting to do in favor of applied science, too long a Cinderella in the British partnership.

But though it is virtually impossible to distinguish pure from applied science by any criterion save the immediate end in view, the case is different for science and technology, which, as has often been pointed out, really are quite dissimilar in their basic structures, their value systems, their respective missions in society, and even in their long histories. Characteristically, technologies supply the bridge



between scientific discovery and the large-scale development of its fruits. They occupy an especially vital position in society, but one that can all too easily be misunderstood. Consonant with their particular function, the criteria of merit and of self-evaluation, for those committed to them, are quite different from the criteria of science. The task of science is basically the creation and the dissemination of new knowledge. And so, characteristically, a major concern of those who work in scientific fields lies with the breadth and depth of new knowledge attained, and its fundamental significance in furthering understanding in a field. The primary concerns of those professionally committed to technology are quite different. Here it is effective and practical new development that counts. As Derek Price has so well pointed out, new developments, if successful, speak eloquently for themselves, and publications about them can take secondary precedence. Thus, though technology indeed serves as a bridge between science and development, its working ties to development are characteristically closer. Though technology constantly turns to science for the substantive bases of its developmental achievements, it is commonly the "older," more established sectors of the scientific panoply, the territory lying somewhat back of the most actively moving fronts, that are the most useful and the most used at any given time.

Again, closely interwoven as science and technology functionally are in all industrially developed countries, it is significant that their historic origins lay far apart. Contemporary historical research makes it abundantly clear that man's basic technological revolutions antedated the scientific revolution by many thousands of years. Indeed, they had transformed ancient civilizations centuries before the scientific revolution appeared quite independently in a tiny and apparently unlikely corner of the western world. Sophisticated technologies of urban development and planning clearly had to be mastered and elaborated before the great prehistoric centers of Asia and Africa could be maintained. There seems unmistakable evidence that in Egypt, in Mesopotamia, in Babylon, in Crete, in the north of India, men were living three thousand years ago in cities as well planned and serviced as do many of their descendants in the same regions today. In China of the first centuries of the Christian era there was evidently a highly developed technology, as the rich panorama of inventions conceived there during that period bears eloquent witness. During much of this time in China there clearly were skilled craftsmen in abundance; there was a wealthy and cultured segment of society with ample leisure for experiment and inquiry; through much of the era there was a peaceful and orderly society, skillfully maintained. If the connection between technology and science were organically close, one would have expected a true scientific revolution at that time and place, perhaps above all others. Yet it was in Europe, remote and ill equipped as it outwardly appeared to be, that the real scientific revolution occurred.

There seems little doubt that there are indeed real and rather deep distinctions between science and technology, despite the closeness of their more recent welding—a welding that perhaps more than any other single element in our economy has ensured our material progress and prosperity over the years. It is important to observe and distinguish the differences, not only in the obvious interest of clarity of understanding but for very practical reasons as well. One particularly practical reason relates directly to the material growth and health of American science over the years immediately ahead, and the part that a more vigorous and discriminating distinction between science and technology in the Federal budgeting process could play in aiding them.



A major element in the climate of unease for science in the United States today, of course, revolves around the question of government support, present and future. The trajectory of that support over the past two years, and its projection for the next several, are in a number of ways disquieting. According to data prepared by the National Science Foundation and recently quoted by Dr. Lee A. DuBridge, for example, Federal obligations for basic research in the nation grew from about \$200 million in 1956 to about \$2 billion by 1967—an astonishing rate of 21 percent a year. But during the years from 1965 to 1970 the average rate of growth dropped precipitously to approximately 7 percent, and for the last three years it has remained essentially static in the sense of formal dollar commitments. In its budget for 1969, the National Science Foundation was allotted \$435 million, including some carryover from the previous year. For the fiscal year 1970 the corresponding total was about \$438 million. These extremely tight restrictions have proved highly disturbing to the equilibrium of federally funded academic teaching and research. The slight dollar increases, to be sure, were made against heavy odds, given the weight of other demands on the purse strings of the nation, and they may have symbolized some commitment to the principle of advance. Furthermore, the total for the current year is \$513 million, and, if recent discussions in the Senate, in which the “sense of the Congress” with respect to the support of the National Science Foundation was explored, should result in action, it is possible that the NSF budget for 1972 may be increased by a further \$100 million. These are encouraging signs. Yet the fact remains that, because of both dollar inflation and the rapidly rising intrinsic costs of research, the overall current result of the funding levels of the past few years has been to constrict expected programs of federally supported research by 20 to 25 percent in some 550 institutions of the country. Far from merely holding a ceiling on expansion, it would appear that the scope of the National Science Foundation for that period was actually less than in 1966. And it seems probable that the level of federally supported research in the nation as a whole fell by approximately a quarter during the past four years.

For several years past it has been evident to many that Federal funding of science in the nation could not—and should not—expand during the coming decade at the rate that characterized the first half of the last. A number of years ago, for example, Derek Price warned explicitly that in the relatively near future a critical point would inevitably be reached, marking a transition from the exponential rate of scientific growth that had characterized the earlier decades to a more nearly linear rate, which would roughly describe the expansion during the years immediately following. But we did not plan for this transition. Now that it is upon us, we have clearly overreacted to it in ways disturbing and indeed perilous. No precipitate measures directed toward achieving an instantaneous and radical readjustment to a new “equilibrium” can avoid wreaking serious and extensive damage to our scientific fabric over the long term. And that would indeed be to court long-term danger. For to diminish the vigor of our scientific progress in the modern world is inevitably to fall behind, as Alfred North Whitehead observed so presciently many years ago.

The need for a consistent and a generally articulated and accepted Federal science policy in the nation has surely never been greater. Yet it comes at a peculiarly difficult time. Not only does it coincide with a period of critical

stringency in the Federal budget. It is affected by at least two other factors in the fabric of current unease for science.

In science, research and education are one. Sound, critical, and balanced programs of graduate—and, more recently, of postgraduate—training, closely coupled with supervised research experience, are absolutely essential in the preparation of future scientists. Yet the balance in the support of such training, like the balance of support for mature scientific investigators, has suffered badly from our overreaction to the shift in the curves of expansion of science that we have been experiencing. Several years ago students of university trends in the United States were pointing to the fact that during the last decade the number of academic doctorates awarded in the sciences was itself increasing roughly exponentially in response to the currently exponentially increasing demand. They warned that in the very nature of the case such a rate could not be maintained uncritically and rigidly without creating a serious waste of human talent and bringing about widespread frustration of human hope. For nearly half a decade we have had the opportunity to initiate a gradual adjustment of pace and scope and quality of training which could have eased the transition. But here again we failed generally to perceive the necessity and failed totally to grasp the opportunity. Now one of the most critical scientific imperatives in the nation is clearly to respond to the new spectrum of needs as rapidly and vigorously as possible: to readjust base and volume, and above all to build opportunities, on as wide a scale as practicable, for the research training of advanced graduate and postgraduate students of closely selected quality in environments where formal training can be closely combined with, and enriched by, daily personal exposure to investigators of the highest caliber. That is a need to which the Carnegie Institution has long devoted especially close attention.

The second factor, which only in the last years has become crucial for science policy, involves a challenge that is on the whole quite novel for us and to which we are still not fully adjusted. Today we are gradually coming to understand that, however rich our resources of wealth and of trained men and women, there are limits to the range and variety of scientific research that we can undertake. In some fields we are already in the area of hard choice. That may be a useful challenge. But our initial reaction to it, as we become more widely aware of it, is all too likely to be one threatening confusion and discouragement. All these factors, and yet others, underline a growing and general conviction that, great as are the difficulties, the United States must give much more urgent attention to formulating and implementing a more cohesive strategy of Federal aid to science, and particularly for developing and supporting facilities and programs of advanced education devoted to the training of the men and women who will be the lifeblood of the nation in that area tomorrow. We must also devote far more concentrated attention to formulating explicit policies to guide the support of research itself: policies that must surely include provisions for setting priorities in fields of work, a task of truly herculean difficulty. It will certainly require at least a decade of hard and challenging work even to approach these huge questions at all effectively, for the unknowns are stupendous at present. Nonetheless, some detailed elements of such a policy that would clearly be helpful can already be discerned.

Accepting, as we must, the limitations by which we shall inevitably be bound over the next few years at least, what immediate moves can we make? For one thing, a controlled, assured expansion of Federal support for science, an

expansion tied to the growth of the gross national product itself, would assist a great deal even if it were relatively modest in absolute terms. What the precise proportion should be is, indeed, debatable. Far more important than absolute magnitudes would be the firm assurance of some long-term growth that such a commitment could provide. It is encouraging that discussions of the future funding of the National Science Foundation have already been conducted within this frame of reference, and that a specific proportion of the gross national product—0.1 percent—has even been proposed.

Dependability in support, permitting consistent research planning over several years ahead, is a greater desideratum than erratic increases of much larger magnitude. The arguments for wise and coherent planning in the Federal support of both research and education, for the architecting of careful projections and their consistent fulfillment over the long term, are very strong indeed. But the very nature of our times, and of the machinery of government, caution against relying too much on such planning for the immediate future, however helpful it can be over the longer term. No better solution for that short-term future seems at hand than to tie the guarantee of a *floor*, a reliable minimum, for the support of science and of the education related to it, to the gross national product of the nation, to which it contributes so much.

For a decade or more, discussions of the forms that the Federal support of scientific education should take have tended to polarize about two patterns: the so-called "institutional" system on the one hand, and the "project" system on the other. The advantages and disadvantages of the two have been extensively debated. It now has become abundantly evident that neither alone can suffice. Combined in judicious proportions, the two patterns provide a far stronger base than either can by itself. Of recent years it has become more and more evident that the terms "project grant" and "institutional grant" are in fact unreal abstractions, merely distinguishing two points on a long spectrum of possible modes through which Federal monies can be channeled to the support of education in science. Indeed, no less than six categories have been defined in the recently issued report of the President's Task Force on Science Policy, including Institutional Sustaining Grants, Departmental Sustaining Grants, Developmental Grants, Graduate Facilities Grants, Graduate Fellowships, and Research Project Grants. Even though all proposed categories must by their very nature be arbitrary, the recognition of a multiple array of needs by formal designation may be of considerable aid in designing more labile and adaptive structures of support: structures more sensitively attuned to the evolving needs of the nation.

But the usefulness—and indeed the practical reality—of any planning must in the end come back to the basis of support. In a year of special stringency on this score, other aspects of support planning ought to be examined with special care. It is here particularly that formal recognition of the real differences between the nature and requirements of science on the one hand and of technology and development on the other become of great practical, as well as theoretical, significance. Real as it is, this distinction has been badly blurred in the planning of Federal expenditures, and the blurring has had consequences of considerable magnitude for the support of science.

That such a distinction between the needs of science and technology can in



fact be made quite successfully at the budgetary level was effectively demonstrated in certain past years, when the budgets for the two categories were kept formally distinct. During that period, curves of Federal support in the two classes varied independently. It has been estimated, for instance, that in the category of "basic" research Federal support grew by 29 percent a year between 1956 and 1964, then dropped to an average 9 percent from that year to 1969. In the "technology" category, the corresponding growth rate for the earlier interval was 21 percent, and for the later, 5 percent. Over both periods, then, the "basic" category received preferential treatment in terms of proportionate growth. But the dollar amounts involved were much larger in the "technology" category. The formal separation of the two items facilitated increase in the support of basic research. Thus in the year 1966-1967 it proved feasible to increase the separated research budget by more than 10 percent, even in the face of circumstances already quite stringent.

But this salutary formal distinction was abandoned during the latter part of the last decade. The change has certainly made the budgeting picture less sharp and informative. More important, it appears to have raised significant new difficulties for future attempts to establish a stable "floor" under the Federal support of scientific research and education.

In the same general context it is interesting to note that early in the last decade a number of large items of Federal expenditure that earlier had been carried under accounts designated for maintenance, operations, and procurement were transferred to the columns of support for technology, and even for research. In the Department of Defense alone, this increased the research and development account five or six times, resulting in a recorded expenditure of the order of \$17 billion a year for "Research and Development." In fact, as the President's Task Force notes in its report, only 26 percent of that figure was actually employed in the support of basic and applied research. Such gross failures of distinction among the claims of science, technology, and development notably increase the problems of securing appropriate and vitally necessary Federal funding for scientific research and education.

But these, of course, are essentially matters of relatively superficial account representation. There is the much more serious question of how we maintain appropriate balance in actual growth among all the categories from innovation in research to final development. The current national budget, for instance, provides about \$1.5 to \$2 billion for the support of scientific research. For technological development, as currently defined, there is available about ten times this amount, \$15 to \$20 billion. To a rough approximation, we have committed \$150 billion for goods and services closely related to or dependent on technology. When the ratios of support for research and technology, and the procurement that intimately depends on both, stand in such striking contrast, there would seem to be excellent opportunities to readjust the balances between them without seriously affecting the dollar commitments made in the larger categories. For example, a transfer into the research column of 5 percent of the funds now allocated for technological development could augment the sums designated for research by half. Reallocations of this kind alone could greatly aid research support, which at present is so acutely in need of supplementation. It would also go a long way toward optimizing the use of available funds. Such evident opportunities to improve the balance of Federal commitments in these areas suggest that less

obvious possibilities may be open too. They emphasize the real and present need for some more effective monitoring and survey mechanisms in this area.

But in the long run, of course, there will be no escape from the other horn of the dilemma, to which we are finally returned—the ultimate necessity for some sort of choice in what we do, in the conduct and support of research as in other facets of our national activity. We badly need more workable mechanisms for the determination of long-range priorities in Federal support of research fields than we have now. The basic underlying question, however, is much more difficult, and far more fundamental. How *can* such choices of priority be made? How is one to determine whether a particular major field of investigation is “better” than another? This is a formidable query. It may well prove meaningless in any logical and possibly even in any practical sense. The very process of planning, as ordinarily understood, implies the weighing of relative merits among quantities whose future significance for the society, whose outcomes ten or twenty years or a quarter of a century from now, can be reasonably well conceived. But it is of the very essence of science that it deals, basically, with *unknowns*, and must always do so. Making selections among technologies is a process having tangible meaning, and it has been done successfully in myriad contexts by men everywhere since the earliest days of invention and manufacture. But can it have real meaning for “pure” science?

Difficult as that question is, it yet must be faced over the next decades. For in some pioneering scientific fields we are already at the point where the sheer costs of instrumentation required if their frontiers are to be projected much further in the basic patterns of the past could tax the nation’s resources so severely that only a few such fields could be adequately supported. Indeed, it now seems quite possible that instrument costs in some of these fields could ultimately rise to the point where no single country, even the most wealthy, could afford them. Already a variety of experiments in international scientific cooperation in such areas are being undertaken, some quite dramatic, some with uneven and uncertain success.

What of the newer buds of science, whose ultimate promise for the society may be even greater? It is worth recalling—and with emphasis—that some of the newer fields of critical human importance today, fields, for example, like that so often epitomized in the rubric “molecular biology,” not only have had a lengthy and continuous history, for long publicly almost unknown, but have achieved some of their most crucial advances—advances leading to all later progress—when they were almost unrecognized officially and received the most modest material support. It is rare that radically new and significant departures in scientific research—especially those conducted along the borderlines of adjacent formal sciences, where the richest dividends of insight and discovery are often reaped—require extensive funding during their critical early growth. Surely it is precisely here that the closest watch must be kept in the decade ahead, and the most enthusiastic and imaginative Federal support must be given. This is a task for which the National Science Foundation is peculiarly adapted. Indeed, this was one of the primary functions intended when the Foundation was established. We must remember this function, and constantly assure ourselves that it is exercised over the years ahead. It may turn out, in the end, to be the best of all possible approaches to the knotty and intractable problems of scientific choice.

This particular and major set of responsibilities for planning will surely

abide with us over the coming decade, and for much longer. Another, quite as vital, finds its prime focus in that even more essential task of scientific education, at every level. The extraordinary need for wisdom in planning for the training of scientific graduates, to maintain their numbers in that subtly correct relation to demand matching our vision of the greatest opportunity for men and women rather than invoking our justifiable fears of wasted talent, requires no further emphasis at this moment. But at another level, the content of that advanced education, and how it is to be conducted, are more significant today than ever before. Never, in the United States or abroad, has postgraduate education been so vital to those who aspire to participate effectively in the front lines of the march of science. We stand at a new leading edge, now, in the design of education for those who will man these future frontiers. We are witness to the latest stage of an evolution that began when we considered that the college graduate had received a highly superior preparation for the demands of the intellectual life. It progressed through the periods when, in our view, it was the attainment of the master's degree that signaled such a preparation, and then the doctorate. Now it is becoming increasingly evident that this degree of training no longer suffices. Informal learning in science is obviously a lifelong activity. But today, in many areas, formal preparatory training must be carried beyond the doctorate. Tomorrow the same may well be true along the whole front of science.

So far we have given too little thought or attention to exploring the most effective ways of meeting this new requirement. Of all the levels of education, this is clearly the most sensitive and critical. It requires the highest ratio of number of teachers to number of those taught. Above all, it requires by far the most continuous and intimate contact between master and pupil. The characteristic pattern of the most glorious chapters of science, as Hans Krebs eloquently pointed out several years ago, is one of a great master in a field seeking out potentially great apprentices and training them closely and rigorously, generation upon generation. This is the process through which such real and continuing greatness is best molded and fostered. And for this process, formal instruction is not enough. It is vital that the apprenticeship be one not only of the study but of the laboratory too.

It is abundantly evident that one of the crucial tasks for science over the next decade will be the designing of modes that structure this pattern most effectively and at the same time are economically viable both in terms of dollars and of our resources of gifted teachers. This is an arena where the Carnegie Institution of Washington, among others, is actively pioneering today. It is an area of pioneering which must be regarded—and which the Institution emphatically does regard—fully as significant for the years ahead as the more traditional scientific mission of exploring the expanding frontiers of substantive new knowledge.

This whole question, of course, has a final and a yet broader aspect which returns us to the beginning. It is worth reiterating that a nation does indeed achieve continuing greatness in the areas where it believes and agrees that potential greatness lies: in the areas, therefore, where it vigorously fosters greatness. That determination is made, not by the devotees or the experts in any given field, but by the nation as a whole. The nation's concept of science, therefore, its vision of the way that the formidable host of new scientific achievements confronting it almost daily in the newspapers or on television are actually achieved—not effortlessly, not by chance, but always as fruits of the most dedicated and prolonged human labor, of the most intense human thought and



devotion—is extraordinarily important. And so is its understanding of the long continuity of science in a great and unbroken tradition, linking the yesterdays of three centuries with the present and with an unknown tomorrow. That understanding of the real nature of science and of scientific discovery, at the level and the breadth of the nation as a whole, will be a critical factor determining the health and prosperity of science and of the nation itself in future decades. The forwarding of that understanding is also an undertaking and an ideal to which the Carnegie Institution of Washington has long been dedicated. It must be addressed, with deep and constant concern, by all of us over the years to come.

---

*There be many shapes of mystery.  
And many things God makes to be,  
Past hope or fear.  
And the end men looked for cometh not,  
And a path is there where no man sought,  
So hath it fallen here.*

EURIPIDES

This is my last Report. A membership of sixteen years on the staff of the Carnegie Institution has brought to me, as the Institution has brought to members of the staff over the sixty-nine years of its life, deep and abiding inspiration. Now I enter upon another kind of relation with the Institution.

Sixty-seven years ago, in May of 1904, Henry S. Pritchett wrote to Major Henry L. Higginson: "I look upon the Carnegie Institution as the most interesting effort the world has known for the development of the national interest in research." The years have proved the sentence prophetic.

When that letter was written, the idea, let alone the practice, of scientific research in America in its truly investigational sense had scarcely been born. Purely in terms of its economic resources relative to the whole field the Institution inevitably took an immediate place of leadership in the nation. But over succeeding years that leadership was to assume a far greater character. In the present national scene it has taken on qualities that are unique.

To visualize the scope of the radical changes that have taken place in American science during the life of the Institution is well-nigh impossible. There have been two world wars when survival was at stake. Since World War II there has been an unprecedented expansion of American science, conducted and supported publicly and privately, pioneered and catalyzed by public institutions many of which were influenced in their form—and indeed in their very establishment—by the record and example of the Institution.

Against this vast and dynamic background of science in the postwar years, the Institution has consistently pursued, and continues to pursue, the goals that have characterized all its working life. Often in the face of considerable difficulties and against considerable odds, it confirms what today may be the most important aspect of its leadership. [The Institution remains today undeviatingly dedicated to the ideal of the pioneering scientific investigator, to his education and preparation for his task at the levels of high and steady consistency of excellence and sophistication, and to the search for truth.] Though many practical "firsts" have followed from the Institution's work—"firsts" in a wide variety of scientific and technical fields—they have come as by-products in the prosecution of its principal mission. For it is clear that the task of scientific research, and of the education and preparation for it, run far deeper than practical results; and, indeed, far deeper than even the winning of new knowledge. That task has a banner to maintain within our national ethos, as one of the professions among our manifold activities most clearly epitomizing our basic values as a people: the values of individual independence and intellectual integrity.

Joyce Carey has observed that freedom and independence of mind involve solitude in thought. In sympathy and in feeling we are communal, but in mind each of us is very much alone. In an increasingly crowded and an increasingly highly organized America, opportunities for the attainment of that quietness and episodic solitude combined with the assurance of intellectual communion and support when it is most needed become increasingly rare. Yet we know from long experience that just such environments vitally foster and nourish the greatness of the individual American, as of the society as a whole. For it is the gifted, unorthodox individual, in the laboratory or the study or the walk by the river at twilight, who has brought to us, and must continue to bring to us, many of the basic resources by which we live. Six hundred years ago Chaucer observed: "Out of the old fields cometh the new corn." In tilling the fields and steadfastly maintaining them, in cultivating them anew and in fostering their productivity,

the Carnegie Institution continues today one of the greatest and most permanent aspects of its leadership.

At the close of this term of duty, I can find no other words than those of my predecessor, Dr. Vannevar Bush, on the same occasion: words as true today as when they were written in 1955: "It is faith that makes us look beyond tomorrow and ever seek to know, because in some mysterious way we realize that only a small portion of the road to knowledge has yet been trod, that matters beyond our present comprehension lie just around the bend, and that it would be folly at any point to abandon the journey in skepticism without striving to surmount the next obstacle and perhaps attain a better view. You are members of a distinguished and worthy company. Treasure the privilege of your association in your hearts."

Caryl P. Haskins

---

*And the pleasure of discovery differs from all other pleasures in this, that it is shadowed by no fear of satiety on the one hand or of frustration on the other. Other desires perish in their gratification, but the desire of knowledge never: the eye is not satisfied with seeing nor the ear with hearing. . . . the sum of things to be known is inexhaustible, and however long we read we shall never come to the end of our story book.*

A. E. HOUSMAN, *Lecture at University College, London, 1892*

*My heart has followed all my days  
Something I cannot name*

DON MARQUIS



## *The Year in Review*

*"Who are the cousins the mind makes?"*

—THOMAS HORNSBY FERRIL,  
*New and Selected Poems*

*"Time and chance happeneth to them all."*

—ECCLESIASTES

Education and research are twins. They are inseparable, and each is likely to thrive in the presence of the other. The objective of education is learning for an individual man. The objective of research is discovery, a special kind of learning, which we might say is learning for mankind. It is, in a sense, an ontogenetic-phylogenetic relation.

From the day when the founding Deed of Trust was drafted by Andrew Carnegie, education and research have been partners at the Carnegie Institution. The education supported by the Institution has always had a specialized objective—the creation of mature scholars likely to become the "exceptional man" and woman in their fields. Through the nearly seventy years of the Institution's existence this relation has evolved until today it fulfills Warren Weaver's dictum that "teaching and research should be equal partners."<sup>1</sup> During the year 1969–1970, 64 postdoctoral Fellows and 38 graduate students shared the instruments in the laboratories and observatories and the experience of discovery with the senior Staff Members of the Institution. For them, learning and discovery were part of a common experience.

For many years past the close relation between education and research has been implied in these reports, and occasionally made explicit. The reports of the Directors of the Departments this year so well illustrate the relation that another explicit statement is particularly appropriate.

What did the 102 students and postdoctoral Fellows seek in the Institution? What do their peers seek at the great universities and other institutions of higher learning? It has been said that "in science, the race is to the young, the swift—and the skeptical."<sup>2</sup> This statement is only partly true; the race is to the young, the swift, and the skeptical who stand on the shoulders of masters. Above all, in determining his place to learn a chosen craft the student seeks association with a master. The master in turn welcomes the promising student, or Fellow, because

<sup>1</sup> Warren Weaver, *A Great Age for Science*, Alfred P. Sloan Foundation, New York, 1960: 25.

<sup>2</sup> Henry Margenau and David Bergamini, *The Scientist*, Time, Inc., New York, 1964: 11.

he sees the future in him. Margenau and Bergamini have noted that scientists as a group "keep no trade secrets and welcome all apprentices."<sup>3</sup> What better way to learn than to participate in discovery under the guidance of a master? Accordingly, the qualities and habits of the master scientist are matters of the highest interest in describing the relation between education and research.

But most of the promising students, the masters of the future, need more than the association with a present-day master, important as that is. For these students are already scientists, and to do their best they need an environment similar to that of their seniors. They need institutional support, as well as the guidance of the senior hand. The advanced student must have a measure of quietness. He must have equipment; even the mathematician no longer escapes this requirement. He must have independence and flexibility. He must have the association of some, but not too many, of his fellow students. He should have the means of acquiring breadth as well as depth during his residence. These are all matters to which the Administration of the Institution pays attention. But they are needs alike for master and student—a first illustration of the naturalness of the relation between education and research.

Good teaching and good research have been much described and analyzed. There are some rather remarkable parallels. One common quality is the dedication of the teacher or research worker, and the associated qualities of patience and optimism. Other most important qualities are a sense of order, a liking for economy, and the aesthetic sensitivity that may accompany them. Imagination on the one hand, and precision on the other, are still other parallels. The good research worker should have two additional qualities that are helpful, but not essential, in good teaching. One is a certain boldness, a willingness to accept, even to enjoy, long-term risks. Successful speculators and successful scientists have this trait in common. A last quality, perhaps associated with imagination, is a sure sense of the right question, the ability to determine where the frontier of one's field is.

The liking of scientists in the Institution, and many of their colleagues elsewhere, for joining teaching and research therefore is no accident. It is understandable that young scholars should find their company and the pattern of their work a cherished opportunity for advanced education.

### *Long-Term Programs*

Every research scientist has two important types of decision to make during his career. The first is his commitment to a field of specialization, the direction of the frontier he will work on. For many scientists this choice is made only once. The long-term commitments are the type of decision in which boldness or speculative courage must be displayed. The second type of decision, the choice of an immediate problem for research, is made repeatedly during a research scientist's career.

In his book, *The Structure of Scientific Revolutions*, T. S. Kuhn has stressed the importance of a paradigm as an organizing force and a source of direction for scientists' long-term programs. The importance of a paradigm (or model, or theory) is appreciated by most successful research workers. In the absence of one a scientist usually attempts to remedy the deficiency by constructing his own. An understanding of the importance of paradigms, the nature of a successful

<sup>3</sup> *Ibid.*: 34.

model, and familiarity with its construction are essential parts of scientific training. Although the work of almost every senior Staff Member and his associated Fellow, or Fellows, could be chosen to illustrate the place of the paradigm in research and training, two examples must suffice for this report.

*Cosmological Theory as a Paradigm.* Of all the endeavors of science perhaps astronomy offers the greatest scope for boldness of concept. For this a price is exacted: the time required for completion of a research program may be long and the dedication intense. Not all astronomers accept the challenge, but many at the Hale Observatories have. For example, Allan Sandage has chosen observational cosmology as a major field of interest.

The paradigm of cosmology is that of a known universe composed of galaxies and clusters of galaxies scattered uniformly over vast distances.<sup>4</sup> These objects recede at increasing speeds with increasing distance from our Galaxy and from each other, their relative velocities being proportional to the intervening distance. Sandage, like some other astronomers and astrophysicists, has further chosen to search for evidence as to which model of the universe is correct. Was there a primeval event of creation, a "big bang" whose energy caused the dispersal of the objects now observed through radio and optical telescopes, or has the universe always existed in a "steady state"? A refinement of the big bang model is that of an oscillating universe, in which the big bang was but a single event, repeated and repeatable. The competing "steady state" model postulates continuous creation. Evidence has been accumulating at the Hale Observatories and elsewhere that favors the "big bang."

A critical parameter in a decision on any of the cosmological models is the deceleration rate ( $q_0$ ) in the expansion of the universe. A positive value of the deceleration rate favors the "big bang," whereas zero or negative values favor other models.

Critical to a calculation of the deceleration rate is the value of the Hubble constant ( $H_0$ ) which, for any remote galaxy, relates the velocity of recession to distance from the observer. The numerical estimates of this basic constant have been crude because of the great difficulty of determining reliable distances to remote galaxies, but Dr. Sandage and other astronomers consider a more precise value of the constant to be essential to a definitive decision on a cosmological model. As H. W. Babcock, Director of the Hale Observatories, explains in his Report, measurement of the redshifts of remote galaxies is relatively straightforward, but distance determination requires great effort. Only observing programs of many years' duration can provide the needed data. Dr. Babcock says further that fundamental distances to a few nearby galaxies of the Local Group are known accurately from photometric observations of Cepheid variable stars made by the late Walter Baade of the Observatories, and others. But Cepheid determined distances are inadequate beyond the Local Group of galaxies, so other distance indicators have been sought. Notable among these have been the H II regions,<sup>5</sup> which are of much larger extent than individual stars.

Since 1950 Dr. Sandage has used nights of exceptionally good seeing on the 200-inch Hale telescope to accumulate plates of numerous galaxies in which

<sup>4</sup>The distribution of matter within the universe is postulated to be statistically homogeneous and isotropic, even though there are local anomalies; there is no preferred direction, no center, no axis.

<sup>5</sup>In the surroundings of hot (O and B) stars, hydrogen gas is ionized and made luminous. The resulting nebulosities are known as H II regions.



H II regions can be measured. Sandage and G. A. Tammann now report hopeful progress on calibrating the sizes of these H II regions. They appear to range from 70 to 300 parsecs<sup>6</sup> in linear extent, and to vary spectrally according to position within a galaxy.

The reach for better distance indicators has been resourceful and varied. Sandage and Tammann also have measured the brightest red and blue supergiant stars, and Sandage has begun photoelectric observations to establish the precise magnitude scales in the resolved field galaxies for which distances are desired.

A third approach has been an estimate of the ages of globular clusters of stars. Sandage has now completed the observation and analysis, begun in 1958, of the faint photometry and color-magnitude diagrams for hundreds of stars in the clusters M3, M13, M15, and M92. Analyses of the four clusters agree well in giving ages of 10 ( $\pm 3$ ) billion years. The indicated error is an outside limit. Such an age, according to Sandage, is compatible with the age of the expanding universe, if the Hubble constant is less than 75 km per second per megaparsec, and if the deceleration parameter ( $q_0$ ) is as great as +1. An upper limit thus has been set for the constant, at a value far less than it was thought to have only a few years ago.<sup>7</sup> Sandage now believes that the newly determined value will fall somewhere between 50 and 75 km per second per megaparsec. However, the efforts at calibrating distance indicators will have to continue, probably for many years, before the precision needed for a decisive test of the cosmological models will have been achieved. But the efforts of these years of painstaking search for data promise to repay astronomy, and the world, handsomely through a more certain insight into universal history.

*A Theory of Gene Regulation as a Paradigm for Biophysical Research.* The appearance of a new paradigm is an infrequent event in science. A biological paradigm, however, has recently been suggested. The "Report of the President 1968-1969" described a new theory of gene regulation for higher cells. R. J. Britten, of the Biophysics Section of the Department of Terrestrial Magnetism, and E. H. Davidson, of Rockefeller University, proposed last year a model of gene regulation for all higher organisms that gave a new means of visualizing the process of evolution. The model arose from the need to take account of observed repetitive DNA sequences in genomes and a previously postulated "saltatory replication of DNAs." The model provides for the conservation of pre-existing useful batteries of genes as evolution proceeds, for new integrative combinations of pre-existing genes, and a mechanism for divergence through base changes in the DNA sequences.

Since its introduction the Britten-Davidson model has received widespread attention in the world of biology. Together with the postulates developed in earlier years by Britten and his colleagues in the Biophysics Section, the model was background for many of the experiments conducted by the Biophysics Section during the year. Their ultimate objective has been nothing less than understanding the evolution of regulatory systems in all life. Experiments at the Section during the year covered the entire range of life systems from viruses to primates.

Nancy R. Rice, a Fellow at the Section,<sup>8</sup> undertook a particularly interesting

<sup>6</sup> One parsec is 3.26 light years.

<sup>7</sup> Estimates of the Hubble constant have been reduced by a factor of seven during the last twenty years.

<sup>8</sup> Fellow of the National Institute of General Medical Sciences.

set of experiments with rodents during the year. In her report she notes the earlier postulate of Britten and D. E. Kohne that repeated DNA sequences exist as "families" in the genomes of organisms with nucleated cells. According to this model, which is subsidiary to the general model of gene regulation, new families of DNAs continually arise during evolution. A DNA family that has recently appeared may be limited to a single species, but a family that arose long ago currently may be found in many species. Using a technique of testing the thermal stability of nucleic acid strand pairs (the temperatures at which pairs dissociate) Dr. Rice obtained experimental results that were in complete accord with the Britten-Kohne postulate of DNA families. Her experiments were conducted with the DNAs of rat, mouse, multimammate mouse,<sup>9</sup> guinea pig, Syrian hamster, and the Chinese hamster. She found that the DNAs of all may be divided arbitrarily into two classes: those common to both members of a pair of different species, and the DNAs found exclusively in one of the pair. In the tests for thermal stability the former DNAs reassociate with low stability and the latter with high stability. This characteristic is clearly illustrated in the experiment on rat and mouse DNAs (Figure 1A). The high thermal stability material is assumed to have appeared in each of the genomes since the mouse-rat species divergence.

Dr. Rice's experiments with other species gave the same conclusions as those drawn from the comparison of rat and mouse DNAs. Whatever species of rodents were paired, some low thermal stability DNA was common to both genomes. However, the greater the evolutionary separation of the two organisms the smaller the amount of DNA held in common. For example, fewer sequences are held in common between mouse and Chinese hamster than between mouse and rat (Figure 1B).

In a series of similar experiments, D. E. Kohne, J. A. Chiscon, and B. H. Hoyer have obtained new insights into evolutionary processes among the primates. Using the same technique of reassociating "hybrid" DNAs, and a time scale provided by paleontology, they have arrived at estimates of the number of nucleotide pair changes per generation of all the possible pairings among man, chimpanzee, gibbon, green monkey, Rhesus monkey, capuchin monkey, and the galago (a primitive primate); see Figure 2. Estimates also were obtained for nucleotide pair changes for mouse and rat, cow and sheep, and cow and pig. Their data suggest that about five to ten base changes per gamete per generation are fixed in the species. The basic mutational mechanism appears to be connected with the DNA replication cycle. Thus a prior assumption that the rate of molecular evolution has been constant over time is not confirmed by the Kohne-Chiscon-Hoyer experiments. Instead, the rate of molecular evolution of DNA nucleotides has probably been constant with generation time.

One interesting, but tentative, conclusion from the Kohne-Chiscon-Hoyer data is that the generation time of the early primate ancestors of man was relatively short. They postulate that evolutionary changes at the organismal level were preceded by quantitative or qualitative change in the DNA, and that the rapid addition, divergence, and mixing of DNA may very well have played a role in the amount of speciation seen during the past eighty million years. This hypothesis forms an interesting basis for further experiment. Dr. Kohne also determined that shorter generation-time creatures added DNA more rapidly than those with longer generation time.

<sup>9</sup> *Mastomys coucha*, a small African rodent, widely distributed south of the Sahara.

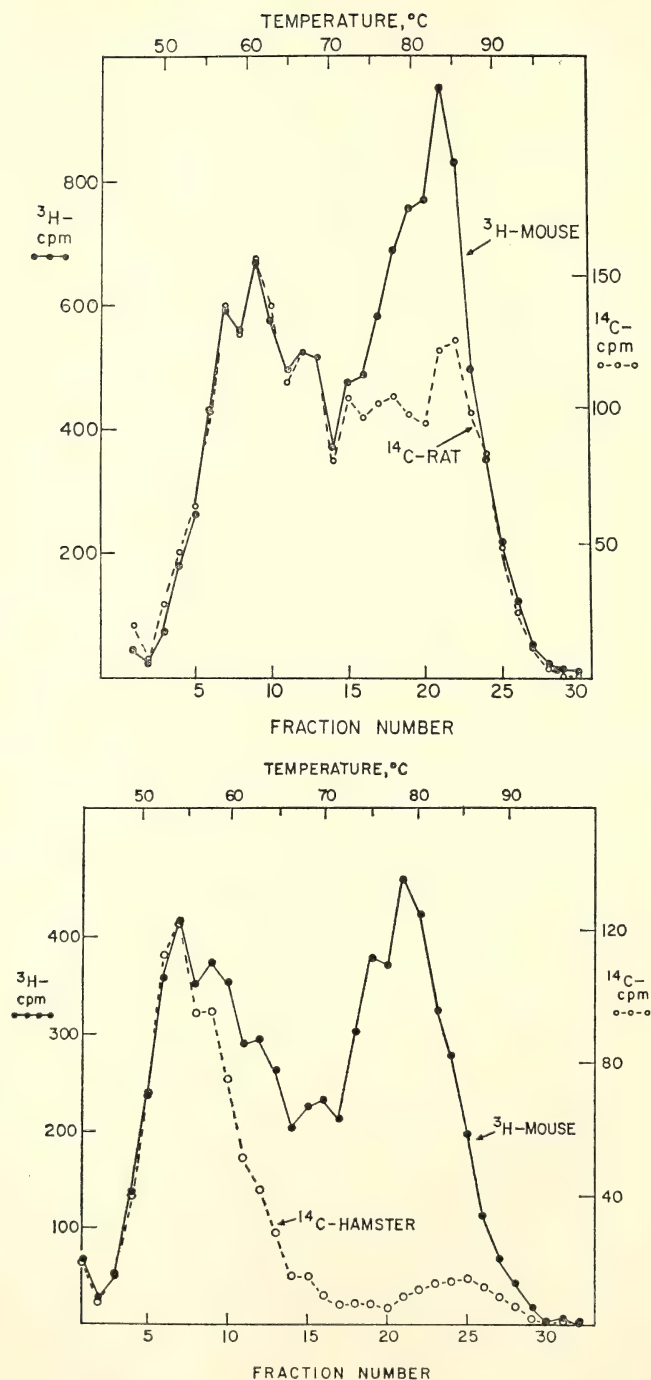


Fig. 1. Thermal DNA-dissociation profiles. Above: Rat and mouse, chromatographed together. Note the dissociation of high-temperature fractions and the stability of low-temperature fractions. Below: Mouse and hamster. The dissociation of low-temperature fractions and the narrow range of stable fractions are to be noted (Dr. Rice's experiments).



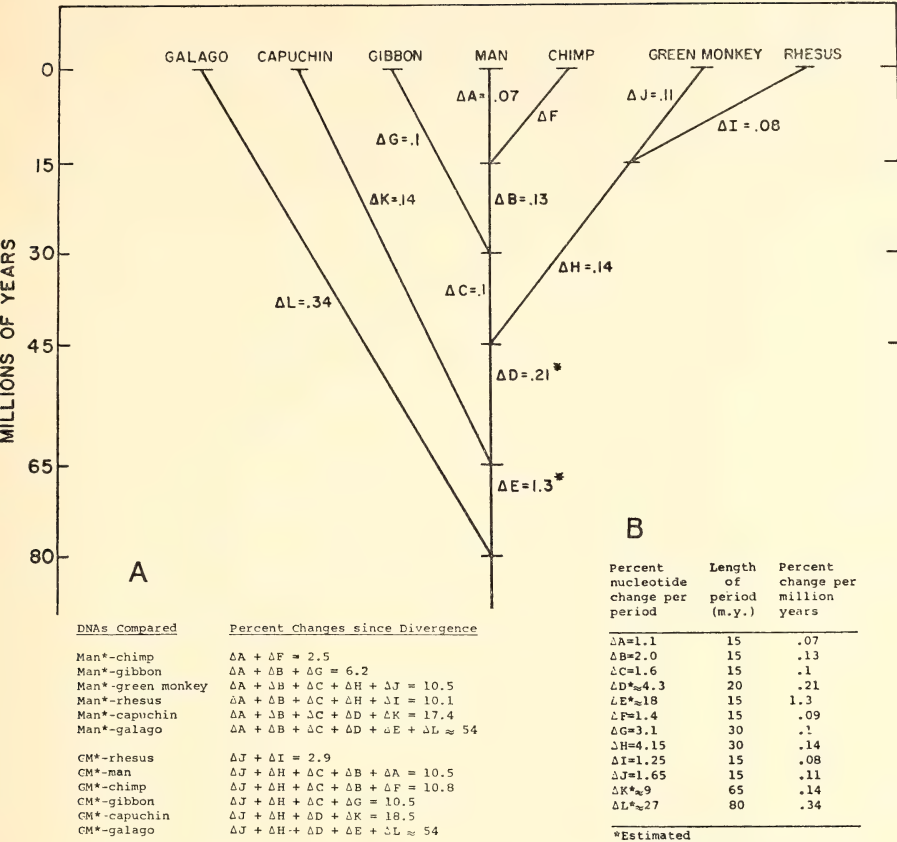


Fig. 2. Primate phylogenetic tree, as postulated by Kohne, Chiscon, and Hoyer, with (A) notations of the percent of change since divergence, and (B) with notation of the percent change of nucleotides per period, and per million years.

Members of the Section conducted a number of other experiments during the year designed to explore the evolutionary DNA relations among related life forms, or to provide answers to technical problems encountered in experiments in DNA relations. D. B. Cowie and R. J. Avery, a Fellow of the Institution, produced a "family tree" for three bacterial phages (T2, T4, and T6) from analysis of the phage DNAs. R. J. Britten and Jean F. Smith found that the slime mold (*Physarum polycephalum*) contains repeated sequences of DNA in the pattern of higher organisms. It is the least complex organism thus far discovered to contain large quantities of typical repeated DNA.

In other work Dr. Britten and Miss Smith studied the relation of a special component of calf DNA [high guanine-cytosine (GC) satellite] with sheep DNA. Dr. Britten also added some conceptual distinctions for describing repeated DNA of all higher organisms according to frequency of repetition, quantity of repeated DNA, and number of sequences represented, in a brief

report on "Sequence Complexity, Kinetic Complexity, and Genetic Complexity." Robert Shleser, a Fellow,<sup>10</sup> studied the homology of the DNAs of a bacteriophage (S13) and its host, the dysentery bacillus (*Shigella dysenteriae*).

All of the evidence accumulated by the Section during the year indicates that the paradigm of a traceable evolutionary relation among the DNAs of higher organisms, and probably of other organisms as well, will continue to be a fruitful one for some time to come.

### *Selection of the Solvable Question*

Dr. Sandage's program, besides illustrating the value of a bold organizing concept, also exemplifies other aspects of research that have high instructional value. The work of Dr. Britten and his colleagues in the Biophysics Section has similar qualities. Research on a frontier must be productive to have its highest educational value. Although we may believe with Francis Bacon that truth comes out of error, the most instructional pattern to follow is one that produces results, that is, answers to questions that have been raised to open further a path on the frontier. Selection of the right questions for immediate attention is vital. Dr. Sandage and his collaborators, and Dr. Britten and his colleagues, consistently have done this. But so have other research groups within the Institution; one of them this year gives a particularly good illustration of problem selection.

The report of James D. Ebert, Director of the Department of Embryology, sets forth very aptly and specifically the place in research and education of selecting the solvable question. In the Introduction of his Report Dr. Ebert quotes from Viktor Hamburger's "Hans Spemann and the Organizer Concept": "the strategy of his research was very well expressed in a letter to me: '. . . to tackle the most immediately solvable question, until, piece by piece, the whole is achieved.'" <sup>11</sup> Dr. Ebert then notes that the Spemann pattern of discovery, the detection of the next "solvable question" with the help of research just completed, is particularly well illustrated by the continuing studies of D. D. Brown, I. B. Dawid, and their colleagues in the Department of Embryology. For several years these Staff Members and Fellows have been studying the mechanisms by which embryos and oocytes of the South African toad, *Xenopus laevis*, synthesize ribonucleic acids (RNAs). The broad objective of the Department is, of course, total understanding of the process of development of an individual organism from gene to mature individual. A more immediate, but still long-range, objective is learning what molecules are involved in coordinating the action of seemingly unlinked genes, which is, as Ebert says, "a salient feature of development."

Within the oocytes and embryo cells of *Xenopus laevis* there are four principal types of RNAs: ribosomal (28S, 18S, and 5S), multiple-transfer RNAs (4S), DNA-like RNAs (messenger RNAs and rapidly turning-over nuclear

<sup>10</sup> Fellow of the American Cancer Society.

<sup>11</sup> Viktor Hamburger, "Hans Spemann and the Organizer Concept," *Experientia*, Vol. 25., 1969: 1124.

RNAs), and mitochondrial RNAs. Dr. Brown and his colleagues are studying the ribosomal RNAs and the multiple-transfer RNAs, and Dr. Dawid and his colleagues are studying the mitochondrial RNAs. There are two genomes to be considered in tracing the RNAs to their origin: the nuclear genes controlling the bulk of cytoplasmic RNAs, and a separate mitochondrial genome. An understanding of the entire function of the limited mitochondrial genome probably is the first prize to be expected, but parallel work on the nuclear genes is also needed and is being pursued.

Past studies at the Department by Brown, Dawid, and their colleagues have shown that the genes responsible for the 28S and 18S ribosomal RNAs are adjacent (Figure 3), and that the 28S and 18S genes are linked, having a co-ordinated transcription. However, the genes for the third ribosomal RNA (5S)

### Anatomy of rDNA

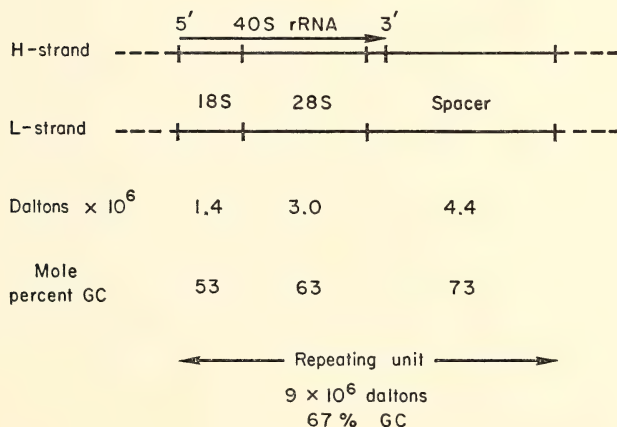


Fig. 3. A model for rDNA. A graphic portrayal of experimental results giving information on the arrangement, length, and base composition of the three nucleotide sequences which comprise a repeating unit of rDNA. GC = guanine-cytosine.

are not intermingled with the repeating pairs for 28S and 18S RNA; but surprisingly the 5S RNA accumulates at the same rate as the 28S and 18S during oogenesis and embryogenesis. When 28S and 18S ribosomal DNA is increased in oocytes, 5S RNA synthesis increases at the same rate as the increase in 18S and 28S synthesis, even though the 5S genes are not amplified. Transcription of the 5S genes is closely coordinated with transcription of the 28S and 18S genes. On the other hand, the multiple-transfer RNAs (4S) are not linked to any of the



ribosomal genes, and their transcription is not coordinated with ribosomal RNA synthesis in the living oocytes.

The mitochondrial ribosomes are another separate system containing 21S and 13S RNAs, and a circular DNA molecule of limited size (16,000 base pairs). Until this year the nature of the 21S and 13S RNAs was unknown.<sup>12</sup>

During the year Dr. Dawid and R. F. Swanson, a Fellow,<sup>13</sup> following a lead given earlier in their studies of protein synthesis in the mitochondria, established the existence of a 60S particle which they conclude is the mitochondrial ribosome. It contains both the 21S and 13S particles of RNA, whose association with the mitochondria now is fully confirmed.

Dr. Ebert notes that the next solvable question can now be perceived, and with it the immediate goal for these studies of DNA-RNA relations. It is "to isolate these genes in pure form and reconstruct their normal controls *in vitro*." He says further that "modest advances . . . on four fronts" were made toward this goal during the year. Not only the results are significant, but also the fact that R. G. Roeder, a Fellow of the American Cancer Society, Yoshiaki Suzuki, a Fellow of the Institution, and Pieter C. Wensink, a graduate student at Johns Hopkins University, shared with Dr. Brown and another Staff Member, R. H. Reeder, in the advances.

Dr. Roeder is purifying and describing RNA polymerases in preparation for testing their ability to transcribe purified genes accurately. Roeder's experiments already have shown that RNA polymerases I and II are similar to their counterparts in other eukaryotic<sup>14</sup> organisms. With this knowledge it became possible to examine the relation between the levels of RNA polymerases and the rate of RNA synthesis during development. Roeder's first experiments along this line during the year showed that RNA polymerases are detectable in significant quantities in embryos where no RNA *synthesis* can be detected *in vivo*. The two polymerases thus cannot account alone for changes in amounts and kinds of RNA that characterize embryogenesis in *Xenopus*. As Dr. Ebert notes, "these observations set the stage for the identification of control factors which endow the enzymes with the specificity attributed to them *in vivo*."

From their earlier studies Brown and his colleagues have developed a model of ribosomal DNA, that is, the part coding for the 18S and 28S RNAs (Figure 3). Dr. Reeder, the Staff Member, and Mr. Wensink have been testing this model. Wensink has studied the structure of rDNAs with the electron microscope. His electronmicrographs of ribosomal DNA thus far show substantial agreement with the length of sequences predicted in the model (Plate 1). In classic scientific fashion, Wensink ends his brief report with a series of four questions that he expects to answer next.

Dr. Reeder's tests of the model are designed to observe the fidelity of initiation of RNA synthesis, as RNA is transcribed from purified genes *in vitro*. It is known that RNA polymerase acting in the living cell begins transcription at

<sup>12</sup> *Carnegie Institution Year Book* 68: 515.

<sup>13</sup> U. S. Public Health Service.

<sup>14</sup> Eukaryotes are all organisms with a true nucleus (enclosed in a well-defined membrane) in their cells.



Plate 1. Electron micrograph of a partially denatured molecule of rDNA, made by P. Wensink, a graduate student at the Department of Embryology.





the unique site on DNA and produces RNA transcripts of exactly the same base sequence. Reeder predicts the same exact transcription of the rRNA *in vitro* as *in vivo*, and is perfecting his experimental design to test the hypothesis.

Meanwhile, Dr. Brown has attempted, with some success, the purification of *Xenopus* 5S DNA. Using a technique that employs silver ions, he has isolated a DNA "satellite," which he says "behaves in many respects like 5S DNA." He has also taken the first steps toward the isolation of 4S DNA, the genes for the multiple-transfer RNAs. They are less abundant than the 5S RNAs. Although Brown has not yet achieved uncontaminated 4S DNA preparation, he has enriched his best precipitates about one hundredfold in 4S DNA.

When the steps started during the year have been completed, the *in vitro* experiments on gene controls of RNA synthesis can be undertaken. Completion of these steps will include verification of the model, isolation of all the rDNAs, and perfection of a method of obtaining specific first nucleotide sequences for RNA synthesis *in vitro*. "The next solvable question" thus is still a question at the Department, but its main components are known and the main steps to its solution are reasonably clear.

Brown, Reeder, and their Fellow and student associates already are thinking ahead to the next and perhaps larger solvable question. Characteristically they have also begun to do something about it. In their report they recognize that "a complete elucidation of the factors regulating the ribosomal and transfer RNA genes may not explain how cell- or tissue-specific genes are controlled in embryogenesis." The genes for the ribosomal RNAs are not characteristic of any tissue or cell type. They may be regulated differently from hemoglobin or antibody genes, for example. For this reason they have also begun to study the genes that function in a specialized tissue; the system chosen is the one for silk fibroin in the Japanese silk worm (*Bombyx mori*). Yoshiaki Suzuki has undertaken the task of isolating this gene, or genes. He is beginning by analyzing the RNA and protein synthesis in the posterior silk gland of *Bombyx mori*. Dr. Suzuki expects to isolate messenger RNA, which can be used as a tool for assay of the gene. During the year techniques for labeling and isolating RNA were developed to the point that detailed analysis now is in progress. Brown and Suzuki then hope to apply the types of analysis now being applied to cytoplasmic RNA genes in *Xenopus* to the *Bombyx* fibroin genes.

When the studies in progress at the Department have been completed the functioning of both the ribosomal genes and a specialized gene for a specific protein should have been charted. Beyond this, Staff Members, Fellows, and students already can discern still another tier of "solvable questions."

### *Precision and Inference in a Sense of Order*

The scientist's sense of order is of course expressed in his choice of a paradigm, or in his invention or discovery of one. But a sense of order reaches much more deeply. Precision gives it the highest meaning—precision in the choice of problem, precision in experimental method, and the precise insight that permits a strong inference. The report of A. D. Hershey, Director of the Genetics Research Unit, gives a very appropriate illustration of all these qualities.

Dr. Hershey describes the research of David H. Parma, Postdoctoral Fellow,<sup>15</sup> and Laura J. Ingraham, Research Assistant, in his laboratory. Parma and Ingraham chose for their recent research a problem in a field where Dr. Hershey's accomplishments are noted—study of bacteriophage genetics. "The point of interest in their work," Hershey says, "lies in the possibility of understanding at the molecular level phenomena known to have their counterparts in higher organisms." He concludes that the Parma-Ingraham research translates prior genetic observations into molecular terms. "Gross aberrations," he adds, "are now part of the molecular chemistry made visible by genetic analyses." The path taken by Brown, Dawid, and their colleagues at the Department of Embryology in their work on higher organisms thus has had further illumination in the research of Dr. Hershey and his colleagues on the simplest of all known organisms.

The Parma-Ingraham experiments were conducted on a phage known as T4. Like other phages, T4 has a genome composed of a single molecule of DNA. About one percent of T4 DNA forms a gene known as rII; it was used by Seymour Benzer in experiments that connected the structure of DNA and the structure of genes with each other. Dr. Hershey describes the rII gene as containing two adjacent DNA segments; they have been designated A and B in rII research. Except for a cooperative function, A and B behave like separate genes, and each mutates from an active (+) to an inactive (−) form. The cooperative function of the two segments is to make T4 growth possible in bacterial strains lysogenic<sup>16</sup> for phage lambda. The two segments, independently or cooperatively, apparently have no other function. Of the four possible permutations (A+B+, A+B−, A−B+, and A−B−) only one (A+B+) can function as an rII gene. However, A+B− and A−B+ can cooperate, if both are present in the same bacterial cell, to perform the rII function. Dr. Hershey notes that the technical importance of the rII gene lies in this bipartite structure, and the ease of recognizing its partial functions.

If phages of the types A+B− and A−B+ are crossed, the progeny contain about one percent of A+B−/A−B+ heterozygotes. Some of these are "terminal hets," that is, having repetitions at the ends of the DNA molecule, marked by genes of different parental origin. By the crossing of appropriate mutants terminal hets can be predictably prepared, and have been used in research on the phage genome since F. W. Stahl first prepared them about 1965. Subsequent experiments showed that such crosses yielded about one particle in ten million that could form a phage clone on plates seeded with the lysogenic bacterial host.<sup>17</sup> Such a clone contains a relatively high number of particles that can be recognized as "hets" of the genotype A+B−/A−B+. The question remained, however, as to whether they were stabilized terminal hets, or whether they carried duplications of another sort. This is the question that Parma and Ingraham chose to investigate.

The "duplications of another sort" hypothetically could be tandem duplications,

<sup>15</sup> National Science Foundation.

<sup>16</sup> In a lysogenic system the genome of an infective phage is carried latent in the genome of a host bacterium and may remain latent for generations, but retains the capacity for eventual infectivity.

<sup>17</sup> Jon Weil, Betty Terzaghi, and Jean Crasemann, "Partial Diploidy in Phage T4," *Genetics*, Vol. 52, 1965: 683–693.

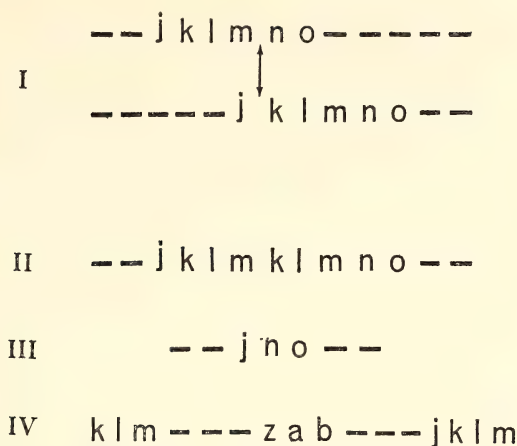


Fig. 4A. Illegitimate crossing-over. Nucleotide sequences corresponding to parts of the genome are represented by alphabetical sequences in which each letter stands for many nucleotides. In I., two molecules are mispaired. An illegitimate cross-over at the double arrow generates a tandem duplication (II) and the corresponding deletion (III). Structure IV is the terminal repetition analogous to II.

inverted duplications, and any possible nontandem duplication. Prior experiment by Sturtevant and Bridges on *Drosophila* had demonstrated the existence of tandem duplication in higher organisms. Dr. Hershey, in his Report, suggests that the evidence provided in the *Drosophila* experiments carries over to the T4 genome, but with one complication.

Tandem duplication is defined by Dr. Hershey as "the product of a single illegitimate crossover." A "legitimate" or typical crossover is the interchange between homologous chromatids of exactly corresponding segments, probably based on complementary nucleotide sequences. Illegitimate crossing over, on the other hand, results in nonhomologous reciprocal products (Figure 4A and Figure 4B).

The complication mentioned by Dr. Hershey for tandem duplication in T4 is the precisely defined molecular limits within which illegitimate crossing-over

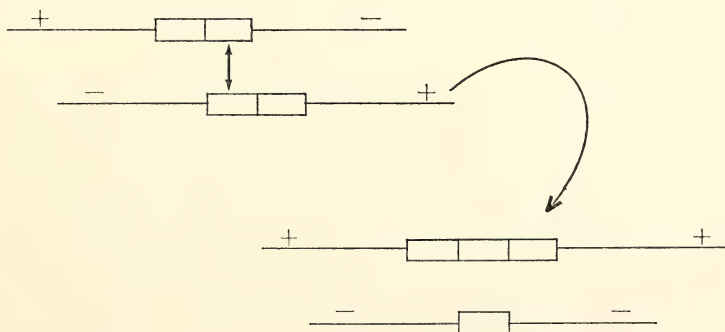


Fig. 4B. Unequal crossing-over between DNA molecules containing a duplication. Each unit of the repeated sequence is indicated by a rectangle. The plus and minus signs signify genetic markers bracketing the repeats.



must be carried out. In *Drosophila* the segregant of an illegitimate crossing-over may be longer than the normal one. Experiments with T4, however, permit detection of recombinant DNA molecules only if they can be put into phage particles. This requirement prohibits lengthening; a DNA molecule containing the unequal product of an illegitimate crossover "must usually suffer deletion of another, dispensable, DNA segment if it is to be recovered in viable form."

Accordingly, the persistent "hets" of the genotype  $A^+B^-/A^-B^+$  were hypothesized by Dr. Hershey and his colleagues to contain tandem duplications of a DNA segment including the rII gene, and to have suffered deletions of non-essential DNA elsewhere in the chromosome. Parma and Ingraham conducted experiments to test this hypothesis. Their results appear to account satisfactorily for the origin of tandem duplications in illegitimate crossing-over. Dr. Hershey summarizes their evidence thus:

1. The persistent hets produce four types of progeny: particles like themselves,  $A^+B^-$  segregants,  $A^-B^+$  segregants, and inviable particles. The segregants make up about 15 percent to 45 percent of the viable particles, and the number of inviable particles equals the number of segregants. The experimenters infer that the inviable particles are the result of crossing-over that generates a gene set too large to go into a phage particle without loss (Figure 4B).

2. Revertants from revertible mutants are haploid, rather than homozygous diploid in structure. This is inferred from the reversion of  $r$  segregants to  $r^+$ , and the low frequency with which persistent hets are regenerated from segregant crosses.

3.  $A^+B^- \times A^-B^+$  crosses from persistent het segregants generate nonpersistent hets at higher than normal frequency. Parma and Ingraham infer from these observations that duplications may be overcompensated by DNA deletions, with the effect of lengthening terminal repetitions.

The same inference is supported by the further observation that the persistent het segregants referred to above regenerate new persistent hets with appreciably higher frequency than the ancestor lines.

4. The Parma-Ingraham persistent hets were prepared from stocks containing multiple genetic markers. The distribution of these markers in the hets shows clearly that the duplications arise by a single crossover in the vicinity of the rII gene, and are usually about a dozen recombination units in length.

5. The recovered markers show a structure in the duplications of  $B^+A^-B^-A^+$  rather than  $B^-A^+B^+A^-$ . From this the survival of short duplications rather than long ones may be inferred.

The Parma-Ingraham experiments, although accounting for the T4 duplications, still do not account for the deletions, whose origin remains an open question. Nevertheless, these precise insights into detailed genetic mechanisms within a single molecule have more than usual significance. Dr. Hershey, in the conclusion to his Report, states: "The mere fact that species exist tells us that genetic replication and genetic recombination are conservative processes. The mere fact that species evolve should tell us that both processes are likely to exhibit limited fidelity. Replication errors (mutations) are better known than recombination errors (illegitimate crossing-over), but only because errors of the first kind are easier to detect." The detection of error in one out of ten million progeny of an appropriate cross of a most minute and highly specialized organism, the T4 phage, supports the strong inference that "gross aberrations," in Hershey's

words, "are now part of the molecular chemistry made visible," and probably applicable to all life forms.

### *Alertness to Chance Opportunities*

Whatever the chosen paradigm, however skillful the choice of solvable questions, and however precise the experiment, the element of chance plays a role in science no less than in other affairs of men. Appreciation of the need for alertness to chance opportunities is a vital component in the training of a young scientist. So is an appreciation of the close connection between adequate preparation and the capacity to profit from chance.

The Staff Members and Fellows of the Geophysical Laboratory during the year had an extraordinary opportunity to profit from an alertness to chance. The chance was none other than the collection of rock samples from the moon's surface by the Apollo 11 and Apollo 12 astronauts. P. H. Abelson, Director of the Geophysical Laboratory, describes it as "one of the most exciting scientific opportunities of this decade." The analysis made at the Laboratory, and at other laboratories in the United States and elsewhere, brought to an end centuries of speculation about the composition of the moon.

Both the similarities and the differences between lunar rocks and those from the earth are interesting. On one hand, rocks from the Apollo landing sites had at one time been molten, and the mineralogy of the specimens collected resembled those of basalts from the earth. On the other hand, the weathering effects commonly found in terrestrial rocks were absent from the lunar specimens, which appeared fresh and unaltered. No water was found in the lunar rocks, even in the form of hydrous minerals. Even the early analyses showed that conditions on the moon had been more highly reducing than those in the earth's crust. It also was found that the moon rocks had a higher content of titanium and chromium than most earth rocks, but were depleted in volatile elements like lead and the alkali metals.

After the first general study of the lunar rock characteristics the staff of the Laboratory concentrated its efforts on a study of opaque minerals. Analyses were made by F. R. Boyd, P. M. Bell, G. Kullerud, and J. F. Schairer, Staff Members; by W. B. Bryan, S. E. Haggerty, H. O. A. Meyer, and L. A. Taylor, Fellows; and by A. Muan, Guest Investigator.

The major phases of the opaque minerals on the moon are ilmenite ( $\text{FeTiO}_3$ ), members of the chromite ( $\text{FeCr}_2\text{O}_4$ )-ulvöspinel ( $\text{FeTiO}_4$ ) series, troilite ( $\text{FeS}$ ), metallic iron ( $\text{Fe}$ ), and minerals of the armalcolite series ( $\text{FeTi}_2\text{O}_5$ - $\text{MgTi}_2\text{O}_5$ ). The mineral armalcolite itself is new,<sup>18</sup> and was named for the astronauts Armstrong, Aldrin, and Collins of Apollo 11. It is intermediate in its series. Armalcolite resembles pseudobrookite, an earth mineral, but it contains no ferric iron.

The composition of armalcolite, like that of many other minerals from the lunar samples, gives an important clue about the lunar environment at the time of the rocks' crystallization. The partial pressure of oxygen must have been very low to produce a mineral of its composition.

Two minerals from the Apollo 12 lavas give some evidence of local tectonic history on the moon. Rocks collected by astronauts Conrad and Bean of

<sup>18</sup> The discovery of armalcolite was made simultaneously at the Geophysical Laboratory and at several other laboratories also studying the lunar samples.

Apollo 12 from the *Mare Procellarum* contain phenocrysts of pigeonite ( $\text{CaMg SiO}_3 \cdot \text{CaFeSiO}_3$ ) with intricately zoned mantles of the pyroxene augite. F. R. Boyd showed that some of the zoning developed in a way similar to tree ring growth. His electron probe studies have made some interpretations of the rocks' eruptive history possible. The pigeonite appears to have been formed at depth within the moon, and the augite mantles in fluid lava streams on the lunar surface. This successive crystallization contrasts with the commonly found simultaneous crystallization of these two minerals in terrestrial rocks.

One of the samples exhibits a rare oscillatory zoning of pigeonite and augite. Dr. Boyd interprets it as being formed in turbulent, rapidly flowing lava streams at the lunar surface.

An indication of lunar rock age also was obtained during the year. D. H. Lindsley, completing study of a newly discovered calcium-iron pyroxenoid, pyroxferroite, established its stability relations. Lindsley's results lead to the conclusion that the lunar pyroxferroite has existed in a metastable state for more than three billion years.

The differences and similarities between rocks from the Apollo 11 collecting area and the Apollo 12 collecting area also were most interesting. A major difference is the low titanium content of the Apollo 12 samples. The modal percentage of titanium in the Apollo 12 rocks is only about half that of the Apollo 11 collection. On the other hand, both sets of samples show high concentrations of refractory elements and low content of volatile elements; in these features lunar materials differ from most terrestrial and meteoritic rocks.

*The Moon Issue of Science.* The great interest of the scientific world in these and other results was reflected in the unique and voluminous "Moon Issue" of the periodical, *Science*,<sup>19</sup> under the general editorial direction of Dr. Abelson, who is Editor of *Science* as well as Director of the Geophysical Laboratory. A very impressive record of a few months of intensive analysis of the moon samples in the United States and abroad was assembled. The instruments placed on the moon by the Apollo 11 astronauts and the 22 kilograms of lunar materials they brought back presented a chance opportunity not only unique in history, but unique in the number of scientists ready to take advantage of it, and the speed with which their results were obtained. As Dr. Abelson explained in his editorial for the Moon Issue, for most investigators the time between receipt of samples and submission of manuscripts was only three months.<sup>20</sup> The Moon Issue was a most impressive demonstration of the capability of American, and world, science. The staff of the Laboratory not only shared in the demonstration, but provided leadership in the massive application of scientific effort brought forth by the return of the lunar materials. Many of the analysts of the lunar samples have been associated with the Geophysical Laboratory in the past, either as Fellows, Guest Investigators, or in other capacities.

### *Preparation as a Prerequisite for Seizing Opportunities*

*Advance Cultivation of a Field.* Members of the staff of the Geophysical Laboratory were able to take advantage of the exciting opportunities offered by the collection of the lunar samples because they were prepared. Their many past analyses of terrestrial basalts and their prior laboratory synthesis of some

<sup>19</sup> January 30, 1970.

<sup>20</sup> *Op. cit.*: 447.



of the lunar materials gave them experience and skills possessed by few other laboratories. The lunar minerals have been synthesized in phase studies of mineral systems that have members important in crustal and mantle rocks of the earth. The materials and structure of volcanic rocks are of course the closest parallel.

In spite of the time devoted to study of the moon samples, an impressive program of volcanic rock investigations continued at the Laboratory during the year.

A tape "library" of published chemical analyses of Cenozoic volcanic rocks was extended so that it now includes more than 9,400 entries from many localities in the world. F. Chayes has shown that the distribution of relative silica saturation is markedly bimodal in the basalts of this library. The Cenozoic basalts of most environments are dominantly either under- or oversaturated in silica. Only the norms of the submarine ridge basalts consistently lack both of the two indicators for over- and undersaturation.

H. S. Yoder, Jr., Staff Member, developed a hypothesis that accounts for the generation of both rhyolitic and basaltic magmas from a single parent material, and that postulates enough material to fit the largest eruptive events known.

W. B. Bryan conducted a field investigation of the volcanic islands of Tonga in the Pacific Ocean, which have been derived from crustal materials but display anomalously low values for alkalis and some trace elements. Bryan's analyses of major and minor elements in these rocks indicate that they could have been derived from a single basaltic andesite by fractional crystallization.

Analyses of mineral systems that are important components of the earth's crust and mantle were also continued. Among them were pressure-temperature stability studies of the jadeite-anorthite system by Ho Kwang Mao, studies of diopside-aegirine melting behavior by R. M. Cassie, studies of the effects of pressure on the thermodynamic mixing properties of orthosilicate systems by L. A. Taylor, P. M. Bell, and A. Muan, and completion of J. F. Schairer's and H. S. Yoder's extensive studies of the  $\text{Na}_2\text{O-MgO-SiO}_2$  system. Many new ternary compounds have been found in the Schairer-Yoder research; one of them has been observed in meteorites.

*Opening an Opportunity by Skilled Technical Manipulation.* Not infrequently skilled technical manipulation opens a path that would have been a blind alley without it. And almost certainly long years of preparation have been essential to the development of that technical skill. The superb record of the Hale Observatories' Mount Wilson and Palomar is as much a record of technical skill by the staff as it is of great instruments and great scientists; the techniques of the Geophysical Laboratory are renowned among geophysicists; equally well known is the technical imagination of the members of the Department of Terrestrial Magnetism; and each of the other departments shares this attribute in some notable manner. Recent work in the Department of Plant Biology provides a particularly happy illustration of the place of technical skills in the most creative research.

The existence of a new carbon dioxide fixation "pathway" in photosynthetic organisms has been established during the past six years in several laboratories. This is now known as  $\beta$ -carboxylation photosynthesis. Members of at least five different families of higher plants, both monocotyledons and dicotyledons, have this pathway, and four different genera contain some species that have

$\beta$ -carboxylation although other species within the given genus do not.<sup>21</sup> Beta-carboxylation is profoundly different from normal photosynthesis in that carbon dioxide is not released by illuminated leaves, and the inhibiting effect of oxygen on the rate of carbon dioxide absorption in normal air is absent.

O. Björkman, E. Gauth, and M. A. Nobs reported in *Year Book 68*<sup>22</sup> that the discovery of the two pathways within plants of the same genus provided a unique opportunity for studying the inheritance of the two. However, exploitation of this opportunity depended on the discovery of species that had enough genetic compatibility to permit hybridization, and then the patient application of plant breeding skills to achieve the hybrids.

Most of the plants belonging to the same genus and having the contrasting pathways appeared to be too distantly related to permit intercrossing. However, a careful search that exploited the wide taxonomic knowledge of the Department turned up two species from the family *Chenopodiaceae* (goosefoot) that appeared promising, *Atriplex patula* and *Atriplex rosea*. The first is a common marsh species in North America, Europe, and Asia, whereas the second favors semi-arid environments on the same continents. In the western United States *Atriplex* species are known as saltbush and greasewood.

Patient experiment with crosses between *Atriplex patula* (normal photosynthesis) and *Atriplex rosea* ( $\beta$ -carboxylation photosynthesis) by M. A. Nobs finally produced a viable cross, using *Atriplex rosea* as the female plant.<sup>23</sup> The production of this  $F_1$  hybrid opened the way for biochemical and physiological experiment that had been hoped for. Some observations from experiments on these  $F_1$  hybrids were reported last year.

During the 1969–1970 year, second-generation hybrids were produced from the  $F_1$ 's of the *Atriplex patula* and *Atriplex rosea* in the Department greenhouses by Dr. Nobs, O. Björkman, Dr. Nobs, and R. W. Percy, an Institution Fellow, continued the analysis of both the  $F_1$  and the  $F_2$  hybrids. They investigated the cytogenetics, leaf anatomy, biochemistry, and photosynthetic characteristics of the *Atriplex* hybrids. The observations made in these studies required technical skills of a high order, since data had to be assembled for a number of individual hybrid plants on: leaf anatomy; phospho(enol)pyruvate (PEP)-carboxylase activity in leaf extracts; carboxydismutase activity in leaf extracts; effect of leaf position on the activity of PEP carboxylase; carbonic anhydrase activity in leaf extracts; distribution of radioactive carbon in individual compounds after photosynthesis; carbon dioxide compensation points; light-saturated rate of carbon dioxide compensation points; light-saturated rate of carbon dioxide uptake; and efficiency of utilization of carbon dioxide at low concentrations in intercellular spaces.

The first results reveal characteristics in the hybrids that might have been anticipated from classical genetics. But others were unanticipated. The first-generation hybrids are diploid, have the same chromosome number as the two parental species, and are generally intermediate in morphology. They also apparently have inherited the carbon dioxide fixation pathways from both parental species; about one-half the initial products of photosynthesis are those of the  $\beta$ -carboxylation pathway and the remainder are those of the normal (Calvin) pathway (Figure 5). The leaf anatomy of hybrids also is intermediate

<sup>21</sup> *Carnegie Institution Year Book 68*: 620–621.

<sup>22</sup> *Ibid.*: 621.

<sup>23</sup> *Carnegie Institution Year Book 68*: 621, 631–633.

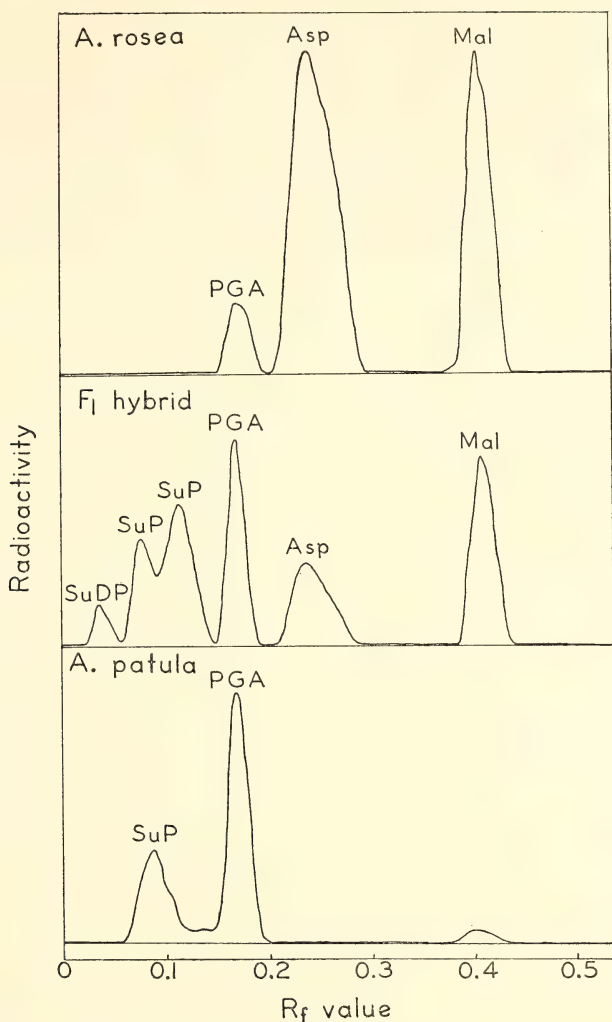


Fig. 5. Biochemical distribution of radioactivity in *Atriplex* leaves after two or four seconds of photosynthesis in air containing  $^{14}\text{CO}_2$ . The products of both in  $\beta$ -carboxylation cycle and normal cycle are shown on the F<sub>1</sub> hybrid curves.

between that of the two parents. However, the peculiar chloroplast structure found in the  $\beta$ -carboxylation plants is not present in the hybrid (Figure 6).

Surprisingly, the intermediate biochemical and leaf anatomical characteristics do not carry over into photosynthetic performance in the F<sub>1</sub> hybrids. The efficiency for using low carbon dioxide concentrations in the hybrids is about one-half that of *Atriplex patula* and about one-third to one-fourth of that of *Atriplex rosea*. The result is much lower light-saturated rate of photosynthesis in the F<sub>1</sub> than in either parent in normal air (Figure 7).

The F<sub>2</sub>, or second-generation hybrids, analyzed by Björkman and Pearcy all have photosynthetic characteristics very similar to the first-generation



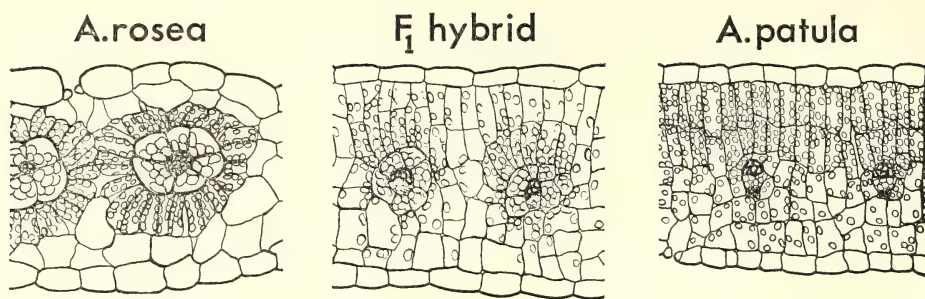


Fig. 6. Camera lucida drawings of living leaf sections of *Atriplex rosea*, *Atriplex patula*, and their first-generation hybrid.

hybrids. This is true in spite of the wide differences among them in the activity of PEP carboxylase, the enzyme responsible for the initial carbon dioxide fixation in the  $\beta$ -carboxylation pathway, as well as wide differences in leaf anatomy. Björkman and Percy thus suggest that the two most distinctive characteristics of the  $\beta$ -carboxylation plants cannot by themselves provide the high photosynthetic efficiency, or the absence of oxygen inhibition found in the  $\beta$ -carboxylation plants. Discovery of the means of coordinating the essential metabolic steps that produce the photosynthetic efficiency of the  $\beta$ -carboxylation plants therefore becomes an interesting, if complex, research problem.

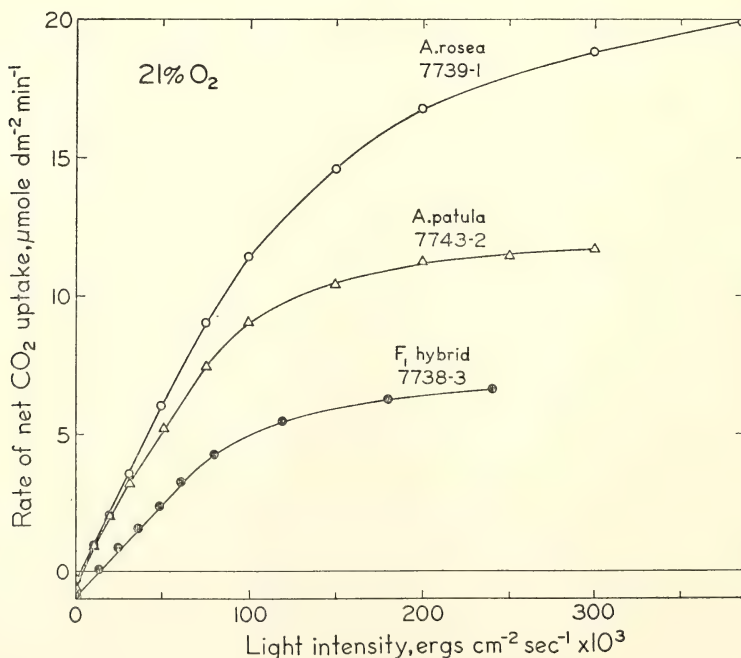


Fig. 7. Photosynthetic carbon dioxide uptake as a function of light intensity in *Atriplex rosea*, *Atriplex patula*, and their  $F_1$  hybrid (under 21 percent  $O_2$  and 0.003 percent  $CO_2$ ). The hybrid is markedly less efficient than either parent.

Studies by J. A. Berry, another Fellow at the Department, suggest that the  $\beta$ -carboxylation pathway probably functions in sequence with the normal pathway of photosynthesis. These and other related reactions take place in separate sites within the leaf. Björkman, Pearcy, and Nobs suggest further that  $\beta$ -carboxylation photosynthesis "involves at least several loci." Although the essential steps of  $\beta$ -carboxylation pathway may be determined by a small number of genes, proper timing and spatial compartmenting of the steps appear highly important.

Björkman, Pearcy, and Nobs drew certain conclusions from their first results that may be applicable to plant breeding. They suggest that the importance of coordination of the  $\beta$ -carboxylation pathway "makes it highly unlikely that plants with desirable characteristics of  $\beta$ -carboxylation photosynthesis can be produced by the application of mutagens to plants lacking the pathway." However, they also believe that their hybridization experiments show that the genetic divergence between species possessing  $\beta$ -carboxylation photosynthesis and those lacking it need not be great. "It may . . . be possible to introduce desirable photosynthetic traits associated with this pathway from species possessing it to related species that are of agricultural importance but which lack the pathway." Thus fundamental research that was made possible by highly skilled plant breeding techniques may in turn open other vistas for practical plant breeders.

### *A Range of Methods—The Usefulness of Field Study*

Scientific research is most commonly associated with the experimental method, and the education of a scientist most often makes liberal use of experimental training. However, field observation is also an important part of science, and its results can be no less vital in the progress of science. All astronomy, in a sense, is a type of field observation, and many sciences depend heavily on a combination of field investigation and experiment. The work in physiological ecology, just described, is a fine illustration. Without the detailed knowledge of species and their geographic distribution brought about through field study, the material used for the *Atriplex* crosses could hardly have been obtained as quickly. The Apollo 11 and Apollo 12 astronauts were part of a field study team, most of whom remained on earth. Of the sciences here represented, perhaps geology and geophysics have the most intimate relationship of field study and experiment.

The scientist in many important fields therefore is at his best if he has some familiarity with field methods as well as the place of field study in his profession. It follows that the education of the young scientist should provide opportunities for acquaintance with field methods. An advanced scientific educational institution therefore does well to include field study subjects within its program.

To illustrate further the value of field study we turn to geology-geophysics, and particularly to seismology, where Staff Members of the Institution have employed field study for many years. More than incidentally, the seismology field program is also a fine example of the inseparability of education and research as conceived within the Institution. A field program, particularly in a foreign country with important field problems, offers an unusual opportunity to establish a continuing advanced training program, which eventually matures into a scientific collaboration.

It has been known for some time that the Andes region of northern Chile, Bolivia, and Peru is of exceptional interest to the interpretation of the crustal and mantle structure of the earth. The towering mountain ranges; the great

altiplano; heat anomalies, electrical conductivity anomalies, and magnetic anomalies; intense seismic activity; and location on the edge of the great Pacific Basin—all these combine to excite the interest of the geophysical research worker. This research opportunity was recognized almost twenty years ago also as an educational opportunity by M. A. Tuve, then Director of the Department of Terrestrial Magnetism, and his associates. South America had a notable lack of physical scientists. A program of field study of Andean structure could be used as a means of advanced training for South American scientists in physics and geophysics.

The first studies of crustal structure under the Andes were undertaken by Dr. Tuve, H. Tatel, and their associates about fifteen years ago. The first reported results were presented in *Year Book 57*. Since that time a succession of field parties has gone out from the Institution and a fruitful set of collaborative relations developed with Chilean, Bolivian, Argentinean, and Peruvian scientists.

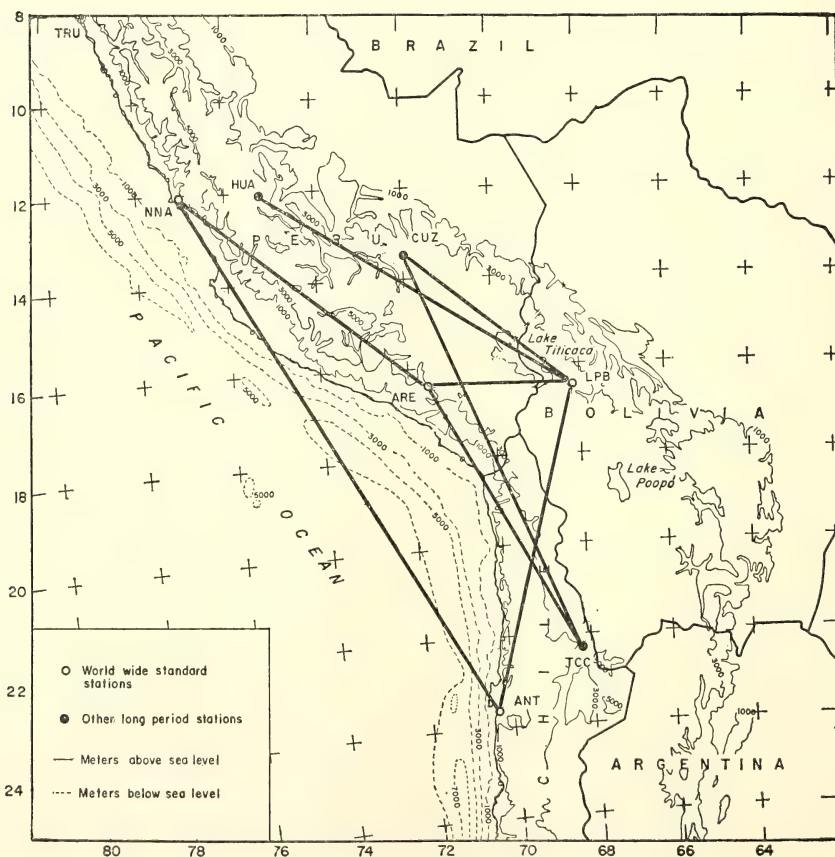


Fig. 8. Profiles of paired stations used in seismic study of earth crustal structure in the Andean region by D. E. James.



During the past year, two South Americans were Research Associates, one a Fellow, and thirteen, collaborators of the Department of Terrestrial Magnetism.

The most notable recent field expedition was that undertaken during the summer of 1968 by the Department and its collaborators to apply explosion seismology in the study of the region. At this time a network of recording seismograph stations was completed at key locations within the region.

The techniques and the equipment developed for past expeditions and collaborators were further applied during the year to interpretations of the crustal and mantle structure of this Andean area. D. E. James, a Staff Member, reports on the interpretation of surface seismic wave velocities recorded as profiles between paired stations in a net crisscrossing the regions (Figure 8). F. Volponi, a Departmental collaborator at the Universidad Nacional de Cuyo, San Juan, Argentina, also reports on studies undertaken with another net. Dr. Volponi's report is particularly interesting as an indication of the progress made within a few years by the South American collaborators.

The problem in both cases is the testing of a model of the crustal and mantle structure underlying the region. Dr. James' results suggest a comparatively normal structure in the coastal area with a thickness of 25-30 kilometers (Figure 9). However, the crust appears to thicken rapidly between the coastal and altiplano regions, attaining a maximum thickness of 70 kilometers or more beneath the western cordillera. Seismic wave interpretation further suggests a thinning of the crust again beneath the eastern cordillera. Dr. James' data thus appear to confirm the existence of a very thick crust postulated by many previous

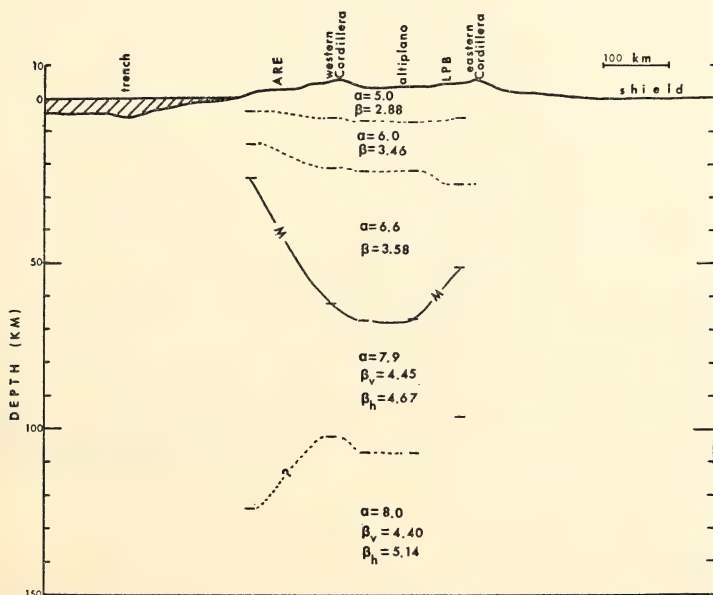


Fig. 9. Cross section of the Andean crustal and upper mantle structure derived from phase velocity measurements of seismic waves.

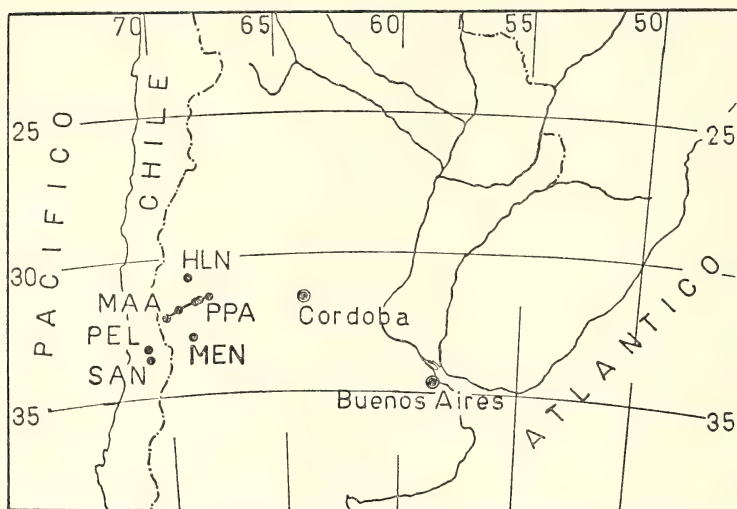


Fig. 10. Seismic observing stations used by F. Volponi for study of earthquake wave anomalies in the Southern Andean region. HLN = Hualilan; MAA = Manantiales; PPA = Pie de Palo; SAN = Santiago; PEL = Peldehue; MEN = Mendoza.

writers on the geology of the region beneath the altiplano. With the possible exception of some fragmentary results on the Himalayas, the crustal thicknesses reported by James for this region are the greatest measured anywhere in the world. In addition, James concludes that this thickness of the crust indicates that the western cordillera was not formed as an island arc, but possibly was formed on pre-existing continental crust.

Studying a cross section of the Andes mountain range in Argentina, Dr. Volponi used a net of field stations (Figure 10) to gather data from 39 earthquakes, including one explosion recording. He found that results from the *P* phases of local earthquakes and the *PKP* phases of more distant earthquakes were very similar. This he interprets to mean that the anomalies observed were caused by differences in the properties of the rocks in the more external layers of the earth, that is, to no more than 200 kilometers' depth. He also draws the conclusion that the earth's interior beyond that depth behaves as a uniform medium with spherical symmetry.

These and other results show that the western South American field geophysics program is producing very significant data about a key section of the earth's crust. However, the results are perhaps even more significant because they illustrate the arrival of a mature collaboration between the scientists of the Andean region and those of the Institution.

### *Equipment—The Essential Substrate*

As the history of science has demonstrated over and over, scientists are by no means helpless without equipment. But without equipment today they are handicapped. A good theoretician may work with pencil and paper, but he must

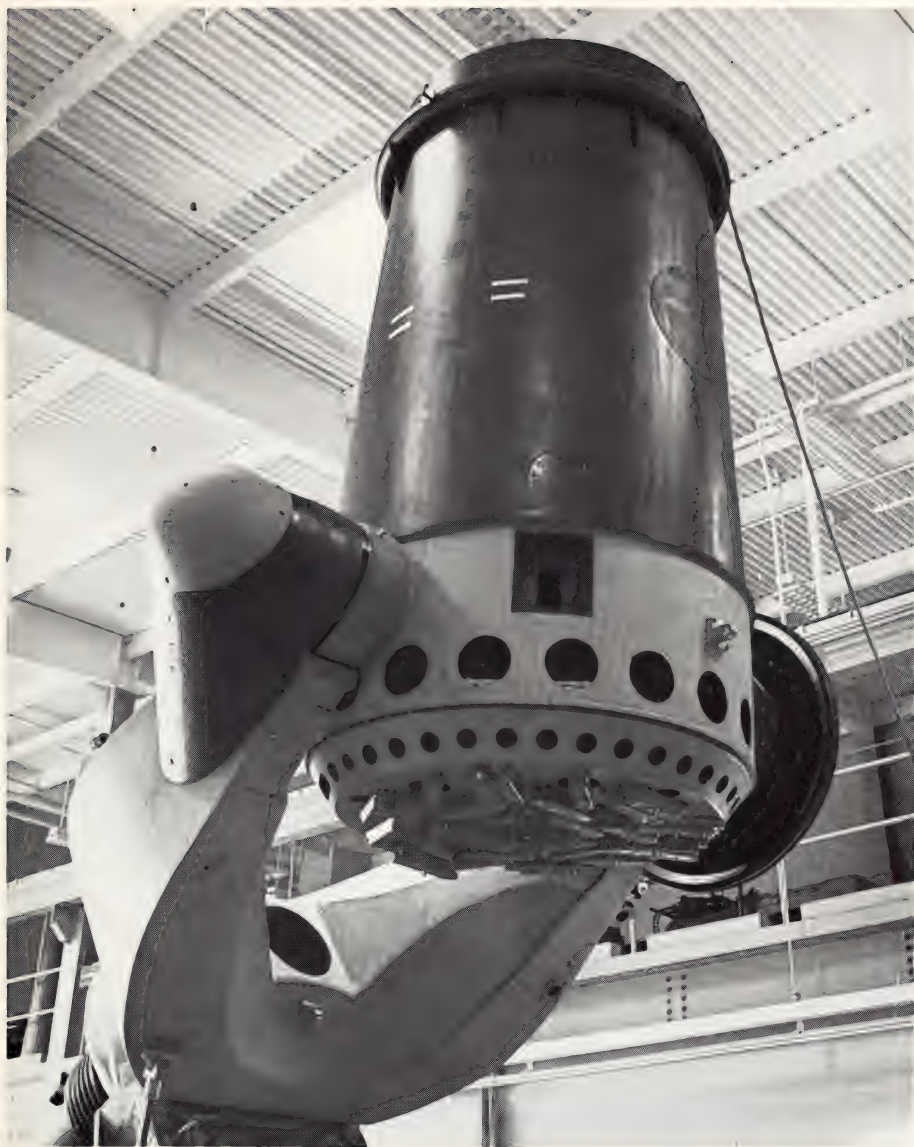


Plate 2. The new 60-inch Palomar photometric telescope was dedicated on October 23, 1970. Equipped with a computer-controlled guidance system and highly sensitive auxiliary instrumentation, it will increase the available telescope time at Palomar very significantly. The telescope was constructed with the aid of National Science Foundation and National Aeronautics and Space Administration grants.





Plate 3. The Oscar G. Mayer Memorial Building and Dome house the new 60-inch photometric telescope and equipment. Gifts from members of the Mayer family made construction possible.



Plate 4. Cerro Las Campanas, Chile, site of the new southern hemisphere observatory, located at latitude  $29^{\circ}$  south. A 20-mile all-weather access road was completed during the summer of 1970, and a 40-inch telescope will be placed in operation on the mountain early in 1971.





be supported by a man, or men, with instruments or his theory eventually languishes. The vast majority of scientists depend heavily on equipment. It follows that the advanced student in science must be exposed not only to the operation of a variety of highly specialized equipment, but also to the process of invention to meet the ever-challenging requirements of frontier research.

All of the Departments of the Institution have a tradition of maintaining up-to-date instrumentation, and permitting Fellows ready access to it. It is also part of the Institution's tradition to aid Fellows in procuring or building equipment when it is not already available. The activities of the Hale Observatories during the year are an excellent example of the normal concerns and practices in a department heavily dependent on equipment.

*Instrumentation at the Hale Observatories.* From the first days of his professional training the astronomer, his telescope, and its auxiliary instruments form an interlocked system. The care of a modern observatory centers largely on the design, procurement, operation, and maintenance of these instruments.

The Hale Observatories, operated jointly by the Institution and California Institute of Technology, have maintained four major telescopes at Mount Wilson and Palomar Mountain since 1948: the 200-inch Hale telescope, the 48-inch schmidt telescope, the 100-inch Hooker telescope, and the Mount Wilson 60-inch telescope. During 1970 a new 60-inch photometric telescope was completed on Palomar Mountain, and was dedicated in October (Plates 2 and 3). It was designed by the Observatories Engineering Staff and built in part at the California Institute of Technology shops. The 60-inch mirror and secondary mirrors were figured in the Mount Wilson optical shop.

Construction of the Big Bear Solar Observatory, a new unit of the Hale Observatories, was completed at Big Bear Lake, California, during the year, adding a new equatorial telescope to the long-used solar tower telescopes on Mount Wilson. At the same time extensive modifications of the fifty-year-old Mount Wilson 60-inch telescope were nearly completed, and a modernization of the Mount Wilson 100-inch begun.

An important part of the instrumentation program at the Hale Observatories in recent years has been the installation of computer controls and associated electronic data systems for each of the telescopes. The new Palomar 60-inch will be completely computer operated, and a similar system was nearing completion at the end of the year on the 200-inch telescope. A complete new data and control system for the 150-foot solar tower telescope at Mount Wilson was designed and construction begun. A number of new auxiliary instruments were developed or applied during the year, including new image intensifiers, an interferometric scanning spectrometer, and a simple new technique for making large objective-transmission "amplitude" gratings.

Finally, construction of the Las Campanas Observatory, about one hundred miles north of La Serena, Chile, was begun, so as to give Observatory Staff and Fellows vitally needed access to southern skies. Site development, including a road to the top of Las Campanas mountain, was well under way by the end of the year, as well as construction on a 40-inch telescope to be installed on Las Campanas during the 1970-1971 year (Plate 4).

An interesting feature of the instrumentation program at the Observatories was the amount of student and Fellow participation in instrument care and

modernization. The modernization of the Mount Wilson 60-inch, for example, was assisted very substantially by volunteer student effort during 1969 and 1970.

Student willingness to volunteer as much as several weeks' time for instrument care and renovation reflects a feeling of commitment to a joint education-research enterprise at the Observatories. Twenty-four students from California Institute of Technology and sixteen Fellows from the California Institute and the Carnegie Institution were associated with the Observatories during the year. In 1969 students and Fellows used the Mount Wilson 100-inch telescope on fifty-four percent of the available nights, and the 60-inch on sixty-seven percent of the available nights. Even the Palomar 200-inch telescope had twenty-one nights of student participation. In addition, and perhaps equally valuable, students acted as the technical assistants for nights of observing by senior astronomers on the 200-inch and other telescopes. Senior astronomers need such assistants to make the best use of electronic data systems and complex auxiliary instruments.

In addition to the major telescopes at Mount Wilson and Palomar there are also three solar telescopes, a 62-inch infrared telescope, a 20-inch photometric telescope, and an 18-inch schmidt that are often used by graduate students and Fellows.

*The Invention of Equipment.* Some scientists consistently prefer to design their own equipment; many do so by necessity at some time or other during their careers. A tradition of resourcefulness is strong within the Institution. Existing practice in the Institution undoubtedly may be traced in part to the long history of its scientific research, extending over nearly seventy years. During the first three decades of the existence of the Institution, Staff Members in many cases would have had to make do without appropriate instruments if they had not designed and built their own. A second influence is inherent in the modest budgets that Institution departments must work with. The search for the economical answer is always a prudent part of experimental design; not infrequently it becomes the elegantly simple and powerful answer. The young scientist who has an opportunity to see this principle in operation has had a priceless experience.

*An Improved Strainmeter.* One elegantly simple invention was described in this report last year (*Year Book 68*). The borehole strainmeter for measuring stresses within the earth is one of the most extraordinarily sensitive instruments ever produced. I. S. Sacks, a Staff Member, and D. W. Evertson and L. M. Dorman, both Fellows at the Department of Terrestrial Magnetism, continued the development of the strainmeter during the year. A second prototype on a new design was produced that enables the resolution of volume strain into areal (horizontal) and vertical strains (Figure 11). This is important because a large share of the "noise" that must be filtered in the volume signal is atmospheric, and is normal to the earth's surface. The new instrument does indeed produce two separate directional signals (Figure 12), thus adding directional resolution to its unusual sensitivity. Sacks, Evertson, and Dorman further found that the atmospheric noise in the vertical signal could be successfully filtered by connecting the strainmeter to a microbarograph. In their tests of a "two-point" microbarograph-strainmeter hook-up, improvements in the signal-to-noise ratio by factors of 5 to 20 were found to be obtainable, the factor depending on the frequency.

*Improved Thermocouple Design.* A good example of the laboratory search for

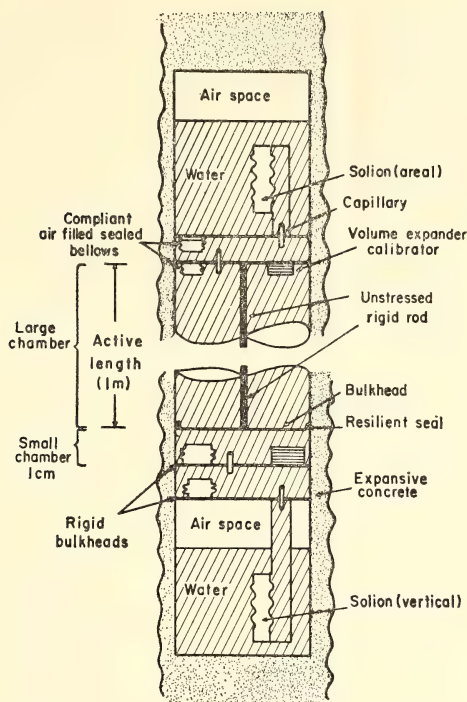


Fig. 11. The improved strainmeter, which can resolve directional signals into their horizontal and vertical components.

precision and the importance of proper instrumentation in arriving at that precision was given in the design of thermocouples by H. K. Mao and P. M. Bell at the Geophysical Laboratory. Dr. Mao is a Fellow there.

Pressure-temperature apparatus is essential to the now widely known program of phase-equilibrium studies on minerals and mineral synthesis at the Laboratory. Some years ago F. R. Boyd and J. L. England of the Laboratory designed the standard pressure cell used in this type of experiment. Pressures of as much as 40 kilobars and temperatures as high as  $1700^{\circ}\text{C}$  may be employed in the cells (Figure 13). The usual means of measuring temperatures within the cells has been through a platinum-rhodium thermocouple. However, it has been known for many years that significant errors occurred in readings from such thermocouples (as much as  $25^{\circ}\text{C}$  at 40 kilobars). These errors are both random and systematic, the latter caused by contamination with elements other than those of the thermocouple and by a hydrostatic pressure effect.

After a number of tests of cells at a wide range of temperatures and pressures, Mao and Bell concluded that the standard platinum-rhodium thermocouple was not as accurate as one based on tungsten-3 percent rhenium/tungsten-25 percent rhenium wires. Certain other design features were explored, including insulation of the thermocouple wires with Pyrex glass to prevent contamination, and the use of weak materials (talc, boron nitride, and Pyrex) in the low temperature parts of the pressure cell. Such a furnace cell is relatively inert chemically for tungsten-rhenium wires and causes a low random error. With this design Mao



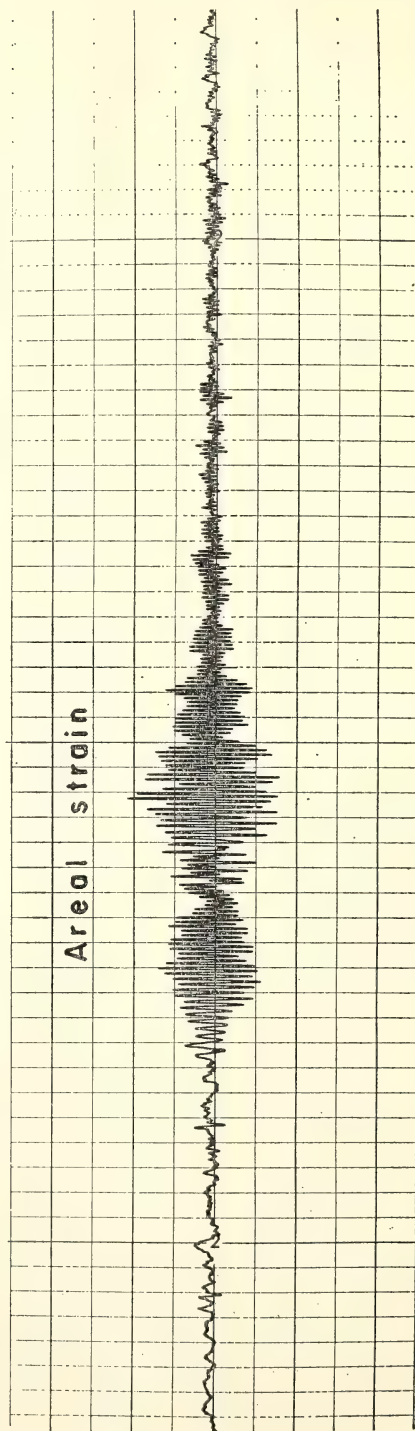
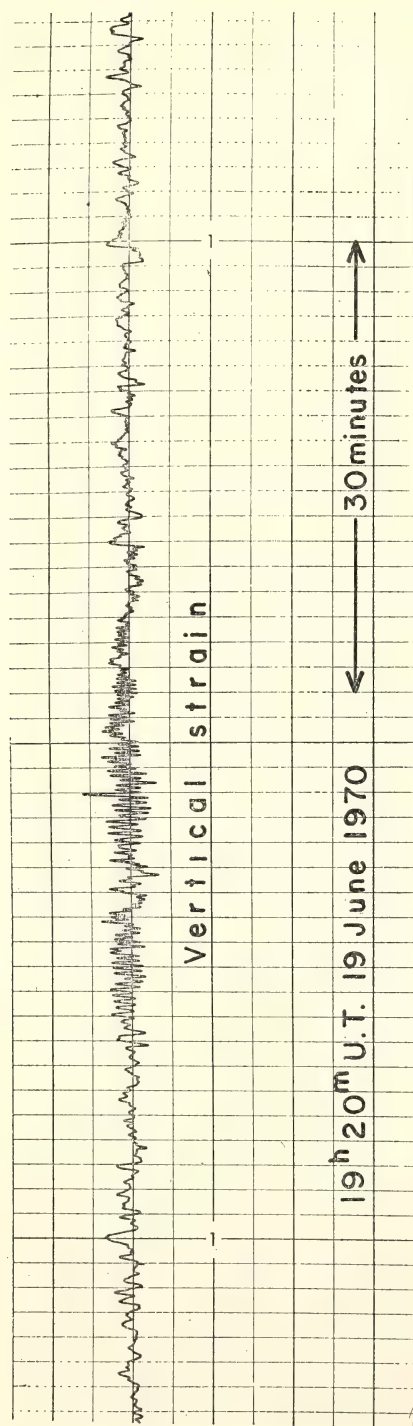


Fig. 12. Rayleigh waves from two earthquakes ( $m_b = 5.3, 5.4$ ) in the Fiji region recorded at the Department of Terrestrial Magnetism, Washington, D.C., on strainmeters. The earthquakes were about 10 minutes apart. The signal-to-noise ratio for the areal recording is about twice that for the vertical.

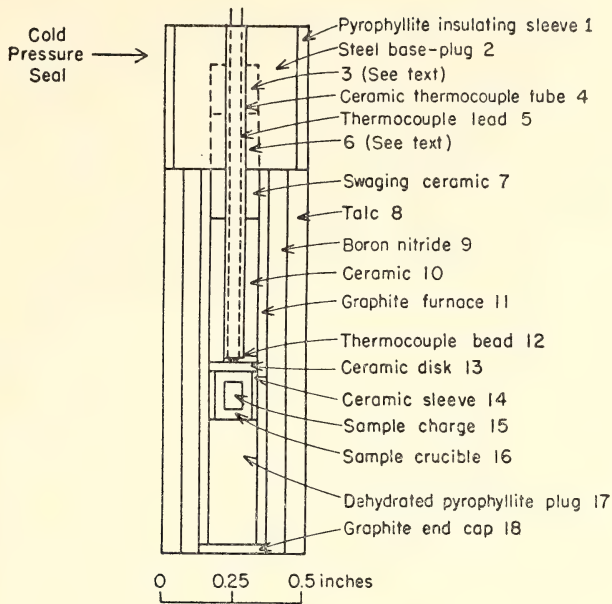


Fig. 13A. High-pressure cell (after Bell and England, 1967). In a regular Boyd-England cell, parts 2, 3, and 6 are a single piece of steel.

and Bell believe that “it should be possible to avoid many of the common errors associated with routine experiments in . . . single-stage apparatus.” Even though the customary errors of using the platinum-rhodium thermocouples were about one percent or less, such errors can be highly significant.

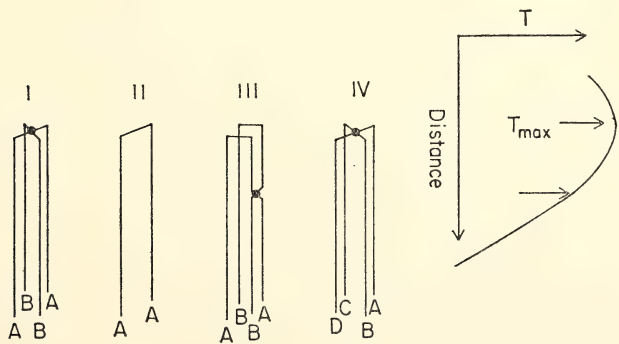


Fig. 13B. Configurations of thermocouple assemblies. A, B, C, and D represent different thermoelectric materials. The upper end of each assembly is placed at the maximum temperature of a high-temperature cell.

*Instrumentation at the Department of Plant Biology.* Specialized instrumentation is no less important in the biological sciences than in the physical. During the administration of C. S. French, instrument development has been a consistent element of the program of the Department of Plant Biology. It has developed several basic instruments that have been highly useful in biophysical-biochemical investigations of photosynthesis and in physiological ecology. Among these have been the French Press for fragmenting chloroplasts, and the small-scale controlled-input growth chambers for plant physiology investigations.

Another basic instrument for the work of the Department has been Dr. French's automatic spectrophotometer, designed and built some years ago for recording action spectra of oxygen evolution from whole plant cells. Because of its size, however, it is usable only in a laboratory. P. Halldal, a former Fellow at the Department and now Professor at Umeå University in Sweden, recently designed and built a portable spectrophotometer for the same purpose. Dr. Halldal has employed it for investigations of marine algae at Umeå and elsewhere. During the year Dr. Halldal returned to the Department as a Senior Fellow. Dr. French and he studied two different recording procedures for measuring the action spectra of any partial reaction of photosynthesis that causes a color change of an added dye. Dr. Halldal's results show promise of a significant improvement over the standard methods. The goal, not yet perfected, is a simple device for measuring action spectra with a precision approaching that which is now routine in absorption spectroscopy.

Over a number of years one of the most important technical objectives in the Laboratory has been the development of improved methods for disintegrating and fractionating chloroplast particles. The French press was an important instrumental contribution to these disintegration techniques. Improved fractionation of chloroplasts by centrifugation on a sucrose density gradient was developed in the Laboratory in 1967-1968 by the Drs. Michel. Renewed interest in this problem has been sparked by the attractiveness of the great variety of pigment systems available in various species of algae. As a possible approach to this problem of chloroplast particle separation for all of the interesting algal systems, Jeanette S. Brown, in collaboration with O. N. Griffith of the Beckman Instrument Company, has tested a zonal rotor centrifuge. A much larger scale preparation of chloroplast fractions than previously possible has now been achieved. At the same time Dr. Brown has employed a large green unicellular alga, *Eremosphaera viridis*, from which chloroplasts may be removed more easily than from the species hitherto employed. The combination of new instrumentation with fresh material affords a new research opportunity which Dr. Brown and her colleagues undoubtedly will exploit more fully in the year to come.

### *A Favorable Environment is the Same for Research and Education*

A scientist's work is generally carried out within a well-defined institutional environment. This institutional ambience is of equal importance to the serious student, particularly the man or woman on the verge of embarking on a scientific career. The conditions for a favorable environment appear to be almost identical for the student and the scientist.

During the seven decades of its life, the Carnegie Institution has developed an institutional environment which may be summarized as affording independence, association, and continuity. The independence of the Institution Staff Member and Fellow is that classically sought in all academic institutions and now so seriously compromised in many of them. First, perhaps, is a degree



of financial independence. As M. A. Tuve, Distinguished Service Member of the Department of Terrestrial Magnetism, often has said, "Mr. Carnegie buys the scientist's time and then gives it back to him." Although salaries at the Institution are modest, they come with few strings attached. The Carnegie scientist is free to pursue knowledge according to his own inspiration. The Staff Member has few duties other than those of his self-chosen program of research and instruction. The student or Fellow is entirely free of extraneous duties, except those for which he may volunteer. The conditions that the Institution has attempted to provide might be called an insulation against what Ellis Bolton recognizes as "a rapidly inflating background of . . . 'cultural noise' [which] covers the whole radiation spectrum and extends even into man's economic and social endeavors."

But the insulation must be that afforded by a permeable membrane with dynamic and constant exchange with the scientific world. Freedom of association within the Institution is particularly important, and it is essential for the student and Fellow. The Staff Member may associate himself with a group, as do the members of the Biophysics Section of the Department of Terrestrial Magnetism or the Physiological Ecology Group of the Department of Plant Biology, and a number of other working groups within the Institution. But the Staff Member is also free to choose only *ad hoc* associations and live a more solitary working life if he chooses. The Staff Member is also free to choose temporary associations in other institutions, at home or abroad. The annual budget always contains travel allotments for this purpose, often unforeseen in a specific way at the time the budget is made up.

Among the associations that the Staff Member of the Institution chooses are those of students and Fellows. Dr. Bolton has put this desire and practice into words which are not easily forgotten: "He [the Staff Member] knows that he cannot accomplish alone what he envisions. He is, therefore, a teacher, a communicator to his peers and to generations that will succeed him."

The Institution is consistently faithful to the ideal of flexibility. But it is a flexibility that keeps the entire structure of the Institution's immediate past, its present, and its future in close view. Continuity is equally important. When, for example, the opportunity came in mid-summer 1970 for I. S. Sacks, co-inventor of the strainmeter described above, to install an array of such strainmeters in Japan, the undertaking was not viewed simply as a field trip for equipment testing. Instead, a comprehensive program was planned for a research-educational visit. Within days the program was ready, an Institution decision was made, and funds were provided. Dr. Sacks' program included not only a collaborative effort with Japanese scientists in testing the strainmeters in one of the most earthquake-prone areas of the world, but also a fundamental study of the attenuation of the "shear" waves from earthquakes, as shown in the data of a number of Japanese seismic stations. It is thought that this study may have a significant bearing on the new paradigm of geophysics and geology, global plate tectonics. An equally important educational mission was seen. A number of young Japanese scientists have been Fellows at the DTM. They are now professors at universities or directors of research institutes in their country. We hope that their students and young colleagues in turn may become Fellows of the Institution. Dr. Sacks' mission will refresh these valued associations.

The continuation of consultation in the Staff Member-Fellow relationship thus extends far beyond the duration of the Fellows' residence at our departments. A continuity between the work of student and Fellow and the later collaborator

and colleague is seen, cherished, and nurtured. The Institution looks upon itself not so much as an endowment and a set of laboratories as a world-wide community of scholars—the teachers, the investigators, and the taught, whose positions are sometimes interchangeable. We believe that these freely chosen associations of independent men and women offer an unusual educational experience, produce consistently valuable research, and are a model for a society of moral men.

### *Losses . . .*

It is with deep regret that I must report the death of one active Staff Member and two retired Staff Members.

Armin J. Deutsch, a Staff Member of the Hale Observatories, died on November 11, 1969. A distinguished stellar spectroscopist, Dr. Deutsch came in 1951 from Harvard College Observatory to the staff of the Mount Wilson and Palomar Observatories. Among his special interests were the theory of electromagnetic processes in stellar atmospheres and spectrum variables of type A stars. One of his major contributions was the elucidation of the oblique rotator model to account for variations in the spectra and magnetic fields of these type A stars. Dr. Deutsch was also well known for his work on mass loss by giant red stars. His courage matched his accomplishments; for several of his last years he had an unrelenting struggle with ill health, yet he continued his work with the same skill and persistence. His quiet manner and brave response to adversity set an example that we shall always remember.

Jens C. Clausen, a member of the Department of Plant Biology from 1931 to 1956, died on November 22, 1969. Dr. Clausen was a pioneer in the study of the evolution of plant species and in plant genetics. His investigations, undertaken with D. D. Keck and W. M. Hiesey and recorded in the series *Experimental Studies on the Nature of Species*, continue to exercise an important influence on students of evolution as well as of plant biology. A scientist of wide international reputation, he was elected to the Danish Academy of Sciences in 1950, and served as President of the Royal Swedish Academy's Society for the Study of Evolution in 1956. Dr. Clausen looked on his formal retirement from the Institution as others look on a graduation. He continued to pursue his field work, experiment and writing uninterruptedly, and with ever greater zeal. Just before his death, he had been one of eleven American botanists named honorary vice-presidents of the XIth International Botanical Congress. Dr. Clausen has left an indelible mark on two generations in the work of plant ecology and taxonomy.

James H. C. Smith of the Department of Plant Biology died January 8, 1970. Joining the Institution in 1927, Dr. Smith was a leading authority on plant pigments. He became particularly distinguished for his work on protochlorophyll, the precursor of chlorophyll in leaves. He was the first to isolate the protochlorophyll holochrome from dark-grown leaves, thus permitting the transformation of protochlorophyll to chlorophyll to be studied outside the leaf for the first

time. Dr. Smith retired as a Staff Member in 1961 but continued his research as an emeritus member of the Department.

All three of these men, so different and yet so alike in their unswerving and single-minded devotion to research, will be deeply missed.

### *. . . and Gains*

It is with the greatest pleasure that I record the reception of several honors by Staff Members of the Institution.

A most signal honor came to Dr. Alfred D. Hershey, Director of the Genetics Research Unit, who received the Nobel Prize in Physiology and Medicine jointly with Dr. Max Delbrück and Dr. Salvador Luria for discoveries concerning the replication mechanism and the genetic structure of viruses. Dr. Hershey was subsequently honored by a resolution adopted by the House of Representatives of the State of Michigan for "opening a new area of genetics"; the Michigan State University also awarded him an honorary degree of Doctor of Medical Science and a distinguished alumni award; the Institute of History of Medicine and Medical Research of New Delhi, India, named Dr. Hershey an honorary fellow.

Dr. Horace W. Babcock, Director of the Hale Observatories, was awarded the Gold Medal of the Royal Astronomical Society.

Dr. Elizabeth M. Ramsey of the Department of Embryology received the John F. Lewis Prize of the American Philosophical Society for her paper on the placenta, presented at the Society's annual meeting (1969) and published in the Society's Proceedings.

Dr. W. Kent Ford of the Department of Terrestrial Magnetism was honored by the Washington Academy of Sciences on February 19, 1970. For achievement in the design and use of image intensification systems in astronomy, Dr. Ford was given an award in the physical sciences.

Dr. Gabrielle Donnay of the Geophysical Laboratory was elected to membership in the Johns Hopkins Society of Scholars.

Dr. Yoshiaki Suzuki, a Fellow at the Department of Embryology, received the Asakawa Annual Award from the Microbiology Society of Japan for work in chloramphenicol-, dihydrostreptomycin-, and kanamycin-inactivating enzymes from multiple drug resistant strains of *E. coli* carrying episome "R."



*Faculty, Fellows, and Students*

1969-1970

DEPARTMENT OF EMBRYOLOGY  
Baltimore, Maryland

*Director*

James D. Ebert

*Staff Members*

Bent B. Böving  
Donald D. Brown  
Igor B. Dawid  
Robert L. DeHaan  
Douglas M. Fambrough  
Elizabeth M. Ramsey  
Ronald H. Reeder

*Research Associates*

Louis B. Flexner  
Arthur T. Hertig  
Irwin R. Konigsberg

*Fellows*

Masako Fukada  
Leonard P. Gage <sup>1</sup>  
Reiji Hirakow  
Harold R. Misenhimer  
Ronan O'Rahilly  
Eijiro Ozawa  
Robert G. Roeder <sup>2</sup>  
Yoshiaki Suzuki  
Ronald F. Swanson <sup>1</sup>

*Students* <sup>3</sup>

John Chase  
John O. Dunning  
H. Criss Hartzell, Jr.  
Mary Kennedy  
Dennis E. Leister  
Edward W. Schaefer  
Malcolm M. Smith  
Ralph Stern  
Thomas G. Storch  
Marjorie A. Tiefert

<sup>1</sup> Fellow, U. S. Public Health Service.

<sup>2</sup> Fellow, American Cancer Society.

<sup>3</sup> Enrolled at Johns Hopkins University.

Doreen Ward  
Pieter C. Wensink

*Student Assistants*

Paul Fishman  
Nancy Kolzak  
Barbara Mann  
Donna S. Minor  
Laureen E. Pepersack  
Jeff Sollins  
Roberta Truitt

GENETICS RESEARCH UNIT  
Cold Spring Harbor  
Long Island, New York

*Director*

Alfred D. Hershey

*Distinguished Service Member*

Barbara McClintock

*Fellows*

Shraga Makover  
David H. Parma <sup>4</sup>  
Irwin Rubenstein <sup>5</sup>  
Anna Marie Skalka  
Hideo Yamagishi

GEOFYSICAL LABORATORY  
Washington, D. C.

*Director*

P. H. Abelson

*Staff Members*

P. M. Bell  
F. R. Boyd  
F. Chayes  
G. L. Davis  
Gabrielle Donnay  
J. L. England  
L. W. Finger  
P. E. Hare  
T. C. Hoering

<sup>4</sup> Fellow, National Science Foundation.

<sup>5</sup> Fellow, National Institute of General Medical Sciences.

T. E. Krogh  
G. Kullerud  
D. H. Lindsley  
J. F. Schairer  
H. S. Yoder, Jr.

*Emeritus Research Associate*

E. G. Zies

*Fellows*

W. B. Bryan  
R. M. Cassie  
S. E. Haggerty  
A. W. Hofmann  
H. G. Huckenholz  
H. K. Mao  
H. O. A. Meyer  
H. R. Puchelt  
D. Rumble  
D. Smith  
L. A. Taylor  
W. Viaene  
J. F. Wehmiller

HALE OBSERVATORIES  
Pasadena, California

*Director*

Horace W. Babcock

*Associate Director*

J. Beverley Oke

*Staff Members*

Halton C. Arp  
Edwin W. Dennison  
Jesse L. Greenstein<sup>6</sup>  
James E. Gunn<sup>6</sup>  
Robert F. Howard  
Jerome Kristian  
Robert B. Leighton<sup>6</sup>  
Guido Münch<sup>6</sup>  
George W. Preston III  
Bruce H. Rule  
Allan R. Sandage  
Wallace L. W. Sargent<sup>6</sup>  
Leonard T. Searle



Maarten Schmidt <sup>6</sup>  
Arthur H. Vaughan, Jr.  
Olin C. Wilson  
Harold Zirin <sup>6</sup>

*Staff Members (Post-Retirement)*

Ira S. Bowen  
Alfred H. Joy  
Henrietta H. Swope  
Fritz Zwicky

*Staff Associates*

John N. Bahcall <sup>6</sup>  
Andrew P. Ingersoll <sup>6</sup>  
Gerry Neugebauer <sup>6</sup>  
James A. Westphal <sup>6</sup>

*Research Associate*

Gustav Tammann

*Fellows*

Arvind Bhatnagar  
David R. Branch  
J. David Bohlin  
Richard A. Defouw  
Peter Foukal  
A. R. Hyland  
William H. Julian  
Keiichi Kodaira  
David L. Lambert  
Michael V. Penston  
Deane M. Peterson  
Stephen W. Prata  
James J. Rickard  
Michael Scholz  
Michal Simon

*Carnegie-Chilean Fellow*

Eduardo Hardy

*Student Observers* <sup>7</sup>

Saul J. Adelman  
William G. Bagnuolo  
John H. Bieging  
Kenneth A. Braly  
Harvey Butcher  
Clark G. Christensen  
Judith G. Cohen

<sup>6</sup> Member of Faculty, California Institute of Technology.

<sup>7</sup> Enrolled at California Institute of Technology.

John Cronin  
Jay A. Frogel  
Sol Giles  
Olav L. Hansen  
Paul M. Harvey  
Gordon Hoover  
Robert Jackson  
Sai Kit Law  
Dennis Matson  
August Oemler, Jr.  
Valdar Oinas  
Bruce Penrose  
Sven E. Persson  
David B. Shaffer  
Larry Soderblom  
Henry Tye  
Glenn J. Veeder, Jr.

DEPARTMENT OF PLANT BIOLOGY  
Stanford, California

*Director*

C. Stacy French

*Staff Members*

Olle Björkman  
Jeanette S. Brown  
David C. Fork  
Malcolm A. Nobs

*Staff Members Emeritus*

Jens C. Clausen  
William M. Hiesey  
James H. C. Smith

*Senior Fellows*

Lars Olof Björn  
Per Halldal  
Günter Jacobi  
Wolfgang Wiessner

*Fellows*

Joseph A. Berry  
John E. Boynton  
Eckhard E. Loos  
Kenneth E. Mantai  
Ernesto Medina  
Norio Murata  
Teruyo Murata  
Robert W. Pearcy  
Colin A. Wraight

*Students*<sup>s</sup>

Lloyd Dunn  
Tyrone Harrison  
Patrice Morrow

DEPARTMENT OF TERRESTRIAL MAGNETISM  
Washington, D. C.

*Director*

Ellis T. Bolton

*Associate Director*

L. Thomas Aldrich

*Section Chairmen*

L. Thomas Aldrich, Geophysics  
Dean B. Cowie, Biophysics  
W. Kent Ford, Jr., Astrophysics

*Distinguished Service Member*

Merle A. Tuve

*Staff Members*

Roy J. Britten  
Louis Brown  
Dean B. Cowie  
W. Kent Ford, Jr.  
Stanley R. Hart  
Bill H. Hoyer  
David E. James  
David E. Kohne  
Richard B. Roberts  
Vera C. Rubin  
I. Selwyn Sacks  
Kenneth C. Turner

*Research Associates*

Mateo Casaverde  
Reynaldo Salgueiro  
Shigeji Suyehiro

*Fellows*

George E. Assousa  
Roger J. Avery  
Willy Z. Barreda R.  
Sandro D'Odorico  
Le Roy M. Dorman  
Joseph W. Erkes  
Dale W. Evertson

<sup>s</sup> Enrolled at Stanford University.



Sandra M. Faber <sup>9</sup>  
Leo J. Grady  
Allan T. Linde  
Nancy R. Rice <sup>10</sup>  
Robert Shleser  
Akhaury Krishna Sinha  
Erich Steiner

<sup>9</sup> Fellow, National Science Foundation.

<sup>10</sup> Fellow, National Institute of General Medical Sciences.

# *Reports of Departments and Special Studies*

Hale Observatories

Geophysical Laboratory

Department of Terrestrial Magnetism

Committee on Image Tubes for Telescopes

Department of Embryology

Department of Plant Biology

Genetics Research Unit





# *Hale Observatories*

Operated by Carnegie Institution of Washington  
and California Institute of Technology

*Pasadena, California*

Horace W. Babcock

*Director*

## OBSERVATORY COMMITTEE

Horace W. Babcock

*Chairman*

Jesse L. Greenstein

Robert F. Howard

J. Beverley Oke

George W. Preston

Wallace L. W. Sargent

Maarten Schmidt

Olin C. Wilson



# Contents

Introduction . . . . .	75	IC 1613 . . . . .	95
Observing Conditions . . . . .	76	Photography of star clusters . . . . .	95
Physics of the Sun . . . . .	77	Coma Cluster . . . . .	96
Polar magnetic fields . . . . .	77	Maffei No. 1 . . . . .	96
Active regions . . . . .	77	Galaxies and cosmology . . . . .	96
Coronal physics . . . . .	78	Peculiar galaxies . . . . .	96
Fine-scan velocity and magnetic fields . . . . .	78	Markarian galaxies . . . . .	97
Synoptic charts . . . . .	79	Masses of galaxies . . . . .	98
Solar activity . . . . .	79	Zwicky compact galaxies . . . . .	98
Magnetic fields and the structure of the chromosphere . . . . .	80	Supernova parent galaxies . . . . .	99
Planets and Comets . . . . .	81	H II regions . . . . .	100
Mars . . . . .	81	Radio galaxies . . . . .	100
Jupiter . . . . .	81	Radio-source identification . . . . .	100
Uranus and Neptune . . . . .	82	Galactic nuclei . . . . .	101
Comet Bennett (1969i) . . . . .	82	Companion galaxies . . . . .	101
Stellar Spectroscopy and Photometry . . . . .	82	Compact galaxies and quasi-stellar sources . . . . .	102
White dwarfs . . . . .	82	Cluster of compact galaxies . . . . .	102
Halo stars . . . . .	83	Infrared radiation . . . . .	102
O-type stars . . . . .	84	Supernovae . . . . .	102
Hot stars deficient in helium . . . . .	85	Pulsars . . . . .	103
Stellar temperatures . . . . .	85	NP 0531 . . . . .	103
Stellar chromospheres . . . . .	85	PSR 0833-45 . . . . .	104
Miscellaneous investigations . . . . .	86	Search for other optical pulsars . . . . .	104
Stellar Magnetic Fields . . . . .	87	X-ray Sources . . . . .	105
Infrared Spectroscopy and Photometry . . . . .	89	Sco X-1 . . . . .	105
Chromospheric helium emission . . . . .	89	Two-color survey of the galactic plane . . . . .	105
Red stars and O II sources . . . . .	90	Quasi-Stellar Sources . . . . .	106
M stars and long-period variables . . . . .	90	Space distribution and luminosity function . . . . .	106
Novae . . . . .	90	Optical positions . . . . .	107
62-inch infrared telescope . . . . .	91	Spectral-energy distribution . . . . .	107
Globular Clusters . . . . .	91	QSO associated with clusters of galaxies . . . . .	108
Interstellar Gas and Gaseous Nebulae . . . . .	92	Infrared measurements . . . . .	108
Galactic emission . . . . .	92	Theoretical Studies . . . . .	109
Planetary nebulae . . . . .	92	Guest Investigators . . . . .	110
Molecular hydrogen emission . . . . .	92	Astroelectronics Laboratory . . . . .	117
Galaxies . . . . .	93	Computer system for Palomar 60-inch telescope . . . . .	117
New calibration of distance indicators . . . . .	93	Computer system for the Hale telescope . . . . .	118
A new preliminary distance to the M101 galaxy group . . . . .	94	Mount Wilson 150-foot tower . . . . .	118
Photoelectric sequences in nearby galaxies . . . . .	94	Big Bear solar telescope . . . . .	119



Instrumentation . . . . .	119	Big Bear Solar Observatory . . . . .	121
General notes . . . . .	119	Las Campanas Observatory . . . . .	121
Mount Wilson 60-inch telescope modernization. . . . .	120	Bibliography . . . . .	122
100-inch telescope engineering study and repair program . . . . .	121	Staff and Organization . . . . .	127

## INTRODUCTION

The name Hale Observatories was adopted this year by the Trustees of the Carnegie Institution of Washington and those of the California Institute of Technology to honor George E. Hale, the founder and first director of the Mount Wilson Observatory, and the man who inspired and planned the building of the 200-inch telescope. The new name supersedes the earlier "Mount Wilson and Palomar Observatories," which had been adopted in 1948 when unified operation of the two observatories was begun. Within the year just past, a somewhat revised agreement for unified operation was formalized by the two sponsoring institutions. It specifies the change of name and provides for certain administrative changes, including enlargement of the Observatory Committee to eight members and the appointment of an Associate Director. Dr. J. Beverley Oke was appointed to the new position.

Important progress is reported this year on two researches relating to the structure of the universe. To both of these the 200-inch telescope contributed indispensably.

First is Sandage's program to improve our knowledge of the expansion rate of the universe by determining reliably the "Hubble constant,"  $H_0$ . This basic constant, which has been drastically reduced in value since Hubble's day, is now believed to be in the vicinity of 50 to 75 km/sec per megaparsec (1 Mpc = 3,260,000 light years). Measurement of the redshifts of remote galaxies showing recession is relatively straightforward, but the determination of their distances is difficult and requires prodigious effort. Fundamental distances to a few nearby galaxies of the Local Group are known from photometric measurements of Cepheid variable stars carried out at the Observatories in previous years by Baade and his associates. But Cepheids do not

suffice at greater distances, so other distance indicators have to be calibrated and used. Sandage and Tammann now report progress on the calibration of sizes of H II regions, which are found to range from 70 to 300 parsecs in linear extent, depending upon the luminosity class of the parent galaxy. Over many years, Sandage has used the 200-inch on nights of exceptional seeing to accumulate plates of numerous galaxies in which H II regions can be measured.

The brightest red and blue supergiant stars in galaxies also serve as distance indicators, and many of these have also been measured by Sandage and Tammann. However, application of this information to distance determination requires precise magnitude scales for photometry of such stars in the various resolved field galaxies for which distances are desired. Therefore, Sandage has begun photoelectric observations to establish magnitude scales near all resolved late-type galaxies whose redshifts are less than 2200 km/sec. About eight stars per sequence are being measured with the 200-inch.

From such comprehensive programs, generally requiring many years for completion, it is expected that a definitive value of the Hubble constant will one day be derived. Meanwhile, an upper limit on  $H_0$  comes from new results on the ages of globular clusters. Sandage has now completed the analysis of faint photometry and the color-magnitude diagrams for hundreds of stars in the four globular clusters M3, M13, M15, and M92. Observations for this monumental work, necessary to determine the cluster ages, have been in progress since 1958. It was necessary to find the helium abundance, the metal abundance, and the absolute magnitude of the cluster evolutionary turnoff point from the standard main sequence. The four clusters agreed

well in giving a best present value for age of  $T = (10 \pm 3) \times 10^9$  years, where the error is an outside limit. This age is not in conflict with the age of the expanding universe if  $H_0$  is less than 75 km/sec/Mpc, provided the deceleration parameter,  $q_0$  is as great as 1.

On another major problem, Schmidt has arrived at a derivation of the space distribution and luminosity function of quasi-stellar objects. This was accomplished through spectroscopic observation of blue stellar objects identified by Sandage and Luyten in two fields. Redshift determinations of objects for which photometry was available are complete to magnitude 18.5.

Schmidt points out that the steep increase, by a factor of about 6 per magnitude, of the number of quasi-stellar objects with magnitude as found by Sandage and Luyten cannot correspond to a uniform distribution. The observed redshift distribution permits making an estimate of the density increase with redshift  $z$  required to explain the steep number-magnitude gradient. On reasonable assumptions—that the density is proportional to a power of  $(1+z)$  and that the deceleration parameter  $q_0 = +1$ —Schmidt finds that the density (or the number per co-moving volume element) varies as  $(1+z)^6$ . With this adopted density law, he now is able to determine the optical (absolute) luminosity function and to derive the total local ( $z=0$ ) density of quasi-stellar objects. This he finds to be  $0.7 \times 10^{-7}$  Mpc $^{-3}$  for the more luminous quasi-stellar objects that at magnitude 18 have redshifts of at least 0.4. (The density may be 10 times greater for less luminous objects having a redshift of at least 0.16 at magnitude 18.) In all, 1.4 million of such luminous quasi-stellar objects having redshifts less

than 2.5 are estimated to be within range of observation down to magnitude 21.5. Because of the decreasing birth rate and relatively short lifetimes of these objects, the total number *now existing* in the universe is expected to be only about 3500. While it is clear that much further work is required on faint quasi-stellar objects, there is reason to believe that the scarcity of such objects with redshifts larger than 2.5 means that the steep increase of density with redshift may terminate at that value.

In honor of Greenstein's sixtieth birthday, a two-day symposium on the relative abundance of the chemical elements in stars was held in Pasadena in January with the support of the United States Air Force Office of Scientific Research. The stellar-composition project, organized informally within the Observatories, had been supported for 13 years by the Air Force. On this occasion, some 50 former associates or students, at various times involved in this work, met to take stock of the present situation on stellar composition. The major differences of opinion related to the reality of the differences in metal abundance as a function of age. Except for the metal-poor stars in the galactic halo, there seems to have been little secular increase in metal abundance in the Galaxy. The controversy on the existence of super-metal-rich old stars was discussed. Examples were given of the decrease in abundances with distance from the center of galaxies, as inferred from CN absorption and the  $[N II]/H\alpha$  emission ratio. Theoretical advances reported in nucleosynthesis emphasized explosions and rapid burning of the elements carbon through silicon as capable of producing the irregularities in nuclear abundances of heavy elements.

## OBSERVING CONDITIONS

Total precipitation on Mount Wilson for the year was 21.69 inches, well below the 66-year average of 36.0 inches. Snow-

fall amounted to 20 inches. A maximum temperature of 90°F was reached on August 5, 1969, and on June 21, 1970; a



minimum of 20° was recorded on April 28, 1970.

Palomar Mountain received 18 inches of snow and a total precipitation of 17.38 inches of water. Maximum and minimum temperatures of 96° and 21° were recorded on August 6 and on December 29, respectively.

On Mount Wilson, the 60-inch telescope was out of service for modernization work for the month of July and 18 days in August; also for 6 days in January. The 100-inch was out of service for engineering studies and repairs for 11

days in March and 12 days in April. With the 200-inch at Palomar, there were no observations on the nights of October 20 through 27, as the mirror was being realuminized. The hours worked with the major telescopes were as shown in the tabulation below.

TABLE 1. Observations

Telescope	Complete Nights	Partial Nights	Total Hours Worked
60-inch	137	83	1964
100-inch	226	79	2669
200-inch	238	74	2731

PHYSICS OF THE SUN

At Mount Wilson, the tower telescopes have been used under the supervision of Howard to accumulate systematic solar records between June 1, 1969, and May 31, 1970, as follows:

Direct photographs	334
H $\alpha$ spectroheliograms, 30-foot focus	606
K2 spectroheliograms, 30-foot focus	606
Full-disk magnetograms	281
Sunspot drawings	320

The most significant are the magnetograms. After several years' development and refinement of the magnetograph, this automated instrument with digital data recording has reached a high level of performance. Magnetic maps of the sun's surface can now be obtained with good resolution and precision by processing the tape-recorded data on a computer.

In a parallel but different program of solar research conducted at the new Big Bear Solar Observatory under the supervision of Zirin, emphasis is on extended sequences of high-resolution narrow-band cinematograms of the sun's surface. These sequences lend themselves to the study of pictorial details on the sun, including filaments, spicules, flares, and active regions. Such data are of special value when correlated with solar magnetic maps obtained at Mount Wilson or elsewhere.

*Polar Magnetic Fields*

The polar magnetic fields of the sun are observed as part of the full-disk magnetogram program. Howard reports that fields near the north and south heliographic poles have remained at a level of a few tenths of a gauss with negative polarity throughout the year. The polar field at the far southern latitudes (poleward of -70°) changed from positive to negative polarity during the summer of 1969, but it is not clear that this change was associated with the expected activity maximum polarity reversal, since the polarity of fields in latitudes 40°-70° in the south has been predominantly negative for several years.

Much of the data reduction of the magnetograms continues to be supported in part by the Office of Naval Research through contract number NR 013-230, N 00014-66-C-0239. The daily magnetograms continue to be published in the monthly ESSA bulletin *Solar Geophysical Data*.

*Active Regions*

The full-disk magnetograms provide a wealth of data concerning the magnetic fields of active regions in recent years. Mrs. Sara F. Smith, of the Lockheed

Solar Observatory, and Howard are continuing their study of the magnetic classification of active regions.

Bhatnagar measured the magnetic flux of all simple bipolar magnetic regions (type B according to the Howard-Smith classification) observed on daily magnetograms obtained during the past three years. From the measured variation of the longitudinal component of magnetic flux, as the region traversed the solar disk, an attempt was made to determine the inclination of the magnetic vector to the solar surface. From the analyzed data no definite conclusion could be derived regarding the inclination of the magnetic axis of the type B bipolar magnetic regions.

Prata traced the development of a sequence of active regions for the period January 14–June 1, 1969. Three such regions emerged in succession at a Carrington longitude of  $258^\circ$ , and at least four emerged in succession at a longitude of about  $270^\circ$ . This series of active regions exhibit an unusually high incidence of inverted polarity. In many cases the inverted polarity was a property of the emerging fields, but in some cases it was a consequence of the interaction of the emerging with the surrounding fields. As far as can be determined, all the large flares occurring in these regions were associated with inverted polarity.

### *Coronal Physics*

One of the most interesting results to come from the solar magnetograph in recent years is the excellent correlation of low-latitude solar magnetic fields with the interplanetary magnetic field measured near the earth. The related problem of the magnetic fields in the corona is being studied in a joint effort by Dr. Gordon Newkirk, Jr., and Dr. Martin Altschuler of the High Altitude Observatory and Howard. The large-scale distribution of magnetic fields is expressed as an expansion in Legendre polynomials. Field lines are then constructed in the

solar corona assuming a current-free situation. Comparisons with eclipse pictures of the solar corona show that many bright coronal features correlate well with the magnetic-field lines.

Observations of the solar corona obtained by *Surveyors 6* and *7* from the moon have been reduced by Bohlin. Polarization and absolute photometry of these data could not be done due to lack of sufficient internal calibration checks, but relative photometry of selected frames was possible by requiring the brightness along the ecliptic to match the mean of published values. The coronal isophotes for *Surveyor 6*, 24 November 1967, were quite symmetric about the ecliptic plane and did not exhibit any distinct streamer structure. However, the *Surveyor 7* data of 23 January 1968 showed an asymmetry in the southeast quadrant which has been attributed to the presence of a large helmet streamer. This streamer's presence and location are corroborated by K-coronameter observations (courtesy High Altitude Observatory). The inferred brightness of this feature is  $\sim 1.25 \times 10^{-11} B_\odot$  at  $15 R_\odot$  and decreases by a factor of 2 over the next  $7\frac{1}{2} R_\odot$ . These brightness values are in reasonable agreement with the extrapolation of eclipse measurements of streamers ( $r_{\max} \sim 10 R_\odot$ ) and represent a two-fold increase in the maximum distance from the sun at which streamer brightness values have been determined.

Bohlin has completed a study of the evolution and structure of coronal streamers. An asymmetric tunnel model for helmet streamers was developed. The model requires the presence of a relatively small active region near the boundary of, and magnetically connected to, an extended bipolar region of magnetic fields.

### *Fine-Scan Velocity and Magnetic Fields*

Fine scans ( $5'' \times 5''$  aperture) were obtained over complex and simple sunspot

groups by Bhatnagar, using both Zeeman sensitive and Zeeman insensitive lines, on several days during good seeing conditions. Besides the mainly horizontal Evershed motion in sunspots, there seems to exist a very strong descending motion of gases over active regions, compared to the surrounding region. Comparison of magnetic maps with the  $H\alpha$  filtergrams shows that there is almost a one-to-one correspondence of the location of the dark markings with the neutral magnetic zone. On fine-scan Dopplergrams obtained on October 25, 1969, over Mount Wilson Group No. 17535, there are regions of strong downward motion corresponding to the location of dark filaments (prominences seen against the disk). These regions of the downward motion perhaps correspond to the position of the "feet" of prominences on the photosphere, where the material is "raining" downward into the photosphere. Thus there seems to be a continuity of the descending motion from the prominences into the photospheric level.

### *Synoptic Charts*

During the year the magnetic-field synoptic-chart computer program was completed by Mrs. Carruthers, and the synoptic charts for 1969, 1968, and the second half of 1967 were drawn by the Caltech computer. These synoptic charts, as well as the current ones, are to be published in the *International Astronomical Union Quarterly Bulletin on Solar Activity*.

### *Solar Activity*

The apparent variation of the rotation rate due to large-scale velocity fields, and possible secular variations in the rotation rate, may be of importance in understanding the activity cycle and even the structure of the solar interior. Solar rotation results from the Doppler data recorded in conjunction with magnetograms have been published by

Howard and Dr. John Harvey of the Kitt Peak National Observatory. These results showed the presence of large-scale velocity fields and gave an indication of a secular change in the rotation velocity. The rotational velocity is about one day per rotation slower than that derived from sunspots.

Another means of investigating the rotation of the sun is to examine the rotational returns of magnetic features on the solar disk. Howard, with Dr. John M. Wilcox of the Space Sciences Laboratory of the University of California, Berkeley, has examined the solar rotation as derived from autocorrelations of digitized magnetic-field data in latitude strips. The data were from 1959 through 1966. The result was that near the equator the rotational velocity is similar to that derived from sunspots, but at higher latitudes the magnetic features rotate faster than sunspots. In a related investigation, Dr. John M. Wilcox, Dr. Kenneth Schatten, Mr. Andrew S. Tanenbaum, and Howard found that, in long autocorrelation analyses of the magnetic data, a 27.0-day period was evident at low latitudes, while for short lags the rotation correlation peak corresponded to a standard differential rotation result. This dual rotation period was pointed out several years ago by Bumba and Howard.

Zirin has continued his studies of the hard X-ray emission in solar flares, in collaboration with Mrs. Joan Vorpahl of the University of California, Berkeley. They have found that the time-dependence of the spectrum of X-ray bursts is complex and can be related to different phenomena in the flare. In a flare on September 11, 1968, photographed with the Caltech photoheliograph, three distinct flare phases were found that corresponded to different X-ray behavior on the UCB detector. In the first stage there was a rapid rise in all energy channels as flare brightening began. A few minutes later, a brilliant kernel of  $H\alpha$  emission appeared with ejection of a great surge.



This was accompanied by a broadband hard X-ray burst up to 80 kv. The X rays from this burst were considerably higher than those already being received. Then the third phase of the flare began, a slow spread of brightness along the neutral line. This was accompanied by an extended maximum in the low-energy X rays, but no hard X rays.

It has been known for some years that three factors are connected with areas showing a high frequency of solar flares: (1) reversed magnetic polarity, violating the Hale-Nicholson law; (2) steep field gradients; and (3) the emergence of new sunspots. Zirin and co-workers now report an additional factor: filaments imbedded in bright plage. The newest high-resolution observations show a continuing marked tendency for flares to spread out from a neutral magnetic line.

### *Magnetic Fields and the Structure of the Chromosphere*

It has been generally believed that strong vertical magnetic fields are concentrated at the boundaries of the chromospheric network, corresponding to regions that appear dark on off-band pictures or bright in the center of H $\alpha$ . The interior of the chromospheric network cells appears devoid of vertical magnetic field, although the possibility of horizontal field cannot be ruled out. Zirin now finds that on high-resolution photographs there appears to be very little intermediate region between vertical and horizontal magnetic fields. In active regions, predominantly horizontal fibrils turn abruptly into the regions of vertical field. Unfortunately, there are very few data on the exact strength of horizontal fields.

The asymmetry found last year by Zirin and Veeder between the H $\alpha$  brightening associated with preceding as contrasted to following polarity is not completely confirmed by more recent high-resolution magnetic observations. In most of these, brightening is found in

every region where there is vertical field. Magnetograms of improved resolution show that there are, in fact, distinct regions of strong preceding magnetic polarity without accompanying bright H $\alpha$  plage, and others that do have H $\alpha$  plage. This matter is still under investigation, and obviously has great significance for our understanding of plages. Regions of emerging flux are always bright no matter what the polarity.

Weart continued his study of the emergence of new magnetic flux on the sun through observations of young arch filament systems (bright regions overlain by dark arches). The orientation of the arches indicates a substantial random component in the solar subsurface magnetic field. However, those arch filament systems that emerge with their magnetic fields tilted so that the preceding part is closer to the solar equator are much more likely to grow into large active regions than are those of opposite tilt. Also, the emergence of two such systems in proximity is particularly likely to herald a major active region. These facts cast fresh light on the mechanisms involved in the development of active regions.

Weart also studied narrow-band movies of spicules, taken previously at Mount Wilson by Zirin and Lambert. He found that spicules move randomly parallel to the solar surface, with an entire spicule occasionally jerking laterally.

Foukal studied the H $\alpha$ , X-ray, and radio data associated with the development of a flare region of inverted polarity, finding very low microwave emission intensity despite very high X-ray flux. He also made use of the new observing facilities at Big Bear in developing a flicker magnetograph. The initial apparatus was built for Zirin, based on a technique suggested by Giovanelli. After some five months of intermittent effort and modification, the latest film shows the equipment to be working well. The apparatus modulates an off-band H $\alpha$



film with a  $\lambda/4$  plate, producing a flicker in intensity of successive frames at points of strong longitudinal field. From the projection of the film the polarity, and to some extent the strength, of the chromospheric longitudinal field may be

seen virtually at a glance. The method is especially valuable since it provides the crucial polarity information that has so far been missing in the high-resolution chromospheric magnetograph information in  $H\alpha$  films.

## PLANETS AND COMETS

### *Mars*

The study of the data returned by the Infrared Radiometer Experiment of the Mariner VI and VII spacecraft, during their encounter with Mars, has been completed by Neugebauer and Münch. The temperatures measured near the equator of the planet are in essential agreement with those obtained previously from ground-based observations, and thus verify the absolute calibration of the 8.5–14  $\mu$  magnitude system. A temperature of 148°K was derived for the polar cap, indicating that it is composed predominantly of  $\text{CO}_2$  frost. The variation of the temperatures characterizing other parts of the planet suggests that the phase angle effect in the thermal infrared is smaller for Mars than for the moon. The thermal energy appears to vary approximately with the power 1/20 of the cosine of the emission angle, rather than with the power 1/6, as for the Moon. The reciprocal thermal inertia of the various terrains viewed varies between 120 and 300  $\text{cm}^2 \text{ sec}^{1/2} \text{ K/cal}$ . The lower value was observed over Syrtis Major and Mare Tyrrhenum, and thus probably is characteristic of the darkest areas on the planet. The larger value, on the other hand, corresponds to the southern edge of the light area Aeria. It seems unlikely, however, that all light areas have an equally low thermal conductivity because the temperatures measured over Deucalionis Regio and Hellas would require radiometric albedos implausibly high (0.4 to 0.5).

### *Jupiter*

The profiles of strong Fraunhofer lines

in the spectra of the sun, the moon, Jupiter, and the blue sky have been obtained by Münch with the photoelectric scanner of the 100-inch coude. Under the resolving power used (about  $10^5$ ), the solar K line appears as deep as that recorded in the *Utrecht Atlas of the Solar Spectrum*, and is identical to that of the moon. The spectrum of Jupiter, on the other hand, definitely exhibits a "filling-in," amounting to about 4% of the continuum, while the sky shows about half as much. The positive measurement of the "filling-in" of the Fraunhofer lines in Jupiter is attributed by Münch to rotational and vibrational Raman scattering of solar light by  $\text{H}_2$ . It should thus provide the means to estimate the number of scatterings involved in the diffuse reflection of the solar light.

In connection with the design of the infrared radiometer experiment of the spacecraft Pioneer F and G, which fly-by Jupiter in 1974 and 1975, respectively, Münch and L. Trafton, of the University of Texas, have constructed a number of models for Jupiter's atmosphere in radiative equilibrium. On this basis, the sensitivity to variations in the helium-to-hydrogen abundance ratio has been established for measurements to be carried out from the spacecraft. With the design value for the signal-to-noise ratio expected for an effective temperature of 130°K, it will be possible to determine the He/H ratio with an uncertainty of 10%. However, the models depend on the opacity produced by the pure rotation band of  $\text{NH}_3$  at 50  $\mu$ , which so far has been incorporated only schematically. Laboratory measurements of this

absorption will be carried out to remove this source of uncertainty.

The spectra of Jupiter and a number of comparison stars in the 4.6–5.2  $\mu$  band have been obtained by Münch and Neugebauer with a grating spectrometer. This work is part of an attempt to find out the origin of the high-brightness temperature shown by the equatorial belt of the planet in this range.

Observations of the thermal flux from Jupiter in a narrow wavelength region centered at 8.5  $\mu$  by Westphal have shown the presence of excess energy over the north equatorial belt where the very intense 5- $\mu$  flux reported in *Year Book 68* (p. 111) was found. The presence of this flux seems to indicate that the Jovian atmosphere has significant transparency in this spectral region.

Polar scans at 6600 Å, 8870 Å, 5  $\mu$ , 8.5  $\mu$ , 9  $\mu$ , 11  $\mu$ , 13  $\mu$ , and 18  $\mu$  were made, almost simultaneously, to test the details of cloud structure suggested by Ingersoll and Cuzzi (*J. Atmos. Scis.*, 26, 981–985, 1969). The details of this study indicate that the Ingersoll-Cuzzi theory is too simple to explain the observational data.

### *Uranus and Neptune*

The planets Uranus and Neptune were observed by Münch photographically with the coudé spectrograph of the 200-

inch telescope. The spectrograms of Uranus, at 6.7 Å/mm dispersion, were for measuring anew the equivalent widths of the S(0) and S(1) quadrupole lines in the (4,0) band of H<sub>2</sub>. The band of CH<sub>4</sub> classified by T. Owen as 5  $\nu_3$  was simultaneously observed. The spectrograms of Neptune, at 13.8 Å/mm, are also for the purpose of measuring the 5  $\nu_3$  band of CH<sub>4</sub>, to be compared with the data for Uranus. An estimate of the temperature at the level of formation of the CH<sub>4</sub> spectrum will be possible on the basis of these measures.

### *Comet Bennett (1969i)*

Westphal, with Toomes, observed this comet on 13 mornings, near the following perihelion, at 1.2, 1.65, 2.2, 3.4, 5, and 8–14  $\mu$  with the 24-inch telescope at Mount Wilson. In general, 1969i was very similar to Comet Ikeya-Seki (1965f, Becklin and Westphal, *Astrophys. J.*, 145, 445–453, 1966) in that the color temperatures were much higher than the local gray-body temperatures due to solar heating, and in the absence of emission bands in the near infrared. Matson, working with the 60-inch on April 4, 1970, independently observed the emission peak near 10  $\mu$  reported by Maas, Ney, and Woolf [*Astrophys. J. (Letters)*, 160, L101–L104, 1970].

## STELLAR SPECTROSCOPY AND PHOTOMETRY

### *White Dwarfs*

Oke has obtained absolute spectral-energy distributions of 32 white dwarfs. These can be compared with model atmospheres by Terashita and Matsushima and with models being calculated here by Shipman. Results so far are as follows:

1. The DA stars have effective temperatures ranging from 13,000°K to 50,000°K.

2. DB stars range from 15,000°K to 25,000°K.

3. Two stars have  $T_e=100,000^\circ\text{K}$ .

4. The DC star L1363–3, which shows no features, has a temperature of approximately 10,000°K.

In general, the effective temperatures are somewhat higher than previous estimates, but the older temperature scales are not seriously in error.

In a continuing investigation of faint blue stars of both large and small proper motion, Greenstein discovered 40 additional white dwarfs. Among the cooler objects, one of a new spectral type has

been found, Giclas 99-37. Possibly related to the carbon-rich stars, G99-37 shows only a shallow G band of CH, but no C<sub>2</sub> or H lines. Continued research for late-type white dwarfs, however, has shown that they are very rare among the peculiar stars of large space motion. Many G, K, and M stars for which *UBV* photometry by Eggen has indicated large ultraviolet excess have been observed spectroscopically. They prove to be weak-lined stars of the halo population with large *U-B* excesses persisting to spectral type M (where TiO is weak and MgH is strong). They cannot be interpreted by conventional methods, using  $\delta(B-V)$  to obtain  $(B-V)_0$  and thence  $M_v$ , since they are so cool that the elementary theory predicts negligible  $\delta(U-B)$  at any metal abundance. In a sample of 70 suspect red degenerate stars, only 2 showed spectroscopic evidence of low luminosity. The space frequency of red degenerates is low, as suggested in an earlier report (*Year Book* 68, p. 113).

### *Halo Stars*

A quantitative analysis of the faint blue stars of the galactic halo has been carried out by Greenstein and Anneila Sargent. A total of 170 stars found by blue color from the Humason-Zwicky, Feige, Tonantzintla, Cowley, and Klemola lists have *UBV* colors and spectra from 18 to 190 Å/mm dispersion. These spectra were analyzed using the colors to obtain temperatures and the H $\gamma$  line profile to obtain *g*, the surface gravity. Model atmospheres provide the latter information and show that the *UBV* colors are insensitive to surface gravity at  $T > 10,000^\circ\text{K}$ . Consequently, it was possible to classify these stars quantitatively, as had been done previously by visual inspection. Certain natural groups can be distinguished—the white dwarfs, the subdwarf O and B stars, the horizontal-branch, and the normal stars. Some of the latter are runaway Population I

stars, but most of the others define an interesting Hertzsprung-Russell diagram for the blue stars of the halo. Greenstein showed that the horizontal-branch A and B stars merge continuously into the subdwarf B stars. Given *T* and *g*, and assuming a constant mass, he finds that a continuous horizontal narrow sequence stretches from 10,000 to 40,000°K. This is far bluer and hotter than in the globular clusters, which usually end below 20,000°K. If the mass is 0.7  $M_\odot$ , the bolometric luminosity is  $10^2 L_\odot$ . The halo stars may have a wider range of age than do the globular clusters, but it is interesting that few models for horizontal-branch evolution are as extreme. Those that reach to high temperatures require a helium burning-core mass of 0.51  $M_\odot$  and a negligible mass in the hydrogen envelope.

At the far left of this sequence, where the *T* determination is poor, are found the sdO stars that occur within a nearly vertical band from just above the horizontal branch down to the brighter, very hot white dwarfs (from  $10^2$  to  $1 L_\odot$ ). Then the white dwarfs cool and follow a line of constant radius down to the typical blue white dwarf at  $10^{-2} L_\odot$ . The so-called "normal" stars may not all be old Population II stars of low mass, and to place them on this diagram we must assume that they follow the mass-luminosity law. (The figure shows the final schematic H-R diagram.)

The most interesting feature provided by the relatively high dispersion of the spectra is the measured strength of lines of He I, He II, Mg II, C II, and Ca II. The entire range of the extended horizontal branch shows weak or no helium lines. Noted by Greenstein and Münch in 1960, the surface helium deficiency is now definite for HBB and sdB stars hot enough to show either He I or He II. Line strengths of He I  $\lambda\lambda 4026, 4471$ , and the singlet-triplet ratio ( $\lambda 4388/\lambda 4471$ ) agree in He/H ratios as low as 0.01 by number. This surface deficiency may indicate a low primordial He/H ratio, and no mix-



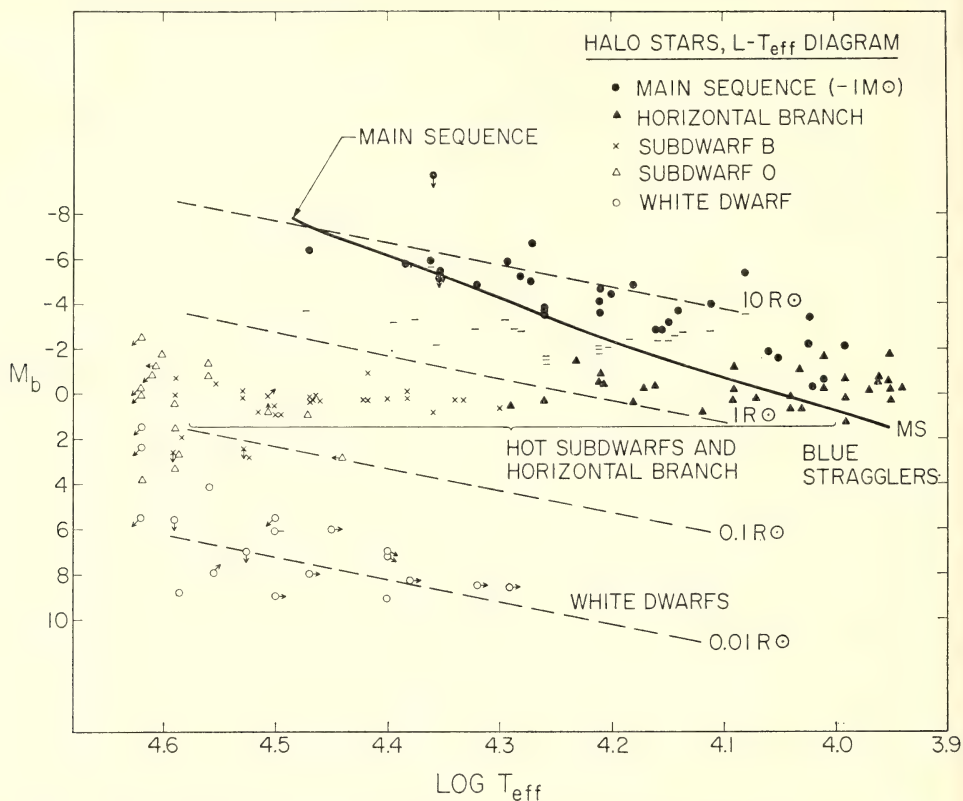


Fig. 1. Schematic Hertzsprung-Russell diagram for faint blue stars in the halo of the Galaxy.

ing with the interior, or it may mean that He settles downwards almost completely. The spectroscopic observations disagree with the theory for the interior, which tends to favor  $\text{He}/\text{H}=0.1$ , with RR Lyrae pulsation theory and with the evolutionary tracks required to explain the horizontal branch. But, since theory does not explain the existence of the long horizontal branch either, it is possible that the case for low (or no) cosmological helium should be re-examined.

The sdO stars, which are very hot, show strong He I and He II, and with their nearly vertical evolution downwards must require quite different occurrences, for example, instability or mixing of core material to the surface and possibly high neutrino luminosity.

A reanalysis of the halo G star, +17°

4708, was carried out by Greenstein and Miss G. Cohen. The star has been called a late-type horizontal-branch star from its Balmer discontinuity, which indicated lower surface gravity than the main sequence. A more careful analysis including the effect of the lower-than-normal line blanketing on the spectrophotometry showed, instead, that it is close to, or just above, the main-sequence turnoff point of the metal-poor sdG stars. The Balmer discontinuity is apparently increased, relative to a normal G star, when the ultraviolet metallic lines are absent or weak. The star has a mean metal deficiency of 10.

#### *O-Type Stars*

D. M. Peterson and M. Scholz have

completed an investigation of the spectra of six O stars with spectral types ranging from O5 to O9.5. Effective temperatures and gravities were obtained from an analysis of the ionization equilibria and hydrogen-line profiles utilizing LTE model atmospheres. The presence of appreciable departures from LTE in both the continuum and hydrogen-line profiles, as predicted by Auer and Mihalas (*Astrophys. J.*, 160, 233, 1970) was confirmed. A comparison of the temperatures obtained for these objects with the  $T_{\text{eff}}$  scale recently proposed by Morton for O stars indicates a substantial discrepancy. This disagreement is in the sense that the models predict a much higher Lyman continuum flux at a given spectral type than might be inferred from observations of H II regions.

Carbon and oxygen abundances appear to be essentially solar for these stars except for 15 Monocerotis (07), which is definitely carbon-deficient. On the other hand, the C/N and O/N as well as the C/Ne and O/Ne ratios are, in general, reduced compared to the sun.

### *Hot Stars Deficient in Helium*

Peterson has been investigating the completeness of the discovery of the hot [ $Q \equiv (U - B) - 0.072 (B - V) \leq -0.40$ ] helium-deficient objects. A  $\lambda 4771$  (He I) index has been defined using the Cassegrain continuum scanner at the Mount Wilson 60-inch telescope. The index has been found to be quite effective when coupled with H $\beta$  photometry and reddening independent colors for discovering these objects. From the photometry of late B stars in the bright star catalogue by Crawford (*Astrophys. J.*, 137, 530, 1963), a list of approximately 100 stars that are too blue by at least two spectral classes for their HD spectral types has been compiled. Many of the apparent discrepancies are removed when the stars are classified at higher dispersion. However, the  $\lambda 4471$  photometry (as yet incomplete) indicates that as many as 40

of these objects are truly helium-deficient.

High-dispersion (10 Å/mm) spectrograms of a small sample of the objects discovered in this manner have been obtained and have confirmed the peculiar nature of their spectra. It would appear that there is a substantially larger percentage of peculiar early B stars than had previously been suspected.

### *Stellar Temperatures*

Oke, D. M. Peterson, and Schild have recently completed a study of the temperature scale for B-type and early A-type stars. A total of 54 stars were included in the study; spectral scans of most of them were obtained with the 4-inch telescope and scanner used for the previous absolute calibration of  $\alpha$  Lyrae. Parameters for  $\alpha$  Lyrae are  $T_e = 10,200^\circ\text{K}$  and  $\log g = 4.05$ . For Sirius the authors found  $T_e = 10,200^\circ\text{K}$  and  $\log g = 4.35$ , which is in excellent agreement with the value of  $\log g$  derived from the mass. The temperature scale deviates only slightly from those published by Morton and Adams, Wolff, Kuhl and Hayes, and Hyland.

### *Stellar Chromospheres*

All of Wilson's work has been directed toward some aspect of stellar chromospheric research. Results during the past year are as follows.

1. Correlation of chromospheric H-K intensity with age in late-type main-sequence stars: Eye estimates of H-K emission intensity for about 300 dK and dM stars have been carefully made from 38 Å/mm spectrograms taken with the 8-inch camera of the Palomar coude spectrograph. A series of spectrograms of 61 Cygni A and B served as standards. In collaboration with Sir Richard Woolley, these estimated intensities have been compared with the orbital eccentricities and inclinations of the stars. Woolley and his co-workers have shown that the

average values of these quantities for groups of stars increase with the age of the groups. On the other hand, there is much evidence that chromospheric activity in main-sequence stars, as measured by the H-K emission strength, decreases with age. It would thus be anticipated that the calcium emission intensity should be inversely correlated with the average orbital eccentricity and inclination. This is indeed found to be true, thus supporting the general picture sketched briefly above.

2. H and K flux measurements in the Hyades main sequence: Wilson has used the scanner of the 100-inch coude to measure the H-K flux in 65 Hyades main-sequence stars with spectral types between F5 and K5. This material has been analyzed with the aid of published photometry of other kinds available for these objects. The major result is that from F5 to K5 the chromospheric emission increases with respect to the total (bolometric) luminosity by a factor of 2.

3. Variability of stellar chromospheric emission: Four years ago, Wilson began a series of measures of the fluxes at the centers of the Ca II H and K lines in a number of main-sequence stars of various types. The purpose was to look for variability in chromospheric emission and especially to seek information on stellar analogs of the solar cycle. This is a lengthy project, still far from complete, but enough material has been accumulated to justify a brief summary of the results to date.

a. Types G5 and earlier. In several of these stars the chromospheric portion of the central H-K flux is half or more of the total. Nevertheless, in none of them is there yet convincing evidence of changes in the measured fluxes from season to season.

b. Types G8 and later. For most of these stars, observations did not begin until 1967. However, there are several that show distinct changes from season to season, the largest variations being of

the order of 20%. The interpretation is still unclear.

c. Scatter versus flux. For all stars, the standard deviation for a single observation (in flux units, not percent) has been computed for each season's observation. When these are plotted against the fluxes, the result is an approximately linear correlation, the fluctuations increasing with the flux. All stars observed, regardless of spectral type, fit this relationship.

### *Miscellaneous Investigations*

Branch and Dr. B. F. Peery, Jr., of Indiana University sought the presence of unstable long-lived  $\text{Al}^{26}$  in the spectra of the long-period variable R Andromedae (S6, 6e) and the irregular variable carbon star 19 TX Piscium (C6, 2). The spectra of both stars show lines of technetium. No isotope shift was detected in absorption lines of AlH, and the ratio  $\text{Al}^{26}/\text{Al}^{27}$  was estimated to be less than 1 to 7.

Branch, with R. A. Bell of the University of Maryland, used model-atmosphere techniques to predict profiles of lines of the (0, 0) band of MgH in the spectrum of Arcturus (K1 III). By comparing the predicted profiles to features seen in R. F. Griffin's *Photometric Atlas of the Spectrum of Arcturus*, the magnesium isotope ratios were found to be  $\text{Mg}^{24}/\text{Mg}^{25}/\text{Mg}^{26} = 80/10/10$ , in agreement with the terrestrial and meteoritic ratios. Significant enhancement (60/20/20) or depletion (100/0/0) of the rarer isotopes was shown to be in conflict with the observations.

A model atmosphere abundance analysis of the ultraviolet-deficient, super-metal-rich dwarf HR 72 was carried out by Branch and Bell. The analysis confirmed the earlier result of Spinrad and Luecke (*Astrophys. J.*, 160, 1141, 1970) that the iron-to-hydrogen ratio in HR 72 is approximately  $2\frac{1}{2}$  times greater than in the sun. The abundances of 14 additional elements were found to be normal, relative to iron. From comparison of ob-



served narrow and broadband colors of HR 72 to those predicted by calculating synthetic stellar spectra and convolving with filter transmission functions, Branch and Bell concluded that either the computed ultraviolet fluxes were too large or HR 72 is helium-rich as well as metal-rich ( $Y \approx 0.66$ ), of small mass ( $0.3 M_{\odot}$ ), and well evolved from the initial helium-rich main sequence.

Miss Cohen has been obtaining profiles of the Li I  $\lambda 6707$  line in G- and K-type field stars with the interferometric spectrometer of the 100-inch coude. The observations will be the main basis of an attempt to determine the  $\text{Li}^6/\text{Li}^7$  abundance ratios. In addition, high-dispersion photographic spectra have been obtained and measured for wavelength. On the theoretical side, the line profiles for a number of model atmospheres have been computed, taking into account the fine structure of both isotopes. Although the work is not yet complete, it appears unlikely that any  $\text{Li}^6$  exceeding in relative abundance a few percent is present in any star so far examined. The reason for the resulting disagreement with previous work of Herbig remains unexplained.

Miss Cohen also completed her analysis of the high-dispersion spectra and scans of  $\alpha^2$  Canum Venaticorum. Her results are consistent with the oblique rotator model and led to more accurate abundance determinations than previously available. She finds a higher temperature ( $12,000^\circ\text{K}$ ) than used by earlier spectroscopists and derives new abun-

dances of the elements. Although the spectrum is variable with phase, in the mean, the iron group Si and Cl are  $10^2$  times and the rare earths from  $10^3$  to  $10^6$  times more abundant than in the sun.

Hyland and M. V. Penston have started a program of observing T Tauri and type B emission stars in  $\text{H}\alpha$  and the near infrared. The line profiles of  $\text{H}\alpha$  have been observed with the coude scanner of the 100-inch telescope, while infrared photometry was performed on the 60-inch at  $2.2 \mu$  and  $1.6 \mu$ . The object of the program is to relate the outflow of matter from the stars as deduced from the line-profiles with the thickness of the circumstellar envelopes responsible for the infrared emission. All the stars show excess infrared emission, which appears to vary roughly 10% from observation to observation.

Kodaira measured 400 spectrograms of standard B3 V stars, taken with the 60-inch, for variability of velocity. These are now being analyzed.

Kodaira and Scholz studied the high-dispersion spectra of  $\iota$  Herculis, a non-rotating B star, compared to  $\eta$  Hydrae, HD 58343,  $\eta$  Ursae Majoris (rotating B stars) using LTE model atmospheres. No composition differences were found, except that Ne I was stronger than expected in  $\iota$  Her, and absent in HD 58343. No other effects of the emission characteristics were found in the rotating stars. The continua systematically indicated temperatures about  $1500^\circ\text{K}$  lower than did the metallic lines.

## STELLAR MAGNETIC FIELDS

Continuing his investigations of stellar magnetism, Preston finds that the mean surface magnetic field of the Sr-Cr-Eu star HD 126515 varies approximately sinusoidally between 10 and 17 kilogauss in a period of 130.0 days. The effective field oscillates between  $-2$  and  $+2$  kilogauss with a single wave in the same period. From the point of view of the

rigid-rotator model, these results are incompatible with a hemispherically symmetric field distribution, but analysis shows that the principal features of the observed variations can be represented by a dipole displaced  $0.36$  radii from the center of the star in a direction opposite to its moment. HD 126515 is also a spectrum variable and the phase rela-

tions between the variations in line intensity and mean surface field indicate in a general way that the heavy elements are concentrated in regions where the surface field is strongest. The asymmetry of the magnetic field of HD 126515 holds promise of providing reasons for the variable line widths encountered in many magnetic variables and for the equality of the magnetic, spectrum, and photometric periods of these objects.

Preston and Dr. Sidney Wolff of the University of Hawaii have accumulated evidence for an extraordinary slow spectrum variation of HD 9996. Comparisons of spectrograms obtained from 1938 through 1969 suggest a period of about 23 years for the antiphase variations of Cr and Eu. The star is now near Eu minimum. Fragmentary magnetic and photometric data are consistent with this very long period. The large range in  $B-V$  ( $\geq 0.15$ ) and small range  $U-B$  resemble those of another rather slow (160 day) spectrum variable, HD 221568, discovered by Osawa. HD 9996 is a single-lined spectroscopic binary with a period of 274 days that is evidently unrelated to the intrinsic variations.

Preston has almost completed a coudé survey of the rotational velocities of virtually all known Ap stars brighter than  $m_v=9$ . These data will be used to construct the rotational velocity distribution functions of Ap stars grouped by colors and by peculiarity subclasses. The results will provide improved information about the slow rotators that populate the main sequence from B5 to F0 and, we hope, will provide new insight into the nature of possible deceleration mechanisms that produce these slow rotators.

The above-mentioned survey has produced a number of auxiliary results of interest:

1. The rotational velocities of 22 *periodic* Ap stars have been used to derive a radius of  $R=3.2 R_\odot$  from consideration

of the period versus line-width relation via the expression

$$R=4/\pi \langle R \sin i \rangle = 2/\pi^2 \langle P v \sin i \rangle.$$

A plot of  $R \sin i$  versus  $B-V$  suggests that the upper envelope of  $R \sin i$  values is reasonably well represented by a zero-age main-sequence  $R[(B-V)]$  relation scaled upward by a factor of 2.

2. Careful examination of line profiles of the sharpest-lined Ap stars at dispersion  $\sim 4\text{\AA}/\text{mm}$  has led to the discovery of resolved Zeeman doublets in the spectra of HD 12288 and HD 165474, marginally resolved doublets in several other stars, and selective Zeeman broadening (as opposed to uniform Doppler broadening) in others. Thus it appears that it will be possible to construct the frequency distribution of mean surface fields for the sharpest-lined Ap stars. The stars with resolved Zeeman patterns are now under surveillance for variations like those of HD 126515.

3. A list of stars with  $V \sin i < 10 \text{ km sec}^{-1}$  provides candidates for longer periods; such objects have not been investigated systematically heretofore. Observations of these objects have already produced a new, unique spectrum variable, HD 24712, for which the lines of neutral and ionized Mg vary in antiphase with those of Y II and Eu II in a provisional period of 26.5 days.

A new differential circular Zeeman analyzer with a long (38 mm) calcite block has been placed in operation so that well-widened Zeeman spectrograms can be obtained with the shorter focal-length cameras of the 200-inch coudé spectrograph. The new analyzer is being calibrated by making new observations of several well-studied periodic magnetic variables.

Preston has called attention to the fact that the quadratic Zeeman effect should produce large violet shifts in the lines of hydrogen for surface magnetic fields greater than about  $5 \times 10^5$  gauss; these are measured in Angstroms at  $10^6$  gauss. The absence of such shifts in the spectra

of dA and dB white dwarfs indicates that these objects generally have mean surface fields less than about  $5 \times 10^5$  gauss, and hence effective fields less than 1 or  $2 \times 10^5$  gauss.

Kodaira and Fomalont observed 12 Ap stars with the 90-foot interferometer at the Owens Valley Radio Observatory. The magnetic stars showed no detectable radio flux at 6.2 cm, with an upper limit of 0.05 flux units. The absence of radio flux shows a relatively steady electromagnetic situation in the Ap stars (unlike the pulsars). If synchrotron radiation exists, the low radio flux shows that it cannot be responsible for the variable component in the optical radiation of the Ap stars.

Following the recent discoveries of lines of heavy elements—Hg I and Hg II, Pt II, Os II, and U II—in the spectra of certain peculiar A-type stars, Sargent and Adelman made an unsuccessful search for lines of ionized and neutral plutonium in the spectra of several Ap stars that show the strong Hg II feature at  $\lambda 3984$ . The longest-lived isotope,  $\text{Pu}^{244}$ , has a half-life of about  $10^8$  years and is expected to be produced by rapid neutron capture processes in about the same abundance as uranium. The discovery of a radioactive element like plutonium would help to discriminate between Michaud's diffusion theory of the origin of Ap stars and the nuclear theories.

Photographic observations with a Zeeman analyzer for stellar magnetic fields normally have a threshold sensitivity of several hundred gauss in sharp-line stars, or even greater in the more rapidly

rotating Ap stars. There are many Ap stars whose fields are too weak to be studied effectively for this reason, and the magnetic properties of these stars remain largely unexplored. Indeed, there is reason to expect that a study of the magnetic fields in the more rapidly rotating Ap stars could help to clarify the nature of stellar magnetism. For this reason, Vaughan and Preston have completed the preliminary design of a photoelectric stellar magnetograph that will have substantially greater sensitivity than the photographic method. They propose to utilize the coudé scanner of the 100-inch telescope and its associated digital data system to record the monochromatic intensities of right and left circularly polarized light. The technique is analogous to the Babcock solar magnetograph, except for complications introduced by the need for seeing-compensation in the stellar observations. Preliminary tests with rudimentary equipment have been carried out. The operational version of the magnetograph remains to be built. In a related program, the design of a birefringent Fabry-Perot interferometer for use in a multi-etalon interferometer under construction by Münch and Vaughan is also being investigated. A first and immediate task to which this instrument will be devoted is the search for very weak general fields in sharp-line solar-type stars and even supergiants [such as  $\gamma$  Cygni, in which a 30–300 gauss field was reported recently by Severny in *Astrophys. J. (Letters)*, 159, L73, 1970].

## INFRARED SPECTROSCOPY AND PHOTOMETRY

### *Chromospheric Helium Emission*

Zirin has continued his spectroscopy of stars in the  $1.08 \mu$  region. Among the interesting phenomena found is the presence of helium emission in the RV Tauri variable R Scuti, as well as the following more normal stars:  $\epsilon$  Corvi,  $\iota$  Aurigae,

$\mu$  Persei, R Leporis (?),  $\theta$  Ceti (?),  $\rho$  Cassiopeiae,  $\alpha$  Cassiopeiae (?),  $\theta$  Herculis, 12 Pegasi,  $\alpha$  Aurigae,  $\alpha$  Aquarii,  $\beta$  Ceti,  $\alpha$  Trianguli,  $\zeta$  Monocerotis, 58 Persei,  $\beta$  Camelopardalis, 61 Cygni A and B,  $\sigma$  Geminorum,  $\beta$  Draconis,  $\beta$  Scuti.



### *Red Stars and O II Sources*

Hyland has continued observations of red stars from 1.2 to 10  $\mu$  on the 60- and 100-inch telescopes. Several of these, which are also OH sources, have been observed many times and show large long-period variations. A simple dust-shell model seems to fit the observations of these very red sources very well. Statistically, it has been established that infrared radiation is associated with and possibly responsible for the OH radio emission. Details of the spectroscopy and photometry of the infrared stars are being studied to understand the physical mechanism that results in OH maser action. The sources are found to be of two types: oxygen-rich M supergiants and long-period variable stars. One common characteristic appears to be a high rate of mass loss, which may lead to the formation of thick dust shells. A joint program with the Harvard College Radio Observatory is under way to monitor both the infrared and radio emission of the OH sources.

The search for infrared sources associated with OH sources in H II regions has also been continued and a source that can be identified with the nebula K3-50 has been found. The equivalent black-body temperature is in the neighborhood of 100°K. This adds strength to the growing realization that the infrared pumping is connected with the OH population inversion even in complex sources.

### *M Stars and Long-Period Variables*

Hyland and Frogel have continued their program of 2- $\mu$  spectroscopy on the 60- and 100-inch Mount Wilson telescopes. The observations of standard late-type stars were virtually completed and an initial spectral-classification scheme utilizing the strength of the molecular bands of CO and H<sub>2</sub>O has been proposed. This scheme makes it possible to distinguish between M-type Mira

variables, S stars, M supergiants, and nonvariable M giant stars. The infrared CN bands have been identified in the spectra of many carbon stars. These stars are indeed easily distinguished from other late-type stars by the bands of CN, C<sub>2</sub>, and other unidentified molecular features probably attributable to carbon compounds.

The spectra of long-period variable carbon stars differ considerably from those with irregular or semiregular variations. The band structure is largely washed out in many long-period variables and is indicative of probable obscuration and thermal emission of solid graphite particles. It appears likely that the very red sources CIT 6 (IRC+30219) and IRC+10216 are extreme cases of this phenomenon.

Several oxygen-rich Mira variables have been observed around their cycles and these show striking variations in the strength of their H<sub>2</sub>O and CO bands. These variables are being studied in detail by Frogel, who has noted a correlation between long-period variables having H<sub>2</sub>O emission at 1.35 cm and strong H<sub>2</sub>O absorption at 1.95  $\mu$ .

In addition, Hyland and Frogel have observed photometrically many standard M stars and Mira variables out to 3.5  $\mu$  as an adjunct to the program of spectroscopy on the same sources. The combination of spectra and photometry of the standard stars enables a temperature scale to be set up involving only the strengths of molecular bands in the spectra.

### *Novae*

In late April 1970 when its visual magnitude was 8.0, Hyland and Neugebauer found that the infrared brightness of Nova Serpens 1970 had greatly increased compared with measurements made a month earlier. The total luminosity was found to be approximately equal to that of the nova at maximum visual

brightness. The April observations showed that more than 90% of the total energy was emitted at wavelengths longer than  $1\ \mu$ . The photometry, together with spectra from  $2.0$  to  $2.5\ \mu$ , was consistent with a  $900^\circ\text{K}$  dust-shell model with a radius of  $\sim 5 \times 10^{14}$  cm. Continued observations by Harvey, Hyland, and Neugebauer confirm that the shell is cooling as it expands.

Observations of Nova Aquila 1970 show that its infrared brightness is also increasing as the visual brightness fades.

### 62-Inch Infrared Telescope

The infrared sky survey has been completed and the telescope, under the supervision of Neugebauer, has been used for photometry of about 440 of the reddest stars on a bimonthly basis. Measurements were at wavelengths of  $1.6$ ,  $2.2$  and  $3.4\ \mu$ . Variations are typically on time scales of years; some of the objects varied by as much as 2 mag at  $2.2\ \mu$ .

The telescope was equipped with a new 62-inch epoxy mirror, but this did not greatly improve the image quality.

## GLOBALAR CLUSTERS

Sandage completed the analysis of faint photometry and the color-magnitude diagrams of the four globular clusters M3, M13, M15, and M92. The program was started in 1958 to obtain data necessary to age-date the clusters.

Ages depend on the helium abundance ( $Y$ ), the metal abundance ( $Z$ ), and the absolute luminosity of the main-sequence turn-off ( $L_{t.o.}$ ). Determination of the helium abundance, discussed in *Year Book 68* (p. 126), was made using Christy's theory, which relates  $Y$  to the blue boundary of the RR Lyrae gap. Metal abundances were found from the observed ultraviolet excess values, calibrated from the direct curve-of-growth data previously obtained in M13 and M92 by Helfer, Wallerstein, and Greenstein. New distance determinations using field subdwarfs with large trigonometric parallaxes were made, with the result  $\langle M_V(RR) \rangle \simeq +0.6 \pm 0.2$  for the absolute magnitude of the RR Lyrae stars.

The calculated ages, using the theory of Demarque, Mengel, and Aizeman, average  $T = 9.5 \times 10^9$  years with very little scatter. An independent theory of Iben and Rood gives ages which average 20% longer at  $\langle T \rangle = 11.5 \times 10^9$  years. These absolute ages can be in error by  $\Delta T/T \simeq 0.3$  from the uncertainties in the input data for  $L_{t.o.}$ ,  $Y$ , and  $Z$ . The present best value for globular-cluster ages is then  $T = (10 \pm 3) \times 10^9$  years,

where the error is an outside limit. This age is not in conflict with Friedmann ages for the expanding universe, considering the present uncertainties of the Hubble constant, but this statement requires  $H_0$  to be less than 75 km/sec/mpc if the deceleration parameter is as great as  $q_0 = +1$ . However, the current best estimate by Sandage puts  $H_0 = 75$  as an *upper* limit. He believes  $H_0$  could be as low as 50 km/sec/mpc, or  $H_0^{-1} = 19 \times 10^9$  years, which would then give a nonconflicting Friedmann time for the big-bang creation at  $T_F = 0.57\ H_0^{-1} = 10.8 \times 10^9$  years if  $q_0 = +1$ .

Although the absolute ages of globular clusters have a large error of 30%, relative ages are better determined. Sandage obtained  $\Delta T/T = 0.015$  by considering the observed correlation of mean RR Lyrae periods in clusters (the Oosterhoff-Sawyer effect) with metal abundance, and relating this correlation to the age-dating equation  $T = f(Y, Z, L_{t.o.})$ . An explanation of the correlation of Oosterhoff-Sawyer cluster-period groups with  $Z$  follows naturally from this equation if the clusters are the same age to within several percent. This small age spread among globular clusters is consistent with the concept of rapid collapse of the protogalaxy at the time of its formation  $10^{10}$  years ago.

Some years ago, Sandage and Walker

(*Astrophys. J.* 143, 313, 1966) showed that stars on the red-giant branch of M92 have a significantly larger ultraviolet excess in the two-color diagram than stars on the asymptotic branch. Oke observed two stars with similar values of  $B-V$  on each branch and found that their continuous energy distributions were very different. The two stars on the asymptotic branch had continua like those of metal-rich K-giant field

stars, quite unlike the continua of the metal-poor giant-branch stars. Sargent obtained image-tube spectra, dispersion 90 Å/mm, of Oke's four stars in order to measure their radial velocities and hence check on cluster membership. He found that on radial-velocity grounds, at least one of the apparently metal-rich stars is a cluster member. Its spectrum is rich in lines. Further observations of the K giants in M92 are planned.

## INTERSTELLAR GAS AND GASEOUS NEBULAE

### *Galactic Emission*

Using the multichannel spectrometer of the 200-inch telescope, Münch and S. Eric Persson have measured in the Orion Nebula the intensities of the emission lines  $H_\alpha$ ,  $H_\beta$ , and  $H_\gamma$ , and He I  $\lambda\lambda 10830$ , 7065, and 5876, as well as those of the continuum in two additional wavelength channels. The measurements were done by continuously scanning the bright part of the nebula along various tracks, with integration times corresponding to a motion of about 1 arc sec. In all, about 20,000 measurements were collected. The internal extinction in the nebula, as measured by the Balmer-line ratio excess over the recombination value, is found to show fast and steep spatial variations, anticorrelated with the brightness fluctuations. The intensity ratio He I  $\lambda 10830/\lambda 5876$  has been found to be anticorrelated with the large-scale reddening. The He I  $\lambda 7065/\lambda 5876$  ratio, in contradistinction, is found to vary nearly in the manner of the Balmer ratios. These facts demonstrate that the anomalous weakness of the He I  $\lambda 10830$  line is not due to an unknown deactivation process of the metastable  $2^3S$  level, but rather to destruction of resonantly trapped  $\lambda 10830$  photons by dust absorption.

### *Planetary Nebulae*

As a thesis project, Persson has mea-

sured a number of planetary nebulae through interference filters and diaphragms of various diameters for the study of spatial variations of the He I  $\lambda\lambda 10830$ , 7065, and 5876, and the  $H_\beta$  lines. The anomalous weakness of the  $\lambda 10830$  line can be accounted for on the hypothesis that dust exists within the nebulae and produces extinction of resonantly trapped photons. The amount of dust required is sufficient to account for the infrared excesses observed in the 8–14  $\mu$  range in some nebulae. The visible effects of the dust, on the other hand, are negligible. Further observations of planetary nebulae, as related to the He I  $\lambda 10830$  problem, will be continued. On the theoretical side, the line radiation transfer problem in a medium with absorbers and differential motions is being studied.

### *Molecular Hydrogen Emission*

Further interferometric observations of the Orion Nebula were carried out by Münch and Rickard to verify the detection of  $H_2$  line emission reported by Werner and Harwitt. On the basis of the data obtained, it appears unlikely that a line at  $\lambda 8748$  is present with the reported intensity, although it cannot yet be definitely ruled out.



### *Cooling Mechanisms*

M. V. Penston studied the role of different cooling mechanisms in the interstellar gas. Fine structure transitions of CI at  $610\mu$  and  $369\mu$  and the  $5201\text{\AA}$  line of NI are found to be significant coolants in addition to those known from earlier work. Observational tests of models of the interstellar medium suggested by the

results are (1) A search for  $\lambda 6300$  of OI and  $\lambda 5201$  of NI from above the atmosphere away from the masking effects of night-sky features, (2) Observation of  $\lambda 156\mu$  of CII in the infra-red, which would determine the heating rate of the interstellar gas, and (3) Observation of interstellar absorption lines of CII at  $\lambda 1334$  and  $1336$  would give the same information.

## GALAXIES

### *New Calibration of Distance Indicators*

The program to determine distances to nearby galaxies has continued as part of the long-range effort to improve the Hubble constant. This is a continuation of the earlier very accurate work of Baade and Swope for M31, and the more recent study of the distance to NGC 2403 in the M81 group reported by Sandage and Tammann in *Year Book 66* (p. 280).

With the completion of work on the M81 group two years ago, a number of galaxies became available from which a new calibration of two primary distance indicators could be made. Linear sizes of the largest H II regions and the absolute magnitudes of the brightest blue and red supergiant stars were determined by Tammann and Sandage for galaxies in the Local Group (M33, IC 1613, LMC, SMC, NGC 6822) and in the M81 group (NGC 2403, NGC 2366, IC 2574, Ho II, and NGC 4236). Fundamental distances to these galaxies are already known from studies of Cepheid variables carried out at the Observatories in previous years.

Restricting the galaxy type to late Sc, Sd, and Sm (Magellanic Cloud type Irr), a well-defined relation was found between the linear size of the largest H II region and the absolute  $B$  magnitude of the parent galaxy. Linear sizes range from 70 parsecs in the dwarf Sm galaxy IC 1613 ( $M_B \simeq -14.4$ ) to greater than 300 parsecs in late-type galaxies brighter than  $M_B = -19$ . Unfortunately, the present calibrating sample contains no super-

giant Sc I galaxies, and the crucial part of the size= $f(M_B)$  relation at bright  $M_B$  cannot be found until distances to supergiant Sc I galaxies such as M101 are determined. A major effort has been started to obtain distances to galaxies in the M101 group, with results reported later in this section.

The difficulty in applying the H II-region size versus absolute-magnitude relation to determine unknown distances to other galaxies is that the slope coefficient of the correlation is  $\Delta \log D / \Delta M_B \simeq 0.14$ , which is close to the coefficient 0.2 that applies if a given galaxy is taken to various distances. Hence, the calibration in the form  $\log D (\text{pc}) = 0.14 M_B (\text{galaxy}) + b$  cannot be used with good accuracy because of its relative insensitivity to distance variations. However, the difficulty was circumvented by correlating linear size of the brightest H II region with luminosity class of the parent galaxy, as defined by van den Bergh. The reformulated calibration shows a moderately well-defined correlation between size and luminosity class with the first-ranked H II region ranging between 70 parsecs and 300 parsecs as the luminosity class changes from Irr V to Sc II.

Brightest red and blue supergiant stars have been measured also in the calibrating galaxies. For the blue supergiants,  $M_B$  (brightest star) ranges between  $-7.5$  for IC 1613 to brighter than  $M_B \simeq -10$  for galaxies as luminous as M101. Curiously,  $M_V$  for the brightest red supergiants does not depend on galaxy lumi-

nosity class (or integrated galaxy magnitude). Its value is  $M_V = -8.1 \pm 0.2$  (A.D.) from six of the available calibrating galaxies that have been measured so far. Arguments advanced by Stothers and by Schild show that this effect is expected if neutrino loss becomes important in the evolution of blue main-sequence stars whose initial luminosity is brighter than  $M_B \simeq -8$ . The red supergiants whose main-sequence progenitors are such massive stars have very short lifetimes due to neutrino loss, and few should be observed. Hence, the effective limit of  $M_V \simeq -8$  observed for red supergiants may define the transition region brighter than which neutrino loss occurs.

### *A New Preliminary Distance to the M101 Galaxy Group*

Fundamental distances are required in the M101 group before the calibration of H II sizes and  $M_B$  (brightest star) can be extended to the most luminous galaxies. Until recently it seemed that galaxies in this group had the same distance as NGC 2403 in the M81 group, or about  $(m-M)_{AB} = 27.8$ . However, analysis of the extensive plate material on M101 itself, taken with the 200-inch from 1950 to 1968, showed that it is much more distant by the following six arguments:

1. No Cepheids have been found despite extensive examination of the more than fifty 200-inch plates. This is in contrast with the many Cepheids found on comparable plates in NGC 2403. From this null result, the apparent blue modulus of M101 is at least 0.5 mag and probably more than 1 mag larger than NGC 2403. This means  $(m-M)_{AB} \geq 28.3$  to 28.8.

2. The general resolvability of stars over the face of M101 and its companion dwarfs (NGC 5204, 5474, and 5585) is considerably less than in comparable members of the M81 group (NGC 2403, NGC 2366, Ho II, and IC 2574). The

resolvability factor is more than 1 mag, which means  $(m-M)_{AB} \geq 28.8$ .

3. No supergiant red stars have been found with  $B-V > 2.0$ . The statement is positive to  $V=20$  and probably to  $V=21$ . With  $M_V = -8.1$ , this means  $(m-M)_{AB} > 28$  and perhaps  $(m-M)_{AB} \geq 29$ .

4. Applying the calibration of linear size of H II regions versus luminosity class, discussed above, to the four M101 dwarf galaxies gives  $(m-M)_0 = 29.0 \pm 0.3$ .

5. Recalibration of van den Bergh's luminosity classes in terms of  $M_B$  via the Local Group and M81 group gives  $(m-M)_0 = 29.1 \pm 0.2$ .

6. Diameters of the M101 dwarfs, calibrated with dwarfs in the Local Group and M81 group, indicate  $(m-M)_0 = 29.5$  to 29.9 with considerable uncertainty.

Sandage and Tammann believe the distance errors to M101 can be considerably reduced next year when their study of the brightest resolved stars and of the newly isolated globular clusters associated with M101 is complete. The present data indicate, however, that  $(m-M)_0 \simeq 29.0$ , which is 1.5 mag more distant than was believed last year and is as much as 5.5 mag more distant than Hubble's 1936 distance scale. The Hubble constant cannot be determined directly from these results because the expansion velocity of the M101 group is too small and may be perturbed by the local anisotropy. The results, however, are a step in the recalibration of the distance indicators that are to be used at larger distances.

### *Photoelectric Sequences in Nearby Galaxies*

The brightest stars constitute one type of distance indicator. To determine their apparent magnitude in various resolved field galaxies requires photometric scales to  $B \simeq 20$ . Sandage began photoelectric observations to determine magnitude scales near all resolved Sc, Sd, Sm galaxies whose redshifts are smaller than

2200 km/sec. Stars for such sequences were observed in the magnitude range  $20 \geq B > 16$  near NGC 247, 925, 1156, 2366, 6384, 6643, 6951, 7640, A 103, Ho II, IC 2574, and WLM. About 8 stars per sequence were measured with the 200-inch telescope. The program is expected to require several years.

### IC 1613

Baade's extensive work on variable stars in the dwarf galaxy IC 1613 in the Local Group has been analyzed and prepared for publication by Sandage. Baade began the work in 1929 and continued to obtain plates through the 1958 observing season. He had completed the determination of periods and magnitude estimates for 25 Cepheid variables relative to a magnitude scale set up through photographic transfers to SA 68. The initial sequence was determined in 1932, was revised in 1939 and again in 1955. Baade was still not satisfied with the systematic accuracy of the sequence fainter than  $B=18$ . At his request, Sandage set up photoelectric standards directly in the galaxy during the 1955 and 1960 observing seasons, and the final reduction of Baade's magnitude estimates has now been made relative to the smoothed photoelectric values. The basic sequence consists of 38 stars measured in *UBV* over the range  $21.7 \geq B > 11.6$ . A total of 309 secondary standards were measured relative to these standards. The secondary stars are in 47 separate regions surrounding the variables, and Baade's estimates on the Argelander scale could be transformed directly into *B* magnitudes. The secondary standards were measured on a series of overlapping plates with an iris photometer by Mrs. Ann Matthews under Baade's direction, and the reduction to magnitudes relative to the photoelectric sequence was done by Sandage and Katem.

A total of 59 variable stars were found by Baade on plates taken with the Mount Wilson 100-inch. Of these, 41 are

Cepheids; periods and light curves are available for 25. There are 12 red irregular variables, 1 blue irregular, 1 eclipser, 1 long-period (446 days) Mira variable whose membership is in doubt, and 3 of unknown type. The Cepheids range in period from 2.87 days to 146 days. The photometry has a cut-off at  $B \simeq 22.2$ , and many suspected Cepheids exist that disappear below plate limit at minimum. The fainter Cepheids at a given period are therefore missing, and this introduces a bias in the slope of the observed period-luminosity relation. Allowing for the bias in fitting to the *P-L* relation discussed by Sandage and Tammann last year gives an apparent blue distance modulus of  $(m-M)_{AB}=24.55$ . The reddening is estimated to be  $E(B-V)=0.03$  from the photoelectric sequence stars, giving a true modulus of  $(m-M)_0=24.43$  under the usual assumption that  $A_B=4.0 E(B-V)$ .

The brightest blue star definitely associated with IC 1613 has  $B=17.00$ ,  $B-V \simeq -0.15$ , or  $M_B = -7.55$ . The brightest red supergiant is one of the irregular variables and reaches  $B=18.5$  at maximum, giving  $M_B = -6.05$ . The colors have not yet been measured accurately, but  $B-V \simeq 2.0$ , giving  $M_V$  (brightest red)  $\simeq -8.0$ , which is the same as in other galaxies. IC 1613 is one of the calibrating galaxies used by Tammann and Sandage for the correlation of size of H II regions and  $M_B$  (brightest star) with luminosity class.

### Photography of Star Clusters

Attempts to measure diameters of star clusters in external galaxies are affected by photographic problems of image spreading. To determine these effects empirically, Sandage began a program of photographing nearby globular clusters in the Galactic System with a 5-inch focal length wide-angle lens. The ratio of this focal length to that of the 100-inch reflector is a factor of 100, which is about the ratio of the distances



to M31 and the Galactic halo clusters. The images on the small camera plates of M2, M3, M5, M10, M13, M15, and M92 look very similar to globular clusters in M31 photographed with the 100- and 200-inch reflectors. The true size distribution of clusters in M31, M33, and M101 is expected to be found from comparison of the plates. The program was begun on an experimental basis by Sandage and Osmer in 1968 and was continued during this report year.

### *Coma Cluster*

Gunn and W. Sargent have undertaken a reinvestigation of the virial mass of the Coma Cluster of galaxies. Spectra at 90 Å/mm of approximately 50 galaxies in the central cluster have been obtained with the image-tube spectrograph. These will be supplemented with data on some 20 or 30 outlying members. Spectra of galactic K giants have been obtained with the same instrument to allow determination of velocity dispersions in the more massive member galaxies.

### *Maffei No. 1*

Gunn and Sargent have obtained image-tube spectra at 90 and 60 Å/mm of the highly reddened local-group object Maffei No. 1, and Gunn obtained a 1-N 48-inch schmidt direct plate of the object. Analysis of the spectra indicates a near-zero radial velocity, a small ( $<200$  km/sec) velocity dispersion, and about 200 km/sec total rotation across about 40" of arc. With reasonable assumptions on the mass-to-light ratio, the distance is about 250 kpc, the mass of the order of  $10^9 M_{\odot}$ .

An intensive infrared study of the object has been carried out by Neugebauer. Although it is essentially invisible to the eye, at  $2.2 \mu$  it is comparable in intensity to M31. In fact, infrared studies combined with optical data have shown it to be remarkably similar to M31 but highly reddened by our own Galaxy. Although

its distance is extremely hard to estimate, its brightness makes it plausible that it is a member of the Local Group of galaxies.

### *Galaxies and Cosmology*

Kristian has begun a program of measuring the energy distributions of the brighter galaxies in clusters as a part of a larger program aimed at determining the cosmological parameters through the Hubble diagram. Redshifts are measured from the total shift of the energy distributions, and magnitudes are measured at all wavelengths. The method was first used by Baum in 1956, and was subsequently used by him to measure several clusters, including the faintest measured to date. The multichannel spectrophotometer enables measurements to be made with better spectral resolution and at a much faster rate. The technique should be particularly useful for fainter clusters for which spectroscopic redshift measurements are difficult or impossible and for which the K corrections required in broadband photometry are especially troublesome.

### *Peculiar Galaxies*

Oke has continued measurements of spectral-energy distributions and line intensities of peculiar galaxies. For the most part, these are N-type galaxies, Markarian galaxies, or Zwicky compact galaxies. The distributions of energy in the continua are generally similar, although two objects have been observed recently that resemble large H II regions.

Shields, Sargent, and Oke are making a detailed analysis of 3C 120. Density and electron temperature for the forbidden-line region are 3000 electrons per  $\text{cm}^3$  and 20,000°K, respectively. Some line ratios are peculiar and suggest substantial reddening within the object.

Zwicky, Oke, Neugebauer, and Sargent have studied the highly variable component galaxy Zw 0039.5+4003. It has

broad emission lines, a redshift of 0.1026, and an absolute visual magnitude of  $-21.6$ . There is no evidence of any stellar contribution. An excellent 200-inch photograph by Arp shows a single arm, or jet, coming out of the object. This object is close to M31 and there are sufficient old photographs to make possible a study of its variability in the past.

Approximately half a dozen peculiar galaxies have been found to have strong Fe II permitted lines. Some of these have already been noted by Sargent. Presence of permitted Fe II lines and absence of forbidden lines of Fe II indicate high densities of the order of  $10^6$  electrons per  $\text{cm}^3$ , or more.

In collaboration with Racine, Arp obtained a spectrum of the stellar object due east of a galaxy which is suspected to be associated with the peculiar radio source OQ 208. The object exhibited a low redshift stellar spectrum, presumably ruling out any connection with the radio source.

Arp has obtained an  $H\alpha$  interference-filter photograph of NGC 3077 which, like M82, is a peculiar companion to the large Sb spiral M81. The hydrogen emission appears to form luminous filaments across the face of the galaxy, increasing its peculiar aspect. Spectra have been obtained at various position angles in this galaxy and Bertola is measuring the redshift of the  $H\alpha$  emission.

In collaboration with Sargent, M. V. Penston obtained a spectrum of NGC 4151 at 20 Å/mm on the 100-inch telescope. This provided confirmation of the variation of the blue-displaced shell absorption in  $\lambda 3889$  of He I, earlier proposed by Cromwell and Weymann. It is interesting to note that this variation may not be due to any variation of material along the line of sight, but could be ascribed to a change in excitation conditions because of the variable non-thermal component. The spectrum also showed indications that  $\lambda 4472$  of He I may be present in absorption.

M. V. Penston has made complete identifications of the radio sources in the Ryle and Neville North Polar Survey. By taking two-color and deep plates on the 48-inch schmidt, he finds 8 quasar candidates and 21 identifications with galaxies. A particularly interesting object is RN 8=3C61.1, which has an ultra-violet excess and lies in a cluster of galaxies.

### *Markarian Galaxies*

Image-tube spectra of 54 objects in Markarian's second list of galaxies with an ultraviolet continuum were obtained by Sargent. Most of the spectra were in the red region from  $\lambda\lambda 4800$  to 6800. Two objects, Markarian 80 and Markarian 113, appear to be galactic stars. Six objects, Markarian Nos. 76, 131, 139, 159, 180, and 194, showed only a blue continuum; it is probable that these objects are white dwarfs, although it is not excluded that they are objects like BL Lacertae or I Zw 1727+50 (variable, lineless, extended objects that are presumed to be extragalactic and to have nonthermal optical continua). Of the 45 Markarian objects with readable spectra, 44 have emission lines. These include 3 Seyfertlike galaxies with broad Balmer emission lines and sharper forbidden lines; namely, Markarian 79 ( $z=0.0221$ ), Markarian 106 ( $z=0.1236$ ), and Markarian 124 ( $z=0.0566$ ). Another object, Markarian 132, is a radio-quiet quasi-stellar object with a redshift of  $z\approx 1.75$ , as given by Lyman- $\alpha$ , C IV  $\lambda 1550$ , and Si IV  $\lambda 1397$  emission lines. This object also has many absorption lines; particularly prominent ones in the blue wings of the above-mentioned emission lines lead to an absorption redshift of about  $z=1.72$ . In the region of  $\lambda 6800$  there is a wide absorption trough that appears to be produced by the Fe II lines around  $\lambda 2500$ , which were found by Lynds, Burbidge, and Stockton in PHL 938. Several other absorption lines were measured, and Sargent is working on

their identification; it seems probable that at least two absorption redshifts are present. Markarian estimated the apparent magnitude of Markarian 132 to be 15 mag; however, on the *Sky Survey* the object appears nearer 16 mag. In any event, the object is exceedingly bright in view of its large redshift. It is hoped to make a detailed analysis of the spectrum of Markarian 132 after suitable spectra have been obtained in the 1970-71 season.

The remaining 40 Markarian galaxies have spectra with sharp emission lines, and in a few cases, with absorption lines as well. These 40 galaxies have redshifts ranging from +270 km/sec for Markarian 178 to 14,500 km/sec for Markarian 83. The absolute magnitudes range from  $M_p = -21.5$  (Nos. 84, 88, and 171) to  $-14$  (Nos. 94 and 178). Sargent is studying the way in which the strength and excitation of the emission lines correlate with the other properties of the galaxies. There is a clear tendency for the galaxies with low intrinsic luminosities to have the most highly excited emission spectra. The Zwicky compact galaxies were found to exhibit similar behavior.

In a separate but related investigation, Sargent is attempting to determine the space densities of the Markarian galaxies of different types by the use of data obtained on objects in Markarian's first and second lists by Weedman and Khachikian and by Sargent himself. The preliminary results indicate that emission-line objects of absolute magnitude  $-14$  to  $-16$  have a space density of about  $0.08 \text{ Mpc}^{-3}$ . This is important in view of Sargent's and Searle's interpretation of Zwicky galaxies of this kind as being possible young galaxies. (See the section on Zwicky compact galaxies.)

### *Masses of Galaxies*

Sargent has embarked on a program to determine velocity dispersions for the stars in the elliptical galaxies for which Fish and others have published light

distributions. As part of this work, two spectrograms were obtained of the nucleus of M32, dispersion  $18 \text{ Å/mm}$ , at the coudé focus of the Hale telescope. Many absorption lines are clearly resolved on the spectrograms, which required exposures of 4 and 6 hours. Reduction of the data is in progress in order to derive an improved estimate of the mass of M32.

### *Zwicky Compact Galaxies*

Following the completion of the survey of the spectra of 141 compact galaxies (see *Year Book 68*, p. 133), Sargent is collaborating with Oke and with Searle on more detailed studies of objects with broad emission lines and those with sharp emission lines, respectively. As part of the work on galaxies with broad emission lines, Sargent obtained  $50 \text{ Å/mm}$  and  $90 \text{ Å/mm}$  image-tube spectra covering the region  $\lambda\lambda 3300-7000$  of II Zw 0119-01, III Zw 0338-01, and II Zw 2130+09. These are being analyzed in conjunction with photoelectric scans obtained by Oke. The galaxy III Zw 0338-01 was found to have *double* sharp emission lines instead of single broad lines on these high-dispersion plates. The components are separated by  $\sim 700 \text{ km/sec}$ , with the one of longer wavelength much the stronger of the two. The 200-inch direct photograph published by Sargent (*Astrophys. J.*, 160, 407, 1970) shows that the nucleus of this object has three small condensations that are evidently in relative motion at very high velocities. The H $\beta$  emission line, which was not detected in the low-dispersion work, now appears as a very weak feature.

Sargent also analyzed the nucleus of the compact galaxy I Zw 1439+53. This object, whose spectrum was described by Zwicky (*Astrophys. J.*, 143, 192, 1966), was found by Sargent to be probably variable and to have spectroscopic features similar to the Seyfert galaxies, although the emission lines are only



about 900 km/sec wide. An analysis of the emission lines, using the new image-tube spectra and scans obtained in 1967, leads to  $T_e=19,000^\circ\text{K}$  and  $30\leq n_e\leq 10^4\text{ cm}^{-3}$  for the hot gas producing the emission lines. The mass of gas is between  $10^8$  and  $10^9 M_\odot$ .

Sargent and Searle are collaborating on a detailed study of two blue compact galaxies, I Zw 0930+55 and II Zw 0553+03, which have been mentioned in *Year Book 66* and *Year Book 67*. They have strong, sharp emission lines of comparatively high excitation, and have low redshifts (about 700 km/sec) which lead to distances of order 10 Mpc and absolute magnitudes of about  $M_p=-14$ . These galaxies have very compact cores, about 100 pc in diameter, which radiate the emission lines. Recently, Heidemann and his associates at Meudon detected 21-cm emission from these objects. They infer a total mass of neutral hydrogen of about  $10^8 M_\odot$  for each galaxy. Sargent and Searle find that the cores of these dwarf galaxies have integrated properties very similar to the O-associations in the outer arms of spiral galaxies such as M33 and M101. They are discussing two possible interpretations: (1) they may be young galaxies with ages of the order of  $10^7$  years; or (2) they may be galaxies  $10^{10}$  years old which have made a preponderance of massive stars throughout most of their lives. (It turns out that the present rate of star formation and the total amount of available neutral gas are consistent with this latter hypothesis.)

In order to set a limit on the population of old stars in such systems, Neugebauer has supplied infrared observations at  $1.6\ \mu$  and  $2.2\ \mu$  of II Zw 0553+03, the only such object bright enough to be observed at these wavelengths. II Zw 0553+03 is surprisingly bright in the infrared; however, Sargent and Searle are unable to interpret Neugebauer's observations until similar ones have been made of a bright O-association in M33 or M101.

In any case, objects such as I Zw 0930+55 and II Zw 0553+03 seem to be among the best candidates yet found for young galaxies. There are many other dwarf emission-line objects in the Zwicky and Markarian lists which would repay searches for 21-cm emission. A preliminary analysis of the scans and spectra of II Zw 0553+03 and I Zw 0930+55 leads to the conclusion that their abundance ratios of He/H, O/H, and Ne/H are the same as those in the Orion nebula within a factor of 2. This is hard to understand according to either hypothesis (1) or (2) above in view of the apparently large mass ratio of gas to stars in these systems. High priority will be put on further work on this intriguing class of objects next season.

In a post-retirement study based on plates obtained between 1936 and 1968, F. Zwicky found that the compact galaxy ZW 0039.5+4003 has varied irregularly in the photographic magnitude range 16.0–18.2. Its spectrum shows both the permitted and forbidden emission lines common in Seyfert galaxies, but it is probably much brighter than a typical object of this type.

Zwicky's work on the compilation of a catalog of about 4000 compact galaxies continues. He estimates that a search over the whole sky to a limit  $m_p=18.5$  would yield about 200,000 such objects.

### *Supernova Parent Galaxies*

Sargent embarked on a program to determine the redshifts of galaxies in which supernovae have occurred. Observations of 16 parent galaxies were made with the Cassegrain image-tube spectrograph on the Hale Telescope; redshifts were obtained for 12 of the galaxies. The relevant supernovae were 1968o, 1968n, 1966i, 1964j, 1955b, 1967e, 1961p, 1968u, 1964h, 1960k, and 1964k. Two of these galaxies are of particular interest. SN 1955b occurred in a faint galaxy close to an aggregate termed the "A-cloud" by Zwicky (*Publ. Astron. Soc. Pacific*, 68,

271, 1956). Humason had earlier determined redshifts of 15440 and 16057 km/sec for two galaxies in the "A-cloud." Zwicky pointed out that if SN 1955b was, in fact, at the same distance as the cloud, then it would have an abnormally bright maximum luminosity. Sargent's redshift for the parent of SN 1955b is 16024 km sec<sup>-1</sup>, which leads to an absolute magnitude at maximum of -20.8 for this apparently Type I supernova.

SN 1964h occurred in NGC 7292, which is a peculiar irregular galaxy with a system of bright fanlike structures around the central core. The spectrum of NGC 7292 shows strong emission lines of H, He I, [O II], [O III], and [Ne III] with unusually high excitation. The object, which has a redshift of +934 km/sec, deserves further study.

### *H II Regions*

Searle completed work begun last year on the spectra of H II regions in nearby galaxies. The image-tube spectrographic survey described in *Year Book 68* (p. 132) was extended to include H II regions in M51, M101, and NGC 1232. A few regions in the irregular galaxy NGC 4214 were observed for comparison. The multichannel spectrometer of the Hale reflector was used to measure the relative line strengths in 30 H II regions in these galaxies and in M33 and in NGC 2403.

In all the spiral galaxies surveyed there is a close correlation between the distance of an H II region from the center of the galaxy and the appearance of its spectrum. After reddening correction, the line ratios [O III]/H $\beta$ , H $\alpha$ /[N II], and [O II]/[N II] all show an increase as one passes from H II regions in the inner spiral arms to regions in the outermost arms. In the extreme case of M101 this increase is by a factor of 100, 10, and 100 for the three ratios, respectively.

The spectral gradient is found in all the spirals surveyed. However, the average spectral type of an H II region is

different in different galaxies and appears to be correlated with morphological type. On the average, the line ratios mentioned increase on going from early Sc galaxies to late Sc galaxies.

An analysis of these results leads to the conclusion that there is a composition gradient across the disk of Sc galaxies and also along the morphological sequence. The N/O abundance ratio (and probably also the O/H abundance ratio) is lowest in irregular galaxies and in the outer parts of late Sc galaxies; it increases toward the centers of the spirals and it is highest in the inner spiral arms of the early Sc galaxies. In contrast, the He/H abundance ratio is constant across the disk of spirals and also along the morphological sequence.

### *Radio Galaxies*

Oke has obtained absolute spectral-energy distributions of a dozen radio galaxies from  $\lambda\lambda 3300$  to 10,000. The data are being analyzed by Oke and Turnrose. Almost all of the objects so far studied resemble ordinary elliptical galaxies. The H and K lines are usually strong and in absorption. Some objects have fairly strong emission lines. There is some evidence that there is an excess of radiation at 10,000 Å; more observations of normal galaxies must be made before this can be shown conclusively.

### *Radio-Source Identification*

A new experimental ITT electrostatically focused image tube was put into service for direct photography at the 200-inch prime focus and the Cassegrain station by Oke and Sandage. The image tube has an S25 cathode and was used to obtain direct plates in a broad band from 6100 to 8500 Å. The gain over conventional photography is about a factor of 20, with no discernible loss of resolution. The tube uses glass fiber input and output optics.

At the end of the report year, Sandage

obtained about 70 photographs of radio-source fields which were empty to the 48-inch schmidt limit. Inspection of the plates by Sandage and Kristian has just begun, but preliminary results indicate a large number of new identifications, mostly with galaxies fainter than  $V \simeq 22$ . Several cluster candidates were found, and the project will be continued as part of the program to obtain a better value of  $q_0$ .

### *Galactic Nuclei*

Searle began a study of emission-line nuclei of normal galaxies. The aim is to find out in what ways the physical conditions in these regions differ from those in the H II regions in spiral arms. A detailed comparison has been made of the nuclei of M101 and M51, which appear to be typical of two physically distinct types of nuclei. In the M101 type, the emission lines are unresolved (on image-tube spectra at 35 Å/mm at  $H\alpha$ ),  $H\alpha$  is stronger than [N II], and the [S II] ratio  $\lambda 6717/\lambda 6731$  exceeds unity. These spectra are indistinguishable from those of normal H II regions. Spectra of the M51 type, on the other hand, all have broad emission lines,  $H\alpha$  weaker than [N II], and frequently show an [S II] ratio less than unity, indicating a high density for the emitting gas. Examples of nuclei of this type are those of NGC 2911, NGC 3998, and NGC 6951. Their spectra are unlike those of H II regions and have certain features in common with the spectra of Seyfert nuclei in supernova remnants.

### *Companion Galaxies*

Arp studied galaxies in groups or clusters with particular emphasis on small galaxies that are nearby companions to large galaxies. The first part of this work involved a statistical study of redshifts of commonly accepted companions to well-known dominant Sb spirals such as M31 and M 81. For these,

Arp found a statistical predominance of positive redshifts with respect to the large galaxy. Among 13 of the accepted and most certain cases of companion galaxies, he showed that in 11 of these the companion had a positive relative redshift. For companions on the ends of spiral arms, where the interaction of companion and arm ensures that both objects are at the same distance, an excess of positive redshifts for the smaller galaxies was again found in 5 out of 6 cases, making 16 positive redshifts of a total of 19 systems.

Previously, Arp had studied the physical characteristics of 6 representatives of a class of galaxy characterized by companions on the ends of spiral arms and had shown that this class was characterized by high surface brightness, early integrated spectral type, red color, and non-equilibrium form. He had suggested that the companions had been ejected from the larger galaxies, initially in compact form, and were now expanding. In April, Arp obtained a deep photograph of Zw 1443+51, a compact galaxy discovered by Zwicky on schmidt plates. Its spectrum had been recorded previously by Sargent. The photograph reveals long luminous filaments emerging on either side of an E0 galaxy. In the filaments are four luminous condensations. Three of these condensations are very compact, and one resembles a star. Nevertheless, spectra by Arp show that even the starlike condensation is also a galaxy with a redshift within about 1% (+200 km/sec) of the central E0 galaxy.

An extensive study has been made of the companions in the vicinity of the disturbed Sb spiral NGC 772 (*Atlas of Peculiar Galaxies*, No. 78). The main galaxy has a redshift of about 2500 km/sec. Two out of the three companions that appear to be connected to the disturbance, however, have redshifts of 20,000 km/sec. Three-hour exposures on IIIa-J plates with the 200-inch telescope have been printed at high contrast and analyzed at various magnifications with



an isodensitometer. These methods indicate that the small companions are connected by luminous filaments and protuberances to the main galaxy despite their very discordant redshifts.

Most recently, Arp has started to reduce photographs taken with the 48-inch telescope of the well-known group of galaxies called Stephan's Quintet. This group is only 30 arc min southwest of the large Sb spiral NGC 7331. The similarity of the redshift of NGC 7331 and the small galaxies immediately surrounding it to the redshifts in Stephan's Quintet has led Arp to believe that the latter is associated with NGC 7331 in a situation similar to that of the companions around Sb spirals investigated in the earlier phases of the project. Previously published radio maps of the region by De Jong show radio extensions from NGC 7331 toward Stephan's Quintet, thereby supporting this interpretation.

#### *Compact Galaxies and Quasi-Stellar Sources*

Arp has photographed in red and blue wavelengths the objects B264 and Ton 256. These were previously supposed to be quasi-stellar objects located in clusters of galaxies. He finds, however, that they have minimum diameters of 6 arc sec and 9 arc sec, respectively, and therefore are more properly classified as compact galaxies of high surface brightness. Photography of additional bona fide quasi-stellar radio sources (optically unresolved) with redshifts between  $z=0.2$  and  $0.3$  supports the view that quasi-stellar radio sources generally do not occur in clusters of galaxies. Previously, Sandage and Miller showed that 3C273 and 3C48 are not in great clusters.

#### *Cluster of Compact Galaxies*

Sargent has applied the virial theorem to 13 red compact galaxies that form an elongated system at the center of the cluster Zw Cl 0152+33. This is the only cluster found by Zwicky and his associates in which all the brighter members and most of the faint ones are compact. The mean redshift of the cluster is 26,390 km/sec, and the brightest galaxy has  $m_p=17.0$  and  $M_p=-21.2$ , only 0.3 mag fainter than the mean absolute magnitude of the brightest galaxy in rich clusters. Application of the virial theorem leads to a mass for the system of  $1.65 \times 10^{13} M_\odot$  and to a mass-to-light ratio of 20–30. The center of the cluster thus appears to be bound.

#### *Infrared Radiation*

A program to measure the infrared radiation from the nuclei of radio galaxies has been carried out with the 100-inch telescope by Neugebauer in collaboration with Becklin of the Smithsonian Astrophysical Observatory and Danziger of Harvard College Observatory. The 1.65, 2.2  $\mu$  radiation has been measured in approximately 30 galaxies, and the 3.5  $\mu$  in about 15. The infrared observations have been combined with scanner observations by Danziger to obtain an energy distribution from 0.35 to 3.5  $\mu$ . Preliminary reduction of the data indicates that most of the galaxies have a distribution similar to the nucleus of M31 (Sandage, Becklin, and Neugebauer, *Astrophys. J.*, 157, 55–68, 1969). Approximately 25% of the galaxies, however, show excess infrared radiation, particularly at 3.5  $\mu$ .

### SUPERNOVAE

The Palomar supernova search was reorganized under the supervision of Oke and Sargent. Fifteen supernovae were discovered here during this report period: 9 by Kowal at the 48-inch, 1 by Fairall

at the 18-inch, and 5 by Zwicky on plates of the *Palomar Sky Survey*. Spectroscopic and photometric observations of these and other supernovae were obtained by Oke, Sargent, Kristian, and

Schmidt. An interesting by-product of the supernova search was the discovery of a common nova in Messier 33 in November 1969. The nova was found by Kowal and additional observations were

obtained by Sandage. The brief period of visibility of common novae in extragalactic systems makes it very difficult to obtain an adequate number of observations of them.

## PULSARS

### *NP 0531*

The central star of the Crab Nebula remains the only pulsar observed optically. Photoelectric photometry and polarization measurements of the object have been made on a continuing basis by Kristian, Visvanathan, and Westphal. Broadband *UBVR* photometry on nine nights between February 1969 and February 1970 show constant intensity and colors for the pulsar of  $V=16.5$ ,  $B-V=0.5$ ,  $U-B=-0.45$ , and  $V-R=-0.75$ , with an accuracy of 10–15% in each pass band. The ratio of the intensity in the main pulse to that in the subpulse is 1.8 in each color, with the same accuracy. In the pass band  $\lambda\lambda 3800\text{--}6000$ , the pulsar intensity repeated within 3% on successive nights and on nights two months apart. Constancy on shorter and longer time scales was discussed in *Year Book 68* (p. 139). The data now available cover time scales from successive pulses to the last 50 years, and with different degrees of accuracy in each case. There is no evidence for any change of intensity, color, or pulse shape.

Linear polarization measurements on four nights in February, August, and October 1969 show repeatable behavior, with the amount of polarization changing smoothly through the pulses from at least 25% to near zero, and the plane of polarization sweeping through  $150^\circ$ , corresponding to  $60^\circ$  of the pulsar's rotation. The discontinuous change of the pulsar's period in September 1969 had no discernible effect upon the intensity, colors, or polarization of the pulses. Also, earlier suggestions of substantial changes in intensity and polarization are not confirmed.

The evidence is by now overwhelming that the pulsars are rotating objects, probably neutron stars; and the secular constancy and precise phase-lock of the intensity and polarization over months leave little doubt that the optical pulses of the Crab pulsar are due to a stable, polarized radiation pattern, fixed in the pulsar, which is being azimuthally scanned as the object rotates.

The observations also imply, in a direct way, the existence in the Crab pulsar of a quasi-permanent, asymmetric magnetic field whose existence has been assumed in much of the theoretical discussion of pulsars. The pulsed nature of the radiation requires localization of the emission, while the observed polarization requires a fixed local direction, and the most natural way to satisfy both of these requirements is, in one way or another, through the agency of a magnetic field.

In addition to a magnetic field, emission mechanisms that are likely to be discussed will also involve high-energy particles, and the observed constancy of the emission and polarization will require a means for maintaining a constant particle flux. The temptation is strong to suppose that this particle flux may itself be generated by the rotating magnetic field.

The sweep of the plane of polarization can be interpreted in terms of a very general geometrical model, wherein the observed plane of polarization is either parallel or orthogonal to the projection on the plane of the sky of a vector that is fixed with respect to the pulsar and rotating with it. The model is quite general and seems likely to be valid, at least to first order, for any physical emission mechanism. If it is valid, then the

projection of the rotation axis on the plane of the sky is found directly from the data, with an ambiguity of  $90^\circ$ . This direction can be determined independently for the data from the main pulse and the subpulse, and agrees between the two. Its value is, with an accuracy of within a few degrees, either parallel or orthogonal to the integrated magnetic field of the nebula itself within 20 arc sec of the pulsar. The agreement between the two angles seems too close to be accidental, and implies that the external field, at least in the vicinity of the pulsar, was produced by the pulsar itself at some stage in its history. The origin of the ordered magnetic field in the Crab Nebula has been a puzzle since it was first recognized that the continuum radiation is due to synchrotron emission. The question is still very much open, but the polarization data discussed above constitute the first direct observational evidence of a simple connection between the collapsed star and the external field.

### PSR 0833-45

The Vela pulsar is particularly interesting because (1) it is the second fastest known pulsar, after the one in the Crab, and in some theories is therefore likely to be the second youngest and second brightest, and (2) it is the only pulsar besides the one in the Crab to be associated with a known supernova remnant. Observations are somewhat difficult because of the low declination, but a few measurements have been made at Palomar by Kristian. The pulsar is located some 7" southeast of a bluish star suggested by Cooke, Disney, and Westerlund as a candidate. This star was found to be not pulsing, and a photoelectric measurement made by synchronously averaging photomultiplier counts from a region several radio error boxes in size, centered on the radio position, sets a limit of about 23 mag for the integrated

optical intensity of a pulsing source analogous to the Crab pulsar.

A 48-inch schmidt plate showing part of the nebulosity surrounding the pulsar and presumably associated with the supernova was taken by Minkowski in 1957 and was repeated by Kristian this year. A first crude estimate, based on blinking the plates, sets a lower limit of 10,000 years for the age of the remnant, assuming a constant expansion rate. This is of the same order as the age of the pulsar in several current theories, and it is likely that a more precise measurement will yield an observational test for some of the models.

### *Search for Other Optical Pulsars*

Kristian has continued the search for optical counterparts of radio pulsars whose positions are accurately known. For objects with position accuracies of a few arc minutes, the procedure has been to search on the best available plates for pulsations of stars visible within several radio error boxes, so the limits are at least that of the *Sky Survey*, about 21 mag. For objects with position accuracies of a few arc seconds or less, the procedure has been to synchronously average photomultiplier pulses from a region of the sky several error boxes in size, centered on the radio position. Integration times of the order of an hour at the prime focus of the 200-inch are sufficient to detect an object whose integrated magnitude is 25, assuming a 10% duty cycle.

Measurements have so far been made in the fields of CP 0329, CP 0808, AP 0823, PSR 0833-45, CP 0834, CP 0950, CP 1133, AP 1237+25, HP 1508, PSR 1749-28, CP 1919, PSR 1929+10, JP 1933, AP 2016+28, and PSR 2045-16. These include most of the known pulsars with good positions that are visible from the northern hemisphere.

The faintest limits,  $m \geq 25$ , have been set for CP 0950 and CP 1133, and  $m \geq 24$  for CP 0329 and HP 1508. All



of these except CP 0329 are at high galactic latitudes, and the first two have small dispersion measures.

The limits on optical emission can be expected to set severe constraints on possible emission mechanisms. An optical magnitude of 25 represents an optical flux density at the earth 2500 times smaller than that measured for the Crab

pulsar. This contrasts strongly with the measured radio flux densities of pulsars, which are generally within an order of magnitude of one another.

In addition to the searches in visible wavelengths, Neugebauer and Kristian have conducted some preliminary searches in the infrared, also with negative results.

## X-RAY SOURCES

### *Sco X-1*

In the course of a series of observations of Sco X-1, in which its energy distribution was measured every minute for intervals of the order of an hour, using Oke's multichannel spectrophotometer on the 200-inch telescope, a flare was observed by Kristian. This lasted about 20 minutes and was very blue, with magnitude changes of 0<sup>m</sup>.4 at  $\lambda$ 3500, 0<sup>m</sup>.33 at  $\lambda$ 5000, and 0<sup>m</sup>.28 at  $\lambda$ 7000.

The best current model for the optical continuum of Sco X-1 is that it, as well as the X-ray emission, is due to thermal bremsstrahlung from a source at about 10<sup>7</sup>°K that is optically thin at X-ray wavelengths, semiopaque in the visible, and optically thick at 2.2  $\mu$  and longward. It is difficult to interpret the observed flare as due to this source: an increase in its temperature, for example, would cause it to become redder rather than bluer, since the wavelengths where it becomes optically thin move further to the red. The added intensity in the flare, however, is a moderately good fit to a blackbody of 50,000°K. It is known that a source in this temperature range must be present in Sco X-1 in order to produce the observed emission lines, and, if the flare were due to an enhancement of this component, one would not expect a corresponding increase in the X-ray intensity. The source was, in fact, observed in the X-ray region for short periods before, during, and after the flare by Dr. Hugh Hudson of the University of California at San Diego, using instrumentation on an OSO satellite, and pre-

liminary reduction of the X-ray data shows no changes, with an accuracy of the order of 30%. This is in marked contrast to the only other flare observed simultaneously at optical and X-ray wavelengths by Hudson with OSO and by Westphal, Sandage, and Kristian from Palomar in 1967. The X-ray flare in this earlier measurement was an order of magnitude larger than the corresponding optical flare. Thus, the frequent flares observed in Sco X-1 appear to be of at least two kinds, with the high-temperature and low-temperature components being capable of brightening independently.

### *Two-Color Survey of the Galactic Plane*

Sandage and Kristian have undertaken to photograph a band 18° wide and centered on the galactic plane with two-image (*U* and *B*) 48-inch schmidt plates. The program is in anticipation of several X-ray satellites to be launched in the next few years, beginning with the American Science and Engineering-NASA satellite in the latter half of 1970. Many new accurate X-ray positions are expected, and the plate file will be used for preliminary screening of optical candidates that will be investigated photoelectrically and spectroscopically to establish identifications. The optically identified X-ray source may also be expected to be bright in the ultraviolet. The plate library is 80% complete and will be completed during the summer of 1970.

## QUASI-STELLAR SOURCES

*Space Distribution and Luminosity Function*

Spectroscopic investigations of blue stellar objects identified by Sandage and Luyten in a number of fields at intermediate and high galactic latitude are being continued by Schmidt. All objects with colors similar to those of quasi-stellar radio sources are observed. Tentative redshift determinations of objects in two fields for which photometry was available are essentially complete to magnitude  $18\frac{1}{2}$ . This material permits a derivation of the space distribution and the luminosity function of quasi-stellar objects to be made.

The steep increase, by a factor of about 6 per magnitude, of the number of quasi-stellar objects with magnitude (Sandage and Luyten) cannot correspond to a uniform distribution in a relativistic cosmological model with zero cosmological constant. The observed redshift distribution allows a quantitative estimate of the density increase (assumed to be independent of luminosity) with redshift  $z$  required to explain the steep number-magnitude gradient. It is assumed that the density is proportional to a power of  $(1+z)$ , which quantity itself is inversely proportional to the scale length of the universe. For a value of the deceleration parameter  $q_0$  of  $+1$ , it is found that the density (or the number per co-moving volume element) varies as  $(1+z)^6$ . This density increase is similar to that derived by Schmidt for 3CR quasi-stellar radio sources and to that derived by Longair for extragalactic radio sources in general.

With the adopted density law, Schmidt now finds it possible to determine the optical luminosity function. It turns out to be rather steep, increasing by a factor of 3 or 4 per magnitude. The total local ( $z=0$ ) density of quasi-stellar objects is found to be  $0.7 \times 10^{-6}$  Mpc $^{-3}$ . This estimate includes all objects sufficiently

luminous to have a redshift of at least 0.16 at magnitude 18. This number is rather uncertain because the fainter part of the luminosity function is poorly determined. A more reliable local density of  $0.7 \times 10^{-7}$  Mpc $^{-3}$  is derived for the more luminous quasi-stellar objects that at magnitude 18 exhibit a redshift of at least 0.4. A total of 1.4 million of such luminous quasi-stellar objects with redshifts of less than 2.5 are estimated to be observable down to magnitude  $21\frac{1}{2}$ . Due to the steep decrease of density with time, the total number of such luminous quasi-stellar objects expected to exist in the universe at the present cosmic time is only 3500.

The redshift distribution of optically selected quasi-stellar objects of magnitude 18 turns out to be statistically the same as that of 3CR quasi-stellar radio sources. This similarity cannot be understood if the radio-luminosity function of quasi-stellar sources is independent of the optical luminosity. Schmidt finds that the radio-luminosity function must be displaced toward higher radio luminosity for optically brighter quasi-stellar sources. He is proposing that the relevant-luminosity function may be of the form  $f(M_r - M_v)$ , where  $M_r$  and  $M_v$  are the radio and optical absolute magnitudes, respectively. Since this distribution function may be written as  $f(m_r - m_v)$ , where  $m_r$  and  $m_v$  are the radio and optical apparent magnitudes, respectively, we would be able to predict the radio-flux density distribution of quasi-stellar sources from the optical magnitude distribution of optically selected quasi-stellar objects, without knowledge of individual redshifts.

The scarcity of quasi-stellar objects with redshift larger than 2.5 suggests that the steep increase of density with redshift may terminate at that redshift. Schmidt has investigated this matter in detail on the basis of redshifts observed for objects with magnitude 19 or fainter.

No conclusion can be drawn yet from optically selected quasi-stellar objects, too few faint ones having been observed. The situation is more favorable if quasi-stellar radio sources are included, for which the redshift distribution at magnitude 19 should be the same as for quasi-stellar objects, according to the preceding paragraph. With a density proportional to  $(1+z)^6$ , some 20% of the quasi-stellar objects at magnitude 19 should have redshifts exceeding 2.5. Since only one (actually of magnitude 18) out of twenty objects has a redshift larger than 2.5, it appears that the density law  $(1+z)^6$  yields an overestimate at a redshift of, say, 3 by a factor of 5. This suggests that the density beyond a redshift of 2.5 may be more nearly constant or decrease rather than increase with redshift, but much further observational work on faint quasi-stellar objects is required to settle this important question.

Schmidt is continuing spectroscopic work on quasi-stellar radio sources in the declination zone  $+20^\circ$  to  $+40^\circ$ . Most of the sources are 4C sources for which identifications have now been published by E. T. Olsen. Further identifications in this declination zone are being supplied by radio astronomers at Parkes and at the National Radio Astronomy Observatory. Eventually, this work should allow further studies of the space distribution and the optical and radio luminosity functions, similar to an earlier study of 3CR sources and to a study of optically selected quasi-stellar objects reported above.

### *Optical Positions*

Kristian and Sandage have completed a program of measuring optical positions of 41 radio sources, mostly quasars, with an accuracy of  $0''.3$ . Measurements were made with respect to AGK standards, with proper motions taken into account. Radio positions of the same objects were measured by Dr. C. M. Wade of the National Radio Astronomy Observatory,

using the three-element interferometer at Green Bank, with an accuracy better than  $1''$ . A new technique was used for the radio observations that produced absolute declinations and differences in right ascension, requiring optical calibrators only to fix the zero point in right ascension. The r.m.s. difference between the radio and optical positions is  $0''.5$  in right ascension and  $0''.6$  in declination, with a systematic difference of  $0''.3$  in declination. The accuracy was sufficiently high that a slight systematic difference of  $1''$  between the radio and optical positions, over a  $90^\circ$  declination range, was detected at one stage of the program and was traced to a slight misalignment of the interferometer elements. The sources are spread over the sky between declinations  $-20^\circ$  and  $+70^\circ$  and should provide a useful grid of calibrators for differential radio-position measurements.

The program led to six new identifications: NRAO 140, PKS 1508-05, and 3C 343 are probably quasars; 3C 256, 3C 343.1, and NRAO 530 are probably galaxies, the last probably being in a cluster. Two previously suggested identifications (3C 256 and 0056-17) were found to be incorrect.

In addition to the identified sources, six fields remained empty to  $m_{pg}=21$  or fainter.

The success in making new identifications was sufficiently high in this program that it is being extended to more than 100 currently empty fields above galactic latitude  $15^\circ$ , in continued cooperation with Wade and G. K. Miley. A major aim of the program is to find clusters of galaxies more distant than 3C 295 in the effort to eventually determine the deceleration parameter  $q_0$ .

### *Spectral Energy Distribution*

Oke has continued to obtain absolute spectral energy distributions of selected quasi-stellar sources. These sources are being measured also in the infrared by Neugebauer. Objects being studied in-



clude the highly variable quasars and also those quasars studied by Oke, Neugebauer, and Becklin for which blue spectral energy distributions were not known.

One object studied specifically by Oke was B264, which Bahcall, Schmidt, and Gunn had shown to be a member of a cluster of galaxies. Arp has reported recently that B264 has an apparent diameter of 6 arc sec and is, therefore, more properly classified as a compact galaxy than as a quasar. The spectral energy distribution and line intensities of B264 are almost identical to those of the N-type galaxy 3C 120 and to those of the much more luminous quasar, 3C 223.1.

The absolute spectral energy distribution from  $\lambda 3220$  to  $\lambda 9000$  has been obtained by Oke for the quasar 4C 05.34. This object has recently been found by Lynds to have a redshift  $z=2.877$ . The energy distribution and line intensities show it to be a typical quasar. The second Lyman line, Ly  $\beta$ , is present and there is a drop of intensity by a factor 2 near the Lyman limit. From a very simple model, it is inferred that the optical depth in the Lyman continuum is of the order of unity and approximately 3 at the center of Ly  $\beta$ . This puts very severe restrictions on the amount of neutral hydrogen near the object. The ratio of photons of Ly  $\alpha$  to the extrapolated number beyond the Lyman limit in quasars PHL 938, 3C9, and PKS 0237-23 also suggests that small optical depths beyond the Lyman limit may be common.

### *QSO Associated with Clusters of Galaxies*

A systematic search for clusters of galaxies associated with small-redshift quasi-stellar objects (QSO) has been conducted by Bahcall and Gunn. The investigation was carried out with the Palomar 48-inch schmidt telescope, using exposures of approximately  $2\frac{1}{2}$  hours

duration on baked Eastman IIIa-J plates behind a Wratten 4 filter. At the outset of this investigation, Bahcall discovered that five of the six objects previously classified as QSO with redshift  $z < 0.2$  lie within the boundaries of known clusters of galaxies. However, Arp finds that two of these, B264 and Ton 256, have apparent diameters of several arc sec, and hence are not typical QSO. Schmidt obtained spectrograms of four galaxies in the direction of B264 which have nearly the same redshift as the object. Similarly, Gunn finds that three galaxies, candidates for cluster membership, have about the same redshift as Ton 256.

Bahcall has listed 21 quasi-stellar objects that are in the direction of clusters of galaxies listed in the catalogues compiled by Zwicky and his associates; 14 quasi-stellar objects that are in the direction of rich clusters in Abell's catalogue were also listed. These objects are interesting candidates for radio and optical absorption observations.

An inspection of the deep IIIa-J plates taken by Bahcall and Gunn for six small redshift QSO fails to reveal any underlying galaxy brighter than  $M_v = -19^m$ .

An interesting item of history is the proof that the 16-mag object Ton 202 is, in fact, a quasi-stellar radio source. Listed as a DC white dwarf by Eggen and Greenstein, it was found by Oke and Greenstein to have weak and very broad emission of Mg II, [O III], H $\alpha$  at redshift  $z=0.36$ . It has been detected as a radio source at Green Bank and Owens Valley, with an overall spectral index of  $-0.4$ . The 200-inch spectrogram of Ton 202 proved to be the first one known taken of any quasi-stellar object. It shows the Mg II line to be 400 Å wide.

### *Infrared Measurements*

The study of the energy distributions of quasars to the infrared wavelengths was extended to  $3.5 \mu$  on several of the brighter sources by Neugebauer. The

measurements show that in general the energy distributions continue smoothly from the visual, near-infrared points. Particular emphasis has been placed on the study of those quasars that show marked variability in the visual wavelengths. The infrared intensity in general seems to vary with the visual intensity,

and the infrared color is apparently relatively constant. The object BL Lacertae has been monitored also in the infrared at every possible opportunity. The variations are almost as large as 2 mag, and are intermediate between those observed in the visual and radio wavelengths.

## THEORETICAL STUDIES

During a visit to the Institute of Theoretical Astronomy, Cambridge University, Sargent studied the nuclei of Seyfert galaxies in collaboration with Dr. Martin Rees. Cromwell and Weymann recently compared spectra of the nucleus of NGC 4151 obtained at the Steward Observatory in 1969 with those obtained by Sargent at Mount Wilson in 1962. They found that weak absorption features had appeared in the blue wings of the Balmer emission lines on a time scale of about a year. This was interpreted as evidence for a small, dense core with a radius of about  $3 \times 10^{15}$  cm in the nucleus of NGC 4151. This core, which has an electron density of about  $10^9$  cm $^{-3}$ , was pictured by Cromwell and Weymann as being the origin of the very broad wings to the permitted emission lines radiated by NGC 4151. On their model, these wings are produced by electron scattering in a gas that is too dense to radiate forbidden lines. Rees and Sargent presented arguments against the electron-scattering hypothesis and suggested instead that the broad permitted lines are produced by *rotation* of the small dense core, which may in fact be a thin disk. The disk of gas would be rotating around a condensed mass of about  $10^7 M_{\odot}$ , which would have a Schwarzschild radius of about  $3 \times 10^{12}$  cm. Rees and Sargent speculate that the gas in lineless objects such as BL Lacertae or I Zw 1727+50 may be rotating so rapidly as to produce no detectable emission lines.

Gunn and J. P. Ostriker of Princeton University Observatory have continued their work on the magnetic-dipole model

for pulsars. Detailed calculations have been made for particle acceleration and radiation in the strong wave field produced by the central rotating neutron star. It is found that cosmic-ray spectra, fluxes, and energies can be satisfactorily explained. Examination of the early phase of pulsar evolution indicated that the intense early radiation might be responsible for the supernova event itself, and this possibility has been followed up with a series of crude numerical models. Many details remain to be investigated, but the results seem promising. Reasonably detailed fits can be made with the Crab Nebula; the agreement in all parameters, including the nebular acceleration and the present pulsar period, is striking.

The gravitational stability of thin, rotating disks of stars with respect to small-scale, axisymmetric disturbances has been re-examined by Julian, taking into account possible overstabilities. These overstabilities are absent whenever the density of stars in phase space is a decreasing function of the size of the Lindblad epicycle. In such cases there exists a maximum wavelength of disturbance and a maximum r.m.s. random velocity beyond which all simple instabilities are avoided. On the other hand, overstability occurs for no rotation if the distribution of stellar velocities in any given direction has a sufficiently high relative maximum at a non-zero velocity. Moreover, overstabilities arise even in the presence of rotation for that velocity distribution wherein all the Lindblad epicycle are equal in size.

This work suggests that stable velocity distributions for the stars in disk galaxies must be similar to the Schwarzschild one.

Electron cyclotron masers have been studied by Goldreich and Julian with possible applications to radio emission from Jupiter and other astrophysical radio sources. The effects on the maser phenomenon of various electron distribution functions were pursued by numerical analysis of the dispersion equation for electromagnetic waves in a plasma.

Goldreich and Julian have investigated

relativistic analytic solutions for the model stellar-wind problem posed by Weber and Davis. These solutions are consistent with the hypothesis of minimum torque proposed by Michel, but do not require it as an additional assumption. The radial momentum equation has three critical points that occur where the radial flow velocity is equal to the propagation speed of infinitesimal disturbances. A unique continuous solution is determined by the requirement that it pass through all these critical points.

### GUEST INVESTIGATORS

Dr. Lawrence H. Aller of the University of California at Los Angeles and Dr. Stanley J. Czyzak of Ohio State University observed a number of planetary nebulae with the 60-inch and 100-inch telescopes. At the 60-inch, they employed the Cassegrain spectrum scanner to measure intensities of the strongest emission lines in the region  $\lambda\lambda 4800\text{--}7600$  for the following objects: NGC 40, IC 418, IC 2003, IC 2165, NGC 2440, IC 4593, IC 3568, NGC 2610, NGC 6720, NGC 6741, NGC 6778, NGC 6818, NGC 6826, and NGC 6886. At the 100-inch, they measured visual-region line intensities in J 900, NGC 1535, NGC 2022, NGC 2440, NGC 3242, IC 2003, IC 2165, and IC 4997. They were able to measure several line ratios in IC 4997 and to establish that the spectral changes in this planetary, first noted at Mount Wilson in 1956, are continuing. The weakening of  $\lambda 4363$  [O III] with respect to  $H\gamma$  suggests that the density of this nebula continues to decrease and that its temperature may be declining also. The photoelectric data are being combined with photographic line-intensity measurements to give observational data which can be compared with predictions of theory, and hence give improved information and density and temperature. These and other investigations demonstrate the importance of small-scale density and temperature fluctuations.

During the year, the authors have prepared or published nine papers on their studies of gaseous nebulae.

Dr. E. E. Becklin of the Smithsonian Astrophysical Observatory and Dr. I. J. Danziger of the Harvard College Observatory collaborated with Neugebauer in measuring the infrared radiation from the nuclei of about 30 radio galaxies (*see Galaxies*).

Dr. F. Bertola of the University of Padua spent two months as a guest investigator at the Hale Observatories during which he collaborated with Arp. Photographs of 5 giant E galaxies in clusters were analyzed with an isodensitometer at the Jet Propulsion Laboratory. Large extensions, similar to those previously found for NGC 4486, were detected. The results suggest that the  $M/L$  ratio for such galaxies is higher, perhaps by an order of magnitude, than had previously been thought, thus reducing the discrepancy between virial theorem determinations of galaxy masses within clusters and rotational masses derived for individual galaxies. In a spectroscopic study of the nucleus of NGC 1808, Bertola and Arp found redshift discontinuities among the six compact condensations. Apparent photographic magnitudes between 21 and 22 were obtained for the supernova that erupted in NGC 1058 in 1961. The supernova appears to be located on the end of



a long thin filament that winds out of the center of the galaxy.

In April Dr. M. Breger of the State University of New York at Stony Brook undertook narrow-band photometric measurements of the Ap star HR 5315 (period 0.521 days) in the region  $\lambda\lambda 3400\text{--}6300$ , using the scanner attached to the 60-inch telescope. The measurements, designed to study the wavelength dependence of the variability throughout the period, are still being analyzed.

Drs. G. Courtes, J. M. Deharveng, and A. Pellet of the Laboratory of Space Astronomy, Marseille, continued an interferometric  $H\alpha$  survey of the nearest galaxies during a run of five nights at the prime focus of the 200-inch telescope. The most extended survey was devoted to chains of H II regions in M31. The high contrast and sensitivity of the Fabry-Perot interferometer, coupled with the resolution of the 200-inch, has shown a much larger extension of the  $H\alpha$  emission along the spiral arms. A preliminary reduction of 828 fields, each one 3 arc sec in diameter, has been made in M31. Similarly, 250 fields have been measured in NGC 628, a "face-on" Sc galaxy that shows general  $H\alpha$  emission over the disk and spiral arms.

Dr. Anthony P. Fairall of the University of Texas participated in the supernova search with the 18-inch and 48-inch schmidt telescopes during the summer of 1969.

Dr. Robert F. Garrison of the David Dunlap Observatory, University of Toronto, used the 60-inch telescope and Newtonian spectrograph for 11 nights, primarily to complete observations of stars in the cluster Trumpler 27 (in I Cephei=Cepheus OB2) and of all B3-B9 stars in the Belt Region of Orion. The spectra are being used for MK classification in these regions. These two programs were initiated during 1966-1968 when Garrison was here working primarily on the spectra of long-period variable stars.

Dr. Hugh M. Johnson of the Lockheed Palo Alto Research Laboratory used the

48-inch schmidt on four nights in August. Plates were taken of fields centered on M31, M33, K 3-50, NGC 6888, the Cygnus Loop, Cygnus X-1, Cygnus X-4, Serpens XR-1, and the field of the temporary X-ray source reported in Centaurus from the Vela Satellite. The two-image plates were exposed through a Wratten 2B filter and an interference filter peaked at He II  $\lambda 4686$ . Relatively scarce peculiar stars, such as Wolf-Rayets and X-ray sources, are sought by this method. Microscopic examination shows that He II-strong stars can be found to magnitude limits that are greater than those reached by objective-prism plates on W-R stars. Trial analysis of the plates is under way on the GALAXY machine at the Royal Observatory, Edinburgh.

Dr. Philip C. Keenan of the Perkins Observatory, Ohio State University, working with the 200-inch telescope and coudé spectrograph, obtained high-dispersion spectrograms of 13 stars. Four were carbon stars and the remainder were supergiants for which accurate radial velocities are needed. A particularly interesting G-type Ia supergiant is AX Sagittarii, which has a spectrum remarkably similar to that of RW Cephei. Variable velocity is indicated.

Observations for a proposed revision of the catalog of the spectra of Mira variables were finished by Deutsch, Garrison, and Keenan in 1969; completion of the work awaits classification of the large number of spectrograms taken by Garrison. The joint program resulted in a paper on "The Anomalous Behavior of Aluminum-Oxide Bands in Mira Variables" (*Astrophys. J.*, 158, 261, 1969).

Dr. Gerald P. Kuiper, Director of the Lunar and Planetary Laboratory, University of Arizona, observed Pluto with special equipment at the prime focus of the 200-inch telescope in the period May 21-24, 1970, for the purpose of improving estimates of the diameter of the planet. Unfortunately, the seeing during this interval was only 1 to 3 on the visual

scale. Nevertheless, it could be stated that the diameter of Pluto was approximately 0.3 arc sec. A similar measurement made by Dr. Kuiper in 1950 under exceptionally fine conditions, when the seeing was rated 6 to 7, resulted in a value of 0.23 arc sec.

For a *Proper Motion Survey*, Dr. W. J. Luyten of the University of Minnesota began in 1965 to obtain with the 48-inch schmidt, plots of 936 fields required for second-epoch comparisons with the original National Geographic Society-Palomar Observatory Sky Survey. During the current year Veeder obtained some 90 plates, leaving only 13 fields yet to be completed.

Dr. Donald Lynden-Bell of the Royal Greenwich Observatory repeated short-exposure plates taken with the 60-inch telescope in 1962 in the hope of finding variability in the nuclei of normal galaxies and of some with mildly excited nuclei. No definite variation was found.

In the course of an extended investigation of the distribution of dust and H II regions in spiral galaxies, Dr. Beverly T. Lynds of the University of Arizona spent some weeks at the Observatory offices studying H $\alpha$  photographs made by Sandage at the 200-inch telescope, as well as blue photographs from the files. Her conclusions, based on 33 galaxies in all, are to be presented at the Uppsala symposium of the International Astronomical Union on External Galaxies and Quasi-Stellar Objects. In brief, the bright H II regions of a galaxy are always found either next to or imbedded in regions of high obscuration. It is found also that the dust lanes of a galaxy better define a spiral pattern than do the H II regions.

The 60-inch and 100-inch telescopes were used several times by Dr. Thomas B. McCord of the Massachusetts Institute of Technology to observe the spectrum from 0.3 to 0.1  $\mu$  of asteroids and satellites. The spectrum of the asteroid Vesta was shown to contain an absorption band near 0.9  $\mu$ , which was interpreted in terms of the composition of

the asteroid. Vesta is compositionally quite similar to a particular class of meteorites, Basaltic Achondrites. A small variation of the absorption feature with phase during rotation was found. Extensive observations of the satellites of Saturn in the spectral region 0.3 to 1.1  $\mu$  have been made and are being prepared for publication. Their spectral reflectivities are generally flat in this region, unlike those for Jupiter's satellites, Saturn's rings, and most of the solar-system bodies. This may indicate a surface composition of ices rather than silicates. The large orbital phase variation for Iapetus was confirmed. A color change with brightness change was discovered.

Spectral reflectivity of the rings of Saturn (0.3–1.1  $\mu$ ) was measured and then analyzed along with the spectrum in the infrared (1.0–1.25  $\mu$ ). The IR spectrum clearly suggests the presence of water frosts, but the visible spectrum suggests that additional material is present. A preliminary analysis indicates a composition of either special mixtures of ices and silicates or radiation-damaged ices.

Many lunar spectral reflectivity measurements of small areas of surface were made with a 24-inch telescope in the range 0.3 to 2.5  $\mu$ . It was shown that mineralogical analysis can be performed using remote measurements. The results have conformed very closely to the Apollo data. Special study was made of proposed future Apollo landing sites to help choose the most scientifically rewarding sites for exploration.

Dr. Walter E. Mitchell, Jr., of the Perkins Observatory, Ohio State University, used the Snow Telescope in September to make photoelectric observations of the cores of the H and K lines and the nearby continuum. The scans were made in the double-pass mode with integrated sunlight to determine the strength and stability of the line reversals during the course of the solar rotation.



Dr. Tobias Owen of the Division of Geological Sciences, California Institute of Technology, used the coudé spectrograph of the 200-inch telescope to obtain spectrograms of comets. In January, two plates of Comet Tago-Sato-Kosaka (1969g) were obtained in the blue-violet region. They are being analyzed to determine the abundance ratio  $^{12}\text{C}/^{13}\text{C}$ . Two spectrograms (4500–7000 Å) of Comet Bennett (1969i) were obtained in April. One of these was at a dispersion higher than any previously published cometary spectra and reveals many new emission lines. Identification of these features is in progress.

Dr. Benjamin F. Peery, Jr., of the University of Indiana obtained coudé spectrograms of several S-type long-period variables in the red for abundance determinations of s-process elements and for zirconium isotopic abundances. Spectrograms were also obtained of several cool carbon stars, including TX Piscium, in the violet for detailed identifications and abundances.

Mrs. M. V. Penston of the Royal Greenwich Observatory, Herstmonceux, has used the 20-inch and 60-inch to obtain photoelectric *UBV* observations of 50 faint A stars in the region of the North Galactic Cap. Recent work at Herstmonceux has indicated that the mean velocity component perpendicular to the galactic plane of main-sequence early A stars increases with height above the plane in the Southern Hemisphere (G. A. Harding, F. Fahim, C. M. Haslam, *Roy. Obs. Bull.*, in press). The dispersion in these velocities also increases with height above the plane in both hemispheres. The stars in the present program were chosen from objective-prism surveys to investigate the motion of early A stars at heights of 500–1000 pc above the plane in the Northern Hemisphere. Radial velocities and accurate spectral types have been determined at Herstmonceux.

In cooperation with C. A. Murray at Herstmonceux, Mrs. Penston has obtained second-epoch plates of Selected

Areas in the region of the North Galactic Pole with the 60-inch as part of project "Pole-Hole" mentioned in *Year Book 65* (p. 141). Photoelectric *UBV* observations have also been made of a selection of stars in seven other Selected Areas down to the observable limit of the 20-inch:  $V \sim 12^m.5$ .

Six blue stragglers in M67 found to have variable velocity by A. J. Deutsch, were examined for light variations with the 20-inch by Mrs. Penston. These were observed at roughly half-hour intervals for about five hours on three out of four consecutive nights, and several isolated observations were made a month later. No variations in excess of 0<sup>m</sup>.1 were found.

Mrs. Penston has also used the coudé scanner on the 100-inch to determine the H and K emission intensity both in main-sequence stars with  $b-y \geq 0.290$  not already investigated by O. C. Wilson and in dwarfs from a recently revised catalog of nearby stars. In both cases the absolute magnitudes of the stars are known, so that by using radial velocities and proper motions, the orbital parameters can be deduced. It is intended to investigate the correlation of emission intensity with the orbital invariants in order to study the progression of both parameters with stellar age.

Dr. A. G. Davis Philip of Dudley Observatory, Albany, New York, has undertaken photometric and spectroscopic investigations of some 50 field horizontal-branch stars identified in regions of high galactic latitude. Strömgren four-color and  $H_\beta$  measures were made of 15 field horizontal-branch stars with the 60-inch telescope. Thirteen spectra of field horizontal-branch stars, as well as numerous spectra of bright, high-velocity standards, were obtained at the Newtonian focus of the 100-inch telescope. Radial velocities for the faintest stars in the group of fifty are being obtained at the Kitt Peak National Observatory. Secondary standards, to be observed at Kitt Peak National Observatory, have been



set up at Mount Wilson. The spectra (dispersion = 86 Å/mm) of the field horizontal-branch stars show sharper hydrogen Balmer lines than do stars of similar spectral type of Population I. The Balmer lines can be seen to  $n=16, 17$  in contrast to  $n=13, 14$  in the spectra of Population I A-stars. Radial velocities for 18 field horizontal-branch stars have been published (*Astrophys. J. (Letters)*, 158, 113, 1970; *Astron. J.*, 75, 246, 1970). The velocity dispersion for the group is over  $\pm 100$  km/sec.

Dr. René Racine of the David Dunlap Observatory, University of Toronto, observed stars associated with galactic nebulae in the range  $20^\circ < \ell^\text{II} < 80^\circ$ . The observations were made photoelectrically in *UBV* down to  $B \simeq 15$  and spectroscopically to  $B \simeq 13$  in an attempt to extend the optical mapping of interstellar matter in this region of the Galaxy. A large opaque nearby cloud of interstellar dust exists up to  $\ell^\text{II} \simeq 60^\circ$  at a distance of 200 to 600 pc. The "Orion Arm" appears to connect to a more or less circular arm at  $\ell^\text{II} \simeq 70^\circ$  at a distance of about 1700 pc.

A survey of the Virgo cluster with the 48-inch schmidt on IIIa-J plates was completed by Racine in May 1970 and supplemented by 200-inch limiting photographs of about 70 Virgo galaxies and *UBV* plates of M87 and NGC 4472. A study of the colors and luminosity functions of the globular clusters associated with Virgo galaxies is in progress. Preliminary results indicate that the M87 clusters are abnormally bright compared to those in other galaxies. Racine also reports that the peculiar radio source V.R.O. 42.22.01 = BC Lacertae, which in many respects is similar to Seyfert nuclei and QSO, exhibited erratic optical variability of a few percent with a time scale of a few minutes.

High-dispersion spectra of several O and F stars were taken by Dr. M. T. Scholz of the Lehrstuhl für Theoretische Astrophysik, Heidelberg. With Dr. J.

Hardorp of Cambridge University, Scholz completed a detailed investigation of  $\tau$  Scorpii (B0 V) and  $\lambda$  Leporis (B0.5 IV). They carried out fine analyses and found that most elements have solar abundances but that neon is overabundant. The ratio of helium to hydrogen is about 0.10 by number of atoms.

Dr. R. Schild of the Smithsonian Astrophysical Observatory continued measurements of standard sources and bright stars, especially  $\alpha$  Lyrae, in the current program of absolute calibration with Oke. This program has recently reached its conclusion with a report in the September 1970 *Astrophysical Journal*, in which generally good agreement is found with the recent calibration by Hayes. The new calibrations depart appreciably from older work in showing a steeper slope for Vega in the Paschen continuum. The absolute flux from a star of apparent visual magnitude  $V=0.00$  at  $\lambda 5840$  has been found to be  $3.65 \times 10^{-20}$  ergs sec $^{-1}$  cm $^{-2}$  Hz $^{-1}$ , a considerable downward revision.

Schild and Oke have extended their investigations of absolute energy distributions to approximately 50 bright stars observed with the same equipment used in the absolute calibration. In a joint publication in preparation with D. Peterson, they report that a Vega model having  $T_{\text{eff}} = 9650^\circ\text{K}$  and  $\log g = 4.05$  fits the slope of the Paschen continuum, the Balmer discontinuity, and the Balmer lines  $H\alpha$ ,  $H\beta$ , and  $H\gamma$ . Moreover, effective temperatures determined from the Balmer discontinuities are in good agreement with those determined from the slopes of the Paschen continua for essentially all of the unreddened B stars observed.

Schild and Oke are continuing their investigations of extended sources, using the calibration equipment to measure energy distributions of the Crab Nebula and of elliptical galaxies in the Virgo cluster. Observations available to date suggest that most of the light in the Virgo ellipticals comes from the nonnuclear re-

gions, which are very much less red than the nuclei. The energy distributions appear to be very similar to one another, as has been known to be true for the nuclear regions. Observations have been extended to 8000 Å to permit K corrections to be computed in the *B*, *V*, and *R* filter bands.

Schild has also measured the energy distribution of M67 and numerous bright stars of late spectral types. An attempt will be made to synthesize the observed energy distribution from energy distributions of the bright stars and the known color-magnitude diagram. It may be possible to assess the contribution of red dwarfs to the energy distribution in this way. Furthermore, the effects of the presence or absence of horizontal-branch stars and blue stragglers should be readily apparent. Age effects on the energy distributions will be investigated.

Dr. G. A. Tammann of the Basel Astronomical Institute, Switzerland, has taken a number of plates of a galactic anti-center field with the 48-inch schmidt telescope and RGU filters. The plates will be measured at Basel for Dr. W. Becker's program to derive a three-dimensional model of the distribution of stars in the galactic disk and halo.

Tammann has investigated the frequency of supernovae in Sb and Sc galaxies within the local supercluster as a function of the integral properties of the parent galaxies. The frequency is a strong function of the luminosity class as defined by van den Bergh, ranging from one observed supernova per 16 years in supergiant Sc galaxies to one supernova per about 200 years in dwarf spirals. The true frequencies are estimated to be about 25% higher. Supernovae are roughly three times less frequent in Sb than in comparable Sc galaxies. The ratio of 1/2 between supernovae of type I and type II seems to be nearly the same for both types of galaxy. For each galaxy type the supernova frequency can be expressed as a linear function of the luminosity or total mass

of the parent galaxy. This and the frequency difference in Sb and Sc galaxies is taken as evidence that the only parameter governing the supernova frequency is the number of massive stars in a galaxy.

From the mass of our Galaxy and an adopted type of Sbc, Tammann predicts a frequency of one type I supernova per  $23 \pm 10$  years and one type II supernova per 35 to 55 years. The latter value corresponds to the present galactic death rate of stars with masses higher than 4–5  $M_{\odot}$ . Recent model calculations for the end phases of a star predict, in fact, above a similar mass limit the occurrence of severe evolutionary instabilities. The frequency of type II supernovae seems also to support the view that all supernovae of type II eventually turn into pulsars.

Dr. S. van den Bergh of the David Dunlap Observatory, University of Toronto, used sixteen 200-inch plates taken by various observers between 1951 and 1968 in a study of the expansion of the optical remnant of the radio source Cassiopeia A. Assuming no deceleration, the explosion of this supernova took place in AD  $1667 \pm 8$  years. No star brighter than  $V=22.5$  is visible within eight standard deviations of this position. For reasonable absorption values, it then follows that any remaining stellar remnant of Cas A must be fainter than the pulsar in the Crab Nebula. The remnant of Cas A is found to be undergoing rapid changes. The average decay time scale for moving knots is about 10 years. The average decay time scale for stationary flocculi appears to be of the order of a few decades. The Cassegrain image-tube spectrograph of the Hale telescope was used to measure the radial velocities of a large number of moving knots. A comparison of these radial velocities with available proper-motion data yields a very uncertain distance of 2.8 kpc. Such a distance would place Cas A slightly beyond the backbone of the Perseus spiral arm as outlined by OB



stars. Individual moving knots in Cas A have space velocities in the range  $4140 < V < 8460$  km/sec. Knots located within a single filament are observed to have velocity differences of up to 3000 km/sec. The cause of this large velocity dispersion remains unknown. Van den Bergh finds that the spectra of moving knots can be adequately represented by a two-temperature model with  $T_e$  (low) = 10,000°K and  $T_e$  (high) = 50,000°K, "normal" abundances, collisional excitation, and  $A_V \simeq 3$  mag. It is difficult to reconcile such a low absorption value with 21-cm measurements and with the lack of 17th century observations of the explosion of Cas A. If  $A_V \simeq 6.8$  is adopted, then both hydrogen and nitrogen must be underabundant by a very large factor. The observation that new knots tend to form in the same general areas in which knots are already present suggests a model in which dense fragments of the exploding supernova become luminous as they plow through tenuous interstellar cloud banks.

A IIIa-J plate of the Crab Nebula obtained by van den Bergh with the 48-inch schmidt shows a jetlike structure pointing away from the center of the nebula. This "jet" has a length of about 100 arc sec, corresponding to a linear size of 1 pc. It is not yet clear whether this "jet" is associated with the filamentary or with the amorphous component of the Crab Nebula. Plates of M82 made with the 200-inch show that the nuclear region of this galaxy contains a number of knots that are extremely prominent in the infrared. The Cassegrain spectrograph of the Hale telescope was used to show that the brightest of these knots has an A-type integrated spectrum. This observation suggests that the nuclear region of M82 contains a number of young and very highly reddened "superstar clusters."

Dr. G. van Herk of the Leiden Observatory inspected the photographs of planetary nebulae in the Observatories' plate files and obtained new direct photographs of a number of planetaries at

the Cassegrain and Newtonian foci of the 60-inch reflector for the purpose of determining proper motions. For a number of so-called ring-shaped stellar associations, several direct photometric plates were also taken to distinguish between early- and late-type stars in and out of the areas occupied by these associations.

Dr. N. Visvanathan of Harvard College Observatory, in collaboration with Kristian and Westphal, observed the Crab pulsar photoelectrically for linear polarization at the prime focus of the 200-inch telescope in February, August, and October, 1969. Most of the data were acquired with time resolution of either 40 or 50  $\mu$ sec. For a summary of the results, see "Pulsars," this Report.

In collaboration with Sandage, Visvanathan made observations of the filaments of the exploding galaxy M82 during the spring of 1970 both at the prime focus of the 200-inch telescope with an S20 photomultiplier and at the Cassegrain focus with the multichannel scanner. Results relate largely to three selected patches.

Analysis of the data shows that the  $H\alpha$  line is linearly polarized and that the percentage of polarization and position angle of the electric vector are the same as in the continuum (24% at  $54^\circ$ ). The polarization of the continuum is constant with wavelength. The equivalent width of  $H\alpha$  is 113 Å, assuming that the ratio of  $H\alpha$  to [N II] 6583 Å is 1/1. It is the same in all the three patches and in the nucleus. No Balmer jump is visible in the continuum of the patches. The continuum in the blue part of the spectrum is nearly flat; it rises in the infrared. The results are consistent with the theory that the spectrum of the patches has its origin in a point source in M82, and that it is probably affected by electron scattering.

On several occasions, Visvanathan observed the peculiar radio source BL Lacertae with the multichannel scanner on the 200-inch for measurements of polarization and intensity from 3400 to



10,000 Å. On July 15, 1969, the continuum between 4300 Å and 10,000 Å had a steep slope proportional to  $\nu^{-3.01}$ . This slope is steeper than the slope obtained on October 19, 1968, when the exponent was 2.78. The visual magnitude on October 19, 1968, was 15.4, while on July 15, 1969, it was 13.9. Thus the continuum of BL Lac is redder during the outburst than when faint. The linear polarization  $P$  and position angle  $\theta$  of the electric vector of the continuum on July 14 and 15, 1969, were 6.2% and  $110^\circ$ .  $P$  and  $\theta$  on October 19, 1968, were 9.8% and  $166^\circ$ . It is interesting to note that the continuum was featureless on these dates. In both the change of slope in the continuum and polarization elements, BL Lac seems similar to the variable QSS 3C 446 (Sandage, A., Westphal, J. A., and Strittmatter, P. A., *Astrophys. J.*, 146, 322, 1966). In the period May to December, 1969, the polarization of BL Lac varied from 10.8% to 3%, and the position angle of electric vector  $\theta$  varied from  $76^\circ$  to  $165^\circ$ .

Dr. George Wallerstein of the University of Washington has obtained high-dispersion spectra (4.5–15.3 Å/mm) of moderately peculiar stars for abundance analyses. The carbon star HD 156074 was observed at 6.7 Å/mm in the visual-red. Atomic lines have been identified in the  $\lambda\lambda 5165$ – $5450$  region, which is relatively free from blends with molecular features. The equivalent widths have been measured and the material is being analyzed by curves of growth. HR 7606 and HR 8626, two bright low-velocity stars with strong CH have been observed at 4.5 Å/mm in the blue. Both CH and CN appear to be enhanced and the lines of ionized elements are quite strong. Line profiles also indicate that these stars are of at least moderately high luminosity. Two high-

velocity G5 stars, HD 175305 and HD 31782, have been observed at 13.5 Å/mm in the visual. Spectrum scans by Spinrad have been employed to assist the analysis. HD 31782 turned out to be an entirely normal star with  $M_V=4$ . HD 175305 is probably metal-poor.

Wallerstein has observed the 27-day Cepheid T Monocerotis to study the depth-dependence of the velocity curve during rising light. The absorption lines appear to follow the pattern of the 41-day star SV Vulpeculae (*Publ. Astron. Soc. Pacific*, 81, 732, 1969), but H $\alpha$  appears to behave as in X Cygni.

In cooperation with Dr. A. H. Batten of the Dominion Astrophysical Observatory, Wallerstein has been observing the double-lined spectroscopic binary HD 27149, which is an F8V star in the Hyades. A tentative period of 75 days has been found.

In addition to extending the spectrograms of VY Canis Majoris to higher dispersion, Wallerstein has started high-dispersion observations of several long-period variables that show microwave OH and H<sub>2</sub>O emission. It is hoped that a kinematic model can be derived by comparing the radial velocities of optical atomic and molecular features with the velocities found from the microwave lines.

Wallerstein has searched unsuccessfully for interstellar lines of lithium in stars located in the direction of the galactic center. As a bonus, an interesting discovery was made of a component of Na I at  $-61$  km/sec (with respect to the local standard of rest) in the A2 Ia<sup>+</sup> star HD 160529. That star is sufficiently distant so that the observed interstellar gas may be part of the flow out from the center of the Galaxy, previously observed at radio wavelengths only.

## ASTROELECTRONICS LABORATORY

*Computer System for Palomar 60-Inch Telescope*

The hardware for the new computer-

operated telescope control and data system for the new 60-inch photometric telescope at Palomar Mountain is essen-

tially complete. The computer programming (software) is nearing completion and, after a final system check, the complete instrument will be ready for installation in July 1970.

Among the novel features of this instrument is the control and display system. The data-gathering process can be controlled by the night assistant in the data room or by the observer at the telescope eyepiece. At either location, four push buttons and one switch are used to operate the entire computer system. These controls have been selected after evaluation of the data systems that have been installed and used here over the past six years. Changes in the data system operational configuration can be made by means of a series of switches located near the night assistant. All of the pertinent data—telescope position, photometer pulse counts, tracking rates, etc.—gathered by the system are displayed to both the night assistant and the observer on television monitors. Control data such as desired tracking rates, data acquisition, and time intervals are entered into the computer by way of a keyboard located near the night assistant and are displayed on the monitors for verification. The night assistant will have a control panel, the computer configuration control, the keyboard and TV monitor, and the strip printer immediately accessible. The observer will be concerned only with a control panel and a television monitor in addition to his observing instrument. This simplicity of operation is intended to minimize human error and improve operational efficiency.

The computer will perform the necessary calculations to control the dome and windscreen positions, adjust the declination and right ascension tracking rates to compensate for refraction, display the coordinate corrections necessary to compensate for refraction-position displacements, and display the air mass for any telescope position. All of these functions will be carried on independently of the data-acquisition process.

In addition to the basic computer with its 8000-word memory and teleprinter, this system as now constructed consists of a civil and sidereal clock, telescope position encoders for hour angle and declination, focus and scan encoders, filter wheel and diaphragm indicators, automatic dome and windscreen position controls, a strip printer, automatic declination and right ascension tracking rate controls, a chopper timer, and acquisition timer and two counters (one of which may be used as a preset counter for ratio measurements). Planned future additions include the hardware and software for a complete computer control of the telescope-setting operation and a digital magnetic tape recorder. Because of the flexible design of the input/output controller, a variety of additional devices can be added in the future to accommodate new observing requirements.

#### *Computer System for the Hale Telescope*

A computer system similar to the 60-inch photometric system is nearing completion for the 200-inch telescope. In addition to those features already described, this system will have a magnetic tape recorder to handle the data from the multichannel spectrometer. Installation is scheduled for the summer of 1970. This system will use much of the same software that is being developed for the new 60-inch telescope.

A new pulse-counting exposure meter was designed, constructed, and installed in the 200-inch coude spectrograph. The older unit had become a serious maintenance problem because of the heavy usage that it had received over the years. The new exposure meter uses a thermoelectrically cooled photomultiplier that has a negligible dark count. Oke coordinated the optical and mechanical components for this project.

#### *Mount Wilson 150-Foot Tower*

A second major project initiated this year was the design and construction,

in coordination with Howard, of a complete new data and control system for the 150-foot solar tower telescope at Mount Wilson. The goal of this project is to provide a system that will not only control the magnetograph and acquire data but also provide on-line reduction of the data, including magnetogram plots. This will enable the solar observers to see magnetogram plots of the sun within an hour after the observations have been completed. The basic plan for the data system and a new all-solid-state tower control system has been completed. The major items of computer hardware have been obtained. These include the computer with 16,000 words of core memory and 800,000 words of disc memory, two magnetic tape recorders, and a digital plotter. A line printer has been ordered

and the interface for the line printer will be designed in the near future.

### *Big Bear Solar Telescope*

A complete control system for the Big Bear solar telescope and its associated spectrograph was designed, built, and installed this year with the cooperation of Zirin. This system provides all the necessary controls for the observer, who has only one hand box with five buttons for all telescope functions at each observing station. Each button activates one unique function, such as telescope guiding, focus, or selection of spectrograph wavelength. In addition to these controls, an automatic spectrograph shutter, film transport, and slit stepping sequencer were designed and built.

## INSTRUMENTATION

### *General Notes*

Under the supervision of Rule, the 200-inch mirror was realuminized in October 1969. Improvements had been made in fore-pump capacity and in leak-testing equipment; otherwise the same multifiring and vacuum equipment was used as in the last coating in 1960. The second attempt, completed on October 27, 1969, resulted in a very good coat with negligibly small haze areas. Evaluation of concurrently run test samples showed 92% reflectance.

The mounting of the new Palomar 60-inch telescope was shipped and installed on the pier in the completed Mayer Building in October 1969. Mechanical items, drives, limits, and temporary control console are ready for operation. Optical figuring of the  $f/2.5$  primary mirror was carried as far as possible in the shop. The mirror was ready for transport to Palomar in July. Hartmann tests will be conducted on stars with the mirror in the telescope, under the supervision of Bowen, to determine whether final corrective figuring is required.

Auxiliary instrumentation for the new 60-inch telescope, which is being funded by a National Science Foundation grant, is progressing satisfactorily. The instrument-mounting base and offset guider are nearing completion. The broadband photometer and cold boxes should be finished in a few more weeks. Plans are being made to adapt the 200-inch prime-focus scanner for use with the 60-inch; this will also be done by August 1970. An image-tube low-dispersion spectrograph has been designed and will be built during the latter half of 1970.

Military and commercial development of image intensifiers led to experiments with various electrostatic, fiber-optic faceplate intensifiers. The most satisfactory has been a 40-mm diameter ITT 4708 with S25 cathode. A photographic plate is pressed into contact with the fiber optics behind the phosphor, and a field-flattener is used to fit the tube to the 18-inch coudé camera of the 200-inch telescope. The tube can be substituted for the photographic devices in a short time and proves quite successful. The resolution loss is by a factor of 2 and the



speed gain is a function of wavelength. In the blue-violet, stars of 13 mag can be observed at  $18 \text{ \AA mm}^{-1}$  in one hour (the limiting exposure, from tube background, is about two hours). Ila-O plates reach 10 mag at higher resolution. However, the real gain is in the red and infrared, where the intensifier loses only slightly and photographic plates lose enormously. To test the performance, Greenstein has taken spectrograms of NGC 1976 and NGC 7027 from 3600 to 8900  $\text{\AA}$ ; in the yellow they show all lines listed by Bowen and Aller, while many new lines have been found in the red and infrared. The most interesting are lines of O I, including the fluorescently excited  $\lambda 8446$ , resulting from a coincidence with Lyman  $\beta$ . Further tests of image tubes will be carried out at the coudé.

A purely interferometric scanning spectrometer is under construction for high-resolution work at the 200-inch and 60-inch telescopes at Palomar, under the supervision of Münch and Vaughan. It consists of a stack of three optically contacted etalons, with 45-mm clear aperture, to be scanned in parallel by varying the pressure in the spacer gas. This instrument is funded through Grant NGC 05-002-140 from the National Aeronautics and Space Administration Office of Planetary Astronomy.

Vaughan developed a simple technique for making crude large objective-transmission "amplitude" gratings that can be used for low-dispersion spectroscopy on the Palomar 48-inch schmidt. They consist of alternate transparent and opaque stripes ruled on thin transparent plastic film. With these gratings on the large schmidt, using baked Ila-O emulsion and no filter, unwidened first-order stellar spectra at  $1100 \text{ \AA/mm}$  can be detected at a magnitude limit of about 15, in an exposure time of 1 hour. The grating spectra compare not unfavorably in definition with the spectra obtained at similar dispersions by means of objective prisms on smaller telescopes. It is expected that the technique will be suit-

able for discovery or classification of dA, gK, late M, S, and C stars, supernovae, and emission-line stars and galaxies. A limited survey program for this purpose is in progress. A basic disadvantage of unblazed amplitude gratings is, of course, their reduced magnitude limit due to the presence of many orders. Thus the need continues for an objective dispersing device that can take full advantage of the largest existing or planned schmidt telescopes. The possible early development of blazed replica gratings for this purpose is under study.

### *Mount Wilson 60-Inch Telescope Modernization*

Extensive modifications of the 1908 Mount Wilson 60-inch telescope, in progress since 1965 under a contract with the National Aeronautics and Space Administration, have largely been completed during the past year, under the general supervision of Vaughan. Most of the main modifications of the telescope itself, including rewiring and the installation of the new electronic drives and other sub-assemblies that had been built in Pasadena, were carried out during a three-month shutdown in the summer of 1969, and the telescope was returned to regular operation in mid-August 1969. It has been in continuous use since that time, although some additional modifications continued through December and January. These included, primarily, the final installation of digital coordinate readouts for right ascension and declination, which are now displayed at the control console; installation of a new hoist; overhauling of the main declination axis bearings, resulting in a substantial reduction in operating torque; realignment of the telescope polar axis with respect to the celestial pole; and installation of new coudé spectrograph. A computer-controlled data acquisition system for use with the telescope was about 50% completed, but additional funding will be required to place this system in opera-

tion. Observers have reported considerable and welcome improvements in most essential aspects of telescope operation as the result of the modernization, particularly in regard to improved setting and tracking accuracy and convenience of use.

### *100-Inch Telescope Engineering Study and Repair Program*

After a half-century of uninterrupted use, the 100-inch telescope has developed serious mechanical problems requiring immediate attention. Consequently, an engineering study was begun by Rule with the aim of defining the principal

requirements involved in a comprehensive repair and modernization program, while at the same time accomplishing emergency repairs to permit current operations to continue with a minimum of interruption. The telescope was removed from the observing program for the interval February 27 through March 11 while data were logged on friction, balance, bearing problems, equipment handling, safety, and operating characteristics. Subsequent improvement programs were recommended for later shutdown periods. The engineering study is expected to result in recommendations for major overhaul and renovation.

## BIG BEAR SOLAR OBSERVATORY

Construction of the Big Bear Solar Observatory was completed in September 1969, and the equatorial telescope was installed. The Observatory was dedicated on May 3, 1970. Although the mechanical work on the spectrograph was finished, its installation awaited completion of the electronic work during the current year. In the meantime, cinematographic observations have been carried out with

the two refracting telescopes under the general supervision of Zirin. The seeing at the Big Bear site has proved to be good for extended periods of time and spectacular new films have been obtained. A number of defects in the design of the telescope are currently being remedied; the declination drive is being completely rebuilt and the mirror cells are being rebuilt to permit adjustment.

## LAS CAMPANAS OBSERVATORY\*

The Institution completed the purchase of the 208-square-kilometer property, including the Las Campanas ridge, from the Government of Chile and proceeded with its development as a site for a major astronomical observatory. Of special importance was the action of the Trustees in appropriating funds for the purchase of a 40-inch general purpose telescope as the initial instrument for the new observatory. The telescope is being built by Boller and Chivens of South Pasadena, and is scheduled for completion in November 1970. It will then be shipped to Chile and installed at a site that is being prepared. Planning for the telescope and its instrumenta-

tion is the responsibility of a staff committee headed by Sandage.

In February 1970 a trip for inspection and planning was made to Las Campanas by a group including Adkison, Babcock, Hoggan, Oke, Rule, and Sandage. Selection of the building sites for the 40-inch telescope and for the generator house was accomplished and road location was approved. The general plan for mountain development was advanced. Microthermal records and other meteorological data are being obtained from six 50-foot towers on the ridge.

The 32-kilometer access road to the mountain top is under construction by the firm of Figalem Ingenieria, S. A. It is scheduled for completion by August 31, 1970. The firm of Mena and Williams,

\*The Las Campanas Observatory is not a part of the Hale Observatories.



Santiago, has signed a contract for the construction of the building and the erection of the dome to house the 40-inch telescope. Adkison made several trips to Chile during the year in connection with these and other matters.

Project personnel under the supervision of Wagner have sunk some 16 test wells and 10 bores in developing and appraising sources of water for the new observatory. These sources are located in the Quebrada las Breas de San Antonio to the south and in the Quebrada Algorrobal to the north. Results are encouraging. A water system for supplying the observatory ridge has been designed and the necessary pipe has been ordered. Orders have been placed also for two diesel-electric generators for supplying the observatory with power.

A detailed topographic map of the Las Campanas ridge, with 1-meter contours, has been produced by the Chilean Air Force. It is proving to be of value in planning future installations. Bonded warehouses have been established on Las

Campanas and at the local project offices at Colina el Pino in La Serena.

The law firm of Carlos Urenda Z. has represented the Institution in Chile and has negotiated with the Government for a law that would give to the Institution franchises and privileges similar to those enjoyed by the European Southern Observatory. (The desired law, No. 17318, Article 48, was passed and published in the *Diario Oficial*, No. 27712, on August 1, 1970.) Mr. Antonio Urrutia A. has represented the Institution in matters relating to mining claims on the Las Campanas land.

On July 31, 1969, a revised agreement was signed between the Carnegie Institution and the University of Chile. This agreement, based on a mutual interest in advancing the science of astronomy, provides that the Institution, in the construction and operation of the observatory, shall benefit from the relevant Chilean law, and that Chilean astronomers shall share in the observing time allotted with the Las Campanas telescopes.

## BIBLIOGRAPHY

- Anderson, Christopher M., The interstellar extinction of stars in H II regions. *Astrophys. J.*, 160, 507-518, 1970.
- Arp, Halton, Distribution of quasi-stellar radio sources on the sky. *Astron. J.*, 75, 1-12, 1970.
- Arp, Halton, Companion galaxies on the ends of spiral arms. *Astron. & Astrophys.*, 4, 418-435, 1969.
- Arp, Halton, Compact companions connected to 3C 371. *Astrophys. Letters* (England), 5, 75-79, 1970.
- Arp, Halton, Companion galaxies connected to NGC 772. *Astrophys. Letters* (England), 5, 257-260, 1970.
- Arp, Halton, Redshifts of very young objects. *Nature*, 223, 386, 1969.
- Arp, Halton, Redshifts of companion galaxies. *Nature*, 225, 1033-1035, 1970.
- Arp, Halton, On the origin of arms in spiral galaxies. *Sky and Telescope*, 38, 2-4, 1969.
- Arp, Halton, and F. Bertola, The large optical extent of M87. *Astrophys. Letters* (England), 4, 23-25, 1969.
- Arp, Halton, and N. Visvanathan, Spectrum and redshift of the optically variable compact radio galaxy 3C 371. *Astrophys. Letters* (England), 5, 73-74, 1970.
- Arp, Halton, *see also* Felten, James E.
- Bahcall, John N., Maarten Schmidt, and James E. Gunn, Are some quasi-stellar objects associated with clusters of galaxies? *Astrophys. J. (Letters)*, 157, L77-L80, 1969.
- Becklin, E. E., and G. Neugebauer, 1.65-19.5-micron observations of the galactic center. *Astrophys. J. (Letters)*, 157, L31-L36, 1969.
- Becklin, E. E., J. A. Frogel, A. R. Hyland, J. Kristian, and G. Neugebauer, An unusual infrared object, IRC + 10216. *Astrophys. J. (Letters)*, 158, L133-L137, 1969.
- Becklin, E. E., *see also* Hyland, A. R.; Oke, J. B.; Sandage, Allan.
- Bergh, Sidney van den, Photometric and spectroscopic observations of globular clusters in the Andromeda Nebula. *Astrophys. J., Suppl. Ser.*, 19, No. 171, 145-174, 1969.
- Bergh, Sidney van den, Photography of the faint outer regions of galaxies. *Astrophys. Letters* (England), 4, 117-119, 1969.



- Bertola, F., *see* Arp, Halton.
- Bhatnagar, A., *see* Howard, Robert.
- Bohlin, J. David, and M. Simon, Coronal densities and magnetic fields from K-coronameter and Type IV radio-burst data. *Solar Physics*, 9, 183-193, 1969.
- Bowen, Ira S., *see* Dennison, E. W.
- Burbidge, G. R., and W. L. W. Sargent, The case of the missing mass. *Comments on Astrophys. & Space Physics*, 1, 220-225, 1969.
- Chase, S., Jr., E. Miner, G. Münch, and G. Neugebauer, Infrared radiometry experiment for Mariner Mars 1971. *Icarus*, 12, 46-47, 1970.
- Chase, S., Jr., *see also* Neugebauer, G.
- Chevalier, R. A., and D. L. Lambert, The excitation of the forbidden coronal lines, I: Fe XIII  $\lambda\lambda 10747$ , 10798, and 3388. *Solar Physics*, 10, 115-134, 1969.
- Chevalier, R. A., and D. L. Lambert, The excitation of the forbidden coronal lines, II: [Ca XV]  $\lambda\lambda 5694$  and 5446. *Solar Physics*, 11, 243-257, 1970.
- Cohen, Judith G., The spectrum of  $\alpha^2$  CVn, II. *Astrophys. J.*, 159, 473-484, 1970.
- Cohen, Judith G., The continuum of M31 in the nuclear bulge. *Publ. Astron. Soc. Pacific*, 82, 760-761, 1970.
- Defouw, Richard J., Thermal-convective instability. *Astrophys. J.*, 160, 659-670, 1970.
- Dennison, Edwin W., Microphotometer design. *Amer. Astron. Soc. Photo Bull.*, No. 2, 7-8, 1970.
- Dennison, E. W., M. Schmidt, and I. S. Bowen, An image-tube spectrograph for the Hale 200-inch telescope, in *Advances in Electronics and Electron Physics*, Vol. 28, pp. 767-771, L. Marton, ed., Academic Press, London and New York, 1969.
- Deutsch, Armin J., Harmonic analysis of rigidly rotating Ap stars. *Astrophys. J.*, 159, 985-1001, 1970.
- Deutsch, Armin J., Mass loss from stars: A review, in *Mass Loss From Stars*, pp. 1-4, M. Hack, ed., Astrophysics and Space Science Library, D. Reidel Publishing Co., Dordrecht-Holland, 1969.
- Deutsch, Armin J., Chromospheric activity in red giants and related phenomena, in *Ultra-violet Stellar Spectra and Related Ground-Based Observations*, Intern. Astron. Union Symp. No. 36, pp. 199-208, L. Houziaux and H. Butler, eds., D. Reidel Publishing Co., Dordrecht-Holland, 1970.
- Deutsch, Armin J., *see also* Keenan, P. C.
- Eggen, Olin J., and Allan Sandage, New photometric data for the old galactic cluster NGC 188: The presence of a gap, chemical composition, and distance modulus. *Astrophys. J.*, 158, 669-684, 1969.
- Eggen, Olin J., *see also* Sandage, Allan.
- Fairall, A. P., *see* Zwicky, Fritz.
- Felten, James E., Halton Arp, and C. R. Lynds, The M87 jet, II, Temperature, ionization, and X-radiation in a secondary-production model. *Astrophys. J.*, 159, 415-423, 1970.
- Frazier, Edward N., *see* Tanenbaum, Andrew W.
- Freeman, Kenneth C., *see* Sandage, Allan.
- Frogel, J. A., *see* Becklin, E. E.
- Garrison, Robert F., *see* Hiltner, W. A.; Keenan, P. C.
- Goldreich, Peter, and William H. Julian, Pulsar electrodynamics. *Astrophys. J.*, 157, 869-880, 1969.
- Goldreich, Peter, and William H. Julian, Stellar winds, *Astrophys. J.*, 160, 971-978, 1970.
- Gott, J. Richard III, James E. Gunn, and Jeremiah P. Ostriker, Runaway stars and the pulsars near the Crab Nebula. *Astrophys. J. (Letters)*, 160, L91-L96, 1970.
- Greenstein, Jesse L., The Lowell suspect white dwarfs. *Astrophys. J.*, 158, 281-294, 1969.
- Greenstein, Jesse L., Mount Wilson and Palomar Observatories; Two rooms with a view, in *Britannica Year Book of Science and the Future*, 1970, pp. 356-363, William Benton, Publisher, Chicago, 1970.
- Greenstein, Jesse L., The symposium on stellar composition and nucleosynthesis. *Comments on Astrophys. & Space Physics*, 2, 85-91, 1970.
- Greenstein, Jesse L., Curve-of-growth method, in *Spectroscopic Astrophysics*, pp. 61-79, G. H. Herbig, ed., University of California Press, Berkeley, 1970.
- Greenstein, Jesse L., Astronomical instruments for faint objects, in *Stellar Astronomy*, Vol. 1, pp. 77-97, Hong-Yee Chiu, John L. Remo, and Robert L. Warasila, eds., Gordon and Breach, New York, 1969.
- Greenstein, Jesse L., Theory and data concerning white dwarfs, in *Stellar Astronomy*, Vol. 2, pp. 83-109, Hong-Yee Chiu, John L. Remo, and Robert L. Warasila, eds., Gordon and Breach, New York, 1969.
- Greenstein, Jesse L., *see also*, Kodaira, Keiichi; Sargent, Anneila I.
- Grygar, J., *see* Heintze, J. R. W.
- Gunn, James E., *see* Bahcall, John N.; Gott, Richard J. III.
- Hardorp, Johannes, and M. Scholz, The atmospheres of Tau Scorpii (B0 V) and Lambda Leporis (B0.5 IV). *Astrophys. J., Suppl. Ser.*, 19, No. 173, 193-233, 1970.
- Harvey, J., *see* Howard, Robert.
- Hatznebeler, H., *see* Neugebauer, G.

- Heintze, J. R. W., On the temperature distribution in the solar atmosphere, in *Theory and Observation of Normal Stellar Atmospheres, Proc. Third Harvard-Smithsonian Conference*, pp. 163-171, Owen Gingerich, ed., The M.I.T. Press, Cambridge, Massachusetts, 1969.
- Heintze, J. R. W., The temperature scale of the B-type stars, in *Theory and Observation of Normal Stellar Atmospheres, Proc. Third Harvard-Smithsonian Conference*, pp. 265-270, Owen Gingerich, ed., The M.I.T. Press, Cambridge, Massachusetts, 1969.
- Heintze, J. R. W., and J. Grygar, Determination of the shape and of the limb darkening at  $\lambda 4230$  of the components of the eclipsing binary SZ Camelopardalis. *Bull. Astron. Inst. Czech.*, 21, 77-91, 1970.
- Hiltner, W. A., R. Garrison, and R. E. Schild, MK spectral types for bright southern OB stars. *Astrophys. J.*, 157, 313-326, 1969.
- Hoag, Arthur A., and William C. Miller, Application of photographic materials in astronomy. *Applied Optics*, 8, 2417-2430, 1969.
- Howard, Robert, and A. Bhatnagar, On the spectrum of granular and intergranular regions. *Solar Physics*, 10, 245-253, 1969.
- Howard, Robert, and J. Harvey, Spectroscopic determinations of solar rotation. *Solar Physics*, 12, 23-51, 1970.
- Howard, Robert, *see also*, Tanenbaum, Andrew W.
- Hudson, Hugh, *see* Zirin, Harold.
- Hyland, A. R., The effective-temperature scale and bolometric corrections for B stars, in *Theory and Observation of Normal Stellar Atmospheres, Proc. Third Harvard-Smithsonian Conference*, pp. 271-279, Owen Gingerich, ed., The M.I.T. Press, Cambridge, Massachusetts, 1969.
- Hyland, A. R., The helium abundance in normal B stars and silicon stars, in *Theory and Observation of Normal Stellar Atmospheres, Proc. Third Harvard-Smithsonian Conference*, pp. 361-364, Owen Gingerich, ed., The M.I.T. Press, Cambridge, Massachusetts, 1969.
- Hyland, A. R., and G. Neugebauer, Infrared observations of Nova Serpentis 1970. *Astrophys. J. (Letters)*, 160, L177-L181, 1970.
- Hyland, A. R., E. E. Becklin, G. Neugebauer, and George Wallerstein, Observations of the infrared object VY Canis Majoris. *Astrophys. J.* 158, 619-628, 1969.
- Hyland, A. R., *see also* Becklin, E. E.
- Ingham, William, *see* Zirin, Harold.
- Julian, William H., *see* Goldreich, Peter.
- Keenan, P. C., A. J. Deutsch, and R. F. Garri-son, The anomalous behavior of AlO bands in Mira variables. *Astrophys. J.*, 158, 261-268, 1969.
- Kodaira, Keiichi, Osawa's peculiar star HD 221568. *Astrophys. J. (Letters)*, 157, L59-L62, 1969.
- Kodaira, Keiichi, The continuous radiation of bright B3V stars. *Astrophys. J.*, 159, 931-944, 1970.
- Kodaira, Keiichi, and M. Scholz, Spectroscopic investigation of B3V stars:  $\iota$  Herculis,  $\eta$  Hydrae, HD 58343. *Astron. & Astrophys.*, 6, 93-113, 1970.
- Kodaira, Keiichi, and W. Unno, New evidence for the oblique-rotator model for  $\alpha^2$  CVn. *Astrophys. J.*, 157, 769-784, 1969.
- Kodaira, Keiichi, Jesse L. Greenstein, and J. B. Oke, The unusual composition of  $+39^\circ 4926$ . *Astrophys. J.*, 159, 485-512, 1970.
- Kowal, Charles T., The structure of the Virgo clusters as determined from supernovae. *Publ. Astron. Soc. Pacific*, 81, 608-612, 1969.
- Kowal, Charles T., Wallace L. W. Sargent, and Fritz Zwicky, The 1969 Palomar supernova search. *Publ. Astron. Soc. Pacific*, 82, 736-740, 1970.
- Kraft, Robert P., Stellar rotation, in *Spectroscopic Astrophysics*, pp. 385-422, George H. Herbig, ed., University of California Press, Berkeley, 1970.
- Kraft, Robert P., W. Krzeminski, and George S. Mumford, Binary stars among cataclysmic variables, XI, Photoelectric and spectroscopic observations of the dwarf nova Z Camelopardalis. *Astrophys. J.*, 158, 589-598, 1969.
- Kristian, Jerome, The central star: photometric optical observations. *Publ. Astron. Soc. Pacific*, 82, 456-469, 1970.
- Kristian, Jerome, *see also* Becklin, E. E.
- Krzeminski, W., *see* Kraft, Robert P.; Mumford, George S.
- Lambert, D. L., Intrinsic reddening of Eta Carinae. *Nature*, 223, 726-728, 1969.
- Lambert, D. L., and E. A. Mallia, The forbidden line [Ca II]  $\lambda 7323$  in the Fraunhofer spectrum. *Solar Physics*, 10, 311-314, 1969.
- Lambert, D. L., and A. D. Thackeray, Forbidden lines of Ni IV in the spectrum of RR Telescopii. *Astrophys. & Space Sci.* 5, 283-288, 1969.
- Lambert, D. L., *see also* Chevalier, R. A.
- Larson, Richard B., Numerical calculations of the dynamics of a collapsing protostar. *Monthly Notices Roy. Astron. Soc.*, 145, 271-296, 1969.
- Larson, Richard B., The emitted spectrum of a protostar. *Monthly Notices Roy. Astron. Soc.*, 145, 297-308, 1969.

- Lasker, Barry M., On the homogeneity of the spectral energy distribution among giant E and S0 galaxies and other results. *Astron. J.* 75, 21-33, 1970.
- Lynds, C. R., *see* Felten, James E.
- McKenzie, David, *see* Zirin, Harold.
- Mallia, E. A., *see* Lambert, D. L.
- Michaud, Georges, Diffusion processes in A-pec stars. *Astrophys. J.*, 160, 641-658, 1970.
- Miller, William C., Cutting plates for astronomical uses. *Amer. Astron. Soc. Photo-Bulletin*, No. 1, 10-12, 1969.
- Miller, William C., Enlarged star charts from prints or plates. *Amer. Astron. Soc. Photo-Bulletin*, No. 1, 13-14, 1969.
- Miller, William C., Reduction of low-intensity reciprocity failure in photographic plates by controlled baking. *Amer. Astron. Soc. Photo-Bulletin*, No. 2, 15-17, 1970.
- Miller, William C., *see also* Hoag, Arthur A.
- Miner, E., *see* Chase, S., Jr.; Neugebauer, G.
- Mumford, George S., and W. Krzeminski, Binary stars among cataclysmic variables, X, Photoelectric observations of EM Cygni. *Astrophys. J., Suppl. Ser.*, 18, No. 166, 429-442, 1969.
- Mumford, George S., *see also* Kraft, Robert P.
- Münch, Guido, Interstellar gas, in *Spectroscopic Astrophysics*, pp. 295-319, George H. Herbig, ed., University of California Press, Berkeley, 1970.
- Münch, Guido, *see also* Chase, S., Jr.; Neugebauer, G.; Trafton, Laurence M.
- Neugebauer, G., G. Münch, S. C. Chase, Jr., H. Hatzenbeler, E. Miner, and D. Schofield, Mariner-Mars 1969: a preliminary report, in *NASA SP-225*, Chap. 8, pp. 105-109, Washington, D.C., 1969.
- Neugebauer, G., G. Münch, S. C. Chase, Jr., H. Hatzenbeler, E. Miner, and D. Schofield, Mariner 1969: Preliminary results of the infrared radiometer experiment. *Science*, 166, 98-99, 1969.
- Neugebauer, G., *see also* Becklin, E. E.; Chase, S., Jr.; Hyland, A. R.; Oke, J. B.; Sandage, Allan; Zwicky, Fritz.
- Newell, E. B., A. W. Rodgers, and Leonard Searle, The blue horizontal-branch stars of  $\omega$  Centauri. *Astrophys. J.*, 156, 597-608, 1969.
- Newell, E. B., A. W. Rodgers, and Leonard Searle, The blue horizontal-branch stars of  $\nu$  Centauri. *Astrophys. J.*, 158, 699-710, 1969.
- Oke, J. B., Photoelectric spectrophotometry of B264. *Astrophys. J. (Letters)*, 158, L9-L10, 1969.
- Oke, J. B., and W. L. W. Sargent, Seyfert galaxies. *Science Journal*, 6, 57-61, 1970.
- Oke, J. B., and R. Schild, Recent absolute calibration work at Palomar Mountain, in *Ultraviolet Stellar Spectra and Related Ground-Based Observations, Intern. Astron. Union Symp. No. 36*, pp. 13-17, L. Houziaux and H. Butler, eds., D. Reidel Publishing Co., Holland, 1970.
- Oke, J. B., G. Neugebauer, and E. E. Becklin, Absolute spectral-energy distribution of quasi-stellar objects from 0.3 to 2.2 microns. *Astrophys. J.*, 159, 341-355, 1970.
- Oke, J. B., *see also* Kodaira, Keiichi; Zwicky, Fritz.
- Ostriker, Jeremiah P., *see* Gott, J. Richard, III.
- Peach, John V., The determination of the deceleration parameter and the cosmological constant from the redshift-magnitude relation. *Astrophys. J.*, 159, 753-764, 1970.
- Preston, George W., Partial resolution of Zeeman patterns in the spectrum of 53 Camelopardalis. *Astrophys. J.*, 157, 247-252, 1969.
- Preston, George W., The periodic variability of 78 Virginis. *Astrophys. J.*, 158, 242-250, 1969.
- Preston, George W., The variability of 21 Persei. *Astrophys. J.*, 158, 251-260, 1969.
- Preston, George W., The mean surface magnetic field of  $\beta$  Coronae Borealis. *Astrophys. J.*, 158, 1081-1084, 1969.
- Preston, George W., The large variable field of HD 126515 and its implications for the rigid-rotator model of magnetic stars. *Astrophys. J.*, 160, 1059-1070, 1970.
- Preston, George W., The quadratic Zeeman effect and large magnetic fields in white dwarfs. *Astrophys. J.*, 160, L143-L146, 1970.
- Preston, George W., The rotation of the Ap stars from the point of view of the rigid rotator model, in *Stellar Rotation, Intern. Astron. Union Coll. No. 4*, pp. 117-126, A. Slettebak, ed., D. Reidel Publishing Co., Holland, 1970.
- Preston, George W., and Sidney C. Wolff, The very slow spectrum, magnetic and photometric variations of HD 9996. *Astrophys. J.*, 160, 1071-1078, 1970.
- Racine, René, Ros 4, a distant open cluster associated with nebulosities. *Astron. J.*, 74, 816-817, 1969.
- Racine, René, Photometric calibration of direct plates. *Astron. J.*, 74, 1073-1078, 1969.
- Rodgers, A. W., *see* Newell, E. B.
- Sandage, Allan, Did the world begin? in *Astronomical Insights*, pp. 71-78, Peter Pockly, ed., published by the Australian Broadcasting Commission, Sydney, 1970.
- Sandage, Allan, The reddening, age difference, and helium abundance of the globular clusters



- M3, M13, M15, and M92. *Astrophys. J.*, 157, 515-532, 1969.
- Sandage, Allan, New subdwarfs, II, Radial velocities, photometry, and preliminary space motions for 112 stars with large proper motions. *Astrophys. J.*, 158, 1115-1136, 1969.
- Sandage, Allan, Cosmology: A search for two numbers. *Physics Today*, 23, 34-41, 1970.
- Sandage, Allan, and Olin J. Eggen, Isochrones, ages, evolutionary deviation curves, and the composite C-M diagram for old galactic clusters. *Astrophys. J.*, 158, 685-698, 1969.
- Sandage, Allan, and G. A. Tammann, The double Cepheid CE Cassiopeiae in NGC 7799: Tests of the theory of the instability strip and the calibration of the period-luminosity-color relation. *Astrophys. J.*, 157, 683-708, 1969.
- Sandage, Allan, and N. Visvanathan, Colors, linear polarization, and preliminary mapping of the magnetic field for the outer filaments in the exploding galaxy M82. *Astrophys. J.*, 157, 1065-1074, 1969.
- Sandage, Allan, E. E. Becklin, and G. Neugebauer, *UBVR/IKL* photometry of the central region of M31. *Astrophys. J.*, 157, 55-68, 1969.
- Sandage, Allan, Kenneth C. Freeman, and N. R. Stokes, The intrinsic flattening of E, S0, and spiral galaxies as related to galaxy formation and evolution. *Astrophys. J.*, 160, 831-834, 1970.
- Sandage, Allan, *see also* Eggen, Olin J.
- Sargent, Anneila I., Jesse L. Greenstein, and Wallace L. W. Sargent, A search for neon in the spectra of peculiar A and B stars. *Astrophys. J.*, 157, 757-768, 1969.
- Sargent, Wallace L. W., The spectra and redshifts of thirty Markarian galaxies with ultra-violet continua. *Astrophys. J.*, 159, 765-772, 1970.
- Sargent, Wallace L. W., A spectroscopic survey of compact and peculiar galaxies. *Astrophys. J.*, 160, 405-428, 1970.
- Sargent, Wallace L. W., K. M. Strom, and S. E. Strom, An analysis of the peculiar A star HD 204411. *Astrophys. J.*, 157, 1265-1278, 1969.
- Sargent, Wallace L. W., *see also* Burbidge, G. R.; Kowal, Charles T.; Oke, J. B.; Sargent, Anneila I.; Zwicky, Fritz.
- Schild, Rudolph E., HDE 310376: A rapid variable star similar to Sco-XR-1. *Astrophys. J.*, 157, 709-716, 1969.
- Schild, R. E., *see also* Hiltner, W. A.; Oke, J. B.
- Schmidt, Maarten, Observed properties of quasi-stellar objects, in *Proc. Intern. Astron. Union Symp. on Contemporary Physics*, (Trieste, 1968), Vol. I, pp. 467-469, published by the International Centre for Theoretical Physics of the International Atomic Energy Agency, Vienna, 1969.
- Schmidt, Maarten, *see also* Bahcall, John N.; Dennison, E. W.
- Schofield, D., *see* Neugebauer, G.
- Scholz, M., *see* Hardorp, Johannes.; Kodaira, Keiichi.
- Searle, Leonard, *see* Newell, E. B.
- Simon, Michal, Particle acceleration during the 1966-1967 radio burst of 3C273. *Astrophys. J.*, 158, 865-869, 1969.
- Simon, Michal, and D. L. P. Strange, Bremsstrahlung radiation in intense magnetic fields. *Nature*, 224, 49-50, 1969.
- Simon, Michal, and Harold Zirin, The coarse structure of the solar atmosphere. *Solar Physics*, 9, 317-327, 1969.
- Simon, Michal, *see also* Bohlin, J. David.
- Stokes, N. R., *see* Sandage, Allan.
- Strange, D. L. P., *see* Simon, Michal.
- Strom, K. M., *see* Sargent, Wallace L. W.
- Strom, S. E., *see* Sargent, Wallace L. W.
- Strong, John, and Fritz Zwicky, Objective transmission gratings for large Schmidt telescopes. *Applied Optics*, 8, 1021, 1969.
- Tammann, G. A., Search for periodic Comet Temple-Swift. *Intern. Astron. Union Circular*, No. 2181, 1969.
- Tammann, G. A., *see also* Sandage, Allan.
- Tanenbaum, Andrew W., John M. Wilcox, Edward N. Frazier, and Robert Howard, Solar velocity fields: 5-minute oscillations and supergranulation. *Solar Physics*, 9, 328-426, 1969.
- Thackeray, A. D., *see* Lambert, D. L.
- Trafton, Laurence M., and Guido Münch, The structure of the atmospheres of the major planets. *J. Atmos. Sci.*, 26, 813-825, 1969.
- Unno, W., *see* Kodaira, Keiichi.
- Veeder, Glenn J., and Harold Zirin, The chromospheric magnetograph. *Solar Physics*, 12, 391-402, 1970.
- Visvanathan, N., *see* Arp, Halton; Sandage, Allan.
- Vorpahl, J., and Harold Zirin, Identification of the hard X-ray pulse in the flare of 11-12 September 1968. *Solar Physics*, 11, 285-290, 1970.
- Warlerstein, George, *see* Hyland, A. R.
- Weart, Spencer R., and Harold Zirin, Round-the-clock solar movies. *Sky and Telescopes*, 37, 296-298, 1969.

- Westphal, J. A., Observations of localized 5-micron radiation from Jupiter. *Astrophys. J. (Letters)*, 157, L63-L64, 1969.
- Wilcox, John M., *see also* Tanenbaum, Andrew W.
- Wilson, Olin C., Dependence of chromospheric emission upon bolometric luminosity for the Hyades. *Astrophys. J.*, 160, 225-232, 1970.
- Wilson, Olin C., and Sir Richard Woolley, Calcium emission intensities as indicators of stellar age. *Monthly Not. Roy. Astron. Soc.*, 148, 463-475, 1970.
- Wolff, Sidney C., *see* Preston, George W.
- Woolley, Sir Richard, *see* Wilson, Olin C.
- Zirin, Harold, The Big Bear Solar Observatory. *Sky and Telescope*, 39, 3-7, 1970.
- Zirin, Harold, Interpretation of XUV spectroheliograms. *Solar Physics*, 9, 77-87, 1969.
- Zirin, Harold, Coronagraph observations of the coronal condensation of 4 Feb 62. *Solar Physics*, 11, 497-512, 1970.
- Zirin, Harold, William Ingham, Hugh Hudson, and David McKenzie, De-occultation X-ray event of 2 December 1967. *Solar Physics*, 9, 269-277, 1969.
- Zirin, Harold, *see also* Simon, Michal; Veeder, Glenn J.; Vorpahl, J.; Weart, Spencer R.
- Zwicky, Fritz, Systems for extracting elements and chemical compounds from lunar materials needed for manned operations on the Moon, in *Applied Sciences Research and Utilization of Lunar Resources, Proc. Fourth Lunar Intern. Lab. (LIL) Symp.*, pp. 187-199, Frank J. Malina, ed., Pergamon Press, Oxford and New York, 1970.
- Zwicky, Fritz, Morphology of justice in the space age and the boundaries of outer space. *Astronomica Acta*, 14, 615-626, 1969.
- Zwicky, Fritz, Circular Letter on Supernovae, No. 10, California Institute of Technology, May 1970.
- Zwicky, Fritz, Katalog von Galaxien und Galaxienhaufen. *Die Sterne*, 45, 115-116, 1969.
- Zwicky, Fritz, Catalogue of galaxies and of clusters of galaxies. *Observatory*, 89, 156, 1969.
- Zwicky, Fritz, Das Morphologische Weltbild. *Proc. Symp. for "Gestalt und Gestaltung,"* published by Schweizerischer Graphikerverband, Zürich, 1970.
- Zwicky, Fritz, Some results of the international search for supernovae, in *Supernovae and Their Remnants*, pp. 1-22, P. J. Brancazio and A. G. W. Cameron, eds., Gordon & Breach, New York, 1969.
- Zwicky, Fritz, J. B. Oke, G. Neugebauer, W. L. W. Sargent, and A. P. Fairall, The variable compact galaxy ZW 0039.5 + 4003. *Publ. Astron. Soc. Pacific*, 82, 93-98, 1970.
- Zwicky, Fritz, *see also* Kowal, Charles T.

## STAFF AND ORGANIZATION

Dr. Armin J. Deutsch died on November 11, 1969. A distinguished stellar spectroscopist, Deutsch came from the Harvard College Observatory to join the staff of the Observatories on February 1, 1951. While at Harvard he had become interested in the peculiar A-type stars and spectrum variables. One of his major contributions was in elucidating the subject and in advancing the oblique rotator model to account for the variations in the spectra and magnetic fields of these stars. Deutsch was also well known for his pioneering work on mass loss by red giant stars. His spectroscopic observations with the 200-inch telescope placed this concept on a firm footing and provided evidence for an essential stage in the evolution of stars. In recent years Deutsch had advanced ideas for basic improvements in the techniques of stellar

spectroscopy through the development of digital image dissector tubes with associated computer systems.

At the time of his death, Deutsch was a member of the Observatory Committee. He had also ably served the Observatory in a number of other capacities.

### Research Division

#### Staff Members

Halton C. Arp  
 Horace W. Babcock, *Director*  
 Edwin W. Dennison  
 Jesse L. Greenstein<sup>1</sup>  
 James E. Gunn<sup>2</sup>  
 Robert F. Howard  
 Jerome Kristian  
 Robert B. Leighton<sup>3</sup>  
 Guido Münch<sup>4</sup>  
 J. Beverley Oke, *Associate Director*<sup>4</sup>  
 George W. Preston III

Bruce H. Rule, *Chief Engineer*  
 Allan R. Sandage  
 Wallace L. W. Sargent <sup>5</sup>  
 Leonard T. Searle  
 Maarten Schmidt <sup>4</sup>  
 Arthur H. Vaughan, Jr.  
 Olin C. Wilson  
 Harold Zirin <sup>6</sup>

*Staff Members Engaged in Post-Retirement Studies*

Ira S. Bowen  
 Alfred H. Joy  
 Henrietta H. Swope  
 Fritz Zwicky

*Research Associate*

Gustav Tammann

*Staff Associates*

John N. Bahcall <sup>7</sup>  
 Andrew P. Ingersoll <sup>8</sup>  
 Gerry Neugebauer <sup>3</sup>  
 James A. Westphal <sup>9</sup>

*Librarian*

Marjorie A. Henderson

*Carnegie Fellows*

Arvind Bhatnagar  
 Michael V. Penston  
 Deane M. Peterson

*Research Fellows*

David R. Branch  
 J. David Bohlin  
 Richard A. Defouw <sup>10</sup>  
 Peter Foukal  
 A. R. Hyland  
 William H. Julian <sup>11</sup>  
 Keiichi Kodaira <sup>12</sup>  
 David L. Lambert <sup>13</sup>  
 Stephen W. Prata  
 James J. Rickard <sup>14</sup>  
 Michael Scholz <sup>11</sup>  
 Michal Simon <sup>13</sup>

*Carnegie-Chilean Fellow*

Eduardo Hardy

*Senior Research Assistants*

Sylvia Burd  
 Dorothy D. Locanthi <sup>15</sup>  
 A. Louise Lowen

Anneila Sargent  
 Grace Vess

*Research Assistants*

John Adkins  
 John E. Boyden  
 Frank J. Brueckel  
 Lucy M. Carruthers <sup>16</sup>  
 Ken D. Clardy  
 Thomas A. Cragg  
 Basil N. Katem  
 Charles Kowal  
 Gary L. McQueary  
 Gail J. Pruss  
 Malcolm S. Riley

*Student Observers*

Saul J. Adelman  
 William G. Bagnuolo  
 John H. Bieging  
 Kenneth A. Braly  
 Harvey Butcher  
 Clark G. Christensen  
 Judith G. Cohen  
 John Cronin  
 Jay A. Frogel  
 Sol Giles  
 Olav L. Hansen  
 Paul M. Harvey  
 Gordon Hoover  
 Robert Jackson  
 Sai Kit Law  
 Dennis Matson  
 August Oemler, Jr.  
 Valdar Oinas  
 Bruce Penrose  
 Sven E. Persson  
 David B. Shaffer  
 Larry Soderblom  
 Henry Tye  
 Glenn J. Veeder, Jr.

*Photographic Department*

John R. Bedke, Photographer  
 John Difley, Photographer <sup>17</sup>  
 William C. Miller, Research Photographer  
 Paula R. Swanson, Solar Photographic Assistant

*Instrument Design and Construction*

Lawrence E. Blakeé, Supervisor Electronic Services  
 Maynard K. Clark, Senior Engineering Assistant  
 John P. Cowley, Laboratory Specialist



Floyd E. Day, Head Optician  
 Stephen Doro, Machinist  
 Raymond Dreiling, Machinist  
 Earle B. Emery, Research Engineer  
 Eugene B. Fair, Optician  
 Robert D. Georgen, Machinist  
 Robert E. Goff, Senior Laboratory Assistant  
 Donn M. Hall, Electronics Engineer  
 H. Robert Hoggan, Design Specialist  
 Joseph P. Hsu, Associate Electronics Engineer  
 William H. Huff, Electronic Technician  
 Fred Idzinga, Senior Electronic Specialist  
 Melvin W. Johnson, Optician  
 Margaret Katz, Technical Assistant  
 Richard E. Kelly, Junior Electronic Technician  
 Leroy M. Kimoto, Electronic Specialist  
 Wilfred H. Leckie, Senior Draftsman  
 Deborah Levin, Technical Assistant<sup>18</sup>  
 Ernest O. Lorenz, Engineering Field Assistant<sup>19</sup>  
 Walter M. Nagao, Junior Mechanic  
 Daniel Netto, Engineering Designer  
 Stephen L. Nowlin, Technical Aide  
 Frederick G. O'Neil, Shop Foreman  
 Martin J. Olsiewski, Electronic Specialist  
 Edward H. Rehnborg, Senior Engineer  
 Rudolf E. Ribbens, Designer and Shop Superintendent  
 Howard G. Sachs, Group Supervisor  
 Neil S. Schwartz, Laboratory Assistant  
 Edward H. Snoddy, Engineering Designer  
 Robert G. Stiles, Optician  
 David Thompson, Senior Technical Assistant  
 William Thompson, Electronics Technician  
 Eli A. Tilajef, Junior Engineer  
 Virgal Z. Vaughan, Electronic Specialist  
 Madeleine B. Williams, Draftswoman  
 Felice Woodworth, Draftswoman-Illustrator  
 George M. Yamamoto, Designer

### *Maintenance and Operation*

#### *Mount Wilson Observatory and Offices*

Fern V. Borgen, Telephone Operator-Typist  
 Clyde B. Bornhurst, Mountain Superintendent  
 Herman E. Carpentier, Carpenter  
 Hugh T. Couch, Superintendent of Buildings and Grounds

Helen S. Czaplicki, Typist-Editor  
 Sue H. DeWitt, Secretary  
 Hazel M. Fulton, Stewardess  
 Elsie E. Hanlon, Stewardess<sup>17</sup>  
 Eugene L. Hancock, Night Assistant  
 Judith A. Harstine, Secretary  
 Laurence B. Herscher, Laborer<sup>20</sup>  
 Rinaldo M. Jacques, Head Steward<sup>21</sup>  
 Peter Mastrosimoni, Night Assistant  
 Alfred H. Olmstead, Custodian  
 Glen Sanger, Driver  
 Henry P. Schaefer, Night Assistant<sup>22</sup>  
 Clair E. Sharp, Accountant  
 William D. St. John, Custodian  
 Benjamin B. Traxler, Mountain Superintendent<sup>22</sup>  
 Frank Trylko, Custodian  
 Warren E. Weaver, Assistant Mountain Superintendent  
 Fredrick P. Woodson, Assistant to the Director

#### *Palomar Observatory and Robinson Laboratory*

Carol N. Anthony, Clerk-Typist  
 Ray L. Ballard, Senior Administrative Assistant  
 Catherine S. Bennett, Secretary<sup>23</sup>  
 Betty Browne, Secretary  
 Jan Adriian Bruinsma, Painter and General Maintenance  
 Maria J. Bruinsma, Stewardess  
 Juan R. Carrasco, Night Assistant  
 Patricia Ebert, Secretary  
 Eleanor Ellison, Librarian  
 Sue A. Elwell, Secretary  
 Beulah Greenlee, Stewardess  
 Frank V. Greenlee, Sr., Custodian  
 Daniel J. Hargraves, Mechanic and Relief Night Assistant  
 Della S. Harris, Department Clerk  
 Liselotte M. Hauck, Secretary  
 Victor A. Hett, Maintenance Mechanic  
 Helen Holloway, Secretary  
 Charles E. Kearns, Assistant Mountain Superintendent  
 J. Luz Lara, Mechanic  
 Carl D. Palm, Night Assistant  
 Anne L. Parrill, Secretary  
 Marilynne J. Rice, Secretary  
 Kenneth R. Robison, Night Assistant and Mechanic  
 Gary M. Tuton, Senior Night Assistant

William C. Van Hook, Mountain Superintendent

Paul Van Ligten, Maintenance Mechanic and Electrical

Ardith V. Walthers, Secretary <sup>24</sup>

*Carnegie Southern Observatory  
Pasadena, California*

Bruce Adkison, Associate for Administration

Wilma J. Berkebile, Secretary

<sup>1</sup> Professor of Astrophysics and Executive Officer for Astronomy, California Institute of Technology.

<sup>2</sup> Assistant Professor of Astrophysics, California Institute of Technology.

<sup>3</sup> Professor of Physics, California Institute of Technology.

<sup>4</sup> Professor of Astronomy, California Institute of Technology.

<sup>5</sup> Associate Professor of Astronomy, California Institute of Technology.

<sup>6</sup> Professor of Astrophysics, California Institute of Technology.

<sup>7</sup> Associate Professor of Theoretical Physics, California Institute of Technology.

<sup>8</sup> Assistant Professor of Planetary Science, California Institute of Technology.

*La Serena, Chile*

Donald L. Buck, Project Supervisor <sup>14</sup>

Manuel Casanova, Field Supervisor

Cecilia Espinoza, Secretary-Receptionist

Jens P. Haahr, Project Supervisor <sup>25</sup>

Pedro La Paz, Utility Employee

Fernando Peralta, Field Supervisor

Leonardo Peralta, Driver

Hernán Santana, Mechanic

Eduardo Toledo, Accountant

Manfred Wagner, Project Supervisor

<sup>9</sup> Senior Research Fellow in Planetary Science, California Institute of Technology.

<sup>10</sup> Resigned June 20, 1970.

<sup>11</sup> Resigned September 15, 1969.

<sup>12</sup> Resigned October 15, 1969.

<sup>13</sup> Resigned August 31, 1969.

<sup>14</sup> Resigned September 30, 1969.

<sup>15</sup> Resigned September 12, 1969.

<sup>16</sup> Resigned June 15, 1970.

<sup>17</sup> Resigned February 28, 1970.

<sup>18</sup> Resigned June 6, 1970.

<sup>19</sup> Resigned March 9, 1970.

<sup>20</sup> Terminated December 30, 1969.

<sup>21</sup> Resigned June 30, 1970.

<sup>22</sup> Retired June 30, 1970.

<sup>23</sup> Resigned May 22, 1970.

<sup>24</sup> Resigned September 22, 1969.

<sup>25</sup> Resigned May 15, 1970.

# *Geophysical Laboratory*

*Washington, District of Columbia*

Philip H. Abelson

*Director*





# Contents

Introduction . . . . .	135	Thermodynamic analysis of phase equilibria in the system $\text{Fe}_2\text{TiO}_4\text{-Fe}_3\text{O}_4\text{-TiO}_2$ (Rumble) . . . . .	198
Experimental Petrology . . . . .	141	Behavior of thermocouples in the single-stage piston-cylinder apparatus (Mao and Bell) . . . . .	207
Contemporaneous rhyolite and basalt (Yoder) . . . . .	141	Investigations of Lunar and Related Materials . . . . .	216
Introduction and diffusion of argon into natural albite (Laughlin and Yoder) . . . . .	145	Anatomy of a mantled pigeonite from <i>Oceanus Procellarum</i> (Boyd) . . . . .	216
Liquidus relations and subsolidus reactions in some plagioclase-bearing systems (Emslie) . . . . .	148	Analysis of olivine crystals in Apollo 12 rocks (Bell) . . . . .	228
Kosmochlor and the chromite-plagioclase association (Yoder and Kullerud) . . . . .	155	Apollo 12: opaque oxides (Haggerty and Meyer) . . . . .	229
The joins $\text{Na}_2\text{O} \cdot 5\text{MgO} \cdot 12\text{SiO}_2$ -sodium disilicate and $2\text{Na}_2\text{O} \cdot 3\text{MgO} \cdot 5\text{SiO}_2$ -sodium disilicate in the system $\text{Na}_2\text{O-MgO-SiO}_2$ (Schairer and Yoder) . . . . .	157	Investigations of Apollo 12 samples (Taylor, Kullerud, and Bryan) . . . . .	238
The compound $3\text{Na}_2\text{O} \cdot 8\text{SiO}_2$ in the system $\text{Na}_2\text{O-SiO}_2$ (Schairer and Yoder) . . . . .	160	Melting relations of materials of lunar composition (Muan and Schairer) . . . . .	243
The system jadeite ( $\text{NaAlSi}_2\text{O}_6$ )-anorthite ( $\text{CaAl}_2\text{Si}_2\text{O}_8$ ) at high pressures (Mao) . . . . .	163	Meteorites (Bryan and Kullerud) . . . . .	245
Subsolidus reactions of jadeite ( $\text{NaAlSi}_2\text{O}_6$ ) and albite ( $\text{NaAlSi}_3\text{O}_8$ ) (Bell and Mao) . . . . .	168	Chemical and Mineralogical Petrography Petrology and geochemistry of volcanic rocks from Tonga (Bryan and Ewart) . . . . .	249
The melting behavior of diopside-aegirite pyroxenes at high pressures (Cassie) . . . . .	170	Coral Sea drift pumice from Eua Island, Tonga (Bryan) . . . . .	258
The join diopside-pyrope- $\text{H}_2\text{O}$ at 10 kb: its bearing on the melting of peridotite, the ACF metamorphic facies, and the gedrite-hornblende miscibility gap (Yoder) . . . . .	176	Mid-Atlantic Ridge near $45^\circ\text{N}$ : magnetism and magnetic mineralogy (Haggerty and Irving) . . . . .	259
Andradite stability in air at 1 atm, $\text{O}_2$ up to 30 kb, and $\text{H}_2\text{O} + \text{O}_2$ up to 20 kb total pressure (Huckenholz and Yoder) . . . . .	182	Petrography and mineral chemistry of a differentiated flow of Picture Gorge basalt near Spray, Oregon. Geologic setting and mechanism of differentiation (Lindsley, Smith, and Haggerty) . . . . .	264
Synthesis and preliminary results on the stability of aenigmatite ( $\text{Na}_2\text{Fe}_3\text{TiSi}_6\text{O}_{20}$ ) (Lindsley) . . . . .	188	Chemical variations in pyroxene and olivine from Picture Gorge basalt (Smith and Lindsley) . . . . .	269
Mössbauer spectroscopy of synthetic Ca-Fe pyroxenes (Dowty and Lindsley) . . . . .	190	Chemical variations in the feldspars (Lindsley and Smith) . . . . .	274
Thermal expansion of pyrophyllite (Taylor and Bell) . . . . .	193	Phase relations of Fe-Ti oxides and aenigmatite: oxygen fugacity of the pegmatoid zones (Lindsley and Haggerty) . . . . .	278
Equilibrium studies in $\text{ZnO}$ -containing silicate systems . . . . .	194	Final products of the differentiation process (Smith and Lindsley) . . . . .	284
The effects of pressure in the $\text{Zn}_2\text{SiO}_4\text{-Co}_2\text{SiO}_4$ system (Taylor, Bell, and Muan) . . . . .	194	Iron-rich pyroxenes (Smith) . . . . .	285
The system $\text{ZnO-CoO-SiO}_2$ at 1 atm (Muan) . . . . .	195	Chloritoid-staurolite quartzites from the Moosilauke quadrangle, New Hampshire (Rumble) . . . . .	290
Notes on the thermal behavior of loughlinite (Schairer and Yoder) . . . . .	197	Computer reduction of electron probe data (Hadidiacos, Finger, and Boyd) . . . . .	294
		Statistical Petrography (Chayes) . . . . .	295
		Distribution of relative silica saturation in Cenozoic basaltic rocks . . . . .	295

Miscellaneous studies in statistical petrography . . . . .	299	Finger) . . . . .	318
Crystallography . . . . .	302	Pyrite-type compounds (Taylor and Kullerud) . . . . .	322
Fe/Mg ordering in olivines (Finger) .	302	A high-pressure polymorph of troilite, FeS (Taylor and Mao) . . . . .	325
Internal equilibrium in a spinel (Finger) . . . . .	305	Biogeochemistry . . . . .	327
Chalcopyrite solid solution (Kullerud and Donnay) . . . . .	306	Reactions of amino acids with natural and artificial humus and kerogens (Abelson and Hare) . . . . .	327
Structural hypothesis for mackelveyite, Ba(Ca,RE,Na, . . .) <sub>1.00</sub> (CO <sub>3</sub> ) <sub>2</sub> (Donnay) . . . . .	309	Humic acids in a Recent marine sediment (Hoering) . . . . .	334
Additional data on chaoite (Whittaker, Donnay, and Lonsdale) . . . . .	311	Isotopic Investigations in Geochemistry and Geochronology (Krogh, Davis, and Hart) . . . . .	337
Biocrystallography . . . . .	312	Isotopic ages along the Grenville Front in the Bell Lake area, southwest of Sudbury, Ontario (Krogh, Davis, and Frarey) . . . . .	337
Minimal surfaces (Donnay) . . . . .	312	Paragneiss studies in the Georgian Bay area 90 km southeast of the Grenville Front (Krogh and Davis) .	339
Crystallographic observations on regenerated shells of <i>Ampullarius</i> (Donnay) . . . . .	313	A simplified technique for the dissolution of zircons and the isolation of uranium and lead (Krogh) . . . . .	341
Crystallographic observations on a naturally occurring branched spine of <i>Strongylocentrotus purpuratus</i> (Donnay and Heatfield) .	314	Staff Activities . . . . .	344
Fractured and regenerated spines of <i>Arbacia punctulata</i> (Donnay and Heatfield) . . . . .	314	Washington Crystal Colloquium . .	344
Corrigendum for "Fifty years of X-ray crystallography at the Geophysical Laboratory, 1919-1969" . . . . .	314	Lectures . . . . .	344
Studies of Sulfides . . . . .	315	Petrologists' Club . . . . .	346
Mineral assemblages in the Cu-Fe-S-O system (Taylor and Kullerud) .	315	Bibliography . . . . .	346
Structural refinement and composition of mackinawite (Taylor and		References Cited . . . . .	348
		Personnel . . . . .	359



## INTRODUCTION

One of the most exciting scientific opportunities of this decade came last year with the return of the successful Apollo missions. The Geophysical Laboratory was among the organizations receiving lunar samples. Very quickly many similarities and differences between lunar and terrestrial rocks were noted. It was evident that at least portions of the moon had at one time been molten and that the mineralogy of the specimens was reminiscent of terrestrial basalts. The differences were more interesting than the similarities. The minerals are entirely fresh and unaltered, with none of the weathering effects commonly found in rocks on earth; indeed, water was not even present in the form of hydrous minerals. It was also evident that conditions on the moon had been more highly reducing than those in the crust of the earth. There were important differences in the bulk composition. The lunar rocks contain relatively abundant titanium and chromium, whereas the more volatile elements, such as the alkali metals and lead, are depleted.

With this quick survey completed a number of the staff members began more detailed investigations using the electron microprobe and other optical and X-ray equipment. Almost every day for many weeks new observations were made and the entire Laboratory shared an atmosphere of stimulating excitement.

In the examination and interpretation of the lunar specimens the Laboratory had many fine assets—skilled staff, excellent equipment, and long experience with the kinds of minerals found on the moon. Some of the lunar minerals have not been found in terrestrial rocks, but they had previously been synthesized and studied at the Laboratory. Since other laboratories were also actively investigating the lunar specimens our staff chose important aspects not likely to be

examined by many other scientists. A major effort was devoted to the study of opaque minerals.

The opaque minerals in the Apollo 11 and Apollo 12 samples form a unique assemblage. The major phase is ilmenite, and members of the chromite ulvöspinel series, members of the armalcolite series, troilite and metallic iron occur in small quantities.

Armalcolite, a new mineral with the pseudobrookite structure, is intermediate in composition between the end members  $\text{FeTi}_2\text{O}_5$  and  $\text{MgTi}_2\text{O}_5$ . It was discovered independently at a number of laboratories, including the Geophysical Laboratory, and its occurrence was first described earlier this year at the Lunar Science Conference in Houston (Haggerty *et al.*, 1970a). It was named in honor of the Apollo 11 astronauts Armstrong, Aldrin and Collins. Armalcolite differs from pseudobrookite-like minerals on earth in that it contains no ferric iron, as a consequence of the very low partial pressure of oxygen that existed on the moon during the crystallization of these lavas.

The lunar spinels are also distinctive in chemical composition and show a wide variability. Haggerty has shown that analyses of spinels from the Apollo 12 lavas fall into two separate and distinct compositional groups along the join ulvöspinel ( $\text{Fe}_2\text{TiO}_4$ )-chromite ( $\text{FeCr}_2\text{O}_4$ ). Optically isotropic spinels are chromium rich and contain 45–60 mole %  $\text{FeCr}_2\text{O}_4$  and 12 to 25%  $\text{Fe}_2\text{TiO}_4$ . Those in the optically anisotropic group are richer in Fe and Ti and contain 60 to 90 mole %  $\text{Fe}_2\text{TiO}_4$ . The latter spinels, or more correctly, chromian ulvöspinels, are the most  $\text{Fe}_2\text{TiO}_4$  rich yet found. The Apollo 11 spinels are intermediate in composition between the two groups of spinels from the Apollo 12 rocks.

Troilite and metallic iron occur in both

Apollo 11 and Apollo 12 rocks, but in the Apollo 11 lavas these minerals are usually intergrown, whereas in the Apollo 12 specimens they are generally not associated. Taylor, Kullerud and Bryan have noted that when intergrown with ilmenite or spinel, troilite contains appreciably more Ti than when associated with silicates. The troilites contain less than 0.02% Cr and with one exception less than 0.02% Ni. The metal phase contains between 4 and 30% Ni when it is included in early crystallized olivine, but in other associations it contains  $4 \pm 0.5\%$  Ni and  $1.6 \pm 0.1\%$  Co. Si and P in the metal range from 0.05 to 0.13% and  $< 0.01$  to 0.03%, respectively.

At least two of the lavas collected by astronauts Conrad and Bean from *Mare Procellarum* contain phenocrysts of pigeonite with intricately zoned mantles of Ca-rich pyroxene. Boyd has shown that a part of this zoning has developed in a manner analogous to the formation of growth rings in trees, and electron probe study of sections cut through these crystals makes it possible to interpret their eruptive history. Because the sequential relations of pyroxene crystallization are clear, these Apollo 12 lavas have provided more insight into the formation of lunar basalts than was gained from the rather chaotic crystallization patterns of the pyroxenes in the Apollo 11 sample.

The basic pattern of pyroxene zoning in lunar rocks 12021 and 12052 consists of euhedral cores of pigeonite, believed to have formed at depth in the moon, with mantles of augite that appear to have crystallized in fluid lava streams on the moon's surface. The augite and pigeonite have crystallized in succession rather than jointly precipitating from the liquid. This relationship contrasts with the usual occurrence of augite and pigeonite in terrestrial rocks where generally these minerals crystallize simultaneously over a considerable temperature interval.

One of the samples that contain mantled pigeonite phenocrysts (12021) is remarkable in that the augite mantles show an oscillatory zoning. There are oscillations in the crystallization of augite and pigeonite, and one crystal studied has three generations of pigeonite separated by augite. There are also oscillations in the progressive zoning toward more Fe-rich compositions. Terrestrial pyroxenes do not generally show oscillatory zoning. It probably formed in turbulent, rapidly flowing lava streams when partially cooled and fractionated lava was mixed with fresh lava at a higher temperature.

The discovery of a Ca-Fe pyroxenoid, subsequently named "pyroxferroite" in Apollo 11 lunar samples, spurred Lindley to complete a study of the stability relations of its synthetic equivalent. His results lead to the conclusion that the Apollo 11 pyroxferroite not only crystallized metastably but also has persisted in a metastable state for a period of more than 3 billion years.

Large crystals of olivine were among the earliest minerals to crystallize in the Apollo 11 and 12 lavas, and they differ from terrestrial olivines by being extraordinarily rich in chromium. Bell's analyses show that the lunar olivines contain 0.2–0.4 wt % Cr as  $\text{Cr}_2\text{O}_3$ , whereas the usual concentration in terrestrial olivines is less than 0.1%. Analysis of the fine structure of crystal-field absorption spectra of Apollo 11 olivines indicates that the chromium is present at  $\text{Cr}^{2+}$ . The reduced state of chromium is another product of the low partial pressure of oxygen present during the crystallization of lunar rocks. Nickel preferentially enters the metal phase in lunar lavas, and accordingly the Ni content of the olivines is much lower than that of terrestrial olivines of igneous origin. Finger's study of the crystal structure of an olivine from lunar rock 10020 has led to the first X-ray detection of Fe/Mg ordering in olivines.



In addition to studying basalt-like materials from the moon, staff members have conducted extensive investigations on similar materials from earth. The Geophysical Laboratory tape library of published chemical analyses of Cenozoic volcanics now contains more than 9400 entries, of which 3340 are analyses of rocks referred to with source references by one of some 60 specific names determined by members of the basalt family. More than 2000 are called simply basalt; most of the rest belong to the tholeiite, alkali-basalt, trachybasalt, or basanite groups. Chayes has recently found that the distribution of silica saturation among those relatively unaffected by surficial oxidation is distinctly bimodal. More than 75% of such analyses are either *Q*- or *ne*-normative, the sample frequency distribution showing well defined point maxima at  $ne_{20}di_{50}ol_{30}$  and  $Q_{10}di_{45}hy_{45}$ . Basaltic rocks whose norms lack both *ne* and *Q* are decidedly subordinate in every major environment except the submarine ridges. Curiously, they are overwhelmingly dominant in this environment; of 79 analyses of relatively unoxidized submarine ridge basalts included in the survey, only two are *Q*-normative and three are *ne*-normative. At present there is no satisfactory explanation for the scarcity of *Q*- and *ne*-normative basalts along the submarine ridges. Their abundance elsewhere, and the markedly bimodal distribution of silica saturation in Cenozoic basalt as a whole, are compatible with remelt hypotheses based upon recent experimental results indicating that invariant points in the relevant simplified systems are indeed either *Q*- or *ne*-normative at pressures at least up to 6 kb.

Yoder demonstrated the miscibility of rhyolitic and basaltic magmas under hydrothermal conditions and the reluctance of those magmas of highly contrasting composition to mix once formed separately. He evolved a hypothesis whereby

both rhyolitic and basaltic magma can be generated from a single parent by fractional melting without giving rise to magmas of intermediate composition. By progressive batch melting of parental material, adequate volumes of magma can be supplied repetitively for the largest eruptive events known. Comagmatic rhyolite and basalt have been observed in eruption, and their joint occurrence has been recognized since the earliest days of petrology.

Lindsley, Smith, and Haggerty collaborated on a field, petrographic, and electron microprobe study of an unusually thick, differentiated flow of Picture Gorge basalt. Pegmatoid segregations in the interior of the flow contain alkali feldspar, aenigmatite, Na-rich and Fe-rich pyroxenes, and fayalite as late-stage residual minerals. Feldspars show an extreme range of compositional zoning; one thin section from the flow interior contains compositions from  $An_{84}Ab_{15.5}Or_{0.5}$  to  $An_{0.3}Ab_{39.9}Or_{59.8}$ . Analyses of pyroxene provide documentation of a well-defined augite "quench trend": compositions of augites from the chilled base and from the more slowly cooled interior of the flow form trends with contrasting directions in the pyroxene quadrilateral. Augite in the pegmatoids in the flow is sector zoned. The discovery of aenigmatite in these rocks has led to a preliminary investigation of its stability field: it is not stable at temperatures much above 900°C. The presence of fayalite, aenigmatite, and Fe-Ti oxides suggests that the oxygen fugacity during crystallization of the flow was about an order of magnitude below that defined by the fayalite-magnetite-quartz buffer.

It has been known for many years that the andesitic and dacitic lavas of the circum-Pacific volcanic belt are chemically and mineralogically similar to common continental crustal rocks. More recently, geophysical studies have indicated that certain volcanic island arcs lying within this belt in the western



and northwestern Pacific are developed wholly or partly within oceanic crust and that they display anomalously low values for alkalis and certain trace elements. During July and August 1969, Bryan conducted a field investigation of the volcanic islands of Tonga, a typical "primitive" island arc for which there are already abundant geophysical data. Major and minor element analyses of rocks and minerals have been completed, and have been used to test various possible fractionation schemes. Preliminary results suggest that basaltic andesite is a suitable parent liquid from which all other more siliceous rock types in Tonga may be readily derived by fractional crystallization. The origin of this parental basaltic andesite can probably be attributed to partial fusion of oceanic basalt, under conditions favorable to crystallization of hornblende as a residual solidus phase.

Mao has been studying the system jadeite-anorthite at pressures up to 40 kb. He synthesized  $\text{NaAlSi}_2\text{O}_6$ - $\text{CaAl}_2\text{SiO}_6$  solid solutions and found that the  $P$ - $T$  stability field of these pyroxenes expands to lower pressures with increasing CaTs content. These pyroxenes can dissolve as much as 8% by weight of excess silica. The solubility of silica depends on the pressure and the CaTs content.

Smith has combined experimental studies of calcium-free pyroxenes with electron microprobe studies of iron-rich pyroxenes and olivines in intrusives associated with a Labrador anorthosite complex. The results help in outlining limits of pyroxene stability at low pressure and suggest that pyroxene in some of the Labrador rocks formed at pressures greater than 5 kb.

Cassie has studied the melting behavior of diopside-aegirine solid solutions at pressures up to 40 kb. The incongruent melting range of these solid solutions is considerably reduced under pressure; at 40 kb the composition  $\text{Di}_{53}\text{Ac}_{67}$  (mole %) was found to melt congruently.

X-ray diffraction data and microscopic observations indicate that the phase relations of these solid solutions are more complex than previously suspected. It appears that no part of the diopside-aegirine join is truly binary at pressures lower than 30 kb (dry).

The low-temperature melting of a peridotite assemblage was observed by Yoder in his study of the diopside-pyroxene- $\text{H}_2\text{O}$  system at 10 kb. In addition he delineated for the first time a two-amphibole assemblage critical to the interpretation of certain metamorphic rocks. The lowest to highest grades of metamorphic assemblages were encountered within an interval of only  $400^\circ\text{C}$ . Of special interest was the demonstration of the stable coexistence of chlorite and clinopyroxene, a key pair in spilitic assemblages, which as yet do not have a place in facies classifications.

Kosmochlor ( $\text{NaCrSi}_2\text{O}_6$ ), the unique chromium clinopyroxene found in meteorites, was synthesized hydrothermally by Yoder and Kullerud, and a complete series of solid solutions with diopside was demonstrated. The coexistence of chromiferous diopside and kosmochlor solid solutions in meteorites suggests that a miscibility gap exists on this join and that kosmochlor should be stable under terrestrial conditions.

An exceedingly large stability field for andradite ( $\text{CaFe}_2^{3+}\text{Si}_3\text{O}_{12}$ ), one of the ubiquitous components of garnet, was found by Huckenholz and Yoder in air at 1 atm, in  $\text{O}_2$  up to 30 kb, and  $\text{H}_2\text{O} + \text{O}_2$  up to 20 kb. A new technique for studying oxy and hydroxy systems was evolved, employing the low-temperature breakdown of  $\text{PtO}_2$ .

During the past year Schairer and Yoder have been preparing a manuscript incorporating their extensive studies on the  $\text{Na}_2\text{O}$ - $\text{MgO}$ - $\text{SiO}_2$  system. This is a limiting ternary system for several major quaternary systems and includes compositions close to natural rocks and minerals. This study has required exten-

sive comparison of thermal and X-ray results on 300 preparations. Many new ternary compounds were found, one of which has been observed in meteorites. In addition, the incongruent melting behavior of the compound  $3\text{Na}_2\text{O} \cdot 8\text{SiO}_2$  in the binary system  $\text{Na}_2\text{O}-\text{SiO}_2$  has been delineated.

The effects of pressure on the thermodynamic mixing properties of orthosilicate systems are virtually unknown. For this reason Taylor, Bell, and Muan chose and studied the  $\text{Zn}_2\text{SiO}_4-\text{Co}_2\text{SiO}_4$  system at 30 kb as a model. Preliminary results indicate a strong dependence upon pressure for the position of the solvus along this join and demonstrate that under pressure olivine structure is highly favored over willemite. It was also found that the melting curve of  $\text{Zn}_2\text{SiO}_4$  has a negative slope in  $P$ - $T$  space—a very unusual feature for silicate minerals.

Rumble has been engaged in a diversified effort to understand the conditions of equilibrium or disequilibrium under which the metamorphic rocks of west-central New Hampshire recrystallized. The Moosilauke quadrangle is especially interesting because (1) it is an example of the world-wide association of recumbent folds, gneiss domes, and regional metamorphism found in orogenic belts of all geologic ages; and (2) the distribution of all three aluminum silicate polymorphs in the Moosilauke quadrangle implies that rocks in that area recrystallized under  $P$ - $T$  conditions close to the  $\text{Al}_2\text{SiO}_5$  triple point. This relationship gives a starting point for construction of a fossilized  $P$ - $T$  grid for the area.

Taylor and Kullerud determined the high-pressure phase relations associated with the newly discovered compound  $\text{CuS}_2$ , a superconductor of special interest to solid state physicists. They found that though all of the X-ray diffraction reflections could be indexed on the basis of the cubic pyrite structure, the optical properties were more sensitive indicators of the noncubic symmetry of  $\text{CuS}_2$ .

Taylor and Kullerud have studied the

quaternary system  $\text{Cu}-\text{Fe}-\text{S}-\text{O}$  to temperatures below  $300^\circ\text{C}$ . Knowledge of this system not only serves to explain the mineral paragenesis found in various types of rocks and ores but also bears directly on the processes of secondary alteration (e.g., oxidation).

It has been known for many years that chalcopyrite, the most important copper-bearing mineral is nonstoichiometric above  $200^\circ\text{C}$ . No information existed, however, on the type of solid solution occurring in this phase. Kullerud and Donnay have been able to determine, by X-ray diffraction studies on natural  $\text{CuFeS}_2$  as well as on synthetic materials containing  $\text{Cu}+\text{Fe}/\text{S}>1$ , that the solid solution must be one of metal addition.

Taylor and Mao have made a new high-pressure polymorph of  $\text{FeS}$  in a diamond-anvil high-pressure cell and have calculated that this phase is stable at  $25^\circ\text{C}$  above  $\sim 55$  kb.

Mackinawite, a low-temperature iron sulfide mineral of near  $\text{FeS}$  composition, is found in certain ore deposits and is a common constituent of the black mud sediment known as "hydrotroilite." Taylor and Finger performed a detailed structural refinement on mackinawite single crystals. They determined that this compound possesses unfilled sulfur sites and thus is the first known example of sulfur deficiency in a naturally occurring sulfide mineral. The structural formula for mackinawite should be  $\text{FeS}_{1-x}$  rather than  $\text{Fe}_{1+y}\text{S}$ , as it is usually written.

Mao and Bell studied the behavior of thermocouples in the single-stage piston-cylinder apparatus. The experiments revealed that a random error caused by differential stress of the individual thermocouple wires exists when a high-strength thermocouple insulating tube is used. This error can amount to as much as  $\pm 15^\circ\text{C}$  with the Pt/Pt 10% Rh thermocouple at  $1700^\circ\text{C}$  and 40 kb. The rate of drift of the Pt/Pt 10% Rh thermocouple in contact with various ceramics has been studied in high-pressure



experiments at temperatures as high as 1700°C. Mao and Bell have measured the effect of hydrostatic pressure on the emf's of single-wire W 3% Re and W 25% Re as well as on the emf of the W 3% Re/W 25% Re thermocouple. The pressure effect on the emf of the W 3% Re/W 25% Re thermocouple at 1000°C and 40 kb is -7°C.

The upper thermal stability of the mineral pyrophyllite,  $\text{Al}_2\text{Si}_4\text{O}_{10}(\text{OH})_2$ , common in certain metamorphic terrains, sets a lower boundary for the stability of  $\text{Al}_2\text{SiO}_5$  (andalusite or kyanite) under high water potential. One necessary set of data for a rigorous thermodynamic analysis of these stabilities is knowledge of the thermal expansion of pyrophyllite. During this past year, Taylor and Bell have determined these data and have found that the improved estimate of the change of volume for the above reaction increased the stability field calculated for pyrophyllite.

Large granite samples analyzed by the Rb-Sr whole-rock, and the U-Pb zircon techniques have provided the information that much of the Grenville province is composed of rocks that are more than 1700 m.y. old. Similar whole-rock analyses of small, closely spaced (2-3 cm) layers in a paragneiss sample show that the major metamorphism occurred (in at least one area) about 1800 m.y. ago. Analyses of minerals in the rock, however, indicate a metamorphism about 900 m.y. ago. Krogh and Davis have interpreted these isotopic relationships to show that diffusion of Sr during the second metamorphic episode did occur but was limited to only a few millimeters.

Krogh has developed a simplified technique for the dissolution of zircons and the extraction of U and Pb for age determinations. The method has been shown to lead to extremely low contamination levels and requires far less glassware and purified reagents than the conventional chemical procedure.

A possible source of error in age K-A

determinations is the migration of argon into or out of minerals. Argon was introduced by Laughlin and Yoder into natural albite under pressures as low as 1 bar in amounts approximating the excess argon reported in some natural albites. Excess argon in plagioclase, therefore, need not necessarily be introduced during growth, but may be introduced during metamorphism and degassing of potassium-rich minerals such as potassium feldspar and the micas.

Work in organic geochemistry was largely devoted to examination of properties of humic acids and kerogen. Hoering has isolated and characterized humic acids in a Recent marine sediment from the continental shelf off Southern California. The material is an organic polymer with a molecular weight of greater than 10,000. Electron-spin-resonance measurements indicate that it contains organic free radicals. Its infrared adsorption spectrum shows the presence of hydroxyl groups, carboxyl groups, and aliphatic carbon to hydrogen bonds. Aromatic carbon-to-carbon and carbon-to-hydrogen bonds are not prominent. The carboxyl groups have acidic hydrogens that can be titrated with bases.

Chemical degradation of humic acid to small recognizable molecules gave small yields of a complex mixture of organic compounds with no one type of molecule predominating. Sodium amalgam reduction gave mainly aliphatic and alicyclic compounds rather than aromatic compounds, in contrast to previous reports in the literature.

Abelson and Hare investigated the reactivity of a wide variety of samples that included humic acid, humus, and kerogen, and represented very different geologic settings. These materials, freed of mineral matter, were tested by exposure to a suite of the principal amino acids. Qualitative similarities were found; in all the experiments, cystine, the dibasic amino acids, and phenylalanine and tyrosine disappeared most rapidly. Substantial quantitative differ-



ences were noted, some of which were traced to the effect of oxygen in promoting reactivity.

Abelson and Hare also synthesized a large number of complex polymers from glucose and single amino acids. In their behavior these polymers resembled very

closely the properties of natural humic acids and kerogen. They can be made to have similar molecular weights, carbon-nitrogen ratios, titratable acid groups, reactivity with free amino acids, sensitivity to oxygen, and electron spin resonance.

## EXPERIMENTAL PETROLOGY

### CONTEMPORANEOUS RHYOLITE AND BASALT

*H. S. Yoder, Jr.*

#### *The Problem*

One of the oldest problems in petrology is the contemporaneous extrusion or intrusion of magmas of great contrast in composition with intermediate members absent or of negligible volume. Bunsen (1851) recognized the association of acid and basic rocks in Iceland and conceived the idea of two primary magmas which if mixed would yield intermediate products. The compositional contrast has been noted on a regional scale, on a formational scale with ash, tuffs, and lava beds of rhyolite interbedded with basalt or andesitic flows, in composite dikes, and on a microscopic scale in welded tuffs, emulsion rocks, and tektites, each having at least two glasses of widely differing index of refraction. There is no doubt that two liquids of acid and basic composition can exist at the same locality; but are they of contemporaneous formation? On-site witnesses have reported abrupt changes in composition of pumice and lava issuing from the same volcano or differences in composition of products issuing simultaneously from different parts of the same volcano. The primary question is, how can two magmas of great compositional contrast be generated and maintained separately? The usual explanation assumes the existence of the magmas stored in separate shallow reservoirs that supply a common conduit

or closely adjoining conduits leading to the summit of a volcano. The composite dikes presumably represent the case of a common conduit. The extent of mixing, if any, presumably depends on the time required for transit and other factors. More recently the concept of two magmas of different composition in a strongly zoned chamber with a mixed zone at the convective interface has been advanced (Schmincke, 1969, p. 91).

The primary question remains, especially after the properties of the two magmas are examined. Because the rhyolites are usually explosive, yielding ash, tuff, and pumice, and the principal propellant is  $H_2O$ , the melting relations of the contrasting rock types with an excess of  $H_2O$  are presented. In Fig. 1 is the minimum melting curve for a rhyolite (=granite) and the beginning of melting and liquidus curves for an olivine tholeiite. Andesites may contain hydrous minerals, such as amphiboles and micas; the basalts are usually relatively free of such phases, however, and their eruption is relatively quiescent. The absence of hydrous minerals does not necessarily mean, of course, that the liquids were anhydrous, merely that the temperatures exceeded the stability of the hydrous phases. The curve representing the formation of amphibole in the olivine tholeiite is also exhibited in Fig. 1. To avoid the complication of amphibole formation in the basaltic liquid it is necessary to consider that region below about 1.5 kb  $P_{H_2O}$ .

The first obvious point is that at the temperatures where rhyolite is just all

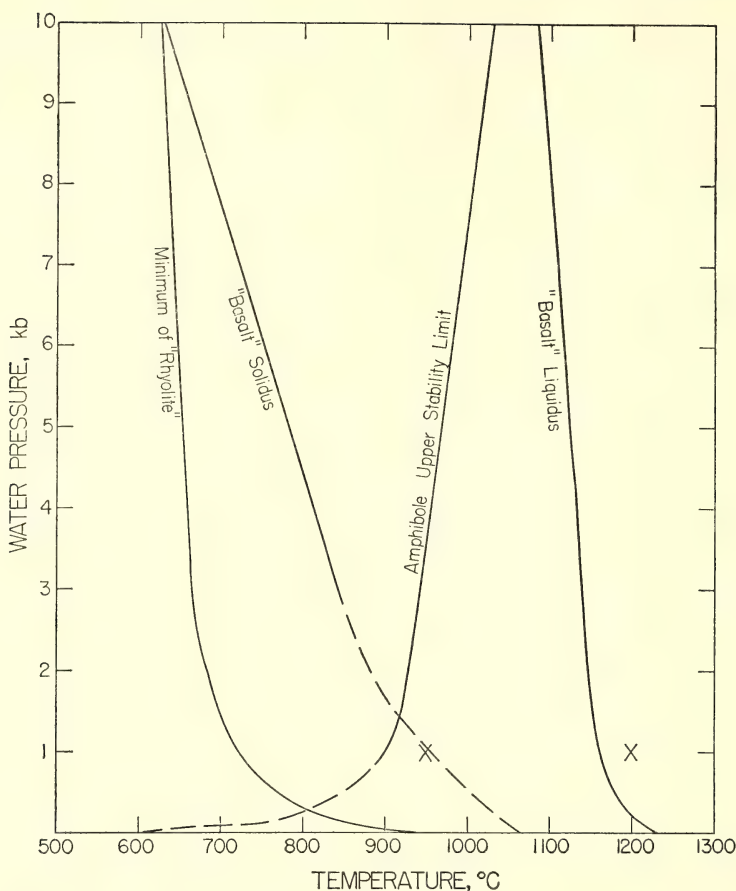


Fig. 1. The minimum melting curve of rhyolite composition (= granite of Tuttle and Bowen, 1958; Luth, Jahns, and Tuttle, 1964) and the liquidus, solidus, and upper stability curve of amphibole for the olivine tholeiite composition (Yoder and Tilley, 1962) in the presence of excess  $H_2O$ . The conditions studied herein with other materials are marked with an X, above the liquidus of rhyolite and basalt, respectively.

liquid,\* basalt is completely crystalline. Second, if basalt is all liquid, then the rhyolite liquid is superheated approximately  $250^{\circ}C$  at 1 atm and  $450^{\circ}C$  at 1 kb  $P_{H_2O}$ . If the liquids coexisted through an immiscibility relationship, the higher temperatures of the basalt would presumably prevail. Superheat is

not considered very likely, particularly in magmas that reach the surface bearing phenocrysts. Alternatively it would be necessary, therefore, to maintain separate reservoirs at or near the liquidus temperature of each magma.

#### *Exploratory Experiments*

\*The solidus and liquidus are identical for the minimum melting composition of rhyolite. A specific rhyolite will have a small melting interval, however, depending on its composition relative to the minimum melting composition, which changes with water pressure.

Some exploratory experiments were carried out at  $P_{H_2O}=1$  kb to ascertain the behavior of rhyolite and basalt under the liquidus conditions most likely to obtain for each, as indicated in Fig. 1. The

intent was to obtain some notion as to the relevant physicochemical parameters and to test their miscibility, if any. The materials used were the G-1 granite of Westerly, Rhode Island, and the W-1 diabase of Centerville, Virginia, used in the test of analytical precision (Fairbairn *et al.*, 1951); obsidian from Lake Naivasha, Kenya (Bowen, 1935); and tachylite from Kilauea, Hawaii (Adams and Gibson, 1926).

Equal proportions by weight of the G-1 granite and W-1 diabase were ground together for 1 hour and placed in a platinum tube with  $H_2O$  in excess of that required for saturating the liquid. After hydrothermal treatment at  $1200^{\circ}C$  for 1 hour a homogeneous brown glass was obtained. Similar results were obtained in the absence of water by Ginsberg and Nikogosyan (1924), who heated mixtures of granite and iron-rich diabase at  $1400^{\circ}C$ . In another hydrothermal run at  $950^{\circ}C$  for 2 hours the products were clinopyroxene, plagioclase, opaques, and a glass of relatively uniform index of refraction. There was no evidence of immiscibility, and it was evident that with intimate mixing intermediate compositions could be obtained.

In another set of experiments powdered G-1 granite and powdered W-1 diabase and  $H_2O$  were packed in a platinum tube so that the separate but equal proportions by weight of the powders lay end-to-end with a single common interface. After hydrothermal treatment at  $1200^{\circ}C$  and 1 hour the products consisted of a clear glass in the position of the granite and a dark brown glass in the position of the diabase with an exceedingly sharp cusped interface convex toward the granitic glass. A photograph of the undisturbed charge after the platinum container had been peeled back is given in Plate 1A. In Plate 1B is shown the basalt-rhyolite contact of the Orónsfjall composite flow in eastern Iceland, photographed from a polished hand specimen by Gibson and Walker (1963)

and reproduced with their kind permission. It is evident that the diffusion process is slow even when the granitic liquid is highly superheated. The interpretation of the cusped interface is complicated, and the initial temptation to conclude that the basaltic liquid is the more viscous must be tempered by considerations of surface tensions and convective instability. Samples similarly packed and held at  $950^{\circ}C$  for 2 hours yielded a clear glass in the position of the granite and a recrystallized hard cake in the position of the diabase. The interface was sharp with some of the granitic liquid flowing around the end of the basaltic cake. On the basis of the lack of coloration of the granitic glass, no reaction appeared to take place during the short duration of the run.

Further experiments were conducted at the same temperatures and time periods with powdered obsidian and tachylite mixed intimately and packed in a platinum tube with excess  $H_2O$ . In addition, cylinders were cut of the two natural glasses and placed end-to-end in the platinum tube with excess  $H_2O$ . The results were comparable to those using the G-1 granite and W-1 diabase. An experiment analogous to that with the cylinders of glass at  $1200^{\circ}C$  was performed under anhydrous conditions by Bowen (1921). He heated at about  $1500^{\circ}C$  a crucible containing a layer of various plagioclase glasses over a layer of diopside glass for periods of 17 to 48 hours and measured the extent of diffusion by the changes of index of refraction from top to bottom of the resulting partially homogenized glass. No comparable diffusion was observed in the short runs with obsidian and tachylite cylinders. Additional experiments are under way on samples from regions such as Katmai (Alaska), Gardiner River (Wyoming), Breiddalur (Iceland), and Gran Canaria, where contemporaneous lavas of high compositional contrast are described.



*Tentative Hypothesis*

On the basis of the above exploratory experiments and the published field interpretations, it is suggested that basaltic and rhyolitic magmas, once formed, would be maintained in a contiguous manner and that a relatively negligible amount of diffusion would take place between eruptive cycles. It is of interest, then, to inquire whether such magmas of high compositional contrast can actually be generated from the same parent without intermediate members rather than having separate origins at different depths.

The data of Kushiro (1969b) on the diopside-forsterite-silica system at  $P_{H_2O}=20$  kb are pertinent to a possible mechanism for the generation of both magmas from a common parent. Con-

sider a parental material of quartz-normative ultrabasic composition analogous to  $X$  in Fig. 2. The pressure of 20 kb may be excessive relative to the depths of origin presumed for such magmas; the principles involved, however, are informative. If the temperature is raised to  $960^\circ\text{C}$ , melting of composition  $X$  in the presence of excess  $\text{H}_2\text{O}$  begins and yields a liquid of the composition at point  $A$  in Fig. 2. Removal of that initial melt as soon as it is formed causes the bulk composition of the parent to move away from the liquid composition. Continuous isothermal removal of liquid of the composition  $A$  eventually causes the bulk composition to move to  $C$ . Here the quartz component of the parental material is exhausted, and melting ceases after about 20% of siliceous liquid has

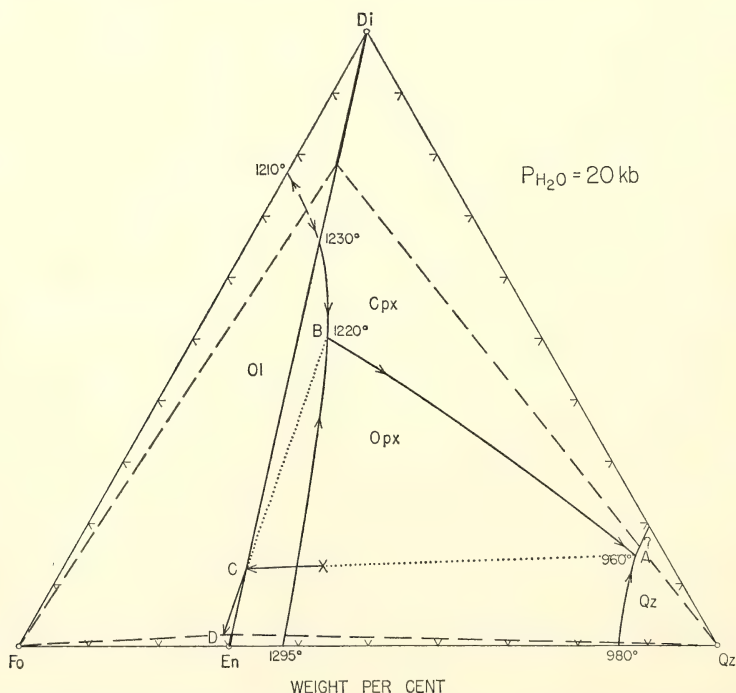


Fig. 2. The diopside-forsterite-silica system at  $P_{H_2O}=20$  kb (Kushiro, 1969). The  $X$  marks an assumed parental composition, and the arrows from it indicate the change of its composition resulting from the continuous removal of liquids  $A$  and  $B$  with heating. The dotted lines are construction lines. Di, diopside; Cpx, clinopyroxene; En, enstatite; Opx, orthopyroxene; Fo, forsterite; Ol, olivine; Qz, quartz.

been removed. It is necessary to raise the temperature to 1220°C (point *B* in Fig. 2) before the resumption of melting of the remaining parental material, which now has the composition *C*.<sup>\*</sup> Continuous removal of liquid *B* in a similar way drives the bulk composition of the remaining parental material toward *D*, where melting again ceases because of the depletion of a phase, diopside solid solution (Cpx). The remaining material could be described as a pyroxenite or a saxonite. About 22% of basic liquid having the composition *B* has been removed from the parental material of composition *D*. In brief, two homogeneous liquids have been removed from a common parent without the production of liquids of intermediate composition. The analogy of rhyolite to point *A* and andesite to point *B* has already been drawn by Yoder (1969). The obvious questions dealing with the assumption of excess H<sub>2</sub>O, the implications of trace element partition, the influence of possible hydrous phases (e.g. tremolite in the simple system described), and the mechanics of storage and eruption of the two magmas will be dealt with in full at a later time. It is important to note that a single eruptive event rarely exceeds 2 cubic km in volume; therefore the partial melting process need involve, on the basis of the simple system described, only 10 cubic km. That small region of parental material could not, of course, contribute further to the production of

rhyolite or basalt. The ever-present problem of providing essentially point-source heating of small batches can possibly be resolved by an advancing wave of heat or volatiles (Bailey, 1970) through heterogeneous parental material having primarily a single "eutectic point" and a single "reaction point." Similar chemography can be applied to the alkali magma series at high pressures. Depletive partial melting or fractional fusion (Presnall, 1969) of nepheline-normative parental material would account for the hiatus between some alkali basalts and trachytes recorded in the oceanic islands (Chayes, 1963).

#### INTRODUCTION AND DIFFUSION OF ARGON INTO NATURAL ALBITE

*A. W. Laughlin\* and H. S. Yoder, Jr.*

The presence of excess radiogenic Ar<sup>40</sup> has been demonstrated in albite crystallizing under pegmatitic conditions (Livingston *et al.*, 1967; Laughlin, 1969a). Albite from the Bob Ingersoll pegmatite, for example, contained  $4.0 \times 10^{-9}$  mole/g of excess Ar<sup>40</sup>. In low-potassium minerals this quantity may lead to apparent ages much older than the true age of the rock; i.e., the true age of the Bob Ingersoll pegmatite is about 1700 m.y., whereas the K-Ar albite age is 4900 m.y. This excess Ar<sup>40</sup> could have been incorporated in the albite either at the time of initial crystallization or during some later thermal event. It was believed that experimental demonstration of incorporation and release of argon would provide a basis for evaluation of the partition functions and the rates of gain and loss as a function of temperature and pressure.

#### *Argon Introduction*

Experiments were conducted to determine if significant quantities of argon

\*The time required for raising the temperature would probably be at least a few thousand years if the temperature interval were 250° and the rate of heating near 0.1° per year. For natural material the temperature interval between the two "points" of liquid generation at the relevant depths is probably double that in the simple system. Cooling of the siliceous liquid in the conduit or in a reservoir would of necessity be minimal because of the minimum melting character of the liquid. A small drop in temperature below the liquidus would produce a large amount of crystallization. The cooling problem is not critical in basaltic or andesitic liquid because of the large temperature interval between liquidus and solidus.

\* Department of Geology, Kent State University, Kent, Ohio.

could be introduced into crystalline albite. The introduction of argon was performed at the Geophysical Laboratory, and the argon determinations, at the Department of Geology, University of Arizona. The albite used was a -80 +100 mesh sample from the Canoa Ranch, Arizona, pegmatite (Livingston *et al.*, 1967). The albite had a potassium content of 0.09%, and before addition of argon, an argon content of  $0.225 \times 10^{-10}$  mole/g. In the introductions conducted at elevated pressures, the samples were placed in unsealed platinum capsules and subjected to high argon pressures. In the experiments at 1 bar, the samples were loaded in double platinum foil cylinders and a continuous stream of argon was passed over them. All runs were conducted at  $1000^\circ \pm 10^\circ\text{C}$ .

Determinations of the 131-131 separation before and after heating indicated that the albite suffered no structural damage.

The results of these experiments are shown in Table 1. Gerling, Pushkarev, and Kotov (1965) concluded from their experiments on pyroxene that saturation at high pressures was attained in less than 1 hour. Because of the difference in structure, however, the high-pressure introductions were run for 24 hours to ensure saturation. The experiments at 1 bar were run for varying lengths of time to determine whether saturation

was also rapidly attained at lower pressures. It is apparent that saturation in albite at that pressure was not attained in 24 hours nor probably even after 338 hours.

During run 6 the argon tank emptied before the experiment was concluded and while the sample was still at  $1000^\circ\text{C}$ . Normal air thus replaced the 1 bar of argon over the sample, effectively reducing the argon partial pressure from 1 bar to 0.01 bar. This reduced pressure was insufficient to retain the argon introduced previously, and an argon loss of 74% occurred.

The results of the high-pressure experiments are somewhat perplexing. Runs 2A and 2B were splits of the same sample, analyzed 8 months apart to determine if argon leakage had occurred. Run 2B, which was analyzed after the 8-month period, is outside the experimental error of about 3%, but on the high side. Clearly argon leakage cannot be the cause of error. Sample inhomogeneity is a likely source of error in that the samples were small. In addition equilibrium may not have been attained. The sample held at 10 kb pressure incorporated less than the 2-kb sample, perhaps owing to the closing of defects in the structure of the albite. These defects have been suggested as one possible site for the excess  $\text{Ar}^{40}$ .

### Argon Diffusion

Diffusion experiments on natural albites and microcline indicated that the argon was held in multiple sites (Laughlin, 1969b). A series of similar experiments was conducted on the albite containing argon introduced in the laboratory under 185 bars of pressure. The results are presented in Table 2 and plotted in Fig. 3. This albite also appears to have multiple sites containing argon. In contrast to natural albites, which contain about 33% of their argon in the low-temperature site, only 14% of the introduced argon was so situated. Sig-

TABLE 1. Introduction of Argon into Natural Albite at  $1000^\circ \pm 10^\circ\text{C}$

Run No.	Time, hours	Argon Pressure, bars	$\text{Ar}^{40}$ Introduced $\times 10^{-6}$ mole/g
1	24	10,000	3.15
2A	24	2000	4.20
2B	24	2000	6.34
3	24	185	0.685
4	24	1	0.00278
5	168	1	0.00407
6	338	1 †	0.00266
7	338	1	0.0101

\* Weighted average = 5.05.

† Pressure decreased to 0.01 bar for the last 2-3 hours.



TABLE 2. Removal of Argon from Natural Albite after Introduction under 185 Bars of Argon Pressure

Run No.	T, °C	Time, min.	Cumulative Time, min.	Ar <sup>40</sup> Removed $\times 10^{-8}$ mole/g	Fraction Ar <sup>40</sup> Remaining
1	770	1	1	1.289	0.9812
2	770	10	11	1.304	0.9622
3	770	30	41	1.806	0.9359
4	770	50	91	1.456	0.9147
5	920	1	92	1.637	0.8908
6	920	10	102	4.998	0.8179
7	920	30	132	1.995	0.7888
8	920	50	182	1.691	0.7641
9	1050	1	183	14.51	0.5524
10	1050	10	193	29.48	0.1223
11	1050	30	223	4.821	0.0520
12	Fusion			3.555	0.0000

Total Ar<sup>40</sup> removed,  $68.542 \times 10^{-8}$  mole/g.

nificant loss of argon did not take place in the artificially treated sample until 1050°C was reached. Heating for 1 minute produced an argon loss of about 21%, and an additional 10 minutes of heating at this temperature removed 43% more of the argon. Insufficient data are available to determine the energy of activation of the sites.

### Conclusions

It has been demonstrated that a large quantity of argon can be introduced into albite at pressures as low as 1 bar, approximating the excess argon reported in natural albites. It may be concluded that excess argon in plagioclase need not

necessarily be introduced during crystallization, but may be introduced during metamorphism and the degassing of potassium-rich minerals such as potassium feldspar and the micas. For example, a low-temperature site in microcline is activated at temperatures below 770°C, releasing about one-third of its total argon. Metamorphism of a rock with coexisting feldspars would, therefore, tend to produce excess argon in high-temperature sites in the plagioclase and a deficiency of argon in the low-temperature sites in the potassium feldspar. It will be necessary to demonstrate this behavior with coexisting feldspars in the temperature range at which metamorphism is believed to take place.

It is also possible that excess argon could be introduced into plagioclase at the time of its initial crystallization if a sufficient partial pressure of argon existed in the gas phase. It is evident from the experiments that suitable sites are available in albite for retention of argon even at temperatures above the solidus of basalt. The fact that phenocrysts in unmetamorphosed lavas have excess argon supports this view.

The drop in pressure in run 6 was useful because it closely duplicated the pressure changes during extrusion of lava at the earth's surface. Before extrusion, lava

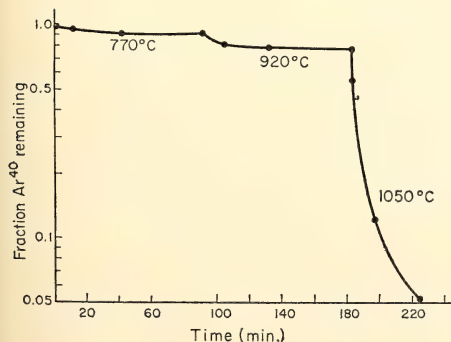


Fig. 3. Fraction of Ar<sup>40</sup> remaining in natural albite containing Ar introduced at 185 bars.

would be subjected to argon partial pressures higher than the 0.01 bar of the atmosphere, and phenocrysts would incorporate some finite quantity of argon. During extrusion with its accompanying decrease in argon partial pressure, the melt and phenocrysts would degas, and only in large phenocrysts is it likely that any argon would be retained. This is an experimental demonstration of the conclusions reached by Damon, Laughlin, and Percious (1967), based on measurements on minerals from volcanic rocks.

#### LIQUIDUS RELATIONS AND SUBSOLIDUS REACTIONS IN SOME PLAGIOCLASE-BEARING SYSTEMS

*R. F. Emslie*

Plagioclase is the most abundant mineral constituent in the earth's crust and is likely present to shallow depths in the upper mantle. Plagioclase must, therefore, play an important role in many processes of fractional crystallization, partial melting, and solid state reaction in these environments. The origin and crystallization of magmas that form plagioclase-rich igneous anorthosites in particular are undoubtedly dependent upon the behavior of plagioclase under *P-T* conditions that occur in the crust and upper mantle. In addition, plagioclase is known to take part in subsolidus reactions during metamorphism of these rocks and basic granulites in general.

Controversy remains rife about the character of the parent magma from which anorthositic plutons crystallize. A parent magma of approximately granodiorite to diorite composition has been regarded favorably by several workers over the years. T. H. Green (1968) has performed some experiments to provide support for this viewpoint. Most workers would agree that production of large volumes of such a magma probably requires close relationship with active orogenic processes. There are, however, some large anorthositic intrusions, notably along the coast of Labra-

dor, Canada, whose character implies formation under anorogenic conditions (e.g. Emslie, 1970). Field evidence there and elsewhere indicates an association with basaltic magma (e.g. Bowen, 1917; Buddington, 1931; Emslie and Lindsley, *Year Book* 67, pp. 110-112). The anorthite content of plagioclase and the compositions of associated ferromagnesian minerals in many anorthositic plutons are consistent with crystallization from basaltic magma. Recent lunar expeditions have made possible the discovery of many anorthositic rock fragments (Wood *et al.*, 1970) together with evidence of solely basaltic magmatism on the moon. These finds clearly suggest a genetic connection. Exploration of the relationship between basaltic magmas and bodies of anorthosite is therefore warranted.

Reactions between plagioclase and pyroxenes or olivine are known to take place over a considerable range of temperature and pressure (Kushiro, 1969a; Kushiro and Yoder, 1966) and have been recognized to be potentially useful indicators of these variables in rocks. The solubility of  $\text{Al}_2\text{O}_3$  as  $\text{CaAl}_2\text{SiO}_6$  in diopside in equilibrium with anorthite and quartz can be substantial even at modest pressures (Kushiro, 1969a).  $\text{Al}_2\text{O}_3$  solubility in enstatite may also be high under favorable conditions (14 wt %  $\text{Al}_2\text{O}_3$  at 18.2 kb, 1400°C, in the system  $\text{MgSiO}_3\text{-Al}_2\text{O}_3$ , Boyd and England, *Year Book* 59, pp. 49-52).

Experiments described below were designed to examine several aspects of the role of plagioclase as it bears on the origin and crystallization of anorthositic magmas and on equilibria in basic granulites. Liquidus relations in the system  $(\text{An}_{60}\text{Ab}_{40})\text{-diopside-enstatite}$  were determined in an attempt to relate generation of anorthosite masses to silica-saturated basaltic magmas. Subsidiary relations in the system enstatite-anorthite were studied at 1212°C and pressures up to 20 kb to examine the behavior of enstatite in equilibrium with

plagioclase under conditions of excess silica. A limit on the maximum depth of crystallization of a large anorthositic intrusion was defined by investigating the upper  $P$ - $T$  stability limits of a natural olivine-plagioclase assemblage. All high-pressure experiments were performed in solid-media, single-stage, piston-and-cylinder apparatus. Starting materials were prepared and 1-atm experiments were performed with the help of J. F. Schairer.

*Liquidus Relations in the System  
Plagioclase ( $An_{60}Ab_{40}$ )-Diopside-  
Enstatite at 1 Atm and  
15 Kb (Dry)*

Most rock assemblages of the anorthosite association have compositions and mineral assemblages that are saturated or nearly saturated with silica. A reasonable assumption, therefore, is that the parent magmas probably began crystallization with compositions that were at or near silica saturation. The join plagioclase-diopside-enstatite has been designated as the plane of silica saturation in the simplified basalt tetrahedron nepheline-diopside-forsterite-silica of Yoder and Tilley (1962). This join was selected to serve as a simplified model with which to examine certain aspects of the derivation and early crystallization of anorthositic magmas.

The plagioclase composition was chosen as  $An_{60}Ab_{40}$  mole % ( $An_{61.4}Ab_{38.6}$  wt%) to approximate an average normative basaltic plagioclase. Because solid solution exists in all the solid phases at high pressure and at 1 atm, the system plagioclase ( $An_{60}Ab_{40}$  mole)-diopside-enstatite is not ternary. The liquidus field boundaries, however, can be accurately portrayed in ternary terms, and they are of principal concern in the present investigation.

At 1 atm the pseudoternary piercing point was determined to lie at ( $An_{60}Ab_{40}$ )<sub>56</sub>Di<sub>31</sub>En<sub>13</sub> at a temperature of  $1235^{\circ} \pm 5^{\circ}\text{C}$  (point *B*, Fig. 4). The

phases present on the liquidus surface at 1 atm are plagioclase, diopside solid solution, and forsterite. The diopside solid solution is expected to contain some alumina, but the amount should be small near the liquidus under silica-saturated conditions at 1 atm (Hytönen and Schairer, *Year Book 60*, pp. 125-141). Plagioclase coexisting with liquid close to the piercing point has a composition of  $An_{77}Ab_{23}$  wt % determined by the electron probe.

At 15 kb (dry) pressure the piercing point has made a significant shift to a composition of about ( $An_{60}Ab_{40}$ )<sub>75</sub>Di<sub>7</sub>En<sub>18</sub> at a temperature of  $1390^{\circ} \pm 20^{\circ}\text{C}$  (point *A*, Fig. 4). At this pressure enstatite melts congruently (Boyd, Englund, and Davis, 1964) and forsterite is no longer stable in the system. The phases appearing on the liquidus surface are plagioclase, diopside solid solution ( $Di_{ss}$ ), and enstatite solid solution ( $En_{ss}$ ). Plagioclase in equilibrium with pyroxenes and liquid near the piercing point has a composition of about  $An_{65}Ab_{35}$  wt % determined by the probe. Because of their small size and rarity near the liquidus, the pyroxenes were not analyzed but are undoubtedly aluminous at this pressure.

At 1 atm the composition ( $An_{60}Ab_{40}$ )<sub>75</sub>Di<sub>7</sub>En<sub>18</sub> lies well within the plagioclase field and has a liquidus temperature of  $1313^{\circ} \pm 2^{\circ}\text{C}$ . The composition of plagioclase close to the liquidus was determined to be  $An_{70}Ab_{30}$  wt % by the probe. For the composition ( $An_{60}Ab_{40}$ )<sub>75</sub>Di<sub>7</sub>En<sub>18</sub>, therefore, liquidus plagioclase is about 5 wt % richer in albite at 15 kb than at 1 atm. This result is consistent with the pressure effect on plagioclase composition reported by T. H. Green (1969) but of somewhat lower magnitude.

Changes in phase relations in the system between 1 atm and 15 kb that are relevant to this investigation may be described simply. With increasing pressure from 1 atm the primary phase field of plagioclase shrinks relative to both



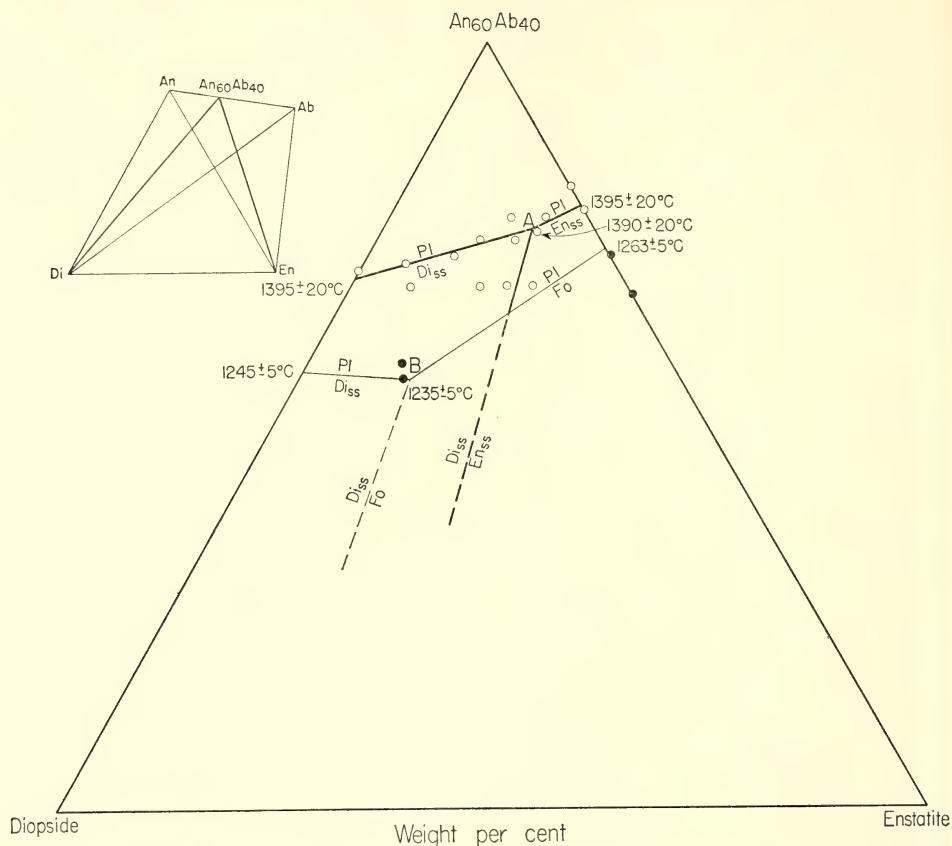


Fig. 4. Liquidus relations in the system  $(\text{An}_{60}\text{Ab}_{40})$ -diopside-enstatite at 1 atm (light lines) and 15 kb dry (heavy lines). Inset shows the position of the  $(\text{An}_{60}\text{Ab}_{40})$ -diopside-enstatite join in the system Di-En-An-Ab. Open circles are compositions run at 15 kb; solid circles are compositions run at 1 atm. Data at 1 atm for the  $(\text{An}_{60}\text{Ab}_{40})$ -diopside join are from Bowen (1915). Points A and B are the pseudoternary piercing points at 15 kb and 1 atm, respectively. Abbreviations: Pl, plagioclase;  $\text{En}_{ss}$ , enstatite solid solution;  $\text{Di}_{ss}$ , diopside solid solution; Fo, forsterite.

$\text{Di}_{ss}$  and Fo. The field of  $\text{Di}_{ss}$  increases at the expense of both plagioclase and Fo. At a pressure of about 5 to 7 kb (Boyd *et al.*, 1964; Kushiro, 1969b) the primary phase volume of forsterite no longer intersects the join  $(\text{An}_{60}\text{Ab}_{40})$ -diopside-enstatite and the Fo field is replaced by  $\text{En}_{ss}$ . Thereafter, as pressure is increased to 15 kb, the plagioclase field continues to decrease in size and the  $\text{Di}_{ss}$  field continues to increase at the expense of plagioclase and  $\text{En}_{ss}$ . At pressures not far above 15 kb the phase relations change radically and become

dominated by garnet and omphacitic pyroxene.

A liquid composition such as A in Fig. 4 on rising into the crust will undergo decompression. Consequently expansion of the primary phase field of plagioclase must cause crystallization of abundant plagioclase on cooling. The level to which the magma rises determines whether the next phase to crystallize will be orthopyroxene (higher pressure) or olivine (lower pressure). In nature the critical pressure constituting this division is probably between 5 and 10 kb judging

from experimental data on basalts (e.g. D. H. Green, 1968). Crystallization at pressures above this critical value may therefore be expected to produce an assemblage of rocks consisting of anorthosite, feldspathic norite, and feldspathic gabbro, whereas crystallization at lower pressure yields anorthosite, troctolite, and gabbro. It is of interest to note that both of these assemblages are common among natural occurrences.

As a model to explain some of the problems of genesis and crystallization of anorthositic intrusions, the system ( $An_{60}Ab_{40}$ )-diopside-enstatite appears to be attractive. In natural magma systems iron is a significant component. Addition of iron to the system ( $An_{60}Ab_{40}$ )-diopside-enstatite would enlarge the primary phase field of plagioclase at both high and low pressures; that is, addition of iron would move points *A* and *B* (Fig. 4) to compositions less rich in plagioclase. Addition of a more sodic plagioclase or the presence of even a small amount of volatiles, however, would have an opposing and perhaps more pronounced effect. In any case, the relative magnitude of the shift in composition of the piercing point with pressure is likely to be similar in direction and magnitude in the synthetic and the natural systems. Fractional crystallization of all liquids lying in the plane ( $An_{60}Ab_{40}$ )-diopside-enstatite leads to silica-saturated residues at 15 kb and at lower pressures.

It is possible for a basic magma to reach a composition similar to *A* (Fig. 4) in at least two ways. For example, a basalt magma brought from depths corresponding to pressures greater than 15 kb must, on rising to the crust, pass through a pressure regime such that a liquid comparable to *A* may form, perhaps by fractional crystallization of pyroxene and/or garnet. Alternatively liquid *A* may form directly by partial fusion of mantle rock at the appropriate depth. Once a liquid of composition *A* has formed, its subsequent rise into the

crust must be accompanied by crystallization of plagioclase. If the magma rise is slow, so that plagioclase crystals can be effectively removed, the liquid will arrive at the earth's surface with a composition similar to *B*, a tholeiitic basalt. On the other hand, if the magma rise into the crust takes place in such a way that the crystallizing plagioclase is carried along in suspension, then the bulk composition *A* may be introduced into a crustal magma chamber. Subsequent concentration of the suspended plagioclase is capable of producing an anorthosite body of sizable proportions (up to 25% by volume of the original magma). The associated basaltic liquid may remain in close spatial relationship with the anorthosite or most of it may move away from the accumulated, solidified plagioclase mass to complete its crystallization elsewhere as normal gabbro or basalt.

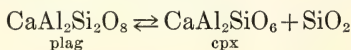
The mechanism described is particularly attractive as applied to the Michikamau intrusion, Labrador (Emslie, 1970). There an anorthosite zone 5 to 6 km thick is underlain by a much thicker troctolitic layered series. The chilled margin of the intrusion is a very nearly silica-saturated basaltic composition (Emslie and Lindsley, *Year Book* 67, p. 110) and may represent basaltic liquid from which a large proportion of plagioclase has already crystallized and separated. Structural and textural evidence at Michikamau suggests that the thick anorthosite zone formed by concentration of plagioclase crystals at the top of the magma chamber in the early stages after intrusion. The density contrast between plagioclase crystals and basaltic magma is unlikely to be great (e.g., Hess, 1960, p. 85). Small variations in magma or plagioclase compositions could be decisive factors allowing plagioclase to sink or float, assuming that the magma viscosity is sufficiently low to permit it. Field evidence supporting flotation of plagioclase in gabbroic magma has been recognized for many years

(Elftmann, 1893; Grout, 1928; von Eckermann, 1938). The lack of any complementary ultramafic zone in the intrusion rules out the possibility that the anorthosite formed by mechanical segregation of plagioclase and mafic minerals from a magma of initially basalt bulk composition. Subsequent to the formation of the anorthosite zone, the remaining basaltic liquid crystallized to form a layered series beneath it.

Speculation involving flotation of plagioclase in basaltic magma has been invoked by several authors (Wood *et al.*, 1970; Anderson *et al.*, 1970) to explain formation of the lunar highlands, which have an albedo and a gravity deficiency consistent with anorthosite. The discovery of anorthosite fragments on the moon's surface lends support to this hypothesis, and a model similar to that just described for terrestrial anorthosites may have application to the lunar environment.

*Subsolidus Reactions in the System  
Enstatite-Anorthite at 1212°C and  
Pressures up to 20 Kb*

The solubility of  $\text{Al}_2\text{O}_3$  in pyroxenes is known to be a function of temperature and pressure (e.g. Boyd and England, *Year Book 59*, pp. 49–52; Kushiro, 1969a). Kushiro has demonstrated the increased solid solution of  $\text{CaAl}_2\text{SiO}_6$  (formed by anorthite breakdown) in diopside with increasing temperature and pressure.  $\text{CaAl}_2\text{SiO}_6$  concentration in diopsidic pyroxenes is known, on the other hand, to be inversely related to silica activity (Kushiro, 1960; LeBas, 1962). For equilibria involving plagioclase and diopsidic pyroxene this relationship is evident from the reaction:



where, at constant  $T$  and  $P$ , a decrease in silica activity causes the reaction to proceed to the right, increasing the  $\text{CaAl}_2\text{SiO}_6$  available for solid solution in diopside.

The system  $\text{CaO-MgO-Al}_2\text{O}_3\text{-SiO}_2$  contains the divariant subsolidus assemblage diopside solid solution ( $\text{Di}_{ss}$ ), enstatite solid solution ( $\text{En}_{ss}$ ), anorthite (An), plus quartz (Qtz). At fixed values of  $T$  and  $P$  the pyroxene compositions of this assemblage are fixed and the anorthite and silica activities are defined. High-Ca and low-Ca pyroxenes coexist with plagioclase in many igneous rocks and metamorphic granulites. It is pertinent, therefore, to inquire whether the compositions of coexisting pyroxenes in terms of  $\text{Al}_2\text{O}_3$  solubility are unique functions of  $T$  and  $P$  and thus useful for determining these variables in rocks.

As a first step toward examining the solubility of  $\text{Al}_2\text{O}_3$  in coexisting pyroxenes it was decided to investigate the system enstatite-anorthite for comparison with the system diopside-anorthite. The composition 1 anorthite : 2 enstatite (mole ratio) has been studied by Kushiro and Yoder (1966). It is richer in anorthite than the range of compositions reported here.

Mechanical mixtures of synthetic crystals of  $\text{MgSiO}_3$  and  $\text{CaAl}_2\text{Si}_2\text{O}_8$  were used as starting materials. These were packed, slightly moistened to hasten reaction, into platinum capsules and used for instroke experiments in piston-and-cylinder apparatus to approach equilibrium from the low-pressure side. For outstroke experiments the high-pressure assemblage was first synthesized and then used as starting material to approach equilibrium from the high-pressure side. The temperature of 1212°C was chosen in anticipation of relatively rapid reaction; however, run times of 24 to 36 hours were still required. As an aid to interpolating the  $\text{En}_{ss} + \text{Qtz}$  field boundary,  $\text{Al}_2\text{O}_3$  contents of enstatite solid solutions were estimated by the X-ray method of Boyd and England (*Year Book 59*, p. 50, Fig. 3, curve A). It was assumed that the small Ca contents of the enstatite solid solutions would not seriously affect the X-ray



method. This assumption was tested by a run of  $\text{En}_{95}\text{An}_5$  composition (containing 1.88 wt %  $\text{Al}_2\text{O}_3$ ) at 17 kb, 1212°C, i.e. under conditions that caused complete breakdown of anorthite so that all of the Ca and Al should have entered enstatite in solid solution. The X-ray method gave 1.9 wt %  $\text{Al}_2\text{O}_3$  for this  $\text{En}_{ss}$ , in excellent agreement with the theoretical value. The composition  $\text{En}_{90}\text{An}_{10}$  (3.76 wt %  $\text{Al}_2\text{O}_3$ ) run at 30 kb and 1212°C yielded an  $\text{En}_{ss}$  with 4.2 wt %  $\text{Al}_2\text{O}_3$  by the X-ray method. It thus appears likely that with increasing Ca content the  $\text{Al}_2\text{O}_3$  in  $\text{En}_{ss}$  tends to be overestimated by the X-ray method. For plotting in Fig. 5 the weight percentage of  $\text{Al}_2\text{O}_3$  deter-

mined by the X-ray method was recalculated into the equivalent weight percentage of  $\text{CaAl}_2\text{Si}_2\text{O}_8$ .

The amount of quartz in run products tended to be somewhat erratic in some experiments. Kushiro (1969a) reported a similar experience and suggested it might be due to the occurrence of excess silica in some of the phases, particularly diopside. Schairer and Kushiro (*Year Book 63*, pp. 130–132) indicated some solid solution of  $\text{SiO}_2$  in diopside at 1 atm. In the present experiments the moistened starting material was contained in tightly crimped, but not welded, platinum capsules, so that some silica loss by vapor transport was possible.

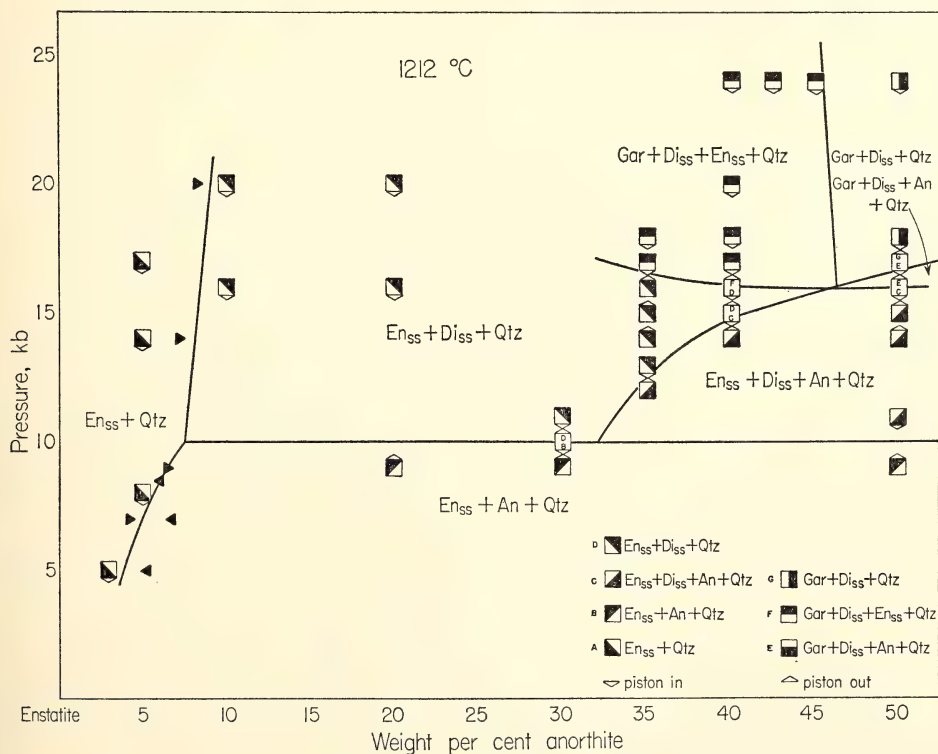


Fig. 5. Isothermal section for the system enstatite-anorthite at 1212°C. Small solid triangles are compositions of  $\text{En}_{ss}$  determined by X-ray. Those with apices pointing to the right were determined by instroke experiments; apices pointing to the left were determined by outstroke experiments. Blank symbols with letters indicate different assemblages obtained in outstroke and instroke experiments; the upper letter designates the outstroke (higher pressure) assemblage, and the lower letter indicates the instroke (lower pressure) assemblage. Abbreviations:  $\text{En}_{ss}$ , enstatite solid solution;  $\text{Di}_{ss}$ , diopside solid solution; Gar, garnet; An, anorthite; Qtz, quartz.

Run products were rather fine grained, making optical examination difficult. X-ray examination of products was therefore heavily relied upon to determine presence or absence and relative abundance of phases.

Results of the experiments are plotted in Fig. 5. In this system solid solution in enstatite may be expressed in several ways. Perhaps the simplest expression is in terms of  $\text{CaSiO}_3$  and  $\text{Al}_2\text{O}_3$ . These two components plus quartz are formed in equimolar amounts by the breakdown of anorthite. At pressures below 10 kb in this system phases other than  $\text{En}_{\text{ss}}$ , An, and Qtz were not detected, and it is assumed that all  $\text{CaSiO}_3$  and  $\text{Al}_2\text{O}_3$  could enter into solid solution in enstatite in 1:1 molar ratio (i.e., as  $\text{CaAl}_2\text{SiO}_6$ ). Figure 5 indicates that solid solution of  $\text{CaAl}_2\text{SiO}_6$  in enstatite at  $1212^\circ\text{C}$  increases with increasing pressure to reach 5.9 wt % (7.5% An equivalent to 2.7%  $\text{Al}_2\text{O}_3$ ) at 10 kb. With further increase in pressure the  $\text{En}_{\text{ss}} + \text{Qtz}$  field expands only slightly relative to the field of  $\text{En}_{\text{ss}} + \text{Di}_{\text{ss}} + \text{Qtz}$ , at least up to 20 kb. At 20 kb the  $\text{En}_{\text{ss}} + \text{Qtz}$  field extends to about  $\text{En}_{91}\text{An}_9$ . Above 10 kb the appearance of  $\text{Di}_{\text{ss}}$  suggests that enstatite reaches saturation with  $\text{CaSiO}_3$ , which must then be accommodated in a new pyroxene phase.  $\text{Al}_2\text{O}_3$  concentration in enstatite, however, undoubtedly continues to increase with pressure. The rapid increase with pressure in the size of the field  $\text{En}_{\text{ss}} + \text{Di}_{\text{ss}} + \text{Qtz}$  relative to that of  $\text{En}_{\text{ss}} + \text{Di}_{\text{ss}} + \text{An} + \text{Qtz}$  indicates that at least one, but more likely both pyroxenes must show strong increases in  $\text{Al}_2\text{O}_3$  with increasing pressure up to the appearance of garnet.

An isothermal invariant point occurs at 16 kb at a composition about  $\text{En}_{54}\text{An}_{46}$  in this system where Gar,  $\text{Di}_{\text{ss}}$ ,  $\text{En}_{\text{ss}}$ , An, and Qtz coexist. At higher enstatite concentrations garnet appears at progressively higher pressures.

A number of authors have indicated that  $\text{Al}_2\text{O}_3$  solubility in pyroxenes may

be sufficiently sensitive to pressure to be a valuable geobarometer. With suitable assemblages it is possible that the temperature effect can be combined to provide a  $P$ - $T$  grid over a geologically useful range. Evaluation of the effect of decreasing anorthite activity by progressive substitution of the albite component will be necessary. Addition of albite permits formation of jadeite ( $\text{NaAlSi}_2\text{O}_6$ ), which may enter into solid solution in clinopyroxene. At moderate temperatures and pressures, however, the concentration of  $\text{NaAlSi}_2\text{O}_6$  relative to  $\text{CaAl}_2\text{SiO}_6$  in clinopyroxene should be low (Kushiro 1969a), possibly low enough to neglect without serious error for  $P$ - $T$  conditions equivalent to the granulite facies. T. H. Green (1969) found only small  $\text{Na}_2\text{O}$  contents in highly aluminous pyroxenes crystallized from high-alumina basalt at pressures between 13.5 and 18 kb. Natural pyroxenes also contain iron whose effect on solubility of  $\text{Al}_2\text{O}_3$  is not known.

#### *Upper P-T Stability of a Natural Olivine-Plagioclase Assemblage*

The upper limits of stability of coexisting olivine and plagioclase define the depths to which troctolites may exist in the earth's crust. Many layered intrusions contain troctolite assemblages, and they can provide useful upper limits on the depths at which the intrusions may have crystallized. The Michikamau intrusion (Emslie, 1970) has a layered sequence that is interpreted as having had an original thickness of not less than 15 km. The lowermost members of the layered series are troctolite. Establishment of the stability limits of this natural assemblage provides a limit to the maximum depth at which the intrusion crystallized.

Kushiro and Yoder (1966) have studied the univariant reaction 2 forsterite + anorthite = forsterite + clinopyroxene + orthopyroxene + spinel over a range of temperature and pressure. Their curve

for this reaction is reproduced in Fig. 6. Under water pressures equal to total pressure the assemblage forsterite-anorthite is not stable at any pressure above 7.5 kb (Yoder, *Year Book 65*, p. 276). Addition of albite to the system increases the stability field of forsterite and plagioclase (Emslie and Lindsley, *Year Book 67*, p. 110), but addition of iron should tend to decrease it. The relative magnitudes of these effects are not readily assessed, and the direct approach was chosen instead.

Analyzed olivine and plagioclase separated from a single specimen of troctolite from the lowermost exposed part of the layered series of the Michikamau intrusion were chosen for the experiment. The olivine composition is  $\text{Fo}_{70}\text{Fa}_{30}$  wt %; the plagioclase is  $\text{An}_{73}\text{Ab}_{27}$  wt %. A 1:1 mixture of these minerals by weight was made, ground finely under acetone, and

thoroughly dried. Experiments were made in platinum capsules.

Because both natural minerals are solid solutions, the reaction between olivine and plagioclase must proceed over a  $P$ - $T$  interval. Of the new minerals formed by reaction, clinopyroxene is most abundant. The curve marking the beginning of reaction was therefore located by determining the first appearance of clinopyroxene in X-ray patterns of the run products. The curve is shown in Fig. 6. The curve has been drawn with a slope parallel to that for the forsterite-anorthite reaction. The present data, however, would permit a slightly steeper slope.

This assemblage of olivine-plagioclase is stable to pressures approximately  $1\frac{1}{2}$  kb higher than forsterite-anorthite at the same temperature. It is possible to argue that this difference is within the experimental limits of uncertainty. Nevertheless, the curve marking the upper stability of the olivine-plagioclase assemblage remains a valid maximum. The experiments at  $958^\circ\text{C}$  probably did not reach equilibrium, although they were run for  $2\frac{1}{2}$  days. The sluggishness of the reaction increases rapidly at temperature below  $1000^\circ\text{C}$ , and reaction kinetics may prevent the higher pressure assemblage from forming at low temperatures in dry rocks. The crystallization temperature of the Michikamau troctolite was probably near  $1200^\circ\text{C}$ . It is certain from these experimental data that the total pressure was not greater than 9 kb and probable that it did not exceed 8 kb. This is equivalent to about 28 km depth, so that assuming a 15-km thickness for the intrusion would permit a maximum thickness of about 13 km for the cover rocks.

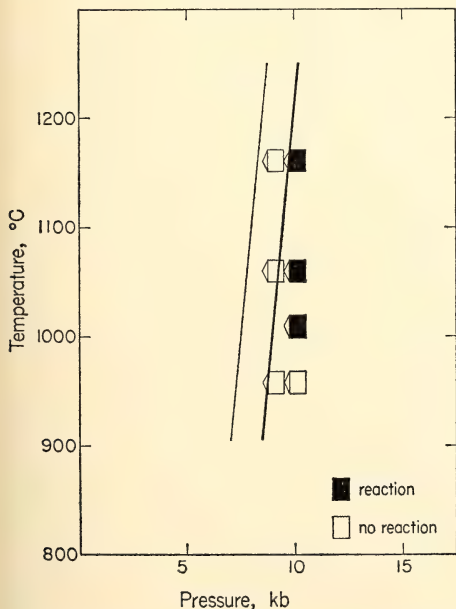


Fig. 6. Subsolidus reaction between olivine ( $\text{Fo}_{70}$  wt %) and plagioclase ( $\text{An}_{73}$  wt %). Light line is the curve of Kushiro and Yoder (1966) for the upper stability of forsterite-anorthite. Heavy line marks the upper stability limit for the natural olivine-plagioclase assemblage.

#### KOSMOCHLOR AND THE CHROMITE-PLAGIOCLASE ASSOCIATION

H. S. Yoder, Jr., and G. Kullerud

Chromium is now recognized as a key element in meteorites, lunar rocks, and



various depth-dependent assemblages in terrestrial rocks. Its appearance in specific minerals is greatly influenced by the prevailing conditions during crystallization. Chromite is the major chromium-bearing phase in terrestrial and meteoritic rocks, whereas in the lunar rocks chromite is a component in titaniferous spinels. Under specific conditions in terrestrial rocks chromium may occur as a major constituent in pyroxene or garnet, or very rarely an oxide ( $\text{Cr}_2\text{O}_3$ ). At moderate depths in the earth chromium is in the pyroxene structure as a minor solid solution in chromiferous diopside and in addition uniquely as a pyroxene close to the end member kosmochlor,  $\text{NaCrSi}_2\text{O}_6$ , in meteoritic material. It is relevant to determine why chromium occupies the same structure in such different proportions in these contrasting environments.

Meteoritic chondrules are unique in that they may consist wholly of chromite and plagioclase or contain minor olivine or pyroxene as well. Some pyroxene was thought by Ramdohr to be possibly "relict" kosmochlor (=ureyite), the laths of which are pseudomorphosed by chromite (Ramdohr, 1967, Figs. 5 and 10). In addition some of the feldspar was described as albite. The close association of plagioclase and chromite in the chondrules of certain meteorites suggests coprecipitation from a liquid by fast cooling (quench), whereas the textures of the same minerals occurring in the Bushveld layered intrusion (Cameron and Emerson, 1959) indicate slow cooling. The chromite is usually considered a "released mineral" (Bowen, 1928, p. 280) from the reaction of a Cr-bearing spinel with liquid to produce mainly olivine and plagioclase. The reaction effect may persist in liquids with normative An as low as 59 (Schairer and Yoder, *Year Book 65*, p. 206). Resorption of aluminous chromites in some troctolites supports this concept (Thayer, 1946, p. 205).

Kosmochlor was discovered by Las-

peyres (1897) in the meteorite from Toluca, Mexico, and was documented by Frondel and Klein (1965) on other material, which they called ureyite, from the same locality, in addition to two other meteorites, and by Neuhaus (1966) on the original material. The mineral is imbedded in sulfides with feldspar, zircon, quartz, and most significantly, with a chromiferous diopside containing "only about 1%  $\text{Cr}_2\text{O}_3$ " (Frondel and Klein, 1965, p. 744). The possibility of kosmochlor occurring in terrestrial rocks and as a precursor of the chromite in layered intrusions is of considerable interest in the light of the low  $\text{Cr}_2\text{O}_3$  content (<3 wt %) of chromiferous diopsides (Ross, Foster, and Myers, 1954; Boyd, 1969).

Kosmochlor was first synthesized by Coes (1955, p. 298) at the optimum conditions of 900°C and 20 kb using  $\text{Na}_2\text{Cr}_2\text{O}_7 + \text{SiO}_2$ . He noted that it was a component of chromiferous diopsides in eclogites believed to have formed at relatively high pressures. Frondel and Klein (1965, p. 742) reported its synthesis at 1 atm from nonstoichiometric mixtures, but they were unable to produce it by fusion from its own composition. In the same year Wurmbach in Neuhaus *et al.* (1965, p. 546) also reported its synthesis at high pressures under anhydrous conditions. The present writers have grown kosmochlor from its own composition hydrothermally at 500°, 600°, and 700°C and 2 kb. At 700°C and 2 kb albite + chromite, as well as albite + eskolaite ( $\text{Cr}_2\text{O}_3$ ), were found to be stable. A mixture of kosmochlor + anorthite + enstatite reacted at the same conditions to form an albitic plagioclase + eskolaite + chromite + clinopyroxene. One possible explanation of the meteoritic assemblage is, therefore, that kosmochlor is a stable product or a metastable quench product that reacts with an anorthitic plagioclase as well as bronzite and possibly olivine, the common associates of chromite, to form albitic plagioclase, chromite, and a clinopyroxene.

It is possible that the kosmochlor may

be inherited from a moderately high-pressure environment (e.g., eclogitic facies). A mixture of albite, chromite, and forsterite yielded a kosmochlor-rich clinopyroxene and a transparent spinel at 30 kb and 1200°C. The results are in accord with the observation that the enstatite + spinel = forsterite + pyrope equilibrium of MacGregor (*Year Book* 63, p. 157, and unpublished data) is raised to higher pressures with Cr. At still higher pressures the mixture may yield a kosmochlor-rich clinopyroxene and a garnet of the pyrope-knorringite series (cf. Nixon and Horning, 1968). On these grounds the Cr would be expected to be found mainly in the spinel structure at low pressures, in the pyroxene structure at moderate pressures, and in the garnet structure at very high pressures (cf. Meyer, 1968). Curiously enough, both the spinel and the pyroxene structures are stable at 1 atm with maximum Cr contents. The synthesis of knorringite at high pressures mentioned by Coes (1955) appears to have been withdrawn because of the presence of Ca in the starting materials (Coes, 1962), leading instead to the formation of a uvarovite molecule.

The coexistence of kosmochlor with chromiferous diopside suggests that  $\text{CaMgSi}_2\text{O}_6$  and  $\text{NaCrSi}_2\text{O}_6$  do not form a complete series of solid solutions under natural conditions. The apparent absence of kosmochlor in terrestrial rocks indicates that the limit of solid solution of kosmochlor in diopside presumably exceeds at least 3 wt %, whereas the limit of diopside in kosmochlor is probably near 30 wt %. Experiments at 700°C and 2 kb with 3:1, 1:1, and 1:3 by weight mixtures of diopside and kosmochlor yielded a continuous series of pyroxenes based on the changes of the 131 and 221 reflections in the powder X-ray diffraction patterns. It is not known whether a solvus can form under other conditions in the laboratory.

Laspeyres noted that "augite" occurred with kosmochlor in his portion of

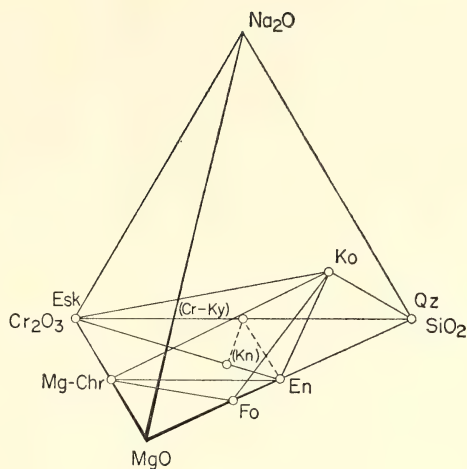


Fig. 7. The system  $\text{Na}_2\text{O-MgO-Cr}_2\text{O}_3\text{-SiO}_2$  and some of the known phases and presumed coexisting assemblages. The dashed joins and phases enclosed in parentheses are probably stable only at very high pressures. Ko, kosmochlor; Kn, knorringite; Qz, quartz; Esk, eskolaite; Mg-Chr, picrochromite; Fo, forsterite; En, enstatite; Cr-Ky, chromium kyanite.

the Toluca meteorite; the analysis listed, however, appears to be that of a bronzite. The relationship of kosmochlor with an orthopyroxene is displayed in Fig. 7 along with other coexisting  $\text{Cr}_2\text{O}_3$ -bearing phases. It would be useful to search more carefully those specimens containing chromiferous diopside and chromite for kosmochlor and to ascertain the exact  $\text{Cr}_2\text{O}_3$  content of those clinopyroxenes now found with kosmochlor. It is especially important to determine the sodium content of the chromiferous clinopyroxenes. Other types of solid solutions involving  $\text{Cr}_2\text{O}_3$  are possible in clinopyroxene.

#### THE JOINS $\text{Na}_2\text{O} \cdot 5\text{MgO} \cdot 12\text{SiO}_2$ -SODIUM DISILICATE AND $2\text{Na}_2\text{O} \cdot 3\text{MgO} \cdot 5\text{SiO}_2$ -SODIUM DISILICATE IN THE SYSTEM $\text{Na}_2\text{O-MgO-SiO}_2$

*J. F. Schairer and H. S. Yoder, Jr.*

During the past year a final manuscript for the system  $\text{Na}_2\text{O-MgO-SiO}_2$  has been in preparation. Schairer, Yoder,

and Keene (*Year Book 52*, p. 64, Fig. 11; *Year Book 53*, p. 124, Fig. 13) and Schairer (1957, p. 227, Fig. 25) gave preliminary phase-equilibrium diagrams for this system. Recently the X-ray patterns on all of the nearly 300 compositions that were prepared were examined and compared. At this time phase-equilibrium diagrams for the joins 1:5:12-Na disilicate and 2:3:5-Na disilicate are presented as Figs. 8 and 9, respectively.

It is interesting to note the successive incongruent melting behavior of  $\text{Na}_2\text{O} \cdot \text{MgO} \cdot 4\text{SiO}_2$ ,  $\text{Na}_2\text{O} \cdot 2\text{MgO} \cdot 6\text{SiO}_2$ , and  $\text{Na}_2\text{O} \cdot 5\text{MgO} \cdot 12\text{SiO}_2$  in the join 1:5:12-Na disilicate (Fig. 8). No evidence for solid solution in the system  $\text{Na}_2\text{O}$ - $\text{MgO}$ -

$\text{SiO}_2$  has been found except possibly in very soda-rich compositions that lie below the line forsterite-Na metasilicate. In this soda-rich region, alkali losses make the determination of the phase-equilibrium relations difficult to interpret. Another interesting aspect of the system of  $\text{Na}_2\text{O}$ - $\text{MgO}$ - $\text{SiO}_2$  as compared with  $\text{K}_2\text{O}$ - $\text{MgO}$ - $\text{SiO}_2$  (Roedder, 1951) is the lack of similarity in compounds, except the compound with the 1:5:12 ratio. There is no correlation in compounds between  $\text{Na}_2\text{O}$ - $\text{MgO}$ - $\text{SiO}_2$  and  $\text{Na}_2\text{O}$ - $\text{CaO}$ - $\text{SiO}_2$  (Morey and Bowen, 1925). Insufficient data are available on the compounds in  $\text{Na}_2\text{O}$ - $\text{FeO}$ - $\text{SiO}_2$  (Schairer, Yoder, and Keene, *Year Book 53*, p. 126,

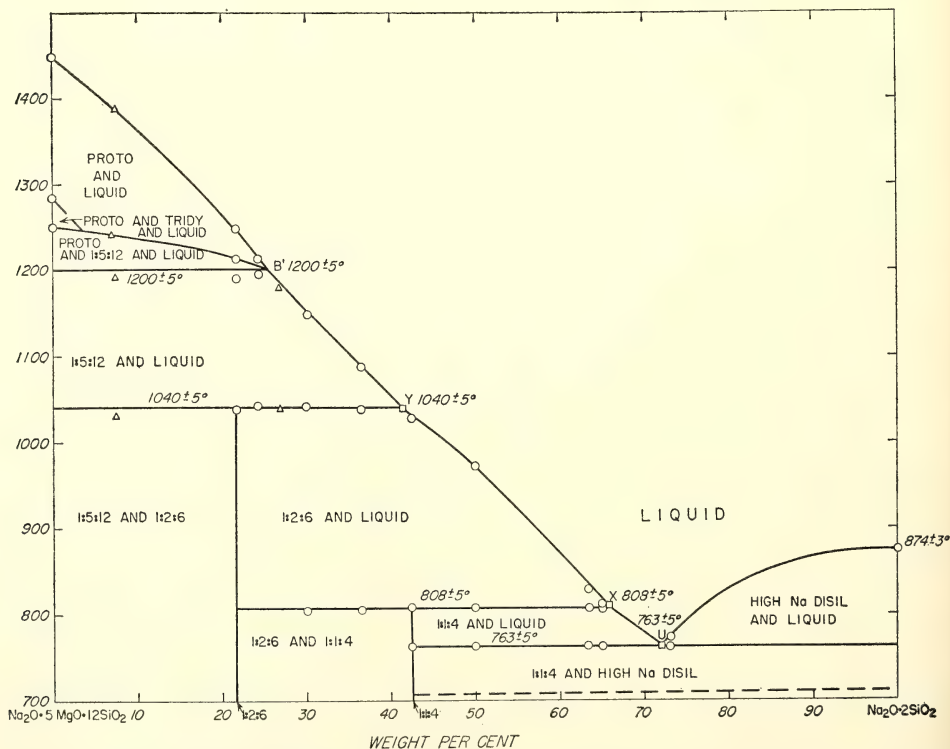


Fig. 8. Phase-equilibrium diagram of the system 1:5:12-sodium disilicate. Open circles represent determined equilibria on preparations that lie on the join; open triangles are for those preparations in the ternary system within a few percent of this join; open squares are lettered invariant points (same as in ternary equilibrium diagram); the point lettered *B'* lies where the join cuts the boundary curve protoenstatite + 1:5:12 + liquid. The ratios are for ternary compounds of soda, magnesia, and silica. The horizontal dashed line for which we have no data marks the inversion between high sodium disilicate and a lower temperature polymorph.



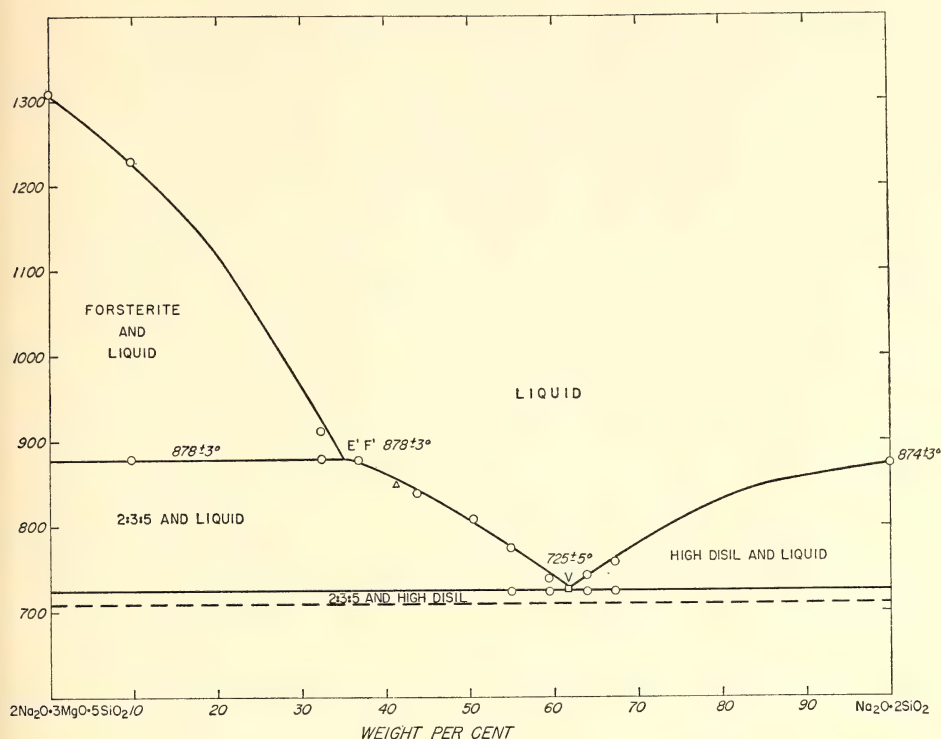


Fig. 9. Phase-equilibrium diagram of the system 2:3:5-sodium disilicate. Symbols and horizontal dashed line as in Fig. 8. The point labeled  $E'F'$  is also a binary invariant point and lies where the join cuts the boundary curve forsterite + 2:3:5 + liquid.

Fig. 14) to make a comparison at this time; however, at least the 1:1:4 compounds are analogous.

The compound  $\text{Na}_2\text{O} \cdot 5\text{MgO} \cdot 12\text{SiO}_2$  is similar structurally to the minerals roedderite (Fuchs, Frondel, and Klein, 1966), merrihueite (Dodd, van Schmus, and Marvin, 1965) osumilite, probably milarite and armenite (Schreyer and Schairer, 1962), and the synthetic compound  $\text{K}_2\text{O} \cdot 5\text{MgO} \cdot 12\text{SiO}_2$  (Roedder, 1951). There appear to be no other structural similarities with the known compounds in the  $\text{K}_2\text{O}$ - $\text{MgO}$ - $\text{SiO}_2$  system even though one compound has the same ratio of oxides as  $\text{Na}_2\text{O} \cdot \text{MgO} \cdot 3\text{SiO}_2$ . The structural similarity of  $\alpha\text{K}_2\text{O} \cdot \text{MgO} \cdot 3\text{SiO}_2$  to kalsilite, recognized by Roedder, implies a most unusual type of solid solution,  $\text{Mg}^{\text{IV}}\text{Si}^{\text{IV}} \rightarrow 2\text{Al}^{\text{IV}}$ . In an analogous

fashion nepheline would presumably have some solid solution toward  $\text{Na}_2(\text{MgSi})\text{Si}_2\text{O}_8$ . Pursuing this line of reasoning further, it may be possible to account for siliceous albite with minor solid solution toward  $\text{Na}_2(\text{MgSi})\text{Si}_6\text{O}_{16}$  and  $\text{Na}_2(\text{Fe}^{2+}\text{Si})\text{Si}_6\text{O}_{16}$  without changing the alkali content.

The eight new ternary compounds identified in the  $\text{Na}_2\text{O}$ - $\text{MgO}$ - $\text{SiO}_2$  system have the ratios 1:5:12, 1:2:6, 1:2:4, 1:1:4, 1:1:3, 2:2:3, 2:3:5, and 2:1:3. Their powder X-ray diffraction patterns are displayed in Fig. 10. The compound 2:2:3 appears to have at least three polymorphs; however, their thermal relations have not as yet been determined satisfactorily. The 1:1:1 compound reported by Hughes (1966) appears to consist of the 2:2:3 (Fig. 10) and an-

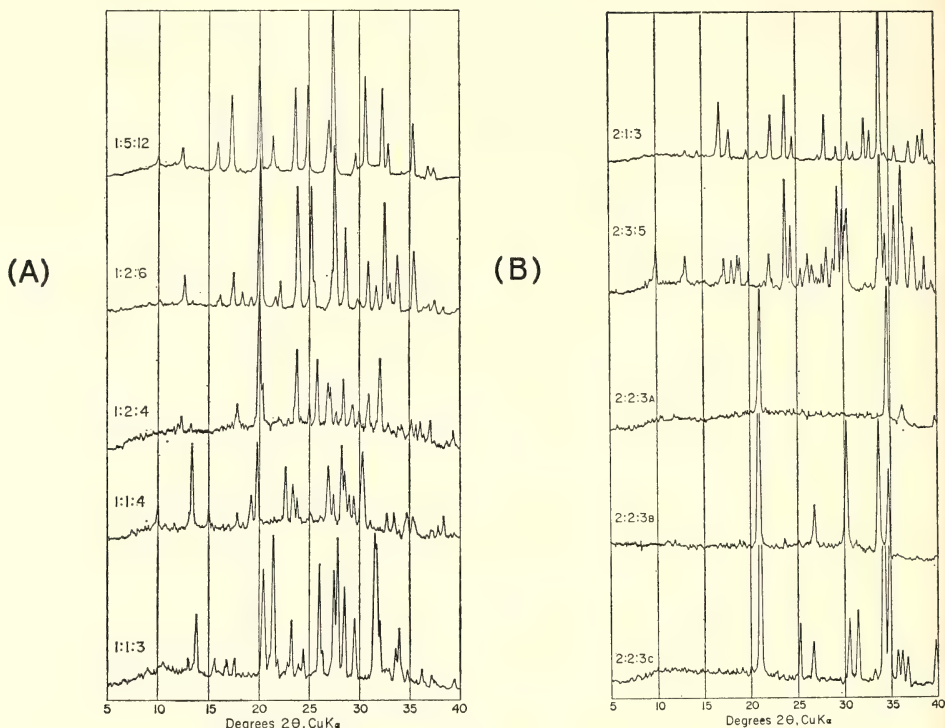


Fig. 10. (A) Powder X-ray diffraction patterns for identified compounds in the  $\text{Na}_2\text{O}$ - $\text{MgO}$ - $\text{SiO}_2$  system having the ratios 1:5:12, 1:2:6, 1:2:4, 1:1:4, and 1:1:3 in the region  $5^\circ$ - $40^\circ$   $2\theta$  ( $\text{CuK}\alpha$  radiation). (B) Powder X-ray diffraction pattern for identified compounds in the  $\text{Na}_2\text{O}$ - $\text{MgO}$ - $\text{SiO}_2$  system having the ratios 2:1:3, 2:3:5, and 2:2:3 in the region  $5^\circ$ - $40^\circ$   $2\theta$  ( $\text{CuK}\alpha$  radiation). Note the similarity of 2:1:3 with some peaks in 2:3:5. The phases with patterns labeled 2:2:3A, B, and C are believed to be related by polymorphism. The two main peaks of 2:2:3A are also contained in 2:2:3B, which therefore may be a mixture; intensity variations in obvious mixtures suggest, however, that 2:2:3B is a single phase.

other unidentified phase. Several other new compounds in compositions more soda rich than the forsterite-sodium metasilicate join have not as yet been identified, and electron probe studies were not successful because of the fine grain size of the crystals. One additional phase was encountered in those compositions in the region 1:1:4-quartz-sodium disilicate in the subsolidus below  $715^\circ\text{C}$ , especially in the crystallized starting materials. The powder X-ray diffraction pattern is related to the "D" polymorph of sodium disilicate reported by Kracek, Morey, and England (*Year Book* 52, pp. 58-60) but may possibly

be that of a low-temperature ternary compound in that region.

#### THE COMPOUND $3\text{Na}_2\text{O} \cdot 8\text{SiO}_2$ IN THE SYSTEM $\text{Na}_2\text{O}$ - $\text{SiO}_2$

*J. F. Schairer and H. S. Yoder, Jr.*

The compound  $3\text{Na}_2\text{O} \cdot 8\text{SiO}_2$  was first described by Williamson and Glasser (1965) and was characterized as having an incongruent melting point at  $808^\circ \pm 2^\circ\text{C}$ , melting to quartz and liquid. Bailey and Schairer (1966, pp. 145-146) reported that a reexamination of the system sodium disilicate-silica indicated that the compound  $3\text{Na}_2\text{O} \cdot 8\text{SiO}_2$  occurs at the binary eutectic quartz- $3\text{Na}_2\text{O} \cdot$

$8\text{SiO}_2$  and the compound melts incongruently at  $794^\circ \pm 2^\circ\text{C}$ , having only a very small liquidus range in the system  $\text{Na}_2\text{O}-\text{SiO}_2$ .

Schairer, Yoder, and Keene (*Year Book 52*, p. 64, Fig. 11; *Year Book 53*, p. 124, Fig. 13) and Schairer (1957, p. 227, Fig. 25) gave preliminary diagrams for the system  $\text{Na}_2\text{O}-\text{MgO}-\text{SiO}_2$ . In these studies problems were encountered with the polymorphic forms of sodium disilicate. At the ternary eutectic ( $M$  of Fig. 11), quartz,  $\text{Na}_2\text{O} \cdot \text{MgO} \cdot 4\text{SiO}_2$ , and the alleged  $W$  form of sodium disilicate were the three solid phases. The

alleged  $W$  form of sodium disilicate is not a polymorph of sodium disilicate but instead has the composition  $3\text{Na}_2\text{O} \cdot 8\text{SiO}_2$ .

Our considerable data on the ternary system  $\text{Na}_2\text{O}-\text{MgO}-\text{SiO}_2$  indicate that there are boundary curves between quartz and  $3\text{Na}_2\text{O} \cdot 8\text{SiO}_2$ ,  $\text{Na}_2\text{O} \cdot \text{MgO} \cdot 4\text{SiO}_2$ , and  $3\text{Na}_2\text{O} \cdot 8\text{SiO}_2$ , and between  $3\text{Na}_2\text{O} \cdot 8\text{SiO}_2$  and the high-temperature form of sodium disilicate. The point  $M'$  of Fig. 11 ( $\text{Na}_2\text{O} \cdot \text{MgO} \cdot 4\text{SiO}_2 + 3\text{Na}_2\text{O} \cdot 8\text{SiO}_2 + \text{high } \text{Na}_2\text{Si}_2\text{O}_5 + \text{liquid}$ ) lies at  $738^\circ\text{C}$ , and the liquidus temperatures along the boundary curve  $M'M$  are at

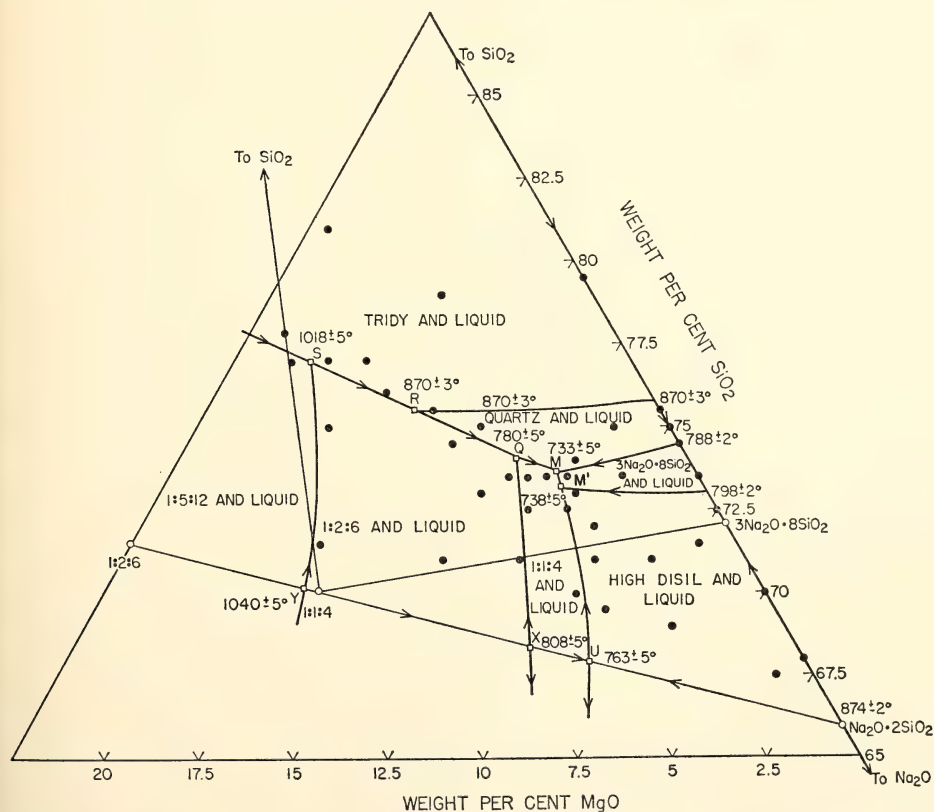


Fig. 11. Phase-equilibrium diagram for the siliceous portion of the system  $\text{Na}_2\text{O}-\text{MgO}-\text{SiO}_2$  lying in the triangles  $\text{Na}_2\text{O} \cdot \text{MgO} \cdot 4\text{SiO}_2-\text{Na}_2\text{O} \cdot 2\text{SiO}_2-3\text{Na}_2\text{O} \cdot 8\text{SiO}_2$  and  $\text{Na}_2\text{O} \cdot \text{MgO} \cdot 4\text{SiO}_2-3\text{Na}_2\text{O} \cdot 8\text{SiO}_2-\text{SiO}_2$ . Black dots indicate the compositions of preparations studied. Heavy curves are boundary curves between the several primary fields on the liquidus surface. The lettered points are squares representing binary or ternary invariant points. Open circles also show the composition of binary or ternary compounds.



slightly lower temperatures, until the ternary eutectic  $M$  is reached at  $733^{\circ}\text{C}$ . These relationships led us to look very carefully into the binary system  $\text{Na}_2\text{Si}_2\text{O}_5\text{-SiO}_2$ , particularly in the region near  $3\text{Na}_2\text{O}\cdot 8\text{SiO}_2$  and the binary eutectic with quartz as one of the solid phases.

The coexistence of  $W$  and high sodium disilicate in the completely crystallized glasses was erroneously interpreted as nonequilibrium; that is, complete inversion of the "polymorph" was not attained. The failure to observe quartz in those compositions between  $\text{Na}_2\text{O}\cdot 2\text{SiO}_2$  and  $3\text{Na}_2\text{O}\cdot 8\text{SiO}_2$  was attributed to its

small amount. In addition the liquidus field of  $3\text{Na}_2\text{O}\cdot 8\text{SiO}_2$  is too small in the ternary system to use the lever principle for determining the composition of the precipitating phase. For these reasons  $W$  was incorrectly assumed in the earlier work to be a polymorph of  $\text{Na}_2\text{O}\cdot 2\text{SiO}_2$  rather than a new compound.

The X-ray patterns on all the compositions and runs in the system  $\text{Na}_2\text{O-MgO-SiO}_2$  were examined and compared. These comparisons indicate that there is a field of the compound  $3\text{Na}_2\text{O}\cdot 8\text{SiO}_2$  on the liquidus surface, and the results for this portion of  $\text{Na}_2\text{O-MgO-SiO}_2$  are given here as Fig. 11. These data indicate that

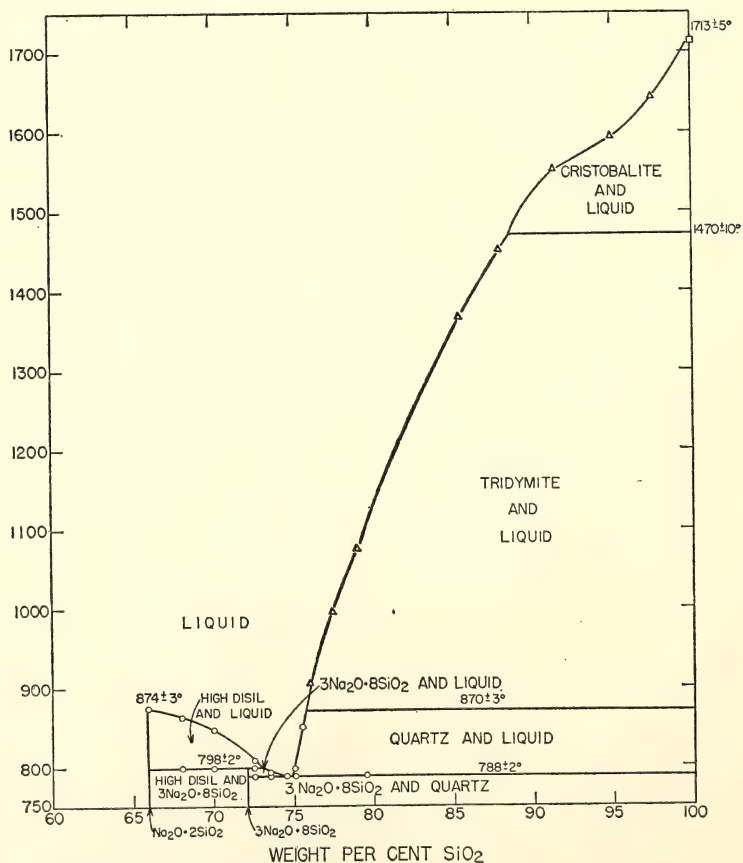


Fig. 12. Phase-equilibrium diagram for the binary system  $\text{Na}_2\text{O}\cdot 2\text{SiO}_2\text{-SiO}_2$ . Open circles are compositions studied by Schairer and Yoder. Triangles are the data of Kracek (1930*a,b*). High disilicate is the high-temperature form of  $\text{Na}_2\text{O}\cdot 2\text{SiO}_2$ .

the compound  $3\text{Na}_2\text{O} \cdot 8\text{SiO}_2$  must melt incongruently to high sodium disilicate (not quartz as suggested by Williamson and Glasser, 1965, 1966) and liquid and that a small field of  $3\text{Na}_2\text{O} \cdot 8\text{SiO}_2$  appears on the liquidus surface in the ternary system.

Additional runs have now been made in the binary system  $\text{Na}_2\text{Si}_2\text{O}_5$ - $\text{SiO}_2$ . The compositions studied were  $\text{Na}_2\text{O}$ - $\text{SiO}_2$  preparations with 68, 70, 72.5, 73.5, 74.5, 75, 75.5, and 79.5 wt %  $\text{SiO}_2$ . The compound  $3\text{Na}_2\text{O} \cdot 8\text{SiO}_2$  has 72.1 wt %  $\text{SiO}_2$  and melts incongruently at  $798^\circ \pm 2^\circ\text{C}$  to a more siliceous liquid and crystals of the high-temperature form of sodium disilicate, with a sodium disilicate liquidus at  $807^\circ\text{C}$ . There is a small field of  $3\text{Na}_2\text{O} \cdot 8\text{SiO}_2$  on the liquidus surface in the binary system, and the eutectic with quartz lies at  $788^\circ \pm 2^\circ\text{C}$ . The data are plotted here in Fig. 12. Dr. F. P. Glasser (personal communication, June 1970) confirms our results. He indicates that his recent studies of the siliceous portion of the system  $\text{Na}_2\text{O}$ - $\text{CaO}$ - $\text{SiO}_2$  show a field of  $3\text{Na}_2\text{O} \cdot 8\text{SiO}_2$  on the liquidus surface and that  $3\text{Na}_2\text{O} \cdot 8\text{SiO}_2$  must melt incongruently to high disilicate and liquid, not to quartz and liquid.

THE SYSTEM JADEITE ( $\text{NaAlSi}_2\text{O}_6$ )-  
ANORTHITE ( $\text{CaAl}_2\text{Si}_2\text{O}_8$ ) AT  
HIGH PRESSURES

H. K. Mao

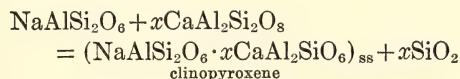
The roles of calcium-Tschermak's molecule and silica in the pressure-temperature stabilization of jadeitic clinopyroxene were studied up to 40 kb and  $1700^\circ\text{C}$ . A study of pure jadeite composition and jadeite with 5, 15, 25, and 35 wt % anorthite composition was begun last year, and a report of their melting relations at 1 atm was given (*Year Book* 68). This year, jadeite-CaTsch clinopyroxene solid solutions were synthesized at high pressures. The jadeite-CaTsch clinopyroxenes were found to be stable in a  $P$ - $T$  region in

which neither end member was stable. These clinopyroxenes were also found to dissolve as much as 7.5 wt % excess  $\text{SiO}_2$ . For a fixed Ca Tschermak's molecule content, the solubility of  $\text{SiO}_2$  in the jadeite-CaTsch clinopyroxene is highly pressure-sensitive, suggesting that the excess  $\text{SiO}_2$  content in the clinopyroxene could be a potential continuous geobarometer. The jadeite-CaTsch clinopyroxenes, like plagioclase (Lindsley, *Year Book* 65, p. 204), melt incongruently to corundum+liquid at high pressures.

The starting materials for the experiments were glass, crystalline plagioclase, and nepheline, and crystalline clinopyroxene for studying various phase boundaries. The starting material was dried in nitrogen at  $800^\circ$  to  $1050^\circ\text{C}$  for 0.5 to 2 hours and welded in a platinum capsule while it was still hot. All runs were performed in a Boyd-England type, single-stage, piston-cylinder apparatus utilizing the outstroke procedure. Temperatures were measured with Pt 10% Rh/Pt thermocouples and were corrected for the effect of pressure on thermocouple emf on the basis of the work of Getting and Kennedy (1970).

*Jadeite-Anorthite Solid Solutions*

$\text{Jd}_{95}\text{An}_5$ ,  $\text{Jd}_{85}\text{An}_{15}$ ,  $\text{Jd}_{75}\text{An}_{25}$ , and  $\text{Jd}_{65}\text{An}_{35}$  glass were held overnight at  $1300^\circ\text{C}$  and 40 kb and then quenched. The expected reaction



did not occur. Instead, in every experiment the result was a single jadeitic clinopyroxene phase, as determined by powder X-ray diffraction and optical examination. No coesite or quartz was found. Electron microprobe analysis also indicated no free silica. Apparently, all excess silica was dissolved in the jadeite-CaTsch clinopyroxene. To check whether

the clinopyroxene was a metastable product, a one-week run with the clinopyroxene as starting material was made at 38 kb and 1200°C. No change was observed.

It should be pointed out that pure synthetic jadeite dissolves very little excess silica in the analogous Jd-Ab system. Similar relationships exist in the diopside-anorthite and diopside-albite systems. In the Di-An system, Kushiro (1969a) obtained a single clinopyroxene phase from a sample containing up to 50 wt % anorthite at 22 kb and 1400°C, whereas in the Di-Ab system he always obtained quartz and/or plagioclase in addition to the clinopyroxene phase. A probable reason is that in jadeite and diopside all tetrahedral (T) sites of the pyroxene structure are occupied by Si ions. For any excess silica to dissolve some Si must be in the octahedral (M2) site, an occurrence that is seldom observed in nature. In Tschermak's molecule, on the other hand, half of the T sites are occupied by Al. To dissolve excess silica merely requires that Si replace the tetrahedral Al and the Al be removed to the M2 site.

When excess silica is dissolved, the total cation-to-oxygen ratio will be less than the ideal ratio for pyroxene, 2:3. A conventional way to calculate the formula for pyroxene is to normalize all cations to six oxygen atoms. All Si is assigned to T, and Al is added if necessary to make  $T=2$ . The remaining Al and other small cations are assigned to M2, and large cations like Na and Ca are assigned to the octahedral (M1) site. The calculated formulas for jadeitic clinopyroxenes with the compositions  $\text{Jd}_{95}\text{An}_5$ ,  $\text{Jd}_{85}\text{An}_{15}$ ,  $\text{Jd}_{75}\text{An}_{25}$ , and  $\text{Jd}_{65}\text{An}_{35}$  are, respectively,  $(\text{Na}_{0.95}\text{Ca}_{0.04})(\text{Al}_{1.00})(\text{Al}_{0.025}\text{Si}_{1.975})\text{O}_6$ ,  $(\text{Na}_{0.85}\text{Ca}_{0.11})(\text{Al}_{1.00})(\text{Al}_{0.07}\text{Si}_{1.93})\text{O}_6$ ,  $(\text{Na}_{0.76}\text{Ca}_{0.18})(\text{Al}_{1.00})(\text{Al}_{0.12}\text{Si}_{1.88})\text{O}_6$ , and  $(\text{Na}_{0.66}\text{Ca}_{0.26})(\text{Al}_{1.00})(\text{Al}_{0.17}\text{Si}_{1.83})\text{O}_6$ . The resultant total M1 value is 0.01 to 0.08 less than 1. The resultant M2 is exactly equal to 1. Coleman and Clark (1968)

observed the calculated M1 values for some clinopyroxenes from the blueschist facies of California to be substantially less than 1. They attributed this result to the inhomogeneity of the sample. As indicated by the present work, however, it is possible that these clinopyroxenes do not have the ideal formulas.

The unit-cell parameters for the Jd-An clinopyroxenes were determined through least-squares refinement of powder X-ray diffraction data with the program of Burnham (*Year Book 61*). The data were collected in the range 20° to 60° with  $\text{CuK}\alpha_1$  and  $\text{CuK}\alpha_2$  radiation and Si internal standard. The variation of the unit-cell parameters with composition is presented in Fig. 13. Parameters of  $\text{CaAl}_2\text{SiO}_6$  pyroxene (Hays, 1966) are plotted at the anorthite end for comparison. All parameters except  $\beta$  of the  $\text{CaAl}_2\text{SiO}_6$  pyroxene are substantially larger than the linear extrapolation of those of Jd-An clinopyroxene.

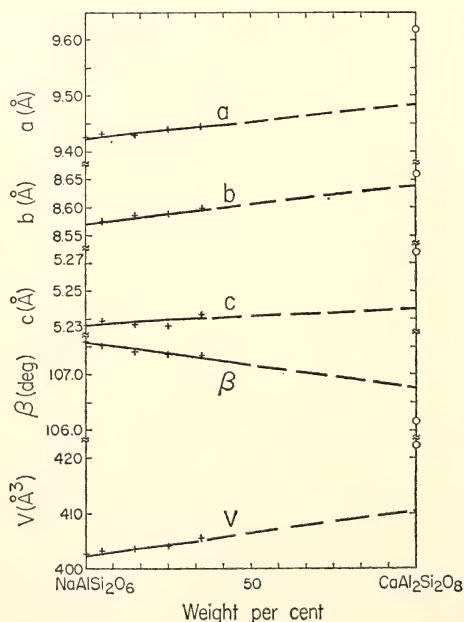


Fig. 13. Unit-cell parameters of jadeite-anorthite clinopyroxenes. The circles at the anorthite end represent data on calcium-Tschermak's molecule (Hays, 1966).



## Phase Equilibrium in the Jd-An System

Pressure-temperature phase diagrams for the fixed bulk compositions  $\text{Jd}_{95}\text{An}_5$  and  $\text{Jd}_{65}\text{An}_{35}$  are presented in Fig. 14A and B. Point *I* is an invariant point of the  $\text{NaAlSi}_3\text{O}_8\text{-SiO}_2$  binary system. Lines *IA* in Fig. 14A and *IS* and *SB* in Fig. 14B are univariant curves in the Jd-An system. All other lines in Fig. 14A and B are compositionally dependent. In the regions where corundum exists the system is quaternary ( $\text{CaO-Na}_2\text{O-Al}_2\text{O}_3\text{-SiO}_2$ ). In other regions the system degenerates to a ternary one ( $\text{NaAlSi}_3\text{O}_8\text{-SiO}_2\text{-CaAl}_2\text{SiO}_6$ ) provided the nepheline solid solution is on the ternary plane.

## Subsolidus Relations

Albite and nepheline form jadeite at high pressure. As the bulk composition changes from pure Jd to Jd-An, the subsolidus equilibrium boundary Plagioclase + nepheline<sub>ss</sub>  $\rightleftharpoons$

jadeitic clinopyroxene shifts to a lower pressure, and the three-phase region (jadeitic clinopyroxene + plagioclase + nepheline<sub>ss</sub>) changes from a line to a band (Fig. 14). The stability field of the clinopyroxene expands to the low-pressure region where neither the end member jadeite nor the end member Ca-Tschermak's molecule is stable (Fig. 15A). An isothermal *P-X* section for

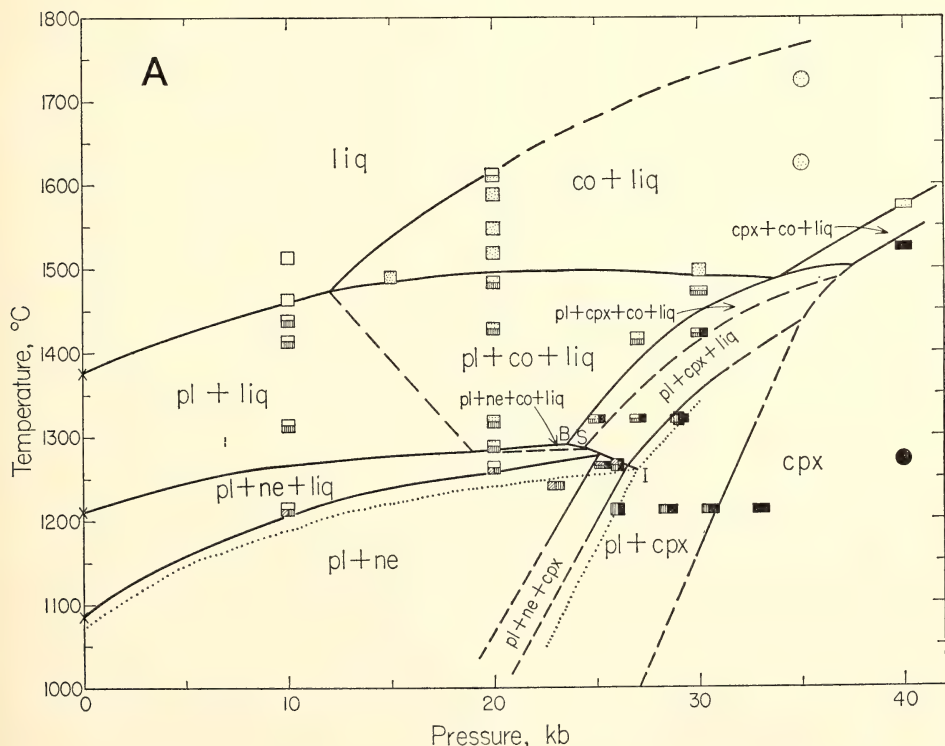
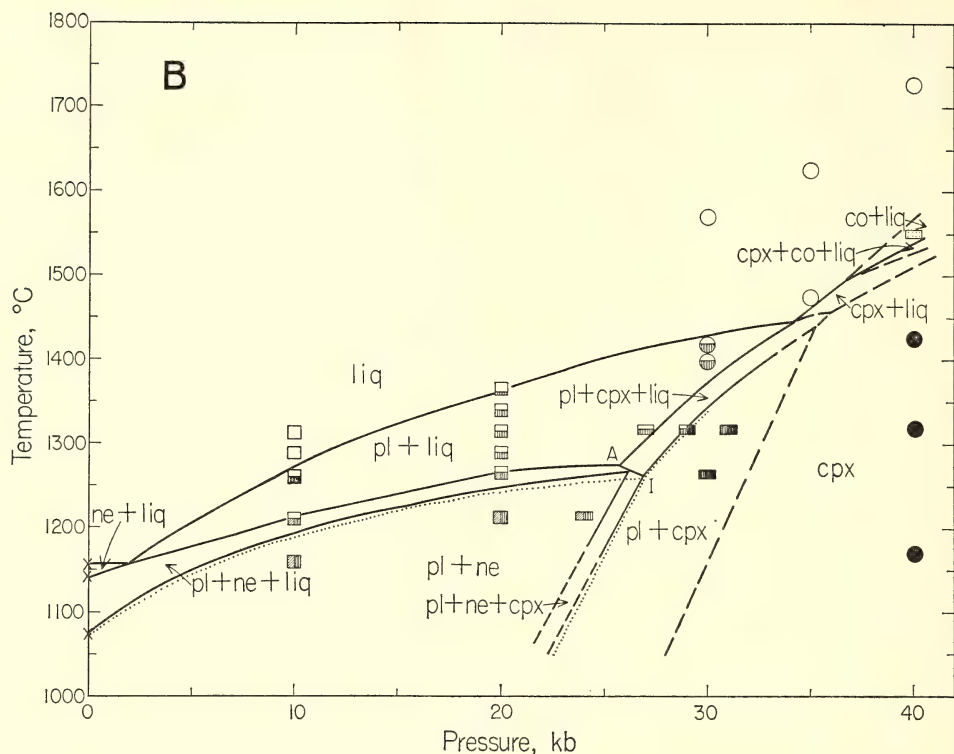


Fig. 14. *P-T* phase diagrams. (A) Bulk composition  $\text{Jd}_{95}\text{An}_5$ . (B) Bulk composition  $\text{Jd}_{65}\text{An}_{35}$  (wt %). Abbreviations: liq, liquid; pl, plagioclase; ne, nepheline solid solution; cpx, clinopyroxene; co, corundum. The shape of the symbol indicates the starting material: circle, glass; square, pl + ne; rectangle, cpx. The content of the symbol indicates the product: blank, liq; vertically shaded, pl; diagonally shaded, ne; dotted, co + liq; solid, cpx. Dotted lines are univariant lines in the  $\text{NaAlSi}_3\text{O}_8\text{-SiO}_2$  system. Dashed lines indicate no data or less reliable data.



Jd-CaTs composition at 1200°C is presented in Fig. 15B to illustrate the situation that the solid solution is stable while both end members are not.

In the Jd-An system at a pressure slightly higher than the (clinopyroxene + plagioclase + nepheline<sub>ss</sub>) three-phase region, the stable phase assemblage is

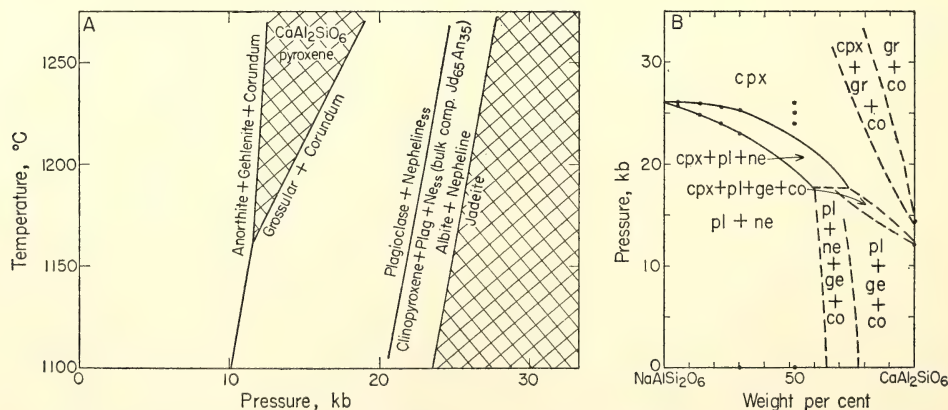


Fig. 15. (A)  $P$ - $T$  stability fields of jadeite-CaTs clinopyroxenes. (B) Isothermal section of jadeite-CaTs at 1200°C. Abbreviations: gr, grossular solid solution; ge, gehlenite solid solution; others as in Fig. 14.

clinopyroxene and plagioclase. Estimated from the plagioclase-to-clinopyroxene ratio, the composition of this clinopyroxene is probably very close to an ideal  $\text{NaAlSi}_2\text{O}_6$ - $x\text{CaAl}_2\text{SiO}_6$  composition. With increasing pressure, the amount of plagioclase decreases. Evidently the clinopyroxene dissolves more and more excess silica. Gradually all excess silica is dissolved and the clinopyroxene shifts to a Jd-An composition. No breakdown components of pure anorthite, such as gross-

sular and kyanite, are found in the  $P$ - $T$  range studied. Isothermal and isobaric sections of the  $\text{CaAl}_2\text{SiO}_6$ - $\text{NaAlSi}_2\text{O}_6$ - $\text{SiO}_2$  ternary system at  $1200^\circ\text{C}$  and 15, 24, 25, 26, and 33 kb are presented in Fig. 16 to show the nature of the subsolidus reactions. A few experiments with  $\text{Ne}_{85}\text{An}_{15}$  composition were made to check these phase diagrams.

Since the solubility of silica in a Jd-CaTsch clinopyroxene is a function of pressure and temperature, the  $P$ - $T$  rela-

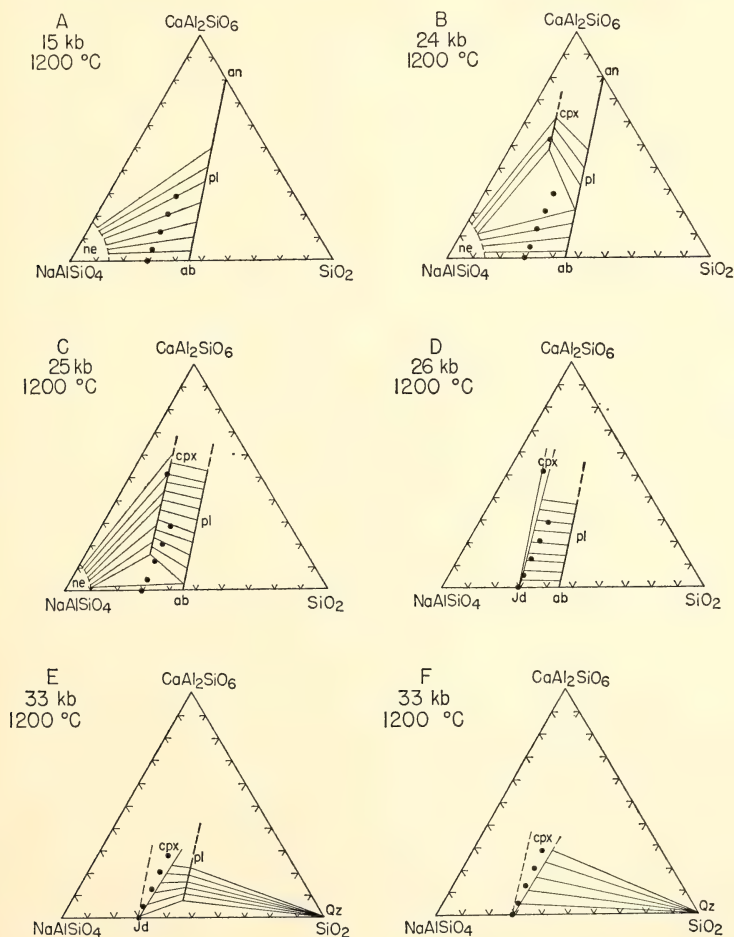


Fig. 16. Isothermal isobaric sections of the  $\text{CaAl}_2\text{SiO}_6$ - $\text{NaAlSi}_2\text{O}_6$ - $\text{SiO}_2$  system at  $1200^\circ\text{C}$ . (A) 15 kb; (B) 24 kb; (C) 25 kb; (D) 26 kb; (E-F) alternatives at 33 kb: (E) if an intermediate plagioclase decomposes to  $\text{cpx} + \text{qz}$  at a higher pressure than albite does, or (F) if an intermediate plagioclase decomposes to  $\text{cpx} + \text{qz}$  at a lower pressure than albite. Abbreviations: ab, albite; an, anorthite; jd, jadeite; qz, quartz; others as in Fig. 14.



tions of a Jd-CaTsch clinopyroxene at the time of its formation can be indicated from the chemical composition of the clinopyroxene alone. The natural clinopyroxene usually contains diopside, aegirine, and hedenbergite, however, and their roles in the solubility of silica must be known before the chemical composition of the clinopyroxene can be used as a geothermometer and geobarometer. It is likely that the solubility of silica in the Di-CaTsch clinopyroxene is also a function of  $P$  and  $T$ , as revealed by inspection of Kushiro's (1969a) data.

### Melting Relations

The plagioclase + nepheline + liquid and plagioclase + jadeite + liquid univariant curves in the  $\text{NaAlSi}_3\text{O}_8$ - $\text{SiO}_2$  binary system become divariant bands in the Jd-An ternary system ( $\text{NaAlSi}_3\text{O}_8$ - $\text{SiO}_2$ - $\text{CaAl}_2\text{SiO}_6$ ) and move to higher temperatures with increasing An contents (Fig. 14). A univariant curve separates the plagioclase + clinopyroxene + liquid divariant band from the plagioclase + nepheline solid solution + liquid and plagioclase + nepheline solid solution + clinopyroxene divariant bands. The plagioclase liquidus and clinopyroxene liquidus also move to higher temperatures with increasing An content.

Plagioclase and jadeitic clinopyroxene begin to melt incongruently to corundum + liquid with increasing pressure and An content. Point S in Fig. 14B is the intersection of a quaternary univariant curve and its degenerated ternary univariant curve and is fixed in  $P$ - $T$  space if the bulk composition varies on the  $\text{NaAlSi}_3\text{O}_8$ - $\text{SiO}_2$ - $\text{CaAl}_2\text{SiO}_6$  plane. The curves that separate  $\text{cpx} + \text{pl} + \text{co} + \text{liq}$  from  $\text{cpx} + \text{pl} + \text{liq}$  and  $\text{pl} + \text{ness} + \text{co} + \text{liq}$  from  $\text{pl} + \text{ness} + \text{liq}$  are not true univariant curves, but they are fixed in  $P$ - $T$  space if the bulk composition varies on the  $\text{NaAlSi}_3\text{O}_8$ - $\text{SiO}_2$ - $\text{CaAl}_2\text{SiO}_6$  plane, and the compositions of plagioclase, clinopyroxene, and nepheline<sub>ss</sub> are all on this plane. Because some of the details of the phase

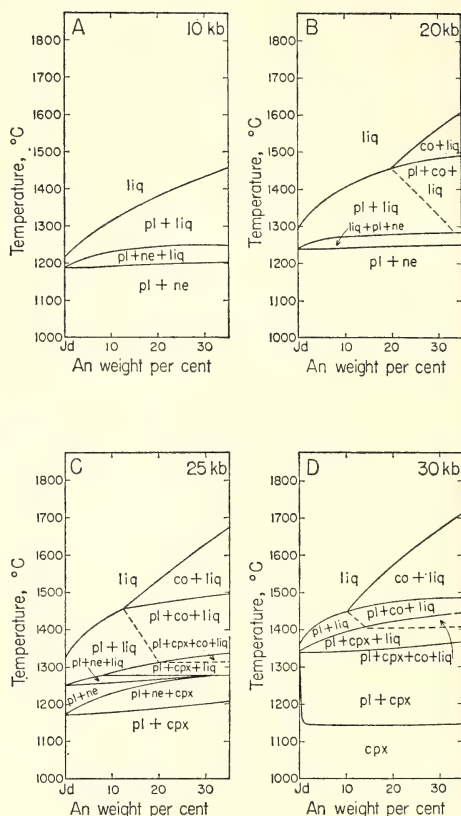


Fig. 17. Temperature-composition section of the Jd-An system. Abbreviations as in Fig. 14.

equilibria occur over too small a  $P$ - $T$  range to be resolved, and the equilibria in the corundum-bearing assemblage are difficult to attain, the incongruent melting to corundum + liquid, especially at the first appearance of corundum, is less well determined. Isobaric temperature-composition sections at 10, 20, 25, and 35 kb are presented in Fig. 17 to show the melting relations.

### SUBSOLIDUS REACTIONS OF JADEITE ( $\text{NaAlSi}_3\text{O}_6$ ) AND ALBITE ( $\text{NaAlSi}_3\text{O}_8$ )

*P. M. Bell and H. K. Mao*

Using special means to speed equilibria, such as the addition of water and

phase seeds, it has been possible to produce rapid and precise reactions in the system jadeite-albite. This system responds so reproducibly that it is now being suggested as a standard for inter-laboratory calibration, and various values of other workers are presented here.



The results are shown in Fig. 18 with the unreduced data of Newton and Kennedy (1968) and Boettcher and Wyllie (1968) and unpublished results of W. Johannes, University of Göttingen, Germany. Johannes also supplied the starting materials, which consist of a 1:1 mixture of analyzed natural jadeite+quartz and albite to which we added excess  $\text{H}_2\text{O}$ . The experiments of this study were run at  $600^\circ\text{C}$  and were made under conditions of instroke and outstroke piston motion in order to evaluate friction. These results show no evidence of piston-cylinder friction.

Agreement is evident with the raw data of Newton and Kennedy and with those of Boettcher and Wyllie, although these two groups applied arbitrary fraction corrections of  $-5\%$  and

8.8%, respectively, in their published reports. Johannes' values are distinctly lower in pressure and may reflect the fact that in his apparatus sodium chloride was the primary pressure medium, whereas talc and boron nitride were employed in the other studies. Positive or negative "anvil" effects can exist in these high-pressure cells, from strength differences of the strong ceramic pieces relative to the weaker talc pieces. The existence of strength differences in the single-stage cell has been demonstrated by Green, Ringwood, and Major (1966). Richardson, Bell, and Gilbert (1968) have shown that the present high-pressure cell gives results 2–3 kb too high in pressure at this temperature range compared with those obtained with purely hydrostatic pressure media. Clearly, a fixed point on albite breakdown determined with hydrostatic equipment would be useful here, but the pressures needed for jadeite formation are beyond the capability of our available hydrostatic pressure vessel.

These results, therefore, serve as a valuable cross-comparison, not only for the upper limit of albite stability, but for all other systems determined with this apparatus.

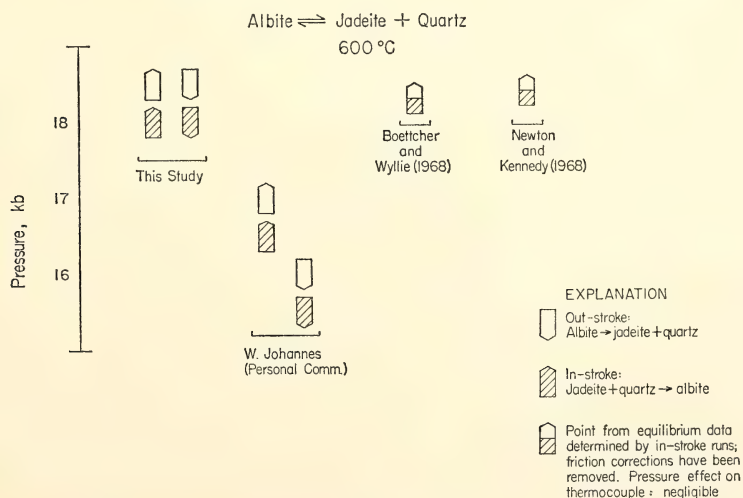


Fig. 18. Experiments with albite  $\rightleftharpoons$  jadeite + quartz.





omphacite. Acmite is perhaps the most important of the subordinate components; it constitutes over 10% of some omphacites (Coleman *et al.*, 1965) and has a large incongruent melting range (322°C at 1 atm, Yagi, 1966, and Fig 20 of this report). Bowen and Schairer (1929) described the incongruent melting of acmite at 1 atm and pointed out its potential role in the generation of soda- and silica-enriched magmas by fractional crystallization and the separation of iron oxides from the reacting magma. Their 1-atm data have since been reproduced with some refinement by Bailey and Schairer (1966), and the incongruent melting was recently shown by Gilbert (1969) to persist to at least 40 kb. The melting curve of diopside was first determined by Yoder (1952) to 10 kb; Boyd and England (1963) extended the congruent melting curve to 50 kb; it has recently been redetermined, with some disagreement at pressures above 30 kb, by Williams and Kennedy (1969).

The melting behavior of diopside-acmite solid solutions at 1 atm was investigated experimentally by Yagi (*Year Book 61* and 1966). The incongruent melting range of Di-Ac solid solutions at 1 atm decreases in general with increasing Di content (Fig. 20). Compositions between pure acmite and  $\text{Di}_{42}\text{Ac}_{58}$  (all compositions in this report are expressed as mole %) melt initially to pyroxene<sub>ss</sub>+hematite+liquid in air at 1 atm. With increasing temperature, either pyroxene<sub>ss</sub> or hematite disappears from this assemblage, depending on the composition. The coexistence of three solid phases+liquid along the solidus of the pseudobinary diopside-acmite join enhances the possibilities of magmatic fractionation during partial melting or crystallization.

Several possible mechanisms of basic magma formation by partial melting of eclogites and garnet peridotites in the upper mantle and subsequent magmatic fractionation have been discussed by

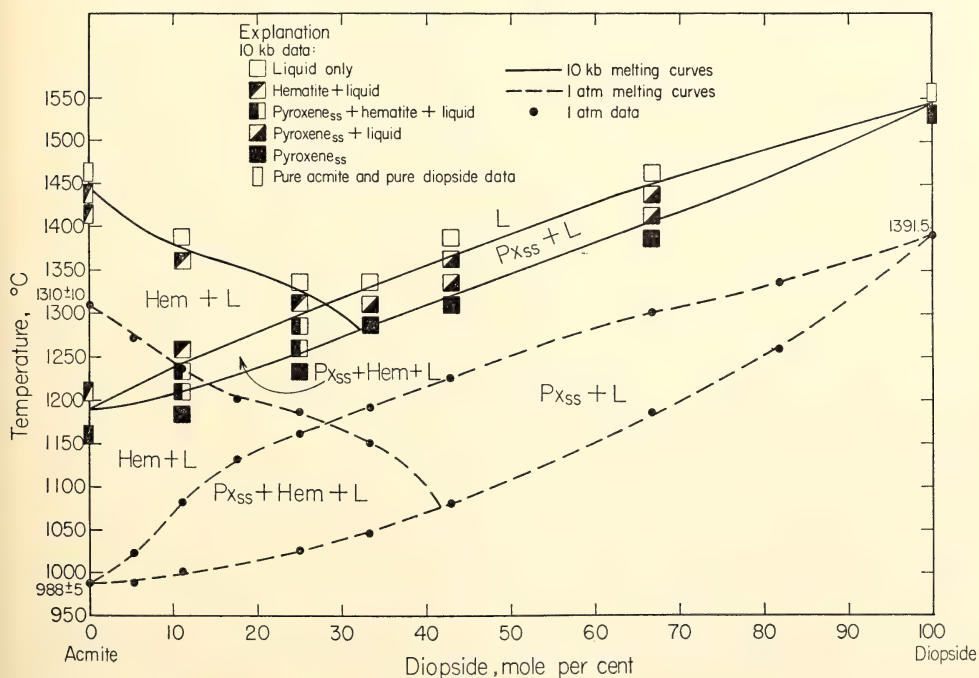


Fig. 20. Melting curves for diopside-acmite at 1 atm and 10 kb.

many authors in the recent literature; a comprehensive review of the various magmatic evolution schemes in the light of experimental work has been presented by O'Hara (1968). Omphacites are major constituents of eclogites, and knowledge of the melting behavior at pressure of the three pairs of omphacite components diopside-jadeite, jadeite-acmite, and diopside-acmite is essential to an understanding of magmatic evolution deep in the earth's crust and upper mantle. A study of the first of these joins at high pressures was reported by Bell and Davis (1969); Gilbert's (1969) work on acmite stability at high pressures was preliminary to a projected study of the jadeite-acmite join. The present study was undertaken to determine the effect of pressure on the temperature range of incongruent melting and the phase-equilibrium relations of diopside-acmite solid solutions, and thereby to gain further understanding of the role of omphacite in magma fractionation.

Glasses were prepared at intervals from pure acmite to pure diopside, with emphasis on the acmite-rich end of the join. A portion of each glass was subsequently crystallized in air as described by Yagi (1966). Precautions were taken to minimize the solution of iron in the platinum crucibles; deviations from the starting compositions were negligible, as will be seen below. The 1-atm data obtained by Yagi were reproduced, within the limits of experimental error, in a series of quenching runs with both glass and crystalline starting materials. Five of these preparations were selected and finely ground for use as starting materials in the high-pressure study of the Di-Ac join.

The piston-and-cylinder high-pressure apparatus designed and modified by Boyd and England (1960, 1963) was used. The magnitude and causes of pressure uncertainty in this experimental system have been discussed in detail by Richardson, Bell, and Gilbert (1968).

The pressure uncertainty in the data presented here is estimated to be not more than  $\pm 1.5$  kb. Experimental temperature and pressure conditions in all runs were approached in a consistent manner (the "piston-out" technique). The reactants in all experimental runs were contained in sealed platinum capsules. The size and position of the capsule in the pressure cell were carefully controlled to minimize the temperature error due to the thermal gradient in the cell (Boyd and England, 1963). Pt/Pt 10% Rh thermocouples were used, and all the temperature data presented here have been corrected for the pressure effect, with the use of working curves based on the study of Getting and Kennedy (1970); the previously determined melting temperatures of acmite (Gilbert, 1969) and diopside (Boyd and England, 1963) (which have been reproduced within the limits of experimental error in this investigation) were similarly corrected.

The effects of oxygen partial pressure on acmite stability were discussed by Yagi (1966) and investigated in detail by Bailey (1969) and Gilbert (1969). Bailey demonstrated by a series of buffered hydrothermal experiments that the melting temperature of acmite is lowered considerably as  $P_{O_2}$  decreases. At the suggestion of H. S. Yoder, Jr.,  $PtO_2$  powder was added to each of the thoroughly dried charges prior to welding the platinum capsule to assure a high  $P_{O_2}$  in the capsule. The high  $P_{O_2}$  should not only maintain the most favorable atmosphere for the stability of the acmite component but also oxidize any  $Fe^{2+}$  in the reactants. Whether or not the latter effect was actually achieved is not known with certainty because no analyses to determine  $Fe_2O_3/FeO$  have been made.

The five selected compositions have been investigated at 10 kb; the composition  $Di_{33}Ac_{67}$  has been further studied at pressures up to 40 kb. The 10-kb data are shown in Fig. 20, as well as the 1-atm

melting curves determined in this study. All experimental products were quenched under conditions as nearly isobaric as possible in the piston-and-cylinder apparatus. The formation of feathery quench pyroxene<sub>ss</sub> crystals was not a significant problem; when quench pyroxene did form, it was seldom abundant and was easily distinguished from primary pyroxene<sub>ss</sub>. The tendency for quench pyroxene formation increased somewhat with increasing diopside content.

The most significant aspect of the 10-kb section is the considerable narrowing of the incongruent melting range of all the solid solution compositions investigated. In addition, the shape of the three-phase field pyroxene<sub>ss</sub> + hematite + liquid changes considerably between 1 atm and 10 kb. The melting of the acmite end member occurred over a narrow range, not well defined, as described by Gilbert (1969); because of the high  $P_{O_2}$  generated by the decomposition of  $PtO_2$  in the sealed capsule, magnetite did not appear in this interval as it did in Gilbert's experiments and acmite coexisted only with hematite + liquid. The solidus for this composition shown in Fig. 20 is therefore based on the complete disappearance of acmite. The composition  $Di_{33}Ac_{67}$  melts to pyroxene<sub>ss</sub> + hematite + liquid at 1 atm; hematite disappears with increasing temperature, leaving the assemblage pyroxene<sub>ss</sub> + liquid near the liquidus. At 10 kb this composition melts to pyroxene<sub>ss</sub> + liquid with no hematite formation.

The pressure-temperature data obtained for  $Di_{33}Ac_{67}$  to 40 kb are shown in Fig. 21. The melting behavior of this composition becomes apparently congruent between 30 and 40 kb; i.e., any region of incongruity that may exist is smaller than the range of uncertainty of temperature measurement in the experimental system. The change from incongruent to congruent behavior with increasing pressure probably corresponds to a minimum on the liquidus surface of

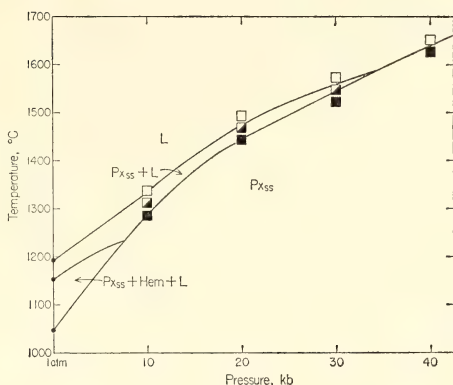


Fig. 21. Pressure-temperature plane for the composition diopside<sub>33</sub>acmite<sub>67</sub>.

the diopside-acmite join in the vicinity of the  $Di_{33}Ac_{67}$  composition. The pyroxene solid solution  $Di_{33}Ac_{67}$  apparently becomes truly binary at about 34 kb (Fig. 21), resulting in the observed congruent melting behavior above that pressure. Those portions of the reaction curves in Fig. 20 that do not involve hematite would be truly binary if the compositions of the pyroxene<sub>ss</sub> phases involved were actually on the Di-Ac join; this is probably not the case at 10 kb, however, as will be discussed below.

All crystalline starting materials and high pressure run products were examined by X-ray diffraction in an attempt to determine the pyroxene<sub>ss</sub> composition, with the use of the determinative curves of Nolan and Edgar (1963). These curves are applicable only to pyroxene<sub>ss</sub> phases that lie on the Di-Ac join. The method employs three diffraction peaks (221, 002, and 13 $\bar{1}$ ), which occur between  $34.5^\circ$  and  $36.5^\circ$   $2\theta$  (CuK $\alpha$  radiation) for members of this series.  $\Delta 2\theta$  002–13 $\bar{1}$  increases linearly with wt % from acmite to diopside, whereas  $\Delta 2\theta$  221–002 decreases linearly toward diopside. Each determination in this study was based on two diffraction scans, one from low- to high-angle  $2\theta$  and one in the opposite direction, at  $\frac{1}{4}^\circ$   $2\theta$  per minute and a chart speed of  $\frac{1}{4}$  inch per minute, essentially



the same instrumental conditions as were used by Nolan and Edgar (1963).

In Fig. 22 are presented the X-ray results for the crystalline starting materials and for sixteen subsolidus run products, none of which showed any apparent signs of chemical reduction (green coloration) or leakage of the charge from the capsule during the run. The results are ambiguous and suggest that the pyroxene<sub>ss</sub> compositions may not lie on the Di-Ac join. There is a consistent disparity between the compositions indicated by  $\Delta 2\theta$  221-002 and by  $\Delta 2\theta$  002-13 $\bar{1}$ : the former parameter gave consistently higher Di values than the latter, i.e.,  $\Delta 2\theta$  002-13 $\bar{1}$  was consistently too small for the associated  $\Delta 2\theta$  221-002; the Di values indicated by  $\Delta 2\theta$  221-002 were generally closer to the ideal compositions of the crystalline materials. Diffraction study of the crystalline products of numerous high-pressure runs in addition to those represented in Fig. 22 revealed that these same relationships were consistently maintained. Microscopically observed zoning of the individual crystals in the products of most experimental runs suggests that complete intracrystalline equilibrium was not attained. All of the

reactions in this study were carried out for at least as long as was found to be adequate by Gilbert (1969) and by Boyd and England (1963) for the acmite and diopside end members. Moreover, several runs of an hour or more did not produce any significant change in the X-ray results or in the zoning.

There are several possible explanations for the ambiguous X-ray results: (1) solid solution toward hedenbergite,  $\text{CaFe}^{2+}\text{Si}_2\text{O}_6$  (Nolan, 1969), or ferrosilite,  $\text{Fe}^{2+}\text{SiO}_3$  (Lindsley, Davis, and MacGregor, 1964), due to the presence of  $\text{Fe}^{2+}$  in the starting materials; (2) disorder of  $\text{Ca}^{2+}$  and  $\text{Fe}^{3+}$  between the  $M_1$  and  $M_2$  structural positions; (3) the presence of ferri-Tschermak's molecule,  $\text{CaFe}_2^{3+}\text{SiO}_6$  (Huckenholz, Schairer, and Yoder, 1969), and enstatite components in the pyroxene<sub>ss</sub> phases.

The first possibility can be effectively ruled out as a significant factor because the discrepancies between the observed  $\Delta 2\theta$  values do not correspond to those that would be caused by the substitution of  $\text{Fe}^{2+}$ .

Several lines of evidence could support the second possibility, that of disorder in the cation distributions: (1) the disparity between the compositions indicated by  $\Delta 2\theta$  221-002 and  $\Delta 2\theta$  002-13 $\bar{1}$ , with the use of Nolan and Edgar's (1963) curves, is larger for the intermediate composition  $\text{Di}_{33}\text{Ac}_{67}$  than for compositions near the end members; (2) the decrease in this disparity with increasing pressure, observed for the  $\text{Di}_{33}\text{Ac}_{67}$  composition, could be the result of increased ordering at the higher pressures; (3) the crystalline materials studied by Nolan and Edgar were synthesized hydrothermally at 750°C, whereas all crystalline materials in this study were formed under dry conditions at much higher temperatures. One would expect the hydrothermal materials to be more highly ordered if disordering does actually occur in this structure. Two hydrothermal runs

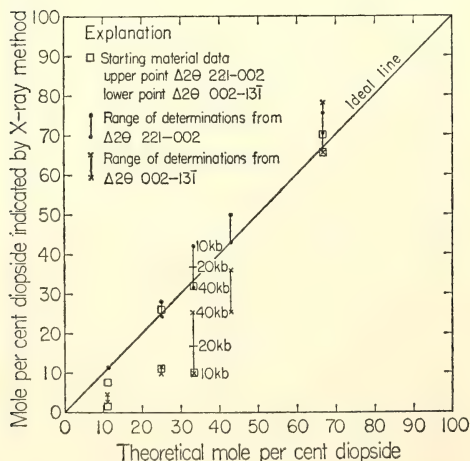
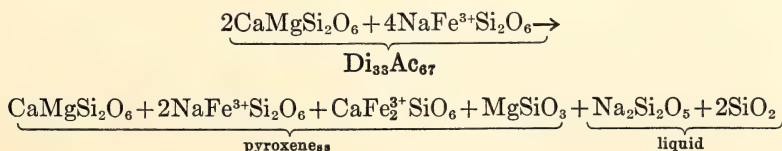


Fig. 22. X-ray diffraction results; the method of Nolan and Edgar (1963) was used.

with  $\text{Di}_{33}\text{Ac}_{67}$  glass and  $\text{Di}_{33}\text{Ac}_{67}$  crystalline starting material were held at  $750^\circ\text{C}$  and 1000 bars  $P_{\text{H}_2\text{O}}$  for 3 days in order to investigate the possibility of disorder in the cation distributions; the oxygen partial pressures of the runs were buffered by the hematite-magnetite pair. Microscopic examination of the products revealed that they were completely crystalline with only traces of intergranular filaments of glass. Application of the X-ray method of Nolan and Edgar (1963) indicated that their compositions corresponded to the theoretical  $\text{Di}_{33}\text{Ac}_{67}$  composition within the precision of the method, using both  $\Delta 2\theta$  parameters. One of these hydrothermally crystallized materials (crystallized from glass) was subsequently used as the charge in a piston-and-cylinder run at 10 kb and  $1275^\circ\text{C}$ ;  $\text{PtO}_2$  was added to the thoroughly dried charge in the usual manner. Subsequent X-ray examination of the crystalline product gave the following results:  $\Delta 2\theta$  221-002, 49 mole % Di;  $\Delta 2\theta$  002-13 $\bar{1}$ , 30 mole % Di. Microscopic examination revealed a definite increase in the abundance of tiny intergranular filaments of glass. Clearly some change had occurred during this dry subsolidus run.

The third possibility described above appears to offer the best means of reconciling both the X-ray data and the microscopic observations. Microscopic examinations of all crystalline pyroxene<sub>ss</sub> run products and crystalline starting materials revealed small amounts of ubiquitous minute interstitial filaments of glass and, in some cases, tiny ( $\sim 1\ \mu\text{m}$ ) spherules of glass inside the crystals. This glass may be a product of a "subsolidus" reaction such as:



If this type of reaction does occur, as suggested by H. S. Yoder, Jr. (personal communication), it is apparently suppressed under hydrothermal conditions. Moreover, no part of the Di-Ac join would be truly binary at pressures lower than about 30 kb, and the join could be properly described only by reference to a quaternary system, e.g.,  $\text{CaSiO}_3\text{-MgSiO}_3\text{-Fe}_2\text{O}_3\text{-Na}_2\text{Si}_4\text{O}_9$ . The ambiguous X-ray data may reflect variations in a complex pyroxene solid solution such as indicated in the above equation; such variations would no doubt be affected by temperature and pressure as well as starting composition. The necessity of detailed electron microprobe analyses of the pyroxene<sub>ss</sub> phases in the further investigation of this problem is apparent.

The present experimental data for diopside-acmite solid solutions indicate a distinct narrowing of the incongruent melting range with increasing pressure. This observation suggests that the effectiveness of partial melting of rocks containing acmite-omphacite in generating soda- and iron-enriched magmas may diminish with depth and that this mechanism may be truly effective only at relatively shallow depths in the mantle. Similar restrictions would apply also to residual magma generation by fractional crystallization of such magmas. Moreover, the X-ray results suggest that the determinative curves of Nolan and Edgar may not be strictly applicable to materials crystallized dry at high temperatures ( $>900^\circ\text{C}$ ) and low to intermediate pressures because of the possibility of increased complexity of the pyroxene solid solutions formed under these conditions and perhaps also because of possible  $\text{Ca}^{2+}\text{-Fe}^{3+}$  disorder in the crystal structure.

THE JOIN DIOPSIDE-PYROPE-H<sub>2</sub>O AT  
10 KB: ITS BEARING ON THE MELTING  
OF PERIDOTITE, THE ACF METAMORPHIC  
FACIES, AND THE GEDRITE-HORNBLEND  
MISCIBILITY GAP

H. S. Yoder, Jr.

Many phase assemblages pertinent to natural rocks appear in the CaO-MgO-Al<sub>2</sub>O<sub>3</sub>-SiO<sub>2</sub>-H<sub>2</sub>O system. Most of the major phases with the exception of quartz lie in a narrow band of composition straddling the anhydrous, iron-free, ACF plane (corundum-wollastonite-enstatite; Al<sub>2</sub>O<sub>3</sub>-CaSiO<sub>3</sub>-MgSiO<sub>3</sub>). Figure 23 illustrates the location, without regard for their H<sub>2</sub>O content, of most of the phases encountered in the present study near that plane. It was anticipated that knowledge of the phase assemblages in

diopside (Di)-pyrope (Py) along with data collected on the join grossularite (Gr)-pyrope (Yoder and Chinner, *Year Book 59*, p. 79, Fig. 25) would lead to a complete description of the relevant phase assemblages in the five-component system in the excess H<sub>2</sub>O region at 10 kb. Both Di-Py and Gr-Py lie in the ACF plane, and data on those joins, therefore, would uniquely define the array of assemblages for a range of temperatures at one pressure. An array of assemblages is required to define a metamorphic (or igneous) facies. One assemblage is not sufficiently unique to serve as the basis of a facies because its stability field normally transcends the stability field of other alleged diagnostic assemblages. The experimental determination of one or more arrays would provide a sound

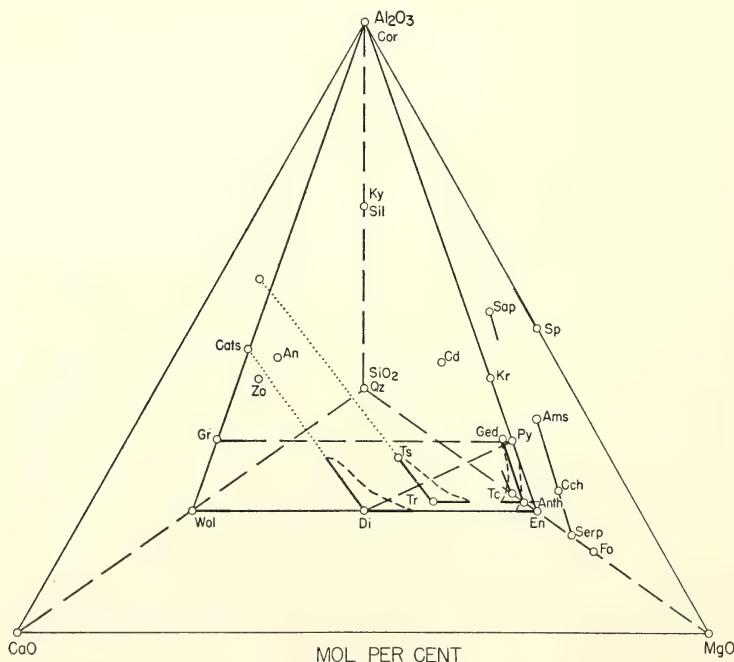


Fig. 23. Projection from H<sub>2</sub>O of phases pertinent to the present study of the CaO-MgO-Al<sub>2</sub>O<sub>3</sub>-SiO<sub>2</sub>-H<sub>2</sub>O system in the region of the ACF plane (Cor-Wol-En). Dashed lines locate the Gr-Py join studied by Yoder and Chinner (*Year Book 59*) and the Di-Py join herein described for  $P_{H_2O} = 10$  kb. Heavy bars indicate directions and rough limits of major known solid solution trends; where two directions are indicated the limits of solid solution are illustrated schematically by short dashed curves. Dotted lines are construction lines to real or fictive end members. Chlorites (Chl) lie along the join Ams-Cch and its extension.



basis for reestablishing quantitative application of the facies principle.

### *Previous Studies*

Data on the melting of diopside in the presence of  $H_2O$  at 10 kb were presented by Yoder (*Year Book 64*, p. 84, Fig. 9) and the behavior of the pyrope composition was reported on by Yoder and Chinner (*Year Book 59*, p. 79, Fig. 25), Fawcett and Yoder (*Year Book 62*, p. 144, Fig. 54), and Schreyer (*Year Book 66*, p. 390, Fig. 27). The diopside-pyrope system was studied at 1 atm by O'Hara and Schairer (*Year Book 62*, p. 107, Fig. 31) and at 30 kb by O'Hara and Yoder (1967); however, no previous hydrothermal studies on the join have been undertaken. The compositions prepared as glass by O'Hara and Schairer were used in the present study.

### *Discussion of Phase Diagram*

The results of the exploratory study are presented in Fig. 24, and the abbreviations used are defined in Table 3. The experimental difficulties are briefly described in the Appendix. The primary liquidus phases of diopside solid solution (Cpx), forsterite (Fo), and spinel (Sp) are comparable with those obtained at 1 atm by O'Hara and Schairer (*Year Book 62*, p. 107, Fig. 31). The major changes are the lowering of the liquidus

temperatures and the reduction of the forsterite field. Because of the quench products noted in the Appendix, the boundaries of the liquidus fields may not be located precisely. Quench clinopyroxene completely obscured the liquidus relations in diopside-rich compositions.

At about 1005°C, Fo reacts with liquid and yields an aluminous orthopyroxene (Opx), an aluminous clinopyroxene (Cpx), and Sp. The temperature is within experimental error of that obtained by Yoder and Chinner for the same reaction in other bulk compositions at the same water pressure. The phases involved approximate those of a spinel-peridotite, and, therefore, the reaction marks the beginning of melting of that assemblage. The temperature is remarkably close to that for the  $H_2O$ -saturated beginning of melting of a natural peridotite (spinel-bearing lherzolite) studied by Kushiro, Syono, and Akimoto (1968). The most important observation is that the liquid compositions must be quartz normative (cf. O'Hara, 1965, p. 35).

The assemblages close to 950°C form a continuous set except for Cpx+Opx+Sp+(?) + G. The presumed unknown phase is required because the known solid solutions of pyroxene and spinel do not enclose the compositions on the Di-Py join. The absence of quench products or glass (provided they are recognizable) precludes liquid. Alumi-

TABLE 3. Abbreviations Used in Text and Figures

Al-Serp	aluminous serpentine	Kr	kornerrupine
Ams	amesite	Ky	kyanite
An	anorthite	L	liquid
Anth	anthophyllite	Oam	orthoamphibole
Cam	clinoamphibole	Opx	orthopyroxene
CaTs	calcium Tschermak's molecule	Py	pyrope
Cch	clinochlore	q	quench
Cd	cordierite	Qz	quartz
Chl	chlorite	Sap	sapphirine
Cor	corundum	Serp	serpentine
Cpx	clinopyroxene	Sil	sillimanite
Di	diopside	Sp	spinel
En	enstatite	Te	talc
Fo	forsterite	Tr	tremolite
G	gas	Ts	tschermakite
Ged	gedrite	Wol	wollastonite
Gr	grossularite	Zo	zoisite

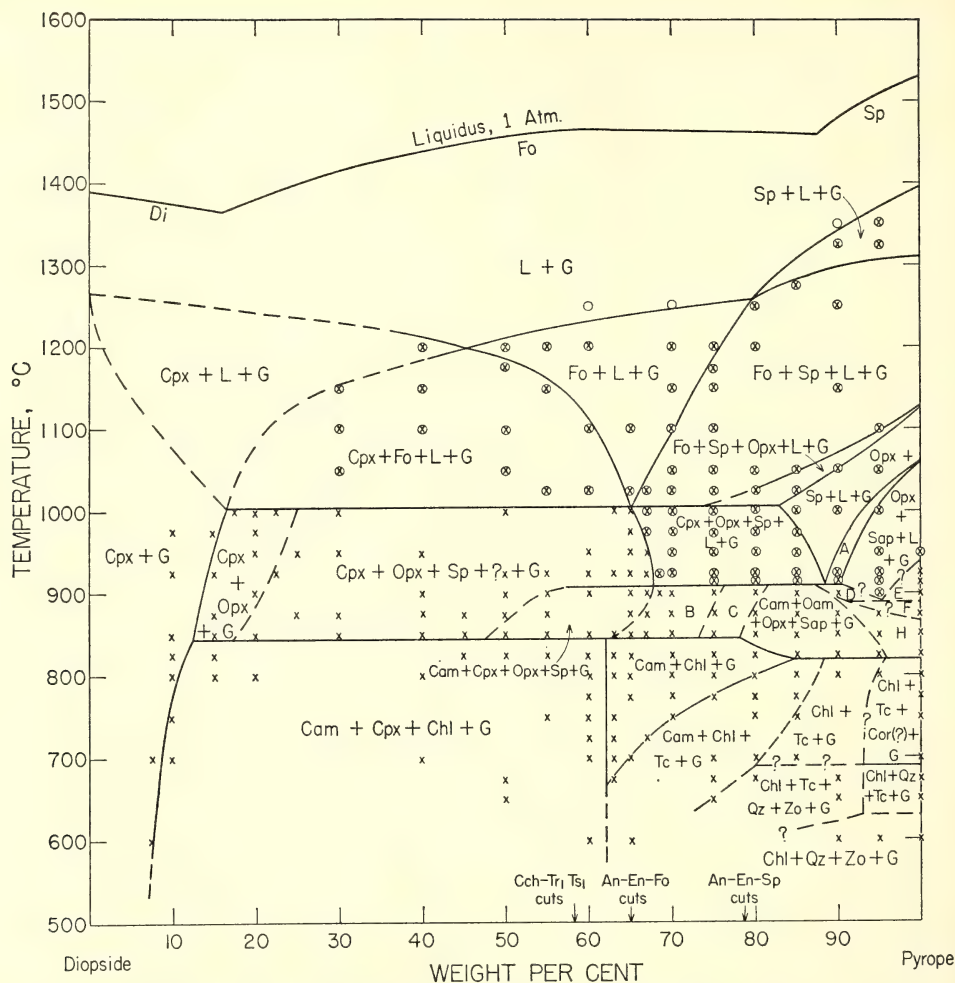


Fig. 24. Exploratory phase diagram for the diopside-pyroxene- $H_2O$  system at 10 kb. The liquidus at 1 atm is from O'Hara and Schairer (*Year Book 62*, p. 107, Fig. 31). Abbreviations are defined in Table 3. Lettered assemblages: (A)  $Opx + Sap + Sp + L + G$ ; (B)  $Cam + Opx + Sap + Sp + G$ ; (C)  $Cam + Opx + Sap + G$ ; (D)  $Oam + Sap + Sp + L + G$ ; (E)  $Cd + Opx + Sap + L + G$ ; (F)  $Cd + Opx + Sap + G$ ; (H)  $Oam + Opx + Sap + G$ . Critical intersections of the join with other joins are noted by a small arrow on the abscissa. Open circles, liquid and gas only; circle with cross, crystals with liquid and gas; cross, crystals with gas.

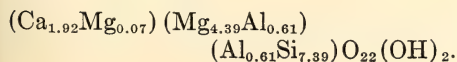
nous amphibole is probably not stable at these temperatures. Anorthite is stable in the subsolidus region with aluminous pyroxenes and quartz in the absence of  $H_2O$  at 10 kb (Kushiro and Yoder, 1966, p. 349, Fig. 3), and presumably would be stable with the aluminous pyroxenes and spinel. The assemblage  $Cpx + Opx + Sp + An + G$  was not encountered by

Yoder and Chinner, who obtained  $An + Cpx + Sp + L + G$  in the pertinent compositions. The nature of the unknown phase cannot be resolved at this time. The absence of a four-phase field between  $Cpx + Opx + G$  and  $Cpx + Opx + Sp + (?) + G$  is the result of the coplanar nature of the pyroxene solid solutions with the Di-Py join. The assemblage A,

Opx+Sp+Sap+L+G, is required, but cannot be demonstrated with satisfaction because of the nucleation difficulties with sapphirine.

The phase relations in the region 910° to 845°C are most difficult to interpret because of the rapid growth of the amphiboles. Excessive amounts of orthoamphibole (Oam) grew in runs of short duration in accord with the experience of Greenwood (1963) on pure anthophyllite. Run times employed here exceeded those in which Greenwood (1963, p. 344, Fig. 7) believed equilibrium was approached at 1 kb. Traces of clin amphibole (Cam) appear some 15° above 910°C even after long runs; it may be a persisting run-up product or a quench product. In the two-amphibole region, the initial assemblage is Cam+Oam+Opx+Sp+G, which gradually changes with time to Cam+Oam+Opx+Sap+G. Toward the more diopside-rich compositions this assemblage presumably passes progressively into Cam+Opx+Sap+G (C), Cam+Opx+Sap+Sp+G (B), Cam+Opx+Sp+G, and then into Cam+Cpx+Opx+Sp+G. An equally consistent set of assemblages can be evolved on the basis of short runs using the initial metastable assemblage Cam+Oam+Opx+Sp+G. Toward the more pyrope-rich compositions a complex series of changes is required, involving, for example, Oam+Sap+Sp+L+G (D), Opx+Sap+L+G, and Cd+Opx+Sap+L+G (E) at 900°C; Oam+Opx+Sap+G (H), Cd+Opx+Sap+G (F) at 880°C; and only Oam+Opx+Sap+G (H) at 860°C. Documentation of these assemblages will require use of more favorable compositions.

On the basis of preliminary electron probe analysis of Ca, Mg, and Al, if an ideal H<sub>2</sub>O content is assumed and the SiO<sub>2</sub> is obtained by difference, the clin amphibole in the two-amphibole region has the composition



It is essentially near the tremolite-tschermakite join with a small aluminous anthophyllite component.\* The Al<sub>2</sub>O<sub>3</sub> content was about 14 wt %.† The coexisting orthopyroxene had about 10 wt % Al<sub>2</sub>O<sub>3</sub> and a minor amount (~0.5) of CaO. The orthopyroxene, therefore, is mainly an enstatite containing some magnesium Tschermak's molecule and diopside in solid solution and may be thought of as containing about 40 wt % of potential pyrope. Analyses of three different samples of sapphirine coexisting with amphiboles and orthopyroxene yielded results that favored a composition close to 2MgO·2Al<sub>2</sub>O<sub>3</sub>·SiO<sub>2</sub> on the join cordierite-spinel rather than 4MgO·5Al<sub>2</sub>O<sub>3</sub>·2SiO<sub>2</sub>. Schreyer and Seifert (1969, p. 424) have reported the synthesis of the 2:2:1 sapphirine at 900°C and 10 kb. Only sapphirine fluoresced sufficiently to aid in identification under the electron probe beam. The orthoamphibole, presumably an aluminous anthophyllite, was too fine grained for electron probe analysis. The *minimum* content of Al<sub>2</sub>O<sub>3</sub> required in orthoamphibole for the pyrope composition to exhibit the assemblage Oam+Opx+Sap+G is about 9 wt % if the 2:2:1 composition of sapphirine is used in the construction. Schreyer (*Year Book 66*, pp. 380-392) and Schreyer and Seifert (1969) indicated that a solid solution

\* According to Robinson *et al.* (1969), natural gedrites have essential Na and a different structure than anthophyllite. In the absence of Na<sub>2</sub>O in the system and with lack of structure data, it is believed more prudent to describe this component as aluminous anthophyllite.

† Short runs on a glass of the Tr,Ts composition (12.81% Al<sub>2</sub>O<sub>3</sub>) prepared by Dr. F. R. Boyd at 875° and 900°C and at 10 kb *P*<sub>H<sub>2</sub>O</sub> yielded mostly clin amphibole with some Cpx and minor An+Sp. Although the assemblage obtained is compatible with recent studies on the grossularite-pyrope join, longer runs may produce more extensive solid solution. On the other hand, the clin amphibole analyzed may represent a metastable solid solution which would decrease in extent with longer runs. Further experimentation will be required to resolve these apparently anomalous results.



member close to  $\text{Mg}_6\text{Al}(\text{AlSi}_7)\text{O}_{22}(\text{OH})_2$  containing 13 wt %  $\text{Al}_2\text{O}_3$  was probably the maximum to be synthesized at 10 kb in the range  $850^\circ$  to  $910^\circ\text{C}$  although complete reaction was not demonstrated. The synthesis of two coexisting amphiboles was readily verified in the presence of orthopyroxene and sapphirine by powder X-ray diffraction patterns and by optical parameters. Preliminary analysis of boron-free kornerupine that appeared in runs in this temperature range in pyrope composition appeared to be closer to the  $4\text{MgO} \cdot 3\text{Al}_2\text{O}_3 \cdot 4\text{SiO}_2 \cdot \text{H}_2\text{O}$  composition rather than to 7:7:7:2. Because the anhydrous boron-free kornerupine composition is colinear with aluminous enstatite, pyrope, and corundum, the appearance of boron-free kornerupine (or corundum) with sapphirine and aluminous enstatite in the pyrope composition suggests metastable growth.

The stability of  $\text{Cam} + \text{Sp}$  has a wide range of implications. Independent of the extent of tschermakite solid solution in tremolite the join  $\text{Cam} - \text{Sp}$  penetrates  $\text{An} - \text{Cpx} - \text{Chl}$ . The possible subsolidus assemblages are therefore  $\text{An} + \text{Cpx} + \text{Cam} + \text{Sp} + G$ ,  $\text{An} + \text{Cam} + \text{Chl} + \text{Sp} + G$ , and  $\text{Cam} + \text{Chl} + \text{Cpx} + \text{Sp} + G$ . If  $\text{Cam}$  and  $\text{Sp}$  were in fact incompatible, the assemblages would be  $\text{An} + \text{Cpx} + \text{Chl} + \text{Sp} + G$  and  $\text{An} + \text{Cpx} + \text{Chl} + \text{Cam} + G$ . The last-named assemblage was obtained by Yoder (*Year Book 65*, p. 276, Fig. 49) in addition to  $\text{An} + \text{Cpx} + \text{Chl} + G$  using the  $\text{An}_1\text{Fo}_1$  (mole) composition. Longer runs at 7.5 and 10 kb on that bulk composition yielded  $\text{Cam} + \text{Chl} + \text{An} + G$  or  $\text{Cam} + \text{Chl} + \text{Zo} + G$ , respectively, whereas at 5 kb the  $\text{An} + \text{Cpx} + \text{Chl} + G$  assemblage persisted after 2 weeks. It appears that  $\text{Cam} + \text{Sp} + G$  reacts to give  $\text{An} + \text{Cpx} + \text{Chl}$  at about 7 kb. This may be the principal relationship between amphibolite and spilite-type facies (cf. Yoder, *Year Book 65*, p. 278).

Below  $845^\circ\text{C}$  for most compositions and below  $820^\circ\text{C}$  for the more pyrope-rich compositions, chlorite becomes a

major phase. Most of the join is occupied by the assemblage  $\text{Cam} + \text{Cpx} + \text{Chl} + G$ . Attention is called to the intersection of the join clinochlore ( $\text{Cch}$ )- $\text{Tr}_1\text{Ts}_1$  with  $\text{Di} - \text{Py}$  in Fig. 24. The range of solid solutions in both chlorite and clinoamphibole is sufficiently large to account for the simple assemblage of  $\text{Cam} + \text{Chl} + G$ ; minor amounts of other phases, however, could easily be missed. The latter is particularly true in the region  $\text{Chl} + \text{Tc} + G$  where excessively high  $\text{Al}_2\text{O}_3$  contents of talc would be required. According to Fawcett and Yoder (1966, p. 375) the maximum  $\text{Al}_2\text{O}_3$  content of talc at 10 kb is about 4 wt %. The evolution of the assemblages toward pyrope is not known in the light of the probable metastability of corundum ( $\text{Cor}$ ). Similar difficulties were experienced by Schreyer (*Year Book 66*, p. 390, Fig. 27A). His presentation of the assemblage  $\text{Chl} + \text{Tc} + \text{Cor}$  in the  $\text{MgO} - \text{Al}_2\text{O}_3 - \text{SiO}_2 - \text{H}_2\text{O}$  system at  $800^\circ\text{C}$  and 10 kb was based on the breakdown of sapphirine and reaction of natural andalusite and synthetic spinel. The  $\text{Cor}$  could be proxying for yoderite, which is stable in this region but most difficult to nucleate.

The next major event observed with decreasing temperature is the appearance of the chlorite + quartz assemblages at about  $690^\circ\text{C}$ . The maximum stability of chlorite + quartz apparently either expands with pressure at the slower rate of about  $15^\circ/\text{kb}$  above 5 kb based on the data of Fawcett and Yoder (1966, p. 372) or indicates that invariant points involving different breakdown products are intercepted as suggested by Schreyer (*Year Book 66*, p. 386, Fig. 25). Zoisite also appeared in some bulk compositions near this temperature; however, anorthite usually appeared first. At and below  $650^\circ\text{C}$ , zoisite was clearly the stable phase in the pyrope-rich compositions. Zoisite was present in assemblages obtained in new experiments on the  $\text{Gr} - \text{Py}$  join up to  $820^\circ\text{C}$  at 10 kb. Extrapolation of Newton's (1965, p. 440) data gives

an upper limit to the stability of zoisite considerably in excess of this value.

### *Major Conclusions*

The following major conclusions may be drawn on the basis of these exploratory runs. No attempt will be made at this time to relate the various assemblages to specific natural occurrences.

1. The beginning of melting of the peridotite assemblage Fo + Opx + Cpx + Sp occurs at a very low temperature in the presence of H<sub>2</sub>O and the liquid is quartz normative. In addition, the last liquid, on cooling or, conversely, the first liquid on partial melting appears to have a very high MgO/CaO ratio.

2. At 10 kb the lowest to highest grades of metamorphism as represented by this five-component system encompass only 400°C, and half of this range includes chlorite-bearing assemblages.

3. The growth of assemblages bearing a clinoamphibole, highly tschermakitic in composition, and an orthoamphibole, presumably an aluminous anthophyllite (or possibly gedrite) appears to be stable based on 1 week runs.

4. The coexistence of clinopyroxene and chlorite, considered to be a key pair in spilitic assemblages, is documented. Their occurrence with anorthite at lower pressures appears to be related by reaction to clinoamphibole and spinel.

### *Appendix: Experimental Difficulties*

The choice of pressure was made primarily because the rates of reaction were believed to be adequate for a survey of the join in a reasonable time period (about 2 years). The rates were adequate under conditions where liquid was present; metastable products formed quickly during run-up, however, and were slow to react in the solidus region. The amphiboles and aluminous clinopyroxene particularly grew rapidly.

Liquids did not quench to glasses but formed clinopyroxenes, montmorillonites, aluminous serpentines, and other structures related to chlorite. Small amounts of stable phases were no doubt missed optically among the quench products. Small amounts of synthetic forsterite are particularly difficult to recognize among masses of stable and quench diopside.

Nucleation problems were encountered with the more aluminous phases. Spinel and sapphirine were not obtained reliably in multiply repeated runs. The joins with corundum are suspect because of its known metastable growth and persistence. In two relatively long runs boron-free kornorupine appeared as the aluminous phase. Zoisite failed to nucleate in some runs, anorthite growing instead, in regions where runs contiguous in composition produced zoisite.

Phases such as talc, chlorite, and the amphiboles grew so quickly that it was not possible to reverse reactions. The consistency test of continuous compositional enclosure was applied. This test is not wholly reliable in that consistent sets of metastable assemblages for given run times were obtained. The runs of longest duration were used to construct the phase diagram when time studies were made. Further work, however, with compositions more advantageous relative to the proportions and number of phases, different starting materials, and run times exceeding 1 week may yield more definitive results.

Some of the assemblages were not intersected at optimum compositions for determining the extent of solid solution. The alumina content of the pyroxenes, amphiboles, and talc was found to be especially large on the basis of electron probe analysis. The three major types of solid solution,  $\text{MgSi} \rightleftharpoons 2\text{Al}$ ,  $\text{Ca} \rightleftharpoons \text{Mg}$ , and possibly  $3\text{Mg} \rightleftharpoons 2\text{Al}$  should be investigated for each major mineral. The exploratory data presented above emphasize that need.



ANDRADITE STABILITY IN AIR AT 1 ATM,  
O<sub>2</sub> UP TO 30 KB, AND H<sub>2</sub>O+O<sub>2</sub> UP TO  
20 KB TOTAL PRESSURE

*H. G. Huckenholz and H. S. Yoder, Jr.*

Andradite, Ca<sub>3</sub>Fe<sub>3</sub><sup>3+</sup>Si<sub>3</sub>O<sub>12</sub>, occurs as a component in garnets of ubiquitous occurrence and reflects the oxidation state under which the garnet has crystallized. A much larger field of stability was suspected than that revealed by its typical occurrence in skarns and thermally metamorphosed calcareous sediments. Because of the important role of H<sub>2</sub>O and O<sub>2</sub> in the formation of andradite, the thermal behavior of pure andradite was studied up to 30 kb under oxidizing conditions with and without H<sub>2</sub>O.

Starting material included two batches of homogeneous glass near the Ca<sub>3</sub>Fe<sub>3</sub><sup>3+</sup>Si<sub>3</sub>O<sub>12</sub> composition having 3.95 and 5.00 FeO, respectively; a mixture of wollastonite (Wo) + hematite (Hem) prepared from the glass at 900°C and 1 day (no andradite formed because of its sluggish growth); synthetic andradite (andr) crystallized from glass at 1135°C and 1 atm for 56 days (contains 0.25% FeO,  $a=12.054 \pm 0.002$  Å,  $n=1.886$ ). In addition, certain equilibria required use of compositions containing hematite or wollastonite in excess of the andradite composition: CaFe<sub>2</sub><sup>3+</sup>SiO<sub>6</sub> and Wo<sub>73</sub>Hem<sub>27</sub>, respectively.

New techniques were devised to carry out the runs under oxidizing conditions at elevated pressures. Use was made of the decomposition of PtO<sub>2</sub>→Pt+O<sub>2</sub> that takes place between 400° and 500°C at 1 atm. Although the pressure effect is not yet known, it was found that the decomposition occurred in the temperature range investigated. The PtO<sub>2</sub> (14.09 wt % O<sub>2</sub>) was either mixed directly with the sample and placed in a sealed Pt tube or held separately but open to the sample in the same sealed Pt tube. Continuous drying of the PtO<sub>2</sub> at 200°C is necessary to eliminate absorbed moisture. A similar technique is used when water is added to the PtO<sub>2</sub>-containing system. Other

oxyhydrous experiments were carried out with equal success with a 30% solution of H<sub>2</sub>O<sub>2</sub>. No ferrous iron was detected by chemical analysis of the products. The PtO<sub>2</sub> technique has been used subsequently to maintain extreme oxygen pressures on other chemical systems that may be contained in platinum.

Andradite produced at 1 atm is very light yellow in color and is a deeper yellow at elevated pressures. Faceted crystals were not observed at 1 atm because if formed initially they were destroyed by the repeated intermittent grindings and did not form again; however, well-formed dodecahedra and less abundant icositetrahedra grew under oxyhydrous conditions. Nucleation of smaller crystals on larger crystals was noted. The average  $a$  is  $12.056 \pm 0.003$  Å and  $n=1.887 \pm 0.002$  for andradite formed at 1 atm;  $a=12.059 \pm 0.003$  Å and  $n=1.887 \pm 0.002$  under anhydrous high-pressure conditions; and  $a=12.061 \pm 0.003$  Å and  $n=1.886 \pm 0.004$  under oxyhydrous conditions. Garnet formed on quenching had  $a>12.067$  Å.

*Relations at 1 Atm*

Andradite is a stable phase on the join CaSiO<sub>3</sub>-Fe<sub>2</sub>O<sub>3</sub> under subsolidus conditions up to 1137°±5°C. The  $T$ - $X$  diagram depicted in Fig. 25 is based on results obtained by Schairer and Bowen (1942) on pure CaSiO<sub>3</sub> and Osborn and Muan (1960) on the liquidus surface of the CaO-"Fe<sub>2</sub>O<sub>3</sub>"-SiO<sub>2</sub> join, and on supplementary data of the present study. Above 1137°C andradite decomposes to pseudowollastonite, hematite, and a garnet. This garnet was first thought by Huckenholz, Schairer, and Yoder (1969) to be an andradite with a small amount of solid solution toward skiaegite (Fe<sub>3</sub><sup>3+</sup>Fe<sub>2</sub><sup>3+</sup>Si<sub>3</sub>O<sub>12</sub>); it is now believed to be residual, however, because of its observed persistence above its breakdown when excess oxygen under pressure is applied. The pseudowollastonite + hematite assemblage begins to melt at 1293°±



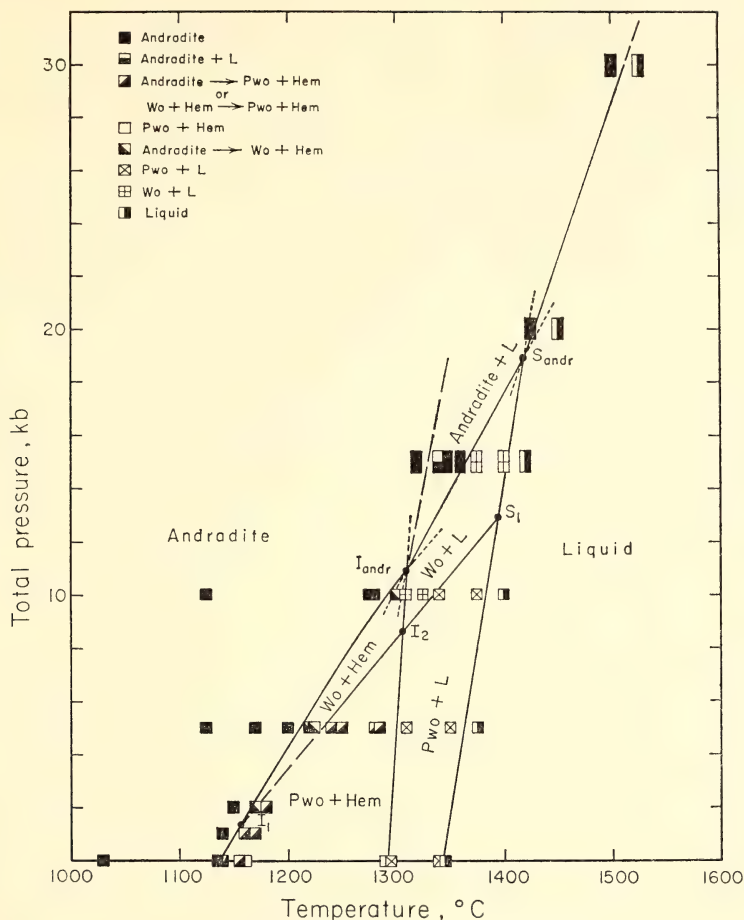


Fig. 25. Plot of temperature versus composition for data obtained on the join  $\text{CaSiO}_3\text{-Fe}_2\text{O}_3$  at 1 atm. Abbreviations of phases encountered: Andr, andradite; Wo, wollastonite; Pwo, pseudowollastonite; Hem, hematite;  $\text{Mt}_{ss}$ , magnetite solid solution.

$3^\circ\text{C}$ , and the  $\text{Ca}_3\text{Fe}_2^{3+}\text{Si}_3\text{O}_{12}$  bulk composition is completely melted at  $1343 \pm 2^\circ\text{C}$ .

#### *Relations of Andradite in the $\text{CaSiO}_3\text{-Fe}_2\text{O}_3\text{-O}_2$ Join from 1 to 30 Kb*

Results on the stability of andradite under anhydrous conditions and in the presence of  $\text{PtO}_2$  are presented in Fig. 26 and in a series of isobaric  $T\text{-X}$  sections of the  $\text{CaSiO}_3\text{-Fe}_2\text{O}_3$  join in Fig. 27A-E. The stability of andradite increases at various rates from  $1137^\circ \pm 5^\circ\text{C}$  at 1 atm to  $1510^\circ\text{C}$  at 30 kb. The breakdown of

andradite yields hematite with either pseudowollastonite or wollastonite, depending on the temperature and pressure below or above, respectively,  $1155^\circ \pm 10^\circ\text{C}$  and 1.3 kb. The pseudowollastonite-wollastonite transition curve cuts the field of the andradite breakdown assemblage with a slope of  $21^\circ/\text{kb}$ , in agreement with the data of Kushiro (*Year Book 63*, pp. 83-84) on pure  $\text{CaSiO}_3$ . Apparently neither pseudowollastonite nor wollastonite takes up ferric iron. Invariant conditions exist at  $1310^\circ \pm 10^\circ\text{C}$

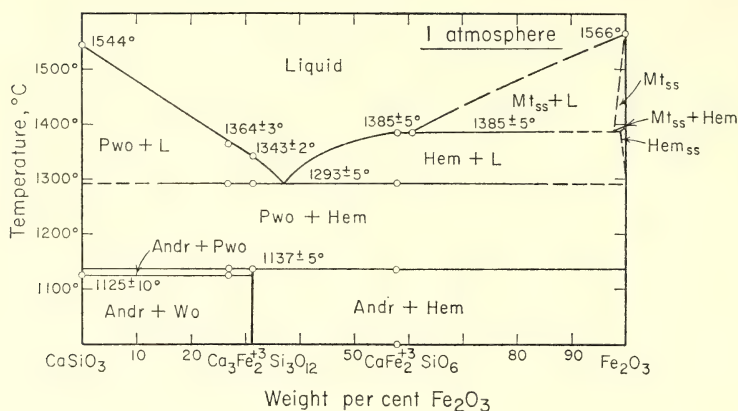
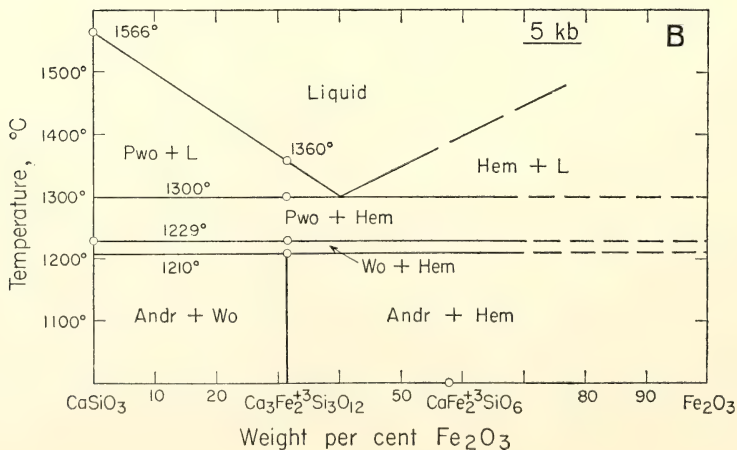
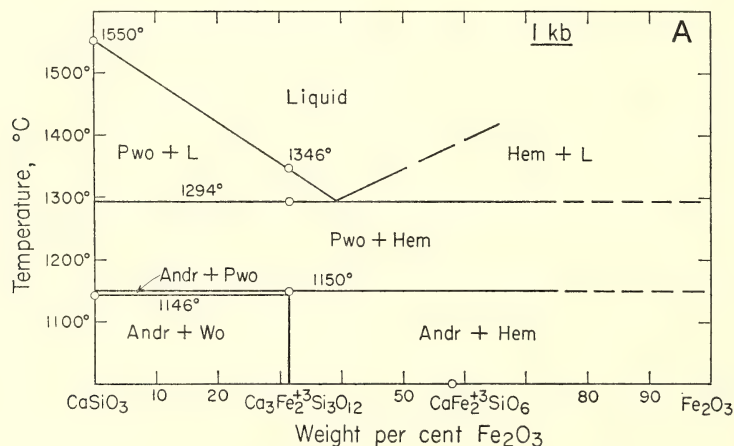


Fig. 26. Pressure-temperature diagram for  $\text{Ca}_3\text{Fe}_2^{+3}\text{Si}_3\text{O}_{12}$  composition in the presence of excess  $\text{O}_2$  at total pressure up to 30 kb. Abbreviations as in Fig. 25.  $I_{\text{and}}$ ,  $I_1$ , and  $I_2$ , invariant points;  $S_{\text{and}}$  and  $S_1$ , singular points.



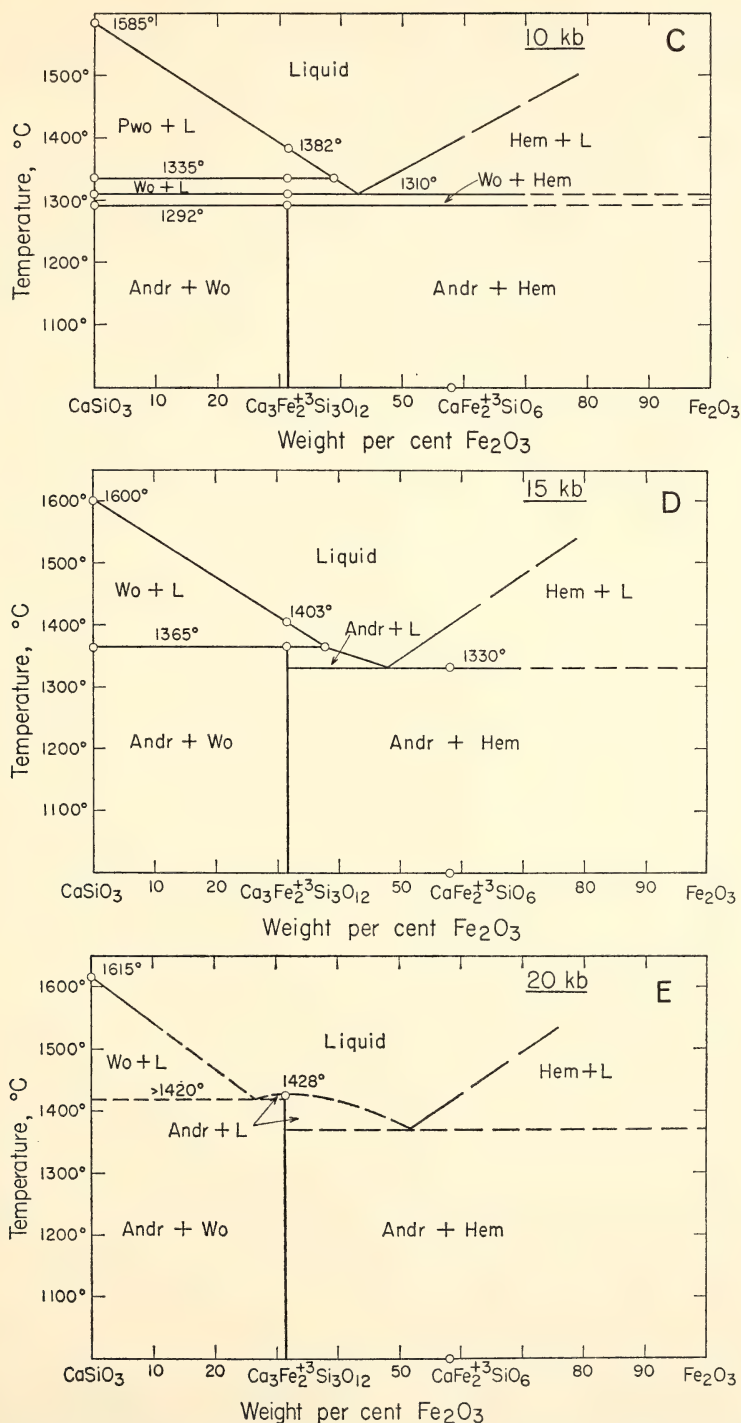


Fig. 27. (A-E) Isobaric temperature-composition sections of the join  $\text{CaSiO}_3\text{-Fe}_2\text{O}_3$  with excess  $\text{O}_2$  at a total pressure of 1, 5, 10, 15, and 20 kb. Abbreviations as in Fig. 25.



and  $11.0 \pm 0.5$  kb ( $I_{\text{andr}}$ ) where andradite, wollastonite, hematite, and liquid coexist. Above these conditions andradite melts incongruently to  $1420^\circ \pm 10^\circ\text{C}$  and  $19 \pm 1$  kb ( $S_{\text{andr}}$ ), where it then melts congruently. The nature of the melting curves lends support to the belief that oxygen is relatively insoluble in silicate melts. Additional singular points occur at  $1155^\circ\text{C}$ , 1.3 kb;  $1305^\circ\text{C}$ , 8.6 kb; and  $1395^\circ\text{C}$ , 13.0 kb as a result of the intersection of the pseudowollastonite-wollastonite transition curve at and above

the solidus of the  $\text{Ca}_3\text{Fe}_2^+\text{Si}_3\text{O}_{12}$  bulk composition. The  $\text{CaFe}_2^+\text{SiO}_6$  bulk composition was used to locate the long-dash curve marking the reaction andradite + hematite  $\rightleftharpoons$  liquid. The arrangement and slopes of the curves about  $I_{\text{andr}}$  are consistent with chemographic principles.

*Relations of Andradite in the Presence of  $\text{H}_2\text{O} + \text{O}_2$  up to 20 Kb Total Pressure*

The  $P$ - $T$  diagram of andradite in the presence of excess  $\text{H}_2\text{O}$  and  $\text{O}_2$  is given in Fig. 28. The thermal stability of

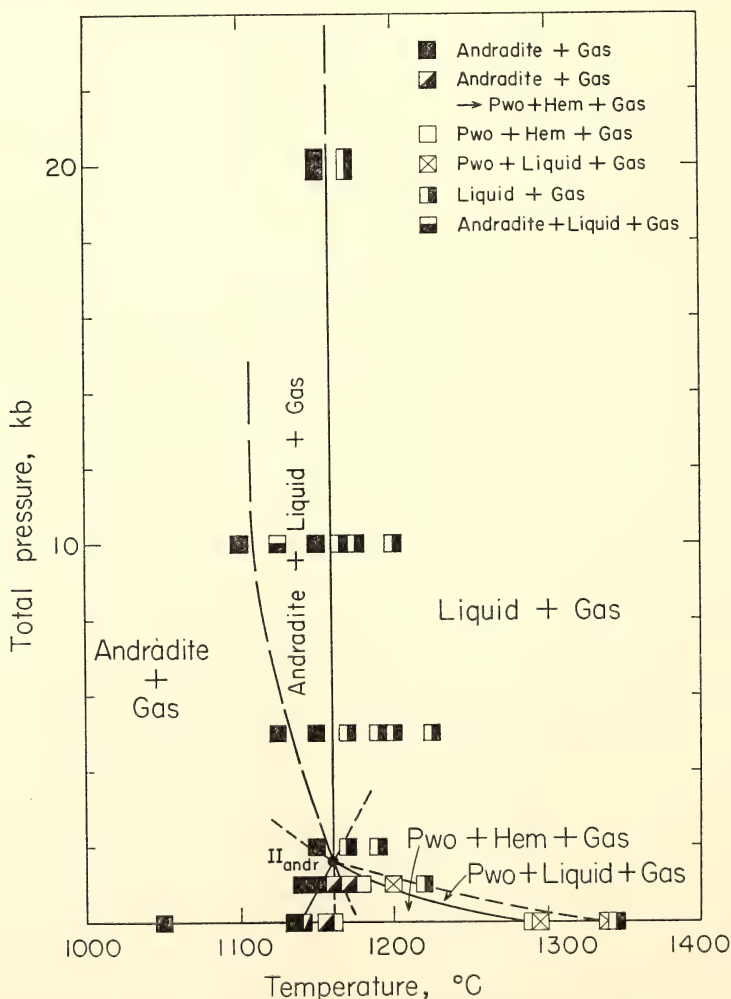


Fig. 28. Pressure-temperature diagram for the  $\text{Ca}_3\text{Fe}_2^+\text{Si}_3\text{O}_{12}$  composition in the presence of excess  $\text{H}_2\text{O} + \text{O}_2$  at total pressures up to 20 kb. Abbreviations as in Fig. 25.  $II_{\text{andr}}$ , invariant point.

andradite increases from  $1137^{\circ} \pm 5^{\circ}\text{C}$  at 1 atm to  $1163^{\circ} \pm 10^{\circ}\text{C}$  at a total pressure of  $1.6 \pm 0.5$  kb ( $\Pi_{\text{andr}}$ ). Andradite melts directly to liquid and gas above the invariant point  $\Pi_{\text{andr}}$ , and the upper stability curve is essentially isothermal to 20 kb. The slope of the garnet breakdown curve below  $\Pi_{\text{andr}}$  is the same as that obtained under anhydrous conditions. The beginning of melting of the andradite bulk composition is drastically lowered by the presence of the volatile phase. On the basis of measurements of the index of refraction and cell dimensions, no hydrogarnet solid solution is believed to have taken place. The long-dash curve represents the beginning of melting for compositions in the join andradite-hematite-gas and was determined using the  $\text{CaFe}_2^{3+}\text{SiO}_6$  bulk composition. The curves about the invariant point  $\Pi_{\text{andr}}$  are consistent with chemographic principles if the system is assumed to be adequately represented by three components— $\text{CaSiO}_3$ ,  $\text{Fe}_2\text{O}_3$ , and gas ( $\text{H}_2\text{O} + \text{O}_2$ ).

The gas is composed mainly of  $\text{H}_2\text{O}$  and  $\text{O}_2$ , and after quenching, the dissolved constituents are represented by fibrous wollastonite, hematite, and sometimes andradite. It is not possible to evaluate the partial pressures of  $\text{H}_2\text{O}$  and  $\text{O}_2$  in these experiments. If the  $\text{O}_2$  is essentially inert, as suggested by the data in Fig. 26, then the activity of  $\text{H}_2\text{O}$  is reduced and the curves presented involving liquid are not the minimum melting relations. A further complication is that hydrogen is continuously diffusing through the Pt tube wall and the composition of the gas phase changing accordingly. It is perhaps noteworthy that previous investigations of the melting of minerals in the presence of alleged stoichiometric  $\text{H}_2\text{O}$  are subject to these same concerns.

### Petrogenetic Conclusions

Results of this study confirm the suspicion that andradite has a much larger

field of stability under highly oxidizing conditions than that revealed by its most abundant occurrences under presumably less oxidizing conditions. The extent of its stability is clearly indicated in Fig. 29, where the anhydrous and hydrous stability limits of andradite are plotted together with those of pyrope (Boyd and England, *Year Book* 58, pp. 83–87; Schreyer and Seifert, 1969), grossularite (Yoder, 1950; Yoder and Chinner, *Year Book* 59, pp. 78–81; Hays, *Year Book* 65, 234–239), almandite (Yoder, 1955; Hsu, 1968), and the hydrous solidus and liquidus curves of alkali basalt (Yoder and Tilley, 1962).

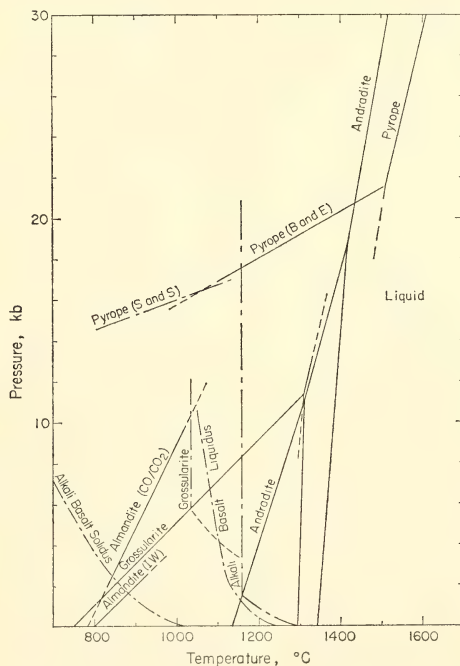
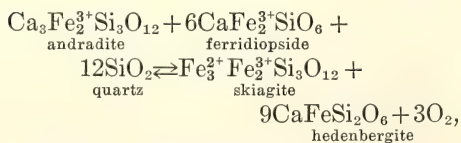


Fig. 29. Pressure(total)-temperature plot of anhydrous (solid line) and hydrous (dot-dash) reaction curves for pyrope (Boyd and England, *Year Book* 58; Schreyer and Seifert, 1969), grossularite (Yoder, 1950; Yoder and Chinner, *Year Book* 59; Hays, *Year Book* 65), almandite (Yoder, 1955,  $\text{CO}/\text{CO}_2$  buffer; Hsu, 1968, iron-wüstite buffer), and the hydrous solidus and liquidus curves of alkali basalt (Yoder and Tilley, 1962). Dashed lines are extrapolations or estimates.

Andradite appears as a primary phase in syenite and nepheline syenite or their volcanic equivalents, trachyte and phonolite. Felsic differentiates of the alkalic rock suite are generally enriched in ferric iron (Yoder and Tilley, 1962, p. 429, Fig. 20), and their liquidus temperatures (Tilley, Yoder, and Schairer, *Year Book 64*, pp. 69–82) are near or below the breakdown temperature of andradite. The formation of andradite (and of Ti-bearing andradite) is favored in these particular rocks.

Figure 30 shows that the higher the oxidation state of skarn rocks, alpine serpentinites, ijolites, and related rocks, the larger the andradite component in the garnet. The small amount of andradite component in garnets from gneiss, mica schist, hornfels, amphibolites, glaucophane schists, granulites, charnockites, eclogites, and peridotites is relatively insensitive to the oxidation state of those rocks. Whereas regional metamorphism does not appear to produce andradite, the contact metamorphic environment will generally be more oxidized, and the oxidation state will be essentially controlled by that of the intruding magma (Chinner, 1960). The formation of andradite in skarns is attributed by some to the transport of  $\text{Fe}_2\text{O}_3$  and  $\text{SiO}_2$  into calcareous sediments with liberation of  $\text{CO}_2$ . Where the dissociation of  $\text{CO}_2 \rightarrow \text{CO} + \frac{1}{2} \text{O}_2$  is the controlling factor, the effect will be oxidizing; if graphite is present, the effect may be reducing. Under the latter circumstances andradite would give way to hedenbergite: first, through solid solutions probably involving skiaquite and ferridiopside such as related by



and eventually through the reaction sug-

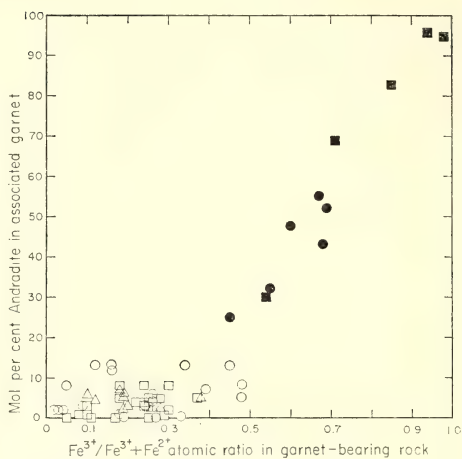
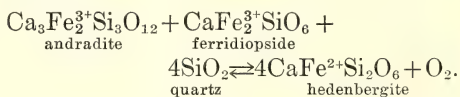


Fig. 30. Correlation of oxidation state of garnet-bearing rocks [expressed as the atomic ratio of  $\text{Fe}^{3+}/(\text{Fe}^{3+} + \text{Fe}^{2+})$ ] with the amount of andradite component ( $\text{Ca}_3\text{Fe}_2^{3+}\text{Si}_3\text{O}_{12}$ ) present in their garnets. Three skarn rocks and two alpine serpentinites (solid square); six ijolites and related rocks (solid circle); ten mica schists and gneisses, ten amphibolites and glaucophane schists, and five hornfels (open circle); ten granulites and charnockites (open triangle); five eclogites and twenty-five peridotites (open square).

gested by Huckenholz (*Year Book 67*, p. 94)



Those skarns in which garnet and hedenbergite occur together usually contain manganese (involving solid solutions with calderite and johannsenite, respectively), which also may account for the coexistence of these minerals which reflect under other circumstances such different oxidation states.

#### SYNTHESIS AND PRELIMINARY RESULTS ON THE STABILITY OF AENIGMATITE ( $\text{Na}_2\text{Fe}_5\text{TiSi}_6\text{O}_{20}$ )

D. H. Lindsley

Thompson and Chisholm (1969) reported the first synthesis of the mineral aenigmatite having the theoretical composition  $\text{Na}_2\text{Fe}_5^{2+}\text{TiSi}_6\text{O}_{20}$  (Kelsey and



McKie, 1964). Guided in part by the findings of Ernst (1962) that a Ti-free "aenigmatite" is stable at the low oxygen fugacity ( $f_{O_2}$ ) of the wüstite-magnetite (WM) buffer but not at that of the fayalite-magnetite-quartz (FMQ) buffer, Thompson and Chisholm reacted a mix of oxide plus fired "gel" hydrothermally at 700°C and 1000 bars  $P_{H_2O}$ , and the  $f_{O_2}$  of the iron-wüstite buffer. Reaction was rapid; there was virtually complete conversion in 48 hours. The results are of interest in view of the rather common occurrence of aenigmatite in peralkaline lavas. Several questions remain: Is aenigmatite stable only at abnormally low  $f_{O_2}$ , as inferred by Kelsey and McKie (1964) and Abbott (1967)? Does it have an upper or lower thermal stability that might put limits on the temperature of the lava precipitating it? Does aenigmatite require structural water, as many older analyses would suggest, or is water only incidental, as most recent analyses and the discussion of the crystal chemistry by Kelsey and McKie (1964) seem to indicate?

The discovery of aenigmatite as a very late-stage mineral in pegmatoids segregated from a thick basalt flow (p. 279) spurred an experimental investigation of aenigmatite stability aimed at answering these questions. In preliminary experiments (Lindsley, Haggerty, and Smith, 1970) on  $Na_2Fe_5TiSi_6O_{20}$  bulk composition\* aenigmatite was synthesized at temperatures from 500° to 750°C, fluid pressure of 500 bars, and oxygen fugacity controlled by the FMQ and nickel-nickel oxide (NNO) buffers. Complete reaction to aenigmatite in a few days was observed in experiments employing the FMQ buffer; those using the NNO buffer yielded mostly aenigmatite, but also minor Ti-Mt, acmite, and quartz. The extreme ease of the

synthesis reported by Thompson and Chisholm was confirmed; indeed, subsequent stability experiments strongly suggest that the synthesis at the  $f_{O_2}$  of the NNO buffer was metastable with respect to a more oxidized assemblage: acmite + Fe-Ti oxide(s) (Ti-magnetite or ilmenite or both) + quartz. Successful synthesis of aenigmatite from the anhydrous starting materials in evacuated silica-glass tubes at 700°C demonstrates that hydrogen is not a necessary component in the aenigmatite structure.

Experiments designed to delineate the stability of aenigmatite are in progress. Experiments *in vacuo* utilized a charge and buffer, each in a crimped but unsealed metal capsule, sealed in an evacuated silica-glass tube. Thus the vapor phase is free to communicate between the capsules, and oxygen can be exchanged. It is possible for other components to be transferred as well, but there have been no indications that this is a serious problem. Aenigmatite *in vacuo* melts incongruently at 880° to 900°C. These experiments on aenigmatite bulk composition give its maximum thermal stability, for water lowers the melting temperature by preferentially entering the liquid, as would most or all the components found in peralkaline lavas. This result places a severe upper temperature limit on lavas containing aenigmatite, unless rather small deviations from the nominal composition (see, for example, Nicholls and Carmichael, 1969, p. 280) drastically increase its stability. Such a possibility should be checked by experiments on aenigmatites of various compositions.

It has generally been assumed—both on the basis of Ernst's experiments on Ti-free "aenigmatite" and because of a preponderance of  $Fe^{2+}$  over  $Fe^{3+}$  in natural samples—that aenigmatite requires abnormally low oxygen fugacities. In contrast Nicholls and Carmichael (1969) have estimated a free energy of formation for aenigmatite and have calculated that it may be stable at oxygen

\* Starting materials were crystalline  $Na_2Si_2O_5$ ,  $SiO_2$  glass, fine-grained  $TiO_2$ ,  $Fe_2O_3$ , and metallic Fe intimately ground together under alcohol in an agate mortar.

fugacities three orders of magnitude above those of the FMQ buffer, well above the NNO buffer. The successful synthesis at the  $f_{O_2}$  of the NNO buffer would seem to give support to this hypothetical stability at relatively high oxygen fugacities; experiments on previously synthesized aenigmatite, lasting several weeks and utilizing the NNO buffer, yielded aenigmatite + acmite + Fe-Ti oxide(s), however, at a variety of temperatures. No other phases were identified and it was initially assumed that the aenigmatite contained some ferric iron (Lindsley, Haggerty, and Smith, 1970). In an experiment that lasted 5 months ( $T=750^\circ\text{C}$ ,  $P_{H_2O}=500$  bars, NNO buffer), however, aenigmatite broke down completely to the more oxidized assemblage acmite + Ti-magnetite + quartz, so it now appears that the aenigmatite had only persisted metastably, rather than being stabilized by ferric iron. The breakdown assemblage was then further reacted for 20 days, one aliquot at the NNO buffer and another at the FMQ buffer. Only the latter showed any reaction, aenigmatite growing at the expense of the oxidized assemblage. Thus, at least at  $750^\circ\text{C}$  and 500 bars, the stability curve for aenigmatite lies between the NNO and FMQ buffer curves. This is the only temperature for which complete breakdown was obtained at the NNO buffer, but the appearance of acmite in runs with that buffer and at temperatures down to  $400^\circ\text{C}$  probably indicates that aenigmatite is unstable at lower temperatures as well. In experiments on aenigmatite with the NNO buffer, a silica mineral is not observed until the breakdown is nearly complete. A possible explanation is that the acmite contains some  $\text{FeSiO}_3$  in solid solution.

This experimental result could be used to provide a more precise estimate for the free energy of formation of aenigmatite (Nicholls and Carmichael, 1969, p. 291), but the estimate would be dependent on data for acmite and also the

mixing properties of the Fe-Ti oxides (see, for example, Rumble, p. 202). The present results do show, however, that the presence of aenigmatite phenocrysts in a lava places upper limits on both the temperature and the oxygen fugacity of its crystallization.

#### MÖSSBAUER SPECTROSCOPY OF SYNTHETIC CA-FE PYROXENES

*Eric Dowty\* and D. H. Lindsley*

Crystal-chemical study of pyroxenes, with the ultimate objective of contributing to the understanding of the genesis of mafic igneous and metamorphic rocks, has been a popular topic in the past few years. A large part of the effort in this field has gone toward the elucidation of order-disorder relationships in the M1 and M2 sites, involving chiefly Mg and Fe. The degree of ordering is presumably dependent on the temperature at which the mineral reached equilibrium, and some possibilities for geothermometry therefore exist in the accurate determination of order-disorder relationships. The first studies in this field were by X-ray structure refinement (e.g., Ghose, 1965), but Mössbauer spectroscopy has emerged as the technique that offers the most promise as a routine and accurate method of measuring distribution of iron and, indirectly, order in pyroxenes with known crystal structure. The orthopyroxenes (enstatite-ferrosilite) were the natural starting place for these studies, since they may be regarded as essentially a binary solid solution, and work by Virgo and Hafner (1969) and Saxena and Ghose (1970) seems to have established ordering patterns in this series as a function of temperature.

Some effort has also been made to relate ordering of clinopyroxenes to the thermal history of the rocks in which they formed (e.g., Bancroft and Burns, 1967; Hafner and Virgo, 1970). There are, however, two factors that make the

\* U. S. Geological Survey.



interpretation of Mössbauer data for clinopyroxenes a good deal more complicated than for orthopyroxenes. First, chemical compositions of clinopyroxenes are more complex. For each new element that reaches significant concentration, such as calcium, aluminum, titanium, or manganese, another constant must be evaluated for thermodynamic calculations. Chemical disorder over the sites in the structure also tends to broaden the Mössbauer lines. It is usually assumed that calcium is strictly ordered into the M2 site; yet there is evidence that under conditions of high temperature (1150°C) and low pressure a considerable amount may be made to take the M1 site in synthetic pyroxenes (Matsui, Maeda, and Syono, 1969). Second, Ca-Mg-Fe clinopyroxenes may crystallize in at least two different symmetries ( $C2/c$  and  $P2_1/c$ ), with complex exsolution relations between them. The pyroxenes studied by Hafner and Virgo (1970), for example, were admittedly multiphase assemblages.

It seems clear that before further interpretation of Mössbauer data for clinopyroxenes is made it is desirable to have some groundwork laid in the form of studies of end-member and binary compositions (i.e., compositions along the edges of the pyroxene quadrilateral). The present study is concerned with the join hedenbergite-ferrosilite. Room-temperature spectra for this series were reported by Dundon and Lindsley (*Year Book* 66, pp. 366-369). Since it is now evident that the M1 and M2 sites are not sufficiently resolved at room temperature to give an accurate measure of the Mössbauer hyperfine parameters and site occupancies, spectra for the present study have been taken at liquid nitrogen temperature (77°K). Another point of departure from the previous study is the nature of the materials themselves: Dundon and Lindsley reported results from clinopyroxenes only, synthesized dry at various temperatures and pressures, whereas we are now concerned

with the phases made hydrothermally in the system at 950°C and 20 kb, which include all three symmetry types of Fe-Ca pyroxenes (hedenbergite,  $C2/c$ ; clinoferrosilite or pigeonite,  $P2_1/c$ ; and orthoferrosilite,  $Pbca$ ). Syntheses were made in piston-cylinder apparatus with large-volume (0.5 g) silver capsules (see Munoz and Lindsley, *Year Book* 67, pp. 88-91, for subsolidus phase relations in the system at 20 kb). In synthesizing the pyroxenes, an effort was made to obtain single crystals large enough for X-ray study, in order to ascertain the space groups. The X-ray examination is currently being carried out by Charles W. Burnham (Harvard University). The compositions of specimens made to date are  $Fs_{50}$ ,  $Fs_{60}$ ,  $Fs_{70}$ ,  $Fs_{75}$ ,  $Fs_{80}$ ,  $Fs_{85}$ , and  $Fs_{90}$ , all optically identified as clinopyroxenes, and  $Fs_{98}$  and  $Fs_{100}$ , both optically identified as orthopyroxenes.

A constant-acceleration "flyback" Mössbauer spectrometer was used in conjunction with a 200-channel analyzer to record the spectra.\* Four peaks, representing doublets for each of the sites M1 and M2, were fitted by least squares to the observed spectra, with the use of a computer program based on the metric minimization method of Davidon (1959); no constraints were applied to the peak parameters. Some of the preliminary data from the spectra are shown in Figs. 31 and 32.

Quadrupole splitting for both of the M sites shows very marked trends over the composition range studied. Splitting for the M1 site (Fig. 31A) shows a fairly continuous increase with iron content, possibly indicating a decrease in "distortion" of this site as the large Ca ion is removed from the structure. Splitting for the M2 site, on the other hand, at first decreases with increasing iron content and then, between  $Fs_{85}$  and  $Fs_{90}$ , makes a sudden jump upward.

\* We thank Dr. J. J. Spijkerman and the National Bureau of Standards for the use of this equipment.



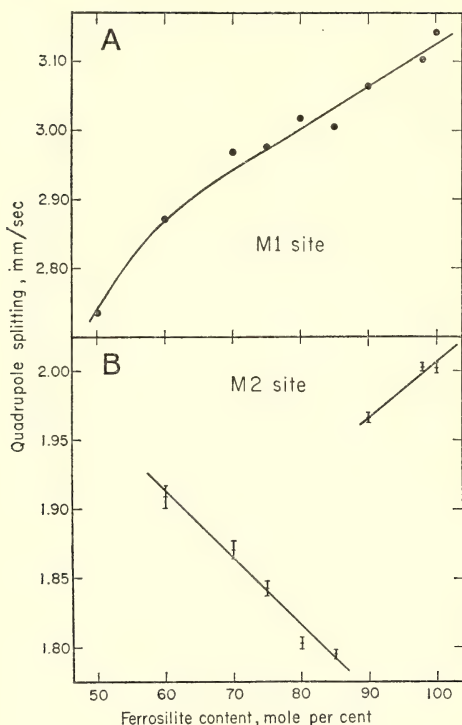


Fig. 31. Quadrupole splitting of M sites in synthetic hedenbergite-ferrosilite pyroxenes. (A) M1 site. Errors for the fitting process are smaller than the size of the points. (B) M2 site. Errors are shown as bars.

The composition  $\text{Fs}_{90}$  probably has  $P2_1/c$  symmetry, although the symmetry has not yet been confirmed by X-ray diffraction. X-ray refinement of the structure of natural pigeonites with

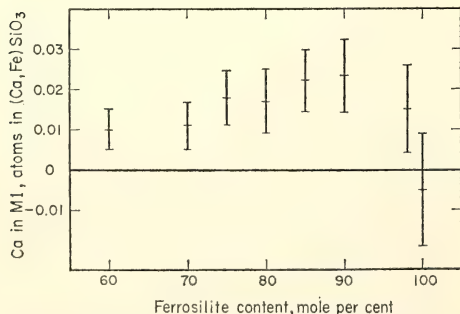


Fig. 32. Amount of calcium in M2 site calculated from Mössbauer area ratios.

$P2_1/c$  symmetry leads to the conclusion that the M2 site is seven-coordinated. Morimoto and Güven (1970) state that this result probably represents only an "average" coordination of the M2 site over the entire structure and that the coordination is expected to be different for each cation, eight-fold for Ca, and six-fold for Fe and Mg. The idea that each type of cation maintains its own coordination number whatever the chemical composition or space-group symmetry, however, is not supported by the data shown in Fig. 31B. These data seem more consistent with the hypothesis that the M2 site has one type of coordination (probably eight-fold) for the compositions with  $C2/c$  symmetry ( $\text{Fs}_{80}$ - $\text{Fs}_{85}$ ), becoming more distorted with increasing iron content, and another type (probably six-fold) for the compositions with  $P2_1/c$  or  $Pbca$  symmetry ( $\text{Fs}_{90}$ - $\text{Fs}_{100}$ ).

There is presently some uncertainty about the above interpretation because one sample of  $\text{Fs}_{85}$  synthesized under the same conditions as those of the present study was previously found by Burnham (written communication, 1968) to have  $P2_1/c$  symmetry, whereas in Fig. 31B,  $\text{Fs}_{85}$  seems to fall on the same trend as the compositions that are assumed to have the hedenbergite structure. Further X-ray work and more syntheses in this critical region are being carried out in an effort to resolve this question.

The results of measurement of the areas under the Mössbauer peaks, shown in Fig. 32, indicate that there is a small, but statistically significant, amount of Ca in M1 in all the specimens except  $\text{Fs}_{100}$ . The fact that the latter, which contains no calcium, has the theoretical distribution of iron within the error of measurement argues against the anomalous measured distribution in the other specimens being the result of an experimental bias. The amount of Ca in M1 is not large on an absolute scale, but in terms of the total amount of Ca present, the disordering is significant; in fact, Ca

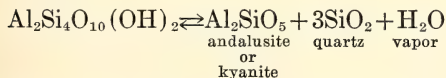
in  $\text{Fs}_{98}$  is apparently completely randomly distributed over M1 and M2, if it is not found preferentially in M1. It does not follow, however, that all natural pyroxenes have Ca in M1. For instance, the presence of Mg would probably promote the ordering of Ca in M2, since Mg has a stronger preference than Fe for the M1 site.

It was found that the M2 doublet was distinctly unsymmetric in all the specimens, including orthopyroxenes: the high-velocity peak was broader and lower than the low-velocity peak. The use of peak heights as opposed to areas in measuring the site occupancies (Hafner and Virgo, 1970) is therefore not justified in very high-iron pyroxenes. Whether or not it is justified for the more commonly occurring pyroxenes containing considerable Mg remains to be decided by carefully controlled studies.

#### THERMAL EXPANSION OF PYROPHYLLITE

*L. A. Taylor and P. M. Bell*

The mineral pyrophyllite  $[\text{Al}_2\text{Si}_4\text{O}_{10}(\text{OH})_2]$  has been considered rare by field petrologists (Zen, 1969), but this may be a reflection of its fine-grained and semi-micaceous character, which makes it difficult to identify. The general reaction



sets a lower boundary for aluminum silicate stability under circumstances of high water potential.

The studies of Althaus (1966) and Kerrick (1968) are the latest attempts to fix the stability of pyrophyllite under  $P_{\text{total}} = P_{\text{H}_2\text{O}}$  conditions. Such hydrothermal results are plagued by sluggishness of reaction in the 400°–500°C range. Zen (1969) has noted that assemblages which should be stable, on the basis of free energies calculated from some of the hydrothermal data, are not, in fact, the common ones found in nature. One necessary set of data lacking for a rigor-

ous thermodynamic analysis was thermal expansion information for pyrophyllite.

Thermal expansion measured by high-temperature X-ray diffraction can be precise only if the crystallographic parameters are well known. Unfortunately, they are not well known for pyrophyllite, but the structure is currently being re-determined (R. Robie, personal communication) on crystals of rare perfection collected in Staley, North Carolina, by E-an Zen. In the present study, thermal expansion of the Staley pyrophyllite was measured, with the space group  $C2/c$  (Zvyagin and Pinsker, 1949), which evidently is slightly incorrect. Indexing caused moderate uncertainties, but these errors were reduced by successive computer iteration techniques and will be greatly lowered when the exact space group is known. High-temperature heat-capacity measurements are also currently being determined by Dr. R. Robie on the same material, so the present values can be applied thermodynamically from the same base.

Powdered pyrophyllite crystals were mounted in a sealed, evacuated silica-glass capillary and X-rayed (FeK radiation) at 50°C intervals with a 19-cm Debye-Scherrer camera, calibrated with Si ( $a_{25^\circ} = 5.4306 \text{ \AA}$ ), on a modified Unicam unit. At least 15 reflections were measured on each film, and the cell data were obtained after a least-squares refinement (LCLSQ) of the X-ray data according to the program of Burnham (*Year Book 61*). These cell data are compiled in Table 4 and shown in Fig. 33. Crystallographic axes  $b$  and  $c$  increase slightly, and  $a$  decreases, as does  $\beta$ . Third-rank least-squares fits (made with a computer program written by L. W. Finger) were made in each case. Only slight volume increase occurs, with a curious, but possibly unreal, dip in the cell parameters at 200°C. The molar volume changes very slightly, from 127.61 cc/mole to 128.06 cc/mole in the 400°C range. Above 400°C, a perceptibly larger expansion occurs, accompanied by

TABLE 4. Pyrophyllite Thermal Expansion Data

$T, ^\circ\text{C}$ ( $\pm 3$ )	$a, \text{\AA}$	$b, \text{\AA}$	$c, \text{\AA}$	$\beta, \text{deg}$	$V, \text{\AA}^3$
22	5.169(4)	8.931(2)	18.639(3)	99.91(2)	847.7(4)
102	5.167(4)	8.935(5)	18.656(5)	99.89(4)	848.5(6)
153	5.158(9)	8.946(7)	18.670(6)	99.82(6)	848.9(7)
210	5.146(10)	8.956(10)	18.678(9)	99.76(8)	848.4(10)
256	5.149(13)	8.958(10)	18.678(9)	99.66(9)	849.2(9)
303	5.137(15)	8.971(13)	18.691(11)	99.60(12)	849.3(12)
402	5.125(14)	8.990(11)	18.716(9)	99.55(9)	850.4(11)

irreversible changes, which we attribute to the beginning of dehydration. These results are consistent with the experimental data of Kerrick (1968) projected to 1 atm.

The thermal expansion of pyrophyllite is at a rate of only about 20% that of andalusite over the temperature range 100–400°C. The absolute change in volume of reaction as temperature increases is small but is in the direction of increasing pyrophyllite stability over andalusite from that calculated without taking into account thermal expansion.

#### EQUILIBRIUM STUDIES IN $\text{ZnO}$ -CONTAINING SILICATE SYSTEMS

##### *The Effects of Pressure in the $\text{Zn}_2\text{SiO}_4$ - $\text{Co}_2\text{SiO}_4$ System*

L. A. Taylor, P. M. Bell, and A. Muan

Several recent papers have been concerned with thermodynamic mixing properties, at 1 atm pressure, of orthosilicate systems; the effects of pressure upon these systems, however, have not been well investigated. The join  $\text{Zn}_2\text{SiO}_4$ - $\text{Co}_2\text{SiO}_4$  was chosen as a model system for this study because the end members represent two different structures at 1 atm pressure— $\text{Co}_2\text{SiO}_4$  with olivine structure and  $\text{Zn}_2\text{SiO}_4$  with willemite structure—and because spinel phases have been reported for both end members,  $\text{Co}_2\text{SiO}_4$  and  $\text{Zn}_2\text{SiO}_4$ , at high pressures. A study of this model system will provide a basis for interpreting natural olivine reactions that are not amenable to direct experiment.

A preliminary study at 1 atm pressure by Muan (following paper and private communication) has shown the existence of extensive solid solubility between the two end members  $\text{Zn}_2\text{SiO}_4$  and  $\text{Co}_2\text{SiO}_4$ , as sketched in Fig. 34. In the present in-

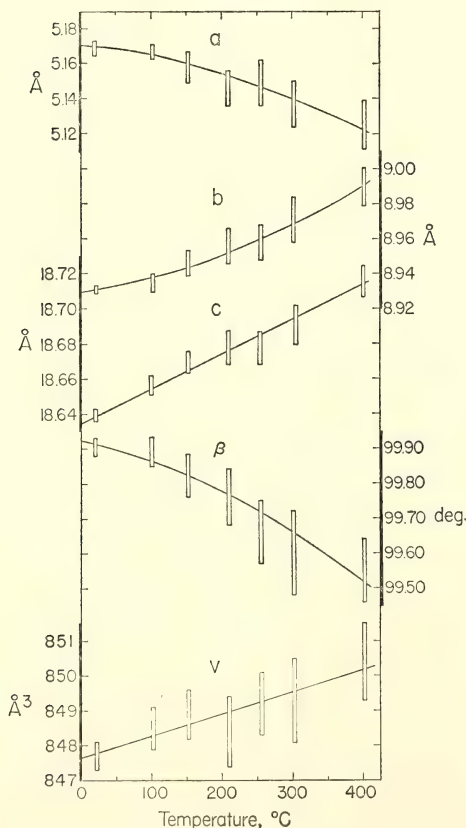


Fig. 33. Thermal expansion data for pyrophyllite, with the space group  $C2/c$ . The procedure used to obtain these data is explained in the text. The dimensions of the individual rectangles represent the precision of these data.



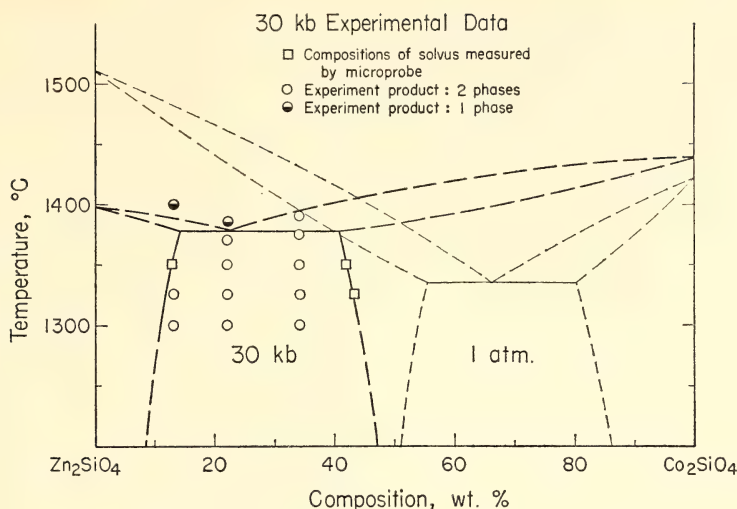


Fig. 34. Sketch showing main effects of pressure on phase relations in the system  $\text{Zn}_2\text{SiO}_4\text{-Co}_2\text{SiO}_4$ . The 1-atm data were determined by Muan (private communication), and the 30-kb data are from this study.

vestigation, experiments were conducted at 30 kb with piston-cylinder pressure apparatus (Boyd and England, 1960), and homogeneous compounds synthesized at 1 atm were used as starting materials. The compositions of the solid phases within the two-phase field were determined by microprobe analyses of the products of several experiments with bulk compositions within this field, as shown in Fig. 34.

Two main effects of pressure on equilibria in the system  $\text{Zn}_2\text{SiO}_4\text{-Co}_2\text{SiO}_4$  are apparent from the sketch in Fig. 34. First, the negative effect of pressure on the congruent melting point of  $\text{Zn}_2\text{SiO}_4$  is evidenced by a lower liquidus temperature and measurements of index of refraction, where  $M_{\text{quenched glass}} > M_{\text{primary crystal}}$ . Increased pressure lowers the melting point from a 1-atm value of  $1510^\circ\text{C}$  to below  $1425^\circ\text{C}$  at 30 kb—an unusual feature for silicate minerals. Second, the two-phase field on the  $\text{Zn}_2\text{SiO}_4\text{-Co}_2\text{SiO}_4$  join is shifted approximately 40 wt % toward the Zn end member at 30 kb. The direction of this shift can be reconciled with the crystal chemistry of the phases involved. The

olivine structure is based on a close-packing of oxygen atoms with associated octahedrally coordinated metal cations, whereas the willemite structure does not have close-packed oxygens and the cations are tetrahedrally coordinated. Pressure, therefore, should and does favor the olivine structure over the willemite. Because of this large expansion of the olivine<sub>ss</sub> field with pressure, it is suspected that the structure will completely span the join at some higher, as yet undetermined pressure.

### *The System $\text{ZnO-CoO-SiO}_2$ at 1 Atm*

*Arnulf Muan*

This study is concerned with the determination of phase relations and thermodynamic properties of a system in which the cations may be interchanged between sites of four-fold and six-fold coordination. The  $\text{Zn}^{2+}$  ion has a strong tendency to assume four-fold coordination in oxide and silicate structures, as demonstrated by the wurtzite structure of  $\text{ZnO}$  and the phenacite structure of  $\text{Zn}_2\text{SiO}_4$ . The  $\text{Co}^{2+}$  ion, on the other hand, has a strong preference for six-fold co-

ordination in oxide and silicate structures, as demonstrated by the chloride structure of CoO and the olivine structure of  $\text{Co}_2\text{SiO}_4$ . If the two oxides ZnO and CoO are combined with  $\text{SiO}_2$  to form the ternary system ZnO-CoO- $\text{SiO}_2$ , there will be only partial mutual solubilities between the end members ZnO and CoO in the oxide solid solution, and between the end members  $\text{Zn}_2\text{SiO}_4$  and  $\text{Co}_2\text{SiO}_4$  in the orthosilicate solid solution. However, the mutual solubilities between the end members in each of the two solid solutions are sufficiently large that the thermodynamic properties of the solutions can be studied over a considerable concentration range. Furthermore, no intermediate compound other than the orthosilicate phase is formed between  $\text{SiO}_2$  and either of the two oxides ZnO and CoO. The system ZnO-CoO- $\text{SiO}_2$

therefore constitutes an unusually simple and attractive model system for studying the energetics involved in the transition between four-fold and six-fold coordination.

The present work is concerned mainly with interrelations among the crystalline phases present in the system, and in particular with the distribution of  $\text{Zn}^{2+}$  and  $\text{Co}^{2+}$  between coexisting solid-solution phases. These relations are illustrated in Fig. 35, showing the 1050°C isothermal section through the system ZnO-CoO- $\text{SiO}_2$  at a total pressure of 1 atm.

The directions of the conjugation lines shown in Fig. 35, in conjunction with the known activity-composition relations in the bounding binary system ZnO-CoO at 1050°C (Navrotsky and Muan, 1970), permit calculation of the activity-composition relations in the  $\text{Zn}_2\text{SiO}_4$ - $\text{Co}_2\text{SiO}_4$

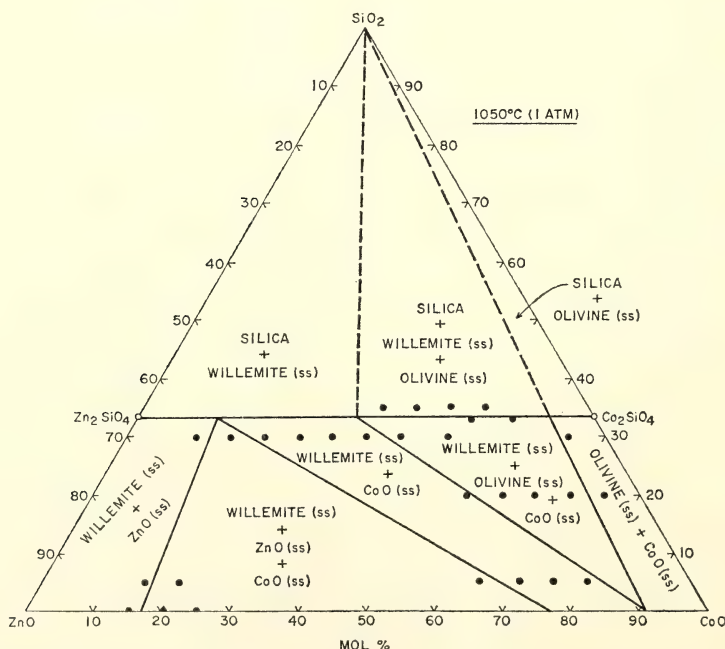
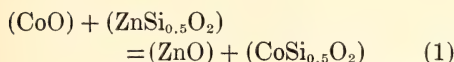


Fig. 35. The 1050°C isothermal section of the system ZnO-CoO- $\text{SiO}_2$  at a total pressure of 1 atm. Solid dots represent compositions of mixtures studied.

solid solution series at the same temperature. The following equations (Muan, 1967) may be derived:

For the reaction



we may express the equilibrium constant  $K$  as

$$\log K = \log C + \log \gamma_{\text{CoSi}_{0.5}\text{O}_2} - \log \gamma_{\text{ZnSi}_{0.5}\text{O}_2} \quad (2)$$

where

$$C = \frac{a_{\text{ZnO}} \cdot N_{\text{CoSi}_{0.5}\text{O}_2}}{a_{\text{CoO}} \cdot N_{\text{ZnSi}_{0.5}\text{O}_2}} \quad (3)$$

By combining the differentiated form of equation (2) with the Gibbs-Duhem equation for the orthosilicate join and rearranging the terms, we obtain the following expressions for the activity coefficients of the components of the orthosilicate solid solution.

$$\log \gamma_{\text{CoSi}_{0.5}\text{O}_2} = -N_{\text{ZnSi}_{0.5}\text{O}_2} \log C + \int_0^{N_{\text{ZnSi}_{0.5}\text{O}_2}} \log C \, dN_{\text{ZnSi}_{0.5}\text{O}_2} \quad (4)$$

and

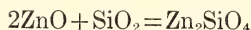
$$\log \gamma_{\text{ZnSi}_{0.5}\text{O}_2} = (1 - N_{\text{ZnSi}_{0.5}\text{O}_2}) \log C + \int_1^{N_{\text{ZnSi}_{0.5}\text{O}_2}} \log C \, dN_{\text{ZnSi}_{0.5}\text{O}_2} \quad (5)$$

The free energies of formation ( $\Delta G^\circ$ ) of the two end members of the orthosilicate solid solution,  $\text{Zn}_2\text{SiO}_4$  and  $\text{Co}_2\text{SiO}_4$ , are related to the above parameters by the equation

$$2.303 RT \log K = \frac{\Delta G^\circ_{\text{Co}_2\text{SiO}_4} - \Delta G^\circ_{\text{Zn}_2\text{SiO}_4}}{2} \quad (6)$$

Because  $\Delta G^\circ_{\text{Co}_2\text{SiO}_4}$  is known from previous work (Brežný and Muan, 1969), we can determine  $\Delta G^\circ_{\text{Zn}_2\text{SiO}_4}$  from the present equilibrium data.

Approximate activity-composition curves along the  $\text{Zn}_2\text{SiO}_4$ - $\text{Co}_2\text{SiO}_4$  join based on these calculations are shown graphically in Fig. 36. The free energy of formation ( $\Delta G^\circ$ ) of the  $\text{Zn}_2\text{SiO}_4$  end member from its oxide components according to the equation



at  $1050^\circ\text{C}$  is calculated to be  $-4.2 \pm 0.5$  kcal.

#### NOTES ON THE THERMAL BEHAVIOR OF LOUGHLINITE

*J. F. Schairer and H. S. Yoder, Jr.*

In the phase diagram for  $\text{Na}_2\text{O}$ - $\text{MgO}$ - $\text{SiO}_2$ , dehydrated loughlinite should lie in the triangle forsterite- $\text{Na}_2\text{O} \cdot 2\text{MgO} \cdot 6\text{SiO}_2$ - $\text{Na}_2\text{O} \cdot 2\text{MgO} \cdot 4\text{SiO}_2$  and should begin to melt at  $913^\circ \pm 5^\circ\text{C}$ . A small sample of natural loughlinite ( $\text{Na}_2\text{O} \cdot 3\text{MgO} \cdot 6\text{SiO}_2 \cdot 8\text{H}_2\text{O}$ ) was obtained from Joseph J. Fahey of the U. S. Geological Survey. When a sample of this material was held 19 hours at  $400^\circ\text{C}$  it gave an X-ray pattern showing loughlinite with several other new peaks. When the sample was held at  $850^\circ\text{C}$  for 6 days the X-ray pattern showed peaks of  $\text{Na}_2\text{O} \cdot 2\text{MgO} \cdot 6\text{SiO}_2$  with five other peaks. When it was held at  $900^\circ\text{C}$  for 7 days the X-ray pattern showed peaks for  $\text{Na}_2\text{O} \cdot 5\text{MgO} \cdot 12\text{SiO}_2$ ,  $\text{Na}_2\text{O} \cdot 2\text{MgO} \cdot 6\text{SiO}_2$ , and enstatite but no peaks for  $\text{Na}_2\text{O} \cdot 2\text{MgO} \cdot 4\text{SiO}_2$ . The remainder of the original sample was melted to a glass at  $1440^\circ\text{C}$ , and a portion of this glass held 7 days at  $900^\circ\text{C}$  showed X-ray peaks for  $\text{Na}_2\text{O} \cdot 5\text{MgO} \cdot 12\text{SiO}_2$  and  $\text{Na}_2\text{O} \cdot 2\text{MgO} \cdot 6\text{SiO}_2$  with a trace of forsterite. A similar sample held for 7 days at  $1000^\circ\text{C}$  showed X-ray



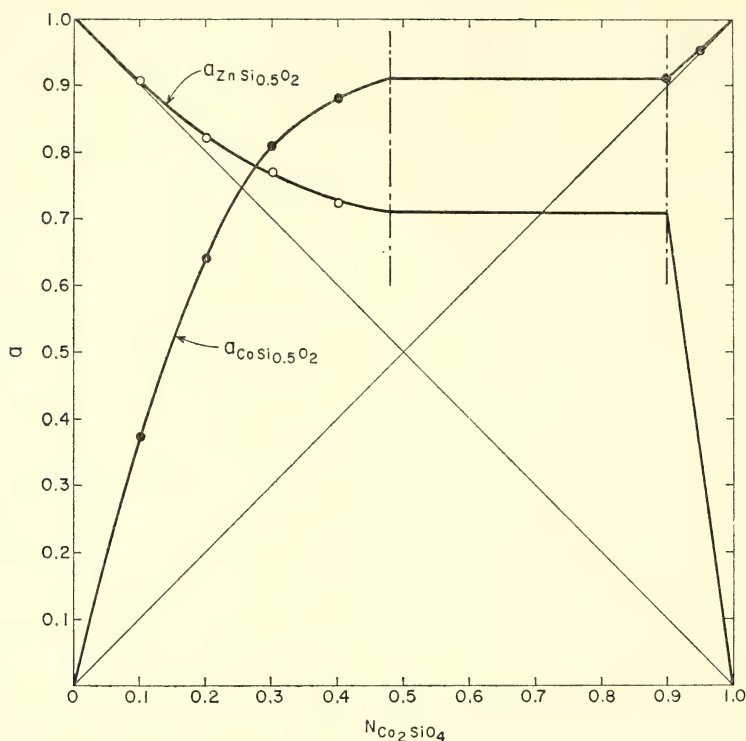


Fig. 36. Activity-composition relations in  $\text{Zn}_2\text{SiO}_4$ - $\text{Co}_2\text{SiO}_4$  solid solutions at  $1050^\circ\text{C}$  and a total pressure of 1 atm.

peaks for forsterite, enstatite, and  $\text{Na}_2\text{O} \cdot 5\text{MgO} \cdot 12\text{SiO}_2$ . Unless a liquid phase is present, equilibrium apparently cannot be attained. In studies of preparations in  $\text{Na}_2\text{O}$ - $\text{MgO}$ - $\text{SiO}_2$ , appropriate compositions also first crystallized enstatite, which disappeared in long heatings at appropriate temperatures higher than those used for the crystallization.

#### THERMODYNAMIC ANALYSIS OF PHASE EQUILIBRIA IN THE SYSTEM $\text{Fe}_2\text{TiO}_4$ - $\text{Fe}_3\text{O}_4$ - $\text{TiO}_2$

*Douglas Rumble III*

The minerals rutile, magnetite, and ilmenite are nearly ubiquitous in igneous and metamorphic rocks. Knowledge of their thermodynamic properties is essential to an understanding of the conditions under which the minerals crystallized

during igneous and metamorphic processes. In the first part of this report the writer calculates the pressure dependence of the two-phase equilibrium ilmenite-magnetite. Equations of state for the binary solutions magnetite-ulvöspinel and hematite-ilmenite are derived in the second part, and phase diagrams have been calculated showing the equilibria between the binary solutions and rutile.

#### *Pressure Dependence of the Partition of Fe and Ti between Coexisting Ilmenite and Magnetite*

The chemical compositions of coexisting natural ilmenite and magnetite have been used to estimate the  $T$  and  $\mu_{\text{O}_2}$  conditions under which the minerals crystallized (Buddington and Lindsley, 1964; Carmichael, 1966). The pressure inde-

TABLE 5. Thermodynamic Equations

	$dT$	$dP$	$(\frac{d\mu_{3I}}{d\mu_{4I}} - \frac{d\mu_{1M}}{d\mu_{2M}})$	$d\mu_{4I}$	$d\mu_{2M}$	$dN_{3I}$	$dN_{1M}$	$d\mu_{O_2}$
(1)	$0 = +\bar{S}_I$	$-\bar{V}_I$	$+N_{3I}$	0	+1	0	0	0
(2)	$0 = +\bar{S}_M$	$-\bar{V}_M$	0	$+N_{1M}$	0	+1	0	0
(3)	$0 = 0$	0	-1	+1	0	0	0	0
(4)	$0 = -(\bar{S}_{3I} - \bar{S}_{4I})$	$+(\bar{V}_{3I} - \bar{V}_{4I})$	-1	0	0	$\bar{G}_{33I}$	0	0
(5)	$0 = -(\bar{S}_{1M} - \bar{S}_{2M})$	$+(\bar{V}_{1M} - \bar{V}_{2M})$	0	-1	0	0	$\bar{G}_{11M}$	0
(6)	$0 = 0$	0	0	0	+3	-2	0	$-1/2$

Notation

$N_{1M}$ , mole fraction  $Fe_2TiO_4$  in magnetite;  $N_{2M}$ , mole fraction  $Fe_3O_4$  in magnetite.  
 $N_{3I}$ , mole fraction  $FeTiO_3$  in ilmenite;  $N_{4I}$ , mole fraction  $Fe_2O_3$  in ilmenite.  
 $\bar{V}_M$ , molar volume of magnetite;  $\bar{V}_{3I}$ , partial molar volume of  $FeTiO_3$  in ilmenite.  
 $\bar{S}_I$ , molar entropy of ilmenite;  $\bar{S}_{2M}$ , partial molar entropy of  $Fe_3O_4$  in magnetite.  
 $\mu_{4I}$ , chemical potential of  $Fe_2O_3$  in ilmenite.  
 $G_M$ , molar Gibbs free energy of magnetite.

$\bar{G}_{11M} = \left( \frac{\partial^2 \bar{G}_M}{\partial N_{1M}^2} \right)_{P,T}$

pendence of the two-phase equilibrium ilmenite-magnetite is critical to its use as a geothermometer and oxygen barometer: if the equilibrium were dependent on total pressure ( $P$ ), then it would not be possible to calculate the three unknown parameters  $P$ ,  $T$ , and  $\mu_{O_2}$  from the two measurable quantities  $N_{1M}$  and  $N_{3I}$  (notation summarized in Table 5). Lindsley (*Year Book 62*, pp. 60-66) has performed experiments at 1 and 2 kb total pressure and at 600°, 700°, 800°, 900°, and 1000°C, indicating that the compositions of ilmenite and magnetite coexisting in chemical equilibrium are a function of  $T$  and  $\mu_{O_2}$  and are independent of  $P$ . Lindsley (*Year Book 64*, pp. 145-

146) estimated the pressure dependence of the equilibrium to be very small on theoretical grounds but did not give an analytical formulation of it.

The writer has calculated the pressure dependence of the compositions of ilmenite and magnetite solutions coexisting in equilibrium as well as the pressure dependence of their equilibrium  $\mu_{O_2}$  (Tables 6 and 7). The results of the calculations confirm the pressure independence of the two-phase assemblage in the pressure range 1-2 kb. The calculations also suggest that the ilmenite-magnetite equilibrium is independent of pressure in the range 1-10 kb.

Equations 1 through 6, used in deriv-

TABLE 6. Pressure Dependence of  $\mu_{O_2}$  for the Two-Phase Equilibrium Ilmenite-Magnetite

$T, ^\circ C$	$N_{1M}$	$N_{3I}$	$\left( \frac{\partial \mu_{O_2}}{\partial P} \right)_{T, N_{1M}, N_{3I}}$ cal/bar	Uncertainty, cal/bar
1000	0.851	0.99	$8.7 \cdot 10^{-3}$	$8.4 \cdot 10^{-3}$
900	0.851	0.99	$9.0 \cdot 10^{-3}$	$8.4 \cdot 10^{-3}$
800	0.85	0.99	$9.3 \cdot 10^{-3}$	$8.4 \cdot 10^{-3}$
700	0.845	0.99	$9.8 \cdot 10^{-3}$	$8.6 \cdot 10^{-3}$
600	0.84	0.99	$10.0 \cdot 10^{-3}$	$8.6 \cdot 10^{-3}$
1000	0.50	0.87	$6.0 \cdot 10^{-2}$	$5.6 \cdot 10^{-3}$
900	0.441	0.90	$5.6 \cdot 10^{-2}$	$6.0 \cdot 10^{-3}$
800	0.34	0.92	$4.5 \cdot 10^{-2}$	$6.0 \cdot 10^{-3}$
700	0.22	0.93	$2.1 \cdot 10^{-2}$	$6.0 \cdot 10^{-3}$
600	0.12	0.94	$-2.4 \cdot 10^{-2}$	$10.8 \cdot 10^{-3}$

TABLE 7. Pressure Dependence of  $N_{1M}$  for Two-Phase Assemblages of Ilmenite and Magnetite on the Ni-NiO Buffer

$T, ^\circ\text{C}$	$N_{1M}$	$N_{3I}$	$\left(\frac{\partial N_{1M}}{\partial P}\right)_{T, \mu_{\text{O}_2}, 2\phi}$ mole fraction/bar	Uncertainty, mole fraction/bar
1000	0.50	0.87	$9.6 \cdot 10^{-7}$	$1.0 \cdot 10^{-4}$
900	0.44	0.90	$9.0 \cdot 10^{-8}$	$1.1 \cdot 10^{-4}$
800	0.34	0.92	$6.4 \cdot 10^{-7}$	$9.5 \cdot 10^{-5}$
700	0.22	0.93	$2.0 \cdot 10^{-7}$	$6.1 \cdot 10^{-5}$
600	0.12	0.94	$-1.3 \cdot 10^{-7}$	$5.9 \cdot 10^{-5}$

ing the formulas for the pressure dependence of the ilmenite-magnetite equilibrium, are given in matrix form in Table 5. In the body of the table are listed the thermodynamic constants that are the coefficients of the differentials given as column headings. The ilmenite solution is defined as a rhombohedral phase made up of the components  $\text{FeTiO}_3$  and  $\text{Fe}_2\text{O}_3$ . The magnetite solution is a spinel phase made of  $\text{Fe}_2\text{TiO}_4$  and  $\text{Fe}_3\text{O}_4$ . Cation deficiency solid solution on the part of either solution, observed at  $1200^\circ$  and  $1300^\circ\text{C}$  (Taylor, 1964; Webster and Bright, 1961), is negligible in the temperature range below  $1000^\circ\text{C}$  (Lindsley, *Year Book 61*, p. 104). Equations 1 and 2 are Gibbs-Duhem equations with the dependent  $N_{2M}$  or  $N_{4I}$  terms eliminated. Equation 3 gives the condition of exchange equilibrium between two binary solutions in a ternary reciprocal system (Thompson and Waldbaum, 1968). Equations 4 and 5 are derived from the total differentials of  $(\mu_{3I} - \mu_{4I})$  and  $(\mu_{1M} - \mu_{2M})$  as functions of  $P$ ,  $T$ , and phase composition and from the relations

$$(\mu_{3I} - \mu_{4I}) = \left( \frac{\partial \bar{G}_I}{\partial N_{3I}} \right)_{P,T}$$

and

$$(\mu_{1M} - \mu_{2M}) = \left( \frac{\partial \bar{G}_M}{\partial N_{1M}} \right)_{P,T}$$

for each binary solution (Prigogine and Defay, 1954, p. 73, eq. 6.47). In equation 6 is stated the condition of equilibrium that must exist between the chemical potentials of the components

$\text{Fe}_2\text{O}_3$  and  $\text{Fe}_3\text{O}_4$  of ilmenite and magnetite and the chemical potential of the system component  $\text{O}_2$ .

The derivation of formulas from Table 5 will be illustrated by an example.\* Let it be required to find a formula for

$$\left( \frac{\partial \mu_{\text{O}_2}}{\partial N_{1M}} \right)_{P,T,2\phi} \quad (7a)$$

where the symbol  $2\phi$  indicates that the partial derivative (7a) refers only to a two-phase assemblage of ilmenite and magnetite. Setting  $dP=0$  and  $dT=0$ , their columns of coefficients vanish from Table 5. Dividing through all the equations by  $dN_{1M}$  and transposing to the left-hand side the column of terms that were formerly coefficients of  $dN_{1M}$ , we obtain six simultaneous equations in six unknowns. We may then solve for the unknown partial derivatives in terms of the known thermodynamic constants:

$$\left( \frac{\partial \mu_{\text{O}_2}}{\partial N_{1M}} \right)_{P,T,2\phi} = 2G_{11M} (2N_{1M} - 3N_{3I}) \quad (7b)$$

Formula 7b is of special interest because of the information it gives on the location of the critical temperature of the magnetite solution solvus at 1 kb. The quantity  $(2N_{1M} - 3N_{3I})$  is always negative (Lindsley, *Year Book 62*, p. 63); therefore, positive values for  $G_{11M}$  cor-

\*The writer is indebted to Professor J. B. Thompson, Harvard University, for developing in class lectures the method of thermodynamic analysis used in this study.



respond to negative values for  $(\partial\mu_{O_2}/\partial N_{1M})_{P,T,2\phi}$ . Should a solvus be present in the magnetite solution, then the spinodal compositions, where  $(\partial^2\bar{G}_M/\partial\bar{N}_{1M}^2)_{P,T}=0$ , correspond to zero values for  $(\partial\mu_{O_2}/\partial N_{1M})_{P,T,2\phi}$ .

Hypothetical curves of  $\mu_{O_2}$  vs.  $N_{1M}$  are given in Fig. 37 for ilmenite-magnetite assemblages (cf. Prigogine and Defay, 1954, pp. 240-241, Figs. 16.12 and 16.13). The hypothetical curves are to be compared with Fig. 38, which shows plots of  $\mu_{O_2}$  vs.  $N_{1M}$  calculated from the two-phase equilibrium data of Lindsley (Year Book 62, p. 63) and the thermodynamic constants of Robie and Waldbaum (1968). The 1000°, 900°, and 800°C isotherms are not consistent with the presence of a miscibility gap in the magnetite solution. The 600°C and possibly the 700°C isotherms are consistent with the existence of a solvus in the magnetite solution. Vincent *et al.* (1957) con-

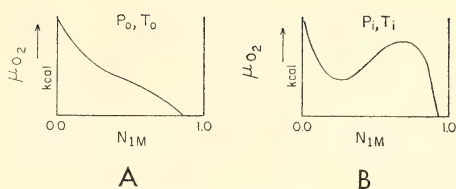


Fig. 37. (A) Hypothetical curves of  $\mu_{O_2}$  vs.  $N_{1M}$  for the two-phase equilibrium ilmenite-magnetite.  $P_0$  and  $T_0$  represent conditions at which there is no miscibility gap in the magnetite solution. (B) Hypothetical curves of  $\mu_{O_2}$  vs.  $N_{1M}$  for the two-phase equilibrium ilmenite-magnetite.  $P_1$  and  $T_1$  represent conditions at which there is a miscibility gap in the magnetite solution.

cluded, on the basis of heating experiments on natural titaniferous magnetites, that the critical temperature of the magnetite solvus lies just above 600°C at 1 bar.

Two additional formulas may be derived from Table 5:

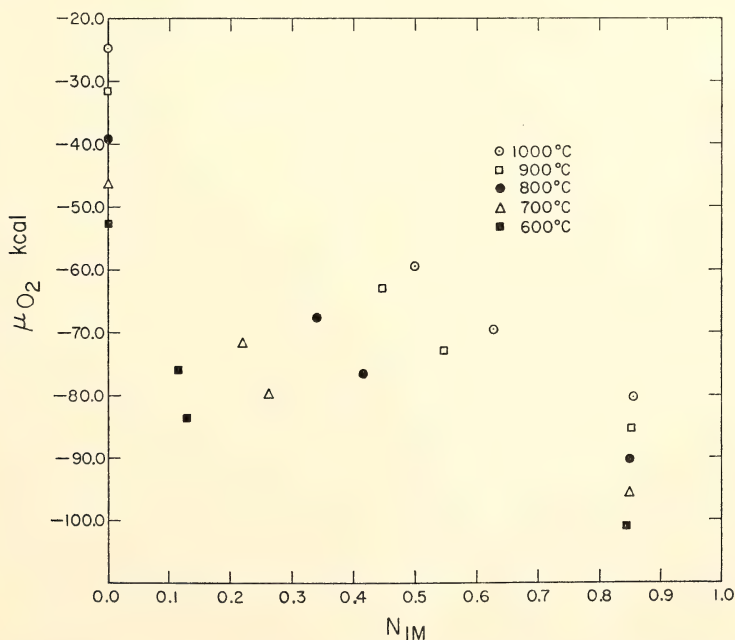


Fig. 38. Calculated values of  $\mu_{O_2}$  (oxygen buffer data from Robie and Waldbaum, 1968) plotted as a function of  $N_{1M}$  for the two-phase equilibrium ilmenite-magnetite determined by Lindsley (Year Book 62, pp. 60-66).

$$\left(\frac{\partial \mu_{O_2}}{\partial P}\right)_{T, N_{1M}, 2\phi} = 2[(2\bar{V}_M - 3\bar{V}_I) + (3N_{3I} - 2N_{1M})(\bar{V}_{1M} - \bar{V}_{2M})] \quad (8)$$

and

$$\left(\frac{\partial N_{1M}}{\partial P}\right)_{T, \mu_{O_2}, 2\phi} = \frac{2\bar{V}_M - 3\bar{V}_I}{G_{11M}(3N_{3I} - 2N_{1M})} + \frac{(3N_{3I} - 2N_{1M})(\bar{V}_{1M} - \bar{V}_{2M})}{G_{11M}(3N_{3I} - 2N_{1M})} \quad (9)$$

Formula 8 gives the pressure dependence of the value of  $\mu_{O_2}$  in equilibrium with a given two-phase assemblage of ilmenite and magnetite at constant  $T$ . Values of formula 8 may be calculated from the molar volume data of Lindsley (*Year Book 64*, pp. 144–148) and Akimoto, Katsura, and Yoshida (1957) and from the compositions of coexisting ilmenite and magnetite solutions determined by Lindsley (*Year Book 62*, pp. 60–66). Compressibilities and thermal expansion of the solid phases are assumed to be negligible. The dependence of  $\mu_{O_2}$  on pressure is approximately 0.01 cal/bar, with an uncertainty of 0.001 cal/bar, for the two-phase tie lines on the wüstite-magnetite and Ni-NiO buffers (Table 6). For a pressure change of 10 kb the value of  $\mu_{O_2}$  for a given ilmenite-magnetite equilibrium will change 0.1 kcal, an insignificant amount.

Formula 9 gives the pressure dependence of the value of  $N_{1M}$  for a two-phase assemblage of ilmenite and magnetite at constant  $T$  and  $\mu_{O_2}$ . Values for formula 9 may be calculated from the data sources given above, as well as the value of the curvature of the molar Gibbs free energy calculated from formula 7b. Values of  $G_{11M}$  were obtained by calculating the slopes of curves derived by least-squares analysis (computer program written by L. W. Finger) of the points plotted in Fig. 38. Because of the paucity of data points, the curves obtained have physical meaning at temperatures of 600°, 700°, and 800°C, only in the range of magnetite

compositions spanned by tie lines on the hematite-magnetite, Ni-NiO, and quartz-fayalite-magnetite buffers. The tie line on the Ni-NiO buffer is bracketed by those on the hematite-magnetite and quartz-fayalite-magnetite buffers at temperatures of 600°, 700°, and 800°C and, therefore, the value of  $G_{11M}$  calculated from formula 7b for this tie line is the least uncertain value of  $G_{11M}$  for these isotherms. The pressure dependence of  $N_{1M}$  is of the order of magnitude of  $10^{-7}$  mole fraction per bar. An increase in pressure from 1 to 10 kb will, therefore, change the composition of magnetite coexisting isothermally with ilmenite by 0.1 mole %. Because of the uncertainty in the value of  $G_{11M}$ , however, the uncertainty of the pressure dependence of  $N_{1M}$  is  $10^{-4}$  mole fraction per bar. The uncertainty in the value of  $G_{11M}$  can be eliminated by the determination of additional tie lines on oxygen buffers other than those available to Lindsley (*Year Book 62*, pp. 60–66).

#### *Equations of State for Magnetite-Ulvöspinel and Hematite-Ilmenite Crystalline Solutions*

Minerals that lie wholly or in part on the binary joins magnetite-ulvöspinel ( $Fe_3O_4$ - $Fe_2TiO_4$ ) and hematite-ilmenite ( $Fe_2O_3$ - $FeTiO_3$ ) are nearly ubiquitous in igneous and metamorphic rocks. Study of these minerals is very rewarding to petrologists because the compositions of coexisting ilmenite and magnetite may be used to estimate the temperature and  $\mu_{O_2}$  during their crystallization (Lindsley, *Year Book 62*; Buddington and Lindsley, 1964). Sufficient experimental data are now at hand for a preliminary calculation of the mixing properties of the binary solutions with the use of the methods of Thompson (1967), Thompson and Waldbaum (1968), and Waldbaum and Thompson (1968). The calculated mixing properties have been used to con-

struct the magnetite-ulvöspinel solvus and to construct isothermal, isobaric phase diagrams of the system  $\text{Fe}_2\text{TiO}_4\text{-Fe}_3\text{O}_4\text{-TiO}_2$ .

In the analysis that follows, we explicitly assume  $\bar{G}_M$  and  $\bar{G}_I$  to be continuous functions of  $P$ ,  $T$ , and phase composition. (For explanation of notations see Table 8.) It is also assumed that the magnetite and ilmenite solutions do not deviate from their binary joins,  $\text{Fe}_2\text{TiO}_4\text{-Fe}_3\text{O}_4$  and  $\text{FeTiO}_3\text{-Fe}_2\text{O}_3$ , respectively. The limited cation deficiency observed in both solutions at  $1200^\circ$  and  $1300^\circ\text{C}$  (Webster and Bright, 1961; Taylor, 1964) is negligible over the temperature range considered herein (Lindsley, *Year Book 61*, p. 104). The term ilmenite will be used to refer to rhombohedral phases made up of  $\text{FeTiO}_3$  and  $\text{Fe}_2\text{O}_3$ , and the term magnetite, to refer to spinel phases made up of  $\text{Fe}_2\text{TiO}_4$  and  $\text{Fe}_3\text{O}_4$ .

The solvus of the ilmenite-hematite crystalline solution has been determined at atmospheric pressure and at temperatures ranging from  $25^\circ$  to  $900^\circ\text{C}$  (Carmichael, 1961). The measurement of the binodal compositions of the ilmenite solvus at given  $P$  and  $T$  gives sufficient information to calculate the Margules parameters  $W_{G3I}$  and  $W_{G4I}$ . The quantities  $W_{G3I}$  and  $W_{G4I}$  are related to the excess Gibbs free energy ( $\bar{G}_{exI}$ ) of a regular asymmetric binary solution by the equation (Thompson, 1967, p. 352, eq. 70a)

$$\bar{G}_{exI} = (W_{G3I}N_{4I} + W_{G4I}N_{3I})N_{3I}N_{4I} \quad (1)$$

The total Gibbs free energy of the ilmenite solution at constant  $P$  and  $T$  is, therefore, equal to (Thompson, 1967, p. 352, eq. 73)

$$\begin{aligned} \bar{G}_I = & N_{3I}\mu_{3I}^0 + N_{4I}\mu_{4I}^0 + \\ & RT(N_{3I}\ln N_{3I} + N_{4I}\ln N_{4I}) + \\ & (W_{G3I}N_{4I} + W_{G4I}N_{3I})N_{3I}N_{4I} \end{aligned} \quad (2)$$

Formulas for calculating  $W_{G3I}$  and  $W_{G4I}$  from the binodal compositions at different temperatures have been derived by Thompson (1967, p. 355, eq. 87a, 87b) using equation 2, above, and the condition of equilibrium for two binodal phases at constant  $P$  and  $T$

$$\text{and} \quad \left. \begin{aligned} \mu_{3A} &= \mu_{3B} \\ \mu_{4A} &= \mu_{4B} \end{aligned} \right\} \quad (3)$$

where  $A$  and  $B$  refer to binodal phases on the ilmenite solvus. Values of  $W_{G3I}$  and  $W_{G4I}$  are plotted as a function of  $1/T^\circ\text{K}$  in Fig. 39. The uncertainty of these values is equal to approximately 60% of their stated value. Their uncertainty may be reduced to an order of magnitude less than their stated values only if the binodal compositions are measured with an uncertainty of  $10^{-3}$  mole fraction or less. A more sophisticated analysis of the ilmenite solvus (cf. Thompson and Waldbaum, 1969) is not justified because of the large uncertain-

TABLE 8. Notation

$N_{1M}$	Mole fraction of $\text{Fe}_2\text{TiO}_4$ in magnetite solution.
$N_{2M}$	Mole fraction of $\text{Fe}_3\text{O}_4$ in magnetite solution.
$N_{3I}$	Mole fraction of $\text{FeTiO}_3$ in ilmenite solution.
$N_{4I}$	Mole fraction of $\text{Fe}_2\text{O}_3$ in ilmenite solution.
$\bar{G}_M$	Molar Gibbs free energy of magnetite solution.
$\bar{G}_I$	Molar volume of ilmenite solution.
$\mu_{1M}$	Chemical potential of $\text{Fe}_2\text{TiO}_4$ in magnetite solution.
$\mu_{3I}^0$	Chemical potential of pure $\text{FeTiO}_3$ ; standard state is formation of compound from the elements at $T$ of interest and $P = 1$ bar.
$W_{G1M}$	Molar Margules parameter of molar Gibbs free energy of magnetite solution.
$W_{VI}$	Molar Margules parameter of molar volume of ilmenite solution (symmetric).
$W_{V1M}$	Molar Margules parameter of molar volume of magnetite solution (asymmetric).



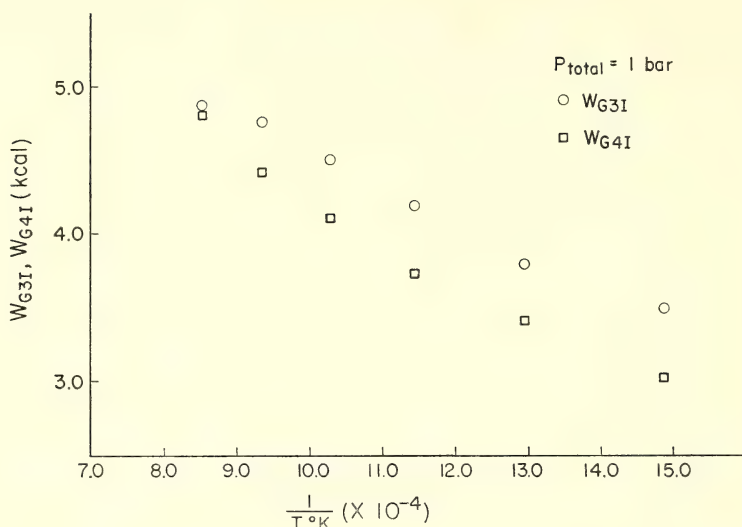


Fig. 39. Margules parameters of Gibbs free energy of ilmenite solution at 1 bar plotted as a function of  $1/T^{\circ}\text{K}$ .

ties in the binodal compositions determined by Carmichael (1961).

The molar volume of the ilmenite solution is a symmetrical function of composition and is given by

$$\begin{aligned} \bar{V}_I = & 0.7243 (\pm 0.0003) + \\ & 0.0223 (\pm 0.0014) N_{3I} + \\ & 0.0111 (\pm 0.0014) (N_{3I})^2 \text{ cal/bar} \end{aligned} \quad (4)$$

The coefficients of the power-series expansion (4) were determined by least-squares analysis (computer program written by L. W. Finger) of Lindsley's molar volume data (*Year Book 64*, pp. 144–148). The Margules volume parameter,  $W_{VI}$ , is equal to  $-0.0111 (\pm 0.0014)$  cal/bar (Waldbaum and Thompson, 1968). Ilmenite solution has a negative excess volume of mixing, and the critical temperature of its solvus, therefore, is expected to decrease with increasing pressure.

The mixing properties of the magnetite-ulvöspinel binary solution may be calculated with the use of the two-phase tie lines determined by Lindsley (*Year*

*Book 62*, pp. 60–66), the condition of exchange equilibrium between binary solutions in a ternary reciprocal system (Thompson and Waldbaum, 1968), and the mixing properties of ilmenite solution derived from Carmichael's (1961) solvus. The mixing properties of ilmenite derived above are valid only for atmospheric pressure and must be corrected to 1 kb by the relation

$$\left( \frac{\partial W_{G1}}{\partial P} \right)_T = W_{VI} \quad (5)$$

(Thompson, 1967, p. 349 equation 54a). The condition of exchange equilibrium between the binary solutions is (at constant  $P$  and  $T$ )

$$(\mu_{1M} - \mu_{2M}) = (\mu_{3I} - \mu_{4I}) \quad (6)$$

Substituting in this relation the Margules expansion for  $(\mu_{1M} - \mu_{2M})$  and  $(\mu_{3I} - \mu_{4I})$  (Thompson, 1967, p. 353, eq. 75) and rearranging terms, we obtain the following equation (cf. Thompson and Waldbaum, 1968, p. 1975, eq. 23)

$$\begin{aligned}
 & RT \ln \frac{N_{3I}N_{2M}}{N_{4I}N_{1M}} + W_{G4I}N_{3I}(3N_{4I}-1) - \\
 & W_{G3I}N_{4I}(3N_{3I}-1) = [(\mu_{1M}^0 - \mu_{2M}^0) - \\
 & (\mu_{3I}^0 - \mu_{4I}^0) + W_{G1M}] + \\
 & 2(W_{G2M} - 2W_{G1M})N_{1M} + \\
 & 3(W_{G1M} - W_{G2M})(N_{1M})^2 \quad (7)
 \end{aligned}$$

The equation is written in a form that facilitates least-squares analysis of the left-hand side as a power series in  $N_{1M}$ :

$$\text{left-hand side} = a + bN_{1M} + c(N_{1M})^2 \quad (8)$$

The coefficients  $a$ ,  $b$ , and  $c$  (8) have been determined by least-squares analysis of the two-phase tie lines measured by Lindsley (*Year Book 62*, pp. 60-66). Coefficients  $b$  and  $c$  give two simultaneous equations in  $W_{G1M}$  and  $W_{G2M}$ . Values of  $W_{G1M}$  and  $W_{G2M}$  are plotted in Fig. 40 as a function of  $1/T^\circ\text{K}$ ; their uncertainties are approximately 60% of the stated values. The uncertainties may be reduced by decreasing the uncertainty in the binodal compositions of the ilmenite solvus

and by measuring the compositions of coexisting ilmenite and magnetite with an uncertainty of  $10^{-3}$  mole fraction. Coefficient  $a$  of equation 8 gives a means of calculating  $\mu_{1M}^0$

$$\mu_{1M}^0 = a - W_{G1M} + (\mu_{3I}^0 - \mu_{4I}^0) + \mu_{2M}^0 \quad (9)$$

Values of  $\mu_{1M}^0$  at 1 kb are plotted as a function of  $T^\circ\text{K}$  in Fig. 41. The extrapolated value for the free energy of formation from the elements at 1 bar and  $298^\circ\text{K}$  of  $\text{Fe}_2\text{TiO}_4$  is  $-333.24$  kcal ( $\pm 3.0$  kcal). This value for  $\bar{G}_{f,\text{Fe}_2\text{TiO}_4}$  is in agreement with the estimate of Verhoogen (1962a,  $-338.0$  kcal ( $\pm 3.0$  kcal)).

The molar volume of magnetite solution is asymmetric with respect to composition and is given by

$$\begin{aligned}
 \bar{V}_M = & 1.0647 (\pm 0.0006) + \\
 & 0.0310 (\pm 0.0049) N_{1M} + \\
 & 0.0627 (\pm 0.0119) (N_{1M})^2 - \\
 & 0.0406 (\pm 0.0079) (N_{1M})^3 \text{ cal/bar} \quad (10)
 \end{aligned}$$

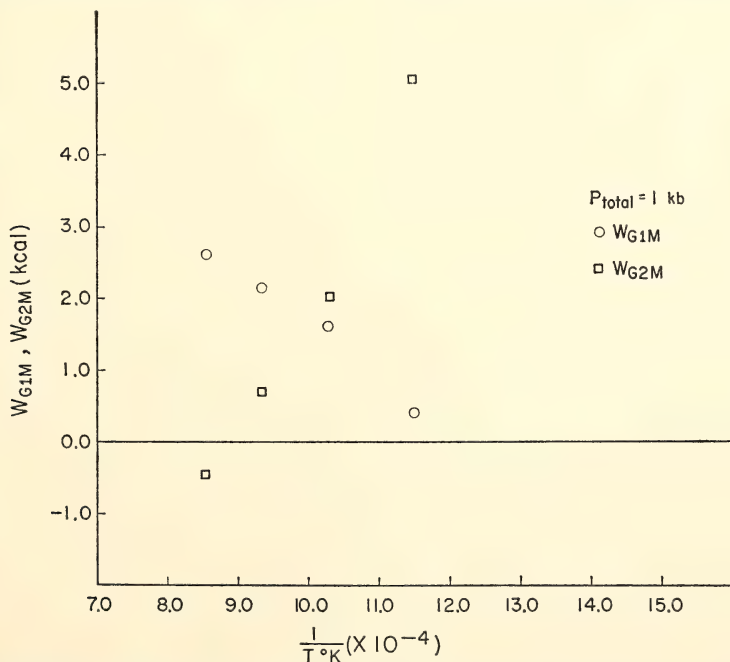


Fig. 40. Margules parameters of Gibbs free energy of magnetite solution at 1 kb plotted as a function of  $1/T^\circ\text{K}$ .

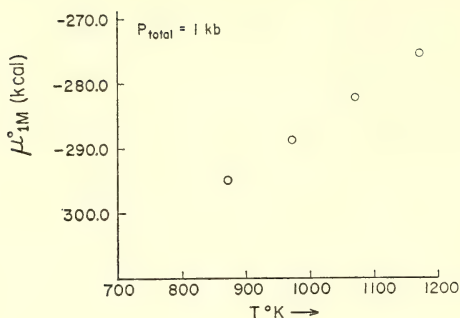


Fig. 41. Values of  $\mu_{1M}^0$  at 1 kb plotted as a function of  $T^\circ\text{K}$ .

Coefficients of equation 10 were determined by least-squares analysis of the molar volume data of Lindsley (*Year Book 64*, pp. 144-148) and Akimoto, Katsura, and Yoshida (1957) (computer program written by L. W. Finger, Geophysical Laboratory). The Margules volume parameters,  $W_{V1M}$  and  $W_{V2M}$ , are equal to +0.0185 cal/bar and -0.0221 cal/bar, respectively. The excess volume of mixing of magnetite solution is negative for  $\text{Fe}_3\text{O}_4$ -rich compositions and positive for  $\text{Fe}_2\text{TiO}_4$ -rich compositions.

Phase-equilibrium diagrams have been calculated from the mixing properties of the ilmenite and the magnetite solutions (Figs. 42, 43, and 44). The magnetite solvus (Fig. 42) shows the binodal compositions that satisfy the conditions of equilibrium

$$\text{and } \left. \begin{aligned} \mu_{1A} &= \mu_{1B} \\ \mu_{2A} &= \mu_{2B} \end{aligned} \right\} \quad (11)$$

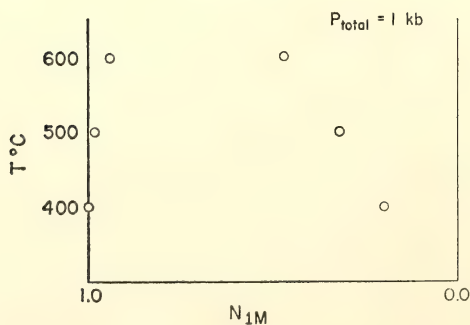


Fig. 42. Calculated magnetite solvus at 1 kb.

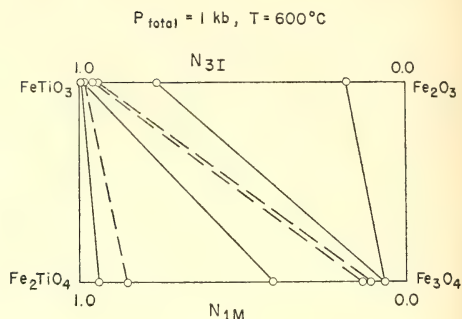


Fig. 43. Calculated phase equilibria in the system  $\text{FeTiO}_3\text{-Fe}_2\text{O}_3\text{-Fe}_2\text{TiO}_4\text{-Fe}_3\text{O}_4$  at  $600^\circ\text{C}$  and 1 kb. Dashed two-phase tie lines are those experimentally determined by Lindsley (*Year Book 62*, pp. 60-66).

where  $A$  and  $B$  refer to conjugate phases on the magnetite solvus. The binodal compositions were determined by plotting the two curves  $\mu_{1A}$  vs.  $\mu_{2A}$  and  $\mu_{1B}$  vs.  $\mu_{2B}$  and noting their point of intersection (Scatchard, 1940).

Two- and three-phase equilibria in the ternary reciprocal system  $\text{FeTiO}_3\text{-Fe}_2\text{O}_3\text{-Fe}_2\text{TiO}_4\text{-Fe}_3\text{O}_4$  are shown in Fig. 43 for  $600^\circ\text{C}$  and 1 kb. The two-phase tie lines ilmenite-magnetite give the phase compositions that satisfy the condition of equilibrium

$$(\mu_{1M} - \mu_{2M}) = (\mu_{3I} - \mu_{4I}) \quad (6)$$

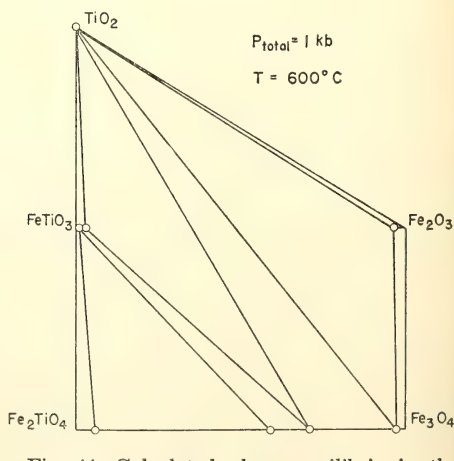


Fig. 44. Calculated phase equilibria in the system  $\text{TiO}_2\text{-Fe}_2\text{TiO}_4\text{-Fe}_3\text{O}_4$  at  $600^\circ\text{C}$  and 1 kb.



The phase compositions were determined by plotting the two curves ( $\mu_{1M} - \mu_{2M}$ ) vs.  $N_{1M}$  and ( $\mu_{3I} - \mu_{4I}$ ) vs.  $N_{3I}$  at the same scale; phase compositions satisfying the condition of equilibrium (6) were read directly from the graphs.

Phase diagrams showing the phase-equilibrium relations between rutile, ilmenite, and magnetite may be calculated with the use of the condition of three-phase equilibrium

$$\mu_{TiO_2, Rutile} = 2\mu_{3I} - \mu_{1M} \quad (12)$$

for the three-phase assemblage rutile-magnetite-ilmenite at constant  $P$  and  $T$ . If we assume rutile to be a pure substance,  $TiO_2$ , then we may substitute

$$\bar{G}_{f, Rutile} = \mu_{TiO_2, Rutile}^* = \mu_{TiO_2, Rutile} \quad (13)$$

in equation 12. The composition of rutile deviates only slightly from  $TiO_2$  at temperatures of 1200° and 1300°C (Webster and Bright, 1961; Taylor, 1964). It is, therefore, reasonable to assume that rutile is pure  $TiO_2$  in the temperature range considered herein. If the value of ( $2\mu_{3I} - \mu_{1M}$ ) for a given two-phase assemblage is less than  $\bar{G}_{f, Rutile}$ , then the two-phase assemblage of ilmenite and magnetite is stable with respect to the three-phase assemblage rutile-ilmenite-magnetite. If the value of ( $2\mu_{3I} - \mu_{1M}$ ), however, is greater than  $\bar{G}_{f, Rutile}$ , then the three-phase assemblage rutile-ilmenite-magnetite is stable with respect to the two-phase assemblage of ilmenite and magnetite. Values of  $\bar{G}_{f, Rutile}$ , corrected to 1 kb, were obtained from the compilation of Robie and Waldbaum (1968). At temperatures of 400°, 500°, and 600°C and a pressure of 1 kb, rutile-magnetite tie lines are stable by about 3 kcal with respect to a two-phase assemblage of the conjugate phases, on the ilmenite solvus (Fig. 44). Natural occurrences of rutile-magnetite assemblages are rare but have been observed in regionally metamorphosed rocks from Maryland (Southwick, 1968) and from western New Hampshire (Rumble, in progress). The

uncertainty in the value of ( $2\mu_{3I} - \mu_{1M}$ ) is 3.0 kcal, and the phase relations shown in Fig. 44, therefore, cannot be accepted as proved. The hypothesis that magnetite-rutile tie lines are stable with respect to the conjugate phases on the ilmenite solvus is now being tested by hydrothermal experiments (Rumble and Lindsley, in progress).

The uncertainties associated with the calculated phase diagrams may be estimated by comparing them with experimental results. The critical temperature of the calculated magnetite solvus is in agreement with the estimates of Vincent *et al.* (1957) and of Kawai (1956; quoted in Vincent *et al.*, 1957) but the sense of asymmetry of the calculated solvus is the opposite of that of Vincent *et al.* (1957) and Kawai (1956). The disagreement between the calculated position of the three-phase field magnetite *A*-magnetite *B*-ilmenite and the ilmenite-magnetite tie line on the WM buffer (Lindsley, *Year Book 62*) (see Fig. 43) may also be taken as evidence that the asymmetry of the calculated magnetite solvus may be incorrect. The asymmetry of the calculated magnetite solvus is critically dependent on the least-squares analysis of equation 8. An equation of rank 3 gives a better fit to the data points than does a rank 2 equation, but with only four ilmenite-magnetite tie lines per isotherm, there is not sufficient redundancy to adequately test the fit of the equations. The question of the asymmetry of the calculated magnetite solvus would be resolved by the determination of additional ilmenite-magnetite tie lines.

#### BEHAVIOR OF THERMOCOUPLES IN THE SINGLE-STAGE PISTON-CYLINDER APPARATUS

H. K. Mao and P. M. Bell

Evaluation of the behavior of a thermocouple in a high-pressure, high-temperature cell is important but difficult. An independent method of accurately measuring temperature in a high-pres-

sure vessel is not available. Starting with Bridgman's (1918) experiments on pressurized single wires in a thermal gradient, attempts have been made to ascertain the magnitude of the error introduced by the pressure effect on thermocouples (Hanneman, Strong, and Bundy, 1970; Birch, 1939). Recently, Getting and Kennedy (1970), Freud and LaMori (1970), and Bell, Boyd, and England (1970) have reinvestigated the pressure effect on the standard Pt/Pt 10% Rh thermocouple. Most of the studies were limited to approximately 10 kb and were done with gas pressure. To examine the effects of higher pressures, Getting and Kennedy employed solid media in their experimental cells. This method possibly introduced errors of uneven pressure distribution but permitted measurements up to 1000°C at 33 kb.

The present calibration study, conducted in the temperature-pressure range 25° to 1700°C and 1 bar to kb, employs the same design of high-pressure, high-temperature cell utilized in routine geochemical experiments. Pressure and contamination effects caused by this particular cell have been measured, leading to useful modifications of the thermocouple element and the cell itself.

Both the standard Pt/Pt 10% Rh thermocouples and thermocouples of W 3% Re/W 25% Re (for higher temperatures) were tested. Systematic errors due to hydrostatic pressure and chemical contamination were measured. The former were compared to extrapolations of the values of Getting and Kennedy on platinum-rhodium. Tests for the latter type of error were confined to platinum-rhodium thermocouples. Contamination was observed at 1600° and 1700°C but was negligible for most applications in this temperature range. Single-wire values and thermocouple corrections for the effects of pressure applied to the tungsten-rhenium thermocouple were significant, of the same order as the error extrapolated for platinum-rhodium thermocouples (~25°C at 1700°C, 40 kb).

Further experiments revealed another type of effect, which appeared to be characteristically random. This error could amount to as much as  $\pm 15^\circ\text{C}$  with the platinum-rhodium thermocouple at 1700°C, 40 kb. It is caused by differential stress of the individual thermocouple wires in a zone where a steep temperature gradient crosses high-strength materials of the cell and can vary from zero to some maximum value higher than those observed. The ensuing analysis encompasses a variety of critical and supporting tests of random and systematic errors. More accurate techniques and more suitable cell materials can be suggested from the results.

### *Random Errors*

Most high-pressure, high-temperature data obtained with the single stage are characterized by appreciable scatter over and above the uncertainties that should be expected from known limits of experimental control. The most precise calibration experiments (Getting and Kennedy, 1970), in special pressure cells designed to relate single-wire emf with calculated pressure, show peculiar hysteresis loops where the equivalent pressure is displaced by as much as 3 kb.

Initially in the present investigation, average random error in temperature was 8°C (40  $\mu\text{V}$ ) for the platinum-rhodium thermocouple (1500°C, 20 kb), and errors as large as  $\sim 15^\circ\text{C}$  were noted. At the same time, the mean scatter for the tungsten-rhenium couple was characteristically much lower (2°C, average;  $\sim 4^\circ\text{C}$ , maximum; both for the conditions 1500°C, 20 kb). The total random error appeared to change in direct proportion to pressure and temperature, but was independent of time.

Random errors can be generated from a great variety of sources. Some possible causes are:

1. Temperature gradient. The thermocouple junction has a finite size, so thermal gradients may cause variable errors

in the temperature of the effective junction.

2. Random contamination.

3. Random pressure differences. High strength of the insulation ceramic can cause the thermocouple wires to be pressurized differently. The effect of pressure on a single wire is significant and would affect the individual thermocouple reading.

It was possible to test for these and other errors with four special thermocouple junctions. They are shown relative to their position in the applied thermal gradient in Fig. 45 (a). The entire pressure-temperature cell with a thermocouple in place (part 12) is shown in Fig. 45 (b). Numerous data points were needed; some of the values measured at 20 kb are shown in Fig. 46 (A, Pt/Pt 10% Rh; B, W 3% Re/W 25% Re).

The categories of temperature gradient and random compositional difference were quickly eliminated as large sources of error. Minute junctions [Fig. 45 (a), type I] mounted in a thick block of Pt for reducing the gradient gave results identical with those in Fig. 46. An emf

of  $60 \mu\text{v}$ , equivalent to about  $8^\circ\text{C}$ , was recorded in an experiment where a single piece of platinum wire was looped through the temperature gradient [Fig. 45 (a), type II]. It effectively acted as a thermocouple. These results could not be explained by thermal gradients.

Observed random scatter is usually reversible in these experiments, although at times the  $\Delta$  emf between two identical thermocouples at the same junction [Fig. 45 (a), type I] showed "overshoot" after the pressure was released by dropping to zero and then changing sign. On the basis of these observations and those previously described, the main source of error can evidently be attributed to a physical effect related to the junctions or wires themselves and not to contamination.

Most materials of a single-stage cell are known to have considerable strength at high pressure and temperature. The high-purity alumina of the thermocouple insulation sheath could easily support a stress difference of 2 kb in the cooler part of the pressure cell. The cool zone is also a part where thermal gradients are high, so differences in single-wire emf's

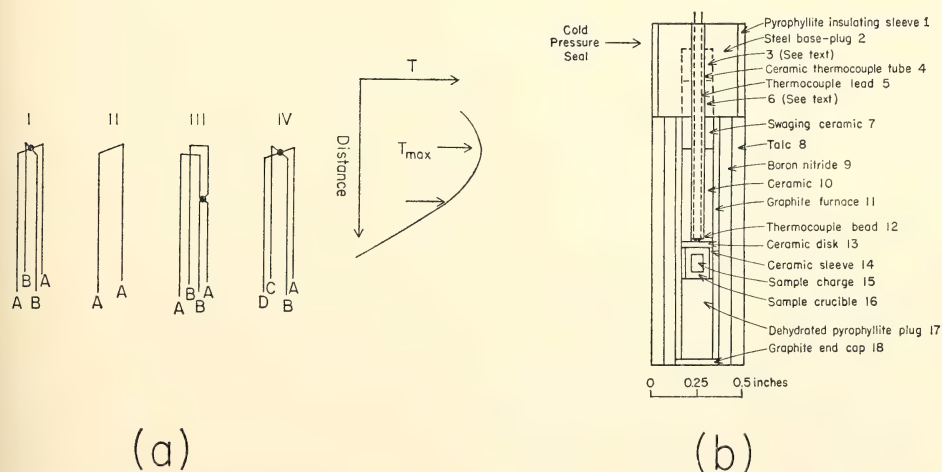


Fig. 45. (a) Configurations of thermocouple assemblies. A, B, C, and D represent different thermoelectric materials. The upper end of each assembly is placed at the maximum temperature of a high-pressure cell. (b) High-pressure cell (after Bell and England, 1967). In a regular Boyd-England cell, parts 2, 3, and 6 are a single piece of steel.



could occur, superimposed upon the hydrostatic pressure effect. From the data of Getting and Kennedy (1970) on platinum-rhodium and the single-wire values determined in this study for tungsten-rhenium, it is clear that a 2-kb pressure difference on the four wires at 20 kb is sufficient to cause the random errors. The observed features are consistent with this concept.

For example, the effect is strongly dependent on pressure and temperature but not on time. One can imagine all pos-

sible pressure gradients from zero to some maximum value dictated by the yield strengths of the materials, so the wide range of scattering observed with high probability at some mean value (Fig. 46A, C) would be expected. Specifically, as the load pressure on the cell is raised, stronger material around one of the thermocouple wires would provide a relative protection from part of the pressure and cause a  $\Delta$  emf if the other three wires [Fig. 45 (a), type I] were pressurized evenly. As pressure was re-

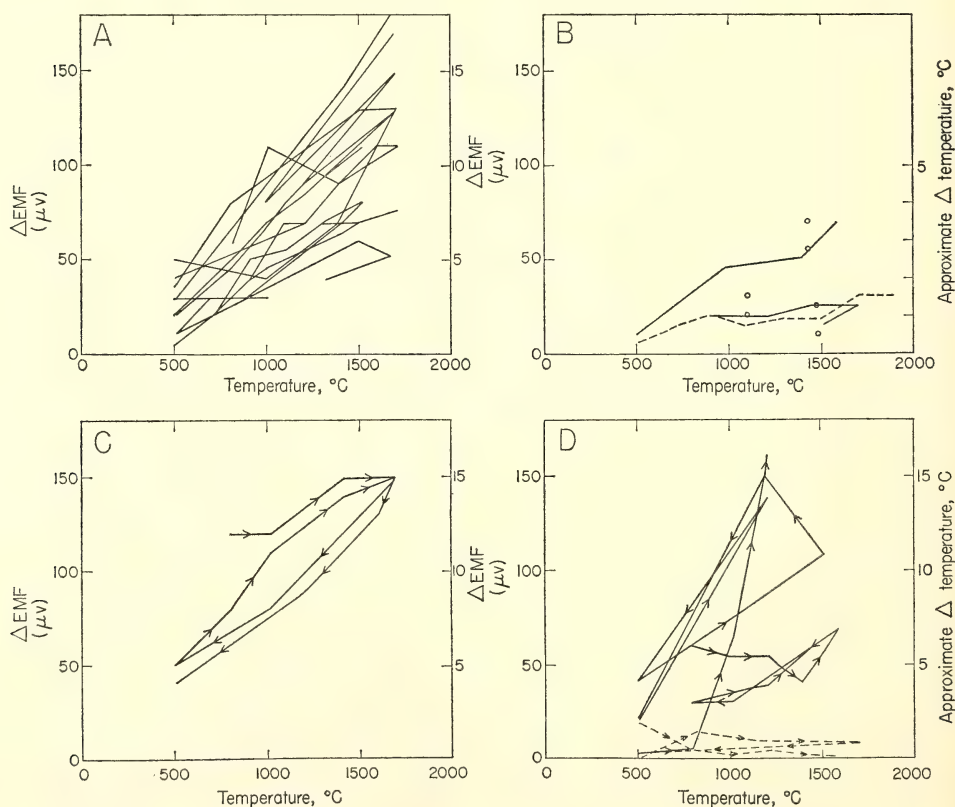


Fig. 46. Random errors.  $\Delta$  emf is the maximum emf difference among four A/B type thermocouples in an assembly of configuration I [Fig. 45 (a)]. The path of  $\Delta$  emf in a temperature excursion is plotted against the temperature at the thermocouple junction. (A) Pt 10% Rh/Pt at 20 kb with a strong, pure  $\text{Al}_2\text{O}_3$  insulator (McDanel 997) tube in a Boyd-England cell. (B) W 3% Re/W 25% Re at 20 kb: solid lines and circles, with an  $\text{Al}_2\text{O}_3$  insulator (McDanel 997) tube in a Boyd-England cell; dashed line, with Pyrex glass insulator. (C) Pt 10% Rh/Pt at 40 kb with an  $\text{Al}_2\text{O}_3$  insulator (McDanel 997) tube in a Boyd-England cell. (D) Pt 10% Rh/Pt at 20 kb: solid lines, with an  $\text{Al}_2\text{O}_3$  insulator (McDanel 997) tube surrounded by glass; dashed lines, with Pyrex glass insulator.

duced the strong material would tend to hold pressure preferentially on one wire and the sign of the  $\Delta$  emf would change; this occurrence would explain the observations of this study. The pressure effect on single wires of the tungsten-rhenium thermocouple is approximately half that on platinum-rhodium, so the observed  $\Delta$  emf's (Fig. 46A, B) for the junctions are of the right order. In terms of temperature, the ratio is  $\frac{1}{4}$  because emf/ $^{\circ}\text{C}$  for tungsten-rhenium is about twice that of the platinum-rhodium thermocouple.

To make certain that no part of the effect was caused by parts of the cell other than the alumina thermocouple insulation, a relatively low-strength Pyrex tubing was substituted for various alumina pieces [Fig. 45 (b), parts 7 and 10], extending into the cold pressure seal [Fig. 45 (b), part 6; part 3, swaging ceramic]. A cell very similar to this modification, described by Williams and Kennedy (1969), was also tested, but in both cells the thermocouple wires are still in contact with strong ceramic, and the usual scatter of data was observed (Fig. 46D, solid lines). It was only when the four-hole ceramic insulator tube itself [Fig. 45 (b), part 4] was replaced entirely with a Pyrex glass piece, or when parts of the ceramic insulator tube were ground away so as to expose the thermocouple wires to a surrounding Pyrex sleeve, that the random errors were reduced to a negligible level (Fig. 46D, dashed lines).

### *Systematic Errors*

By minimizing random errors with the modified pressure cell, systematic errors caused by contamination and by the hydrostatic pressure effect could be measured free of serious scatter. Determinations of the two effects were made separately, the former being a series of critical tests to gauge the magnitude of error from contamination and the latter

being a thermocouple calibration experiment.

*Contamination.* Possible contamination of a thermocouple in the single-stage apparatus is frequently worrisome because it is practically impossible to be certain whether temperature drift has occurred during a quenching experiment. Williams and Kennedy (1969) have shown that tungsten-rhenium thermocouples are relatively unaffected by contamination. They made numerous DTA excursions on a high-temperature melting curve with the same thermocouple, recording no apparent drift. Most experiments still use platinum-rhodium thermocouples, so it was essential to explore the problem, with tungsten-rhenium for control. In other tests, two platinum-rhodium thermocouples were compared with each other while they were subjected to different contaminants.

Self-diffusion could possibly occur between the thermocouple wires. This type of contamination would produce the same type of drift as any point source, so the special junctions shown in Fig. 45 [(a), III] were designed to test for the effect. Contamination from widely dispersed sources in the cell was measured with four different wires welded at a common junction [Fig. 45 (a), IV], and in a separate series of experiments hematite and graphite were introduced as contaminants in a configuration where two platinum-rhodium thermocouples were welded into a common junction [Fig. 45 (a), I].

The rationale for most of these experiments is shown diagrammatically in Fig. 47. It is possible to critically test for and categorize most types of contamination at the junction. Generalized results of the experiments are plotted in Fig. 48. No diffusion at the junction occurred below  $1600^{\circ}\text{C}$ ; the maximum effect, observed at  $1700^{\circ}\text{C}$  with the junction located in a steep part of the thermal gradient, was equivalent to approximately  $13^{\circ}\text{C}$ . This effect required 20 hours, and would be of lesser magnitude

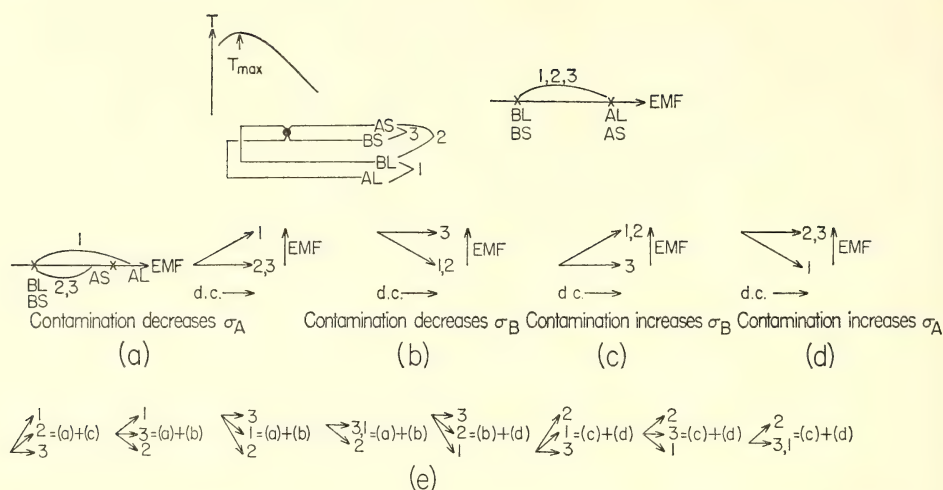


Fig. 47. Diagrammatic analysis of the thermocouple self-diffusion and point-contamination experiments, using thermocouple assembly III [Fig. 45(a)]. Top left: AL, A long leg; BL, B long leg; AS, A short leg; BS, B short leg. 1, 2, and 3 represent three independent thermocouples. In the thermal gradient, each leg (AL, BL, AS, or BS) is an independent source of emf. The thermocouple emf is the difference of two single-leg emf's. Top right: the sequence of single-leg emf's without point contamination. The span indicates thermocouple emf. (a)–(e) A point source of contamination exists at the junction. Contaminant diffuses from the junction along each leg. (a) The contamination decreases the Seebeck coefficient ( $\sigma = d \text{ emf}/dT$ ) of A,  $\sigma_A$ . Because AL and AS approach the junction in thermal gradients of opposite signs, the contamination increases the single-leg emf of AL, but decreases that of AS. (a) Left, the sequence of single-leg emf's. (a) Right, emf's of thermocouples 1 and 2 with reference to 3 as a function of degree of contamination (d.c.). (b)–(d) Emf's of thermocouples 1 and 2 with reference to 3, when the point contamination decreases  $\sigma_B$ , increases  $\sigma_B$ , and increases  $\sigma_A$ , respectively. (e) Any sequence of emf's of thermocouples 1, 2, and 3 can be expressed as a unique combination of the four basic types—(a), (b), (c), and (d). Self-diffusion between A and B tends to increase  $\sigma_B$  and decrease  $\sigma_A$ ; thus it belongs to the first case of (e). The emf's of thermocouples 1 and 2 with reference to 3 are experimentally observable. With the help of the present figure, the type of point contamination can be determined.

in a normal experiment where the junction is placed at the flat part of the thermal gradient.

Using the junction of four different wires [Fig. 45 (a), IV] and assuming the two tungsten-rhenium wires to be free of measurable contamination during an experiment, we established that the platinum-rhodium wires were contaminated from the conventional ceramic parts of the high-pressure cell. Drift of the platinum-rhodium thermocouple progressed at a rate of  $-2^\circ\text{C}/\text{hour}$  at  $1600^\circ\text{C}$  (Fig. 49A) and  $-20^\circ\text{C}/\text{hour}$  at  $1700^\circ\text{C}$  (Fig. 49B, C). When a purer ceramic material was used, the drift rates were reduced to  $-1^\circ\text{C}/\text{hour}$  and

$-2.5^\circ\text{C}/\text{hour}$  at  $1600^\circ$  and  $1700^\circ\text{C}$ , respectively (Fig. 49A, B, C). Rates are much higher than those obtained when hematite and graphite were deliberately placed in contact with Pt and Pt 10% Rh wires (Fig. 50A, B).

*Hydrostatic pressure effect.* In order to obtain an abundant redundancy of information concerning the behavior of thermocouple elements, a four-wire junction of Pt, Pt 10% Rh, W 3% Re, and W 25% Re [Fig. 45 (a), type IV] was employed. Six thermocouples could be read in rapid sequence. Observations were conducted at temperatures up to  $1500^\circ\text{C}$  and pressures to 40 kb. Several temperature cycles were made at each



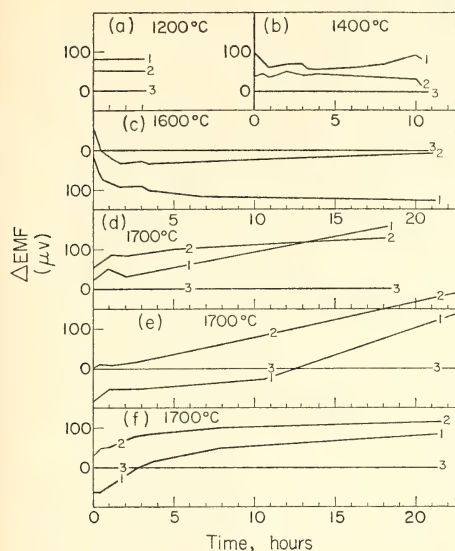


Fig. 48. Results of self-diffusion and point-contamination experiments of Pt 10% Rh/Pt at 20 kb, using a thermocouple assembly of configuration III. The emf of thermocouple 3 (Fig. 47) was held constant and used as a reference. The differences between thermocouple 1 and 3 and between 2 and 3 are  $\Delta$  emf's. Their drift with time is plotted. (a) and (b) with low-strength, impure porcelain insulator (McDaniel H.T.); (c)–(f) with  $\text{Al}_2\text{O}_3$  insulator (McDaniel 997) surrounded by a porcelain sleeve (McDaniel H.T.). The porcelain sleeve is in contact with the junction and acts as a point-contaminant. In (f) a 0.01-inch cube of graphite was placed at the junction as a point-contaminant. Below 1600°C [(a)–(c)] no significant self-diffusion. At 1700°C [(d)–(f)] the emf of thermocouple 1 increases rapidly and the emf of thermocouple 2 increases slowly with respect to 3, indicating self-diffusion [Fig. 47(e)]. (c)–(f) The initial emf sequence of 2-3-1 or 2-1-3 indicates that the contamination of porcelain increases  $\sigma_{\text{Pt}}$  and  $\sigma_{\text{Pt}10\% \text{Rh}}$ . (f) is not significantly different from (d) and (e), indicating that Pt/Pt 10% Rh is not sensitive to graphite point-contaminant.

pressure, with frequent checks on reproducibility being made by lowering the pressure to 5 kb between measurements. Only small random fluctuations were noted, and by careful observation of their direction it was concluded that a  $\Delta$  emf could be caused by slight axial tension of the wires during temperature

cycling even though the confining pressure was high. These emf's are of no great significance, but account for the uncertainty bands of the measured data. Single-wire values of the pressure effect on W 25% Re and W 3% Re are plotted in Fig. 51A, B. The pressure effect on a tungsten-rhenium thermocouple is plotted in Fig. 51C. The values were determined with the use of the single-wire/emf curves of Getting and Kennedy (1970) for Pt-Rh at 20 and 40 kb. Getting and Kennedy constructed these curves by plotting data measured to 1000°C and extrapolated to approximately 1800°C.

The single-wire pressure effect for W-Re wires increased much more rapidly than linearly with pressure. At 1500°C and 20 kb the single-wire effect for W 3% Re was 100  $\mu\text{V}$ , whereas at 40 kb the effect was 420  $\mu\text{V}$ . The single W 25% Re showed a similar effect. When the two wires were combined as a thermocouple, however, the pressure effect at 20 kb was 140  $\mu\text{V}$  and that at 40 kb was 275  $\mu\text{V}$ .

### Conclusions

In the light of the results of this study, it should be possible to avoid many of the common errors associated with routine experiments in the single-stage apparatus. The following conclusions can be drawn from the data:

**Thermocouples.** (1) W 3% Re/W 25% Re has proved to be a superior thermocouple in all cells tested because of its inherently low random error and its relative chemical inertness. (2) Pt/Pt 10% Rh is sensitive to contamination above 1600°C and is subject to strong random effects. Short experiments at these temperatures need not be greatly in error if strong insulating materials are avoided.

**Materials of the high-pressure cell.** (1) Random errors from high-strength materials in the cell can be reduced by keeping Pyrex glass in contact with the thermocouple wires. (2) Random errors can be further minimized if materials are

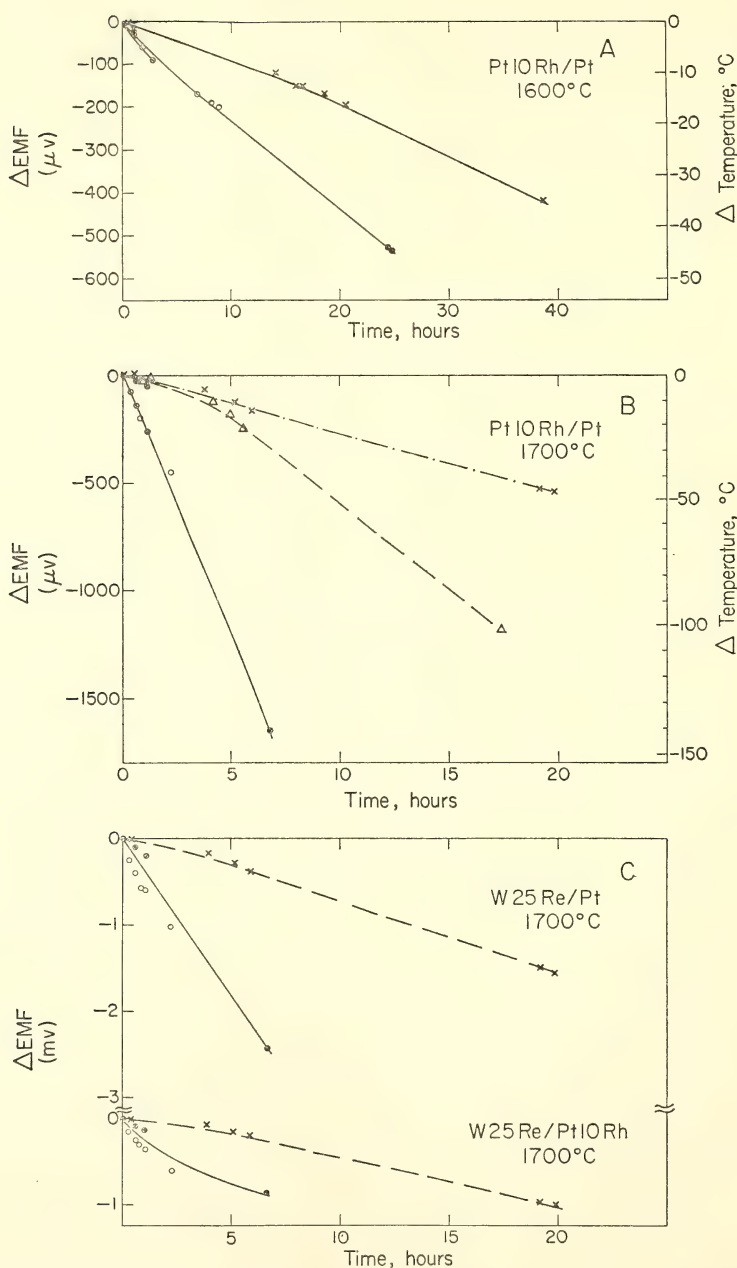


Fig. 49. Emf drift experiments at 20 kb, using thermocouple assembly IV [Fig. 45(a)]. Pt 10% Rh, Pt, W 3% Re, and W 25% Re are the four thermoelements. Emf of W 3% Re/W 25% Re was held constant and used as a reference. The drifts of emf's of other thermocouples are plotted. Crosses:  $\text{Al}_2\text{O}_3$  insulator (McDaniel 997). Open and solid circles: porcelain insulator (McDaniel H.T.). Triangles: emf of Pt 10% Rh/Pt was held constant. The drifts of Pt 10% Rh/Pt, W 25% Re/Pt, and W 25% Re/Pt 10% Rh referring to W 3% Re/W 25% are obtained by calculation;  $\text{Al}_2\text{O}_3$  insulator (McDaniel 997).

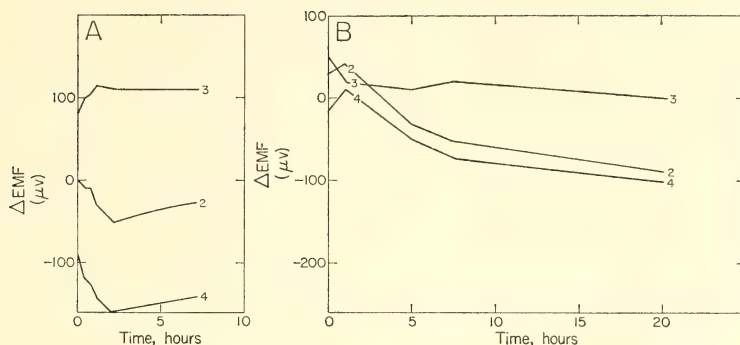


Fig. 50. Hematite and graphite contamination experiments of Pt/Pt 10% Rh at 1700°C and 20 kb, using a thermocouple assembly I [Fig. 45 (a)]. Two of the four holes of the  $\text{Al}_2\text{O}_3$  insulator (McDanel 997) were deliberately contaminated with hematite or graphite. The contaminant covers  $\frac{1}{40}$  of the hole's surface. Four thermocouples were read: 1, clean Pt/clean Pt 10% Rh; 2, contaminated Pt/contaminated Pt 10% Rh; 3, clean Pt/contaminated Pt 10% Rh; 4, contaminated Pt/clean Pt 10% Rh. The emf of 1 was held constant and used as the reference.  $\Delta$  emf's, the differences between the emf's of 2, 3, and 4 and the emf of 1, are plotted as a function of time. (A) Contaminant is hematite; during the first 3 hours, the contamination increases the Seebeck coefficients of the single-leg Pt and Pt 10% Rh and decreases the Seebeck coefficient of the Pt/Pt 10% Rh thermocouple. (B) Contaminant is graphite; no significant effect.

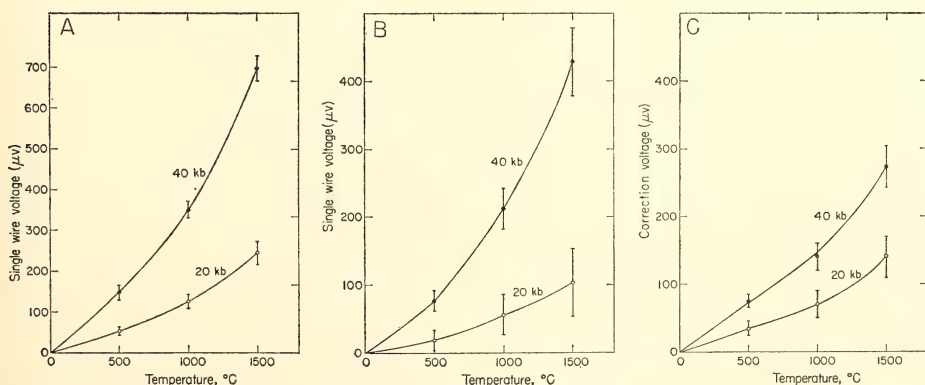


Fig. 51. (A) The effect of pressure on single-wire emf of W 25% Re. (B) The effect of pressure on single-wire emf of W 3% Re. The single-wire voltage is the emf of pressurized wire (positive) versus wire at 1 bar (negative). (C) The effect of pressure on emf of W 3% Re/W 25% Re thermocouple. The correction voltage is, at a given temperature, the emf of the thermocouple at 1 bar minus the emf of the pressurized thermocouple. Cold-seal temperature of A, B, and C is 0°C.



used that are weak at the low-temperature part of the pressure cell. A combina-

tion of materials—such as talc, boron nitride, and Pyrex—seems suitable.

## INVESTIGATIONS OF LUNAR AND RELATED MATERIALS

### ANATOMY OF A MANTLED PIGEONITE FROM *Oceanus Procellarum*

F. R. Boyd

The pyroxenes in the basaltic rocks collected in the Apollo 11 and Apollo 12 missions have provided some insights into the nature of lunar volcanism, but they have also provided some challenging problems in interpretation and analysis. These pyroxenes are characterized by extreme fractionation toward Fe-rich compositions, with individual crystals ranging over as much as 60 mole % in  $\text{FeSiO}_3$  content. Sectorial zoning, in which segments of crystals that have formed by growth on particular crystallographic faces show compositions that differ from adjacent segments, is also beautifully developed. Moreover, at least one of the Apollo 12 rocks (12021) contains pyroxenes with a remarkable oscillatory zoning, which appears to be unlike any yet described in terrestrial or meteoritic pyroxenes.

Analytical data for pyroxenes from the Apollo 11 lavas provide a rather chaotic picture in that Ca, Mg, and Fe analyses determined for points with a single crystal or for a group of associated crystals scatter across the pyroxene quadrilateral rather than forming a coherent trend. Both pigeonite and augite are present in primary intergrowths (e.g., Kushiro *et al.*, 1970), but their sequential relationship is not evident in many cases. These relations are clarified by study of certain of the Apollo 12 lavas that contain pigeonite phenocrysts mantled by zones of more Ca-rich and Fe-rich pyroxene in regular growth patterns. The cores of these crystals are believed to have formed at depth in the moon, and the mantles grew as the lavas flowed

over the moon's surface. The crystallization of these phenocrysts and their mantles can thus be deciphered in a manner analogous to the determination of the history of a tree from its growth rings.

The strong fractionation shown by the pyroxenes in both the Apollo 11 and Apollo 12 lavas suggests very rapid cooling, especially by analogy with studies of the Makaopuhi lava lake in Hawaii (Evans and Moore, 1968). Weill *et al.* (1970) estimate the viscosity of the lunar lavas to be equivalent to glycerine, or an order of magnitude more fluid than terrestrial basalts. Probably the lunar lavas were erupted in thin sheets which spread rapidly and cooled quickly, except where they ponded in impact craters on the mare surfaces. Discussion hereafter suggests that the Ca-rich mantles on pigeonite phenocrysts in the Apollo 12 samples crystallized in turbulent lava streams where partially cooled and fractionated lava was being mixed with fresh lava.

The pyroxene phenocrysts in the Apollo 12 lavas consist essentially of pigeonite mantled by augite, although this relationship is sometimes complicated by oscillatory zoning. It appears that the crystallization of these pyroxenes has been controlled by a pigeonite-augite peritectic. The existence of a peritectic in the crystallization of Fe-rich pyroxenes from terrestrial magmas has been postulated by Muir (1954) and others. However, lunar pyroxenes which appear to show a peritectic relation contain as little as 28 mole %  $\text{FeSiO}_3$ . Common terrestrial pyroxenes in this composition range have textures which indicate coprecipitation of augite and pigeonite from liquid. The reason for this difference in the crystallization of lunar

and terrestrial pyroxenes is not presently clear, but is believed to be related to differences in composition between the liquid phases in terrestrial basaltic magmas and their lunar counterparts.

The basalts collected in the Apollo 11 and Apollo 12 missions have cooled sufficiently quickly that there has been little opportunity for solid state reaction. Electron photomicrographs of pyroxenes from the Apollo 11 samples (Bailey *et al.*, 1970; Ross *et al.*, 1970) show exsolution lamellae of Ca-rich and Ca-poor pyroxene which are on the order of only 500 Å thick. X-ray studies by Prewitt, Papike, and Bence (1970) on pyroxenes from rock 12021 (which have been studied in this investigation) show exsolution of augite and pigeonite, but the lamellae are submicroscopic. However, there are visible lamellae of a brownish phase in these pyroxenes which may be ilmenite (M. Ross, personal communication). The chemical variations which are revealed by electron probe scans are believed to be produced during crystallization from liquid and not by subsequent solid state reaction. This interpretation is supported by the fact that the patterns of zoning are completely unlike those developed by exsolution in more slowly cooled pyroxenes.

Electron probe studies which are described in this report were carried out primarily on a thin section (no. 7) of rock 12021. This specimen is a porphyritic gabbro and it is the most coarse-grained rock thus far returned from the moon. Phenocrysts of pigeonite mantled by Ca-rich pyroxenes form crystals up to 2–3 cm parallel to *c* and 2–4 mm in diameter. The groundmass is predominantly pyroxene, anorthite, ilmenite, and minor chromian ulvöspinel with patches of residual crystallization products. The grain size of the groundmass ranges from 0.2 to 1.0 mm and its texture is ophitic and variolitic. As seen in thin section, patches of anorthite and pyroxene form sheafs which resemble quench crystals formed in laboratory experiments, al-

though the lunar sheafs are much more coarse grained.

Electron probe data were obtained by step scans with a M.A.C. model 400 probe.\* Counts were taken at 10 μm intervals with an X-ray spot size in the range 2–3 μm. Results for more than three elements were obtained by repeating a scan as closely as possible. These data were reduced with a computer program written by D. H. Lindsay and D. Smith and modified by the author. The principal modification is a simplified matrix correction for pyroxenes which is set up as a function of the Fe content. Fe must thus be measured with each scan, along with two other elements which may include Ca, Mg, Al, Ti, Si, Cr, and Mn. The simplified matrix correction provides an accuracy which is generally better than ±1 relative %, but other errors inherent in step scanning reduce the overall accuracy to around ±3 relative %.

Values of the molar proportions of Ca, Mg, and Fe which are plotted in the pyroxene quadrilateral are calculated directly from the corrected weight percentages of these elements. This is the conventional method of calculation, but an alternative method is to allot some Ca for  $\text{CaAl}_2\text{TiO}_6$ ,  $\text{CaAl}_2\text{SiO}_6$ , etc. before calculating  $\text{CaSiO}_3$ . There is some uncertainty in identifying the coupled substitutions involving Al, Ti, and Cr, as discussed hereafter, and it is a problem to understand how best to make the calculation for  $\text{CaSiO}_3$ . Some minor variations in the component  $\text{CaSiO}_3$  which appear in plots in the pyroxene quadrilateral are probably only apparent and are actually due to variations in the components  $\text{CaAl}_2\text{TiO}_6$ ,  $\text{CaAl}_2\text{SiO}_6$ , etc.

Most of the scans described hereafter were carried out on a phenocryst in section 12021,7 which has its *c* axis at a high angle to the plane of the section. A photograph of a portion of this crystal

\* Purchased with the assistance of the National Science Foundation under grant GP 4384.

in Plate 2 shows the pigeonite core bounded by ( $\bar{1}\bar{1}0$ ) and ( $\bar{1}\bar{1}0$ ) and a euhedral mantle, 300–350  $\mu\text{m}$  thick. A ( $\bar{1}00$ ) face has developed on the mantle in addition to ( $\bar{1}\bar{1}0$ ) and ( $\bar{1}\bar{1}0$ ). Universal stage measurements by W. B. Bryan give an optic angle for the pigeonite core of  $+19.5^\circ$  and  $Z \wedge c = 39^\circ$ . The optic plane is parallel to (010). The mantle is predominantly Ca-rich pyroxene, and it has a beautifully developed sector zoning which is clearly shown in Plate 2. The locations of most of the probe scans described hereafter are also shown in Plate 2.

The simplest relations are found on ( $\bar{1}\bar{1}0$ ) and are illustrated by a probe scan for Ca, Mg, and Fe (E, Plate 2) plotted in the pyroxene quadrilateral in Fig. 52. The pigeonite core is relatively homogeneous, but there is a detectable zoning from approximately  $Wo_{10}En_{62}Fs_{28}$  in the central portion to  $Wo_{13}En_{59}Fs_{28}$  near the boundary with the mantle. Proceeding from the core into the mantle there is an abrupt change to a more Ca-rich augite with an average composition of  $Wo_{35}En_{53}Fs_{22}$ . Figure 52 shows a few points which are transitional between the mean composition of the pigeonite and the predominant range of

augite composition, but they are not reproducible in detail in parallel profiles. About 30  $\mu\text{m}$  from the outer edge of the mantle on ( $\bar{1}\bar{1}0$ ) there is a second, abrupt transition back to a pigeonite which is more Fe-rich than the core. The average composition of the pigeonite in the rim is  $Wo_{12}En_{50}Fs_{38}$ . The pigeonite rim and core extinguish together on rotation under crossed nicols, and the rim can be seen as a dark band in the photograph in Plate 2. A profile parallel to that shown in Fig. 52 but displaced about 150  $\mu\text{m}$  along ( $\bar{1}\bar{1}0$ ) shows compositional relations very similar although not precisely identical to those in Fig. 52.

The pigeonite rim is locally absent on ( $\bar{1}\bar{1}0$ ), possibly due to partial resorption prior to crystallization of augite in the groundmass. Two probe scans approximately perpendicular to ( $\bar{1}\bar{1}0$ ) and about 100  $\mu\text{m}$  apart (A and B, Plate 2) differ from each other in their trends of compositional zoning. Figure 53 shows the variation in Ca, Mg, and Fe across the mantle in an area where the pigeonite rim is missing. As previously described for the ( $\bar{1}\bar{1}0$ ) sector there is an abrupt transition from the pigeonite core to augite in the mantle. The mantle is about 300  $\mu\text{m}$  thick on this face, and along

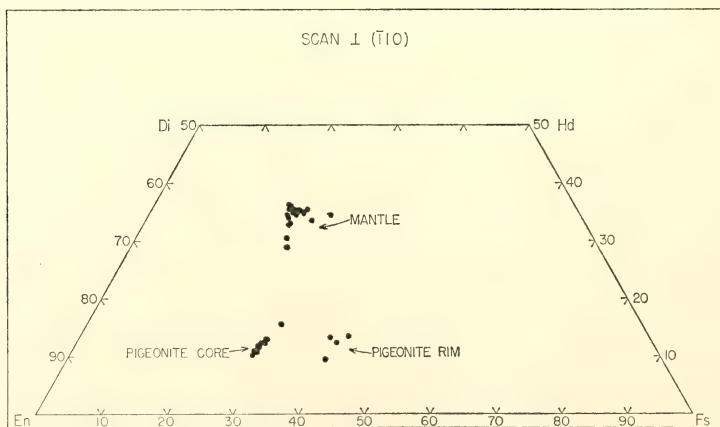


Fig. 52. Ca, Mg, and Fe analyses on a scan normal to ( $\bar{1}\bar{1}0$ ) plotted in the pyroxene quadrilateral. Scan is E in Plate 2. Analyses are spaced at 10- $\mu\text{m}$  intervals, and the length of the scan is about 700  $\mu\text{m}$ .



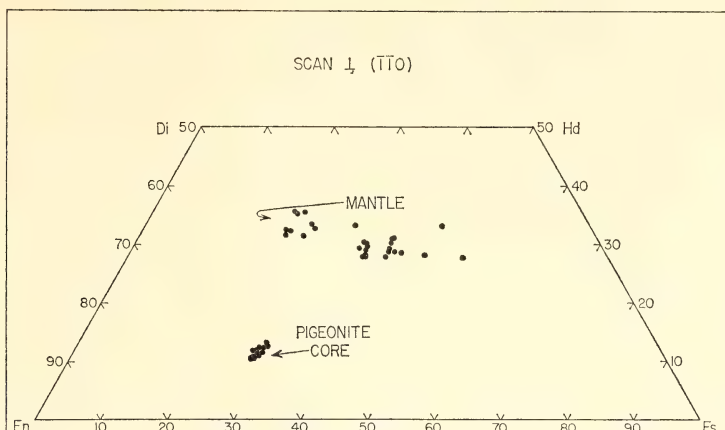


Fig. 53. Ca, Mg, and Fe analyses on a scan normal to  $(\bar{1}\bar{1}0)$  plotted in the pyroxene quadrilateral. Scan is *A* in Plate 2; and Al, Ti, and Cr analyses for this scan are in Fig. 58. Analyses are spaced at 10- $\mu$ m intervals, and the length of the scan is about 600  $\mu$ m.

step-scan *A* (Plate 2 and Fig. 53) it is composed entirely of Ca-rich pyroxene which is zoned discontinuously toward the hedenbergite-ferrosilite join. The ferrosilite concentration in the mantle ranges from a minimum of 22 mole % to a maximum of 50 mole %. The most Fe-rich pyroxenes are in the outer part of the mantle, but the overall increase in the  $\text{FeSiO}_3$  component proceeding from

the core boundary to the  $(\bar{1}\bar{1}0)$  face of the mantle is interrupted by reversals.

Ca, Mg, and Fe analyses are shown in Fig. 54 for step-scan *B* in the  $(\bar{1}\bar{1}0)$  sector in a region where the pigeonite rim is present. Again there is an abrupt discontinuity between the pigeonite core and the more Ca-rich pyroxene in the inner part of the mantle. However, the outer part of the mantle is complexly

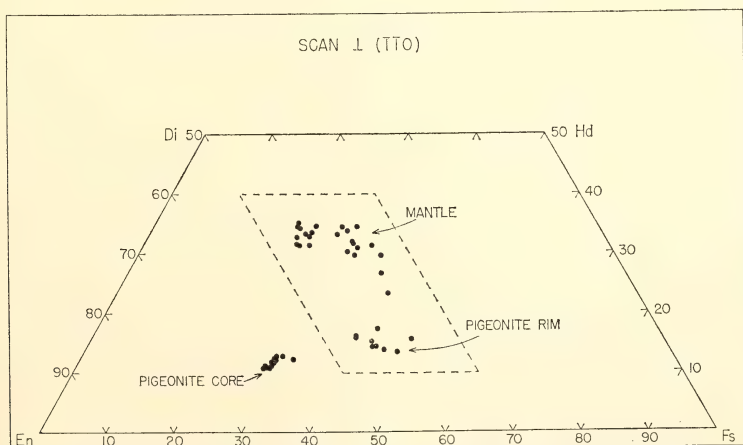


Fig. 54. Ca, Mg, and Fe analyses on a scan normal to  $(\bar{1}\bar{1}0)$  plotted in the pyroxene quadrilateral. Scan is *B* in Plate 2. Analyses are spaced at 10- $\mu$ m intervals, and the length of the scan is about 650  $\mu$ m. Area surrounded by dashed line is expanded in Fig. 55.

zoned to pigeonite with a considerable range in  $\text{FeSiO}_3$  content. The compositional zoning in the mantle in this scan is illustrated in an expanded plot in Fig. 55, and the analytical points are connected by arrows to show the sequence of variations proceeding from the core boundary (A, Fig. 55) to the intersection of the scan with the  $(\bar{1}\bar{1}0)$  face of the mantle (B, Fig. 55). In the inner mantle the zoning is toward more Fe-rich compositions with pronounced oscillations in  $\text{FeSiO}_3$  concentration. This trend is similar to that shown for the inner part of the mantle in Fig. 53. In the outer mantle, however, there is an abrupt transition to a more Fe-rich pigeonite, followed by a reversal of trend back to augite and then crystallization of a third generation of pigeonite which terminates at the  $(\bar{1}\bar{1}0)$  face of the mantle. The zoning shown by this scan is thus oscillatory with respect to the crystallization of augite and pigeonite but it is also

oscillatory with respect to the  $\text{FeSiO}_3$  contents of both phases.

Yet a different kind of compositional zoning is found in the sector which has formed by growth of the  $(\bar{1}00)$  face. In the plane of the thin section this sector has the shape of a wedge with its apex at the junction of the  $(\bar{1}\bar{1}0)$  and the  $(\bar{1}10)$  faces of the pigeonite core (Plate 2). Extinction in this sector is undulate, but the range is intermediate between the extinction position of the core and that of the mantle sectors on  $(\bar{1}\bar{1}0)$  and  $(\bar{1}10)$ . Parallel probe scans (C and D, Plate 2) normal to  $(\bar{1}00)$  and spaced about  $10\ \mu\text{m}$  apart are shown in Fig. 56. The two scans are very similar and they reveal a gradational change in composition from the pigeonite in the core to a subcalcic augite containing about 30 mole %  $\text{CaSiO}_3$  in the mantle with a further gradational change back to a more iron-rich pigeonite in the rim. The abrupt discontinuities which mark the

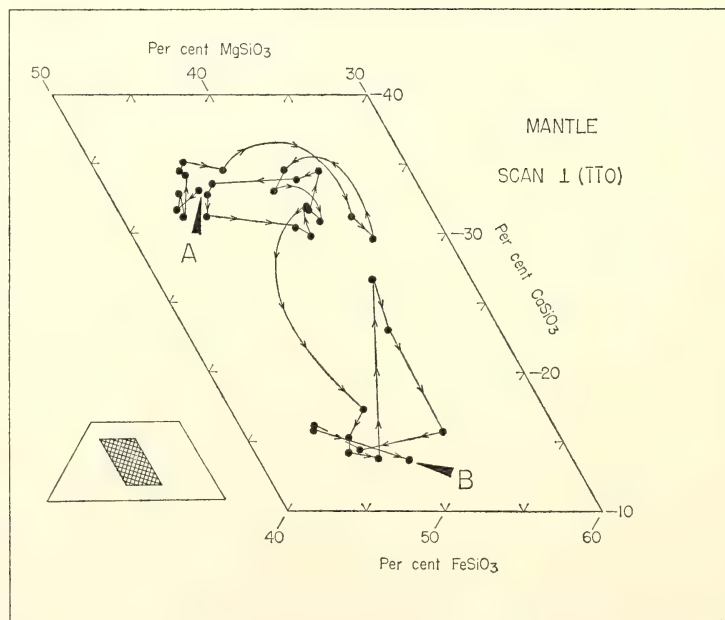


Fig. 55. Scan of the mantle in the  $(\bar{1}\bar{1}0)$  sector expanded from Fig. 54. Sequence of crystallization of points on this scan is shown by arrows starting at the core-mantle boundary (A) and ending at the outer edge of the mantle (B).

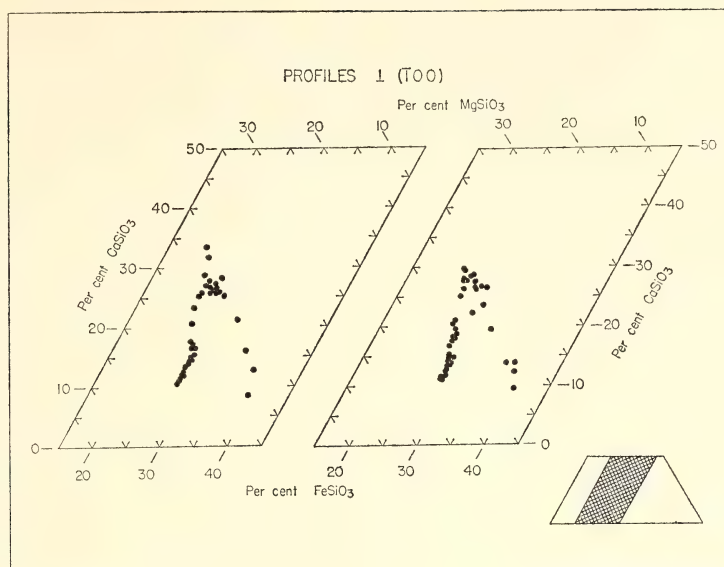


Fig. 56. Ca, Mg, and Fe analyses in two parallel scans in the  $(\bar{1}00)$  sector. These scans are about  $10\ \mu\text{m}$  apart and are marked *C* and *D* in Plate 2. Analysis are spaced at  $10\text{-}\mu\text{m}$  intervals, and the lengths of the scans are  $600\text{--}700\ \mu\text{m}$ .

transitions from pigeonite to augite or vice versa in the  $(\bar{1}10)$  and  $(\bar{1}\bar{1}0)$  sectors are thus replaced by progressive changes in composition over intervals as large as  $200\ \mu\text{m}$  in the  $(\bar{1}00)$  sector. Nevertheless, the overall pattern of the zoning from pigeonite to augite and back to a more iron-rich pigeonite is the same on  $(\bar{1}00)$  as on  $(\bar{1}10)$  and on portions of  $(\bar{1}\bar{1}0)$ .

It is interesting to note that the progressive change in composition from pigeonite to augite on  $(\bar{1}00)$  starts at a point which appears optically to be inside the core about  $100\ \mu\text{m}$  from the junction of the  $(\bar{1}10)$  and  $(\bar{1}\bar{1}0)$  faces (Plate 2 and Fig. 56). The composition of the outer portion of the pigeonite core in the  $(\bar{1}10)$  and  $(\bar{1}\bar{1}0)$  sectors contains uniformly about 13 mole %  $\text{CaSiO}_3$ , but at the junction of these faces the composition of the pyroxene in what appears optically to be the outer portion of the core is in the range 20–25 mole %  $\text{CaSiO}_3$ . The  $\text{CaSiO}_3$  content drops progressively along a line normal to  $(\bar{1}00)$

and reaches 13 mole % at a point about  $100\ \mu\text{m}$  inside the junction. Hence it is evident that the pigeonite core had a small  $(\bar{1}00)$  face. This face disappeared during the initial stages of the growth of the mantle in the  $(\bar{1}00)$  sector, but a  $(\bar{1}00)$  face developed again as crystallization of the mantle continued. The true core boundary is thus about  $100\ \mu\text{m}$  inside the junction of the  $(\bar{1}10)$  and  $(\bar{1}\bar{1}0)$  faces as seen optically (Plate 2). The true core-mantle boundary in the  $(\bar{1}00)$  sector cannot be seen under the microscope because of the gradual nature of the zoning toward Ca-rich compositions.

Compositions of pyroxenes at points which were selected at random in the groundmass of section 12021,7 (Fig. 57) scatter across the Fe-rich portion of the pyroxene quadrilateral. In this respect they much resemble the pyroxenes from the Apollo 11 samples. Compositions of the groundmass pyroxenes overlap those found in the outer part of the mantle of the phenocryst which has been studied



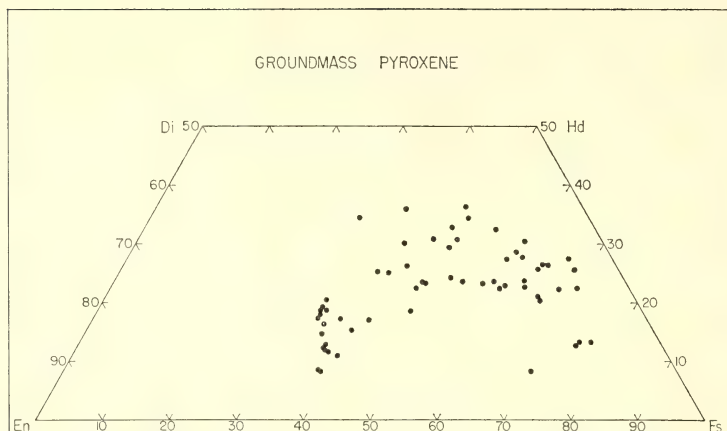


Fig. 57. Ca, Mg, and Fe analyses for a series of points selected at random in the groundmass pyroxenes of section 12021,7.

in detail (Plate 2 and Figs. 52–56). There is a group of analyses of groundmass pyroxenes in Fig. 57 centering around  $Wo_{15}En_{48}Fs_{37}$  that correspond in composition to the pigeonite rim and the more Fe-rich augites in the groundmass. However, the groundmass pyroxenes with  $FeSiO_3$  contents over about 50 mole % have apparently crystallized from residual liquids after growth of the phenocryst ceased.

Thus, there are three stages in the crystallization of the pyroxenes in section 12021,7, two of which overlap. The pigeonite cores which formed first are euhedral and they are relatively homogeneous, being zoned only about 3 mole % in  $CaSiO_3$  content between their central and outer portions. It is reasonable to suppose that these pigeonite cores are phenocrysts which formed at depth in the moon under relatively quiescent conditions or at least sufficiently slowly to allow diffusion to eliminate primary inhomogeneities. The mantles are strongly zoned in systematic patterns. They have also developed euhedral forms but they clearly have crystallized too rapidly to permit crystals to maintain equilibrium with the liquid. Diffusion has not dissipated initial inhomogeneities. Crystallization of the interstitial, groundmass

pyroxene began while the mantles were still growing and continued after they reached their final form. Weill *et al.* (1970) have estimated that liquid lunar basalt is an order of magnitude more fluid than terrestrial basaltic lava and accordingly the lunar basalts probably erupted in thin, fast-moving flows. The extreme zoning of the groundmass pyroxene toward the hedenbergite-ferrosilite join implies that their crystallization was sufficiently rapid to prevent reaction between residual liquids and early formed crystals. Possibly the crystallization of the groundmass pyroxenes and feldspars took place after the lavas had come to rest.

Evans and Moore (1968) have demonstrated a relationship between cooling history and zoning toward more Fe-rich compositions in the fossil lava lake in Makaopuhi crater. They found that rapidly cooled specimens collected 7 feet from the surface contained augites with  $FeSiO_3$  contents ranging from 10 to 36 mole %. However, augites which crystallized more slowly at a depth of 190 feet have a reduced zoning in  $FeSiO_3$  content from only 14 to 19 mole %. In large intrusions such as the Skaergaard, strong fractionation toward Fe-rich residual liquids is possible because crystals are

removed from possible reaction with the liquid by settling. But in basaltic lava flows crystal-liquid reaction and solid diffusion can only be inhibited by rapid cooling. The lunar basalts show a greater fractionation than do terrestrial basalts, probably because the lunar lavas were more fluid and crystallization could more effectively keep pace with rapid cooling.

The crystallization of pyroxenes in the phenocrysts in sample 12021 described above seems to show an "either/or" relationship for augite and pigeonite. Both have not crystallized together, except for the curious sectorial zoning on (100) where a metastable solid solution between pigeonite and augite precipitated at the same time that augite was crystallizing on (110) and ( $\bar{1}$ 10). Both augite and pigeonite are present in the groundmass, but the composition of the bulk of the groundmass pigeonite corresponds to that present in rims on the phenocrysts and it is thus probable that the crystallization of the more Mg-rich pigeonite in the groundmass preceded the Fe-rich augite.

Examples of augite mantling Fe-rich pigeonite are known in various terrestrial occurrences. Poldervaart (1944) has described early pigeonite mantled by augite with late pigeonite rims in dolerite from the New Amalfi sheet. This occurrence appears to have considerable similarity to the lunar pyroxenes described herein, but meaningful comparison is impossible in the absence of electron probe data on the New Amalfi material. Wheeler (1970) has found pigeonite crystals with augite mantles in monzonite associated with anorthosite, and an electron probe study of samples from this occurrence is presented by D. Smith elsewhere in this report.

Weill *et al.* (1970) found pigeonite mantled by augite in rock 10022 of the Apollo 11 sample and noted that this texture was consistent with a peritectic reaction. The possible influence of a peritectic in the crystallization of Fe-rich pyroxenes was apparently first sug-

gested by Muir (1954), and his hypothetical diagram for pyroxene phase relations has been reproduced in Deer, Howie, and Zussman (1963). Muir (*op. cit.*) did not use the term "peritectic" in his discussion, but his diagram for equilibria in the Fe-rich portion of the quadrilateral (*op. cit.*, Fig. 4c) clearly shows such a relation.

The basic textural relations of augite mantles on pigeonite cores are thus known in terrestrial occurrences as well as in the lunar lavas. In both the lunar and the terrestrial occurrences the texture can be interpreted as due to a reaction relationship in which pigeonite is the phase stable with liquid at temperatures above the peritectic. Nevertheless the terrestrial pyroxenes which show this texture are considerably more Fe rich than those in the lunar occurrences. Pigeonite in the cores of the phenocrysts in rock 12021 contains about 28 mole %  $\text{FeSiO}_3$ , whereas most mantled pigeonites of terrestrial origin contain more than 60 mole %  $\text{FeSiO}_3$  (e.g., D. Smith, this report).

Terrestrial basalts commonly crystallize pyroxenes with about the same Fe  $\text{SiO}_3$  content as the pigeonite cores in the lunar rock 12021, but the textural relations in terrestrial basalts show that augite and pigeonite have precipitated together. These textures indicate cotectic crystallization rather than the peritectic relation suggested by the lunar lavas and by more Fe-rich terrestrial pyroxenes. As Muir (1954) has suggested, a cotectic relation in the Mg-rich part of the pyroxene quadrilateral may transform into a peritectic as the Fe content is increased. If this interpretation is correct, then the transformation must occur in the crystallization of lunar basalts under circumstances such that the precipitating pyroxenes contain much less  $\text{FeSiO}_3$  than do mantled pyroxenes in terrestrial rocks. The reason for this difference in the crystallization of lunar and terrestrial pyroxenes is not clear, but it may well

be related to the marked differences in composition of the liquid phases.

Experimental data on crystal-liquid equilibria within the pyroxene quadrilateral are not yet sufficiently complete to help resolve this problem, but it is interesting to note that Kushiro (1969b) has found evidence for a pigeonite-augite peritectic in the system  $\text{CaMgSi}_2\text{O}_6\text{-MgSiO}_3$  at 20 kb.

It is a further problem to understand the cyclic nature of the augite-pigeonite relationship found in section 12021,7. Examination of a simple peritectic in a binary system will show that if the system is chemically closed and at constant pressure, it is impossible to crystallize a second generation of the liquidus phase by reheating and cooling unless the phase stable with liquid below the peritectic is *completely* resorbed. In a multicomponent system involving ternary or higher order solid solutions a peritectic reaction will take place over a temperature interval rather than at a fixed temperature. However, the interval may be small, particularly under disequilibrium conditions. Even in a multicomponent system it seems unlikely that the liquidus phase could be crystallized in a cyclic fashion by simple reheating and cooling without complete resorption of the solid phase stable with liquid below the peritectic. Nevertheless, a number of the phenocrysts in 12021,7 show two generations of pigeonite *separated by augite*, and evidence for three generations of pigeonite with interlaminated augite is shown in Fig. 55. Textural evidence for resorption is difficult to establish, but if there has been resorption of the augite, the resorption has clearly not been complete.

Changes in hydrostatic pressure caused by convection in a magma chamber might in principle produce cycles of crystallization of pigeonite and augite. Carr (1954) has suggested this mechanism to account for oscillatory zoning in plagioclase crystals in the Skaergaard Complex. Nevertheless, it is questionable

whether this mechanism would be very effective on the moon. Changes in hydrostatic pressure on the order of 1 kb are required to produce significant changes in crystal-liquid equilibria. The variation of pressure with depth in a magma whose density is  $\sim 3 \text{ g/cm}^3$  is approximately 0.3 kb per kilometer in the earth and about 0.05 kb per kilometer in the moon. Vertical movement of crystals in a magma chamber of 20 km or more is improbable enough in itself and it clearly would allow time for diffusion and reaction to eliminate the zoning patterns which have been preserved.

It is more probable to believe that the cyclic zoning is produced when crystals and liquid which have partially cooled, crystallized, and differentiated are mixed with fresh magma at a higher temperature during eruption. Under such circumstances the system is not chemically closed. Partially cooled lava can be reheated above the peritectic temperature by contact with fresh lava and the compositions of partially differentiated liquids can be changed by mixing to allow for precipitation of second or third generations of pigeonite without complete resorption of augite. Such mixing could reasonably be supposed to occur during turbulent flow in a thin, highly fluid lava stream. Thus the complexly zoned, Ca-rich mantles on pigeonite cores have most likely crystallized in flowing lava on the moon's surface. The oscillatory reversals in the trend of differentiation of the augite toward more Fe-rich compositions shown in Fig. 55 are also explained by this model.

Probe scans presented in Figs. 52-56 show that the transition from pigeonite to augite or *vice-versa* involves an abrupt compositional break in traverses normal to  $(\bar{1}\bar{1}0)$  and  $(\bar{1}10)$ , but that there is a gradation in composition for crystal growth on  $(\bar{1}00)$ . The crystal thus appears to show a complete solid solution between Ca-rich and Ca-poor pyroxene in growth parallel to  $a$  but a miscibility gap in the  $\{110\}$  sectors.



Crystallization through a peritectic should lead to a compositional break, and the relations on ( $\bar{1}\bar{1}0$ ) and ( $\bar{1}10$ ) are thus believed to represent the closest approach to equilibrium. Understanding the nature of this crystallographic control on composition is a fascinating problem. Sector zoning in lunar pyroxenes has been described and discussed (e.g. Hargraves, Hollister, and Otalora, 1970; Bence, Cameron, and Papike, 1970), but this particular relationship has not yet been interpreted. Obviously, additional probe scans normal to  $\{010\}$  and  $\{001\}$  are needed. The  $P2_1/c$  structure type of these pigeonites transforms on heating to the  $C2/c$  structure type (e.g., Prewitt, Papike, and Bence, 1970) and it may be that the structure of the primary, high-temperature parent of these pigeonites will have to be worked out in detail before an explanation of this sector zoning can be provided.

The minor elements Al, Ti, and Cr show considerable fluctuations in concentration across the mantle of the crystal shown in Plate 2, and it is clear that they also are involved in the sector zoning. Variations in the contents of Al, Ti, and Cr in a traverse normal to ( $\bar{1}\bar{1}0$ ) are shown by a probe scan in Fig. 58. The pigeonite core is relatively homogeneous in the contents of these minor elements as well as Ca, Mg, and Fe. However, there is an abrupt increase in Al, Ti, and Cr relative to the core in the innermost layers of the mantle. The outer part of the mantle, where it is zoned to a Fe-rich augite, shows a decrease in these elements. Data obtained in a scan normal to ( $\bar{1}10$ ) show the same abrupt increase in Ti and Al in the mantle at the core boundary, but there are also some areas with high Al (up to 3.6 wt %) and high Ti (up to 1.8 wt %) in the range 50–100  $\mu\text{m}$  from the outer edge of the mantle. The abrupt changes in Ti and Al at the core-mantle boundary which characterize the  $\{110\}$  sectors are not present in a scan perpendicular to ( $\bar{1}00$ ). Here there is a smooth increase in Al and Ti con-

centration from the core into the central layers of the mantle and then a decrease in the outer mantle where it is zoned to a more Fe-rich pigeonite. Maximum values for Al and Ti on ( $\bar{1}00$ ) correspond to high values for Ca. Thus the progressive variations in Al and Ti on ( $\bar{1}00$ ) mirror the gradual changes shown by the major elements. Relatively low concentrations of Al, Ti, and Cr in the outermost part of the mantle are present in all scans regardless of whether the outer rim of the mantle is zoned to Fe-rich augite or to pigeonite.

The increase in Al, Ti, and Cr contents in the inner part of the mantle relative to the core (Fig. 58) probably reflects the fact that these components have a greater solubility in Ca-rich pyroxenes than they do in Ca-poor pyroxenes. For example, Boyd and Brown (1969) have analyzed a clinohypersthene lamella and augite host from the Bushveld and found that Al, Ti, and Cr are concentrated in the Ca-rich augite by a factor of 2 or more over the Ca-poor lamella. Evans and Moore (1968) show similar enrichments for these elements in augite which crystallized with pigeonite and hypersthene in the Makaopuhi lava lake. Why Ca-rich pyroxenes dissolve more Al, Ti, and Cr than do Ca-poor pyroxenes (either  $P2_1/c$  inverted from  $C2/c$ , or  $Pbca$ ) is not clear, but such fractionation seems to be the general rule.

The  $\text{Al}_2\text{O}_3$  contents of the augite mantles in these lunar phenocrysts range up to higher values than are found in terrestrial pyroxenes which have crystallized from basaltic magmas. Bence, Papike, and Prewitt (1970) report up to 7.9%  $\text{Al}_2\text{O}_3$  in augite mantling pigeonite from rock 12052, whereas the maximum value found in the present study for augite from section 12021,7 is 6.8%. Bence *et al.* (*op. cit.*) note that the amount of Al in the most aluminous augites is considerably more than that required to charge compensate the Ti and that a Tschermak-type solid solution is thus present. They suggest that

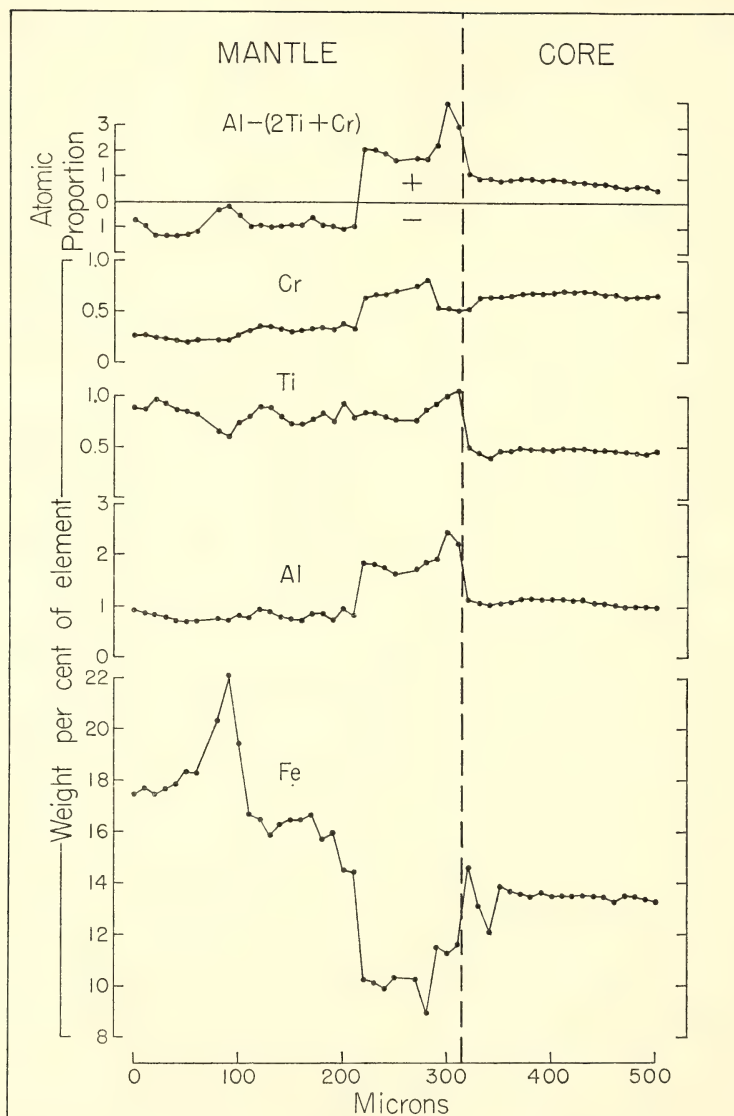


Fig. 58. Probe scans for Al, Ti, Cr, and Fe in the  $(\bar{1}10)$  sector. This scan is marked A in Plate 2, and associated variations in Ca, Mg, and Fe are given in Fig. 53. Atomic proportions shown in this figure were obtained from the weight percentages of each element by dividing by the molecular weight and multiplying by 100. An error of 5 relative % in the analysis of Al, Ti, or Cr leads to an error in the atomic proportion in the range 0.1–0.2. Thus the negative values for  $\text{Al} - (2\text{Ti} + \text{Cr})$  are quite significant.

these pyroxenes have either crystallized from a liquid at elevated pressure or from a melt with low silica activity, or that both these factors are operative.

Speculations outlined heretofore indicate that the oscillatory zoning in the augite mantles is most easily explained on the assumption that the mantles have formed

in turbulently flowing lava on the moon's surface. The high alumina contents of these augites are not necessarily inconsistent with this hypothesis. For example, Yagi and Onuma (1967) have studied the join  $\text{CaMgSi}_2\text{O}_6$ - $\text{CaTiAl}_2\text{O}_6$ , finding that the maximum solubility of  $\text{CaTiAl}_2\text{O}_6$  in diopside at atmospheric pressure is 11 wt %, corresponding to 3.7%  $\text{TiO}_2$  (2.2% Ti) and 4.7%  $\text{Al}_2\text{O}_3$  (2.5% Al). Their experiments show that pressure reduces the solubility of Ti in diopside from this maximum value. De Neufville and Schairer (*Year Book 61*) have shown that up to 20 wt % of  $\text{CaAl}_2\text{SiO}_6$  will dissolve in diopside at atmospheric pressure, corresponding to 9.3 wt %  $\text{Al}_2\text{O}_3$  (4.9% Al). The latter solid solution is of the Tschermak-type and is extended by pressure (Clark, Schairer, and de Neufville, *Year Book 61*). Hence, the Al and Ti contents of these Ca-rich pyroxenes synthesized at atmospheric pressure are quite comparable with those found in the lunar augites.

Bence *et al.* (*op. cit.*) further suggest that the decrease in Al in the outer part of the augite mantles is due to depletion in the liquid of Al caused by crystallization of anorthite. This interpretation seems valid because anorthite is intergrown with the Ca-rich mantles, but not with the primary pigeonite in the cores. Some of the pigeonite cores have formed as hollow crystals and the central cavities are now filled with late-stage augite, anorthite, and opaque phases. In some cases there is a visible channel from the original cavity through to the exterior of the crystal. In cases where such channels are not apparent, it is reasonable to suppose that they exist in some plane other than that cut by the thin section.

A number of studies of Apollo 11 and 12 pyroxenes (e.g. Kushiro, *et al.*, 1970; Ross *et al.*, 1970; Hargraves, Hollister, and Otalora, 1970; Bence, Papike, and Prewitt, 1970) have shown that the solid solution of Ti in the pyroxenes is principally effected by the coupled substitu-

tion  $[(\text{Ti}^{4+})^{\text{VI}} + 2\text{Al}^{\text{IV}}]$  for  $[(\text{R}^{3+})^{\text{VI}} + 2\text{Si}^{\text{IV}}]$ , confirming the analysis of Verhoogen (1962b). Nevertheless, in order to understand the Al and Ti relations one must also consider Cr. Augites in section 12021,7 contain up to 0.8% Cr (1.2%  $\text{Cr}_2\text{O}_3$ ). The effective ionic radii of  $\text{Cr}^{3+}$  and  $\text{Ti}^{4+}$  in six-fold coordination are respectively 0.615 and 0.605 Å (Shannon and Prewitt, 1969) and there should be a reluctance for  $\text{Cr}^{3+}$  to enter the tetrahedral site in augite which is comparable to that for  $\text{Ti}^{4+}$ . A possible substitution for  $\text{Cr}^{3+}$  in the octahedral site is  $[(\text{Cr}^{3+})^{\text{VI}} + \text{Al}^{\text{IV}}]$  for  $[(\text{R}^{2+})^{\text{VI}} + \text{Si}^{\text{IV}}]$ . Figure 58 shows a plot of the atomic proportion  $\text{Al} - (2\text{Ti} + \text{Cr})$  across the Ca-rich mantle normal to (110). Where this proportion is positive, it means that there is more than sufficient Al to compensate any possible octahedral substitution of  $\text{Ti}^{4+}$  and  $\text{Cr}^{3+}$ . The surplus of Al could then be dissolved in a Tschermak-type substitution. However, a negative value for this proportion means that the substitutions involving these ions are not wholly of the types proposed. As can be seen in Fig. 58 the proportion  $\text{Al} - (2\text{Ti} + \text{Cr})$  is positive for the pigeonites in the core and for the augites in the inner part of the mantle, but it is uniformly negative in the outer mantle. Hence, at least in the outer mantle some other substitution(s) must be involved, and there are a number of possibilities. Some  $\text{Ti}^{4+}$  and  $\text{Cr}^{3+}$  might be in tetrahedral coordination. Alternatively some of either or both these ions might be in reduced form, as  $\text{Ti}^{3+}$  and  $\text{Cr}^{2+}$ . Then there is a possible couple suggested by Verhoogen (1962) which is  $[(\text{Ti}^{4+})^{\text{VI}} + \text{Mg}^{\text{IV}}]$  for  $[\text{Mg}^{\text{VI}} + \text{Si}^{\text{IV}}]$ . It seems most reasonable to suppose that Cr is present as  $\text{Cr}^{2+}$  in the  $\text{M}_1$  site. Haggerty *et al.* (1970a) have found evidence for the presence of  $\text{Cr}^{2+}$  in olivines from the Apollo 11 rocks, and elsewhere in this report Bell describes even larger concentrations of  $\text{Cr}^{2+}$  in Apollo 12 olivines. Nevertheless, even if all the Cr is assumed to be present as  $\text{Cr}^{2+}$ , the



atomic proportion Al-2Ti is negative for many of the analyses shown in Fig. 58 for the outer mantle on (TiO). This relationship suggests that some Ti<sup>3+</sup> is also present.

ANALYSIS OF OLIVINE CRYSTALS IN  
APOLLO 12 ROCKS

P. M. Bell

Olivine crystals from Apollo 12 rocks 12052, 12004, 12022, and 12040 have been analyzed by electron microprobe and can be evaluated in light of the analyzed olivine from rock 10020 of Apollo 11 (Haggerty *et al.*, 1970a).

Olivine is one of the liquidus phases (with chrome ulvöspinel) in these rocks, and forms apparent phenocrysts of large dimension (up to 2.5 mm). Generally the crystals are only slightly zoned at the margins and contain information on the initial part of the crystallization process.

Haggerty *et al.* described a large (1.8 mm) crystal from Apollo 11 that was not zoned and gave a value of Fo<sub>72</sub> Fa<sub>28</sub>. Its chromium content was the highest ever observed in a natural olivine (0.21% Cr<sub>2</sub>O<sub>3</sub>), and measurements of optical absorption spectra in the near infrared region suggested that all chromium was present as octahedrally coordinated Cr<sup>2+</sup>. From these results combined with data on other minerals, it was concluded that the rock had crystallized under extremely reducing conditions (*P*<sub>O<sub>2</sub></sub> ~ 10<sup>-13</sup> atm). The olivines from Apollo 12 rocks can be interpreted in much the same way, although differences in bulk chemistry and in phase composition are significant.

Fifteen olivine crystals from 12052 (Apollo 12) were analyzed for three major (Fe, Mg, Si) and three minor (Ca, Mn, Cr) elements. The results given in Table 9A show little variation; the compositions closely approximate Fo<sub>70</sub> Fa<sub>30</sub>. Each crystal was analyzed five times, first with one standard then with another, the values listed representing 150 analyses. It is significant, therefore, that the values for Cr<sub>2</sub>O<sub>3</sub> come close to 0.4%. This value is a factor of 2 greater

TABLE 9. Quantitative Analysis of Apollo-12 Olivines by Electron Microprobe

Grain	A															B			C	
	1	2	3	4	5	6	7	8	9	10	11	12	13	14	15	1	1A	1	1A	1
MgO	35.50	35.62	36.30	35.16	36.25	36.31	35.74	35.85	34.38	35.56	35.32	36.29	34.67	35.05	35.42	39.08	38.76	39.08	38.76	32.50
SiO <sub>2</sub>	37.34	37.44	37.59	37.14	37.46	37.83	37.44	37.73	37.21	37.21	37.47	37.84	37.26	37.32	37.45	...	...	...	...	...
CaO	0.30	0.30	0.30	0.30	0.31	0.30	0.30	0.30	0.30	0.30	0.33	0.30	0.28	0.30	0.33	...	...	...	...	...
Cr <sub>2</sub> O <sub>3</sub>	0.40	0.42	0.42	0.41	0.30	0.39	0.39	0.39	0.39	0.34	0.38	0.38	0.40	0.35	0.39	0.36	0.38	0.36	0.38	0.23
MnO	0.31	0.32	0.32	0.31	0.34	0.32	0.31	0.31	0.32	0.32	0.40	0.32	0.30	0.34	0.34	...	...	...	...	...
FeO	27.23	26.99	25.69	26.87	25.52	25.92	26.39	26.50	27.77	26.51	26.89	25.82	27.64	27.27	26.35	22.34	23.95	22.34	23.95	28.86
Totals	101.08	101.09	100.62	100.19	100.28	101.08	100.58	101.08	100.37	100.24	100.79	100.96	100.55	100.62	100.28					

A. Rock 12052.  
B. 1, Rock 12004; 1A, rock 12022.  
C. Rock 12040.

than the chromium content in the crystals from Apollo 11. The difference may be the result of a higher bulk value for the rock (0.52%  $\text{Cr}_2\text{O}_3$  in 12052 as opposed to 0.32%  $\text{Cr}_2\text{O}_3$  in 10020). Again, low  $P_{\text{O}_2}$  values of crystallization are consistent with these abnormally high chromium contents.

Magnesium, iron, and chromium were analyzed in olivines from rocks 12004 and 12022. The values are listed in Table 9B. Although somewhat richer in magnesium, the approximate values of  $\text{Fo}_{7.5}\text{Fa}_{25}$  and  $\text{Fo}_{74}\text{Fa}_{26}$  are not significantly different. Slight zoning in the margins of crystals is toward iron enrichment. The chromium values are very similar to those of 12052.

Bulk spectrographic analyses of the Apollo 12 rocks are listed in the Lunar Sample Information Catalog Apollo 12 (NASA-MSC-01512). The rocks are coarse grained, and spectrographic analyses of small samples may not be representative. The data for 12052, 12004, and 12022 are consistent with the olivine compositional variations, which should be chemically diagnostic of the original liquid from which the rocks crystallized. This is not true of rock 12040. The Fe/Mg ratio is close to 2.0 or higher for 12052, 12004, and 12022 but is approximately equal to 1.6 for 12040. The  $\text{Cr}_2\text{O}_3$  content is 0.23% in the olivines but is reported as 0.7% for the whole-rock spectrographic analysis, the highest value reported for Apollo 12 rocks.

This relative enrichment in Mg, if real, suggests higher liquidus temperatures. The olivines should reflect this as well. Electron probe measurements show the olivines in 12040 to be strongly zoned, giving an average composition of  $\text{Fo}_{50}\text{Fa}_{50}$ . Iron is enriched, not magnesium, as would be expected from the spectrographic analyses. The strong zoning makes an average composition meaningless, so the measured values are not listed in Table 9. The most Mg-rich core of an olivine in this rock, however, is homogeneous for a radius of approxi-

mately 30  $\mu\text{m}$ . The analysis of this core (measured by L. A. Taylor) is given in Table 9C. The composition is close to  $\text{Fo}_{61}\text{Fa}_{39}$ , still more iron rich than olivines from the other rocks.

Other checks on the discrepancy between spectrographic and electron probe analysis of the olivines were made by observation of the olivine composition as deduced by X-ray diffraction and of the compositions of chromium ulvöspinel that occur as inclusions in olivine. G. Warner (personal communication) of the NASA Lunar Receiving Laboratory reports that X-ray diffraction parameters give an average olivine composition of  $\text{Fo}_{50}\text{Fa}_{50}$ , entirely consistent with the present results.

The spinels in olivines have been analyzed by Haggerty and Meyer (p. 144). Clearly the spinels are the most Fe rich and Cr poor of those analyzed. The spinels in 12052 (Haggerty and Meyer, *op. cit.*) show this same consistency with the olivine compositions.

One can safely conclude that the olivine-spinel pairs are primary liquidus phases in the Apollo 12 rocks. They are diagnostic of the "basaltic" liquid from which they crystallized. The high chromium content signifies a low  $P_{\text{O}_2}$  of crystallization, and the general composition reflects the total iron-rich composition. That Ni was not detected in these olivines is another difference from their terrestrial counterparts. Taylor, Kullerud, and Bryan (p. 241) have noted the presence of Ni in metallic phase assemblages that were entrapped in olivine crystals.

#### APOLLO 12: OPAQUE OXIDES \*

*S. E. Haggerty and H. O. A. Meyer*

A comparison of the Apollo 12 samples from *Oceanus Procellarum* with the Apollo 11 samples from *Mare Tranquillitatis* reveals certain chemical similarities. Both suites show distinctive features

\*Supported in part by National Aeronautics and Space Administration contract no. 09-140-(006).

of high concentrations of *refractory* elements and low contents of *volatile* elements; these features most clearly distinguish lunar material from terrestrial or meteoritic material. One of the major differences between the two sites is the lower abundance of Ti, in both the crystalline rocks and fine material, in the Apollo 12 samples. The range in composition is 1.2 to 5.1% TiO<sub>2</sub> compared with 7 to 12% TiO<sub>2</sub> for the Apollo 11 material (Lunar Sample Preliminary Examination Team, 1970). This difference is reflected in the opaque minerals; ilmenite forms 10 to 20 modal % of the crystalline rocks of Apollo 11, whereas the concentration is 5 to 10% in Apollo 12 rocks.

The opaque minerals in the lunar material form a unique assemblage (Haggerty *et al.*, 1970*a,b*; Cameron, 1970; Ramdohr and El Goresy, 1970). The major phases are ilmenite (FeTiO<sub>3</sub>), members of the chromite (FeCr<sub>2</sub>O<sub>4</sub>)–ulvöspinel (Fe<sub>2</sub>TiO<sub>4</sub>) series, members of the armalcolite series (FeTi<sub>2</sub>O<sub>5</sub>–MgTi<sub>2</sub>O<sub>5</sub>), troilite (FeS), and metallic iron (Fe). This assemblage reflects the highly reducing lunar environment and permits estimation of oxygen fugacity, tempera-

ture of formation, and fractionation trends during crystallization.

### Ilmenite

Ilmenite forms between 5 and 10 modal % of the crystalline rocks examined. Optically, ilmenite is distinctly anisotropic and in oil immersion shows the deep reddish tan color that is characteristic. Extremely thin plates of ilmenite are translucent. Ilmenite grains in the crystalline rocks form (1) blocky, euhedral to subhedral crystals; (2) thin plates parallel to {0001} with rhombohedral terminations; and (3) more rarely, coarse skeletal crystals with trapped pyroxene, troilite, and metallic iron. Electron microprobe analyses (Table 10) show ilmenite to be almost stoichiometric FeTiO<sub>3</sub>; SiO<sub>2</sub>, Al<sub>2</sub>O<sub>3</sub>, Cr<sub>2</sub>O<sub>3</sub>, MgO, CaO, and MnO total less than 1%.

Most of the ilmenite is homogeneous, but a few individual grains of ilmenite contain lamellae of rutile, <10 μm thick, oriented along {0112} and lensoidal rods of a dark gray spinel phase, aligned along {0001}.

The secondary spinel and rutile invariably coexist within ilmenite, and they are often intimately associated,

TABLE 10. Electron Probe Analyses of Ilmenite in Samples from Apollo 12 Rocks

	12020,10 1	12064,6 2	12064,6 1
SiO <sub>2</sub>	...	0.20	0.12
TiO <sub>2</sub>	52.3	52.8	53.1
Al <sub>2</sub> O <sub>3</sub>	0.15	0.04	0.07
Cr <sub>2</sub> O <sub>3</sub>	0.22	0.08	0.22
FeO	46.9	46.8	46.7
MgO	0.12	0.11	0.20
CaO	0.10	0.01	0.01
MnO	0.34	0.28	0.37
Totals	100.1	100.3	100.8
Number of Cations on the Basis of 3(O)			
Si	...	0.005	0.003
Ti	0.992	0.997	0.997
Al	0.005	0.001	0.002
Cr	0.004	0.002	0.004
Fe	0.988	0.982	0.974
Mg	0.004	0.004	0.007
Ca	0.003	0.000	0.000
Mn	0.007	0.006	0.008

1.001

1.005

1.006

1.002

0.992

0.989



with no clear-cut textural evidence as to their order or sequence of formation. Both spinel and a second generation of ilmenite have been observed as oriented lamellae within the exsolved rutile, suggesting that the rutile was enriched in iron when it formed. The textures of these various intergrowths indicate that the phases are interrelated by a complex rather than a simple exsolution process, with possibly one phase triggering nucleation and growth of the other. In some instances, exsolution intergrowths are confined to ilmenite grain boundaries but contact with troilite, metallic iron, crystalline silicates, glass, or chromian ulvöspinel appears to have promoted exsolution. Such intergrowths in ilmenite have not been reported in terrestrial rocks, but chromite and rutile have been observed in ilmenite from meteorites (Buseck and Keil, 1966).

The process by which rutile and spinel are formed in ilmenite is not fully understood. In terrestrial basalts growth of rutile in ilmenite is generally the result of oxidation (Watkins and Haggerty, 1967), but Ramdohr (*Year Book 63*) has suggested that in meteorites reduction could also cause the generation of rutile by the breakdown of ilmenite in environments of low oxygen fugacity. The breakdown  $2\text{FeTiO}_3 \rightarrow 2\text{TiO}_2 + \text{O}_2 + 2\text{Fe}$  was not observed in lunar ilmenite. The rutile intergrowths have a texture suggesting exsolution rather than alteration, because they are oriented parallel to  $\{01\bar{1}2\}$  and have well-defined contacts that taper at the intersection of two or more lamellae. Furthermore, the orientation of spinel parallel to the basal plane is characteristic of magnetite lamellae in ilmenite (Buddington and Lindsley, 1964). The fact that rutile and spinel are either crosscutting or intimately associated suggests that this is a complex, crystallographically controlled breakdown.

It is possible that both reduction and exsolution from a supersaturated host have caused the growth of these lamellae.

The sparse distribution of exsolved grains suggests a selective nonequilibrium reduction process rather than simple exsolution. Evidence of reduction in the form of reduced phases is lacking in ilmenite, however, but is present in chromium ulvöspinel from the same samples.

### *Spinel*

A group of new variety minerals, variously described as chromian ulvöspinel (Haggerty *et al.*, 1970*a,b*), titanian chromite (Cameron, 1970), and aluminian chromite (Agrell *et al.*, 1970) were discovered in a restricted number of samples from the Apollo 11 material. These spinels are not new minerals but are compositionally distinct from terrestrial and meteoritic analogues and for purposes of comparison may be regarded either as Cr-rich titanomagnetites (e.g., 23.5%  $\text{Cr}_2\text{O}_3$ ) or Ti-rich chromites (e.g., 20.9%  $\text{TiO}_2$ ). There is a restricted solid solution between ulvöspinel and chromite in terrestrial and meteoritic occurrences. Terrestrial titanomagnetites contain between 0.1 and 0.38%  $\text{Cr}_2\text{O}_3$  (Deer, Howie, and Zussman, 1962*b*; Carmichael, 1967). Chromites generally have small concentrations of  $\text{TiO}_2$ , although both rutile (Ramdohr, 1963; Buseck and Keil, 1966) and ilmenite (Ramdohr, 1963; Legg, 1969) have been observed as exsolution intergrowths. Among terrestrial chromites those richest in  $\text{TiO}_2$  are usually found in basaltic lavas and contain 1.3 to 2.5%  $\text{TiO}_2$  (Babkina *et al.*, 1965; Haggerty, 1968). An unusual chromite occurrence in the Bushveld, however, has a reported  $\text{TiO}_2$  content of 12.8% (Frankel, 1942). A meteoritic chromite analyzed by Buseck and Keil (1966) contains 2.9%  $\text{TiO}_2$ . A complete solid solution series exists between magnetite ( $\text{Fe}^{2+}\text{Fe}^{3+}_2\text{O}_4$ ) and chromite ( $\text{FeCr}_2\text{O}_4$ ) and also between magnetite and ulvöspinel ( $\text{Fe}_2\text{TiO}_4$ ). Although a solid solution series has not been experimentally demonstrated be-

tween  $\text{Fe}_2\text{TiO}_4$  and  $\text{FeCr}_2\text{O}_4$ , the reported analyses from Apollo 11 (Agrell *et al.*, 1970) indicate that such a series exists, supporting the suggestions of Evans and Moore (1968) and Legg (1969).

Members of the series chromite (Cr)-ulvöspinel (Usp), somewhat similar to the chromian ulvöspinel described above, occur extensively throughout the Apollo 12 samples (Haggerty and Meyer, 1970) but differ in several respects from those in Apollo 11. The Apollo 12 spinels are mineralogically distinct, fall into two well-defined compositional groups on either side of the Apollo 11 spinels along the join  $\text{Fe}_2\text{TiO}_4$ - $\text{FeCr}_2\text{O}_4$ , show a wide variety of unusual optical properties and textures, and also show the first evidence of subsolidus reduction reactions in the lunar material.

### *Optical Properties*

Five optically distinct spinels have been identified in the Apollo 12 crystalline rocks (Plate 3A-D). These spinels may be divided into two groups, optically isotropic chromites and optically anisotropic chromian ulvöspinel. The isotropic group are either blue or gray in color, whereas the anisotropic group are tan, pink, or khaki in color. Estimated reflectivity values for the isotropic group are 12-15%, those for the anisotropic tan and pink minerals 18-20%, and for the khaki phase 22-25% (cf. ilmenite 20-22%). The isotropic group are harder than the anisotropic group and both are harder than ilmenite. Terrestrial and synthetic ulvöspinel and chromites are optically isotropic, but the lunar chromian ulvöspinel are consistently anisotropic. The crystalline rocks examined in this study are unshocked, and so anisotropy due to lattice distortions is unlikely. Anionic deficiencies are possible under the highly reducing lunar environment, but such defects would not be observed optically. It is therefore suggested that the chromian ulvöspinel are a new group of nonisometric phases along the

join  $\text{Fe}_2\text{TiO}_4$ - $\text{FeCr}_2\text{O}_4$  and are therefore not true spinels.

### *Textures and Paragenesis*

The isotropic blue and gray spinels are the earliest crystallization products and occur in olivine and pyroxene as euhedral crystals in the size range 20-100  $\mu\text{m}$ . Isotropic spinels in the groundmass are *always* rimmed (Plate 3A-B) by overgrowths of anisotropic spinels of the tan or pink variety and never of the khaki type; the khaki phase is anhedral and occurs in complex intergrowths with metallic iron and ilmenite (Plate 3D). The overgrowths vary in thickness from <10 to 150  $\mu\text{m}$ . Contacts between core and overgrowths are generally gradational, although sharp, optically well-defined contacts are also observed. In terrestrial basalts chromite is also the first mineral to form; chromite in the groundmass is always rimmed by titanomagnetite, whereas chromite in olivine or pyroxene is unzoned (Haggerty, 1968). By contrast the Apollo 11 chromian ulvöspinel are rimmed by ilmenite (Haggerty *et al.*, 1970a,b). In Plate 3A the paragenetic sequence for the Apollo 12 opaque minerals is illustrated; chromite forms the core of the assemblage, followed by chromian ulvöspinel, ilmenite, and finally metallic iron plus troilite (eutectoid-type intergrowth). Ilmenite overgrowths on chromite were not observed. The oxide overgrowths are interpreted as progressive zoning that has developed as a result of reaction with liquid. A consequence of this interpretation, and the paragenetic sequence, is that an early depletion of Cr and an enrichment of Fe and Ti in the liquid are indicated during crystallization.

Crystallization trends for the opaque oxides from Apollo 11 and 12 missions and for typical terrestrial basalts are summarized and contrasted in Fig. 59 in terms of the system  $(\text{FeMg})\text{O-TiO}_2\text{-(CrAl)}_2\text{O}_3$ .

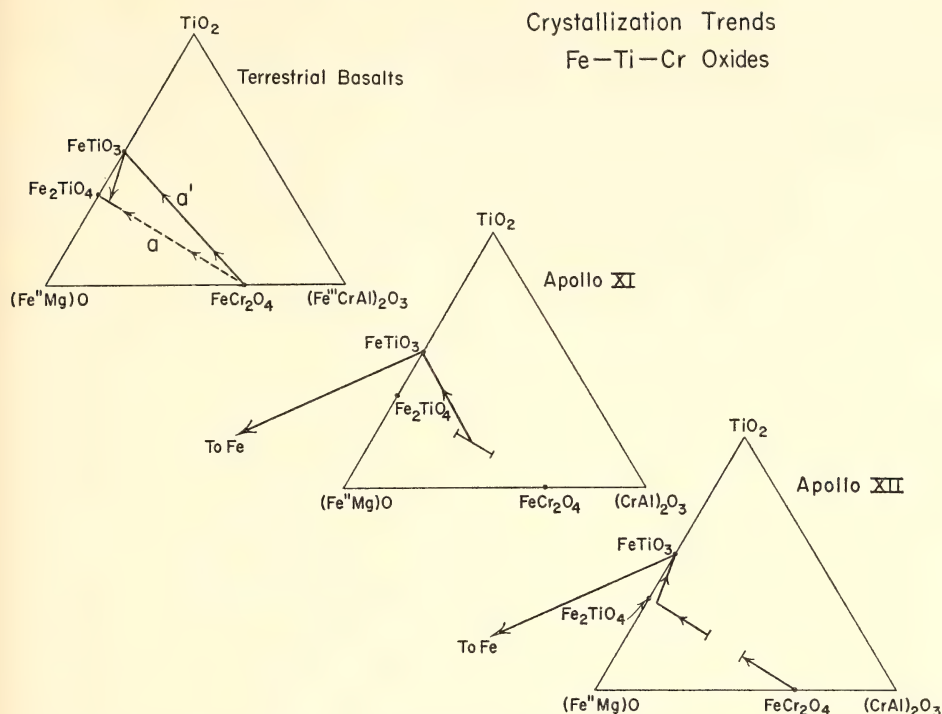


Fig. 59. Simplified crystallization trends for the Fe-Ti-Cr oxides in terrestrial basalts compared with those in rocks from the Apollo 11 and 12 lunar missions.

### *Subsolidus Reactions*

Exsolution lamellae of ilmenite and minute blebs of metallic iron occur along (111) planes in chromian ulvöspinel (Plate 3E). The lamellae are tapered, pinch on intersection, and have all the oxidation-exsolution features of ilmenite in titanomagnetite. The presence of metallic iron, however, is a direct indication that a process of reduction rather than oxidation has been operative. Ilmenite is commonly observed along cracks and grain boundaries in chromian ulvöspinel. Each ilmenite lamella is flanked by a gradational gray Cr-rich lamella, which is also gradational on contact with Cr ulvöspinel. The distribution of  $\text{FeO}$ ,  $\text{TiO}_2$ , and  $\text{Cr}_2\text{O}_3$  across two ilmenite lamellae is shown in Fig. 60. The ilmenite is well defined in terms of high  $\text{TiO}_2$  and low  $\text{Cr}_2\text{O}_3$  but note the

4–5 wt % increase in chromium at the ilmenite lamellae contacts; this Cr residuum is the result of preferential migration of Fe and Ti from the spinel to form ilmenite during subsolidus reduction. It is generally accepted that  $P_{\text{O}_2}$  decreases during crystallization, but whether these intergrowths formed deuterically or by some postdeuteric process is not known. On the basis of Fe-Ni ratios in metals from the Apollo 12 samples, Reid *et al.* (1970) have suggested that the metal is reduced from the melt as crystallization proceeds; this possibility would support a deuteric origin for the exsolved ilmenite.

### *Chemistry*

Fifteen electron microprobe analyses on the five Fe-Ti-Cr oxides (gray, blue, tan, pink, khaki) have been carried out



## APOLLO XII

Exsolved Ilmenite in Cr-Ulvöspinel

Analyses: 1  $\mu\text{m}$  intervals

12040-4

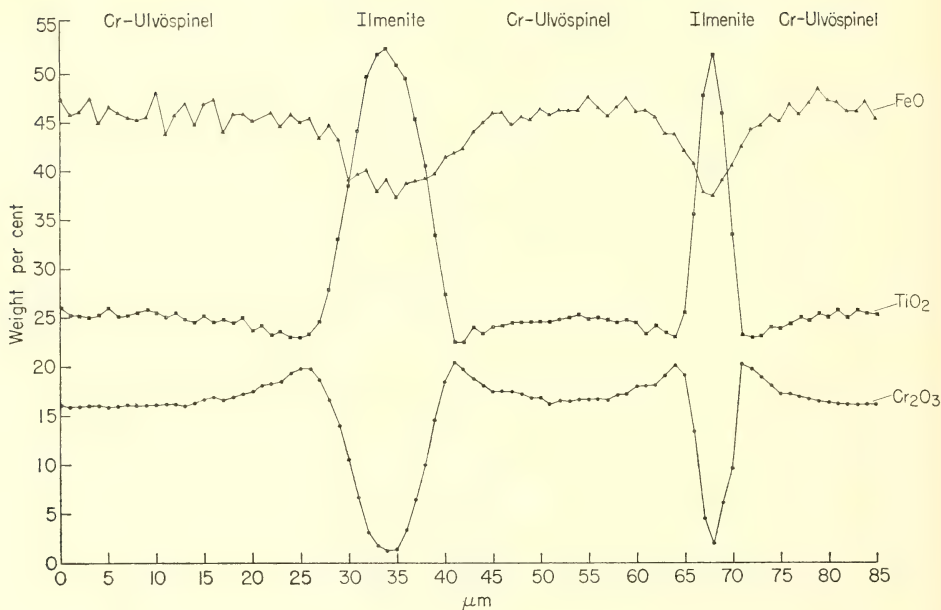


Fig. 60. Single traverse of uncorrected electron probe analyses at 1- $\mu\text{m}$  intervals across exsolved lamellae of ilmenite in chromium ulvöspinel.

on four polished thin sections (12020,10; 12040,4; 12052,6; 12064,6) of unshocked microgabbros. The data are presented in Tables 11 and 12 and Fig. 61. Data on coexisting ilmenite are also presented (Table 10).

The spinel analyses fall into two separate and distinct compositional groups along the join  $\text{Fe}_2\text{TiO}_4$  (Usp)- $\text{FeCr}_2\text{O}_4$  (Cr) in the ternary system  $(\text{FeMg})\text{O}-\text{TiO}_2-(\text{CrAl})_2\text{O}_3$  (Fig. 62). The isotropic (gray and blue) spinels are Cr rich ( $\text{Usp}_{90}\text{Cr}_{91}$ - $\text{Usp}_{25}\text{Cr}_{75}$ ), whereas the anisotropic (tan, pink, khaki) chromian ulvöspinel are richer in Fe and Ti ( $\text{Usp}_{74}\text{Cr}_{26}$ - $\text{Usp}_{90}\text{Cr}_{10}$ ). These oxides are in direct contrast to spinels from the Apollo 11 samples ( $\text{Usp}_{45}\text{Cr}_{55}$ - $\text{Usp}_{63}\text{Cr}_{37}$ ). The distribution and separation of the

Apollo 12 analyses, on either side of the Apollo 11 spinels, suggest that a miscibility gap may be present along the join ulvöspinel-chromite. The Apollo 11 samples fall within this gap. If a solvus is present it would suggest either that the Apollo 11 spinels crystallized metastably or that these rocks were quenched from a higher temperature than those of Apollo 12. The miscibility gap extends from  $\text{Usp}_{42}\text{Cr}_{58}$ - $\text{Usp}_{66}\text{Cr}_{34}$ , although further work on other samples may narrow the extent of the chromite-rich limb.

The gradational overgrowths of chromian ulvöspinel on chromite, discussed above, are interpreted as continuous reaction with liquid during slow crystallization; such overgrowths provide further evidence for the suggested solvus.

TABLE 11. Electron Probe Analyses of Chromian Ulvöspinels in Samples from Apollo 12 Rocks\*

Sample Color	12040,4 Tan	12040,4 Tan	12040,4 Pink	12064,6 Pink	12020,10 Tan	12064,6 Tan	12064,6 Khaki
SiO <sub>2</sub>	...	...	...	0.19	...	0.33	0.17
TiO <sub>2</sub>	22.8	23.8	25.6	28.0	28.7	31.1	32.2
Al <sub>2</sub> O <sub>3</sub>	5.06	4.88	3.84	2.64	2.67	2.66	2.32
Cr <sub>2</sub> O <sub>3</sub>	17.9	17.5	13.3	9.34	8.61	3.64	1.50
FeO	51.9	51.8	55.0	58.6	58.8	61.8	62.9
MgO	2.44	2.86	2.31	0.21	0.41	0.17	0.13
CaO	0.00	0.01	0.02	<0.01	0.05	<0.01	<0.01
MnO	0.53	0.52	0.50	0.27	0.30	0.16	0.29
Totals	100.6	101.4	100.6	99.3	99.5	99.9	99.5
Number of Cations on the Basis of 32(O)							
Si	...	...	...	0.055	...	0.097	0.049
Ti	4.895	5.068	5.555	6.250	6.382	6.895	7.200
Al	1.704	1.625	1.305	0.924	0.931	0.926	0.813
Cr	4.053	3.906	3.032	2.192	2.015	0.849	0.352
Fe	12.409	12.235	13.267	14.555	14.544	15.239	15.626
Mg	1.037	1.205	0.991	0.092	0.182	0.075	0.059
Ca	0.000	0.004	0.007	0.000	0.015	0.000	0.000
Mn	0.128	0.124	0.121	0.068	0.075	0.039	0.072
Totals	24.226	24.167	24.278	24.136	24.144	24.120	24.171

\* Analyses are listed in increasing concentrations of TiO<sub>2</sub>. These spinels are optically anisotropic and are contrasted from those in Table 12, which are optically isotropic.

Uncorrected microprobe analyses for FeO, Cr<sub>2</sub>O<sub>3</sub>, and TiO<sub>2</sub>, taken at 1- $\mu$ m intervals, across an ilmenite+Cr-Usp (pink)+Cr-Usp (tan)+chromite (gray) assemblage are illustrated in Fig. 62. Units of five or ten analyses were aver-

aged for points across the gradational contact, and typical values for MgO and Al<sub>2</sub>O<sub>3</sub> were used in the final microprobe corrections. These data are plotted in Fig. 63 as mean values for nine gradational-contact analyses. In spite of the

TABLE 12. Electron Probe Analyses of Chrome Spinels in Samples from Apollo 12 Rocks\*

Sample Color	12052,6 Gray	12052,6 Gray	12052,6 Gray	12020,10 Gray	12052,6 Gray	12020,10 Blue	12040,4 Gray	12064,6 Gray
SiO <sub>2</sub>	0.12	0.14	0.14	...	0.09	...	...	0.26
TiO <sub>2</sub>	4.22	4.31	4.43	4.72	5.54	6.89	7.39	9.14
Al <sub>2</sub> O <sub>3</sub>	12.02	11.83	11.86	12.3	11.88	13.5	12.2	12.5
Cr <sub>2</sub> O <sub>3</sub>	48.30	48.84	48.90	45.0	45.99	42.2	40.4	37.9
FeO	26.02	26.87	25.95	31.2	29.41	30.9	35.2	33.8
MgO	7.43	7.74	7.43	4.94	6.46	6.93	4.59	5.29
CaO	0.04	0.04	0.01	0.10	0.06	0.01	0.06	0.01
MnO	0.75	0.76	0.76	0.17	0.64	0.23	0.72	0.21
Totals	98.9	100.5	99.4	98.4	100.0	100.7	100.6	99.1
Number of Cations on the Basis of 32(O)								
Si	0.032	0.037	0.038	...	0.025	...	...	0.070
Ti	0.857	0.862	0.893	0.980	1.178	1.375	1.513	1.870
Al	3.822	3.708	3.747	4.007	3.769	4.224	3.914	4.003
Cr	10.298	10.269	10.365	9.812	9.784	8.840	8.702	8.152
Fe	5.869	5.977	5.818	7.211	6.617	6.860	8.004	7.688
Mg	2.984	3.067	2.968	2.033	2.591	2.740	1.862	2.148
Ca	0.011	0.011	0.004	0.029	0.017	0.003	0.018	0.004
Mn	0.171	0.171	0.172	0.040	0.145	0.051	0.166	0.049
Totals	24.044	24.102	24.005	24.112	24.126	24.093	24.179	23.986

\* Analyses are listed in increasing concentrations of TiO<sub>2</sub>.

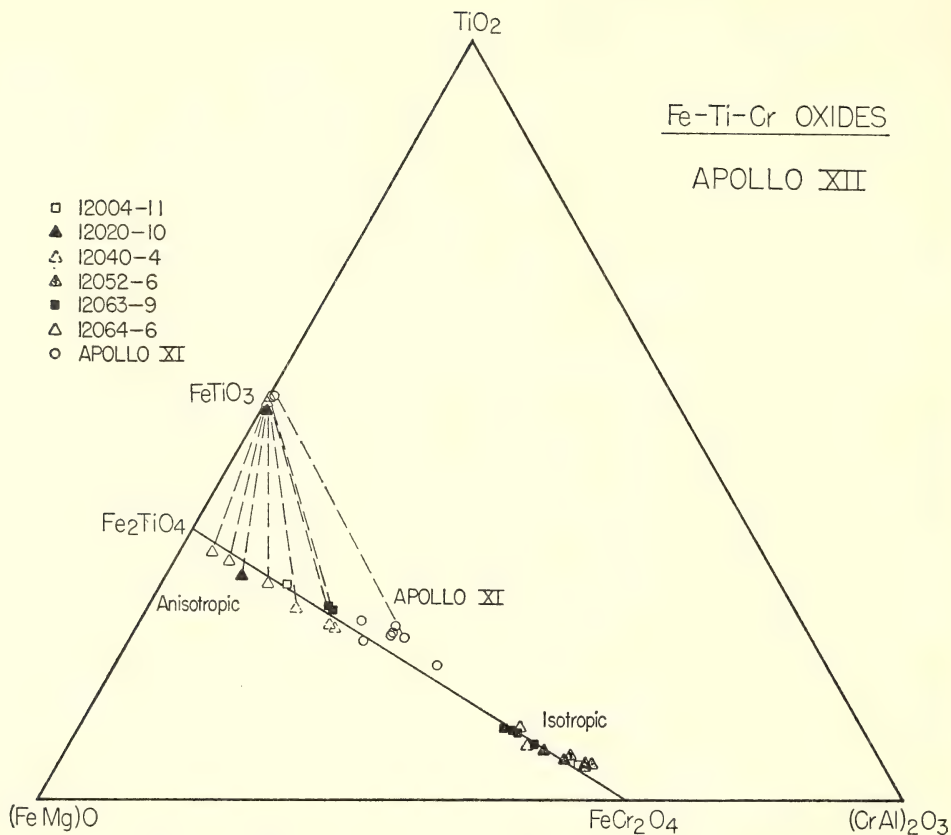


Fig. 61. (FeMg)O-TiO<sub>2</sub>-(CrAl)<sub>2</sub>O<sub>3</sub> plot of spinel analyses from Apollo 12 samples. Full and open squares are from Table 16 (Taylor, Kullerud, and Bryan, p. 243). Apollo 11 results are shown for comparison; data drawn from Agrell *et al.*, 1970.

observed optical gradation, it is noted that none of these data points falls within the miscibility gap.

The presence of approximately 90% of the Fe<sub>2</sub>TiO<sub>4</sub> molecule in the khaki chromian ulvöspinel (12064,6) defines this phase as being the most Fe<sub>2</sub>TiO<sub>4</sub>-rich mineral yet found in nature. Terrestrial ulvöspinel, possibly comparable in Fe<sub>2</sub>TiO<sub>4</sub> to the above material, may occur in ulvöspinel exsolution lamella within magnetite. Analyzed terrestrial material (usually titaniferous magnetites) contains less than 50% of the Fe<sub>2</sub>TiO<sub>4</sub> molecule (Deer, Howie, and Zussman, 1962b, p. 74), however, whereas in the Apollo 12 lunar ulvöspinel 60% is the minimum value.

Recalculations of the analyses in Tables 11 and 12 into possible spinel molecules indicates the presence of excess Fe<sup>2+</sup>. In order to retain charge balance on the basis of 32 oxygen atoms some of this excess Fe<sup>2+</sup> must be considered as Fe<sup>3+</sup>, thus allowing the formation of Fe<sup>2+</sup>Fe<sup>3+</sup>O<sub>4</sub>-magnetite. In general the amount of the magnetite molecule is not greater than 4%, corresponding roughly to a maximum of 4% by weight of Fe<sub>2</sub>O<sub>3</sub> in the original analyses. The presence of this small amount of Fe<sub>2</sub>O<sub>3</sub> when added to the (Al,Cr)<sub>2</sub>O<sub>3</sub> corner of Fig. 61 allows the individual ulvöspinel analyses to move closer to or onto the join Fe<sub>2</sub>TiO<sub>4</sub>-FeCr<sub>2</sub>O<sub>4</sub>.



# APOLLO XII

Analyses : 1  $\mu\text{m}$  intervals

12020-10

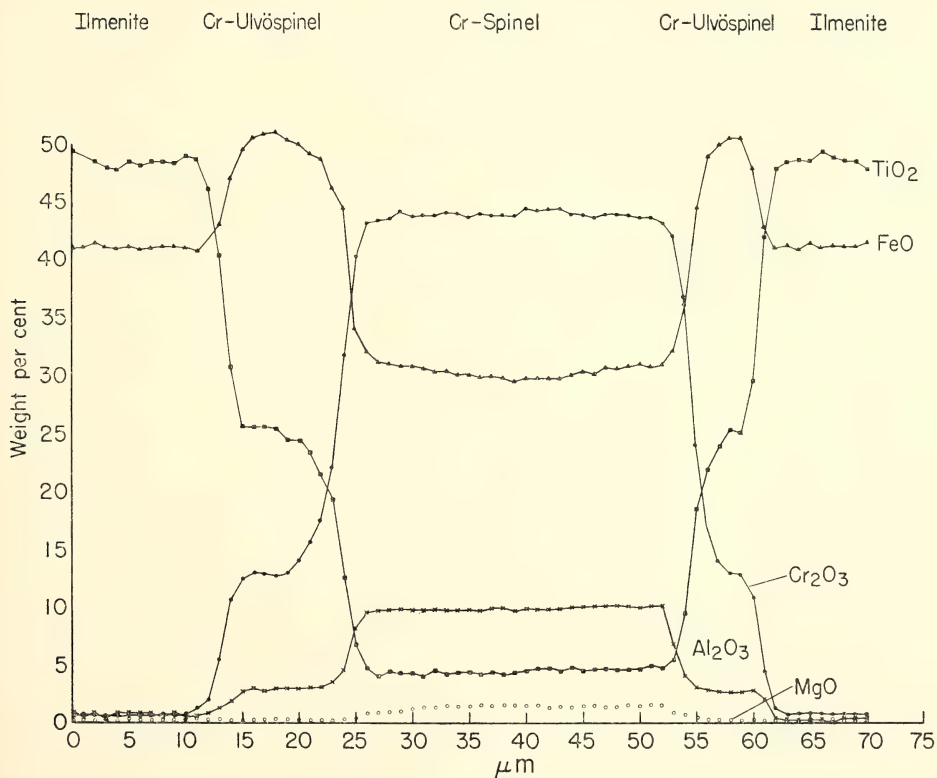


Fig. 62. Traverse of uncorrected electron probe analyses at 1- $\mu\text{m}$  intervals across chrome spinel, chromium ulvöspinel, ilmenite complex. Chrome spinel forms the core of the assemblage with gradational and consecutive overgrowths of chromium ulvöspinel and ilmenite.

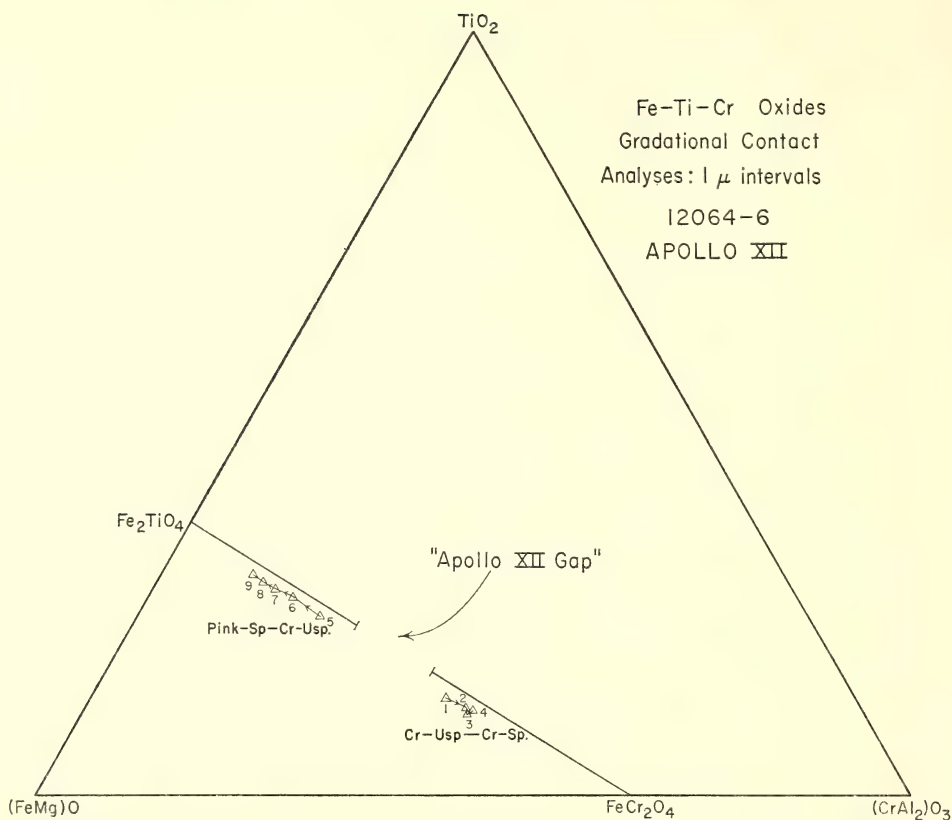


Fig. 63. Corrected electron probe analyses obtained from data presented in Fig. 62. The coordinates of this plot are similar to that of Fig. 61. Contacts between phases are optically gradational, but compositionally a distinct miscibility gap is present along the join ulvöspinel-chromite.

The abundance of  $\text{Fe}^{3+}$  in lunar whole-rock analyses is small, and because of the presence of free metallic iron, has been considered suspect. Taylor (1964), however, in studying the system  $\text{FeO-Fe}_2\text{O}_3\text{-TiO}_2$  at  $1300^\circ\text{C}$ , has shown the possible presence of ulvöspinel containing some magnetite in equilibrium with wüstite and metallic iron. Undoubtedly these relationships will be affected by the addition of Cr, Mg, and Al, but at present no experimental data applicable to this discussion are available.

INVESTIGATIONS OF APOLLO 12 SAMPLES  
L. A. Taylor, G. Kullerud, and W. B. Bryan

The lunar samples provide an unprecedented opportunity to study phase relations in rocks crystallized under highly reducing conditions. The lunar

rocks differ from meteorites both in bulk composition and in the nature and composition of individual mineral phases. Because in effect the rocks represent a natural experiment in a different portion of the complex sulfide-oxide-metal-silicate "system" than has previously been available for study, our initial investigations were designed mainly to define mineralogical and chemical relationships on which to base detailed experiments in portions of the natural system.

We have determined major and minor element concentrations in coexisting metal, sulfide, oxide, and silicate phases.\*

\* The microprobe used for these analyses was purchased with the support of NSF grant GP 4384. Some of the data were reported by Taylor, Kullerud, and Bryan (1970).

Variations in these concentrations may be related to fractionation taking place during magmatic crystallization or may represent postdepositional reequilibration. Laboratory experiments have been initiated to clarify whether the elemental distribution displayed by lunar samples is of primary or secondary origin.

The results presented below were obtained from polished thin sections of two Apollo 12 rocks, samples 12063,9 and 12004,11, a microgabbro and a melano-cratic olivine basalt, respectively. A more comprehensive and complete discussion of the findings will be presented elsewhere.

### Shock Features

Sample 12063,9 contains abundant evidence of having undergone considerable shock. Much of the plagioclase feldspar ( $An_{90}$ ) is not associated with apparent shock features, but locally a twinned plagioclase extends into a patch of untwinned, presumably recrystallized plagioclase, which was apparently melted by shock. It is thus possible to distinguish three feldspars as (1) unshocked, (2) shocked but unmelted, and (3) shock-melted.

Microprobe analysis (Table 13) shows that all three types of feldspar are deficient in alkalies and are very similar in composition, but the shock-melted feldspar has a slightly lower refractive index, perhaps due to structural adjustment during recrystallization.

In 12063,9 fayalite and cristobalite are commonly closely associated in areas interstitial to pyroxene and plagioclase. Fayalite (Table 13) usually contains marginal inclusions of glass rich in Ca, Al, and Si; these inclusions are generally absent where fayalite is in contact with cristobalite. Small amounts of troilite, Fe metal, and ilmenite are commonly associated with the fayalite and cristobalite, and are probably of secondary origin. These areas appear to be due to very localized shock, the fayalite-cristobalite association probably being derived from melting and recrystallization of iron-rich pigeonite, whereas the glass contains components derived from plagioclase and augite. Other evidence of shock in the silicates is provided by occasional pressure shadows in pyroxene. In addition, the ilmenite grains commonly display sigmoidally deformed, translation-twin

TABLE 13. Silicate Analyses of Lunar Sample 12063,9

Unshocked				Shocked, Unmelted				Shocked, Melted						
a. Plagioclase														
SiO <sub>2</sub>	48.9	Si	8.925	}	A	47.0	Si	8.756	}	A	48.2	Si	8.979	
Al <sub>2</sub> O <sub>3</sub>	32.1	Al	6.899			32.2	Al	7.068			31.2	Al	6.850	
TiO <sub>2</sub>	0.08	Ti	0.011			0.07	Ti	0.009			0.05	Ti	0.007	
FeO	0.70	Fe	0.106			0.70	Fe	0.108			0.72	Fe	0.112	
MgO	0.24	Mg	0.066			0.20	Mg	0.054			0.16	Mg	0.045	
CaO	17.4	Ca	3.399			17.6	Ca	3.509			17.0	Ca	3.389	
Na <sub>2</sub> O	1.14	Na	0.404	}	B	1.04	Na	0.374	}	B	1.08	Na	0.390	
K <sub>2</sub> O	0.05	K	0.011			0.07	K	0.017			0.09	K	0.022	
	100.6	O	≡ 32			98.9 *					98.5 *			
ΣA			16.007 †			15.995 †					15.993 †			
ΣB			3.814			3.900					3.801			
b. Fayalite														
SiO <sub>2</sub>	30.0	Si	1.002	}	1.993									
TiO <sub>2</sub>	0.11	Ti	0.003											
FeO	67.2	Fe	1.881											
MnO	0.77	Mn	0.022											
CaO	0.75	Ca	0.027											
MgO	1.21	Mg	0.060											
	100.0													

\* Low total may be due to cation deficiency as reported by Weill *et al.* (1970).

† See discussion of allocation in feldspar of Ashmore chondrite. Weill *et al.* (1970) put Fe and Mg with the alkalies and assume substitution for Ca.



lamellae, usually considered to result from high shock pressures.

The typical, locally intense, shock effects described above from sample 12063,9 are not displayed in sample 12004,11. The fayalite+cristobalite assemblage is not present. Much of the pyroxene shows undulatory extinction, and "ophitic" pyroxene grains when viewed in polarized light appear to have been broken into blocky aggregates. Both the undulatory extinction and the formation of aggregates were possibly caused by shock, which, however, was of much lower intensity and of more uniform distribution than that imposed on the 12063,9 sample. The ilmenite grains are usually free of the intense deformation observed in the ilmenite of the more severely shocked 12063,9 sample, but some of the ilmenite grains contain very small amounts of exsolved rutile that may be a result of shock.

### *Troilite*

Troilite, FeS, a common opaque mineral in Apollo 11 rocks, was reported as always associated with Fe metal in a eutectic texture (Skinner, 1970). In the Apollo 12 rocks troilite is present in this association and texture where it is late in the crystallization sequence. It commonly occurs without Fe metal, however, and is paragenetically related to the oxide minerals (i.e., ilmenite and the spinels). Microprobe analyses of troilite, given in Table 14, demonstrate

that troilite coexisting with ilmenite or spinel contains appreciably more titanium than troilite coexisting with silicates. This apparently is associated with the partitioning of titanium between these phases. The amount of titanium in troilites of 12004,11 is greater than in sample 12063,9 (Table 14).

Troilite in sample 12004,11 associated with spinel and ilmenite (Table 14) contains more Ni ( $\sim 0.1$  wt %) than that coexisting with silicates (Table 16), and this troilite is the only one in either sample that contains detectable Ni (i.e.,  $\geq 0.02$  wt %). In sample 12004,11 the cobalt content appears to be nearly constant in the troilite but higher than in sample 12063,9. In meteorites, troilites occasionally have been reported to contain appreciable chromium (Keil, 1968), but in this lunar sample they always contain less than 0.02% Cr.

### *FeNi Metal*

The Fe metal phase in the Apollo 11 rocks was always associated with troilite (Skinner, 1970), but in the Apollo 12 specimens the metal phase has a much more complicated paragenesis. It most commonly is *not* associated with troilite. For example, in sample 12063,9 it occurs with the oxides, pyroxene and plagioclase, with troilite and ilmenite in the shock-produced fayalite+cristobalite assemblage, and in the end-stage eutectic intergrowth with troilite. In sample 12004,11 the metal phase is associated

TABLE 14. Electron Probe Analyses of Troilites\*

Association †:	Sample 12063,9			Sample 12004,11	
	1 il or sp	2 px + plg	3 fa + gl	4 il + sp	5 plg + crist
Fe	63.2	63.4	63.1	63.4	63.4
S	36.4	35.9	36.0	36.4	36.3
Co	0.03	0.08	0.06	0.12	0.12
Ti	0.15	0.02	0.05	0.24	<0.02
Ni	<0.03	<0.03	<0.03	0.10	<0.03
Mn	0.01	0.01	0.01	...	...
Cr	<0.02	<0.02	<0.02	...	...
Totals	99.8	99.4	99.2	100.3	99.8

\* 1, 3, 4, and 5 represent the averages of two analyses; 2, the average of four analyses.

† Abbreviations: il, ilmenite; sp, spinel; px, pyroxene; plg, plagioclase; fa, fayalite; crist, cristobalite.

with all of the minerals, including the early-formed olivine, unlike 12063,9.

Reid *et al.* (1970) report that in rock 12004 the metal phase contains from <1 wt % to as much as 30 wt % nickel. A considerable number of metal grains have been analyzed in a variety of associations (Table 15). The metal phase occurring in the olivine of sample 12004,11 ranges in nickel content from 4 to 30 wt %, whereas the metal phase enclosed by opaque minerals or silicates other than forsteritic olivine contains nearly constant amounts of nickel (3.5 to 4.5%) and cobalt (1.5 to 1.7%). These latter values are also representative of the approximate compositions for all FeNi metal analyzed from sample 12063,9 (Table 15).

The nickel-to-cobalt ratio in the metal phase always exceeds unity.\* Whereas this ratio in the 12063,9 sample varied only from 2.4 to 3.0, it varies from 2.4 to 12.5 in the metal enclosed by olivine in the 12004,11 sample but only from about 2.2 to 2.8 when the metal occurs within opaque minerals or silicates other than olivine. Inasmuch as the cobalt content of the metal phase is relatively constant regardless of its association, the higher ratios for the metal associated with the early-formed olivine evidently reflect the

preference of nickel for the early-formed metal (Reid *et al.*, 1970).

The nickel content of the forsteritic olivine containing metal grains was determined by microprobe analyses to be always less than 0.05%, i.e. 0.04 to <0.01% (the measured detectability limit).

Ringwood (1956) has demonstrated that complete solid solution exists between  $Mg_2SiO_4$  and  $Ni_2SiO_4$ , and terrestrial olivines have been reported with ~0.5% nickel (Deer, Howie, and Zussman, 1962a), so it is curious that the nickel partitioning in sample 12004,11 is strongly in favor of the metal phase. Equilibrium did not exist between individual metal particles coexisting in olivine grains, as evidenced by the large compositional differences between the metals even within the same olivine grains. In consequence, equilibrium did not exist between the olivine and the metal phases, and this apparent nickel partitioning is not representative of equilibrium crystallization.

According to the phase relations in the iron-nickel system, the metal grains containing more than a small percentage of nickel should consist of a mixture of kamacite and taenite, provided subsolidus reequilibration has taken place in the primary metal phase. In sample 12004,11, however, the metal grains occurring in olivine are very small (i.e.,

\* The other opaque minerals and the silicates show the reverse trend, i.e., Ni/Co < 1.

TABLE 15. Electron Probe Analyses of Metal\*

Association †:	Sample 12063,9			Sample 12004,11			
	1 px	2 sp	3 tr	4 px	5 px + sp	6 ol	7 ol
Fe	93.6	94.4	95.4	94.8	92.6	94.4	67.4
Ni	3.97	4.28	3.24	4.14	3.81	4.11	29.7
Co	1.49	1.66	1.08	1.60	1.47	1.67	2.37
Ti	0.06	0.14	0.06	0.05	0.40	0.02	<0.03
Cr	<0.03	0.07	<0.03	<0.03	0.42	...	...
Mn	0.01	0.01	...	<0.03	<0.03	...	...
Totals	99.1	100.6 ‡	99.8	100.6 §	98.7 §	100.2	99.5

\* Analysis 2 represents the average of three analyses; 4, the average of six; 5, the average of two. Analysis 6 is a lower limit and 7 is an upper limit for Ni content of the metal phase in olivine with seven additional analyses of 4.65, 4.93, 5.32, 11.0, 15.4, 19.8, and 22.1% Ni.

† Abbreviations: px, pyroxene; sp, spinel; tr, troilite; ol, olivine.

‡ Includes Si = 0.05 and P = 0.03%.

§ No detectable V, i.e., <0.01%.

1–10  $\mu\text{m}$ ) and the plessite (kamacite-taenite) intergrowth textures, common in meteoritic material, have not been observed in normal reflected light.

Microprobe analyses of three metal grains in the 12063,9 sample give silicon values ranging from 0.05 to 0.13 wt % and phosphorous values ranging from <0.01 to 0.03 wt %.\* The metal phase also contains detectable amounts of chromium when it is associated with spinel, but less than the limit of detection when the metal phase occurs in or with silicates, thus demonstrating a measurable partitioning of this element between spinel and metal. A similar relationship also was found for the Ti content of the metal phase associated with spinel.

There are other important differences between the metals in the Apollo 11 and 12 samples. The metal from the Apollo 11 samples was found to be essentially free of nickel but contained up to 0.7% cobalt (Ramdohr and El Goresy, 1970; Simpson and Bowie, 1970) and was always one of the last minerals in the paragenetic sequence. In fact, the presence of nickel in the metal was usually considered indicative of meteoritic contamination. In view of the composition of the metal phase in the Apollo 12 samples where nickel could not be due to such contamination, the interpretations concerning the origin of the metal phase in the Apollo 11 samples should be reconsidered.

### Oxides

Three optically distinct "spinel" occur in sample 12063,9. One of these appears gray in reflected light; it occurs in tiny grains inside pyroxene and is sometimes associated with metallic iron. These isotropic gray spinel grains are too small for microprobe analysis. Of

the remaining two "spinel,"\* one is brown and anisotropic, whereas the other is isotropic and blue in reflected light. The latter two spinels almost invariably occur together; blue spinel commonly occurs as cores rimmed by brown spinel. Occasionally patterns of mutual intergrowth of brown and blue spinel are displayed. The phase boundaries between these spinels are sometimes sharply defined but more generally tend to be diffuse or poorly resolved by the microscope. The textures closely resemble those described by Haggerty and Meyer (this report). Ilmenite\* is commonly in physical contact with brown spinel; such contact also occurs, though rarely, between blue spinel and ilmenite.

In sample 12004,11 there are two optically distinct "spinel"; one is blue and isotropic and the other is pink and clearly anisotropic as viewed in reflected light. The blue and pink phases coexist; cores of blue spinel are rimmed by pink spinel resembling the association of blue and brown spinel in 12063,9. The amount of blue relative to nonblue spinel in 12004,11 is two to three times greater than in 12063,9, however, so that many grains of the blue phase have little or no rim of the pink spinel phase. Also some of the blue spinel in this sample is associated with olivine, as well as with the other minerals.

Microprobe analyses were performed on coexisting blue and brown spinels in sample 12063,9 and on coexisting blue and pink spinels in sample 12004,11 (Table 16). The compositions of these phases are plotted on Fig. 61 of the report by Haggerty and Meyer (pp. 229–238), and our conclusions concerning

\*The brown "spinel," an Fe-Ti-Cr oxide, is distinctly anisotropic and thus not a true cubic spinel; however, because its composition is near  $\text{AB}_2\text{O}_4$  and it is usually associated with the blue spinel, it will be designated brown spinel.

\*These values are much lower than those reported by Keil (1968) for kamacite in enstatite chondrites, but are similar to those obtained for the Ashmore chondrite described elsewhere in this report.

\*The ilmenite phase in this lunar sample is always stoichiometric regardless of its mineral association. One typical analysis is given in Table 15 showing that  $\text{TiO}_2$  and FeO together account for nearly 99 wt % of the mineral.



TABLE 16. Electron Probe Analyses of Opaque Oxides \*

	Sample 12063,9							Sample 12004,11	
	Blue Spinel				Brown Spinel		Ilmenite	Blue Spinel	Pink Spinel
	1	2 †	3 †	4	2A †	3A †	5	6	6 A †
TiO <sub>2</sub>	8.71	9.22	6.74	8.89	25.6	25.8	52.7	4.66	28.3
FeO	36.3	39.0	36.6	36.9	50.7	51.3	46.1	30.0	55.5
MgO	3.40	2.26	1.89	3.30	2.08	1.70	0.32	4.58	0.88
Cr <sub>2</sub> O <sub>3</sub>	40.0	38.3	42.2	39.6	16.4	16.3	0.32	48.5	11.0
Al <sub>2</sub> O <sub>3</sub>	10.6	10.3	11.1	10.1	4.52	4.37	0.09	11.5	2.77
MnO	0.58	0.38	0.40	0.59	0.36	0.36	0.37	0.42	0.39
V <sub>2</sub> O <sub>5</sub>	0.99	0.86	0.97	0.87	0.70	0.62	...	0.98	0.48
CoO	0.05	0.04	0.04	0.05	0.07	0.07	0.04	0.06	0.13
NiO	<0.02	<0.02	<0.02	<0.02	<0.02	<0.02	<0.02	<0.02	<0.02
CaO	0.03	0.04	0.05	0.02	0.05	0.04	<0.02	0.03	0.04
Totals	100.7	100.4	100.0	100.3	100.5	100.6	99.9	100.7	99.5

\* The compositions of these phases are plotted on Fig. 61 in the lunar section by Haggerty and Meyer (this report).

† Coexisting spinels: 2 + 2A, 3 + 3A, 6 + 6A.

the spinel mineralogy are similar to those mentioned by them.

The occurrence of the blue spinel commonly rimmed by brown or pink spinel is suggestive of a reaction of the blue spinel with the magma to produce brown or pink spinel. If the compositional separation of these spinels is caused by a peritectic along the join (FeMg)<sub>2</sub>TiO<sub>4</sub>-Fe(Cr,Al)<sub>2</sub>O<sub>4</sub> as suggested by Kushiro, Nakamura, and Akimoto (1970), it would be difficult to explain the compositions of spinels in Apollo 11 rocks (see Fig. 61 of Haggerty and Meyer, this report). These plot compositionally between the two Apollo 12 spinel groups, thereby effecting an almost complete sequence of compositions along this join. It is possible that a peritectic or a solvus may exist on or to the FeO side of the join but that the immiscibility gap does not extend appreciably to the TiO<sub>2</sub> side of the join.

#### MELTING RELATIONS OF MATERIALS OF LUNAR COMPOSITION

*Arnulf Muan and J. F. Schairer*

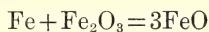
Lunar rocks were at least partly molten at some stage of their development. In attempting to understand the

origin and mechanism of formation of these rocks, it is necessary to ascertain the temperature range over which crystals and liquids would coexist in them and the sequence of appearance of the various crystalline phases under equilibrium conditions. Toward this end, we have used "synthetic moon" samples to develop experimental methods for studying liquid-solid equilibria in lunar materials under conditions approximating those thought to prevail on the moon. The method consists of equilibrating prereduced mixtures in iron crucibles sealed into silica-glass capsules under vacuum and quenching the capsules rapidly to room temperature for phase identification.

The experiments were performed on a mixture of the following composition (weight %) synthesized from reagent-grade chemicals: SiO<sub>2</sub>, 43.0; Al<sub>2</sub>O<sub>3</sub>, 13.0; TiO<sub>2</sub>, 7.0; FeO, 17.0; MgO, 8.0; CaO, 11.5; Na<sub>2</sub>O, 0.5. This composition is similar to that reported for lunar rocks from the Apollo 11 mission (Lunar Sample Preliminary Examination Team, 1969). The mixture was heated five times to 1300°C in air in a platinum crucible, to yield a homogeneous glass, which was then heated in a 70% Ag 30% Pd con-

tainer at 1100°C for 18 hours in a CO<sub>2</sub>-H<sub>2</sub> atmosphere with a CO<sub>2</sub>/H<sub>2</sub> ratio of 14, corresponding to an oxygen pressure of  $\sim 10^{-10}$  atm. The second heat treatment served to reduce most of the iron to the divalent state and to partly crystallize the mixture prior to the final equilibration runs. Samples of this pre-reduced mixture were then placed in small iron crucibles, sealed under vacuum in silica-glass capsules, and equilibrated for various lengths of time (4 hours to 30 days) in a vertical-tube quench furnace in the temperature range between the liquidus and the solidus (approximately 1075°–1200°C).

Chemical analyses for divalent and trivalent iron (Ingamells, 1960) were performed on the prereduced mixture and on a sample equilibrated in an iron crucible within a sealed silica capsule at a temperature slightly above the liquidus. It is seen that there is a moderate increase in the total iron oxide content during the equilibration in the iron crucibles as carried out in the present investigation (Table 17), but that the compositions of the samples after equilibration are still a good approximation of those reported for the Apollo 11 lunar samples. The increase in FeO during the equilibration runs can be ascribed mainly to the reaction between Fe of the crucible and the Fe<sub>2</sub>O<sub>3</sub> still remaining in the prereduced mixture ( $\sim 3\%$ , see Table 17) according to the reaction:



This increase in the FeO content can be eliminated or minimized in future ex-

periments on synthetic mixtures by carrying out the prereduction step at a somewhat higher temperature and at a somewhat lower CO<sub>2</sub>/H<sub>2</sub> ratio than those used in the present investigation. An increase in FeO content during equilibration in the Fe crucibles within sealed silica tubes is not expected to occur in experimentation with actual lunar samples because the latter contain essentially no ferrie iron.

The use of a closed system rather than an open system in the final equilibration runs has the following advantages: The method provides a ready means of imposing controlled vacuum conditions on the samples during equilibration; volatilization of oxide components with relatively high vapor pressures (e.g., alkali oxides) is minimized; the sealed-tube technique permits the addition of sulfur to our synthesized mixtures, or the study of sulfur-containing "real" lunar materials, without serious losses of this element.

The results of the equilibration runs (Table 18) may be summarized as follows. The liquidus temperature determined for samples equilibrated in contact with metallic iron is 1185°C. The primary crystalline phase is clinopyroxene. Plagioclase appears as a crystalline phase at only a slightly lower temperature (1180°C), and a third crystalline phase, ilmenite, appears at approximately 1125°C. Determination of the solidus temperature is difficult because of the high viscosity of the liquid and the sluggishness of the reactions at the lowest temperatures used in this investi-

TABLE 17. Results of Chemical Analysis for Divalent, Trivalent, and Total Iron

	Original Mixture	Sample Prereduced at 1100°C in CO <sub>2</sub> /H <sub>2</sub> = 14	Sample Equilibrated in Fe Crucible in Sealed Silica Capsule
FeO	...	13.88	19.06
Fe <sub>2</sub> O <sub>3</sub>	18.9	2.96	...
Total iron as FeO	17.0	16.54	19.06

TABLE 18. Results of Equilibration Runs for Samples in Equilibrium with Metallic Iron

Initial Condition	Temperature, °C	Time	Phases Present *
Crystallized at 1100°C CO <sub>2</sub> /H <sub>2</sub> = 14)	1200	19 hours	Liq
	1900	24 hours	Liq
	1185	4 days	Pyr (tr.) + Liq
	1180	3 days	Pyr (s.a.) + Plag (s.a.) + Liq
	1175	19 hours	Pyr (s.a.) + Plag + Liq
	1150	23 hours	Pyr + Plag + Liq
	1135	3 days	Pyr + Plag + Liq
	1125	4 days	Pyr + Plag + Ilm (s.a.) + Liq
	1115	8 days	Pyr + Plag + Ilm + Liq
	1100	4 days	Pyr + Plag + Ilm + Liq (s.a.)
	1090	10 days	Pyr + Plag + Ilm + Liq (tr.)
	1075		Pyr + Plag + Ilm
Held at 1200°C for complete melting	1200-1090	30 days	Pyr + Ilm + Liq

\* Abbreviations: Pyr, pyroxene; Plag, plagioclase; Ilm, ilmenite; Liq, liquid; s.a., small amount; tr., trace.

gation. It appears, however, that the solidus temperature is somewhere in the range of 1075°-1090°C.

Supplementary equilibration runs were made in air to show the drastic effect of oxygen-potential variation on liquidus temperatures and on the crystallization process. At the relatively high oxygen potential of air (0.2 atm), the liquidus temperature is about 100°C higher than it was in contact with metallic iron (1298° versus 1185°C), and similarly the solidus temperature has increased by ~50°C (~1130° versus ~1080°C). Furthermore, the sequence of appearance of crystalline phases has changed. Whereas in contact with metallic iron, clinopyroxene was the primary crystalline phase (1185°C), followed by plagioclase (1180°C), and ilmenite (1125°C), the sequence of appearance of crystalline phases in air is hematite (1298°C), pseudobrookite (1293°C), plagioclase (~1195°C), and clinopyroxene (~1180°C).

The liquidus and solidus temperatures obtained in the present investigation of a simulated lunar sample are in general accord with crystallization data at 1 atm total pressure reported for specific Apollo 11 lunar rocks or synthetic mixes by O'Hara, Biggar, and Richardson (1970), by Ringwood and Essene (1970), and by Kushiro, Nakamura, and Haramura

(1970). Differences in the results of these three groups of investigators are caused partly by differences in the individual samples studied and partly by differences in the types of containers and in the nature of the atmosphere used in the equilibrations. The present authors believe that equilibrations under vacuum in iron crucibles in sealed silica capsules provide conditions most closely resembling those that are likely to have been in effect during development of lunar rocks and also provide the most reproducible experimental conditions for studying the crystallization behavior of lunar rocks. Because of the remarkable uniformity in composition of the Apollo 11 rocks, the data on one synthesized mixture as obtained in the present investigation provide valuable background information for interpretation of the formation of one suite of lunar rocks.

METEORITES

W. B. Bryan and G. Kullerød

Chondrites are the most common of all meteorites, comprising about 85% of all known falls. Although these "stony meteorites" are composed of 80% or more silicate minerals, there is almost no information on the relative proportions of silicates and other nonopaque phases, in contrast to the considerable



body of data on opaque mineral proportions obtained by point-counting in reflected light (Keil, 1962, 1968). Accordingly, a special effort was made to estimate mineral proportions in one of the samples studied this year, with the use of microprobe traverses as described below. Quantitative microprobe analyses\* were also made on the principal mineral phases, in order to permit classification of our samples according to the compositional and textural scheme recently proposed by Van Schmus and Wood (1967). These authors recognize five major compositional groups, designated E, C, H, L, and LL. The C group includes the so-called carbonaceous chondrites, and the remainder are most readily distinguished by the increasing Fe/Mg ratio of the olivine and pyroxene, going from E to LL. Each group in turn is divided into six textural groups, recognized by the varying degree of recrystallization of matrix and chondrules, type 6 being the most coarsely and completely recrystallized and also the most completely "equilibrated," as evidenced by uniformity of composition of individual mineral phases.

Work this year has been centered on two olivine-bronzite chondrites, which have not previously been studied in detail or precisely classified. One of these, the Ashmore meteorite, was recently discovered in a plowed field in Texas and may be a new find (Craig *et al.*, 1969). Preliminary examination showed that the Ashmore meteorite is relatively unweathered, is well crystallized, and is an equilibrated chondrite, with little or no compositional variation within individual mineral phases. Thus, the Ashmore chondrite seemed especially well suited for estimates of silicate proportions by means of traverses with the electron microprobe. Quantitative mineral analyses were also carried out to establish the classification of this meteorite and to

provide data on relative count rates to aid in identification during the probe traverses. The elements Ca, Mg, and Si were found to be most useful for this purpose. These elements were continuously recorded on chart paper, at a sample traverse rate of 60  $\mu\text{m}$  per minute, with a corresponding chart rate of 1 inch per minute. Each of the major mineral phases was identified from its characteristic peak heights on the chart paper, and the total length of traverse within each phase, divided by the total traverse length, gives its estimated volume proportion.

The Brownfield meteorite was studied only in sufficient detail to establish its classification and its possible relation to the Ashmore meteorite. It has proved to be much finer grained and relatively more weathered than the Ashmore meteorite, and thus a detailed modal analysis was not attempted. It is clearly a different fall, and appears identical with the Brownfield no. 2, found in Texas in 1964 (E. P. Henderson, personal communication).

### *The Ashmore Meteorite*

Texturally, the Ashmore meteorite shows features typical of types 5 and 6 of Van Schmus and Wood (1967). Chondrules are recognizable, but much of the matrix is recrystallized to grains  $>0.1$  mm in diameter. Augite could be detected only with the aid of a finely focused probe beam, however, and feldspar similarly was recognized mainly by its fluorescence under the probe beam; a few grains were clearly visible under the microscope. There is little variation in composition of individual mineral phases from grain to grain, as indicated by nearly constant count rates for all major elements. Accordingly, quantitative analyses of olivine, pyroxene, and opaque phases were made on single grains, chosen for freedom from impurities or cracks, and for sufficient surface area to avoid overlapping of

\*The microprobe was purchased with assistance from National Science Foundation grant GP 4384.

TABLE 19. Compositions of Analyzed Minerals, Compared with Average Mineral Compositions of Group H Chondrites \*

	Olivine		Orthopyroxene			Feldspar			Chromite		
	Fo	Fa	En	Fs	Wo	Or	An	Ab	Fe	Mg	Mn
Ashmore chondrite	81.2	18.8	81.9	16.6	1.5	5.6	12.1	82.3	80.2	17.3	2.5
Average group H	80.7	19.3	81.6	16.8	1.6	5.8	12.3	81.9	83.1	14.0	2.9

\* Van Schmus, 1969.

analyzed spots. The feldspar analysis, however, is a composite of counts taken from a dozen grains chosen at random because of their very small size. These, too, showed little grain-to-grain variation. On the basis of mineral compositions (Table 19) and textural criteria, the Ashmore meteorite is readily classified as an "equilibrated" group H, type 5 chondrite. In Table 20 the modal mineral proportions in the Ashmore meteorite are compared with the typical values for the group H chondrites. In accordance with the practice of Keil (1962, 1968) the mode has been expressed in weight percent, with the use of mineral densities appropriate to the compositions determined by microprobe analyses (Table 21); because the densities are not precisely known, however, the mode as measured directly in volume percent is also given (Table 22).

The area used to estimate silicate mineral proportions was limited to about 5 mm<sup>2</sup> because of both mechanical restrictions on traverse length (about 4 mm) and the time required (about 1 hour) for a complete traverse. Three traverses totaling about 11 mm were run

across this area, which was selected as being reasonably representative of the finer grained matrix on the basis of optical examination. Thus, the silicate proportions must be regarded as representative only of the matrix; a similar area selected within a large chondrule or including a large olivine grain could clearly lead to different results. Apatite forms relatively large but widely scattered grains, which were identified both optically and by semiquantitative counts for Ca and P. It was encountered in only one of the three traverses, however, and the volumetric estimate is probably generous.

Other minerals observed include lawrencite, which is readily identified from its deliquescence in air. Subsequent decomposition of lawrencite to limonite and HCl rapidly produces distinctive rusty patches on freshly cut surfaces. Lawrencite is entirely removed during the washing and polishing of the thin section, and its removal leaves pits in which other minerals are exposed, so it may not be adequately accounted for under "other" in the modal data. Small amounts of copper, chalcopyrrhotite, ilmenite, and taenite in kamacite, were observed. Augite, identified by simultaneously strong counts for Ca, Mg, and Si in the probe traverse, is not readily distinguished optically. It is confined to poorly crystallized interstitial matrix material associated with olivine in remnants of partly recrystallized chondrules.

The analyzed minerals conform closely in composition to the averages for group H, type 5 chondrites (Van Schmus, 1969). The complete olivine analysis

TABLE 20. Modal Proportions of Major Opaque Minerals and Total Silicate, wt % \*

	Ashmore Olivine- Bronzite Chondrite	Average H Group Chondrite †
Kamacite	15.3	16.80
Troilite	6.3	5.03
Chromite	0.9	0.22
Silicate	77.5	77.95

\* Densities assumed: kamacite, 8.0; troilite, 5.0; chromite, 4.8; silicate, 3.4.

† Data from Keil, 1962, p. 4059.

TABLE 21. Microprobe Analyses of Oxide and Silicate Phases, Ashmore and Brownfield Chondrites

	Hypersthene *	Olivine †	Plagioclase *	Chromite *
SiO <sub>2</sub>	56.7	40.3	64.6	0.14
Al <sub>2</sub> O <sub>3</sub>	0.19	0.00	21.5	6.19
TiO <sub>2</sub>	0.19	...	...	2.28
FeO	11.3	17.10	0.21	29.3
MnO	0.55	0.51	...	0.87
MgO	31.3	42.5	0.07	3.47
CaO	0.81	0.04	2.58	...
Na <sub>2</sub> O	0.00	...	9.70	...
K <sub>2</sub> O	...	...	1.01	...
Cr <sub>2</sub> O <sub>3</sub>	...	...	...	56.4
Totals	101.04	100.45	99.67	99.73 ‡
Cations/Oxygen	4.006/6	2.98/4	20.07/32	24.05/32

\* Ashmore meteorite.

† Brownfield meteorite.

‡ Includes V<sub>2</sub>O<sub>5</sub>, 0.72; ZnO, 0.36.

given is for the Brownfield meteorite; partial Fe and Mg analyses of olivine in the Ashmore meteorite gave an almost identical composition, Fa 18.8. The plagioclase analysis yields an almost stoichiometric formula if Mg and Fe<sup>2+</sup> are allotted to the tetrahedral sites and a formula unit of the type Ca(Fe,Mg)Si<sub>3</sub>O<sub>8</sub> is assumed. This allocation does not account for the deficiency in silica, however. The slight apparent departure from stoichiometry could be due to small errors in standards, instrumental drift, and contributions to the counts from olivine or pyroxene adjacent to these very small grains. The kamacite grain analyzed was chosen for its apparent lack of zoning or exsolution. It contains 93.2% Fe, 4.79% Ni, 0.69% Co, 0.05%

Si, 0.02% Mn, and <0.01% P. Elsewhere, however, kamacite sometimes shows irregular patches of taenite, distinguished by a more pinkish color in reflected light; variations in the intensity of the color imply considerable variation in nickel content, but this particular feature has not been investigated in detail. Troilite is essentially stoichiometric, with 0.09% Co, <0.03% Ni, and 0.38% Si. Of the minerals analyzed, the chromite is of most interest, being somewhat lower in FeO and higher in MgO than the typical H5 chromites reported by Bunch, Keil, and Snetsinger (1967). The chromite standard 52NL11 was used for these elements. The Ashmore chromite contains appreciable amounts of ZnO, resembling some terrestrial chromites in this respect.

TABLE 22. Modal Mineral Proportions in Ashmore Meteorite, volume %

Orthopyroxene	24.1	} 87.2 Nonopaque *
Olivine	38.1	
Feldspar	11.1	
Augite	7.1	
Apatite	0.4	
Other	6.4	} 12.8 Opaque
Kamacite	7.3 *	
Troilite	4.8 *	
Chromite	0.7 *	
	100.0	

\* Total silicate and opaque mineral proportions by point count in reflected light, count area = 13 mm<sup>2</sup>, 4354 points.

Minerals observed in polished section include graphite, blue ilmenite, copper, pentlandite, magnetite, and goethite in addition to those already noted. Graphite (microcliftonite) may be observed at high magnification in many grains of kamacite, oriented along the octahedral (111) planes of the metal. It probably forms by breakdown of cohenite (Fe<sub>3</sub>C). Some ilmenite grains enclosed by troilite contain bluish areas, resembling the blue ilmenite produced when stoichiometric synthetic ilmenite is heated with sulfur.



The blue color may be due to loss of iron to form iron sulfide. Metallic copper occurs in tiny grains associated with kamacite and troilite, and may result from breakdown of chalcopyrrhotite. Pentlandite occurs between grains of kamacite and troilite and in tiny fissures in troilite. It apparently formed by reaction between troilite and the Fe,Ni alloy. The latter two minerals also extend into fractures in the silicate matrix, indicating the relative mobility of the nickel-iron and sulfide phases in comparison with the silicates. Magnetite and goethite are restricted to a weathered rim <2 mm thick on the outer surface of the meteorite.

### *The Brownfield Meteorite*

The Brownfield meteorite differs considerably in texture from the Ashmore meteorite. The chondrules are much more distinct and less completely recrystallized than those in the Ashmore meteorite. Some are porphyritic, others are of the barred olivine type, and some finely barred varieties appear to consist mainly of radiating orthopyroxene with narrow lamellae of augite. Still others are spherical aggregates of fine dusty material. The diameters of the chondrules range from several millimeters to less than 0.5 mm. In general, the texture is that of closely packed chondrules of varying size, showing varying degrees of crystallization, with angular silicates less

than 0.1 mm in diameter as interstitial matrix. Comparisons of count rates for Fe, Mg, and Ca on orthopyroxene and chromite, and quantitative analysis of the olivine, show that the major minerals are almost identical in composition with those in the Ashmore meteorite. Kamacite is the most abundant opaque phase and is much coarser than in the Ashmore meteorite, averaging about 0.5 mm but extending outward into the silicate matrix, as irregular wirey stringers. This kamacite appears to be free of graphite. Troilite shows pressure lamellae due to shock. There are small amounts of ilmenite, chromite, and a second spinel, possibly aluminous. There is evidence of brecciation and the spontaneous melting texture described by Ramdohr and Kullerud (*Year Book 61*, p. 163). These features would place the Brownfield chondrite in group H, type 4, of Van Schmus and Wood (1967).

There is no evidence of lawrencite in the Brownfield meteorite. In addition to a weathered surface zone, perhaps 1-2 mm thick, this meteorite displays relatively strong weathering throughout the sample, indicated by troilite oxidized to magnetite, goethite, and even maghemite, sometimes with traces of covellite and a gel-type pyrite. Secondary pentlandite is observed in some troilite grains, where it is occasionally associated with chalcopyrrhotite, chalcopyrite, and even bornite.

## CHEMICAL AND MINERALOGICAL PETROGRAPHY

### PETROLOGY AND GEOCHEMISTRY OF VOLCANIC ROCKS FROM TONGA

*W. B. Bryan and A. Ewart\**

Compared with other island arc regimes along the western Pacific margin, the Tonga area shows some unique features. The trench and associated volcanoes define a virtually straight line,

which can be traced from just north of New Zealand almost to Samoa, in contrast to the arcuate pattern so well displayed by the Japanese islands or the Marianas. The trench appears to bend sharply to the west near Samoa, and Sykes (1966) has shown that this abrupt change in direction is reflected in an equally abrupt bend in the associated Benioff zone. Recent studies (Selater and Menard, 1967) have shown that the Fiji

\* Dept. of Geology and Mineralogy, University of Queensland, Brisbane, Australia.

plateau west of Tonga is an area of unusually high heat flow. The implied structural and crustal peculiarities might be expected to impose unusual petrographic or geochemical properties on the lavas of Tongan volcanoes, but there are almost no descriptions of the rocks of these remote islands other than those originally given by Harker (1891). With the exception of the brief descriptions by Lister (1891) and the study of Eua Island by Hoffmeister (1932), there have been no systematic geologic investigations of the islands.

During July and August 1969 field studies were carried out on the predominantly coral islands of Eua, Tongatapu, and Vavau, and the volcanic islands of Hunga Ha'apai, Late, and Fonualei in order to make a representative collection of volcanic rocks for chemical and mineralogical study. Sample locations and geological features were recorded on topographic sketch maps prepared from aerial photographs. A sample of the dacite from the 1967 eruption of Metis shoal (Melson, Jarosewich, and Lundquist, 1970) was provided by W. G. Melson and has been included in the laboratory studies. Trace-element analyses by optical spectrography were carried out in the Department of Geophysics and Geochemistry, Australian National University, in collaboration with Dr. S. R. Taylor. Electron microprobe analyses\* were made at the Geophysical Laboratory, with standards and correction procedures as described by Boyd (*Year Book 66*, pp. 327-334) and by Boyd, Finger, and Chayes (*Year Book 67*, pp. 210-215). Field work was sponsored by the Smithsonian Institution and was supported by research grants from the National Geographic Society and the University of Queensland. Hyphenated numbers (111547-20) refer to specimens placed in the collection of the U. S. National Museum.

\* The microprobe was purchased with the assistance of National Science Foundation grant GP 4334.

### *Geological Summary*

The Tonga group consists of an eastern line of coral islands along a submarine ridge 60-80 miles west of the trench and active volcanic islands and seamounts arranged along a second ridge about 100 miles west of the trench. These relationships have been well illustrated in a recent paper by Karig (1970). Volcanic rocks appear to be absent on the coral islands with the exception of Eua, where a dike complex intruding slightly metamorphosed basic lavas, gabbros, and tuffs is exposed near sea level on the eastern shore. Fossiliferous limestone overlying the volcanic rocks is of Eocene age (Hoffmeister, 1932, p. 33). A younger sequence of very weathered volcanic tuffs is exposed along the central highlands of Eua.

Each of the volcanic islands is distinctive both in morphology and in the petrography and chemistry of its rocks. Fonualei is essentially a dacite volcano, consisting of an outer tuff ring about 1 mile in diameter, which overlies thick dacite flows and encloses a central caldera, now largely filled by dacite flows, and a pyroclastic cone, which rises to about 600 feet. This cone is breached on its eastern side and contains a deep explosion pit. A partly collapsed scoriaceous dacite dome fills the area between the cone and the inner wall of the caldera to the southwest. Very rough, scoriaceous lavas fill most of the depression between the cone and the caldera wall on the north and west. Late Island is an almost circular, symmetrical andesite volcano about 4 miles in diameter, rising to a central peak about 1800 feet above sea level. A deep, steep-walled central crater is breached to the southwest. There is a group of small cinder cones on the northwest side of the summit crater, and two large pit craters in a graben-like depression on the northeast coast, one of which contains a salt-water lake. The main summit area is covered with welded glassy spatter. Blocks imbedded in the

splatter and flows along the north coast are all composed of andesite or basaltic andesite. A more siliceous andesite capping the low sea cliff on the northwest coast apparently originated from vents associated with the cinder cones. Hunga Ha'apai, and its companion island, Hunga Tonga, appear to be the western and northern remnants of a formerly larger island, which may have enclosed a large caldera centered on the rocky shoals southeast of the islands. Hunga Ha'apai is made up of interbedded siliceous andesite flows and scoria that dip gently to the west away from the supposed caldera center, as originally suggested by Lister.

### *Petrography*

Most of the volcanic rocks of Tonga are characterized by very simple mineralogy, with calcic plagioclase, augite, and hypersthene accounting for the bulk of all the rocks. Rocks from Eua show varying degrees of deuteric alteration or uranalitization, but rocks from the other islands are free of weathering or other secondary alteration. Magnetite appears as scattered microphenocrysts only in the dacites and more siliceous andesites. In the basalts and basaltic andesites, magnetite appears as skeletal crystals in the groundmass or may be completely absent. In these rocks plagioclase and augite are typical phenocrysts, with or without hypersthene. Either hypersthene or pigeonite invariably appears in the groundmass, and hypersthene is a typical phenocryst mineral in the more siliceous andesites. It is the only phenocryst pyroxene in one of the dacites of Fonualei. The range of composition in the phenocryst minerals is relatively small, and they are not strongly zoned, in contrast to phenocrysts of many calcalkaline provinces. Plagioclase varies from anorthite ( $An_{85}$ ) in the high-alumina basalt of Eua to sodic bytownite ( $An_{80}$ ) in the dacites of Fonualei and Metis shoal. Augite ranges from about  $Ca_{43}Mg_{47}Fe_{10}$  in the

basalt and basaltic andesite to about  $Ca_{40}Mg_{35}Fe_{25}$  in the dacite; similarly the hypersthene varies from  $Ca_4Mg_{75}Fe_{21}$  in andesite to about  $Ca_4Mg_{51}Fe_{45}$  in the dacites. The plagioclase contains appreciable amounts of iron and magnesium, these elements being somewhat greater in the more calcic plagioclase of the andesites and lower in the dacites. Alumina and titanium are low in all pyroxenes. Hornblende has not been observed in any of the lavas.

The groundmass is extremely fine grained in the samples studied and only a few groundmass phases have been examined in detail. Pigeonite has been identified and analyzed in one rock, andesite 111547-20 from Late (Table 23, column 4). In this rock the pigeonite forms granular rims around augite phenocrysts and discrete subhedral crystals in the groundmass, where it is the principal pyroxene. Qualitative scans with the electron microprobe indicate that small crystals of potash-rich feldspar are present in the groundmass of many rocks, especially the more coarsely crystalline dacites, but even in these rocks it is not abundant. Although the rocks are normatively oversaturated, a silica phase appears in the mode only in the more siliceous dacites, and there only as tiny patches in the groundmass or as fillings in small miarolitic cavities. Most appear to be quartz rather than cristobalite or tridymite. Microprobe analyses of typical minerals are given in Table 23.

The dacite from Metis shoal has proved to be one of the most unusual and mineralogically distinctive of all rocks so far studied. The polished thin section provided by W. G. Melson includes a large rounded crystal of forsteritic olivine in addition to abundant phenocrysts of bytownite, augite, and hypersthene. The phenocrysts are subhedral in outline except where they are intergrown in glomeroporphyritic clusters. These clusters may contain a few grains of magnetite. Many plagioclase and hypersthene



TABLE 23. Electron Microprobe Analyses of Typical Minerals  
(W. B. Bryan analyst)

	1	2	3	4	5	6
SiO <sub>2</sub>	46.7	54.4	53.3	53.6	52.2	0.31
Al <sub>2</sub> O <sub>3</sub>	33.1	1.32	2.01	1.01	0.77	3.40
TiO <sub>2</sub>	...	0.10	0.18	0.11	0.19	9.22
FeO	0.79	13.3	8.35	16.9	26.5	84.7*
MnO	0.00	0.36	0.23	0.46	0.90	0.39
MgO	0.18	28.6	17.7	23.3	18.4	0.85
CaO	17.6	2.18	18.2	4.79	1.97	0.03
Na <sub>2</sub> O	1.36	0.02	0.15	0.06	0.02	...
K <sub>2</sub> O	0.04	...	...	...	...	...
Totals	99.77	100.28	100.12	100.23	100.95	99.77
O	32.000	6.000	6.000	6.000	6.000	32.000
Si	8.636	1.946	1.954	1.966	1.975	0.093
Al	...	0.054	0.046	0.034	0.025	...
Ti	7.209	0.002	0.041	0.010	0.009	1.192
Fe	...	0.003	0.005	0.003	0.005	2.065
Mn	0.123	0.399	0.256	0.518	0.840	19.957
Mg	0.000	0.011	0.007	0.014	0.029	0.098
Ca	0.049	1.526	0.968	0.188	1.038	0.378
Na	3.494	0.084	0.715	1.273	0.080	0.009
K	0.489	0.001	0.010	0.004	0.001	...
	0.008	...	...	...	...	...

\* FeO, 38.8; Fe<sub>2</sub>O<sub>3</sub>, 45.9, calculated from total Fe assuming ideal magnetite-ulvöspinel solid solution.

1. Bytownite phenocryst, basaltic andesite (111547-2C), Late Island.
2. Hypersthene phenocryst, basaltic andesite (111547-2C), Late Island.
3. Augite phenocryst, basaltic andesite (111547-5), Late Island.
4. Pigeonite, typical groundmass grain, basaltic andesite (111547-20), Late Island.
5. Hypersthene phenocryst, dacite (111548-41), Fonualei Island.
6. Magnetite microphenocryst, dacite (111548-4), Fonualei Island. Includes V<sub>2</sub>O<sub>5</sub>, 0.87.

crystals contain rounded blebs of glass, similar in composition to the glass matrix. The phenocrysts are of virtually constant composition, with little or no zoning.

A few crystals of hypersthene are zoned from an enstatite-rich core to a rim that is similar in composition to the typical hypersthene phenocrysts. These more magnesian hypersthene are rounded or irregular in outline and lack glass inclusions. Similar hypersthene mantles the olivine. The olivine and rounded magnesian hypersthene are tentatively interpreted as xenocrysts that are only partly equilibrated with the dacite magma. Possibly the xenocryst hypersthene has been formed entirely by reaction between olivine and the dacite magma. The olivine encloses small crystals of chrome spinel but none appear in the hypersthene.

The groundmass of the Metis shoal dacite is almost entirely glass, containing tiny microlites of feldspar and pyroxene. There are rather widely scattered large oval vesicles, giving the glass a scoriaceous rather than a pumiceous aspect, and indeed the rock contains insufficient voids to float, the samples having been obtained by diving on the shoal.

Microprobe analyses of the minerals are given in Table 24, along with a chemical analysis of the glass. The major element proportions of phenocryst hypersthene, plagioclase, and augite are almost identical with those reported by Melson, Jarosewich, and Lundquist (1970). A least-squares fit of the compositions of the phenocryst minerals and the glass to the bulk composition of the dacite is given in Table 25. An excellent approximation to the bulk composition may be obtained without including the

TABLE 24. Chemical Composition of Minerals and Glass of  
Metis Shoal Dacite

	1	2	3	4	5	6	7
SiO <sub>2</sub>	48.6	52.7	55.9	52.7	41.3	0.22	73.65
Al <sub>2</sub> O <sub>3</sub>	32.3	0.92	1.03	1.89	0.00	7.31	12.71
TiO <sub>2</sub>	...	0.14	0.06	0.18	0.00	0.18	0.45
FeO	0.77	21.3	11.4	9.39	7.10	17.6	3.85
MnO	0.00	0.53	0.24	0.31	0.13	0.28	0.06
MgO	0.08	22.6	28.9	15.5	50.6	14.3	0.84
CaO	16.8	1.63	1.85	20.6	0.14	0.01	3.80
Na <sub>2</sub> O	1.76	0.02	0.00	0.15	...	...	3.10
K <sub>2</sub> O	0.05	...	...	...	...	...	1.53
Cr <sub>2</sub> O <sub>3</sub>	...	...	...	...	...	59.8	...
Totals	100.36	99.84	99.38	100.72	99.62	99.84	99.99

- 1. Bytownite phenocryst.
- 2. Hypersthene phenocryst.
- 3. Hypersthene xenocryst, average of zoned crystal.
- 4. Augite phenocryst.
- 5. Olivine xenocryst, includes NiO = 0.35%.
- 6. Chromite inclusion in olivine, includes V<sub>2</sub>O<sub>3</sub> = 0.08, ZnO = 0.06.
- 7. Groundmass glass, recalculated to 100%, all Fe as FeO.
- 1-6, Electron microprobe analyses by W. B. Bryan; 7, gravimetric analysis by E. Jarosewich.

composition of olivine, chromite, xeno-cryst hypersthene, or magnetite, indicat-ing that these minerals are sufficiently rare to make only trivial contributions to the bulk composition of the rock. The weight fractions so computed differ somewhat from the volumetric mode given by Melson, Jarosewich, and Lund-quist (1970), but reasonable agreement

TABLE 25. Calculated and Observed Composi-tion of Metis Shoal Dacite, and Weight Fractions of Major Phases

	A	B	C	D
SiO <sub>2</sub>	64.01	64.01		
Al <sub>2</sub> O <sub>3</sub>	12.97	12.95		
TiO <sub>2</sub>	0.30	0.32	Glass	0.5731
FeO	6.61	6.79	Plagioclase	0.1660
MnO	0.15	0.13	Hypersthene	0.1521
MgO	5.65	5.47	Augite	0.1100
CaO	7.46	7.51		
Na <sub>2</sub> O	2.09	1.83		
K <sub>2</sub> O	0.89	0.95		
P <sub>2</sub> O <sub>5</sub>	0.00	0.06	Σ R <sup>2</sup> = 0.1390	

- A. Calculated least-squares estimate of dacite composition.
- B. Metis shoal dacite, actual composition.
- C. Glass and mineral components used in calculation (columns 1, 2, 4, 7, Table 24).
- D. Calculated weight fractions of compo-nents in column C.
- All data recalculated to 100%, minus H<sub>2</sub>O, CO<sub>2</sub>, and with all Fe as FeO.

can be obtained by deleting the vesicles and assuming reasonable densities for the mineral phases and glass of their mode.

Glass inclusions in hypersthene and plagioclase phenocrysts are almost iden-tical in composition with the groundmass glass of the dacite. Similarity between inclusion compositions, lack of zoning in phenocrysts, and similarity in composi-tion between outer zones of hypersthene xenocrysts and hypersthene phenocrysts all suggest that the phenocrysts have grown in equilibrium with a liquid rep-resented by the groundmass glass.

A plot of analyzed pyroxenes (Fig. 64) clearly reveals that the pyroxene of the Metis shoal dacite is unusually mag-nesian compared with pyroxene of other dacites from Tonga. The tendency to-ward a compositional hiatus between dacite and andesite, evident in the bulk chemical analyses discussed below, is also reflected in the mineralogy. Pyroxenes from the Coral Sea drift pumice, which has been attributed to a source on Tonga (Bryan, 1968, 1970), are also very simi-lar to the pyroxenes in the dacites of Fonualei.

The volcanic rocks of Tonga do not readily fit into existing schemes of clas-

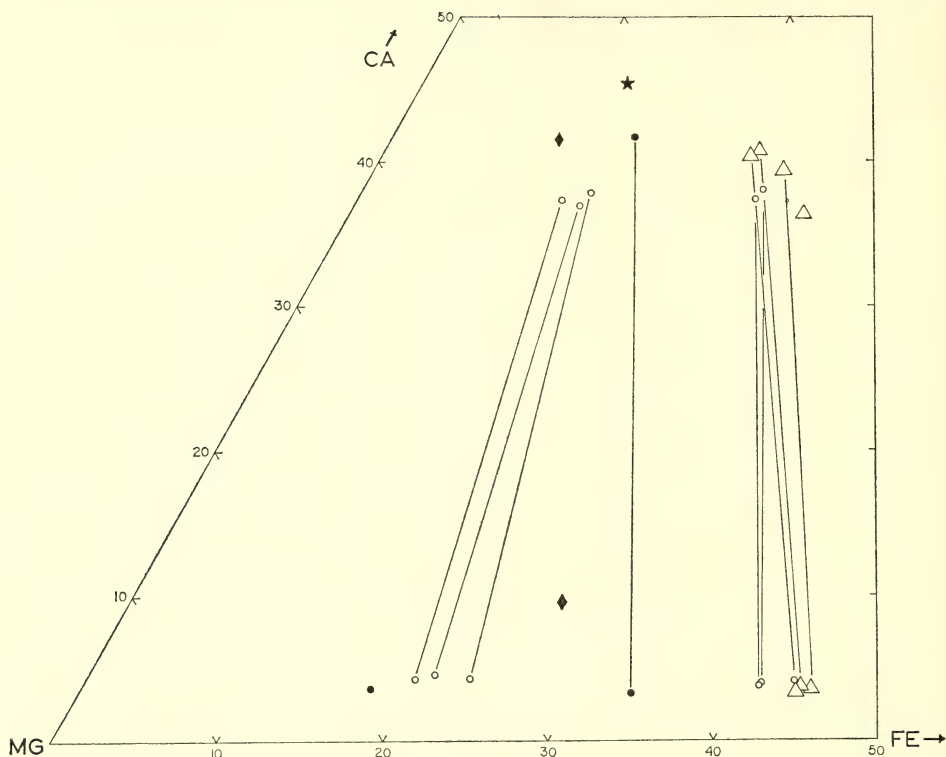


Fig. 64. Coexisting pyroxenes in Tongan lavas: Star, augite of high-alumina basalt 111549-7, Eua Island. Diamonds, augite and pigeonite of basaltic andesite 111547-20, Late Island. Solid circles, augite and hypersthene of Metis shoal dacite; tie line connects phenocrysts. Open circles, augite and hypersthene phenocrysts of andesites of Late and Hunga Ha'apai, and dacites of Fonualei Island. Open triangles, augite and hypersthene of Coral Sea drift pumice (Bryan, 1970).

sification or nomenclature. Rather than impose additional place-name nomenclature on an already overburdened literature, we prefer to retain common rock names combined with mineral or chemical modifiers. Thus, the basalt of Eua Island can be adequately described as an anorthite basalt; most of the andesites are bytownite-augite andesite; and the dacites are more precisely described as bytownite-augite-hypersthene dacite.

### *Geochemistry*

Major element analyses are presented for representative lavas in Table 26. The characteristic features throughout the suite are low alkalies,  $\text{TiO}_2$  and  $\text{P}_2\text{O}_5$ ,

relatively low  $\text{MgO}$ , and moderately high iron. The range of variation is most readily portrayed in the AFM diagram (Fig. 65), which clearly shows the distinct iron enrichment characteristic of this suite, often thought to be atypical of calcalkaline rock suites. However, iron enrichment, like these other chemical characteristics, is probably typical of the earliest volcanic products of island arc development (Jakes and White, 1969; Baker, 1968). Bulk compositions enclosed between dashed lines in the figure are considered on petrographic criteria to be possible liquid compositions. The two compositions lying outside these lines are probably modified by crystal accumulation or contamination. The



TABLE 26. Volcanic Rocks from Tonga and an Average Australite

	1	2	3	4	5
SiO <sub>2</sub>	49.19	53.86	57.57	64.79	63.3
Al <sub>2</sub> O <sub>3</sub>	20.61	16.95	14.14	14.48	16.5
TiO <sub>2</sub>	0.42	0.58	0.80	0.55	0.58
Fe <sub>2</sub> O <sub>3</sub>	2.93	2.74	3.60	1.91	...
FeO	5.63	7.15	8.62	6.07	5.89
MnO	0.18	0.16	0.22	0.16	0.10
MgO	5.93	4.85	3.29	1.45	3.83
CaO	11.78	11.23	8.42	6.04	4.87
Na <sub>2</sub> O	1.21	1.74	2.42	3.03	3.51
K <sub>2</sub> O	0.24	0.49	0.70	1.11	1.05
P <sub>2</sub> O <sub>5</sub>	0.04	0.07	0.12	0.11	...
H <sub>2</sub> O <sup>+</sup>	1.63	<0.10	0.26	<0.10	...
H <sub>2</sub> O <sup>-</sup>	0.43	0.04	0.12	0.10	...
Totals	100.22	99.86	100.11	99.80	99.53

- 1. High-alumina basalt (111549-7), boulder from Liku beach trail, Eua Island. B. D. Kay, analyst.
- 2. Basaltic andesite (111547-5), north coast of Late Island. E. Jarosewich, analyst.
- 3. Andesite (111547-13), uppermost flow on northwest coast of Late Island. B. D. Kay, analyst.
- 4. Bytownite dacite (111548-20), pre-caldera flow, northwest coast of Fonualei Island. E. Jarosewich, analyst.
- 5. Average high Na/K australite (Chapman and Scheiber, 1969, p. 6741). Numbers in parentheses refer to samples in the collection of the U. S. National Museum.

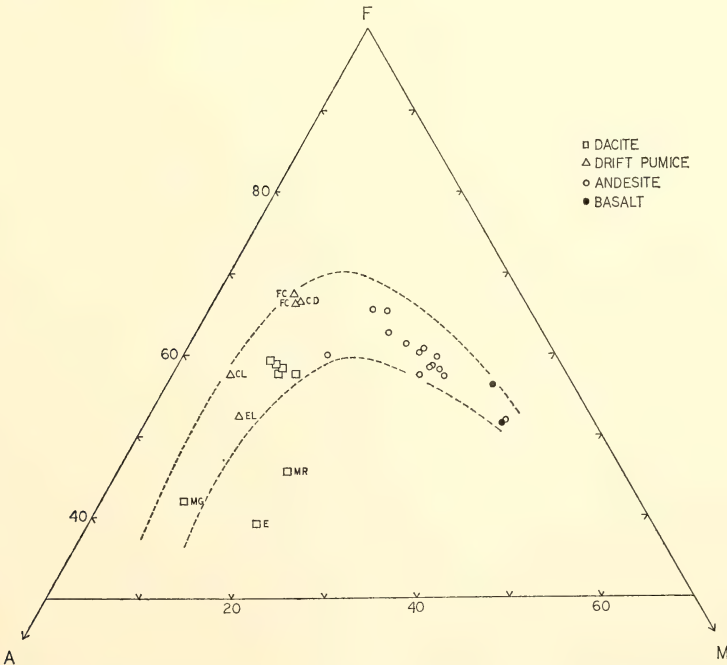


Fig. 65. AFM diagram of volcanic rocks from Tonga. Unlabeled symbols, lavas of Eua, Fonualei, Late, Hunga Ha'apai, and Tofua (Bryan, Stice, and Ewart, 1970). Fc, Falcon Island pumice (Lacroix, 1939); CD, Coral Sea dark pumice (Bryan, 1968); CL, Coral Sea light pumice (Bryan, 1968); EL, light pumice, Eua Island (Bryan, 1970); MG, dacite glass, Metis shoal (Melson, Jarosewich, and Lundquist, 1970); MR, bulk rock composition, Metis shoal (Melson, Jarosewich, and Lundquist, 1970).

Metis shoal rock composition (MR) contains an unusual abundance of phenocrysts and is thus considered to be a mixture of liquid (glass MG) and crystal cumulates. The Eua dacite tuff (E) contains fragments of dark rock, probably of basaltic composition. Excluding the drift pumice analyses plotted for comparison, it can again be seen that most of the volcanic rocks collected *in situ* fall into two distinct groups. The Metis shoal dacite composition falls distinctly away from the main composition field of the Tongan lavas, although the glass (MG) appears to represent a reasonable extension of the late-stage alkali enrichment trend.

Minor element concentrations appear similar to those reported for other island arcs of the western Pacific. The high V/Ni (generally >10) and low Ni/Co ratios of the Tongan lavas are especially typical of calcalkaline andesites and dacites. The low K, Ba, and Zr are shared by some other island arc lavas, such as the Marianas and South Sandwich Islands (Taylor *et al.*, 1969; Baker, 1968). It is interesting that there are generally only small differences between whole-rock and groundmass compositions. This may in part reflect the low phenocryst content of some of the lavas, and also the absence of magnetite or spinels except in the more siliceous lavas. For example, vanadium shows marked depletion only in the dacite groundmass relative to the whole-rock composition (111548-20, Table 27), whereas in those andesites in which magnetite is mainly a groundmass phase, vanadium is concentrated in the groundmass (111547-20). Where magnetite is present both as phenocrysts and as an abundant groundmass phase, as in the siliceous andesites (111547-13), there is little or no fractionation of vanadium.

Rare-earth data for samples of basalt, andesite, and dacite are presented in Fig. 66, with data for a basalt from Hawaii for comparison. The Tongan

TABLE 27. Typical Volcanic Rocks from Tonga: Minor Element Analyses, Parts per Million (A. Ewart, analyst)

	1	2	3	4
	Rock			
Ga	13	15	19	18
Cu	51	150	215	28
Y	12	15	25	25
Ni	25	26	8.8	3
Zr	21	26	40	50
Co	30	33	31	14
Sc	34	40	41	25
Cr	75	78	6	4
V	230	295	410	100
Sr	115	215	225	305
Ba	14	96	165	270
Rb	<2	6	9	14
	Matrix			
Ga	17	17	18	17
Cu	26	240	110	18
Y	23	26	27	20
Ni	24	9.6	7.6	...
Zr	38	46	46	46
Co	30	32	33	10
Sc	45	37	41	14
Cr	27	9	5	3
V	220	460	430	38
Sr	99	225	230	295
Ba	27	180	160	290
Rb	49	12	8	15

1. High-alumina basalt (111549-7), Eua Island.
2. Basaltic andesite (111547-20), Late Island.
3. Andesite (111547-13), Late Island.
4. Dacite (111548-20), Fonualei Island.

lavas average 5 to 10 times the average chondrite values, with only minor fractionation, being among the most "primitive" of terrestrial rocks in this respect.

Melson, Jarosewich, and Lundquist (1970) comment on the similarity between the Metis shoal dacite glass and the composition of some tektites. In particular, the Tongan dacites closely resemble the high Na/K australites (Table 26, column 5) although the most common tektites typically show an excess of K<sub>2</sub>O over Na<sub>2</sub>O. The high Na/K tektites are somewhat lower in rare earths than other tektites (Chapman and Scheiber, 1969, p. 6759) but are still considerably enriched in the lighter rare earths compared with the Tongan dacites.

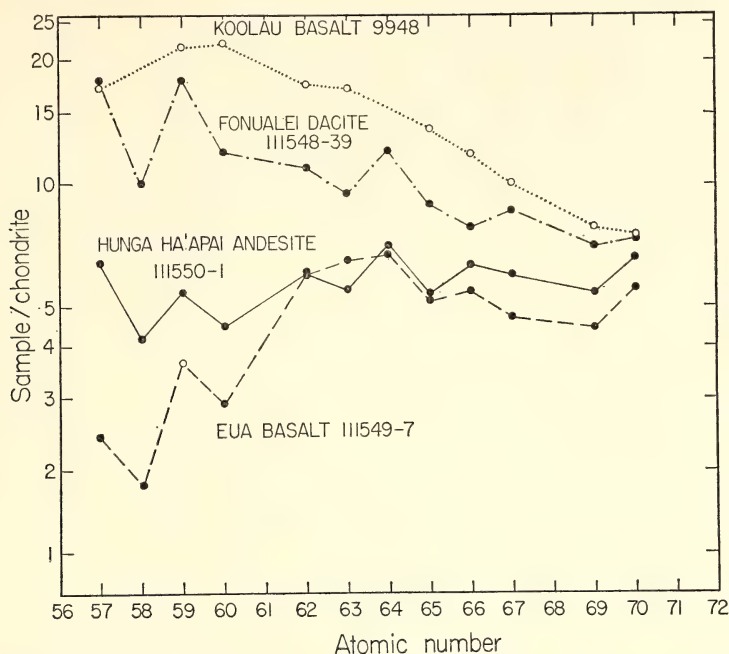


Fig. 66. Rare-earth distribution in Tongan dacite, andesite, and basalt. Analyses by S. R. Taylor and A. L. Graham, Australian National University, using spark source mass spectrography. Koolau basalt 9948 for comparison (Schilling and Winchester, 1969).

### Petrogenesis

The very strong differential partitioning of Mg and Fe between pyroxenes and groundmass glass, and of Ca and Na between plagioclase and groundmass glass, in the Metis shoal dacite indicate crystallization under conditions favorable to extreme fractionation. Similarly strong fractionation was implied in the basalt-pantellerite relation described last year (Bryan, *Year Book* 68, p. 199), and in the gabbro-microsyenite fractionation discussed previously (Bryan, *Year Book* 67, pp. 247-250). Relatively strong fractionation is also implied in differences between whole-rock and groundmass compositions of some New Zealand andesites (Ewart, 1969, p. 375, see especially P.29166 and P.17171); and evidence has been presented that in these rocks also there is a systematic relation between calcic feldspars and overall modal and trace element data (Ewart,

1968; Ewart and Taylor, 1969) that argues against a xenocrystic origin for these feldspars. In the Metis shoal dacite, the abrupt transition from virtually unzoned phenocrysts to a glassy matrix almost devoid of crystals minimizes the usual uncertainty in distinguishing crystalline phases from coexisting liquid. Apparently, under appropriate conditions crystallization of calcic plagioclase and magnesian pyroxenes can produce the strong single-stage fractionation required to pass directly from an andesite composition to a dacite or rhyolite. Yoder (1969) has suggested that calcic plagioclase may reflect crystallization at elevated water pressure. The composition of a typical Fonualei dacite is readily explained in this way (Table 28) if a typical andesite from Late Island is used as parent magma and the composition of that parent is expressed as the sum of appropriate amounts of its phenocryst



TABLE 28. Derivation of Dacite F-20 from Andesite L-5

	A	B	Variable	Weight Fraction
SiO <sub>2</sub>	54.11	54.11	Dacite F-20	0.4259
Al <sub>2</sub> O <sub>3</sub>	17.03	17.03	Augite L-5	0.1737
FeO	9.65	9.64	Hypersthene L-5	0.0378
MgO	4.87	4.88	Plagioclase L-5	0.3166
CaO	11.28	11.28	Magnetite F-4	0.0477
Na <sub>2</sub> O	1.75	1.82		
K <sub>2</sub> O	0.49	0.49		
MnO	0.16	0.14		
TiO <sub>2</sub>	0.58	0.71		
P <sub>2</sub> O <sub>5</sub>	0.07	0.05		

$$\Sigma R^2 = 0.0234$$

A. Andesite L-5, Late Island.

B. Estimated composition of andesite L-5, calculated as a linear combination of dacite F-20, augite L-5, hypersthene L-5, plagioclase L-5, and magnetite F-4.

compositions and the composition of the dacite. Titaniferous magnetite must be included in the mineral assemblage to obtain a suitable solution. This is in agreement with the petrographic observation that magnetite appears as a phenocryst phase in the more siliceous andesites; presumably, magnetite would have appeared as a phenocryst phase in 111547-5 by the time the residual liquid reached the composition of dacite.

Genesis of the basalt and andesite is less readily explained. So far, tests of fractionation schemes for deriving andesites from the high-alumina basalt of Eua Island with various combinations of observed phenocryst minerals have been unconvincing. Possibly the basalt has suffered sufficient change in bulk composition during uralitization that it no longer adequately represents the bulk composition of the parent magma. It is possible that the andesite is a product of partial melting at depth and is unrelated to the basalt, which may represent a much older phase of volcanic activity, unrelated to the presently active volcanic islands.

In accord with the plate-tectonic concept it is possible that the volcanic rocks of Tonga are derived by partial melting of sea-floor basalt thrust downward beneath the arc along the Benioff zone.

Taylor *et al.* (1969) have discussed alternative models for deriving andesite from typical ocean ridge basalts, which they note appear too low in alkalis to serve as an appropriate parent composition. However, the alkali-deficient lavas of Tonga actually require a mechanism of partial melting by which alkalis are retained in the crystalline phases if they are to be derived from oceanic basalts. Amphibole or mica might be appropriate phases, and might also preferentially retain rare earths and other trace elements, thus accounting for some of the compositional peculiarities of these rocks. Green and Ringwood (1969) reported preliminary experiments on partial melting of high-alumina quartz tholeiite at about 10 kb water vapor pressure, in which a tschermakitic hornblende was an important crystal phase. With the possible exception of the Metis shoal olivine and hypersthene, xenoliths or xenocrysts of possible mantle origin have not been found in the Tongan lavas, and we thus have little direct evidence for the nature of crystalline phases actually present at depth.

#### CORAL SEA DRIFT PUMICE FROM EUA ISLAND, TONGA

W. B. Bryan

Pumice collected from a beach on the east side of Eua Island, Tonga, during field studies in July 1969 is megascopically identical with pumice originally described from Herald Cays 2500 miles to the west in the western Coral Sea (Bryan, 1968) and the pumice from One Tree Island described last year (Bryan, *Year Book* 68). Local inquiry indicates that the pumice was stranded during or after a severe storm early in 1969. Again, the pumice from Eua can be divided into light- and dark-colored varieties. Augite, orthopyroxene, plagioclase, and occasional magnetite form glomeroporphyritic clusters. The compositions of these minerals in samples of the light pumice

are virtually identical with those reported last year.

Refractive indices of pumice glass provide the best single quantitative comparison between pumice fragments. Refractive indices were measured by a single variation procedure, with a Bausch and Lomb grating monochromator to establish a matching wavelength for the glass-liquid dispersion curve intersection at constant temperature. Glass dispersion curves were projected to the *D*-line position on Hartmann paper to obtain the reported refractive index. Crushed samples of pumice glass from One Tree Island, Queensland, were used as internal standards to eliminate any possible effects of differences in operating procedures for comparative purposes. The mean values are Eua light pumice, 1.5079; One Tree Island light pumice, 1.5075, Eua dark pumice, 1.5311; One Tree Island dark pumice, 1.5309.

No pumice resembling the drift pumice was found *in situ* on any of the volcanic islands of Tonga. The close mineralogical and chemical similarity to the dacites of Tongan volcanoes suggested previously (Bryan, 1968), however, has been confirmed by the new data for Tongan volcanic rocks described in the previous section. An intermittently active submarine volcano in the Tonga area still appears to be the most likely source for this pumice. Alternatively all of the pumice may have originated in a single eruption during 1964; and a portion of this raft may have escaped into the southern Pacific and have moved with the westwind drift to South America, north with the Humboldt current, and west again with the south equatorial current. At an average speed of about 10 nautical miles a day, a reasonable speed based on other studies (Richards, 1958; Coombs and Landis, 1966), the approximately 15,000-mile round trip would have required about 4 years. This is just about the time that has elapsed since the last documented stranding of

the pumice on the Fiji Islands in March 1965 and its appearance on Eua Island.

MID-ATLANTIC RIDGE NEAR 45°N:  
MAGNETISM AND MAGNETIC  
MINERALOGY \*

*S. E. Haggerty and E. Irving †*

Compared with continental rocks and with ocean sediments, very little is known about the paleomagnetism and the magnetic mineralogy of submarine basalts. It is known that the natural remnant magnetization (n.r.m.) of dredged basalts greatly exceeds that induced by the present field (Ade-Hall, 1964) and that the remanence is, in some instances, stable (Opdyke and Hekinian, 1967) and of about the correct magnitude to explain the observed anomalies over oceans (see, for example, Serson and Hannaford, 1957). But there are many outstanding problems. For example, it is not known whether the magnetic polarity at the axis of the Mid-Atlantic Ridge actually corresponds to that required by the Vine-Mathews hypothesis. The Mid-Atlantic Ridge is well defined magnetically by a large axial anomaly, which rapidly decreases in intensity with distance from the axis. This decrease is not the result of viscous decay, and the present work was therefore undertaken in an attempt to explain the attenuation of the magnetic anomaly pattern on the basis of magnetic mineralogy.

At 45°N the Mid-Atlantic Ridge has a median valley 9 km in width at an average depth of 2900 m. Between 45°N and 46°N the valley trends in a direction 019°E of N. The valley has deep depressions and ridges elongated in the direction of the valley (Fig. 67). A line defining the topographic axial depression (called the axis) of the ridge can be drawn to an accuracy of 1 or 2 km. The crest mountains, on either side of the median valley, have an average width

\* Samples were obtained from the Bedford Institute, Halifax, Nova Scotia.

† Dominion Observatory, Ottawa, Canada.

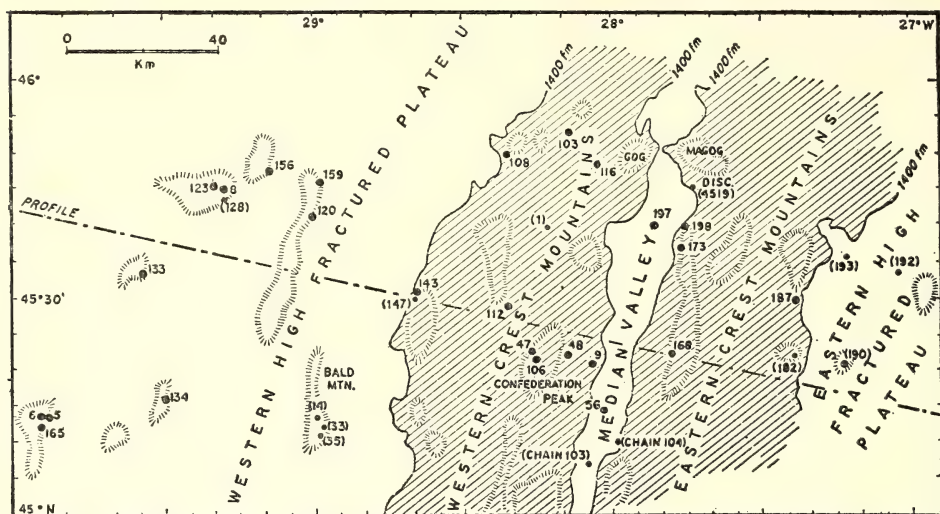


Fig. 67. Sketch map of the Mid-Atlantic Ridge at 45°N. Physiographic units are delineated at the 1400 fathom (2520 m) isobath. All dredge stations in the area are marked.

of 50 km. The peaks are commonly 1800 m above the median valley. The high fractured plateaus form the flanks of the ridge.

Results from 27 dredge hauls (65 samples) spaced from 150 km west to 70 km east of the median valley of the Mid-Atlantic Ridge at about 45°N (Fig. 67) are reported. Forty-seven of the samples are considered to be *locally derived*; the remaining eighteen are *erratics* deposited during Pleistocene glaciations. Erratics are typically rounded and often striated, have thin manganese coatings (3 mm maximum), have never been dredged from the median valley, and have radiometrically dated ages ranging from middle Precambrian to Cambrian (Wanless *et al.*, 1967; York, Baski, and Aumento, 1969). Locally derived rocks have ages less than 16 m.y. (Aumento, 1969) and many have thick manganese coatings that increase with distance from the axis. Only the locally derived basalts will be considered.

Basalts, gabbros, serpentinized peridotites, diorites, and greenstones are present. Only basalts occur in the median valley; the first nonbasaltic rocks (ser-

pentinized peridotite) were dredged at 44 km west of the axis.

The basalts occur mostly as lava pillows (Aumento, 1968), many of them with glassy margins. Their remanent magnetization is due to the iron-titanium oxides that amount to a small percentage by volume. The magnetic properties of these minerals depend on their oxidation state, and it is appropriate, therefore, before considering these properties, to review briefly the relevant chemical properties and follow this by a review of the salient characteristics of the iron-titanium minerals themselves.

The total iron oxide content ( $\text{FeO} + \text{Fe}_2\text{O}_3$ ) falls mostly in the range 7–11%, and there is no systematic variation with distance from the axis (Fig. 68). In axial basalts the oxidation ratio  $\text{FeO}/\text{Fe}_2\text{O}_3$  falls between 5 and 10, whereas beyond 20 km the basalts are more oxidized and the ratio decreases. The variation in water content shows an increase from about 0.5% at the axis to over 8% in the high fractured plateaus. It is, therefore, likely that at least part of the increase in oxidation state is due to reaction with sea water. This conclusion is in agree-



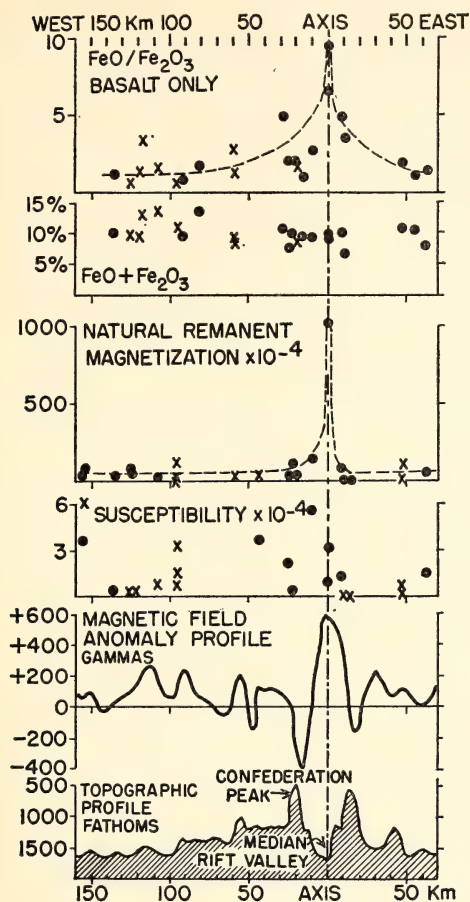


Fig. 68. Chemical and magnetic results plotted as a function of distance from the axis of the Mid-Atlantic Ridge.

ment with results of oxygen-isotope ratio measurements (Muehlenbachs and Clayton, 1970). The value of  $\delta O^{18}$  changes from about 6 at the axis to about 18 at 150 km. Such changes have been found to be characteristic of sea water alteration of basalts.

### *Magnetic Mineralogy*

The Fe-Ti oxides in the basalts are fine grained, ranging from  $<1$  to  $25 \mu m$  in size. Both titanomagnetite and ilmenite are anhedral to subhedral, but the

development of skeletal crystals is ubiquitous, especially in the ultra-fine fraction. Most samples contain one generation of Fe-Ti oxides, but a few specimens contain more than one generation. The formation of skeletal crystals in oceanic basalts is undoubtedly related to rapid quenching that follows extrusion of a lava on the sea floor. In continental volcanics, skeletal crystals of titanomagnetite and ilmenite are commonly found in fine-grained lavas, in thin pahoehoe flow units, at the cooling surfaces of thick individual flows, within the chilled margins of dykes, and in basaltic fragments in lithic tuffs. Skeletal crystals are by no means restricted to rocks that have undergone rapid chilling; they may be phenocrystic or coarse grained ( $100$ – $200 \mu m$ ) and are known to occur in gabbros and in basaltic pegmatites (p. 278), although the association of glass and recognizable pillow structures in oceanic basalts indicates supercooling.

At present we are not aware of any unusual magnetic effects in skeletal titanomagnetite crystals, but several considerations may be important. Coercivity is a measure of stability and depends on grain size and shape, being greater for small grains of the same shape and for elongated grains of the same volume. The most stable remanence is developed in grains that contain a single domain (for magnetite this value is  $0.03 \mu m$ ). Skeletal crystals are characterized by complicated dendritic arrays that are often only a micrometer or less in thickness; these crystals have large surface areas and when subjected to high-temperature subsolidus oxidation, formation of ilmenite lamellae effectively subdivides the host crystal into even smaller magnetite particles (magnetic-effective grain size) that may approach single domain size. Skeletal crystals have a variable geometry, and because they have been quenched may also contain lattice distortions, both of which will affect coercivity.

### *Oxidation Effects*

Variations in magnetic properties are dominantly related to the oxidation state of the Fe-Ti oxides.

*High-temperature oxidation.* All samples have been classified on the high-temperature oxidation scale, which is the same as that used for continental lavas (Wilson and Haggerty, 1966; Watkins and Haggerty, 1967). The classification is based on the paragenetic sequence of mineral assemblages that develop when primary homogeneous members of the magnetite-ulvöspinel solid solution series and primary homogeneous members of the ilmenite-hematite solid solution series are oxidized. The classification is directly related to the  $\text{FeO}:\text{Fe}_2\text{O}_3$  ratios of the rock (Haggerty, 1968).

Of the 32 basaltic samples examined microscopically 23 show no evidence of high-temperature oxidation (oxidation index: C1, R1), five samples contain exsolved ilmenite (oxidation index: C2 or C3, R1), and the remaining four samples show the incipient formation of ferri-rutile, rutile, and titanohematite (oxidation index: C4, R4). The more highly oxidized samples are also coarse grained, indicating that they may have originated near the central portion of a lava where deuteric oxidation is at a maximum (Watkins and Haggerty, 1967; Sato and Wright, 1966). Samples within the median valley are unoxidized (C1, R1); deuterically oxidized samples show no correlation with distance from the ridge.

*Oxidation at low to intermediate temperatures.* The recognition of post-deuteric alteration products at low to intermediate temperatures permits distinctions to be made between primary magmatic oxidation variations and oxidation variations that probably relate to age and hence distance from the median valley.

The degree or intensity of maghemitization that develops is extremely variable within any one polished section or indeed within any one grain; 75%

of the basalts show some degree of maghemitization, and samples within the median valley are unoxidized. Where titanomagnetite grains contain thin lamellae of ilmenite, large grains are effectively subdivided into large numbers of smaller grains (magnetic effective grain size) with each subgrain behaving as a separate oxidation unit. The overall effect is that a wide variation in intensity of maghemitization occurs within distances of 5  $\mu\text{m}$  or less; for this reason accurate analyses of mineral content of these derived oxidation products are not only difficult to obtain, but replicate estimates are also inconsistent.

The groundmass glass, however, passes through a sequence of color changes that reflects the degree of maghemitization and is also related to the overall  $\text{FeO}:\text{Fe}_2\text{O}_3$  ratio of the rock (Fig. 69). Furthermore, Irving, Robertson, and Aumento (1970) have shown that the degree of oxidation increases as a function of distance from the axis of the ridge (Fig. 68); intensity of maghemitization is, therefore, related to age.

### *Magnetic Properties*

The basalts have a mean remanent intensity of  $92 \times 10^{-4}$  and a mean susceptibility of  $0.9 \times 10^{-4}$  egs  $\text{cm}^{-3}$ . The remanence varies with distance from the axis,

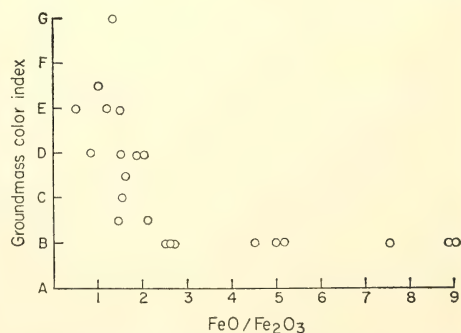


Fig. 69. Groundmass color index as a function of  $\text{FeO}/\text{Fe}_2\text{O}_3$ . A represents the lowest state of oxidation and is dark gray; B, light gray; C, pale yellow; D, straw yellow; E, orange-brown; F, red-brown; G, red.

samples from the median valley (mean  $574 \times 10^{-4}$ ) being ten times more magnetic than samples at a greater distance (Fig. 68). Most of this decrease of intensity occurs within a few kilometers (less than 6 km) of the central axis and within the zone of active volcanism. These high intensities of magnetization are almost as strong as those associated with lightning strikes, a process that obviously cannot occur at the bottom of the sea. It is suggested that the dramatic drop in intensity is caused by chemical change enhanced by reheating in the narrow volcanic axial zone. In contrast, the susceptibility (Irving *et al.*, 1970) and saturation isothermal remanent magnetization (Carmichael, 1970; Irving and Park, 1970) show no large systematic variations across the ridge, although there is some indication that both properties have somewhat higher values in the median valley.

The coercivity of remanence is generally high, and there is no systematic variation with distance from the axis. The distribution of coercivities falls roughly into two sets, one centered at 180 oe and another at 480 oe. A similar bimodal distribution has been observed in subaerial basalts (Larson *et al.*, 1969). Secondary components of viscous origin have an average magnitude of 8% of the total intensity, which is several times less than that commonly found in subaerial basalts (Irving and Park, 1970).

Curie temperatures increase with distance from the axis; median valley samples have values ranging from 100° to 150°C and increase to about 350°C in samples from the crest mountains and high fractured plateau. Schaeffer and Schwarz (1970) have shown experimentally that thermal cycling to progressively high temperatures produces an increase in Curie temperature from 100° to 525°C, the first changes being noticeable at 200°C. They interpret this increase as due to oxidation of titanomagnetite to titanomaghemite.

The blocking temperature (the tem-

perature at which total remanence is lost) also shows a marked variation with distance from the axis. At the axis the values are always low and average 230°C. On the flanks of the median valley the values rise, and on the high fractured plateau and crest mountains they average 450°C. The increase in blocking temperature (and also Curie temperature) does not occur smoothly but shows an abrupt jump at the edge of the median valley. The increase in both properties occurs further out than most of the decrease in natural remanent magnetism (n.r.m.) intensity. Blocking temperatures are systematically 50° to 100°C higher than Curie temperatures, indicating that during thermal demagnetization of remanence a new material is being formed by oxidation at the higher blocking temperature and upon cooling it becomes magnetized in the same direction as the parent material.

### Discussion

The main features of the variations in properties of these basalts are an increase in low-temperature oxidation and Curie and blocking temperatures with distance from the axis and a decrease of n.r.m. intensity with distance. It is reasonable therefore to relate the magnetic parameters to a process of progressive oxidation with age (distance from the axis).

The high axial remanence may be explained as follows: Glassy margins on pillow basalts and quenched skeletal titanomagnetite crystals indicate rapid cooling on the ocean floor. The blocking temperatures of the axial rocks may initially have been as low as 100° or 200°C and did not exceed 300°C, so that it is likely that the titanomagnetites were in their present form when remanent magnetization was acquired. This situation is the most favorable in nature to the formation of thermoremanent magnetization (t.r.m.), that is, the acquisition of remanence by cooling of



already-formed crystals through their critical blocking temperature. The rarity of subsolidus exsolution that might have occurred at temperatures below the characteristic blocking temperatures indicates that there is no substantial component of chemical remanent magnetization (c.r.m.). Therefore, we suggest that to a first approximation the very high intensities in these axial submarine basalts are due to their having a t.r.m.

With reference to the decrease in n.r.m., we conclude that the variations of all the magnetic properties with distance from the axis can be explained by secondary oxidation, and there is no need to appeal to either physical (e.g., viscous decay) or geophysical (e.g. changes in the geomagnetic field) processes. Magnetic viscosity decreases with the logarithm of time, whereas the observed decay is more rapid (Fig. 68). Furthermore, there is no evidence from paleointensity determinations that the strength of the geomagnetic field has changed by a factor of 10 or so in the past  $10^6$  years (Smith, 1967).

The model we propose for the attenuation of the magnetic anomaly pattern with distance from the axis is as follows. Initially, a strong t.r.m. is acquired by these basalts during quenching. They undergo little or no deuteric alteration. Basalts extruded in the median valley are dry (0.5%  $H_2O$ ) and while at the surface begin to absorb oxygen from sea water with the result that titanomagnetite becomes partially oxidized to titanomaghemite. We propose that by this process an initial strong t.r.m. is exchanged in parts of crystals for a c.r.m. of lower intensity. Most flows will not remain near the surface, however, but will be covered by later flows, which will remain in the vicinity of the volcanic vent for some period of time, and may undergo *mild* reheating. Their environment will remain an oxidizing one because of trapped sediment and sea water. We propose that this oxidation, occurring under mild hydrothermal conditions, is

the second contributory cause of the decrease in amplitude of the geomagnetic anomalies away from the axis. Furthermore, experiments show that this secondary remanence will be in the same direction as the initial remanence, so the record of the field at the time of extrusion will be preserved. As sea floor spreading proceeds, the temperature falls and the magnetization stabilizes. Covered flows altered in this way would not be sampled in the median valley, but as the mass spreads sideways and is up-faulted into the crest mountains, they will be exposed along the infacing escarpments where they will form the bulk of the outcrop and hence provide the major source of grab samples. It is argued, therefore, that the reason for the increase in the Curie and blocking temperatures at the margins of the median valley is not that the oxidation occurs at that point, but simply that covered flows are exposed for the first time in the up-faulted escarpments bordering the valley.

Thus progressive irreversible oxidation, occurring in surface flows or in covered flows near the axial vent, can explain the observed magnetic and mineralogical variations. It is not yet clear whether the mineralogical process involved is maghemitization alone or whether a degree of unmixing is also involved. We suggest that both occur and ascribe the former to surface absorption of sea water and the latter to very mild hydrothermal alteration near the axial vent.

#### PETROGRAPHY AND MINERAL CHEMISTRY OF A DIFFERENTIATED FLOW OF PICTURE GORGE BASALT NEAR SPRAY, OREGON

##### *Geologic Setting and Mechanism of Differentiation*

*D. H. Lindsley, Douglas Smith, and  
S. E. Haggerty*

The Miocene Picture Gorge basalt (Waters, 1961) is exposed along the John

Day River near Spray, Oregon. Three flows—each about 90 m thick and extending over tens or hundreds of square kilometers—contain pegmatoids (segregation veins) in their interior portions. Previous work has shown that the pegmatoids have differentiated *in situ* from the host basalts. During July 1969 Haggerty, Lindsley, and Smith collected 355 samples of Picture Gorge basalt; use of a portable, gasoline-powered core drill permitted collection of fresh samples from critical portions of each outcrop. Following petrographic examination, four samples from the uppermost of the three thick flows were selected for detailed study of their mineral chemistry with the electron microprobe. The resulting data are reported here and are used, together with the stratigraphic, optical, and chemical data of Lindsley (1960), to interpret the petrogenesis of these thick flows and to apply the results to the differentiation of basaltic magma at low pressures.

The three thick pegmatoid-bearing flows were named flows 2, 3, and 6 on the basis of their sequence above the base of the Picture Gorge basalt (Lindsley, 1960). A generalized section of flow 6 is given in Fig. 70; flows 2 and 3 are closely similar. Between the jointed lower zones and the flow top lies a "pegmatoid zone," 30–40 m of massive, coarse-grained basalt ("host rock") that contains pegmatoids ranging from 2 cm to 1.5 m thick. Most pegmatoids are horizontal to subhorizontal, with matching top and bottom contacts, suggesting that they formed as crack fillings rather than by replacement of the host basalt. Individual pegmatoids are lens shaped and can rarely be traced laterally for more than 10 m; typically they pinch out as other *en echelon* pegmatoids thicken, so that the total thickness (1.5 to 3.0 m) of pegmatoid material in any vertical section is similar to that in nearby sections. Pegmatoids are distinguished from the enclosing host rock by their coarser grain size and especially

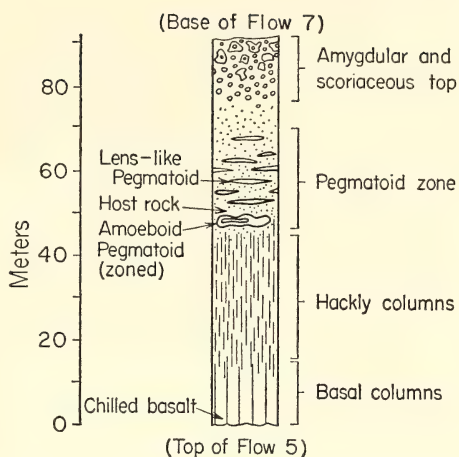


Fig. 70. Schematic section through flow 6. Stippled region indicates interior zone of coarsely crystalline basalt, including host rock of pegmatoid zone.

by their lighter color, which is due mainly to abundant (up to 50%) zeolite-filled amygdules. The proportion of amygdules is greatest in thin pegmatoids and near the tops of thick pegmatoids. Coarse crystals of olivine and pyroxene are concentrated at the base of some pegmatoids.

There are many similarities between these thick flows and the prehistoric Makaopuhi lava lake in Hawaii (Moore and Evans, 1967; Evans and Moore, 1968). For example, the pegmatoids in the lava lake also have matching walls and *en echelon* distribution, which Moore and Evans (p. 205) interpret as indicating that the host rock tore open while still plastic. In contrast, however, the lava lake (where studied) is only 68 m thick, and the thickest pegmatoids in it are of the order of 0.25 m. Whereas the thick Picture Gorge basalts are capped by scoriaceous rubble approximately 15 m thick, with upper columnar jointing typically absent, the lava lake has a well-developed set of upper columns and apparently only a thin vesicular top.

The pegmatoid zones of flows 2 and 3 (and to a lesser extent in flow 6) are cut by a series of vertical joints that outline

huge "columns," 3 to 10 m across. For 10 to 60 cm adjacent to these joints, the basalt weathers in relief. These "joint selvages" are typically lighter in color than the surrounding host rock; they may have a pinkish cast that reflects the presence of hematite, maghemite, goethite, and pseudobrookite, a highly oxidized assemblage. The structures are much larger than, but essentially similar to, those described by Fuller (1938) in the Steens basalt.

The occurrence of pegmatoids in Picture Gorge basalt appears to be restricted to the vicinity of an east-west Miocene stream valley. To the best of our knowledge, abundant pegmatoids are not found more than a few kilometers either to the north or to the south of this valley (although poorly formed pegmatoids occur in the Picture Gorge quadrangle about 12 km south of Kimberly). It is possible that pegmatoids were an inherent characteristic of the three thick flows, which, being near the bottom of the basalt sequence, were constrained to the valley by topography. In addition, the restriction of these flows to the valley area may actually have contributed to the development of pegmatoids through the addition of abundant water from lakes and streams inundated by the lava. The model for the development of pegmatoids to be presented here requires the presence of water trapped in or dissolved in the lava. It is relatively unimportant, however, whether that water was juvenile, was added to the magma on its ascent to the surface, or was contributed at the surface.

The following lines of evidence bear on the origin of the pegmatoids in flows 2, 3, and 6 (for greater detail see Lindsley, 1960):

1. The existence of a thin layer of tuffaceous sediments containing charred plant material between flows 2 and 3 suggests that flow 2 had crystallized before being buried by later flows. Although direct evidence is lacking, it is

assumed that flows 3 and 6 likewise crystallized before being buried. Thus the only overburden during pegmatoid formation is that due to the upper portion of each flow.

2. Pegmatoids are restricted to an interior zone, lying just above the center of each flow, in which the average grain size of the basalt reaches a maximum. If it is assumed that the zone of maximum grain size was also the zone of slowest cooling, then these thick flows cannot have cooled in accord with the assumptions of Jaeger (1961), for they must have lost heat more readily through the bottom than through the top. Probably the thick (15 m) flow tops of scoria inhibited cooling from the upper surface.

3. Contacts of pegmatoids with host rock are sharp but unchilled; any transition zone is less than 1 mm in thickness.

4. Matching upper and lower contacts indicate that many pegmatoids occupy horizontal to subhorizontal dilatant fractures in the host rock.

5. The ubiquitous occurrence of gas bubbles (now amygdules) in the pegmatoids shows that the pegmatoid material was emplaced as a liquid and that a gas phase either was present at the time of emplacement or was formed prior to solidification. The pressure of the gas phase must have been approximately 8–10 bars to balance the weight of the overlying portions of the flow.

6. The plagioclase and clinopyroxene in the pegmatoids are strongly zoned; their compositions correspond to those of the outermost zones of similar phases in the host rock. Detailed discussion of these relationships is deferred to the sections on mineral chemistry.

7. Enrichment of the pegmatoids in  $\text{SiO}_2$ , alkalis,  $\text{TiO}_2$ , and  $\text{P}_2\text{O}_5$  and depletion in  $\text{MgO}$  relative to the host rock (Lindsley, 1960, Table 8) indicate derivation of the pegmatoids from residual liquids of the crystallizing basalt.

8. Pegmatoids occupy approximately 5 to 10% of the volume of the pegmatoid



zone. Therefore, at least that proportion of liquid must have been present at the time the pegmatoids formed. Materials-balance calculations for flows 2 and 3 made by T. L. Wright (written communication, 1970) indicate that the pegmatoids formed when the host rock was approximately 50 to 75% crystallized.

At the base of the three thick flows the pressure due to the weight of the overlying lava approached 30 bars, sufficient to retain some water in the flow, either as a gas phase at that pressure or dissolved in the lava, or both. As cooling and crystallization proceeded inward from flow top and bottom, the dissolved water would be trapped. As more and more lava crystallized, the dissolved water would be restricted to an ever-decreasing proportion of liquid, and its vapor pressure would increase. If the vapor pressure exceeds that of the overburden while the interior of the flow still behaves as a fluid, the excess pressure can be released by uplift of the flow top, either in stages just sufficient to compensate the pressure or in an explosive removal of the flow top.

The situation is somewhat different if even the most slowly cooled zone of the flow has crystallized sufficiently to form a rigid network of crystals—which on the basis of Hawaiian lava lake observations (T. L. Wright, oral communication) occurs at about 50% crystallization—before the vapor pressure matches that of the overburden. Pressure relief by uplift of the flow top can then take place only when the vapor pressure is equivalent to the weight of the overburden *plus* the tensile strength of the crystal network, and only by the opening of horizontal or subhorizontal cracks in that network. Once such a crack forms, a part of the interstitial liquid is forced into the crack, which may continue to open until the local pressure is balanced. As pressure on the liquid phase is released, some of the dissolved water boils, forming gas bubbles in the fluid-filled cracks (which will of course become

pegmatoids on crystallization). Within the crystal network (which will become host rock) the evolving gas will displace liquid, forcing its migration into the nearby cracks, and leaving behind diktytaxitic cavities (Fuller, 1938). This model for pegmatoid formation, which is similar to that proposed by Bailey (in a discussion of a paper by Tyrrell, 1928, p. 568), is supported by data from Makaopuhi lava lake (T. L. Wright, written communication, 1970). The surface of the cooling lava lake initially subsided in response to thermal contraction. At about the stage of crystallization where pegmatoids began to appear (as shown by drilling), however, this downward trend was reversed and the upper surface began to rise.

It is possible that the cracks form solely in response to the pressure exerted by the confined melt, but it seems more plausible that they may originate in response to thermal contraction of the flow. However they form, it is necessary that one or more cracks continue to widen as crystallization continues, at least until the gas pressure is reduced in some other fashion. The pressure might be lowered either by diffusion of gas through the flow top or along vertical joints extending into the pegmatoid zone. The mutual interaction of the escaping gas, the atmosphere, and the basalt adjacent to the joints produces the oxidized joint selvages.

The ratio of length to maximum observed thickness in pegmatoid lenses is rarely less than 10:1 and usually closer to 20:1. Evidently, increases in the thickness of a given lens are accomplished mainly by horizontal extension, with minimum deformation of the surrounding crystal framework. Presumably, the pegmatoid lens will continue to grow in this fashion until the vapor pressure within the pegmatoid no longer exceeds that of the overburden (either by formation of adjacent pegmatoids or by escape of gas), or until the pegmatoid itself forms a rigid crystal framework.

The migration of interstitial melt from the host rock into the pegmatoid may well take place over a period of time. As the pegmatoid grows in this fashion, fractionational crystallization continues in the crystal network (host rock), so that increasingly differentiated liquids are added to the pegmatoid. Thus the striking chemical zoning in the pegmatoid minerals probably reflects fractional crystallization in the host rock as well as in the pegmatoid itself.

The lens-shaped pegmatoids that fill obvious tension cracks comprise 90% or more of those observed; it is from this type that the optical and bulk chemical data of Lindsley (1960) were obtained. During the 1969 field work, a somewhat different pegmatoid from flow 6 was found exposed in a recent road cut: its shape is amoeboid rather than lens-like (although it was still flattened in the horizontal plane) and it contains two distinct zones. The outer (and apparently older) zone is darker in color than the inner part, and it everywhere separates the inner, lighter zone from the host rock. The contacts between host rock and outer zone and between inner and outer zones are both sharp. Evidently, this zoned pegmatoid formed at an earlier stage of crystallization than the lens-shaped pegmatoids. Its amoeboid shape is interpreted as indicating that it formed before the enclosing host rock had achieved *rigid* framework but yet was sufficiently coherent to permit segregation of interstitial liquid into a body with irregular but sharp boundaries.

The four samples whose mineral chemistry is detailed in the following sections all are from flow 6, and include (1) the inner, light pegmatoid, (2) the outer dark pegmatoid, (3) the adjacent host rock, and (4) the chilled margin. All four samples contain the same principal magmatic minerals: plagioclase, augite, olivine, titanomagnetite, and ilmenite. The proportions of phases in all but the light pegmatoid are similar, and modal analysis (1000 points) of the

analyzed sample (Table 33) from the basal chill zone yielded these percentages: plagioclase, 49; augite, 32; olivine, 8; oxides, 5; and remainder (mainly clay minerals), 6. Mineral proportions in the light pegmatoid are variable on the scale of outcrop, hand specimen, and thin section; in general, the light pegmatoid contains a higher proportion of feldspar relative to mafic phases than the other three rock types. Traces of pigeonite were identified in the chilled margin, host rock, and light pegmatoid. Apatite and alkali feldspar occur in host rock and pegmatoid. Minor aegirine-augite and aenigmatite are chiefly restricted to pegmatoids, though traces of aenigmatite were recognized in host rock. Montmorillonoid clay minerals are present in all four rock types, both replacing olivine and in pockets of residual material, perhaps replacing glass; they are particularly abundant in the host rock. Chabazite occurs in the pegmatoids and host rock filling amygdules and diktytaxitic cavities.

Each of the four rocks is texturally distinct. The sample from the chilled flow base has an ophitic texture and an average grain size of 0.1–0.2 mm; it contains sparse plagioclase phenocrysts, commonly in glomeroporphyritic clots, and rare anhedral olivine phenocrysts. The host rock specimen has a subophitic texture and an average grain size of about 1 mm; it contains scattered diktytaxitic cavities. Both pegmatoid facies are distinctly coarser in average grain size than host rock, and they also contain more abundant chabazite-filled amygdules and diktytaxitic cavities. Both contain relatively large grains of early plagioclase and augite and smaller grains of late-stage alkali feldspar and Na-rich and Fe-rich pyroxene; the late-forming phases are typically concentrated in pockets. These pockets of residual material are more abundant and larger in the light pegmatoid than in the dark one, though even in this facies they constitute only 5 to 10% of the



rock. Crystal habits differ in the two rock types. Titanomagnetite and olivine occur in skeletal crystals in light pegmatoid; these habits are less well developed in the dark facies. Some augite in light pegmatoid forms intricate ophitic crystals up to 15 mm in maximum diameter, whereas in the dark pegmatoid augite forms generally smaller, subophitic to equant grains.

*Chemical Variations in Pyroxene and Olivine from Picture Gorge Basalt*

*Douglas Smith and D. H. Lindsley*

The wide range of compositions of olivine and pyroxene in flow 6 are matched only in differentiated stratiform intrusions and lunar basalts, and the flow provides an unusual opportunity to study crystallization of pyroxene and olivine in liquids derived from differentiation of a basalt at low pressure. The three different crystallization environments in the flow—chilled margin, slowly cooled interior, and pegmatoid—also provide an opportunity to study the influence of kinetics on pyroxene crystallization. Results of these studies can be applied to interpret compositional variations in pyroxenes from other environments, such as the lunar mares, where we have little direct knowledge of crystallization rates because the positions of samples within their parent rock masses are not known. Augite, the principal pyroxene, and olivine are present throughout the flow, as are traces of late-crystallizing pigeonite. Aegirine-augite and aegirine occur in trace quantities in the pegmatoids.

Calcium-rich pyroxene compositions extend from compositions as magnesian as  $\text{Ca}_{44}\text{Mg}_{43}\text{Fe}_{13}$  in host rock to compositions as iron rich as  $\text{Ca}_{40}\text{Mg}_{10}\text{Fe}_{50}$  in adjacent pegmatoid (Fig. 71). The most magnesian augite composition is  $\text{Ca}_{43}\text{Mg}_{42}\text{Fe}_{15}$  in dark pegmatoid and  $\text{Ca}_{42}\text{Mg}_{38}\text{Fe}_{20}$  in light pegmatoid. This indication that the dark pegmatoid predates the light one is corroborated both by

field relations and by feldspar compositions (p. 276). Numerous six- and eight-element analyses were made on points in augite crystals from chilled basalt, host rock, and pegmatoids (examples, Table 29); Al markedly decreases in augite with iron enrichment and Ti remains approximately constant. The aluminum and titanium contents of the more magnesian augites are similar to those of augites with similar Fe/Mg ratios from the Skaergaard intrusion (Brown, 1957).

Compositional trends of pyroxenes in host rock and dark pegmatoid (Fig. 71 B, C) are approximately parallel to the early part of the Skaergaard trend and to the augite trends in numerous other differentiated intrusions of basaltic rock. Crystals are progressively zoned to more iron-rich margins; a maximum zoning of 14 mole % ferrosilite was observed in a single crystal. The pyroxenes are slightly more calcic than those in the Skaergaard intrusion, a fact consistent with the observation that most of the augite in the flow did not coprecipitate with calcium-poor pyroxene, perhaps due to a somewhat lower silica activity in the magma of the basalt flow. The trends are presumed to reflect equilibrium crystallization of pyroxene from successively more iron-rich liquids formed by normal fractional crystallization.

The trend established by compositions of pyroxene in the chilled basal portion of the flow (Fig. 71A) is at a sharp angle to the normal trends. It reflects Ca-Fe substitution at a nearly constant proportion of Mg; it is approximately parallel to the sequence outlined by Kuno (1955) in a study of volcanic pyroxenes and subsequently called a "quench trend" by Muir and Tilley (1964). There is little chemical difference between the chilled base and the slowly crystallized interiors of similar thick flows in the area (Lindsley, 1960), and the distinction between the pyroxene trends can best be ascribed to a differ-



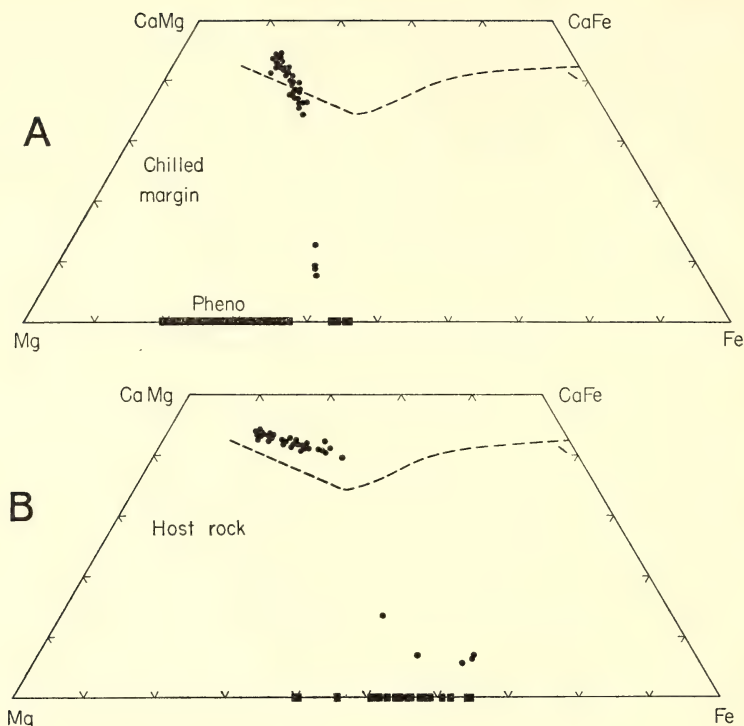
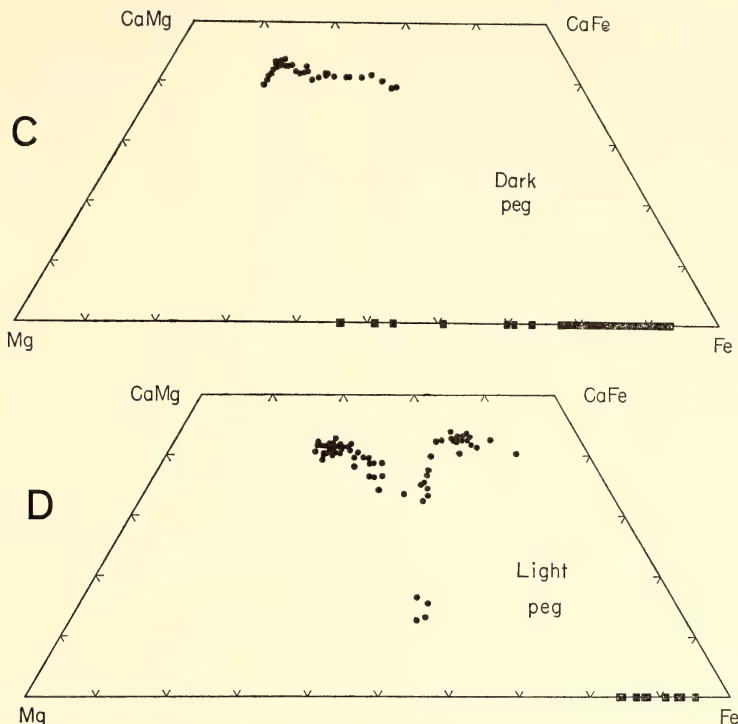


Fig. 71. Compositions of pyroxene (dots) and olivine (squares and solid bars) in samples of chilled margin (A), slowly cooled interior (B), dark pegmatoid (C), and light pegmatoid (D) from the differentiated basalt flow, as determined with an electron microprobe. The solid bars represent ranges of olivine compositions in single, continuously zoned crystals; the bar in (A) represents compositions in a zoned phenocryst. The dashed lines in (A) and (B) represent the augite trend in the Skaergaard intrusion (Wager and Brown, 1968). Sodic pyroxene compositions are not plotted on these diagrams. Only trace amounts of pigeonite are present, and most of the augite did not coprecipitate with a calcium-poor pyroxene.

ence in crystallization rate. The contrast between the trends in two parts of the same flow verifies the concept of the "quench trend" and illustrates the role kinetics can play in determining compositions of igneous phases. The fact that pyroxene compositions in the chilled base form a distinct trend in the quadrilateral rather than a random pattern suggests the operation of a well-defined process, such as either a metastable (as opposed to a nonequilibrium or random) crystal-liquid partition or an equilibrium partition together with a disequilibrium diffusion zone in the liquid around the growing crystal. The compositions of the pyroxenes that define the calcium-poor

end of the quench trend are evidence of another type of metastability in the quench pyroxenes; since these compositions fall within the two-pyroxene field defined by analyses of Skaergaard pyroxenes (Fig. 71A), they probably formed metastably with respect to two phases, a more calcium-poor and a more calcium-rich pyroxene. Further evidence suggests both that this quench trend reflects a metastable crystal-liquid fractionation and that pyroxene compositions at the calcium-poor end of the trend formed metastably with respect to two pyroxenes (Smith and Lindsley, 1970).

The crystal habits of augite reflect the



different rates and environments of crystallization. In chilled rock near the base of the flow, augite forms intricately shaped ophitic crystals, whereas in the more slowly crystallizing host rock the crystals are more nearly equant and distinctly less ophitic. In the less differentiated dark pegmatoid, augite crystals are much larger than in the host rock but are similar in habit. Augite in the more differentiated light pegmatoid forms still larger crystals (up to 15 mm in extent) with much more pronounced ophitic tendencies. The light pegmatoid also contains small, iron-rich augite grains, which formed later than the larger ophitic crystals.

Most of the augite in the large crystals in light pegmatoid shows little Fe-Mg-Ca zoning and is near  $\text{Ca}_{41}\text{Mg}_{36}\text{Fe}_{23}$  in composition: these large crystals comprise the bulk of clinopyroxene in the light pegmatoid, and a separate of all clinopyroxene from this rock would have an

average composition only slightly more iron rich than this value. Some of the large crystals have very thin marginal zones with more iron-rich, less calcic compositions; compositions in these zones form the trend of decreasing Ca in Fig. 71D. Some of these marginal zones are bordered by selvages of pigeonite several tens of micrometers thick. The bulk of augite in the small, late crystals is near  $\text{Ca}_{43}\text{Mg}_{17}\text{Fe}_{40}$  in composition. One iron-rich crystal in the light pegmatoid was zoned from a less calcic core ( $\text{Ca}_{33}\text{Mg}_{27}\text{Fe}_{40}$ ) to a more typical calcic composition ( $\text{Ca}_{44}\text{Mg}_{18}\text{Fe}_{38}$ ); compositions from this crystal are also plotted in Fig. 71D. The causes of these unusual pyroxene variations in the light pegmatoid are not understood. They may be related to an influx of new pegmatoid material or they may reflect disequilibrium or metastable pyroxene crystallization.

Large pyroxene crystals in pegmatoids

TABLE 29. Microprobe Analyses of Pyroxene and Olivine in Flow 6

	1	2	3	4	5	6	7
SiO <sub>2</sub>	50.5	50.5	49.4	49.0	48.7	52.2	30.4
TiO <sub>2</sub>	0.20	1.3	2.0	0.97	0.65	0.06	0.11
Al <sub>2</sub> O <sub>3</sub>	0.08	1.9	3.1	0.70	0.14	0.04	0.04
Fe as Fe <sub>2</sub> O <sub>3</sub>	...	...	...	...	7.0	33.6	...
Fe as FeO	35.5	11.7	13.6	22.9	22.7	...	62.8
MnO	0.88	0.29	0.33	0.60	0.66	0.04	1.4
MgO	11.1	13.4	13.0	5.9	2.3	0.02	4.5
CaO	2.7	20.5	18.4	19.5	14.6	0.08	0.46
Na <sub>2</sub> O	0.11	0.40	0.43	0.39	2.7	13.2	...
Totals	101.1	100.0	100.3	100.0	99.4	99.2	99.7
O	6	6	6	6	6	6	4
Si	2.00	1.91	1.87	1.95	1.98	2.02	0.998
Al	0.004	0.083	0.140	0.032	0.007	0.002	0.002
Ti	0.006	0.037	0.057	0.029	0.020	0.002	0.003
Fe as Fe <sup>3+</sup>	...	...	...	...	0.213	0.976	...
Fe as Fe <sup>2+</sup>	1.18	0.370	0.431	0.764	0.769	...	1.72
Mn	0.029	0.009	0.010	0.020	0.023	0.001	0.040
Mg	0.657	0.758	0.731	0.352	0.141	0.001	0.219
Ca	0.114	0.831	0.746	0.835	0.635	0.004	0.016
Na	0.009	0.029	0.031	0.030	0.213	0.989	...

1. Pigeonite grain at edge of diktytaxitic cavity in host rock (351-69, E4).
2. Augite in host rock (351-69, E5).
3. Augite in large crystal in light pegmatoid (368-69, E2).
4. Augite in small, late crystal in light pegmatoid (368-69, C3); the crystal is intergrown with the olivine represented by analysis 7.
5. Aegirine-augite associated with aenigmatite and alkali feldspar in light pegmatoid (368-69, I4). Ferric iron calculated to balance sodium.
6. Aegirine in light pegmatoid (368-69, M13).
7. Olivine in light pegmatoid (368-69, C2).

contain geometrically bounded volumes of augite with distinctly different aluminum and titanium contents from the augite around them. The volumes, distinguishable in thin section by slightly different extinction and birefringence, appear to be crystal sectors, using "sector" in the sense applied to staurolite by Hollister and Bence (1967) and to pyroxene by Scott (1914), Strong (1969), and others. These volumes are most apparent in sections nearly perpendicular to *c*, and they may represent the (001) sector; differences between other sectors are not readily apparent. Perhaps because many crystals in pegmatite are intricately shaped and ophitic, the familiar hour-glass sector zoning so commonly described for pyroxene (e.g., Strong, 1969; Hargraves, Hollister, and Otalora, 1970) is poorly developed and was observed in only a few grains. There are distinct differences in Al, Ti, and Si

between the presumed (001) sector and surrounding augite, whereas differences in Ca, Fe, and Mg are relatively smaller, as illustrated by the microprobe traverses across one of the geometric boundaries shown in Fig. 72. The most likely explanation for such zoning is that it reflects preferential incorporation of selected elements into different crystal sectors because of different atomic configurations on growth faces, as advanced by Hollister (1970). This explanation implies both chemical disequilibrium between adjacent sectors and a disequilibrium crystal-liquid partitioning for some elements. Though the sectors are common in pegmatoid augite, they were not observed in crystals in the host basalt. The environment of crystallization in the pegmatoids was distinctly different from that in the host basalt, as reflected not only by the larger, more ophitic augite crystals but also by the



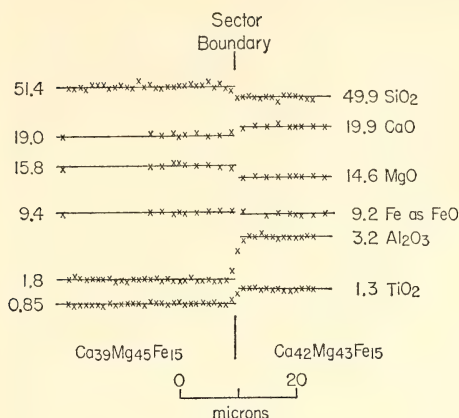


Fig. 72. Results from microprobe traverses on a single augite crystal across the boundary between the presumed (001) sector (left) and an unidentified sector (right). The oxide weight percentages were calculated from the lines drawn through the points in each sector.

spectacular skeletal magnetite<sub>ss</sub> crystals (Plate 4A) and the skeletal olivines in the former. The pegmatoids are amygdaloidal, and pegmatoid magma presumably was nearly or completely saturated with volatiles throughout its crystallization. The volatiles not only would have increased the fluidity of the melt but also may have promoted rapid crystallization due to the removal of their heat of vaporization. The pegmatoid augite may have crystallized more rapidly and from a more fluid magma than the host rock augite.

The assumption that mineral composition trends reflect a stable equilibrium fractionation of elements between crystals and melt underlies most studies of igneous rocks. The crystallization of calcic pyroxene in the flow is of particular interest because the several types of metastable or disequilibrium fractionation that occurred can be related to specific crystallization environments. Augite in basalt in the central part of the flow apparently precipitated in equilibrium with a melt changing in composition because of fractional crystallization. Larger and perhaps more rapidly formed

crystals in the pegmatoids have sector zoning, which implies a disequilibrium fractionation of elements between augite and the melt on at least some of the crystal growth faces. The trend formed by compositions of small ophitic augite grains near the chilled flow base, presumably the grains that crystallized most rapidly, defines a systematic variation in the major elements, Ca, Fe, and Mg distinctly different from the trend of variation in the more slowly formed crystals in the host rock. Compositional variations in pyroxene that crystallized rapidly, as pyroxene may have in the fluid lunar basalts, may be best interpreted in light of such disequilibrium fractionation processes.

Only trace quantities of pigeonite are present in the flow. It is a late-stage crystallization product in the chilled margin and host rock, where it forms small crystals at the borders of cavities and pockets of residuum. In light pegmatoid, pigeonite forms rare overgrowths several tens of micrometers thick on parts of some ophitic augite crystals. Pigeonite compositions are plotted together with augite and olivine analyses in Fig. 71; it is clear from textural evidence, however, that most of the augite and olivine did not coprecipitate with the calcium-poor pyroxene.

Olivine formed early in the basalt magma, with phenocryst cores as magnesian as (Mg<sub>0.80</sub>Fe<sub>0.19</sub>Ca<sub>0.004</sub>)<sub>2</sub>SiO<sub>4</sub> in the chilled flow base. It continued to crystallize until the most differentiated magma solidified in the pegmatoids, where crystals as iron rich as (Mg<sub>0.05</sub>Fe<sub>0.32</sub>Ca<sub>0.005</sub>Mn<sub>0.02</sub>)<sub>2</sub>SiO<sub>4</sub> occur with other late-stage phases. Some of the iron-rich crystals in the light pegmatoid have well-developed skeletal habits. There is no evidence for a crystallization break in the olivine series, and an apparently continuous range of compositions from Fo<sub>54</sub> to Fo<sub>7</sub> was found in a single thin section of dark pegmatoid. Most crystals are zoned; the maximum zoning observed was 18 mole % forsterite in a rimmed

phenocryst in the chilled margin. Even in the slowly cooled host rock an analyzed crystal was zoned by 14% forsterite over a distance of 0.4 mm, suggesting that postcrystallization diffusion in olivine (Moore and Evans, 1967) could have produced only limited effects in the flow.

Minor aegirine-augite, containing 12 to 45 calculated % acmite molecule, is associated with other late-forming phases in the pegmatoids. The aegirine-augite occurs both as apparent reaction rims or overgrowths on iron-rich augite and as small independent crystals. Microprobe data suggest a slight compositional discontinuity between augite and aegirine-augite in these rocks; the most sodic augite analyzed, tan in thin section, contained 0.51%  $\text{Na}_2\text{O}$ , and the least sodic aegirine-augite, green in thin section, contained 1.5%  $\text{Na}_2\text{O}$ . Nearly pure aegirine, containing less than 0.1 wt %  $\text{MgO}$  and  $\text{CaO}$  (Table 29, analysis 6), was found in one diktytaxitic cavity as a

colorless overgrowth on aegirine-augite associated with aenigmatite, fayalite, and alkali feldspar. This pure aegirine may have formed from the pegmatoid vapor phase.

### *Chemical Variations in the Feldspars*

*D. H. Lindsley and Douglas Smith*

An extreme range of feldspar compositions provides the most striking evidence of differentiation in the thick flows of Picture Gorge basalt. Indeed, one thin section (no. 351-69) of host rock from flow 6 contains feldspar ranging from  $\text{An}_{84}\text{Ab}_{15.5}\text{Or}_{0.5}$  through  $\text{An}_{11.5}\text{Ab}_{77.5}\text{Or}_{11}$  to  $\text{An}_{0.3}\text{Ab}_{99.9}\text{Or}_{59.8}$  with few gaps in between (Fig. 73).

Although detailed optical studies have not been made on the samples used for microprobe analysis, it is likely that the optical results of Lindsley (1960, pp. 57-67, 117-124) are representative, and they are summarized here. On the basis of universal stage measurements and the

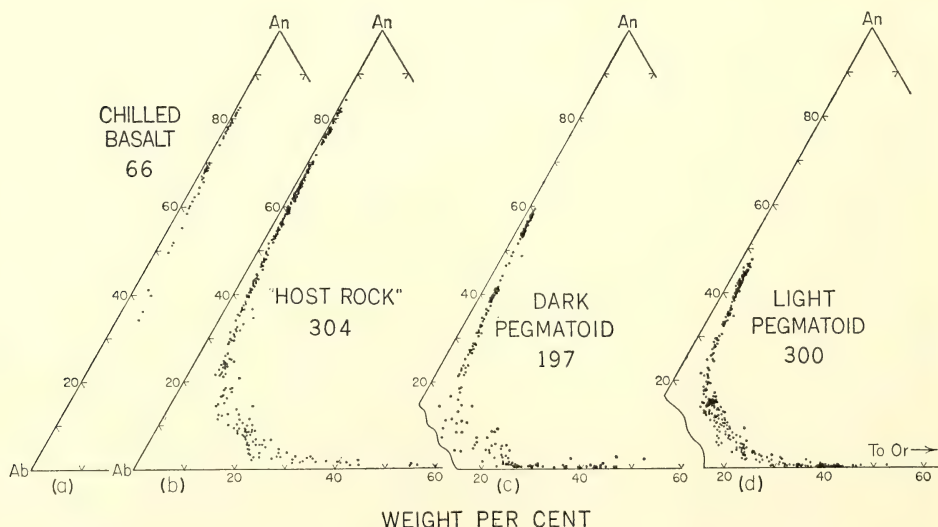


Fig. 73. Compositions as determined on points of zoned feldspar crystals with the electron microprobe. Number of points analyzed is given below each rock name. Most points are based on analyses for K, Na, and Ca only, which are then converted to Or, Ab, and An, assuming stoichiometry. Chilled basalt, no. 346-69, from 1.5 m above base of flow 6. Host rock, no. 351-69; dark pegmatoid, no. 367-69; light pegmatoid, no. 368-69, all from approximately 45 m above the base of flow 6, and within 1.2 m of each other.

method of Köhler (1941; Van der Kaaden, 1951; Kano, 1955), all plagioclase from pegmatoids and most from host rock and other zones of the flows are in the "high" structural state. Of the remainder, most are "intermediate" and only a very few are in the "low" state. All parts of the flows *except* the pegmatoids contain phenocrysts with optically distinct cores of calcic plagioclase and with rims identical in composition with that of groundmass laths. There is a compositional gap between phenocryst cores and rims extending from approximately An<sub>65</sub> to An<sub>75</sub> as determined optically. Pegmatoid feldspars range from An<sub>48</sub> to An<sub>53</sub> in the cores and are progressively zoned toward albite and alkali feldspar. Most plagioclase twinning in the pegmatoids is according to the simple albite law, whereas that from the host rock is dominantly by the simple Carlsbad or combined albite-Carlsbad laws. Alkali feldspar in the pegmatoids has two main occurrences: as outer zones on plagioclase and as independent euhedral grains—sometimes hollow—intergrown with iron-rich olivine and clinopyroxene and with a residuum now mainly altered to clay minerals.

Unlike the prehistoric Makaopuhi lava lake (Evans and Moore, 1968), the lava forming the thick Picture Gorge flows was saturated with plagioclase at the time of their eruption. As a result, we did not find the correlation of maximum An content with depth reported for the lava lake.

Because of nearly ubiquitous compositional zoning, most feldspar analyses presented here are of a single point only; averaging values for several points would be meaningless. Most of the 867 points in Fig. 73 are partial analyses for K, Na, and Ca only; they were converted to Or, Ab, and An, assuming stoichiometry of Al and Si. [More complete analyses (K, Na, Ca, Al, Si, Fe) for selected samples (Table 30) show that this assumption is good but not perfect.] In order to avoid loss of sodium during analysis the maxi-

TABLE 30. Microprobe Analyses of Feldspars from Picture Gorge Basalt

	1	2	3	4
SiO <sub>2</sub>	49.8	52.9	61.7	67.7
Al <sub>2</sub> O <sub>3</sub>	31.3	29.0	23.4	18.1
Fe as FeO	0.72	0.82	0.54	0.57
CaO	16.3	12.4	5.1	0.01
Na <sub>2</sub> O	2.3	4.3	8.2	7.0
K <sub>2</sub> O	0.07	0.26	1.03	6.7
Totals	100.5	99.7	100.0	100.1
8 oxygens				
K	0.004	0.015	0.06	0.38
Na	0.20	0.38	0.71	0.61
Ca	0.80	0.61	0.24	0.001
Si	2.27	2.41	2.75	3.03
Al	1.68	1.56	1.23	0.96
Fe	0.03	0.03	0.02	0.02

1. Core of plagioclase phenocryst, chilled margin of flow 6. Point E2, no. 346-69.

2. Groundmass plagioclase, chilled margin of flow 6. Point C1, no. 346-69.

3. Na-rich feldspar from groundmass of host rock, flow 6. Point C18, no. 351-69.

4. Euhedral, residual alkali feldspar, light pegmatoid, flow 6. Point C10, no. 368-69.

imum exposure time to the electron beam (15 kv, 0.05  $\mu$ a, 8–12  $\mu$ m spot) was determined before Na loss became obvious; then final analyses were made with counting times about one-half that value. The K standard was an orthoclase containing 12.39 wt % K; synthetic An<sub>50</sub> (mole) glass (Lindsley, 1968, pp. 43–44), which had been carefully checked against other plagioclase glasses, was used for Na, Ca, Al, and Si. The An<sub>50</sub> glass standard was constantly moved during readings to minimize effects of Na loss. The use of these standards resulted in very small correction terms for matrix effects on K, Na, and Ca.

Well over half the analyses plotted in Fig. 73 are based on step-scan traverses across zoned crystals. Examination of Fig. 73 shows several points of interest. The optically detected compositional gap between phenocryst cores on the one hand and phenocryst rims and ground mass plagioclase on the other is confirmed (Fig. 73), although the microprobe data show a narrower gap (An<sub>70–74</sub>). The width of the gap is prob-



ably more accurately determined by optical methods, for whereas the break between phenocryst cores and rims is sharp ( $<1\ \mu\text{m}$  in width), the  $8\text{--}12\ \mu\text{m}$  spot size used to minimize Na loss undoubtedly resulted in hybrid values when the beam overlapped core and rim during step-scan traverses of the phenocrysts. The compositional trends in Fig. 73 are similar to those reported for feldspars from a Hawaiian lava lake (Evans and Moore, 1968), although the Hawaiian alkali feldspars tend to contain more calcium.

Large numbers of analyses were made of feldspars from the host rock, dark pegmatoid, and light pegmatoid in an attempt to detect sympathetic or antipathetic relations among them. Although the distribution of analyzed points is *not* rigorously proportional to the volume of feldspar having a given composition (the sampling was biased toward sodic and potassic feldspars), the dominance of points from step-scan traverses gives meaning to variations in point density *for adjacent compositions*. Thus if traverses across eight or ten crystals in a given sample all show a gap in the same compositional range, it is likely that feldspar of that composition crystallized sparsely, if at all, in that sample. A concentration of points, on the other hand, may indicate an abundance of feldspar of that composition, but may also represent the results of a traverse across a grain sectioned parallel to a growth surface rather than through its center. Thus concentrations of points indicate relative abundance in the sample only if they appear on two or more traverses.

Several features are evident in comparing the compositions of feldspars from the host rock and the pegmatoids. (1) The pegmatoid feldspars show restricted range of composition compared with that of feldspars from the host rock. This is particularly so for the more Ca-rich feldspars but is also true for the potassic compositions. (2) The high-calcium end of each pegmatoid trend is rather sharply

defined ( $\text{An}_{59.5}$  for the dark pegmatoid,  $\text{An}_{47.5}$  for the light pegmatoid), and there is a concentration of points within 10% An of each initial composition. This is ascribed to the initial rupture of the host rock and the rapid emplacement of abundant liquid of nearly uniform composition in each case (note that the dark pegmatoid is the host for the light one). (3) The compositional trend in the dark pegmatoid (Fig. 73C) shows a break at the composition of the most calcic feldspar in the light pegmatoid. We interpret this to mean that the removal of liquid from the crystallizing dark pegmatoid to form the light pegmatoid resulted in a temporary volumetric decrease of feldspar crystallizing in the host. (4) There is no evidence for coprecipitation of plagioclase and alkali feldspar: in crystals from all three samples there is progressive (but not always continuous) core-to-rim zoning from plagioclase to approximately  $\text{An}_1\text{Ab}_{61-64}\text{Or}_{35-38}$ . All traverses show a break in approximately that composition range (although the composite plots in Fig. 73 tend to mask the break) which is very near the minimum in the Ab-Or system at low water pressures (Tuttle and Bowen, 1958). We feel confident from textural evidence that the progressive zoning to that composition reflects crystal-liquid partitioning. Compositions more potassic than  $\text{Or}_{35-38}$ , however, show a less orderly distribution; the zoning is erratic rather than progressive. They may well have been modified by crystal-vapor exchange or perhaps even have been precipitated from the gas phase. (5) The An content of  $\text{Or}_{30-45}$  feldspars in both pegmatoids is distinctly lower than that in the host rock. As temperature and pressure were unlikely to have varied between pegmatoids and host rock, the difference is attributed to a gradient in the activity of  $\text{CaAlSi}_2\text{O}_6$ , suggesting that the pegmatoids were effectively isolated from the host rock at this late stage of crystallization.

Twenty-seven feldspar points from the

chilled margin, host rock, and light pegmatoid were chosen for analysis of Al, Si, and Fe as well as K, Na, and Ca. Fe was found in all samples, ranging from 0.4 to 0.9 wt %; it was assumed to be trivalent, substituting for  $\text{Al}^{3+}$ . For most of the 27 analyses, K, Na, and Ca sum to  $1.00 \pm 0.02$ , and Al, Si, and Fe to  $4.00 \pm 0.01$  atoms per 8 oxygens, in excellent agreement with theoretical feldspar compositions. For plagioclase, however, the number of trivalent ions in tetrahedral sites ( $\text{Al}^{3+} + \text{Fe}^{3+}$ ) should equal 1.0 plus the number of Ca ions per 8 oxygens. Preliminary measurements indicated that this rule was violated for the plagioclases from flow 6, so very careful measurements were made (Fig. 74). All analyses plotted in Fig. 74 were repeated once and several were repeated twice. Furthermore, a number of synthetic glasses were analyzed in parallel with the unknowns; their analyses plot close to the theoretical  $45^\circ$  line, so that there appear to be no significant systematic errors in the analysis procedure. For the natural plagioclases, Al+Fe is consistently less than  $1.0 + \text{Ca}$  per 8 oxygens (Fig. 74A). It seems clear that the natural plagioclases are deficient in Al+Fe; they must also have an excess of Si, since the sum of Al+Fe+Si closely approaches the theoretical value. An excess of Si in plagioclase is traditionally ascribed to the presence of "Schwanke's molecule" ( $\text{Ca}_{1/2}\square_{1/2}\text{AlSi}_3\text{O}_8$ ), but that component requires the same ratio of Ca to Al as does anorthite, and cannot explain the excess of Ca over Al reported here. An intriguing alternative is that all or some of the Fe occupies tetrahedral sites as  $\text{Fe}^{2+}$  and results from solid solution toward a hypothetical  $\text{CaFe}^{2+}\text{Si}_3\text{O}_8$  end member. To test this possibility Ca versus Al+2.0 Fe per 8 oxygens is plotted in Fig. 74B. The points for  $0.4 \leq \text{Ca} \leq 0.8$  fall much closer to the theoretical curve. Although Fig. 74B provides permissive evidence for solid solution toward  $\text{CaFe}^{2+}\text{Si}_3\text{O}_8$ , careful X-ray work will have to be done to test its existence.

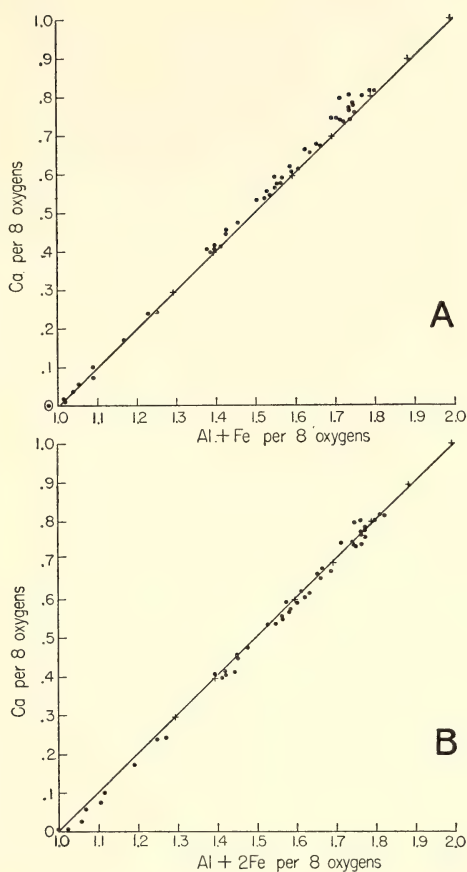


Fig. 74. Plots of Ca versus Al and Fe per 8 oxygens based on two different assumptions regarding the occurrence of Fe in these basaltic plagioclases. Data are plotted only for points where K, Na, Ca, Al, Si, and Fe were determined, and the oxide sum falls between 99 and 101%. Dots, plagioclase from flow 6; crosses, plagioclase glasses. The  $45^\circ$  lines express the stoichiometric condition  $\text{Al} = 1.0 + \text{Ca}$ . (A) It is assumed that Fe is trivalent and substitutes for Al in tetrahedral sites. Note that there is insufficient Al+Fe to balance Ca for  $0.4 \leq \text{Ca} \leq 0.8$ . (B) It is assumed that Fe is divalent and occurs as the hypothetical component  $\text{CaFe}^{2+}\text{Si}_3\text{O}_8$ ; that is,  $\text{Fe}^{2+} + \text{Si}$  replaces 2Al in anorthite. A better fit in the range  $0.4 \leq \text{Ca} \leq 0.8$  provides permissive evidence for the existence of this component.

Ferrous iron in tetrahedral coordination in silicates is known (Shannon and Prewitt, 1969) but is sufficiently rare

that its suspected occurrence should be confirmed.

Mg was looked for in four samples from the light pegmatoid and was found in two intermediate plagioclases (0.07 wt % in  $\text{Ab}_{57}\text{An}_{41}\text{Or}_2$ ; 0.09 wt % in  $\text{Ab}_{53}\text{An}_{45}\text{Or}_2$ ). Somewhat similar contents of Fe and Mg have been found in lunar samples (see paper by Bryan *et al.*, this report). No Mg was found in two alkali feldspars ( $\text{Ab}_{65}\text{An}_1\text{Or}_{34}$ ,  $\text{Ab}_{61}\text{An}_1\text{Or}_{38}$ ).

Ba, Rb, and Sr were looked for in an alkali feldspar ( $\text{Ab}_{61}\text{Or}_{39}$ ) from the light pegmatoid. Rb and Sr were not detected, but 0.1 wt % Ba was found (compared with 0.03 wt % Ca).

### *Phase Relations of Fe-Ti Oxides and Aenigmatite; Oxygen Fugacity of the Pegmatoid Zones*

*D. H. Lindsley and S. E. Haggerty*

The iron-titanium oxide minerals in the three thick flows of Picture Gorge basalt are typical of those from many basalts. In the bottom half and the pegmatoid zone of each flow, discrete homogeneous plates of ilmenite coexist with titaniferous magnetite containing lamellae of ilmenite lying in its (111) planes (ilmenomagnetite). It is now rather generally accepted that such ilmenomagnetites result from oxidation of initial homogeneous ulvöspinel-magnetite solid solutions ( $\text{Mt}_{\text{ss}}$ ); on the oxidation scale of Watkins and Haggerty (1967), most of these grains are class III (where class I is unoxidized and class VI is very highly oxidized). Buddington and Lindsley (1964, pp. 318-321) have pointed out that in many rock bodies this degree of oxidation will normally be obtained during the cooling of  $\text{Mt}_{\text{ss}}$ , particularly if a water-rich vapor is present. The oxidation occurs because the maximum stability curve in the  $f_{\text{O}_2}$ - $T$  plane for  $\text{Mt}_{\text{ss}}$  of any given composition is steeper than those for common iron-bearing silicates (such as augite and olivine) or for water-rich vapor of a constant  $\text{H}_2/\text{H}_2\text{O}$  ratio. Thus a sub-

solidus regime that is moderately oxidizing with respect to  $\text{Fe}_2\text{TiO}_4$ -rich  $\text{Mt}_{\text{ss}}$  will not necessarily be oxidizing with respect to ilmenite and the coexisting ferromagnesian silicates. The compositions—determined by electron microprobe—of coexisting ilmenomagnetite and discrete ilmenite from the host rock in flow 6 are listed in columns 4 and 3 of Table 31. The bulk composition of the ilmenomagnetite was determined by averaging data from a large number of points. In the normative calculations the iron not needed to form  $\text{Fe}_2\text{TiO}_4$  ( $\text{Mt}_{\text{ss}}$ ) and  $\text{FeTiO}_3$  (in ilmenite) is assigned to  $\text{Fe}_3\text{O}_4$  and  $\text{Fe}_2\text{O}_3$ , respectively.

The host magnetite of ilmenomagnetite grains is oxidized in patches to maghemite in the pegmatoid zone and to a lesser extent in the bottom half of each flow. This must reflect low-temperature oxidation, but it is unclear whether the oxidation took place upon the initial cooling or whether it might have accompanied a subsequent zeolitization of the flows upon burial.

In contrast to the host rock, the joint selvages in the pegmatoid zones contain a highly oxidized assemblage. The common presence of pseudobrookite in the selvages indicates that oxidation took place at relatively high temperatures (Year Book 68, p. 249) and so must reflect part of the initial cooling history of the parent flows. Figure 75 shows a decrease in mean oxidation class for the oxide minerals away from a joint into host rock. Lindsley (1960, pp. 147-151) had previously ascribed this gradient to a preferential escape of hydrogen by diffusion from the basalt adjacent to the vertical joints. Although this mechanism may well have been contributory, it is also possible that much of the oxidation resulted from the introduction of water or atmospheric oxygen from the flow surface through the system of vertical joints. Zones of anomalously high oxidation in the interior portions of other basalts are known (Watkins and Haggerty, 1967; Sato and Wright, 1966), but



TABLE 31. Analyses of Ilmenomagnetite, Ilmenite, and Aenigmatite

	1	2	3	4	5
SiO <sub>2</sub>	...	...	...	...	40.7
TiO <sub>2</sub>	24.7	51.1	52.8	23.4	8.7
Fe as FeO	67.1	47.9	45.2	68.1	41.5
MnO	0.97	0.78	0.65	0.58	0.44
MgO	1.6	0.12	1.61	1.00	0.55
Al <sub>2</sub> O <sub>3</sub>	2.0	...	...	...	0.29
Cr <sub>2</sub> O <sub>3</sub>	0.16	...	...	...	...
CaO	...	...	...	...	0.31
Na <sub>2</sub> O	...	...	...	...	6.8
Totals	96.5	99.9	100.3	93.1	99.3
Cations	4 oxygens	3 oxygens	3 oxygens	4 oxygens	20 * oxygens
Fe <sup>2+</sup>	1.58	0.95	0.92	1.30	4.98
Fe <sup>3+</sup>	0.51	0.06	0.02	0.93	0.04
Ti	0.70	0.97	0.99	0.69	0.95
Mn	0.03	0.02	0.01	0.02	0.05
Mg	0.09	0.01	0.06	0.06	0.12
Al	0.09	...	...	...	0.05
Cr	0.005	...	...	...	...
Na	...	...	...	...	1.91
Ca	...	...	...	...	0.05
Si	...	...	...	...	5.91

\* Fe<sup>3+</sup> arbitrarily taken as 1. — (Si + Al).

1. Skeletal ilmenomagnetite from light pegmatoid no. 368-69. Mean of 226 points taken with broad (15–25  $\mu$ m) electron beam.

2. Ilmenite (Plate 4B) associated with aenigmatite in column 5. Light pegmatoid, no. 371-69, approximately 20 cm away from no. 368-69.

3. Discrete ilmenite adjacent to ilmenomagnetite (column 4). Host rock, no. 351-69.

4. Ilmenomagnetite adjacent to discrete ilmenite (column 3). Host rock, no. 351-69. Mean of 42 points taken with broad (10–12  $\mu$ m) electron beam.

5. Aenigmatite occurring as overgrowth (Plate 4B) on ilmenite (column 1). Light pegmatoid no. 371-69.

in those basalts the oxidation was not so clearly controlled by a joint system as in these Picture Gorge basalts.

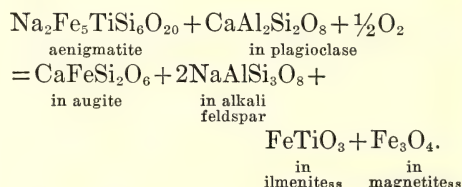
Large skeletal crystals of ilmenomagnetite are easily the most spectacular minerals in the pegmatoids (Plate 4A). The "ribs" of the skeletons lie in the spinel (111) planes; abundant lamellae of ilmenite are included in them and lie in the same planes. The cavities within these skeletal crystals are typically filled with late-stage phases such as alkali feldspar, fayalitic olivine, Fe- and Na-rich clinopyroxene, apatite, and clays that may have formed by devitrification of an original glass. Other less spectacularly skeletal grains are included in early-formed augite. The composition of a large skeletal ilmenomagnetite grain

from the light pegmatoid—determined by averaging data obtained from 226 points with a microprobe spot size of 15–25  $\mu$ m—is given in Table 31, column 1. Discrete plates of ilmenite also occur in the pegmatoids. They are much poorer in MgTiO<sub>3</sub> but slightly richer in MnTiO<sub>3</sub> and Fe<sub>2</sub>O<sub>3</sub> than the host rock ilmenites (Table 31, columns 2 and 3).

Examination of samples from pegmatoids in reflected light revealed that much ilmenite is partly replaced by a phase having reflective properties intermediate between those of Fe-Ti oxides and Fe-rich silicates (Plate 4B). Subsequent study in transmitted light and microprobe analysis showed it to be aenigmatite (ideal formula, Na<sub>2</sub>Fe<sup>2+</sup><sub>5</sub>Ti Si<sub>6</sub>O<sub>20</sub>; chemical analysis in Table 31,

column 5). Aenigmatite also occurs as overgrowths on ilmenite and ilmenomagnetite, and as euhedral, apparently primary, discrete grains. Aenigmatite is considered typical of peralkaline lavas, and this first reported occurrence in a basalt flow underscores the extreme differentiation that has taken place within the pegmatoids: aenigmatite is not found in contact with plagioclase or with alkali feldspar less potassic than approximately  $\text{Or}_{35}$ . The aenigmatite also occurs with Na-rich clinopyroxene; generally they appear to have crystallized simultaneously, but in one occurrence aenigmatite forms an oriented overgrowth on a crystal of Na-rich augite projecting into a diktytaxitic cavity and is clearly younger. Ilmenomagnetite grains with aenigmatite selectively replacing the (111) ilmenite lamellae indicate that the replacement occurred subsequent to the oxidation—"exsolution" of the ilmenite. All these indications of very late-stage formation of aenigmatite are consistent with experimental studies (p. 188) that show the maximum thermal stability of synthetic aenigmatite with the theoretical composition to be below

900°C. The reason aenigmatite does not coprecipitate with the most sodic feldspars (which also have moderate contents of  $\text{CaAl}_2\text{Si}_2\text{O}_8$ ) is not clear. It is possible that the most sodic feldspars crystallized at temperatures above the maximum thermal stability of aenigmatite; but it is equally likely that aenigmatite is incompatible with the anorthite component of plagioclase. D. R. Wones (written communication, 1970) has suggested the possibility of a reaction such as:



This possibility is being tested experimentally.

The replacement of ilmenite by aenigmatite has not been previously reported. Nicholls and Carmichael (1969), however, have noted a generally antipathetic relationship between Fe-Ti oxides and aenigmatite in peralkaline lavas, and they calculate a hypothetical "no-oxide field" in the  $f_{\text{O}_2}$ - $T$  plane within which pyroxene and aenigmatite occur rather than the oxide minerals. Our mineralogical data lend partial support to this concept, but we have observed no textural evidence for replacement of *titanomagnetite* by aenigmatite, although it does selectively replace ilmenite *lamellae* in ilmenomagnetite. Furthermore, our experimental results indicate that the aenigmatite field calculated by Nicholls and Carmichael extends to too high values of  $f_{\text{O}_2}$ . We find that synthetic  $\text{Na}_2\text{Fe}_5\text{TiSi}_6\text{O}_{20}$  is not stable at oxygen fugacities much above the fayalite-magnetite-quartz buffer, and Ernst (1962) reported that a Ti-free synthetic aenigmatite is stable only at oxygen fugacities *below* that buffer. Inasmuch as the main compositional variation reported for natural aenigmatites is their

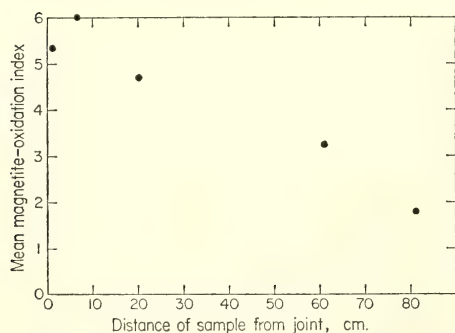


Fig. 75. Variation in mean oxidation index for original titanomagnetites as a function of distance from a vertical joint in the pegmatoid zone approximately 60 m above the base of flow 2. The "joint selvage"—a layer of rock, adjacent to the joint, that weathers in relief—is approximately 7 cm thick here. The oxidation index is obtained by assigning to each original titanomagnetite in a section 2.54 cm in diameter a numerical value corresponding to the oxidation classes of Watkins and Haggerty (1967).

Fe/(Fe+Ti) ratio (Nicholls and Carmichael, 1969, p. 280), it seems unlikely that they could have precipitated at oxygen fugacities much above those of the FMQ buffer.

Because the pegmatoid aenigmatite reported here rather closely approaches the theoretical composition (Table 31, column 4), the fayalite-magnetite-quartz buffer (Wones and Gilbert, 1969) serves as an approximate upper limit to the oxygen fugacity during the late stages of crystallization. It is possible to verify that limit and to estimate a lower limit in several ways.

The compositions of coexisting ilmenomagnetite and ilmenite can be used to estimate the temperature and oxygen fugacity at which they ceased exchanging Fe and Ti (*Year Book 62*, p. 60; Buddington and Lindsley, 1964). The experimental data relate *compositions* of coexisting pure synthetic phases in the system FeO-Fe<sub>2</sub>O<sub>3</sub>-TiO<sub>2</sub> to the oxygen fugacity and temperature of their formation. The optimum method of applying these data to complex natural oxides would be through knowledge of activity coefficients of both the synthetic and natural phases. But because these coefficients are not now known, a less precise method must be used: the calculation of compositions of natural Fe-Ti oxides in such a way as to minimize the effect of other constituents. Buddington and Lindsley (1964, pp. 327-329) suggested a calculation procedure based on the assumption that cations other than Fe<sup>2+</sup>, Fe<sup>3+</sup>, and Ti<sup>4+</sup> act only as inert diluents. Thus, for example, MgO in titanomagnetite was to be apportioned between Mg<sub>2</sub>TiO<sub>4</sub> and MgFe<sub>2</sub>O<sub>3</sub> and these "molecules" were to be discarded. Experimental investigations in the system MgO-FeO-Fe<sub>2</sub>O<sub>3</sub>-TiO<sub>2</sub> (Speidel, 1967), however, have indicated that better results will be obtained if all MgO is discarded as Mg<sub>2</sub>TiO<sub>4</sub> (for titanomagnetite) and MgTiO<sub>3</sub> (for ilmenite). Unfortunately, no data are available as to the best calculation procedures for other

constituents such as MnO, Al<sub>2</sub>O<sub>3</sub>, and Cr<sub>2</sub>O<sub>3</sub>; nor is it clear, for magnetites containing both MgO and Al<sub>2</sub>O<sub>3</sub>, whether MgO should first be used to form Mg Al<sub>2</sub>O<sub>4</sub> with the remainder, if any, allotted to Mg<sub>2</sub>TiO<sub>4</sub>. Fortunately, for the Fe-Ti oxide pairs considered here, variations in the calculation procedure have but a small effect on the calculated Fe<sub>3</sub>O<sub>4</sub> contents of the titanomagnetites and the Fe<sub>2</sub>O<sub>3</sub> contents of the ilmenites. We have adopted the calculation procedure of Buddington and Lindsley (1964, pp. 327-329) with the modification that any RO remaining after the formation of RO·R<sub>2</sub>O<sub>3</sub> is discarded as 2RO·TiO<sub>2</sub>. The calculated compositions are given in Table 31, columns 1-4. It is emphasized that the magnetite compositions represent hypothetical original magnetite-ulvöspinel solid solutions that were subsequently oxidized to ilmenomagnetites.

The analyzed magnetite and ilmenite from the host rock occur in mutual contact and almost certainly represent an equilibrium pair. The rather low temperature indicated for this pair (820° ± 50°C;  $f_{O_2} = 10^{-15.8 \pm 1.0}$  atm) suggests that subsolidus reaction—perhaps granule-"exsolution"—has taken place (Buddington and Lindsley, 1964, pp. 322-323). If so, the primary spinel contained more Fe<sub>2</sub>TiO<sub>4</sub> than is indicated in Table 31. Even though subsolidus reaction appears to have occurred, this pair helps set limits on the oxygen fugacity that obtained in the host rock at subsolidus temperatures: slightly less than one order of magnitude below that of the FMQ buffer.

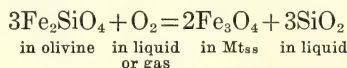
Because much of the ilmenomagnetite in the light pegmatoid has undergone extensive maghemitization, it has not been possible to analyze an unaltered ilmenomagnetite in *contact* with discrete ilmenite. The ilmenomagnetite and discrete ilmenite whose compositions are given in Table 31, columns 1 and 2, occur approximately 20 cm apart, and in view of the extreme compositional zoning of the silicates, one might question whether



they can represent an equilibrium pair. Unlike the silicates, however, the oxides show little zoning; and because they crystallized in the presence of a water-rich gas phase, they may represent a close approach to equilibrium. The indicated temperature is  $900^\circ \pm 50^\circ\text{C}$ , and the oxygen fugacity is  $10^{-13.7 \pm 1.0}$  atm—slightly less than one order of magnitude below that of the FMQ buffer. These values are in good agreement with the limits indicated by the presence of aenigmatite in the pegmatoid.

Once again it is emphasized that these are the conditions at which the oxide pairs effectively ceased to exchange Fe and Ti, and are not necessarily those of their formation. Thus the original  $\text{Mt}_{\text{ss}}$  and ilmenite in the host rock undoubtedly crystallized at a higher temperature than  $820^\circ\text{C}$ , but it is reasonable to assume that the  $f_{\text{O}_2}$  was approximately one order of magnitude below that for FMQ, or  $10^{-14}$  atm at, say,  $900^\circ\text{C}$ , a temperature at which liquid was probably still present in the pegmatoids. To simplify comparison, the following calculations are based on the temperature  $900^\circ\text{C}$ , although it is not claimed that this value has special significance.

We may also estimate oxygen fugacity on the basis of fayalitic olivine ( $\text{Fa}_{92}$ ) in the pegmatoids. The oxidation of olivine is governed by the reaction



with the equilibrium constant (Wones and Gilbert, 1969)

$$K_{900^\circ\text{C}} = 10^{12.96} = \frac{a_{\text{Fe}_3\text{O}_4}^2 \cdot a_{\text{SiO}_2}^3}{a_{\text{Fe}_2\text{SiO}_4}^3 \cdot f_{\text{O}_2}} \quad (1)$$

The *maximum*  $f_{\text{O}_2}$  is obtained by setting  $a_{\text{Fe}_2\text{SiO}_4} = a_{\text{SiO}_2} = 1$  and substituting a value for  $a_{\text{Fe}_2\text{SiO}_4}$ . Although the  $\text{Fe}_2\text{SiO}_4$ - $\text{Mg}_2\text{SiO}_4$  olivine series is slightly non-ideal (Nafziger and Muan, 1967; Kitayama and Katsura, 1968; Williams, 1970), for an olivine as iron rich as  $\text{Fa}_{92}$  it is a good assumption that the activity equals the square of the mole fraction,

$a_{\text{Fe}_2\text{SiO}_4} = X_{\text{Fe}_2\text{SiO}_4}^2 = 0.846$ . (See Albee, 1965a, p. 275, for a discussion of why the mole fraction is squared.) Substitution of this value in equation 1 yields a maximum  $f_{\text{O}_2}$  of  $10^{-12.60}$  atm, very slightly above that for pure FMQ. This is valid as a *maximum* value for  $f_{\text{O}_2}$ , inasmuch as it would obtain only if pure crystalline  $\text{Fe}_3\text{O}_4$  and  $\text{SiO}_2$  were present, which they are not. Thus the presence of both fayalite and aenigmatite in the light pegmatoid suggests *maximum* oxygen fugacities at or slightly above that of the FMQ buffer, whereas the Fe-Ti oxides yield values slightly less than one order of magnitude below that buffer: i.e.,  $10^{-13.7}$  atm at  $900^\circ\text{C}$ . Note that if the temperature is arbitrarily chosen (for purposes of calculation) as exactly  $900^\circ\text{C}$ , then the uncertainty associated with the oxygen fugacity is less than plus-or-minus one order of magnitude;  $10^{-13.7 \pm 0.5}$  atm seems reasonable.

The  $f_{\text{O}_2}$  value can be substituted in equation 1 to yield an estimate of  $a_{\text{Fe}_3\text{O}_4}$  in the pegmatoid. In addition to the estimate for  $a_{\text{Fe}_2\text{SiO}_4}$  already given, a value for silica activity is needed. Williams (1970) has presented arguments that the silica activity in tholeiitic magma is high, and for these quartz-normative pegmatoids (Lindsley, 1960, Table 8) we adopt a value of 0.98 (relative to quartz as a standard state). Substitution of these values in equation 1 yields a nominal value for  $a_{\text{Fe}_3\text{O}_4}$  of 0.35 (Table 32). The maximum and minimum values for  $a_{\text{Fe}_3\text{O}_4}$  in Table 32 correspond to the uncertainty of plus-or-minus one-half order of magnitude in  $f_{\text{O}_2}$ . The values of  $X_{\text{Fe}_3\text{O}_4}$ ,  $X_{\text{Fe}_3\text{O}_4}^2$ , and  $X_{\text{Fe}_3\text{O}_4}^3$  in Table 32 correspond to the values of  $a_{\text{Fe}_3\text{O}_4}$  predicted by three simple models of the  $\text{Fe}_3\text{O}_4$ - $\text{Fe}_2\text{TiO}_4$  solid solution series.

The only value to fall within the range of  $a_{\text{Fe}_3\text{O}_4}$  calculated from equation 1 is  $a_{\text{Fe}_3\text{O}_4} = X_{\text{Fe}_3\text{O}_4} = 0.25$ , which involves the assumptions—neither of which can be valid—that the  $\text{Fe}_3\text{O}_4$ - $\text{Fe}_2\text{TiO}_4$  series is both molecular and ideal. Although there is no direct evidence to support a

TABLE 32. Values of  $a_{\text{Fe}_3\text{O}_4}$  Calculated from Equation Compared with those Predicted by Three Simple Models

Reference	$a_{\text{SiO}_2}$ *	$a_{\text{Fe}_3\text{SiO}_4}$ $= X_{\text{Fe}_3\text{SiO}_4}^2$	$T, ^\circ\text{C}$	$\log f_{\text{O}_2}$ , atm	Calculated $a_{\text{Fe}_3\text{O}_4}$			$X_{\text{Fe}_3\text{O}_4}^2$	$X_{\text{Fe}_3\text{O}_4}^2$	$X_{\text{Fe}_3\text{O}_4}^2$
					Nominal	Minimum	Maximum			
(1)	0.98	0.85	900	$-13.7 \pm 0.5$	0.35	0.20	0.62	0.25	0.06	0.02
(2)	0.99	0.86	915	$-12.9 \pm 0.5$	0.61	0.34	1.0	0.37	0.14	0.05
(3)	1.0	0.79	810	$-14.7 \pm 0.5$	0.77	0.43	1.0	0.56	0.31	0.17
(4)	1.0	0.81	790	$-15.1 \pm 0.5$	0.84	0.47	1.0	0.59	0.35	0.21

\* Values of  $a_{\text{SiO}_2}$  are estimated for nos. 1 and 2. Nos. 3 and 4 contain quartz phenocrysts.

(1) This report; (2) sample no. 2; (3) sample no. 5; (4) sample no. 6, all from Carmichael (1967).

molecular solution model for the  $\text{Fe}_3\text{O}_4$ - $\text{Fe}_2\text{TiO}_4$  series, some workers (e.g. Lindsley, Brown, and Muir, 1969; Nash, Carmichael, and Johnson, 1969) have tacitly assumed this model in calculating oxygen fugacities.

There is abundant evidence that the  $\text{Fe}_3\text{O}_4$ - $\text{Fe}_2\text{TiO}_4$  substitution is ionic rather than molecular, and a number of models of the ionic distribution have been proposed (Akimoto, 1954; Néel, 1955; Chevallier, Bolfa, and Mathieu, 1955; O'Reilly and Banerjee, 1965; Stephenson, 1969). As an extreme case, assume that the distribution of the cations is random, that is, there is an equal probability that each of the cations  $\text{Fe}^{2+}$ ,  $\text{Fe}^{3+}$ , and  $\text{Ti}^{4+}$  will occupy the one tetrahedral site and two octahedral sites per four oxygens in the spinel formula. Further assume that the only contribution to the entropy of mixing is the configurational entropy of three types of cations on three sites; then  $a_{\text{Fe}_3\text{O}_4} = X_{\text{Fe}_3\text{O}_4}^3 = 0.017$ , a value that is incompatible with the calculated range for  $a_{\text{Fe}_3\text{O}_4}$ . It is highly likely, however, that  $\text{Ti}^{4+}$  is restricted to the octahedral sites (Blasse, 1964), so that this extreme case is unrealistic. The restriction of  $\text{Ti}^{4+}$  to octahedral sites modifies the calculation of  $a_{\text{Fe}_3\text{O}_4}$ . Finger (p. 305) has applied the techniques of Thompson (1969, 1970) to this problem using the assumption that there is only one internal reaction,  $\text{Fe}_{\text{Tet}}^{2+} + \text{Fe}_{\text{Oct}}^{3+} = \text{Fe}_{\text{Tet}}^{3+} + \text{Fe}_{\text{Oct}}^{2+}$ , which corresponds to the high-temperature model of Stephenson (1969). This, of course, is equivalent to the transfer of an electron between the sites. There is also one external reaction—the coupled substitution of  $\text{Fe}^{2+}\text{Ti}^{4+}$  for  $2\text{Fe}^{3+}$ —and, again on the assumption that only configurational entropy contributes to the entropy of mixing,  $a_{\text{Fe}_3\text{O}_4} = X_{\text{Fe}_3\text{O}_4}^2$ . This value also falls well below the calculated minimum (Table 32). Thus although the ideal, molecular model ( $a_{\text{Fe}_3\text{O}_4} = X_{\text{Fe}_3\text{O}_4}$ ) is incompatible with both experimental and crystal chemical data, it nevertheless yields the best estimate of  $a_{\text{Fe}_3\text{O}_4}$  in this

case. The same result holds true for a range of  $X_{\text{Fe}_3\text{O}_4}$  (Table 32, nos. 2-4) as calculated for rocks from which fayalitic olivine, titanomagnetite, and ilmenite have been analyzed and for which  $a_{\text{SiO}_2}$  is unity or can be estimated (Carmichael, 1967). Evidently the  $\text{Fe}_3\text{O}_4$ - $\text{Fe}_2\text{TiO}_4$  solid solution series is considerably more complex than has been assumed.

### *Final Products of the Differentiation Process*

*Douglas Smith and D. H. Lindsley*

The compositional change of the liquid during crystallization was unusually great for magma in a surface extrusion, as evidenced by the exceptionally large range of solid solutions in the feldspar, pyroxene, and olivine series. Samples from the chill zone near the base of the flow contain only a small percentage of phenocrysts, and the initial basaltic liquid of the flow is represented approximately by an analysis (Table 33) of a sample from 5 feet above the flow base; the rock has the normative characteristics of an olivine tholeiite magma (Yoder and Tilley, 1962), with 15% normative hypersthene and 6% normative olivine. On a plot of  $(\text{Na}_2\text{O} + \text{K}_2\text{O})$  against  $\text{SiO}_2$  the analysis falls just into the field defined by the analyses of

Hawaiian tholeiitic rocks by Macdonald and Katsura (1964). Calcium-poor pyroxene, however, only in trace quantities in the flow, and quartz was not recognized even among residual crystallization products; both facts indicate that the magma did not have pronounced tholeiitic affinities.

The most differentiated residual liquid in the flow crystallized in irregular pockets in the light facies of the pegmatoid; because of extreme mineral zoning its composition cannot be measured but must be inferred from the late-crystallizing mineral assemblage there. The assemblage present in these pockets includes alkali feldspar ( $\text{Ab}_{65-56}\text{Or}_{35-43}\text{An}_{0.1-0.6}$ ), fayalitic olivine ( $\text{Fo}_{16-5}$ ), ferroaugite ( $\text{Ca}_{43}\text{Mg}_{18}\text{Fe}_{39}$  to  $\text{Ca}_{40}\text{Mg}_{10}\text{Fe}_{40}$ ), titanomagnetite, ilmenite, and apatite. This mineral assemblage is that of a trachyte or syenite; it is very similar, for instance, to the assemblage in the ferrosyenite that represents the most fractionated residual liquid in the layered Kiglapait intrusion (Morse, 1969). It is interesting to note that the ranges of feldspar, olivine, and clinopyroxene compositions in this single flow are almost as great as in the entire Kiglapait intrusion; almost all of each of the ranges is covered by analyses of the three phases from specimens of host rock and pegmatoid collected from an interval only 1.3 meters thick in the central part of the flow.

Aegirine-augite, clearly subordinate in amount to ferroaugite, occurs in pockets of residual phases both as alteration rims or overgrowths on ferroaugite and as small independent crystals. Aenigmatite, occurring both as a replacement product of ilmenite intergrown with magnetite and in apparently primary crystals, commonly is spatially associated with aegirine-augite. Though the magma from which these two phases crystallized may have been in equilibrium with a vapor phase, as implied by the numerous amygdules and diktytaxitic cavities in the pegmatoid, textural evidence suggests

TABLE 33. Composition and Norm of the Chilled Margin of Flow 6\*

Chemical Analysis		CIPW Norm	
$\text{SiO}_2$	47.4	Or	2.36
$\text{TiO}_2$	1.7	Ab	22.00
$\text{Al}_2\text{O}_3$	16.0	An	30.81
$\text{Fe}_2\text{O}_3$	3.3	Di	13.57
FeO	8.5	Hy	14.55
MnO	0.19	Ol	5.96
MgO	7.6	Mt	4.78
CaO	10.0	Il	3.23
$\text{Na}_2\text{O}$	2.6	Ap	0.74
$\text{K}_2\text{O}$	0.40		
$\text{P}_2\text{O}_5$	0.32		
$\text{H}_2\text{O}$	2.4		
Totals	100.4		

\* U.S. Geological Survey rapid rock analysis, no. 154735, by P. L. D. Elmore, S. D. Botts, I. H. Barlow, and G. Chloe (Lindsley, 1960).



that the aenigmatite and aegirine-augite formed at least in part by magmatic crystallization. The presence of these phases, both with a large molecular excess of Na over Al, indicates that the last liquid may have had a composition like that of a peralkaline trachyte. Bailey (1969) has suggested that acmite may form only from liquids containing excess sodium silicate, a condition implying peralkalinity. Aenigmatite also seems characteristic of peralkaline environments (Nicholls and Carmichael, 1969). The final apparently compatible magmatic mineral assemblage is then alkali feldspar, fayalite, aegirine-augite, aenigmatite, titanomagnetite, and apatite.

Crystallization may have continued from the gas phase after solidification of residual magma. It is likely that the nearly pure aegirine (Table 29, analysis 6) formed during this vapor crystallization stage, as the small analyzed crystal occurs as an overgrowth on aegirine-augite projecting into a diktytaxitic cavity. The aegirine is considerably more sodic than the aegirine-augite in contact with it, and the exceptional purity of this end member suggests that it formed at a lower temperature than the aegirine-augite of probable magmatic origin. Zeolites are found in cavities in the pegmatoid and host rock and in veins replacing plagioclase. Chabazite was the only zeolite identified in the samples studied in detail here, but analcite, philipsite, thomsonite, heulandite, and apophyllite were recognized in pegmatoids in similar flows in the area by Lindsley (1960). Though it is possible on the basis of our present knowledge of the area that chabazite was deposited from the vapor phase during cooling of the flow, it is equally possible that the zeolite was deposited from circulating groundwater, as suggested for other chabazite occurrences by Walker (1951).

In summary, the mineral assemblages in the basalt flow provide a superb illustration of the derivation of a syenitic or trachytic liquid from an olivine

tholeiite magma. The final residual liquid was probably peralkaline. The differentiation took place at the earth's surface under a maximum pressure of several tens of bars. This evidence that a peralkaline liquid can be derived from a basalt parent at low pressure is relevant to problems of the origin of peralkaline lavas, such as those discussed by Bryan (*Year Book* 68, pp. 194-200). Vapor, predominantly  $H_2O$ , may have been interchanged with the environment of the flow during differentiation, but there is no evidence that assimilation of any non-volatile component influenced the chemistry of the differentiation process. The oxygen fugacity during at least most of the differentiation was almost an order of magnitude below that defined by the fayalite-magnetite-quartz buffer (pp. 278-282).

## IRON-RICH PYROXENES

*Douglas Smith*

Iron-rich pyroxenes and olivines are major minerals in terrestrial iron-rich differentiates of basaltic magmas and in some metamorphosed iron formations; they are also present in many samples of lunar basalt. Further experiments to determine the relative stability of calcium-free orthopyroxene (*Year Book* 68, pp. 229-231) have been conducted. Electron microprobe studies of natural olivine-pyroxene-quartz assemblages have also been made to test the validity of extrapolating results on the stability of synthetic orthopyroxene to the calcium-poor, iron-rich pyroxenes found in nature. In addition, compositions of pyroxene pairs have been determined with the electron microprobe in an attempt to delineate boundaries of the two-pyroxene fields in the iron-rich portion of the pyroxene quadrilateral.

The rocks selected for this study were provided by E. P. Wheeler, who collected and described them as part of his study of the rock suite associated with the Nain, Labrador, anorthosite mass

(Wheeler, 1965, 1968). Electron microprobe studies were made of the ferro-magnesian silicates in four rocks—three quartz monzonites and one monzonite. The rocks are from two intrusions associated with the anorthosite complex. Field and chemical studies suggest that the bodies were derived from the same parent magma as the anorthosite (Wheeler, 1968), but recent strontium isotope data indicate that the intrusions do not belong to a simple, uncontaminated differentiation series (Heath and Fairbairn, 1968).

### *Experimental Results in the Calcium-Free System*

Experiments with pressures at and below 7 kb were made at 900°C in hydro-

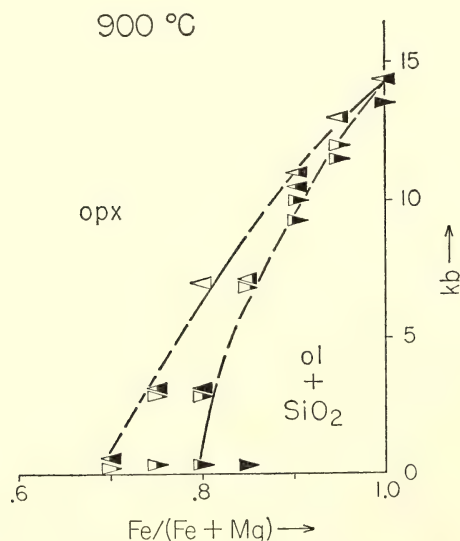


Fig. 76. Experiments with compositions on the enstatite-ferrosilite join. Triangles pointing right show orthopyroxene of the indicated composition reacted to yield olivine plus quartz, whereas triangles pointing left show olivine of the indicated composition reacted with silica to yield orthopyroxene. The amount of shading is approximately proportional to the abundance of olivine plus quartz in the reaction products. Experiments at pressures of 7 kb and below were made at oxygen fugacities of the fayalite-magnetite-quartz buffer.

thermal and internally heated gas apparatus at oxygen fugacities of the fayalite-magnetite-quartz buffer. Those at higher pressures were made in a piston-and-cylinder, solid-media apparatus in sealed silver capsules. The width of the three-phase field as shown in Fig. 76 is defined here only by those experiments in which complete or nearly complete reaction was attained. The width of the field has been drawn to be consistent with the experiments of Medaris (1969) on the Fe-Mg partition between olivine and orthopyroxene at 900°C. The microprobe data on the Labrador specimens suggest, however, that the partition for these iron-rich compositions may be somewhat greater than indicated by his experiments. If the effects of calcium and minor elements are neglected, the results in Fig. 76 may be used as an approximate geobarometer for magmatic rocks containing the three-phase assemblage orthopyroxene-olivine-quartz.

### *Iron-Rich Stability Limit for Natural Pyroxenes*

All four of the natural samples contain convincing textural evidence of the partial or complete breakdown of calcium-poor pyroxene to yield olivine, quartz, and a calcium-rich pyroxene (Wheeler, 1965)—a reaction directly analogous to the olivine-orthopyroxene-silica reaction studied experimentally. One rock contains both crystals of orthopyroxene that have partly broken down to olivine, quartz, and ferroaugite, and other crystals in which the reaction did not occur. Textures suggest that all the orthopyroxene formed by inversion of pigeonite. Representative mineral compositions from this rock are listed in Table 34 and are plotted in Fig. 77A. Orthopyroxene in crystals that have partly broken down to ferroaugite, olivine, and quartz is distinctly more magnesian than orthopyroxene in unreacted crystals. These latter crystals must have persisted metastably, as orthopyroxene

TABLE 34. Representative Mineral Compositions in a Quartz Monzonite (2-1299) Associated with the Nain Anorthosite \*

	1	2	3	4	5
SiO <sub>2</sub>	48.5	30.7	49.5	47.4	48.9
TiO <sub>2</sub>	...†	...	...	0.12	0.27
Al <sub>2</sub> O <sub>3</sub>	0.31	n.d.‡	0.61	0.25	0.75
Fe as FeO	41.2	64.5	22.2	45.0	26.0
MnO	0.78	0.88	0.35	0.76	0.36
MgO	6.4	3.4	5.9	4.0	3.7
CaO	3.3	0.05	21.9	3.0	20.2
Na <sub>2</sub> O	...	...	...	0.02	0.16
Totals	100.5	99.5	100.5	100.5	100.2

\* Analyses 1, 2, and 3 are from an orthopyroxene-olivine-quartz-ferroaugite intergrowth resulting from the breakdown of a single crystal of pigeonite: (1) calcium-poor pyroxene, Ca<sub>7</sub>Mg<sub>20</sub>Fe<sub>72</sub>; (2) olivine, Mg<sub>50</sub>Fe<sub>60</sub>Mn<sub>1</sub>; (3) ferroaugite, Ca<sub>46</sub>Mg<sub>17</sub>Fe<sub>37</sub>. Analyses 4 and 5 are of a lamella and calcium-poor host: (4) host, Ca<sub>7</sub>Mg<sub>13</sub>Fe<sub>80</sub>; (5) lamella, Ca<sub>44</sub>Mg<sub>11</sub>Fe<sub>44</sub>.

† ..., not analyzed.

‡ n.d., not detected.

in the four-phase assemblage has the most iron-rich composition stable at the pressure and temperature of equilibration. The partly reacted crystals contain two sets of exsolution lamellae, suggesting that they inverted from pigeonite, as well as blebs of ferroaugite formed by granule exsolution; microprobe analyses show a range of calcium contents in these crystals, apparently due to locally different concentrations of exsolution lamellae that could not be resolved with the microprobe. The compositions of less

calcic orthopyroxene and associated olivine and ferroaugite occurring with quartz in another rock are shown in Fig. 77B, together with the compositions of unreacted orthopyroxene crystals in yet another specimen.

Data on ferrosilite contents of orthopyroxene from the Labrador rocks are plotted in Fig. 78 together with data from the literature on other unusually iron-rich, calcium-poor terrestrial pyroxenes. Compositions of pyroxene occurring with olivine plus quartz in the Labrador

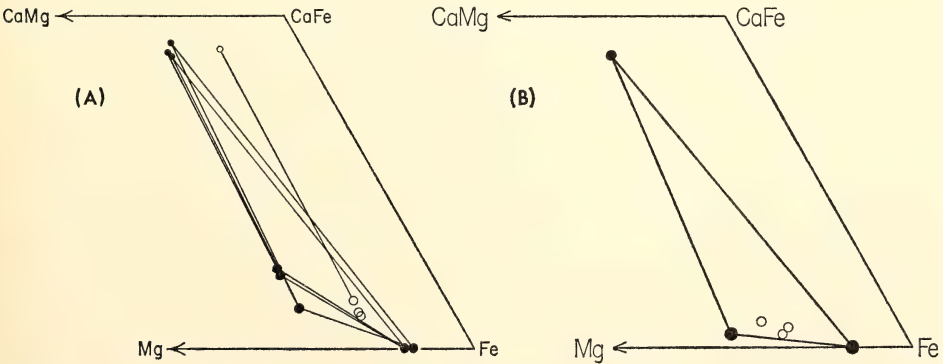


Fig. 77. (A) Pyroxene and olivine compositions in rock 2-1299. Filled circles represent pyroxene and olivine in partly reacted orthopyroxene crystals; open circles represent compositions of unreacted calcium-poor pyroxene crystals and ferroaugite lamellae in them. (B) Filled circles represent compositions of olivine and pyroxene occurring with quartz in rock 2-1568. Open circles represent orthopyroxene in rock 2-1451.



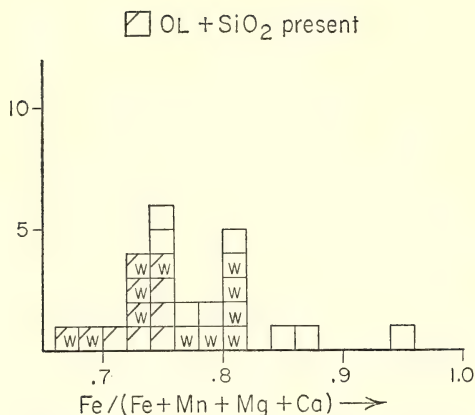


Fig. 78. Histogram of iron-rich pyroxene compositions. Pyroxenes in the Labrador rocks studied here are identified by a W. Other data for pyroxenes coexisting with olivine plus quartz are from Bonnicksen (1969). The most iron-rich composition shown is volcanic clinoferrrosilite studied by Bowen (1935) and Bown (1965).

specimens are similar to those in the low-pressure, contact metamorphic rocks described by Bonnicksen (1969), the ferrosilite content in both sets falling in the range 66 to 76 mole %. Studies with calcium-free synthetic phases indicated that low-pressure iron-rich limits of orthopyroxene stability are more magnesian than  $\text{Fs}_{70}$  and  $\text{Fs}_{75}$  at 900° and 800°C, respectively (Year Book 68). The natural pyroxenes have a range of calcium contents, and the similarity between the natural and experimental compositions suggests that calcium does not have much effect on the iron-rich stability limits of orthopyroxene and pigeonite. Calcium-poor pyroxenes more iron rich than  $\text{Fs}_{75}$  in magmatic rocks must have been either stabilized by pressure or crystallized metastably. All available analyses of calcium-poor pyroxenes with values of the ratio  $\text{Fe}/(\text{Fe} + \text{Mn} + \text{Mg} + \text{Ca})$  greater than 0.75\* have been plotted

\* A number of iron-rich orthopyroxenes with values of the ratio only slightly less than 0.75 have been described from metamorphosed iron formations (e.g. Butler, 1969; Kranck, 1961). These pyroxenes do not occur together with both olivine and quartz, and they have not been plotted in Fig. 78.

in Fig. 78. Those pyroxenes in the Labrador rocks were presumably stabilized by pressure; if they formed stably at or above 900°C, and if the effects of minor elements were negligible, the pressure must have been in excess of 5 kb. More iron-rich, calcium-poor pyroxenes that formed at low pressures, such as the clinoferrrosilite in obsidian described by Bowen (1935) and Bown (1965), must have crystallized metastably. Appreciable contents of Mn might act to stabilize iron-rich pyroxene, since the Mn pyroxenoid, rhodonite, is stable at atmospheric pressure. However, the analyzed Labrador pyroxenes all contain less than 2%  $\text{MnSiO}_3$  molecule. Lindsley (Year Book 64, p. 150) demonstrated that the clinoferrrosilite in obsidian could not have been stabilized by its Mn content, equivalent to 5%  $\text{MnSiO}_3$  molecule.

### *The Two-Pyroxene Fields for Iron-Rich Compositions*

The Labrador rocks contain unusually iron-rich pyroxene pairs. Microprobe analyses were made of three basically different associations: (1) pigeonite rimmed by ferroaugite, (2) closely associated orthopyroxene and ferroaugite grains, and (3) ferroaugite exsolution lamellae in host crystals of orthopyroxene inverted from pigeonite. The pyroxene pairs in this last association are the most iron rich known to the author. These pairs provide an unusual opportunity to outline parts of the two-pyroxene fields in the quadrilateral near the ferrosilite-hedenbergite join.

The crystals of pigeonite rimmed by ferroaugite are in an olivine-clinopyroxene monzonite described by Wheeler (1968, pp. 194-195, sample 2-1599). The ferroaugite rims are fairly homogeneous, with compositions near  $\text{Ca}_{42}\text{Mg}_{14}\text{Fe}_{45}$ ; the cores of two crystals examined in detail have sparse exsolution lamellae, 2 to 4  $\mu\text{m}$  wide, of approximately rim composition in a less calcic host. Average analyses of lamellae plus host in the two

cores obtained with broad microprobe beams are  $\text{Ca}_{18}\text{Mg}_{15}\text{Fe}_{67}$  and  $\text{Ca}_{17}\text{Mg}_{15}\text{Fe}_{68}$ . A microprobe traverse across one core-rim boundary indicates that the transition zone is less than  $10\ \mu\text{m}$  wide. The average core and rim compositions plotted in Fig. 79A (A–A') apparently represent pyroxene compositions precipitated from the melt, and they may reflect a reaction relationship like that suggested in Fig. 79B.

Compositions of pyroxene lamellae and their host crystals define points on

the boundaries of the two-pyroxene field reached by subsolidus reactions. Orthopyroxene crystals (rock 2-1299) contain one set of sparse lamellae  $5$  to  $12\ \mu\text{m}$  wide, presumably parallel to (001) of original pigeonite, in a host streaked by a different set of very fine lamellae, so closely spaced and so thin that the host appears homogeneous with the smallest microprobe beam. Compositions of "host pyroxene" represent orthopyroxene plus the unresolved fine lamellae, and they are interpreted (Fig. 79B, C) as pigeonite compositions. Compositions of lamellae-host pairs from three crystals are plotted in Fig. 79A (B'–C), and complete analyses of one pair are listed in Table 34. All elements appear to have participated in the exsolution process, as noted by Boyd and Brown (1969) in a study of more magnesian lamella-host pairs. One crystal with typical host and coarse lamellae,  $\text{Ca}_6\text{Mg}_{15}\text{Fe}_{70}$  and  $\text{Ca}_{44}\text{Mg}_{14}\text{Fe}_{43}$ , contains an area of less calcic pyroxene with a uniform composition of  $\text{Ca}_{1.4}\text{Mg}_{15}\text{Fe}_{84}$ , presumably that of orthopyroxene from which diffusion has removed the fine lamellae included in the other analyses; the two calcium-poor pyroxenes are metastable with respect to a pyroxene-olivine-quartz assemblage.

Compositions of orthopyroxene without visible exsolution lamellae and associated ferroaugite from an olivine quartz monzonite (Wheeler, 1968, Table 1, 2-1568) are also plotted in Fig. 79A (B–B'). Textures in this rock suggest a history of subsolidus deformation, and some of the small grains of ferroaugite associated with the analyzed orthopyroxene may have formed by granule exsolution. If so, these orthopyroxene-ferroaugite pairs equilibrated at subsolidus conditions.

The calcium-poor pyroxene rimmed by ferroaugite is significantly more calcic than pigeonites in less iron-rich basaltic rocks, though pyroxene crystallization

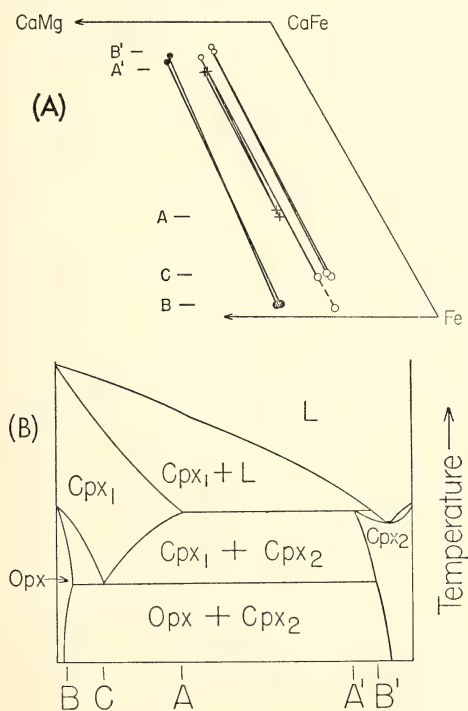


Fig. 79. (A) Pyroxene pairs from Labrador specimens 2-1299 (open circles), 2-1568 (filled circles), and 2-1599 (crosses). Letters A, A', B, B', and C refer to points in Fig. 79B. (B) Schematic cross section across the iron-rich part of the pyroxene quadrilateral parallel to an orthopyroxene-ferroaugite tie line, after Muir (1954). Letters indicate the presumed subsolidus relationships giving rise to the pyroxene pairs. Even in the simpler system,  $\text{CaO-FeO-MgO-SiO}_2$ , the liquid composition would not lie in the plane of the section. Liquidus and solidus temperatures may have been very different for the three rocks.

temperatures in the monzonite should be lower than those in basalts. These facts imply that the inferred crest of the two-pyroxene field is at considerably lower temperatures in this iron-rich part of the quadrilateral than at the more magnesian compositions where less calcic pigeonites crystallize at higher temperatures. This inference is consistent with the suggestion of Lindsley and Munoz (1969) that the critical temperature of the metastable two-pyroxene field on the ferrosilite-hedenbergite join should lie near 820°C at low pressure. The Labrador orthopyroxene-ferroaugite pairs, however, have calcium contents similar to those of much more magnesian pyroxene pairs that underwent subsolidus equilibration in the Bushveld gabbro (Boyd and Brown, 1969). Since there is no *a priori* reason to assume that equilibration should continue to lower temperatures for more iron-rich compositions, the similarity of calcium contents suggests that there is no significant difference in the width of the two-phase field at subsolidus temperatures for iron-rich and magnesian pyroxene compositions. Evidently, with increasing iron content the critical temperature of the two-pyroxene field becomes progressively lower, but the width of the field at lower temperatures does not change significantly.

CHLORITOID-STAUROLITE QUARTZITES  
FROM THE MOOSILAUKE QUADRANGLE,  
NEW HAMPSHIRE

*Douglas Rumble III*

The regionally metamorphosed rocks of central-western New Hampshire afford well-exposed examples of the worldwide association of recumbent folds and gneiss domes (Thompson *et al.*, 1968). The writer is now measuring the chemical compositions of coexisting minerals in these rocks with the electron microprobe in order to determine the conditions of equilibrium or disequilibrium under which they crystallized. The results of the study of chloritoid-staurolite

assemblages collected in the area are sufficiently unusual to justify reporting them at this time.

The mineral assemblage chloritoid-staurolite is found in regionally metamorphosed, aluminous, ferruginous pelitic schists and quartzites. Most reported occurrences lie in the middle grades of Barrovian-type successions of metamorphic mineral zones (Halferdahl, 1961; Espenshade and Potter, 1960). The stability of the association has been questioned in the past, and chloritoid was believed to be present as a metastable relict of lower grade metamorphism. Recent work, however, on the partition of Fe and Mg between coexisting chloritoid and staurolite has raised the possibility that the assemblage is stable in certain regionally metamorphosed terranes (Albee, 1965*b*; Schreyer and Chinner, 1966; Frey, 1969). The existence of a stability field for two-phase assemblages of chloritoid and staurolite has been demonstrated experimentally by Richardson (1968), Hoschek (1969), and Ganguly (1969). The chloritoid-staurolite assemblages of the Moosilauke quadrangle, New Hampshire, are characterized by mutually consistent partition of elements between coexisting minerals (Table 35), implying that the minerals crystallized in chemical equilibrium; there is no textural evidence of disequilibrium.

Three specimens of chloritoid-staurolite quartzites have been collected from outcrops of the Early Silurian Clough formation in the Moosilauke quadrangle, New Hampshire.\* The chemical compositions of staurolite, chloritoid, and garnet in these rocks have been measured on the MAC 400 electron microprobe † following the procedures of Boyd, Finger, and Chayes (*Year Book* 67, p. 210). Well-polished grains in polished thin sec-

\* The writer is grateful to Professor M. P. Billings, Harvard University, for supplying rock samples from the Moosilauke quadrangle. Sample L-534 was collected by him.

† Purchased with the assistance of the National Science Foundation under grant GP 4384.



TABLE 35. Electron Microprobe Analyses of Coexisting Minerals

	L-534 Staurolite	L-534 Chloritoid	68-44 Staurolite	68-44 Chloritoid	69-1 Staurolite	69-1 Chloritoid	69-1 Garnet
MgO	0.39	0.70	0.49	0.92	0.34	0.67	0.40
Al <sub>2</sub> O <sub>3</sub>	55.86	40.70	55.40	40.00	55.16	40.33	20.61
SiO <sub>2</sub>	28.27	24.13	28.18	23.89	28.13	24.05	36.03
CaO	0.00	0.00	0.00	0.00	0.00	0.00	1.45
TiO <sub>2</sub>	0.35	0.00	0.36	0.00	0.27	0.26	0.03
MnO	0.22	0.45	0.08	0.18	0.01	0.03	0.34
FeO *	13.35	26.88	13.30	26.75	13.73	26.87	40.09
ZnO	0.00	0.00	0.00	0.00	0.09	0.00	n.d.
Anhydrous total	98.43	92.86	97.80	91.73	97.77	92.22	98.93
Cation Proportions (Staurolite, per 30 cations; chloritoid and garnet, per 8 cations)							
Mg	0.16	0.09	0.21	0.12	0.14	0.08	0.05
Al	18.58	4.00	18.54	3.98	18.50	3.99	2.016
Si	7.98	2.01	8.00	2.02	8.00	2.02	2.99
Ca	0.00	0.00	0.00	0.00	0.00	0.00	0.13
Ti	0.07	0.00	0.08	0.00	0.06	0.02	0.002
Mn	0.05	0.03	0.02	0.01	0.001	0.002	0.02
Fe	3.15	1.87	3.16	1.89	3.28	1.89	2.79
Zn	0.00	0.00	0.00	0.00	0.02	0.00	n.d.

\* Total Fe as FeO.

tions, 1 inch in diameter, were selected for analysis. In addition, three to five other grains were partially analyzed to test for homogeneity. No significant deviations from chemical homogeneity have been found in the analyzed minerals.

The outcrops of chloritoid-staurolite quartzite are located near the outcrop trace of "the fossil isobaric surface corresponding to the pressure of the kyanite-andalusite-sillimanite triple point" (Thompson and Norton, 1968, p. 324). Aluminum silicate occurrences and sample locations are given in Fig. 80 (Billings, 1937; Rumble, reconnaissance sampling in the summers of 1968 and 1969). Samples L-534 and 68-44 are located within the outcrop area of kyanite occurrences. Mineral assemblages of adjacent pelitic schists are characterized by the presence of staurolite-chlorite-biotite-quartz-muscovite and the absence of kyanite-biotite. Sample 69-1 occurs within the band of uncertainty in the location of the kyanite-sillimanite isograd. The sillimanite schists lying east of sample 69-1 are characterized by the

assemblage sillimanite-(with or without andalusite)-staurolite-garnet-biotite-ilmenite-rutile-pyrrhotite-muscovite-quartz.

Estimated modes of the polished thin sections of the specimens are given in Table 36. In all the specimens, chloritoid, staurolite, and muscovite exhibit a strong preferred orientation that defines the foliation of the rock; quartz grains are equigranular anhedral and show three-grain intersections of 120°. Kyanite, staurolite, and chloritoid of sample 68-44 (only staurolite and chloritoid in sample 69-1) are intergrown in single grains with no textural evidence whatever of replacement of one mineral by another. The Fe-Ti oxide assemblage of sample L-534 consists of primary grains of ilmenite and magnetite that have been partially oxidized to a mixture of rutile and hematite. In sample 68-44 primary grains of ilmenite (and rutile?) have been partially oxidized to a granular aggregate of rutile and hematite. Primary grains of rutile and ilmenite in sample 69-1 show no traces of secondary oxidation.

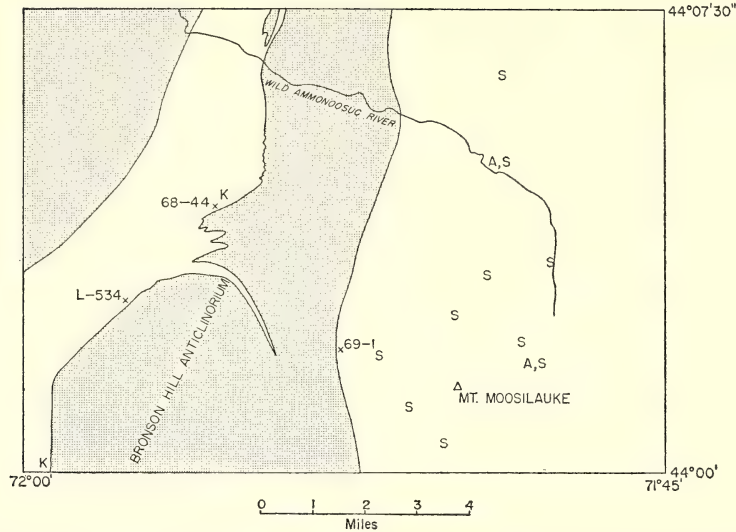


Fig. 80. Geologic map of southern half of the Moosilauke quadrangle, New Hampshire, showing sample locations (L-534 X) and distribution of aluminum silicate occurrences (A, andalusite; K, kyanite; S, sillimanite). Outcrop areas of pre-Silurian rocks are stippled; of Siluro-Devonian rocks, blank.

Chemical analyses of the minerals and their cation ratios are given in Table 35. The garnet and chloritoid analyses give cation proportions corresponding to the ideal formulas of these minerals. The staurolite analyses, however, show cation proportions higher in Al and lower in the sum (Fe+Mg+Mn+Zn) than the ideal formula,  $H_2Fe_4Al_{18}Si_8O_{48}$  (Náray-Szabó and Sasvári, 1958). This result is in accord with that of other workers (Schreyer and Chinner, 1966; Richardson, *Year Book 66*, pp. 397-398; Smith, 1968; Hollister, 1970), who have found not only

that staurolite's composition varies through substitution of the type  $Fe=Mg=Mn=Zn$  but that the proportions  $R^{1+}:R^{2+}:R^{3+}:R^{4+}$  also depart from their ideal values. In order to test the accuracy of the staurolite analyses, two staurolite samples,\* previously analyzed by Professor Arden Albee, California Institute of Technology, were analyzed by the same technique used to obtain the analyses reported above. The analyses of each sample agree within 1-2 relative wt % for  $Al_2O_3$ ,  $SiO_2$ ,  $FeO$ , and  $MgO$ .

Compositions of coexisting staurolite and chloritoid from the Moosilauke quadrangle, New Hampshire, are plotted in Fig. 81 in the AFM projection (Thompson, 1957). The  $Fe/(Fe+Mg)$  atomic ratios of coexisting chloritoid and staurolite are equal: 0.95 for sample L-534, 0.94 for sample 68-44, and 0.96

TABLE 36. Estimated Modes

	L-534	68-44	69-1
Quartz	90	80	89
Muscovite	3	5	5
Kyanite	...	5	...
Staurolite	2	5	1
Chloritoid	5	3	2
Garnet	...	...	3
Tourmaline	tr	...	...
Rutile	tr	1	tr
Ilmenite	tr	1	tr
Magnetite	tr		
Hematite	tr	tr	

\* One of the specimens is from a staurolite-chloritoid schist collected near Madoc, Ontario, by Dr. J. M. Moore, Carleton University. The other specimen is an aliquot of the staurolite separated from the Gassetts schist, Gassetts, Vermont, by Dr. Jun Ito, Harvard University.

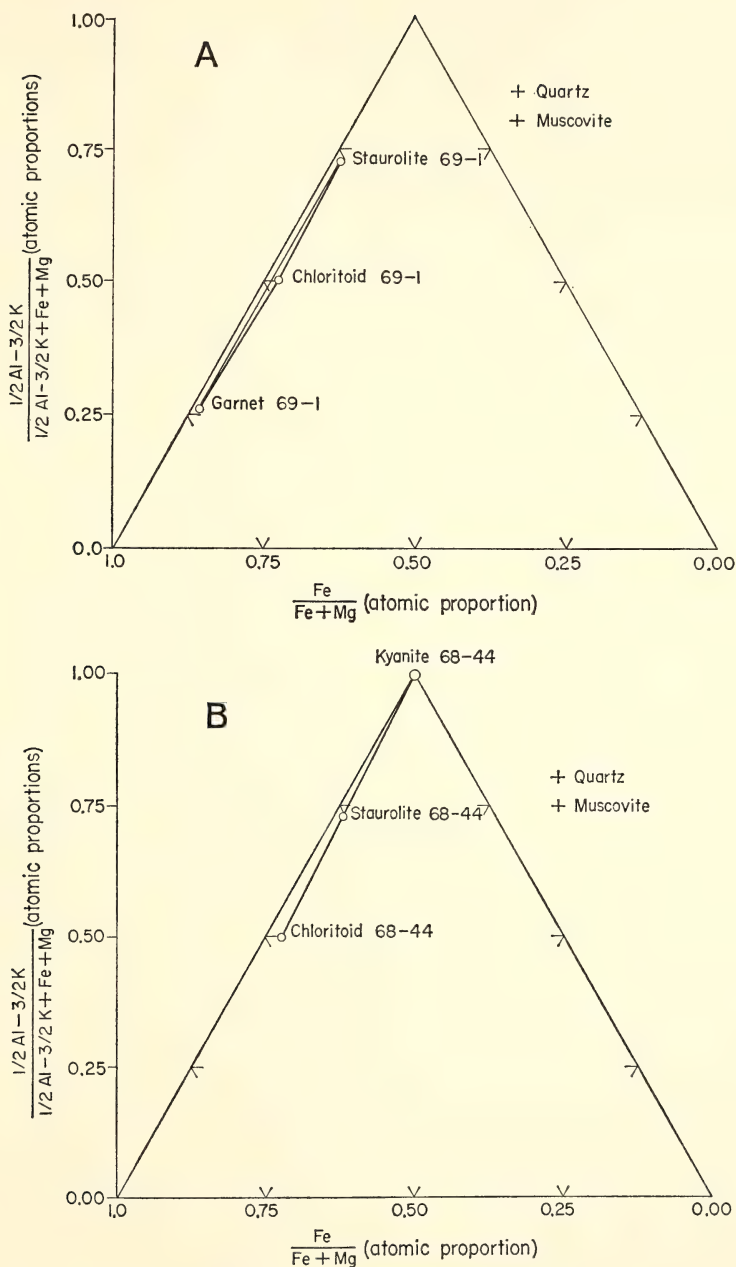


Fig. 81. (A) AFM projection (Thompson, 1957) of compositions of coexisting staurolite, chloritoid, and garnet in sample 69-1. (B) AFM projection (Thompson, 1957) of compositions of coexisting staurolite, chloritoid, and kyanite in sample 68-44. The minerals of sample L-534, not plotted, correspond to a two-phase assemblage of chloritoid and staurolite in the projection.



for sample 69-1. The  $\text{Fe}/(\text{Fe}+\text{Mg})$  atomic ratio for the garnet of sample 69-1 equals 0.98. The compositions of the chloritoid-staurolite pairs are collinear, therefore, with the aluminum silicate corner of the AFM projection. The assemblages are of greater variance than that implied by the AFM projection. The preferential substitution of Ti in staurolite and of Mn in chloritoid introduces two additional degrees of freedom to the compositional variability of the system.

If the Fe-Mg partition between garnet, staurolite, and chloritoid shown by sample 69-1 is found by future work to be of general occurrence, then one source of uncertainty now present in deriving "petrogenetic grids" representing Fe-Mg partition in the AFM projection will be eliminated. That the staurolite-garnet tie line of sample 69-1 lies on the Fe-rich side of coexisting chloritoid makes impossible reaction relationships of the type  $\text{quartz} + \text{chloritoid} = \text{aluminum silicate} + \text{staurolite} + \text{garnet} + \text{H}_2\text{O}$ . Instead, reaction relationships occur of the type  $\text{quartz} + \text{chloritoid} + \text{aluminum silicate} = \text{garnet} + \text{staurolite} + \text{H}_2\text{O}$ .

#### COMPUTER REDUCTION OF ELECTRON PROBE DATA

*C. G. Hadidiacos, L. W. Finger, and F. R. Boyd*

The reduction of electron probe data and its correction for matrix effects involve complex and tedious calculations, which can only be effectively handled with a large computer. Boyd, Finger, and Chayes (*Year Book 67*) described two programs designed to process probe analyses that have been widely used at this Laboratory in the past few years. Program CONE is used to make instrumental corrections, averages, and statistical calculations, and program ABFAN is used to carry out matrix corrections. Recently we have rewritten these programs, extending the range of

elements that can be handled and correcting an error in the formulation of the atomic number correction that appeared in ABFAN.

Most of the modifications have been made to ABFAN, which in revised form has been named ABFAN2. The range of elements for which matrix corrections can be made has been extended from atomic numbers 11 (Na)–28 (Ni) in ABFAN to 11 (Na)–57 (La) in ABFAN2.  $K\alpha$  lines are used in the analysis of elements in the atomic number range 11–36, and  $L\alpha$  lines are used in the range 37–57. Reed's (1965) full expression for characteristic fluorescence is used in ABFAN2 and the program corrects for all possible  $K$ - $K$ ,  $L$ - $L$ ,  $K$ - $L$ , and  $L$ - $K$  fluorescence.

An error that appeared in the formulation of the atomic number corrections in ABFAN has been called to our attention by E. D. Glover and has been corrected in ABFAN2. The backscatter ( $R$ ) and stopping power ( $S$ ) corrections of Duncumb and Reed (1968) are used. In the original version of ABFAN,  $S_i$  and  $R_i$  for an individual element in a multielement target were calculated using  $E_K$  for that particular element rather than  $E_K$  for the element being analyzed. In ABFAN2,  $E_K$  is the excitation potential for the element being analyzed and  $R_{AB}$  and  $S_{AB}$  depend on the element being analyzed in a given target at a given  $KV$ .

An additional program (CONETR) has been written to process probe scans by D. H. Lindsley and Douglas Smith and modified by F. R. Boyd. CONETR can be used to make corrections for background, drift, and deadtime for individual counts in step scans and to reduce each count to an element or oxide analysis. Single-point analyses for Na, Ca, and K in feldspars and Ca, Mg, and Fe in pyroxenes are given approximate matrix corrections and reduced for plotting in the ternary feldspar system and the pyroxene quadrilateral.

## STATISTICAL PETROGRAPHY

*Felix Chayes*

The first section of this report describes current—and far from complete—work on a matter of very general interest to petrologists, the distribution of silica saturation in Cenozoic basalt. Based on examination of nearly 2000 published analyses, this study establishes beyond reasonable doubt that the distribution of silica saturation in analyzed specimens of Cenozoic basaltic rocks is markedly bimodal. Although nearly all the analyzed basalts of the mid-ocean ridges are saturated with regard to silica, the Cenozoic basalts of all other environments seem to be dominantly either under- or oversaturated. This curious distribution invites speculation along the lines proposed at the close of the section, but no satisfactory explanation of it is currently available.

During the report year studies have also been completed concerning the estimated compositions of successive residual liquids of the Skaergaard series, the appropriate null values to be used in testing the ratio correlations so common in petrology and geochemistry, the effect of a single nonzero open covariance on the behavior of a recently proposed test of simple closure correlation, and the problem of deciding whether a polynomial surface of order  $(k+1)$  is or is not an improvement over one of order  $k$ . Since all of these either have already appeared in print or will soon do so, there is no need here for more than the brief discussion of them given in the second section below.

*Distribution of Relative Silica Saturation in Cenozoic Basaltic Rocks*

There is extensive mineralogical and chemical variation among basaltic rocks, and their subdivision into feldspathoidal, or alkaline, and nonfeldspathoidal varieties was suggested before the turn of the century. No consistent geographic or

satisfactory genetic rationalization of the occurrences of these compositional variants was forthcoming, however, and by the mid-twenties many prominent petrologists began to feel that the distinction was arbitrary and unrewarding. The desirability of a dichotomous classification was soon urged once more in the provocative early work of W. Q. Kennedy. Until about 1950, however, and despite considerable discussion, the profession remained undecided; indeed, for much of this period there seemed little practical basis for firm commitment. In 1950, Tilley's adaptation and rather severe modification of Kennedy's classification attracted immediate attention and support. The ensuing terminological embroglio has been reviewed elsewhere (Chayes, 1966, which contains pertinent bibliography).

For decades it has been rather widely considered that alkaline rocks as a whole are scarce and volumetrically trifling, and, as a corollary, that alkaline basalts are far less abundant than subalkaline ones. Discovery that the basalts of the submarine ridges, in sharp contrast to those of most oceanic islands, are not *ne-normative* has probably reinforced this conviction. Whatever may be the case with regard to plutonic rocks or pre-Cenozoic volcanics, however, this view of the relative abundances of alkaline and subalkaline rocks seems to me mistaken and misleading as regards the voluminous products of Cenozoic and Recent basaltic volcanism. In this time interval, about 70 million years, alkaline basaltic volcanism seems of about the same general order of importance as the subalkaline variety, not only on the continents, but also both in Mediterranean areas and on islands rising from the ocean basins. It is only along the deeply submerged crests of the mid-ocean ridges and on the immediately

shoreward flanks of the deep trenches that margin so much of the open ocean, i.e., where the tectonic plates of current geophysical speculation are supposed to appear and disappear, that alkaline basalts are rare or lacking.

This note reports preliminary results of a study of the abundance of published chemical analysis of Cenozoic basaltic rocks of varying "alkalinity." What is at issue, of course, is not richness in alkalis in any absolute sense, but the molar balance—or lack of it—between alkalis and alkaline earths as opposed to silica. Applying the initially mineralogical or modal terminology of Shand (1943, pp. 187–189) directly to chemical composition, we may distinguish three levels of "silica saturation." A rock containing more silica than is required to permit the casting of all alkalis, alkine earths, and molar excess of FeO over  $(\text{Fe}_2\text{O}_3 + \text{TiO}_2)$  as a mixture of feldspar and alumina-free pyroxene will be referred to as "oversaturated" with silica, and one with silica sufficient or insufficient to permit recasting of these oxides as a mixture of pyroxene, olivine, and feldspar will be called, respectively, "saturated" or "undersaturated." In the simple basalt tetrahedron of Yoder and Tilley (1962), the "plane of saturation" separates our saturated and oversaturated classes and the "plane of critical undersaturation" separates the saturated and undersaturated classes.

### *On Determining the Level of Silica Saturation in a Basalt Analysis*

In the CIPW combining conventions, the norm of an oversaturated basalt will contain *Q*, the norm of an undersaturated basalt will contain *ne*, and the norm of a saturated basalt will contain neither. A more direct molar statement of the rules determining the saturation class of a particular analysis may be of interest to readers who are not petrologists. The molar inequalities

$$\text{FeO} > (\text{Fe}_2\text{O}_3 + \text{TiO}_2) \quad (1)$$

and

$$\begin{aligned} \text{K}_2\text{O} + \text{Na}_2\text{O} + \text{CaO} - 3\text{P}_2\text{O}_5 > \\ \text{Al}_2\text{O}_3 > \text{K}_2\text{O} + \text{Na}_2\text{O} \end{aligned} \quad (2)$$

apply almost without exception to basaltic rocks which have escaped extensive surficial or hydrothermal oxidation, and it is these with which we shall be concerned. When (1) and (2) hold, the CIPW rules for the appearance of *Q*, *ol* and *ne* may be put in the surprisingly simple form shown in Table 37, where, if  $\text{R}_2\text{O} = \text{K}_2\text{O} + \text{Na}_2\text{O}$ ,  $\text{RO} = \text{CaO} + \text{MgO} + \text{FeO}$ , and  $\text{R}_2\text{O}_3 = \text{Al}_2\text{O}_3 + \text{Fe}_2\text{O}_3 + \text{TiO}_2 + \text{P}_2\text{O}_5$ ,

$$\begin{aligned} A = 5\text{R}_2\text{O} + \text{RO} + \text{R}_2\text{O}_3 - \\ 2(\text{Fe}_2\text{O}_3 + \text{TiO}_2 + 2\text{P}_2\text{O}_5), \end{aligned} \quad (3)$$

and

$$\begin{aligned} B = \frac{1}{2}(\text{R}_2\text{O}_3 + \text{RO} - \text{R}_2\text{O}) - \\ (\text{CaO} + \text{Fe}_2\text{O}_3 + \text{TiO}_2 + 2\text{P}_2\text{O}_5), \end{aligned} \quad (4)$$

all quantities in (3) and (4) being molar amounts.\*

Each line of Table 37 defines one of the silica saturation classes. The norm of an analysis satisfying condition I will contain *Q*, the norm of one satisfying II will contain neither *Q* nor *ne*, and the norm of one satisfying III will contain

\*In the interest of simplification the ratio  $\text{CaO}:\text{P}_2\text{O}_5=3:1$ , instead of the more exact 10:3, has been assumed for *apatite*, which is rarely more than a very minor part of the norm. It has also been tacitly assumed that less CaO than  $(\text{FeO} + \text{MgO})$  is available for  $(px + ol)$ , certainly a safe assumption in rocks of this sort.

TABLE 37. Molar Conditions Determining Silica-Saturation Levels\*

	Presence (+) or Absence (0) of Normative Parameters		
	<i>ne</i>	<i>ol</i>	<i>Q</i>
I. $\text{SiO}_2 > A$	0	0	+
II. $A \geq \text{SiO}_2 \geq (A - B)$	0	+	0
III. $(A - B) > \text{SiO}_2$	+	+	0

\**A* and *B* as defined in relations (3) and (4) of text.



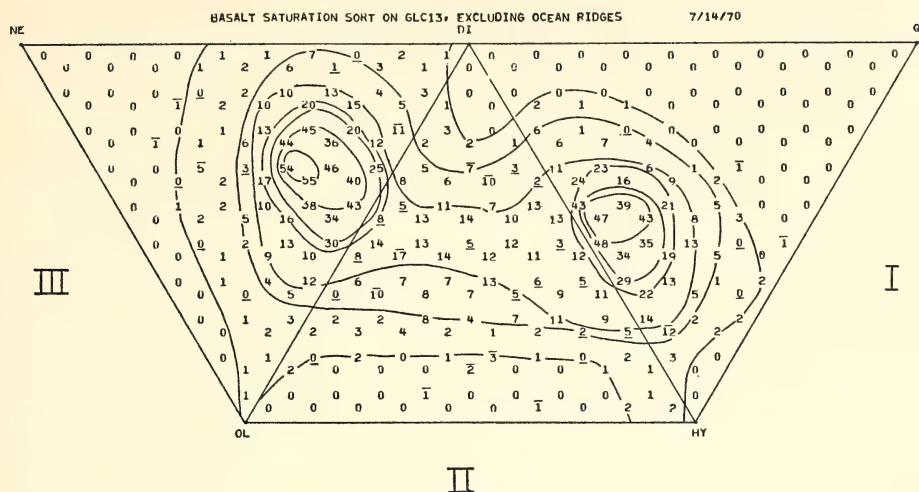


Fig. 82. Distribution of relative silica saturation in analyses of Cenozoic basaltic rocks exclusive of those from submarine ridges. For definition of symbols and contours see text.

*ne*. The classification may be represented graphically, as in Fig. 82, by three ternaries, one of which has a common edge with each of the others. All members of class I project in the ternary *Q-hy-di*, all members of II in *hy-di-ol*, and all members III in *di-ol-ne*. The *ol-hy-Q-di-ne* diagram seems to have been proposed first by Tilley and Muir (1962).

### *Data, Data Reduction, and Data Display*

The data are published analyses, collected from the literature and now incorporated in the Geophysical Laboratory tape library of analyses of Cenozoic volcanic rocks. For present purposes the tape was searched for analyses satisfying the following conditions:

1. The name given the analyzed rock in the source reference contains one of the following as principal or only noun: ankaramite, ankaratrite, basanite, basalt, crinanite, dolerite, etindite, hawaiiite, lamproite, limburgite, nephelinite, oceanite, orvietite, tachylyte, tephrite, tholeiite,\* trachybasalt.

2. The analysis includes values for

$\text{SiO}_2$ ,  $\text{Al}_2\text{O}_3$ ,  $\text{Fe}_2\text{O}_3$ ,  $\text{FeO}$ ,  $\text{MgO}$ ,  $\text{CaO}$ ,  $\text{Na}_2\text{O}$ ,  $\text{K}_2\text{O}$ ,  $\text{MnO}$ ,  $\text{TiO}_2$ ,  $\text{P}_2\text{O}_5$ ,  $\text{H}_2\text{O}$ .

3. The weight percentage of  $\text{SiO}_2$  is less than 54.

4. The molar ratio  $\text{Fe}_2\text{O}_3/(\text{Fe}_2\text{O}_3 + \text{FeO})$  is less than  $\frac{1}{4}$ .

5. The norm contains no corundum.

Of the 9500 analyses included in the current version of the tape library, 1832 † satisfy these conditions.

The normative parameters *Q*, *di*, *hy*, *ol*, and *ne* for each accepted analysis, retained in a mass storage file, were next processed by a separate program that first determined the saturation triangle to which the analysis belonged and then recorded the 10% subtriangle in which it lay. By "10% subtriangle" we mean here a triangle each of whose edges is 10% of the analogous edge of a main saturation triangle of Fig. 82. There are 100 such nonoverlapping subtriangles in any ternary. Each subtriangle is thus 0.33% of the area of the saturation diagram.

The sample frequency distribution is printed out in two forms. In the first (Fig. 82) the actual cell frequencies are

† Excluding 79 analyses of ocean ridge basalts.

\* In the sense of Tilley.

recorded, the units digit of each frequency lying at the center of its cell. In the second, each nonzero frequency is replaced by the smallest integer whose square it exceeds. The map of coded frequencies can be contoured more rapidly, less subjectively, and possibly also less accurately, than the map of actual frequencies. A density interval linear in the square roots of frequencies was suggested to me, for other reasons, by J. Tukey.

The rule used in drawing the contours shown in Fig. 82 (but prepared on a coded frequency map) is that each cell whose center falls on or within contour number  $n$  should contain not less than  $n^2$  analyses. Violations of this convention, where consistency could only have been preserved either by creating local maxima (or minima) or by introducing what seemed excessive inversions of curvature, are marked on the diagram by over- or under-lining of the frequencies concerned, the former indicating that the observed frequency is greater than the square of the next overlying contour, the latter that it is less than the square of the next underlying one. In triangles I and III most of these discrepancies involve points lying on what appears to be the wrong side of contour number 1, i.e., in the vicinity of the boundary between the occupied and empty regions of the diagram, where data density is low and uncertainty correspondingly large, and there are a number of these in II as well. More centrally located discrepancies are rare in I and III but common in II. With three exceptions, each of the 32 discrepancies could be eliminated by relocating no more than one contour.

On the whole, the contouring provides a rather consistent summary of the sample frequency distribution, and the pattern it suggests is abundantly clear. Strong point maxima are centered near  $Q_{10}di_{45}$  in triangle I and  $ne_{20}di_{50}$  in triangle III. There is no indication of a maximum in triangle II; indeed, there

are numerous negative deviations along the crest and upper flanks of the low ridge which cuts across this triangle, connecting the maxima in I and III. Of the 1832 data points, 592 fall in I, 445 in II, and 795 in III.

### *Conclusions*

For a uniform parent density the expected number of items in each cell is  $1832/300=6.1$ , but of course the parent density cannot be uniform, for the rock names themselves, however imprecisely defined or irresponsibly used, preclude occupancy of most of triangle I and large parts of II and III. The average content per cell in the region within contour number 1 is 13.4 in triangle I, 11.4 in III, and only 6.1 in II.

Making every allowance for real or imagined sampling bias, it seems a reasonable inference from Fig. 82 that there are two distinctly different immediate parent materials for the bulk of Cenozoic basalt, one a little oversaturated, the other appreciably undersaturated, in silica. There is at present little persuasive reason for either believing or disbelieving that these two "proximate" parents themselves have a common parent of homogeneous composition. If current speculation about the depths at which they form is correct, basalts must be generated by local melting of normally solid crust or upper mantle. If this melting goes to completion in a closed system, the composition of the resulting magma must of course be that of its parent. It may be that the maxima of Fig. 82 represent essentially complete melts of different parental materials in crust or upper mantle, for there is surely no reason to suppose that either of these regions is more homogeneous compositionally than the observable lithosphere. But whether the parent materials are presumed to occur at different depths, as has been suggested, or haphazardly throughout the zone of basalt formation, there seems no reasonable explanation of why the

compositions of those that are actually melted and ejected at the surface should follow such a markedly bimodal distribution. This, it seems to me, is a nearly fatal objection to the complete melt conjecture. The hypothesis can assume, but cannot account for, the observed bimodality.

If we are to start from a solid and refrain from melting it completely, however, it is obvious that we must derive basalts by an incomplete or partial melting. From anhydrous experiments on natural and synthetic charges, Yoder and Tilley (1962, p. 509) concluded that "there are wide ranges of [eclogitic and peridotitic—F.C.] bulk compositions capable of producing the two principal basalt magma trends by varying the pressure," and the results of extensive experimental study (see especially Schairer and Yoder, *Year Book 63*, pp. 64–74; Kushiro, 1968) of simplified haplobasaltic systems imply that *initial* melts would usually be either *ne-* or *Q-*normative whatever the relative silica saturation of the parental mantle materials. If basalts are indeed derived by partial melting of mantle materials, the distribution described here is clearly compatible with such an inference.

#### MISCELLANEOUS STUDIES IN STATISTICAL PETROGRAPHY

##### *The Skaergaard Model and the Skaergaard Series*

Application of the calculation scheme implicit in the "Skaergaard model" (*Year Book 68*, pp. 200–201) to the available data for the Skaergaard layered intrusive is the subject of an essay in the *Journal of Petrology* (Chayes, 1970a). The work indicates that the 1960 value for the magnitude of the "hidden zone" may well be a serious underestimate and that the graphically derived compositions of the successive Skaergaard "residual liquids" are inconsistent with what is known about the

compositions of the proposed parent magma and partition products. In successive liquids whose compositions are consistent with current information about these matters there appears to be no tendency toward end-stage alkali enrichment. In the conventional AFM projection the only trend of any importance seems to be a linear inverse variation of FeO and MgO at virtually constant alkali content.

##### *Ratio Correlation in Petrography and Geochemistry*

Ratio correlations, widely used throughout earth science but perhaps most critical in petrography and geochemistry, have been the subject of recurrent study over many years (see, for instance, *Year Book 65*, pp. 372–374). A manuscript summarizing the results of this study, in the form of a manual designed for self- or formal-instruction at the advanced undergraduate or beginning graduate level, has recently been accepted by the University of Chicago Press. During the report year the adequacy of certain of the approximations needed in an early stage of the argument was tested by simulation experiments. The approximations in question are of the famous "spurious correlations" of Karl Pearson, *viz.* the correlations to be anticipated between fractions having either common numerator or common denominator when the "absolute" variables, the variables from which the terms of the fractions are formed, are themselves uncorrelated. There are in all five distinguishable cases: correlations of a ratio with its own numerator or denominator, correlations between ratios of common numerator or denominator, and correlations between ratios the denominator of one of which is the numerator of the other. The approximate null correlations, shown in Table 38, are readily derived by procedures outlined in *Year Book 65*.

The experimental study indicates that



TABLE 38. Approximate Null Correlations between Simple Ratios Formed from Uncorrelated Variables,  $x_i$ , with means  $\mu_i$  and standard deviations  $\sigma_i$ ,  $i = 1, 3$

Ratio Pair $Q_i; Q_j$	Approximate Null Correlation between $Q_i$ and $Q_j$
$X_1/X_2; X_1$	$\mu_2\sigma_1/(\mu_2^2\sigma_1^2 + \mu_1^2\sigma_2^2)^{\frac{1}{2}}$
$X_1/X_2; X_2$	$-\mu_1\sigma_2/(\mu_2^2\sigma_1^2 + \mu_1^2\sigma_2^2)^{\frac{1}{2}}$
$X_1/X_2; X_3/X_2$	$\mu_1\mu_3\sigma_2^2/\{(\mu_2^2\sigma_1^2 + \mu_1^2\sigma_2^2)(\mu_2^2\sigma_3^2 + \mu_3^2\sigma_2^2)\}^{\frac{1}{2}}$
$X_2/X_1; X_2/X_3$	$\mu_1\mu_3\sigma_2^2/\{(\mu_2^2\sigma_1^2 + \mu_1^2\sigma_2^2)(\mu_2^2\sigma_3^2 + \mu_3^2\sigma_2^2)\}^{\frac{1}{2}}$
$X_1/X_2; X_2/X_3$	$-\mu_1\mu_3\sigma_2^2/\{(\mu_2^2\sigma_1^2 + \mu_1^2\sigma_2^2)(\mu_2^2\sigma_3^2 + \mu_3^2\sigma_2^2)\}^{\frac{1}{2}}$

these approximations are excellent if all relative standard deviations are less than 0.05, and are still useful for many practical purposes if they are less than 0.15. If any one of the relative standard deviations exceeds 0.15, however, the approximation, which is only of first order, may often be unsatisfactory. It will then be necessary to use either a higher order approximation or a Monte Carlo solution. Given the existence of a suitable computer program, the latter will usually be simpler to reach.

*Behavior of the Simple Closure Test when There is a Single Nonzero Covariance in the Parent Open Array*

In another and more complicated example of ratio correlation, it has recently been argued (Miesch, 1969) that when the closure correlation test proposed by Chayes and Kruskal (1966) leads to rejection of the null hypothesis \* "no information is obtained regarding the statistical or geochemical significance of individual correlations" and even "the pairs of variables that are correlated geochemically cannot be identified." The published criticism is based entirely on closure, in a single large simulation experiment, of a four-variable open array in which two of the variables are correlated, but all other covariances remain

zero. Its substance seems to be that under these circumstances the test is hypersensitive, indicating departures from random association between open variables known to be uncorrelated. Effects of this sort are bound to occur in large enough simulations, however, for the null values of *all* closed correlations are indeed shifted by the introduction of even a single nonzero open covariance; a large simulation is then in effect a Monte Carlo solution for a model different from that envisaged in  $H_0$  and ought to lead to its rejection, as indeed happened in Miesch's experiment. But the test was primarily intended for use on small samples.

On small samples drawn from the open parent used by Miesch, the test, far from being hypersensitive, turns out to be woefully *insensitive*, invariably failing to detect the known nonzero covariance and only infrequently indicating correlation between variables known to be uncorrelated in the parent. In retrospect this weakness seems almost self evident, but it was not previously suspected, and might have remained undetected had Miesch's work not shown the need for further experimentation. The difficulty arises because one of the four variables in the test array hardly varies, i.e., one of the variances is very much smaller than the others. The effective number of variables is thus closer to three than to four, and for a strictly ternary array, as pointed out in the original paper (Chayes and Kruskal, 1966, p. 695), the null correlations are precisely those observed in

\* That correlation observed in a closed array might have been generated by closure of a sample drawn from an open array of uncorrelated variables, referred to below as  $H_0$ .

the sample, so the test can only give trivial results. Considerable experimentation suggests that if the number of variables is large enough and variances are homogeneous, the test will nearly always correctly identify a single non-zero open covariance and that the incidence of misidentifications will then be just about that appropriate to the significance level being used. The first effect of inhomogeneous partition of variance, the number of variables still being adequate, appears to be an increase in the frequency with which  $H_0$  is rejected for the wrong reason, i.e., because the test indicates departures from random association between variables whose parent open covariance is known to be zero.

In the current experiments, however, this effect hardly seemed strong enough to warrant blanket condemnation of the test—when, for instance, one supposed he was accepting a 1% probability of rejecting  $H_0$  for the wrong reason, the actual probability of such a rejection might be 3 or 4 or even 5%. But no general theoretical basis for estimating the power or efficiency of the test is yet available, nor does it seem likely that a reasonable amount of experimentation will provide a widely applicable practical solution. The work reviewed here is described in detail in the published proceedings of the 1970 Geostatistics Colloquium of the Geological Survey of Kansas, before which it was presented as an invited paper.

*On Deciding Whether Trend Surfaces of Progressively Higher Order are Meaningful*

The only commonly used statistical justification of petrographic trend surfaces of order  $(k+1)$  is a test of the mean square for variation associated with *all* terms of order  $(k+1)$  against the mean square for residual variation at order  $(k+1)$ . It is not at all likely,

however, that a level of significance firmly established at order  $k$  will be seriously lessened by inclusion of terms of higher order, and with inclusion of each set of such terms a further portion of the total sum of squares is removed from the residual by assignment to specific sources, or, as trend-mappers say, “explained.” In a recently published example, for instance, this “explained” variation increases steadily from 22% in the first-order surface to 56% in the fourth-order surface, but as many of the data points are misclassified by the latter as by the former. The test, in short, is no test at all.

An obvious modification of the test ordinarily applied in the empirical fitting of polynomials would appear to be both more germane to the issue and intrinsically sounder. In this procedure, unless the mean square associated with terms of order  $(k+1)$  *only* is significantly larger than the mean square for residual variation at this order, the fitting terminates at order  $k$ . The rationale of the test is simply that terms of order  $(k+1)$  are not worth having unless they significantly reduce the residual variation remaining at order  $k$ ; accordingly, the residual variance of order  $k$  is split into two parts, that accounted for by terms of order  $(k+1)$  and that not accounted for by such terms, and the former is tested against the latter.

Shortly after a note advocating this procedure appeared in the Bulletin of the Geological Society (Chayes, 1970b), a reader pointed out that precisely the same suggestion had been made earlier by Allen and Krumbein (1962), and again by Krumbein and Graybill (1965). Appropriate methods not described in the geological journal or text literature often remain unexploited by statistical geologists, but it seems curious that a sound method readily available in both journal and text form is so roundly ignored.

## CRYSTALLOGRAPHY

## Fe/Mg ORDERING IN OLIVINES \*

L. W. Finger

The data from refined crystal structures are necessary for calculation of the nonideal terms needed in the thermochemical equations for predicting phase equilibria. In a solid solution series, for example, the ordering of cations into non-equivalent positions, reduces the configurational entropy from the maximum value associated with the fully disordered structure. If this entropy term and the excess volume and heat of mixing are known, the deviation of the free energy from a linear combination of the components can be calculated. This detailed knowledge of the thermochemical behavior of phases is necessary for prediction and mathematical modeling of homogeneous and heterogeneous phase equilibria. Preliminary calculations of liquidus relations in ternary systems have been performed by Barron (1970) using experimentally determined binary phase diagrams; however, the crystal structure data are necessary to extend these calculations into the subsolidus region.

The olivine series forsterite-fayalite,  $(\text{Mg,Fe})_2\text{SiO}_4$ , has long been regarded as exhibiting "ideal" behavior. The determinative curves of Yoder and Sahama (1957) and Jambor and Smith (1964) empirically relate selected  $d$  values as linear functions of the composition. A more complete treatment, which includes the effects of Ca and Mn, has been presented by Louisnathan and Smith (1968), with linear functions describing the variation in unit cell parameters. Proof of nonideal mixing was provided by the studies of Nafziger and Muan (1967) and Kitayama and Katsura (1968). The effect of this nonideality was investigated by Fisher and Medaris (1969),

who found a nonlinear relationship between the unit cell parameters and the composition.

Although the olivine structure has two distinct cation positions with different sizes and distortions, no deviation from a disordered cation population has been detected by X-ray studies, although Burns (1969) reported ordering effects in the infrared spectrum. A thorough summary of the previous investigations of the olivine structure has been presented by Birle *et al.* (1968). Recent advances in the techniques of the refinement of cation distributions (Finger, *Year Book 67*, pp. 216-217), when combined with an electron microprobe analysis of the same crystal, make possible a much more sensitive determination of the degree of ordering. Accordingly, olivine samples of widely differing thermal history were selected for analysis to determine if ordering could be detected.

The first sample studied was an olivine from a specimen collected by the astronauts of Apollo 11. The sample was from a phenocryst in rock chip 10020,41, which is a fine-grained vesicular crystalline igneous rock (type A) (Lunar Sample Preliminary Examination Team, 1969). The crystal studied was selected from an olivine concentrate prepared by Dr. Edwin Roedder, of the U. S. Geological Survey, Washington, D. C. A terrestrial sample, C15-64, of contrasting thermal history from a volcanic neck in the Carnarvon Range, Australia, has been described by Bryan (*Year Book 67*, pp. 247-250). Since the sedimentary rocks around this neck show metamorphic effects to a distance of approximately 0.1 km (Bryan, personal communication), it is likely that the rock cooled slowly, in probable contrast to the lunar sample.

The chemical and crystal data for the materials studied are presented in Table 39 with the unit cell data, refined from

\* This research was partially supported by National Aeronautics and Space Administration contract no. NAS 9-9988.



TABLE 39. Chemical Analyses and Crystal Data for Two Olivines \*

	10020 Olivine, wt %	C15-64 Olivine, wt %
<u>Oxide:</u>		
SiO <sub>2</sub>	38.6	33.8
MgO	37.9	22.5
FeO †	24.2	41.5
CaO	0.30	0.23
MnO	0.30	0.65
Cr <sub>2</sub> O <sub>3</sub>	0.25	n.d. ‡
Totals	101.5	98.7
<u>Formula Used in Refinement</u>		
<u>Cation:</u>		
Si	1	1
Mg	1.463	0.980
Ca	0.008	0.007
Fe' = Fe + Mn + Cr	0.529	1.013
O	4	4
<u>Crystal Data</u>		
<i>a</i> , Å	4.759(2)	4.795(3)
<i>b</i> , Å	10.285(2)	10.361(2)
<i>c</i> , Å	6.0168(8)	6.0480(9)
<i>V</i> , Å <sup>3</sup>	294.5(1)	300.4(2)
Space group	<i>Pbnm</i>	<i>Pbnm</i>
<i>Z</i>	4	4

\* The standard deviation of the final digit is in parentheses.

† Total iron as FeO.

‡ Not determined.

zero-level Weissenberg films about the *a* and *c* axes with the use of the program LCLSQ of Burnham (*Year Book 61*, pp. 132–135). No evidence of the extra reflections and resulting supercell reported by Eliseev (1958) was observed. The chemical data were obtained on the electron microprobe by mounting and polishing the crystals used for the single-crystal intensity collection; no zoning or inhomogeneity was observed in either specimen. Although the chromium con-

tent is reported as Cr<sub>2</sub>O<sub>3</sub>, the optical absorption spectrum (Haggerty *et al.*, 1970a) shows that this metal is present as Cr<sup>2+</sup> in the lunar crystal. The intensity data were collected on the Supper-Pace automated equi-inclination diffractometer with Mo radiation ( $\lambda=0.71069$  Å) and a Nb filter. The diffractometer was operated in the step-scan mode with the scan angle computed according to Finger and Burnham (1968). A step increment of 0.04° and a counting time of 3 seconds were used. The resulting data for the terrestrial olivine were corrected for dead time ( $\tau=6 \times 10^{-6}$  sec), and the data were converted to integrated intensities. The intensities of (*hkl*) and (*hk* $\bar{l}$ ) were measured for both crystals, providing a check on the reliability of the measurements and corrections. The intensities were corrected for the Lorentz-polarization and absorption effects with the program GNABS of Burnham (1966), modified to calculate the isotropic extinction factor of Zachariasen (1968), and the structure factors for equivalent reflections were averaged. The pertinent details of the data collection and correction are given in Table 40. The reflections with an intensity less than twice the standard deviation of the intensity based on counting statistics are specially marked and have been excluded from the refinement.

Refinement was accomplished with the use of the neutral scattering factors of Cromer and Mann (1968), the anomalous dispersion coefficients of Cromer (1965), and the atomic parameters of forsterite (Birle *et al.*, 1968) as starting values. The cation occupancies were assigned as

TABLE 40. Data Collection Information for Two Olivines

	10020 Olivine	C15-64 Olivine
Rotation axis	<i>a</i>	<i>a</i>
Crystal size	0.07 × 0.21 × 0.27 mm	0.16 × 0.30 × 0.34
Radiation/filter	Mo/Nb	Mo/Nb
Linear absorption coefficient, cm <sup>-1</sup>	37.0	54.8
No. of independent reflections collected	967	448
No. with $ F_o  \geq  F_{min} $	815	395

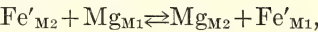
TABLE 41. Atomic Parameters for Olivine \*

Atom	10020 Olivine				C15-64 Olivine			
	<i>x</i>	<i>y</i>	<i>z</i>	<i>B</i> <sub>eq</sub>	<i>x</i>	<i>y</i>	<i>z</i>	<i>B</i> <sub>eq</sub>
M1	0	0	0	0.64(2)	0	0	0	0.46(2)
M2	0.98834(22)	0.27824(9)	1/4	0.64(2)	0.98737(20)	0.27892(10)	1/4	0.49(2)
Si	0.42746(22)	0.09509(10)	1/4	0.58(2)	0.42877(25)	0.09582(15)	1/4	0.41(2)
O1	0.76596(57)	0.09174(27)	1/4	0.67(3)	0.76667(62)	0.09283(39)	1/4	0.57(6)
O2	0.21917(62)	0.44868(26)	1/4	0.72(3)	0.21444(68)	0.45054(38)	1/4	0.58(6)
O3	0.28064(41)	0.16367(18)	0.03445(31)	0.75(2)	0.28296(48)	0.16403(28)	0.03625(40)	0.60(4)

\* The standard deviation of the final digit is in parentheses.

follows: (1) the available Ca was placed in the position (M2) that it assumes in the isostructural monticellite, CaMgSiO<sub>4</sub> (Onken, 1965), and glaucochroite, CaMnSiO<sub>4</sub> (Caron, Santoro, and Newnham, 1965); (2) all Fe<sup>2+</sup>, Fe<sup>3+</sup>, Mn, and Cr were called Fe'; and (3) the initial Fe'/(Mg+Fe') ratios were the same for both cation positions. After convergence with fixed occupancies, the cation distributions were refined, with the bulk chemistry held constant. The significance test of Hamilton (1965) was applied, and the model improved. The following hypotheses were tested: (1) the cations exhibit anisotropic thermal motions; (2) all atoms vibrate anisotropically; and (3) the data are affected by extinction. All hypotheses turned out to be correct. In Table 41 are given the atomic parameters and equivalent isotropic temperature factors for these structures. Note that the temperature factors for M1 and M2 are very nearly equal, a fact that has been used to argue in favor of disordered cation populations. Any ordering of cations in the structure results from the

exchange reaction



which is written for one atom of iron in M2 interchanging with a magnesium atom in M1. The observed occupancies may be used to calculate a distribution coefficient *K<sub>D</sub>* for the above reaction with

$$K_D = \frac{X_{\text{Mg}}^{\text{M2}} X_{\text{Fe}'}^{\text{M1}}}{X_{\text{Fe}'}^{\text{M2}} X_{\text{Mg}}^{\text{M1}}} = \frac{X_{\text{Mg}}^{\text{M2}}(1 - X_{\text{Mg}}^{\text{M1}})}{X_{\text{Mg}}^{\text{M1}}(1 - X_{\text{Mg}}^{\text{M2}})}$$

*X<sub>Mg</sub><sup>M1</sup>* denotes the Mg/(Mg+Fe') ratio for M1. In Table 42 are listed the final value of the extinction parameter, the residuals with  $R = \Sigma ||F_o| - |F_c|| / \Sigma |F_o|$  and weighted  $R = [\Sigma \omega (|F_o| - |F_c|)^2 / \Sigma \omega |F_o|^2]^{1/2}$ , the cation occupancies, and the values of *K<sub>D</sub>* for each crystal studied. If the Mg and Fe' cations were fully disordered, the value of *K<sub>D</sub>* would be 1, so the deviation from that value indicates the extent of ordering. Clearly neither sample is very strongly ordered, but certain consistent relationships strengthen the possibility that the effect is real. The degree of order is less in the lunar sample, which

TABLE 42. Residuals and Occupancies for Two Olivines

Parameter	10020 Olivine	C15-64 Olivine
Extinction coefficient, cm	$(5.7 \pm 0.3) \times 10^{-5}$	$(8.7 \pm 0.4) \times 10^{-6}$
<i>R</i> , $F_o \geq F_{\text{min}}$	0.048	0.026
Weighted <i>R</i> , $F_o \geq F_{\text{min}}$	0.053	0.025
<i>R</i> , all data	0.059	0.031
Weighted <i>R</i> , all data	0.065	0.025
Occupancy of M1	0.729 ± 0.005 Mg 0.271 ± 0.005 Fe'	0.477 ± 0.004 Mg 0.523 ± 0.004 Fe'
Occupancy of M2	0.734 ± 0.005 Mg 0.258 ± 0.005 Fe'	0.503 ± 0.004 Mg 0.490 ± 0.004 Fe'
	0.008 Ca	0.007 Ca
<i>K<sub>D</sub></i>	1.06 ± 0.05	1.13 ± 0.04

cooled rapidly, than in the terrestrial sample, which was more slowly cooled. In addition, the sense of the ordering is the same in both samples, i.e. M1 is enriched in Fe' relative to M2. This conflicts with the predictions based on cation size (Table 43), since the M2 octahedron has a larger mean size. In addition, the sense of the ordering also conflicts with the findings of Burns (1969) who found Fe enrichment in M2. This discrepancy has not been explained, although it may be due to an incorrect interpretation of the infrared spectrum studied by Burns. The minor amounts of Mn and Cr that were treated as Fe in this study will affect the value of  $K_D$ . The study of Gordon Brown (personal communication) on knebelite,  $(\text{Fe,Mn})_2\text{SiO}_4$ , shows that roughly two-thirds of the Mn occurs in M2. This degree of fractionation would increase the value of  $K_D$  by reducing the Fe content of M2. A procedure for determining the occupancies of three species will be tested in the near future. This procedure will involve holding the Mg content determined above while refining the Fe-Mn distribution.

This study suggests that there may be detectable Fe/Mg ordering in olivines; it will be necessary to investigate samples with a history of slower cooling, however, to determine whether they show a larger degree of ordering.

#### INTERNAL EQUILIBRIUM IN A SPINEL

*L. W. Finger*

The subject of chemical reactions in crystals has been covered extensively by Thompson (1969). Lindsley and Haggerty (this report) are investigating the activity of magnetite in magnetite-ulvöspinel solid solutions, and this contribution describes the application of Thompson's equations to the titanomagnetites.

In Table 44 the site occupancies for this series are listed in the form given by Thompson. Sites *A* and *B* are tetrahedrally and octahedrally coordinated

TABLE 43. Selected Interatomic Distances (Å) in Olivine \*

Atoms	10020	C15-64
<u>Si Tetrahedron</u>		
Si-O1	1.611(3)	1.620(4)
Si-O2	1.660(3)	1.654(4)
Si-O3 (2x)	1.633(2)	1.631(3)
Mean	1.634	1.634
O1-O2	2.738(4)	2.738(5)
O1-O3 (2x)	2.750(3)	2.756(4)
O2-O3 † (2x)	2.564(3)	2.562(5)
O3-O3 ‡	2.594(4)	2.585(5)
Mean	2.660	2.660
<u>M1 Octahedron</u>		
M1-O1 (2x)	2.096(2)	2.113(2)
M1-O2 (2x)	2.080(2)	2.103(2)
M1-O3 (2x)	2.159(2)	2.186(3)
Mean	2.112	2.134
O1-O2 † (2x)	2.858(4)	2.892(5)
O1-O3 (2x)	3.143(3)	3.184(4)
O1-O2 (2x)	3.045(1)	3.067(1)
O2-O3 ‡ (2x)	2.564(3)	2.562(5)
O1-O3 † (2x)	2.869(3)	2.889(4)
O2-O3 (2x)	3.377(3)	3.441(4)
Mean	2.976	3.006
<u>M2 Octahedron</u>		
M2-O1	2.191(3)	2.199(4)
M2-O2	2.069(3)	2.085(4)
M2-O3 (2x)	2.065(2)	2.075(2)
M2-O3 (2x)	2.237(2)	2.258(3)
Mean	2.144	2.158
O1-O3 † (2x)	2.869(3)	2.889(4)
O1-O3 (2x)	3.043(3)	3.058(4)
O2-O3 (2x)	3.219(3)	3.254(5)
O2-O3 (2x)	2.936(3)	2.947(4)
O3-O3 ‡ (2x)	2.594(4)	2.585(5)
O3-O3 (2x)	2.998(2)	3.019(4)
Mean	2.943	2.959
<u>Oxygen Bonds</u>		
O1-Si	1.611(3)	1.620(4)
O1-M1 (2x)	2.096(2)	2.113(2)
O1-M2	2.191(3)	2.199(4)
O2-Si	1.660(3)	1.654(4)
O2-M1 (2x)	2.080(2)	2.103(2)
O2-M2	2.069(3)	2.085(4)
O3-Si	1.633(2)	1.631(3)
O3-M1	2.159(2)	2.186(3)
O3-M2	2.065(2)	2.075(2)
O3-M2	2.237(2)	2.258(3)

\* The standard deviation of the final digit is in parentheses.

† Edge shared with An octahedron.

‡ Edge shared with Si tetrahedron.

by oxygens, respectively. The correct value of  $q$  to use should be clarified. It



TABLE 44. Site Occupancy of Titanomagnetite

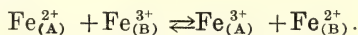
Site	A	B	O
$q$	2	4	8
Species $Q$	$\text{Fe}^{3+}$	$\text{Fe}^{3+}$	$\text{O}^{2-}$
Other species	$\text{Fe}^{2+}$	$\text{Fe}^{2+}$ $\text{Ti}^{4+}$	
$(\sigma - 1)$	1	2	0

is the number of sites of a given kind,  $q$ , in a unit quantity of crystal, and therefore  $q$  equals the multiplicity of the position in the unit cell (*International Tables*, 1952, Vol. 1) divided by the largest common factor of the multiplicities of the unique positions of the space group.

If the values of  $(\sigma - 1)$  from Table 44 are used in Thompson's equation 5, we find that

$$\tau = \sum_q (\sigma - 1) + 1 - \pi = 3.$$

The correct value of  $\pi$  is unity because there are positions in the crystal that have species with more than one valence. The above equation indicates that there are three independent quantities needed to specify the state of a crystal in this system:  $n_{\text{Ti}(B)}^{4+}$ ,  $\mathbf{n}$ , and  $n_{\text{Fe}(A)}^{2+}$ . In a closed crystal with no coupled creation and destruction of vacancies, the first two are fixed; therefore, one internal degree of freedom corresponds to the exchange reaction



Stephenson (1969) attempted to investigate the thermal dependence of the above reaction on titanomagnetites quenched from near the melting point and discovered a completely random distribution at the temperature studied. This random distribution was attributed to insufficient time for ordering. The study showed no appreciable titanium in the tetrahedral position (A); thus the assumptions of Table 44 are satisfied.

#### CHALCOPYRITE SOLID SOLUTION

G. Kullerud and Gabrielle Donnay

Chalcopyrite is one of the most com-

mon sulfide minerals. When separated from ore samples and chemically analyzed it is invariably found to have stoichiometric  $\text{CuFeS}_2$  composition. Donnay *et al.* (1958) determined the magnetic structure of natural chalcopyrite and found copper and iron to be present as  $\text{Cu}^+$  and  $\text{Fe}^{3+}$ , respectively.

Merwin and Lombard (1937) and Yund and Kullerud (1966) observed that synthetic chalcopyrites are stoichiometric only below  $200^\circ\text{C}$ . Above this temperature the stable chalcopyrite composition is nonstoichiometric, with a metal-to-sulfur ratio always greater than 1:1. The purpose of the present study is to determine whether this solid solution is one of omission, addition, or a combination of the two.

Omission solid solution is designated  $\text{CuFeS}_{2-x}$  or  $\text{Cu}^+\text{Fe}_{1-2x}^{3+}\text{Fe}_{2x}^{2+}\text{S}_{2-x}$  if we wish to draw attention to the fact that some ferric iron must be reduced to ferrous in order to maintain the formal balance of charges. The cell volume is expected to decrease with increase in  $x$ . The density is expected to decrease if, and only if, the relative decrease in formula weight exceeds the increase in cell volume.

Addition solid solution is designated  $\text{Cu}_{1+y}\text{Fe}_{1+y}\text{S}_2$  or  $\text{Cu}_{1+y}\text{Fe}_{1-3y}^{3+}\text{Fe}_{2y}^{2+}\text{S}_2$  if we wish to show the formal charges. The cell volume should increase with increasing value of  $y$ . The relative rates of increase in cell volume and formula determine whether the density increases, remains unchanged, or decreases with increasing departure from stoichiometry.

A combined solid solution,  $\text{Cu}_{1+y}^{+}\text{Fe}_{1-2x-3y}^{3+}\text{Fe}_{2x+2y}^{2+}\text{S}_{2-x-y}$ , would show a deficit of sulfur in some unit cells, whereas other cells would have additional copper or iron atoms in positions such as  $8(c)$ ,  $00z$ , in  $I42d$ , which are vacant in the regular chalcopyrite cell. This combination solid solution has, of course, the previously considered solid solutions as end members: for  $x=0$  it reduces to the metal-addition type; for  $y=0$  it becomes the

sulfur-omission type. Thus the determination of the solid solution type cannot be based on a cell-volume curve alone. Additional data such as very accurate densities, powder line intensities, structure factors, and Mössbauer or NMR spectra are needed.

The solid solution under discussion exists in two polymorphic forms. The low-temperature form is tetragonal, and the high-temperature form is cubic (ZnS-type structure). The inversion temperature varies with composition, occurring at 547°C when the phase is saturated with sulfur (Yund and Kullerud, 1966) and at decreasing temperatures with increasing metal-to-sulfur ratio. The cubic-tetragonal inversion is rapid and can readily be recorded in D.T.A. experiments when the chalcopyrite composition lies near the sulfur-rich solid solution boundary. With increase in the metal-to-sulfur ratio the inversion becomes sluggish, and the cubic form with high metal-to-sulfur ratios is readily quenchable. The cubic-tetragonal inversion is always accompanied by the so-called "Oleander-Blatt" twinning described by Ramdohr (1960).

In an attempt to produce untwinned crystals large enough for single-crystal X-ray work, chalcopyrite was synthesized with sulfur-to-metal ratios of 0.96 and 0.90. Appropriate amounts of high purity copper, iron, and sulfur were used as starting materials, and the procedure described by Yund and Kullerud (1966) was followed. The mixtures were

heated to temperatures between 365° and 500°C for 22 months with frequent regrindings at room temperature to insure homogenization. At the end of this period, representative samples were studied in polished sections. They showed chalcopyrite as the only phase. A solid lump of the sample, mounted in a powder camera and exposed to FeK $\alpha$  radiation, gave sharp powder lines of uniform intensities, which proved the material to be polycrystalline, with a grain size of about 0.1  $\mu$ m and with no preferred orientation. The attempt to grow single crystals had thus failed. A Debye-Scherrer camera, of radius (180/ $\pi$ ) mm, equipped with a calibration device for film-shrinkage correction, was used for obtaining cell dimensions. The films were read on a Picker film reader, which had a micrometer scale reading to 0.01 mm. The measurements were corrected for film shrinkage, and the twelve measurable reflections were used to refine the cell constant with Burnham's LCLSQ program (*Year Book* 61, pp. 132-135) (Table 45). The same procedure was used for obtaining cell dimensions of natural chalcopyrite samples from Transvaal, Africa, from Akita, Japan, and from the Magma copper mine in Arizona (Table 45).

An increase in cell volume with decrease in sulfur-to-metal ratio was observed and can only be interpreted as a predominance of metal addition over sulfur omission. Powder intensity measurements were chosen as a second cri-

TABLE 45. Chalcopyrite Crystal Data

	Transvaal, Africa	Akita, Japan	Magma Copper Mine	Average Mineral CuFeS <sub>2</sub> Cell	S(Cu + Fe) = 0.960(1) Cu <sup>+1.04</sup> Fe <sup>3+</sup> <sub>0.88</sub> Fe <sup>2+</sup> <sub>0.16</sub> S <sub>2</sub>	S(Cu + Fe) = 0.900(1) Cu <sup>+1.11</sup> Fe <sup>3+</sup> <sub>0.67</sub> Fe <sup>2+</sup> <sub>0.44</sub> S <sub>2</sub>
<i>a</i> , Å	5.288(1)	5.293(3)	5.285(1)	5.289	5.297(5)	5.290(2)
<i>c</i> , Å	10.416(2)	10.426(17)	10.417(2)	10.420	10.441(18)	10.732(6)
<i>V</i> , Å <sup>3</sup>	291.2(1)	292.1(4)	291.0(1)	291.5	292.9(5)	300.3(3)
<i>c</i> / <i>2a</i>	0.9849	0.9849	0.9855	0.9851	0.9856	1.0144
Formula weight	183.521	183.521	183.521	183.521	188.297	196.654
<i>D<sub>s</sub></i>	4.185	4.172	4.188	4.181	4.268	4.349
No. of reflections used	11	12	9		10	9

terion to distinguish between metal-addition and metal-addition+sulfur-omission solid solution. The films were read at the National Institutes of Health on a Joyce-Lobell double-beam microdensitometer, Mark III. Only peak intensities were used, since the peaks were too sharp for measurement of integrated intensities. The accuracy of these measurements is therefore low. An inspection of the chalcopyrite crystal structure (Pauling and Brockway, 1932) shows only one likely position where cations can be added, namely,  $8(c)$ ,  $00z$ , with  $z \approx \frac{3}{4}$ . The powder line intensities were calculated, therefore (using the modified D. K. Smith program UCRL 7196), assuming pure addition solid solution, for the compositions  $\text{Cu}_{1.04}\text{Fe}_{1.04}\text{S}_2$  and  $\text{Cu}_{1.11}\text{Fe}_{1.11}\text{S}_2$ , corresponding to the synthesized compositions  $\text{S/Me}=0.96$  and  $0.90$ , and setting  $z=0.75$ . Owing to the pseudo-cubic subcell of dimensions  $2a \sim c$ , reflections appear in the powder pattern in closely adjacent pairs, which are well suited for intensity comparisons. It should be noted (Table 45, row  $c/2a$ ) that there is a reversal in  $c/2a$  value from less than 1 to greater than 1 with increasing departure from stoichiometry, resulting in changes in relative positions of neighboring lines. For example, the stoichiometric mineral sample and the  $\text{Cu}_{1.04}\text{Fe}_{1.04}\text{S}_2$  composition show 132 at

$2\theta$  of  $74.86^\circ$  and  $74.61^\circ$  with considerably stronger intensities than 116 at  $2\theta$  of  $75.61^\circ$ , respectively. Composition  $\text{Cu}_{1.11}\text{Fe}_{1.11}\text{S}_2$ , on the other hand, has line 116 at  $73.65^\circ$  of  $2\theta$  with weak intensity and 132 at a  $2\theta$  of  $74.57^\circ$  with strong intensity. At composition  $\text{Cu}_{1.06}\text{Fe}_{1.06}\text{S}_2$  a cubic pattern is predicted because  $c/2a \approx 1$ . At first the need for reindexing was not taken into account; even so it was possible to obtain all dimensions for  $\text{Cu}_{1.11}\text{Fe}_{1.11}\text{S}_2$  which gave reasonably good agreement for  $d_{\text{obs}}$  and  $d_{\text{calc}}$  values. Only the radical change in intensity of lines gave cause for suspicion. We thank J. D. H. Donnay for pointing out the possibility of a mistake in the indexing. With correct indexing, the intensity ratios of neighboring lines are in reasonable agreement with the calculated intensities based on the assumption of metal-addition solid solution (Table 46). As a measure of this agreement a discrepancy index is listed:

$$R_I = \frac{\sum \left| \left( \frac{I_1}{I_2} \right)_{\text{obs.}} - \left( \frac{I_1}{I_2} \right)_{\text{calc.}} \right|}{\sum \left( \frac{I_1}{I_2} \right)_{\text{calc.}}}$$

This index, obtained by summing, over all observed pairs of reflections, has the value 0.14 for the Transvaal mineral and  $\text{Cu}_{1.04}\text{Fe}_{1.04}\text{S}_2$  composition and the value 0.09 for  $\text{Cu}_{1.11}\text{Fe}_{1.11}\text{S}_2$ .

TABLE 46. Observed and Calculated Intensity Ratios for Neighboring Powder Lines of Chalcopyrites

Miller Indices	$I_1/I_2$					
	$\text{CuFeS}_2$ (Transvaal)		$\text{Cu}_{1.04}\text{Fe}_{1.04}\text{S}_2$		$\text{Cu}_{1.11}\text{Fe}_{1.11}\text{S}_2$	
	Obs.	Calc.	Obs.	Calc.	Obs.	Calc.
220						
024	0.72	0.51	0.57	0.51	0.60	0.48
132						
116	2.1	2.1	2.3	2.1	2.3	1.9
040						
008	1.8	2.0	2.0	2.0	1.6	1.8
332						
136	0.77	0.50	0.72	0.49	0.55	0.49
244						
228	1.6	1.9	2.4	1.9	2.0	2.0
152						
336	1.4	1.6	...	...	2.0	2.0



Addition solid solution is exceptional for sulfide minerals; omission solid solution such as  $\text{Fe}_{1-x}\text{S}$ , pyrrhotite, is the rule. It appears likely that metal addition raises the lattice energy of the structure, so that the stoichiometric composition is energetically favored. Therefore, it is not surprising that the non-stoichiometric chalcopyrite compositions are not encountered in nature: during cooling, recrystallization keeps taking place, moving the crystalline composition closer and closer to stoichiometry.

We hope to carry out a neutron-diffraction study with the two nonstoichiometric synthetic compositions and to check the present conclusion by determining the change in magnetic scattering intensities that should result from the drop in ferric iron concentration (see column headings, Table 45).

To test the stability of the mineral composition at elevated temperatures, samples of the Transvaal material were heated from 10 hours to 20 days at temperatures ranging from 200° to 600°C. No changes in cell dimensions were observed. The powder lines did not shift measurably, although at the highest temperature, yellow sulfur was visible, mixed in with the specimen at the end of the run. The powder lines increase in sharpness, owing to increase in grain size as a result of heating for 10 hours at 400°C or 10 days at 300°C. At 200°C recrystallization is slower. The original sample has an estimated grain size of 0.1  $\mu\text{m}$  or less; the heated samples show at least a 10-fold increase in grain size.

Dr. R. W. G. Wyckoff, of the University of Arizona, kindly permitted us the use of his Transvaal chalcopyrite sample and critically read the manuscript. Dr. David Davies of the National Institutes of Health permitted and showed G. Donnay the use of his microdensitometer instrument, on which all intensity measurements were made. Dr. G. Tunell discussed the subject matter with us.

# STRUCTURAL HYPOTHESIS FOR MACKELVEYITE, $\text{Ba}(\text{Ca}, \text{RE}, \text{Na}, \dots)_{1.00}(\text{CO}_3)_2$

Gabrielle Donnay

The solution of the ewaldite crystal structure (Donnay and Preston, 1970) has provided a promising hypothesis for the crystal structure of mackelveyite. As first reported in *Year Book 67* (pp. 218–

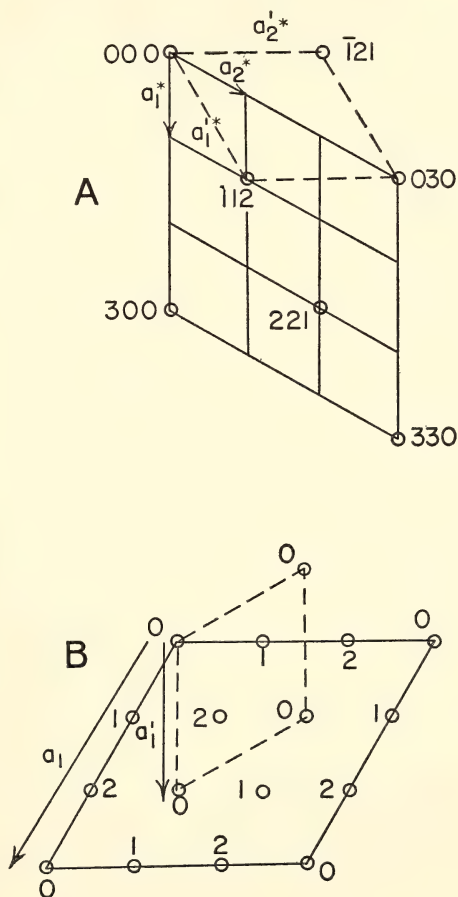


Fig. 83. Reciprocal and direct cells and subcells of mackelveyite. (A) True reciprocal cell with repeat distance  $a^*$ . Open circlets show the observed, sharp reflections with their Miller indices. Dashed lines outline the smallest reciprocal cell with repeat distance  $a^{*'}.$  (B) True cell with edge  $a$  and subcell, corresponding to only sharp reflections with edge  $a'.$  Solid circles show positions of nine barium atoms at heights given in thirds of the cell height  $c.$

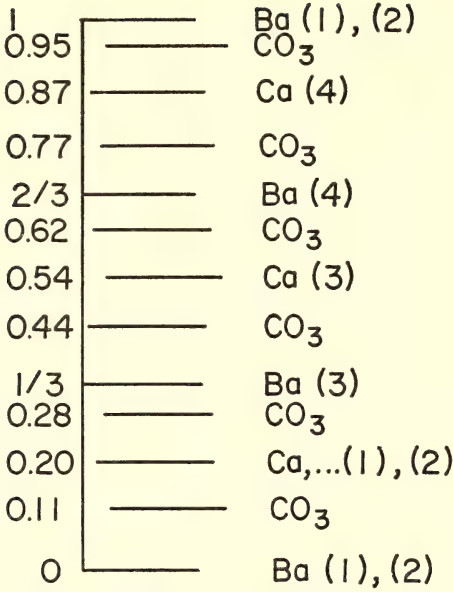


Fig. 84. Sequence of atomic layers parallel to (0001) in mackelveyite. Contact of layer line with vertical line indicates fixed origin for the layer. Numbers on left side are *z* coordinates.

219), mackelveyite has space group *P*31*m*; cell dimensions *a*=9.164(10), *c*=19.126(18) Å; and sharp X-ray reflections *hkl* only for Miller indices *h*, *3p*+*h*, *3r*-*h*, where *p* and *r* are any integers. All other reflections are drawn out into continuous rods of diffuse X-ray intensity in reciprocal space parallel to *c*\*. Beginning with the observed sharp reflections only (Fig. 83A), it is noted that they outline, in direct space, a smaller cell with dimensions *a'*=*a*√3, *c'*=*c*, *V'*=1/3*V*, *Z'*=*Z*/3=3, and space

group *R*3*m* (Fig. 83B), where the reverse description of the rhombohedral lattice must be used. On the basis of the observed intensity relations between sharp and diffuse reflections of mackelveyite, the barium atoms are placed at 0, 0, 0; 1/3, 2/3, 1/3; 2/3, 1/3, 2/3 in the small cell, and thus nine barium atoms are obtained in the true mackelveyite cell (Fig. 83B, Table 47).

All other ions, cations as well as carbonate groups, are placed in layers parallel to (0001), in the same sequence as in ewaldite (Fig. 84). They are, however, randomly displaced from each other along vectors lying in the horizontal plane, thus leaving constant spacings between atomic planes. With this arrangement, they will contribute scattered X-ray intensity to the diffuse rods only apart from 000*l* reflections (Kathleen Lonsdale, private communication). Half the carbonate groups could, as in ewaldite, be contributing to the sharp Bragg reflections rather than to the diffus scattering, provided their atomic planes were in fixed, rather than random, relation with respect to the barium planes.

This hypothesis appears satisfactory because, in addition to accounting for the cell size and geometry, it gives mackelveyite a structure so closely related to that of ewaldite that the morphological evidence for mackelveyite as a forerunner of ewaldite is accounted for (Donnay and Donnay, 1970). It explains equally well the generally observed coexistence of ewaldite and mackelveyite; mackelveyite crystals are

TABLE 47. Proposed Atomic Coordinates for Cations of Mackelveyite

Wyckoff Position	Symmetry Point	Atom	Coordinates *		
			<i>x</i>	<i>y</i>	<i>z</i>
1( <i>a</i> )	3 <i>m</i>	Ba(1)	0	0	0.00
2( <i>b</i> )	3	Ba(2)	1/3	2/3	0.00
3( <i>c</i> )	<i>m</i>	Ba(3)	0.33	0	0.33
3( <i>c</i> )	<i>m</i>	Ba(4)	0.67	0	0.67
1( <i>a</i> )	3 <i>m</i>	Ca,...(1)	δ	ε	0.20
2( <i>b</i> )	3	Ca,...(2)	1/3 + δ	2/3 + ε	0.20
3( <i>c</i> )	<i>m</i>	Ca,...(3)	0.33 + δ	ε	0.54
3( <i>c</i> )	<i>m</i>	Ca,...(4)	0.67 + δ	ε	0.87

\* δ and ε are variables, differing from cell to cell for each atomic layer.

observed pure, whereas ewaldite is always found in syntactic intergrowth with mackelveyite. The disordered structure forms first and changes, in the solid state, to the more—but still not completely—ordered form, giving ewaldite pseudo-morph crystals after mackelveyite.

Calculations to check the above structural hypothesis are under consideration, thanks to helpful suggestions from Dame Kathleen Lonsdale.

#### ADDITIONAL DATA ON CHAOITE

*A. G. Whittaker,\* Gabrielle Donnay, and  
Kathleen Lonsdale†*

The latest allotropic form of carbon, first observed in nature in the Ries Crater, Germany (El Goresy and Donnay, 1968), and then produced from graphite in the laboratory (Whittaker and Kintner, 1969), has also been found in a carbon-containing meteorite (Vdovykin, 1969). Although the quantities of chaoite so far produced in the laboratory are very small, they have yielded some additional experimental data.

Flakes of chaoite sink slowly in methylene iodide, thus setting a lower limit of  $3.33 \text{ g/cm}^3$  for their density. X-ray powder data and single-crystal electron-diffraction data both give hexagonal cell dimensions  $a = 8.948 \pm 0.010$ ,  $c = 14.078 \pm 0.018 \text{ \AA}$ . The cell volume together with the minimum observed density give a minimum cell content of 163.0 carbon atoms. The diamond density of  $3.52 \text{ g/cm}^3$  would correspond with 172.3 carbon atoms per cell. The refractive index of diamond is 2.41. Chaoite is birefringent; its refractive index along the  $c$  direction is found to be greater than 1.80. Electron-probe tests of the

purity of artificial chaoite show from 0 to 2.5 wt % Si as the only impurity.

Transmission electron-microscope photographs of synthetic chaoite crystals (Plate 5) show euhedral specimens up to  $0.5 \mu\text{m}$  in largest dimension. They are very thin, white, transparent plates (0001), with ditrigonal or hexagonal outlines. It has not been possible to discern whether they are bordered by prism or pyramid faces, but by correlating a photograph with the diffraction pattern from the same crystal, Miller indices  $\{10\bar{1}0\}$  or  $\{10\bar{1}l\}$  can be assigned to the lateral faces, if the crystal is assumed to have a six-fold axis so that six faces belong to the given form. For the more likely possibility of an axis of order 3, two lateral forms are observed,  $\{10\bar{1}l\}$  and  $\{01\bar{1}l\}$ , where  $l$  may or may not be zero.

Electron-diffraction patterns have been obtained of nets other than (0001)<sub>o</sub>\*. Miller indices  $hk \cdot O$  obey the  $R$ -lattice criterion;  $hk \cdot l$  reflections do not. The structure is therefore rhombohedral only in projection on (1000). In contrast to the X-ray powder pattern, which showed no basal reflections, reflections  $000l$  with  $l = 3, 6, 9, 12$ , and 15 have all been observed on the electron-diffraction patterns. This difference is explained by the extreme thinness of the chaoite flakes.

It is observed that the  $c$  axis of chaoite lies in the plane perpendicular to the  $c$  axis of pyrolytic graphite from which chaoite is formed. Attempts to grow chaoite on single-crystal graphite are under way, so that the mutual orientations of  $a$  axes from graphite and chaoite can also be learned.

The following relations of chaoite cell dimensions to  $C$ - $C$  interatomic distances as observed in diamonds are of interest:

$$a_{\text{Ch.}} \approx 6 \left( \frac{\sqrt{3}}{4} a_{\text{Diam.}} \sin 70^\circ 32' \right) = 6 \times C-C \text{ sp}^3 \text{ bond length projected from one body diagonal of the cube onto any other body diagonal}$$

$$8.948 \text{ \AA} \approx 8.737 \text{ \AA}$$

$$c_{\text{Ch.}} \approx 9 (C-C \text{ sp}^3 \text{ bond length})$$

$$14.078 \text{ \AA} \approx 13.901 \text{ \AA}$$

\* Aerospace Corporation, Los Angeles, California.

† Bexhill-on-Sea, Sussex, England.



BIOCRystallography

Minimal Surfaces

Gabrielle Donnay

The unique ability of echinoderms to grow their single-crystal calcite plates with a *minimal surface* as interface between amorphous organic stroma and inorganic crystalline calcite is most intriguing. Michael Goldberg (private communication) gives a mathematician's introduction to minimal surfaces as follows:

If a closed loop of wire, of arbitrary shape, is dipped into a soap solution, and then removed, a soap film is found to bridge the opening. Because of the surface tension in the film, the surface contracts to a position to minimize the total area. Mathematicians call this film a minimal surface, since it has less area than any other surface that may be stretched across the wire to close the opening.

Erect a perpendicular at some point of the surface. Pass a plane through this perpendicular. Then this plane cuts the surface in a curve that has curvature *k* at the point. As the plane is turned about the perpendicular, the curvature *k* varies and even changes sign. The two extreme curvatures are equal and opposite in sign. Hence, the sum of the two extremes, which is called the mean curvature, is zero. This property of zero mean curvature characterizes a minimal surface.

If a skeletal triperiodic structure, containing a large number of equal chambers, is dipped into a soap solution, the soap film obtained is a periodic minimal surface, which may have different lattice symmetries (translation groups). So far, only cubic and hexagonal symmetries have been observed on scanning electron-microscope photographs of echinoderm plates.

Botanists are apparently dealing with the same type of surface in prolamellar bodies of plants, but have not been aware of the mathematical nature and fame of their membranes. Gunning (1965) of

Queen's University of Belfast, northern Ireland, for example, gives a schematic drawing of the membrane system of the *Avena* prolamellar body, which is a perfect illustration of a cubic periodic minimal surface.

A hypothesis that follows from the concept of a minimal-surface interface has been tested experimentally. The growth of an echinoderm plate is due to precipitation of additional  $\text{Ca}^{2+}$  and  $\text{CO}_3^{2-}$  ions from the stroma onto the single-crystal phase, so that the ratio of crystalline to amorphous volume should rise with increasing age of the plate. The densities of calcite and stroma differ sufficiently, so that an increase in density with plate age should be observable.

D. L. Pawson supplied an adolescent living specimen of *Strongylocentrotus droebachiensis* (Müller), about 39 mm in body diameter, and removed from it a column of interambulacral plates labeled 1 to 16, going from the apical system to the peristome of the animal. Increasing numbers thus correspond to increasing age of the plate. The densities of individual plates were measured in the usual way on the Berman balance (Table 48). They increase slightly with age. If the magnesium content of the calcite is assumed to be 13.5 atomic %, as determined from cell dimensions and calibration curve in the literature for plates of the same species (Donnay and Pawson, 1969), a calculated density of  $D_x = 2.761 \text{ g/cm}^3$  is derived for the crystalline phase. If the density of the stroma is assumed to be  $1.0 \text{ g/cm}^3$ , the volume

TABLE 48. Measured Densities and Volume Fraction Stroma of Interambulacral Plates of *Strongylocentrotus droebachiensis* (Müller)

Plate No.	Density, g/cm <sup>3</sup>	Volume Fraction of Stroma for Stroma Density, g/cm <sup>3</sup>		
		0.9	1.0	1.2
2	2.48 ± 0.01	0.15	0.16	0.18
8	2.51 ± 0.01	0.13	0.14	0.16
15	2.54 ± 0.01	0.12	0.12	0.14

fraction of stroma drops from 0.16 to 0.12 in shells 2 to 15 (Table 48).

P. E. Hare studied the amino acids in the stroma of plates 2, 3, 10, and 14 of the above column and found no significant changes in the amino acid contents. His data indicate collagen-like stroma throughout.

*Crystallographic Observations on  
Regenerated Shells of  
Ampullarius*

*Gabrielle Donnay*

Dr. K. M. Wilbur suggested this X-ray study and supplied the specimens, which had been prepared as follows: three living specimens of the gastropod *Ampullarius* had a piece removed from their shells and were then allowed to regenerate the shell for periods of 3, 4, and 7 days before being sacrificed. The transmission Laue technique, with MoK radiation, was used to study the degree and type of preferred orientation. For this purpose an area of the shell, which included all of the regenerated region, was removed with a dental drill and mounted on a goniometer head. The

translation motions were used to bring different regions into diffracting position without changing the orientation relation of shell and film. Afterwards smaller pieces of shell were studied in a Debye-Scherrer powder camera, with CuK $\alpha$  radiation, to permit phase identification and determination of cell dimensions.

Aragonite is the only observed crystalline phase. Cell dimensions remained unchanged from specimen to specimen. Preferred orientation (Table 49) is a minimum when the shell is first regenerated, but increases to the extent observed in the original shell in only 7 days. There is a striking lowering of density when the shell is regenerated: the original shell of the "7-day" specimen has a density of  $2.82 \pm 0.01$  g/cm<sup>3</sup>, whereas the regenerated shell of the same specimen gives a value of  $1.33 \pm 0.02$  g/cm<sup>3</sup>. It must be concluded that during the process of rapid regeneration the volume ratio of organic to inorganic matter in the shell increases considerably. Changes in amino acid components between original and regenerated shells have also been observed in another gastropod, *Helix pomatia*, by Saleuddin and Hare (1970).

TABLE 49. X-ray Study of Preferred Crystal Orientation in Aragonite Shells of *Ampullarius*

Specimen Description	1 Original Shell		2 Original Whole Shell	3 Regenerated Shell
	Inner Layer	Outer Layer		
3 days	?	?	very pronounced L	minimal L, P
4 days	?	?	very pronounced (preferred orientation) L	on the increase L
7 days	strongest of all layers examined P	pronounced L, P	very pronounced L	pronounced, like that of outer layer in original shell L, P

L refers to Laue pattern, taken with a precession camera used as a Laue camera, crystal-to-film distance 60 mm, MoK, 50 kv, 20 ma, 3.0-hour exposure. Specimen plate about perpendicular to X-ray beam.

P refers to powder pattern, taken with Debye-Scherrer camera,  $R = (180/\pi)$  mm, CuK $\alpha$  (Ni filter), 10.0-hour exposure. Specimen rotated in beam.

? indicates layers could not be separated for study.

*Crystallographic Observations on a Naturally Occurring Branched Spine of Strongylocentrotus purpuratus*

Gabrielle Donnay and B. M. Heatfield\*

The branched or Siamese-twin type of spine is a very rare occurrence in nature. Its two branches, 2.3 mm and 3.5 mm long, separate just above the milled ring. The specimen was kept intact during the X-ray study; it was mounted on a specially designed sample holder that fits into a Supper goniometer head. Different regions of it were successively exposed to an MoK X-ray beam (50 kv, 20 ma, 0.7-hour exposures) of 1.2 mm diameter, on the precession camera. Six orientation patterns with  $\mu=10^\circ$  told the following history of this abnormal feature.

At the socket end of the spines only one calcite phase is present. Its  $c$  axis, as usual, extends normal to the circular cross section. The specimen was adjusted so that the  $a^*c^*$  net was centered in the beam. When the milled ring is centered in the beam, an additional calcite phase appears for the first time. Its  $c$  axis lies in the  $a^*c^*$  plane of the first phase, the two  $c$  axes subtend an angle of  $43^\circ$ ; the  $a^*$  axis of the second phase does not fall in this net. Right above the milled ring, the two phases separate bodily into the two distinct spines, each one again showing the normal calcite orientation with  $c$  along the length of the spine. The shorter of the two spines is the one whose crystalline phase extends back through the milled ring. The cell dimensions of the two calcite crystals are found to be the same within 0.1%.

It is concluded that some interference with the normal growth process led to the formation of a branch in the milled ring region, which continued growing normally. An irregular contact surface should be observable within the milled ring.

\*Zoology Department, Duke University, Durham, North Carolina.

*Fractured and Regenerated Spines of Arbacia punctulata*

Gabrielle Donnay and B. M. Heatfield

Primary, interambulacral spines of the sea urchin *Arbacia punctulata* were fractured 2–3 mm above their milled ring. They were then allowed to regenerate for 60 days under constant conditions in the laboratory. The regenerated portion was more heavily pigmented than that portion of the spine below the fracture. The spines were mounted with their length along the axis of the goniometer head and were studied with precession orientation patterns ( $\mu=10^\circ$ , MoK radiation, 50 kv, 20 ma, 1.3 hours). The specimen was made to fill only the lower half of the X-ray beam, whose diameter is 1.2 mm. Successive exposures were taken of adjacent regions of the spine from 5 mm below the fracture to 6 mm above it.

No evidence of any kind on the diffraction patterns revealed the fact of the past fracture. Cell dimensions remained constant within the observable 0.1% and the orientations of the crystallographic axes remained unchanged within  $1'$  of arc. The pigmentation of the fractured region cannot be due to inclusions in the calcite phase but must be caused by changes in the noncrystalline organic phase.

The picture of the spine as a two-phase body with a periodic minimal-surface interface (Donnay and Pawson, 1969) is in line with the above observations. The fracture leaves enough of the single-crystal and stroma phase in contact so that crystal growth can continue without permanent scar effect.

CORRIGENDUM FOR "FIFTY YEARS OF X-RAY CRYSTALLOGRAPHY AT THE GEOPHYSICAL LABORATORY, 1919–1969"

In *Year Book 68* (p. 279) it was incorrectly stated that prior to 1919 crystal-structure work in the United States was limited to the Massachusetts Insti-



tute of Technology, the General Electric Company, and Cornell University. We thank Professor Linus Pauling for pointing out to us that this type of research was begun at the California Institute of Technology late in 1916. Indeed, the

first American crystal-structure determination based on single-crystal data, that of chalcopyrite, was published early in 1917 by C. L. Burdick and J. H. Ellis, as publication no. 3 of the California Institute of Technology.

## STUDIES OF SULFIDES

### MINERAL ASSEMBLAGES IN THE Cu-Fe-S-O SYSTEM

*L. A. Taylor and G. Kullerud*

In most sulfide ore deposits, whether of magmatic, hydrothermal, metamorphic, or sedimentary origin, one or both of the iron oxides magnetite and hematite are associated with the sulfides. In magmatic, hydrothermal, and metamorphic deposits, magnetite is typical as a primary phase. Hematite is commonly a primary phase in sedimentary deposits but sometimes also in metamorphic and even hydrothermal ones. Subsequent to original deposition many ores are exposed to various degrees of secondary oxidation. The mechanisms of such oxidation are complicated and very insufficiently understood.

Of the ternary systems bounding the quaternary one, the most important economically and with respect to frequency of mineral occurrences is that involving the elements copper and iron in addition to sulfur. The minerals of this system occur under an exceedingly wide range of geologic conditions. The phase relations in this system are well known from liquidus temperatures down to about 200°C (Yund and Kullerud, 1966). In order to facilitate the investigation of the quaternary system, studies have also been performed on the phase relations in the copper-iron-oxygen system (Yund and Kullerud, 1964), the copper-oxygen-sulfur system (Kullerud and Yund, *Year Book 61*; Taylor and Kullerud, *Year Book 68*), and the iron-oxygen-sulfur system (Kullerud, *Year Book 56*).

In the present study the behaviors of the compounds of the copper-iron-sulfur system when heated at various temperatures with magnetite and/or hematite have been investigated. Phase assemblages in the quaternary system copper-iron-sulfur-oxygen have also been synthesized by heating mixtures of pure copper, iron, and sulfur with the oxides. In addition, presynthesized sulfides were heated at various temperatures in a stream of pure oxygen, at a pressure slightly exceeding that of the atmosphere, and their behaviors were studied as a function of time. This study did not produce quaternary compounds, and to the best of our knowledge minerals containing copper, iron, sulfur, and oxygen as the four major components have never been reported. Because of this lack of quaternary compounds, tie lines always represent connections between binary or ternary phases.

The phase relations at 300°C as derived by these experimental procedures are shown in Fig. 85. Vapor is always a phase in coexistence with all the phases and phase assemblages that are shown in this and the following figure. To facilitate diagrammatic presentation and to avoid overcrowding the figure with tie lines, a number of phases not essential to the following discussion have been omitted. These are Cu<sub>2</sub>O (cuprite), CuO (tenorite), CuFeO<sub>2</sub> (delafossite), and CuFe<sub>2</sub>O<sub>4</sub>, which are all situated on the Cu-Fe-O plane.

At 300°C, where wüstite is not stable on the Fe-O join, magnetite, iron, copper, and pyrrhotite form a univariant assemblage. This pyrrhotite, having stoichio-

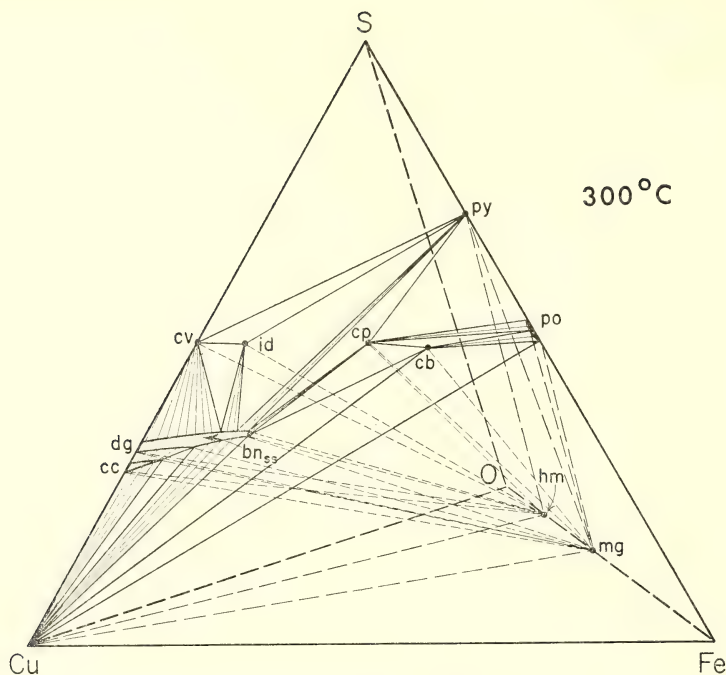


Fig. 85. Phase relations in the Cu-Fe-S-O system at 300°C. Phases such as  $\text{Cu}_2\text{O}$  (cuprite),  $\text{CuO}$  (tenorite),  $\text{CuFeO}_2$  (delafossite), and  $\text{CuFe}_2\text{O}_4$  are not shown. Abbreviations: cv, covellite; dg, digenite; cc, chalcocite;  $\text{bn}_{ss}$ , bornite solid solution; id, idaite; cp, chalcopyrite; cb, cubanite; py, pyrite; po, pyrrhotite; hm, hematite; mg, magnetite.

metric FeS composition, is the troilite end member of the pyrrhotite solid solution series. This assemblage sometimes occurs in meteorites. Magnetite, copper, cubanite, and pyrrhotite (of near FeS composition) and magnetite, copper, bornite, and cubanite form univariant assemblages that are rare on earth but have been reported in several meteorites. At 300°C the bornite solid solution, which is very extensive at high temperature, is intersected by a solvus, so that chalcocite and bornite appear as two distinct phases. Magnetite, chalcocite, bornite, and copper form a univariant assemblage, as noted in Fig. 85. This assemblage and those discussed below are not clearly distinguishable in Fig. 85. For this reason the quaternary system has been "exploded" in Fig. 86 to show the individual univariant tetrahedra and some of the wedge-shaped divariant

volumes. Again, in order to facilitate presentation, only the most extensive solid solution fields are shown in the "exploded" diagram.

In Fig. 86 the copper-magnetite-pyrrhotite surface is common to both the copper-iron-magnetite-pyrrhotite and the copper-magnetite-pyrrhotite-cubanite volumes, and similarly the copper-magnetite-cubanite surface is common to the copper-magnetite-pyrrhotite-cubanite and copper-magnetite-cubanite-bornite volumes. The curved lines in the "exploded" diagram of Fig. 86 were drawn in an effort to show the correlations between pairs of univariant volumes that share one surface plane and to orient these volumes relative to each other.

In addition to the assemblages already discussed, it is noted in Fig. 86 that the magnetite-bornite-cubanite-chalcopyrite and magnetite-pyrrhotite-chalcopyrite-

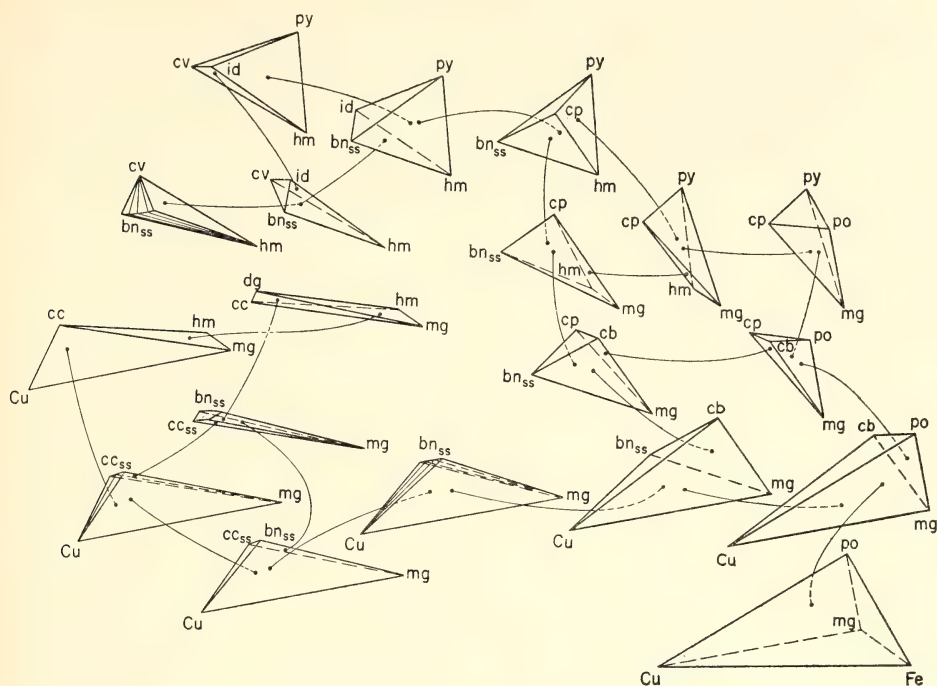


Fig. 86. "Exploded" diagram showing phase relations in the Cu-Fe-S-O system at 300°C. Abbreviations as in Fig. 85.

pyrite assemblages are stable. Of these two, the latter is particularly common in hydrothermal ores.

If a copper-iron sulfide assemblage has a bulk composition situated on the sulfur side of an approximate composition line running from chalcocite to bornite, to chalcopyrite, and on to pyrite, it cannot coexist with magnetite alone. Hematite must appear as a phase. Typical univariant assemblages involving the two oxides are copper-chalcocite-magnetite-hematite, chalcocite-digenite-magnetite-hematite, bornite-chalcopyrite-magnetite-hematite, and chalcopyrite-pyrite-magnetite-hematite. Figure 86 also demonstrates that magnetite cannot coexist stably with sulfide assemblages containing covellite or idaite, whereas hematite can. The very important bornite-chalcopyrite-pyrite sulfide assemblage is stable with hematite and not with magnetite. Assemblages

commonly resulting from secondary oxidation are represented in the upper portion of Fig. 86. They are covellite-idaite-bornite-hematite, covellite-idaite-pyrite-hematite, and bornite-idaite-pyrite-hematite. Covellite and idaite do not coexist stably with chalcopyrite.

The established phase diagram can be usefully employed to obtain some information on the change in any mineral assemblage as a result of oxidation. If, for example, magnetite associated with chalcopyrite, pyrrhotite, and pyrite is oxidized to hematite, pyrrhotite would become unstable and bornite might appear instead, establishing the bornite-chalcopyrite-pyrite-hematite assemblage. If magnetite, in coexistence with bornite, is oxidized to hematite, the bornite composition must change toward sulfur across the bornite solid solution field. Oxidation slightly beyond that required to convert all magnetite will lead to for-



mation of idaite and/or covellite rims on bornite. This process may be very common. Ramdohr (1960), who has observed idaite from hundreds of localities, points out that in each instance the idaite phase is apparently the first oxidation product of bornite.

The volume of sulfide ores deposited from magmatic rocks is small compared to the volume of the entire sulfide-silicate system. For this reason the sulfide system can be considered to be buffered by the rock components. The sulfide minerals that form are those that can exist under the oxygen fugacity conditions that are buffered by the rock constituents. Magnetite is a common mineral in such rocks, and the copper-iron sulfides that can occur stably with magnetite are illustrated in Fig. 85. The most common of these assemblages is that involving chalcopyrite, pyrrhotite, pyrite, and magnetite. The composition tetrahedron formed by these phases has a broad base, so that even considerable variation in bulk composition will not produce variation in mineralogy. Addition of nickel as a fifth component will produce pentlandite as a phase that is stable with chalcopyrite, pyrrhotite, pyrite, and magnetite below about 200°C. It is also noted in Fig. 85 that if the copper-to-iron atomic ratio exceeds 1:1, if the sulfur concentration is high, or if hematite is stable in the rock system rather than magnetite, then assemblages such as bornite-chalcopyrite-pyrite-hematite will result. This is exemplified in the large deposits of the Magma Mining district.

The copper-iron-sulfur-oxygen system can be used to relate the most common sulfides with the iron oxides. The phase relations displayed at 300°C are not in complete accordance with the sulfide and oxide mineral associations observed in nature, where equilibration among minerals in this quaternary system takes place to well below 200°C. The mineralogically important changes in phase relations below 300°C are being studied, and with these data it will be

possible to decipher the reequilibration processes that take place during cooling of ores. Knowledge of this system not only serves to explain the mineral assemblages found in various types of rocks and ores but also bears directly on the processes of secondary alteration.

#### STRUCTURAL REFINEMENT AND COMPOSITION OF MACKINAWITE

*L. A. Taylor and L. W. Finger*

Mackinawite is an iron-sulfide mineral, commonly occurring with troilite (FeS), cubanite ( $\text{CuFe}_2\text{S}_3$ ), chalcopyrite ( $\text{CuFeS}_2$ ), and pentlandite [ $(\text{Fe}, \text{Ni}, \text{Co})_9\text{S}_8$ ] in certain ore deposits that have reequilibrated to low temperatures. Berner (1962) has found that the substance described as "hydrotroilite"—an amorphous, fine-grained, black, iron-sulfide mixture, which is a common constituent of many Tertiary and Recent sediments—is, in large part, poorly crystallized mackinawite.

The name mackinawite was proposed by Evans *et al.* (1962, 1964) for natural occurrences of a tetragonal compound near FeS in composition. A phase possessing the properties of this mineral had previously been described by Milton and Milton (1958), Kouvo and Vuorelainen (1959), and Kouvo, Vuorelainen, and Long (1963). Although the composition of mackinawite was originally given with a metal-to-sulfur ratio of 1:1, most chemical analyses show a slight excess of metal, and thus mackinawite and troilite (FeS) are not polymorphs; the composition is usually written as  $(\text{Fe}, \text{Ni}, \text{Co})_{1+x}\text{S}$ , with  $x \cong 0.06$  (Clark, 1966). Most mackinawite specimens found in ore deposits contain some Ni and Co; Berner (1962) has synthesized this phase in aqueous Fe-S solutions, however, demonstrating that Ni and Co are not essential components of the structure.

Berner (1962) also discovered that mackinawite could be satisfactorily indexed on a primitive tetragonal cell and that the structure closely resembled that

of FeSe, described by Hägg and Kindström (1933) as having an anti-PbO type structure. Kouvo *et al.* (1963) described mackinawite crystals from Outokumpu, Finland, which they examined by the Weissenberg method, finding a tetragonal unit cell in probable space group  $P4/nmm$ , in agreement with Berner's conclusions based on powdered samples.

The chemical data for mackinawite are consistent with three possible hypotheses for the deviations from stoichiometry in mackinawite. There may be extra metal positions that are partially occupied, giving the formula  $M_{1+x}S$ ; there may be only one metal position that is completely occupied, with vacancies replacing some of the sulfur, leading to  $MS_{1-x}$  as the structural formula; or the true description of the structure may be a combination of both possibilities. To resolve this question, a crystal from Outokumpu, Finland, was obtained through the courtesy of Dr. O. Kuovo. Morphologically the crystal is a perfect dipyrmaid,  $\{111\}$ , with  $\{100\}$  and  $\{001\}$  as minor forms. The diffraction symmetry and subsequent refinement are compatible with space group  $P4/nmm$ . The unit cell constants were refined from Weissenberg films taken at 22°C with Fe radiation ( $\lambda_{K\alpha}=1.93728$  Å) by program LCLSQ of Burnham (*Year Book 61*, pp. 132-135). The following results were obtained:  $a=3.6795\pm0.0008$  Å,  $c=5.030\pm0.002$  Å,  $V=68.1\pm0.1$  Å<sup>3</sup>, and  $c/a=1.3670\pm0.0007$  Å. There are two formula units per unit cell, in agreement with the observed density. Single-crystal intensities were measured on the Supper-Pace equi-inclination automated diffractometer with levels collected normal to the  $a_1$  axis. All reflections with  $h\geq0$  and  $\sin\theta/\lambda<0.65$  Å<sup>-1</sup> were collected with the use of Nb-filtered MoK $\alpha$  radiation. A total of 337 reflections were measured and corrected for the Lorentz-polarization and absorption ( $\mu_t=128$  cm<sup>-1</sup>) effects, with the program GNABS of Burnham (1966); and the symmetrically related structure factors were averaged,

yielding 62 independent reflections. Four of them had intensities that were less than the minimum observable and were subsequently excluded from the normal equations matrix during the refinement, although their structure factors were computed and found to have low values.

Refinement of the structure was begun with the parameters of Kouvo *et al.* (1963) transformed to place the origin at a center of inversion, neutral scattering factors from Cromer and Mann (1968), and the anomalous dispersion coefficients of Cromer (1965). The model was converged with isotropic temperature factors, and a difference electron density map was prepared. This map indicated the presence of a highly significant anisotropic thermal motion for all atoms; the model was converged with anisotropic temperature factors, therefore, and a new map was prepared with a much smaller noise level. This map had no significant peaks in the interstices of the sulfur framework, and thus no evidence for metal excess could be found.

The crystal studied by X-rays was now mounted for the electron microprobe. The natural surface was not smooth enough for a proper analysis, however, and an attempt to polish it would have destroyed the crystal because of the perfect (001) cleavage. As a result, only the metal ratios from the analysis could be used. The normalized metal composition is  $Fe_{0.90}Ni_{0.08}Co_{0.02}$ , and these values were used in all further refinement.

In the final stages of refinement, the sulfur occupancy and an isotropic extinction correction (Zachariasen, 1968) were included with the anisotropic thermal parameters and the  $z$  coordinate for sulfur. The results are shown in Table 50.  $B_{eq}$  is the equivalent isotropic temperature factor of Hamilton (1959),  $R=\Sigma||F_o|-|F_c||/\Sigma|F_o|$ , and  $R_w=[\Sigma w(|F_o|-|F_c|)^2/\Sigma wF_o^2]^{1/2}$ .

Since sulfur has fewer electrons associated with it than the metal position, the standard deviation of its occupancy

TABLE 50. Atomic and Experimental Parameters for Mackinawite \*

Atom	$x$	$y$	$z$	$B_{eq}$	$\beta_{11} \dagger = \beta_{22}$	$\beta_{33}$	$\beta_{12} = \beta_{13} = \beta_{23}$
Fe, Ni, Co	$\frac{3}{4}$	$\frac{1}{4}$	0	1.82(8)	0.0247(16)	0.0276(13)	0
S	$\frac{1}{4}$	$\frac{1}{4}$	0.2555(10)	1.74(12)	0.0257(26)	0.0241(21)	0
Parameter				Value			
Sulfur occupancy				0.975(18)			
Extinction				$1.6(5) \times 10^{-6}$			
$R$				4.7% for $F_o > F_{min}$			
				5.1% for all data			
$R_w$				2.6% for $F_o > F_{min}$			
				2.6% for all data			
Thermal vibration (rms amplitude):							
Metal, normal to $c$				0.130(3) Å			
parallel to $c$				0.188(4) Å			
Sulfur, normal to $c$				0.133(7) Å			
parallel to $c$				0.176(8) Å			

\* The numbers in parentheses are the estimated standard deviations of the last digit presented.

† Anisotropic temperature factor =  $\exp \{-\sum_i \sum_j h_i h_j \beta_{ij}\}$ .

is large, even though the correlation coefficients with the temperature factors are relatively small (0.55 and 0.43); the change from an occupancy of unity to 0.975, however, would change the density from 4.30 to 4.26 g/cm<sup>3</sup>. The density of the crystal was measured, therefore, and found to be  $4.26 \pm 0.01$  g/cm<sup>3</sup>, apparently confirming the results of the refinement. If true, this is the first known case of sulfur deficiency in a naturally occurring sulfide mineral.

The structure consists of a distorted cubic close-packed array of sulfur atoms with some of the tetrahedral interstices filled with metal atoms. The stacking direction is approximately parallel to [101]\*. The important interatomic distances for this structure are presented in Table 51, which may be interpreted with the aid of Fig. 87. Each metal atom is at the center of a slightly distorted tetrahedron of sulfur atoms, which share edges to form sheets of tetrahedra. These sheets are stacked normal to  $c$  with only Van der Waals forces between them and lead to the perfect (001) cleavage observed. The metal-metal distance of 2.602 Å across the shared edge is very near the distance in the body-centered cubic form of iron (2.59 Å) and indicates

a degree of metal-metal bonding in the structure. This metal-metal bonding could possibly reduce the strength of metal-sulfur bonds and leave the sulfur underbonded. The underbonding could be compensated by the occasional omission of a sulfur atom.

In this structure, the ellipsoids of thermal motion are required to be uniaxial with the unique axis parallel to  $c$ . The values determined and shown in Table 50 are reasonable; each atom has

TABLE 51. Interatomic Distances (Å) and Angles (degrees) in Mackinawite \*

Atoms	Distance
M-S (4x)	2.244(3)
M-M' (4x)	2.602(1)
Within a layer	
S-S' (4x)	3.657(7)
S-S'' (4x)	3.680(1)
Between layers	
S-S' (4x)	3.581(7)
Atoms	Angle
S-M-S'' (2x)	110.1(2)
S-M-S' (4x)	109.1(1)
M-S-M'' (2x)	110.1(2)
M-S-M' (4x)	70.9(1)

\* The numbers in parentheses represent the estimated standard deviation of the last digit presented.



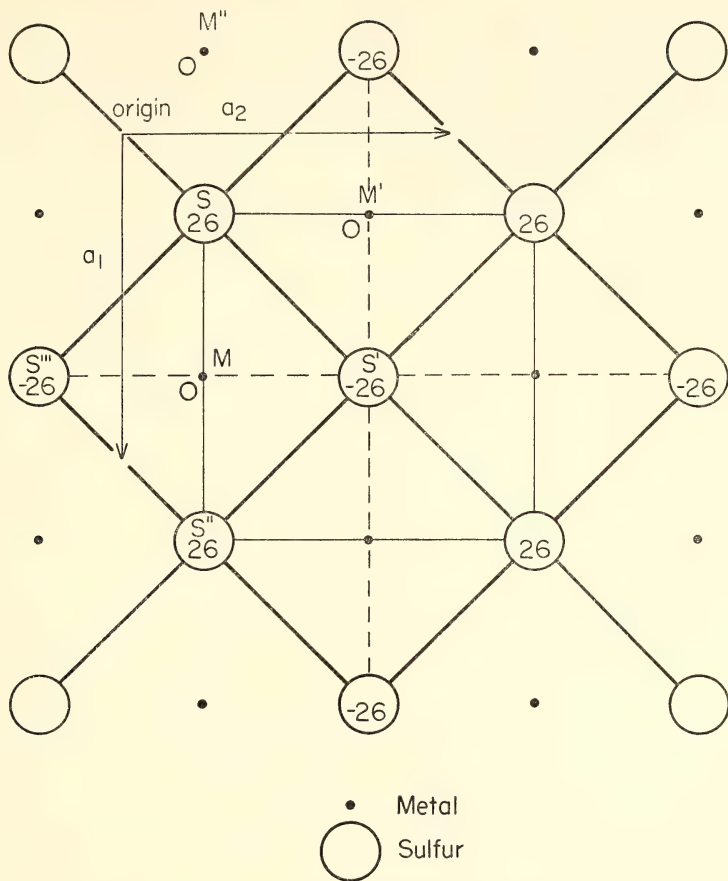


Fig. 87. One tetrahedral sheet of the mackinawite structure projected parallel to *c*. The heavy lines represent shared edges, the light and dashed lines represent unshared edges, and the numbers correspond to the altitude in hundredths of the *c*-axis length.

its maximum amplitude of vibration parallel to *c* and normal to the plane of the sheets although the amplitudes of vibration are large. For the metal position, the direction of maximum amplitude of vibration is away from the short metal-metal distance.

Two other crystals from the Outo-

TABLE 52. Chemical Composition of Mackinawite from Outokumpu, Finland

	Weight %	Atomic %	Metal/Sulfur *	Σ Metals = 1 †
Fe	60.29	48.45	1.042	0.906
Ni	5.63	4.30	0.093	0.080
Co	0.99	0.75	0.016	0.014
S	33.21	46.49		0.869
	100.12 ‡			

\* Resulting formula,  $\text{Fe}_{1.042}\text{Ni}_{0.093}\text{Co}_{0.016}\text{S} = \text{M}_{1.151}\text{S}$ .  
† Resulting formula,  $\text{Fe}_{0.906}\text{Ni}_{0.080}\text{Co}_{0.014}\text{S}_{0.869} = \text{MS}_{0.869}$ .  
‡ Cu, Cr, Ti, and Se each <0.05 wt %.

kumpu mackinawite were mounted, polished, and analyzed on the electron microprobe. The two analyses being very similar, the average results are presented in Table 52. These crystals are more sulfur deficient than any reported previously, but because of the extremely small grain size ( $<30\text{ }\mu\text{m}$ ), their density could not be measured.

### PYRITE-TYPE COMPOUNDS

*L. A. Taylor and G. Kullerud*

A considerable number of sulfide- and arsenide-type minerals and compounds display a cation-to-anion ratio of or near 1:2. The sulfide-type\* compounds when synthesized in the presence of vapor have the hexagonal cadmium iodide ( $\text{CdI}_2$ ), the orthorhombic marcasite, or the cubic pyrite crystal structures. The arsenide-type compounds synthesized in the presence of vapor, however, show a much larger variety of crystal structures. We shall here concern ourselves mainly with the crystal structures of the sulfide-type compounds.

Some of these compounds have physical properties, such as semi- or superconductivity, magnetic susceptibility, that are of special interest to solid state physicists. Considerable effort has been expended recently to produce in the laboratory not only synthetic analogues of disulfide-type minerals but also new compounds that may have even more desirable physical properties than the minerals. The developments of a whole series of intermediate- and high-pressure experimental techniques have facilitated synthesis of a large number of such compounds.

It is interesting to note that of the

\* We are here using the terms sulfide type and arsenide type as defined by Kullerud (*Year Book 68*). The sulfide type involves all sulfides and selenides and only a few tellurides; the arsenide type involves all arsenides and antimonides as well as almost all tellurides and bismuthides.

sulfide-type compounds synthesized in the presence of vapor, those involving Ti, Zr, and Hf of the IVB group; Nb and Ta of the VB group; and Mo and W of the VIB group all appear to have the cadmium iodide crystal structure. A number of such compounds, for instance those involving Fe and Ni, are known to have the marcasite structure. The largest number, by far, of such compounds have the pyrite-type crystal structure, which is represented by compounds and minerals involving Mn from the VIIB group and Fe, Ru, Co, Ni, etc., from group VIII.

It has been found that a number of these compounds invert from one crystal form to another under high confining pressure or sometimes simply by being heated. For instance, marcasite ( $\text{FeS}_2$ ) inverts to pyrite when heated to about  $400^\circ\text{C}$  or when exposed to high confining pressures.

The pyrite-type polymorph has slightly higher density than the marcasite type which in turn has higher density than the cadmium iodide type. In other words increasing pressure can be expected to first transform the cadmium iodide structure to that of marcasite and then invert the marcasite structure to that of pyrite. The pyrite structure apparently is stable even at the highest pressures attainable in laboratory experiments.

High-pressure experiments have also demonstrated that disulfide-type compounds are stable at high confining pressures in many systems which in their condensed states do not contain such compounds. For instance,  $\text{CuS}_2$ ,  $\text{ZnS}_2$ ,  $\text{CdS}_2$ , and the corresponding selenides (and some of the tellurides), all having the pyrite structure, are stable at high pressures. Reactions whereby the monosulfide or monoselenide of the pertinent metals incorporate sulfur (or Se) to form the appropriate disulfide or diselenide can readily be visualized. In our studies, however, we are interested not only in the

synthesis of phases but in their stability fields and stability limits as well. For that reason we are primarily concerned with univariant reactions defining stability curves of the phases in question. The only known and experimentally determined univariant reaction pertaining to the disulfides under discussion is that involving the copper sulfides.

### $CuS_2$

Covellite ( $CuS$ ) melts incongruently to digenite ( $Cu_9S_5$ ) and liquid at  $507^\circ C$  as shown by Kullerud (1965), who also determined the upper stability curve of  $CuS$  to 2 kb. The further course of this curve, which delineates the reaction  $CuS \rightleftharpoons Cu_9S_5 + L$ , was determined to about 11 kb by Kullerud, Bell, and England (*Year Book 66*).

The study of Munson (1966) indicated that  $CuS$  is not stable at temperatures above  $\sim 350^\circ C$  at pressures in excess of about 30 kb. The first few experiments conducted during the present study produced  $CuS_2$  as a phase and demonstrated that the  $CuS + Cu_9S_5 + L_S$  univariant curve terminates in an invariant point situated below 25 kb. At this invariant point, which consequently was found to be situated at  $647^\circ C$  and 18 kb, the four phases  $CuS$ ,  $Cu_9S_5$ ,  $CuS_2$  and  $L_S$  coexist (Fig. 88). The  $CuS + Cu_9S_5 + L_S$  curve, therefore, has a slope of  $140^\circ C$  over 18 kb, or about  $8^\circ C/kb$ . This slope compares well with that given by Kullerud (1965) as  $9^\circ C/kb$  up to 2 kb and that given by Kullerud, Bell, and England (*Year Book 66*) as  $10^\circ C/kb$  up to 11 kb.

Four univariant curves originate at the invariant point. The sequence of the

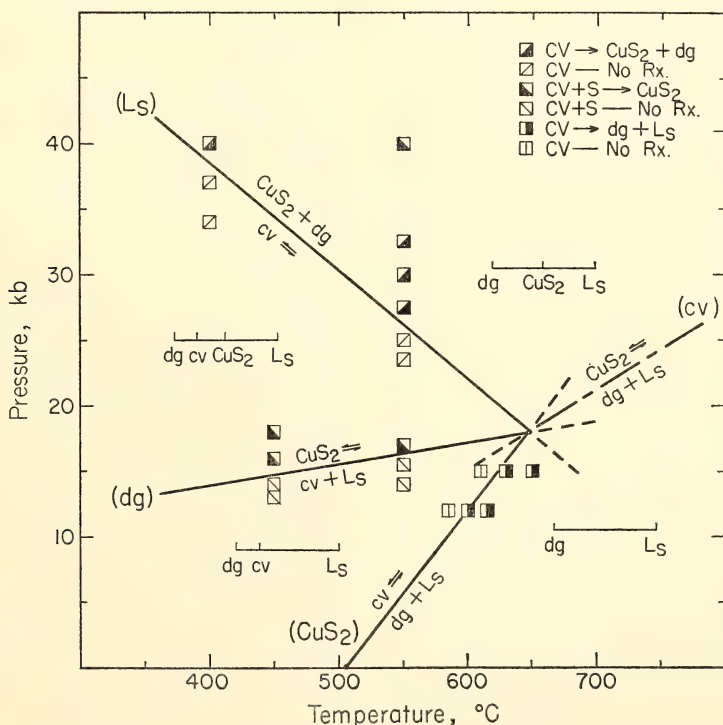


Fig. 88. Pressure-temperature diagram depicting the univariant curves associated with the invariant point at  $647^\circ C$  and 18 kb involving the phases  $CuS_2$ ,  $cv$ ,  $dg$ , and  $L_S$ . Abbreviations:  $dg$ , digenite ( $Cu_9S_5$ );  $cv$ , covellite ( $CuS$ );  $L_S$ , liquid of near-S composition.



curves about this point was deduced from the principles of Morey and Williamson (1918) and the Morey-Schreinemaker coincidence theorem (*Year Book* 56, p. 246). Experimental determination of the ( $L_s$ ) and (dg) curves, in addition to the ( $\text{CuS}_2$ ) curve discussed above was accomplished by employment of the piston-cylinder pressure apparatus described by Boyd and England (1960). The experimental charges were contained in capsules made of platinum/30 rhodium alloy or of gold. The charges consisted of  $\text{CuS}$  and/or  $\text{Cu}_9\text{S}_5$ , which were synthesized from high purity (i.e., 99.99+%)  $\text{Cu}$  and  $\text{S}$ , and which were mixed with various amounts of pure  $\text{S}$ . The experimental results outlining the ( $L_s$ ), (dg), and ( $\text{CuS}_2$ ) univariant curves are plotted in Fig. 88. The reversibility of each univariant reaction was also established in these experiments.

Several attempts were made to determine the (cv) univariant curve (see Fig. 88). Difficulties were encountered, however, since a eutectic liquid exists at relatively low temperatures in the  $\text{Au-Cu-S}$  system. The exact position of this univariant curve, therefore, could not be fixed, but its relative position based on theoretical considerations is known. The curve must lie between the metastable extensions of the ( $\text{CuS}_2$ ) and (dg) curves and its metastable extension must lie between stable portions of these curves. Because of the uncertainty in the position of this curve, it is dashed in Fig. 88.

It is noted from Fig. 88 that  $\text{CuS}_2$  is stable only in the region above the (dg) and (cv) curves. The slope of the (dg) curve is approximately  $63^\circ\text{C/kb}$ , and extrapolation of this curve indicates that  $\text{CuS}_2$  at room temperature is stable only under confining pressures exceeding 8 kb. The  $\text{CuS}_2$  phase is readily preserved at room temperature and under atmospheric pressure, however. When heated in a sealed, evacuated silica-glass tube at  $130^\circ\text{C}$ , it gradually breaks down to give  $\text{CuS} + L_s$ , but this process is only 90% complete even after  $4\frac{1}{2}$  months.

Munson (1966) reported that the copper disulfide he synthesized contained considerably less sulfur than required by the  $\text{CuS}_2$  formula. Electron microprobe analyses were performed on two of the synthetic samples with synthetic  $\text{CuS}$ ,  $\text{Cu}_2\text{S}$ , and  $\text{Cu}_9\text{S}_5$  as standards. The results, presented in Table 53, demonstrate that the composition of the disulfide does not depart measurably from that of stoichiometric  $\text{CuS}_2$ . It was also found that covellite composition remains  $\text{CuS}$  whether it is in contact with digenite or  $\text{CuS}_2$ .

The  $\text{CuS}_2$  phase displays the cubic pyrite-type crystal structure in X-ray powder diffraction patterns (Munson, 1966). The cell edge of synthetic  $\text{CuS}_2$  was determined at  $22^\circ\text{C}$  as  $a = 5.7897 \pm 0.0002 \text{ \AA}$  utilizing 25 reflections measured against  $\text{Si}$  ( $a = 5.4300 \text{ \AA}$ ) as an internal standard and employing the least-squares refinement program (Burnham, *Year Book* 61). All observed reflections indexed on the cubic symmetry.

Examination of  $\text{CuS}_2$  in polished sections clearly demonstrates that this phase is *not* cubic. In plane polarized light,  $\text{CuS}_2$  is pink and possesses moderate pleochroism, ranging in color from orange to light purple. With crossed nicols, under oil immersion,  $\text{CuS}_2$  is strongly anisotropic with birefringence colors ranging from orange-tan to light blue-gray. When the nicols are positioned  $2^\circ$  from being completely crossed, the anisotropism is even more striking and varies from aquamarine to orange. These colors are very distinct, and the change from one color to another is sharp.

The possible effects of polishing on the optical properties of  $\text{CuS}_2$  were investi-

TABLE 53. Electron Microprobe Analyses of Synthetic  $\text{CuS}_2$

	1	2	Theoretical $\text{CuS}_2$
Cu	50.09	50.31	49.8
S	49.94	50.12	50.2
Totals	100.03	100.43	100.0

gated. Preparation of polished sections by various techniques (both wet and dry), with differing intensities of polishing and for different periods of time, invariably resulted in the same optical features. Comparison of X-ray powder diffraction patterns made on the original  $\text{CuS}_2$  and on  $\text{CuS}_2$  that had been polished showed no detectable differences. It appears that  $\text{CuS}_2$  is *pseudocubic* and in reality possesses a crystal structure of lower symmetry than that of pyrite.

The mineral pyrite commonly displays anisotropic behavior in polished sections. This anomalous feature is usually attributed to surface deformation induced by polishing (e.g., Gibbons, 1967). The  $\text{CuS}_2$  crystal structure is identical with or at least very similar to that of pyrite. Since the optical properties of  $\text{CuS}_2$  are definitely not compatible with cubic symmetry, the possibility exists that some pyrites in reality are not cubic. Apparently the optical properties of a mineral are much more sensitive in detection of noncubic symmetry than the X-ray powder diffraction technique.

### A HIGH-PRESSURE POLYMORPH OF TROILITE, $\text{FeS}$

*L. A. Taylor and H. K. Mao*

Troilite, the end member of the pyrrhotite solid solution series, is stoichiometric  $\text{FeS}$ . This mineral is common in certain terrestrial deposits and most meteorites, and is ubiquitous to all lunar samples from the Apollo 11 and 12 missions. Many of the rocks containing troilite have been exposed to high pressure either during or subsequent to their formation (e.g., shock features of lunar samples), and it is thus important to establish the stability region of troilite in  $P$ - $T$  space.

Troilite is the polymorph of  $\text{FeS}$  stable below the  $\alpha$  transition that occurs at  $140^\circ\text{C}$  and approximately 1 atm pressure. This polymorph has a supercell based on the NiAs-type (B-8) structure. Above  $140^\circ\text{C}$ , hexagonal pyrrhotite, with

the simple hexagonal B-8 structure or some minor supercell modification thereof (Taylor, *Year Book 68*), is the stable phase at low pressures.

Kullerud, Bell, and England (*Year Book 64*) determined by differential thermal analysis the effect of pressure on this  $\alpha$  transition from about 2 to 19.7 kb and found that pressure lowers the transition temperature by about  $2.2^\circ\text{C}/\text{kb}$ , indicating a negative  $\Delta V$  for the transition from low to high temperature. Taylor (*Year Book 68*), on the basis of a high-temperature X-ray diffraction study resulting in a plot of cell volume versus temperature, reported a  $\Delta V$  associated with the  $\alpha$  transition of  $\approx +0.22 \text{ \AA}^3/\text{mole-FeS}$ . He calculated the effect of pressure on the transition, using the value for  $\Delta H$  from Robie and Waldbaum (1968), to be  $+2.3^\circ\text{C}/\text{kb}$ , i.e., increased pressure should raise the transition temperature. Taylor (*Year Book 68*) suggested that this apparent discrepancy could be explained by the presence of a high-pressure polymorph of  $\text{FeS}$  with an approximate arrangement of univariant curves as shown in Fig. 89.

$\text{FeS}$  was synthesized from the elements, of 99.99+ wt % purity, in sealed, evacuated silica-glass tubes annealed at

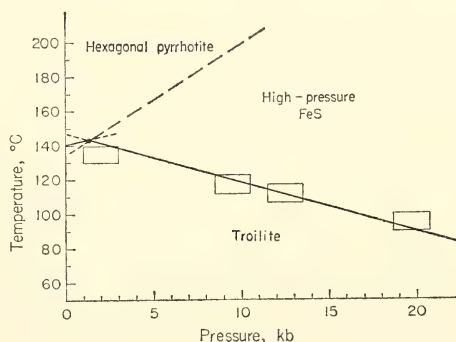


Fig. 89. Pressure-temperature diagram of  $\text{FeS}$ . The curve associated with the data of Kullerud, Bell, and England (*Year Book 64*) is consistent with their data but is slightly different from their curve. This modification was made in order to draw in the schematic phase relations.

700°C for 2 days, followed by quenching, grinding, and resealing in a new silica tube with additional annealing for 14 days. The  $d_{102}$  value of this material was  $2.0932 \pm 0.0009$  Å, identical to the value commonly accepted for FeS (Toulmin and Barton, 1964). Optical examination of this starting material in polished section did not reveal the presence of Fe or any other phase besides troilite. This polycrystalline FeS sample was compressed in a diamond-anvil, high-pressure cell (Bassett, Takahashi, and Stook, 1967) and X-rayed at pressure with the use of  $\text{MoK}\alpha$  radiation and exposure times of approximately 14 days. Experiments at  $120 \pm 40$  kb and  $22^\circ\text{C}$  and at  $50 \pm 20$  kb and  $120^\circ \pm 30^\circ\text{C}$  revealed the presence of a new high-pressure form of FeS. X-ray powder diffraction data are recorded in Table 54, but the pattern has not been indexed. Subsequent X-ray diffraction analyses and optical examination of polished sections of these products at 1 atm did not reveal any evidence for a breakdown reaction. The products consisted entirely of troilite. An experiment in the piston-cylinder type press

(Boyd and England, 1960) at  $40 \pm 1$  kb and  $100^\circ \pm 5^\circ\text{C}$  followed by a quench to  $22^\circ\text{C}$  in  $\sim 5$  seconds contained only troilite. Obviously the transition from the high-pressure polymorph to troilite is so rapid that the high-pressure form is nonquenchable by the techniques employed.

It was possible to microscopically examine the FeS at pressure in the diamond cell with reflected light. The FeS is present between the polished diamond faces as a thin, flat layer, which is optically similar to a normal polished section of the material. In contrast to the brown color and moderate anisotropism of troilite, the high-pressure polymorph is a beige color and displays little or no anisotropism.\*

Plate 6 shows both of these polymorphs of FeS at pressure. The pressure gradient across the diamond surface is large so that the center of the surface is at a pressure above the inversion and the outer portions of the surface are at pressures below; therefore, the low-pressure polymorph, troilite, occurs as a rim around the high-pressure polymorph. The exact pressure of this inversion at  $22^\circ\text{C}$  is not known, but extrapolation of the  $P$ - $T$  curve of Kullerud, Bell, and England (*Year Book 64*) indicates a pressure on the order of  $55 \pm 10$  kb.

This new high-pressure form of FeS may occur naturally as a mineral. The effects of trace elements such as Ni, Co, Ti, and Cr upon the kinetics of the transition to troilite are unknown; it is possible, however, that small amounts of certain elements can slow down the transformation rate sufficiently so that the high-pressure form of FeS can be retained at room temperature and pressure. The effect of extreme pressures of short duration, i.e. shock pressures, are also unknown but should be considered.

TABLE 54. X-ray Diffraction Data for High-Pressure FeS

120 $\pm$ 40 Kb, 22°C		50 $\pm$ 20 Kb, 120° $\pm$ 30°C	
<i>d</i> , Å	<i>I</i> *	<i>d</i> , Å	<i>I</i>
3.645	1	...	
3.236	1	3.366	1
2.843	10	2.869	10
2.582	6	2.617	4
2.444	6	2.475	4
2.250	2	2.278	2
2.113	6	2.155	3
1.979	10	2.015	5
1.881	4	1.909	1
...		1.845	1
1.754	5	1.770	5
1.632	6	1.644	9
1.502	3	...	
1.412	2	1.425	3

\* Some preferred orientation was present in this sample at pressure, evidenced by the non-uniform density of the reflections as recorded on the film.

\* The optical interference due to the presence of the diamond in the optical train makes it difficult to give any definite statement concerning the anisotropism.



## BIOGEOCHEMISTRY

REACTIONS OF AMINO ACIDS WITH  
NATURAL AND ARTIFICIAL HUMUS  
AND KEROGENS*P. H. Abelson and P. E. Hare*

Most organic substances in nature participate in the carbon cycle and are quickly oxidized to carbon dioxide and water. A small fraction has a different fate. On land it is converted into humic acid and humus and is important to the fertility and texture of soils. In the marine environment a part of the organic productivity of the oceans is incorporated in the bottom sediments in the form of humic acid and kerogen.

Humic acid, humus, and kerogen are reactive mixtures of complex chemicals. Last year we reported on uptake of various amino acids by a marine kerogen. In effect the individual amino acids were probes that tested the reactivity of kerogen.

These explorations have been extended to include samples from the Black Sea, the Gulf of Mexico, Long Island Sound, the Drummer Loam of Illinois, the 11,000-year-old Murray Springs formation of Arizona, and the Pleistocene Wailes Bluff formation in southern Maryland. In addition tests have been made with a number of synthetic humic acids and kerogens. The artificial humic acids and kerogens, prepared by the action of glucose with amino acids, behave in remarkably similar ways to the natural materials. We have also discovered that exposure of humic acids, humus, and kerogen to oxygen or to a reducing agent markedly changes reactivity of these substances.

The kerogens, humus, and humic acids used in these studies were prepared from sediments and soils. On the basis of wet weight of the starting material, the organic contents ranged from 1 to 10%. Direct experiments with the muds were only marginally feasible because of contamination of the amino acid analyzer

with cations such as iron. Accordingly, the crude materials were demineralized by repeated treatments with hydrochloric and hydrofluoric acids. The organic matter remaining was partly soluble in alkali. Thus the product was a mixture of kerogen and humic acid or humus and humic acid. For most experiments the crude mixture was employed. Experiments last year had shown that the behavior of the crude mixture and that of the organic components were similar.

The Black Sea sediment was obtained through the courtesy of John Hunt of the Woods Hole Oceanographic Institution. The core was obtained at the WHOI station 1479 during a 1969 cruise. The C/N ratio of the demineralized kerogen was 22. The Wailes Bluff mud was collected at the type locality in southern Maryland. It is of late Pleistocene age (40,000–100,000 years?). The C/N ratio of the kerogen was 33. The Aransas Bay mud was collected off St. Joseph Island, Texas, by T. C. Hoering and P. L. Parker. The C/N ratio of the kerogen was 23. The specimen from Long Island Sound was collected by T. C. Hoering and Gerald Friedman offshore from the mouth of the Connecticut River. The C/N ratio of the kerogen was 43. The San Pedro mud was collected by T. C. Hoering in the San Pedro Basin off the California coast. The C/N ratio of the kerogen was 15. The Murray Springs specimen was collected in southern Arizona by Vance Haynes, of Southern Methodist University. The specimen bore his sample number B3-11 and was obtained at his Boguillas station. The material represents a black sedimentary layer that was deposited 11,000 years ago at a site of considerable archeological interest. The C/N ratio of the kerogen was 37. The sample of Drummer Loam, collected in Illinois, was obtained from George Stanford, of the U. S. Depart-

ment of Agriculture. The C/N ratio of the humus was 38.

For most of the experiments a consistent set of procedures was employed. Samples of the kerogen or humic acid containing 50 mg organic matter were added to 2 ml of a standard  $10^{-4}$  molar amino acid mixture. The pH was adjusted to 8.5, and the contents were sealed in a glass tube under nitrogen. After incubation the pH was found to be 6–8. The suspension was adjusted to pH 1 and centrifuged. An aliquot of the supernatant was dried *in vacuo* and redissolved, and a portion was taken for analysis.

In a first set of experiments, incubations were conducted at 105°, 80°, and 52°C. Drawing on last year's experience with San Pedro kerogen, we estimated that reaction rates would not be very sensitive to temperature, and accordingly the respective incubation times were 15½ hours, 3 days, and 18 days. Data are presented in Tables 55, 56, and 57. Although there are differences in the reactivities of the organic matter, there are important similarities. In all these ex-

periments cystine disappeared without corresponding appearance of another ninhydrin positive product. Next in order of reactivity were the dibasic amino acids, followed by tyrosine and phenylalanine. In general the hydrophilic amino acids were least reactive. For purposes of comparison the values in the tables are adjusted so that aspartic acid is 100. Considerable differences were noted in the behavior of the organic matter, the Murray Springs sample being most reactive. In the presence of this material even the hydrophilic amino acids disappeared rapidly; the original data show that aspartic acid reacted also. Thus the adjustment of the data understates the overall reactivity of the Murray Springs material by a factor of 1.5 in Table 55, 1.2 in Table 56, and 1.1 in Table 57.

Another unusual feature in the Murray Springs material is the substantial reactivity of glycine in comparison with its homologue alanine. Comparison of the reactivities of the various samples of organic matter (Tables 55, 56, and 57) shows that the effect of temperature is consistent; that is, the Murray Springs

TABLE 55. Percentage Recovery of Amino Acids from Various Kerogen-Amino Acid Mixtures,\* 105°C, 15½ Hours

	B.S.	W.B.	P.A.	L.I.	S.P.	M.S.	D.L.
Lysine	31	33	5	7	4	1	0
Histidine	63	17	0	15	2	2	0
Arginine	22	15	11	14	0	0	0
Threonine	80	100	100	95	94	36	67
Serine	86	100	95	100	90	35	67
Glutamic acid	100	100	62	100	100	100	100
Glycine	100	100	82	93	100	16	40
Alanine	100	100	100	100	95	46	84
Cystine	0	0	0	0	0	0	0
Valine	95	100	88	98	85	55	73
Methionine	90	93	56	82	55	26	37
Isoleucine	79	97	77	94	71	48	64
Leucine	83	93	66	93	56	41	54
Tyrosine	88	91	52	83	44	13	27
Phenylalanine	84	80	39	68	31	13	26

\* Initially 0.1 micromole/ml of each amino acid. Data expressed as percentage recovered with aspartic acid normalized to 100%.

Abbreviations: B.S., Black Sea; W.B., Wailes Bluff, Maryland; P.A., Port Aransas, Texas; L.I., Long Island Sound, Connecticut; S.P., San Pedro, California; M.S., Murray Springs, Arizona; D.L., Drummer Loam, Illinois.

TABLE 56. Percentage Recovery of Amino Acids from Various Kerogen-Amino Acid Mixtures,\* 80°C, 3 Days

	W.B.	P.A.	L.I.	S.P.	M.S.	D.L.
Lysine	28	5	9	2	0	0
Histidine	16	1	17	2	0	0
Arginine	12	4	4	0	0	0
Threonine	100	91	97	98	48	70
Serine	100	89	100	97	51	73
Glutamic acid	90	63	96	70	99	88
Glycine	93	71	91	100	18	47
Alanine	99	87	100	100	69	86
Cystine	0	0	0	0	0	0
Valine	93	78	96	82	63	74
Methionine	82	51	72	51	23	39
Isoleucine	88	68	86	70	59	64
Leucine	87	61	83	60	55	54
Tyrosine	83	48	73	42	17	29
Phenylalanine	73	37	63	27	20	29

\* Initially 0.1 micromole/ml of each amino acid.

Abbreviations as in Table 55.

material is the most active in all the experiments, and its reaction pattern is about the same at the various temperatures. The Wailes Bluff material is relatively inert at all temperatures, but insofar as it reacts, the pattern is consistent with that of other kerogens.

We searched for an explanation for the differing reactivities of the various specimens and found a major factor. Some samples, such as the Black Sea specimen, had come from a very reducing

environment. Others, such as the Murray Springs sample, had been exposed to oxygen during dry storage. The Drummer Loam was a well aerated soil. Accordingly experiments were devised to test effects of oxygen and of a reducing agent,  $\text{Na}_2\text{S}_2\text{O}_4$ . In one procedure, specimens of kerogen were exposed to air in an oven at 105°C for a day before the usual treatment with amino acids. Results of some of the experiments are shown in Table 58. Comparison with

TABLE 57. Percentage Recovery of Amino Acids from Various Kerogen-Amino Acid Mixtures,\* 52°C, 18 Days

	W.B.	P.A.	L.I.	S.P.	M.S.	D.L.
Lysine	41	8	10	7	2	4
Histidine	29	2	9	1	1	1
Arginine	31	3	9	3	2	4
Threonine	83	80	77	73	55	65
Serine	91	88	89	81	57	70
Glutamic acid	91	74	97	89	96	90
Glycine	94	78	82	86	31	57
Alanine	94	91	91	85	76	84
Cystine	0	0	0	0	0	0
Valine	88	83	83	79	75	79
Methionine	86	59	68	53	41	48
Isoleucine	80	71	76	67	68	66
Leucine	80	67	75	58	66	63
Tyrosine	88	53	71	43	31	38
Phenylalanine	83	44	61	26	37	39

\* Initially 0.1 micromole/ml of each amino acid.

Abbreviations as in Table 55.



TABLE 58. Percentage Recovery of Amino Acids from Partially Oxidized Kerogen-Amino Acid Mixtures,\* 105°C, 16 Hours

	B.S.	W.B.	P.A.	L.I.	S.P.	M.S.	D.L.
Lysine	6	6	0	2	1	2	0
Histidine	17	3	0	2	0	2	0
Arginine	0	0	0	0	0	0	0
Threonine	72	79	58	33	71	22	42
Serine	67	70	52	25	65	20	38
Glutamic acid	82	64	31	85	71	78	79
Glycine	100	100	54	97	100	8	29
Alanine	96	94	67	90	82	37	67
Cystine	0	0	0	0	0	0	0
Valine	87	94	56	84	68	34	60
Methionine	68	40	24	29	26	12	13
Isoleucine	72	79	42	66	44	27	47
Leucine	65	63	33	48	26	22	34
Tyrosine	63	46	21	26	15	4	11
Phenylalanine	45	30	13	19	7	5	10

\* Kerogens oxidized in oven in air for 1 day prior to incubation with amino acids (initially 0.1 micromole/ml).

Abbreviations as in Table 55.

Table 55 shows that the oxidized samples reacted more completely than the unoxidized counterparts. For example, in the Black Sea kerogen 22% of original arginine was recovered after exposure to the unoxidized specimen and no arginine remained after exposure to the oxidized material.

In another study we chose to concentrate on materials from the Murray Springs formation. The original preparation had been very reactive, and it was suspected that oxidation during processing might have had a role. Accordingly a second preparation was made, and the crude kerogen was extracted with NaOH to yield humic acid and kerogen free of humic acid. For the oxidation step, oxygen was bubbled through the kerogen-amino acid mixture for an hour prior to sealing under oxygen. To test the effect of a reducing agent, samples were exposed to 5 ml of 0.1 molar  $\text{Na}_2\text{S}_2\text{O}_4$  at room temperature for an hour. Most of this reagent was removed by centrifugation before addition of the amino acid mixture.

The experiments summarized in Table 59 demonstrated that exposure to oxygen increases the reactivity of kerogen or

humic acid, whereas treatment with a reducing agent diminishes it. For nearly every reaction of organic matter with individual amino acids it can be noted that the reduced organic matter is less reactive than the oxidized sample. The differences among the two kerogens and the humic acid point to a problem of quantitative reproducibility of behavior from preparation to preparation. This problem was also noted in comparisons of the behavior of different kerogen preparations obtained from San Pedro muds. Nevertheless, the qualitative trends described earlier remain valid.

#### *Artificial Humic Acids and Kerogens*

In another part of this report Hoering tells of efforts to degrade natural humic acids and to characterize them. Many other workers have previously addressed themselves to the matter but have not obtained very satisfying information. The results seem to show that natural humic acids are complex mixtures of substances produced by unknown reactions among a large number of starting materials. In a recent review of the chemistry of humic acids, Stevenson and

TABLE 59. Percentage Recovery of Amino Acids from Amino Acid Mixtures\* with Oxidized and Reduced Specimens of Murray Springs Kerogen and Humic Acid, 105°C, 15 Hours

	MS-1 R	MS-1 U	MS-1 O	MS-2 R	MS-2 U	MS-2 O	HA U	HA O
Lysine	5	0	0	30	9	3	17	1
Histidine	11	7	0	47	37	3	18	1
Arginine	1	0	0	12	2	0	14	0
Threonine	45	34	11	74	90	47	71	35
Serine	36	30	9	62	74	41	64	29
Glutamic acid	86	86	83	91	88	86	87	91
Glycine	36	17	4	99	94	53	85	43
Alanine	69	51	21	97	96	79	86	65
Cystine	0	0	0	0	0	0	0	0
Valine	66	49	28	100	95	72	90	54
Methionine	38	18	1	81	80	22	60	27
Isoleucine	57	39	21	86	82	55	76	40
Leucine	44	28	12	78	68	38	65	28
Tyrosine	17	13	0	58	58	17	50	11
Phenylalanine	21	18	0	51	47	11	48	11

\* Initially 0.1 micromole/ml of each amino acid.

Abbreviations: MS-1, original preparation of Murray Springs kerogen; MS-2, second preparation of Murray Springs kerogen; HA, humic acid extract of MS-2; R, reduced; U, untreated; O, oxidized.

Butler (1969) summarized their view of the state of the topic by saying that "A completely satisfactory scheme for the synthesis of humic substances in geologic environments has not yet been developed." They discuss some of the proposed mechanisms, such as production from lignin and leaf litter, but point out that algae, lichens, and mosses, which do not contain lignin, give rise to humic substances. Stevenson and Butler appear to lean slightly toward formation of humic acid by condensation of sugars and amines.

Preparation of humic acids from known starting materials would have evident advantages provided that the behavior of the artificial substances was similar to that of the natural ones. In approaching this matter we decided to employ reactions between carbohydrates and amino acids. These substances are major constituents of living matter and likely candidates. Moreover, in experiments reported last year we had confirmed observations of others that amino acids are slowly released from humic

acid and kerogen by lengthy 6 *N* HCl hydrolysis.

It has long been known that carbohydrates and amino acids react, particularly at neutral and slightly alkaline pH, to form dark, complex products. We have explored the matter using glucose as the carbohydrate and have tested most of the conventional amino acids. As a result we have produced synthetic products that resemble in many respects natural humic acids and kerogens.

Most of the preparations were made as follows: Equimolar portions of glucose and the respective amino acids were dissolved in enough water and NaOH to produce 1.0 molar solutions at pH 8.5. The mixture was refluxed gently. Almost immediately the solutions became brown, and soon an appreciable drop in pH occurred. After 24 hours the pH dropped to about 5.0. The pH was adjusted to 8.5 daily, and after a few days further changes were minimal. It is not certain that this pH adjustment is essential. In some experiments production of humic acid was rapid. Thus with glucose and phenylalanine, substantial (25%) yields

could be obtained in a day. Even with long incubation none of the yields was greater than 60%. Hydrophobic amino acids incubated with glucose tended to yield humic acids faster than the hydrophilic ones. With longer incubations (a month or more) insoluble solids were formed that fit the description of kerogen. In this respect the combination of lysine and glucose was different from other pairs, which formed kerogen quickly. With some combinations, for example, glucose and alanine, yields of only 20% humic acid were obtained, even after 6 months, and practically no kerogen formed. However, all 15 amino acids tested gave rise to substantial yields of humic acids or kerogens.

Proportions other than equimolar can be employed. Sets of components ranging from 1 phenylalanine-5 glucose to 2 phenylalanine-1 glucose and including intermediate compositions all yielded humic acids.

The C/N ratios of some of the synthetic materials were examined. Humic acids that were produced from 1:1 proportions of amino acids and glucose, and refluxed at 100°C for 6 months, had the following C/N ratios: alanine, 6.5; isoleucine, 9.3; phenylalanine, 13.5; tyrosine, 12.5. An equimolar glucose-lysine kerogen, refluxed for 6 months, had a C/N ratio of 5.6. Humic acids, prepared in 10 days from various proportions of phenylalanine and glucose, had the following C/N ratios: 2 phenylalanine-1 glucose, 12.5; 1 phenylalanine-3 glucose, 16; 1 phenylalanine-5 glucose, 25.

The soluble artificial humic acids fit within the rather loose operational limitations used to characterize natural humic acids. They are soluble in alkali and insoluble in acid. They have titratable acid groups much like the natural products. By choice of starting materials and length of incubation one could produce humic acids of a wide range of C/N ratios, molecular weights, and titratable acid groups. We have chosen to examine the behavior of the artificial humic acids

when incubated with standard mixtures of amino acids. Most of the experiments were conducted with preparations resulting from equimolar proportions of glucose and the respective amino acids. In the absence of oxygen these preparations were not quite so reactive as the most reactive of the natural humic acids and kerogens discussed earlier.

Several of the synthetic humic acids were, however, very comparable in their behavior to, for example, the Black Sea and Wailes Bluff kerogens. The similarity can be noted in Table 60. In all the results shown, cystine disappeared completely and the diabasic amino acids were next in reactivity; in all the incubations that were conducted in the presence of oxygen, reactivity was enhanced.

Artificial humic acids and kerogen are also similar to the natural products in their response to prolonged acid hydrolysis. Last year we described results of a sequence of incubations of the natural products with 6 *N* HCl at 108°C in which it was found that even after 5 weeks amino acids were being released. When similar procedures were employed with artificial humic acids and kerogen derived from phenylalanine and glucose, a comparable slow release of amino acid was observed.

We are indebted to Drs. T. C. Hoering and Subrata Ghose for another kind of measurement that indicates a similarity of the artificial and natural humic acids—a comparison of electron spin resonance (e.s.r.). Natural humic acids display e.s.r. effects. Accordingly Hoering and Ghose examined samples of artificial humic acids both before and after exposure to oxygen. The amount of e.s.r. was comparable to that of a natural specimen, and the e.s.r. of both types of specimen was enhanced by exposure to oxygen. Qualitatively the magnitude of the e.s.r. effect paralleled the reactivities of the artificial humic acids toward amino acids. A large e.s.r. and a high reactivity went together.

One would not expect the artificial



TABLE 60. Percentage Recovery of Amino Acids from Mixtures\* of Amino Acids and Artificial Kerogens and Humic Acids (Oxidized and Unoxidized), 105°C, 16 Hours

	B.S.	W.B.	PHE 1-5	PHE 2-1	ALA	TYR	ISO	O PHE 1-5	O PHE 2-1	O ALA	O TYR	O ISO
Lysine	31	33	3	75	32	58	76	3	40	9	72	26
Histidine	63	17	38	50	35	49	51	2	45	16	26	33
Arginine	22	15	2	50	26	40	58	0	20	10	49	25
Threonine	80	100	72	100	92	99	100	62	100	72	97	80
Serine	86	100	78	100	90	84	93	62	83	73	88	81
Glutamic acid	100	100	86	93	74	93	97	81	85	88	51	72
Glycine	100	100	76	85	94	87	92	64	83	71	98	72
Alanine	100	100	95	97	...	97	100	89	100	...	100	93
Cystine	0	0	0	0	0	0	0	0	0	0	0	0
Valine	95	100	100	100	97	100	100	85	100	79	100	95
Methionine	90	93	63	95	85	88	87	29	85	61	83	87
Isoleucine	79	97	93	80	98	96	...	68	78	74	97	...
Leucine	83	93	68	75	82	87	88	39	65	63	85	65
Tyrosine	88	91	51	80	57	...	73	25	60	32	...	58
Phenylalanine	84	80	...	...	69	65	85	...	...	44	69	60

\* Initially 0.1 micromole/ml of each amino acid.

Abbreviations: B.S. (Black Sea) and W.B. (Wailes Bluff) from Table 55 for comparison. PHE 1-5, phenylalanine humic acid from reaction mixture of 1 part amino acid and 5 parts glucose. PHE 2-1, phenylalanine humic acid from reaction mixture of 2 parts amino acid and 1 part glucose. ALA, alanine humic acid. TYR, tyrosine humic acid. ISO, isoleucine kerogen. O, oxidized specimens.

humic acids that we have prepared to behave identically with those found in nature, the latter being formed from a more complex mixture of original constituents. Nevertheless, the similarity of the artificial and natural products is striking. The humic acids synthesized from known constituents will be useful in helping us to understand the more complex natural materials.

#### HUMIC ACIDS IN A RECENT MARINE SEDIMENT

*T. C. Hoering*

Humic acid is a complex mixture that represents a substantial fraction of the organic matter in a soil. It can be extracted into dilute alkaline solutions and subsequently precipitated by mineral acids. This material has received much attention because of its relation to soil fertility. Humic acid is derived from detrital plant material that has been only partially metabolized by microorganisms and condensed into a polymer that is rather resistant to further biological attack. The chemical structure and fate of humic acid is poorly known.

This report describes research on humic acids isolated from a Recent marine sediment. Comparatively little is known about this class of materials in the marine environment, but it is of importance since it probably represents the initial stage of the formation of kerogen. The great bulk of the organic matter on the surface of the earth exists in the form of insoluble, polymerized material dispersed in sedimentary rocks of marine origin. The name kerogen is given to this organic matter.

The sediments used in this work were surface grab samples collected in 2440 feet of water in the San Pedro Basin off Southern California at 33°39' N, 118°26' W. The samples were frozen from the time of collection until used and contain 4.3% organic carbon on a dry weight basis.

Marine humic acids were isolated by

extraction of the sediment with sodium hydroxide and by precipitation with hydrochloric acid. They were hydrolyzed in 6 *N* HCl and were dialyzed in cellophane against distilled water until neutral and free of chloride ion. At this stage, the marine humic acids were a gel-like mass, containing a very large percentage of water and closely resembling soil humic acids. When vacuum-dried at 100°C, they formed a black friable solid with 12% ash content. Approximately 15% of the organic matter in the sediment could be isolated in this way.

The dried marine humic acid was dispersed in potassium bromide, a pellet was formed, and its infrared absorption spectrum was measured. A portion of it was methylated with alkaline dimethyl sulfate and esterified with methanol. The material was washed, dialyzed, and dried. Its spectrum was measured. Reduced humic acid, formed by the sodium amalgam reduction described below was similarly measured. The spectra are shown in Fig. 90. They have many features that are similar to those reported in the literature for humic acids from soils.

The broad band at 2.90  $\mu$ m is due to hydrogen bonded hydroxyl groups in carboxyl, alcoholic, or phenolic functions, or tightly bonded water. The band at 3.45  $\mu$ m is due to aliphatic carbon-to-hydrogen bonds. The broad band at 5.72 to 6.25  $\mu$ m in the original humic acid is split into two bands on methylation and esterification. The one at lower wavelengths is due to carbon-to-oxygen double bond vibrations in ester groups. The origin of the band from 6.25 to 6.17  $\mu$ m in humic acids is not known. None of the absorptions can be definitely assigned to aromatic carbon-to-carbon vibrations. The reduction by sodium amalgam causes only small changes in the spectra. The infrared studies show that marine humic acids have functional groups similar to those found in soils.

The molecular weight of the marine

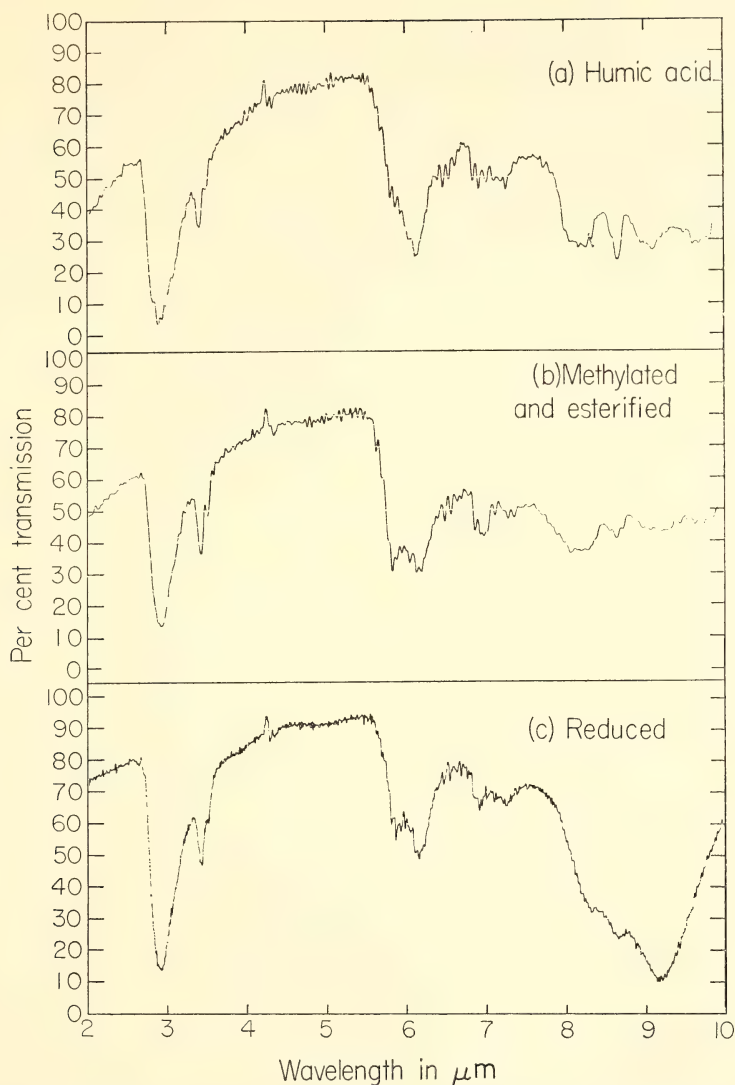


Fig. 90. Infrared adsorption spectra of (a) humic acid from San Pedro Basin sediment, (b) after methylation and esterification, (c) after sodium amalgam reduction.

humic acid was estimated by gel permeation chromatography on a series of Sephadex media at pH 9. The material passes through G 25 and G 50 gels without retention, but is partially retained by G 75 gel. A molecular weight greater than 10,000 is indicated. This weight is typical of the molecular weights observed for soil humic acids.

Humic acids contain in their structure acidic hydrogen atoms that can be titrated with bases. The method of discontinuous titration was applied to the marine humic acids, and an equivalent weight of 220 g/mole of acidic hydrogen was obtained. This weight is only slightly higher than that reported for soil humic acids.



Soil humic acids are organic free radicals that give an easily measurable absorption in electron spin resonance spectroscopy. Measurements on dried marine humic acids by this technique gave absorptions whose position, shape, and intensity were qualitatively very similar to those from a soil humic acid.

Humic acids can be degraded chemically into small, recognizable molecules. Many of the methods reported in the literature for this purpose are drastic and leave some doubt as to the extent to which the products bear resemblance to the component parts of the original material. Burges, Hurst, and Walkden (1964) reported that mild reduction of soil humic acids with sodium amalgam yielded up to 30% of a mixture of phenols and phenolic acids. They identified ten compounds by paper chromatography. Their method was applied to the marine humic acid. It reacted similarly but only a very small amount of it could be obtained as compounds that could be separated as distinct peaks by gas-liquid chromatography. The mixtures formed by sodium amalgam reduction were fractionated by silica-gel chromatography and found to be extremely complex. Chromatographic fractions were examined by combined gas chromatography and mass spectrometry, and the mass spectra of over a hundred pure compounds were measured. Only a small fraction of them could be completely identified but very few gave spectra of phenols or phenolic acids. The bulk of them gave mass spectra characteristic of aliphatic or alicyclic molecules with oxygenated functional groups rather than the spectra of aromatic compounds. Mendez and Stevenson (1966) reached the same conclusion in an infrared spectroscopic study of the products of sodium amalgam reduction of soil humic acid.

During the silica-gel chromatography of the reduction products, a bright red band traversed the column. It was collected, and its optical absorption spectrum was characteristic of free porphyrin

compounds. Apparently chlorophyll residues are bonded onto the marine humic acids and are liberated as porphyrins on reduction. One of the column chromatography fractions, accounting for 0.1% of the starting material, consisted of a mixture of methyl esters of fatty acids having predominantly an even number of carbon atoms in the range 14 to 26.

The bulk of the carbon remained in the form of humic acids after repeated reduction. This residue was oxidized for 4 hours with an excess of alkaline potassium permanganate at ice temperature. The humic acid was completely solubilized. Extraction of the reaction mixture with ether yielded about 1% of the carbon as organic acids. Most of the sample was oxidized to carbon dioxide, volatile acids, or water-soluble compounds that were lost during sample work-up. The ether soluble acids were esterified with diazomethane and fractionated by silica-gel chromatography. One fraction, accounting for 0.02% of the starting material, consisted of methyl esters of fatty acids with a smooth distribution of carbon atoms in the range 15 to 24. Another fraction, amounting to 0.3% of the starting material, contained methyl esters of normal dicarboxylic acids. Only small amounts of benzenoid acids could be detected.

Attempts were made to chemically degrade marine humic acids by several other procedures, including hydrolysis in strongly alkaline solutions, oxidation by alkaline copper sulfate solutions at elevated temperatures, and reaction with hydrogen iodide and red phosphorous in acetic anhydride. The results were similar. Only a small percentage of the humic acid could be isolated in a form that would pass through a gas chromatography column. The mixtures were very complex with no one class of compound predominating.

Research this year has shown that a significant fraction of the organic matter in a Recent marine sediment exists in

the form of humic acids. This material has been examined by a wide range of physical and chemical methods and has properties similar to those of soil humic acids. The material has a very complex chemical structure.

Many of the inorganic constituents of the Recent sediments on the continental shelf off Southern California have been transported from the land, and it is

possible that some of the organic matter has a similar history. There are areas of high biological productivity in the oceans of the area, and some of the organic chemicals in the living organisms of the sea should be deposited in the sediments. The research reported here gives no strong evidence on the relative proportions of the organic matter from these possible sources.

## ISOTOPIC INVESTIGATIONS IN GEOCHEMISTRY AND GEOCHRONOLOGY

*T. E. Krogh, G. L. Davis and S. R. Hart\**

### ISOTOPIC AGES ALONG THE GRENVILLE FRONT IN THE BELL LAKE AREA, SOUTHWEST OF SUDBURY, ONTARIO

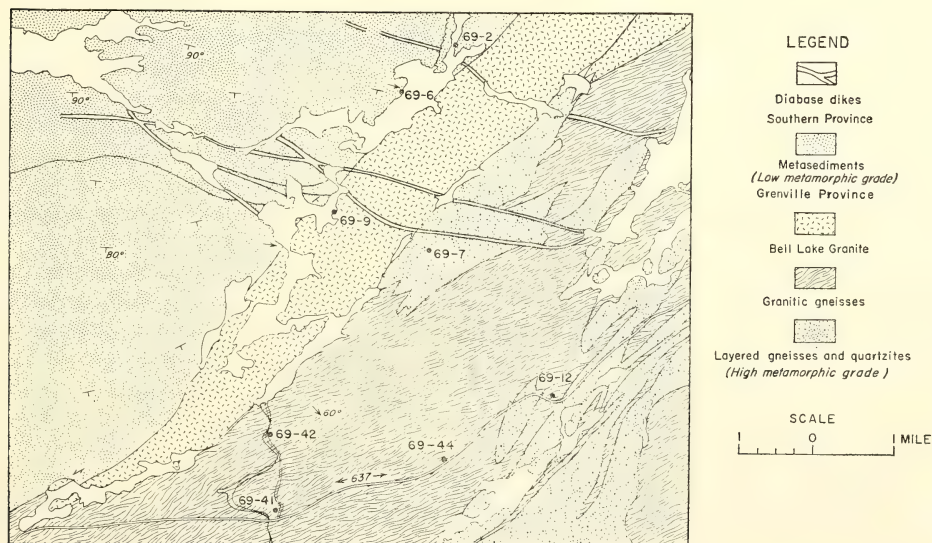
*T. E. Krogh, G. L. Davis, and M. J. Frarey†*

Recent geological mapping indicates that the transition from the low-grade metamorphic rocks of the Southern province to the high-grade metamorphic

rocks of the Grenville province is very well displayed in the Bell Lake area (Fig. 91). As the Grenville Front is approached from the north, the rocks no longer conform to the general east-west fold patterns, but rather develop a northeast-trending foliation and a lineation that plunges steeply to the south-east. Thermal metamorphism along the north side of the Bell Lake granite has produced metamorphic minerals that developed later than this foliation at loca-

\* Department of Terrestrial Magnetism.

† Geological Survey of Canada, Ottawa, Canada.



SAMPLE LOCATIONS AND GEOLOGICAL RELATIONSHIPS ALONG THE GRENVILLE FRONT AT BELL LAKE

Fig. 91. Generalized geological map of the Grenville Front in the Bell Lake area in the Sudbury-Georgian Bay region of Ontario, from Frarey and Cannon (1968).

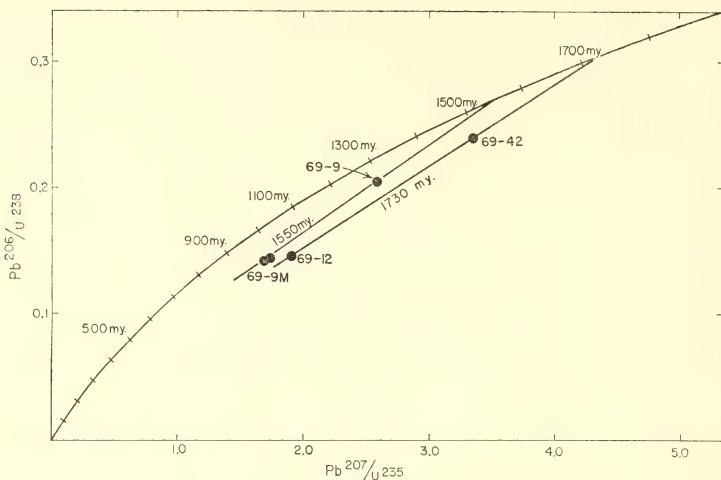


Fig. 92. Concordia diagram for zircons from the Bell Lake granite (69-9 and 69-9M) and the granitic gneiss (69-12 and 69-42).

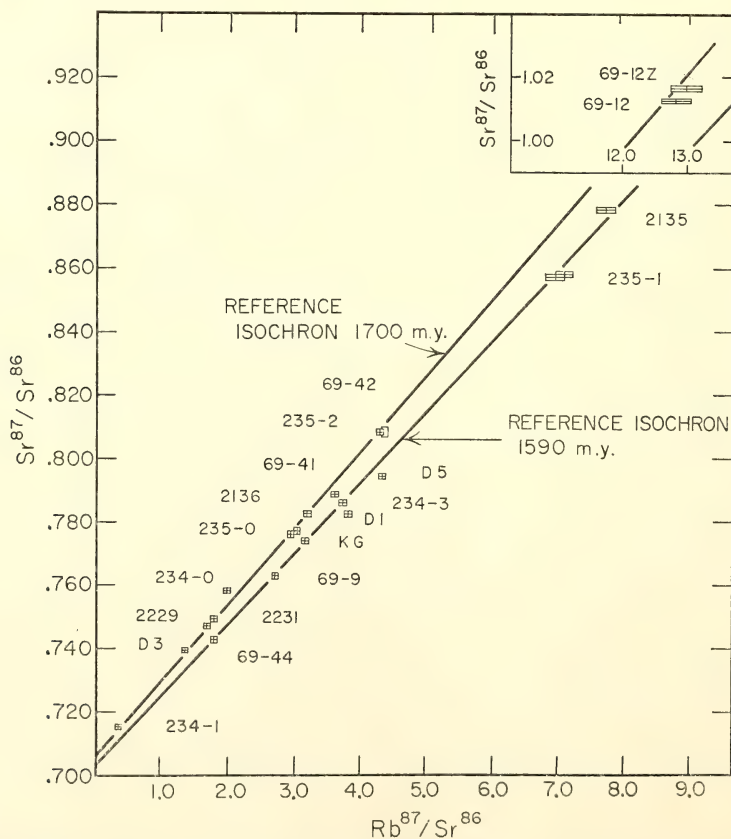


Fig. 93. Isochron plot for granite samples from along the Grenville Front in the Georgian Bay-Sudbury area. Sample designated KG is from the Killarney granite collected a few miles from the Bell Lake granite sample 69-9. Granitic gneiss samples were collected at locations 69-12, 69-41, 69-42, and 69-44.



tion 69-2. Similarly, pegmatites spatially related to this granite, and probably coeval with it, intrude rocks that had previously been foliated and lineated, at locations 69-2 and 69-6. Similar pegmatites at location 69-7 intrude and hence postdate the development of a foliated gneissic quartzite. The Bell Lake granite certainly was emplaced during or after the geological event that brought the high-grade metamorphic rocks from the Grenville province to the same crustal level as the Southern province rocks. South of the Bell Lake granite a geologically older granitic gneiss is intermixed with layered paragneiss and is plastically deformed in a northeast trending zone (locations 69-12, 69-41, 69-42, 69-44). The granite rocks in this zone were emplaced either before or during the deformation and recrystallization typical of this part of the Grenville Front.

The uranium-lead ages for two fractions of zircon from the Bell Lake granite, collected at location 69-9, indicate an age of emplacement of about 1550 m.y. (Fig. 92). Zircons from the orthogneiss yield an age of emplacement of about 1730 m.y. for samples collected at locations 69-42 and 69-12 (Fig. 92). Whole-rock Rb-Sr data for these rocks are plotted in Fig. 93 along with data for other granites that occur along the Front in this area. The data for whole rocks are ambiguous because many different bodies are represented and because intense shearing of some of the samples probably has contributed to migration of the dating elements. The data imply, however, that at least two periods of granite emplacement have occurred.

These isotopic data combined with the geological field relationships indicate that the Front zone formed at least 1550 m.y. ago when the Bell Lake granite was emplaced, and perhaps was an

active zone of plastic deformation 1730 m.y. ago when the granitic gneisses were emplaced. These results agree with our previous studies in the area (*Year Book 68*) but are incompatible with the commonly accepted conclusion based on mineral age data that the Front formed about 1000 m.y. ago.

#### PARAGNEISS STUDIES IN THE GEORGIAN BAY AREA 90 KM SOUTHEAST OF THE GRENVILLE FRONT

*T. E. Krogh and G. L. Davis*

In previous studies in the northwest part of the Grenville province, large whole-rock samples from homogeneous granite outcrops were examined and it was shown by the Rb-Sr whole-rock dating technique that much of the region was at least 1700 m.y. old. More recently adjacent 2- to 3-cm layers in a single paragneiss block collected 90 km southeast from the Grenville Front were studied, and it was concluded that the major metamorphism of this rock occurred about 1800 m.y. ago (*Year Books 66 and 67*). This provided a unique opportunity to determine the limits of strontium migration because this area underwent a regional metamorphism about 1000 m.y. ago. To accomplish this, analyses were made on large (9-kg) whole-rock samples from the outcrop and smaller (2- to 3-mm) slices from the original paragneiss block.

In Fig. 94 the data for the 2- to 3-cm layers are plotted as circles (80-2, 80-4, 80-5, 80-7, 80-8, 80-9) and data for four (9-kg) whole-rock samples are shown as rectangles (68-13, 68-14, 68-15, and 66-88). A best-fit isochron for the six layers in the paragneiss block ( $1790 \pm 95$  m.y.) is shown for reference. The data for large whole rocks conform to the reference isochron but suggest a degree of scatter greater than that found for

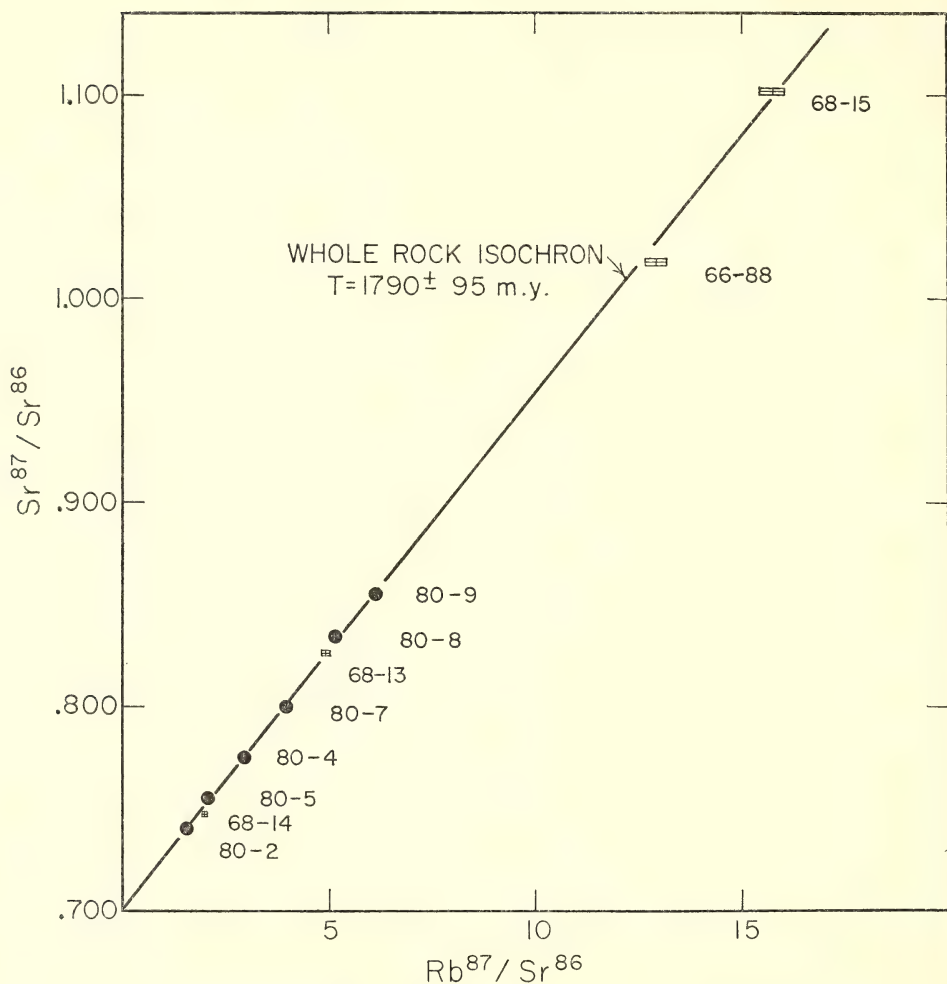


Fig. 94. Isochron plot for the Georgian Bay, Pointe au Barile paragneiss. Rectangular data points represent 9-kg whole-rock samples; circles represent data from 2- to 3-cm whole-rock slices from a single 20-cm block.

the individual layers. Their conformity to the age line previously described as a time of local isotopic mixing suggests that similar isotopic mixing occurred throughout the sampled outcrop area or that the metamorphic age indicated is also close to the true deposition age of the rock.

Results for analyzed 2- to 3-mm (micro) layers are shown in Fig. 95 as rectangular data points. Circled points represent data for the previously de-

scribed 2- to 3-cm layers, and crosses indicate data obtained by analyzing single minerals. Data for microlayers 17 and 18 from the contact of layers 80-4 and 80-5 indicate local isotopic mixing between these local adjacent rock volumes at the time of isotopic mixing among coexisting minerals. It is interesting to note that microlayer 17 was analyzed as part of layer 80-5, and hence this layer has not been a closed system for 1800 m.y. Similarly microlayer 16

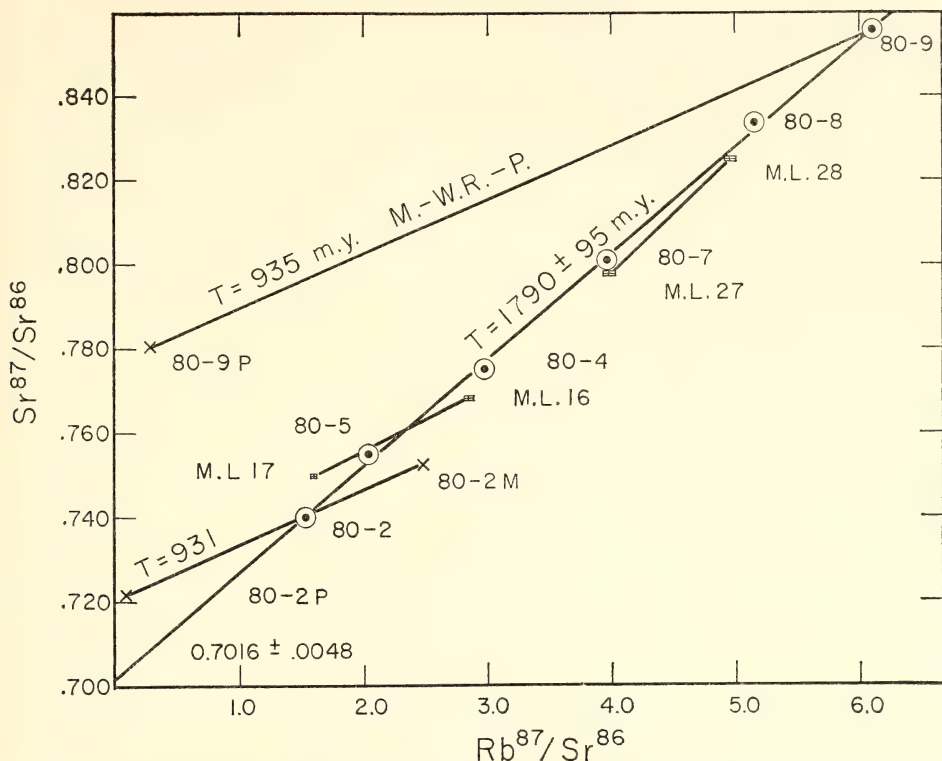


Fig. 95. Isochron for the Georgian Bay, Pointe au Barile paragneiss. Rectangular points represent data from 3-mm whole-rock slices, circled points represent data from 2- to 3-cm layers, and crosses indicate data obtained from the analysis of single minerals.

accounts for the deviation of data for layer 80-4 from the isochron. Micro-layers 27 and 28 occur at the edge of layers 80-7 and 80-8. They do not represent the edge of two homogeneous regions but rather reflect small lenses alternately rich in plagioclase and microcline that occur within a more general gradient in the rubidium-to-strontium ratio (*Year Book 67*). In this case isotopic mixing of strontium takes place on a gradient in the  $\text{Sr}^{87}\text{-Sr}^{86}$  ratio, and local rock volumes do not easily attain the same isotopic composition.

It is concluded that the 1790 m.y. isochron indicates the time of most intense metamorphism of the paragneiss block and that the same age is obtained by analyzing large whole rocks from this outcrop. A scale of local isotopic mixing

during the second metamorphism on the order of a few millimeters is suggested by the isotopic mixing of strontium between the two adjacent 3-mm layers. This small limit of isotopic mixing is remarkable, considering that the second metamorphism has imposed an amphibolite metamorphism on some rocks in this region believed to be less than 1300 m.y. old.

#### A SIMPLIFIED TECHNIQUE FOR THE DISSOLUTION OF ZIRCONS AND THE ISOLATION OF URANIUM AND LEAD

*T. E. Krogh*

U-Pb age determination has been established as one of the most reliable methods of determining true geological ages; it is, however, not widely used as



compared to other methods. The laborious chemical methods used in the dissolution of zircon and the extraction of uranium and lead are limiting factors. For this reason an effort has been made to simplify the method by utilizing a Teflon-lined stainless steel bomb for dissolution and an ion-exchange column technique for the extraction of U and Pb. Compared with the techniques now in use, this method offers much lower contamination levels, requires fewer purified reagents and less attention, and is suitable for batch processing. The technique also avoids the possibility of lead loss by volatilization during the borax fusion at 1000°C. So far the contamination levels are extremely low, the column separations have been shown to be effective, and it has been demonstrated that U, Th, and Pb are not lost through the Teflon walls owing to the formation of volatile compounds. Ultimately, it is expected that this technique together with the new method for the mass spectrometric analysis of submicrogram quantities of lead (Cameron, Smith, and Walker, 1969) will make possible U-Pb determinations of extremely small samples as well as zircon samples with very low contents of uranium.

High-pressure dissolution techniques using either a sealed glass tube or a stainless steel chamber with an inert liner of Teflon or platinum have been developed by analytical chemists to determine ferrous iron and silica as well as to dissolve refractory materials. Ito (1961) reported that zircons could be completely dissolved in hydrofluoric acid at temperatures as low as 240°C in as little as 10 hours in a Teflon-lined vessel, and May and Rowe (1965) described a platinum-lined container in which small amounts of zircon were dissolved in 20 hours at 425°C. The reaction vessels used by each of these investigators were unsuitable for use in routine zircon analysis for isotopic dating because the contents of the Teflon container could not be isolated from the stainless steel

of the confining vessel and the platinum vessel could hold only 1 to 2 ml of acid.

In the initial attempts to design a larger, completely sealed Teflon liner certain designs were found to be unsatisfactory, not only because they leaked at high pressures but also because the Teflon tended to flow when under the sealing load, so that the useful life of the capsule was limited. It was also discovered that hydrofluoric acid, when contained at 220°C, diffuses readily through the 5-mm Teflon wall in a 25-ml capsule at a rate of 0.013 g/hr. The rate of HF loss has been reduced by a factor of 5 in the latest design by utilizing an internally produced sealing pressure.

### *Description of Apparatus*

A Teflon vessel of the type shown in Fig. 96 has been in operation for approximately 60 days at 220°C without any significant changes in its performance. It is now a few hundredths of an inch shorter, and a slight bulge has developed on the inside wall below the cylindrical plug of the lid. Tests carried out by wrapping the vessel in aluminum foil before inserting it into the bomb show no etching due to leakage of HF along the seal but indicate a general loss of HF gas by diffusion through the Teflon.

This vessel provides contamination-free pouring from the lip and is used on a hot plate during the first stages of chemical treatment of the sample. Besides the long path of the seal, the sample is further isolated from the stainless steel bomb by a sleeve of "shrink Teflon," which has been preformed to fit exactly over the cylindrical dissolution vessel. It should be noted that the Teflon stock as received changes shape and should be annealed overnight at 220°C before final machining. Our next generation of vessels will have a thicker wall to reduce the loss of HF gas by diffusion.

The metal jacket of 316 stainless steel shown in Fig. 96 is designed to provide

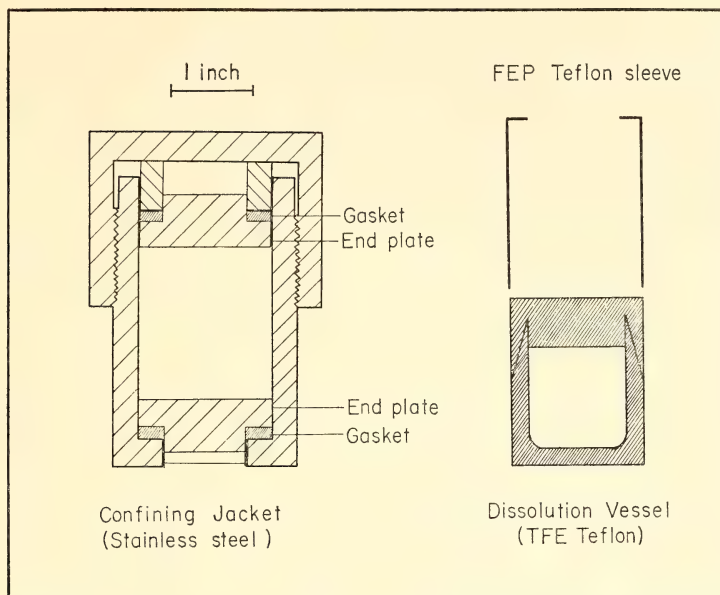


Fig. 96. The Teflon dissolution vessel and the stainless steel confining jacket (bomb) used for the dissolution of zircons.

a pressure seal that reduces gas leakage from the Teflon container and to apply a load to seal the lid of the container. In this regard it differs from all other containers now in use for similar purposes. The seals, made of FEP Teflon, which flows at the pressures encountered, are placed inside each end-plate. Pressures in the seal are always greater than the pressure acting on the end-plate because the support area of the seal is only about 40% of the area of the end-plate. This seal reduces by a factor of 5 the rate at which HF gas leaks from the dissolution chamber. Any further improvement will require a new gasket material that is not permeable to HF gas or else a thicker Teflon gasket on the top of the bomb.

#### *The Chemical Procedure*

The sample is weighed into the Teflon vessel and moistened with concentrated nitric acid, and 48% hydrofluoric acid is added (10 ml of HF will dissolve at least

1 g of zircon). For dissolution the stainless steel lid is tightened by hand, and the bomb is placed in a conventional drying oven at 220°C for 5 to 6 days. More rapid dissolution rates can be achieved by grinding the zircon sample, but this grinding is inconvenient for routine analysis and can be a source of contamination. If grinding is to be used, a steel mortar is recommended, so that mortar material can be removed from the sample with hydrochloric acid without affecting the zircon.

After decomposition the sample requires further treatment to insure a perfect solution. Silica gel is eliminated by a double evaporation with HF, and the fluoride ion is eliminated by fuming the sample twice with sulfuric acid. The sample is then dissolved in 3.1 N HCl, and two aliquots are prepared, one for the concentration of U and Pb and another for the determination of the lead isotopic composition.

After isotopic spikes are added, the

aliquots are adjusted to 4 ml with 3.1 *N* HCl and placed on an anion ion-exchange column (Dow 1×8 resin). A 6-cm column containing 1.5 ml of resin made from a shrink Teflon tube is satisfactory. A 3-ml wash with 3.1 *N* HCl removes Zr, which is not absorbed on the resin, and moves U and Pb a short distance down the column. Pb is not absorbed in 6.2 *N* HCl and can be removed

in 4 ml. In this acid, U is strongly held but it can be easily removed with 4 ml of H<sub>2</sub>O. A satisfactory method for the separation of Th, which passes through the column with Zr, has not been found. The samples from the column are ready for mass spectrometric analysis after they have been dried down with one or two drops of both nitric and perchloric acid to destroy any resin that may be present.

## STAFF ACTIVITIES

### *Washington Crystal Colloquium*

The Washington Crystal Colloquium, an informal monthly assembly of crystallographers from the Baltimore-Washington-Virginia area, met ten times during the report year. The following lectures were presented:

"Some geometrical theorems relevant to crystal structures," by A. F. Wells (University of Connecticut), September 25, 1969.

"Epitaxy," by Kathleen Lonsdale (Ohio State University), October 24, 1969.

"Crystal structure study of the decamolybdocobaltate ion," by Howard T. Evans, Jr. (U.S. Geological Survey, Washington, D.C.), November 21, 1969.

"Applications of the electroneutrality principle to crystal structure problems," by Gabrielle Donnay and R. Allmann (Geophysical Laboratory and Mineralogical Institute, Marburg), December 19, 1969.

"The structure of lamprey hemoglobin at 2.5 Å resolution," by Wayne Henrickson (Naval Research Laboratory) and Warner E. Love (The Johns Hopkins University), January 30, 1970.

"The structure of  $\gamma$ -chymotrypsin at 2.7 Å resolution," by D. R. Davies, G. H. Cohen, E. W. Silvertown, J. Richardson, H. Braxton, and D. Segal (National Institutes of Health), February 20, 1970.

"Studies of antimalarial drugs," by Hugh Preston (University of Maryland), March 27, 1970.

"Recent developments in the structural aspects of mixed-metal bonding," by Robert F. Bryan (University of Virginia), April 24, 1970.

"What is the silicon-oxygen bond?" by D. W. J. Cruickshank (Virginia Polytechnic Institute), May 22, 1970.

"Determination of cation ordering in minerals and the refinement of a crystal structure of an olivine from the moon," by Larry W. Finger (Geophysical Laboratory), June 12, 1970.

### *Lectures*

During the report year Staff Members and Fellows were invited to present lectures as follows:

P. H. Abelson made a total of 16 invited public appearances. He made speeches in the following capacities: As Robert Kennedy Duncan Memorial Lecturer ("Toward a More Livable Environment") on the occasion of receipt of the Mellon Institute Award for 1970 at Carnegie-Mellon University, Pittsburgh; as a member of panels on "Science and Man in Space" and "Science and the Future of Man" at the annual meeting of the American Association for the Advancement of Science at Boston; as speaker ("Evolution of Proteins") at dinner of North American Paleontological Convention, Chicago; as participant ("The Coming Struggle for International Solvency") in a Symposium on the Relationship of Science and Society at the 158th National Meeting of the American



Chemical Society at New York; as speaker ("American Policy towards the Exploration of Space") at the Jonathan Edwards College, Yale University, New Haven; as speaker ("Research Climate of the Seventies") at the Massachusetts General Hospital, Boston; and as a participant in a Seminar on "Exploration of the Moon and the Planets" sponsored by the Southern Newspaper Publishers Association Foundation and the Department of Astronomy at the University of Virginia, Charlottesville.

P. M. Bell lectured at the Department of Geochemistry, Pennsylvania State University.

F. R. Boyd, Jr. presented an invited paper at the Symposium on the Upper Mantle at the 50th Anniversary Meeting of the Mineralogical Society of America at Atlantic City.

W. B. Bryan addressed the Department of Geology at the University of Massachusetts, the Department of Geochemistry at Woods Hole Oceanographic Institution, and the Department of Geology at the University of Cincinnati. He served as editor of "Pyroclastic Rocks" and "Textures and Structures," revised edition of *American Geological Institute Glossary of Geology*.

F. Chayes attended the IAVC Oxford Symposium on Volcanoes and Their Roots, at which he lectured on methods of estimating compositions of residual liquids of the Skaergaard layered series. He also lectured on petrographic ratio correlation before the Geology Department of the University of Pennsylvania, contributed a paper on the performance of a proposed test of closed correlations in simulation experiments to the Annual Geostatistics Colloquium of the Kansas Geological Survey, and has been invited to participate in a Royal Society discussion meeting on "Volcanism and the Structure of the Earth."

Gabrielle Donnay lectured at the Department of Chemistry, University of Maryland; the Ledgemont Laboratory of the Kennecott Copper Corporation at

Lexington, Mass.; the Department of Geological Sciences, McGill University; the Chemistry Department, Howard University; the Department of Geological Sciences, University of California at Los Angeles; the chemistry and geology departments, California Institute of Technology; and the Dental Research Center, University of North Carolina.

S. E. Haggerty addressed the departments of geology at Virginia Polytechnic Institute, the University of Massachusetts, and Dalhousie University; the departments of geophysics at the University of Pittsburgh and the University of Toronto; and the Geological Society of Washington.

P. E. Hare lectured at the Department of Geosciences, University of Texas, Dallas, and addressed the student body at Atlantic Union College, South Lancaster, Massachusetts.

T. E. Krogh gave an invited lecture at the Geology Department, University of Western Ontario, Canada.

G. Kullerud continued as Adjunct Professor in Geochemistry at Lehigh University where he supervised the sulfide research program and lectured on sulfide phase equilibria. He served as Consulting Professor to the Department of Geosciences, Texas Technological University, Lubbock, Texas, and as a Visiting Professor at Heidelberg University, where he also lectured on ore deposits. On the occasion of the 50th Anniversary of the Mineralogical Society of America he organized a Sulfide Symposium and presented one of the six lectures given at the symposium. He was also an invited lecturer at the Symposium on Erz und Nebengestein held in Heidelberg on the occasion of Prof. Ramdohr's 80th birthday. In addition, he presented one lecture at the University of Ruhr, Bochum, Germany, and two lectures at Université de Louvain, Belgium.

D. H. Lindsley addressed the Franklin and Marshall Geological Society.

H. O. A. Meyer participated in a

meeting of the International Association of Volcanology and Chemistry of the Earth's Interior at Oxford, England. He also visited the University of Ruhr, Bochum, and presented an invited lecture at the Max-Planck Institut für Kernphysik, Heidelberg.

D. Rumble lectured at the Department of Geology, Oberlin College; the Department of Geological and Geophysical Sciences, Princeton University; and the U.S. Geological Survey, Washington, D.C.

J. F. Schairer delivered the Horizons of Knowledge lecture ("Chemistry of the Earth's Crust") sponsored by the chemistry and geology departments at Indiana University, and gave two seminar talks in their Geology Department. He also addressed the chemistry and geology departments at Acadia University, Wolfville, Nova Scotia, and gave a series of three seminar talks to students in their Geology Department.

D. Smith addressed the geology departments at the University of Massachusetts and the State University of New York at Binghamton.

H. S. Yoder, Jr. presented a lecture at Lehigh University on "Alkali Magma Fractionation Problems." He coauthored a paper for the Pyroxene and Amphibole Symposium held at the Virginia Polytechnic Institute, Blacksburg; participated in the Apollo 11 Lunar Science

Conference in Houston, Texas; and attended the Francis Birch Symposium at Harvard University. Yoder again served on the M.I.T. Visiting Committee on the Earth Sciences.

### *Petrologists' Club*

Five meetings were held during the 59th year of the Petrologists' Club and the following lectures were presented:

"Synthesis and stability of andradite and Ti-bearing garnet," by H. G. Huckenholz (University of Munich), October 14, 1969.

"Partial fusion products in Alpine-type peridotites: Serrania de la Ronda and other examples," by John S. Dickey (Smithsonian Astrophysical Observatory, Cambridge, Massachusetts), November 18, 1969.

"Discussion of paper on 'Contact metamorphism in the Kwoiek, B.C., area: an end-member of the metamorphic process,' by Lincoln Hollister" (Princeton University), January 20, 1970.

"Applications of nuclear magnetic, electron paramagnetic, and Mössbauer resonance techniques in petrology," by Subrata Ghose (NASA, Goddard Space Flight Center), April 2, 1970.

"Equilibrium studies in the plagioclase<sub>ss</sub>-NaCl-CaCl-H<sub>2</sub>O system," by Philip M. Orville (Yale University), May 19, 1970.

## BIBLIOGRAPHY

Allmann, R., *see* Donnay, G.

Anderson, A. T., T. E. Bunch, E. N. Cameron, S. E. Haggerty, F. R. Boyd, L. W. Finger, O.B. James, K. Keil, M. Prinz, P. Ramdohr, and A. El Goresy, Armalcolite: a new mineral from the Apollo 11 samples, in *Proceedings of the Apollo 11 Lunar Science Conference*, Vol. 1, A. A. Levinson, ed., Pergamon Press, New York, 55-63, 1970 (G. L. Paper 1566).

Bell, P. M., and E. H. Roseboom, Jr., Melting relationships of jadeite and albite to 45 kb with comments on melting diagrams of binary systems at high pressures, *Mineral. Soc. Amer. Spec. Pap.*, 2, 151-161, 1969 (G. L. Paper 1543).

Bell, P. M., *see also* Brett, P. R.; Haggerty, S. E.

Boyd, F. R., and G. M. Brown, Electron-probe study of pyroxene exsolution, *Mineral. Soc. Amer. Spec. Pap.*, 2, 211-216, 1969 (G. L. Paper 1544).

Boyd, F. R., *see also* Anderson, A. T.; Haggerty, S. E.

Brett, P. R., and P. M. Bell, Melting relations in the Fe-rich portion of the system Fe-FeS at 30 kb pressure, *Earth Planet. Sci. Lett.*, 6, 479-482, 1969 (G. L. Paper 1550).

Brown, G. M., *see* Boyd, F. R.

Bryan, W. B., *see* Haggerty, S. E.

- Bunch, T. E., *see* Anderson, A. T.
- Burnham, C. W., *see* Lindsley, D. H.
- Cameron, E. N., *see* Anderson, A. T.
- Chayes, F., The chemical composition of Cenozoic andesite, *Oreg. Dep. Geol. Miner. Ind. Bull.*, 65, 1-11, 1969 (G. L. Paper 1541).
- Chayes, F., On estimating the magnitude of the hidden zone and the compositions of the residual liquids of the Skaergaard layered series, *J. Petrology*, 11, 1-14, 1970 (G. L. Paper 1555).
- Chayes, F., On deciding whether trend surfaces of progressively higher order are meaningful, *Geol. Soc. Amer. Bull.*, 81, 1273-1278, 1970 (G. L. Paper 1559).
- Craig, J. R., and G. Kullerud, Phase relations in the Cu-Fe-Ni-S system and their application to magmatic ore deposits, *Econ. Geol. Monogr.*, 4, 344-358, 1969 (G. L. Paper 1512).
- Davis, G. L., *see* Krogh, T. E.
- Donnay, G., and R. Allmann, How to recognize  $O^{2-}$ ,  $OH^{-}$ , and  $H_2O$  in crystal structures determined by X-rays, *Amer. Mineral.*, 65, 1003-1015, 1970 (G. L. Paper 1568).
- Donnay, G., and D. L. Pawson, X-ray diffraction studies of echinoderm plates, *Science*, 166, 1147-1150, 1969 (G. L. Paper 1553).
- Donnay, G., J. M. Stewart, and H. Preston, The crystal structure of sonoraite,  $Fe^{3+}Te^{4+}O_8(OH) \cdot H_2O$ , *Tschermaks Mineral. Petrogr. Mitt.*, 14, 27-44, 1970 (G. L. Paper 1552).
- El Goresy, A., *see* Anderson, A. T.
- Finger, L. W., The crystal structure and cation distribution of a grunerite, *Mineral. Soc. Amer. Spec. Pap.*, 2, 95-100, 1969 (G. L. Paper 1545).
- Finger, L. W., *see also* Anderson, A. T.; Haggerty, S. E.
- Haggerty, S. E., F. R. Boyd, P. M. Bell, L. W. Finger, and W. B. Bryan, Iron-titanium oxides and olivine from 10020 and 10071, *Science*, 167, 613-615, 1970 (G. L. Paper 1558).
- Haggerty, S. E., F. R. Boyd, P. M. Bell, L. W. Finger, and W. B. Bryan, Opaque minerals and olivine in lavas and breccias from *Mare Tranquillitatis*, in *Proceedings of the Apollo 11 Lunar Science Conference*, Vol. 1, A. A. Levinson, ed., Pergamon Press, New York, 513-538, 1970 (G. L. Paper 1565).
- Haggerty, S. E., *see also* Anderson, A. T.
- Huckenholz, H. G., J. F. Schairer, and H. S. Yoder, Jr., Synthesis and stability of ferri-diopside, *Mineral. Soc. Amer. Spec. Pap.*, 2, 163-177, 1969 (G. L. Paper 1546).
- James, O. B., *see* Anderson, A. T.
- Keil, K., *see* Anderson, A. T.
- Krogh, T. E., and G. L. Davis, Old isotopic ages in the northwestern Grenville province, Ontario, *Geol. Ass. Can. Spec. Pap.*, 5, 189-192, 1969 (G. L. Paper 1538).
- Kullerud, G., *see also* Craig, J. R.; Puchelt, H.
- Kullerud, G., R. A. Yund, and G. H. Moh, Phase relations in the Cu-Fe-S, Cu-Ni-S, and Fe-Ni-S systems, *Econ. Geol. Monogr.*, 4, 323-343, 1969 (G. L. Paper 1511).
- Kushiro, I., Clinopyroxene solid solutions formed by reactions between diopside and plagioclase at high pressures, *Mineral. Soc. Amer. Spec. Pap.*, 2, 179-191, 1969 (G. L. Paper 1547).
- Lindsley, D. H., Melting relations of plagioclase at high pressures, *N. Y. State Museum Sci. Serv. Mem.*, 18, 39-46, 1968 (G. L. Paper 1563).
- Lindsley, D. H., and C. W. Burnham, Pyroxferroite: stability and X-ray crystallography of synthetic  $Ca_{0.15}Fe_{0.65}SiO_3$  pyroxenoid, *Science*, 168, 364-367, 1970 (G. L. Paper 1567).
- Lindsley, D. H., and I. D. Muir, Conditions of the ferrowollastonite-ferrohedenbergite inversion in the Skaergaard intrusion, east Greenland, *Mineral. Soc. Amer. Spec. Pap.*, 2, 193-201, 1969 (G. L. Paper 1548).
- Meyer, H. O. A., Géochimie des inclusions minérales dans les diamants naturels, *Bull. Ass. Franc. Gemmologie*, 22, 8-10, 1970 (G. L. Paper 1557).
- Moh, G. H., The tin-sulfur system and related minerals, *Neues Jahrb. Mineral., Abh.*, 111, 227-263, 1969 (G. L. Paper 1540).
- Moh, G. H., *see also* Kullerud, G.
- Muir, I. D., *see* Lindsley, D. H.
- Munoz, J. L., Stability relations of  $LiAlSi_2O_6$  at high pressures, *Mineral. Soc. Amer. Spec. Pap.*, 2, 203-209, 1969 (G. L. Paper 1549).
- Naldrett, A. J., A portion of the system Fe-S-O between 900 and 1080°C and its application to sulfide ore magmas, *J. Petrology*, 10, 171-201, 1969 (G. L. Paper 1531).
- Pawson, D. L., *see* Donnay, G.
- Presnall, D. C., Pressure-volume-temperature measurements on hydrogen from 200° to 600°C and up to 1800 atm, *J. Geophys. Res.*, 74, 6026-6033, 1969 (G. L. Paper 1551).
- Preston, H., *see* Donnay, G.
- Prinz, M., *see* Anderson, A. T.
- Puchelt, H., and G. Kullerud, Sulfur isotope fractionation in the Pb-S system, *Earth Planet. Sci. Lett.*, 7, 301-306, 1970 (G. L. Paper 1556).
- Ramdohr, P., *see* Anderson, A. T.
- Roseboom, E. H., Jr., *see* Bell, P. M.
- Schairer, J. F., *see* Huckenholz, H. G.
- Stewart, J. M., *see* Donnay, G.
- Taylor, L. A., The significance of twinning in



- Ag<sub>2</sub>S, *Amer. Mineral.*, 54, 961-963, 1969 (G. L. Paper 1539).
- Taylor, L. A., The system Ag-Fe-S: phase equilibria and mineral assemblages *Miner. Deposita*, 5, 41-58, 1970 (G. L. Paper 1554).
- Yoder, H. S., Jr., Calcalkalic andesites: experimental data bearing on the origin of their assumed characteristics, *Oreg. Dep. Geol. Miner. Ind. Bull.*, 65, 77-89, 1969 (G. L. Paper 1542).
- Yoder, H. S., Jr., Experimental studies bearing on the origin of anorthosite, *N. Y. State Museum Sci. Serv. Mem.*, 18, 13-22, 1968 (G. L. Paper 1562).
- Yoder, H. S., Jr., *see also* Huckenholz, H. G.
- Yund, R. A., *see* Kullerud, G.

## REFERENCES CITED

- Abbott, M. J., Aenigmatite from the ground-mass of a peralkaline trachyte, *Amer. Mineral.*, 52, 1895-1901, 1967.
- Adams, L. H., and R. E. Gibson, The compressibilities of dunite and of basalt glass and their bearing on the composition of the earth, *Proc. Nat. Acad. Sci. U. S.*, 12, 275-283, 1926.
- Ade-Hall, J. M., The magnetic properties of some submarine oceanic lavas, *Geophys. J. Roy. Astron. Soc.*, 9, 85-92, 1964.
- Agrell, S. O., F. R. Boyd, T. E. Bunch, E. N. Cameron, M. R. Dence, J. A. V. Douglas, S. E. Haggerty, O. B. James, K. Keil, A. Peckett, A. G. Plant, M. Prinz, and R. J. Trail, Titanian chromite, aluminian chromite and chromian ulvöspinel from Apollo 11 rocks, in *Proceedings of the Apollo 11 Lunar Science Conference*, Vol. 1, A. A. Levinson, ed., Pergamon Press, New York, 81-86, 1970.
- Akimoto, S., Thermo-magnetic study of ferromagnetic minerals contained in igneous rocks, *J. Geomagn. Geoelec.*, 6, 1-14, 1954.
- Akimoto, S., T. Katsura, and M. Yoshida, Magnetic properties of TiFe<sub>2</sub>O<sub>4</sub>-Fe<sub>3</sub>O<sub>4</sub> system and their change with oxidation, *J. Geomagn. Geoelec.*, 9, 165-178, 1957.
- Albee, A. L., Phase equilibria in three assemblages of kyanite-zone pelitic schists, Lincoln Mountain quadrangle, central Vermont, *J. Petrology*, 6, 246-301, 1965.
- Albee, A. L., A petrogenetic grid for the Fe-Mg silicates of pelitic schists, *Amer. J. Sci.*, 263, 512-536, 1965.
- Allen, P., and W. C. Krumbein, Secondary trend components in the top Ashdown pebble bed, a case history, *J. Geol.*, 70, 507-538, 1962.
- Althaus, E., Die bildung von pyrophyllit und andalusite zwischen 2000 und 7000 bar H<sub>2</sub>O druck, *Naturwissenschaften*, 53, 105-106, 1966.
- Anderson, A. T., Jr., A. V. Crewe, J. R. Goldsmith, P. B. Moore, J. C. Newton, E. J. Olsen, J. V. Smith, and P. J. Wyllie, Petrologic history of Moon suggested by petrography, mineralogy, and crystallography, *Science*, 167, 587-589, 1970.
- Aumento, F., Report of activities, *Geol. Surv. Can. Pap.*, 69-1A, 253-257, 1968.
- Aumento, F., The Mid-Atlantic Ridge near 45°N. V. Fission track and ferromanganese chronology, *Can. J. Earth Sci.*, 6, 1431-1440, 1969.
- Bailey, D. K., The stability of acmite in the presence of H<sub>2</sub>O, *Amer. J. Sci.*, Schairer Vol., 267A, 1-16, 1969.
- Bailey, D. K., Volatile flux, heat-focusing and the generation of magma, *Geol. J. Spec. Issue no. 2*, 177-186, 1970.
- Bailey, D. K., and J. F. Schairer, The system Na<sub>2</sub>O-Al<sub>2</sub>O<sub>3</sub>-Fe<sub>2</sub>O<sub>3</sub>-SiO<sub>2</sub> at 1 atm, and the petrogenesis of alkaline rocks, *J. Petrology*, 7, 114-170, 1966.
- Bailey, J. C., P. E. Champness, A. C. Dunham, J. Esson, W. S. Fyfe, W. S. MacKenzie, E. F. Stumpf, and J. Zussman, Mineralogical and petrological investigations of lunar samples, *Science*, 167, 592-594, 1970.
- Baker, P. E., Comparative volcanology and petrology of the Atlantic island-arc, *Bull. Volcanol.*, 32, 189-206, 1968.
- Bancroft, G. M., and R. G. Burns, Distribution of iron cations in a volcanic pigeonite by Mössbauer spectroscopy, *Earth Planet. Sci. Lett.*, 3, 125-127, 1967.
- Barron, L. M., Thermodynamic multicomponent silicate phase equilibrium calculations (abstract), *Trans. Amer. Geophys. Union*, 51, 437, 1970.
- Bassett, W. A., T. Takahashi, and P. W. Stook, X-ray diffraction and optical observations on crystalline solids up to 300 kb, *Rev. Sci. Instrum.*, 38, 37-42, 1967.
- Bell, P. M., F. R. Boyd, and J. L. England, Effects of hydrostatic pressure on Pt/Pt 10 Rh and chromel-alumel thermocouples, Symposium on the Accurate Characterization of the High-Pressure Environment, Carnegie Institution of Washington-National Bureau of Standards, Gaithersburg, Maryland, October 14-18, 1968, in press, 1970.
- Bell, P. M., and B. T. C. Davis, Melting relations in the system jadeite-diopside at 30

- and 40 kb, *Amer. J. Sci., Schairer Vol.*, 267A, 17-32, 1969.
- Bell, P. M., and J. L. England, High-pressure experimental techniques, in *Researches in Geochemistry*, Vol. 2, P. H. Abelson, ed., John Wiley and Sons, Inc., 619-637, 1967.
- Bell, P. M., and E. H. Roseboom, Jr., Melting relationships of jadeite and albite to 45 kilobars with comments on melting diagrams of binary systems at high pressures, *Mineral. Soc. Amer. Spec. Pap.*, 2, 151-161, 1969.
- Bence, A. E., K. L. Cameron, and J. J. Papike, Sector zoning in calcic clinopyroxenes (abstract), *Trans. Amer. Geophys. Union*, 51, 435, 1970.
- Bence, A. E., J. J. Papike, and C. T. Prewitt, Apollo 12 pyroxenes: Chemical trends (abstract), American Geophysical Union, 51st Annual Meeting, Supplementary Program, 1970.
- Berner, R. A., Tetragonal iron sulfide, *Science*, 137, 669, 1962.
- Billings, M. P., Regional metamorphism of the Littleton-Moosilauke area, New Hampshire, *Geol. Soc. Amer. Bull.*, 48, 463-566, 1937.
- Birch, F., Thermoelectric measurement of high temperatures in pressure apparatus, *Rev. Sci. Instrum.*, 10, 137-140, 1939.
- Birle, J. D., G. V. Gibbs, P. B. Moore, and J. V. Smith, Crystal structures of natural olivines, *Amer. Mineral.*, 53, 807-824, 1968.
- Blasse, G., Crystal chemistry and some magnetic properties of mixed metal oxides with spinel structure, *Philips Res. Rep. Suppl.*, 3, 1964.
- Boettcher, A. L., and P. J. Wyllie, Jadeite stability measured in the presence of silicate liquids in the system  $\text{NaAlSi}_3\text{O}_8\text{-SiO}_2\text{-H}_2\text{O}$ , *Geochim. Cosmochim. Acta*, 32, 999-1012, 1968.
- Bonnichsen, Bill, Metamorphic pyroxenes and amphiboles in the Buivabik iron formation, Dunka River area, Minnesota, *Mineral. Soc. Amer. Spec. Pap.*, 2, 217-239, 1969.
- Bowen, N. L., The crystallization of haplobasaltic, haplodioritic, and related magmas, *Amer. J. Sci.*, 40, 161-185, 1915.
- Bowen, N. L., The problem of the anorthositic, *J. Geol.*, 25, 209-243, 1917.
- Bowen, N. L., Diffusion in silicate melts, *J. Geol.*, 29, 295-317, 1921.
- Bowen, N. L., *The Evolution of the Igneous Rocks*, Princeton University Press, 1928.
- Bowen, N. L., "Ferrosilite" as a natural mineral, *Amer. J. Sci.*, 30, 481-494, 1935.
- Bowen, N. L., and J. F. Schairer, The fusion relations of acmite, *Amer. J. Sci.*, 18, 365-374, 1929.
- Bown, M. G., Re-investigation of a clinofersilite from Lake Maivasha, Kenya, *Mineral. Mag.*, 34, 66-70, 1965.
- Boyd, F. R., Electron-probe study of diopside inclusions from kimberlite, *Amer. J. Sci., Schairer Vol.*, 267A, 50-69, 1969.
- Boyd, F. R., and G. M. Brown, Electron-probe study of pyroxene exsolution, *Mineral. Soc. Amer. Spec. Pap.*, 2, 211-216, 1969.
- Boyd, F. R., and J. L. England, Apparatus for phase-equilibrium measurements at pressures up to 50 kb and temperatures up to 1750°C, *J. Geophys. Res.*, 65, 741-748, 1960.
- Boyd, F. R., and J. L. England, Effect of pressure on the melting of diopside,  $\text{CaMgSi}_2\text{O}_6$ , and albite,  $\text{NaAlSi}_3\text{O}_8$ , in the range up to 50 kb, *J. Geophys. Res.*, 68, 311-323, 1963.
- Boyd, F. R., J. L. England, and B. T. C. Davis, Effects of pressure on the melting and polymorphism of enstatite,  $\text{MgSiO}_3$ , *J. Geophys. Res.*, 69, 2101-2109, 1964.
- Brežný, B., and A. Muan, Phase relations and stabilities of compounds in the system  $\text{CoO-TiO}_2$ , *J. Inorg. Nucl. Chem.*, 31, 649-655, 1969.
- Bridgman, P. W., Thermo-electromotive force, Peltier heat, and Thompson heat under pressure, *Proc. Amer. Acad. Arts Sci.*, 53, 269-386, 1918.
- Brown, G. M., Pyroxenes from the early and middle stages of fractionation of the Skaergaard intrusion, east Greenland, *Mineral. Mag.*, 31, 511-543, 1957.
- Bryan, W. B., Low-potash dacite drift pumice from the Coral Sea, *Geol. Mag.*, 105, 431-439, 1968.
- Bryan, W. B., A new occurrence of Coral Sea drift pumice from Eua Island, Tonga, *Geol. Soc. Amer. Bull.*, in press, 1970.
- Bryan, W. B., G. D. Stice, and A. Ewart, Geology, petrography, and geochemistry of the volcanic islands of Tonga, *J. Geophys. Res.*, in press, 1970.
- Buddington, A. F., The Adirondack magmatic stem, *J. Geol.*, 39, 240-263, 1931.
- Buddington, A. F., and D. H. Lindsley, Iron-titanium oxide minerals and synthetic equivalents, *J. Petrology*, 5, 310-357, 1964.
- Bunch, T. E., K. Keil, and K. G. Snetsinger, Chromite composition in relation to chemistry and texture of ordinary chondrites, *Geochim. Cosmochim. Acta*, 31, 1569-1582, 1967.
- Bunsen, R. W., Über die Prozesse der vulkanischen Gesteinsbildungen Islands, *Ann. Phys.*, 83, 197-272, 1851.
- Burges, N. A., H. M. Hurst, and B. Walkden, The phenolic constituents of humic acid and their relation to the lignin of the plant cover,

- Geochim. Cosmochim. Acta*, **28**, 1547-1554, 1964.
- Burnham, Charles W., Computation of absorption corrections, and the significance of end effect, *Amer. Mineral.*, **51**, 159-167, 1966.
- Burns, R. G., Evidence for cation ordering in olivine minerals from crystal field spectra (abstract), *Acta Crystallogr., Sect. A*, **25**, S59, 1969.
- Buseck, P. R., and K. Keil, Meteoritic rutile, *Amer. Mineral.*, **51**, 1506-1515, 1966.
- Butler, P., Mineral compositions and equilibria in the metamorphosed iron formation of the Gagnon region, Quebec, Canada, *J. Petrology*, **10**, 56-101, 1969.
- Cameron, A. E., D. H. Smith, and R. L. Walker, Mass spectrometry of nanogram-size samples of lead, *Anal. Chem.*, **41**, 525-526, 1969.
- Cameron, E. N., Opaque minerals in certain lunar rocks from Apollo 11, in *Proceedings of the Apollo 11 Lunar Science Conference*, Vol. 1, A. A. Levinson, ed., Pergamon Press, New York, 221-245, 1970.
- Cameron, E. N., and M. E. Emerson, The origin of certain chromite deposits of the eastern part of the Bushveld complex, *Econ. Geol.*, **54**, 1151-1213, 1959.
- Carmichael, C. M., The magnetic properties of ilmenite-hematite crystals, *Proc. Roy. Soc. London, Ser. A*, **263**, 508-530, 1961.
- Carmichael, C. M., The Mid-Atlantic Ridge near 45°N. VII. Magnetic properties and opaque mineralogy of dredged samples, *Can. J. Earth Sci.*, **7**, 239-256, 1970.
- Carmichael, I. S. E., The Fe-Ti oxides of salic volcanic rocks, *Contrib. Mineral. Petrol.*, **14**, 36-64, 1966.
- Carmichael, I. S. E., The iron-titanium oxides of salic volcanic rocks and their associated ferromagnesian silicates, *Contrib. Mineral. Petrol.*, **14**, 36-64, 1967.
- Caron, L. G., R. P. Santoro, and R. E. Newnham, Magnetic structure of  $\text{CaMnSiO}_4$ , *J. Phys. Chem. Solids*, **26**, 927-930, 1965.
- Carr, J. M., Zoned plagioclases in layered gabbros of the Skaergaard intrusion, east Greenland, *Mineral. Mag.*, **30**, 367-375, 1954.
- Chapman, D. R., and L. C. Scheiber, Chemical investigation of Australasian tektites, *J. Geophys. Res.*, **74**, 6737-6776, 1969.
- Chayes, F., Relative abundance of intermediate members of the oceanic basalt-trachyte association, *J. Geophys. Res.*, **68**, 1519-1534, 1963.
- Chayes, F., Alkaline and subalkaline basalts, *Amer. J. Sci.*, **264**, 128-145, 1966.
- Chayes, F., On estimating the magnitude of the hidden zone and the compositions of the residual liquids of the Skaergaard layered series, *J. Petrology*, **11**, 1-14, 1970a.
- Chayes, F., On deciding whether trend surfaces of progressively higher order are meaningful, *Geol. Soc. Amer. Bull.*, **81**, 1273-1278, 1970b.
- Chayes, F., and W. Kruskal, An approximate statistical test for correlations between proportions, *J. Geol.*, **74**, 692-702, 1966.
- Chevallier, R., J. Bolfa, and S. Mathieu, Titanomagnetites et ilménites ferromagnétiques. (1) Étude optique, radiocristallographique, chimique, *Bull. Soc. Fr. Mineral. Cristallogr.*, **73**, 307-346, 1955.
- Chinner, G. A., Pelitic gneiss with varying ferrous-ferric ratios from Glen Cova, Angus, Scotland, *J. Petrology*, **1**, 178-217, 1960.
- Clark, A. H., Some comments on the composition and stability relations of mackinawite, *Neues Jahrb., Monatsh.*, **10**, 300-304, 1966.
- Coes, L., Jr., High-pressure minerals, *J. Amer. Ceram. Soc.*, **38**, 298, 1955.
- Coes, L., Jr., Synthesis of minerals at high pressures, in *Modern Very High Pressure Techniques*, R. H. Wentorf, ed., Butterworths, Washington, 137-150, 1962.
- Coleman, R. G., and J. R., Clark, Pyroxenes in the blueschist facies of California, *Amer. J. Sci.*, **266**, 43-59, 1968.
- Coleman, R. G., D. E. Lee, L. B. Beatty, and W. W. Brannock, Eclogites and eclogites: their differences and similarities, *Geol. Soc. Amer. Bull.*, **76**, 483-508, 1965.
- Coombs, D. S., and C. A. Landis, Pumice from the South Sandwich eruption of March 1962 reaches New Zealand, *Nature*, **209**, 289-290, 1966.
- Craig, J. R., R. L. Harris, G. Kullerud, and D. A. Howe, The Loop meteorite: a new olivine-bronzite chondrite (abstract), *Abstracts with Programs for 1969, Geol. Soc. Amer.*, pt. 7, 40, 1969.
- Cromer, D. T., Anomalous dispersion corrections computed from self-consistent field relativistic Dirac-Slater wave functions, *Acta Crystallogr.*, **18**, 17-23, 1965.
- Cromer, D. T., and J. B. Mann, X-ray scattering factors computed from numerical Hartree-Fock wave functions, *Acta Crystallogr., Sect. A*, **24**, 321-324, 1968.
- Damon, P. E., A. W. Laughlin, and J. K. Percious, Problem of excess argon-40 in volcanic rocks, in *Radioactive Dating and Methods of Low Level Counting*, International Atomic Energy Agency, Vienna, 463-479, 1967.



- Davidon, W. C., Variable metric method for minimization, Argonne National Laboratories, ANL 5990, 1959.
- Deer, W. A., R. A. Howie, and J. Zussman, *Rock-Forming Minerals*, Vol. 1, John Wiley and Sons, Inc., New York, 1962a.
- Deer, W. A., R. A. Howie, and J. Zussman, *Rock-Forming Minerals*, Vol. 5, John Wiley and Sons, Inc., New York, 1962b.
- Deer, W. A., R. A. Howie, and J. Zussman, *Rock-Forming Minerals*, Vol. 2, John Wiley and Sons, Inc., New York, 1963.
- Dodd, R. T., R. W. van Schmus, and V. B. Marvin, Merrihueite, a new alkali-ferromagnesium silicate from the Mezö-Madaras chondrite, *Science*, **149**, 972-974, 1965.
- Donnay, G., L. M. Corliss, J. D. H. Donnay, N. Elliott, and J. M. Hastings, Symmetry of magnetic structures: Magnetic structure of chalcopyrite, *Phys. Rev.*, **112**, 1917-1923, 1958.
- Donnay, G., and J. D. H. Donnay, Ewaldite, a new barium calcium carbonate. I. Occurrence of ewaldite in syntactic intergrowth with mackelveyite, *Tschermaks Mineral. Petrogr. Mitt.*, in press, 1970.
- Donnay, G., and D. L. Pawson, X-ray diffraction studies of echinoderm plates, *Science*, **166**, 1147-1150, 1969.
- Donnay, G., and H. Preston, Ewaldite, a new barium calcium carbonate. II. The structure determination, *Tschermaks Mineral. Petrogr. Mitt.*, in press, 1970.
- Duncumb, P., and S. J. B. Reed, The calculation of stopping power and back-scatter effects in electron probe microanalysis, *Nat. Bur. Stand. (U. S.) Spec. Publ.*, **298**, 133-154, 1968.
- Eckermann, H. von, The anorthosite and kenningite of Nordingrån-Rödö region: A contribution to the problem of the anorthosites, *Geol. Fören. Stockholm Förh.*, **60**, 243-284, 1938.
- Elftmann, A. H., Preliminary report of field work during 1893 in northeastern Minnesota, *Geol. Nat. Hist. Surv. Minn.*, **22nd Ann. Rep.**, 141-180, 1893.
- El Goresy, A., and G. Donnay, A new allotropic form of carbon from the Ries Crater, *Science*, **161**, 363-364, 1968. (German translation by El Goresy, A., *Naturwissenschaften*, **56**, 493-494, 1969.)
- Eliseev, E. N., New data on the crystal structure of olivine, *Kristallografiya*, **3**, 167-174, 1958; English translation in *Sov. Phys.-Crystallogr.*, **3**, 163-170, 1958.
- Emslie, R. F., The geology of the Michikamau intrusion, *Geol. Surv. Can. Pap.*, **68-57**, 1970.
- Ernst, W. G., Synthesis, stability relations, and occurrence of riebeckite and riebeckite-arfvedsonite solid solutions, *J. Geol.*, **70**, 689-736, 1962.
- Espenshade, G. H., and D. B. Potter, Kyanite, andalusite, and sillimanite deposits of the southeastern states, *U. S. Geol. Surv. Prof. Pap.*, **336**, 121 pp., 1960.
- Evans, B. W., and J. G. Moore, Mineralogy as a function of depth in the prehistoric Makaopuhi tholeiitic lava lake, Hawaii, *Contrib. Mineral. Petrol.*, **17**, 85-115, 1968.
- Evans, H. T., Jr., R. A. Berner, and C. Milton, Valleriite and mackinawite, *Geol. Soc. Amer. Spec. Pap.*, **73**, 147, 1962.
- Evans, H. T., Jr., C. Milton, E. C. T. Chao, I. Adler, C. Mead, B. Ingram, and R. A. Berner, Valleriite and the new iron sulfide, mackinawite, *U. S. Geol. Surv. Prof. Pap.*, **475-D**, D64-D69, 1964.
- Ewart, A., The petrography of the central North Island rhyolitic lavas, part 2, *N. Z. J. Geol. Geophys.*, **11**, 478-545, 1968.
- Ewart, A., Petrochemistry and feldspar crystallization in the silicic volcanic rocks, central North Island, New Zealand, *Lithos*, **2**, 371-388, 1969.
- Ewart, A., and S. R. Taylor, Trace and minor element geochemistry of the rhyolitic volcanic rocks, central North Island, New Zealand, phenocryst data, *Contrib. Mineral. Petrol.*, **22**, 127-146, 1969.
- Fairbairn, H. W., et al., A cooperative investigation of precision and accuracy in chemical, spectrochemical, and modal analysis of silicate rocks, *U. S. Geol. Surv. Bull.*, **980**, 1951.
- Fawcett, J. J., and H. S. Yoder, Jr., Phase relationships of chlorites in the system  $MgO-Al_2O_3-SiO_2-H_2O$ , *Amer. Mineral.*, **51**, 353-380, 1966.
- Finger, L. W., and C. W. Burnham, Peak-width calculations for equi-inclination goniometry, *Z. Kristallogr.*, **127**, 101-109, 1968.
- Fisher, G. W., and L. G. Medaris, Jr., Cell dimensions and X-ray determinative curve for synthetic Mg-Fe olivines, *Amer. Mineral.*, **54**, 741-753, 1969.
- Frankel, J. J., Chrome-bearing magnetic rocks from the eastern Bushveld, *S. Afr. J. Sci.*, **38**, 152-157, 1942.
- Frarey, M. J., and R. T. Cannon, Notes to accompany a map of the geology of the Proterozoic rocks of Lake Panache-Collins inlet map-areas, Ontario, *Geol. Surv. Can. Pap.*, **68-63**, 1968.
- Freud, P. J., and P. N. LaMori, The effect of pressure on thermoelectric power of thermocouple materials, Symposium on the Accurate Characterization of the High-Pressure Environment, Carnegie Institution of Wash-

- ington-National Bureau of Standards, Gaithersburg, Maryland, October 14-18, 1968, in press, 1970.
- Frey, M., Die Metamorphose des Keupers vom Tafeljura bis zum Lukmanier-Gebiet, *Beitr. Geol. Karte Schweiz, N. F.*, 137, 160 pp., 1969.
- Frondel, C., and C. Klein, Jr., Ureyite,  $\text{NaCrSi}_2\text{O}_6$ : a new meteoritic pyroxene, *Science*, 149, 742-744, 1965.
- Fuchs, L., C. Frondel, and C. Klein, Roedderite, a new mineral from the Indarch meteorite, *Amer. Mineral.*, 51, 949-955, 1966.
- Fuller, R. E., Deuteric alteration controlled by the jointing of lavas, *Amer. J. Sci.*, 35, 161-171, 1938.
- Ganguly, J., Chloritoid stability and related parageneses; theory, experiments, and applications, *Amer. J. Sci.*, 267, 910-944, 1969.
- Gerling, E. K., Yu. D. Pushkarev, and N. V. Kotov, Behavior of certain minerals when heated under conditions of higher argon pressures, *Izv. Akad. Nauk SSSR, Ser. Geol.*, 11, 3-13, 1965.
- Getting, I. C., and G. C. Kennedy, The effect of pressure on the emf of chromel-alumel and platinum-platinum 10% rhodium thermocouples, *J. Appl. Phys.*, 41, 4552-4562, 1970.
- Ghose, S.,  $\text{Mg}^{2+}$ - $\text{Fe}^{2+}$  order in an orthopyroxene  $\text{Mg}_{0.85}\text{Fe}_{1.07}\text{Si}_2\text{O}_6$ , *Z. Kristallogr.*, 122, 81-99, 1965.
- Gibbons, G. S., Optical anisotropy in pyrite, *Amer. Mineral.*, 52, 359-370, 1967.
- Gibson, I. L., and G. P. L. Walker, Some composite rhyolite/basalt lavas and related composite dykes in eastern Iceland, *Proc. Geol. Ass.*, 74, 301-318, 1963.
- Gilbert, M. C., High-pressure stability of acmite, *Amer. J. Sci., Schairer Vol.*, 267A, 145-159, 1969.
- Ginsberg, A. S., and C. S. Nikogosyan, The fusion of diabase and granite, *Bull. Geol. Comm. Leningrad*, 43, 735-765, 1924 [in Russian; French summary].
- Green, D. H., Effects of high pressure on basaltic rock, in *Basalts: The Poldervaart Treatise on Rocks of Basaltic Composition*, Vol. 1, H. H. Hess and A. Poldervaart, ed., Interscience Publishers, New York, 401-443, 1968.
- Green, T. H., High pressure experimental studies on the origin of anorthosite, *Can. J. Earth Sci.*, 6, 427-440, 1969.
- Green, T. H., Experimental fractional crystallization of quartz diorite and its application to the problem of anorthosite origin, *N. Y. State Mus. Sci. Serv. Mem.*, 18, 23-29, 1968.
- Green, T. H., and A. E. Ringwood, High pressure experimental studies on the origin of andesites, *Oreg. Dep. Geol. Miner. Ind. Bull.*, 65, 21-32, 1969.
- Green, T. H., A. E. Ringwood, and A. Major, Friction effects and pressure calibration in a piston-cylinder apparatus at high pressure and temperature, *J. Geophys. Res.*, 71, 3589-3594, 1966.
- Greenwood, H. J., The synthesis and stability of anthophyllite, *J. Petrology*, 4, 317-351, 1963.
- Grout, F. F., Anorthosite and granite as differentiates of a diabase sill on Pigeon Point, Minnesota, *Geol. Soc. Amer. Bull.*, 39, 555-578, 1928.
- Gunning, B. E. S., The greening process in plastids, *Protoplasma*, 60, 111-130, 1965.
- Hafner, S. S., and D. Virgo, Temperature-dependent cation distributions in lunar and terrestrial pyroxenes, in *Proceedings of the Apollo 11 Lunar Science Conference*, Vol. 3, A. A. Levinson, ed., Pergamon Press, New York, 2183-2193, 1970.
- Hägg, G., and A. L. Kindström, X-ray study of the system iron-selenium, *Z. Phys. Chem., Abt. B*, 22, 453-464, 1933.
- Haggerty, S. E., The Fe-Ti minerals of Icelandic basic rocks and their significance in rock magnetism, unpublished Ph.D. thesis, University of London, 1968.
- Haggerty, S. E., F. R. Boyd, P. M. Bell, L. W. Finger, and W. B. Bryan, Iron-titanium oxides and olivine from 10020 and 10071, *Science*, 167, 613-615, 1970a.
- Haggerty, S. E., F. R. Boyd, P. M. Bell, L. W. Finger, and W. B. Bryan, Opaque minerals and olivine in lavas and breccias from *Mare Tranquillitatis*, in *Proceedings of the Apollo 11 Lunar Science Conference*, Vol. 1, A. A. Levinson, ed., Pergamon Press, New York, 513-538, 1970b.
- Haggerty, S. E., and H. O. A. Meyer, Apollo 12: opaque oxides, American Geophysical Union, 51st Annual Meeting, Supplementary Program, 1970.
- Halferdahl, L. B., Chloritoid: its composition, X-ray and optical properties, stability, and occurrence, *J. Petrology* 2, 49-135, 1961.
- Hamilton, W. C., On the isotropic temperature factor equivalent to a given anisotropic temperature factor, *Acta Crystallogr.*, 12, 609-610, 1959.
- Hamilton, W. C., Significance tests on the crystallographic *R* factor, *Acta Crystallogr.*, 13, 502-510, 1965.
- Hanneman, R. E., H. M. Strong, and F. P. Bundy, A critical review of the effect of pressure on thermocouple emf's, Symposium on the Accurate Characterization of the High-Pressure Environment, Carnegie In-

- stitution of Washington-National Bureau of Standards, Gaithersburg, Maryland, October 14-18, 1968, in press, 1970.
- Hargraves, R. B., L. S. Hollister, and G. Otalora, Compositional zoning and its significance in pyroxenes from three coarse-grained lunar samples, *Science*, **167**, 631-633, 1970.
- Harker, A., Notes on a collection of rocks from the Tonga Islands, *Geol. Mag.*, **8**, 250-258, 1891.
- Hays, J. F., Stability and properties of the synthetic pyroxene  $\text{CaAl}_2\text{SiO}_6$ , *Amer. Mineral.*, **51**, 1524-1529, 1969.
- Heath, S. A., and H. W. Fairbairn,  $\text{Sr}^{87}/\text{Sr}^{86}$  ratios in anorthosites and some associated rocks, *N. Y. State Mus. Sci. Serv. Mem.*, **18**, 99-110, 1968.
- Hess, H. H., Stillwater igneous complex, Montana: A quantitative mineralogical study, *Geol. Soc. Amer. Mem.*, **80**, 1960.
- Hoffmeister, J. E., Geology of Eua, Tonga, *Bernice P. Bishop Museum Bull.*, **96**, 1932.
- Hollister, L. S., Origin, mechanism, and consequences of compositional sector-zoning in staurolite, *Amer. Mineral.*, **55**, 742-766, 1970.
- Hollister, L. S., and A. E. Bence, Staurolite: sectoral compositional variations, *Science*, **158**, 1053-1056, 1967.
- Hoschek, G., The stability of staurolite and chloritoid and their significance in metamorphism of pelitic rocks, *Contrib. Mineral. Petrol.*, **22**, 208-232, 1969.
- Hsu, L. C., Selected phase relationships in the system  $\text{Al-Mn-Fe-Si-O-H}$ : a model for garnet equilibria, *J. Petrology*, **9**, 40-83, 1968.
- Huckenholtz, H. G., J. F. Schairer, and H. S. Yoder, Jr., Synthesis and stability of ferri-diopside, *Mineral. Soc. Amer. Spec. Pap.*, **2**, 163-177, 1969.
- Hughes, H., Formation of alkali silicates and aluminosilicates and their occurrence in blast furnaces, *Trans. Brit. Ceram. Soc.*, **65**, 661-679, 1966.
- Ingamells, C. O., A new method for "ferrous iron" and "excess oxygen" in rocks, minerals, and oxides, *Talanta*, **4**, 268-273, 1960.
- International Tables of X-ray Crystallography*, Vol. 1, Kynoch Press, England, 1952.
- Irving E., and J. K. Park, The Mid-Atlantic Ridge near 45°N. Coercivity of remanence and other magnetic properties of dredge samples, *Can. J. Earth Sci.*, in press, 1970.
- Irving, E., W. A. Robertson, and F. Aumento, The Mid-Atlantic Ridge near 45°N. VI. Remanent intensity, susceptibility, and iron content of dredged samples, *Can. J. Earth Sci.*, **7**, 226-238, 1970.
- Ito, J., A new method of decomposition for refractory minerals and its application to the determination of ferrous iron and alkalies, *Sci. Pap. Coll. Gen. Educ., Univ. Tokyo*, **11**, 47-68, 1961.
- Jaeger, J. C., The cooling of irregularly shaped igneous bodies, *Amer. J. Sci.*, **259**, 721-734, 1961.
- Jakes, P., and A. J. R. White, Structure of the Melanesian arcs and correlation with distribution of magma types, *Tectonophysics*, **8**, 223-236, 1969.
- Jambor, J. L., and C. H. Smith, Olivine composition determination with small diameter X-ray powder cameras, *Mineral. Mag.*, **33**, 730-741, 1964.
- Kano, H., High-temperature optics of natural sodic plagioclase, *Mineral. J.*, **1**, 255-277, 1955.
- Karig, D. E., Ridges and basins of the Tonga-Kermadec island arc system, *J. Geophys. Res.*, **75**, 239-254, 1970.
- Kawai, N., Exsolution of titanomagnetite and its time effect on rock-magnetism. III. Effects of enduring temperature and slow cooling. *Proc. Jap. Acad.*, **32**, 464-468, 1956.
- Keil, K., On the phase composition of meteorites, *J. Geophys. Res.*, **67**, 4055-4061, 1962.
- Keil, K., Mineralogical and chemical relationships among enstatite chondrites, *J. Geophys. Res.*, **73**, 6945-6976, 1968.
- Kelsey, C. H., and D. McKie, The unit-cell of aenigmatite, *Mineral. Mag.*, **33**, 986-1001, 1964.
- Kerrick, D. M., Experiments on the upper stability limit of pyrophyllite at 1.8 kb and 3.9 kb water pressure, *Amer. J. Sci.*, **266**, 204-214, 1968.
- Kitayama, K., and T. Katsura, Activity measurements in orthosilicate and metasilicate solid solutions. I.  $\text{Mg}_2\text{SiO}_4$ - $\text{Fe}_2\text{SiO}_4$  and  $\text{MgSiO}_3$ - $\text{FeSiO}_3$  at 1204°C, *Bull. Chem. Soc. Jap.*, **41**, 1146-1151, 1968.
- Köhler, A., Die Abhängigkeit der Plagioklasoptik vom vorangegangenen, *Mineral. Petrogr. Mitt.*, **53**, 24-49, 1941.
- Kouvo, O., Y. Vuorelainen, On valleriite, *Geologi*, **11**, 32-33, 1959.
- Kouvo, O., Y. Vuorelainen, and J. V. P. Long, A tetragonal iron sulfide, *Amer. Mineral.*, **48**, 511-524, 1963.
- Kracek, F. C., the system sodium oxide-silica, *J. Phys. Chem.*, **34**, 1583-1598, 1930a.
- Kracek, F. C., The cristobalite liquidus in alkali oxide-silica systems and the heat of fusion of cristobalite, *J. Amer. Chem. Soc.*, **52**, 1436-1442, 1930b.



- Kranck, S. H., A study of phase equilibria in a metamorphic iron formation, *J. Petrology*, **2**, 137-184, 1961.
- Krumbein, W. C., and F. Graybill, Evaluation of the "strength" of a trend, in *An Introduction to Statistical Models in Geology*, McGraw-Hill Book Co., Inc., New York, 333-337, 1965.
- Kullerud, G., Covellite stability relations in the Cu-S system, *Freiberg. Forschungsh.*, **C**, 186, 145-160, 1965.
- Kuno, H., Ion substitution in the diopside-ferropigeonite series of clinopyroxenes, *Amer. Mineral.*, **40**, 70-93, 1955.
- Kushiro, I., Si-Al relation in clinopyroxenes from igneous rocks, *Amer. J. Sci.*, **258**, 548-554, 1960.
- Kushiro, I., Compositions of magmas formed by partial zone melting of the earth's upper mantle, *J. Geophys. Res.*, **73**, 619-634, 1968.
- Kushiro, I., Clinopyroxene solid solutions formed by reactions between diopside and plagioclase at high pressures, *Mineral. Soc. Amer. Spec. Pap.*, **2**, 179-191, 1969a.
- Kushiro, I., The system forsterite-diopside-silica with and without water at high pressures, *Amer. J. Sci.*, **267A**, 269-294, 1969b.
- Kushiro, K., Y. Nakamura, and S. Akimoto, Crystallization of Cr-Ti spinel solid solutions in an Apollo 12 rock, and source rock of magmas of Apollo 12 rocks (abstract), American Geophysical Union, 51st Annual Meeting, Supplementary Program, 1970.
- Kushiro, I., Y. Nakamura, and H. Haramura, Crystallization of some lunar mafic magmas and generation of rhyolitic liquid, *Science*, **167**, 610-612, 1970.
- Kushiro, I., Y. Nakamura, H. Haramura, and S. Akimoto, Crystallization of some lunar mafic magmas and generation of rhyolitic liquid, *Science*, **167**, 610-612, 1970.
- Kushiro, I., Y. Syono, and S. Akimoto, Melting of a peridotite nodule at high pressures and high water pressures, *J. Geophys. Res.*, **73**, 6023-6029, 1968.
- Kushiro, I., and H. S. Yoder, Jr., Anorthite-forsterite and anorthite-enstatite reactions and their bearing on the basalt-eclogite transformation, *J. Petrol.*, **7**, 337-362, 1966.
- Lacroix, A., Composition minéralogique et chimique des laves des volcans des îles de l'Océan Pacifique situées entre l'Équateur et le tropique du Capricorne, le 175° de longitude ouest et le 165° de longitude est, *Mem. Acad. Sci. Paris*, **63**, 1-97, 1939.
- Larson, E. E., Mitake Ozima, Minoru Ozima, T. Nagata, and D. Strangway, Stability of remanent magnetization, *Geophys. J. Roy. Astron. Soc.*, **17**, 263-292, 1969.
- Laspeyres, H., Die steinigen Gemengtheile im Meteoriten von Toluca in Mexico, *Z. Kristallogr.*, **27**, 586-600, 1897.
- Laughlin, A. W., Excess radiogenic argon in pegmatite minerals, *J. Geophys. Res.*, **74**, 6684-6690, 1969a.
- Laughlin, A. W., Excess radiogenic argon in pegmatite minerals, Ph.D. thesis, University of Arizona, 1969b.
- LeBas, M. J., The role of aluminum in igneous clinopyroxenes with relation to their parentage, *Amer. J. Sci.*, **260**, 267-288, 1962.
- Legg, C. A., Some chromite-ilmenite associations in the Merensky Reef, Transvaal, *Amer. Mineral.*, **54**, 1347-1354, 1969.
- Lindsley, D. H., Geology of the Spray quadrangle, Oregon; with special emphasis on the petrography and magnetic properties of the Picture Gorge basalt, Ph.D. thesis, The Johns Hopkins University, 1960.
- Lindsley, D. H., Melting relations of plagioclase at high pressures, in "Origin of Anorthosite and Related Rocks," *N. Y. State Museum Sci. Serv. Mem.*, **18**, 39-46, 1968.
- Lindsley, D. H., G. M. Brown, and I. D. Muir, Conditions of the ferrowollastonite-ferrohedenbergite inversion in the Skaergaard intrusion, east Greenland, *Mineral. Soc. Amer. Spec. Pap.*, **2**, 193-201, 1969.
- Lindsley, D. H., B. T. C. Davis, and I. D. MacGregor, Ferrosilite (FeSiO<sub>3</sub>) synthesis at high pressures and temperatures, *Science*, **144**, 73-74, 1964.
- Lindsley, D. H., S. E. Haggerty, and D. Smith, Occurrence of aenigmatite in differentiated basalt (abstract), *Trans. Amer. Geophys. Union*, **51**, 435, 1970.
- Lindsley, D. H., and J. L. Munoz, Subsolidus relations along the join hedenbergite-ferrosilite, *Amer. J. Sci.*, *Schäfer Vol.*, **267A**, 295-324, 1969.
- Lister, J. J., Notes on the geology of the Tonga Islands, *Quart. J. Geol. Soc. London*, **47**, 590-617, 1891.
- Livingston, D. E., P. E. Damon, R. L. Mauger, R. Bennett, and A. W. Laughlin, Argon-40 in cogenetic feldspar-mica mineral assemblages, *J. Geophys. Res.*, **72**, 1361-1375, 1967.
- Louisenathan, S. J., and J. V. Smith, Cell dimensions of olivine, *Mineral. Mag.*, **36**, 1123-1134, 1968.
- Lunar Sample Preliminary Examination Team, Preliminary examination of the lunar samples from Apollo 11, *Science*, **165**, 1211-1227, 1969.
- Lunar Sample Preliminary Examination Team, Preliminary examination of lunar samples from Apollo 12, *Science*, **167**, 1325-1339, 1970.

- Luth, W. C., R. H. Jahns, and O. F. Tuttle, The granite system at pressures of 4 to 10 kb, *J. Geophys. Res.*, **69**, 759-773, 1964.
- Macdonald, G. A., and T. Katsura, Chemical composition of Hawaiian lavas, *J. Petrology*, **5**, 82-133, 1964.
- Matsui, Y., Y. Maeda, and Y. Syono, The Mössbauer study of synthetic calcium-rich pyroxenes, *Techn. Rep. Inst. Solid State Phys., Univ. Tokyo, Ser. A*, no. 400, 1969.
- May, I., and J. J. Rowe, Solution of rocks and refractory minerals by acids at high temperatures and pressures, *Anal. Chim. Acta*, **33**, 648-654, 1965.
- Medaris, L. G., Jr., Partitioning of Fe<sup>2+</sup> and Mg<sup>2+</sup> between coexisting synthetic olivine and orthopyroxene, *Amer. J. Sci.*, **267**, 945-968, 1969.
- Melson, W. G., E. Jarosewich, and C. A. Lundquist, 1967-1968 Eruption of Metis shoal, Tonga: description and petrology, *Smithson. Contrib. Earth Sci.*, in press, 1970.
- Mendez, J., and F. J. Stevenson, Reductive cleavage of humic acids with sodium amalgam, *Soil Sci.*, **102**, 85-93, 1966.
- Merwin, H. E., and R. H. Lombard, The system, Cu-Fe-S, *Econ. Geol.*, **32**, 203-284, 1937.
- Meyer, H. O. A., Chrome pyrope: an inclusion in natural diamond, *Science*, **160**, 1446-1447, 1968.
- Miesch, A. T., The constant sum problem in geochemistry, in *Computer Applications in the Earth Sciences*, Plenum Press, New York, 161-176, 1969.
- Milton, C., and D. J. Milton, Nickel-gold ore of the Mackinaw mine, Snohomish County, Washington, *Econ. Geol.*, **53**, 426-447, 1958.
- Moore, J. G., and B. W. Evans, The role of olivine in the crystallization of the prehistoric Makaopuhi tholeiitic lava lake, Hawaii, *Contrib. Mineral. Petrol.*, **15**, 202-223, 1967.
- Morey, G. W., and N. L. Bowen, The ternary system sodium metasilicate-calcium metasilicate-silica, *J. Soc. Glass Technol.*, **9**, 226-264, 1925.
- Morey, G. W., and E. D. Williamson, Pressure-temperature curves in monovariant systems, *J. Amer. Chem. Soc.*, **40**, 59-84, 1918.
- Morimoto, N., and N. Güven, Refinement of the crystal structure of pigeonite, *Amer. Mineral.*, **55**, 1195-1209, 1970.
- Morse, S. A., The Kiglapait layered intrusion, Labrador, *Geol. Soc. Amer. Mem.*, **112**, 1969.
- Muan, A., Determination of thermodynamic properties of silicates from locations of conjugation lines in ternary systems, *Amer. Mineral.*, **52**, 797-804, 1967.
- Muehlenbachs, K., and R. N. Clayton, O<sup>18</sup>/O<sup>16</sup> studies of fresh and weathered submarine basalts (abstract), *Trans. Amer. Geophys. Union*, **51**, 444, 1970.
- Muir, I. D., Crystallization of pyroxenes in an iron-rich diabase from Minnesota, *Mineral. Mag.*, **30**, 376-388, 1954.
- Muir, I. D., and C. E. Tilley, Iron enrichment and pyroxene fractionation in tholeiites, *Geol. J.*, **4**, 143-156, 1964.
- Munson, R. A., The synthesis of copper disulfide, *Inorg. Chem.*, **5**, 1296-1297, 1966.
- Nafziger, R. H., and A. Muan, Equilibrium phase compositions and thermodynamic properties of olivines and pyroxenes in the system MgO-FeO-SiO<sub>2</sub>, *Amer. Mineral.*, **52**, 1364-1385, 1967.
- Náray-Szabó, I., and K. Sasvári, On the structure of staurolite, *Acta Crystallogr.*, **11**, 862-865, 1958.
- Nash, W. P., I. S. E. Carmichael, and R. W. Johnson, The mineralogy and petrology of Mount Suswa, Kenya, *J. Petrology*, **10**, 409-439, 1969.
- Navrotsky, A., and A. Muan, Activity-composition relations in the systems CoO-ZnO and NiO-ZnO at 1050°C, *J. Inorg. Nucl. Chem.*, in press, 1970.
- Néel, L., Some theoretical aspects of rock magnetism, *Advan. Phys.*, **4**, 191-243, 1955.
- Neuhaus, A., Über Kosmochlor (Ureyit), *Int. Mineral. Ass. Symposia (Cambridge, England)*, 329-333, 1966.
- Neuhaus, A., C. Ballhausen, H. J. Meyer, and R. Steffen, Arbeiten und Betrachtungen sur Synthese und Kristallchemie anorganischer Verbindungen bei hohen Drücken und Temperaturen, *Jahrb. Landesamtes Forsch. Landes Nordrhein-Westfalen*, 487-548, 1965.
- Newton, M. S., and G. C. Kennedy, Jadeite, analcite, nepheline, and albite at high temperatures and pressures, *Amer. J. Sci.*, **266**, 728-735, 1968.
- Newton, R. C., The thermal stability of zoisite, *J. Geol.*, **73**, 431-441, 1965.
- Nicholls, J., and I. S. E. Carmichael, Peralkaline acid liquids: a petrologic study, *Contrib. Mineral. Petrol.*, **20**, 268-294, 1969.
- Nixon, P. H., and G. Horning, A new chromium garnet end member, knorringite, from kimberlite, *Amer. Mineral.*, **53**, 1833-1840, 1968.
- Nolan, J., Physical properties of synthetic and natural pyroxenes in the system diopside-hedenbergite-aegirite, *Mineral. Mag.*, **37**, 216-229, 1969.
- Nolan, J., and A. D. Edgar, An X-ray investigation of synthetic pyroxenes in the system aegirite-diopside-water at 100 kg/cm<sup>2</sup> water-vapour pressure, *Mineral. Mag.*, **33**, 625-634, 1963.

- O'Hara, M. J., Primary magmas and the origin of basalts, *Scot. J. Geol.*, **1**, 19-40, 1965.
- O'Hara, M. J., The bearing of phase-equilibria studies in the synthetic and natural systems on the origin and evolution of basic and ultrabasic rocks, *Earth-Sci. Rev.*, **4**, 69-133, 1968.
- O'Hara, M. J., G. M. Biggar, and S. W. Richardson, Experimental petrology of lunar materials: the nature of mascons, seas, and the lunar interior, *Science*, **167**, 605-607, 1970.
- O'Hara, M. J., and H. S. Yoder, Jr., Formation and fractionation of basic magmas at high pressures, *Scot. J. Geol.*, **3**, 67-117, 1967.
- Onken, H., Verfeinerung der Kristallstruktur von Monticellit, *Tschermak's Mineral. Petrogr. Mitt.*, **10**, 34-44, 1965.
- Opdyke, N. D., and R. Hekinian, Magnetic properties of some igneous rocks from the Mid-Atlantic Ridge, *J. Geophys. Res.*, **72**, 2257-2260, 1967.
- O'Reilly, W., and S. K. Banerjee, Cation distribution in titanomagnetites ( $1-x$ )  $\text{Fe}_3\text{O}_4$ - $x\text{Fe}_2\text{TiO}_4$ , *Phys. Lett.*, **17**, 237-238, 1965.
- Osborn, E. F., and A. Muan, Phase-equilibrium diagrams of oxide systems. Plate 10. The system  $\text{CaO}$ - $\text{Fe}_2\text{O}_3$ - $\text{SiO}_2$ , American Ceramic Society, Columbus, Ohio, 1960.
- Pauling, L., and L. O. Brockway, The crystal structure of chalcopyrite,  $\text{CuFeS}_2$ , *Z. Kristallogr.*, **82**, 188-194, 1932.
- Poldervaart, A., The petrology of the Elephant's Head dike and the New Amalfi sheet (Matatiele), *Trans. Roy. Soc. S. Afr.*, **30**, 85-119, 1944.
- Presnall, D. C., The geometrical analysis of partial fusion, *Amer. J. Sci.*, **267**, 1178-1194, 1969.
- Prewitt, C. T., J. J. Papike, and A. E. Bence, Apollo 12 clinopyroxenes: Crystal chemistry and phase transitions, American Geophysical Union, 51st Annual Meeting, Supplementary Program, 1970.
- Prigogine, I., and R. Defay, *Chemical Thermodynamics*, Longmans, Green, and Co., Ltd., London, 1954.
- Ramdohr, P., *Die Erzminerale und ihre Verwachsungen*, Akademie-Verlag, Berlin, 2nd ed., 1960.
- Ramdohr, P., The opaque minerals in stony meteorites, *J. Geophys. Res.*, **68**, 2011-2036, 1963.
- Ramdohr, P., Chromite and chromite chondrules in meteorites, I, *Geochim. Cosmochim. Acta*, **31**, 1961-1967, 1967.
- Ramdohr, P., and A. El Goresy, Opaque minerals of the lunar rocks and dust from *Mare Tranquillitatis*, *Science*, **167**, 615-618, 1970.
- Reed, S. J. B., Characteristic fluorescence corrections in electron-probe microanalysis, *Brit. J. Appl. Phys.*, **16**, 913-926, 1965.
- Reid, A. M., C. Meyer, Jr., R. S. Harmon, P. Butler, Jr., and R. Brett, Metal in two Apollo 12 igneous rocks (abstract), American Geophysical Union, 51st Annual Meeting, Supplementary Program, 1970.
- Richards, A. F., Transpacific distribution of floating pumice from Isla San Benedicto, Mexico, *Deep-Sea Res.*, **5**, 29-35, 1958.
- Richardson, S. W., Staurolite stability in a part of the system  $\text{Fe-Al-SiO}_2\text{-H}_2\text{O}$ , *J. Petrology*, **9**, 467-488, 1968.
- Richardson, S. W., P. M. Bell, and M. C. Gilbert, Kyanite-sillimanite equilibrium between 700° and 1500°, *Amer. J. Sci.*, **266**, 513-541, 1968.
- Ringwood, A. E., Melting relationships of Ni-Mg olivines and some geochemical implications, *Geochim. Cosmochim. Acta*, **10**, 297-303, 1956.
- Ringwood, A. E., and E. Essene, Petrogenesis of lunar basalts and the internal constitution and origin of the moon, *Science*, **167**, 607-610, 1970.
- Robie, R. A., and D. R. Waldbaum, Thermodynamic properties of minerals and related substances at 298.15°K (25.0°C) and 1 atmosphere (1.013 bars) pressure and at higher temperatures, *U. S. Geol. Surv. Bull.*, **1259**, 256 pp., 1968.
- Robinson, P. W., H. W. Jaffe, C. Klein, and M. Ross, Equilibrium coexistence of three amphiboles, *Contrib. Mineral. Petrol.*, **22**, 248-258, 1969.
- Roedder, E. W., The system  $\text{K}_2\text{O-MgO-SiO}_2$ , *Amer. J. Sci.*, **249**, 81-130, 224-248, 1951.
- Ross, C. S., D. M. Foster, and A. T. Myers, Origin of dunites and of olivine-rich inclusions in basaltic rocks, *Amer. Mineral.*, **39**, 693-737, 1954.
- Ross, M., A. E. Bence, E. J. Dwornik, J. R. Clark, J. J. Papike, Lunar clinopyroxenes: Chemical composition, structural state, and texture, *Science*, **167**, 628-630, 1970.
- Saleuddin, A. S. M., and P. E. Hare, Amino acid compositions of normal and regenerated shells of *Helix*, *Can. J. Zool.*, **48**, in press, 1970.
- Sato, M., and T. L. Wright, Oxygen fugacities directly measured in magmatic gases, *Science*, **153**, 1103-1105, 1966.
- Saxena, S. K., and S. Ghose, Mg-Fe distribution isotherms at 500 and 800°C in orthopyroxenes (abstract), *Trans. Amer. Geophys. Union*, **51**, 436, 1970.
- Seatchard, G., The calculation of the compositions of phases in equilibrium, *J. Amer. Chem. Soc.*, **62**, 2426-2429, 1940.



- Schaeffer, R. M., and E. J. Schwarz, The Mid-Atlantic Ridge near 45°N. IX. Thermomagnetism of dredged samples of igneous rocks, *Can. J. Earth Sci.*, **7**, 268-273, 1970.
- Schairer, J. F., Melting relations of the common rock-forming oxides, *J. Amer. Ceram. Soc.*, **40**, 215-235, 1957.
- Schairer, J. F., and N. L. Bowen, The binary system  $\text{CaSiO}_3$ -diopside and the relations between  $\text{CaSiO}_3$  and akermanite, *Amer. J. Sci.*, **240**, 725-742, 1942.
- Schilling, J. G., and J. W. Winchester, Rare earth contribution to the origin of Hawaiian lavas, *Contrib. Mineral. Petrol.*, **23**, 27-37, 1969.
- Schmincke, H.-U., *Petrologie der Phonolithischen bis Rhyolitischen Vulkanite auf Gran Canaria, Kanarische Inseln*, Ruprecht-Karl Universität zu Heidelberg, 1969.
- Schreyer, W., and G. A. Chinner, Staurolite-quartzite bands in kyanite quartzite at Big Rock, Rio Arriba County, New Mexico, *Contrib. Mineral. Petrol.*, **12**, 223-244, 1966.
- Schreyer, W., and J. F. Schairer, Metastable osumilite- and petalite-type phases in the system  $\text{MgO-Al}_2\text{O}_3\text{-SiO}_2$ , *Amer. Mineral.*, **47**, 90-104, 1962.
- Schreyer, W., and F. Seifert, High-pressure phases in the system  $\text{MgO-Al}_2\text{O}_3\text{-SiO}_2\text{-H}_2\text{O}$ , *Amer. J. Sci.*, *Schairer Vol.*, **267A**, 407-443, 1969.
- Slater, J. G., and H. W. Menard, Topography and heat flow of the Fiji plateau, *Nature*, **216**, 991-993, 1967.
- Scott, A., Augite from Bail Hill, Dumfriesshire, *Mineral. Mag.*, **17**, 100-110, 1914.
- Serson, P. H., and W. L. W. Hannaford, A statistical analysis of magnetic profiles, *J. Geophys. Res.*, **62**, 1-18, 1957.
- Shand, S. J., *Eruptive Rocks*, Murby and Co., London, 2nd ed., 1943.
- Shannon, R. D., and C. T. Prewitt, Effective ionic radii in oxides and fluorides, *Acta Crystallogr., Sect. B*, **25**, 925-946, 1969.
- Simpson, P. R., and S. H. V. Bowie, Quantitative optical and electron-probe studies of the opaque phases, *Science*, **167**, 619-621, 1970.
- Skinner, B. J., High crystallization temperatures indicated for igneous rocks from Tranquillity Base, *Science*, **167**, 652-654, 1970.
- Smith, D., and D. H. Lindsley, Stable and metastable augite crystallization trends in a single basalt flow, *Amer. Mineral.*, in press, 1970.
- Smith, J. V., The crystal structure of staurolite, *Amer. Mineral.*, **53**, 1139-1155, 1968.
- Smith, P. J., The intensity of the ancient geomagnetic field: a review and analysis, *J. Geophys. Res.*, **12**, 321-362, 1967.
- Southwick, D. L., Mineralogy of a rutile- and apatite-bearing ultramafic chlorite rock, Hartford Co., Maryland, *U. S. Geol. Surv. Prof. Pap.*, **600-C**, C8-C44, 1968.
- Speidel, D. H., Effect of  $\text{MgO}$  on hematite-ilmenite magnetite-ulvöspinel equilibria (abstract), *Trans. Amer. Geophys. Union*, **48**, 225, 1967.
- Stephenson, A., The temperature dependent cation distribution in titanomagnetites, *Geophys. J. Roy. Astron. Soc.*, **18**, 119-210, 1969.
- Stevenson, F. J., and J. H. A. Butler, Chemistry of humic acids and related pigments, in *Organic Geochemistry: Methods and Results*, G. Eglinton and M. T. J. Murphy, ed., Springer-Verlag, New York, 534-557, 1969.
- Strong, D. F., Formation of the hour-glass structure in augite, *Mineral. Mag.*, **37**, 472-479, 1969.
- Sykes, L. R., The seismicity and deep structure of island arcs, *J. Geophys. Res.*, **71**, 2981-3006, 1966.
- Taylor, L. A., G. Kullerud, and W. B. Bryan, Apollo 12 sample 12063.9 (abstract), American Geophysical Union, 51st Annual Meeting, Supplementary Program, 1970.
- Taylor, R. W., Phase equilibria in the system  $\text{FeO-Fe}_2\text{O}_3\text{-TiO}_2$  at 1300°C, *Amer. Mineral.*, **49**, 1016-1030, 1964.
- Taylor, S. R., A. C. Capp, A. L. Graham, and D. H. Blake, Trace element abundances in andesites. II. Saipan, Bougainville, and Fiji, *Contrib. Mineral. Petrol.*, **23**, 1-26, 1969.
- Thayer, T. P., Preliminary chemical correlation of chromite with the containing rocks, *Econ. Geol.*, **41**, 202-217, 1946.
- Thompson, J. B., Jr., The graphical analysis of mineral assemblages in pelitic schists, *Amer. Mineral.*, **42**, 842-858, 1957.
- Thompson, J. B., Jr., Thermodynamic properties of simple solutions, in *Researches in Geochemistry*, Vol. 2, P. H. Abelson, ed., John Wiley and Sons, Inc., New York, 340-361, 1967.
- Thompson, J. B., Jr., Chemical reactions in crystals, *Amer. Mineral.*, **54**, 341-375, 1969.
- Thompson, J. B., Jr., Chemical reactions in crystals: corrections and clarification, *Amer. Mineral.*, **55**, 528-532, 1970.
- Thompson, J. B., Jr., and S. A. Norton, Paleozoic regional metamorphism in New England and adjacent areas, in *Studies of Appalachian Geology*, E-an Zen et al., eds., John Wiley and Sons, Inc., New York, 319-327, 1968.
- Thompson, J. B., Jr., P. Robinson, T. N. Clifford, and N. J. Trask, Nappes and gneiss domes in west-central New England, in *Studies of Appalachian Geology*, E-an Zen

- et al., eds., John Wiley and Sons, Inc., New York, 203-218, 1968.
- Thompson, J. B., Jr., and D. R. Waldbaum, Mixing properties of sanidine crystalline solutions: I. Calculations based on ion-exchange data, *Amer. Mineral.*, **53**, 1965-1999, 1968.
- Thompson, J. B., Jr., and D. R. Waldbaum, Analysis of the two-phase region halite-sylvite in the system NaCl-KCl, *Geochim. Cosmochim. Acta*, **33**, 671-690, 1969.
- Thompson, R. N., and J. E. Chisholm, Synthesis of aenigmatite, *Mineral. Mag.*, **37**, 253-255, 1969.
- Tilley, C. E., Some aspects of magmatic evolution, *Quart. J. Geol. Soc. London*, **106**, 37-61, 1950.
- Tilley, C. E., and I. D. Muir, The Hebridean plateau magma type, *Trans. Edinburgh Geol. Soc.*, **19**, 208-215, 1962.
- Toulmin, P., III, and P. B. Barton, Jr., A thermodynamic study of pyrite and pyrrhotite, *Geochim. Cosmochim. Acta*, **28**, 641-671, 1964.
- Tuttle, O. F., and N. L. Bowen, Origin of granite in the light of experimental studies in the system  $\text{NaAlSi}_3\text{O}_8\text{-KAlSi}_3\text{O}_8\text{-SiO}_2\text{-H}_2\text{O}$ , *Geol. Soc. Amer. Mem.*, **74**, 1958.
- Tyrrell, G. W., On some dolerite-sills containing analcite-syenite in central Ayrshire, *Quart. J. Geol. Soc. London*, **84**, 540-569, 1928.
- Van der Kaaden, G., Optical studies on natural plagioclase feldspars with high and low temperature optics, Pub. van het Min. Geol. Inst. Ryks, Univ. Utrecht, Holland, 1951.
- Van Schmus, W. R., The mineralogy and petrology of chondrite meteorites, *Earth-Sci. Rev.*, **5**, 145-184, 1969.
- Van Schmus, W. R., and J. A. Wood, A chemical-petrologic classification for the chondritic meteorites, *Geochim. Cosmochim. Acta*, **31**, 747-765, 1967.
- Vdovykin, G. P., A new hexagonal modification of carbon in meteorites [in Russian], *Geokhimiya*, no. 9, 1145-1148, 1969.
- Verhoogen, J., Oxidation of iron-titanium oxides in igneous rocks, *J. Geol.*, **70**, 168-181, 1962a.
- Verhoogen, J., Distribution of titanium between silicates and oxides in igneous rocks, *Amer. J. Sci.*, **260**, 211-220, 1962b.
- Vincent, E. A., J. B. Wright, R. Chevallier, and S. Mathieu, Heating experiments on some natural titaniferous magnetites, *Mineral. Mag.*, **31**, 624-655, 1957.
- Virgo, D., and S. S. Hafner,  $\text{Fe}^{2+}$ -Mg order-disorder in heated orthopyroxenes, *Mineral. Soc. Amer. Spec. Pap.*, **2**, 67-81, 1969.
- Wager, L. R., and G. M. Brown, *Layered Igneous Rocks*, Oliver and Boyd, Ltd., London, 1968.
- Waldbaum, D. R., and J. B. Thompson, Jr., Mixing properties of sanidine crystalline solutions: II. Calculations based on volume data, *Amer. Mineral.*, **53**, 2000-2017, 1968.
- Walker, G. P. L., The amygdale minerals in the Tertiary lavas of Ireland. I. The distribution of chabazite habits and zeolites in the Garron plateau area, County Antrim, *Mineral. Mag.*, **29**, 773-791, 1951.
- Wanless, R. K., R. D. Stevens, G. R. Lachance, and C. M. Edmunds, Age determinations and geological studies, *Geol. Surv. Can. Pap.*, **67-2A**, 140-141, 1967.
- Waters, A. C., Stratigraphic and lithologic variations in the Columbia River basalt, *Amer. J. Sci.*, **259**, 583-611, 1961.
- Watkins, N. D., and S. E. Haggerty, Primary oxidation variation and petrogenesis in a single lava, *Contrib. Mineral. Petrol.*, **15**, 251-271, 1967.
- Webster, A. H., and N. F. H. Bright, The system Fe-Ti-O at 1200°C and oxygen partial pressures between 1 atm and  $2 \cdot 10^{-4}$  atm, *J. Amer. Ceram. Soc.*, **44**, 110-116, 1961.
- Weill, D. F., I. S. McCallum, Y. Bottinga, M. J. Drake, and G. A. McKay, Petrology of a fine-grained igneous rock from the Sea of Tranquillity, *Science*, **167**, 635-638, 1970.
- Wheeler, E. P., Fayalitic olivine in northern Newfoundland-Labrador, *Can. Mineral.*, **8**, 339-346, 1965.
- Wheeler, E. P., Minor intrusives associated with the Nain anorthosite, *N. Y. State Museum Sci. Serv. Mem.*, **18**, 189-206, 1968.
- Whittaker, A. G., and P. L. Kintner, Carbon: Observations on the new allotropic form, *Science*, **165**, 589-591, 1969.
- Williams, D. W., and G. C. Kennedy, Melting curve of diopside to 50 kb, *J. Geophys. Res.*, **74**, 4359-4366, 1969.
- Williams, R. J., Reaction constants in the system Fe-Mg-O-SiO<sub>2</sub> between 1300° and 900° at one atmosphere: theory, experiment, and application, Ph.D. thesis, The Johns Hopkins University, 1970.
- Williamson, J., and F. P. Glasser, Phase relations in the system  $\text{Na}_2\text{Si}_2\text{O}_7\text{-SiO}_2$ , *Science*, **148**, 1589-1591, 1965.
- Williamson, J., and F. P. Glasser, The crystallization of  $\text{Na}_2\text{O} \cdot 2\text{SiO}_2\text{-SiO}_2$  glasses, *Phys. Chem. Glasses*, **7**, 127-138, 1966.
- Wilson, R. L., and S. E. Haggerty, Reversals of the earth's magnetic field, *Endeavour*, **25**, 104-109, 1966.
- Wones, D. R., and M. C. Gilbert, The fayalite-magnetite-quartz assemblage between 600°

- and 800°C, *Amer. J. Sci., Schairer Vol.*, 267A, 480-488, 1969.
- Wood, J. A., J. S. Dickey, U. B. Marvin, and B. N. Powell, Lunar anorthosites, *Science*, 167, 602-604, 1970.
- Yagi, K., The system acmite-diopside and its bearing on the stability relations of natural pyroxenes of the acmite-hedenbergite-diopside series, *Amer. Mineral.*, 51, 976-1000, 1966.
- Yagi, K., and K. Onuma, The join  $\text{CaMgSi}_2\text{O}_6\text{-CaTiAl}_2\text{O}_6$  and its bearing on the titanagites, *J. Fac. Sci. Hokkaido Univ., Ser. 4*, 13, 463-483, 1967.
- Yoder, H. S., Jr., Stability relations of grossularite, *J. Geol.*, 58, 221-253, 1950.
- Yoder, H. S., Jr., Change of melting point of diopside with pressure, *J. Geol.*, 60, 364-374, 1952.
- Yoder, H. S., Jr., Role of water in metamorphism, *Geol. Soc. Amer. Spec. Pap.*, 62, 505-524, 1955.
- Yoder, H. S., Jr., Calcalkalic andesites: experimental data bearing on the origin of their assumed characteristics, *Oreg. Dep. Geol. Miner. Ind. Bull.*, 65, 77-89, 1969.
- Yoder, H. S., and Th. G. Sahama, Olivine X-ray determinative curve, *Amer. Mineral.*, 42, 475-491, 1957.
- Yoder, H. S., Jr., and C. E. Tilley, Origin of basaltic magmas: An experimental study of natural and synthetic rock systems, *J. Petrology*, 3, 342-532, 1962.
- York, D., A. K. Baski, and F. Aumento, K-Ar dating of basalts dredged from the North Atlantic (abstract), *Trans. Amer. Geophys. Union*, 50, 353, 1969.
- Yund, R. A., and G. Kullerud, Stable mineral assemblages of anhydrous copper and iron oxides, *Amer. Mineral.*, 49, 689-696, 1964.
- Yund, R. A., and G. Kullerud, Thermal stability of assemblages in the Cu-Fe-S system, *J. Petrology*, 7, 454-488, 1966.
- Zachariasen, W. H., Experimental tests of the general formula for the integrated intensity of a real crystal, *Acta Crystallogr., Sect. A*, 24, 212-216, 1968.
- Zen, E-an, Free energy of formation of pyrophyllite from hydrothermal data: Values, discrepancies, and implications, *Amer. Mineral.*, 54, 1592-1606, 1969.
- Zvyagin, B. B., and Z. G. Pinsker, Electronographic determination of the elementary cells of pyrophyllite and talc, and their structural relations to montmorillonite, *Dokl. Akad. Nauk SSSR*, 68, 505-508, 1949.

## PERSONNEL

### Scientific Staff

*Director:* P. H. Abelson  
*Emeritus Research Associate:* E. G. Zies, Chemist  
*Physical Chemists:* F. R. Boyd, T. C. Hoering,<sup>1</sup> J. F. Schairer  
*Petrologists:* F. Chayes, D. H. Lindsley, H. S. Yoder, Jr.  
*Geochemists:* G. L. Davis, T. E. Krogh, G. Kullerud  
*Organic Geochemist:* P. E. Hare  
*Geophysicist:* P. M. Bell  
*Physicist:* J. L. England  
*Crystallographers:* Gabrielle Donnay, L. W. Finger<sup>2</sup>  
*Fellows:* W. B. Bryan, University of Queens-

land, Brisbane, Australia; R. M. Cassie, State University College at Brockport, N. Y.;<sup>3</sup> S. E. Haggerty, Imperial College of Science and Technology, University of London, England; A. W. Hofmann, Brown University;<sup>4</sup> H. G. Huckenholz, University of Munich, Germany;<sup>5</sup> H. K. Mao, University of Rochester; H. O. A. Meyer, University College, London;<sup>6</sup> H. R. Puchelt, University of Tübingen, Germany;<sup>7</sup> D. Rumble, Harvard University;<sup>3</sup> D. Smith, California Institute of Technology; L. A. Taylor, Lehigh University; W. Viane, University of Louvain, Belgium;<sup>4</sup> J. F. Wehmler, Lamont-Doherty Geological Observatory.<sup>2</sup>

<sup>1</sup>On leave of absence at Space Sciences Laboratory, University of California, Berkeley, through August 31, 1969.

<sup>2</sup>Appointment from July 1, 1969.

<sup>3</sup>Appointment from September 1, 1969.

<sup>4</sup>Appointment from April 1, 1970.

<sup>5</sup>Appointment from September 1 through November 30, 1969.

<sup>6</sup>Appointment terminated August 1, 1969, to accept position as Senior Resident Research Associate, NASA Goddard Space Flight Center, Greenbelt, Maryland.

<sup>7</sup>Appointment from March 15 through April 30, 1970.



*Guest Investigators:* M. Bird, U. S. Geological Survey; K. L. Cameron, Virginia Polytechnic Institute; Maryellen Cameron, Virginia Polytechnic Institute; J. D. H. Donnay, Johns Hopkins University; E. Dowty, U. S. Geological Survey; R. F. Emslie, Geological Survey of Canada; L. K. Fink, Jr., University of Maine; M. C. Gilbert, Virginia Polytechnic Institute; K. King, Lamont-Doherty Geological Observatory; A. Long, University of Arizona; N. D. MacRae, University of Western Ontario; H. O. A. Meyer, NASA Goddard Space Flight Center; A. Muan, Pennsylvania State University; W. Salomons, State University, Groningen, Netherlands; Judy Sever, University of Texas at Port Aransas; A. Shinyayev, Soviet Academy of Sciences, Baikov Institute of Metallurgy, Moscow; A. C. Turnock, University of Manitoba.

### *Operating and Maintenance Staff*

*Executive Officer:* A. D. Singer  
*Accountant:* C. B. Petry  
*Editor and Librarian:* Dolores M. Thomas  
*Stenographers:* Patricia S. Hart (née Garrett), Marjorie E. Imlay  
*Clerk:* H. J. Lutz  
*Electronic Technician:* C. G. Hadidiacos  
*Research Assistants:* J. F. Kocmanek, W. D. Stanbro<sup>\*</sup>  
*Chief Mechanician:* F. A. Rowe  
*Instrument Makers:* C. A. Batten, L. C. Garver, W. H. Lyons, G. E. Speicher  
*Mechanic and Carpenter:* E. J. Shipley  
*Machinists:* W. R. Reed, J. R. Thomas  
*Building Engineer:* H. L. Moore  
*Mechanic's Helper:* M. Ferguson  
*Janitor:* L. B. Patrick

<sup>\*</sup> Appointment on a part-time basis through June 19, 1970.

PLATES





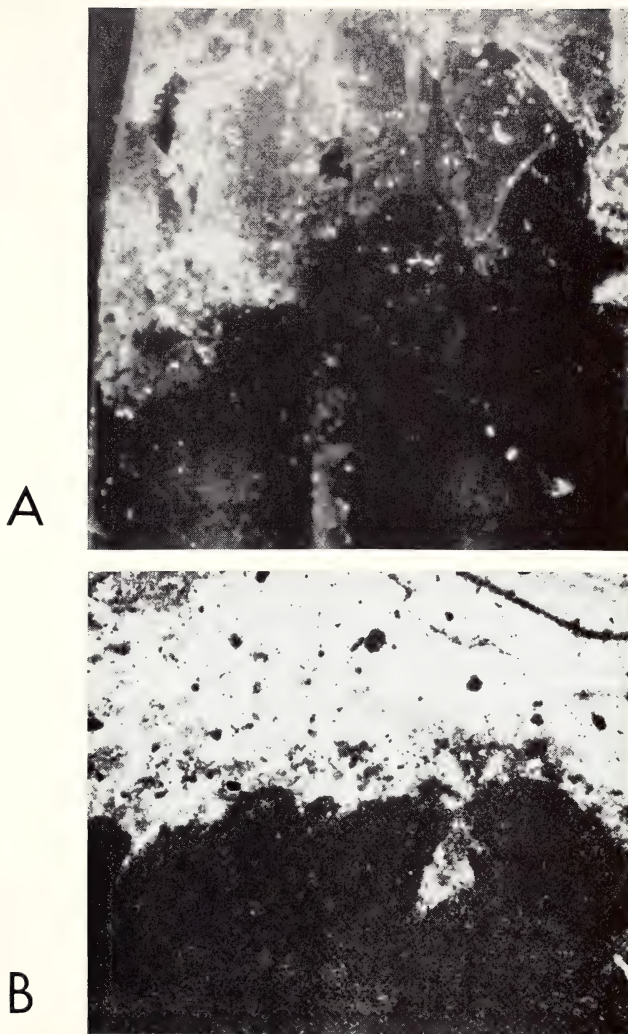


Plate 1. (A) Photograph of products resulting from the hydrothermal treatment of G-1 granite (top) and W-1 diabase (bottom). Turned 90° from run position for comparison below. Width, 3 mm. (B) Photograph of rhyolite-basalt contact of the Ornólfsfjall composite flow in eastern Iceland reproduced from Gibson and Walker (1963) with permission of the authors and the publisher. Width, 5 cm.

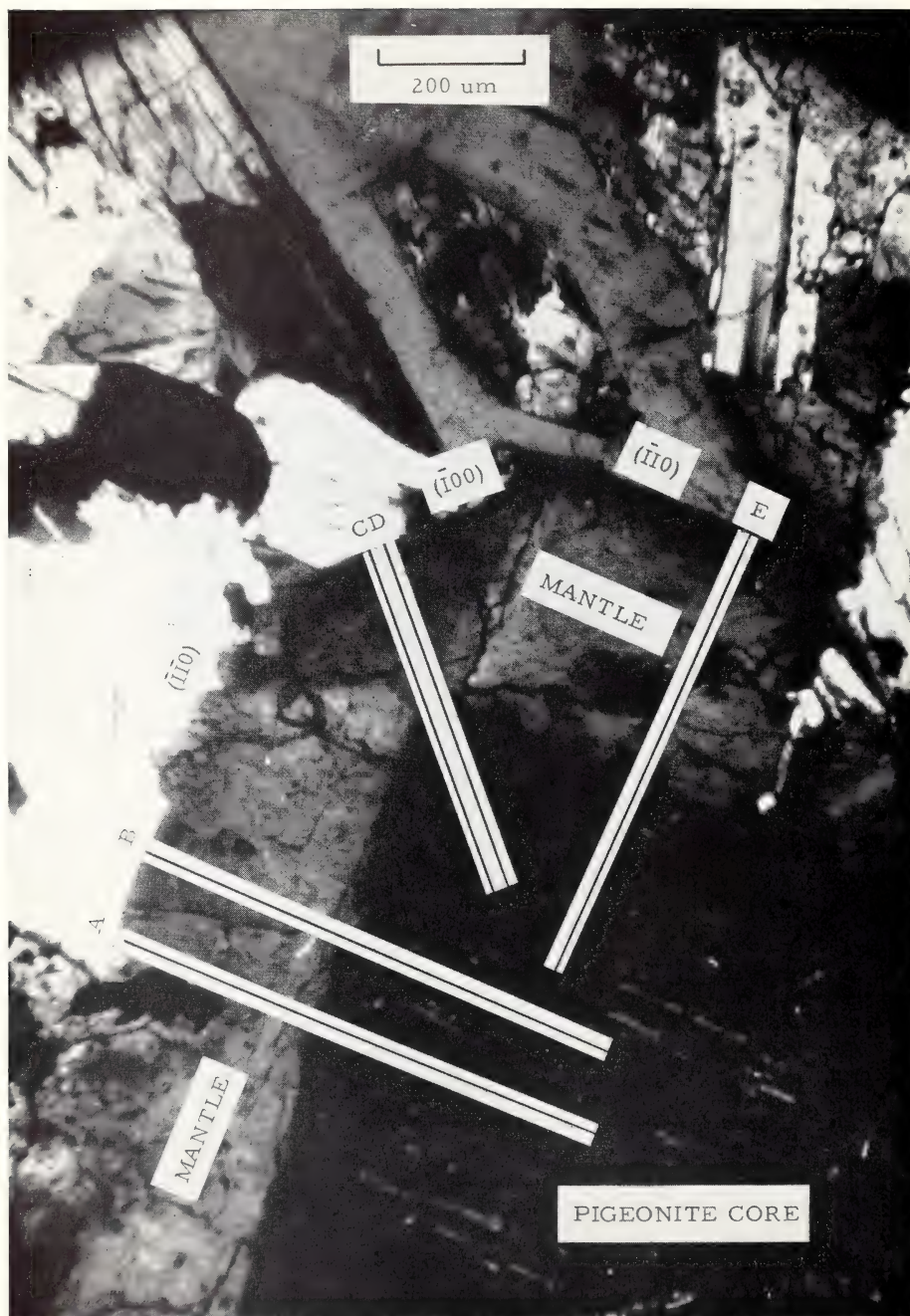


Plate 2. Phenocryst in section 12021,7 consisting of a pigeonite core and a dominantly Ca-rich mantle photographed under crossed nicols. There is a rim of more Fe-rich pigeonite on  $(\bar{1}10)$  and  $(\bar{1}00)$  in optical continuity with the core. This rim is discontinuous on  $(\bar{1}10)$ . Locations of probe traverses are indicated by vectors. A, Figs. 53 and 58; B, Figs. 54 and 55; C and D, Fig. 56; E, Fig. 52.



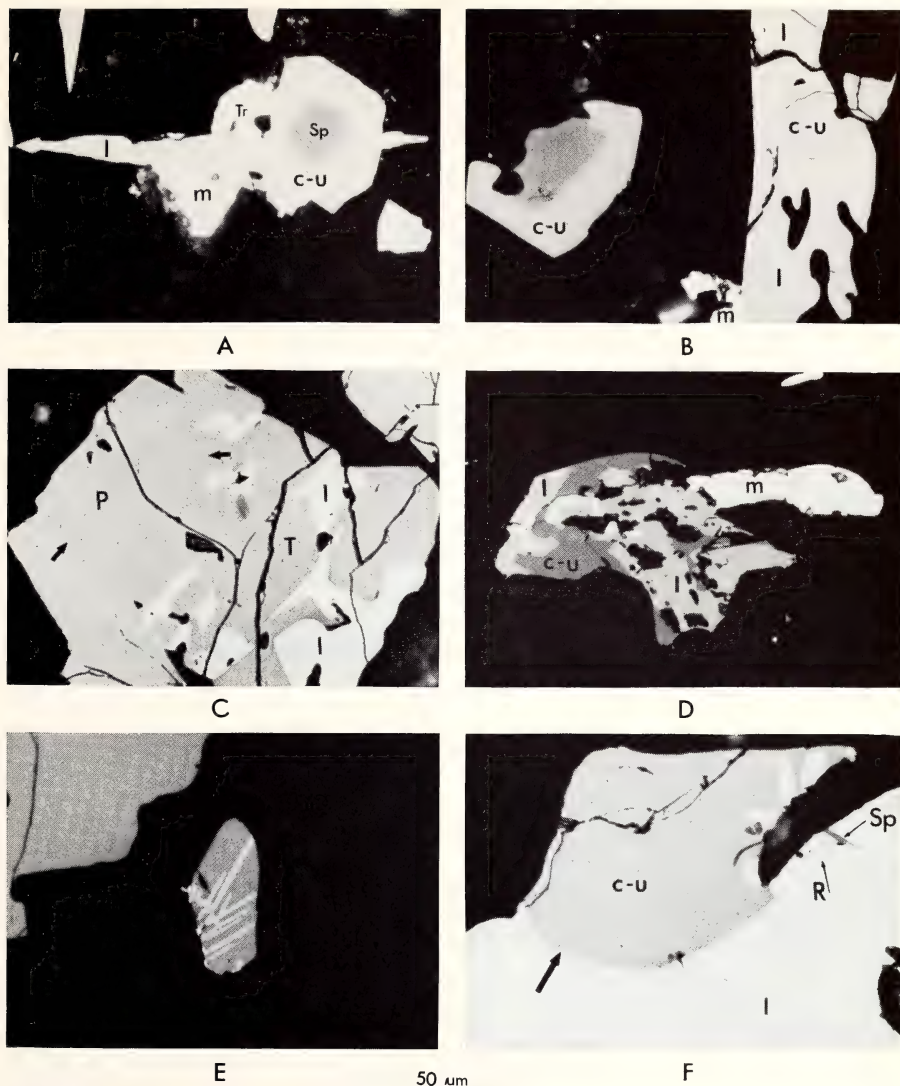


Plate 3. (A) Chrome spinel (Sp) core with a chromian-ulvöspinel (C-U) overgrowth. Ilmenite (I), metallic iron (M), and troilite (Tr) are also present. The order in which the minerals are named is the order of paragenesis (12020,10). (B) Chrome-spinel core with a chromian-ulvöspinel (C-U) overgrowth. In the assemblage to the right ilmenite (I) forms an overgrowth on chromian-ulvöspinel (C-U). Metallic iron (M) is present in the groundmass (12020,10). (C) An assemblage of pink (P) and tan (T) varieties of chromian ulvöspinel associated with exsolved ilmenite (I). Note the crenulate contact between the chromian ulvöspinel, and also that ilmenite is confined to the tan variety. Electron probe analyses are given in Table 11 (12040,4). (D) An intergrowth of khaki chromian ulvöspinel (C-U), ilmenite (I), and metallic iron (M). This chromian ulvöspinel contains the highest concentration of  $\text{Fe}_2\text{TiO}_4$  yet found in nature. The mineral is strongly anisotropic and is considered to be a new nonisometric phase along the join  $\text{Fe}_2\text{TiO}_4\text{-FeCr}_2\text{O}_4$ . Analyses are presented in Table 11 (12064,6). (E) Chromian ulvöspinel with exsolved lamellae of ilmenite along  $\{111\}$  planes. Note the fine blebs of associated metallic iron. This assemblage is considered to have formed by subsolidus reduction (12040,4). (F) Chromian ulvöspinel (C-U) with fine ilmenite lamellae along  $\{111\}$  planes. Note that the exsolved ilmenite is confined to grain boundaries and cracks within the chromian ulvöspinel. The chromian ulvöspinel abuts against discrete ilmenite (I). Ilmenite contains rutile (R) along  $\{01\bar{1}2\}$  and spinel (Sp) along  $\{0001\}$  planes. Note the dark chrome-rich reaction rim between the chromian ulvöspinel and the ilmenite, marked by an arrow (12040,4).



A

2.5 mm

B

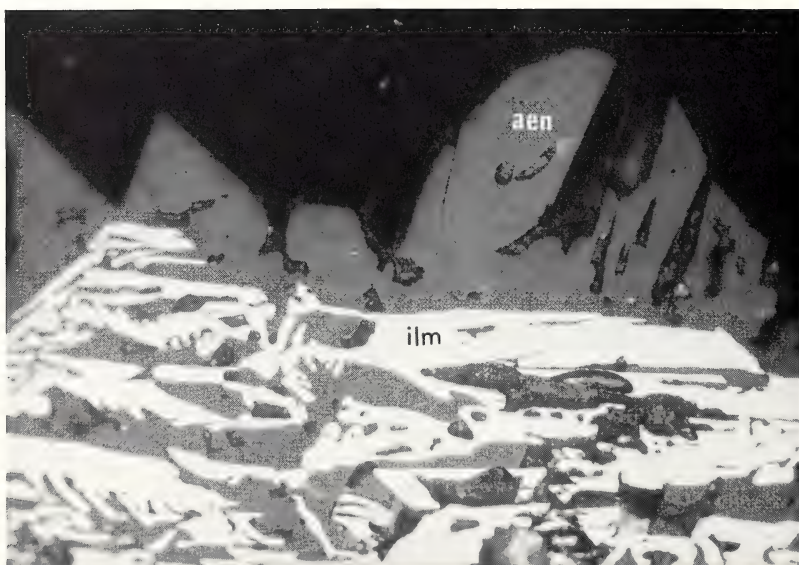
100  $\mu$ m

Plate 4. (A) Skeletal crystal of ilmenomagnetite from light pegmatoid, no. 368-69. Late-stage silicates fill the interstices. (B) Aenigmatite (dark gray, aen) replacing and forming euhedral overgrowths on ilmenite (light gray, ilm) in light pegmatoid no. 371-69. The labels are on the portions analyzed by electron microprobe (Table 31). Dark minerals are transparent.

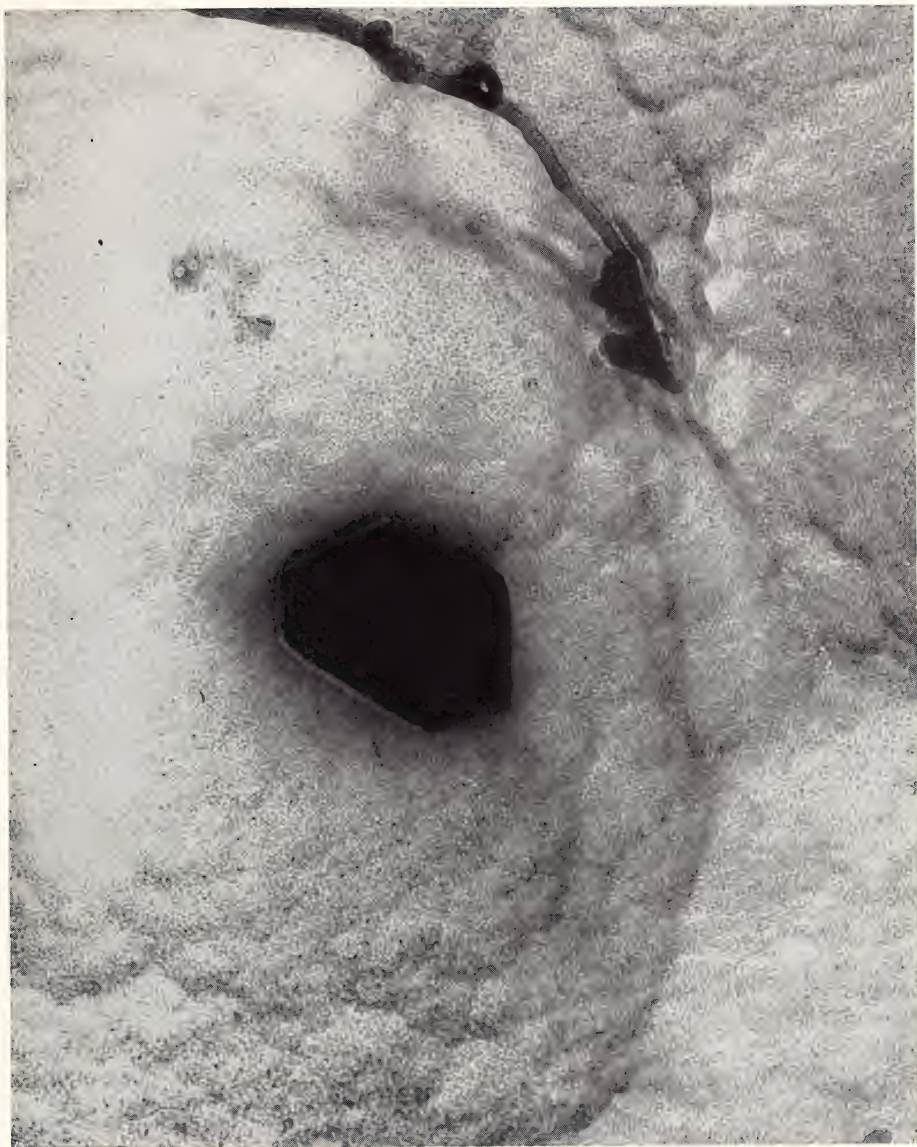


Plate 5. Transmission electron micrograph of chaoite crystal. Magnification,  $14 \times 10^5$ .

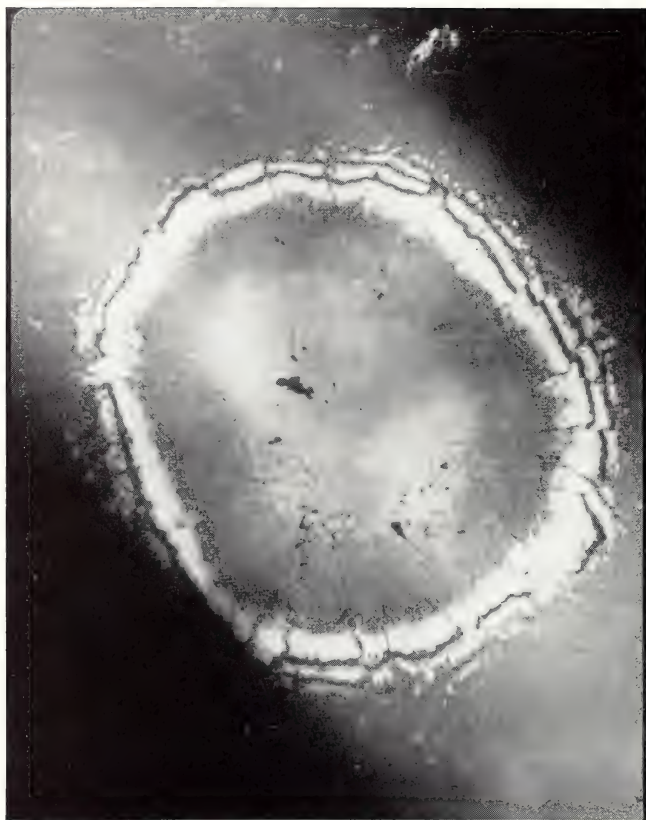


Plate 6. Coexisting high-pressure FeS (light gray core) and troilite (dark gray rim) as photographed at pressure in a diamond-anvil press. The center of the diamond cell is at approximately 70 kb, and the pressure decreases toward the edges (see text). The white-and-black rings around the outside are Newton spectra due to diffraction at the diamond interfaces. Magnification,  $\times 180$ .



# *Department of Terrestrial Magnetism*

*Washington, District of Columbia*

Ellis T. Bolton  
*Director*

L. Thomas Aldrich  
*Associate Director*



# Contents

Introduction . . . . .	367
Astrophysics . . . . .	367
Optical astronomy . . . . .	367
Image tubes . . . . .	370
Radio astronomy . . . . .	371
Atomic physics . . . . .	377
Nuclear physics . . . . .	382
Geophysics . . . . .	383
Geochemistry and geochronology . . . . .	383
Analytical equipment and techniques . . . . .	383
Ocean floor basalts . . . . .	388
Geochemistry of Franciscan volcanic and sedimentary rocks from California . . . . .	394
Ancient and modern volcanic rocks: a trace element model . . . . .	400
Primary differences in U/Pb ratios in two primitive crustal blocks . . . . .	405
U/Pb dating of volcanism in the central Piedmont (Carolina slate belt) . . . . .	408
The Glenarm series and related rocks . . . . .	412
Seismology . . . . .	413
Core phase nomenclature: suggested changes . . . . .	413
Anelasticity of the outer core . . . . .	414
Anelasticity of the inner core . . . . .	416
The structure of the transition zone between the inner core and the outer core . . . . .	419
Borehole strainmeters . . . . .	426
Frequency analysis of seismic body waves . . . . .	430
Earthquake body wave radiation and source dimensions . . . . .	439
Pseudodispersion in body waves . . . . .	442
Andean crustal structure . . . . .	447
Anomalous Love wave phase velocities . . . . .	460
Time anomalies and structure beneath the Andes . . . . .	464
Electrical conductivity . . . . .	470
Biophysics . . . . .	471
Introduction . . . . .	471
Thermal stability of reassociated repeated DNA from rodents . . . . .	472
Some observations on interspersion of DNA sequences . . . . .	479
Reassociation profiles of rodent DNAs . . . . .	482
Pattern of DNA acquisition during evolution . . . . .	485
Nucleotide sequence change in nonrepeated DNA during evolution . . . . .	488
The probability of occurrence of accidental sequence homologies . . . . .	501
Sequence complexity, kinetic complexity, and genetic complexity . . . . .	503
Cattle, sheep, and satellites . . . . .	506
Phosphate gradient elution of reassociated DNA fragments absorbed to hydroxy-apatite . . . . .	507
A possible role of adrenergic neurones in memory . . . . .	515
The nuclear satellite in slime mold . . . . .	518
Measurements of the rate of growth of the polynucleotide chains of ribosomal RNA in <i>Bacillus subtilis</i> . . . . .	521
Bacteriophage DNAs . . . . .	528
Functional homology between phage S13 and its hosts . . . . .	536



References cited . . . . .	538
Bibliography . . . . .	545
Major publication . . . . .	547
Personnel . . . . .	547

## INTRODUCTION

When we set about accounting for a Napoleon or a Shakespeare or a Raphael or a Wagner or an Edison or other extraordinary person, we understand that the measure of his talent will not explain the whole result, nor even the largest part of it; no, it is the atmosphere in which the talent was cradled that explains; it is the training which it received while it grew, the nurture it got from reading, study, example, the encouragement it gathered from self-recognition and recognition from the outside at each stage of its development: when we know all these details, then we know why the mind was ready when his opportunity came. . . . Broadly speaking, genius is not born with sight, but blind; and it is not itself that opens its eyes, but the subtle influence of a myriad of stimulating exterior circumstances.

We all know this to be not a guess, but a mere commonplace fact, a truism.

—MARK TWAIN

“In Defense of Harriet Shelley and Other Essays,” 1894.

The Department has enjoyed a highly productive year, as the body of the report that follows demonstrates. It is, nevertheless, increasingly difficult to function at such a level of effectiveness while struggling against a rapidly inflating background of what has been aptly termed “cultural noise.” This noise covers the whole radiation spectrum and extends even into man’s economic and social endeavors. There is no escape from it for the scientist and teacher, nor for that matter for persons in other walks of life. As long as we insist upon explosive development of the technology which follows upon basic scientific discovery, we shall have this problem daily to live with, and to learn to solve, for any particular scientific goal intended. The scientist attempts to ascertain what portion of all this noise can be put into a meaningful and relevant framework for his comprehension in order that the sig-

nals he seeks will stand out in support of his mission.

As a member of the Institution he knows he must choose most wisely some special part of all the static so he can work through it. Even so, he is a problem seeker far more than a problem solver. He knows he cannot buy his window facing the unknown by massive monetary expenditure. He knows that he cannot accomplish alone what he envisions. He is, therefore, a teacher, a communicator to his peers and to generations that will succeed him. By his response to the challenge posed, he stamps his imprint upon the future.

We believe that we continue to provide for our students, our Fellows, one of the finest environments for intellectual advancement and scholarly adaptive radiation. Their accomplishments in concert with this staff lend substance to the quotation from Mark Twain and the comments above.

## ASTROPHYSICS

*G. E. Assousa, L. Brown, S. D’Odorico, J. W. Erkes, W. K. Ford, Jr., V. C. Rubin, E. Steiner, K. C. Turner, M. A. Tuve, and C. M. Varsavsky*

“What do you expect to find with the 200-inch?” he was asked, and he replied “We hope to find something we hadn’t expected”—E. P. Hubble as described by N. U. Mayall, *National Academy of Sciences Biographical Memoirs*, p. 183, 1970.

## OPTICAL ASTRONOMY

*S. D’Odorico, W. K. Ford, Jr., and Vera C. Rubin*

For the past five years, we have been obtaining spectra of galaxies by using the image tube spectrograph of the De-

partment of Terrestrial Magnetism on the 72-inch Perkins telescope at Lowell Observatory and on the 84-inch telescope at the Kitt Peak National Observatory. During these five years, the velocity resolution of the spectra has consistently improved. This was initially achieved by the acquisition of improved optics. More recently, we have gone to higher and higher dispersions, and consequently, longer and longer exposures with the image tube system. At these higher dispersions we have already been rewarded with unexpected results. This surely is the hope of any observing program. In astronomy, as in all science, the truly rewarding experiment is often the one that gives results other than the expected ones.

During the past year, our efforts have been divided about equally between studying the rotational velocities of galaxies in general, and studying one, the Andromeda galaxy, in particular. In all cases, we are concerned with deriving accurate radial velocities, and obtaining the relative strengths of the lines of various elements and ionizations, as a step in understanding the physics of the ionized gas in the nuclei of galaxies.

*The Andromeda galaxy.* From spectra of 70 emission regions in M31—the innermost at 3 kpc from the nucleus, the outermost at 24 kpc from the nucleus—we have studied the velocity field in the galaxy, the mass distribution, and compared the results obtained from the optical observations with the 21-cm results for M31 and for our own galaxy. This study was published early in 1970 (Rubin and Ford).<sup>1</sup> We are presently using these spectra for determining the relative line strengths for emission regions at various distances from the nucleus. For this purpose, a microphotometer has been connected to a card punch through a scanner-coupler designed and built by Mr. Poe, and a digitized record of the transmitted light is obtained. Using the calibrated step

wedge for each plate, this is processed in the IBM 1130 to produce line profiles and integrated intensities for each line.

The emission regions near the nucleus,  $3 \text{ kpc} < r < 5 \text{ kpc}$ , define two classes, as indicated by their spectra. For the first class, the metal abundance, deduced from the lines of [SII], [NII], [OI], [OII], and [OIII], is high. The second class exhibits more normal nuclear abundances. The great strength of the [SII] doublet in some regions near the nucleus is the most striking feature yet detected. For regions more distant from the nucleus,  $r > 5 \text{ kpc}$ , the spectra generally exhibit line ratios  $I(\text{H}\alpha)/I(\text{NII})$ ,  $I(\text{OIII})/I(\text{H}\beta)$ , and  $I(\text{H}\alpha)/I(\text{SII})$  which increase with increasing distance from the nucleus, but with a considerable range in values at each  $r$ . The helium abundance varies from region to region, but the mean value does not vary with  $r$ .

Closer than 3 kpc to the center of M31, the integrated starlight from the high stellar density makes observations difficult. No emission regions have been identified in this region. Last year, working with plates taken at a dispersion of  $135 \text{ \AA/mm}$ , we detected the emission line of [NII]  $\lambda 6583$  at distances of 0.4 to 4 kpc from the nucleus, indicating the presence of ionized gas near the nucleus. Previously, only the OII  $\lambda [3727]$  line had been detected (Münch, 1960).<sup>2</sup> Our most recent spectra at a dispersion of  $28 \text{ \AA/mm}$  and  $66 \text{ \AA/mm}$  reveal narrow emission lines of [NII]  $\lambda\lambda 6548, 6583$ ,  $\text{H}\alpha$ , [SII]  $\lambda\lambda 6717, 6731$ , and [OIII]  $\lambda 5007$ , all superimposed on the continuous spectrum from the stars in the nuclear region (see Plate 1). The presence of the [OIII] line indicates that a higher state of excitation exists in the nucleus of M31 than had been thought. The velocities measured from this excited gas, in 16 position angles around the nucleus, are not at all compatible with a simple dynamical model of rotation or rotation plus expansion or contraction. The velocities are strikingly



asymmetric across the nucleus, often showing (at a single position angle) steep velocity gradients on one side of the nucleus, and zero velocity gradients on the other. These observations have led us to study the general problem of three-dimensional motions near the nuclei of galaxies, in order to predict the observed velocities if gas is ejected, or is falling, into the nuclear regions. For M31, the extreme narrowness of the lines (less than 75 km/sec) makes it appear unlikely that we are here dealing with motions outside of the principal plane.

The emission line strengths from this excited gas are generally as follows:  $H\alpha = \frac{1}{2} [NII]$ ,  $[SII] \lambda 6731 > \lambda 6717$ , indicating a high ( $\sim 10^5$  e/cm<sup>3</sup>) electron density. However, these ratios can change abruptly in distances of the order of 200 parsecs, with  $[SII] \lambda 6731 = \lambda 6717$ ,  $H\alpha = [NII]$ . One of these abrupt changes can be identified with a dust lane crossing the inner part of M31.

Perhaps the best summary of these observations of the nucleus is that we know how little observational knowledge we have about the nucleus of M31 and galactic nuclei in general. We hope that the observations at hand will help answer the questions: (1) what is the source of energy for the excitation of the emission lines in the nucleus? (2) how do the asymmetric velocities arise? (3) what is the mass of gas involved in the phenomena? "Explosive event," a term often used in astronomy today to describe unknown phenomena, is probably too strong a term to explain the somewhat gentler activity we are observing, but certainly the nucleus of M31 has undergone some activity in the observable past.

Finally, we note two observational facts. First, it is only by observing at high dispersions, and thus reducing the signal-to-noise ratio (i.e., the ratio of emission line intensity to stellar background continuum) that the emission

lines near the nucleus can be detected. Second, at a dispersion of 28 Å/mm, with the Kitt Peak 84-inch telescope, exposure times of 6 hours are necessary for us to obtain a well-exposed image tube spectrum of regions of M31 just 500 pc from the nucleus.

*Other galaxies.* Several years ago Morton Roberts, at the National Radio Astronomical Observatory, compiled a list of relatively bright late-type galaxies; for each galaxy the radial velocity determined from 21-cm HI observations differed significantly from the optical radial velocity. Many of these earlier optical radial velocities came from measures of the Ca II H and K absorption lines, although in some cases emission lines were also measured. We have obtained spectra centered near  $H\alpha$ , at a dispersion of 135 Å/mm, and have measured velocities for 16 galaxies of this list. For these galaxies, the difference between the 21-cm and the old optical velocities had values  $\Delta V$  ranging up to  $\Delta V = -664$  km/sec, with a mean value (without regard to sign) of  $\langle |\Delta V| \rangle = 120$  km/sec. From our new radial velocities this quantity has been reduced to  $\langle |\Delta V| \rangle = 33$  km/sec. Clearly, errors in some of the previously published values of radial velocities of galaxies have been underestimated. This fact may be significant in statistical studies of velocities of galaxies.

Detailed studies of emission line strengths and radial velocities in interesting galaxies have also been made. For the pathological interacting galaxies NGC 4038-4039, a study of 18 emission knots reveals a pattern in the radial velocities which may be interpreted as two interacting rotating galaxies. A comparison of the theoretical  $H\alpha/H\beta$  ratios and the observed line ratios in the emission knots indicates the presence of large amounts of dust within these objects. Helium is observed in both pairs of galaxies, with an average He/H ratio of about 0.1. Together with the line

strength data from M31, these studies contribute significantly to the available information concerning excited gas in galaxies.

A spectroscopic study of the double galaxy NGC 3395-3396 was made by S. D'Odorico, a Carnegie postdoctoral Fellow on leave from the Astrophysical Observatory, Asiago, Italy. Spectrograms were obtained with the DTM image tube spectrograph attached to the 72-inch Perkins telescope of Ohio State and Ohio Wesleyan Universities at Lowell Observatory. These spectrograms show emission lines of H I, He I, [O II], [O III], [N II], and [S II]. It was found that within 1.5 kpc of the nucleus NGC 3395 rotates as a solid body and has an approximate mass of  $1.2 \times 10^9 M_{\odot}$ . The velocity measurements for NGC 3396 show no appreciable rotation. The general velocity field is consistent with the hypothesis that NGC 3396 rotates around NGC 3395.

### IMAGE TUBES

*W. K. Ford, Jr., and L. Brown*

Photographic plates obtained with the aid of cascaded image intensifiers are increasingly being used for the determination of relative intensities of lines in the spectra of faint sources. Photographic integration of the light from an image tube is a powerful technique and is well suited for problems where only rough ( $\sim 20\%$  accuracy) relative intensities are required. On the other hand, the electronographic devices developed by Lallemand, McGee, Kron, Walker, *et al.* are better suited to problems requiring precision photometry because of the linear or very nearly linear response of the tube-emulsion system. However, these devices tend to be more complex in operation and are more difficult to maintain; consequently, their use has thus far been limited to a few large, well-manned observatories.

The high gain of a new ceramic-en-

velope cascaded tube (RCA type C33063) offers the possibility of an alternative method of efficiently obtaining a linear recording of low-light-level images. When viewing an image at lower and lower light levels with the aid of one of the intensifiers, one sees the image break up into randomly arriving point scintillations, each originating from a single primary photoelectron. The rise and decay in brightness of one of these single photoelectron scintillations is the result of the rate of electron excitation and the convolution of the persistences of the two phosphor screens. (The time-of-flight of the electrons at 10 or 15 kv per stage is a few nanoseconds and is negligibly small by comparison.) We have measured the time distribution of randomly occurring single photoelectron scintillations in the new C33063 tube and find a duration of the order of one millisecond for decay to 10 percent of the peak brightness.

A tube with a radiant energy gain of 20,000 (as measured at the wavelength of peak sensitivity and operated at 30 kv total voltage) and with a cathode having a peak responsive quantum efficiency of 0.15 photoelectrons per photon produces a total of  $20,000/0.15 = 1.3 \times 10^5$  photons in each primary photoelectron scintillation. Currently available transfer lenses are only about 3% efficient (including transmission losses) in collecting and re-imaging these photons so that on the order of  $20,000/0.15 \times 0.03 = 4000$  photons are available in the focal plane of the transfer system. If a plane photocathode of 15% efficiency is used here as a second detector, then  $4,000 \times 0.15 = 600$  electrons are produced with the same distribution in time as the original single photoelectron scintillation. Any one of these 600 electrons in the second detector if multiplied in a conventional electron multiplier can, with high probability, produce a pulse that can be used to signal the occurrence of a single photoelectron scintillation in the image tube.

A rapidly scanning photomultiplier, such as the common magnetic deflection image dissector, can be used as the second detector to sample a line image, such as a spectrum, with a repetition rate comparable to the scintillation decay. The pulses thus produced can be accepted or rejected according to their amplitude and uniformly shaped in a single channel pulse-height analyzer and counted in a multichannel scaler that is locked in synchronism with the repetitive scans of the second detector. Since each pulse indicates the presence of a primary photoelectron scintillation in the image tube, the counts recorded in the multichannel analyzer are a linear measure of the light intensity in the original spectrum. For light levels of interest in astronomical observations the counting rate is sufficiently low that problems caused by pulse pile-up are relatively minor.

A "breadboard" setup of this system has been assembled at DTM and is currently being tested. Thus far we have observed pulses from the photoelectrons in the second detector caused by single randomly occurring photoelectron scintillations in a prototype sample C33063. These measurements confirm the estimates based on the gain and lens efficiency cited above and indicate the practical limits of the storage capacity of the phosphor screens. A substandard image dissector has been obtained on loan and put into operation with an improvised deflection yoke. A slow 400-channel multiscaler has been used in some initial scanning experiments. Its speed limitation as multiscaler has been largely circumvented for these initial tests by a variable-gain pulse amplifier. This device uses the current through the deflection yoke of the second detector to bias the amplifier so that the uniform pulses fed into the device are given a pulse amplitude proportional to their position in the scan. These pulses are then sorted by pulse height to give a display of the input spectrum. There is

a dead-time associated with the operation of the pulse-height analyzer, but for low light levels the dead-time corrections are small. These experiments confirm the feasibility of using the short-term ( $\sim 1$  millisecond) storage of the tube to permit counting scintillations in a line image due to primary photoelectrons.

## RADIO ASTRONOMY

*K. C. Turner, J. W. Erkes, M. A. Tuve,  
E. T. Ecklund, and C. A. Little*

Major emphasis this year has been placed on the development of new equipment and the analysis of previously obtained observations. New observations of both supernovae remnants and the Small Magellanic Cloud were also made. A modest increase in our nonpostdoctoral educational activities was effected.

It is a pleasure to express again our thanks to the Office of Naval Research for the continuing loan, under contract number Nonr-3021(00), of the 38 tons of pig lead that serve as counterweights for our Derwood telescope.

## Equipment

For the most part, the new equipment devised this year is meant to extend our observing capabilities in two directions: toward greater sensitivity, and toward other areas of the electromagnetic spectrum.

Our receiver has for many years used simple RC integrators with time constants of 400 seconds on the output of each of the channels of our hydrogen line spectrometer. These are satisfactorily linear up to integration times of about 100 seconds. For the detection of very faint sources of line radiation longer periods are necessary. As usually operated, a single channel of our receiver exhibits per single observation a standard deviation of about  $\frac{1}{2}^{\circ}\text{K}$ . To reduce this by tenfold requires that we integrate for more than two hours. To reduce the



number of cards we must handle, as well as to provide an "on-line" view of the average as it builds up, a nuclear physics type multichannel analyzer, kindly loaned us by Professor J. C. Walker of the Physics Department of Johns Hopkins University, has been adapted for use as a digital integrator.

This instrument, a Nuclear Data ND-110, has 128 channels of memory, each with a capacity of 99,999. Since each 100-second scan adds about 200 counts to each of 60 channels, integrations of as long as 10 hours may be performed with this instrument. Either the first or the second half of the 128-channel memory may be selected for storage so that there is room for observations both of the object of interest and for a piece of "cold sky" for comparison. Observations may be collected until there is a clear difference between the two halves of the memory as read out visually on an oscilloscope. At this point the data may be automatically punched onto cards for further analysis. This device will be used primarily in the southern hemisphere for studies of extragalactic hydrogen, but a similar instrument will be constructed for use in the northern hemisphere in conjunction with both our hydrogen line spectrometer and our new K-band receiver.

To further enhance our sensitivity in studying hydrogen in other galaxies, 30 of our old set of medium-band filters have been retuned to 100 KHz bandwidth and spacing of 24 km/sec at 21 cm wavelength. Since the filters span a velocity interval of 720 km/sec, the detection of neutral hydrogen is possible in systems that do not have well-determined velocities without very time consuming searches.

A K-band receiver is being constructed for use primarily in studies of the  $\text{H}_2\text{O}$  line at 22.2 GHz, although it should be useful with minor modifications throughout the region between 18 and 24 GHz. It will utilize our existing spectrometer

back end and the Derwood 60-foot telescope. The principal difficulty in beginning such a project is to obtain adequate stability in the local oscillator system. We have solved this problem by using a double phase-lock system applied to a Hewlett-Packard K-band sweep oscillator. The system is locked to a combination of a crystal oscillator in the 300-Mc region and an extremely stable 3-6 Mc variable frequency oscillator. The measured stability of the system is better than 10 Hz over periods of the order of one hour at 300 MHz. As part of our continuing program of modernization and maintenance of our Derwood Observatory we have this year replaced our rather unsatisfactory relay type scanner-coupler with an extremely versatile and reliable solid state device that uses integrated circuits. Designed at the DTM, it eliminates all moving parts from this part of the digital output system.

### *Analysis and Observations*

In attempting to understand the significance of previous observations of the distribution of neutral hydrogen between the two Magellanic Clouds, three principal avenues have been explored.

1. Since the Small Magellanic Cloud seems most intimately connected with the intercloud material, a quite complete survey of the Small Cloud has been made to study in some detail the transition region, if such can be defined, between the Small Cloud and the intercloud medium.

In order to have observations evenly spaced on the Magellanic system, a new Cartesian coordinate system (Fig. 1) has been defined, whose center is at the optical center of the Small Magellanic Cloud, and whose  $x$ -axis increases positively in the direction of the Large Magellanic Cloud. Observations of the brightest regions of the Small Magellanic Cloud have been made at  $\frac{1}{4}^\circ$  intervals in this coordinate system; the extremi-

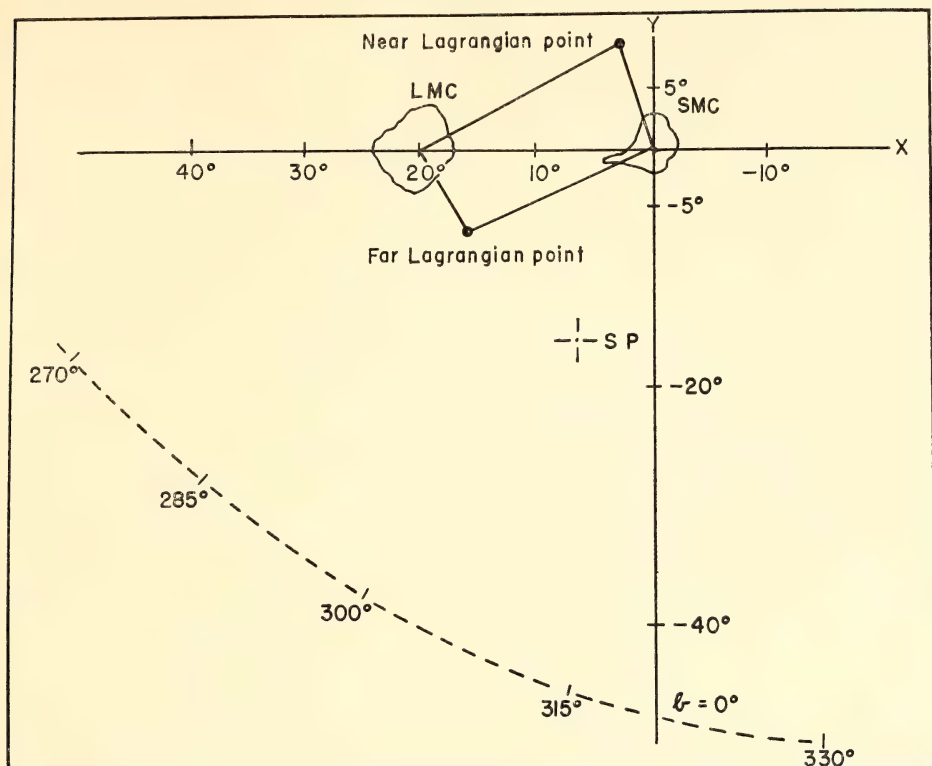


Fig. 1. Coordinate system used in Magellanic Cloud observations. Observed position of assumed Lagrangian points are indicated.

ties have been explored with a  $\frac{1}{2}^\circ$  spacing.

The data are being prepared for presentation in several different types of contour maps: (1) maps showing the distribution of neutral hydrogen as a function of  $x$  and  $y$ , for various velocity intervals; (2) maps showing the brightness temperature as a function of  $x$  and velocity, for constant  $y$ ; (3) maps showing the variation of brightness temperature as a function of  $y$  and velocity, for constant  $x$ ; (4) special maps showing, for example, the distribution of neutral hydrogen velocities along the major axis. Preliminary construction of these maps indicates that neutral hydrogen exists at greater distances from the center of the Small Magellanic Cloud than had been anticipated. Further observations are in

progress to extend the coverage of the maps.

2. Optical observations of stars in the "wing region" of the Small Cloud have been published by Sanduleak.<sup>3</sup> These reveal a strong association with the double peaked velocity feature, the most striking part of the intercloud material. Figure 2 shows this association. The presence of these stars clearly indicates that this hydrogen has not been ejected in such a state as to inhibit star formation. It is unfortunate that our present ignorance of the conditions necessary for the formation of stars makes a stronger statement impossible.

3. The idea that the two Magellanic Clouds are really a single permanent system leads, of course, to speculation on the form of this system before it

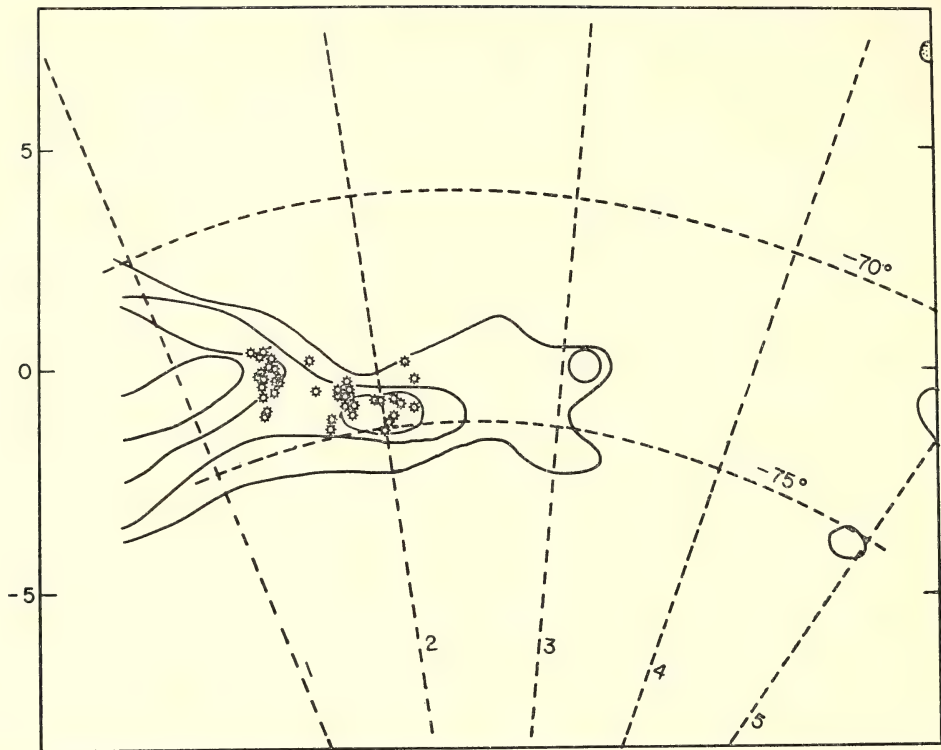


Fig. 2. Position of bright stars observed by Sandulear, superimposed on contours of neutral hydrogen density. Contours are successive multiples of  $1375 \times 10^6$  Mo/beam area.

began to interact with our own galaxy. (Since the force due to our galaxy upon the two Clouds is an order of magnitude stronger than the forces they exert upon one another, one cannot imagine both that they are one system and that they are permanent satellites of our galaxy.) The question of the intercloud material then becomes whether it is of recent or of primeval origin. The placement and velocity suggest that a primeval origin is not impossible. It is possible to imagine that the features near  $x=2$ ,  $y=8$ , and  $x=16$ ,  $y=-7$  (Fig. 3) represent material near the equilateral Lagrangian points of the 2-body system of the two Clouds. Under this assumption, if one knows the masses of the Magellanic Clouds and assumes circular motion for

the pair, the space motion of the whole system may be determined from the observed radial velocities. Figures 1 and 4 indicate the geometry. Our galaxy will, of course, perturb this system to a considerable extent, but not enough to imply that it was not a single system in the past. If one then turns the picture around and assumes an originally circularly symmetrical system, one can find that set of histories which will produce the presently observed set of positions and velocities. Although this work is still in preliminary stages, it is possible to state that under these assumptions, the two "Trojan" objects should lie at significantly different distances from us than do the two Magellanic Clouds. If sufficient stellar material can be observed in



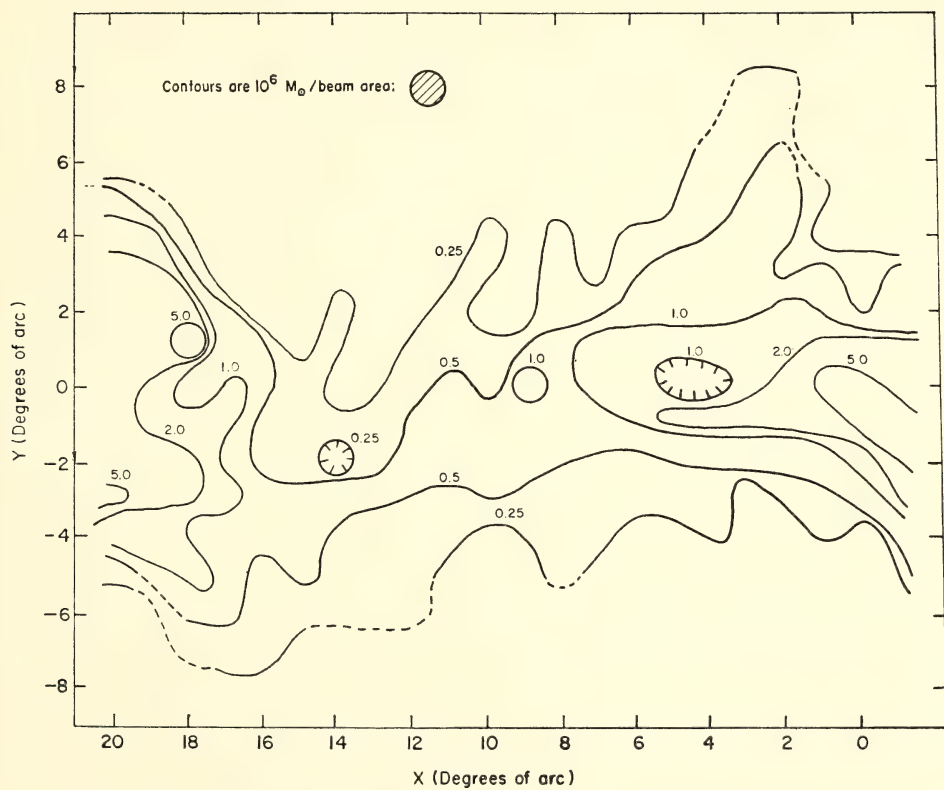


Fig. 3. Contours of neutral hydrogen surface density in the Magellanic Cloud system.

*The Neutral Hydrogen  
near Supernova Remnants*

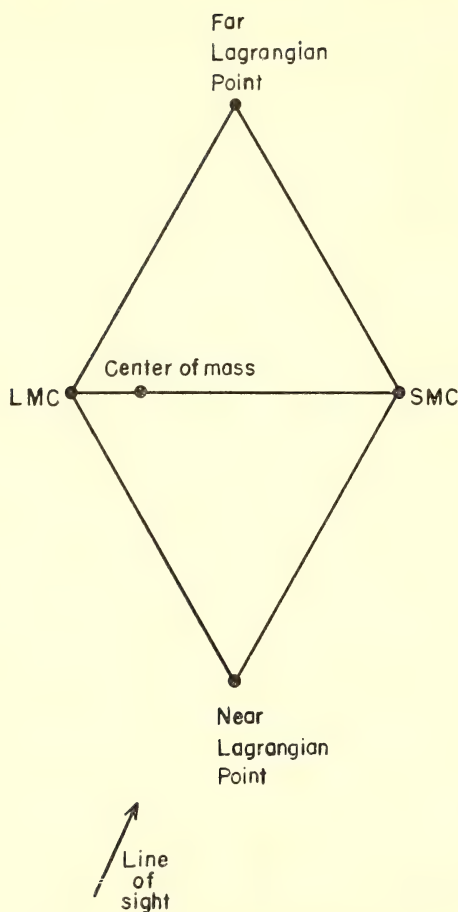


Fig. 4. Hypothetical geometry of Magellanic Cloud system.

these objects to enable an estimate of distance to be made, these notions can be tested.

*HB 21.* Observations of neutral hydrogen near supernova remnant HB 21 have been completed and reduced. These observations show the strong influence of the supernova remnant on the surrounding interstellar medium, and suggest that the neutral hydrogen in the direction of HB 21 has the structure and kinematics of an expanding shell. The expanding shell of neutral hydrogen appears to have a diameter slightly greater than that of the radio continuum radiation from HB 21, and is well aligned with the radio continuum contours. In addition, an elongated bar of neutral hydrogen seen on the far side of the expanding shell agrees very well in location and position angle with the flattened northern edge of HB 21, suggesting a causal linkage.

Table 1 shows estimates of the total mass of hydrogen involved in the shell, as well as other parameters of interest. Since the true distance to HB 21 is unknown, the mass of the expanding shell has been calculated for several sample distances. The mass estimates become quite unreasonable for the greater distances; the energy required to form expanding shells of this size is extremely large, as is shown by the very large ejected masses required. In all cases, however, the interstellar densities required are comparable to those found in interstellar clouds.

TABLE 1. Some Interesting Parameters for the Supernova Remnants HB 21

Distance, pc	Height Above Plane, pc	Radius (pc)		V Expan- sion Veloc- ity, km/s	$M_{\text{HI}},$ $M_{\odot}$	$M_{\text{total}},^*$ $M_{\odot}$	Local Inter- stellar Den- sity, H atoms/ $\text{cm}^3$	$M_e$ (Ejected Mass) $^{\dagger}$	
		Radio Con- tinuum	HI					$V_e =$ 7500 km/s	$V_e =$ 10,000 km/s
650	53	11.3	13.5	20	1650	2887	6.4	7.7	5.7
1300	106	22.6	27.1	20	6600	11550	3.2	31	23
2600	213	45.2	54.2	20	26400	46200	1.6	123	92

\* Assumes H/He  $\sim 7$ .

$^{\dagger}$  Calculated by momentum conservation:  $M_e V_e = M_{\text{total}} V$ .

In summary, it appears that the supernova remnant HB 21 has expanded within an interstellar cloud that has considerably retarded the expansion of the supernova remnant. The distance to the remnant is probably considerably less than has been previously suggested.

*Vela X.* Observations of neutral hydrogen near Vela X supernova remnant were begun in January and February of 1970 with the 100-foot Instituto Argentino de Radioastronomía-Carnegie Institution of Washington (IAR-CIW) dish. The Vela X remnant is particularly suitable for studies of this type because its large angular diameter permits telescopes of moderate apertures to easily resolve shell features. In addition, it exhibits large inhomogeneities in the surface brightness of individual shell segments.

Observations of other old supernova remnants (HB 21, IC443, Cygnus Loop) show that shell segments that have interacted strongly with the interstellar medium have higher surface brightness than shell segments that have collided with less dense regions of the interstellar medium. It is felt, therefore, that the neutral hydrogen near Vela X may show the effects of interaction with the supernova remnant. Reductions of the observations are proceeding.

### *Other Activities*

For the second year our Derwood Observatory was used by the students of the University of Maryland course in observational astronomy. We were able to provide these students with the opportunity to make for themselves observations of galactic neutral hydrogen, thus giving them a very personal feeling for both the pleasures and problems of "hands on" radio astronomy.

Our Derwood Observatory was also visited by Professor J. C. Walker's class in general astronomy at Johns Hopkins University. Although the galaxy's plane was not visible at the time of their visit,

a set of profiles in the galactic plane was collected earlier in the day for their later study.

### *Dish Parameter Measurement*

The aperture efficiency and beam shape of the 60-foot Derwood telescope were measured in collaboration with George Reed, a visiting graduate student from the University of Pennsylvania. A neon noise bulb was first calibrated by comparing its signal contribution with the contributions from a cold load (78° K) and a hot load (273.5° K). An antenna temperature of 77.5° K was measured for Cygnus A using the neon noise source as a calibrator. A flux density for Cygnus A of 1400 flux units was adopted; this yielded an aperture efficiency of 59.8%. The half power beam shape was found to be slightly elliptical, with a half power width of 42.5 arc minutes in declination and 49.5 arc minutes in right ascension.

### ATOMIC PHYSICS

*G. E. Assousa, L. Brown, and W. K. Ford, Jr.*

Our primary goal in this work is the determination of the lifetimes of excited atomic states with a foil-excitation technique that was invented by Stanley Bashkin and has been used successfully by several groups. Our first work of this kind was an observation of the spectrum of a beam of sodium (*Year Book 66*, pp. 66-68). This experiment startled us with the number of unclassified spectral lines observed, many of which probably originate from levels having more than one excited electron. It also convinced us that we could use the image tube spectrograph to measure the lifetimes of the excited states.

This preliminary experiment thus pointed out two courses open to us: (1) investigating the structure of the multi-electron excited states and (2) measuring the lifetimes of those states that decay through a classified transition. The



former course tempts us with unknown structures of atoms to map but would give us at the moment rather meager information for such an undertaking. The difficulties of such investigations will no doubt yield to improvements in experimental method in the future. The present limitations are poor resolution in wavelength and the small portion of the spectrum that can be observed in a single exposure. The statistical approach described earlier (*Year Book 67*, pp. 299–300) is an intermediate way of describing matters and will be used again when a large number of spectra have been recorded. The second course, the measurement of lifetimes, has immediate and important application to spectroscopy and astronomy and can be accomplished with the image tube spectrograph for spectral regions only poorly accessible by other techniques. Lifetime measurements test the accuracy of wave functions. They are required in abundance determinations, since one obtains from them the oscillator strengths that are needed to convert the intensities of spectral lines into the quantity of radiating matter. It is appropriate to remark here that there is little point in determining the lifetimes of states that have not been classified, since for such states there

are neither wave functions to test nor ways to get the oscillator strengths.

We began using our equipment to measure lifetimes. The technique was untried with our method, so we first attempted an element for which lifetime measurements had been made with another technique that we considered good. This other technique uses pulsed electron beams<sup>4</sup> to excite the atoms. It is limited, however, to elements that can be put into a gaseous state. Comparing our data with those obtained with pulsed electron beams was a sound beginning, for it forced us to locate systematic errors in our method that might have eluded us.

Neon was the element selected for this test, and this was the work in progress when fire seriously damaged our Van de Graaff machine and cost us so dearly in time (*Year Book 68*, p. 374). The first work after repair was the remeasurement of neon with improvements in technique that analysis of the first results suggested. This gave good agreement with the pulsed electron technique, as can be seen in Table 2.<sup>5, 6</sup> We then observed a beam of argon, primarily because the ion source that produced the neon beam could just as well produce argon. Many lifetime measurements have been made

TABLE 2. Lifetimes of 3p Levels in Neon I

Level	Paschen Notation	Transition Wave-length, nm	Beam-foil	Measured Mean Life, nanoseconds	
				Pulsed Electron Beams <sup>3</sup>	Beam-gas <sup>13</sup>
1s <sub>0</sub>	2p <sub>1</sub>	585.3	14.9 ± 2.6	14.7 ± 0.5	14.5
3p <sub>1</sub>	2p <sub>2</sub>	588.2	18.0 ± 3.2	16.3 ± 0.6	
		616.4	19.2 ± 3.4	16.8 ± 0.7	
		659.9			19.8
3p <sub>0</sub>	2p <sub>3</sub>	607.4	18.8 ± 3.3	23.3 ± 4.8	25.4
3p <sub>2</sub>	2p <sub>4</sub>	609.6	21.4 ± 3.8	22.4 ± 4.4	26.0
		594.5	21.1 ± 3.9		
		667.8	22.6 ± 4.0		26.5
3d <sub>1</sub>	2p <sub>7</sub>	638.3	18.8 ± 3.3	20.3 ± 1.6	20.2
1d <sub>2</sub>	2p <sub>8</sub>	633.4	26.3 ± 4.6	24.3 ± 2.0	
		650.7	25.6 ± 4.5		27.8
3d <sub>3</sub>	2p <sub>9</sub>	640.2	29.3 ± 5.2	22.5 ± 1.9	30.5

TABLE 3. Lifetimes \* of 4p and 4p' Levels in Ar II

Level	Transition Wave- length, nm	Experiment				Theory	
		Present Work	Bennett <i>et al.</i> <sup>7</sup>	Bakos <i>et al.</i> <sup>8</sup>	Matilsky & Hesser <sup>9</sup>	Schnappauff <sup>10</sup> & Popenoe <sup>11</sup>	Schunaker, Garstang <sup>12</sup> & Trusty <sup>13</sup>
4p <sup>2</sup> P <sub>3/2</sub>	476.5	11.7 ± 2.1	9.4 ± 0.5	8.5 ± 0.1	3.9 ± 0.4	≤ 11.7 ± 2.6	9.9
4p <sup>2</sup> D <sub>3/2</sub>	472.7	11.6 ± 2.1	9.8 ± 0.2	9.9 ± 0.2		≤ 12.9 ± 2.8	10.5
4p <sup>2</sup> D <sub>5/2</sub>	496.5	10.0 ± 1.8	9.8 ± 0.2				
4p <sup>2</sup> P <sub>1/2</sub>	484.8	11.4 ± 2.0					
4p <sup>2</sup> P <sub>3/2</sub>	473.6	11.6 ± 2.1		9.6 ± 0.1		6.4 — 6.5	9.3
4p <sup>2</sup> P <sub>5/2</sub>	480.6	12.2 ± 2.2		10.3 ± 0.2		6.4 — 6.5	11.2
4p <sup>2</sup> D <sub>1/2</sub>	438.0	10.6 ± 1.9		10.3 ± 0.2	10.6 ± 1.1	6.2	10.7
4p <sup>2</sup> D <sub>5/2</sub>	442.6	10.8 ± 1.9	7.5 ± 0.5	10.3 ± 0.2	10.6 ± 1.1	6.8	7.9
4p <sup>2</sup> D <sub>3/2</sub>	434.8	11.6 ± 2.1		9.9 ± 0.2	10.6 ± 1.1	4.9	8.6
4p <sup>2</sup> P <sub>3/2</sub>	423.7	5.5 ± 1.0			4.7 ± 0.5	≤ 6.1 ± 1.4	7.8
4p <sup>2</sup> D <sub>5/2</sub>	448.2	10.0 ± 1.8					
4p <sup>2</sup> F <sub>5/2</sub>	459.0	14.3 ± 2.5		9.0 ± 0.2	1.2 ± 0.1	≤ 12.0 ± 2.4	5.4
4p <sup>2</sup> F <sub>7/2</sub>	461.0	14.4 ± 2.5			1.2 ± 0.1		5.6
							8.0
							8.0

\* Mean life in nanoseconds.

for argon but there is disagreement with other measurements, some of it serious. The experimental and theoretical situation for Ar II, i.e., singly ionized argon, is summarized in Table 3.<sup>7-13</sup>

A complete description of the experiment is available elsewhere,<sup>14</sup> and only a brief treatment is suitable here. A singly ionized beam is produced by an rf ion source located in the terminal of the Van de Graaff accelerator. The accelerated beam is deflected by a magnet to eliminate unwanted ionic species from the beam, and then enters the target chamber where it passes through a thin, self-supporting carbon foil. After passing through the foil the beam glows as a result of the radiative de-excitation of the excited states created by the collision of the atoms of the beam with the foil. The glowing beam is imaged onto the slit of the spectrograph, as shown schematically in Fig. 5. The resulting spectrograms show lines decaying in intensity downstream from the foil. In order to

extract information concerning the relative light intensity along the beam, a photometric calibration of the plate is necessary. Although at low light levels the image tube response is a linear function of the incident light intensity, the response of the photographic emulsion is not. A calibration plate is made simultaneously with each spectrogram by exposing the emulsion through a step wedge to a faint source of blue light. Following wavelength calibration and line identification, unblended lines are scanned with a microphotometer. Background contributions owing to general plate fogging, thermal electrons in the image tube, and light scattered from nearby lines are evaluated by tracing the plates along the direction of dispersion. The upper half of Fig. 6 shows a microphotometer tracing of the 4380 Å transition in Ar II. The ordinate is the transmission,  $T$ , relative to clear glass. The abscissa is the time in nanoseconds following excitation of the beam. The

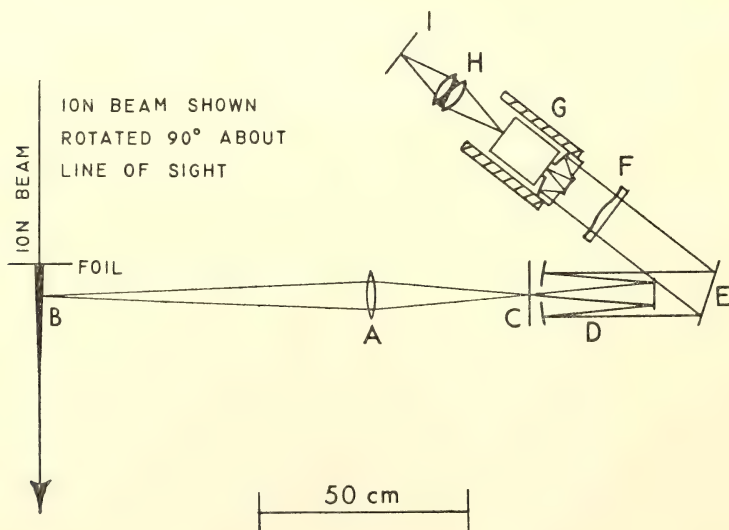


Fig. 5. Optical system. Light from the glowing beam (B) is imaged on the spectrograph slit (C) by a 25-mm aperture telescope (A). On passing the slot, the light is collimated by an  $f/16$  Cassegrain system (D), and dispersed by a Bausch and Lomb 600 line/mm grating (E) and focused by an  $f/1.4$  semisolid cassegrain-schmidt camera (F) of 140 mm focal length on the photocathode of the image intensifying tube (G). The light from the phosphor is imaged on the photographic plate (I) by the transfer lens (H).



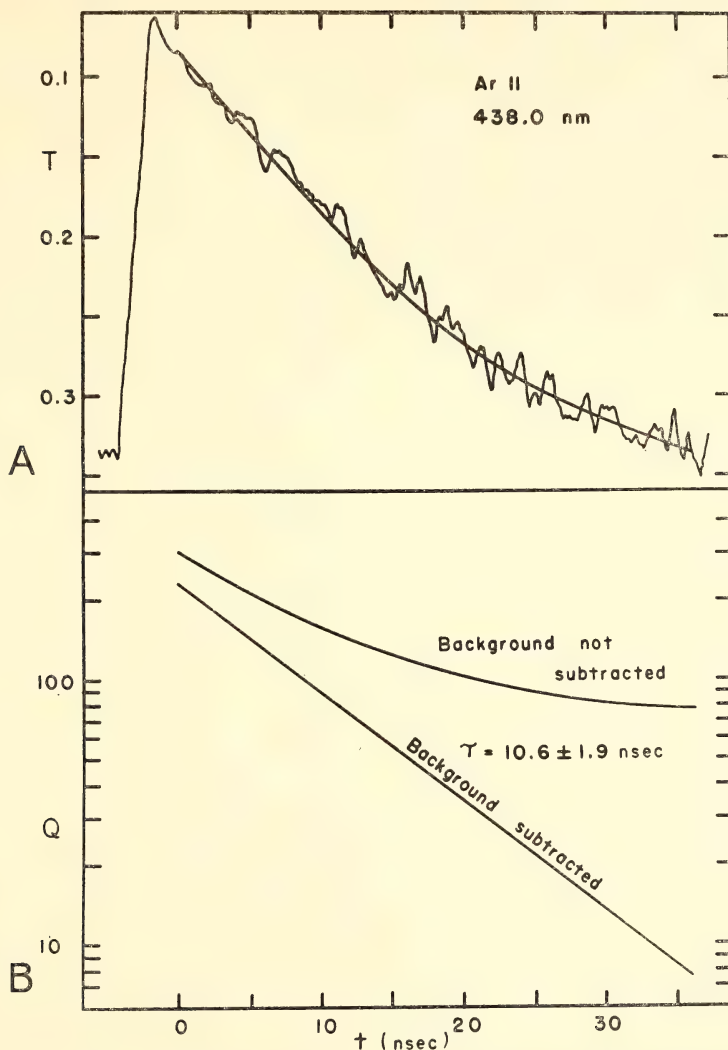


Fig. 6 A. Microphotometer tracing of the 438-nm transition in singly ionized argon. The ordinate is the transmission,  $T$ , relative to clear glass. The abscissa is the time in nanoseconds following excitation of the beam. The smooth curve is a visual fit to the tracing. B. The lower half of the figure shows a plot of the integrated light intensity,  $Q$ , as a function of time. The transmission,  $T$ , is converted to  $Q$ , using a calibration curve for the plate, which is not shown. With background subtracted this curve has an exponential decay which determines a characteristic lifetime.

smooth curve is an eye fit to the tracing. The lower half of the figure shows a plot of the integrated light intensity,  $Q$ , as a function of time. The transmission,  $T$ , is converted to  $Q$  using a calibration curve for the plate, which is not shown.

With background subtracted this curve has an exponential decay, which determines a characteristic lifetime.

Our interest in the processes that take place when atoms collide at high speeds prompted us to collaborate in the use of

our Van de Graaff machine with students of Prof. Werner Brandt of New York University. Mr. Roman Laubert and Mr. Dieter Carstanjen, who is visiting from the University of Munich, measured the X-ray yield of aluminum targets bombarded with beams of neon and argon. These measurements are described nicely by a theory of inner-penetrating electron shells, which Brandt and Laubert call Pauli excitation.<sup>15</sup>

## NUCLEAR PHYSICS

*L. Brown and E. Steiner*

Last year we described the analysis of our measurements of the elastic scattering of polarized protons by lithium-6 (*Year Book* 68, pp. 370-373). We were able to reproduce all cross section and polarization data with phase shifts, which are the fundamental quantum mechanical parameters that describe collision between microscopic particles. These results surprised us because the number of phases required for the complete description of the interaction was smaller and their behavior as functions of energy simpler than expected. Nature takes fewer liberties here than the general laws of physics permit. We had feared that complications might have arisen from the large number of

states that can be formed from a spin-half particle (the proton) and a spin-one particle (lithium-6). This simplicity has caused us to undertake similar studies for the scattering of protons by nuclei of spin- $\frac{3}{2}$ .

Figure 7 shows the S, P, and D states and the parameters that mix them for protons interacting with isotopes of spin- $\frac{3}{2}$ . D-states, which have orbital angular momentum  $\ell=2$  are seldom excited with beams of our energy, so D-phases can be neglected or set to very small values; mixing between them and other states must, of course, be correspondingly small. A comparison of states shown in Fig. 7 with those for protons and spin-one nuclei (*Year Book* 68, p. 371, Fig. 7) discloses that the spin- $\frac{3}{2}$  system has only one more state for the dominant S and P terms than has the spin-one system. It is this that suggests to us that perhaps elastic scattering of protons on isotopes of spin- $\frac{3}{2}$  may also behave in the simple manner found in lithium-6. Three light isotopes are obvious choices for such a study: lithium-7, beryllium-9, and boron-11. All three have a small nuclear charge, so nuclear forces dominate at energies attainable with our accelerator, and the structures of the systems are simple, a consequence of the small number of nucleons in-

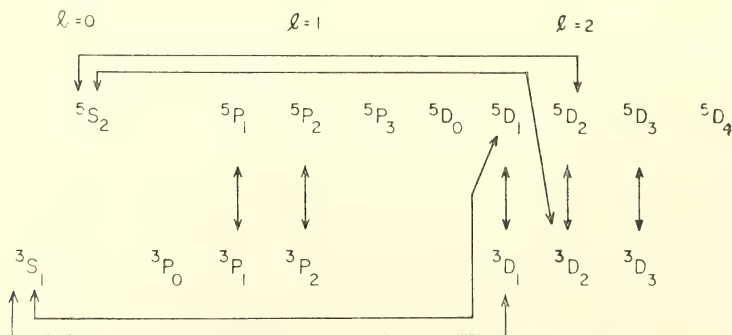


Fig. 7. Parameters describing the states for the elastic scattering of protons by  ${}^7\text{Li}$ . For orbital angular momentum  $\ell_{\max}=2$ , there are 18 phase shifts associated with the 18 states. The arrows represent mixing parameters coupling states of the same total angular momentum and parity. Previous experiment leads us to believe that states with  $\ell=2$ , D-states, can be neglected, as can mixing between triplet and quintuplet states. This reduces the parameter to a manageable number.

volved. Further, it seems likely that the phases of the three isotopes may be similar functions of energy except for the resonances, which are superimposed on the resonating phases and easily recognized.

We have begun taking data with lithium-7 as target nucleus and should have all of the data required within a few months. Neither of the other isotopes seems to offer serious experimental difficulties. Most of the computer program for the phase shift analysis, based as before on the equations of Dr. Richard Seyler, has been written; analysis should thus follow shortly after acquisition of the data.

During the fall semester Dr. Brown conducted a seminar in nuclear physics at DTM. Three graduate students at Howard University received credit at their university for participating in this seminar with Drs. Brown, Assousa, and Steiner. During the spring semester Dr. Assousa and Dr. Brown conducted an Atomic Physics Seminar with essentially the whole Astrophysics Section participating.

Dr. Rubin taught a college-level course in modern astronomy (3 hrs. per week) to qualified seniors at a local District of Columbia public high school. Special lectures to the class were presented by Drs. Erkes, Ford, and James.

## GEOPHYSICS

*S. R. Hart, I. S. Sacks, L. T. Aldrich, D. E. James, M. A. Tuve, L. M. Dorman, D. W. Evertson, A. T. Linde, K. Sinha, S. E. Forbush, G. L. Davis, T. E. Krogh, M. Casaverde, R. Salgueiro, S. Suyehiro, C. Brooks, L. Glover III, M. W. Higgins, W. S. Kirk, G. Saa, A. Rodriguez, D. Simoni, L. Tamayo, A. A. Giesecke, Jr., E. Kausel, E. Gajardo, F. Volponi, J. Mendiguren, R. Cabre, S. del Pozo, J. Bannister*

Included below is the product of both the scientific activities and the deductions of ten students of geophysics at the Department. The other names on our masthead include our colleagues in the United States and abroad who have made substantive contributions to this product. That this number of colleagues approximately equals those of us here at the DTM is a continued and deliberate attempt to amplify both the scope and depth of our geophysical studies. Our weekly seminars have measurably contributed to our understanding of current problems in geophysics and to the relationships, occasionally unsuspected, of our local activities.

The use of isotopic tracers to try to understand the origins of modern and ancient basalts; the application of modern analytical techniques to the spectra of seismic waves to learn more about both the mechanism by which earthquakes release seismic energy and the properties of our region of intense study

in the South American altiplano; the improvement of the borehole strainmeter and the correlation of the noise from this meter with that measured by a microbarograph; the improvement in precision and resolution of our mass spectrometers—these are samples of the reports included below. Not included is our continued analysis of data from and concern for the three cosmic ray meters operating near Washington, D.C., Huancayo, Peru, and Christchurch, New Zealand. The cosmic ray data will be accumulated for another five years in order that the variation in the diurnal change in cosmic ray intensity as the solar magnetic field reverses may be observed.

## GEOCHEMISTRY AND GEOCHRONOLOGY

## ANALYTICAL EQUIPMENT AND TECHNIQUES

Usually our reports deal mainly with the results and interpretations of our



scientific studies. In recent years the demands for precision and accuracy in these studies have greatly increased, resulting in a new generation of equipment and techniques which we feel warrants presentation in this report.

### *Mass Spectrometry*

*S. R. Hart, K. Burrhus, L. T. Aldrich, and T. Krogh*

This year saw completion of a new mass spectrometer of nine inch radius of curvature (Plate 2) equipped with a programmable automatic data acquisition system that permits data to be taken and processed rapidly and with high precision. The main support for the flight tube is a table in the form of an equilateral triangle constructed of aluminum plates. The magnet is supported within this table by three jack-screws, and three-dimensional positioning is provided by suitable drive-screws. Anti-parallax windows and scales are provided for complete position reference. The source and collector housings are machined from solid stainless steel forgings, and are joined by a copper flight tube. The source block contains an in-line beam valve so that vacuum can be maintained in the analyzer region during sample changing. Rough pumping is accomplished with a standard forepump operating through a molecular-sieve trap. The vacuum in the analyzer is maintained with a 15-lps Vacion pump attached to the source block behind the in-line valve. High speed source-pumping is accomplished with an 80-lps Vacion working through a four-inch valve attached directly to the source block. With this pumping system, the analyzer region is held continuously below  $1 \times 10^{-8}$  torr, and the source region will reach  $2 \times 10^{-7}$  torr within ten minutes of changing samples.

We are currently using a thick-lens Z-focusing source modified from that of Dietz<sup>16</sup> and Wasserburg *et al.*<sup>17</sup> The lens is assembled on a rigid base with

the deflection plates aligned and supported by ceramic rods and spacers. A clamping ring on the end of the source allows changes in plate position as well as changes in overall length of the lens so that experimental source modifications are easily tested. Normally, the source assembly remains fixed in the source housing; the first drawing-out plate is easily removable for cleaning, though the filament geometry of this source is such that cleaning has only rarely been necessary. The sample filaments are mounted on single, double, or triple-pin A. E. I. filament beads, and the loaded bead is simply supported on the vacuum flange by the electrical connectors. With our present source and machine geometry and vacuum, the overall resolution is such that strontium or lead peaks contribute in general less than one part in  $10^5$  to the neighboring peaks.

The collector assembly uses an adjustable width slit and a movable Faraday cup mounted on a sapphire rod, so that either direct collection or electron-multiplier collection may be utilized. Ion-currents are amplified with a Cary model 401 electrometer modified so that polarization and time-constant residuals due to a given signal decay to less than 0.01% of the signal within 2.5 seconds after the signal is switched off. (As received, these electrometers are frequently damped with capacitors which show excessive polarization.) The signal from the VRE is sent through a Hewlett-Packard 2212A voltage-to-frequency converter to a H-P 5216A counter. The BCD output of this counter is interfaced with an IBM 029 card-punch through a DTM designed scanner-coupler with noise filter. Final processing of the data cards is done on the Department's IBM 1130 computer.

Linearity of the recording system is calibrated with a high precision voltage decade monitored by a L&N K3 potentiometer. We have found the V-F con-

verter to be highly stable and linear, with nonlinearities consistently less than 0.01% of the signal for signals down to 2–3% of full scale. One of our Cary electrometers (serial 300) was equally good, allowing high precision recording without the need for signal attenuation. However, another 401 electrometer we have tested (serial 4) showed serious nonlinearity (irrespective of the input resistor, which we will discuss later). The nonlinearity is such that signals at 10% and 3% of full scale were found to be low by 0.04% and 0.20%, respectively.

Peak switching is done by a five-channel magnet-jump-scanner using either a fixed-point or a scanning-point mode. In the first case the magnet is incremented to a given part of each peak top, and up to five successive one-second counts taken. In the scanning-point mode the magnet is incremented to one edge of the peak top and slowly scanned across the peak while successive one-second counts are taken. In typical operation we read four counts on each peak top and four counts on a zero for each scan of the spectrum, with at least six seconds allowed between each set of readings due to the time requirements of magnet hysteresis and electrometer time-constant.

### *Isotopic Analysis of Strontium*

*S. R. Hart, T. Krogh, and K. Burrhus*

Purified strontium samples are normally loaded on single Ta or Re filaments, usually with tantalum-oxide powder as an activator. The advantages of this procedure over triple-filament techniques—ability to run small samples ( $<10^{-7}$ – $10^{-8}$  g) and lack of isobaric rubidium contamination—are partly offset by the greater difficulty involved in achieving highly stable emission. Runs can usually be handled so that the deviations from interpolated linearity of successive peaks will fall in the range 0.05%–0.15%. However, this appears to

be dependent on chemical purity, and occasional runs will be much worse than this. Generally, the emission stability is the limiting factor in our final precision, so the length of the run must be matched to the ion-beam stability. For runs of high stability we generally collect 20–30 spectrum scans; for unstable runs, or where the highest precision is sought, 50–100 scans may be required. Thus, to a certain extent, our precision for isotopic analysis is not a fixed value but varies with the characteristics of each run and the user demands on the mass spectrometer. For analysis of the Eimer and Amend  $\text{SrCo}_3$  isotope standard (which runs very stably) 20–30 scans result in 95% confidence-level precision of about  $\pm 30$  ppm (for normalized  $\text{Sr}^{87}/\text{Sr}^{86}$  ratios), on a daily-to-weekly time scale. For samples, however, it is generally difficult to maintain precision of better than 100 ppm without unduly long runs.

Reproducibility can be maintained at this level only as long as machine and operational characteristics are held constant. Over a period of six months, during periodic machine modifications and under various operating schemes, our value for the E&A standard has varied between 0.70785 and 0.70815. Our uncorrected value for runs taken with our “nonlinear” electrometer was 0.70775. Specification of the absolute value of  $\text{Sr}^{87}/\text{Sr}^{86}$  to better than  $\pm 0.0001$  obviously requires absolute calibration of electrometer linearity to better than 0.01% and detailed knowledge of the voltage coefficient of the input resistor. Because this latter measurement is difficult to perform with test equipment we have measured it indirectly with a strontium standard artificially prepared to have  $87/86 \sim 1$  and  $88/86 \sim 8$ . Sets of data were taken on this sample at various ion current levels (ranging from 1v to 30v on a  $10^{11}$  ohm resistor), and all data were normalized to a common value for  $87/86$ , as this ratio is unaffected by

voltage coefficients. The deviations of the 86/88 ratio, plotted against the 88 voltage, gave us a value for the voltage coefficient of 0.014% per volt. Taking account of the various linearity corrections, our best value for the E&A standard would be about 0.70800. However, we wish to emphasize the fact that it is very difficult to demonstrate knowledge of this value to better than  $\sim 0.01\%$ . As a final comment on Sr isotope measurement, we can foresee short-term precision for Sr samples of 10–20 ppm in the near future. Valid or useful intercomparison of different samples at this level, however, begins to put extreme demands on the assumption of constancy of  $\text{Sr}^{86}/\text{Sr}^{88}$  ratios in nature, an assumption which can perhaps no longer be justified theoretically at this level of precision.

### *Lead Isotopic Analysis*

*A. K. Sinha, G. L. Davis, S. R. Hart, and T. Krogh*

Almost all lead runs are now made using the silica gel-phosphoric acid activator technique of Cameron.<sup>18</sup> With this technique we are able to obtain strong runs on  $10^{-7}$ – $10^{-8}$  g samples of lead, and though emission stability is occasionally difficult to achieve with the gel technique, our runs normally will show satisfactory interpolated linearities (in the range 0.05%–0.20%).

Precision for lead isotope analysis is generally limited by fractionation effects,

since there are no fixed isotope pairs with which to normalize as there are with strontium. While lead standards run with the silica gel technique commonly show less absolute fractionation than with sulfide runs, the between-run variability in fractionation is not greatly different. For high precision in our common lead and zircon-lead runs, we have developed a mixed 207/204 lead spike similar to that used by Compston and Oversby.<sup>19</sup> The computations for this procedure are done non-iteratively by a direct-solution method kindly supplied to us by M. J. Dallwitz. This double-isotope lead spike was calibrated against the absolute 1:1 NBS lead standard, and the value for the 207/204 ratio found to be 5.817. To assess the precision and accuracy of this spike, several mixtures were made up with the California Institute of Technology common lead standard, and the results from the mixtures used to correct the fractionation effects on a series of 32 unspiked ratio measurements of the Cal Tech lead standard (7 runs as sulfide, 25 runs by silica gel technique). The results are given in Table 4 for the mean corrected value of the Cal Tech standard and the standard deviation of the 32 corrected runs. For comparison, the mean and precision of 25 unspiked runs as analyzed by our silica gel technique are also given, along with the value for this standard reported by Catanzaro<sup>20</sup> and by Compston and

TABLE 4. Analysis of Cal Tech Lead Standard Using a Two-Isotope Lead Spike

	$Pb^{206}/Pb^{204}$	$Pb^{207}/Pb^{204}$	$Pb^{208}/Pb^{204}$	$Pb^{206}/Pb^{207}$	$Pb^{206}/Pb^{208}$
Mean value, mix 1 (32 unspiked runs)	16.6472	15.5003	36.3541	1.07399	0.45792
Mean value, mix 2 (32 unspiked runs)	16.6478	15.5011	36.3563	1.07398	0.45790
Mean value, 25 unspiked runs by silica gel technique	16.6148	15.4552	36.213	1.07503	0.45881
Catanzaro <sup>20</sup>	16.625	15.475	36.301	1.0743	0.45798
Compston and Oversby <sup>19</sup>	16.600	15.443	36.181	1.07492	0.45880
Standard deviation, mix 1	0.091%	0.098%	0.084%	0.045%	0.020%
Standard deviation, mix 2	0.053%	0.072%	0.055%	0.036%	0.003%
Standard deviation, silica gel	0.20%	0.32%	0.42%	0.12%	0.22%
Standard deviation, Compston and Oversby <sup>19</sup>	0.045%	...	...	0.025%	0.045%



Oversby. The agreement between our average values derived from the two mixtures is quite good, with the largest difference being 0.006%. Our values are quite different (0.1–0.5%) from Compston and Oversby's, and different from the unspiked gel runs. However, our agreement with Catanzaro is excellent, with only the ratios involving 204 outside (0.17%) the error limits quoted by Catanzaro (0.11%). Our precision or reproducibility, based on intercomparison of the 32 corrected unspiked runs, is better than 0.11% for all ratios and is a factor of 2–10 better than that obtained by the gel technique. The precision quoted by Compston and Oversby for their double spike technique is somewhat better than ours, but is highly unrealistic as it is based on comparison of 15 spike-normal mixtures with only one unspiked run. Clearly, the precision of actual sample analyses is largely controlled by the unspiked run with its unfavorably small 204 peak. The spike-normal mixtures are amenable to much more precise measurement (for example, compare the differences between our two mixtures), and therefore we feel our quoted precision is a much more relevant estimate than that of Compston and Oversby.

We have not completed our analysis of the error propagation effects due to various measurement errors, such as variable contamination between spiked and unspiked runs. However, it appears that these effects are not serious for reasonable spike-normal mixtures of either common or radiogenic lead, and the effects due to variable lead blank are only slightly worse (50%) than they would be in unspiked analyses. Our analyses of the Cal Tech standard demonstrate that the fractionation of lead follows a theoretical fractionation law very precisely, as shown in Fig. 8. This result is contrary to that of Ozard and Russell<sup>21</sup> who, on the basis of relatively few analyses, stated that Pb fractiona-

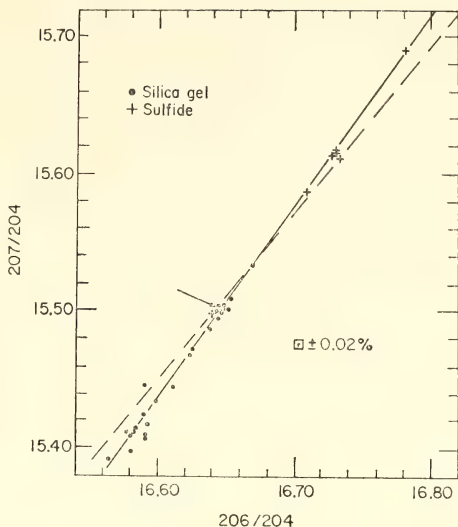


Fig. 8. 207/204–206/204 plot of Cal Tech lead standard analyses. Solid line is theoretical fractionation line; dashed line is fractionation trend proposed by Ozard and Russell.<sup>21</sup> Mean value after normalization with double-spike shown by arrow.

tion on rhenium filaments did not follow the simple fractionation law.

With the high sensitivity of the silica gel technique, it is now possible to run much smaller samples than before, and the limiting factor now becomes the level of lead contamination during chemical processing. We have monitored the environmental lead levels, and find a contribution of  $\sim 0.0005$  micrograms per day in the clean lab (averaged over a period of 26 days) and a contribution of  $\sim 0.0003$  micrograms per hour in the source loading and mass spectrometry lab (for 7 cm<sup>2</sup> surface area). Total lead blanks during HF-HClO<sub>4</sub> dissolution of 3–4 gram samples of whole rock and subsequent processing run about 0.07 micrograms; most of this is contributed by the HClO<sub>4</sub> dissolution of whole rocks in Teflon bombs. This dissolution, using H<sub>2</sub>SO<sub>4</sub>+HNO<sub>3</sub>, is expected to yield blanks of  $\leq 0.01$  microgram.

Recently we have applied the silica gel-phosphoric acid technique to anal-

ysis of uranium and thorium and find that stable ion beams of these two elements can be achieved at levels similar to or better than those using multiple-filament ionization techniques. The general technique, as modified in this lab, is to take a single drop of silica gel from the water-gel interface (after agitating and settling for 10–20 seconds) and apply it to an outgassed 20 mil flat rhenium ribbon, while heating at 0.5 amps. When the gel has evaporated to a fine film (5–10 minutes), a mixed sample of U, Th and Pb, picked up in 0.75 *M* phosphoric acid, is added to the filament and the current increased to 1.1 amperes. At the first sign of bubbling, the current is reduced to 0.7 amperes and then slowly raised to 1.5 amperes until all the phosphoric acid evaporates. The load will turn brown or black if more than a few micrograms of lead are present. With this technique, the concentration analysis for U, Th and Pb in a rock or zircon can be completed from a single filament load. The filament temperature and current ranges necessary to produce satisfactory ion beams ( $>10^{-12}$  amperes) for these elements are: Pb, 950–1330°C (1.1–1.5a); U, 1300–1650°C (1.6–2.0a); Th, 1700–1900°C (2.4–2.7a). To demonstrate that no unusual fractionation effects occur because of the mixing of these elements, a mixture of Cal Tech lead standard, thorium spike, and normal uranium was made and analyzed by this technique. The lead ratios obtained from this mixture were within 0.1% of the average Cal Tech gel value shown in Table 4; the uranium and thorium ratios were within 0.2% of values obtained in the usual way on single- or multiple-filament runs.

## OCEAN FLOOR BASALTS

*S. R. Hart*

Last year we reported studies of the alteration of dredge basalts caused by interaction with sea water. The results

showed that the amounts of the trace elements K, Rb, and Cs are particularly susceptible to this type of alteration, whereas the Sr content is relatively resistant to alteration. As a result of these investigations, criteria were developed which now enable us to select fresh samples for further study of these trace elements. During the past year we have looked into the effect of crystal differentiation on the alkali and alkaline earth elements in dredge basalts; we have searched for correlations of trace element chemistry with the dynamics of the sea floor spreading process; and we have carried out high precision Sr isotope analyses to test for differences in mantle evolution in the source regions of ridge basalt as compared to oceanic island basalt.

### *Differentiation Effects*

Puzzling discrepancies have been apparent in trace element analyses of various samples from Amphitrite, dredge 3 (Scripps Institute of Oceanography). We have determined the major element content of thirteen fragments from this dredge and a histogram of the results, Fig. 9, clearly demonstrates the presence of both basaltic and andesitic rock types. The andesite is clearly calcalkaline in nature and has a Peacock alkali-lime index of about 60. This is the first record of an andesitic rock type dredged from the sea floor, although Aumento (1969)<sup>22</sup> has recently reported an occurrence of diorite on the mid-Atlantic ridge and Kay, Hubbard, and Gast (1970)<sup>23</sup> have reported an analysis of a "basaltic" glass from the bottom of a sediment core from the East Pacific Rise which is very similar to the Amphitrite 3 andesite. The concept of a near-surface differentiation of alkali basalt from tholeiite as suggested by Engel *et al.* (1965)<sup>24</sup> is clearly inconsistent with these findings of calcalkaline differentiates on the ocean floor.

Only one of the 13 analyses does not fit

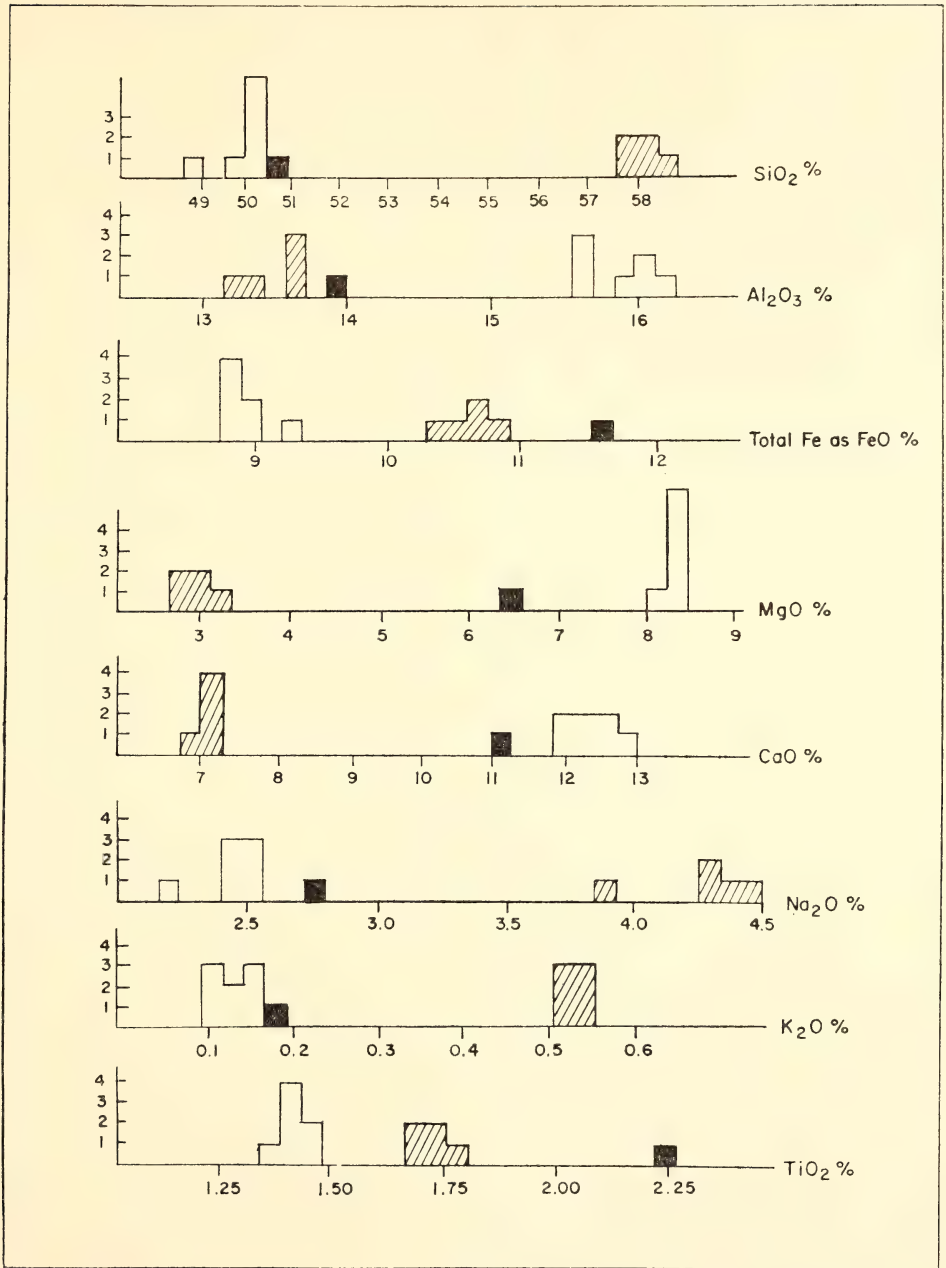


Fig. 9. Histogram of major element variations in the Amphitrite 3 basalt-andesite suite.



the bimodal grouping of basalt and andesite shown in Fig. 9. This sample is similar to the tholeiites in  $\text{SiO}_2$ ,  $\text{CaO}$ ,  $\text{MgO}$ , and  $\text{K}_2\text{O}$  and similar to the andesites in  $\text{Al}_2\text{O}_3$  and  $\text{Na}_2\text{O}$ ; however, it has a higher content of  $\text{FeO}$  and  $\text{TiO}_2$  than either the tholeiite or the andesite groups. The basalts and the andesites may both exhibit glassy surfaces, although the andesites generally are found as thin fracture-bounded plates. Even these latter, however, show only very fine-grained variolitic and arborescent textures, demonstrating that they cooled very rapidly. Aside from occasional olivine microphenocrysts and a few large rounded crystals of plagioclase, phenocrysts are rare. (One plagioclase grain in an andesite sample gave a composition of An 69 by microprobe analysis.) All samples appear very fresh, with no microscopic evidence of alteration and with only minor surface and crack coatings and fillings.

The average compositions of the tholeiite group and the andesite group are given in Table 5. A computed "model andesite" is also shown in Table 5, calculated from the tholeiite composition by subtraction of 30% plagioclase (An

80), 22% clinopyroxene, 8% olivine (Fo 85), and 2.3% titanomagnetite. This differentiation scheme is obviously not unique, and a better fit might be obtained by using the least-squares technique of Bryan *et al.* (1969);<sup>25</sup> it is sufficient, however, to show that the andesite composition can be derived in a relatively simple way from the tholeiite composition. It is interesting to note that Kay *et al.* (1970) concluded that the minor compositional variations found among dredge basalts could be explained by crystallization of plagioclase and olivine in proportions of about 4:1, essentially the same proportions derived from the computation of Table 5. It is possible that the clinopyroxene enters into the crystallization sequence only after more extreme degrees of crystallization than those described by Kay *et al.* (1970).

The only elements whose distributions are difficult to reconcile with this simple differentiation model are  $\text{K}_2\text{O}$  and  $\text{H}_2\text{O}^+$ , both of which are concentrated in the andesite by a factor of two more than the model would predict. All attempts to fit these two elements into a model based solely on crystal-liquid equilibria have been unsuccessful. I am forced to conclude that some form of concentration mechanism involving partitioning and transfer in a vapor phase is required. (This applies to the trace elements Rb and Cs as well.)

The K/Rb-K/Cs relationships of 6 samples from Amphitrite 3 are shown in Fig. 10. The K/Cs ratios in the tholeiites and andesites are very similar, lying in the range 55,000–75,000. The intermediate sample 3J has a distinctly lower K/Cs ratio (40,000). While 3J appears as fresh as the other samples, Cs is so sensitive to alteration that there are no reliable criteria to prove that this sample is unaltered. The K/Rb data are more clear-cut and show that this ratio is essentially unaffected by differentiation (of the type proposed in Table 5). The

TABLE 5. Comparison of Chemical Analyses of Amphitrite-3 Samples with a Crystal Differentiation Model (Number of analyses averaged, in parenthesis)

Sample	Tholeiite (7)	Andesite (5)	Com- puted †
$\text{SiO}_2$ , %	50.1	58.1	57.8
$\text{Al}_2\text{O}_3$ , %	15.8	13.4	13.3
$\text{FeO}^*$ , %	8.9	10.6	11.6
$\text{MgO}$ , %	8.3	2.9	3.2
$\text{CaO}$ , %	12.2	7.1	7.9
$\text{Na}_2\text{O}$ , %	2.5	4.3	4.8
$\text{K}_2\text{O}$ , %	0.10	0.54	0.24
$\text{H}_2\text{O}^+$ , %	0.16	1.02	0.42
$\text{TiO}_2$ , %	1.4	1.7	1.7
Sr, ppm	115	106 ‡	105
Ba, ppm	13 §	39 ‡	30

\* Total iron calculated as  $\text{FeO}$ .

† By subtracting 30% An 80, 22% Cpx, 8% olivine, and 2.3% titanomagnetite from tholeiite average.

‡ From Philpotts *et al.*, 1970.<sup>28</sup>

§ Average of 8 East Pacific Rise basalts.

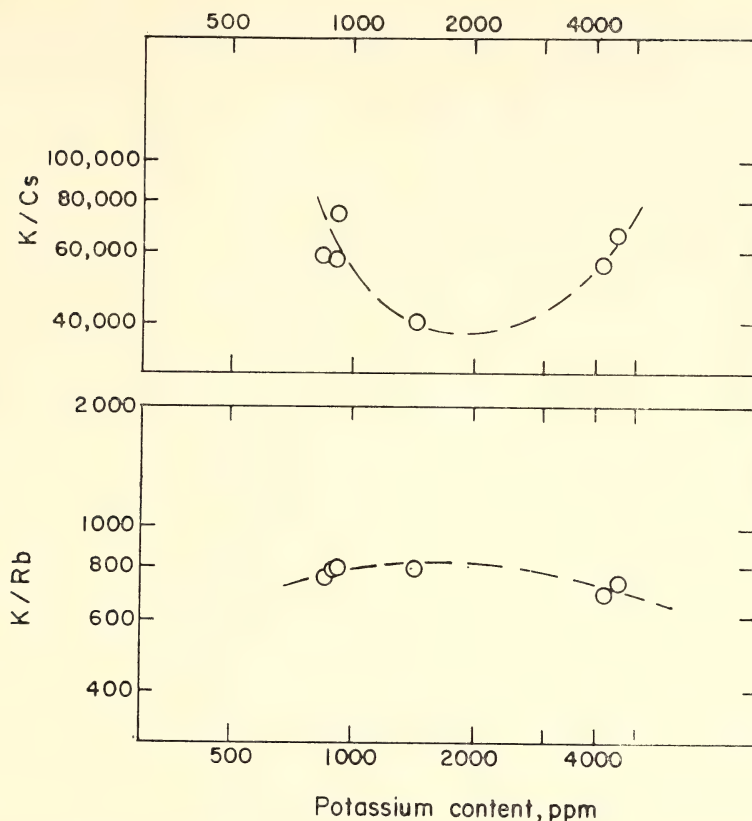


Fig. 10. K/Rb and K/Cs versus K content in basalt-andesite dredge suite from Amphitrite 3, Scripps Institution of Oceanography.

maximum variation in K/Rb is 15% over a range in K content of more than a factor of 5.

Consideration of partition coefficients strongly supports this observed decoupling of K/Rb ratio from the differentiation process. The K/Rb partition coefficients for plagioclase, clinopyroxene, and olivine reported by Philpotts and Schnetzler (1970),<sup>26</sup> coupled with a fractional crystallization model (using the mineral abundances shown in Table 5) predict a K/Rb ratio in the andesite only 5% lower than that in the tholeiite starting melt. This is largely because both K and Rb are strongly partitioned into the melt. I have already noted above, however, that a crystal fractionation

scheme (either equilibrium or fractional) which satisfies the major elements is insufficient to produce the observed  $H_2O^+$  and  $K_2O$  concentration factors; thus the K/Rb-K/Cs relationships may involve other mechanisms in addition to simple crystal-liquid equilibria. For example, if concentration takes place by a vapor transport mechanism, then the K/Rb-K/Cs ratios would be dependent in detail on the nature of the liquid-vapor equilibria as well.

The results for Sr and Ba in Table 5 show that the concentrations of these elements in the andesite can be accounted for by the simple crystal-liquid differentiation model. The rare earth elements in one of the Amphitrite 3 ande-

sites have been reported by Frey *et al.* (1968).<sup>27</sup> Both analyses show a large depletion anomaly for europium (35–40%), which is qualitatively consistent with crystallization and removal of substantial quantities of plagioclase. Philippotts *et al.* (1970)<sup>28</sup> have shown how the europium concentrations of a number of dredge basalts, including the Amphitrite 3 andesite, can be interrelated in terms of a simple fractional crystallization model involving plagioclase.

The trace element parameters that are useful in "seeing through" differentiation effects are thus the K/Rb ratio, perhaps the K/Cs ratio, and Sr concentration. Concentrations of K, Rb, Cs, and Ba are all strongly affected by differentiation. Barium apparently does not follow the alkalis particularly well during differentiation, as it can be modeled by crystal-liquid equilibria, whereas the alkalis seem to require some additional mechanism of concentration such as vapor transport. Thus, the K/Ba ratio shows some dependence and the K/Sr ratio a large dependence on the differentiation processes that are known to modify the compositions of dredge basalts (Miyashiro, 1969;<sup>29</sup> Kay *et al.*, 1970).

### Regional Trace Element Variations

The concentrations of the alkali metals in dredge basalts show variations of up

to a factor of ten, and part of this variation may be due to high level differentiation effects. Variations in ratios, such as K/Rb, are difficult to account for in this way. In the five cases where more than one fragment was analyzed from a single dredge, it is apparent that K/Rb is not even uniform in a single dredge haul, though the range is generally much smaller than that between different dredge hauls. These variations could arise in several ways. First, the suboceanic mantle is demonstrably non-uniform (Gast *et al.*, 1964;<sup>30</sup> Tatsumoto, 1966)<sup>31</sup> and thus may yield basaltic melts which reflect this nonuniformity. Secondly, the partial melting process itself may be variable, due either to different degrees of melting or to the effects of partitioning among different mineral assemblages. Griffin and Murthy (1969)<sup>32</sup> have shown that, while it is difficult to generate variable K/Rb ratios from an amphibole peridotite by different degrees of partial melting, addition of minor amounts of phlogopite is quite effective in this regard.

To what extent are mantle heterogeneities and/or variations in partial melting processes related to plate dynamics? While the quantity and geographic coverage of fresh samples are hardly adequate to settle this problem, I have assembled my samples into two composites: one representing 6 localities

TABLE 6. Data on Composite Samples from Mid-Ocean Ridges  
(All element concentrations in ppm)

	K	Rb	Cs	Sr	Ba	K/Rb	K/Cs	Rb/Sr	Sr <sup>87</sup> /Sr <sup>86</sup>
<i>Slow Spreading Ridges</i> *	1260	1.16	.018	140	7.8	1080	69,000	.0083	0.70277
Mid-Atlantic, Carlsberg 7 samples, 6 localities									
<i>Fast Spreading Ridges</i> †	1060	1.06	.015	131	13.2	1040	71,000	.0081	0.70248 ‡
East-Pacific, Juan de Fuca 8 samples, 5 localities									
<i>Difference, %</i>	20	10	25	7	50	4	3	2	0.041

\* Samples AD5-5, AD5-18, AD2-1, AD3-3, Chain 44-2-1, 5111.7, GE 159.

† Samples Amph 1-PDIP, Amph 3-PD3, DIO-SRH 1, DIOA-I, Amph 1-DIC, Amph 4A, Amph 4B, D2-SRHA.

‡ Values normalized to 86/88 = 0.1194 and relative to E and A standard value of 0.70810. Error, 95% confidence limits = ± 0.0001.



on ridges of slow (normal) spreading rate, and one representing 5 localities on ridges with high spreading rates. Table 6 shows a summary of data for these composites. Considering the small number of samples involved and the large individual variations in concentration, it is clear that the K, Rb, Cs, and Sr concentrations are indistinguishable in basalts from the two types of ridges. The Ba data seem rather different in the two composites, but in the absence of values on the individual samples this cannot be evaluated statistically. The ratios K/Rb, K/Cs, and Rb/Sr are almost identical in the two composites. The  $\text{Sr}^{87}/\text{Sr}^{86}$  ratios, while clearly distinct analytically, are nevertheless very similar; again, in the absence of individual values for all the samples, this small difference cannot be evaluated statistically. These data clearly show that mantle chemistry, while variable, is very effectively decoupled from the dynamic processes involved in plate movement. Insofar as U and Th levels can be inferred from the alkali metal contents, it would appear that the general level of radioactivity in the upper mantle is also unrelated to plate dynamics.

#### *Strontium Isotope Evolution in the Mantle*

There is considerable disagreement between the two Sr isotope analyses reported in Table 6 and other values reported previously in the literature. Tatsumoto, Hedge, and Engel (1965)<sup>33</sup> obtained an average value for three mid-Atlantic Ridge samples of 0.7024 and for two East Pacific Rise samples of 0.7016. Evidence from other published papers of these authors suggest that their values are systematically low and, to be compatible with the E and A Sr standard reported in Table 6, should be raised by about 0.001. This correction would bring their Pacific value into line

with the "fast" composite value; their Atlantic value, however, ends up considerably higher than that of the "slow" composite. Gast (1967)<sup>34</sup> reported three values for Atlantic dredge samples (0.7032 average) and three values for Pacific dredge samples (0.7030 average). Both of these averages are higher than the values in Table 6, though there is, unfortunately, no way to compare them in an absolute sense, as Gast (1967) did not report a value for the Sr standard. Bence (1966)<sup>35</sup> analyzed four Atlantic basalts (0.7035 average) and seven Pacific basalts (0.7034 average) along with a carefully controlled value for the Sr standard which is the same as that used as a basis in Table 6. Bence's basalt values should be directly comparable then with the composite values of Table 6; however, it is clear that they are systematically higher by 0.0008. As each composite contains three samples from dredge hauls also analyzed by Bence (1966), it seems unlikely that these isotope ratio differences can be attributed to sampling variations or differences in state of alteration. Most of Bence's analyses were calculated from spiked runs and it is possible that some of the discrepancy arises from this approach. (For example, two of the three dredge basalts which were analyzed unspiked gave values  $\sim 0.0008$  lower than values calculated from the spiked runs.) I feel that the Sr isotopic analyses in Table 6 should supplant previous values for ocean floor basalts, partly because the samples were carefully picked for freshness and partly because the samples were run, along with the Sr standard, under conditions of ultra-high precision. An accurate Sr isotopic value for ocean floor basalts is necessary if meaningful comparisons are to be made with the basalts of the oceanic islands. Bence (1966) concluded from his study that alkali basalts from oceanic islands have very similar Sr isotopic ratios to ocean floor basalts, and suggested that similar

mantle source materials might supply both magma types. Gast (1968)<sup>36</sup> has stressed the necessity for deriving ocean floor basalts from a mantle depleted in the dispersed elements relative to that from which alkali basalts are generated. If the depletion event(s) has occurred at a much earlier time, as advocated by Tatsumoto (1966), then Sr developed in the depleted mantle should be less radiogenic than that in "undepleted" mantle, and dredge tholeiites should be less radiogenic than alkali basalts. The new Sr isotope values of Table 6 show that this is true. The average Sr of oceanic islands is about 0.7036, for both alkali basalt and tholeiitic basalt. The lowest well-documented value for a single island is for Iceland (Moorbath and Walker, 1965),<sup>37</sup> where 12 basalts average 0.7029 (relative to Sr standard of Table 6). Other islands range considerably higher, as for example, Hawaii, where analyses tabulated by Gast (1967) average 0.7043. Thus, while there is a real variation of Sr isotope ratio between different islands, all islands appear to show higher values than the dredge basalt average of 0.7026 (Table 6). I believe this strongly argues for generation of ocean floor basalts from a mantle source region which has undergone depletion of the dispersed elements, especially Rb, Cs, and Ba, at some considerably earlier time in the earth's history. If the K/Rb ratio of basalts is used as an index of relative depletion, then it appears that the depletion factor is about 2-3 times. I infer from this that the Rb/Sr ratio of the mantle region from which submarine ridge basalts are generated is a factor of 2-3 lower than that in the "undepleted" mantle regions. This difference has existed for a relatively long time, and may have been produced in a single episode (Tatsumoto, 1966), in multiple episodes (Gast, 1968),<sup>38</sup> or essentially continuously (Hart and Brooks, 1969).<sup>39</sup>

# GEOCHEMISTRY OF FRANCISCAN VOLCANIC AND SEDIMENTARY ROCKS FROM CALIFORNIA

*A. K. Sinha and T. E. Davis*

The Franciscan assemblage on the western margin of the United States is a complex mélange of volcanic and sedimentary rocks. The rock assemblage of graywackes, cherts, pillow basalts, greenstones, peridotite, and dunite suggests a eugeosynclinal environment.

Numerous workers have attempted to evaluate the geology and the nature of the Franciscan basement. Reed (1933)<sup>40</sup> proposed deposition of Franciscan rocks in local basins underlain by granitic basement. Taliaferro (1943)<sup>41</sup> suggested that metamorphic rocks of the Paleozoic Sur series underlie the Franciscan eugeosynclinal assemblage. Bailey, Irwin, and Jones (1964)<sup>42</sup> hypothesized "basalt substratum or ultramafic rock" for the basement material. Ernst (1965)<sup>43</sup> emphasized the absence of continental type crustal inclusion in presumably diapiric serpentinites, which he suggested to be hydrated mantle material. Hsu (1966)<sup>44</sup> postulated an "older granitic basement" which was subsequently remobilized to form the coast range batholith. Besides, the Franciscan assemblage and associated ultramafics, according to Hsu, have been thrust or gravity slid from a root zone near the western margin of Sierra Nevada and represent a highly deformed allochthonous mass of mixed rocks. Hatherton (1969)<sup>45</sup> modified an earlier hypothesis of Irwin and Bath (1962)<sup>46</sup> and suggested an ultramafic basement for the Franciscan eugeosyncline. This ultramafic layer was supposedly deformed upward into a ridge now exposed as a continuous belt of serpentinite separating the eugeosynclinal Franciscan from the miogeosynclinal Great Valley sequence rocks. Moreover, this ridge appeared prior to the eugeosynclinal-miogeosynclinal sedimentation and functioned as a buffer during subsequent deformation of the basin. Ernst (1970)<sup>47</sup>

and Page (1970)<sup>48</sup> have proposed sea floor spreading and continental margin tectonics to explain the distribution of the Franciscan. Their models indicate that the basement is oceanic crust.

The purpose of the present study is to determine the nature of the basement of the Franciscan by using Rb, K, Sr, and Pb as tracers. Earlier Sr isotopic ratios and abundance ratios of K and Rb have been used with success in determining whether volcanic rocks in a given area have continental or oceanic affinities. The average  $\text{Sr}^{87}/\text{Sr}^{86}$  ratio for oceanic basalt is 0.7038, and for continental tholeiites the  $\text{Sr}^{87}/\text{Sr}^{86}$  ratios show a large spread, although overlap with oceanic basalts is common.

The  $\text{Sr}^{87}/\text{Sr}^{86}$  ratios and Sr, K, Rb concentrations for some Franciscan rocks are given in Table 7. The average  $\text{Sr}^{87}/\text{Sr}^{86}$  of the Franciscan tholeiites is 0.7069, a value much too high to prove that the

basement is basaltic. The spread in the ratios obtained would suggest partial contamination with a continental crust. We, however, propose a model which relates variations in strontium isotopic composition to the concentration of strontium in a basic rock. The process is equilibration with sea water and the amount of change in  $\text{Sr}^{87}/\text{Sr}^{86}$  is related to the concentration. Fig. 11 is a plot of  $\text{Sr}^{87}/\text{Sr}^{86}$  measured in basalts and andesites against concentration. The upward trend in  $\text{Sr}^{87}/\text{Sr}^{86}$  seen is real (all the data have been normalized to one standard value of Eimer and Amend at 0.7082) and is directly related to the observed concentrations. This model, however, does not propose equilibration with sea water for all oceanic tholeiites, but is applicable to only those which are related to island arc or trench systems. We believe that Fig. 11 adequately shows degrees of partial equilibration.

TABLE 7. K, Sr, Rb, and  $\text{H}_2\text{O}^+$  Concentrations and  $\text{Sr}^{87}/\text{Sr}^{86}$  of Some Volcanic, Metamorphic, and Sedimentary Rocks from the Franciscan Assemblage, California

Sample	$\text{Sr}^{87}/\text{Sr}^{86}$	Sr, ppm	Rb, ppm	K, ppm	K/Rb	K/Sr	Rb/Sr	$\text{H}_2\text{O}^+$ , %
<i>Volcanics</i>								
AC-SB-20V	0.7069	142.1	142.1	900	660.6	6.33	.0096	4.1
PS-SB-6V	0.7078	151.3	30.2	10,080	358.1	66.6	.200	4.9
NA-SC-5V	0.7066	221.8	22.1	8,600	389.9	38.8	.057	2.6
SS-S-7V	0.7078	188.7	4.60	3,300	710.2	17.5	.024	4.9
L-M-IV	0.7038	229.4	2.23	1,600	728.7	6.97	.009	4.2
SS-S-2V	0.7073	77.0	0.57	700	1166.7	9.1	.007	4.4
CI-LA-IV	0.7076	60.3	0.90	300	340.0	5.63	.015	5.02
RP-M-IV	0.7083	108.9	12.6	7,265	576.6	11.93	.116	5.2
SM-SLO-IV	0.7072	66.7	0.47	200	535.0	2.99	.007	4.3
<i>Blue Schists</i>								
BR-SB-21BS	0.7469	7.73	52.76	9,188	174.1		6.82	4.9
RR-S-1BS	0.7064	128.2	7.20	1,373	196.0		.056	4.8
PF-M-6BS	0.7218	39.0	87.1	24,151	277.0		2.24	5.6
<i>Graywacke</i>								
PF-M-7G	0.7060	141.4	2.77	1,165	420.6		.020	5.3
<i>Average</i>								
Franciscan	0.7069	138	5.3	2,600	500	19.3	.038	
Archaean *	0.7018	150	5.9	1,900	330	13.0	.040	
Orogenic								
Archaean *	0.70	260	45	1,1000	360	42.0	.017	
Tholeiite *	0.7038	450	17	6,000	340	12.9	.004	
Submarine								
Basalt *	0.7033	125	1.8	1,600	900	13.0	.014	
<i>Trench</i>								
Basalt †	0.7033	128 to	2.55 to	1,871 to	732 to	14.6 to	.020 to	
(Puerto Rico)	to 0.7062	124	1.86	2,441	1,310	19.6	.015	

\* Values from Hart *et al.*, 1969.<sup>49</sup>

† Values from Hart and Nalwalk, 1970.<sup>50</sup>



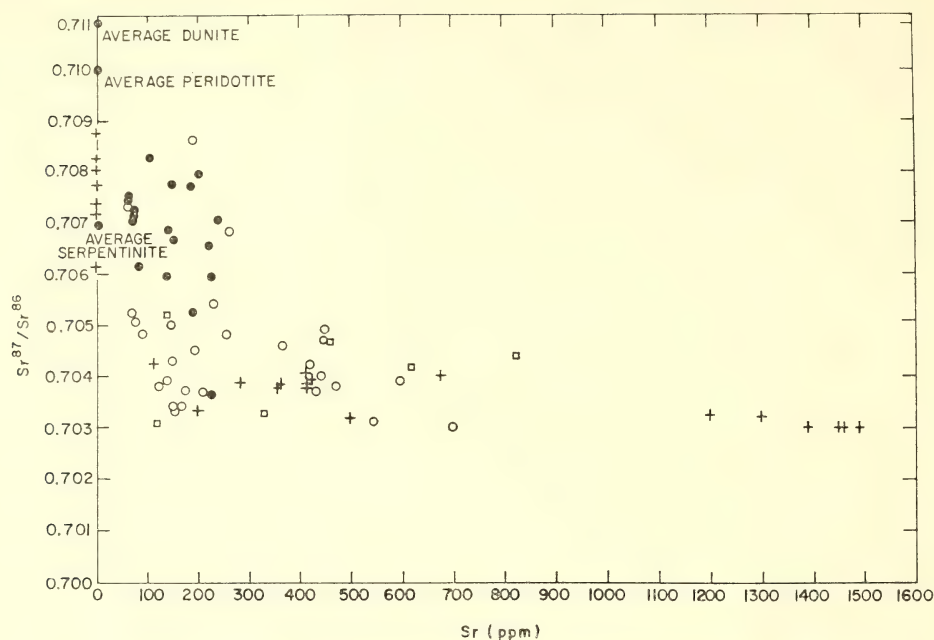


Fig. 11. Strontium concentration versus  $\text{Sr}^{87}/\text{Sr}^{86}$  of modern tholeiites and andesites.

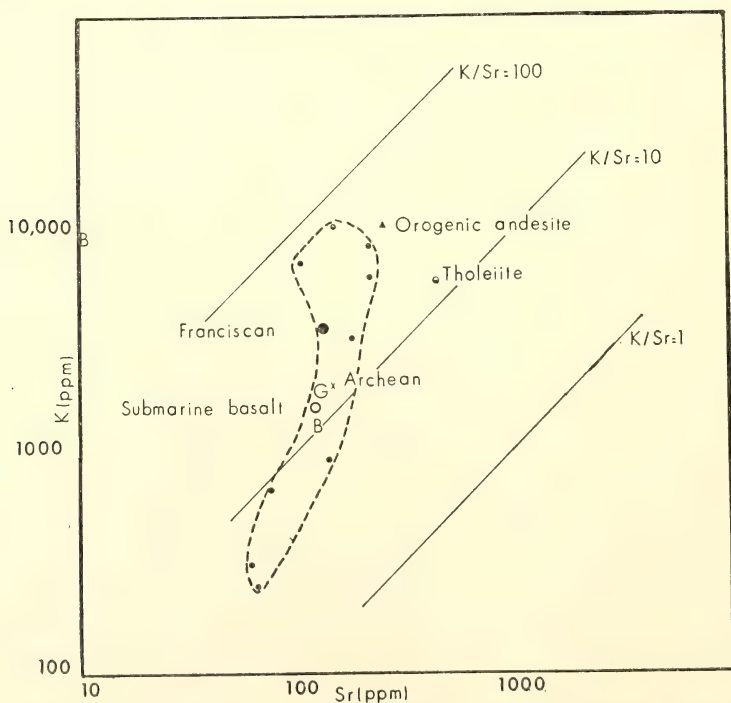


Fig. 12. Log-log plot of strontium and potassium concentrations. Dashed outline indicates limits to Franciscan tholeiites. G = graywacke; B = blueschists.

This model seems more plausible when one considers the variations in the  $\text{Sr}^{87}/\text{Sr}^{86}$  ratios of sea water since Cambrian times. There is a marked lowering of the isotopic ratios during Jurassic and Cretaceous ages ( $\text{Sr}^{87}/\text{Sr}^{86}=0.7065$  to  $0.7075$ ) (Peterman *et al.*, 1970).<sup>51</sup> These ages also coincide with the most voluminous onpouring of tholeiites since the Cambrian. The conclusion based on this hypothesis is that the high  $\text{Sr}^{87}/\text{Sr}^{86}$  ratios obtained on basalts of possible oceanic affinity should not be interpreted as crustal (radiogenic Sr) contamination, but rather as isotopic equilibration (partial to complete) with sea water Sr. The concentration of  $\text{H}_2\text{O}^+$  determined on some of the basalts is extremely high (4–5%) indicating the presence of a wet system to facilitate isotopic exchange.

The K, Rb, and Sr concentrations are given in Table 7. Fig. 12 is a log-log plot of Sr against K. The dashed line outlines the variations in all the analyzed samples. The average Franciscan tholeiite lies in the same region as Archaean tholeiites and has the same trend as oceanic basalts. It is possible that such close similarities indicate a noncontaminated mantle type basalt. The blueschist (B) and graywacke (G) are in the same field, but as will be shown later in discussion of lead isotopic data, they are

not wholly (genetically) related to the basalts. In a plot of potassium versus strontium concentrations, the similarity with other volcanic rocks of known oceanic and arc affinities is striking. We interpret these similarities as partly indicative of a noncontinental substratum below the Franciscan assemblage.

### Lead Isotopes

Lead isotopic studies have also been used to decide between an oceanic and a continental source for these basalts. The absence of uranium concentrations on our samples (used to correct for *in situ* decay of uranium) does not change the common lead interpretation. Since these basalts are only 130–150 million years old, corrections for radiogenic lead would not be greater than 1–2% (Tatsunoto and Snively, 1969).<sup>52</sup>

Figure 13 is a  $\text{Pb}^{206}/\text{Pb}^{204}$  versus  $\text{Pb}^{207}/\text{Pb}^{204}$  plot of the observed ratios as given in Table 8. The range in  $\text{Pb}^{206}/\text{Pb}^{204}$  is in the order of nearly 3–4% and of  $\text{Pb}^{207}/\text{Pb}^{204}$  is only 0.5%. The data points lie for the most part on an extension of a growth curve with  $\mu (=U^{235}/\text{Pb}^{204})=8.7$ . It is not possible from the data we have to construct a meaningful secondary isochron and so we interpret the leads as derived from a single-stage

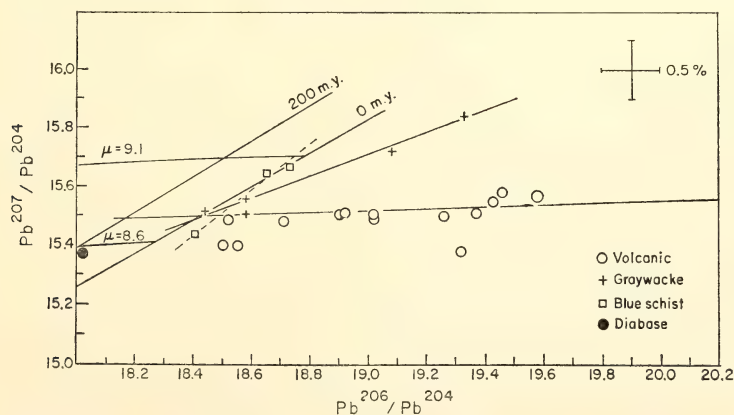


Fig. 13.  $\text{Pb}^{206}/\text{Pb}^{204}$  versus  $\text{Pb}^{207}/\text{Pb}^{204}$  of Franciscan tholeiites, graywackes, blueschists and diabase.

TABLE 8. Lead Isotopic Composition of Selected Volcanic, Sedimentary, and Metamorphic Rocks from the Franciscan Assemblage, California

Sample Number	Pb <sup>206</sup> /Pb <sup>207</sup>	Pb <sup>206</sup> /Pb <sup>208</sup>	Pb <sup>206</sup> /Pb <sup>204</sup>	Pb <sup>207</sup> /Pb <sup>204</sup>	Pb <sup>208</sup> /Pb <sup>204</sup>
<i>Volcanics</i>					
AC-SB-20V	1.2482	0.4949	19.46	15.58	39.31
PS-SB-6V	1.2186	0.4947	18.90	15.50	38.20
LL-M-IV	1.2419	0.4949	19.26	15.50	38.91
NA-SC-5V	1.3195	0.4889	18.92	15.51	38.69
SS-S-7V	1.2487	0.4994	19.43	15.55	38.90
PS-S13-6V	1.2219	0.4985	19.02	15.55	38.16
L-M-IV	1.2485	0.4997	19.37	15.51	38.76
BR-SB-24V	1.2569	0.5047	19.58	15.57	38.79
NI-SBE-10V	1.2046	0.4928	18.55	15.40	37.65
GR-SBE-4V	1.1953	0.4879	18.52	15.49	37.96
UD-SC-6V	1.2009	0.4883	18.50	15.40	37.89
SS-S-2V	1.2288	0.4987	19.02	15.49	38.17
CI-LA-IV	1.4869	0.6063	23.28	15.77	38.39
RC-SB-S9SZ	1.1699	0.4823	18.01	15.40	37.35
RP-M-IV	1.2560	0.5139	19.32	15.38	37.49
MD-CC-2462V	1.2087	0.4930	18.71	15.48	37.96
<i>Graywacke</i>					
PF-F-7G	1.1976	0.4837	18.58	15.51	38.41
M-SLO-5G	1.1880	0.4847	18.44	15.52	38.06
SB-M-3G	1.2183	0.4895	19.33	15.84	39.48
NA-SC-2G	1.2136	0.4897	19.08	15.72	38.97
PP-SBE-1G	1.1878	0.4858	18.48	15.56	38.04
<i>Blue Schist</i>					
BR-SB-21BS	1.1913	0.4832	18.40	15.44	38.08
RR-S-1BS	1.1900	0.4832	18.65	15.66	39.50
H-SBE-3BS	1.1956	0.4883	18.63	15.68	38.14
PF-M-6BS	1.1952	0.4816	18.73	15.67	38.89

process. Tatsumoto and Snavely's data on Oregon basalts (Eocene to Miocene in age) have indicated the possibility of a two-stage evolution of lead with secondary isochron ages of 180–55 m.y. The lead isotopic ratios of the Franciscan leads suggest a single primary extraction at different times from the mantle and no contamination from a granitic basement. This is also supported by the low apparent  $\mu$  values found which are directly comparable to  $\mu$  values obtained on sea floor tholeiites. The extension of points along the Pb<sup>206</sup>/Pb<sup>204</sup> axis can be adequately explained by an open system model for lead evolution, and those which lie beyond Pb<sup>206</sup>/Pb<sup>204</sup> > 19.0 indicate heterogeneity in U/Pb in the mantle along the western margin of the United States.

The hypothesis that has been advanced most recently to explain the mélange nature and metamorphic grade

of the Franciscan rocks proposes sea floor spreading and trench tectonics (Ernst, 1970). If this is true, then the analyses of lead seen in the sediments preclude any mixing of sediment lead with basalts. The slope of the sediment lead line is distinct from that of the basalts, and therefore the sediment leads appear to have a different history. Most of the graywackes in the Franciscan contain certain amounts of argillite, to which we attribute this slope. The blueschists, although shown in Fig. 13 on a separate line, are apparently more closely related to the graywacke type of lead than lead from basalts.

Figure 14 shows a plot of Pb<sup>206</sup>/Pb<sup>204</sup> versus Pb<sup>208</sup>/Pb<sup>204</sup>. The basalts are spread around a line with a  $\mu$  = 8.7 and K (=Th/U) = 3.6. The sediments and blueschists indicate a minimum K of 3.8. This variation leads to similar arguments presented earlier.



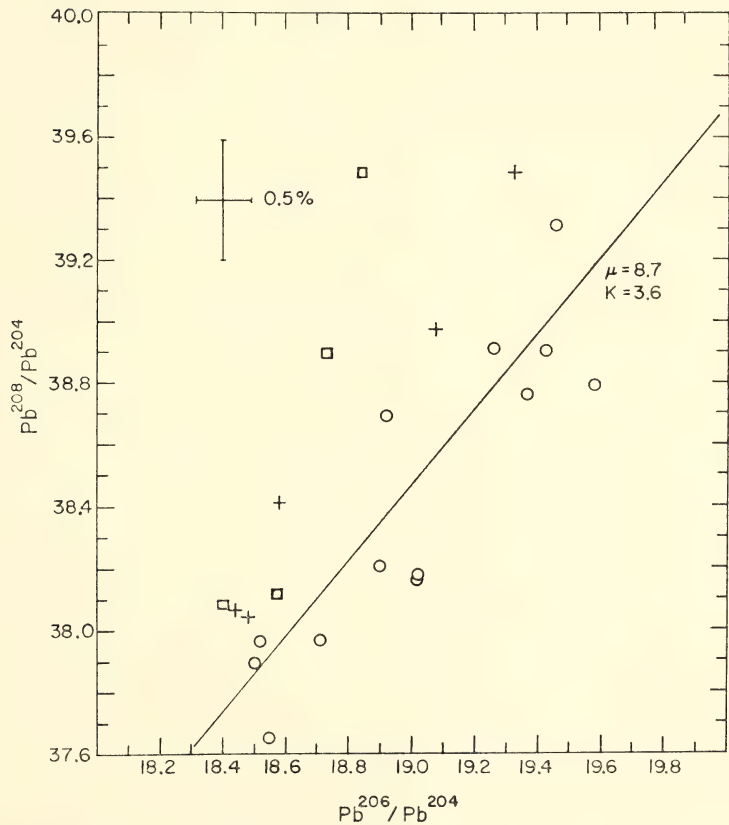


Fig. 14.  $Pb^{208}/Pb^{204}$  versus  $Pb^{206}/Pb^{204}$  of Franciscan rocks. Symbols are the same as in Fig. 13.

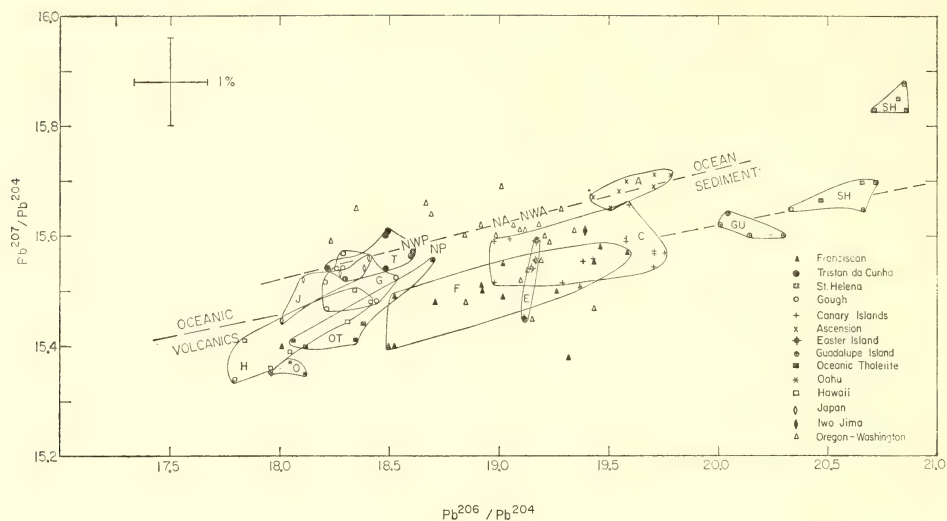


Fig. 15.  $Pb^{208}/Pb^{204}$  versus  $Pb^{207}/Pb^{204}$  plot of all recent volcanic rocks taken from the literature. The sediment line as shown in Fig. 13 would go between *NWP*—*NP* (Northwest Pacific—North Pacific sediments).

### Conclusions

The strontium isotopic composition of the Franciscan tholeiites is significantly higher than those observed in oceanic tholeiites. Instead of crustal contamination, we propose partial equilibration with sea water Sr to explain the high  $Sr^{87}/Sr^{86}$  ratios. The K, Rb, and Sr concentration data on log-log plots define trends similar to those observed in oceanic and arc basalts.

Figure 15 shows a plot of  $Pb^{206}/Pb^{204}$  versus  $Pb^{207}/Pb^{204}$  of tholeiites and alkali basalts from known oceanic sources. The sediments of the ocean floor on such a plot define a line different from the all "volcanic" line, and the Franciscan data indicate no significant mixing of sediments with the basalts.

### ANCIENT AND MODERN VOLCANIC ROCKS: A TRACE ELEMENT MODEL

S. R. Hart, C. Brooks, T. E. Krogh, and  
G. L. Davis

In *Year Book 68*, pp. 429–433 we reported on a series of K, Rb, Cs, and Sr

analyses of Archaean (2.7 b.y.) volcanic rocks and discussed possible explanations for the differences in the abundance of these elements in ancient and modern volcanics. Since that time we have analyzed the Archaean volcanics for barium, and have surveyed a number of modern volcanics for these elements. Table 9 lists our best estimates for the geochemical properties of various modern basalt types with the Archaean values (and lunar values) given for comparison.

We have restricted the modern data to oceanic and volcanic-arc materials and have excluded continental or cratonic basalts to avoid complexities introduced by crustal contamination. The data in Table 9 should not be construed as evidence that modern basalts fall into four discrete geochemical groups. To emphasize this point, these four groups of data are plotted in Fig. 16 so the progressive change in element concentrations between alkali basalt and tholeiite is evident.

It has been thought that ocean-floor basalts, which are highly depleted in all

TABLE 9. Comparison of Selected Elements in Basaltic Rocks, ppm

Rock Type	K	Rb	Cs	Sr	Ba	K/Rb	K/Sr	K/Ba	Sr/Ba
Alkali basalt <sup>a</sup>	13,800	33	~2	815	498	420	17	28	1.6
Tholeiite <sup>b</sup>	4,000	8	~0.2	330	160	500	12	25	2.1
Tholeiite, low potassium <sup>c</sup>	2,170	3.2	~0.04	250	100	680	8.7	22	2.5
Archaean basalt <sup>d</sup>	2,120	5.9	0.36	175	70	360	12	30	2.5
Lunar basalt <sup>e</sup>	1,510	3.0	0.10	165	190	500	9.2	8	0.9
Ocean floor basalt <sup>f</sup>	1,160	1.10	0.016	136	10.5	1050	8.5	110	13

- a. Average oceanic alkali basalt; Engel *et al.*<sup>44</sup>
- b. Average tholeiitic basalt of oceanic and island arc regions; Manson,<sup>70</sup> Prinz,<sup>71</sup> Kuno,<sup>65</sup> Hart (unpublished).
- c. Average of 8 low potassium basalts from Japan, California, Hawaii, and Iceland; Griffin and Murthy,<sup>32</sup> Philpotts and Schnetzler,<sup>30</sup> Hart (unpublished).
- d. Composite B of Table 9.
- e. Average of 7 Apollo 11 basalts; Gast.<sup>72</sup>
- f. Average of 15 basalts dredged from 11 localities; Hart.<sup>60</sup>

the dispersed trace elements, were a geochemically uniform group found only in the spreading ridge environment. The trends in Fig. 16 argue rather for ocean floor basalts being an “end-member” case of which close representatives may also

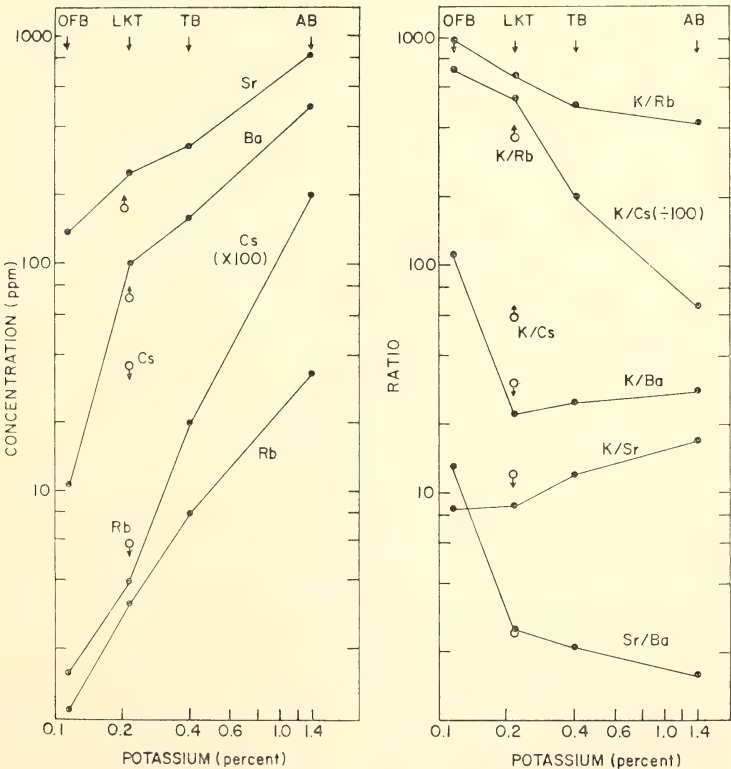


Fig. 16. Trends of element concentrations and ratios in modern basalts relative to potassium content. OFB, ocean floor basalt; LKT, low potassium tholeiite; TB, tholeiitic basalt; AB, alkali basalt. Open circles are average values for basic Archaean volcanics; arrows point to the relevant modern trend.



be found in island-arc environments; these are the low-K tholeiites of Table 9. Included in this low-K tholeiite group are individual samples which match ocean-floor basalt even more closely than the group average—a Japanese tholeiite with 1330 ppm K, K/Rb of 1570 and 35 ppm Ba<sup>3</sup>, and a Californian basalt with 800 ppm K, K/Rb of 1400 and 0.02 ppm Cs<sup>13</sup>, for example. The Ba contents of these basalts generally run higher than the 10 ppm found in ocean-floor basalts. However, Japanese tholeiites with low U and Th contents similar to ocean-floor basalts have been reported;<sup>53</sup> and a number of basalts have been reported from Japan which show low concentrations of rare earth elements and depletion of light elements characteristic of ocean-floor basalts.<sup>54</sup>

How do the Archaean basalts fit into this gradational series of modern basalts? The Archaean data are plotted on Fig. 16 as separate points, and in terms of K, Sr, and Ba concentrations (and ratios involving these elements), the Archaean data fit fairly closely to the gradational series. The only anomaly arises with Rb and Cs, where the Archaean basalts are somewhat higher in Rb and much higher in Cs than their counterparts of similar K content. We will treat this anomaly later when we come to discussion of the processes by which the modern trends of Fig. 16 are produced.

### Modern Basalt Geographic Trends

Kuno<sup>55</sup> and Sugimura<sup>56</sup> have shown a regular progression of volcanic types in the Japanese arc, from tholeiite on the trench side to alkali basalt on the mainland side. Dickinson and Hatherton<sup>57</sup> showed that this progression produces a striking relationship between the K content of the volcanic rocks and either the depth to the Benioff (seismic) zone or the distance from the trench axis. They found this relationship to be true for Japan as well as for other volcanic

arcs which would be associated with a seismic zone. Since the trace-element trends of Fig. 16 are essentially those related to the progression alkali basalt → tholeiite, a general relationship should exist between all of these elements and the geometry of the seismic zone. Of the elements represented in Fig. 16 (including K), Sr is perhaps most ideal for testing this relationship, as its concentration is relatively unaffected by differentiation and, as we will show later, by sediment contamination effects. Our compilation of relevant literature data is plotted in Fig. 17. Even though the number of useful analyses in the literature is limited, and obvious Sr variability exists between samples from a given location, and the seismic plane is poorly delineated ( $\pm 100$  km) in some regions, the relationship of Sr content to depth of the seismic zone is extremely good. We have used data only from island arcs; the sparse data which exist for continental margins do not fit the trend of Fig. 17 but will perhaps define a trend of much shallower slope. It is interesting to note that ocean-floor basalts, with their low Sr content of 135 ppm, form on the mid-ocean ridges which, while having no well-defined seismic plane, are

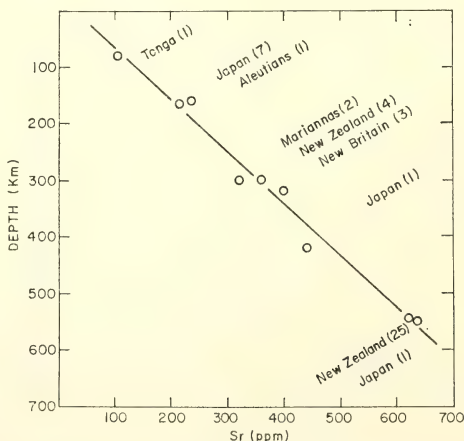


Fig. 17. Sr content of modern island arc basalts related to depth to seismic (Benioff) zone.

nevertheless zones of generally shallow seismicity. Our suggestion of a relationship between ocean-floor basalts and arc basalts is in this way compatible with the trend in Fig. 17.

Does the comparison of Archaean basalt chemistry with the trends of Fig. 16 and 17 imply that Archaean volcanics formed in island arcs over shallow Benioff zones? This depends rather strongly on the explanation of the modern basalt trends and we must therefore consider possible mechanisms for these trends.

### *Models for the Derivation of Basalt*

These may be broken down into the following categories:<sup>58</sup> chemical and mineralogical effects in the mantle source region; effects due to different degrees of partial melting; effects due to crystal fractionation during magma ascent; and less well-defined effects such as wall-rock reaction<sup>59</sup> and transfer in a vapor phase. Basically the problem is to explain why alkali basalts have 5–100 times the concentration of the dispersed trace elements as do the “depleted” tholeiites.

It is obvious that extreme degrees of differentiation would be required to produce the enrichments observed in alkali basalts, and Gast<sup>36</sup> has argued strongly against this mechanism. Mineralogical zoning of the mantle, for example, from amphibole-plagioclase-phlogopite bearing rocks at shallow depths to simple peridotites at greater depth, would result in magmas from the deeper zone which were at best 2–4 times enriched in the dispersed elements over magmas of shallow derivation. This is insufficient to explain the variations shown in Fig. 16. Gast developed a model in which the differences between tholeiite and alkali basalt are produced by different degrees of partial melting. Kay, Hubbard, and Gast<sup>23</sup> showed that trace quantities of water in the mantle would have a buffering effect on the degree of partial melt-

ing, so that large volumes of the deeper mantle would contain small amounts (1–3%) of melt and the degree of melting would increase rapidly toward shallower depths. Using the lowest available partition coefficients, the difference of concentration of dispersed elements in a 1% melt and a 30% melt would be no greater than a factor of 20. Thus this mechanism, especially when more reasonable values are chosen for partition coefficients, is insufficient to explain more than half of the concentration differences shown in Fig. 16. Considerations of this sort have led most authors<sup>23, 33, 35, 36</sup> to conclude that ocean floor basalts must be derived from a “residual” mantle, one from which most of the dispersed elements have been previously extracted. Insofar as certain arc basalts are similar to ocean-floor basalts, and since ocean-floor basalts are exceedingly uniform throughout the world,<sup>23, 58, 60</sup> then this “depleted” mantle source region must be uniformly present on a world-wide scale. The relationship of these basalts to depth of seismicity (Fig. 17) suggests that this depleted mantle is tapped only at very shallow depths (<50 km), either in a ridge or an arc environment.

Various authors<sup>53, 61, 62, 63</sup> have proposed that volcanic rocks of the island arcs may be produced by melting of the oceanic lithosphere in a subduction zone. Since the upper part of this lithosphere is ocean-floor basalt, remelting of this would explain the presence in island arcs of basalts which are very similar to ocean-floor basalts. Tatsumoto<sup>53</sup> and Armstrong<sup>63</sup> have proposed from lead isotopic measurements that ocean sediment is involved in this process as a contaminant. Because sediments are enriched in just those elements (Pb, Rb, Cs, and Ba) which are characteristically depleted in ocean-floor basalts, very minor amounts of contamination will quickly destroy this characteristic. The presence of basalts with high K/Rb and K/Cs ratios (see discussion of Table 9)

in island arcs argues against sediment contamination. On the other hand, we have analyzed several of the basalts from Oshima Island, Japan, which appeared most contaminated in Tatsumoto and Knight's study.<sup>53</sup> The high Cs and Ba contents of these basalts strongly suggest large amounts (~5–10%) of sediment contamination (Table 10). It is thus possible that the tholeiite (and related andesite) of island arcs is derived by re-melting of the oceanic lithosphere during burial in the subduction zone, and that these melts may sometimes, but not always, be contaminated with sediment.

We would conclude our discussion of modern basalts by synthesizing the data into two models, a direct model and a secondary or indirect model, and by noting that a real choice cannot be made between these models at this time.

*Direct model.* The mantle is chemically nonuniform with depth on a world-wide scale, varying gradationally from a primitive (or enriched) zone to a zone highly depleted (factors of 2–10) in the dispersed elements. Tapping of the depleted zone occurs only at very shallow depths on spreading ridges and on the extreme trenchside of island arcs. (This does not necessarily mean that the depleted zone always lies at a shallow depth in the mantle, as this depends on the nature of mantle upwelling in these two regions.) The depleted zone undergoes a high degree of partial melting

under conditions of adiabatic decompression<sup>23</sup> perhaps aided by shear-strain heating<sup>64</sup> and by the possible introduction of water from the underlying subduction zone.<sup>65</sup> Alkali basalts are derived further from the trench and at a greater depth, by low degrees of partial melting of the "primitive" mantle. The relationship of Sr (and K) to the depth of the seismic zone (Fig. 17), which we attribute largely to variations in the degree of partial melting, in no way implies magma derivation from those depths. Magmas are probably derived from a shallower (but dipping) zone, whose depth would be consistent with (1) the control by pressure of major element content,<sup>59, 66</sup> (2) the control by water content and depth of the degree of partial melting,<sup>23</sup> and (3) the seismic evidence showing that volcanic foci lie considerably above the seismic plane.<sup>67</sup>

*Indirect model.* The mantle is zoned (at least laterally) into depleted and nondepleted regions, but the depleted regions are tapped only on the mid-ocean ridges. In island arcs, the volcanic rocks nearest the trench are produced by partial or total melting (if eclogite is involved) of the upper oceanic lithosphere as it travels into the subduction zone; these magmas may occasionally or frequently be contaminated with oceanic sediment material. Further from the trench these two-stage magmas yield gradationally to primary magmas, and

TABLE 10. Sediment Contamination Model for O-Shima Basalts

	Average Oceanic Sedi- ment *	Ocean Floor Basalt Plus 10% Sediment †	Basalts, O-Shima Island, Japan		
			Ja 26 Pre- historic	Ja 25 1778 Flow	Ja 27 1951 Flow
K (ppm)	20,000	2900	2940	3466	3318
Rb	70	7.4	5.30	6.48	6.20
Cs	7	0.63	0.645	...	0.77
Sr	200	140	186	182	170
Ba	2,800	265	254	...	219
Sr <sup>87</sup> /Sr <sup>86</sup>	~0.71	~0.7035	0.70373 ‡	...	0.70375 *

\*Sediment values from 73, 74, 75.

† Average ocean floor basalt values from 60.

‡ Error (2σ) ~ .0001 relative to E & A standard = 0.70800.



the indirect model concepts then follow those of the direct model.

By either of these models, the basic trace element patterns of oceanic and arc basalts would be created by differing degrees of partial melting of a mantle which is not chemically uniform, ranging from residual or depleted mantle to primitive or perhaps even "enriched" mantle.

### *Discussion of Archaean Volcanism*

The major element and certain trace element compositions (K, Sr, and Ba) of Archaean basalts are very similar to that of tholeiitic basalts of modern island arcs which occur on the extreme trench side of the arc (and above a shallow seismic zone). Rb and Cs contents of Archaean basalts are higher than those of the arc basalts by factors of 2 and 10, respectively. Aside from absolute concentrations, however, the Archaean basalts are more like modern alkali basalts than tholeiites in having "nondepleted" trace element ratios (see Fig. 16). By postulating that the mantle had not yet become depleted in Archaean time, we can reconcile the low K/Rb, K/Cs and K/Ba ratios of Archaean basalts relative to the arc tholeiites which they resemble in most other respects.

Our model for the genesis of Archaean basalt, based on this analogy with arc tholeiites, invokes magma derivation from very shallow depths (<50 km) by high degrees (>30%) of partial melting. A shallower melting level during the Archaean is reasonable, since the heat production by natural radioactivity at 2.7 b.y. was twice that at present. As a corollary to this, we suggest that the lithosphere during the early Precambrian was considerably thinner and weaker than at present. The absence of alkali basalts in the Precambrian<sup>24, 68</sup> is consistent with this view, as modern alkali basalts probably require a thick lithospheric lid for their derivation. Thus there would be no mechanism during the

Precambrian for tapping magmas from the great depths where the degree of melting is naturally buffered to small amounts.

The Archaean has been noted as having a rather characteristic geostructural style<sup>68, 69</sup> which may be most easily visualized in terms of thin-plate tectonics. Archaean volcanics occur not in long continuous belts but in multiple, discontinuous, arcuate belts. One model for these, proposed by Anhaeusser *et al.*<sup>68</sup> envisions a series of "strongly oriented parallel downwarps or fault-bounded troughs on an unstable, thin, primitive sialic crust" which becomes filled with volcanic and sedimentary material. We would alter this model by proposing that the fault-bounded troughs be considered as arc-trench features with a shallow and perhaps poorly developed subduction zone, and that the thin crust be not sialic, but essentially a mafic crust on a thin lithosphere. The multiple belts would result from the fact that a thin plate could not maintain large-scale mechanical integrity, and would break into many small plates, each having a subduction zone for one boundary.

### PRIMARY DIFFERENCES IN U/Pb RATIOS IN TWO PRIMITIVE CRUSTAL BLOCKS

*A. K. Sinha*

The study and interpretation of common lead in minerals and rocks are strongly dependent on the existence of a unique growth curve. Using over 300 analyses from different laboratories, but normalized to one reference standard (Cal Tech shelf lead), it is possible to suggest that there may not be a unique growth curve for the entire earth. The data used suggest the existence of two primordial continental nuclei with differing U/Pb ratios. Heat flow and sea-floor spreading rates in the northern and southern hemispheres can also be explained on the basis of differing concentrations of radioactive and heat producing elements like U, Th and K.

The systematics of lead isotopes are based on derivations which relate the changes in lead isotope ratios to the time and relative amount of lead, uranium, and thorium. Since the addition of lead in a chemically closed system is only by radioactive decay, the  $\text{Pb}^{206}$ ,  $\text{Pb}^{207}$ , and  $\text{Pb}^{208}$  show a relationship to each other based on the decay rates of the parents. Graphically,  $\text{Pb}^{206}$  and  $\text{Pb}^{207}$  with nonradiogenic  $\text{Pb}^{204}$  as a common denominator, can be shown as a growth curve (Fig. 18). Leads derived from a closed system at the same time but with differing U/Pb ratios bear a linear relationship in an  $\alpha$ - $\beta$  plot. The age obtained from such a plot is analogous to the Pb/Pb age of a mineral and is called the model age.

In many cases ores or rocks with single-stage primary leads are affected by a later metamorphism that effectively changes the lead isotopic composition by mixing or contamination. Such leads are considered anomalous and can be recognized by a large spread in their isotopic composition. Kanasawich (1962)<sup>76</sup> lists the criteria for the recognition of multistage leads. However, his consideration that model ages should agree with radiometric ages, assuming closed system evolution and 4550 m.y. as the age of the earth, is debatable. (Tilton and Steiger, 1965;<sup>77</sup> 1969a;<sup>78</sup> Chow and Patterson, 1962;<sup>79</sup> Gast, 1967;<sup>80</sup> and Sinha, 1969c<sup>81</sup>). As such, this paper is limited to the discussion of the growth curve itself. Lead isotopic analyses of leads from galenas, feldspars, and whole rocks (generally basalts) Sinha, 1969a,<sup>82</sup> 1969b,<sup>83</sup> 1969c; Tilton and Steiger, 1969a; Tilton and Sinha, 1969b;<sup>84</sup> Zaartman and Wasserburg, 1969;<sup>85</sup> Doe, *et al.*, 1965;<sup>86</sup> Tatsumoto, 1966a,<sup>87</sup> 1966b;<sup>88</sup> Cooper, 1968;<sup>89</sup> Catanzaro, 1960;<sup>90</sup> Chow and Patterson, 1962; Oversby, 1969;<sup>91</sup> and Gast, 1967, 1969<sup>92</sup> when normalized to one standard value of Cal Tech shelf lead (values of Tilton and Steiger, 1965) show a very systematic

spread in the  $\alpha$ - $\beta$  plot. The variations are seemingly related to the geographic location of the samples, more precisely to the northern (Laurasia) and southern (Gondwanaland) hemispheres. Figure 18 is an  $\alpha$ - $\beta$  plot of all the data used in this work. Two distinct growth curves seem to fit the data from the two hemispheres. The average  $\mu$ 's for the growth curves are 8.9 and 9.3 for the northern and southern hemispheres, respectively. The growth curves are treated for both closed and open system isotopic evolution of lead.

*Southern hemisphere.* The average closed system growth curve for samples from South Africa, Australia, and India indicate a range of  $\mu$  values from 9.1 to 9.5 with a best fit curve of 9.3. Two time periods need special attention. The samples older than 2900 m.y. range from  $\mu$ 's of 9.4 to 9.9 with the majority of the samples around 9.9. Samples younger than 1000 m.y. show a range from 9.5 to 9.0. These samples (>1000 m.y.) indicate the possibility of recycling and mixing of large heterogeneities in the mantle. Another possibility is that samples older than 2900 m.y. evolved in a system of very high  $\mu$  (9.9) and at the time of first major crustal fractionation, depleted the mantle in uranium to drop the  $\mu$  to 9.3. Since then evolution proceeded in this  $\mu$  environment until nearly 500 m.y. ago when apparently the effects of recycling and mixing with lower  $\mu$  systems effectively changed the observed  $\mu$ .

The best fit open system growth curve (not shown in Fig. 18) is one with a  $t_0$  of 4750 m.y. and  $K$  of 2.5 (terminology of Tilton and Steiger, 1969). It is proposed that this curve more adequately defines the evolution of common lead and indicates a higher rate of uranium transport than in the northern hemisphere.

*Northern hemisphere.* Samples from Canada, United States, Japan, Europe, and some of the Pacific islands are shown in Fig. 18. These samples indicate

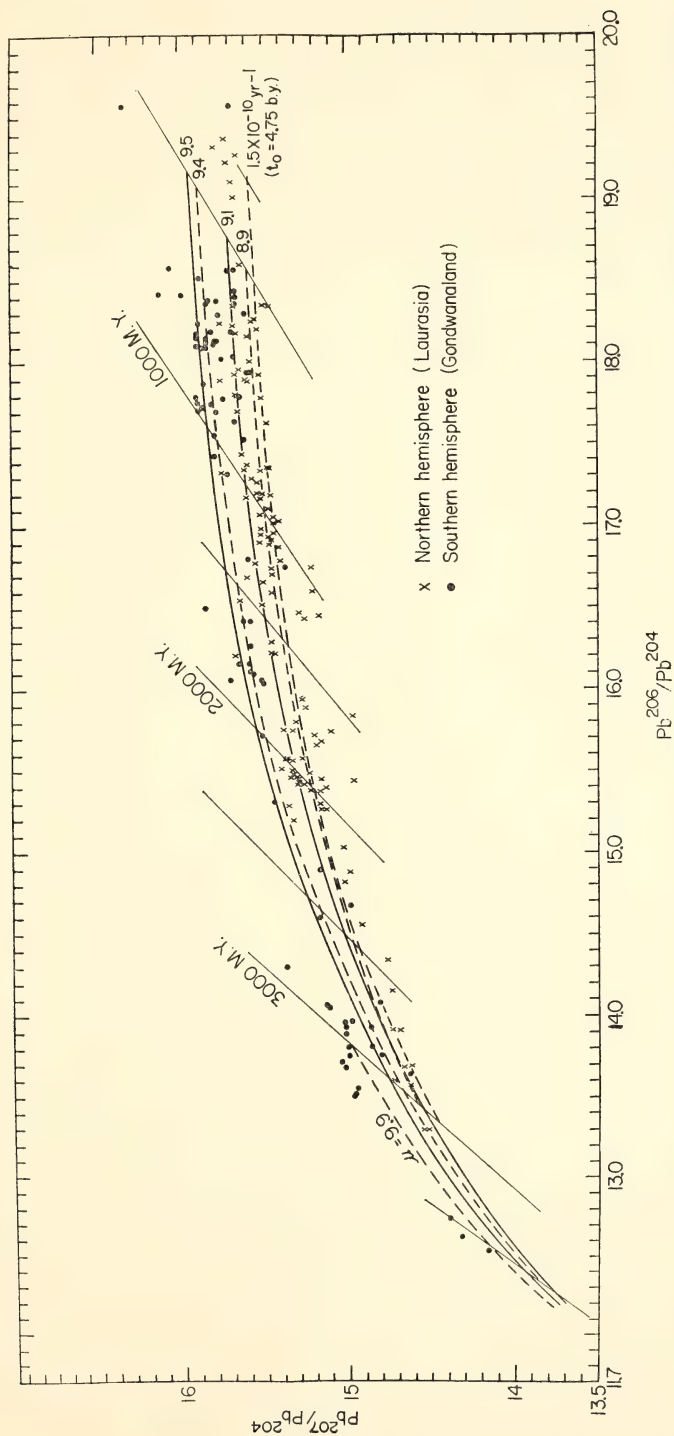


Fig. 18.  $Pb^{207}/Pb^{204}$  versus  $Pb^{206}/Pb^{204}$  of galenas and feldspars. The data points have been taken from the literature and are documented in Sinha, 1969.



a  $\mu$  distinctly lower than for the southern hemisphere, and an average  $\mu$  of 9.0 is indicated. If an episodic model (closed system) is used, then samples evolved in a  $\mu$  condition of 9.4, and after crustal differentiation and mantle depletion in uranium they evolved further with a  $\mu$  of 8.9. As indicated in a previous section, an open system evolution model with a  $K$  of 2.0 best fits the data.

The variations in the two growth curves indicate three possibilities: (1) the difference in U/Pb ratios in the two hemispheres is primary; (2) the rate of transport of uranium (and associated elements like K and Th) relative to lead is higher in the southern hemisphere; and (3) a combination of (1) and (2) with vastly different ages of crustal differentiation in the two hemispheres. There is no unique way to test the first possibility, but if the rate of transport of uranium (with Th+K) is higher in the south, then differences in heat flow, especially in the old stable shield areas should be seen. Lee and Uyeda (1965)<sup>93</sup> have averaged heat flow values for shield areas (see Table 11).

Lambert and Heier (1967)<sup>94</sup> have shown that the average Th, U, and K abundances in surface rocks of the southwest Australian Shield are higher than the values obtained by Eade, *et al.* (1967)<sup>95</sup> for the Quebec Shield region in Canada. This need not indicate deeper levels of erosion as suggested by Heier *et al.*, but primary differences in concentration of the heat producing elements. The only other indication of large regional variations between the two hemi-

spheres is suggested by the work of Rickwood (1969).<sup>96</sup> He found variations in chromium and iron in garnet peridotite xenoliths from Russia and South Africa and suggested a chemical heterogeneity of the upper mantle on a continental scale.

In conclusion, I have attempted to show that major differences in the chemistry of the earth can exist on a much larger scale than ever proposed before. The data seem to indicate that variations in  $\mu$  from the two hemispheres call for a very careful approach for bad isotope ratios. It is possible that with more normalized data the strength of this hypothesis may increase. It will be interesting to compare major element chemistry of basalts to determine possible differences in distribution of other elements.

#### U/PB DATING OF VOLCANISM IN THE CENTRAL PIEDMONT (CAROLINA SLATE BELT)

A. K. Sinha,\* L. Glover III,† M. W. Higgins,†  
S. R. Hart,\* G. L. Davis,‡ W. S. Kirk†

The age of rocks of the volcanic-rich Carolina slate belt has long been in doubt. Early workers considered these rocks Precambrian, but more recently, most have considered them early Paleozoic. In 1965, St. Jean<sup>97</sup> described an Early or Middle Cambrian trilobite from the upper part of the sequence in central North Carolina. This is the only fossil known in the slate belt throughout its extent from central Virginia to Georgia. Mineral age dates in the area where the trilobite was found are in conflict with the fossil evidence. White and others (1963)<sup>98</sup> reported 440 to 470±60 m.y. (Ordovician?) zircon lead-alpha ages from beds that are known from physical

TABLE 11. Average Heat-Flow Values from Precambrian Shield Area (Number of Values in Parentheses)

Southern hemisphere shield areas:	
	Heat flow units:
Australia (7)	1.02
South Africa (5)	1.03
India (1)	0.66
Northern hemisphere shield areas:	
Canada (10)	0.88
Ukraine (3)	0.69

\* Department of Terrestrial Magnetism, Carnegie Institution of Washington.

† U. S. Geological Survey, Beltsville, Maryland.

‡ Geophysical Laboratory, Carnegie Institution of Washington.

stratigraphy to be older than the Cambrian trilobite. Hills and Butler (1968)<sup>99</sup> reported Rb-Sr ages of  $494 \pm 14$  m.y. and  $535 \pm 50$  m.y. on rocks that subsequent work has also indicated to underlie the fossil-bearing unit. The age of rocks of the slate belt and of adjacent higher rank gneisses (Charlotte belt) is an important aspect of southern Piedmont geology. An adequate time frame is essential in establishing the stratigraphic and structural relations between belts and in dating the great central Piedmont axis of volcanism.

Geologic mapping in progress along the Virginia-North Carolina line (Plate 2), about 100 miles north of the dated slate-belt sequence, provides an opportunity to date rocks across a seemingly conformable boundary between the slate belt and the higher grade Charlotte belt to the west. The rocks of the slate belt in this area consist of a lower felsic pyroclastic unit and an upper mafic pyroclastic unit separated by a phyllitic quartz-feldspar metasandstone of mixed volcanic-sedimentary parentage. The

low-grade slate belt is deformed into a synclinorium. Prior to the metamorphic maximum the slate belt was intruded by granodiorite and quartz monzonite. At the western margin of the Virgilina synclinorium, a conformable sequence of higher grade mixed mafic and felsic gneisses of probable volcanic parentage dips below the felsic pyroclastic unit and appears to form the core of a large recumbent fold-nappe. The nappe was extruded westward just before the metamorphic thermal maximum and subsequently was refolded into an antiform. Metamorphism increases abruptly but systematically westward (Tobisch and Glover, 1969)<sup>100</sup> across the slate-belt boundary, rising from the biotite zone to the sillimanite zone in about 7 miles (Plate 2). Detailed structural studies indicate that no major discontinuity exists and that the western slate-belt boundary at the Virginia-North Carolina line is primarily an isograd.

We have analyzed seven zircon samples including two fractions from one rock to determine the ages of volcan-

TABLE 12. Analytical Data and Isotopic Ages for Zircons and Sphene from the Carolina Slate Belt and the Glenarm Series, Maryland. Common lead corrections for the slate belt zircons are for 500 m.y.  $\alpha$   $\beta$  values; for the Glenarm, 1,100 m.y. No common lead corrections have been made on 518 sphene sample.

Sample Number	U, ppm	Pb, ppm	Ratios			Ages in m.y.		
			$\frac{\text{Pb}^{206}}{\text{U}^{238}}$	$\frac{\text{Pb}^{207}}{\text{U}^{235}}$	$\frac{\text{Pb}^{207}}{\text{Pb}^{206}}$	$\frac{\text{Pb}^{206}}{\text{U}^{238}}$	$\frac{\text{Pb}^{207}}{\text{U}^{235}}$	$\frac{\text{Pb}^{207}}{\text{Pb}^{206}}$
<i>Carolina Slate Belt</i>								
515	812.8	78.6	0.07837	0.63468	0.05876	490.9	505.6	573.5
516	535.9	84.5	0.08704	0.71578	0.05967	543.0	555.4	607.3
517	403.9	60.5	0.12073	1.0059	0.06046	741.6	716.1	636.1
518 *	466.7	36.9	0.06299	0.48032	0.05533	397.4	403.6	439.2
518 †	512.9	38.3	0.06294	0.48045	0.05539	397.1	403.7	441.6
518 Sp	...	...	...	...	0.80186	...	...	~20
519	562.3	26.7	0.03306	0.27328	0.05997	211.7	248.6	618.4
520	1,110.6	107.9	0.04898	0.37065	0.05490	311.17	324.4	421.6
<i>Glenarm Series</i>								
1	715.2	61.3	0.07462	0.60018	0.05836	468.3	483.7	558.4
2 (2.5°) ‡	487.5	73.4	0.13721	1.50829	0.07977	836.6	946.1	1,214.5
2 (5°) ‡	458.3	69.9	0.13994	1.52889	0.07928	852.2	954.5	1,202.2
2 †	...	...	...	...	0.07805	...	...	1,168.2
2 *	...	...	...	...	0.07591	...	...	1,113.

Sp = sphene.

\* Sample retained on 200-mesh sieve.

† Sample passed through 200-mesh sieve.

‡ Magnetic fraction from Frantz Isodynamic Separator; 2.5°, 5° are tilt values.

ism and metamorphism. An attempt to correlate weathering (based on  $H_2O^+$ ) with loss of lead or uranium has also been made. Locations of the samples are shown on Plate 2.

Table 12 gives the isotopic ages, and Fig. 19 is a concordia plot (Wetherill, 1956).<sup>101</sup> Samples 516, 517, and 519 are zircon from felsic tuff-breccia from the top of the lower pyroclastic unit (Plate 2). These samples lie on an episodic lead loss line primarily due to contemporary weathering effects, and indicate a primary age of  $620 \pm 20$  m.y. Sample 518 from layered paragneiss in the root

zone of the nappe gives a Pb/Pb age of 440 m.y. Field relations, however, indicate that the mixed gneiss sequence that contains sample 518 dips conformably beneath the felsic pyroclastic unit that contains samples 516, 517, and 519. The younger Pb/Pb age of 518, therefore, is anomalous, unless the felsic pyroclastic sequence has been thrust over younger rocks of the Charlotte belt. If so, this event must have occurred before the metamorphism and deformation that produced the synclinorium. Clearly, more samples from the mixed gneisses are needed.

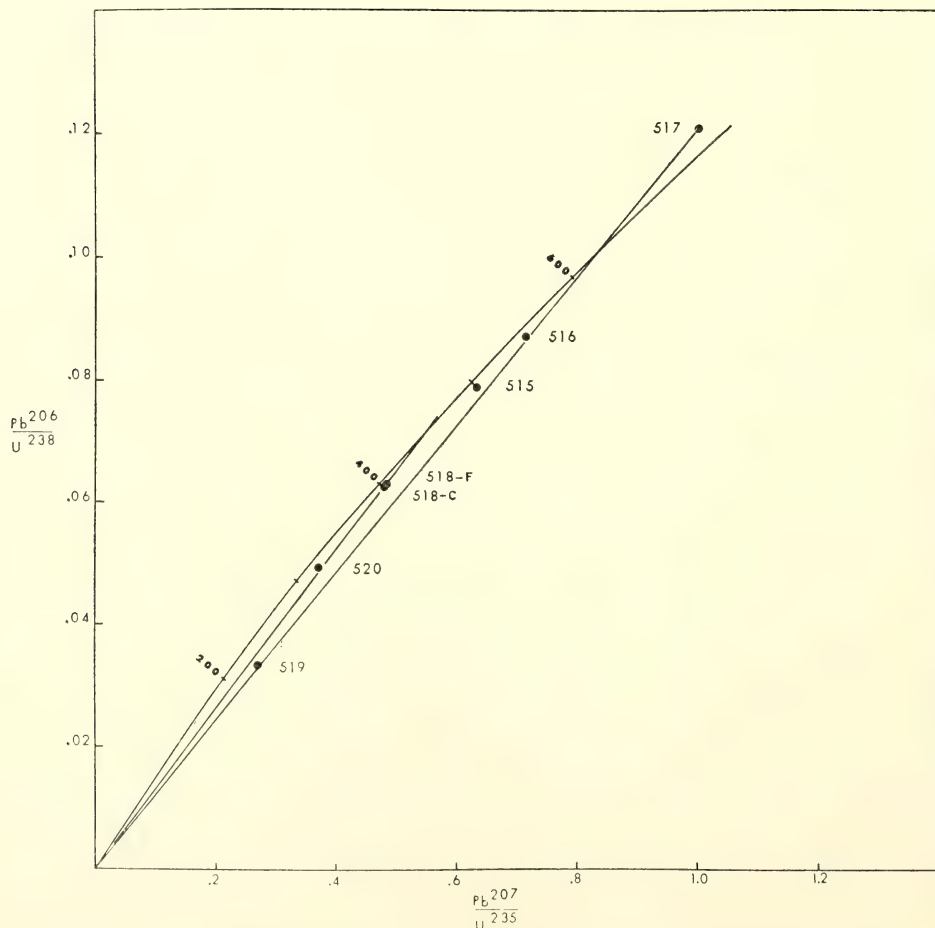


Fig. 19. Concordia plot of Carolina slate belt zircons. Sphegne sample is not shown.



Sample 520 has a Pb/Pb age of 422 m.y., similar to sample 518. This agreement may be fortuitous if sample 520 represents a concordant pluton. However, if it is from a metamorphosed pyroclastic unit essentially coeval with 518, then the discordia age for these two samples could be nearly 460 m.y.

Figure 20 is an  $\alpha$ - $\beta$  diagram of the analyzed zircons, showing two distinct chords. Samples 516, 517, and 519 give an age of about 700 m.y., slightly older than the age obtained by the concordia intercept. The two fractions of sample 518, however, give an age of 480 m.y., a little older than the Pb/Pb ages of the samples. We do not consider this  $\alpha$ - $\beta$  plot to be strong evidence because the two zircon fractions may be unrelated. One (518c) is a coarse, rounded form that may be detrital; the other (518f) is a fine euhedral form that may be of volcanic origin. When coupled with more data from the same unit, the slope of the line and the age may change significantly.

Sample 515 is from a large granodio-

rite pluton that is younger than all of the slate-belt sequence. Its  $\text{Pb}^{207}/\text{Pb}^{206}$  age of 573 m.y. is slightly younger than the pyroclastic unit and is in good agreement with its geological position. If this age stands when more samples are obtained, it will also postdate the youngest pyroclastic unit in the area and define a minimum age for the stratigraphically recorded volcanism.

On the basis of  $\text{H}_2\text{O}^+$  (whole rock) determinations made and uranium concentrations (zircons) measured, we propose a tentative correlation of weathering to the degree of discordancy. A single sample of Norbeck quartz diorite (no. 1) has been included because of the availability of  $\text{H}_2\text{O}^+$  data. Fig. 21 is a plot of U concentration against  $\text{H}_2\text{O}^+$  for the total rock. It seems that a correlation is possible, i.e., samples with lower uranium have more  $\text{H}_2\text{O}^+$  (except for sample 519, which is rather weathered). The higher concentration of water remaining in the rock system under metamorphic conditions may, under conditions of weathering, remove uranium to the ex-

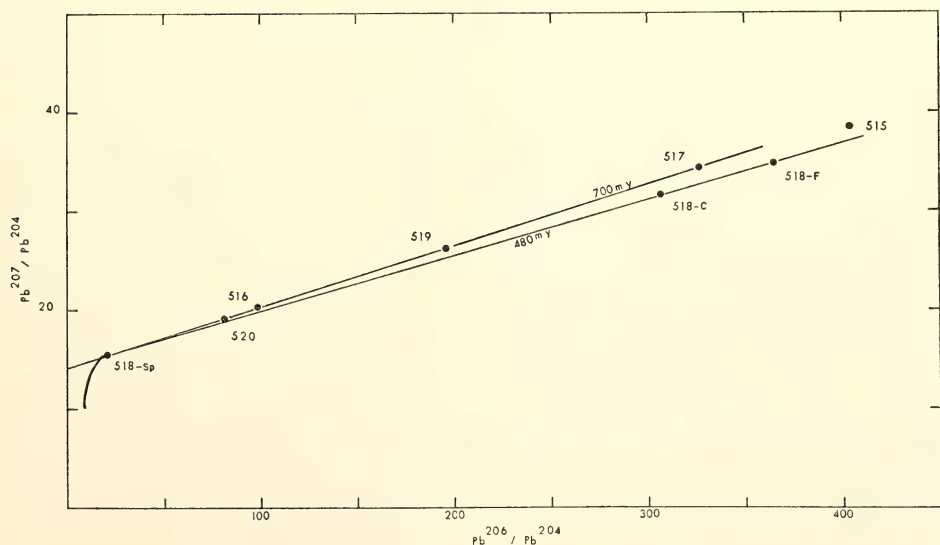


Fig. 20.  $\text{Pb}^{206}/\text{Pb}^{204}$  versus  $\text{Pb}^{207}/\text{Pb}^{204}$  plot of Carolina slate belt zircons and sphene. The common lead growth curve is shown.

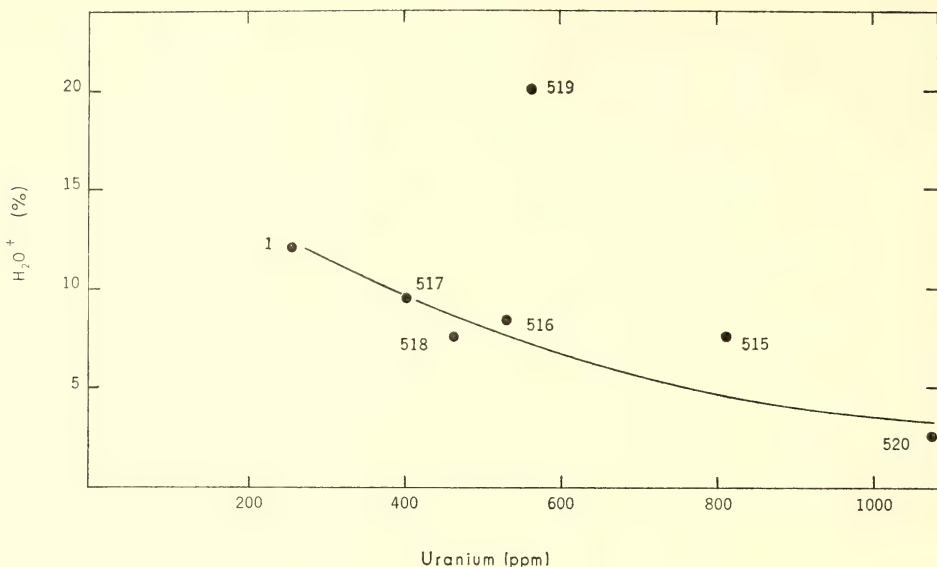


Fig. 21. Uranium concentration (ppm) versus  $H_2O^+$  (total rock). Sample 519, which is weathered, shows no apparent relationship to other samples.

tent that it lies above the concordia curve (sample 517).

#### THE GLENARM SERIES AND RELATED ROCKS

*A. K. Sinha, M. W. Higgins, G. L. Davis,  
S. R. Hart, and W. S. Kirk*

The Glenarm Series is a thick sequence of metasedimentary and meta-volcanic rocks that underlies most of the Maryland, Pennsylvania, and Delaware Piedmont and extends into northern Virginia. The basal unit of the series, the Setters Formation, is a transgressive quartzite that rests unconformably upon a 1000–1300 million-year-old basement complex called Baltimore Gneiss. The Setters is conformably overlain by the Cockeysville Marble, and the marble by the thick Wissahickon Formation. The Wissahickon Formation consists of at least five facies: pelitic schist, meta-graywacke, quartzite, conglomerate, and large submarine slide deposits of pebbly paragneiss called the diamictite facies. Recent mapping indicates that the

Wissahickon grades eastward into a sequence of metamorphosed volcanic, volcanoclastic, and volcanic-epiclastic rocks—the James Run Formation in Maryland and Chopawamsic Formation in northern Virginia.

The age of the Glenarm Series has been a subject of controversy for more than 60 years (see Swartz, 1948;<sup>102</sup> Hopson, 1964,<sup>103</sup> for summaries). Interpretation of important structural features (i.e., Martie overthrust, Peach Bottom fold) depends on the age of the Glenarm. The age of the Glenarm and events affecting it also bear strongly on the interpretation of the nature and development of the Appalachian geosyncline and on the theories of continental drift and sea-floor spreading with regard to the geosyncline. A lower Paleozoic age for the series would support the view of a contemporaneous “double” geosyncline, with a miogeosynclinal basin to the west (unmetamorphosed Paleozoic Appalachians) and a eugeosynclinal trough or basin to the east (crystalline Appalachians). It would

also be strong support for an "intra-cratonic" Appalachian geosyncline, developed between eastern North America and Africa before these continents were drifted apart, and for a post-middle Paleozoic formation of the Atlantic Ocean Basin. On the other hand, a Precambrian age for the series would suggest that geosynclinal growth was already well advanced by latest Precambrian, would greatly reduce the width of the early Paleozoic part of the geosyncline, and would deprive it of the zone of thickest graywacke sedimentation, ophiolite intrusion, volcanism, strong regional metamorphism, and granite emplacement (the eugeosyncline), thus indicating successively developing, but temporally related miogeosynclines and eugeosynclines.

We have dated four fractions of zircon from the diamictite facies (sample 2, Table 12) of the Wissahickon Formation (Sykesville Formation of Hopson, 1964) in an attempt to find young zircons that would place a maximum age on this part of the Glenarm Series. We have so far been unsuccessful, and all of the zircons thus dated appear to be detrital components from the Baltimore Gneiss. The data does have value, however, even though it does nothing to define the maximum age of the Wissahickon Formation. It shows: (1) that 1100–1300 m.y.-old zircons can be eroded, transported, and metamorphosed to amphibolite facies without significantly affecting their Pb/Pb ages; (2) it supports the idea that the source area for this part of the Wissahickon was rugged, tectonic terrain, and that erosion and deposition were very rapid—too rapid for there to have been much weathering effect on the zircons; (3) it supports earlier data on the age of the Baltimore Gneiss; and (4) it proves the sedimentary origin of the diamictite facies.

We have also dated zircon from a felsic metavolcanic rock (sample 1,

Table 12) near the base of the Chopawamsic Formation in northern Virginia. The Chopawamsic has gradational contacts with both the Quantico Slate (Ordovician) and the Wissahickon Formation. Our data here are consistent with a Cambrian age for the Chopawamsic, and suggest a late Precambrian-Cambrian age for the Wissahickon.

## SEISMOLOGY

### CORE PHASE NOMENCLATURE: SUGGESTED CHANGES

*I. S. Sacks*

The standard designation of core phases is somewhat unsatisfactory because from this it is not apparent which region of the core the rays actually traverse or whether reflections or refractions are involved. In order to avoid this confusion a system is suggested in which the notation directly indicates the ray path through the core. It is based on the divisions of the earth by Bullen.<sup>104</sup> He has divided the earth into a series of shells ranging from *A*, the outermost, to *G*, the inner core.

For a refracted core phase, the standard three-letter notation is followed by either *E*, *F*, or *G*, indicating the deepest zone of penetration: *E* for the outer core, *F* for the transition zone, *G* for the inner core. If the phase is reflected, the standard core notation is followed by the two letters designating the zones above and below the reflector. Thus, for example, if a *P* wave core phase has its point of deepest penetration in region *F*, the phase is designated *PKPF*. If it is reflected from the surface of the inner core, it will be designated *PKPFG*.

Both the above nomenclature and the previous notation are used in all appropriate figures. Figure 22 shows all the travel-time branches which are discussed. (Reflections are not indicated by lower case characters because, in gen-



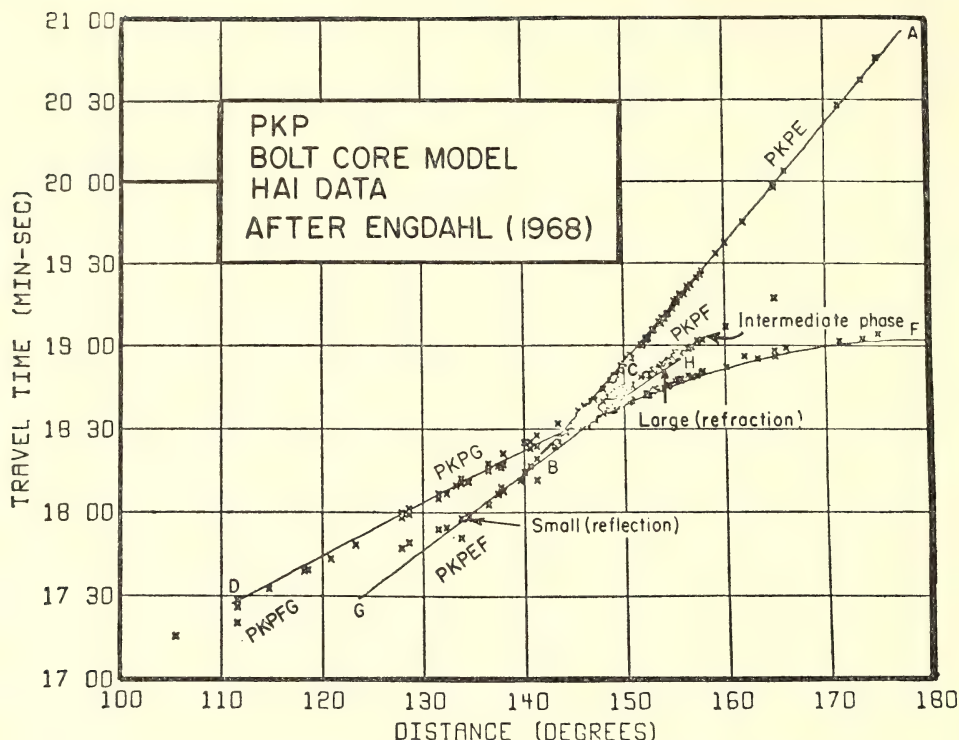


Fig. 22. *P* wave travel times in the earth's core. (Engdahl, 1968).<sup>105</sup>

eral, these are not available on line printers.)

#### ANELASTICITY OF THE OUTER CORE

*I. S. Sacks*

Seismologists have long noted that seismograms of compressional elastic waves which travel through the earth's outer core have substantial high-frequency content. This suggests that there is little absorption of elastic energy in this region, since the effect of absorption is to attenuate selectively the higher frequencies. The determination of the anelasticity in a low absorption (i.e., high *Q*) region is difficult because the wave character changes but little while traversing such a region. When the region of interest is the outer core, the problem is further aggravated, since the seismic waves traverse the whole mantle

(a region of relatively high absorption) at least twice.

The factors which determine the spectral content in the recording of a seismic phase are: (1) the source radiation spectrum; (2) propagation effects, particularly anelasticity along the ray path (the parameter of interest in this study) and crustal layering effects; and (3) the frequency response of the seismograph. Correction for the seismograph response presents little difficulty, but determination of the source radiation spectrum and the crustal layering effects are major studies in their own right. Rather than attempt to calculate these (and suffer from the resulting errors), a different approach has been used. Two ray paths (see Fig. 23) are chosen (*P* and *PKPPKP*) such that both phases originate from the same earthquake and are recorded by the same seismograph. Tak-

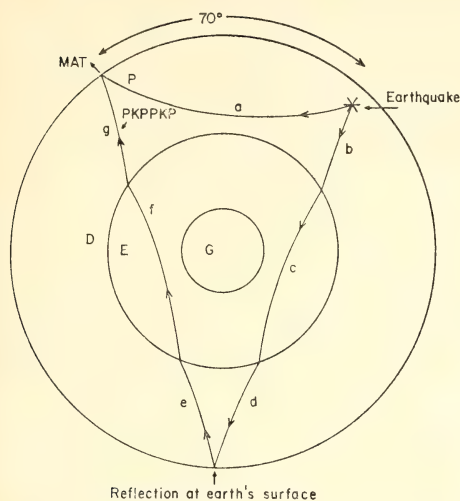


Fig. 23. Ray paths studied to determine the anelasticity of the outer core.

ing a spectral ratio over a sufficiently wide frequency range results in cancellation of the effects of the source spectrum and of crustal layering under the recording seismograph. This does not, however, allow for attenuation in the mantle path.

Recordings of the Fiji large deep earthquake ( $m=7.0$ ,  $h=654$  km) of 9 October 1967, on the DTM large-range seismograph in Matsushiro, central Japan ( $\Delta=70^\circ$ ) permitted the application of this technique. The travel time for the direct  $P$  wave was 10 minutes 10 seconds, and the travel time for  $PKPPKP$  was 38 minutes 3 seconds. This earthquake radiated so much seismic energy that the  $PKPPKP$  arrival at Matsushiro was greater than the local noise over the frequency range 0.05 to 2.7 Hz (Plate 3). The arrival amplitude of  $P$  at MAT is very large, above noise from 0.02 to 4.0 Hz, so that the range over which spectra can be compared is limited by the  $PKPPKP$  arrival. The spectral ratio  $PKPPKP/P$  is shown in Fig. 24.

From the data one can determine the excess attenuation of the high-frequency energy relative to that at lower frequencies. This can be done with some confidence because of the wide frequency range over which the signals are re-

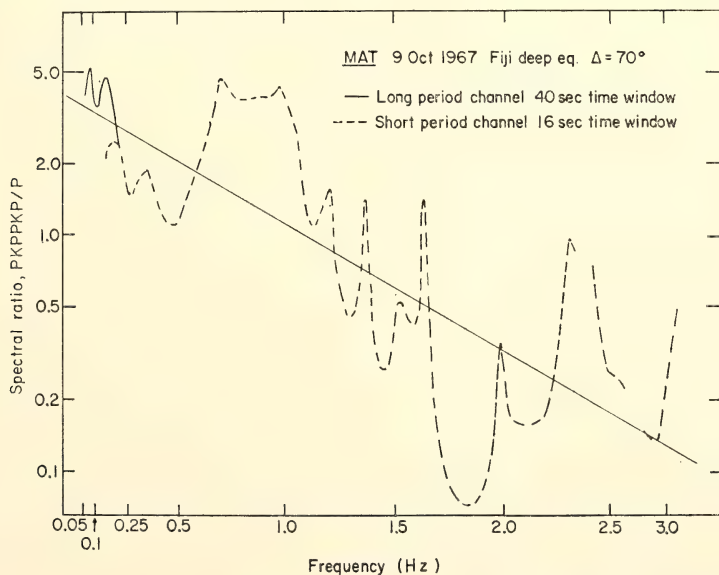


Fig. 24. Spectral ratio of  $PKPPKP/P$ . Both signals are at least twice noise where the ratio is plotted. The noise was determined by analyzing an equal length of record just prior to the arrival.

corded. It remains, however, to apportion the attenuation between the mantle and the core. In order to simplify this calculation it is assumed that the attenuation of the direct  $P$  arrival along path marked  $a$  in Fig. 23 may be taken to be approximately the same as that suffered by the rays along segments  $b$  and  $g$ . The travel time along  $a$  is 10 minutes 10 seconds and the sum of the time  $b+g=8$  min. 44 sec. The ray  $a$  samples the upper two-thirds of the mantle, whereas the rays  $b$  and  $g$  sample the whole mantle with a somewhat smaller angle of incidence than ray  $a$ . The effect of the lower third of the mantle on  $b+g$  is not expected to be substantial because there is no suggestion from the change of frequency content of  $P$  waves traveling in the lower one-third of the mantle (i.e., at distances between 70 and 95°) that there is anomalous or rapid change in attenuation near the base of the mantle until the ray grazes the core (distance > 95°). If the above assumption, i.e., that there is equivalent absorption on rays  $a$  and  $b+g$ , is permitted, then the spectral ratio determined is dominated by the attenuation of core paths  $c$  and  $f$  and whole mantle paths  $d$  and  $e$ .

The range of possible values of  $Q$  in the mantle and the core satisfying the data are given in Table 13. Some interesting limiting cases should be considered. If one assumes that the mantle is perfectly elastic and that all the attenuation occurs in the core, this gives the minimum possible  $Q$  for the core. The value is  $Q=3000$ . If one makes the opposite assumption that all the loss occurs

in the mantle and that the core is perfectly elastic, the minimum  $Q$  of the mantle is 1365. Thus, we have determined that the  $Q$  of the core lies in the range of 3000– $\infty$ , and that the  $Q$  of the mantle is in the range 1365– $\infty$ . The mantle  $Q$  can be determined independently but this has not yet been done with sufficient accuracy. (Sacks, *Year Book 66*, pp. 28, 29, determined a value of 1500 based on the attenuation over a path of 50°). It is likely that the mean  $Q$  of the whole mantle will be slightly higher, and if a value of 2000 is taken as a probable value, this leads to a derived  $Q$  of the outer core of about 10,000.

It is clear from the above discussion that an accurate mantle  $Q$  must be determined before the outer core  $Q$  can be known with great precision. However, it is also clear that the  $Q$  of the outer core is much higher than that of any other region in the earth.

#### ANELASTICITY OF THE INNER CORE

*I. S. Sacks*

The anelasticity of the inner core has been determined by comparing the spectra of waves that travel in the inner core with that of those which travel just outside it, in the high  $Q$  outer core. We have found that the outermost region of the inner core has a very low  $Q$  value (for  $P$  waves), and that  $Q$  increases rapidly with depth in the inner core.

Core phases from a number of earthquakes over the distance range 130–170° have been studied on the DTM broadband seismographs. Figure 25 shows the ray paths of the arrivals compared in order to evaluate the  $Q$  of the inner core. The study was facilitated by the fact that rays traveling just inside and those traveling just outside the inner core have rather similar paths through the mantle;

at a distance of 150°,  $\frac{dT}{d\Delta}$  for the inner core phase is 1.5, and that for the nearest outer core phase is 2.25 sec/km. This means that the mantle path absorption

TABLE 13.  $Q$  Value Combinations That Satisfy Spectral Data

Mantle	Core
	3,000
6,000	3,960
4,000	4,630
3,000	5,500
2,000	9,600
1,500	33,500
1,365	



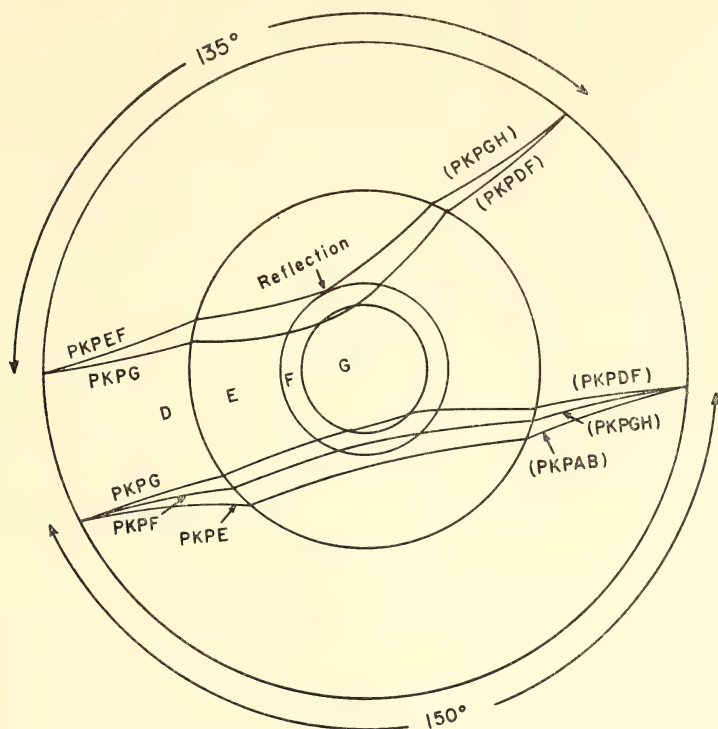


Fig. 25. Ray paths studied to determine anelasticity as a function of depth in the inner core. The ray *PKPG* first penetrates the inner core at a distance of about  $125^\circ$ . From  $130$  to  $140^\circ$  *PKPEF* and *PKPG* may be used to determine the  $Q$  of the outermost region of the inner core. From  $148$  to  $155^\circ$  *PKPF* and *PKPG* are used to determine  $Q$  at a greater depth.

is essentially the same for both phases. The difference in travel time for the two phases is also rather small, being about 4 seconds at the same distance. Therefore, any difference in the spectra of two such phases recorded on the same seismograph from the same earthquake is due to differences in the anelasticity of the outer core and inner core segments of the paths. The travel time in the inner core is shown in Fig. 23.

Plate 4 shows a filtered seismogram of an arrival at an epicentral distance of  $154^\circ$ . It is apparent that at low frequencies (upper traces) the inner core phase (*PKPG*) has an amplitude comparable with those of the phases traveling in the outer core (*PKPF*, *PKPE*). But at higher frequencies (lower traces) the outer core phases have substantially

larger amplitudes. The spectral ratio of the first two phases (*PKPG*: *PKPF*) is shown in Fig. 26. If one ascribes all the absorption to the inner core path, a  $Q$  value of 600 is obtained. Since the outer core  $Q$  has been determined to be about an order of magnitude greater, its effect on the attenuation determination will be less than 10%. This is less than the error in the determination and may be ignored. Figure 27 shows spectral ratios of three different earthquakes recorded on the Cuzco station at epicentral distances of about  $151^\circ$ . The similarity of these ratios illustrates the consistency of the results. At distances less than  $145^\circ$ , the outer core phase available for comparison with that traveling through the inner core is *PKPEF* (*GH*); see Fig. 22. This is known to travel wholly in the outer core

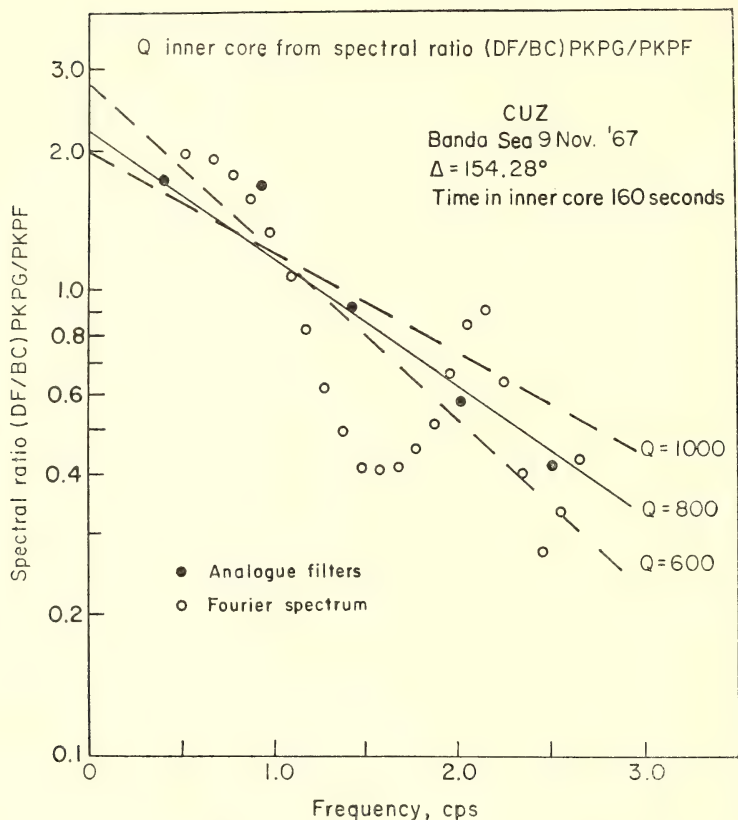


Fig. 26. Spectral ratio of *PKPG* to *PKPE*. Since the  $Q$  of the liquid outer core is so high, the slope of the spectral ratio is due to anelasticity in the inner core. The spectral ratio at zero frequency is the geometrical amplitude ratio of the two phases.

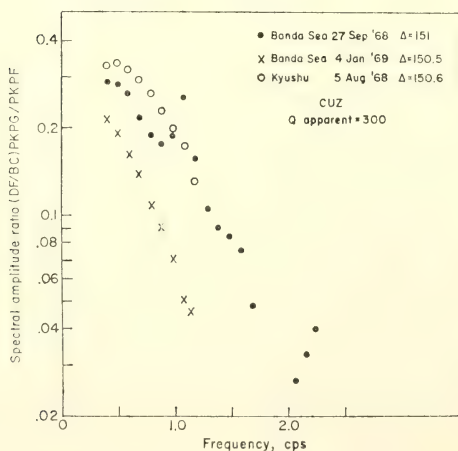


Fig. 27. Spectral ratios of *PKPG* to *PKPE*.

from its  $\frac{dT}{d\Delta}$  value of 2.75 (Bolt, 1968).<sup>106</sup> Phases traveling in the inner core must have  $\frac{dT}{d\Delta}$  values less than 1.9.

Spectral ratios of inner core and outer core phases over the distance range  $130^\circ$ – $155^\circ$  enable a determination of apparent  $Q$  vs. travel time, and hence  $Q$  vs. depth of penetration in the inner core.  $Q$  is  $170^\circ$  at the outer edge, rising to  $600^\circ$  at a depth penetration of 15%. Figure 28 shows a  $Q$  structure that would satisfy the apparent  $Q$  vs. distance determination. A simple two-shell structure over a constant  $Q$  sphere is adequate to explain the data. It is not

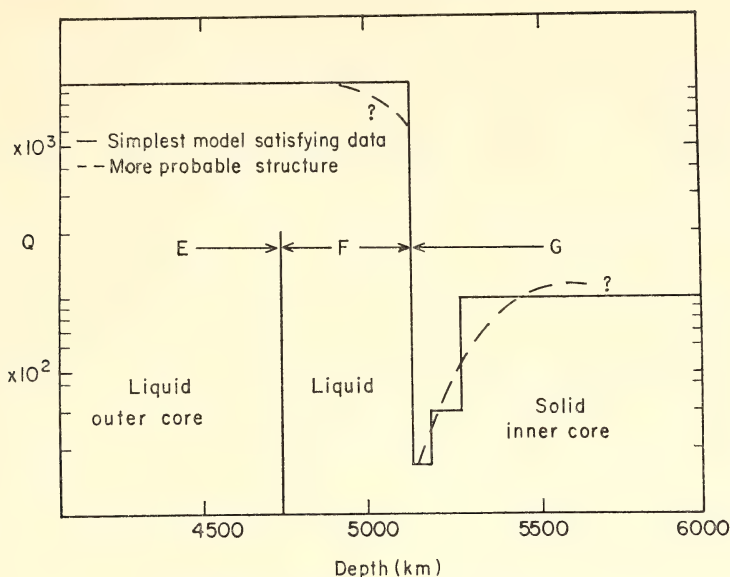


Fig. 28.  $Q$  structure of the earth's core.

suggested that there are discrete shells in the inner core; a more likely structure is one in which the  $Q$  value increases rapidly but continuously with depth.

One may conjecture that the low  $Q$  edge of the inner core indicates a zone of partial melting. The relatively low  $Q$  of the inner core implies that detection of higher frequency shear waves which travel through that region ( $PKJKP$ ) is rather unlikely.

#### THE STRUCTURE OF THE TRANSITION ZONE BETWEEN THE INNER CORE AND THE OUTER CORE

*I. S. Sacks and G. Saa*

Velocity structures of the core as determined by Jeffreys and also by Gutenberg were for many years the authori-

tative core models. Bolt (1959)<sup>107</sup> found that small amplitude arrivals earlier than those on the  $DF$  branch ( $PKPG$ ), which were previously the earliest accepted core arrivals, necessitated modification of the core models. He suggested a step-like velocity increase in a region outside the inner core. Since then the use of digital computers has enabled workers to calculate a large variety of core models that satisfy the travel-time data (see Engdahl, 1968).<sup>105</sup>

All these suggested models would have the amplitude of the  $GH$  phase (Fig. 22) of the same order as those of the  $DF$ ,  $AB$ , and  $BC$  phases, since all phases are presumed to be the result of refraction in regions of moderate to zero velocity gradients. On this basis, however, observed  $GH$  amplitudes exhibit an anoma-

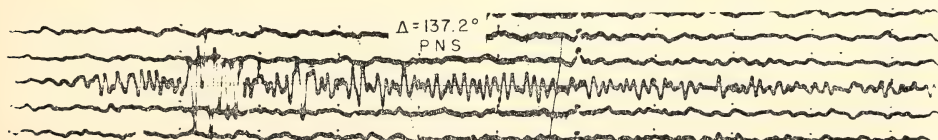


Fig. 29. Core phases at distance of  $137.2^\circ$ . The first arrival is  $GH$  phase ( $PKPEF$ ), followed by the larger  $DF$  ( $PKPG$ ) inner core phase.



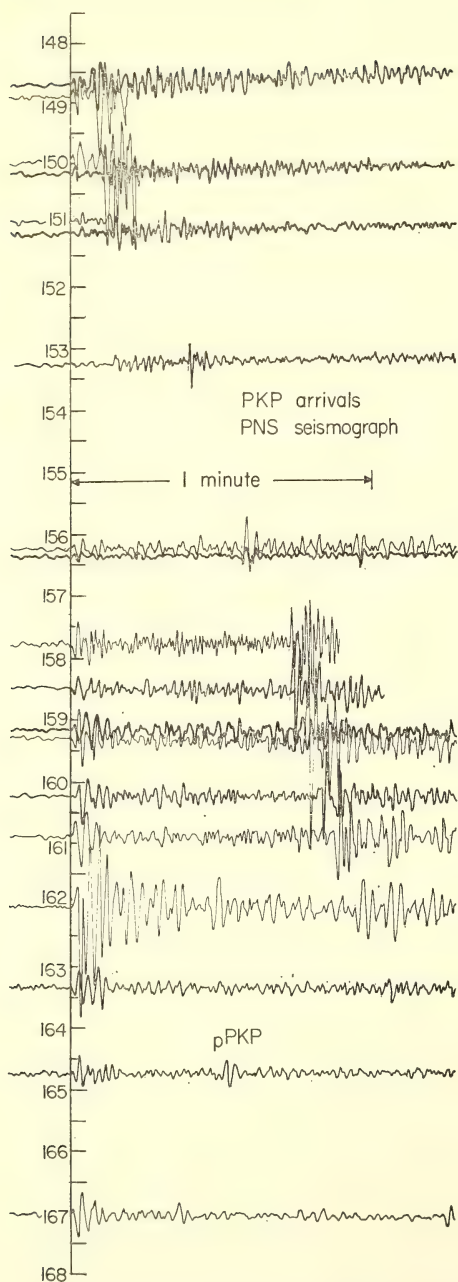


Fig. 30. Core phases in the distance range  $148^{\circ}$  to  $167^{\circ}$ . These are recorded on the same seismograph as Fig. 32. The large amplitude of the second arrival (*PKPGH?*, *PKPBC?*) *PKPF* relative to that of the first arrival *DF* (*PKPG*) at distances less than  $154^{\circ}$  is apparent.

lous behavior. Over the distance range  $125^{\circ}$  (*G* point) to  $144^{\circ}$ , they are very small relative to those of the *DF* phase (see Fig. 29), but, over the remainder of the presumed continuous travel-time curve ( $144^{\circ}$  to the *H* point at  $157^{\circ}$ ), amplitudes are much larger than the corresponding *DF* amplitudes (Fig. 30). Therefore, previously determined velocity models cannot be correct. Rather, the travel-time and amplitude data must be interpreted in terms of a model which for the so-called *GH* branch, gives rise to two distinct ray families with travel times apparently continuous. The model proposed here leads to a reflected phase, *PKPEF*, which satisfies the small amplitude section of the *GH* branch, while the large amplitude section is accounted for in forms of the refracted phase *PKPF*. To avoid further confusion, we will anticipate this result and use these designations to denote the travel-time branches previously referred to as *GH*.

#### Data and Analysis Techniques

Use was made of records from 22 of the DTM direct writing seismographs in Peru, Bolivia, and Chile in addition to seismograms from the World Wide Standard Seismic Network station NNA and ARE (Peru), LPB (Bolivia), and ANT (Chile). Spectral data, necessary to provide corrections for absorption in the inner core, were derived from the DTM broad-band stations in Chile (TCC), Peru (CUZ and TRU), and New Guinea (PMG).

The study of amplitudes and arrival times on an absolute basis requires a very large number of seismograms because one must evaluate the effects of station residuals and of errors in earthquake location and origin time. In a study in which one determines amplitude ratios and differences in arrival times for two (or more) phases, these errors are considerably reduced. In this study the *PKPG* (*DF*) branch was chosen as the normalizing phase. Of all core phases, its travel times are the best determined,

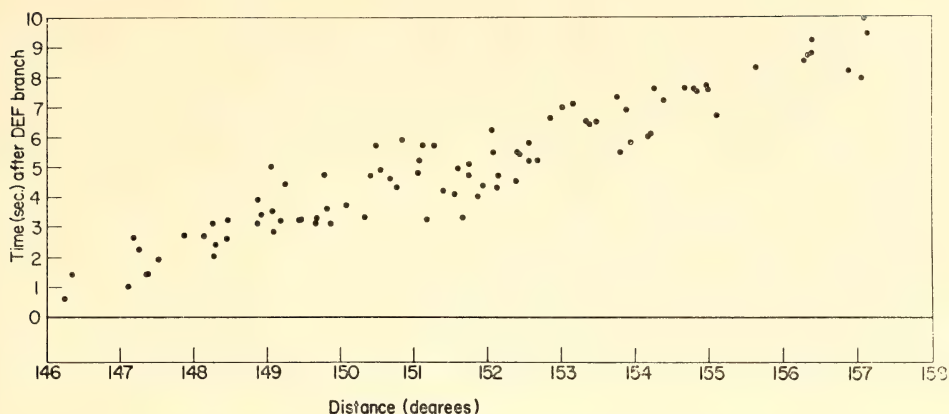


Fig. 31. Arrival time differences vs. distance between the first arriving core phase, (*PKPDF*) *PKPG* and the second arrival, (*PKPGH?*, *PKPBC?*) *PKPF*.

so that probably one can rely on both first and second derivatives of the travel-time curve. Bolt's (1968) travel times for *PKPG* were used, but use of the Jeffreys-Bullen travel times could not have led to substantially different conclusions.

Arrival times for *PKPF* were determined with the use of records from the stations given above. A seismogram section is presented in Fig. 30 and arrival time differences between *PKPF* and *PKPG* are plotted in Fig. 31.

In Fig. 32 amplitude ratios *PKPF*/

*PKPG*, calculated from records of the above stations, are shown as a function of distance. These data, however, are from instruments peaked in the range 1–2 Hz, and so correction for absorption *PKPG* in the relatively low *Q* inner core (see preceding article) is necessary in order to determine the amplitude ratio due solely to the different ray geometrics. The true geometric amplitude ratio may be obtained from the records of the broad-band magnetic recording seismographs. These records enable calculation

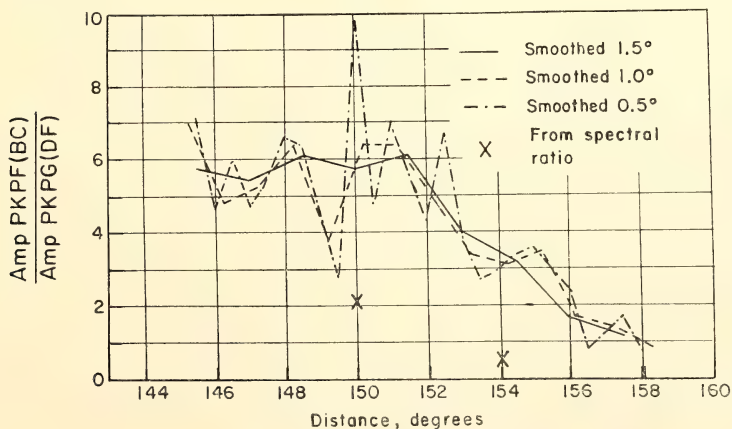


Fig. 32. Uncorrected amplitude ratios of *PKPF*/*PKPG* (*PKPBC*/*PKPDF*) vs. distance. The effect of anelasticity of the inner core on the relatively short period arrivals has not been removed.

of the ratio of the spectrum of *PKPG* to that of *PKPF* over a wide frequency range. The slope of this spectral ratio gives the apparent  $Q$  of the inner core (see preceding article) and the projection of the slope to zero frequency gives the geometric amplitude ratio (Fig. 26). This was done for a number of distances, and the uncorrected amplitudes of Fig. 32 were used to interpolate between the rigorously determined values. For the *PKPEF* phase the only geometric amplitude ratios used were these calculated from spectral ratios.

### Determination of $dT/d\Delta$

In order to calculate a velocity versus depth model we need to know values of the first derivative ( $dT/d\Delta$ ) of the travel-time curves. Despite the technique of measuring time differences, the spread of values in the time-distance plot (Fig. 31) is too large for a reliable estimate of the shape of the curve. Amplitudes are proportional to the second derivative,  $d^2T/d\Delta^2$  (see below), and thus an unknown constant results from the integration to calculate  $dT/d\Delta$ . By combining these two methods, however, we

are able to calculate a reliable curve for  $dT/d\Delta$  vs.  $\Delta$ . The technique is described in detail below.

The vertical component of the amplitude ( $A_v$ ) of a refracted ray may be calculated in terms of  $I$ , the energy leaving the source per unit solid angle, by use of the expression derived by Bullen (1959)<sup>108</sup>

$$A_v^2 \propto \frac{I \tan^2 e \sec^2 e}{\eta_1 \sin \Delta (\eta_1^2 \tan^2 e - \eta_0^2 \sin^2 e)^{1/2}} \cdot \frac{(1 + 3 \tan^2 e)^2}{\{4 \tan e \tan f + (1 + 3 \tan^2 e)^2\}^2} \left| \frac{d^2 T}{d\Delta^2} \right|$$

where  $e$  is the angle between the emerging  $P$  ray and the horizontal,  $f$  is the angle between the reflected  $S$  ray and the horizontal,  $\Delta$  is the epicentral distance,  $\eta_0$  is the radius/velocity at the surface, and  $\eta_1$  is radius/velocity at the focal depth. Amplitude ratios of *PKPF*/*PKPG* have been determined, so that knowledge of the various angles and  $d^2T/d\Delta^2$  for *PKPG* allows calculation of the second derivative for *PKPF* (Fig. 33). (The assumption that  $I$  is constant for the two ray paths considered is reasonable, since the angles of departure from the source are little different.) In-

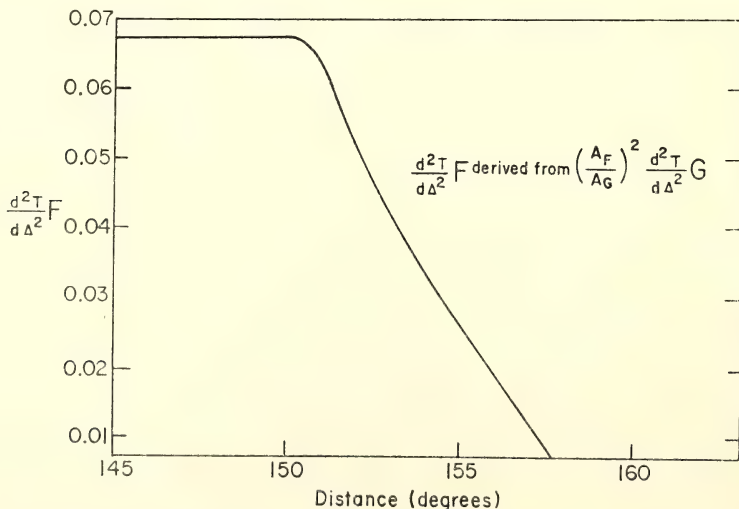


Fig. 33.  $d^2T/d\Delta^2$  of the second arrival core phase *PKPF* ( $\Delta > 144^\circ$ ). It is derived from the amplitude of *PKPF* and *PKPG* (*PKPDF*) and the observed travel times of *PKPG*.



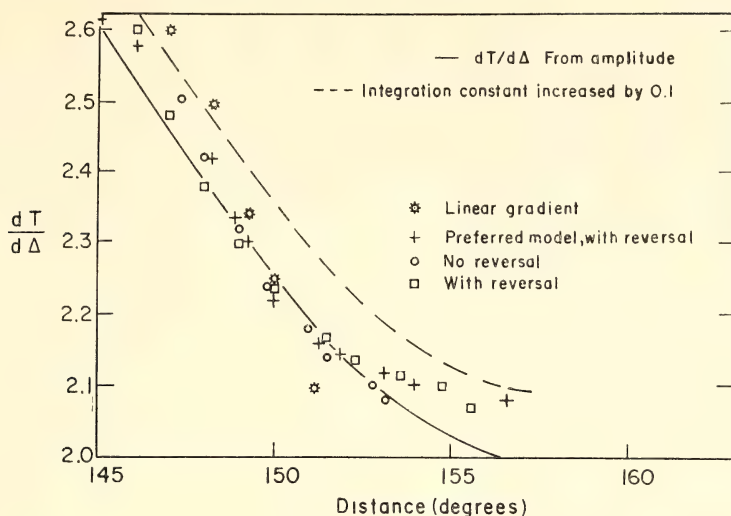


Fig. 34.  $dT/d\Delta$  of the second arrival core phase *PKPF* ( $\Delta > 144^\circ$ ) vs. distances.  $dT/d\Delta$  values calculated from models in Fig. 37 are also plotted.

tegration yields the shape of the  $dT/d\Delta$  curve (Fig. 34), with the level being arbitrary because of the unknown constant of integration. By using the independently determined travel-time data, however, this constant of integration can be estimated. A tentative estimate is ob-

tained from the least-squares fit of a straight line to a  $2^\circ$  segment of the travel-time curve (Fig. 35). The value finally selected for the constant is such that, on further integration of the  $dT/d\Delta$  curve, a travel-time curve is obtained whose shape best fits the observed data.

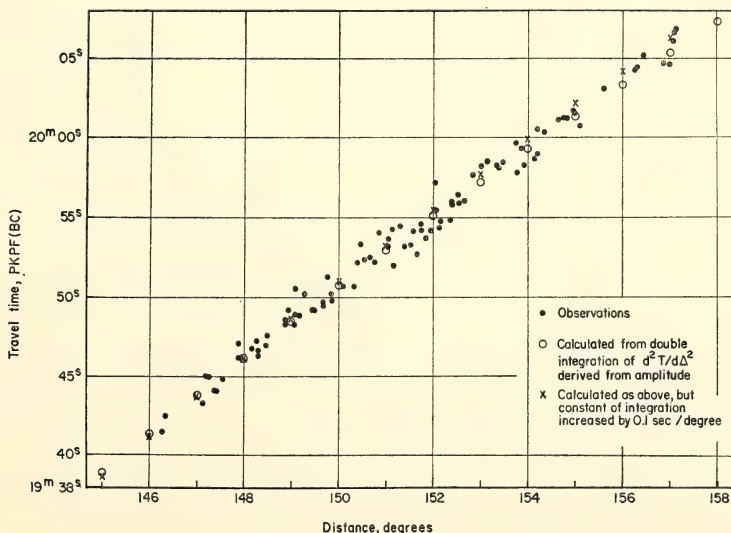


Fig. 35. Observed travel time curve of the second arrival core phase *PKPF* ( $\Delta > 144^\circ$ ).

The constant calculated by this technique is believed to have an accuracy of  $\pm 0.1$  sec/km (see Fig. 35).

### Velocity Models

It has been shown above that the amplitudes of *PKPEF* are small relative to those of *PKPG* (Fig. 29). Therefore, this phase is unlikely to be due to refraction. Interpretation of these arrivals in terms of wide-angle reflection at the outer boundary of the transition zone (*F*) satisfies both the amplitude behavior and the first derivative of the travel-time curve. The depth of the reflecting surface is determined by the observed  $dT/d\Delta$  (Bolt 1968)<sup>106</sup> for the phase, while the discontinuity in velocity is calculated from observations of the decrease in amplitude as the angle of reflection decreases. (At the angles of reflection appropriate here ( $>75^\circ$ ), the

reflection coefficient is insensitive to density contrast.)

Figure 36 shows, as a function of distance, the observed amplitudes together with those calculated as a result of reflection from a velocity discontinuity of 0.5% at a depth of 4773 km. The lack of reported observations of this phase at distances less than about  $125^\circ$  (see Fig. 22) is compatible with the amplitude behavior calculated from the model, since the reflection coefficient for this distance is only 0.028.

A further constraint on the velocity model of the transition zone is provided by the maximum distance at which the *PKPF* phase is observed. Generally, *PKPF* is not discernible on seismograms recorded at distances greater than  $157^\circ$ . If the ray penetrates any deeper, it encounters the core and is reflected to the *D* point (see Fig. 22). It is possible that as a result of diffraction around the

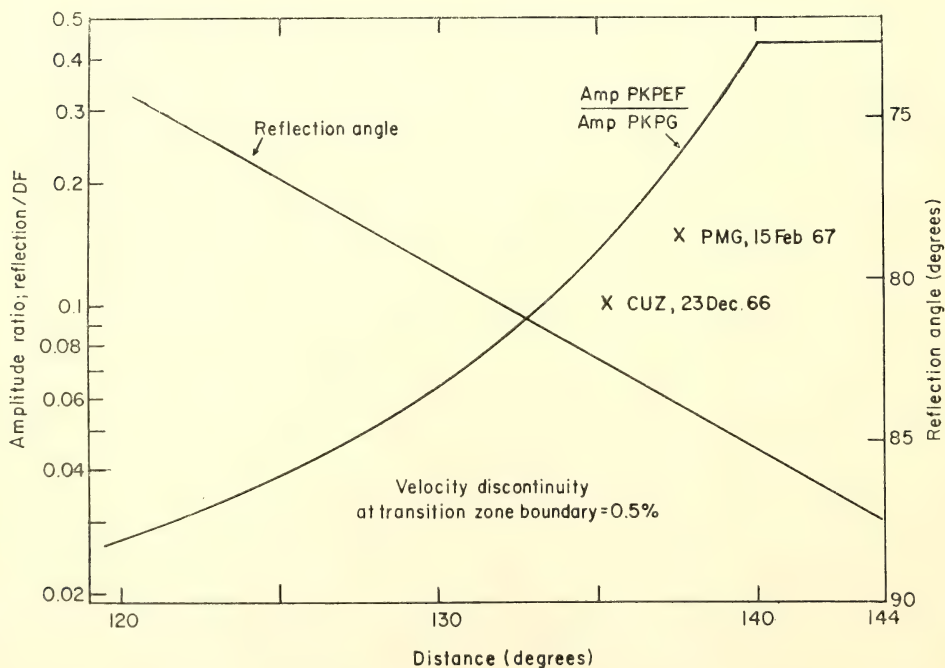


Fig. 36. Calculated and observed amplitude ratios of the first arriving *GH* phase (*PKPEF*) to the phase *DF* (*PKPG*). The calculated amplitude ratios are based on a velocity step of 0.5% at the transition zone boundary. Anelasticity effects have been removed.

inner core, the range of observations of *PKPF* has been extended beyond the growing distance by a degree or so. Thus  $157^\circ$  should be regarded as an upper limit to the maximum distance of observation of *PKPF*.

A range of velocity models is presented in Fig. 37, while Fig. 34 shows the comparison of  $dT/d\Delta$  calculated from these models and  $dT/d\Delta$  derived experimentally from the amplitude and travel-time data for *PKPF*.

The simplest model (A) has a linear velocity gradient of 0.07 km/sec/100 km throughout the whole transition zone. This velocity gradient is too small and the ray strikes the inner core at a distance of only  $151^\circ$ .

Model (B), the preferred model (see discussion below), has a linear gradient of 0.08 km/sec/100 km to a depth of 5080 km. In the deepest 56 km, this velocity gradient decreases and finally reverses. Amplitudes and travel times calculated from this model are in satisfactory agreement with observations.

Model (C) has an initially positive gradient which decreases to zero at the inner core boundary. The calculated  $dT/d\Delta$  agrees fairly well with observations, but the ray grazes the core at a distance of only  $153.5^\circ$ .

Model (D) has an initial velocity gradient of 0.1 km/sec/100 km which decreases with depth, and eventually reverses in the last 50 km. Calculated amplitudes and travel times agree satisfactorily with the observed values.

### Discussion and Conclusions

A difficulty in the structure determination is due to uncertainty in the velocity of the outer core material outside the transition zone. The travel times of the phase which samples this region, *PKPE*, are not well determined (Bolt 1968). The outer core velocity bounding the transition zone (x in Fig. 37) may therefore need modification when improved data are available. For this reason, exact matching of the calculated travel times with the observations for transition zone refracted (*PKPF*) and reflected (*PKPEF*) phases may not be significant. Thus, for the transition zone, the velocity model (B) is the preferred one because it is the simplest model compatible with the observed travel times and amplitudes.

Conclusions which may be drawn from this study are:

1. Arrivals previously considered to belong to one travel-time branch called

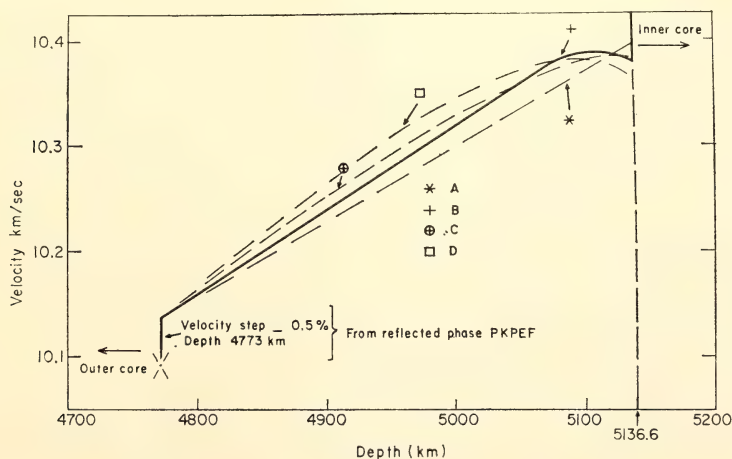


Fig. 37. Velocity models of the transition zone between the inner and outer cores.



*GH* are explained more satisfactorily in terms of two branches; one phase (*PKPEF*) being reflected from the outer boundary of the transition zone, the other (*PKPF*) resulting from refraction through the transition zone.

2. The transition zone between the inner core and the outer core is bounded on the outside by a sharp velocity increase of 0.5% and has a thickness of 364 km.

3. The velocity gradient over most of the transition zone is 0.08 km/sec/100 km.

4. The velocity gradient is rapidly reduced and probably reversed in the 60 km just outside the inner core.

One might conjecture that the velocity decrease, or at least disappearance of the positive velocity gradient outside the inner core is due to a mixture of some higher density inner core material into this region.

#### BOREHOLE STRAINMETERS

*I. S. Sacks, D. Evertson, and L. M. Dorman*

A high-sensitivity omnidirectional borehole strain-rate meter was described

in *Year Book 68*, p. 448. It was shown at that time that the ultimate sensitivity of buried strainmeters was limited by atmospheric noise (rock strains induced by atmospheric pressure variations in space and time). The marked similarity between the noise on the strainmeter and a co-located microbarograph suggested the possibility of improving the signal-to-noise (S/N) ratio by subtracting a suitably filtered signal from the microbarograph from the strainmeter output. Figure 38 shows the result of such a subtraction. The S/N improved by about 5, so the approach was deemed profitable.

During the past year we connected the strain instruments and the microbarograph to the seismic digitizing system used for replay of the broad-band seismic tapes. Thus, when the IBM 1130 computer would otherwise be idle (usually at night and on weekends) we are able to accurately and conveniently record data from these instruments.

Having these data in convenient digital form, it becomes possible to compute the pertinent statistics from the data. We have computed digitally the coher-

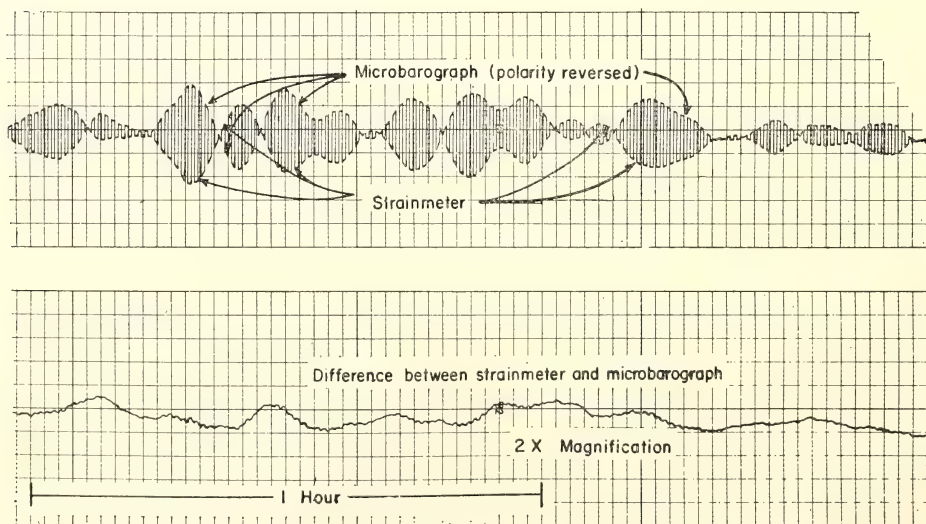


Fig. 38. Example of analog subtraction of coherent noise from strainmeter signal.

ence ( $\gamma$ ) (Foster and Guinzy, 1967;<sup>109</sup> Haubrich, 1965<sup>110</sup>) between the barograph and the volume strainmeter (see Fig. 39). The value of this statistic is that  $\gamma^2$  at any given frequency is the proportion of the power in the strainmeter signal at that frequency which is coherent with the microbarograph signal. Since the coherent noise can be removed by linear filtering and subtraction,  $1/\gamma^2$  is the easily obtainable improvement in the signal-to-noise ratio at that frequency. Thus, at frequencies where  $\gamma^2$  is 0.8, we can obtain an improvement in S/N of a factor of 5 (7 dB), and where it is 0.95, an improvement of a factor of 20 (30 dB).

The coherence drops sharply for periods shorter than about 40 seconds. This drop is due in part to the increase in microseismic noise at these shorter periods and in part to the lack of spatial coherence at the higher frequencies.

When the spatial coherence of the atmospheric pressure fluctuations is high, a microbarograph sampling pressure at one or two points near the strainmeter will be adequate for making the noise corrections. However, in order to make the best of all possible atmospheric noise corrections in an incoherent pressure field, we must use as a noise reference a

barograph that averages the surface pressure with a weighting proportional to the sensitivity of the strainmeter. The barograph used in the coherence measurements samples the atmospheric pressure at two points separated by about 50 meters.

The fact that the "two-point" barograph works as well as it does tells us that the surface atmospheric pressure is quite coherent across the surface area sampled by the strainmeter. It is as though there were a pressure pattern "frozen" into the air and the air were moving over the surface at a uniform speed. This is in agreement with the findings of Priestley (1965)<sup>111</sup> of high coherence for periods longer than 30 or 40 seconds. The only applicable work we have found in the open literature is that of Priestley, so we do not know how much or how rapidly the spatial coherence and the frequency-wave number spectra of atmospheric noise vary. We are still studying this subject.

### *Directional Strainmeters*

The simplest borehole strainmeters respond to volume strain (omnidirectional). However, since atmospheric pressure is normal to the earth's surface,

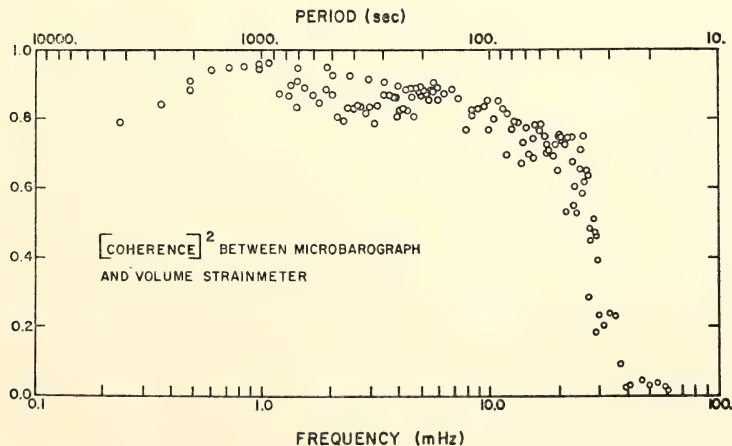


Fig. 39. Coherence squared between barograph and strainmeter.

one might expect to reduce the sensitivity to atmospheric pressure by measuring only the horizontal strain components. Indeed, Ozawa (1957)<sup>112</sup> had shown that the areal strain (the sum of the two horizontal strains) at the surface due to a normal load was identically zero when the loaded area did not include the strainmeter. We have computed (see Fig. 40) the vertical, areal, and volume strains which would be detected by a buried strainmeter as a result of a normal concentrated load on the surface as a function of distance from the borehole to the load. From these curves we can compute the strain at a depth due to any prescribed atmospheric stress distribution by taking a weighted average of the surface atmospheric pressure. By considering the problem in Fourier transform space, we can calculate the sensitivity of the earth-strainmeter system to the atmospheric pressure as a function of wave number. Figure 41 shows the response of a buried strainmeter to the atmospheric pressure field as a function of wave number. The wave number is the inverse of wavelength measured in units of the burial depth. The dominant component of atmospheric noise at  $\sim 100$ -

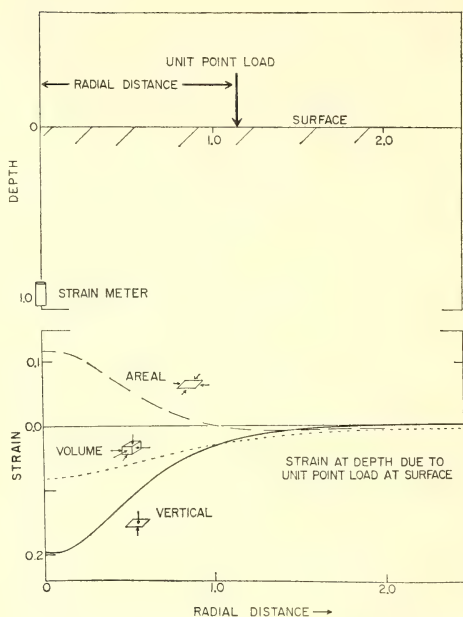


Fig. 40. The strain seen by a buried strainmeter due to a unit concentrated load at the surface as a function of distance from the load to the borehole. The strainmeter is buried at unit depth.

second period is due to turbulence in the boundary layer at the earth's surface. These disturbances travel at  $\sim 5$

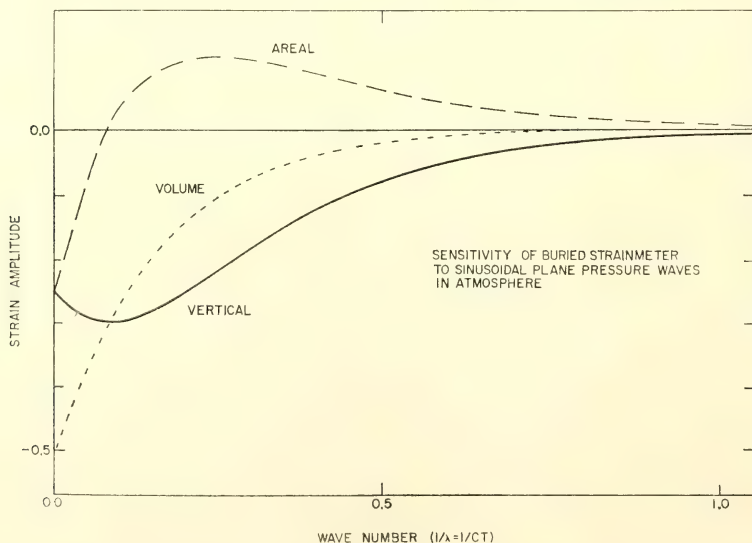


Fig. 41. The sensitivity of a buried strainmeter to sinusoidal plane pressure waves in the atmosphere.



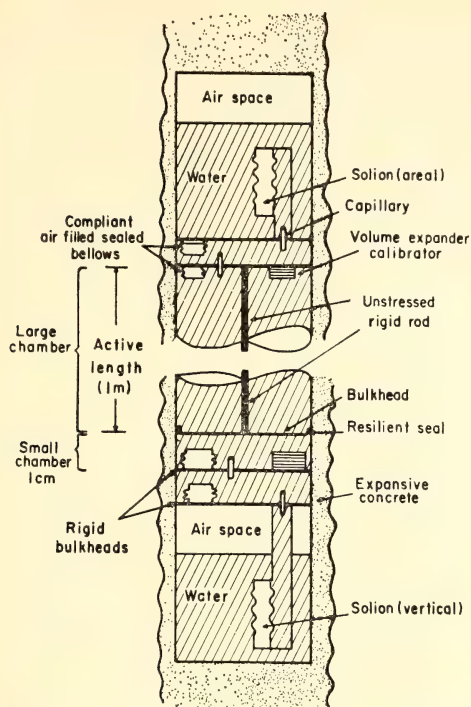


Fig. 42. Schematic of combined vertical and areal strain-rate meter.

meters/sec, giving a scaled wave number of 0.1, which, according to Fig. 41, is the value for which the areal strain component is least sensitive. Hence, the areal component is indeed the least sensitive to this principal source of noise. With this as motivation, the next strainmeter (2) was constructed with the same principal features as (1) except for the following points.

1. The response was shaped with high-cut hydraulic filters in order to reduce the possibility of ion depletion in the solion caused by large signals at moderate periods ( $\sim 20$  seconds). Hydraulic filtering was chosen over electronic filtering because of the large dynamic range obtainable and because the filter had to be in the system ahead of the sensor.

2. In the second instrument, volume strain is resolved into the vertical and areal strains by connecting the sensors so that they measure the volume changes in two separate chambers that are effectively decoupled from the walls or the bottom of the tube, respectively. The large chamber (see Fig. 42) responds

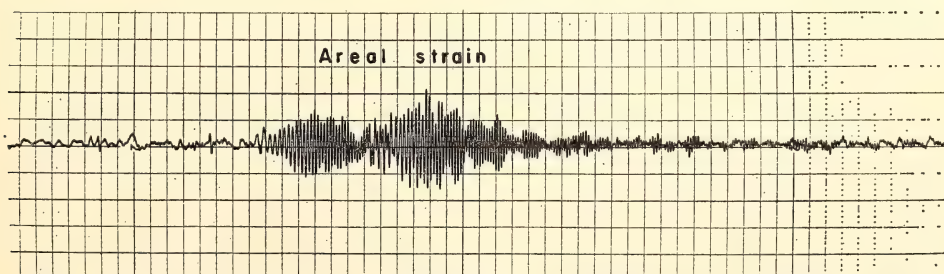
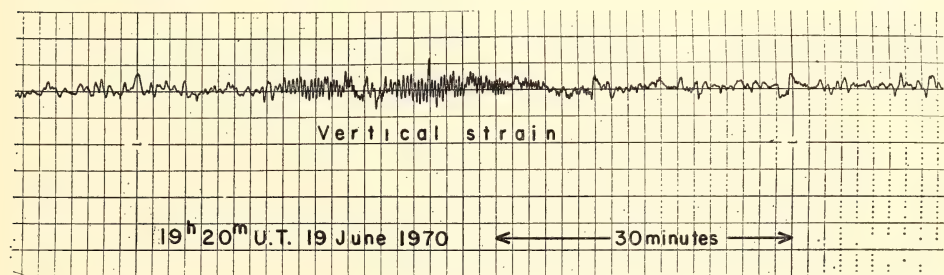


Fig. 43. Rayleigh waves from two earthquakes ( $m_b = 5.3, 5.4$ ) in the Fiji region, recorded at DTM, Washington, D. C., on vertical and areal strain-rate meters. The earthquakes were about 10 minutes apart. Note that the signal-to-noise ratio for the areal meter is about twice that for the vertical meter.

only to areal strain, since the height of the volume is maintained by an unstressed column connecting the movable bottom piston with the fixed top of the chamber. The small chamber at the bottom of the instrument has a movable piston as a top and the fixed end of the tube as a bottom. Since the piston is connected to the top of the tube by a fixed length member, the length change due to vertical strain on the active length is reflected in a height change in the lower volume. Thus the volume change in the small chamber is the volume change due to vertical strain for the active length ( $\sim 1$  meter) plus that due to areal strain in the relatively insignificant ( $\sim 1$  centimeter) small chamber.

Our early results from this second meter have largely borne out the predictions. Figure 43 shows a sample of noise from both the vertical and areal components. The short-period ( $< 200$  seconds) noise is indeed lower on the areal than on the vertical (or the omni). An unexpected finding is that the noise on the vertical component is small at periods longer than  $\sim 500$  seconds. We as yet have no explanation for this.

#### FREQUENCY ANALYSIS OF SEISMIC BODY WAVES

*A. T. Linde and I. S. Sacks*

The Fourier integral transform

$$F(\omega) = \int_{-\infty}^{\infty} f(t) e^{-i\omega t} dt$$

is, in the case of temporal signals sampled at discrete intervals, replaced by the series transform with coefficients

$$A_r = \sum_{k=0}^{N-1} f(k) W^{rk} \quad r=0, 1, \dots, N-1$$

where

$$W = \exp(-2\pi i/N)$$

and  $f(k)$  is the  $k^{\text{th}}$  sample of the time series consisting of  $N$  samples. The series transform has found wide application for frequency analysis; seismic arrivals, for

instance, are transformed to the frequency domain for studying phenomena such as earthquake and explosion radiation and earth anelasticity. Theoretically, however, the substitution of the series transform of a finite interval for the integral transform is valid only under very restrictive conditions: when the signal is repetitive, or, when a nonzero signal exists for a finite duration. Often neither condition is satisfied. Recordings of seismic arrivals are not repetitive and noise is always present. By suitable selection of a sample of the record and by weighting the data according to an appropriately chosen window function it is possible, in the case of a seismic arrival, to approximate the limited nonzero signal condition. This approximation, however, must result in some error. Further, a truncation effect, due to the presence of arrivals other than the one of interest, may preclude analysis of a sufficient signal length.

In practice, a suitable sample of the data has to be selected for analysis and the type of window to be applied has to be chosen. Ideally the sample length used should include the whole of the recorded arrival, which means that the effect of the instrument response in the time domain must be considered. As discussed below this often presents a major problem when a standard long-period seismometer is the recording instrument. The choice of window type is not a simple one. Its effect in both the time and frequency domain must be considered. In general, a window which does not distort the time domain, e.g., a box-car window, has severe side lobes in its transform (Fig. 44) and since multiplication in the time domain corresponds to convolution in the frequency domain, a false spectrum may result. Choosing a window with small side lobes, e.g., a Hamming window (Fig. 45), in order to minimize this problem results in a modified time domain record. Attempts at a compromise between these two types of

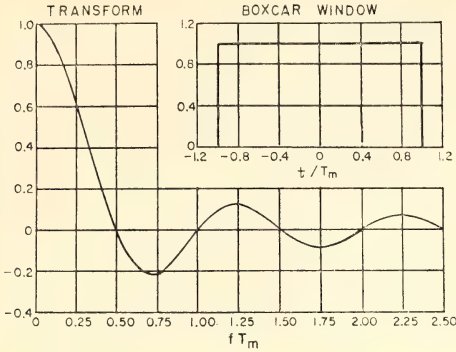


Fig. 44. The boxcar window and its transform.

time domain windows (the flat boxcar window and the smoothly varying Hamming—or the similar Hanning—window) are unsuccessful. Bracewell (1965)<sup>113</sup> considers this problem and comments: “If such a function undergoes a large change in a short interval of abscissa as in [Fig. 46, this Report] Fig. 8.11

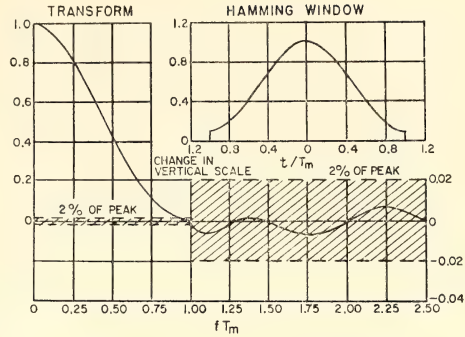


Fig. 45. The Hamming window and its transform.

[Bracewell, p. 153] (that is, it has a very large slope in this interval), it may for some practical purposes be effectively discontinuous. Its spectrum will indeed be found to behave appropriately. The fact that ultimately the asymptotic behavior appropriate to a continuous function sets in is then not of practical

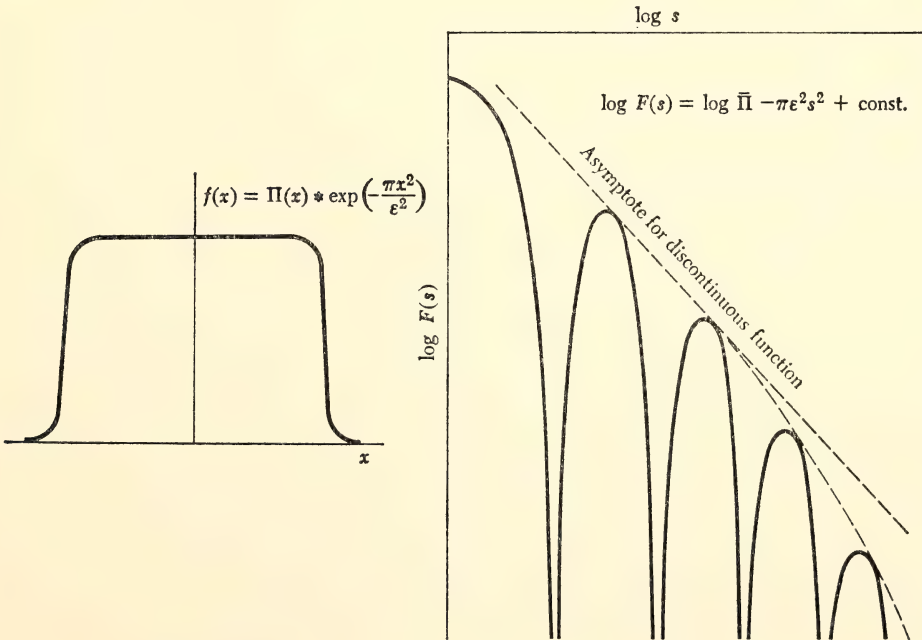


Fig. 46. A continuous function with all continuous derivatives, which for certain purposes is effectively discontinuous, and its transform. (From *The Fourier Transform and Its Applications*, by R. Bracewell. Copyright 1965, McGraw-Hill, Inc. Used with permission of McGraw-Hill, Inc.)



concern, since only periodic components of periods short compared with the above mentioned short interval exhibit the expected behavior, and they are beyond the limit of interest, for we have said that for the purpose the change is effectively discontinuous." \* There are, however, numerous instances in the literature of the use of such compromises in the window choice. A compromise often used is to modify a boxcar window by cosine tapering the last, and sometimes also the first, 10% to 20% of the window. The rationalization is that the effects of truncation are thereby reduced. This ignores the fact that the problem is basically one of convolution in the fre-

quency domain, not one of first-order discontinuity in the time domain. (The compromise windows described above have side lobes little different from those of the boxcar window.

We are, therefore, forced to the conclusion that, in the case of real seismic signals, it is impossible to recover without error the frequency spectrum of the ground signal by means of Fourier analysis. If extreme care is not taken, the subtle but crucial errors introduced may be so large that interpretation of the results can lead to erroneous geophysical conclusions.

#### *Model Study—Fourier Analysis of Long-Period Body Waves*

As is demonstrated below, the shape of the long-period body wave displace-

\* *The Fourier Transform and its Applications*, by R. Bracewell. Copyright, 1965, McGraw-Hill, Inc. Used with permission of The McGraw-Hill Book Co.

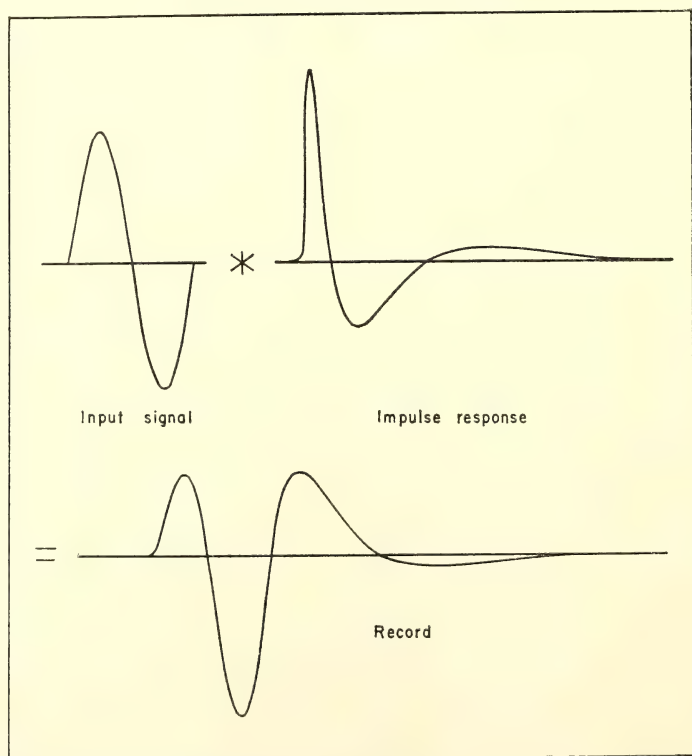


Fig. 47. Convolution of a single-cycle sinusoidal wave with the impulse response of a long-period seismometer.

ment spectrum radiated by earthquakes is diagnostic of the volume from which energy is released. However, there is a fundamental difficulty in "windowing" a long-period seismic arrival recorded by standard instruments when the arrival consists essentially of a single cycle and is followed by later arrivals which limit sample length. In order to investigate the effects of truncation and noise, various simple signals were convolved with the impulse response of a 30-second seismometer-100-second galvanometer system (Fig. 47), the former World Wide

Standard Seismic Network long-period instrument; and sections of the record thus obtained were Fourier transformed.

Figure 48 shows the record that would be obtained from the long-period instrument when the incident signal is a single cycle of a 20-second sinusoidal wave. This is a record that has no noise present. After cessation of the input signal 60 seconds are required for the instrument to complete its response, although the amplitude of the last trough is small, being somewhat less than 6% of the maximum amplitude recorded. The

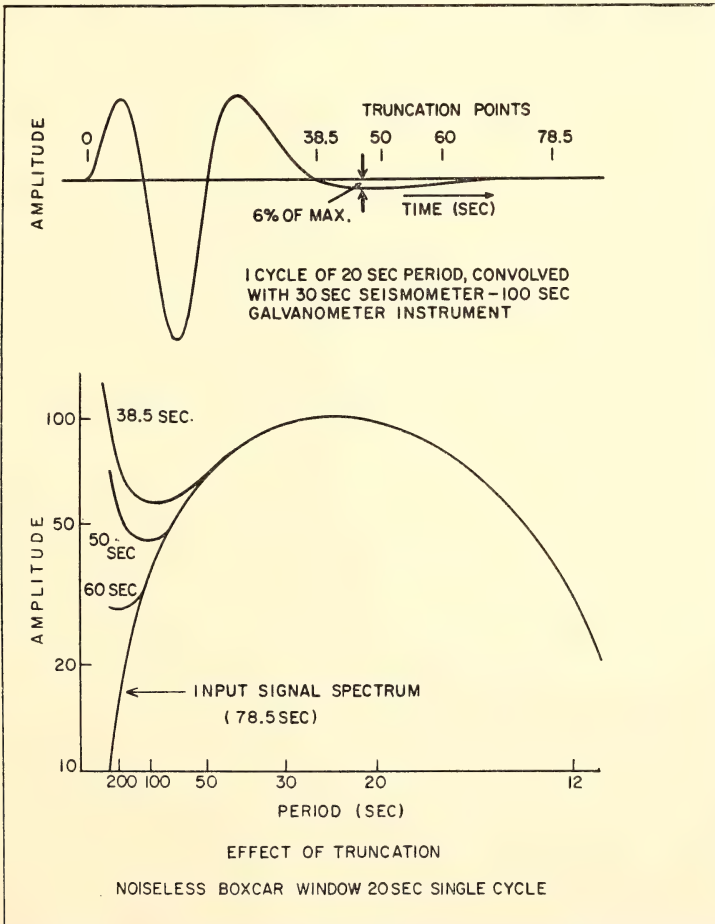


Fig. 48. Effect of truncation (boxcar window) of the record resulting from a 20-second single-cycle sinusoid input signal in the absence of noise.

spectra shown in Fig. 48 result from transforming the record after the application of boxcar windows starting at time zero and ending at the indicated truncation points. The instrument response has been removed in the frequency domain. The actual input spectrum (the curve corresponding to the 78.5-second window, outside of which the signal is zero) has further structure at shorter periods, but this is not of

interest in the present study. The effect of increasing truncation is to increasingly exaggerate the long-period amplitude, even though the amplitude of the truncated part of the signal is small.

Addition of white noise to the signal, such that the signal-to-noise recorded amplitude ratio is 10 to 1, results in the record shown in Fig. 49. In the frequency domain, the long periods are enhanced even though the signal has not been

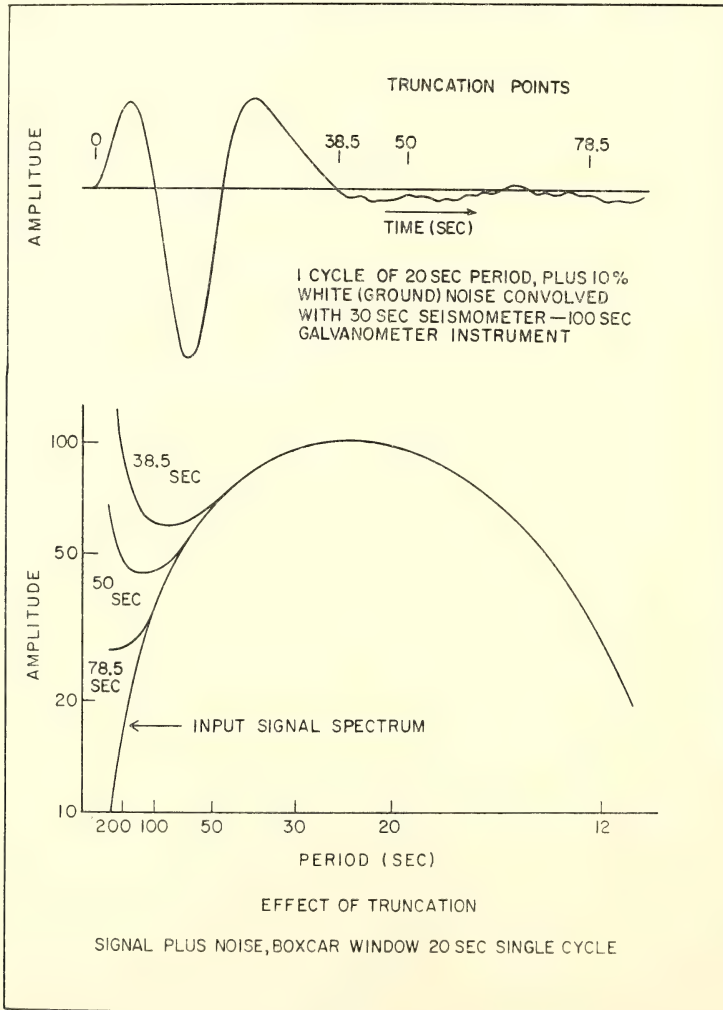


Fig. 49. Effect of truncation (boxcar window) of the record resulting from a 20-second single-cycle sinusoid input signal in the presence of white ground noise.



truncated. Again the error increases as the window is shortened.

As discussed above, the Hamming window is often used to overcome the ringing effects of side lobes in the frequency domain. It is simply a cosine wave on an 8% pedestal. In Fig. 50 this window has been centered on the region of maximum disturbance, with truncation points as before. The frequency domain results show that the long-period error is further increased by application of the Hamming window.

The variation of the truncation effect with the period of the incident single cycle is illustrated in Fig. 51. Records due to incident single cycles of 10, 20, 40, and 80 seconds are shown, but with

different time scales. For convenience of comparison, the spectra shown correspond to time domain truncation at the third zero crossing of the signal. Boxcar windows have been used. The spectra are now plotted on a normalized period scale, with  $T$  being the period of the incident single cycle. The trends shown in Figs. 48, 49, and 50 apply to all wavelets, the error increasing with the period of the wavelet.

In Fig. 52 the window length required to show the existence of a peak in the spectrum is shown as a function of the period of the input single cycle. The criterion used here is that the amplitudes must decrease by a factor of two at periods longer than that at which the

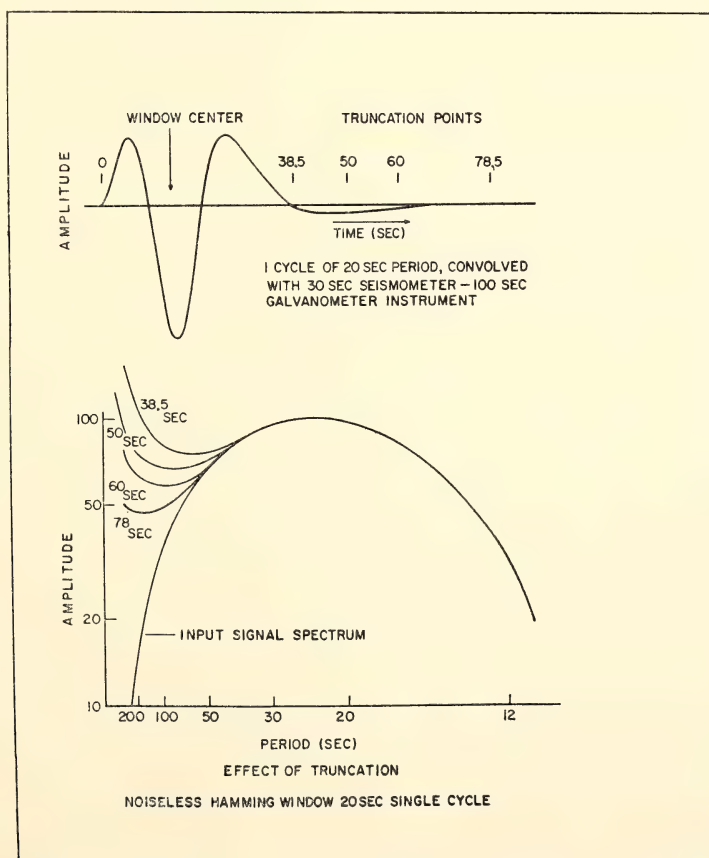


Fig. 50. Effect of truncation (Hamming window) for the same record as in Fig. 51.

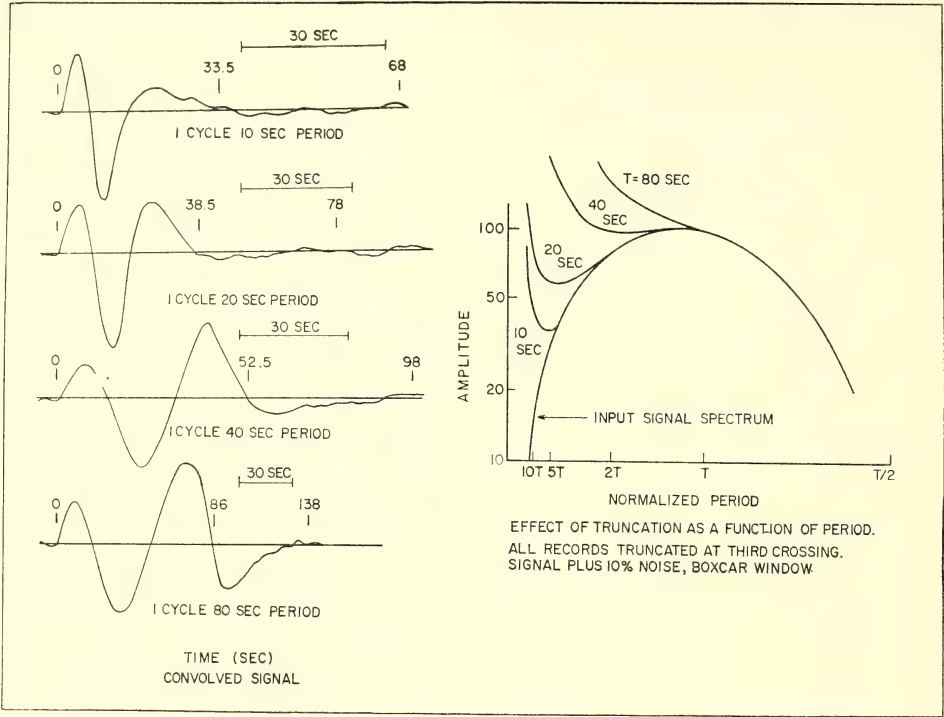


Fig. 51. Effect of truncation as a function of period. A boxcar is used to truncate all records (which include noise) of the third zero crossing of the signal.

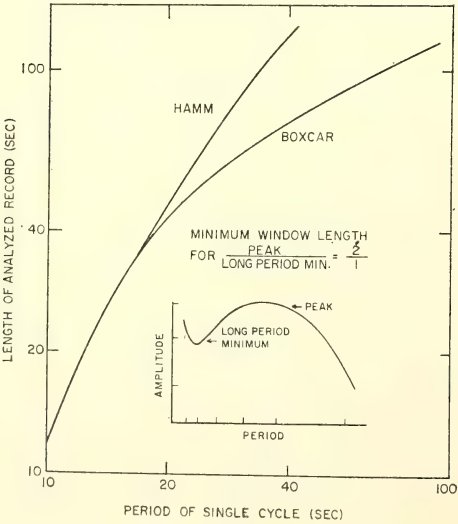


Fig. 52. Window length required to show the existence of a peak in the spectrum as a function of period of the input single cycle.

maximum of the input spectrum occurs. The window length has to be approximately twice the dominant period in order for this requirement to be met. For the long-period end of the spectrum, the time-domain distortion caused by the Hamming window outweighs the advantages resulting from the small side lobes of its transform. In general, for analysis of long periods, such smoothing windows should be avoided since they require excessive window lengths.

The reason that the Hamming window is such a disadvantage is obvious when we consider the cause of the long-period spurious effect. The instrument has no zero frequency response and, therefore, any incident signal must give net zero area under the appropriate duration of the record curve. Noise and truncation destroy this property and introduce an

added contribution to the spectrum with amplitudes increasing with increasing period.

Simple removal of a mean before analysis will not eliminate the error. This can affect only the zero frequency term if the transform includes only the section of the signal under consideration. However, with the use of the fast Fourier transform it is convenient to transform  $2^n$  points, and the usual procedure adopted is to add zeros to the data so that the required number of points can be transformed. Under these conditions (which applied in the examples shown) removal of a mean from the signal section may decrease the very rapidly rising portion of the spectrum at very long period. Removal of both mean and slope from the signal section can result in severe distortion of the whole spectrum. Figure 53 shows the result of this procedure when the input signal is a half-

cycle sinusoid. Removal of a pseudo-slope results in a false peak in the spectrum.

Thus, if a pseudo-slope is not removed, the effect of truncation and noise in the record is to increase spuriously the amplitudes of the longer periods when a Fourier transform is performed. If large instrument corrections have to be applied at these periods, they may then dominate the spectrum. It is often not possible to isolate the complete signal. In that case, a signal whose actual amplitude spectrum decreases as period increases may, on analysis, appear to have a constant amplitude for the longer periods; one-sided pulses, which do have constant amplitude at long periods, will appear to have these amplitudes increasing with the period.

#### *Techniques for Minimizing the Long-Period Error*

Once the problem of long-period spectral distortion is appreciated, there are a number of techniques available which may help to reduce the errors to acceptable levels.

Obviously, the use of a sufficiently long window will yield a spectrum correct except for noise effects. Unfortunately, later arrivals frequently prevent this. It is appropriate to note here two points which are important in routine analysis. It is inviting error to attempt to determine the baseline from a relatively short section of signal; as standard practice we determine the baseline by considering a digitized section of the record which is long compared with the signal duration. Further, with the use of long windows, or indeed whenever Fourier analysis is performed on real data in the presence of noise, the resulting spectrum should not be interpreted until its relation to the noise spectrum is known. Our experience has shown that it is not possible to examine a record visually to determine whether an acceptable signal-to-noise ratio exists, ex-

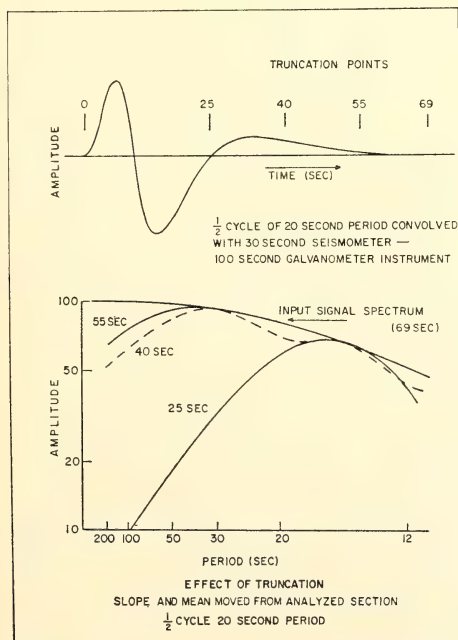


Fig. 53. Effect of truncation (boxcar window) on the record resulting from a 20-second period half-cycle sinusoid after removal of a mean and linear trend from the analyzed section.



cept perhaps at the dominant frequency of the signal. As standard practice we analyze a noise sample immediately before the arrival (with the same window as used for the signal if possible) and then compare signal and noise amplitudes throughout the spectrum.

By staying in the time domain the difficulties associated with the transform are avoided. It is possible to make an estimate of the character of the incident signal spectrum by examining the duration and relative amplitudes of the various half-cycles in the record, and comparing this with records generated from known input signals. The time domain records shown in Fig. 51 illustrate these variations for a range of input single sinusoids. Our results from analysis of earthquakes (presented below) show that, for the long-period spectrum, a single cycle is a reasonable approximation to a seismic body wave. Also Bollinger (1970),<sup>114</sup> in a study of a Japanese earthquake, determined from the ratio of amplitudes of the first peak to the first trough and from the duration of the first half cycle that only a two-sided pulse could satisfy the data.

The long-period errors in the spectrum

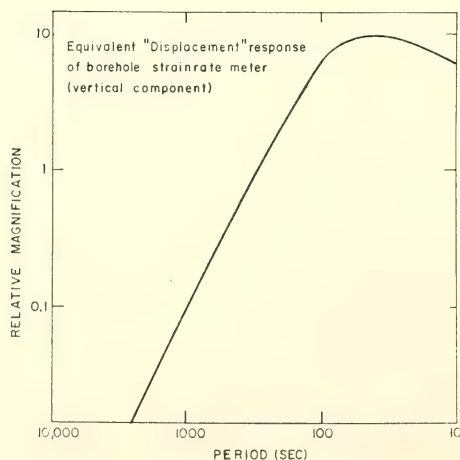


Fig. 54. Equivalent "displacement" response of the borehole strainrate meter (vertical component).

are decreased if small instrument corrections have to be applied at these periods. Sacks and Evertson (*Year Book 68*, pp. 448–452) have developed high gain, long-period borehole strainmeters with an equivalent displacement response as shown in Fig. 54. This response curve is flat to within a factor of less than 2 in the period range of interest, 10 to 100 seconds, with its peak at 50 seconds. The very long-period slope is less than that of standard seismometers. Analysis of signals recorded on these instruments leads to a more reliable long-period determination.

The technique we have used most frequently is to examine magnetic tape playbacks of events recorded on broadband seismometers. By appropriate analogue filtering it is possible to band-pass a narrow range of frequencies and hence determine the spectral content of the arrival by successive filtering at different pass bands. Figure 55 shows the results of such filtering on a deep South American earthquake, magnitude 6.5, recorded at DTM. The top trace is for a filter setting at 75 seconds, yielding a system response that peaks at about 60 seconds; the next two traces are for filter settings at 37.5s and 19s, with the unfiltered trace below these. The upper trace indicates that the amplitudes are decreasing for periods longer than about 40s in the case of the *S* wave. Similarly the *P* wave spectrum must decrease for periods longer than about 30s. The results of Fourier analysis, applying box-car windows as shown, are in agreement with the filtered results, provided a sufficiently long window is used. Analyses of this event at other stations differing greatly in distance and azimuth yield essentially the same values for the spectral peaks. These spectra illustrate the relevance of the model study.

An awareness of the problems involved shows that caution must be exercised if reliable long-period analysis is required. Unfortunately, in practice,

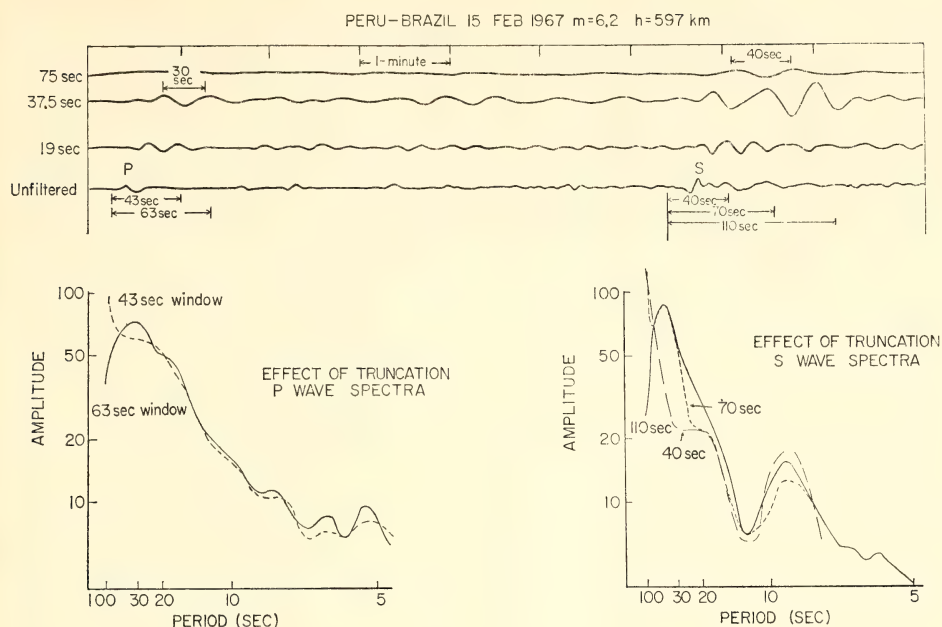


Fig. 55. Time and frequency domain records of a South American deep earthquake recorded at DTM.

there are conditions that make large errors inevitable and these situations must be recognized and avoided. However, when conditions are more favorable, we believe that our techniques result in a reliable determination of the long-period spectrum.

#### EARTHQUAKE BODY WAVE RADIATION AND SOURCE DIMENSIONS

*A. T. Linde and I. S. Sacks*

##### *Theories*

Several different theories of earthquake radiation have been proposed in the literature. Theories based on a system of point forces distributed as double couples over a fault plane (e.g., Ben-Menahem, 1961,<sup>115</sup> 1962<sup>116</sup>) and those based on a distribution of point dislocations over a fault plane (e.g., Haskell, 1964,<sup>117</sup> 1966;<sup>118</sup> Aki, 1967;<sup>119</sup> Savage, 1966<sup>120</sup>) are equivalent, as has been shown by Maruyama (1963).<sup>121</sup> These theories consider the rupture as a propa-

gating process and lead to radiated spectra, which, at frequencies lower than a value dependent on the fault length, exhibit the same characteristic—a displacement amplitude spectrum that is constant. In the following, this limiting frequency will be used as the demarcation between high and low frequencies. At high frequencies there are differences between various models, depending on whether or not the rupture process is uniform. Coherent models display an interference effect with minima in their spectra at periods that are a function of fault length, rupture velocity, and azimuth of the observing station from the fault. In incoherent models these interference effects are smeared out.

A theory due to Archambeau (1968)<sup>122</sup> predicts a different type of radiated spectrum in that the displacement amplitude rises to a peak and then falls to smaller values as the period increases. This theory considers the earthquake as a relaxation source and analytically

solves the phenomenon as an initial value problem. Because of the complexity of the mathematics only a very simple model, an expanding spherical rupture zone in a shear field, is discussed. Consequently, the high frequency portion of the spectrum is smooth, but the author points out that a consideration of more realistic nonsymmetric models would produce structure in the high frequency spectrum. This would be comparable to the interference effects produced by the propagating models discussed above.

There are numerous examples of applications of the theories based on point forces or dislocations distributed over a fault plane. The interference effects have been used (Ben-Menahem and Toksöz, 1962,<sup>123</sup> 1963a,<sup>124</sup> 1963b;<sup>125</sup> Khattri, 1969<sup>126</sup>) to estimate fault length and rupture velocity. The results for surface event dimensions are in reasonable agreement with the values obtained by independent means. The predictions of these theories as to the behavior of high frequencies are therefore supported by the observations. This is not incompatible with Archambeau's theory; the conflict occurs in the long-period portion of the spectrum. Aki (1966)<sup>127</sup> introduced the moment of the equivalent double couple as a quantity which can be calculated in terms of these theories. The moment is shown to be related to the fault plane area and the displacement across the fault. Berckhemer and Jacob (1968),<sup>128</sup> Wyss and Brune (1968),<sup>129</sup> and Wyss (1970)<sup>130</sup> have obtained stress estimates by combining moment and energy determination. However, as pointed out by Archambeau, the moment is defined by the zero frequency or static component of the field, and the determinations made are based on an extrapolation assuming that the amplitude of the long-period displacement spectrum is constant as predicted by the theory. Since their experimental results appear to agree with theory, the extrapo-

lation is seemingly valid. If, however, Archambeau's theory is correct, the estimates obtained by this technique will be seriously in error. The results obtained from body wave spectra have been based on only 40 to 50 seconds of the wave train because of interference by later arrivals, and, on standard long-period seismometers, this must result in some truncation of the signal. As shown above, under conditions like these, the long-period portion of the spectrum is very poorly determined and in general will be overestimated.

#### *Relation between Dominant Period and Source Dimensions*

Our analyses invariably show the existence of a dominant period in the radiated displacement spectrum of body waves. We believe that these results are reliable because we find good agreement by analyzing the same arrival with different techniques and different types of instruments. Further, for the event in Fig. 55, we obtained essentially the same results at stations differing greatly in distance and azimuth.

These results, then, are in good agreement with Archambeau's theory. Therefore, theories that predict a constant amplitude long-period displacement spectrum for body waves must be in error. There is here no indication that for higher frequencies these theories are incorrect, since the error may well be frequency dependent.

Archambeau presents a sample of numerical results graphically. Table 14 illustrates the dependence of the domi-

TABLE 14. Calculated Values of  $T_{\max}$  at  $R_s = 100$  km for  $P$  waves, sec.

$R_s/R_r$	$V_p = 8$ km/s $V_r$ (km/s)			$V_r = 3$ km/s $V_p$ (km/s)	
	2	3	4	6	10
2	37.0	28.6	25.6	34.5	26.3
3	28.6	25.0	23.3	30.3	21.3
4	25.6	23.3	22.2	29.4	19.7
5	23.8	22.2	21.7	28.6	18.5



nant period,  $T_{\max}$ , of the  $P$ -wave spectrum on the parameters involved;  $R_s$ , radius of the volume from which energy is released;  $R_r$ , radius of the rupture volume;  $V_p$ , the wave velocity; and  $V_r$  the rupture velocity. If the velocities and the ratio  $R_s/R_r$  are held constant, then  $T_{\max}$  is directly proportional to  $R_s$ . The table shows that  $T_{\max}$  varies slowly with  $V_r$  and with the ratio  $R_s/R_r$ , provided we consider the energy released from a volume with radius 3 or more times that of the rupture volume. Essentially, then,  $T_{\max}$  depends only on  $V_p$  and  $R_s$  if we take  $R_s/R_r \geq 3$  and, to a good approximation,

$$2 R_s = T_{\max} V_p$$

*Experimental Results*

A set of South American deep earthquakes has been partially analyzed. The importance of a noise analysis is shown in Fig. 56. These spectra, obtained from a Trujillo, Peru, record of the  $S$  arrival from a magnitude 5.5 event, are remarkably similar to those obtained in Washington, D. C., at the DTM station. The variation of dominant period with magnitude is shown in Fig. 57.

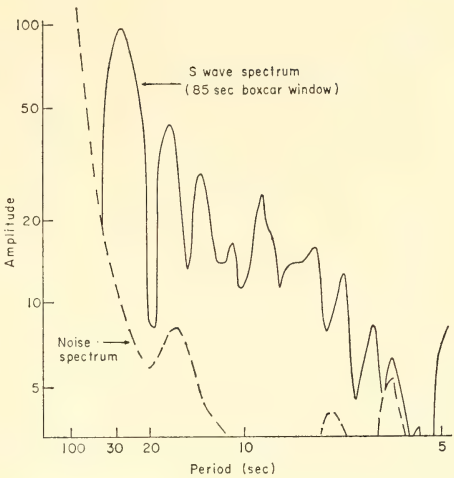


Fig. 56. Signal-to-noise spectral amplitude comparison from the TRU record of the  $S$  arrival from an Argentine deep event of magnitude 5.5.

For  $P$  waves, this dominant period varies from about 1.5 seconds to 30 seconds for magnitudes ranging from 4 to 6. In terms of Archambeau's theory, this indicates release of strain energy from (assumed) spherical volumes with diameters ranging from 15 to 300 km. The dimensions of the actual rupture

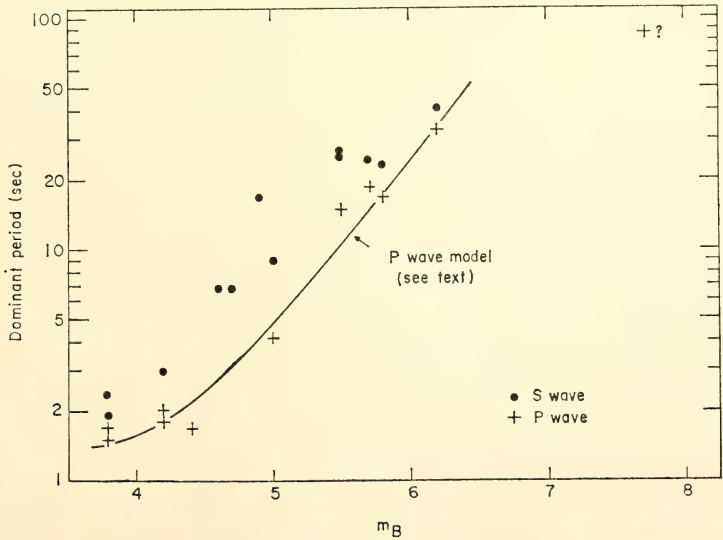


Fig. 57. Variation of dominant period in the radiated spectrum as a function of magnitude.

region, however, are less than these by a factor of at least 3. A linear variation of  $\log T_{\max}$  with  $m_B$  is consistent with these data, but interpretation of a linear variation in terms of simple concepts of strain release and nonradiative energy losses does not seem possible. We have, therefore, attempted to fit the data in terms of the following model.

For deep earthquakes, strain may be released as a result of slip across a zone of localized melting (Griggs and Baker, 1968).<sup>131</sup> If this is so, it appears reasonable to assume that the stress drop is complete and that the energy lost in nonradiative processes is that required to melt a thin disk. Then, if stress conditions are the same for all events (different magnitudes corresponding simply to different volumes of energy release), we expect

$$m_B \propto \log \left( T^3 \left\{ 1 - \frac{T_0}{T} \right\} \right)$$

where  $T_0$  is the period corresponding to an earthquake of minimum dimensions. For South American deep events, 3.5 is a lower limit to observed magnitudes and thus we have chosen  $T_0 = 1.4$  sec. This leads to the curve shown as a fit of this model to  $P$ -wave results.

The peak period determined for the event of magnitude 7.7 obviously does not lie on this curve (nor does it lie near the best linear fit to the remainder of the data). Because the event was so energetic and only records from World Wide Standard Seismic Network stations have been available to us thus far, analysis of a phase which has been sufficiently attenuated to allow digitization was necessary. The phase used was *PKPPKPPKPPK* and the signal-to-noise ratio was not good because of the background of free oscillations. Thus this determination was not reliable. We hope to find a more suitable recording in order to improve the reliability of this determination. However, it is difficult to imagine that, in terms of Archambeau's theory, the peak period could be

much longer; this would require release of energy from an unrealistically large volume. Instead, we suggest that for large deep events (which occur infrequently) the stress release is greater than that for smaller events.

It would be possible to determine quantities such as stress drop by using these results in conjunction with an empirical relation between magnitude and radiated energy of the type

$$\log E = A + B \cdot m$$

where  $A$  and  $B$  are constants. However, it is well known that such energy determinations are very approximate. Therefore, we intend to estimate the radiated energy by integrating over the recorded signals and correcting for the ray path. It should then be possible to estimate the stress conditions with some reliability.

## PSEUDODISPERSION IN BODY WAVES

*Shigeji Suyehiro*

The phenomenon of high-frequency energy arriving later than low-frequency energy was studied and reported for earthquakes in South America by I. S. Sacks, *Year Book* 64, pp. 282-285. The same behavior was recognized for earthquakes in Japan which were recorded on the DTM broad-band seismograph at Urakawa, Hokkaido. The aftershocks of the Tokachi earthquake of May, 1968, off the Pacific coast of northeast Japan were used to study the attenuation and time delay of high-frequency energy of  $P$  and  $S$  waves in relation to epicentral distance, focal depth, magnitude, and geographical location.

## Method of Analysis

To read arrival times and compare energy contents of different frequencies, short- and long-period channels were replayed through a set of bandpass filters. The filters have an attenuation of -24 db/octave outside the pass-band. Fre-

quencies, recording channel, and corresponding filter settings are as follows:

Trace (1) 6 hz or higher: Short-period channels with  $F_L=6$  hz and  $F_H=open$

Trace (2) 2-4 hz: Short-period channels with  $F_L=open$  and  $F_H=3$  hz

Trace (3) 1-2 hz: Short-period channels with  $F_L=open$  and  $F_H=3$  hz

Trace (4) 0.5 hz or lower: Long-period channels with  $F_L=open$  and  $F_H=1$  hz

Trace (5) high frequency in general: Short-period channels with no filter.

( $F_L$ : low-cut frequency,  $F_H$ : high-cut frequency)

Arrival times of different frequencies for  $P$  and  $S$  waves were read. The spectral energy content of the  $S$  waves was estimated from the mean amplitude of the wave train for a 3- to 5-second time interval after the onset of  $S$ .

### *Pseudodispersion in P and S*

Figure 58 shows an example of almost simultaneous arrival of low and high frequencies both in  $P$  and  $S$  from a

nearby earthquake of normal depth. Figure 59 shows an example of delayed arrival of high-frequency waves both for  $P$  and  $S$  from a more distant earthquake. Note that in Figure 59 the direction of first motion is compressional as seen on the LPH-V channel, whereas it is dilatational on the SPH-V channel. Delay times of more than 0.5 sec in  $P$  arrival between the traces (2) and (4) or (5) are plotted vs. epicentral distance in Figure 60. The signal-to-noise ratio of lower frequencies depends on the magnitude of earthquakes, and seemingly also on focal depth. Consequently, the scatter is fairly large. Nevertheless, the tendency of the delay time to increase with epicentral distance is clearly seen. The solid line is an approximate fit through the  $P$  wave delay times, and the broken line shows the expected delay times for  $S$ , assuming the  $S$  velocity to be  $\frac{3}{5}$  that of  $P$ . As expected, the scatter for  $S$  delay times is much larger than for  $P$ . It is obvious, however, that the

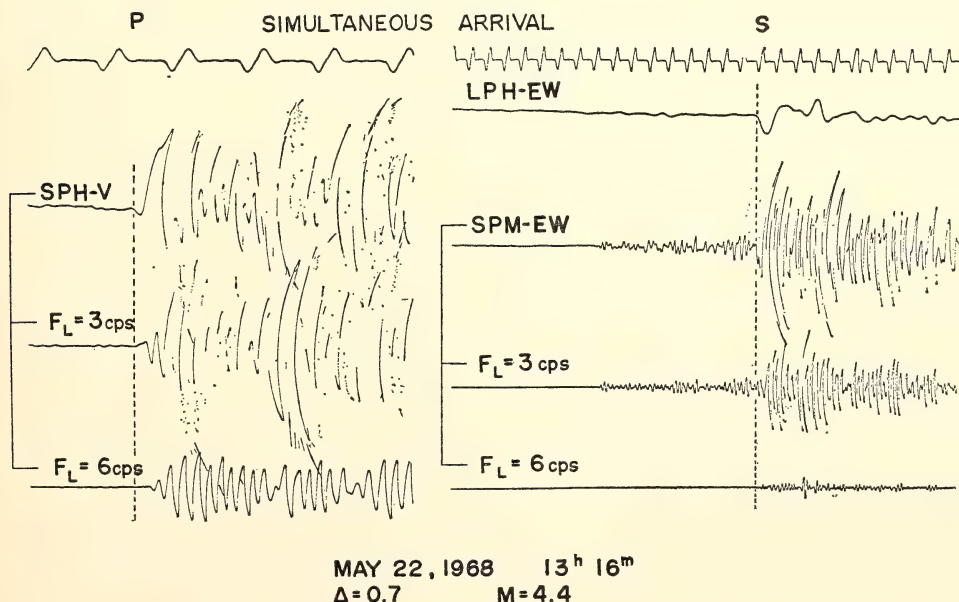


Fig. 58. Example of simultaneous arrival of high and low frequencies from a nearby earthquake. Time marks: seconds;  $F_L$ : low-cut frequency.



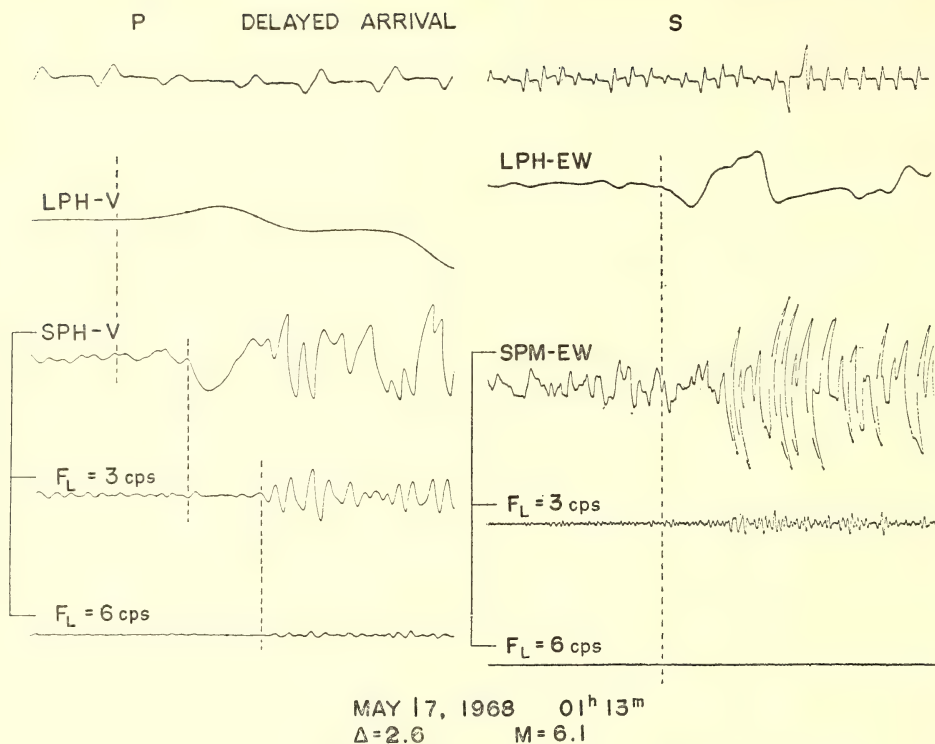


Fig. 59. Example of delayed arrival of high frequency from a more distant earthquake.

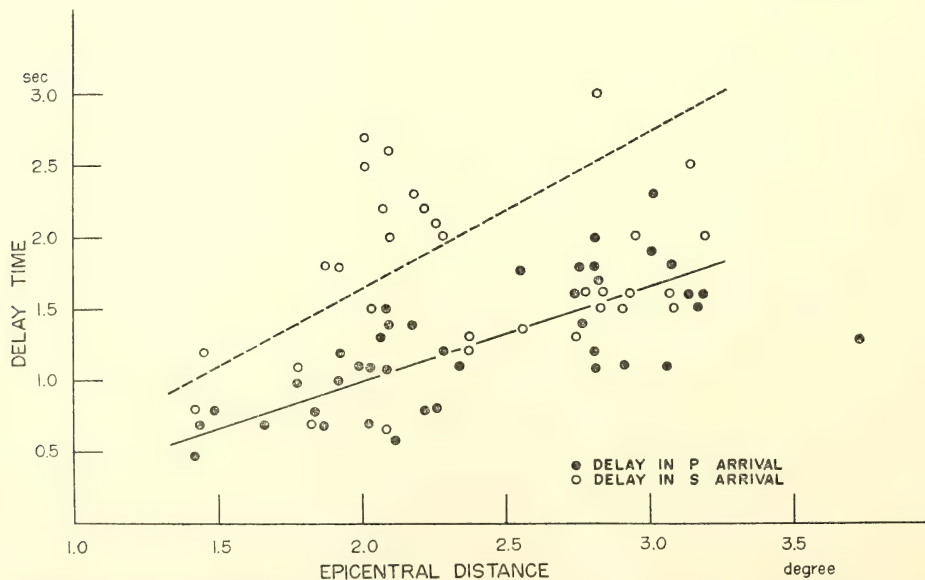


Fig. 60. Delay time of high frequency in *P* and *S* arrivals vs. epicentral distance. The solid line shows the mean delay time for *P* waves, and the broken line shows the expected delay time for *S* waves.

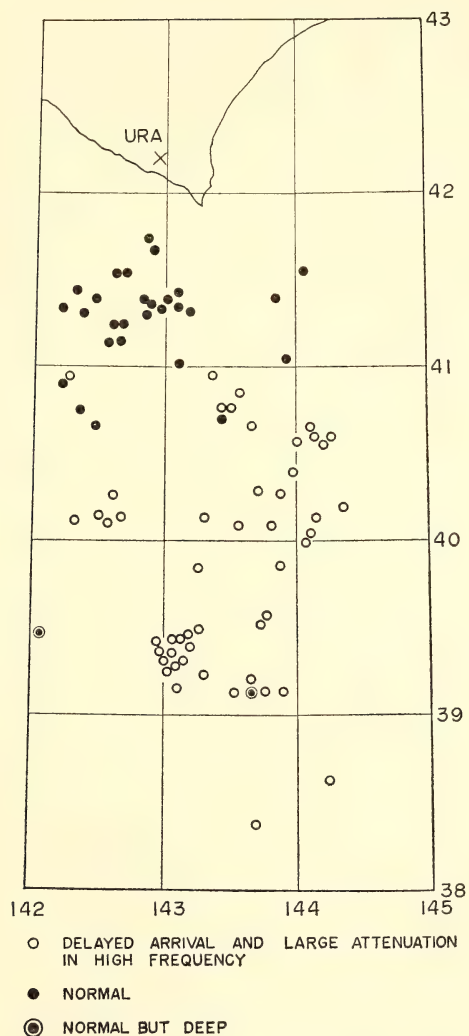


Fig. 61. Epicenters of the Tokachi aftershocks that were studied. Solid circles show earthquakes that gave no delay or a very small delay, and open circles show earthquakes that gave delay times greater than 0.5 sec.

delay times for  $S$  are greater than for  $P$  and become even larger with increasing epicentral distance. In Figure 61, epicenters of earthquakes that gave delay times of less than 0.5 sec in high-frequency for  $P$  are shown by solid circles; those that gave delay times of more than 0.5 sec are indicated by open circles. As inferred from Figures 60 and 61, the delay time associated with the Tokachi aftershocks depends primarily on distance from the station. There are two earthquakes, however, that are distant and should therefore show delays but do not. These earthquakes are 70 km or more in depth (the deepest in the group), suggesting that only earthquakes at shallower depths show time delays of high-frequency energy.

#### *Attenuation of High Frequency*

Earthquakes that gave delayed arrivals of high-frequency energy also showed a large attenuation of high-frequency energy. The attenuation contrast between near and distant earthquakes is readily seen by comparing Figures 58 and 59. In Figure 62 the ratio of the mean  $S$  amplitude of trace (1) (high

frequency) to trace (3) (low frequency) is plotted against epicentral distance. The  $Q$  of the high-frequency energy (about 6 hz) is estimated from the mean attenuation with distance, shown in Figure 62 to be about 330. Again, the distant but deep earthquakes indicated by open circles in Figure 62 show much smaller attenuation.

#### *Earthquakes before the Main Shock and in Other Regions*

Earthquakes within 4 degrees in epicentral distance from Urakawa before the Tokachi main shock of May 1968 were examined, using the same technique. Those regions that showed pseudodispersion and large attenuation of high-frequency energy for the Tokachi aftershocks also exhibited these phenomena for earthquakes prior to the main shocks.

Pseudodispersion and high attenuation, however, could not be found even for distant shallow earthquakes in other regions. In Figure 63 epicenters of earthquakes with and without these effects are shown.

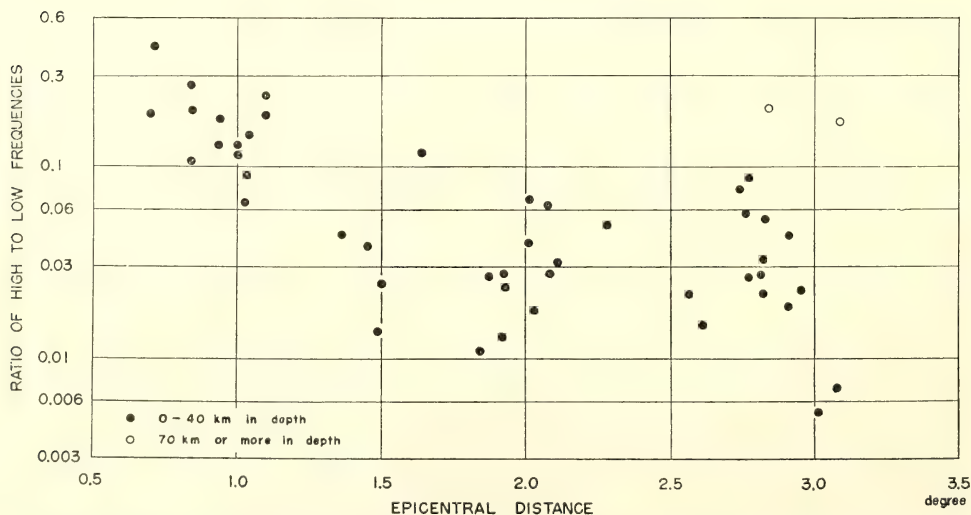


Fig. 62. Ratio of mean  $S$  amplitude of trace 1 (high frequency) to trace 3 (low frequency) and epicentral distance.



### Discussion

(1) When there is a time delay for high-frequency  $P$ -wave energy, there is also a somewhat greater delay for high-frequency  $S$  waves. (2) The delay times become larger with increasing epicentral distance. (3) Earthquakes that exhibit time delays range in depth from 0 to 40 km, whereas the depth to the  $M$ -discontinuity in that region is estimated from explosion observations to be about 20 km. Hence, earthquakes both above and below the  $M$ -discontinuity show this effect. These observational facts imply that there exists an unusual region probably containing scatterers that cause time delays of the high-frequency energy. The fact that two distant but deep earthquakes showed no such effect indicates that the region of unusual scatter lies only in the crust and uppermost part of the mantle.

$P$ - and  $S$ -wave arrivals for which pseudodispersion was observed also exhibited large attenuation of high-frequency energy. That region producing time delays, therefore, must also be a region of large attenuation for high-frequency energy. This region appears to exist only off the Pacific coast of Northeast Japan and is confined to the area indicated by the broken line in Figure 63.

The preceding seismological studies would not have been possible without the cooperation and assistance of the following:

Drs. Utsu and Motoya of Hokkaido University; Dr. Suyehiro and the Japan Meteorological Agency, Tokyo, Japan; Dr. Denham and the Geophysical Observatory, Port Moresby, New Guinea; Dr. Rodriguez and Ing. Simoni at Characato Geophysical Observatory, Arequipa, Peru; Ing. Chadwick and Universidad del Norte, Antofagasta, Chile.

The development and installation of the broad-band magnetic tape seismo-

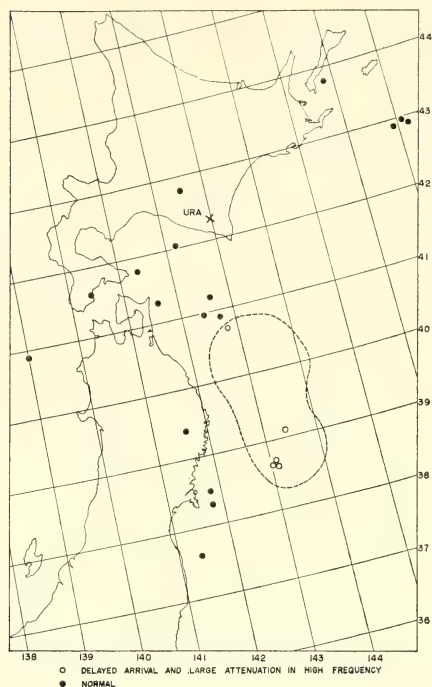


Fig. 63. Epicenters of earthquakes before the main shock and in other regions which were similarly studied. Open circles show delayed arrival and large attenuation of high frequencies, and solid circles show normal arrivals. The Tokachi aftershocks, which occurred in the area indicated by the broken line, exhibited the pseudodispersion and large attenuation of high frequency energy.

graphs were supported in part by a grant from the National Science Foundation.

### ANDEAN CRUSTAL STRUCTURE

*D. E. James*

The surface wave phase velocity studies reported here are part of a long-term study of the earth beneath the Andes Mountains of South America. The location of the stations used in the determination of phase velocities is shown in Fig. 64; the lines between stations indicate the station pairs used in determining either Rayleigh or Love wave velocities. A summary of the station coordinates and elevations is given

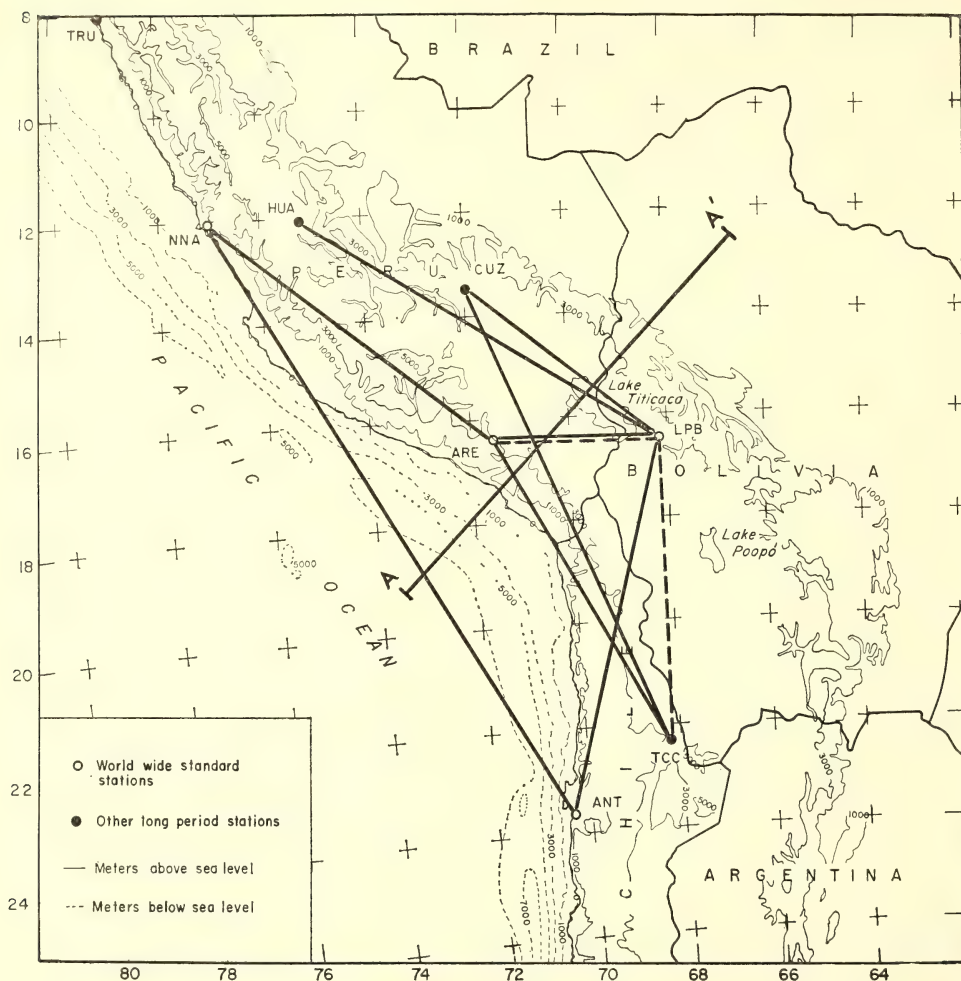


Fig. 64. Station location map. Solid lines indicate Rayleigh wave paths, and dashed lines denote Love wave paths.

TABLE 15. Station Data

Station	Latitude	Longitude	Elevation, m	Location
ANT	-23.699	-70.415	5	Antofagasta, Chile
ARE	-16.462	-71.491	2452	Characato, Peru
CUS	-13.563	-71.877	3240	Cuzco, Peru
HUA	-12.038	-75.323	3313	Huancayo, Peru
LPB	-16.533	-68.098	3292	La Paz, Bolivia
NNA	-11.988	-76.842	575	Naña, Peru
TCC	-22.275	-68.172	3300	Toconce, Chile
TRU	-8.078	-78.861	280	Trujillo, Peru

in Table 15. Distances, azimuths (angle east of north, station 1→station 2), and back bearings (angle east of north, station 2→station 1) between station pairs for which phase velocities were determined are given in Table 16.

Epicentral data of the earthquakes used to determine phase velocities are given in Table 17. In all instances, the deviation of the great circle propagation path from the great circle path connecting the station pairs is less than 3½ degrees. Distances and azimuths have been computed using the formulas developed by Thomas which incorporate both first- and second-order ellipticity corrections.

Previous studies of crustal structure beneath the Andes were performed by Tatel and Tuve and their co-workers. The first reported results were presented in *Year Book 57* (1958). Comparatively good results to distances of 500 km were obtained along the western flanks of the western cordillera in both Peru and Chile, but no records of arrivals of any kind were obtained beyond about 200 km in directions crossing the cordillera and altiplano. The failure to observe arrivals was attributed to extreme crustal attenuation. The data collected in these experiments were re-examined and reinterpreted by Woollard (1960),<sup>132</sup> making greater use of secondary arrivals. The principal features of Woollard's highly speculative summary of the Carnegie explosion results include a crustal thickness beneath the cordillera of about 65 km and a steep dip in the M-discon-

TABLE 16. Station Data

Station Pair	Dist. (km)	Azimuth (Stat. 1 → Stat. 2)	Back- bearing (Stat. 2 → Stat. 1)
ARE → NNA	760.5	309.9	131.2
LPB → ARE	362.3	270.8	91.7
LPB → CUS	522.5	308.5	129.4
LPB → HUA	924.5	301.6	123.4
LPB → TCC	635.6	180.7	0.7
TCC → ARE	731.7	331.0	152.1
TCC → CUS	1040.8	337.2	158.4

TABLE 17. Epicenter and Azimuth Data

Date	Time of Origin, GMT	Lat.	Long.	Depth, km	Mag.	Stat. Pair	Stat. 1		Stat. 2	
							Dist.	Az.	Dist.	Az.
3/20/66	01:42:49.9	06°N	30.2°E	24	6.2-7.25	LPB → ARE	109220.	91.9	11234.2	92.9
9/9/66	18:39:57.8	10.8°N	69.5°W	8	5.0-5.6	LPB → TCC	3026.3	357.0	3661.1	357.6
9/14/66	23:18:40.8	60.2°S	27.2°W	22	6.3-6.75	TCC → CUS	5280.	153.6	6318	155.2
9/15/66	11:51:56.4	60.2°S	26.8°W	33	5.6-6.5	TCC → ARE	5295.4	153.5	6027.1	154.4
4/19/68	09:04:27.3	42.6°S	16.0°W	33	5.6	LPB → CUS	5700.9	131.7	6222.6	132.5
						ARE → NNA	5977.8	131.1	6738.2	132.3
9/29/69	20:03:32.8	32.9°S	19.7°E	N	5.9-6.3	LPB → HUA	8831.9	121.3	9756.3	123.1



tinuity ( $\sim 18^\circ$  slope) from west to east beneath the flanks of the western cordillera. As will be shown below, the results from surface wave phase-velocity measurements confirm to a surprising degree the model proposed by Woollard.

Another explosion expedition supported in part by the Harry Oscar Wood Fund was undertaken during the summer of 1968 by the Carnegie Institution and collaborators from both South America and North America. The study was centered in the region of the altiplano of Bolivia and southern Peru and was chiefly intended as a reconnaissance experiment to determine the requirements of future explosion experiments in that region. The preliminary and rather fragmentary results are presented in *Year Book 68*, p. 459.

*Regional geology.* More than for most areas, the regional geology of the Andean region has direct bearing upon interpretations of crustal structure. The Andes of southern Peru and Bolivia consists of three major parts: the cordillera (eastern cordillera), the altiplano, and the cordillera occidental (western cordillera). The eastern and western cordilleras merge both to the north and to the south of the altiplano. A complete description of the geology within the area of study is given by Morrison (1970),<sup>133</sup> and his work forms the basis of the summary given below. A complete set of references is also supplied by Morrison.

The results reported in this paper pertain primarily to the eastern and western cordilleras and to the high plateau region lying between these mountain belts. The plateau within the region of study is termed the altiplano, although in the southern part of the area (northern Chile and Argentina) it is termed the Puna de Atacama. I shall refer to the entire region as the altiplano.

The geology of this part of South America is not well known. In particular, the geology of the two cordilleran belts is almost unknown. Beneath the alti-

plano, the geology is better known, and it appears that at least 20 km of post-Devonian sedimentary rocks have accumulated in the Lake Titicaca region. In southern and central Bolivia, the lower paleozoic sections (Devonian and earlier) are exposed and aggregate at least 10 km. If this lower paleozoic section also exists in the Lake Titicaca region (where only post-Devonian rocks are exposed), the total thickness of sedimentary rocks beneath the altiplano may total 30 km. This enormous thickness of sedimentary rocks may be a primary cause of the high seismic attenuation that has been observed.

### *Reduction and Interpretation of Data*

The techniques used in the analysis of data are similar to those developed at the Southwest Center for Advanced Studies by Dziewonski, *et al.*, 1969<sup>134</sup> and by Block and Hales, 1968,<sup>135</sup> and are summarized briefly below. The reader is referred to the original papers for a detailed description of the techniques. A very generalized flow chart of the procedures followed is shown in Fig. 65.

The Carnegie magnetic tape station data were digitized at a nominal value of 1 pt./sec and the analog paper records at about 0.5 pts./sec. The data were interpolated to yield a digitizing rate of exactly 1 pt./sec. Both a 60-point sinc ( $\sin x/x$ ) interpolation (see Bracewell, 1965)<sup>113</sup> and a 4-point cubic interpolation were tried. Both of these interpolation routines yielded identical final results, and for most of the work I used a cubic interpolation.

Group velocities were determined by multiple filtering of the digitized records (see Dziewonski, *et al.*, 1969). Multiple filtering produces a display of instantaneous spectral amplitude and phase as a function of time and period. In brief, the method may be described as follows: The digitized seismic record is Fourier analyzed, windowed, and then filtered in the frequency domain at specified

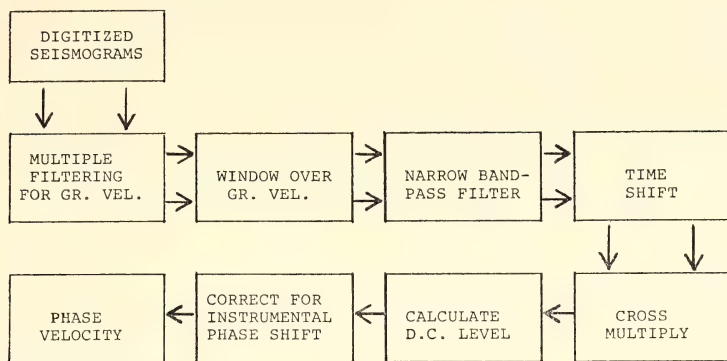


Fig. 65. Simplified flow diagram for phase velocity measurement technique used in this paper.

periods. The filter is a zero phase-shift Gaussian function that provides near optimum resolution. The filtered signal is inverse-transformed and the instantaneous amplitudes and phases graphically displayed.

The phase velocities between a given station pair are computed by the method of cross-multiplication described by Block and Hales (1968). This technique is as follows: The group velocity dispersion diagrams are used to determine the range of periods over which phase velocity measurements may be meaningful. The two seismograms are windowed with a  $\cos^2$  window of length five times the period and centered on the group velocity at the period of interest. The windowed seismograms are filtered with a very narrow bandpass filter and time-shifted and cross-multiplied for a specified range of phase velocities. As shown by Block and Hales, if two seismograms are bandpass filtered at a frequency,  $\omega$ , they may be described as  $A \cos \omega t$  and  $B \cos (\omega t + \phi)$ ; where  $\phi$  is the phase difference between the seismograms at frequency,  $\omega$ . The product seismogram is given as  $AB/2 [\cos (\omega t + \phi) + \cos \phi]$ , where the D. C. term,  $\cos \phi$ , is a maximum when  $\phi$  is zero. The D. C. levels are computed for specified periods over a given range of phase velocities and normalized values are displayed vs. period and phase velocity.

Because the South American long-period stations are not generally matched, a phase correction is applied and corrected phase velocities are obtained. The procedures for obtaining instrumental phase delays are discussed in the next section.

#### *Instrumental Phase Delay*

For any phase velocity study in a region where the stations are not widely separated, it is essential to know precisely the instrumental phase delay, even for station pairs for which the instruments are nominally matched. The phase delays for the DTM magnetic tape stations were measured experimentally to a precision of  $\pm 0.01$  radians in the period range 20–120 sec. At periods less than 20 sec, the precision is on the order of  $\pm 0.05$  radians. As the system employs no galvanometer, I believe the phase delay to be comparatively stable with time.

For WWSSN stations, I found that significant phase drift occurred, and phase delays were computed for the days of interest by digitizing and Fourier-analyzing the calibration pulses on the records. Unfortunately, the calibration pulses are put on the record at the same time every day and thus yield no information as to diurnal drift. In addition, the precise time of the calibration pulse

break is difficult to determine on noisy days, and any timing errors of this nature will result in a constant time shift of the phase delay curve. I believe this error is, for the most part, small, probably less than 1 or 2 seconds.

### *Inversion*

Trial and error have been used in this study for the derivation of structural models; for the available data, this technique has proved satisfactory in obtaining adequate agreement between theoretical and observed curves.

As emphasized by Block and Hales (1968), group and phase velocity determination of fundamental and higher modes for both Rayleigh and Love are necessary to deduce reliable velocity models. In the absence of such complete data, however, one is obliged to seek the most reasonable class of models from the many that can be generated. For this reason, I have employed a number of rather subjective constraints on model parameters.

Initial trial models were designed to agree as closely as possible with the models based on explosion experiments discussed in the previous section. All models have been simplified as far as possible, in the belief that the data do not justify additional complexity. Although the models presented are by no means unique, they are reliable indicators of variability within the region of a study. Whereas individual layer parameters can change significantly, the crustal thickness, mean crustal velocity, and uppermost mantle velocities appear to change very little for most reasonable layer velocity assumptions.

As the Rayleigh wave inversion is insensitive to *P*-wave velocities and comparatively insensitive to density, both these parameters are constrained to follow shear velocity. A variable Poisson's ratio was assumed in determining com-

TABLE 18. Poisson's Ratio for Different Rock Types

Rock Type	Compressional Velocity Range	Poisson's Ratio
Granitic (sed.)	5.0-6.4	0.25
Gabbroic	6.5-7.2	0.283
Ultramafic	7.8-8.5	0.262

pressional velocities. The values of Poisson's ratio for granitic (sedimentary in the case of lower velocities), gabbroic, and ultramafic rock types were calculated from laboratory velocity measurements tabulated by Press (1966).<sup>136</sup> The Poisson's ratios are given in Table 18. Densities for crustal rocks are taken from the Nafe-Drake curve. For mantle (and probably lower crustal) rocks the Nafe-Drake velocity-density relationship is not applicable, as it does not incorporate thermal coefficients. Compressional and shear velocity as a function of temperature for the Twin Sisters dunite is shown in Fig. 66. Although the mantle is certainly not wholly dunite, similar curves for ultramafic rocks consisting in part of minerals other than olivine are not available. At 20 kb and a hypothetical 1200°C, the velocities are characteristic of the upper mantle. In the absence of a suitable velocity-density relationship for high temperatures and pressures, I have assumed that the curves shown in Fig. 66 are more or less applicable and have taken the density to be about 3.3 g/cc for a compressional velocity of 8.0 km/sec. Birch (1969, Table 7)<sup>137</sup> shows that at the *P-T* conditions assumed here (20 kb, 1200°C) the density for olivine is nearly the same as the density measured at room temperature and pressure.

The phase velocity curves were computed according to the usual flat earth formulation of Haskell (1953).<sup>138</sup> The earth flattening approximation of Alterman *et al.* (1961)<sup>139</sup> was used to correct



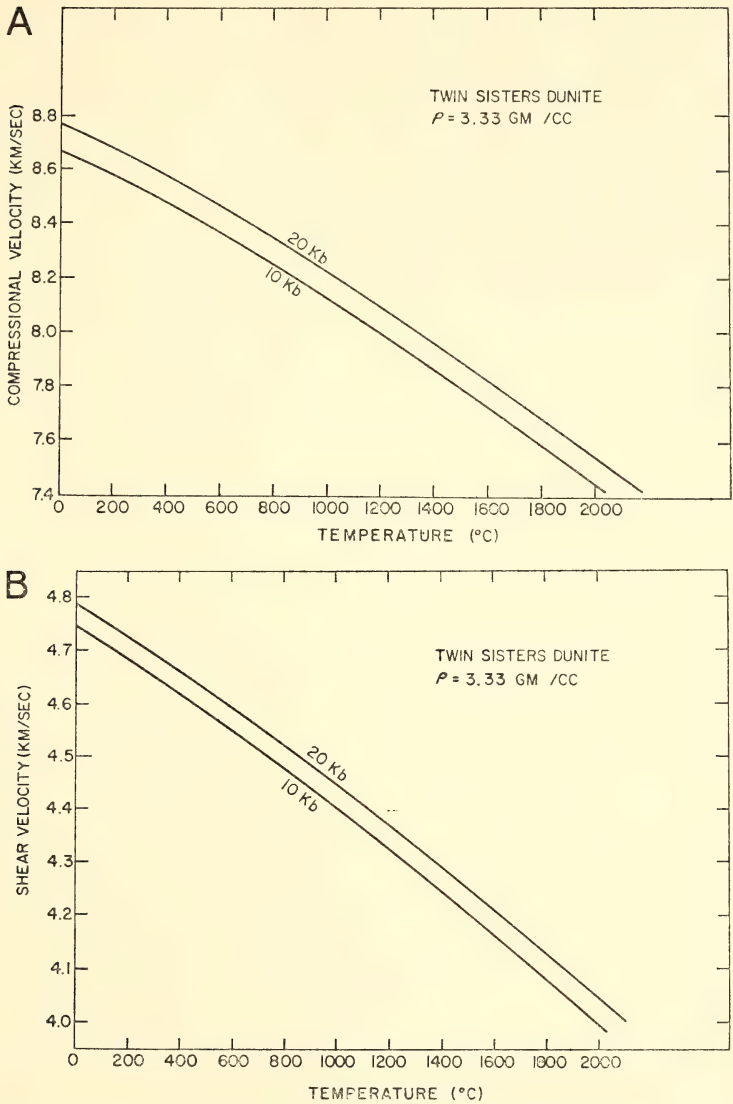


Fig. 66. Compressional and shear wave velocities of Twin Sisters dunite as a function of temperature (A) and pressure (B).

for sphericity of both Rayleigh and Love modes.

*Results and Interpretation*

Station pairs between which phase velocities have been measured are indicated in Fig. 64 by solid (Rayleigh

waves) or dashed (Love waves) lines. Attempts to obtain tripartite solution (e.g., Knopoff, *et al.*, 1966)<sup>140</sup> have not been successful. It appears that the extreme structural variations within the area of study make difficult any assumptions as to the shape of the wavefront incident upon the network. In particular,

we cannot assume that the wavefront is straight when it encounters the vertex of the network closest to the epicenter. I have limited the measurement of phase velocities to those events arriving from directions which appear to exhibit the least amount of refraction (as indicated, for example, by the relative amplitudes of the horizontal components). Along the azimuths of the various station pairs used in this study, all surface waves from earthquakes in the Pacific region show strong refraction at the South American coastline and could not be used in determining phase velocities. This fact severely limits the number of

usable events. Only earthquakes in the hemisphere to the east of the array have been used in this study. In most instances, the great circles are normal to the coastline and at a high angle to the trend of the Andes Mountains. The paucity of events has made it impossible to obtain much redundancy for the individual station pairs.

The phase velocities for the various station pairs are shown in Figs. 67 through 72. The solid line curves have been derived from the model parameters presented in the table on the right-hand part of the figure. The station pair is indicated in the map inset.

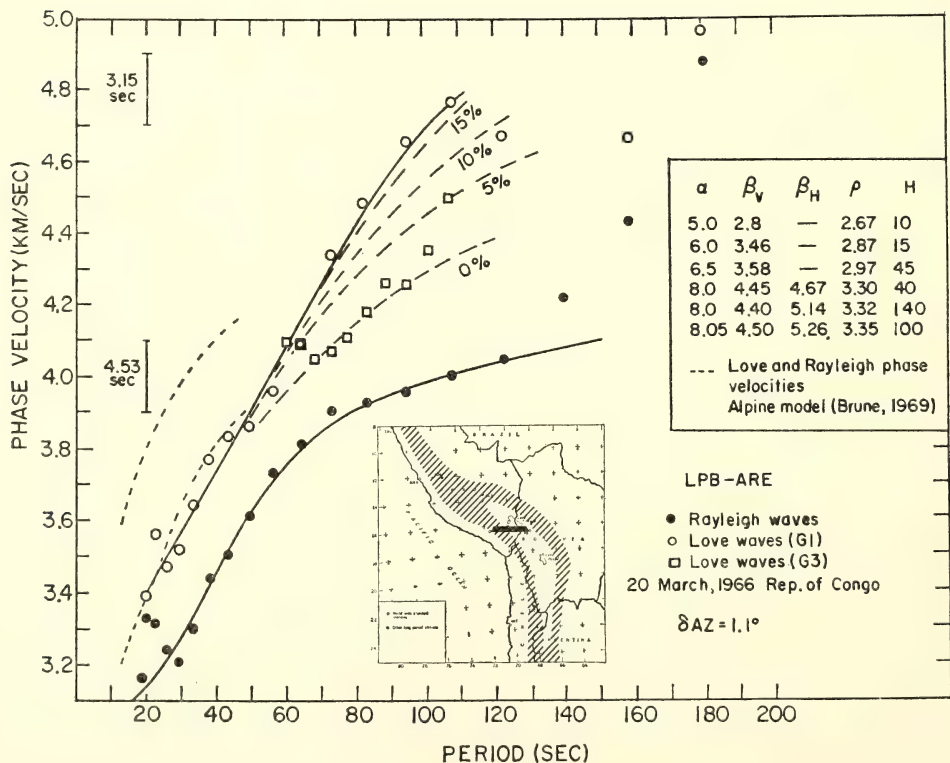


Fig. 67. Rayleigh and Love wave phase velocity computed for R1, G1, and G3. Model parameters which produce the solid curves are given in the table on the right. Dashed lines for Love wave phase velocity denote varying degrees of anisotropy. Except for the zero anisotropy curve, the uppermost mantle layer anisotropy is held to 5%. The 0.2 km/sec vertical bars indicate the velocity uncertainty implied by the time uncertainty printed to the left of the bar. The short dashed lines are Alpine model phase velocities for Love and Rayleigh waves given by Brune (1969).<sup>140</sup>

**LPB-ARE line.** Both Love and Rayleigh waves from the African earthquake of March 20, 1966, are recorded over a wide period range (see Fig. 67). The propagation path is due east-west so that there is complete separation of Love and Rayleigh components. As the NS and EW seismograph components rarely have identical phase responses, the fact that Love waves are present only on the NS component has enhanced the accuracy of the phase velocity measurements over those that could be obtained by rotation of axes. Little significant refraction appears to have occurred, as no Rayleigh waves for periods greater than 40 seconds could be identified by multiple filtering of the NS seismogram and at periods less than 40 seconds the amplitudes were very small. The propagation path is about one-half altiplano and one-half western cordillera.

The most striking aspect of the dispersion curves shown in Fig. 67 is the anomalously high phase velocity of Love waves in the period range 60–110 seconds. The G3 phase velocities shown in the same figure do not show the anom-

alous velocities of the G1 arrivals. This fact has led me to conclude that the G1 phase velocities above 60 second period are due to higher mode interference as proposed by Thatcher and Brune (1969).<sup>141</sup> A complete discussion of the anomalous Love wave velocities is given in a later section of this annual report.

The apparent anomalous behavior of both Love and Rayleigh velocities at periods greater than about 120 seconds is probably due to a poor S/N ratio. As the station separation is only about 360 km, very small errors in phase at long periods become very important. The vertical bars 0.2 km in height are shown on the left-hand side of the illustration, together with the time difference (or error) implied by that velocity contrast. The anomalous Love wave velocities do not extend to periods less than about 60 seconds, and the structure model was derived on the basis of Love wave velocities in the period range to 60 seconds and Rayleigh wave velocities to 120 seconds.

The interpretation of these phase velocities produces a remarkably thick

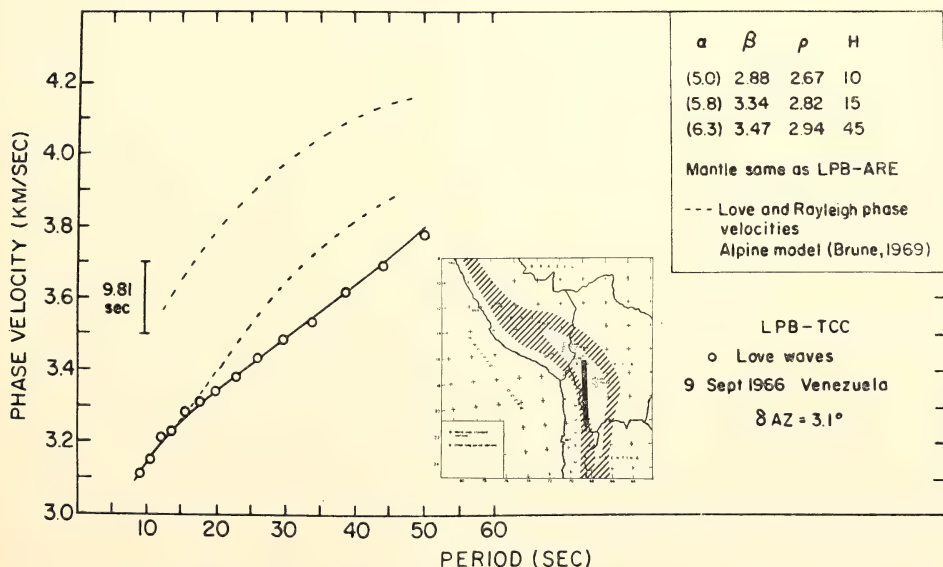


Fig. 68. Phase velocity measurements for Love waves between the LPB-TCC station pair. See legend to Fig. 67 for explanation of other features shown on illustration.



crust of about 70 km thickness and a comparatively low mean crustal velocity. The shear velocity (4.45 km/sec) in the uppermost mantle is comparatively normal for tectonic regions. Of interest is the fact that no significant low velocity channel is required in the upper mantle to a depth of at least 300 km to explain the observed phase velocities. As we shall see, this result holds generally for all profiles in the Andean region. There is a hint of a very minor shear velocity reversal at a depth of slightly more than 100 km, but this is not required to produce an adequate fit to the data.

**LPB-TCC line.** Love wave phase velocities to 50 seconds have been measured along the La Paz-Toconce profile (see Fig. 68). No Rayleigh wave velocities have been measured. The propagation path is almost entirely within the altiplano. The velocities are slightly lower but still very close to those measured along the LPB-ARE line described above. Because the period range covered

does not depend very greatly upon the structure of the mantle, the LPB-ARE model for the mantle was assumed. As for the LPB-ARE profile, the crustal thickness is on the order of 70 km and the mean crustal velocity is very low.

**TCC-CUS line.** The Toconce-Cuzco profile is confined almost entirely to the western cordillera, although the propagation path covers a short section of altiplano just south of Cuzco. The phase velocities are somewhat higher than those measured for the LPB-ARE line (see Fig. 69). The crustal model is similar to that found for the LPB-ARE line; crustal thickness is approximately 65 km and mean crustal velocity is low. Surprisingly, a 10-km thick layer of 5.0 (2.88) km/sec rock is necessary to explain the low phase velocities at short periods. Whereas such a layer was expected in the altiplano with its thick sedimentary section, it was not expected along the mountain profile. The rapidly increasing phase velocities at long periods preclude the existence of any sig-

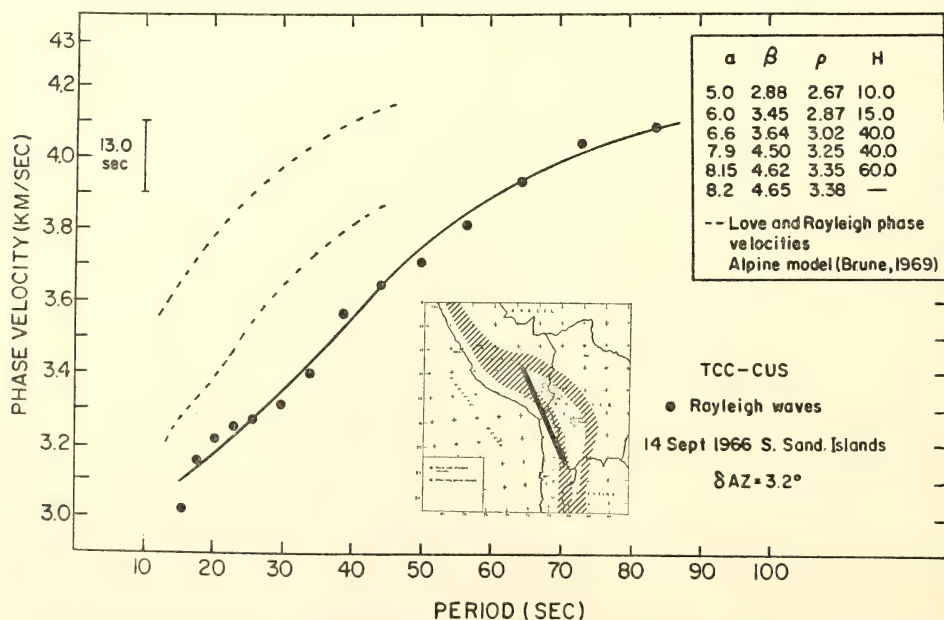


Fig. 69. Phase velocity measurement for Rayleigh waves between the TCC-CUS station pair. See legend to Fig. 67 for explanation of other features shown on illustration.

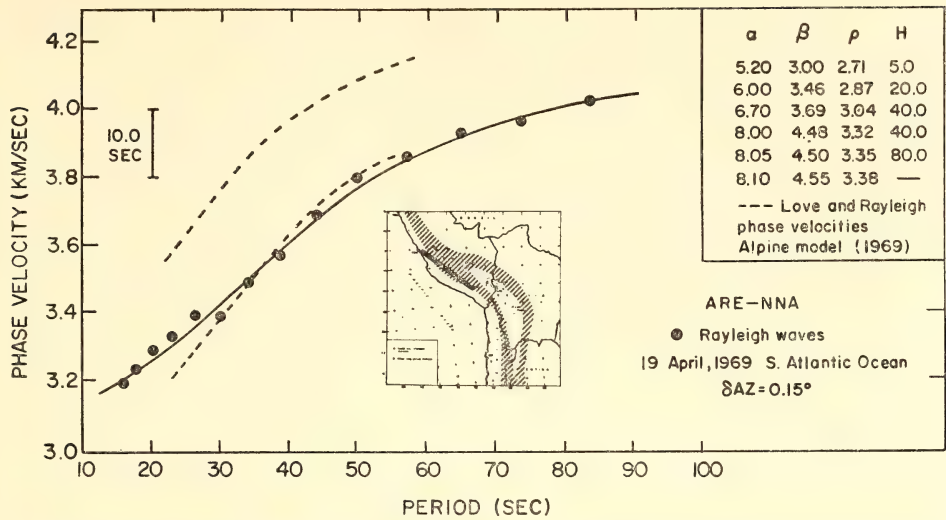


Fig. 70. Phase velocity measurement for Rayleigh waves between the ARE-NNA station pair. See legend to Fig. 67 for explanation of other features shown on illustration.

nificant low velocity channel in that part of the mantle above 200 km depth.  
*ARE-NNA line.* The Arequipa-Nana profile extends primarily along the crest

of the western cordillera. The dispersion curve is similar to that measured along the TCC-CUS line (see Fig. 70). The low-velocity uppermost crustal layer is

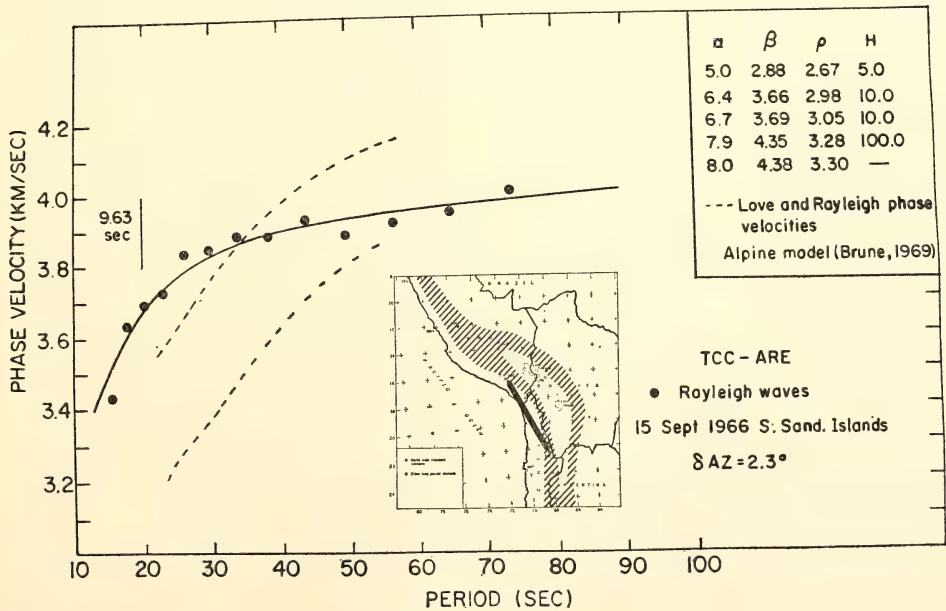


Fig. 71. Phase velocity measurements for Rayleigh waves between the TCC-ARE station pair. See legend to Fig. 67 for explanation of other features shown on illustration.

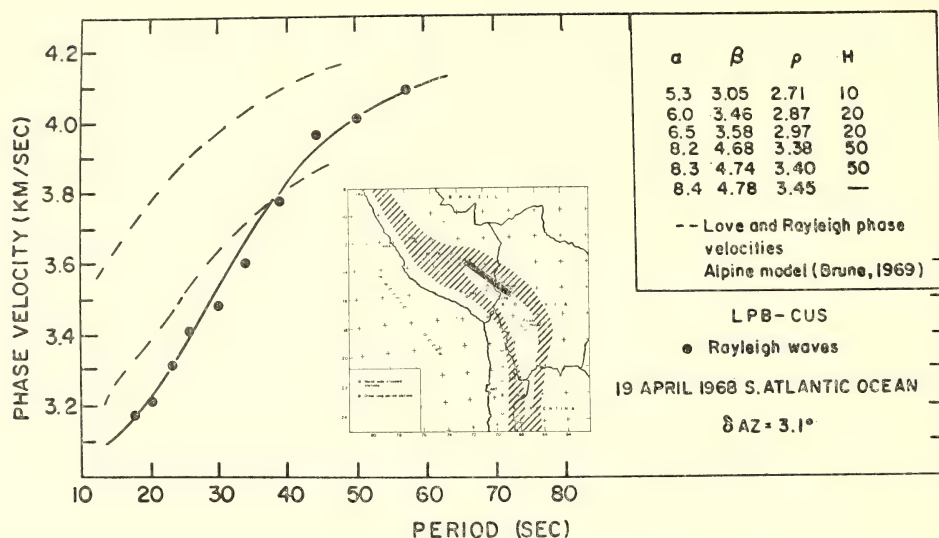


Fig. 72. Phase velocity measurements for Rayleigh waves between the LPB-CUS station pair. See legend to Fig. 67 for explanation of other features shown on illustration.

much thinner than that found for the TCC-CUS profile, although the remainder of the crustal section is essentially identical. Upper mantle velocities do not increase as rapidly as those derived from the TCC-CUS line phase velocities, but again there is no velocity reversal in the upper mantle, at least to depths of about 150 km.

**TCC-ARE line.** The very thin crust ( $\sim 25$  km) implied by the phase velocities along this profile is a very surprising result. The profile is a combination of cordillera flank and coastal topography, and it was expected that the profile would show phase velocities appropriate to structure along the flank of the western cordillera. Additional data will be needed to verify the dispersion curve shown in Fig. 71. Upper mantle velocities are somewhat lower than those measured along other profiles, but again there is no low velocity layer required.

**LPB-CUS line.** The La Paz-Cuzco profile extends along the western flank of the eastern cordillera. The dispersion curve is shown in Fig. 72. The derived model differs strikingly from those de-

scribed above for the central and western parts of the Andes. The crustal velocities are only slightly higher than those obtained for the other mountain profiles, but the crust is significantly thinner, about 50 km. The upper mantle velocities are high and appear to increase rapidly with depth.

### Discussion and Results

The results given above are summarized in the form of an approximate cross-sectional profile along the line A-A' shown in Fig. 73. The cross-section displays the principal features of the structure of the crust and upper mantle that have been obtained in this study. The features of greatest importance can be summarized as follows: (1) The crustal structure of the coastal areas is comparatively normal with a thickness of 25–30 km and a mean crustal velocity in the range of 6.2–6.3 km/sec for  $P$  waves and about 3.5 km/sec for  $S$  waves. The upper mantle velocity near the coast is slightly low ( $V_s \approx 4.35$  km/sec), but no low velocity channel is suggested.



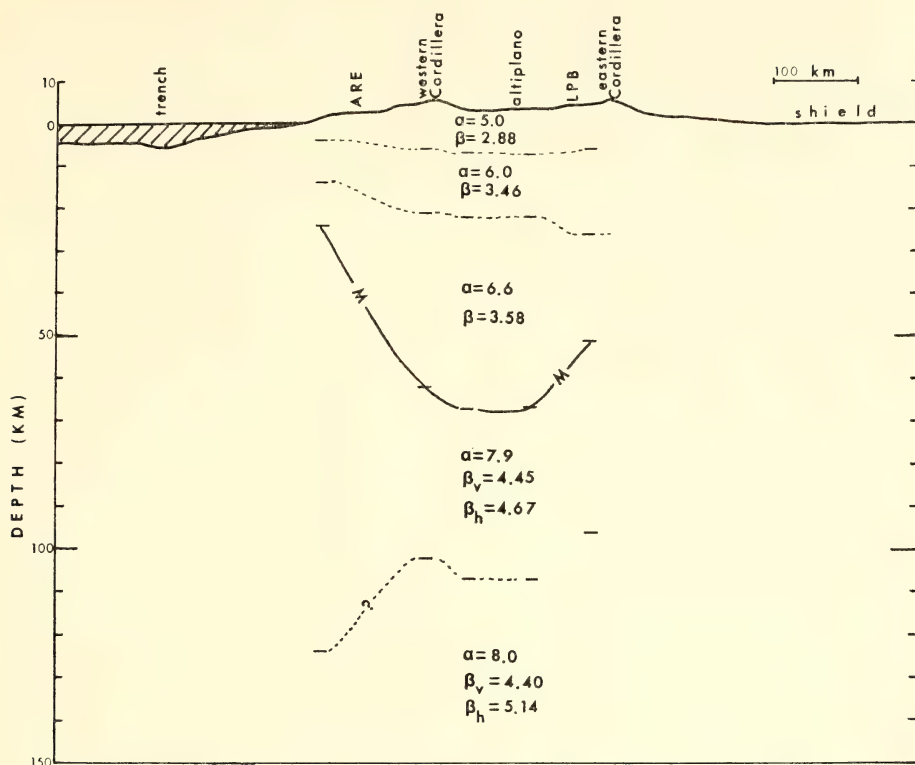


Fig. 73. Cross-section of Andean crustal and upper mantle structure as inferred from phase velocity measurements and derived structural models presented in Figs. 67-72. The results have been simplified and projected onto the line A-A' in Fig. 67.

(2) The crust thickens rapidly between the coastal and altiplano regions, attaining a maximum thickness of 70 km or more beneath the western cordillera and western edge of the altiplano. The sub-crustal velocities are slightly higher than those found for the coastal area, and a very small reversal in  $S$ -wave velocity may occur at depths of 130 km or more.

(3) On the basis of the one profile (LPB-CUS) it would appear that the crust thins beneath the eastern cordillera to about 50 km beneath the western flanks of that cordillera. The upper mantle velocities are considerably higher than those found beneath the altiplano and western cordillera, and increase rapidly with depth.

In the absence of additional phase velocity measurements to verify the data

now available, most conclusions as to the geologic or tectonic significance of the results are somewhat speculative. Nonetheless, a number of pertinent observations can be stated.

The generally low velocities in the upper part of the crust beneath the altiplano suggest that the thick (20-30 km) sedimentary section proposed by many writers (see Morrison, 1970, for a summary of the geology) for the altiplano does exist. The great overall thickness of 70 km, however, indicates that these sedimentary rocks were deposited on a continental crust of average or greater than average thickness. Thus, the altiplano cannot be compared to areas such as the Great Valley of California in which the sediments appear to have been deposited on oceanic crust. It is a re-

markable fact that the crustal section lying between the two active volcanic chains of the eastern and western cordillera appears to have been very little disturbed.

The thinning of the crust beneath the eastern cordillera is in agreement with the gravity data which exhibit a maximum negative Bouguer anomaly along the western side of the altiplano and show a considerably reduced anomaly in the area of the eastern cordillera. Near-vertical residuals (Sacks, *et al.*, p. 452, *Year Book 68*) indicate that the mean velocity beneath LPB is higher than beneath CUS and HUA. This could suggest that beneath the eastern altiplano the crust is thinner and/or the velocity in the upper mantle is higher than beneath the western cordillera.

With the exception of some fragmentary results reported by Russian geophysicists working in the Himalayas, the crustal thicknesses reported here are the greatest measured anywhere in the world. The thickness of the crust beneath the altiplano indicates that the western cordillera did not form as an island arc, but formed immediately adjacent to and possibly on pre-existing continental crust.

ANOMALOUS LOVE WAVE  
PHASE VELOCITIES

D. E. James

Anomalously high Love wave phase velocities in the period range 60–110 seconds have been measured across the

station pair La Paz, Bolivia (LPB) and Arequipa, Peru (ARE) of the World Wide Standard Station Network for an earthquake in the Republic of Congo on March 20, 1966. The station geometry and epicentral data are given in Table 19 and a map showing station locations is given in Fig. 74. The measured phase velocities for both Love and Rayleigh waves are shown in Fig. 67.

These anomalous Love wave velocities are similar to those found elsewhere in the world, e.g., Aki and Kaminuma, 1963,<sup>142</sup> and McEvelly, 1964.<sup>143</sup> The velocities are considered anomalous in the sense that it is impossible to generate a simple plane-layered model that fits both Love and Rayleigh phase velocities.

At least three explanations have been advanced to resolve the apparent discrepancy in phase velocities. (1) Anisotropy has been proposed by Aki and Kaminuma (1963) and McEvelly (1964). By assuming that the *SH* velocity is 6–10% higher than *SV*, both Love and Rayleigh phase velocities can be reconciled. Takeuchi, *et al.* (1968)<sup>144</sup> suggest that elliptical magma pockets in the upper mantle could produce such anisotropy. Preferential olivine orientation could also produce appreciable anisotropy in the upper mantle. (2) Aki (1968)<sup>145</sup> and Hales and Block (1969)<sup>146</sup> have shown that models with alternating thin laminations of “rigid” and “soft” layers can produce phase velocities that satisfy both Love and Rayleigh data. (3) Thatcher and Brune (1969) have

TABLE 19. Station Data

Station		Coordinates	
La Paz, Bolivia (LPB)		16.53 S	68.10 W
Arequipa, Peru (ARE)		16.46 S	71.49 W
ARE → LPB:		Δ = 362.2 km	Az (east of north) = 91.7
Epicentral Data			
Date: March 20, 1966		T <sub>0</sub> : 01:42:49.9	epicenter: 0.6 N, 30.2 E
Focal depth: 24 km		magnitude: 6.2–7.25	
LPB → epicenter:		Δ = 10922.0 km	azimuth = 91.9
ARE → epicenter:		Δ = 11284.2 km	azimuth = 92.9

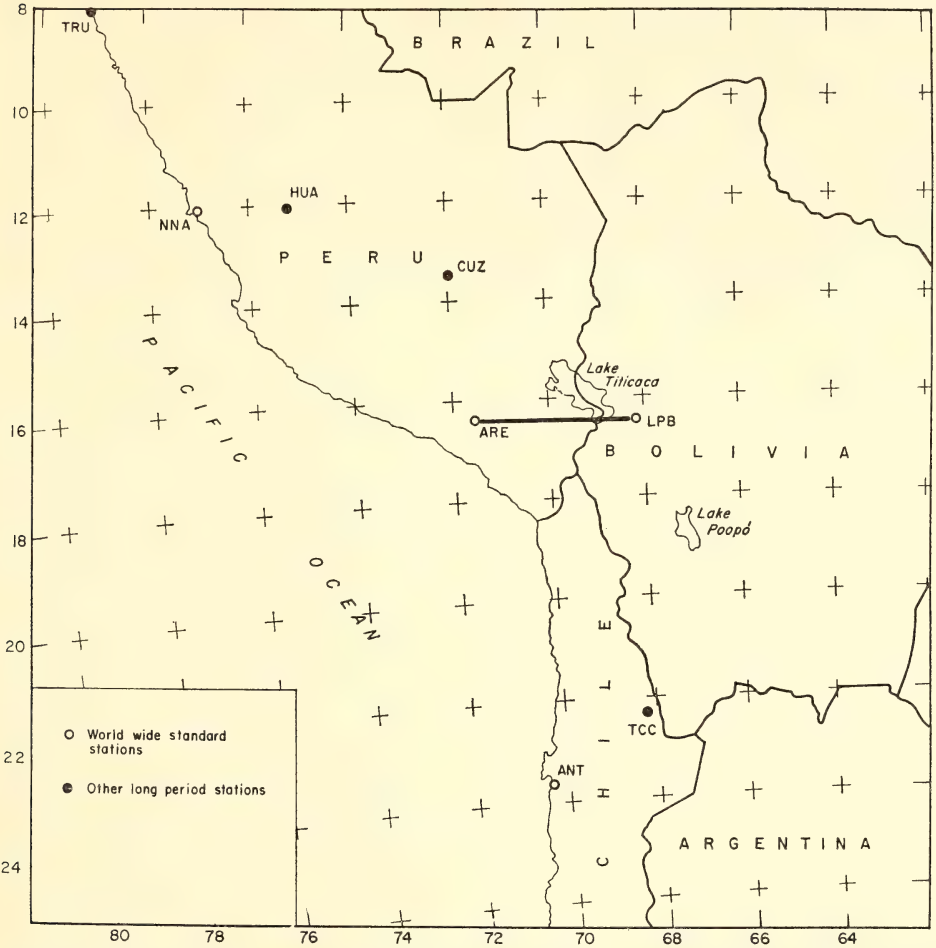


Fig. 74. Station location map. Solid line connects stations Arequipa, Peru (ARE) and La Paz, Bolivia (LPB).

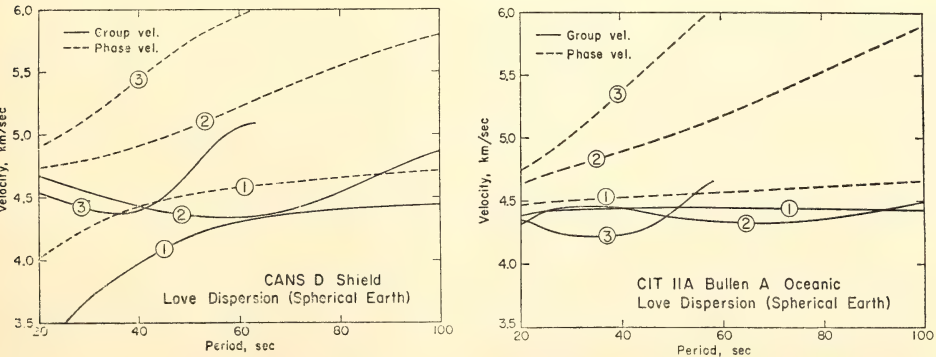


Fig. 75. Love wave phase and group velocity curves for a shield and oceanic model for the first three modes. (From Thatcher and Brune, 1969).<sup>141</sup>



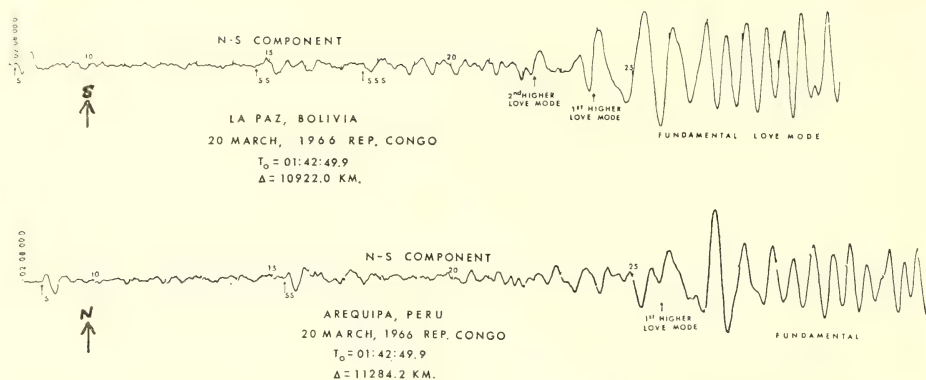


Fig. 76. Seismograms for the N-S component of stations LPB and ARE. Note the first higher Love mode immediately preceding the start of the fundamental mode wave train.

proposed that the anomalous Love wave observations are the result of higher mode interference. They show that such interference could be a consequence of the fact that both the fundamental and first higher Love modes have nearly identical group velocities in the period range  $\sim 50$ – $100$  seconds for a large class of earth models (see Fig. 75). It should be noted that whereas Thatcher and Brune show that anomalously high phase velocities can result from interference, Boore (1969)<sup>147</sup> in a similar study on

the effects of higher mode contamination emphasizes that such interference should not systematically bias the phase velocities for an ensemble of events, although for any single event the dispersion curve may be significantly biased.

#### *Data and Group Velocities*

The 1966 earthquake in the Republic of Congo provided an opportunity to test the above proposals. The propagation vector is almost precisely due east-west

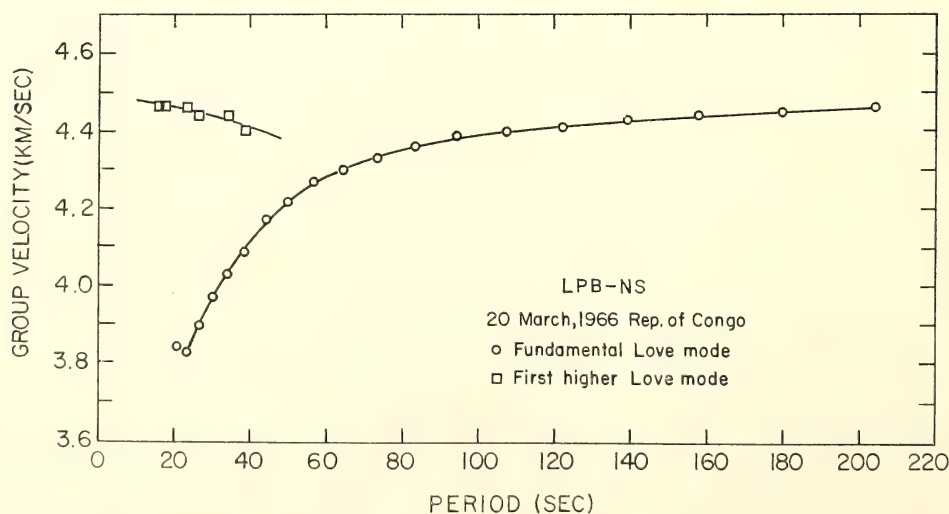


Fig. 77. Group velocity curves measured by multiple filtering are shown for the fundamental and first higher Love modes.

and deviates only  $1.1^\circ$  from the LPB-ARE great circle path (see Table 19). Thus the Love waves recorded on the N-S component are virtually free of Rayleigh wave contamination. In the period range of interest (60–110 seconds) it is unlikely that any significant refraction occurs. The wave trains cross both the African and South American coastlines at nearly normal incidence.

The propagation path from the Congo earthquake is part shield and part oceanic; hence, if the Thatcher and Brune (1969) curves shown in Fig. 75 are applicable, higher mode interference could be important in the period range 60–100 seconds. Tracings of the LPB and ARE records are shown in Fig. 76. The first higher Love mode can be clearly identified on LPB and ARE, and there is an arrival at the expected time for the second higher Love mode on LPB, although the evidence for that mode is not so convincing on ARE. Group velocities for the fundamental and first higher Love mode as measured by multiple filtering (see Dziewonski, *et al.*, 1969, for details) are shown in Fig. 77. Although the first higher mode group velocity curve can be followed reliably only to about 40 seconds, its projected shape indicates that the higher mode could start interfering with the fundamental at about 60 seconds.

### *Phase Velocity Results*

The phase velocities were computed using the technique summarized in Fig. 65 in the form of an abbreviated flow chart. The seismograms are digitized at 1 point/second. Multiple filtering is performed to obtain the group velocity curve. The phase velocities are computed by the method of cross-multiplication described by Block and Hales (1968). The instrumental phase delay for the station pair has been determined by Fourier analysis of the calibration pulses on the two records. All distances and azimuths have been calculated using the

formulas of Thomas (1965),<sup>148</sup> which incorporate both first- and second-order ellipticity corrections.

Because the station separation is only 362 km, phase velocities measured for periods greater than about 100 seconds are unreliable due to the decrease in S/N ratio and the increased phase resolution necessary to maintain precision at longer periods. Nonetheless, phase velocities for G1 and R1 are plotted for periods as great as 180 seconds. Phase velocity oscillations at periods greater than 110 seconds are probably due to loss of resolution, although interference cannot be entirely excluded.

To establish that the anomalous Love wave velocities between 60 and 110 seconds are not an artifact of the method of phase velocity analysis, I have experimented with different windows centered on the group delay times and find no significant change. Attempts to disguise the higher mode arrivals by zeroing all amplitudes in that part of the records immediately prior to the beginning of the fundamental wave train have not altered the results. To satisfy both Rayleigh and Love velocities in terms of a simple layered model, an anisotropy of 5% is required in the uppermost mantle layer and greater than 15% in the underlying layers. No crustal anisotropy is required. Dashed lines indicating varying degrees of anisotropy (with the uppermost mantle layer held to 5% in all cases except for zero anisotropy) are shown in Fig. 67. Other simple models which satisfy the data can be generated, but all involve considerable anisotropy. The *SH* velocities required (see model parameters in Fig. 67) are very high, considerably in excess of those which would be expected in common ultramafic rocks at the *P-T* conditions likely to exist beneath the Andes Mountains.

To ascertain whether the anomalous velocities are caused by the velocity structure of the earth or are only the result of higher mode interference, G3 phase velocities in the period range 60–

110 seconds were measured for the LPB-ARE station pair. The G3 wave train is comparatively free of complications because the fundamental should be well separated in time from the higher modes (the group velocities are not identical).

Phase velocities for G3 between 60 and 110 seconds are shown in Fig. 67 and contrast sharply with the velocities shown for G1. The G3 velocities are "normal" and tend to lie along the zero anisotropy line, particularly for periods between 70 and 100 seconds where the signal-to-noise ratio is greatest.

### Conclusions

The results presented above strongly suggest that higher mode interference, not anisotropy or complex layered models, is responsible for the anomalous Love wave velocities reported in this paper. It is quite possible that other kinds of interference, such as multipath interference, can also significantly perturb the phase velocities, although one would expect such interference to be as important for Rayleigh waves as for Love waves. It is impossible on the basis of this single set of results to state whether or not interference is the cause of anomalous Love wave phase velocities reported elsewhere in the world. In this regard, however, Thatcher and Brune (1969) suggest that many of McEvilly's (1964) anomalous Love wave phase velocities could be caused by higher mode interference. In the light of Boore's (1969) observation that the phase velocities should not be systematically biased by interference, it is surprising that anomalously low phase velocities have not been reported. Although Thatcher and Brune (1969) assert that mixed mode trains that produce smooth (i.e., "good") phase velocity curves will generally exhibit anomalously high phase velocities, this conclusion is not entirely obvious from the examples they present. Certainly the question as to whether or not higher mode interference

will systematically produce high phase velocities has not been completely answered and should be examined further. Nonetheless, it is clear that contamination of the fundamental by higher modes does occur and severely limits the usefulness of Love wave phase velocity results for periods between 50 and 100 seconds.

### Acknowledgments

I wish to thank W. Thatcher and D. Boore who first pointed out to me the possibility that anomalous Love wave velocities could be the result of higher mode interference. They have also provided many stimulating discussions and important suggestions.

### TIME ANOMALIES AND STRUCTURE BENEATH THE ANDES

*F. Volponi*

Several researchers during the last few years used groups of stations (arrays) to study the crust and the mantle, and it is important to mention that there are at least two different ways of using such stations: the first one investigates the deeper layers through which the seismic ray passes. In this case the array stations must be set up in a region where the crust is uniform and well known, and the ray theory is used to determine the *P* or *S* wave velocity of propagation in the deepest point of the ray (L. R. Johnson, 1967;<sup>150</sup> A. L. Hales *et al.*, 1968;<sup>151</sup> R. L. Kovack and R. Robinson, 1969<sup>152</sup>). The second, which is used in this study, is based on a model of the spherical symmetry of the interior of the earth to investigate the outer layers of the crust and the upper mantle. A similar study was reported by G. Saa and I. S. Sacks in *Year Book 68*, pp. 452-459.

We have studied a cross-section of the Andes Mountain range between 31 and 32 degrees southern latitude. We installed a series of seismological stations



along a line that crosses the cordillera, whose locations are given in Figure 78. As it was necessary to use existing roads, the line was not drawn at a right angle with the cordillera axis, but came out inclined to the southwest. Our first idea was to get to the Pacific Coast (and even farther, setting a receiver at the bottom of the ocean), but for the time being it has only been possible to record the data on the east side of the mountains.

Figure 79 shows more details of the location of the stations whose names are, from east to west: Pie de Palo (PPA), Zonda (ZON), Cerro Negro (CEN), Leoncito (LEO), and Manantiales (MAA). Away from the line, farther north, the Hualilan (HLN) station has been installed as a means of control. All these stations are listed in *Seismological Station Abbreviations*, Coast and Geodetic Survey, 1968, where their geographical coordinates can be found. The greatest distance between one station and the next is about 60 kilometers. It has been proved that with this distance it is possible to pass from one station seismogram to that of another by correlation and thus prevent the possibility

of committing mistakes in the readings. By means of artificial explosions, we have tried to profit from the advantages offered by the arrays that have such a wide application in seismographic prospecting. The location of each station has been carefully chosen in places with a low level of noise in order to permit the use of great amplifications.

In each station we have installed a vertical component short-period ( $T_0 = 1$  sec) seismograph. The equipment consists of a Wilson-Lamson receiver, a high gain (DTM) electronic amplifier, a visible trace recorder, and a quartz crystal chronometer. The seismogram paper speed is 12 cm per minute and has time marks for seconds besides the common marks for minutes and hours.

All the stations worked with amplifications of around 250,000, except Zonda which, in a way, has been replaced by that at nearby Cerro Negro for this work. Some stations have instruments for horizontal as well as vertical components to widen the range of frequencies and amplifications of the recording.

Table 20 summarizes the 39 earthquakes used for this work. Number 1,

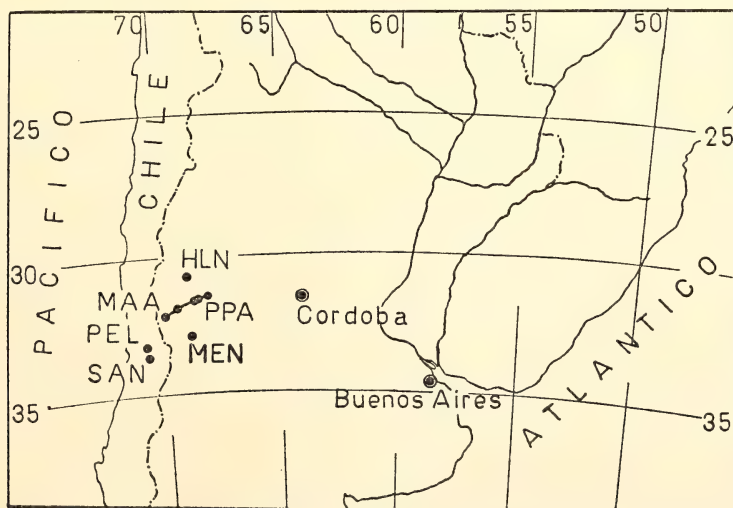


Fig. 78. Map showing location of the seismological stations along a line on the east side of the Andes between 31 and 32 degrees south latitude.

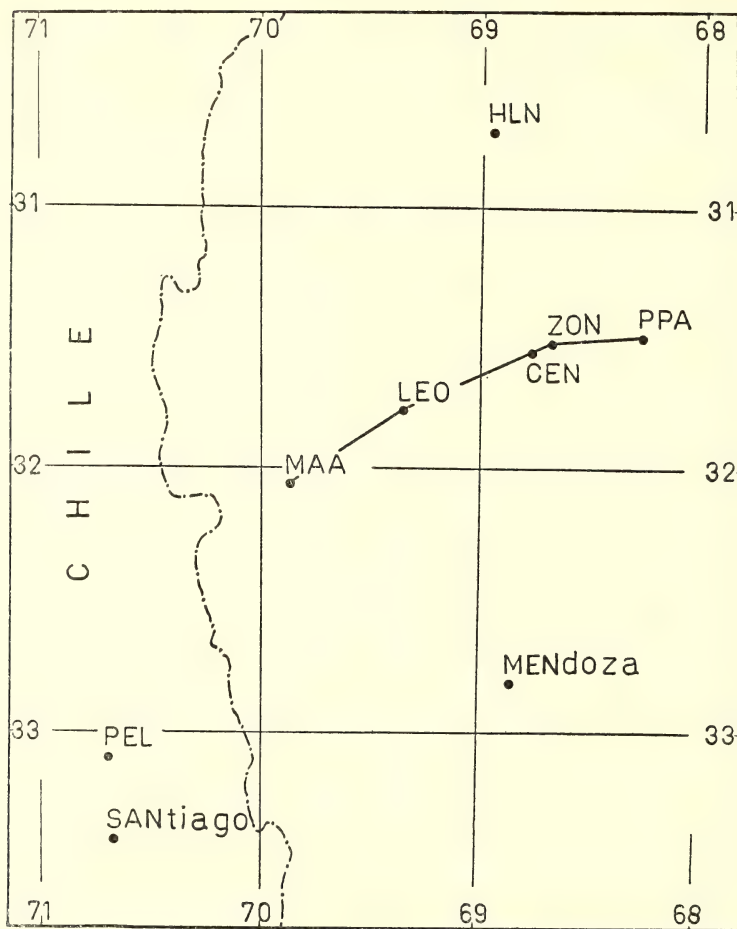


Fig. 79. Details of the locations of the seismological stations. PPA = Pie de Palo, ZON = Zonda, CEN = Cerro Negro, LEO = Leoncito, and MAA = Manantiales. Farther north HLN = Hualilan.

April 26, 1968, is an artificial explosion. The table shows coordinates, depth, and magnitude, all these values taken from *Earthquake Data Reports*, U.S. Coast and Geodetic Survey. The last two columns give the epicenter distances and the azimuths refer to Cerro Negro (CEN) station, data calculated using the 1130 IBM computer of the Instituto de Calculo of the Facultad de Ingeniería of the Universidad Nacional de Cuyo. We have proved that the magnitude of the earthquakes has to be higher than 5

in the Richter scale in order to obtain good *PKP* records. Earthquakes 14 and 30 are of magnitude 5.1; all the others are greater.

We have read the seismograms with the greatest care, applying the criterion of correlation. We have seldom read the time of the first observed deflection of the perturbation, but rather have used the time of some characteristic, well-defined detail of the seismogram that may be clearly identified in the seismograms of the other stations. This com-

TABLE 20. Epicentral Distances and Azimuths of Earthquakes

Number	Date	Origin Time (GMT)			Latitude, deg.	Longitude, deg.	Depth, km.	Magni- tude	Epicentral Distance, deg.	Azi- muth, deg.
		H	M	S						
1	Apr 26	15:00:00.1			36.300N	116.500W	00	6.3	81.76	323
	May									
2	1	08:43:47.4			38.610N	143.090E	60	5.3	153.10	294
3	2	05:29:38.2			18.776N	69.636W	82	5.8	50.07	359
4	3	05:32:54.7			25.140N	124.580E	98	5.8	166.62	245
5	14	14:05:06.0			29.930N	129.373E	168	5.9	164.32	269
6	15	07:51:17.4			15.890S	25.942E	33	6.1	85.72	106
7	16	06:36:51.0			41.078N	142.955E	35	5.7	152.88	299
8	16	07:49:01.5			41.307N	142.623E	38	5.1	153.08	300
9	16	08:58:11.1			41.432N	142.718E	15	5.4	153.00	300
10	16	16:13:45.1			39.680N	143.554E	29	5.6	152.63	296
11	16	18:43:21.0			40.709N	142.112E	59	5.7	153.57	299
12	17	13:02:37.3			41.481N	142.771E	45	5.6	152.93	300
13	17	18:17:07.3			39.627N	143.035E	32	5.2	153.04	296
14	19	22:16:44.8			40.891N	143.183E	18	5.1	152.73	299
15	20	03:16:19.6			39.966N	143.981E	31	5.5	152.27	297
16	20	06:53:35.2			40.281N	143.705E	33	5.2	152.44	297
17	21	08:20:00.9			44.906N	150.151E	33	5.7	147.00	305
18	22	10:51:53.3			41.508N	142.761E	40	5.9	152.94	300
19	24	14:06:24.2			40.933N	143.029E	38	5.6	152.85	299
20	26	04:01:57.8			00.357S	123.991E	106	5.3	146.01	203
	Jun									
21	7	11:57:29.4			01.780S	120.128E	20	5.9	145.77	196
22	7	21:30:50.3			02.126S	120.521E	23	5.5	145.35	196
23	8	05:29:46.5			43.421N	147.071E	43	5.3	149.44	303
24	8	23:24:05.2			48.751S	31.531E	33	5.6	73.16	137
25	12	04:29:22.6			24.867N	91.931E	44	5.3	161.72	107
26	12	17:52:01.2			39.145N	142.913E	30	5.5	153.19	295
27	12	21:57:41.3			39.289N	142.773E	36	5.7	153.28	295
28	14	19:03:27.8			41.911S	171.886E	25	5.3	88.02	221
29	15	07:08:48.1			05.602N	82.570W	16	6.0	39.24	338
30	17	04:26:31.9			22.418N	121.356E	39	5.1	167.18	227
31	17	11:53:00.4			40.977N	142.082E	48	5.7	152.87	299
32	19	05:05:57.3			49.960N	79.094E	00	5.5	149.82	43
	Jul									
33	5	00:45:17.2			34.120N	119.703W	6	5.7	81.07	319
34	8	13:14:29.9			38.033N	67.676E	28	5.2	143.82	67
35	19	04:56:27.2			08.683N	93.570E	33	5.3	151.90	140
	Aug									
36	3	04:54:32.7			25.626N	128.498E	18	6.4	163.73	253
37	3	06:25:05.8			16.479N	122.309E	37	5.9	161.90	216
38	4	11:41:24.8			06.593N	126.758E	107	5.7	151.21	213
39	5	16:17:04.8			33.289N	132.179E	41	6.3	162.24	281

parative study of the records has been useful to prove that if a well-defined correlation between the seismograms is not found, little value can be attached to the time differences obtained. Plates 5 and 6 are examples of seismograms from the array.

From the third to the sixth column in Table 21, the readings made from the seismograms are given. In the seventh, the value of gradient  $dt/d\Delta=f(\Delta)$ , taken

from the seismological tables by Herrin (1968),<sup>153</sup> is given, after having correctly identified the corresponding phase.

All the aftershocks of the May 16 earthquake have an epicentral distance of between 150 and 153 degrees. For this distance three branches of *PKP* arrive at the stations, separated by small intervals of time: the *AB* branch (*PKP*<sub>2</sub>), the *GH* branch (Bolt's notation), and the *DF* branch (*PKP*<sub>1</sub>). It is important



TABLE 21. Seismogram Readings and Anomalous Time Differences

No.	Phase	Readings				$\frac{dT}{d\Delta}$ , $\frac{\text{sec}}{\text{deg}}$	Differences		
		PPA, h m s	CEN, s	LEO, s	MAA, s		C-P, .1s	L-C, .1s	M-L, .1s
1	P	15:12:21.9	21.9	21.4	21.5	5.3	11	2	3
2	PKP	09:03:43.7	43.9	43.3	43.3	2.6	10	2	6
3	P	05:38:25.7	26.9	28.5	31.5	7.5	8	0	9
4	PKP <sub>2</sub>	05:52:48.5	47.5	45.2	43.1	4.4	11	4	6
5	PKP	14:24:52.0	52.1	51.9	52.1	1.0	6	3	7
6	P	08:03:55.2	57.6	60.1	62.2	4.9	6	4	5
7	PKP	06:56:46.5	46.7	46.1	46.3	2.6	11	2	7
8	PKP	08:08:57.1	57.3	56.5	56.8	2.6	10	0	10
9	PKP	09:18:72.4	72.6	72.0	72.0	2.6	10	3	6
10	PKP	16:33:41.8	42.1	41.4	41.6	2.0	10	2	8
11	PKP	19:03:15.3	15.4	14.7	14.9	2.6	10	2	8
12	PKP	13:22:20.1	32.4	31.5	31.6	2.6	14	—1	8
13	PKP	18:36:63.2	63.8	62.8	62.9	2.6	13	—2	7
14	PKP	22:36:43.1	43.5	42.8	43.1	2.6	12	3	8
15	PKP	03:36:15.3	15.6	14.9	15.1	2.6	11	2	8
16	PKP	07:13:31.9	32.2	31.5	31.7	2.6	12	1	9
17	PKP	08:39:39.7	40.5	40.2	40.4	1.6	12	2	5
18	PKP	11:11:49.4	49.7	48.9	49.2	2.6	11	1	9
19	PKP	14:26:20.2	20.6	19.6	19.6	2.6	12	—2	7
20	PKP	04:21:28.7	29.5	28.4	27.7	2.7	13	—1	5
21	PKP	12:16:70.6	71.2	70.0	69.1	2.7	11	—2	3
22	PKP	21:50:28.9	29.3	28.5	27.5	2.7	9	2	3
23	PKP	05:49:30.8	31.5	30.5	30.3	2.6	...	...	4
24	P	23:35:24.9	27.2	28.4	29.5	5.9	10	3	6
25	PKP	04:49:21.1	22.3	23.1	24.1	1.0	9	3	6
26	PKP	18:11:58.3	58.9	58.3	58.2	2.6	14	1	7
27	PKP	22:17:37.2	37.6	37.7	37.6	2.6	14	0	8
28	P	19:16:19.1	18.6	16.3	14.8	4.7	10	0	8
29	P	07:16:18.3	18.2	18.2	20.1	8.3	9	2	6
30	PKP	04:46:36.7	37.1	37.0	36.9	0.8	10	2	4
31	PKP	12:12:58.2	58.5	57.7	57.7	2.6	12	1	7
32	PKP	05:25:50.2	51.6	53.3	55.0	2.6	6	2	7
33	P	00:57:37.0	37.0	36.3	36.1	5.3	12	2	2
34	PKP	13:33:60.5	62.5	64.6	67.1	3.3	6	3	8
35	PKP	05:16:15.3	16.3	17.1	17.5	1.5	10	3	4
36	PKP	05:14:37.3	38.1	37.4	37.7	1.0	12	—1	7
37	PKP	06:45:67.3	68.0	67.5	67.6	1.0	10	—1	6
38	PKP	12:00:62.8	63.4	62.1	62.5	1.5	10	—2	7
39	PKP	16:36:65.9	66.6	66.3	66.5	1.0	11	2	7

to observe here that all this group of aftershocks gave a strong impulse to the phase corresponding to the *GH* branch, whose gradient is 2.6 sec/deg. The phase *PKP*<sub>1</sub> appears some seconds before, but with lesser amplitude.

The last three columns give the time anomalies expressed in tenths of seconds and calculated by the formula

$$\Delta t_{AB} = \frac{1}{n} \sum_{i=1}^n \left( t_B - t_A - \frac{dt}{d\Delta} D_{AB} \right)_i$$

where *A* and *B* are any two consecutive stations,  $dt/d\Delta$  is the normal gradient of the travel-time curve,  $D_{AB}$  the dis-

tance between the two stations measured in the direction of the seismic ray, and *n* the total number of seismic events used. These columns give values of relative time anomalies of one station with respect to the previous one, having taken Pie de Palo station as a base. Thus C—P means Cerro Negro anomaly with respect to Pie de Palo, L—C, the Leoncito anomaly with respect to Cerro Negro, and M—L, the Manantiales anomaly with respect to Leoncito.

We have considered the distribution of error of these results as normal (although we have proved that it is not

exactly so); we have calculated the average values of each series and its respective standard deviations. We have obtained:

$$\text{CEN—PPA} = (1.05 \pm 0.05) \text{ sec}$$

$$\text{LEO—CEN} = (0.12 \pm 0.08) \text{ sec}$$

$$\text{MAA—LEO} = (0.64 \pm 0.03) \text{ sec}$$

The total values of the anomalies referred to Pie de Palo are then,

$$\text{CEN—PPA} = 1.05 \text{ sec}$$

$$\text{LEO—PPA} = 1.17 \text{ sec}$$

$$\text{MAA—PPA} = 1.81 \text{ sec}$$

Using these values, we have drawn Figure 80, which shows the anomalous values in relation to a transverse section of the cordillera on its eastern side on which the line was located.

Figure 81 was drawn with the sole object of showing graphically the reliability of the readings. The five figures on the left are aftershocks of the May 16,

1968, earthquake. The others correspond to earthquakes of different epicentral distances and different azimuths. Number 1 corresponds to the atomic explosion of April 26, 1968, and no. 33, to an earthquake that occurred in California on July 5, 1968, which was a Richter magnitude of 6.

The most important conclusions from this work are the following:

1. In the Cordillera de los Andes there occurs a delay in the time of arrival of the seismic waves, and this delay shows a tendency to increase approaching the cordillera axis.

2. Between the extremes of the line, which is 160 km long, the anomaly reaches the value of 1.80 sec.

3. The time anomaly measured does not depend on the epicentral distance of the earthquakes (for distances greater than 40 degrees, in this paper). It has

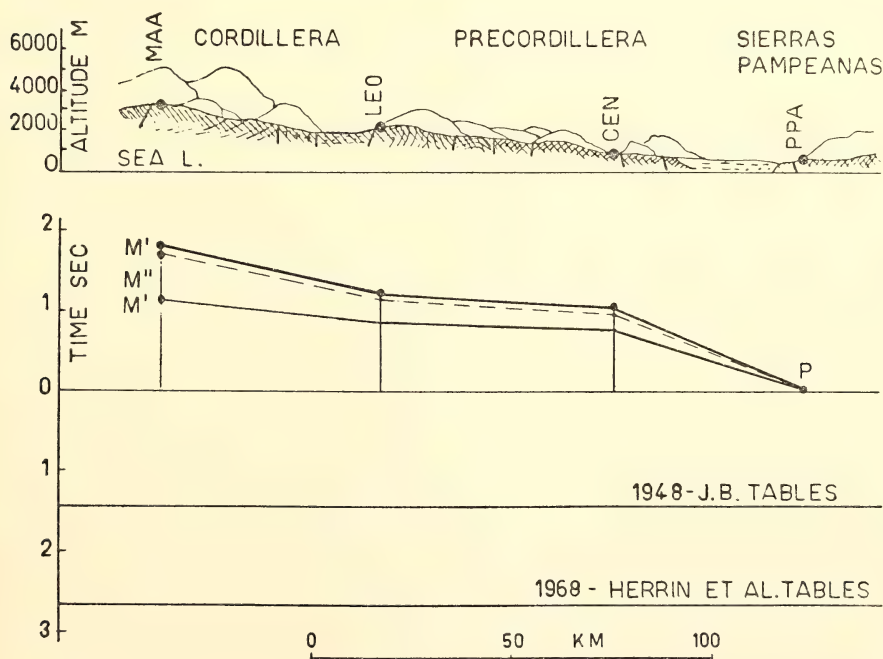


Fig. 80. Graphic representation of the anomalies in correspondence with a transverse section of the cordillera on its eastern side. The line  $PM'$  represents the anomalies corrected to the Pie de Palo level, and the line  $PM''$  represents the anomalies obtained using only phases  $P$  of nearer earthquakes.

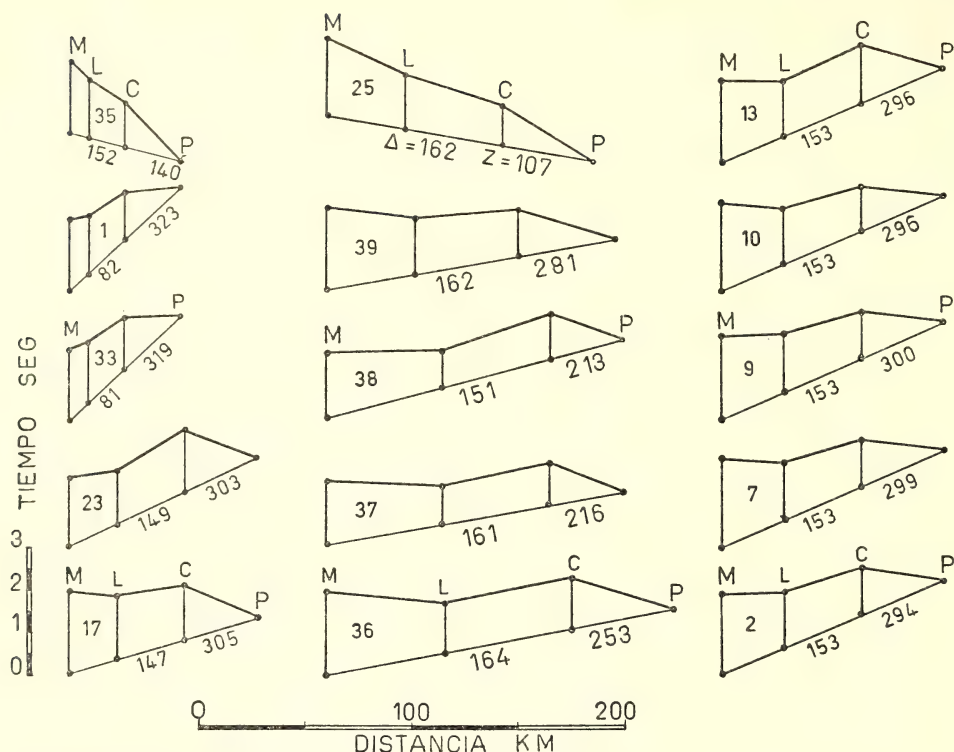


Fig. 81. This figure shows the reliability of the readings. The five diagrams on the right side correspond to aftershocks of the earthquake of May 16, 1968. The others correspond to different earthquakes with different epicentral distances and azimuths, as indicated. The diagram no. 1 on the left corresponds to the BOXCAR artificial explosion.

been proved that we come practically to the same results (the differences are smaller than the error of measurements), using either *P* phases of relatively near earthquakes or employing *PKP* phases of more distant earthquakes.

4. The preceding point has a double significance: first, that the lateral variation of the elastic properties of the rocks, which produces the anomalies, is in the more external layers of the earth, that is, in the crust and the upper mantle, and no more than 200 km deep; second, that (within the degree of accuracy of this work) the earth's interior behaves as a uniform medium of spherical symmetry. The gradient  $dt/d\Delta = f(\Delta)$  keeps itself constant for each earthquake within the limits of the line. The curvature of the

travel-time curve that corresponds to radial variations of the velocity in the deeper part of the seismic rays, gives place to differences that are smaller (smaller than the measurement errors) than those that correspond to the irregularities in the earth's more external layers.

This work has been supported in part by a National Science Foundation grant to the Department of Terrestrial Magnetism.

#### ELECTRICAL CONDUCTIVITY

*L. T. Aldrich, M. Casaverde, R. Salgueiro, A. Rodriguez, S. del Pozo, L. Tamayo, and J. Bannister*

Renewed efforts to characterize more completely the anomalously high electri-



cal conductivity region in the Peru-Bolivia altiplano were undertaken in May of last year. The previous efforts in these studies have been reported in several *Year Books*. Additional data have been obtained at about eight new locations, and sites for an additional twelve are presently either complete or being surveyed. After an initial start using Carnegie resources, added effort in South America was made possible with funds from the National Science Foundation.

The work planned will provide one of two reconnaissance profiles in northern Peru (the other was made inaccessible by the recent earthquake in Peru) and one on an E-W line across the suspected anomaly in southern Bolivia and northern Chile. Added data in Peru and Bolivia along  $-6^\circ$  magnetic latitude will provide details of a profile crossing the anomaly which may aid in deducing a probable conductivity structure. All these data will be obtained from three-component magnetic variographs from

which a description of the inducing magnetic field and the induced magnetic field due to the abnormal conducting media may be obtained.

It has been shown by Vozoff and Swift (1968)<sup>154</sup> that distributions of shallow (0-10 km) conductivity can produce induced magnetic effects that look just like those of distributions deep (100 km) in the earth. In order to verify that our South American studies are of the mantle and not the crust of the earth, we are now preparing for direct measurement of the conductivity of the surface material. The railroad companies in Peru and Bolivia have graciously offered us the use of their telegraph lines at night in order that we may inject current into the earth at points separated by as much as 30 km. The separation will be varied by a factor of 10 and the conductivity measured as a function of the separation of injection points. This may then be interpreted to give the conductivity as a function of depth.

## BIOPHYSICS

*R. J. Avery, E. T. Bolton, R. J. Britten, D. B. Cowie, B. H. Hoyer, D. E. Kohne, N. J. Rice, R. B. Roberts and R. Shleser*

### INTRODUCTION

It is an amusing fact that the writing of an introduction for these reports has often been the final effort for their completion. And frequently, these introductions have been brief recapitulations of the results presented. In a symphony, recapitulation follows the exposition and development of the principal themes but is not used for its opening movement. These annual reports however, do not deal exclusively with the year just past but represent a part of a continuing and enlarging history of scientific achievement. It is an awareness of that history, its relationship to the achievements of the present, that make each report a current recapitulation of that history.

This year's findings emphasize the potential for understanding the relation-

ships and evolution of living creatures through similarities in their DNAs. Results enlarging upon the taxonomy of primates, mammals, slime molds, bacteria, and even the viruses are here presented, reflecting indeed, the earlier work of this laboratory in which mammals and bacteria were examined for taxonomic relationships by the measurement of nucleotide sequence similarities.

Again, as in the past, the thermal stability of nucleic acid strand pairs (the temperatures at which they dissociate) has been used to indicate the degree of divergence in biological systems. For example, this year in studies of rodent DNAs, it was observed that as evolutionary separation of the DNAs increased, fewer families of repeated nucleotide sequences were held in com-

mon. Studies involving the reassociation of the DNA of these families held in common showed that the same thermal stability was observed whether heterologous or homologous DNAs were reacted. Those results imply that, among the species tested, the families undergo the same mutation rate regardless of lineage.

Significantly, in other studies, analyzing the rates of nucleotide sequence change among a large variety of animals gave results strongly indicative that the mutational events seen in evolution are *generation-time dependent*. The basic mutational mechanism therefore is probably involved in some way with the DNA replication cycle.

We have become increasingly aware that the nucleic acids of many organisms are complex, and that specific fractions can be recognized, characterized by their roles in nature or by physical-chemical isolation procedures. This recognition provides opportunities to appreciate the organization and some of the functional aspects of components of this basic genetic material.

For the past decade our joint interests with the Flexners have centered on the biochemical basis of long-term memory. Established memory can be blocked by intracerebral injection of puromycin, and current emphasis for study has been the possibility that this drug acts by blocking receptor sites for norepinephrine or epinephrine in the central nervous system. The involvement of the adrenergic system in the formation of the memory trace was also suggested by the similarity of the O-methyl-tyrosine moiety of puromycin, the structure of norepinephrine, and various mescaline-like drugs. Experiments designed to reverse the block established by puromycin were carried out using a variety of drugs known to influence the adrenergic system. These drugs, of widely differing chemical structure, were shown to have the ability to restore or to improve memory blocked by puromycin. These

collaborative studies on the biochemistry of memory have continued to be one of the highlights of our annual investigations.

#### THERMAL STABILITY OF REASSOCIATED REPEATED DNA FROM RODENTS

Nancy Rice

Britten and Kohne (1968)<sup>155</sup> have suggested that the repeated sequences of the eukaryotic genome exist as "families," each family consisting early in its history of more or less identical elements (and hence capable of reassociating with high thermal stability). These elements become increasingly dissimilar (and hence reassociate with decreasing thermal stability) as mutations accumulate through time. According to this model, new families continually arise during evolution; one that has appeared very recently may be limited to only one species, while a family that arose very long ago may be found today in many species. Thermal dissociation profiles of the repeated DNA of various rodents have been obtained over the past year and are here reported. The data they provide are in complete accord with the Britten-Kohne model.

These experiments consist of measurements of the thermal stability of reassociated homologous and heterologous DNA duplexes. DNAs from two sources are reassociated together, one (e.g., <sup>3</sup>H-mouse DNA) at very high concentration, the other (e.g., <sup>14</sup>C-rat DNA) at very low concentration. Because of its low level, self-reaction of the latter is essentially prevented, and it reassociates predominantly with the heterologous (mouse) DNA. After incubation sufficient to reassociate most of the repeated sequences of the mouse DNA, ( $C_{ot} \sim 100$ , in 0.14 M phosphate buffer at 50°C) the sample is applied to a water-jacketed hydroxyapatite column at 50°C. Reassociated material is eluted according to thermal stability (in 0.14 M phosphate buffer) by using a linear tempera-

ture gradient from 50° to 100°C, and the fractions are assayed for the two radioactive labels.

*Inbred mice.* Results of an experiment testing similarity between DNAs of two strains of inbred mice are illustrated in Fig. 82 and show the type of elution profile obtained by this method. Low levels of  $^3\text{H}$ -C3H DNA were incubated with excess  $^{14}\text{C}$ -DBA/2 DNA and the product chromatographed as described above. Of the total C3H DNA that entered into a duplex product, it can be estimated that at least 65% reassociated with heterologous (DBA) DNA; the actual value is probably close to 100%. The general shape of the elution profile and the two large peaks, one at about 60° and the other at over 80°C, are

typical of the repeated sequences of mouse DNA and are reproducible from experiment to experiment; smaller secondary fluctuations within this general pattern may vary with the experiment. It is clear that the thermal elution of the  $^3\text{H}$ -C3H-DBA duplex is essentially indistinguishable from that of the  $^{14}\text{C}$ -DBA-DBA duplex. Thus, not surprisingly, C3H DNA apparently contains virtually all of the repeated elements found in DBA DNA, and the heterologous duplexes are quite as stable as the homologous.

The same is true of the unique sequences, as shown in Fig. 83. Again, the elution profiles of heterologous and homologous duplexes are superimposable. Since a difference in  $T_m$  of less than

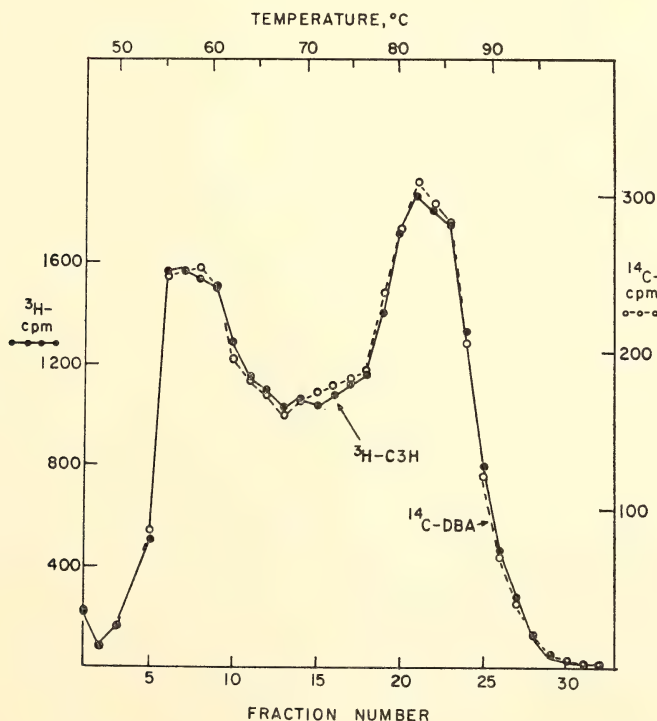


Fig. 82. Thermal dissociation of the repeated sequences of mouse DNA. A mixture of denatured  $^{14}\text{C}$ -DBA/2 DNA (2.14 mg/ml) and  $^3\text{H}$ -C3H DNA (2.1  $\mu\text{g}/\text{ml}$ ) was incubated in 0.14 *M* phosphate buffer at 50°C for 3.7 hours and applied to hydroxyapatite at 50°C. The bound material ( $\sim 55\%$  of the total) was eluted in 0.14 *M* phosphate buffer during a linear temperature gradient, and the fractions were assayed for acid-precipitable radioactivity.



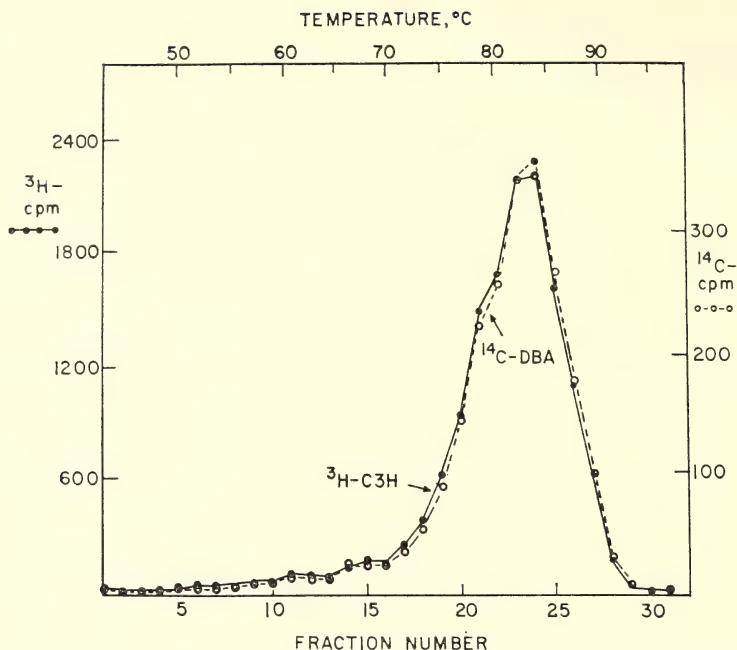


Fig. 83. Thermal dissociation of the nonrepeated sequences of mouse DNA. The DNA which did not bind to hydroxyapatite following the incubation described in Fig. 82 was incubated at about 1000  $\mu\text{g}/\text{ml}$  in 1.0  $M$  phosphate buffer, 0.0025  $M$  EDTA at 65°C for 76 hours. The sample was cooled, diluted to 0.14  $M$  buffer, applied to hydroxyapatite at 51°C (85.2% of the C3H DNA and 85.7% of the DBA DNA were bound), and eluted during a linear temperature gradient.

1°C could be detected, it can be estimated that the unique DNA of the two strains differs in base sequence by less than 1.5% (Laird, *et al.*, 1969).<sup>156</sup> Thus, any differences arising either from mutation or from their different ancestries are not detectable in this way.

**Rat-mouse.** In contrast to the great similarities exhibited by the DNAs of the two inbred mouse strains, the repeated sequences of the rat and mouse differ strikingly.  $^{14}\text{C}$ -rat DNA was annealed with high levels of  $^3\text{H}$ -mouse DNA, as described earlier. The  $^{14}\text{C}$ -rat DNA elution profile thus represents the thermal stability of the heterologous duplex; that of  $^3\text{H}$ -mouse DNA represents the homologous. As shown in Fig. 84, the two major peaks of mouse DNA are again evident, and elution spans a temperature range from 50° to over 90°C in 0.14  $M$  phosphate buffer.

The heterologous duplex, however, elutes over a more restricted range, 50° to about 80°C (the small amount of  $^{14}\text{C}$ -rat DNA that elutes above 80° is attributable to self-reaction). Further, within the range of 50° to about 70°C, the elution profiles of the homologous and heterologous duplexes are *coincident*, indicating identical thermal stabilities of homologous and heterologous reassociated products. This, in turn, must mean that DNA families common to both the rat and mouse have undergone the same *average* mutation rate in each line since the rat-mouse divergence some ten million years ago. Thus, while the thermal stability of the *total* homologous reassociated repeated sequences is higher than that of the heterologous, thermal stability of DNA elements held in common appears to be identical.

There appears to be little or no rat

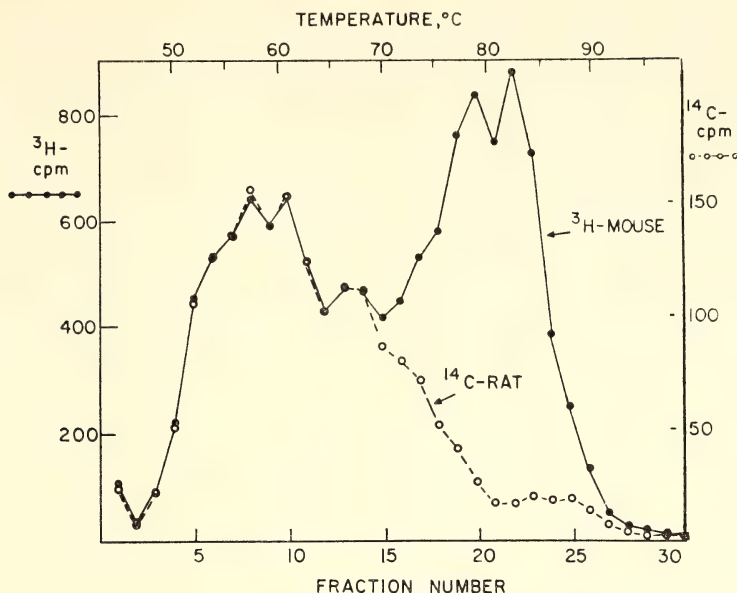


Fig. 84. Thermal dissociation of the repeated sequences of mouse DNA. A mixture of denatured  $^3\text{H}$ -mouse DNA (290  $\mu\text{g}/\text{ml}$ ) and  $^{14}\text{C}$ -rat DNA (0.086  $\mu\text{g}/\text{ml}$ ) in 0.14  $M$  phosphate buffer was annealed at  $51^\circ\text{C}$  for 18.3 hours. 58.3% of the total mouse DNA and 51.6% of the rat DNA subsequently bound to hydroxyapatite and were eluted during the linear temperature gradient.  $^{14}\text{C}$ -rat DNA which elutes above about  $80^\circ\text{C}$  (3.2% of the total) results from self-reaction. To emphasize the constant mouse DNA:rat DNA ratio which is observed during the first half of the gradient, the cpm scales have been selected so as to produce coincident elution profiles in this region. If, instead, the data for each species is plotted as percent of total DNA, the curves are not coincident; fraction 10, for example, contained 3.0% of the total mouse DNA, but 4.37% of the total rat DNA. The basis of this phenomenon is not yet clear, but such factors as slight differences in genome or family size, or fine-scale interspersions of DNA sequences may contribute to it.

DNA capable of reacting with high thermal stability with repeated mouse DNA. Two explanations for this phenomenon can be envisioned: (1) the high thermal stability mouse sequences are represented, if at all, only at a very low level in the rat genome; (2) rat DNA does react with the high stability mouse sequences, but with a reduced thermal stability. The identical thermal stabilities of homologous and heterologous duplexes in the lower temperature range of the profile make the second possibility seem unlikely. Further, Flamm, *et al.* (1969)<sup>157</sup> have directly searched for sequences in rat DNA capable of reacting with mouse satellite DNA, which comprises a substantial fraction of the

mouse high thermal stability material, and have concluded that at best they can be present at very low levels. This very substantial fraction of the mouse genome, then, appears to be without measurable counterpart in rat DNA.

Precisely the same conclusion apparently pertains in the reverse case; namely, rat DNA sequences capable of reassociating with high thermal stability with rat DNA cannot be detected in mouse DNA. One experiment illustrating this point has been performed with the non-reassociated material from the  $^{14}\text{C}$ -rat- $^3\text{H}$ -mouse incubation described above. This fraction consists mainly of single-copy rat and mouse DNA, and any repeated rat DNA that was incap-

able of reacting with mouse DNA. Incubation of this fraction with excess rat DNA (to  $C_{ot}$  13) resulted in the appearance of a significant amount of  $^{14}\text{C}$ -rat DNA in reassociated products which dissociated above  $70^\circ\text{C}$ . There is repeated rat DNA, therefore, that is capable of reacting with high thermal stability with rat DNA. Since this DNA remained unreassociated after a rather exhaustive incubation with mouse DNA, it can be concluded that similar sequences are present, if at all, at a much lower level in mouse DNA.

The repeated sequences of rat or mouse DNA can thus be arbitrarily divided into two classes, those common to both rat and mouse, and those found only in mouse or in rat. The former reassociate with rather low thermal stability, the latter, with quite high stability. If this interpretation is correct, these differences should be apparent in the elution profile of  $^{14}\text{C}$ -rat and  $^3\text{H}$ -mouse DNAs annealed *separately* (each to  $C_{ot}$  60, sufficient to reassociate most of the repeated sequences), but applied to the same column and eluted

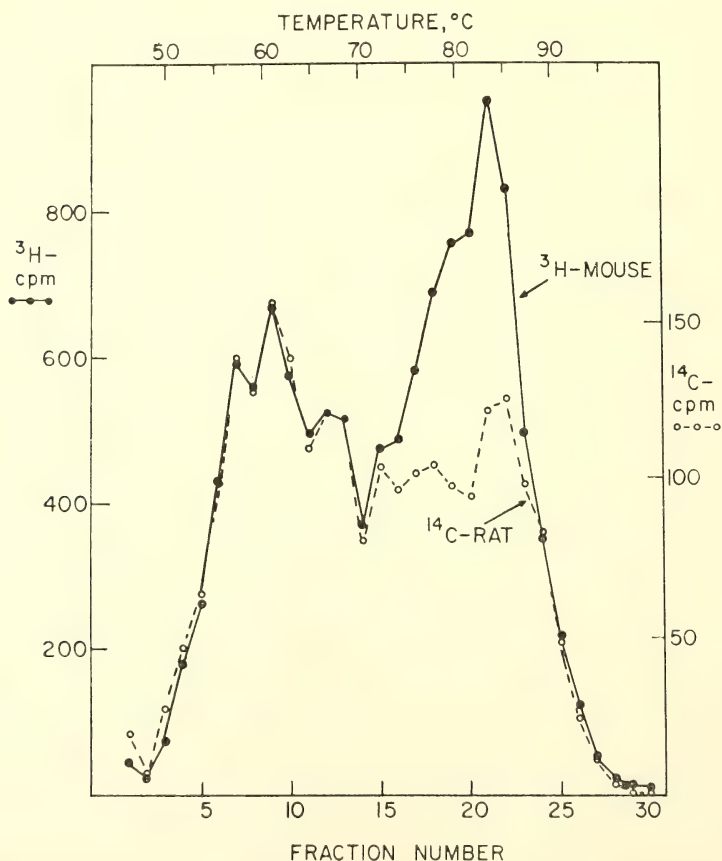


Fig. 85. Thermal dissociation of rat and mouse DNAs chromatographed together.  $^3\text{H}$ -C3H DNA, incubated to  $C_{ot}$  66 in  $0.14\text{ M}$  phosphate buffer at  $51^\circ\text{C}$ , was applied to hydroxyapatite; the column was thoroughly washed to eliminate all non-reassociated material. 56% of the total mouse DNA was bound.  $^{14}\text{C}$ -rat DNA, incubated to  $C_{ot}$  59, was then applied, 51.7% of the total was bound, the column was again washed, and bound material was eluted during a linear temperature gradient.



together. The elution profile of each isotope in this experiment represents dissociation of the homologous duplex *only*. On the basis of the results presented in Fig. 84, one would expect the two profiles to be similar from 50° to about 70° and to differ markedly in the higher temperature region where the rat-specific or mouse-specific material is expected to elute. Further, this profile should differ from that of Fig. 84 in the occurrence of significant <sup>14</sup>C-rat DNA in the high stability region.

As shown in Fig. 85, these expectations are fulfilled. Moreover, rat and mouse DNAs again elute *identically* in the low temperature regions. The simplest explanation of these observations—the identical elution profiles of the heterologous product and both of the homologous products in the low temperature range—is that *all* the families of mouse DNA that reassociate with low thermal stability (50°–70°C) are present in rat DNA, and *vice versa*. Again, since the profiles are identical in this region, a family must undergo the same average mutation rate in each line. The elution profiles differ in the high temperature region, both in the amount (20% of total rat DNA, 27% of mouse DNA) and pattern of material that elutes higher than 75°C. Much of this high thermal stability material, detectable in the homologous genome only, has presumably appeared in each genome since the mouse-rat divergence.

*Other rodents.* Experiments have been performed with a number of other rodent DNAs, and in each case the conclusions are the same as those drawn from the comparison of rat and mouse DNAs. DNAs compared include rat with Syrian hamster, rat with guinea pig, rat with *Mastomys coucha* ("multimammate mouse"), mouse with Syrian hamster, mouse with Chinese hamster, mouse with *Mastomys coucha*, and Syrian hamster with Chinese hamster. Whatever the pair, some amount of low thermal stability material appears to be held

in common; the greater the evolutionary separation of the two organisms, the smaller is the amount of this material. Rat DNA shares fewer sequences with Syrian hamster DNA than with mouse DNA, as shown in Fig. 86, and still fewer with guinea pig DNA. Chinese hamster DNA appears to share fewer sequences with mouse DNA (Fig. 87) than it does with Syrian hamster DNA. In each case, furthermore, thermal stability of the common sequences appears very similar in the homologous and heterologous products, suggesting quite comparable average mutation rates in each line.

Finally, while each DNA tested has material capable of reassociating with high thermal stability with homologous DNA, heterologous duplexes of high thermal stability could not be detected in any of the rodent DNA pairs. Just as argued above for rat and mouse DNAs, therefore, new DNA families seem to have been added to each of these rodent DNAs over the past many million years.

*Conclusions.* Many aspects of the results of these experiments are predicted by the Britten-Kohne model of saltatory genome growth and gradual decline in intrafamily relatedness with time. It should be kept in mind, however, that these experiments deal not with a specific pure family of rodent DNA, but with the total DNA fraction of repeated sequences. One does not measure, for example, a particular family that has been newly produced and consists of very similar members, but rather, an aggregate of material that reassociates to products of high thermal stability. It is the apparent absence of similar sequences in the DNA of another species that permits the conclusion that this high thermal stability material has been produced since the divergence of the two lines. Its high thermal stability points to the presence of very similar copies. Similarly, it is the remarkable coincidence in thermal stability of the homologous and heterologous duplexes in those regions where cross-reaction does occur

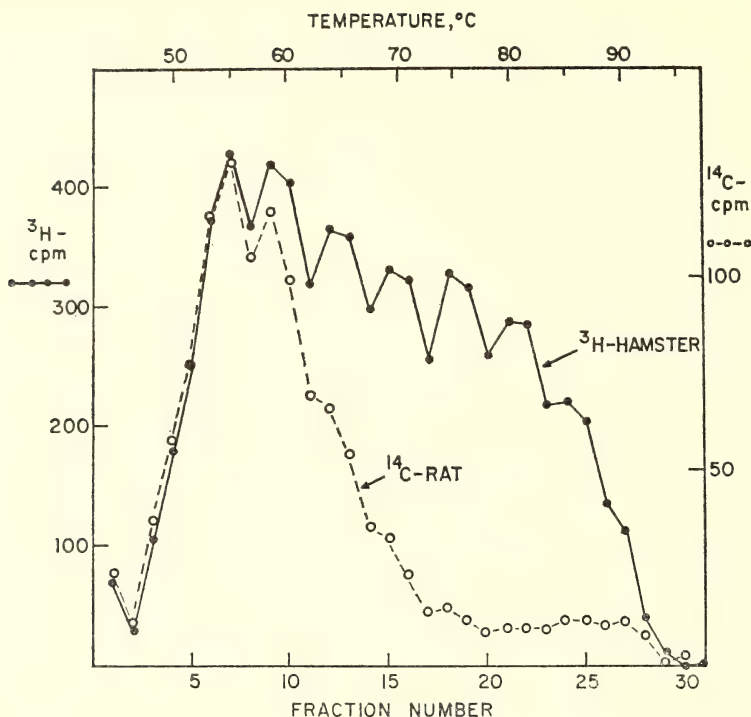


Fig. 86. Thermal dissociation of the repeated sequences of hamster DNA. A mixture of denatured  $^3\text{H}$ -Syrian hamster DNA ( $144 \mu\text{g}/\text{ml}$ ) and  $^{14}\text{C}$ -rat DNA ( $0.035 \mu\text{g}/\text{ml}$ ) was incubated in  $0.14 M$  phosphate buffer at  $51^\circ\text{C}$  for 23 hours. 53.1% of the total hamster DNA and 36.9% of the rat DNA subsequently bound to hydroxyapatite and were eluted during the linear temperature gradient.  $^{14}\text{C}$ -rat DNA which elutes above about  $72^\circ\text{C}$  (43% of total) results from a small amount of self-reaction.

that renders most reasonable the interpretation that the same families are being examined in each line and that they possess very similar average thermal stabilities.

Finally, all of these experiments have been performed with rodent DNAs, and the conclusions apply only within this framework. Greater evolutionary separation and widely differing generation times may complicate the interpretation of experiments performed with DNAs of different orders.

With these reservations, then, the following conclusions may be drawn: (1) DNA families held in common by two or more of the rodents tested reassociate with low to moderate thermal stability. (2) The greater the evolutionary separation of two DNAs, the fewer the families held in common and the lower their reassociated average thermal stability.

(3) Among the mice, rats, and hamsters tested, these common families appear to exhibit the same reassociated thermal stability in the heterologous as in the homologous reaction. This suggests that among those species a family undergoes the same average mutation rate regardless of lineage. (4) A substantial fraction of each DNA tested is capable of reassociating with high thermal stability with homologous DNA. Among pairs of rats, mice, and hamster DNAs, however, heterologous duplexes of high thermal stability are not observed. Reasoning from (2), above, and from Flamm's studies of the mouse satellite, the most

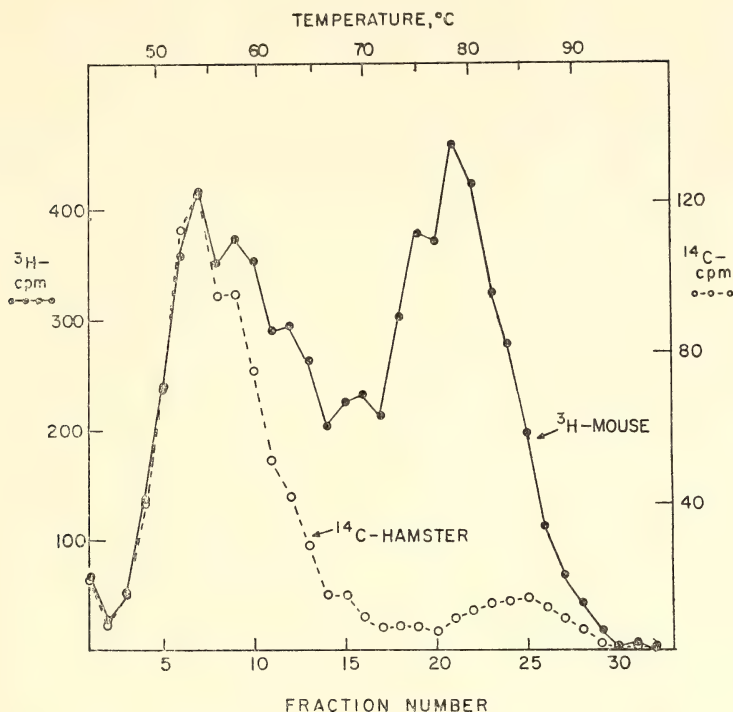


Fig. 87. Thermal dissociation of the repeated sequences of mouse DNA. A mixture of denatured  $^3\text{H}$ -mouse DNA (310  $\mu\text{g}/\text{ml}$ ) and  $^{14}\text{C}$ -Chinese hamster DNA (0.15  $\mu\text{g}/\text{ml}$ ) was annealed at  $50^\circ\text{C}$  for 18 hours in 0.14  $M$  phosphate buffer. 49.6% of the mouse DNA and 25.9% of the hamster DNA subsequently bound to hydroxyapatite and were eluted during the linear temperature gradient.  $^{14}\text{C}$ -hamster DNA which elutes above about  $70^\circ\text{C}$  (3.5% of total) results from a small degree of self-reaction.

reasonable explanation seems to be that the heterologous DNA contains few, if any, sequences complementary to these very stable homologous regions. (5) The high thermal stability material that can be detected in homologous but not in heterologous DNA has presumably appeared in the former since the divergence of the two species. The greater the evolutionary separation of any pair tested, the more of this material is found.

#### SOME OBSERVATIONS ON INTERSPERSION OF DNA SEQUENCES

*Nancy Rice*

The thermal dissociation profiles reported above have suggested that families common to the DNA of both rat and

mouse will associate with comparable stability with either the heterologous or homologous DNA. An alternative method of demonstrating this, however, led to apparently conflicting results.  $^{14}\text{C}$ -mouse DNA (previously incubated to  $C_0t$   $2 \times 10^{-2}$  and then fractionated to remove the most rapidly reassociating material, about 21% of the total DNA) was annealed with excess rat DNA at  $50^\circ\text{C}$  in 0.14  $M$  phosphate buffer, and the reassociated material was isolated on hydroxyapatite. Thus, virtually all of the  $^{14}\text{C}$ -mouse DNA in the isolated fraction was capable of reacting with rat DNA. To determine whether this  $^{14}\text{C}$ -DNA would display the same melting behavior when reassociated with



mouse or rat DNA, aliquots of the fraction were denatured and reassociated with and without added excess mouse DNA. It was found that the  $^{14}\text{C}$ -mouse DNA reacted with significantly greater thermal stability with mouse DNA than with rat DNA. As shown in Fig. 88, the homologous duplex melts over a broader range and with a higher  $T_m$ . Furthermore, when this experiment was performed in the opposite way, namely, with radioactive rat DNA and unlabeled rat and mouse DNA, it was again found that the homologous duplex is more

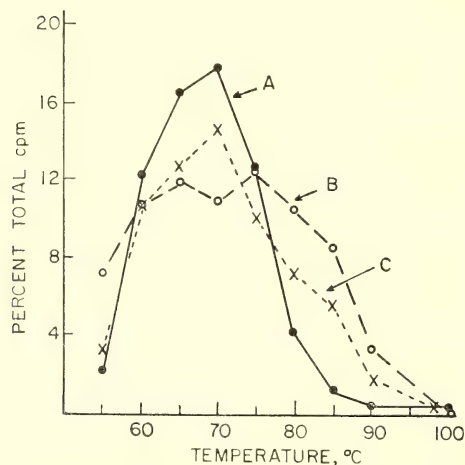


Fig. 88. Thermal stability of homologous and heterologous reassociated DNAs.  $1.6 \mu\text{g}$   $^{14}\text{C}$ -mouse DNA (25,000 cpm/ $\mu\text{g}$ ), sheared at 50,000 psi, was reassociated to  $C_{ot} 1.7 \times 10^{-2}$  in  $0.13 \text{ M}$  phosphate buffer at  $50^\circ\text{C}$ ; the reassociated material (20.7%) was discarded.  $400 \mu\text{g}$  rat DNA was added to the remainder, and the mixture was incubated to  $C_{ot}$  (rat) 1.2. The material retained by hydroxyapatite (19% of total cpm) was collected, divided into three aliquots, treated as follows, and thermally chromatographed on hydroxyapatite. (A) Denatured and reassociated with no additional DNA (69% of cpm reassociated). (B) Denatured and reassociated after addition of  $1900 \mu\text{g}$  mouse DNA, incubation to  $C_{ot}$  (mouse) 2.4 (75% of cpm reassociated). (C) Denatured, reassociated, and the reassociated material isolated in duplex form by  $0.4 \text{ M}$  phosphate buffer elution;  $880 \mu\text{g}$  denatured mouse DNA was added to this fraction and the mixture was incubated in  $0.14 \text{ M}$  phosphate buffer to  $C_{ot}$  (mouse) 3.6.

stable than the heterologous:  $^{14}\text{C}$ -rat DNA that reacted with mouse DNA reacted with even greater average stability with rat DNA.

One possible explanation of these results is that some of the DNA fragments that contain sequences common to both rat and mouse also contain *other* sequences capable of binding only to homologous DNA. Since the thermal stability of reassociated species-specific sequences may be quite high, these DNA fragments would react with greater thermal stability with homologous DNA than with heterologous DNA. Such sequence-coupling, the extent of which should be piece-size dependent, has been demonstrated by isolation of the  $^{14}\text{C}$ -mouse-rat duplex, as described above, followed by incubation of the undenatured duplex with excess denatured mouse DNA. As before, addition of mouse DNA results in increased thermal stability of a portion of the  $^{14}\text{C}$ -mouse DNA, as shown in Fig. 88. In this case, however, the mouse DNA must have reacted with unreassociated portions of an already duplex molecule. Thus, some (possibly up to 25%) of the  $^{14}\text{C}$ -mouse DNA molecules that reacted with rat DNA apparently contained additional sequences able to bind to mouse DNA only. Since the piece size of the  $^{14}\text{C}$ -DNA was quite small (400–500 nucleotides), these results suggest a significant degree of fine-scale sequence interspersion within the mouse genome. (An alternative explanation, that a fragment contains only *one* type of sequence and that the added mouse DNA *displaces* rat DNA from the heterologous duplex to form a more stable homologous duplex, cannot at present be ruled out, but appears unlikely.)

The same phenomenon, namely, the occasional association of sequences of quite different properties, can also be inferred from experiments with rat DNA. As shown in Fig. 85, incubation of  $^{14}\text{C}$ -rat DNA with excess rat DNA results in considerable  $^{14}\text{C}$ -material of

high thermal stability. In contrast, very few duplexes of high thermal stability are formed between  $^{14}\text{C}$ -rat DNA and mouse DNA (Fig. 84). Given the heterologous reaction, one can inquire into the fate of those  $^{14}\text{C}$ -rat DNA sequences capable of forming well-matched products with rat DNA. If these sequences are completely unlinked to those able to bind to mouse DNA, they should appear in the unreassociated fraction (not retained by hydroxyapatite). However, incubation of the unreassociated material with excess rat DNA resulted in only one-half to two-thirds the expected  $^{14}\text{C}$ -material of high thermal stability. It must be presumed, therefore, that the remainder of the sequences in question are coupled to those able to bind to mouse DNA.

To summarize: it appears that a significant fraction of the mouse (or rat) DNA molecules that contain sequences able to bind to heterologous rat (or mouse) DNA under the conditions employed here (DNA piece size of several

hundred nucleotides, incubation at  $50^\circ\text{C}$  in  $0.14\text{ M}$  phosphate buffer) also contains sequences able to reassociate only with the homologous DNA.

The high thermal stability of the species-specific reassociated material provides a basis for its separation from sequences common to rat and mouse DNA. In view of results presented earlier, reassociated  $^{14}\text{C}$ -mouse DNA of low thermal stability might be expected to react equally well (in both extent and stability) with either rat or mouse DNA. Reassociated  $^{14}\text{C}$ -mouse DNA of high thermal stability, on the other hand, can be expected to react with heterologous DNA only to the extent that species-specific and nonspecific sequences coexist on the same DNA molecule. The thermal stability of the heterologous product, furthermore, may be much reduced from that of the homologous. As illustrated in Fig. 89, A and B, these predictions are largely fulfilled.  $^{14}\text{C}$ -mouse DNA (again, previously incubated to  $C_0t\ 3 \times 10^{-2}$  and the reassociated ma-

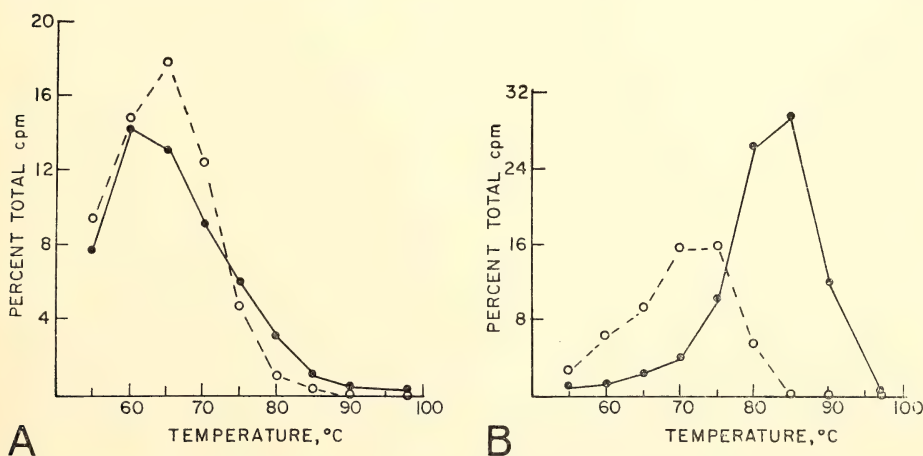


Fig. 89. Reassociation of thermal fractions of mouse DNA.  $2\ \mu\text{g}$   $^{14}\text{C}$ -mouse DNA was incubated to  $C_0t\ 2.8 \times 10^{-2}$  at  $50^\circ\text{C}$  in  $0.12\text{ M}$  phosphate buffer and the reassociated material (21%) discarded. The remainder was incubated to  $C_0t\ 2.1$  and the reassociated material (19.4%) thermally fractionated on hydroxyapatite. One fraction consisted of DNA eluting between  $51^\circ$  and  $70^\circ\text{C}$  (11.3%); a second, of DNA eluting above  $76^\circ\text{C}$  (5.5%). Aliquots of the low stability fraction were incubated with no additional DNA, or with  $625\ \mu\text{g}$  rat (open circles) or mouse (closed circles) DNA to  $C_0t\ 3$  (A). Aliquots of the high stability fraction were incubated with no additional DNA or with  $925\ \mu\text{g}$  rat (open circles) or mouse (closed circles) DNA to  $C_0t\ 3$  (B). Each was then thermally chromatographed on hydroxyapatite.

terial, 21% of the total DNA, removed) was incubated to  $C_0t$  2 (50°C, 0.14 *M* phosphate buffer) and the reassociated material (19.4% of the total) thermally fractionated on hydroxyapatite. Molecules that eluted between 51° and 70°C (11.3% of the total DNA) constituted one fraction; those dissociating at 76°C or above (5.5% of the total DNA) made up a second fraction. Aliquots of each were incubated with excess rat or mouse DNA to  $C_0t$  3. As expected, the low stability fraction displayed a similar thermal stability and extent of reaction with both rat and mouse DNA (56% reacted with mouse DNA, 61% with rat). Reaction of the high stability fraction, however, was very different with rat and mouse DNA. Ninety-one percent of the fraction could reassociate with mouse DNA, with a  $T_m$  over 80°C; but about 55% reassociated with rat DNA, with a  $T_m$  below 70°C. Thus, while most of the DNA molecules in this fraction contain sequences able to bind to mouse DNA with quite high thermal stability, it appears that many also contain sequences able to bind to rat DNA with significantly lower stability. In contrast, the low stability fraction appears relatively free of species-specific sequences and displays similar behavior upon reassociation with either rat or mouse DNA.

This effect, the occasional association of sequences of high and low reassociated thermal stability on a single DNA molecule, is presumably responsible for the results reported previously (*Year Book* 68, pp. 386–388) that thermal fractions of rat DNA show extensive cross-reaction. It is hoped that further studies will quantitate the extent of this interspersion and clarify the effect of DNA piece size.

#### REASSOCIATION PROFILES OF RODENT DNAs

Nancy Rice

The kinetics of reassociation of an organism's DNA provide a useful tool in its characterization and an important

first step in the detailed analysis of its component families. Some aspects of the reassociation of rat and mouse DNAs, monitored both optically and by hydroxyapatite fractionation, have been determined over the past year and are here reported.

The reassociation profile of rat DNA, sheared at 50,000 psi, incubated at widely varying concentrations and times at 50°C in 0.14 *M* phosphate buffer, and fractionated on hydroxyapatite, is displayed in Fig. 90. At this criterion about 50% of rat DNA is found to be composed of repeated sequences. Further, the span of the measurements is extensive ( $C_0t$   $10^{-5}$  to  $C_0t$   $10^4$ ) and indicates a considerable range of repetition frequencies among the elements of the rat genome. Some sequences, which reassociate at  $C_0t$ 's higher than about  $2 \times 10^2$ , appear to be present only once; others, which reassociate at very much lower  $C_0t$ 's, may be present in thousands of copies.

The reassociation profile of rat DNA differs from that of calf DNA (Britten and Smith, *Year Book* 68, pp. 378–386) in the occurrence of material reassociating between  $C_0t$ 's 2 and 200. Thus, whereas calf DNA has no observable element with a repetition frequency less than several hundred, a substantial fraction of rat DNA appears to fall in this class. In this respect, rat DNA resembles salmon DNA (Britten and Kohne, *Year Book* 66, pp. 73–88) rather than that of another mammal, the calf.

A portion of the reassociation profile of mouse DNA is also given in Fig. 90. While of the same general shape and range as that of rat DNA, it reveals significantly more material reassociating during the early stages of the reaction. At  $C_0t$   $3 \times 10^{-2}$ , for example, 20% of mouse DNA, but only 13% of rat DNA, binds to hydroxyapatite. (The mouse satellite, of course, constitutes a substantial fraction of this very rapidly renaturing material.) During the later stages of reaction, from  $C_0t$   $10^{-1}$  to  $10^2$ , the profiles of rat and mouse DNA ap-



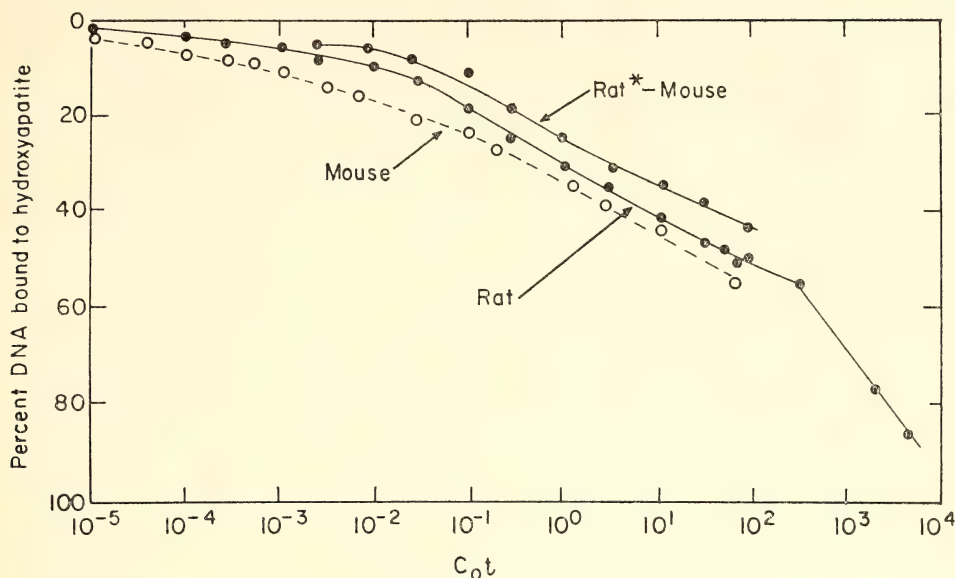


Fig. 90. Reassociation of rat and mouse DNAs.  $^{14}\text{C}$ -rat DNA (closed circles) or  $^{14}\text{C}$ -mouse DNA (open circles) was reassociated at widely varying concentrations and times in  $0.14\text{ M}$  phosphate buffer at  $50^\circ\text{C}$  (with the exception of the two samples of rat DNA falling between  $C_0t$ s  $10^3$  and  $10^4$ , which were incubated in  $0.82\text{ M}$  phosphate buffer at  $63^\circ\text{C}$ ). In each case the amount of material retained by hydroxyapatite was determined. To measure the heterologous reaction,  $^{14}\text{C}$ -rat DNA (held to  $C_0t \approx 10^{-3}$ , self-reaction about 5–8%) was incubated with increasing amounts of mouse DNA in  $0.14\text{ M}$  phosphate buffer at  $50^\circ\text{C}$ , and the amount of  $^{14}\text{C}$ -rat DNA bound by hydroxyapatite was determined.

pear more similar, reassociated rat DNA increasing only slightly faster than mouse DNA.

The families common to both rat and mouse DNA appear to reassociate over a considerable range ( $C_0t \sim 10^{-2}$  to at

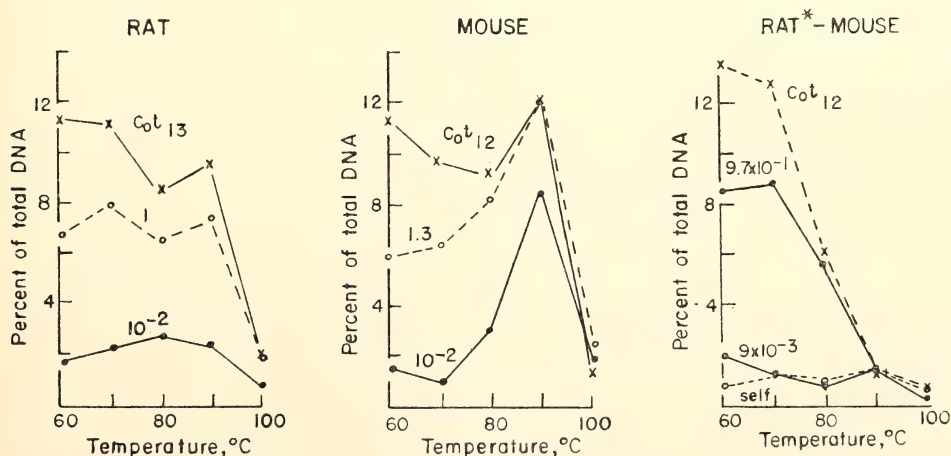


Fig. 91. Thermal dissociation of rat and mouse DNAs at various stages of reassociation. DNAs were annealed as described in Fig. 90, applied to hydroxyapatite in  $0.14\text{ M}$  phosphate buffer at  $50^\circ\text{C}$ , and the amount of material eluting at  $60^\circ$ ,  $70^\circ$ ,  $80^\circ$ ,  $90^\circ$ , and  $100^\circ\text{C}$  measured.

least  $C_0t$   $10^2$ ). As shown in Fig. 90, radioactive rat DNA at low levels has been incubated with mouse DNA at varying concentrations and/or times, and reassociation of the rat DNA determined on hydroxyapatite. Self-reassociation of the rat tracer, held to  $C_0t \sim 10^{-3}$ , ranged from 5% to 8%; reassociation higher than this level is due to formation of heterologous duplexes with the added mouse DNA. It is found that at  $C_0t$ 's greater than  $10^{-2}$  there is a steady increase in the binding of rat DNA, indicating that the elements common to the two genomes are not restricted to a narrow segment of the re-

association profile, but rather represent a considerable range of frequencies.

Homologous and heterologous reassociated duplexes have been characterized according to their thermal stability after varying annealing periods. Each sample was applied as usual to hydroxyapatite at  $50^\circ\text{C}$ ; the temperature was then raised in  $10^\circ$  increments and the amount of material eluted at each step was measured. With rat DNA subjected to any  $C_0t$  value between about  $10^{-3}$  and  $10^2$ , it was found that quite similar amounts of DNA dissociated at  $60^\circ$ ,  $70^\circ$ ,  $80^\circ$ , and  $90^\circ\text{C}$ . These amounts increased with increasing  $C_0t$ , as shown in Fig. 91, but in a roughly parallel way

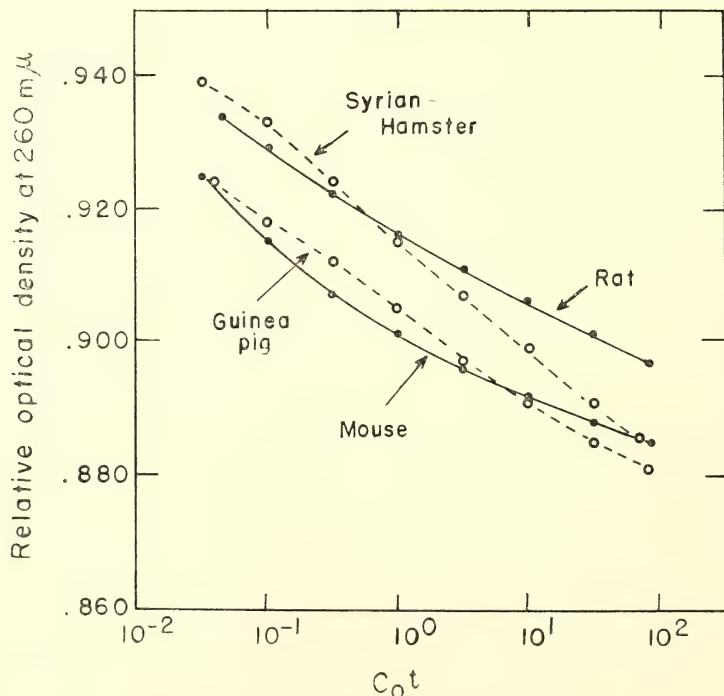


Fig. 92. Optical reassociation profiles of several rodent DNAs. The temperature of each DNA sample (in  $0.28\text{ }M$  phosphate buffer at  $\sim 60\mu\text{g/ml}$ ) was raised to  $98^\circ\text{C}$  in the Gilford recording spectrophotometer and quickly cooled to  $55^\circ\text{C}$  (equilibration time  $< 1.5$  minutes). Reassociation was monitored continuously at  $260\text{ }m\mu$  for about 48 hours. Data is given as Relative Optical Density, taking O.D. at  $98^\circ\text{C}$  to be 1.000; single-stranded DNA under these conditions exhibits a relative O.D. of 0.950. The calculated  $C_0t$  values were corrected for the effect of increased salt concentration on reassociation rate (see Britten and Smith, *Year Book 68*, pp 378-386); the above curves thus represent the decrease in relative O.D. with increasing  $C_0t$  in  $0.14M$  phosphate buffer.

for each thermal fraction. Such is not the case for mouse DNA, where considerable amounts of high thermal stability material (mostly mouse satellite) form at quite low  $C_0t$ 's. By  $C_0t\ 2 \times 10^{-1}$ , in fact, about 14% of the total DNA elutes above 80°C (in 0.14 *M* phosphate buffer); longer  $C_0t$ 's result in little further increase in this very stable material, but in continued accumulation of low thermal-stability products at much the same rate as was observed in rat DNA. Thus, rat and mouse DNAs appear very similar in the amount and frequency of the material that reassociates with low thermal stability; they appear to differ markedly in the amount and frequency of the material that renatures with high stability.

These observations are confirmed by the thermal dissociation profiles of the heterologous duplexes. As seen in Fig. 91, all the DNA common to rat and mouse dissociates at quite low temperatures regardless of the length of incubation. In each case at least 80% of the heterologous product eluted at 70°C or below; there was no detectable material (above the background self-reaction of the rat tracer) eluting at 90° or above. Thus, though heterologous duplexes form over a wide  $C_0t$  range, they are exclusively of rather low thermal stability.

The optical reassociation profiles of several rodent DNAs also show both similarities and differences. In each case unfractionated DNA (sheared at 50,000 psi) was annealed at about 60  $\mu\text{g/ml}$  at 55°C in 0.28 *M* phosphate buffer for about two days, sufficient to allow reassociation of most of the repeated sequences. The results, shown in Fig. 92, are plotted as the fractional decrease in optical density with time, taking the O.D. at 98°C to be 1.000. The very rapidly renaturing components of rat DNA result in a modest decrease (6.6%) in relative O.D. by  $C_0t\ 5 \times 10^{-2}$ . (Single-stranded DNA in 0.28 *M* phosphate buffer exhibits a 5% O.D. drop upon lowering the temperature from 98° to

55°C.) Thereafter, the relative O.D. gradually declines, the profile generally paralleling the increase in hydroxyapatite binding. The profile of mouse DNA is of the same general shape, but the decrease in relative O.D. by  $C_0t\ 2 \times 10^{-2}$  is significantly greater (7.5%). Thus, predictably, the very rapidly reassociating material of high thermal stability exhibits considerable hyperchromicity. Thereafter, as in the hydroxyapatite assay, the profile of mouse DNA roughly parallels that of rat.

Syrian hamster DNA, like rat DNA, possesses a comparatively small amount of very rapidly renaturing material. Guinea pig DNA, on the other hand, resembles mouse DNA in this respect. With both hamster and guinea pig DNA the decline in relative O.D. in the later stages of reassociation ( $C_0t > 3 \times 10^{-1}$ ) is greater than that observed for either rat or mouse DNA. This indicates either a very sizable fraction of the DNA reassociating in this range, or a high degree of sequence similarity among members of families of modest size.

It is hoped that the resolution of these DNAs into specific families will provide useful information regarding their nature and origin. The reassociation profiles described above represent the initial steps in this direction.

#### PATTERN OF DNA ACQUISITION DURING EVOLUTION

*D. E. Kohne*

Families of repeated DNA sequences held in common between two species presumably have been inherited from their most recent common ancestor. These families are composed of member sequences that are more divergent than the member sequences of families *not* held in common between two species. The best evidence yet for this is presented in an earlier section (Nancy Rice, page 472). Repeated DNA *not* held in common between two species has ap-



TABLE 22. Rate of Addition of Repeated DNA to Specific Mammalian Genomes during Evolution  
(For technical reasons the hydroxyapatite measurements should give more accurate values  
than those derived from DNA-agar).<sup>†</sup>

Animal DNAs Compared	Fraction of Repeated DNA Not Held in Common	Fraction of Total Radio- active DNA as Repeated DNA	Present- day Genome Produced since Diver- gence, %	Years since Diver- gence, $\times 10^6$	DNA Added per 10 <sup>6</sup> Years since Diver- gence, %	Source of Data	Criterion	Radioactive DNA Piece Size and Method of Reassociation
Mouse *-rat	0.37	0.35	13	10	1.3	Hoyer & Roberts 1967	0.4 M Na <sup>+</sup> , 60°C	$\sim 5 \times 10^5$ daltons DNA-agar
Mouse *-rat	0.44	0.35	16	10	1.6	McClaren & Walker, 1965	0.4 M Na <sup>+</sup> , 60°C	$\sim 5 \times 10^5$ daltons DNA-agar
Mouse *-rat	0.36	0.53	20	10	2.0	Rice ( <i>Year Book 69</i> )	0.21 M Na <sup>+</sup> , 51°C	$1.3 \times 10^5$ daltons hydroxyapatite
Rat *-mouse	0.20	0.50	10	10	1.0	Rice ( <i>Year Book 69</i> )	0.21 M Na <sup>+</sup> , 51°C	$1.3 \times 10^5$ daltons hydroxyapatite
Rat *-mouse	0.19	0.35	6.7	10	0.67	McClaren & Walker, 1965	0.4 M Na <sup>+</sup> , 60°C	$5 \times 10^5$ daltons DNA-agar
Mouse *-hamster	0.46	0.35	16	35				
Mouse *-guinea pig	0.65	0.35	22.7	55				
Human *-gibbon	0.06	0.35	2.1	30		Hoyer & Roberts, 1967	0.4 M Na <sup>+</sup> , 60°C	$5 \times 10^5$ daltons DNA-agar
Human *-rhesus	0.12	0.35	4.2	45				
Human *-capuchin	0.17	0.35	6.0	65				
Human *-galago	0.42	0.35	14.7	75				
Human *-tree shrew	0.79	0.35	28	100				

\* Radioactive DNA.

<sup>†</sup> Where differences in repeated DNA held in common between species can be detected, the fixation rate can be more accurately measured for closely related species comparison. The known sources of error are such that fixation rates for distantly related species are likely to be underestimated because: (1) some members of families produced since the divergence of the two species may be lost from the repeated DNA fraction by nucleotide sequence divergence; (2) members of older families of repeated sequences tend to be interspersed to a greater extent among the other sequences of the genome (see earlier section). This leads to a single piece of DNA containing both an old and a new family member. In this case the "new" sequence will be carried along in the reaction of the "old" sequence with the DNA of another species. This will result in an underestimate of the amount of repeated DNA *not* held in common between two species. Both these factors lead to underestimating the amount of repeated DNA fixed since the time of divergence of two distantly related species. Therefore, the factor of 3 seen between the fixation rates observed for the man-gibbon versus the man-galago periods is believed to be quite significant (see Table 23).

parently been introduced since the time of divergence of the two species. The ratio of the quantity of repeated DNA *not* held in common and the time since divergence yields a measure of the rate of introduction of new families of repeated DNA sequences into the genome. The interpretation of this rate is influenced by several considerations: (1) This is an *average* rate and reflects the amount of DNA added since the time of divergence of two species lines. The time needed for the production of a repeated family is probably much shorter than the divergence time. The actual rate of addition during the time when a new family was being introduced is not known. The *average* rate observed very probably reflects several events of new family production since the time of divergence. (2) The observed rate reflects only those families of repeated DNA that have been *fixed* in species line. The

actual rate of production of repeated sequences is not known, since many new families may not become fixed in the species line. (3) The rate observed cannot be interpreted as the rate of genome growth, since nothing is known about rates of loss of DNA from the genome during the evolution of a species. The rate observed is then the average *rate of fixation* of repeated DNA into the genome of a species line.

Since the time of divergence of mouse and rat, the rate of repeated DNA fixation into the mouse genome has been about twice as fast as in rat (Table 22). Most of this difference could be accounted for by the satellite fraction of mouse DNA which comprises 10–15% of the total DNA. Both mouse and rat genomes have experienced a much higher rate of fixation over the last 10–20 million years than have primates (Table 23). The magnitude of the difference in

TABLE 23. Rates of Addition of Repeated DNA to Mouse and Human Genomes during Different Evolutionary Periods.\*

Evolutionary Period	Length of Period, years $\times 10^6$	Percent of Present-Day Genome Added During This Period	Average Rate of Addition During This Period, percent per $10^6$ years
TOD † man-gibbon to now	30	2.1	0.07
TOD man-rhesus to now	15	2.1	0.14
TOD man-gibbon to now	20	1.8	0.09
TOD man-rhesus to now	10	8.7	0.87
TOD man-galago to now	25	13.3	0.53
TOD man-capuchin to now	10	13	1.3
TOD mouse-rat to now	25	3	0.12
TOD mouse-rat to now	20	6.7	0.33
TOD mouse-guinea pig to now			
TOD mouse-hamster to now			

\* DNA-agar data from Hoyer and Roberts, 1967 (see Table 22) were used for the above calculations.

† Time of divergence.

fixation rate between rodents and primates is comparable to the magnitude of the difference between the rates of nucleotide sequence change for these creatures (see the following section, Tables 24, 25).

The pattern of rates of fixation of repeated DNA for various primate species lines is also similar to the pattern seen for the rates of nucleotide sequence change (seen in the next section) for primates. Both parameters show an apparently decreasing rate of change with time. The rate of nucleotide sequence change appears to be generation-time dependent (see next section). The similarity of the patterns of rates of nucleotide sequence change and fixation of repeated DNA suggests that the rate of fixation is also generation-time dependent.

### *Genome Growth*

It seems clear that many events of new repeated DNA family formation have occurred during the evolution of most higher organisms. These saltatory replication events (*Year Book 65*, p. 103) have probably been the source of the majority of higher organism DNA sequences. The average rate of DNA fixation in the mouse genome (since its divergence from rat) has resulted in the addition of a quantity of DNA equal to 1.4% of the present-day genome every million years. At this rate the mouse genome would double its present size in about 50 million years. Other mechanisms for genome growth, such as polyploidy or polyteny would tend to amplify the contribution due to the saltatory events.

The striking difference between primates and rodents in the rate of DNA addition is probably due to a generation-time dependence of some aspect of the saltatory replication event. The available evidence (Table 22) does indicate that the shorter generation-time creatures add DNA more rapidly than those

species with longer generation times. There should then be predictable differences between the genome sizes of different existing mammalian species. The available genome size data has too much variation and is not accurate enough to test this prediction. If more accurate determinations show no differences in the genome sizes of various mammals, this would strongly suggest that a significant DNA loss mechanism has been working during mammalian evolution. Comparison of patterns of DNA addition and of fossil cell sizes with present-day cell sizes may corroborate any genome size differences observed, since the size of present-day cells is roughly proportional to their DNA content.

### NUCLEOTIDE SEQUENCE CHANGE IN NONREPEATED DNA DURING EVOLUTION

*D. E. Kohne, J. A. Chiscon, and B. H. Hoyer*

Much information about the evolution of DNA has been gained by using DNA reassociation techniques to compare the DNA of different species. Studies of this type permit the correlation of information derived from fossil records with that obtained biochemically. From this synthesis new insights into evolutionary processes have been gained. The following section examines the divergence patterns of nonrepeated and repeated DNA of certain mammals.

### *Rationale of Experiments*

To determine the rate of nucleotide sequence change since the divergence of various species one must know: (1) the time since the divergence of the species in question, and (2) the number of nucleotide changes that have occurred during that time. Paleontology provides us with estimates of (1), and the number of nucleotide changes can be experimentally determined. Complementary DNA strands from different animal species can interact to form a "hybrid"



reassociated double-strand DNA molecule. One strand of this "hybrid" molecule is radioactive and is from one species, while the other is nonradioactive and from a different species. If the two strands are only partially complementary in the reassociated region, the "hybrid" reassociated DNA will have a lower thermal stability than perfectly base-pair matched DNA. The difference in thermal stability between the "homologous" and "hybrid" double-strand DNA is a measure of the extent of nucleotide changes that have occurred since divergence of the two species in question (Year Book 66, p. 80; Laird, *et al.*, 1969). A reasonable estimate of the actual percentage of nucleotide changes can be obtained by using the relationship: a 1.5% nucleotide pair mismatch lowers the thermal stability 1°C (Fig.

93). The value for percent base changes that have occurred since divergence is an average divergence value for the many different nucleotide sequences present in the DNA used for the experiment.

A primary requirement for comparing the DNAs of different species is that the DNA of one species forms predominantly "hybrid" double-strand DNA molecules during the incubation period. This requirement can be met by properly adjusting the radioactive and nonradioactive DNA concentrations to control the rates of reassociation. The radioactive DNA used must be kept at a low enough concentration so that the collision of two radioactive complementary strands is very improbable. The nonradioactive DNA concentration must be high enough so that virtually all of the nonradioactive DNA sequences will

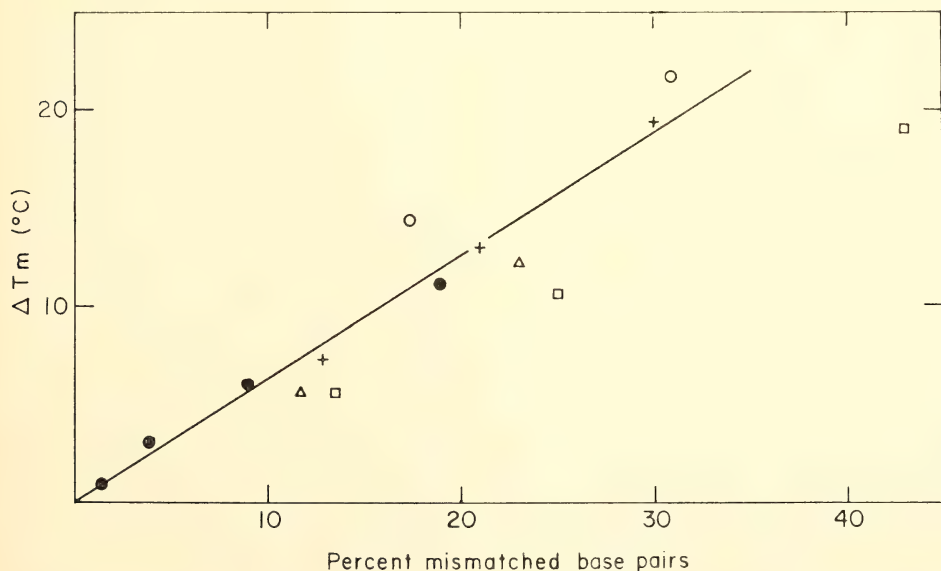


Fig. 93. Relationship between thermal stability and mismatched base pairs for various polynucleotides. The difference between the thermal stability of untreated reassociated polynucleotides and that of altered reassociated polynucleotides is plotted against the percent of mismatched base pairs caused by the altered polynucleotides. The thermal stabilities of duplexes between co-ribopolymers AU (+), AG (□, Δ) or AC (O) with poly U was taken from Bautz and Bautz,<sup>185</sup> and Uhlenbeck *et al.*<sup>186</sup> and illustrates the effect of particular non-complementary base pairs. Data on the thermal stability of nitrous acid treated *B. subtilis* R-RNA reassociated with *B. subtilis* DNA (O) was obtained from Laird. The line drawn is purposely biased toward the situation seen for ribosomal RNA and poly AU, AC values, since it is believed that these data are more representative of the situation for DNA of normal (42% G + C) composition.

find complementary sequences and re-associate during the time of incubation. Thus, a radioactive DNA strand will form a stable double-strand "hybrid" molecule only *if there is a complementary sequence for it in the nonradioactive DNA*.

Not all of the DNA of higher organisms is suitable for such experiments. The fraction containing repeated sequences is diverse even within one species, and the differences observed between the repeated sequences of two species cannot be assumed to have occurred since the time of divergence of these species.

Nonrepeated DNA sequences, on the other hand, comprise a large fraction of mammalian DNA (40–60%) and each sequence occurs only one time per haploid cell. Reassociated, nonrepeated DNA has a thermal stability that indicates that essentially perfect nucleotide pair matching is present. Nonrepeated DNA sequences held in common between species must be the descendants of the same common ancestor sequence that was present in the most recent common ancestor. Nonrepeated DNA is therefore highly suitable for determining the extent of nucleotide change since the divergence of two species.

#### *Probable Nature of Nucleotide Changes*

Point mutations result in the exchange of one base of the DNA for another. Depending on the function of the particular segment of DNA affected, such a change may have a wide range of possible effects on the organism. We can visualize one class of DNA that has no function whatsoever. Any mutation occurring in this DNA has no effect on the organism and all such changes can be passed on to the progeny. After a long period of evolution such DNA could be expected to retain only 25% of its nucleotides in common with its ancestral sequence.

At the other extreme there may be classes of DNA involved in regulation or in acting as templates for certain classes

of RNA wherein any change in the sequence is significant. A large share of these changes can be expected to be deleterious and therefore eventually eliminated from the population. Such a class of DNA can be expected to suffer as many "hits" as any other class but the changes will not be passed along. The genes for ribosomal RNA may be examples of this class of highly conserved DNA where the sequence differences are minimal, even after long periods of evolution (Sinclair and Brown, 1968;<sup>160</sup> *Year Book* 67, p. 404).

Another class of DNA can be defined as that DNA which determines the templates for proteins requiring an unchanged sequence of amino acids. Due to the redundancy of the code, however, some changes in such DNA could be tolerated. One-third of the possible mutations will occur in the third position of the codons and a considerable proportion of these will only change the transfer RNA needed to carry the same amino acid. Thus, roughly one-fourth of the mutations can produce changes to be propagated, and the resulting difference after a long period of evolution will approach 17%. The histone protein that is carried in common by calf and pea may be an example of the product of this type of DNA. Presumably, the DNAs coding for these would differ by 17%.

Finally, the remainder of the DNA can be considered in a class intermediate between these more readily defined extremes. Some changes could be tolerated because of redundancy in the code, or because the replacement of one amino acid by another made no difference, while in adjacent locations any change might be lethal. The proportions of allowed and prohibited changes might vary from one extreme to the other in this class of DNA.

A crude estimate of the quantities of DNA in these various classes can be derived from the stability of the hybrid DNAs formed between two diverged species, as will be explained below.

### *Extent of Nucleotide Change Since the Divergence of Various Mammals*

The basic experiments involve reassociating radioactive nonrepeated DNA from various animals with total non-radioactive DNA prepared from the same or from other organisms. These reaction mixtures are then assayed for the extent of reassociation and the thermal stability of the reassociated fraction.\*

\*The basic experimental procedure followed for these studies was: Mix a large amount of nonradioactive DNA (2-4 mg in less than 1 ml) with a small amount of nonrepeated radioactive DNA (1-2  $\mu$ g). Add EDTA ( $pH=8.0$ ) to a final concentration of 2.5 mM and dissociate the DNA by placing the vial in boiling water bath for one minute. EDTA helps prevent degradation of the DNA during incubation. Care should be taken to heat the DNA for as short a time as possible when the DNA is in a solution of a low salt concentration. After heating, make the DNA to 0.8 M PB (1.2 M  $Na^+$ ) and incubate the mixture at 63°C. The DNA was incubated to a DNA *Cot* equivalent to 10,000 in 0.14 M PB 51°C (at 2 mg/ml of nonradioactive DNA in 0.8 M PB, this involves incubating the DNA for about 90 hours at 63°C). The final volume was 1 ml. At the end of the incubation period freeze the samples for later analysis. For analysis take an aliquot of the sample (about 400 micrograms of DNA) and adjust the salt concentration to 0.14 M PB and pass this sample over a water-jacketed hydroxyapatite (2 grams of Bio Rad HTP) column equilibrated to 51°C and 0.14 M PB. Wash the unreassociated DNA off the column. The thermal stability of these samples was measured by raising the temperature of the column automatically (0.9°C rise in 2.5 min.) and collecting, with a fraction collector, the effluent (0.14 M PB) which pumped through the column at about 5 ml/minute. Each point on Figs. 94 and 95 represents 40 ml of effluent (0.14 M PB) and a 1.8°C temperature rise. After collection, precipitate each fraction, collect on a filter, and assay for radioactivity with a scintillation spectrometer. In order to gain maximum reproducibility, the thermal elution procedure was completely automated. Thermal stabilities were easily reproduced to  $\pm 0.4^\circ C$ . For the sake of efficiency some of the incubation mixtures contained nonrepeated DNA from two different species ( $H^3$ -man DNA and  $C^{14}$ -green monkey DNA). These DNAs were at such low concentration that they were unable to react significantly with themselves (i.e.,  $H^3$ -DNA with  $H^3$ -DNA) or with each other ( $H^3$ -DNA with  $C^{14}$ -DNA).

Radioactive nonrepeated DNAs can be obtained by reassociating the radioactive DNA (human, green monkey, mouse) for a sufficient time to reassociate the repeated DNA sequences. The DNA is then fractionated on hydroxyapatite and the nonrepeated fraction isolated.

Figures 94 and 95 present thermal stability profiles obtained in these experiments, while Tables 24 and 25 summarize the data of these experiments. The stability profiles of human-chimp and human-gibbon hybrids show several qualitative features of significance. Almost all the human DNA reacted with the DNA of either species. Thus, no large class of DNA has diverged so rapidly that hybrids cannot be formed at this temperature of incubation. At the

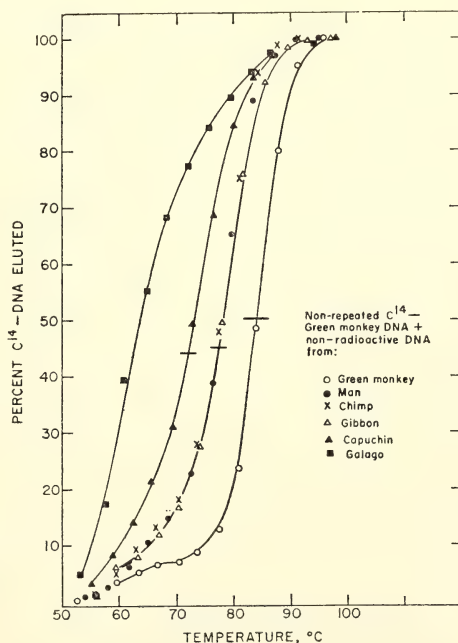


Fig. 94. Thermal stability profile of "hybrid" double-stranded DNA molecules formed between radioactive ( $H^3$ ) nonrepeated DNA of man and other nonradioactive primate DNAs.<sup>166</sup> Control thermal stability profiles ( $H^3$ -human nonrepeated DNA plus nonradioactive human DNA and  $C^{14}$ -green monkey nonrepeated DNA plus nonradioactive green monkey DNA) are also shown.



TABLE 24. Absolute Time-Based Rates of Change

DNAs Reacted	Molecular Data			Interpretation Based on Paleontological Evidence				
	Percent Binding †	Percent Normalized Reaction	T <sub>50</sub> R	ΔT <sub>50</sub> R	Percent Nucleotide Change	Millions of Years since Divergence	Total Divergence Time	Percent Nucleotide Change per Million Yrs. ‡
Man * to man	81	100	82.9	0	0	0	0	...
Man * to chimp	76.5	94.6	81.2	1.7	2.6	~15	30	~.09
Man * to gibbon	73.7	91	78.8	4.1	6.2	~30	60	~.1
Man * to green monkey	71	88	76	7	10.5	~45	90	~.12
Man * to rhesus	72	89	76.2	6.7	10.1	~45	90	~.11
Man * to capuchin	67	83	71.3	11.6	17.4	~65	130	~.13
Man * to galago	32	39.6	~47	~36	~54	~80	160	~.36
Man * to rat	10.3	13	...	...	...	~80-100	...	...

\* Radioactive nonrepeated DNA.

† The binding observed for radioactive DNA alone (2%) incubated for a comparable period of time has been subtracted and the remaining values presented.

‡ Assumes unique genome size =  $2 \times 10^9$  NTP.

TABLE 25. Absolute Time-Based Rates of Change

DNAs Reacted	Molecular Data			Interpretation Based on Paleontological Evidence				
	Percent Binding †	Percent Normalized Reaction	T <sub>50</sub> R	ΔT <sub>50</sub> R	Percent Nucleotide Change	Millions of Yrs. since Divergence	Total Divergence Time	Percent Nucleotide Change per Million Yrs.
GM * to GM	84.5	100	84.4	0	0	0	0	
GM * to rhesus	82.7	98	82.5	1.9	2.9	~15	30	0.1
GM * to man	78.5	93	77.4	7.0	10.5	~45	90	0.12
GM * to chimp	76.4	90.5	77.2	7.2	10.8	~45	90	0.12
GM * to gibbon	77.2	91.4	77.4	7.0	10.5	~45	90	0.12
GM * to capuchin	73.1	86.6	72.1	12.3	18.5	~65	130	0.14
GM * to galago	36.6	43.4	~47	~36	~54	~80	160	~0.36
Mouse * to rat	60	70	63.4	22.3	33.4	~10	20	1.67
Cow * to sheep ‡	84	93	78	7	10.5	~25	50	.21
Cow * to pig ‡	50	59.5	65	20	30	55	110	.27

\* Radioactive nonrepeated DNA.

† The value obtained for radioactive DNA incubated alone (4%) has been subtracted to give the values presented.

‡ Data from Laird, *et al.* (4).

§ Assumes unique genome size  $\approx 2 \times 10^9$  nucleotide pairs.

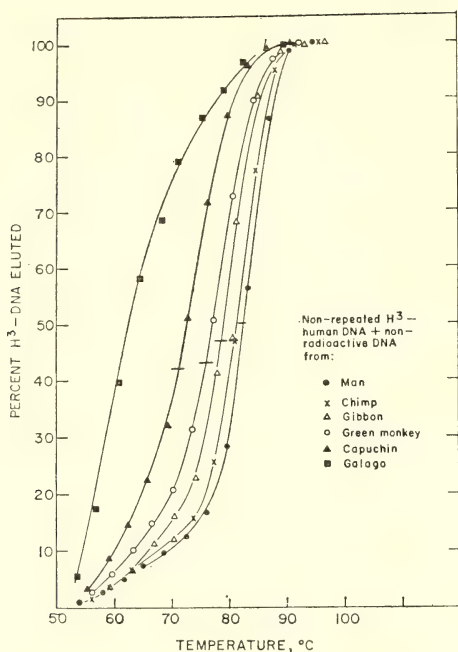


Fig. 95. Thermal stability profile of "hybrid" double-stranded DNA molecules formed between radioactive ( $C^{14}$ ) nonrepeated green monkey DNA and other nonradioactive primate DNAs. Control as in Fig. 94.

other extreme almost all the DNA has diverged appreciably, so there is very little of the highly conserved class of DNA. The widths of the hybrid melting curves are slightly greater than would be expected from a statistical spread, indicating that some fractions of the DNA may be slightly conserved relative to the rest of the DNA.

In comparing the divergence of DNAs of different pairs of species the same sequences must be compared. For the purposes of the calculations and considerations to follow, we have compared the average divergence of *all* the non-repeated DNA. This is estimated from the temperature at which 50% (normalized to the homologous reaction) of the total radioactive DNA is in a hybrid form ( $T_{50R}$ ). For the human-galago hybrids this is estimated to be 47°C. This estimate is based on the assumption

that differences between human and galago are due to divergence and not to the addition of unrelated sequences.

Both the extent of reassociation between the various primate DNAs and the thermal stability measurements agree with the classical paleontological view of the relationships between the primates tested (Simons, 1964).<sup>161</sup> As expected, for example, chimp is most closely related to man, and rhesus to green monkey. Tables 24 and 25 also present the calculated values for the rates of nucleotide sequence change since the divergence of various species.

Figure 96 depicts the present-day view of the phylogenetic relationships among the primates studied here. Chimp and man diverged from their most recent common ancestor about 10–20 million years ago. The extent of divergence for the DNAs is then the sum of changes occurring since divergence in the chimp line, plus those occurring in the human line. The difference seen between chimp and human DNAs today ( $\sim 2.5\%$ ) is equal to  $\Delta A$  (the percent of nucleotide changes occurring in the human line) plus  $\Delta F$  (the percent changes occurring in the chimp line). An average rate of change is then  $\Delta A + \Delta F$  divided by the total divergence time (30 million years) since chimp and man separated. The rate values in Tables 24 and 25 are calculated on this basis and are average values, not individual values of  $\Delta A$  and  $\Delta F$ .

Figure 96 and Table 26 also present the data of Tables 24 and 25 in terms of the above discussion and assign symbols for various evolutionary time periods as defined by divergence points.

The values of  $\Delta A$ ,  $\Delta B$ ,  $\Delta C$ ,  $\Delta F$ ,  $\Delta G$ ,  $\Delta H$ ,  $\Delta I$ ,  $\Delta J$  can be directly determined, while the values for  $\Delta D$ ,  $\Delta E$ ,  $\Delta K$ , and  $\Delta L$ , can be estimated. Table 27 presents the calculations and summarizes the results obtained. Again, by using paleontological data on times of divergence of these primates, the rates of change of nucleotide sequences can be calculated



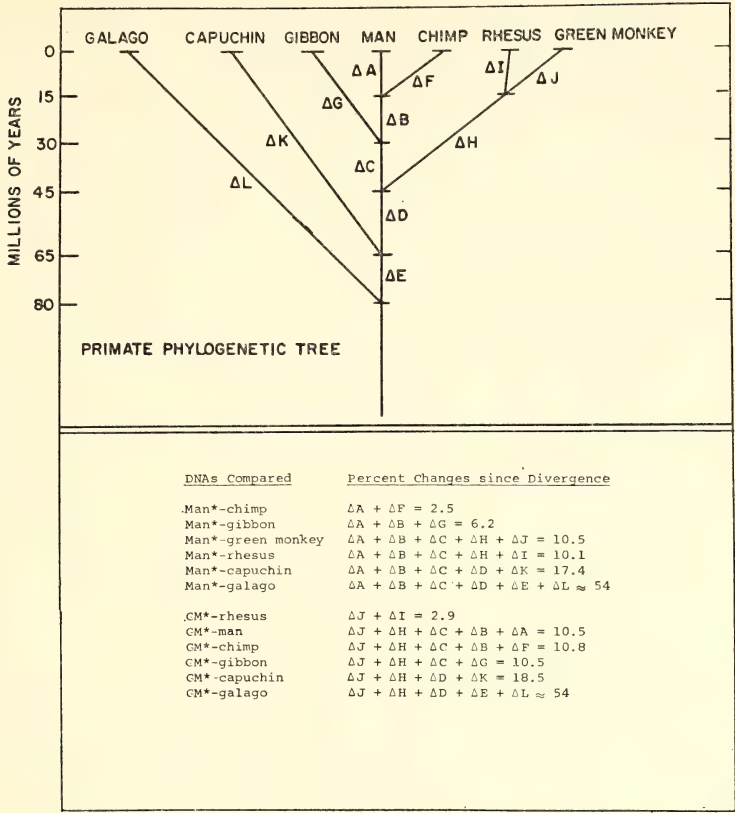


Fig. 96. Primate phylogenetic tree with symbols assigned to various time periods of the primate evolutionary history. Also shown are the equations resulting from the data shown in Figs. 94 and 95 and Tables 23 and 24. Each value represents the average of two or more thermal stability profiles. Values were reproducible to  $\pm 0.4^{\circ}\text{C}$ .

TABLE 26. Equations Representing the Observed Primate Nucleotide Sequence Differences

DNA's Compared	Percent Changes since Divergence
Man *-chimp	$\Delta A + \Delta F = 2.5$
Man *-gibbon	$\Delta A + \Delta B + \Delta G = 6.2$
Man *-green monkey	$\Delta A + \Delta B + \Delta C + \Delta H + \Delta J = 10.5$
Man *-rhesus	$\Delta A + \Delta B + \Delta C + \Delta H + \Delta I = 10.1$
Man *-capuchin	$\Delta A + \Delta B + \Delta C + \Delta D + \Delta K = 17.4$
Man *-galago	$\Delta A + \Delta B + \Delta C + \Delta D + \Delta E + \Delta L \approx 54$
GM *-rhesus	$\Delta J + \Delta I = 2.9$
GM *-man	$\Delta J + \Delta H + \Delta C + \Delta B + \Delta A = 10.5$
GM *-chimp	$\Delta J + \Delta H + \Delta C + \Delta B + \Delta F = 10.8$
GM *-gibbon	$\Delta J + \Delta H + \Delta C + \Delta G = 10.5$
GM *-capuchin	$\Delta J + \Delta H + \Delta D + \Delta K = 18.5$
GM *-galago	$\Delta J + \Delta H + \Delta D + \Delta E + \Delta L = 54$

\* Radioactive DNA.

for times early in the development of the primates as well as late.

Estimates of  $\Delta D$ ,  $\Delta E$ , and  $\Delta K$  were made by assuming that after divergence the number of changes in each line was approximately the same. This clearly is the case in periods where definite data are available (Table 27). For example, after the divergence of human and green monkey lines, the extent of change in

the human line and in the green monkey line is roughly the same. A similar situation exists for the human-chimp and human-gibbon lines. The estimated value for  $\Delta E$  is probably low due to multiple changes which have occurred at many of the nucleotide sites.

Figure 97 presents these calculations superimposed on the primate phylogenetic tree. These values indicate that

TABLE 27. Solutions for Equations of Figure 96 (from Kohne *et al.*, 1970)

(1)	$\frac{\Delta A + \Delta B + \Delta C + \Delta H + \Delta J = 10.5\%}{\Delta A + \Delta B + \Delta C + \Delta H + \Delta I = 10.1\%}$ <p>(man-green monkey) (man-rhesus)</p> $\Delta J - \Delta I = 0.4\%$
(2)	$\frac{\Delta J + \Delta I = 2.9\%}{\Delta J - \Delta I = 0.4\%}$ <p>(green monkey-rhesus)</p> $2\Delta J = 3.3\%$ $\Delta J = 1.65\% \quad \text{Therefore } \Delta I = 1.25\%$
(3)	$\frac{\Delta J + \Delta H + \Delta C + \Delta B + \Delta F = 10.8\%}{\Delta J + \Delta H + \Delta C + \Delta B + \Delta A = 10.5\%}$ <p>(green monkey-chimp) (green monkey-man)</p> $\Delta F - \Delta A = 0.3\%$
(4)	$\frac{\Delta F + \Delta A = 2.5\%}{\Delta F - \Delta A = 0.3\%}$ <p>(man-chimp)</p> $2\Delta F = 2.8\%$ $\Delta F = 1.4\% \quad \text{Therefore } \Delta A = 1.1\%$
(5)	$\frac{\Delta J + \Delta H + \Delta C + \Delta G}{\Delta J + \Delta H + \Delta C + \Delta B + \Delta A} = \frac{10.5\%}{10.5\%}$ <p>(green monkey-gibbon) (green monkey-man)</p> $\Delta G - \Delta B - \Delta A = 0$
(6)	$\frac{\Delta A + \Delta B + \Delta G = 6.2\%}{\Delta A - \Delta B + \Delta G = 0}$ <p>(man-gibbon)</p> $2\Delta G = 6.2\%$ $\Delta G = 3.1\% \quad \text{Therefore } \Delta B = 2.0\%$
(7)	$\frac{\Delta J + \Delta H + \Delta D + \Delta K}{\Delta A + \Delta B + \Delta C + \Delta D + \Delta K} = \frac{18.5\%}{17.4\%}$ <p>(green monkey-capuchin) (man-capuchin)</p> $\frac{\Delta J + \Delta H - \Delta A - \Delta B - \Delta C = 1.1\%}{1.65 + \Delta H - 1.1 - 2.0 - \Delta C = 1.1\%}$ $\Delta H - \Delta C = 2.55\%$
(8)	$\frac{\Delta J + \Delta H + \Delta C + \Delta G = 10.5\%}{\Delta H + \Delta C = 5.75\%}$ <p>(green monkey-gibbon)</p>
(9)	$\frac{\Delta H + \Delta C = 5.75\%}{\Delta H - \Delta C = 2.55\%}$ $2\Delta H = 8.30\%$ $\Delta H = 4.15\% \quad \text{Therefore } \Delta C = 1.60\%$
(10)	<p>Since <math>\Delta A + \Delta B + \Delta C \simeq \Delta H + \Delta J</math> and <math>\Delta G \simeq \Delta B + \Delta A</math> Assume that <math>\Delta K \simeq \Delta A + \Delta B + \Delta C + \Delta D \simeq 9\%</math> Then <math>\Delta D \approx 4.3\%</math></p>
(11)	<p>Assume also that: <math>\Delta L \simeq \Delta E + \Delta D + \Delta C + \Delta B + \Delta A \simeq 27\%</math> Then <math>\Delta E = 18\%</math></p>

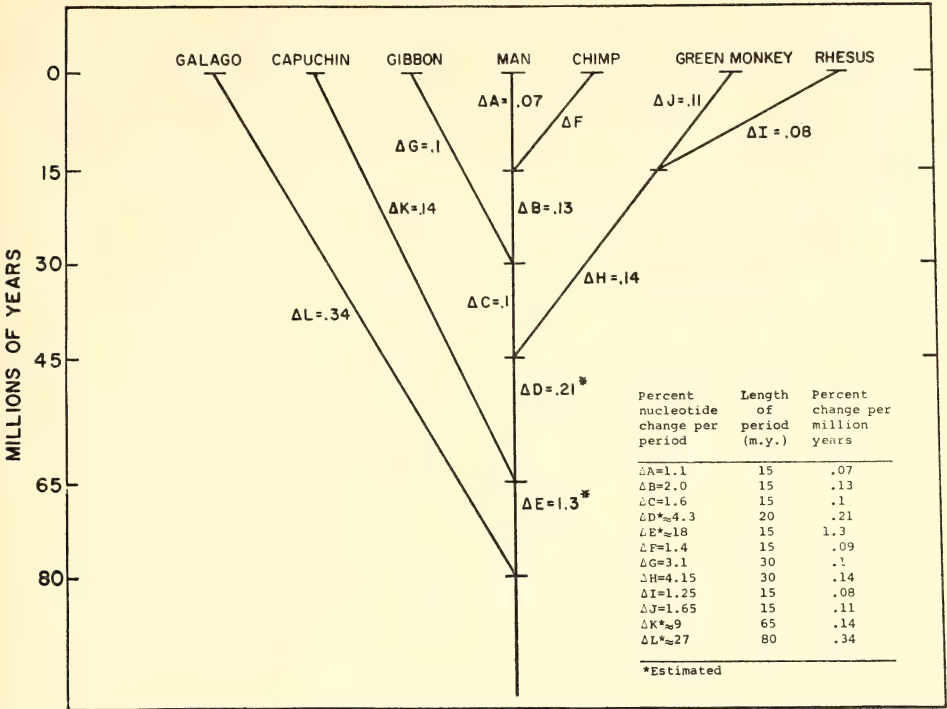


Fig. 97. Primate phylogenetic tree with nucleotide pair rate of change values calculated for the different periods of primate evolutionary development.

when calculated on an absolute time basis the rate of nucleotide sequence change in the primate line leading to man has been decreasing. The rate of nucleotide sequence change has apparently slowly decreased during the last 65–70 million years for the whole primate line. Rhesus and green monkey diverged from each other at roughly the same time as man and chimp diverged. The rate of change of the DNAs of rhesus and green monkey since their divergence is quite comparable to that of the chimp and man since their divergence and again suggests the slowing of the rate of change.

Table 25 also presents rodent DNA divergence data and data obtained (Laird, *et al.*, 1969) for the bovine line. Rat and mouse diverged about 5–10 million years ago. During that time many nucleotide changes have occurred.

Calculated on an absolute time basis the rate of change of rodent nucleotide sequences is about 10 times faster than the rate for the primate or bovine line. This is a fascinating observation, since rodents are known to have undergone extensive radiative speciation in recent evolutionary times (Simpson, 1959).<sup>162</sup> Fossil evidence suggests that primates underwent extensive radiative speciation about 60 million years ago (Romer, 1966).<sup>163</sup> It is of interest to note that during that time (ΔE on Fig. 97) the rate of change in the line leading to primates is comparable to that of the rodents during present evolutionary times. It will be of interest in other species lines to determine whether this greatly increased rate of nucleotide change is a characteristic feature of extensive speciation.



*Generation Time Correlation of  
Rate of Nucleotide Change*

Table 28 shows the values obtained when the rate of nucleotide sequence change is calculated in terms of generation time. The generation time used for the calculation was in each case the shortest generation time of the two animals compared. The rates calculated on this basis are surprisingly similar. Table 28 also includes data for the rat-mouse nonrepeated DNA comparisons and data on cow-sheep and cow-pig comparisons done by Laird, *et al.*, 1969. The rates of divergence seen in these lines are very similar to the primate value, even though wide differences in generation times exist.

The data of Table 28 give very strong indication that the mutational events seen in evolution are generation-time dependent. It seems highly improbable that fluctuating mutational events in each of the three groups could fortuitously give essentially the same result. Implied in the values calculated for Table 28 is that the present-day generation times provide reasonable estimates

of the generation-time history of the various species lines.

If mutational events are generation-time dependent, the basic mutational mechanism is probably involved with the DNA replication cycle in some way. Since it is known that the number of mutations observed in bacteria appear to be dependent upon the number of cell divisions the bacteria undergo, it is reasonable to assume that a similar situation exists in mammalian cells. In light of this an approximate value for the number of base changes per germ cell division is also presented in Table 28. This assumes that about 50 cell divisions occur in the germ lines in going from zygote to zygote. Since the formation of each sperm involves about twice as many divisions as oocyte formation, each sperm should contain twice as many mutations as an egg. This suggests that the male is the major source of mutationally induced variability arising during evolution.

The numbers of Table 28 indicate that at least about 5-10 nucleotide pair changes have been present in each zygote. Each generation has produced a

TABLE 28. Nucleotide Change Rates Calculated in Terms of  
Generation Time\*

DNAs Compared	Nucleotide Pair Changes per Year Since Divergence	Shortest Generation Time of Pair †, Years	Nucleotide Pair Changes per Generation	Nucleotide Pair Changes per Germ Cell Division (~50)
Man †-chimp	2.0	~10	20	.4
Man †-gibbon	2.0	~10	20	.4
Man †-green monkey	2.4	2-4	5-10	.1-2
Man †-rhesus	2.2	2-4	4-9	.08-18
Man †-capuchin	2.8	~2-4	6-11	.12-22
Man †-galago	7.2	1-2	7-14	.14-28
GM †-rhesus	2.0	2-4	4-8	.08-16
GM †-human	2.4	2-4	5-10	.1-2
GM †-chimp	2.4	2-4	5-10	.1-2
GM †-gibbon	2.4	2-4	5-10	.1-2
GM †-capuchin	2.8	2-4	6-11	.12-22
GM †-galago	7.2	1-2	7-14	.14-28
Mouse †-rat	33.0	0.25	8	.16
Cow †-sheep	4.2	1-2	4-8	.08-16
Cow †-pig	5.4	1-2	5-10	.1-2

\* Data from Kohne *et al.*, 1970.

† The generation time is taken as the gestation time plus the time needed to reach a fertile state. (Anderson and Jones, 1967).

population of gametes that contain roughly 5 base changes per gamete that would be fixed in the species. The total number of base changes per gamete should not be greatly different and is probably at most 2-4 times greater. On this basis the probability of any one base changing per germ cell division would be about  $10^{-10}$ .

*The Molecular "Clock" Approach*

The primate times of divergence utilized in Tables 24 and 25 and in Figures 96 and 97 were determined from fossil evidence. Wilson and Sarich (1969)<sup>164</sup> have recently questioned the classically determined times of divergence for man-chimp, man-gibbon and man-old world monkey. They contend from amino acid sequence and immunological evidence that the actual times of divergence of these species have been much more recent than the bulk of the fossil evidence indicates (Wilson and Sarich, 1969). The assumption basic to their interpretation is that *the rate of molecular evolution has been constant over absolute time*. Obviously, if this can be shown to be true the degree of molecular change can be used as an evolutionary clock, and times of divergence can be calculated with good accuracy from biochemical data if just one fairly accurate time of divergence is known. Wilson and Sarich

TABLE 29. Data Calculated Using More Recent Divergence Times

Period	Percent Nucleotide Pair Change per Period *	Length of Period, Million Years †	Percent Change per Million Years
A	1.1	5	0.22
B	2.0	5	0.4
C	1.6	20	0.08
F	1.4	5	0.27
G	3.1	10	0.31
H + J	5.8	30	0.19
ΔD	4.3	15	0.38
ΔK	9	45	0.2
ΔE	~18	~5-25	3.8-0.7

\* Data obtained from Fig. 103.

† Divergence times taken from Wilson and Sarich, 1969.<sup>164</sup>

used their data and a time of divergence of 23 million years for old world monkeys (e.g., rhesus and green monkey) and man to calculate that the man-chimp and man-gibbon divergence times were about 5 and 10 million years ago, respectively.

Tables 29 and 30 present nucleotide pair change rate data calculated with the divergence times of Wilson and Sarich. With these values Table 29 indicates that the absolute time-based rate of nucleotide sequence change has not been constant during primate evolution. The rate of change during period B is about five times that of period C, while

TABLE 30. Data Calculated Using More Recent Divergence Times

DNAs Compared ‡	Million Years Since Divergence	Total Divergence Time, Million Years	Percent Nucleotide Pair Change per Million Years	Percent Change per Generation $\times 10^{-6}$ (Use shortest generation time of pair.)
Man * + chimp	5	† 10	0.26	2.6
Man * + gibbon	10	† 20	0.31	3.1
Man * + green monkey	30	† 60	0.17	0.34-0.68
Man * + capuchin	45	† 90	0.19	0.38-0.76
Man * + galago	50-70	† 100-140	0.5-0.4	0.5-0.4
Mouse * + rat	10	20	1.65	0.41
Cow * + sheep	25	50	0.21	0.21-0.54
Cow * + pig	55	110	0.27	0.27-0.54

\* Labeled DNA.

† Divergence times taken from Wilson and Sarich, 1969.<sup>164</sup>

‡ Data taken from tables 24 and 25.

the rates for most of the other periods differ significantly. Further, Table 30 indicates that wide variations occur between the absolute time-based rates of nucleotide change of rodents, primates, and bovids.

The classically derived times of divergence and the immunologically derived times of divergence of Wilson and Sarich. With these values Table 29 indicates the current views for the divergence times of various primates. When coupled with the nucleotide change data neither of these views will support a general assumption of a constant absolute time-based rate of molecular evolution. Furthermore, these data also indicate that a restricted assumption of a constant absolute time-based rate of molecular evolution within the primate line is untenable. These nucleotide change data suggest that the rate of molecular evolution of DNA has probably been constant with generation time.

### *Comparing DNA and Protein Changes during Evolution*

Much work has been done on determining the amino acid sequences of similar proteins from different species and comparing these sequences. From these data investigators have constructed phylogenetic trees and have calculated rates of changes for amino acid replacements in these proteins. Different proteins were found to have widely differing rates of amino acid sequence change. Comparing the rates of change of proteins to those of nucleic acids is of some interest (Laird, *et al.*, 1969). These comparisons are, however, difficult to interpret for several reasons. Rates of change of DNA have been determined for a very large fraction of the DNA, which presumably represents a great many proteins. The function of this non-repeated DNA is not known. It is not known how much of the DNA is actually used, and it is possible that a large fraction of the DNA being studied had no

genetic expression and hence was not conserved. The proteins under study all have definite cellular functions and are therefore genetically important and more apt to be conserved.

It was stated earlier that a basic requirement for utilizing the comparison of DNAs to calculate rates of nucleotide sequence change is that one must be able to compare the *direct descendants* of a nucleotide sequence present in the most recent common ancestor. In comparing amino acid sequences of a protein from two different animals the same strict requirement holds. In order to interpret properly the rate of amino acid replacement data it must be known that the two proteins are products of two genes, one in each species, both of which are direct descendants of the same common ancestor gene in the most recent common ancestor. This requirement may be difficult to meet when working with some proteins. Many proteins are known to exist in several variant or "polymorphic" forms in the same animal or population of animals. Thus, in comparing the proteins of two different species we may be comparing proteins which had already diverged in the common ancestor.

*DNA evolution vs. fossil evolution.* The current view of the role of DNA indicates that evolutionary changes at the organismal level must have been preceded by some quantitative or qualitative change in the DNA. Detectable in the DNA are repeated DNA sequences, nonrepeated DNA sequences, base changes, and translocations. These are the present-day records of historical events that occurred during the evolutionary history of the DNA. Correlating molecular changes with organismal changes is always a difficult task. Comparison of the pattern and character of these DNA records with the patterns derived from the classical fossil record should, however, provide new insight into the nature of evolutionary forces. The evidence available thus far allows a very tentative correlation to be made.



During the period when the classical fossil record indicates that extensive speciation occurred in the primates, it appears that (1) DNA was added to the presumptive human genome at a much faster rate than during other periods for which data are available, and (2) the rate of nucleotide sequence divergence was also much higher relative to other periods. It is not known whether these increased rates are the result or the cause of the extensive speciation seen during this period. The correlation of nucleotide sequence change with generation time suggests that the generation time of the early primate ancestors of man, which lived during this period, was relatively short. The rate of mixing of genetic material to provide new genetic combinations (e.g., translocations, inversions, etc.) should also be generation-time dependent. It does not seem unreasonable to speculate that the rapid addition, divergence, and mixing of the DNA may have played a role in the burst of speciation seen during this period. Much more extensive work needs to be done, however, before any strong conclusions can be made.

#### THE PROBABILITY OF OCCURRENCE OF ACCIDENTAL SEQUENCE HOMOLOGIES

*R. J. Britten and R. B. Roberts*

In the design and interpretation of measurements of sequence homologies among nucleic acids, the possibility of chance occurrence of sequence relationships must be considered. This is particularly true when distant relationships are measured and experiments are performed with low criteria for sequence complementarity. Sequence similarities that are purely due to chance would, of course, not imply historical or functional relationships, and thus represent a kind of background noise underlying the interpretation of sequence homologies.

While it appears that experimental determination of this "noise" will ultimately be necessary, very little data is

now available and calculations are of some use. Here we describe the results of some new calculations in which the effect of various degrees of sequence divergence or precision of match are included. The following equation gives the probability of occurrence at each position in a long random series of a sequence, matching a fraction  $D$  or better of the bases of a given sequence of length  $N$ .

$$P = \sum_{m=0}^{m=DN} \frac{3^m N!}{4^N m! (N-m)!}$$

Since all degrees of mismatch up to a given level are included, this equation represents the conditions of typical measurements in which all degrees of thermal stability of strand pairs are included which are stable in particular experimental conditions. Figure 98 gives the results of calculations from this equation.

In preliminary estimates of accidental homology only the expectation of occurrence of perfectly matching sequences was calculated. The lowest curve ( $P = 4^{-N}$ ) on Fig. 98 gives this case. As expected, the effect of including imperfectly complementary sequences is very large. Compare for example the curve, including up to 20% mismatch ( $D = .2$ ) with the curve ( $D = 0$ ) for perfect matching. For 25-long segments the probability is  $10^{-8}$  for this degree of mismatch. In this case only 20 of the bases actually match, so that comparison can be made with perfectly matched, 20-long sequences that have a probability of  $10^{-12}$ . It is clear that imperfectly complementary accidental homologies are much more common than perfect ones. But are they common enough to cause difficulties in the interpretation of re-association experiments?

In order to simplify the comparison with experiments, the calculations are plotted as curves of constant probability on Fig. 99. It appears that the curve for a probability of  $10^{-12}$  represents the boundary below which observation of

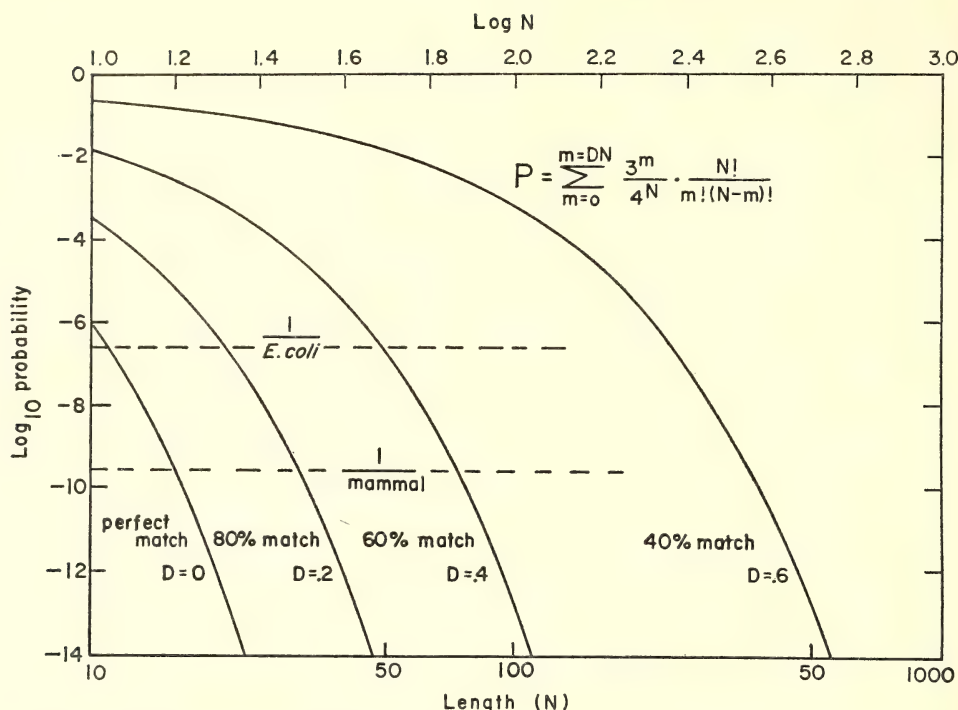


Fig. 98. Accidental sequence homology as a function of fragment length and precision of match. Calculated for equal quantities of the four bases (50% GC). The curves represent the probability of occurrence in a random series of any particular sequence, matching to the indicated degree of accuracy or better. The lowest curve is for perfectly matching sequences and is calculated from the familiar relationship  $4^{-N}$ . It is apparent that very much greater probabilities of accidental pairing may occur with customary experimental criteria which permit 20 to 30% nonmatched bases. However, as indicated by the discussion in the text, most measurements are not significantly affected.

accidental homology would be difficult or impossible. Consider a hypothetical experiment in which the homology is being measured between two genomes that are unrelated except by chance. We assume that both are the size of a typical mammalian genome, about  $3 \times 10^9$  nucleotide pairs. If the experimental criterion were such that there was a probability of  $10^{-12}$  for chance relationship, then about .3% ( $3 \times 10^9 \times 10^{-12}$ ) of the DNA of one species would bind to that of the other. If the fragments were larger than the region over which the chance homology occurred, then a somewhat larger fraction of the DNAs would react. Thus, for most experimental purposes where only homologies greater than 1%

are significant,  $10^{-12}$  is the practical boundary.

The principal difficulty in making direct use of these calculations is that the effect on thermal stability of length and precision of sequence matching is not well known. It does not appear likely under usual experimental criteria that a probability of  $10^{-12}$  would arise. For example, a stretch of nucleotides 40-long with 80% matching would probably melt at least  $40^\circ$  below native DNA. Also, other examples lying on the  $10^{-12}$  curve (such as 55% matching for 120 bases) would appear to be quite unstable. However, the lack of calibration measurements makes it necessary at present to carry out control measure-

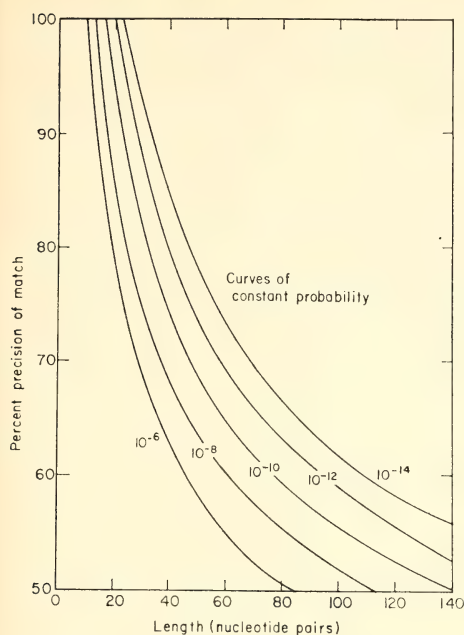


Fig. 99. Curves of constant probability of accidental sequence homology. The calculations used in Fig. 98 have been plotted in a way that is more convenient for some purposes.

ments to estimate the degree of accidental sequence homology that may be observed under particular experimental conditions. In addition, there is the possibility that DNA sequences differ from random order in such a way as to affect the results of these calculations.

It might be suggested that repeated sequences could to some extent be due to accidental sequence homology rather than to past events of multiplication. As it turns out, a simple argument shows that this cannot be the case. Suppose, for example, that at some experimental criterion, chance sequence relationship had a probability of  $10^{-7}$  in a genome of  $3 \times 10^9$  nucleotides. One would expect under these conditions that each sequence would show relationship to about 300 other sequences. Most of the DNA would appear repetitive. However, under such conditions the DNA of all other species would also show a chance rela-

tionship of the same order of magnitude. In other words, if repetition were due to chance relationship almost complete cross reaction would be observed with all higher organism DNA. This is not observed at ordinary criteria of precision, although such phenomena might well occur at very low temperatures of incubation. The answer to one question of fundamental interest awaits the exploration of this region of distantly related DNA sequences. Did all, or the great majority, of higher cell DNA originate in the massive events of multiplication that we term saltatory replications?

The probability of occurrence curves on Figs. 98 and 99, of course, gives the expectations for any specific sequence in a long random series. They are thus useful for other purposes besides estimating chance homologies. For example, the probabilities of occurrence of local regions of extreme base composition can also be estimated. Thus the probability that a segment of DNA 20 bases long contains more than 80% G on one strand can be read as  $3 \times 10^{-7}$ . Thus, if the DNA were fully random in sequence, a mammalian genome might be expected to have almost a thousand such high GC regions. Depending on fragment size they would perhaps add up to only 0.01% of the DNA but nevertheless might be observable. Measurements with pure homopolymers (Lipsett, 1964)<sup>167</sup> suggest that such "almost homopolymer regions" would be stable, for example, at 60°C in .12 M PB. Of course, these calculations were made for DNA that is 50% GC and a somewhat smaller amount of such regions can be expected in mammalian DNA with a base composition of about 40% GC.

#### SEQUENCE COMPLEXITY, KINETIC COMPLEXITY, AND GENETIC COMPLEXITY

*R. J. Britten*

Enough observations have been made to begin the descriptions of the repeated



DNA of higher organisms in terms of the frequency of repetition, quantity of repeated DNA, and the number of sequences represented. This description has raised a number of important and difficult issues. For example, even the boundary between repeated and non-repeated is not obvious. This section represents an attempt to clarify the meaning of some concepts and terms while avoiding rigid definitions that might obscure the underlying and unknown relationships that must ultimately be recognized in order to understand the function and evolutionary history of the DNA of higher cells.

We propose to use the term *sequence complexity* to express the amount of diverse sequence in a given sample of DNA. It is customarily expressed in nucleotide pairs. The word complexity has been used in the past but the term sequence complexity is more specific and permits useful distinctions. The meaning is clear for simple cases such as the DNA of a virus that does not contain terminal redundancy or other significant internal sequence relationship. In such a case the sequence complexity is just the amount of DNA per virus particle or the genome size. The relative genome size or sequence complexity can be measured by determining the rate of reassociation of the DNA. It has been shown that the  $C_0t$  required for half reassociation of bacterial and viral DNA is directly proportional to the DNA content per cell nucleus or the DNA content per virus particle. For such measurements the fragment size, salt concentration, and temperature must be controlled, and there is a small correction for base composition of the DNA.

The extension of this definition to the case of repeated DNA in higher organisms is feasible, but the members of these families of sequences are usually not identical to each other. As well as supplying some potential information on the function and history of the repeated DNA, the divergence of the sequences

creates a conceptual problem. At the present time the rate of reassociation is the only available measure of the complexity of sets of repeated DNA. Since this rate is an operational measure or definition, a specific term is needed and we have chosen *kinetic complexity*. While certain assumptions and simplifications are involved in estimating the actual sequence complexity, the kinetic complexity is directly calculable from measurements and may depend on the specific conditions under which the measurements were made. The following example shows the method of calculation of the kinetic complexity ( $L_i$ ) of a particular pure repeated fraction of DNA:

$$L_i = (C_0t_{1/2} \text{ of sample} / C_0t_{1/2} \text{ of } E. coli \text{ DNA}) \times (\text{genome size of } E. coli)$$

Since this discussion is only intended to bring out the principal issues, the detailed corrections (fragment size, non-optimal temperature, etc.) will not be considered. However, one potential source of error must be mentioned, namely, the effect of the sequence divergence on the rate of reassociation. It seems likely that the presence of non-complementary bases will reduce the rate of reassociation. But adequate control measurements have not yet been made and the effect of noncomplementary bases is a source of uncertainty in the interpretation of the kinetic complexity in terms of actual sequence complexity.

Of course, there is a basic difficulty in describing the complexity of a set of related but not identical DNA sequences. Since each member sequence of a typical set presumably differs somewhat from all of the others, the literal total sequence complexity might be a very large number. If we knew how to estimate the total sequence complexity and if the various member sequences carried out different functions, some biological significance

might ultimately be associated with the total sequence complexity. However, at the present time the kinetic complexity seems to be the most useful and comprehensible measure for repeated DNA. It presumably gives a measure of the length of sequence that must originally have been extensively replicated to form a family of repeated DNA.

The sequence complexity of non-repeated DNA is a much simpler concept. Even for higher organism DNA it is about \* equal to the observed kinetic complexity. For quite a large number of organisms the result agrees with that expected from the known genome size. In other words, when total nuclear DNA is allowed to reassociate and the slowly reassociating component is identified, the  $C_0t_{1/2}$  is found to be proportional to the nuclear DNA content of haploid cells. There is, however, one problem. The fraction of the DNA observed to be repetitive depends upon the criterion of precision of strand pairing established in the measurement. Thus the amount of DNA which appears to be nonrepetitive is determined by the conditions of measurement and can be varied over a wide range. The apparent sequence complexity of the single copy DNA is just equal to the amount of single copy DNA that is observed, under the conditions of measurement. There appears to be an arbitrary boundary between the repetitive and the nonrepetitive DNA because of the types of measurement that are now available. We hold the position that this arbitrariness is more apparent than real. A reasonable view is that a large fraction of the DNA of most organisms exhibits repeated sequences owing to past events of multiplication of DNA segments (saltatory replications). From a historical point of view practically all of the DNA might appear to be repetitive. From a functional point of view

we do not yet have very much information. It would be very valuable to know whether the similarities among repeated sequences are useful to the cells and to what extent the divergence of the member sequences has brought them to a point at which they function independently. These are difficult questions but fortunately there is a direct approach, in the case of single copy DNA, to the question of how much of it is actually functional. That approach is to measure the *extent* of the sequences that are transcribed into RNA; and initial results are available. Before mentioning the results it is necessary to consider the meaning of the third term in the heading of this section—*genetic complexity*. This term cannot properly be defined until we know more about the actual kinds of functions of various regions of the DNA. If the functions were restricted to coding for structural genes which specify proteins, it would conceptually be a straightforward matter to measure the total length of these regions of the DNA and consider the result to be the genetic complexity of that genome. The measurements should, of course, be done throughout the life cycle of the organism, and all cell states should be represented. However, there are other functions, such as gene regulation, which may be ascribed to regions of the DNA, and the complete total of all the active regions may be difficult to obtain. Nevertheless, the extent to which the DNA sequences are transcribed into RNA forms a probable lower limit to the genetic complexity. We do not know the function of all of the RNA, but it seems to be a useful working hypothesis that transcribed sequences are functional. Other hypotheses have been made, but it seems likely that there would be great selective advantage in not transcribing useless DNA sequences.

In two situations experimental estimates have been made of the extent of transcription of single copy DNA; that is, the complexity of the DNA sequences

\* The divergence of the two sets of DNA in diploid organisms and the sex chromosomes has minor effects that may ultimately need to be considered.



that are actually transcribed. While these only supply lower limits of the genetic complexity, they give strikingly large numbers. For newborn mice (*Year Book 67*, p. 320) it appears that for single copy DNA more than 12% of the genome is transcribed and thus the genetic complexity of the mouse genome is at least  $4 \times 10^8$  nucleotide pairs. This very large number is not yet interpretable, since if all of this RNA were messenger, it would code for nearly a million different hemoglobin-sized proteins. In the other available set of measurements (Davidson-Hough)<sup>168</sup> the evidence indicates that the RNA stored in the *Xenopus* oocytes represents at least 1% of the single copy DNA. Therefore, the complexity of this RNA is such that it could code for 40,000 different hemoglobin-sized proteins if that were its function. Thus, it appears that a significant portion of the potential information content of these genomes is actually expressed. Whether there exist large unexpressed regions remains for future measurements to determine.

It appears appropriate to end this somewhat abstract discussion on a practical note. The physical separation of repeated from nonrepeated DNA is limited unless very special techniques are available. One copy, at least, of each of the families of repetitive sequences will remain in the nonrepeated fraction. At this degree of purification the sequences of course will be observably nonrepetitive. In the animals that have been examined such sequences do not appear to represent a significant fraction of the total nonrepeated DNA nor do they contribute appreciably to the total complexity.

#### CATTLE, SHEEP, AND SATELLITES

*R. J. Britten and Jean F. Smith*

The DNA of the calf contains a component that is very rich in guanine and cytosine. Since it has been resolved from the principal DNA by density gradient

centrifugation (Polli, Correo Ginelli, and Bianchi),<sup>169</sup> it is identified as a satellite. It has been recognized as a repeated element in the DNA because the rate of reassociation is rapid, but the actual rate constant has not previously been determined. A peculiar correlation with a component in sheep DNA led us to investigate the two components and their relationship. Each is observable by simply melting native unfractionated DNA in the spectrophotometer. A small and rather sharp step amounting to about 3% of the total hyperchromicity occurs at about 7° above the bulk DNA  $T_m$  or at 93° when each DNA is melted in 0.12 *M* PB. On cooling and remelting without delay ( $C_0t$  about 0.1) both are again visible as steps but melt at reduced temperature ( $T_m = 91^\circ$ ). Both have reassociated, but not perfectly. Since sheep and calf are reasonably closely related (about 25 million years since the most recent known common ancestor), it appeared possible that this component was held in common between the two species. The sequences of the single copy DNA of these two species are known to have diverged from each other to the extent that the  $T_m$  of hybrid DNA pairs has been lowered by 7°. Thus an opportunity was presented, if indeed the two satellites showed homology to each other, to compare the divergence of specific families of repeated sequences with the single copy DNA divergence. However, somewhat to our surprise two components did not appear to have any measurable homology to each other. Nevertheless, this observation is of interest, since it suggests the independent occurrence of similar saltatory replications of high GC components in the two separate species lines, and the measurements will be briefly described.

The high melting temperature of these components makes it possible to purify them very simply on hydroxyapatite. For this purpose the hydroxyapatite column temperature was set so high that all of the principal components of the DNA



were dissociated and did not bind, while the undissociated high GC component was efficiently bound. Preliminary tests showed that the best temperature for fractionation was 95°, somewhat above the  $T_m$  of the component observed in the spectrophotometer. The probable reason for this is that some regions of the components remained associated and maintained the registration of the double-stranded DNA. With this technique a large quantity of DNA could be prepared on a relatively small HAP column since the principal DNA was not bound. About 10 mg of native sheared DNA (Virtis blender, 15,000 rpm, one-half hour) was passed over the column at 95°; the column was washed with 0.12 *M* PB and the satellite was eluted with 0.4 *M* PB, also at 95°. The DNA recovered was still in the native state as judged by its  $T_m$  and hyperchromicity. Six percent of the calf DNA was recovered and 4.5% of the sheep DNA.

Using the above method, labeled sheep DNA and unlabeled DNA from both species were prepared and the rates of reassociation and extent of cross species homology were measured. When measured in the spectrophotometer the calf component appeared to be half reassociated at a  $C_0t$  of 0.02 and had a hypochromicity for the reaction of 11%. This measurement suggested that at least half of this fraction was made up of the high GC satellite which melted quite sharply at 91°. Similar results were obtained for the sheep fraction except that it reassociated more rapidly. The results suggested that the lengths of the repeated element or the sequence complexity for the calf and sheep components were 4000 and 1000 nucleotide pairs. The fact that the calf component appeared to be somewhat more complex than that of the sheep suggested that there could not be complete sequence homology between the two.

The labeled sheep tracer exhibited a moderate amount of binding (11%) to HAP at very small  $C_0t$  and was freed of

this component by denaturing in 0.12 *M* PB, cooling to 60° and immediately passing it over HAP at 60° in 0.12 *M* PB. The material removed is similar to the components previously described (*Year Book* 68, pp. 378–386) which appear in the DNA of many species. The enriched labeled sheep satellite tracer was incubated alone and mixed with calf or sheep satellite DNA to a  $C_0t$  of 0.04. The mixtures were then passed over HAP at 60° in 0.12 *M* PB. The added sheep DNA, as expected, reassociated with the tracer and caused it to bind to the HAP (49%). However, the added calf DNA barely increased the binding over that observed with the tracer alone (1.5–3%). Therefore, we can conclude that the calf high-GC satellite exhibits little or no sequence homology to that of the sheep.

#### PHOSPHATE GRADIENT ELUTION OF REASSOCIATED DNA FRAGMENTS ADSORBED TO HYDROXYAPATITE

*B. H. Hoyer and N. W. van de Velde*

This report describes the phosphate gradient elution of reassociated bacterial and animal DNA fragments adsorbed to hydroxyapatite (HAP). The usual analytical HAP procedures use a two-step adsorption elution with two concentrations of phosphate buffer (PB, an equimolar mixture of  $\text{Na}_2\text{HPO}_4$  and  $\text{NaH}_2\text{PO}_4$ ) to separate single-stranded DNA fragments from wholly or partially double-stranded DNA fragments (*Year Book* 65, pp. 89–91). The phosphate gradient procedure has been developed to use adsorption to and elution from HAP as an indicator of the degree of "double-strandedness" of reassociated DNA fragments.

The quantitative applications of the HAP methodology have been possible through the recognition of the necessity to use single-stranded DNA fragments of small size (about 500 nucleotides in length) and to employ controlled conditions of reassociation (*Year Book* 64,

pp. 324-327 and *Year Book 65*, pp. 78-85). Previous studies (Bernardi, 1969<sup>170</sup> and Becker, 1970<sup>171</sup>) have indicated the potential of phosphate gradient elution from HAP to fractionate reassociated nucleic acids on the basis of the proportion of base-paired nucleotides, but fragment size or reassociation conditions were not controlled and the results are difficult to interpret.

In the present study bacterial DNAs were used in comparison with several selected animal DNAs to indicate the phosphate gradient elution properties of reassociated DNA fragments adsorbed to HAP. The bacterial DNAs are essentially free of repeated nuclear DNA sequences, while animal nuclear DNAs contain repeated sequences as well as nonrepeated sequences (*Year Book 66*, pp. 73-76). The repeated sequences of animal DNAs are composed of "families" which reassociate to form duplexes that have varied proportions of double-stranded and partially double-stranded regions. Therefore, bacterial and animal DNAs provide material for comparison of phosphate gradient elution behavior of reassociated DNAs that comprise a spectrum of single-stranded to almost native, double-stranded configurations.

#### Gradient Elution of *Escherichia coli* DNA

*E. coli* DNA, labeled with  $P^{32}$ -phosphate and sheared by passage through an orifice at 50,000 psi (50 K sheared), was denatured and reassociated to about one-half completion ( $C_{ot}/2$ ) (*Year Book 65*, pp. 81-85). The DNA was then adsorbed to HAP in 0.03 M PB (0.03 M PB allows the adsorption of both single- and double-stranded DNA) and eluted by means of a linearly increasing phosphate gradient, Fig. 100. The elution profile obtained indicated a separation of DNA fragments; single-stranded DNA eluted with a peak at 0.15 M PB and double-stranded with a peak at 0.28 M PB. Between the two peaks was a

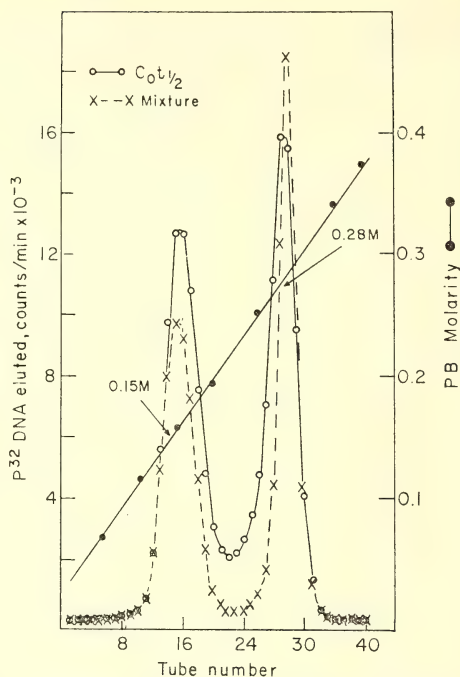


Fig. 100. Phosphate linear gradient elution of *Escherichia coli* DNA fragments adsorbed to hydroxyapatite.  $P^{32}$ -labeled *E. coli* DNA was sheared by passage through an orifice at 50,000 psi (50 K sheared). Of this DNA 166  $\mu$ g was denatured at 85°C and subsequently incubated at 35°C for 1 hour in 3 ml of a mixture of 0.01 M  $Na_2EDTA$ , 50% formamide (v/v), and sufficient phosphate buffer (an equimolar mixture of  $NaH_2PO_4$  and  $Na_2HPO_4$ , designated PB) and NaCl to make the solution 1.2 M in  $Na^+$ . The  $C_{ot}=2$  and the equivalent  $C_{ot}$  (0.12 M PB, 60°C) = 4. This is sufficient to about  $1/2$  reassociate *E. coli* DNA fragments. One ml of the above mixture was removed and diluted in 49 ml of a solution containing sufficient PB to make it 0.03 M. The remaining 2 ml was incubated an additional 141.5 hours at 35°C;  $C_{ot}=285$ . One ml was diluted to yield 50 ml 0.03 M PB. The remaining ml was heated to 85°C for 3 min, diluted to 0.03 M PB, and mixed with the diluted, unheated sample (this preparation is designated "mixture"). The 50% reassociated DNA fragments and the mixture were separately adsorbed at 50°C to hydroxyapatite columns prepared from 2 g Bio-Gel HTP (Bio-Rad, Richmond, Calif.) contained in 1.9 cm I.D. jacketed columns. After adsorption the DNA was eluted at 50°C by a linear gradient of PB, 0.03-0.40 M, formed in 1 liter. PB was pumped through the columns at a constant flow of 4.5 ml/min and fractions were collected at 5 min intervals.

valley that did not extend to the baseline, indicating differential elution of DNA fragments at intermediate stages of reassociation when adsorbed to HAP (Year Book 65, p. 86).

It seemed possible that concatenation of DNA fragments, after their  $C_0t_{1/2}$  is greatly exceeded, may form extensive complexes that have altered elution characteristics. To test this possibility *E. coli* DNA fragments were reassociated to  $C_0t=287.5$ , which is about  $100 \times C_0t_{1/2}$  under the conditions employed. A portion of this DNA was dissociated, diluted, mixed with the reassociated DNA, adsorbed to HAP, and eluted by a linear phosphate gradient (see "mixture," Fig. 100). The positions of the elution peaks were the same as those observed for *E. coli* DNA fragments reassociated to  $C_0t_{1/2}$ , but the intermediate region approached the baseline and the peak eluting at 0.28 M PB was less broad. Therefore, concatenation does not markedly alter the elution position of reassociated DNA fragments. Also, comparison of the elution profile of the "mixture" with that of *E. coli* DNA reassociated to  $C_0t_{1/2}$  affirmed that the elution procedure detected reassociation products intermediate to single- and double-stranded DNA.

*Actinobacillus mallei* is a microorganism whose DNA contains 67 mole percent guanine plus cytosine (Rogul, et al., 1970).<sup>175</sup> *E. coli* DNA contains, in comparison, 50 mole percent guanine plus cytosine and has few polynucleotide sequences in common with *A. mallei*. This pair of DNAs was used to investigate the effect of base composition on phosphate gradient elution of DNAs from hydroxyapatite.  $P^{32}$ -labeled *E. coli* DNA fragments were mixed with  $C^{14}$ -labeled *A. mallei* fragments, dissociated, and partially reassociated. Phosphate gradient elution from HAP indicated that the unassociated *A. mallei* single-stranded DNA eluted at higher PB concentrations (0.17 M PB) than that of *E. coli*, but that the reassociated, double-stranded DNA fragments both eluted at

0.28 M PB. Presumably, the unassociated *A. mallei* DNA fragments had a greater degree of intramolecular structure than those of *E. coli* under the adsorption conditions; the reassociated DNAs had similar elution peaks, indicating little influence of base composition on their elution characteristics.

#### *Elution behavior of E. coli-Salmonella typhimurium DNA hybrids*

*E. coli* DNA contains some polynucleotide sequences similar to those of *S. typhimurium* LT2, but the hybrid duplexes are less stable to thermal dissociation than are the homologous duplexes (McCarthy and Bolton, 1963;<sup>172</sup> Brenner et al., 1967;<sup>173</sup> and Brenner and Cowie, 1968,<sup>174</sup> and Year Book 66, pp. 106-110). The phosphate gradient elution of the DNA-DNA hybrids formed between the above two DNAs and their thermal stability was examined in comparison with previous results.  $P^{32}$ -labeled *E. coli* DNA fragments were incubated with unlabeled *S. typhimurium* DNA fragments in proportions so that less than 2% of the *E. coli* fragments and greater than 90% of the *S. typhimurium* fragments would self-reassociate. In good agreement with the previous results<sup>172, 173</sup> about 40% hybrid formation was indicated (Fig. 101). However, the DNA-DNA hybrids were eluted with a peak at 0.23 M PB instead of at 0.28 M as found for reassociated *E. coli* DNA fragments.

Thermal elution (see legend, Fig. 104, for details) from HAP of DNA hybrids recovered from the ascending and descending portions of the 0.23 M PB elution peak (as indicated in Fig. 101) yielded  $T_{e_{50}}$ 's (midpoints of the integral thermal elution curves) of 71° and 76°C, respectively. This is compared with the homologous *E. coli* DNA reassociation products that have a peak elution at 0.27-0.28 M PB and  $T_{e_{50}}$ 's of 81° and 85°C at comparable positions of their phosphate elution profiles. Therefore,



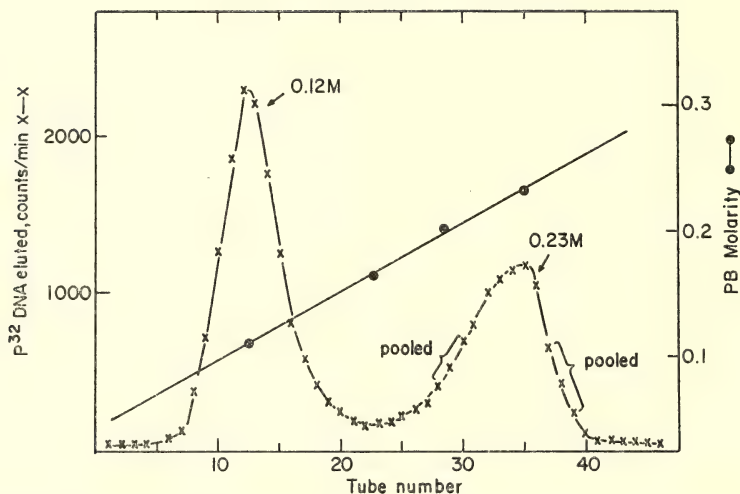


Fig. 101. Phosphate gradient elution of *E. coli*-*Salmonella typhimurium* DNA hybrids. One  $\mu\text{g}$   $P^{32}$ -labeled, 50 K sheared *E. coli* DNA was mixed with 850  $\mu\text{g}$  50 K sheared, unlabeled *S. typhimurium* LT2 DNA and alkali denatured. After neutralization the mixture was incubated 2.5 hours at  $60^\circ\text{C}$  in a solution 0.18 M in  $\text{Na}^+$ . The resulting  $C_{ot} = 0.03$  for the labeled *E. coli* DNA and 25.6 for the unlabeled *S. typhimurium* DNA. Adsorption of the incubated DNAs to hydroxyapatite and elution by a 0.03 to 0.35 M PB linear gradient was done as described in the legend of Fig. 100. Of the  $P^{32}$ -DNA 60% was eluted by less than 0.17 M PB and 40% by 0.17–0.275 M PB. Eluates in tubes 28, 29, and 30 were mixed together as were those in tubes 37, 38 and 39. After adsorption to hydroxyapatite at  $60^\circ\text{C}$  in 0.14 M PB, the thermal stability of the reassociated DNAs in each of the mixtures was individually determined as described in Fig. 103.

fragments eluted at lower PB concentrations have lower thermal stability than those eluted at higher PB concentrations. Again, these observations indicate that phosphate gradient elution of DNA fragments adsorbed to HAP fractionates re-associated DNAs on the basis of the proportion of base pairs in their duplexes.

### Mouse DNA Elution

Since the reassociation characteristics of mouse DNA are well known (*Year Book 65*, p. 103), it was first used in the study of the phosphate gradient elution characteristics of animal DNA adsorbed to HAP. Mouse DNA, as detailed in the legend of Fig. 102, was reassociated to a  $C_{ot}$  of 0.134 (in 0.12  $M$  PB at 60°C) which is sufficient to allow duplexing of sequences with repetition frequencies of about  $10^4$  or greater. The phosphate gradient elution of this reassociated DNA

after its adsorption to HAP, Fig. 102, indicated two main elution peaks at 0.12  $M$  PB and 0.28  $M$  PB, similar to the principal peaks obtained with half re-associated *E. coli* DNA, Fig. 100. However, in addition to the principal peaks, an elution shoulder was found at 0.15  $M$  PB as well as DNA that was eluted between 0.15 and 0.28  $M$  PB, again similar to that found for one-half reassociated *E. coli* DNA. The DNA that eluted with a peak at 0.28  $M$  PB was most likely mouse satellite; when the DNA in the fractions comprising this elution peak was readsorbed and again eluted, reproducible chromatography and a purification were indicated, Fig. 102.

### Elution Characteristics of Reassociated Green Monkey DNA

A further investigation of PB gradient elution of animal DNA was made with

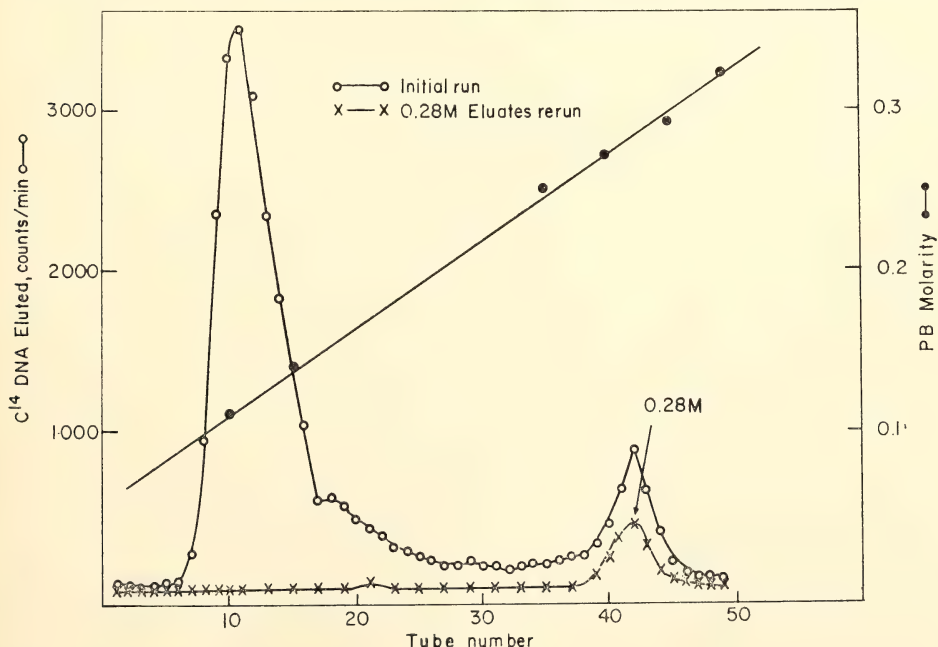


Fig. 102. Phosphate gradient elution of reassociated mouse DNA.  $C^{14}$ -thymidine-labeled, 50 K sheared mouse DNA fragments, 21  $\mu$ g, were denatured by heat and incubated 0.53 hr. at 60°C in a solution containing 0.18  $M$   $Na^+$ ;  $C_{ot}$  = 0.135. The DNA fragments were adsorbed to hydroxyapatite and exposed to a linear gradient, 0.07–0.35  $M$  PB, formed by 1200 ml of solution. See Fig. 100 for procedural details. DNA in fractions 41, 42, and 43 was adsorbed to hydroxyapatite in 0.03  $M$  PB and again eluted by a 0.07–0.35  $M$  PB gradient.

reassociated,  $P^{32}$ -labeled, 50 K sheared green monkey DNA fragments. Green monkey DNA is known to have rapidly reassociating DNA families that comprise about one-half of the total DNA and a major component that is 20–40%

of the rapidly reassociating DNA (J. J. Maio, personal communication; Kohne, *et al.*, this *Year Book*). Following reassociation to  $C_{ot}=30$  (0.12 M PB, 60°C) and adsorption to HAP at 50°C in 0.03 M PB, a phosphate elution profile

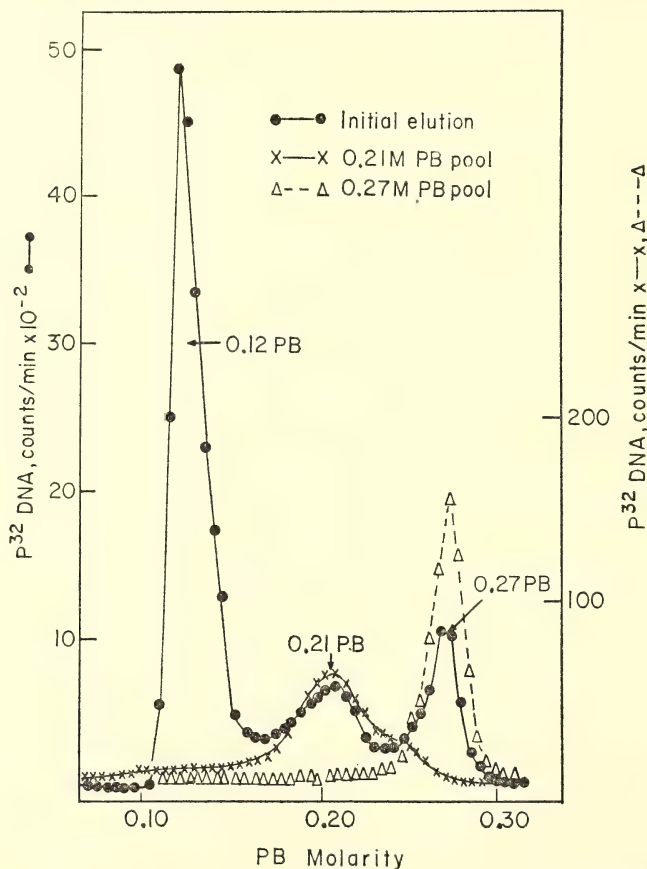


Fig. 103. Reassociation of green monkey DNA fragments previously fractionated by phosphate gradient elution.  $P^{32}$ -labeled, 50 K sheared green monkey DNA fragments, 1100  $\mu$ g, were denatured at 85°C and incubated for 17.4 hours at 35°C in 9 ml of a solution which contained 50% formamide (v/v), 0.01 M  $Na_3$  EDTA, and sufficient NaCl and PB to make the solution 1.2 M in  $Na^+$ . The DNA  $C_{ot}$  was 25.6 and the equivalent  $C_{ot}$  (0.12 M PB, 60°C) was 51.2. Three ml of the incubated DNA was then adsorbed to hydroxyapatite from 150 ml of a solution 0.03 M in PB at 50°C. Linear gradient elution by one liter of 0.05–0.35 M PB was done as described in the legend of Fig. 100. The results obtained are designated initial elution. The DNA fragments in the 10 fractions comprising the 0.21 M PB peak were concentrated, mixed with a fivefold excess of unlabeled, unfractionated 50 K sheared green monkey DNA fragments, dissociated, and reassociated to an equivalent  $C_{ot}$  (0.12 M PB, 60°C) = 104. The  $P^{32}$ -DNA elution profile, designated 0.21 M PB pool, was determined following adsorption to and phosphate gradient elution from hydroxyapatite. Similarly, DNA fragments from the nine fractions comprising the 0.27 M PB peak were mixed with a fivefold excess of unlabeled green monkey DNA fragments, dissociated, and reassociated to an equivalent  $C_{ot}$  (0.12 M PB, 60°C) = 104. The profile designated 0.27 M PB pool was determined.



was observed similar to that shown for unfractionated DNA in Fig. 103. Three principal fractions of unassociated and reassociated DNA were eluted by 0.12, 0.22, and 0.27 *M* PB, respectively. The 0.12 *M* PB peak is probably composed of unique DNA sequences that could not

reassociate at the  $C_0t$  used. The 0.22 and 0.27 *M* PB eluates contain rapidly reassociating DNA sequences that have sufficiently different proportions of base pairs to allow differential elution after adsorption to HAP. The thermal stability of the DNA fractions eluted near the

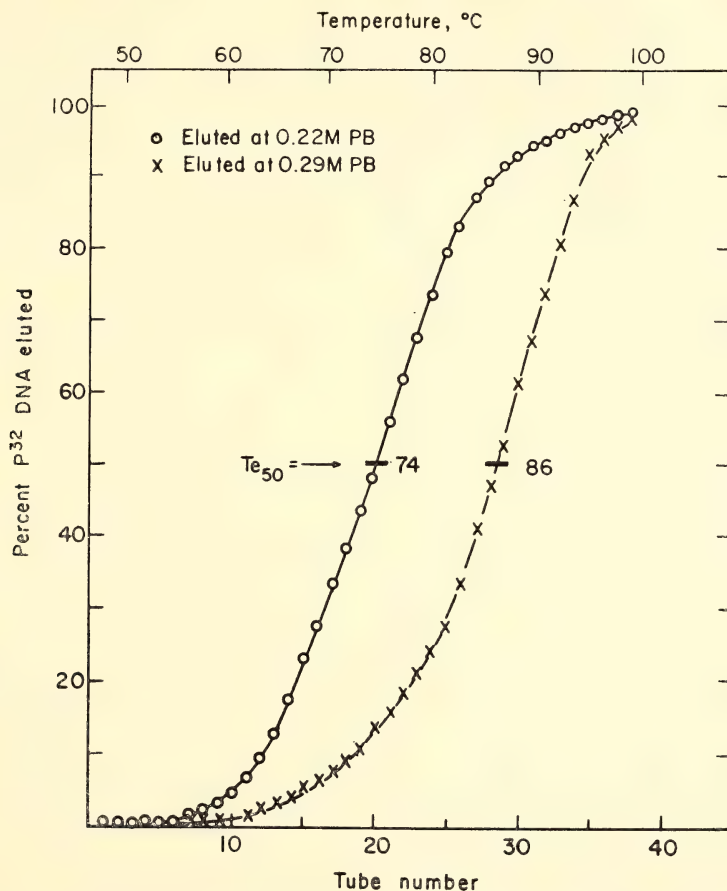


Fig. 104. Thermal stability of reassociated green monkey DNA fractionated by phosphate gradient elution.  $P^{32}$ -labeled green monkey DNA (66  $\mu$ g), alkali denatured and 50 K sheared, was neutralized and incubated for 2.46 hours at 72°C in 2.0 ml of a solution containing 1.2 *M* Na<sup>+</sup>. This is equivalent to  $C_0t = 75$  in 0.12 *M* PB at 60°C. Three fractions collected at the 0.22 *M* PB elution peak (similar to the intermediate peak of the initial elution profile, Fig. 103) were diluted to 0.14 *M* PB and adsorbed to hydroxyapatite. The adsorbed DNA was exposed to a constant flow, 4.5 ml/min, of 0.14 *M* PB and the temperature was increased linearly 0.2°C/min. Fractions were collected every 4 min. The radioactivity of each fraction was determined and an integral plot of percent radioactivity eluted versus temperature was constructed. The midpoint of the integral thermal elution curve ( $Te_{50}$ ) for the DNA initially eluted by about 0.22 *M* PB was 74°C. Fractions collected at 0.28–0.30 *M* PB (similar to those of the descending portion of the 0.27 *M* PB elution peak, Fig. 103) were also adsorbed to hydroxyapatite and eluted thermally. The  $Te_{50}$  of the 0.28–0.30 *M* PB fraction was 86°C.

0.22 *M* PB peak was determined. This DNA was collected, adjusted to 0.14 *M* PB, and adsorbed to HAP at 60°C. After adsorption the DNA fragments were exposed to a linear temperature gradient, an increase of about 0.2°C per minute, in a constant flow of 0.14 *M* PB. Radioactivity of eluates obtained at temperature increments of about 0.8°C was determined and integral plot of DNA eluted versus temperature was constructed (Fig. 104). A  $T_{e50}$  of 74°C was indicated. Fractions with a PB concentration of 0.29 *M* were similarly diluted, adsorbed and re-eluted. The  $T_{e50}$ , indicated by the integral thermal elution curve on the right side of Fig. 104, was 86°C. The difference in the thermal elution midpoints of the green monkey DNA reassociation products was 12°C. The elution position (0.22 *M* PB) and thermal stability of the reassociated green monkey DNA sequences, which were selectively eluted in the intermediate portion of the elution profile, were roughly comparable to those of the *E. coli*-*S. typhimurium* DNA-DNA hybrids (see Fig. 101). These results and those presented earlier leave little doubt that phosphate gradient elution selectively fractionates reassociated DNAs on the basis of their proportions of base pairs.

The reproducibility of elution of reassociated mouse DNA fragments was indicated (see Fig. 102). However, the utility of the phosphate gradient procedure would be enhanced if reassociated fragments from a defined elution region could be dissociated, reacted with unlabeled fragments, and still retain similar elution characteristics. As indicated in Fig. 103, the reproducibility of the elution position of fractionated, radio-labeled green monkey DNA fragments reassociated with an excess of unlabeled, homologous DNA fragments is excellent. This was true for DNA fragments that were initially eluted by PB with peaks at either 0.12 *M* or 0.27 *M*.

### Gradient Elution Profiles of Animal DNAs

A limited survey of the PB gradient elution profiles of animal DNAs has been made (Fig. 105). The primate DNAs from green and capuchin monkeys exhibit the cleanest separations into repeated and unique DNA fractions. The unique DNA is eluted at 0.11–0.12 *M* PB and is distinctly separated from the repeated sequences which are eluted at 0.22–0.28 *M* PB. Mouse and calf DNAs also exhibit three distinct peaks in their elution profiles, but the separation of the region containing unique DNA se-

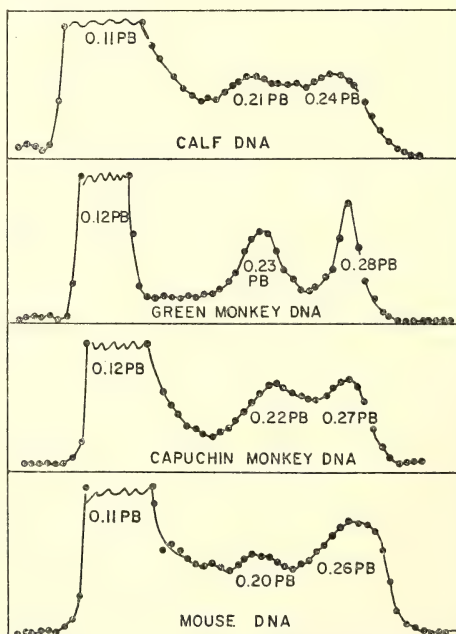


Fig. 105. Comparison of phosphate gradient elution profiles of reassociated animal DNA fragments. DNA fragments from the indicated sources were dissociated and reassociated for an equivalent *Col* (0.12 *M* PB, 60°C) = 100. The reassociated DNA was then adsorbed to and eluted from hydroxyapatite as described in the legend of Fig. 100. The phosphate concentrations at the peaks of the elution profiles are indicated. The amounts of DNA eluted by greater than 0.14 *M* PB were 30–40% of the total amount adsorbed. The abscissae and ordinates are dimensionless to simplify presentation.

quences from those containing repeated sequences was less distinct. In addition, a greater proportion of their repeated DNA was eluted by lower PB concentrations. In view of the results presented by Reed (*Year Book 68*, pp. 386-388) and Rice (*Year Book 69*) on relationships of repeated DNA sequences, it is interesting to speculate that major and more recent saltatory events (*Year Book 66*, p. 85) have taken place in the primate genomes as compared to those of the cow and mouse. Alternatively, the primate genome may now be evolving more slowly because of the longer generation times of the primates (Kohne, *et al.*, *Year Book 69*). In either case this could account for the somewhat more base-paired and better separated repeated DNA sequences of the two primates as compared to those of the mouse and calf.

### *General Considerations*

The phosphate gradient procedure is obviously more useful for separating "satellite" DNAs from other DNA sequences than ultracentrifugation or the usual HAP fractionations. DNA reassociation products with intermediate degrees of base-pairing may be readily selected or eliminated. Also, knowledge of the gradient elution characteristics of reassociated DNA fragments from a defined animal source will allow clean batchwise separation of its unique and repeated DNA elements.

The limited number of fragmented animal DNAs thus far examined contain repeated sequences that elute from HAP with bimodal distributions. Those sequences which elute at higher PB concentrations are apparently more extensively base-paired than those which elute at lower PB concentrations. The elution position is, in addition, reproducible. Therefore, animal DNA sequences fractionated by selective reassociation coupled with gradient elution offer further probes for the examination of intra-

species and interspecies DNA-DNA and DNA-RNA interactions.

### A POSSIBLE ROLE OF ADRENERGIC NEURONES IN MEMORY

*R. B. Roberts*

The collaboration of this department with Drs. L. B. and J. R. Flexner is long standing. The first joint paper was published in 1939, with eighteen more in the subsequent years. For the past decade our joint interest has centered on the biochemical basis of long-term memory. Most of the experimental work has been carried out by the Flexners at the University of Pennsylvania, but for the last four years there has been a small experimental effort in this Department. In addition, collaboration is maintained with Dr. Adrian Rake, a former Carnegie Fellow now at the Pennsylvania State University.

The experimental activity here for the last two years has centered around the possibility that the adrenergic system is involved in the formation of the memory trace. It was postulated that norepinephrine (commonly known as noradrenalin; for summary of relevant biochemical pathways involving norepinephrine, see below) was released from some of the neurones activated during

#### Summary of Norepinephrine Pathways

1. Synthesized in nerve ending from exogenous tyrosine. Tyrosine  $\rightarrow$  dopa  $\rightarrow$  dopamine  $\rightarrow$  norepinephrine. Conversion of tyrosine to dopa, catalyzed by tyrosine hydroxylase, is rate limiting step. This exogenous dopa increases rate of synthesis of NE. Conversion of tyrosine to dopa is inhibited by alpha-methyl-paratyrosine.
2. NE is stored in vesicles. Free NE in nerve end is degraded by monamine oxidase. Monamine oxidase can be inhibited by tranlycypromine. Vesicles can be disrupted by reserpine.
3. NE is released from vesicles to synaptic receptors. Action is terminated when NE in cleft is degraded by catechol-O-methyl transferase or is reabsorbed into nerve end. Re-uptake can be inhibited by imipramine.



the events of training and thereby the neurones involved in a particular pathway could be sensitized. Electrical activity could then continue in this pathway releasing more norepinephrine to sustain reverberation and possibly to initiate protein synthesis by stimulating the formation of cyclic AMP.

This approach continues to appear promising. Reserpine and alpha-methyl-para-tyrosine, drugs that lower the level of norepinephrine, are known to eliminate a conditioned avoidance response in a well-trained mouse (Seiden and Peterson, 1968,<sup>176</sup> and Schoenfeld and Seiden, 1969<sup>177</sup>). In this situation the response returns when the norepinephrine level has been restored. Work here has indicated that if the reserpine is given immediately after training or if alpha-methyl-para-tyrosine is given before training, the memory of the training is permanently reduced. These and similar experiments with other drugs that affect the adrenergic system are continuing both here and at Pennsylvania State University, but the results are not sufficiently complete to report in detail at present.

The work of the Flexners at the University of Pennsylvania over the past decade has followed a different approach,

(Flexner and Flexner, 1969).<sup>179</sup> Inhibition of protein synthesis by cycloheximide has no effect on established memory (Flexner and Flexner, 1966).<sup>180</sup> Furthermore, the puromycin blocks the expression of memory, but the trace is not destroyed because the blockage can be removed by intracerebral injection of saline solution. After this treatment memory is restored, but the mechanism remains a mystery (Flexner and Flexner, 1967,<sup>181</sup> and Flexner and Flexner, 1970<sup>182</sup>).

In *Year Book 68* we reported, "Our present activity is focused on exploring the possibility that puromycin acts by blocking receptor sites for norepinephrine or epinephrine in the central nervous system." This thought was partly derived from our conviction that norepinephrine was involved in memory formation and partly from the similarity of the structure of the O-methyl-tyrosine moiety of puromycin and the structures of norepinephrine and various mescaline-like drugs. It seemed possible that the O-methyl-tyrosine end of puromycin adsorbed to norepinephrine receptors and that the attachment was stabilized by van der Waals forces from the peptide moiety. If so, it might be possible to reverse the block established by puromycin by use of drugs known to influence the adrenergic system. Experiments to test this possibility were carried out by the Flexners.

Mice were trained to a criterion of 9/10 in a single session on day one in a Y-maze. On day two, according to their weight, they were injected bitemporally at each site with 90 or 120  $\mu$ g of puromycin 2-HCl (neutralized with NaOH) dissolved in 12  $\mu$ l of saline. Intraperi-

#### Schedule of Training and Injections

<u>Day 1</u>	<u>Day 2</u>	<u>Day 10</u>	<u>Day 18</u>	<u>Day 32</u>
Train	Inject	Inject	Test	Final test
	puromycin (i.c.)	drugs (i.p.)	memory	of memory

but now the two lines of effort seem to be converging. They have shown that even a well-established memory can be blocked by intracerebral injection of puromycin. This drug was first chosen as an inhibitor of protein synthesis, but it now appears that its action in blocking *established* memory occurs after the puromycin is converted to a puromycin-peptide. Such molecules persist in the brain for periods up to three months

toneal or subcutaneous injection of drugs was given on day 10. On day 18 when the mice had recovered from the adverse effect of the drugs they were tested to determine their memory of training. A final test of retention of relearning was made two weeks later.

The procedures for training, injecting puromycin, and retention testing have been described in detail (Flexner and Flexner, 1963).<sup>178</sup> Furthermore, this technique for disruption of memory by puromycin has been in use for eight years and has resulted in consistent loss of memory.

The following drugs were used in an attempt to restore memory blocked by puromycin:

L-dopa was chosen on the chance that it, or its metabolic products, dopamine and NE, might displace puromycin bound to adrenergic sites.

Reserpine was chosen because of its action in releasing NE from storage vesicles. Its further action in depleting the level of NE would not be expected to be useful in displacing puromycin.

Imipramine was selected because of its action in blocking the synaptic uptake of NE, presumably by competing with NE for the uptake sites. It might

consequently be effective in displacing puromycin.

D-amphetamine was used as it causes marked changes in the central nervous system possibly by mimicking NE, by releasing NE, by inhibiting monamine oxidase, by inhibiting re-uptake of NE, or by other yet unrecognized actions (Iversen, 1967).<sup>183</sup>

Tranlycypromine is a monamine oxidase inhibitor and hence could be expected to raise the level of NE, which, in turn, might displace puromycin. In addition, it may discharge NE and act like imipramine in interfering with the re-uptake of NE (Schildkraut, 1969).<sup>184</sup>

These drugs were injected in an amount only slightly below the lethal limit as roughly estimated in preliminary tests. Other tests showed that the drugs had no effect on the memory of mice that had not received puromycin.

The results are given in Table 31. In accord with previous experiments, the control group showed complete loss of memory. Since the drugs were used at a high dosage a number of deaths occurred. Among the survivors, however, recovery, as judged by cage and maze behavior, was complete 8 days after treatment. As shown in the table, resto-

TABLE 31. Effect of Drugs on Memory Restoration after Memory Blockage with Puromycin

Drug	Dose, mg/kg	Number of Mice Surviving with Memory		Lost	Died
		Restored	Impaired		
Reserpine	2.5 i.p.	0	3	3	1
L-dopa	175 i.p.	1	1	1	0
Imipramine	100 i.p.	8	0	0	6
Tranlycypromine	25 s.c.	3	0	0	1
	12.5 s.c.	3	0	1	0
D-amphetamine	25 i.p.	3	1	0	4
	12.5 i.p.	1	0	0	1
Saline	i.p.	0	0	9	0

All animals injected bitemporally with 12  $\mu$ l puromycin, 90  $\mu$ g per site for mice of 29–33 g; 120  $\mu$ g per site for mice of 34–41 g. Puromycin injections made one day after training. Drug or saline injections 8 days after puromycin. Retention tests 8 days and 22 days after drug injections.

i.p. = intraperitoneal

s.c. = subcutaneous

Average savings of mice with memory classified as: restored, 89%; impaired, 45%; lost, 0.5%.

ration of memory following injection of imipramine, tranlycypromine, and D-amphetamine was striking. Two groups of mice were treated with these drugs at different times, and the results were highly consistent. Reserpine and L-dopa on their first trial gave a relatively weak indication of restoring memory and were not tested further. Three mice used in these experiments had impaired memory on their final retention tests; the remainder showed retention of relearning at a high level.

In spite of the limited number of mice tested we believe that these experiments are sufficient to establish the efficacy of imipramine, D-amphetamine, and tranlycypromine in restoring the memory of mice treated with puromycin. In view of the consistent amnesia produced by puromycin we consider that even the partial restoration caused by reserpine and L-dopa may be significant. Thus, a group of drugs of widely different chemical structure which share the ability to cause drastic changes in the adrenergic system also appear to share the ability to restore or to improve memory blocked by puromycin.

This result suggests, then, that (1) puromycin peptides may be absorbed to adrenergic sites in the central nervous system and so block expression of memory, and (2) a stable modification of adrenergic sites may be involved in the formation and persistence of the memory trace. This view is consistent with the observation mentioned above, that reserpine and alpha-methyl-para-tyrosine, both of which cause reduction of the NE level, can produce a temporary impairment of the performance of a well-established conditioned avoidance response.

Deutsch has presented experiments that he interprets to indicate that the cholinergic system is involved in memory of maze learning in rats (Deutsch, 1969).<sup>185</sup> The involvement of both systems is not inconsistent if it is considered that the adrenergic system acts as a

modulator to increase the sensitivity of the cholinergic system, or, as proposed by Burn 1968,<sup>186</sup> that acetylcholine is responsible for the release of NE.

Further experiments are in progress to determine whether the drugs we have used cause a release of radioactive puromycin peptides from the brain.

## THE NUCLEAR SATELLITE IN SLIME MOLD

*R. J. Britten and Jean F. Smith*

The DNA of the myxomycete *Physarum polycephalum* contains a component with properties that suggest that it might supply evidence on the production of repeated sequences. This component has been studied in some detail by Braun and Evans<sup>187</sup> at Case Western Reserve University, who reported the following list of properties. (1) It is restricted to the cell nucleus. (2) It has a high GC content at the extreme range of the principal nuclear DNA, and thus can be enriched by CsCl density gradient centrifugation. (3) It is extracted from nuclei under conditions that extract little of the principal components of the DNA. (4) Most interestingly, this component is synthesized throughout the cell cycle and its synthesis is not coordinated with that of the principal nuclear DNA which is made during an S-phase that lasts only about 20% of the cell cycle.

As we became aware of these properties it seemed likely that this component, which we term for convenience the nuclear satellite, would be a repeated DNA component. A cooperative research project developed with Dr. Evans, and he sent to the Department of Terrestrial Magnetism samples of total nuclear DNA and labeled nuclear satellite. Study of the reassociation of these samples showed that this organism indeed contains repeated DNA in large quantities and that the nuclear satellite was also made up of repetitive sequences. A brief description of the measurements follows.



The reassociation of these DNAs was studied in several ways, first examining the principal nuclear DNAs. Reassociation of the total, unsheared DNA in the spectrophotometer showed the presence of rapidly reassociating DNA, indicating that repeated sequences were present. The total nuclear DNA was then sheared (at 50,000 psi), denatured, and incubated in 0.12 *M* PB at 60°C to a  $C_0t$  of 38 and passed over hydroxyapatite at 80°C in 0.12 *M* PB. The bound fraction (55% of the DNA) was eluted in the double-stranded form with 0.4 *M* PB. The bound fraction consisting of most of the repeated sequences was placed in the spectrophotometer in 0.12 *M* PB and melted and reassociated. The result is shown in Fig. 106. The melting curve was very broad, rising linearly from 62°C

to 85°C and the hyperchromicity was 15.9%. These characteristics are typical of the repeated sequences of higher organism DNA and thus this myxomycete takes the position (probably temporary) of being the "lowest" or least complex organism with large quantities of typical repeated DNA.

The reassociation kinetics of the repetitive fraction are complex as measured in the spectrophotometer. There is a large initial drop in optical density followed by a small component reassociating in the range of 0.02  $C_0t$  (20,000 copies), and then by a large component that is not complete at the end of the run and probably has a half reaction  $C_0t$  of about 3 to 10. There are probably of the order of 100 copies of this major component and its complexity is some-

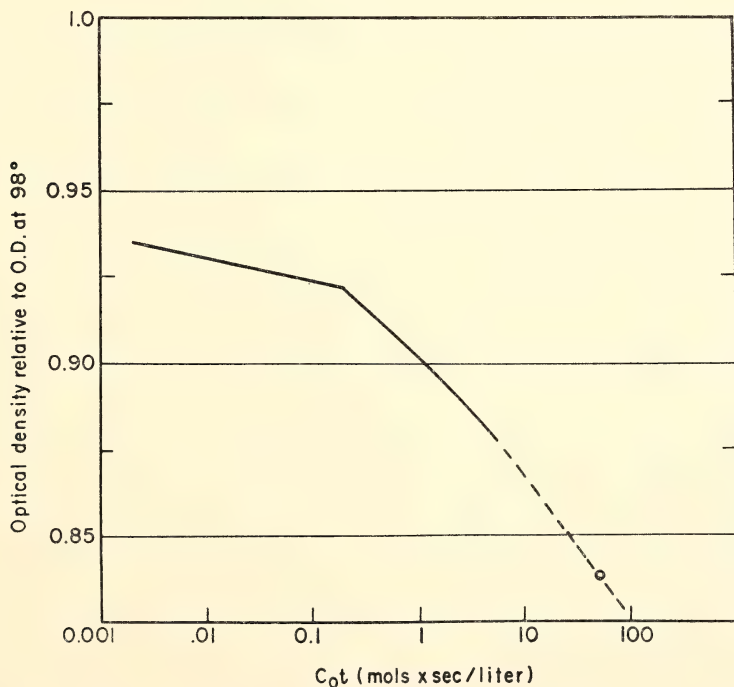


Fig. 106. The reassociation of the repeated sequence fraction of *Physarum polycephalum* DNA measured in the spectrophotometer. The optical density at 260  $m\mu$  is shown relative to that observed at 98°. Incubation was at 60° in 0.12 *M* PB at a concentration of about 40  $\gamma$ /ml. The preparation of the repeated sequence fraction on hydroxyapatite is described in the text. The final point is derived from the initial melt of this fraction and is plotted at the  $C_0t$  used for its preparation.

what less than that of a bacterial genome. This numerical coincidence, of course, raises the question of whether this might be DNA from a symbiotic bacterial "contaminant." This possibility is ruled out by the very broad melting curve of this repeated DNA component.

The reassociation of the nuclear satellite was measured in the presence of a great excess of total nuclear DNA. Both DNAs were sheared at 50,000 psi and denatured and incubated together in 0.12 M PB at 60°C at a ratio of about 250/1. This method of incubation was chosen because it should give a direct measure of the number of copies of the satellite present in the total nuclear DNA, even though the specific radioactivity of the satellite was not well known. Little radioactivity was present in DNA other than that of the satellite because of the method of labeling and preparation. Taking advantage of the phased growth of this organism, the H3 thymidine tracer was added during G2 phase, when little

or no principal nuclear DNA was being synthesized. The satellite was selectively extracted and finally purified by CsCl density gradient centrifugation. Samples of the incubation mixture were taken after incubations to various  $C_0t$ s and diluted into 10 ml of 0.12 M PB at 60° and passed over hydroxyapatite (0.12 M PB, 60°C). Figure 107 shows the results of these measurements. The lower curve shows the fraction of the radioactive satellite DNA that was bound. The upper curve is constructed from several kinds of data and shows the expected binding of the principal nuclear DNA. The two points show actual hydroxyapatite binding measurements done exactly under the described conditions. The later part of the curve is based on the known genome size ( $5 \times 10^{-13}$  g per cell haploid), which implies that single copy DNA would reassociate with a half-reaction  $C_0t$  of 500. The early part of the curve is based on the optical reassociation measurement described above. The single

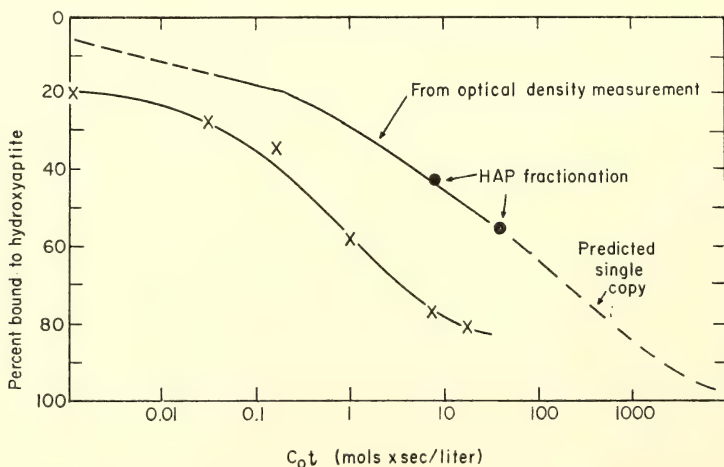


Fig. 107. The reassociation of *Physarum polycephalum* nuclear satellite (lower curve). Purified labeled nuclear satellite incubated at 60° in 0.12 M PB in the presence of a great excess of total nuclear DNA. Samples analyzed by hydroxyapatite under standard conditions. For comparison purposes the upper curve represents a reconstruction of the expected curve for total nuclear DNA. The two points represent the results of actual hydroxyapatite fractionations at the  $C_0t$ s shown, and the curve is therefore well determined in the center region. The early part of the curve is transferred from the previous figure and fitted in the center region. It is quite uncertain below  $C_0t = 0.1$ . The later part of the curve is calculated from the known genome size and again fitted to the data in the center region.

copy region of the curve is probably quite well determined by these data but the  $C_0t$  0.1 to 1 region is somewhat uncertain and the earliest part of the curve is not yet known at all. In spite of these uncertainties this curve supplies a perfectly adequate reference for judging the repetition frequency of the satellite. The satellite appears to contain components with repetition frequencies in the range of from a few hundred to a few thousand copies. The complexity of the satellite is not easy to estimate, since there appears to be more than one component. Evans estimates that the satellite amounts to more than 1% of the total nuclear DNA. If this were so there would be components ranging in complexity from 1000 to 10,000 nucleotide pairs.

Thus it is clear that the nuclear satellite of *Physarum* is an example of a set of repeated DNA sequences whose synthesis is not under the same set of controls as the principal nuclear DNA. While these data are very suggestive of an example of an event of saltatory replication caught *in flagrante delicto*, further measurements are obviously required. It would be valuable to know whether the quantity is constant or varies with growth conditions or strain and species of *Physarum*. If there were such variations, the content of hybrid progeny would probably be informative. It would, of course, be important to know how it is organized in the nucleus and how its synthesis is controlled. It would also be valuable to know whether any of the copies are yet interspersed among the sequences of the principal nuclear DNA. There are some interesting speculative possibilities for future investigation. Is this satellite DNA an analog in higher cells of a bacterial episome or is it virus-like?

## MEASUREMENTS OF THE RATE OF GROWTH OF THE POLYNUCLEOTIDE CHAINS OF RIBOSOMAL RNA IN *Bacillus subtilis*

Roger J. Avery

Hybridization studies have indicated<sup>188, 189, 190, 191</sup> that in *E. coli* the RNA extracted from the two ribosomal subunits have nucleotide sequences in common. No such sharing of nucleotide sequences has been found on investigation of the ribosomal RNAs from the organism *Bacillus subtilis*.<sup>192, 193, 194, 195, 196</sup> One question arising from these findings is whether the process of ribosomal RNA transcription might also differ in these bacteria. The time required for the actual process of synthesis of a 16S or 23S ribosomal RNA chain is a diagnostic feature of the transcription event and can be measured. Estimates in *E. coli*<sup>189, 197, 198</sup> have indicated that an equal time is required for synthesis of a molecule of either RNA type. This report describes measurements of the rate of synthesis of 23S and 16S ribosomal RNA chains in exponentially growing cultures of *Bacillus subtilis*.

*Theoretical considerations.* If an exogenous source of a radioactively labeled precursor of nucleic acids, e.g., [5-<sup>3</sup>H] is added to steadily growing and dividing bacterial cultures, the precursor passes through incomplete RNA chains before entering the completed fraction of ribosomal RNA, later to be incorporated into the ribosomes. If the progress of entry of labeled precursor into completed chains of RNA is monitored over a suitable time interval, the curve obtained shows a rapid change of slope to a constant rate of incorporation of radioactivity. When the steady state is reached, all pre-existing unlabeled material has been "washed out" of the pool of uncompleted chains, and this pool is now saturated with materials having the same specific radioactivity as the added exogenous precursor. The time interval between addition of the exogenous precursor and the abrupt change



in rate of incorporation is a measure of the time required for synthesis of a completed ribosomal RNA chain.

The latter statement is correct only if there is no appreciable delay in the appearance of label in polynucleotide chains due to earlier passage of the precursor through the intracellular nucleotide pools, or to the effects of recycling material from unstable RNAs. Several authors have demonstrated that in *E. coli* radioactivity appears without delay in an RNA fraction that is not rapidly turning over and has the base composition and hybridization characteristics of ribosomal RNA.<sup>199, 200, 201, 202, 203</sup> Recently Midgley<sup>204</sup> has made similar observations for *B. subtilis*. Thus, the influence of nucleotide pools and messenger RNA stability on the incorporation of an exogenous precursor into ribosomal RNA can be excluded, at least at early times.

**Kinetic analysis.** If  $T$  is the time required for the formation of a complete molecule of 23S ribosomal RNA, it is convenient to analyze separately the entry of label into the RNA before and after  $T$ . Initially, chains that are being completed will be labeled only in the terminal nucleotides. The rate of appearance of radioactivity in completed chains will then increase linearly with time ( $t$ ), until, at time  $T$ , the chains that are being completed are maximally labeled. Thereafter, the rate of incorporation of radioactivity into the fraction comprising completed RNA chains will remain constant.

The rate of incorporation of radioactivity into finished chains will, therefore, be in two stages given by

$$\frac{dR}{dt} = \frac{C}{T} t \quad (0 < t < T) \quad (1)$$

$$\frac{dR}{dt} = C \quad (t > T) \quad (2)$$

where  $R$  is the amount of labeled 23S RNA and  $C$  is the constant rate of incorporation of radioactivity into total

23S RNA, i.e., unfinished as well as finished chains ( $C$  is actually increasing exponentially with time owing to bacterial growth, but over the brief period considered in this analysis, the assumption that  $C$  is constant introduces an error of less than 5%).

Integrating (1) over the limits of time between 0 and  $t$ , we obtain

$$R = \frac{C}{2T} t^2 \quad (0 < t < T) \quad (3)$$

This predicts that the rate of uptake of label into finished chains will increase with the second power of time at times earlier than  $T$ . When  $t = T$ , then from (3)

$$R = \frac{CT}{2} \quad (4)$$

Thereafter, equation (2) is obeyed, so that for times later than  $T$ , we have

$$\begin{aligned} R &= \frac{CT}{2} + C(t - T) \\ &= Ct - \frac{CT}{2} \quad (t > T) \quad (5) \end{aligned}$$

If we set  $R = 0$ ,  $CT/2 = Ct$ , indicating that the linear portion of a plot of  $R$  versus  $t$  should intersect the abscissa at  $T/2$ . These relationships have been used to determine the time of synthesis of 23S and 16S RNAs in *B. subtilis*.

**Results.** Cultures of *B. subtilis* 168  $T^-$  were grown exponentially at 37°, with forced aeration in "c" medium<sup>205</sup> fortified with 0.1 g yeast extract, 0.9 g casein hydrolysate and 50 mg thymine per liter. When the cultures had a turbidity at 650  $m\mu$  of 0.60, a small amount of unlabeled uracil was added in order to make the experiments strictly comparable to earlier ones performed on *E. coli*.<sup>198</sup> The amount added was such that it was nearly all incorporated in about 10 min. After this time had elapsed, <sup>3</sup>H-labeled uracil, thoroughly mixed with sufficient unlabeled carrier to ensure continuous uptake throughout the experiment, was vigorously injected with rapid stirring.

At appropriate intervals samples were removed both for freezing and the subsequent preparation of RNA, and to follow the time course of incorporation of [5- $H^3$ ] uracil into the cellular nucleic acids (Fig. 108). Growth of the cells was also followed during the uptake of isotope by measurement of turbidity to ascertain that the exponential growth rate of the cultures was maintained during the course of the experiments. Labeled samples of cells were broken in the French press at about 3° and deproteinized. DNA was removed by DNAase treatment, which was followed by further cycles of deproteinization and alcohol precipitation. The pellet from the final alcohol precipitation was extracted twice with ice cold 2*M* NaCl. This removed any polysaccharide, DNA, and

transfer RNA remaining in the preparation.

The components of the mixture were then separated by centrifugation in 5 to 20% sucrose density gradients at 3°. Fractions were assayed for extinction at 260  $m\mu$  and monitored for radioactivity. Messenger RNA contamination of each 16S and 23S peak was estimated by subjecting fractions to the procedure described in detail by Pigott.<sup>206</sup> This involved hybridizing the RNA with DNA bound to cellulose nitrate membrane filters<sup>207</sup> at DNA:RNA ratios of about 5:1 (w/w). (150  $\mu$ g DNA/filter incubated in 1.5 ml of 6 $\times$ SSC for 16 hours at 66°C.) At this level essentially all of the messenger RNA and essentially none of the ribosomal RNA will hybridize. Thus, the hybridization obtained gave

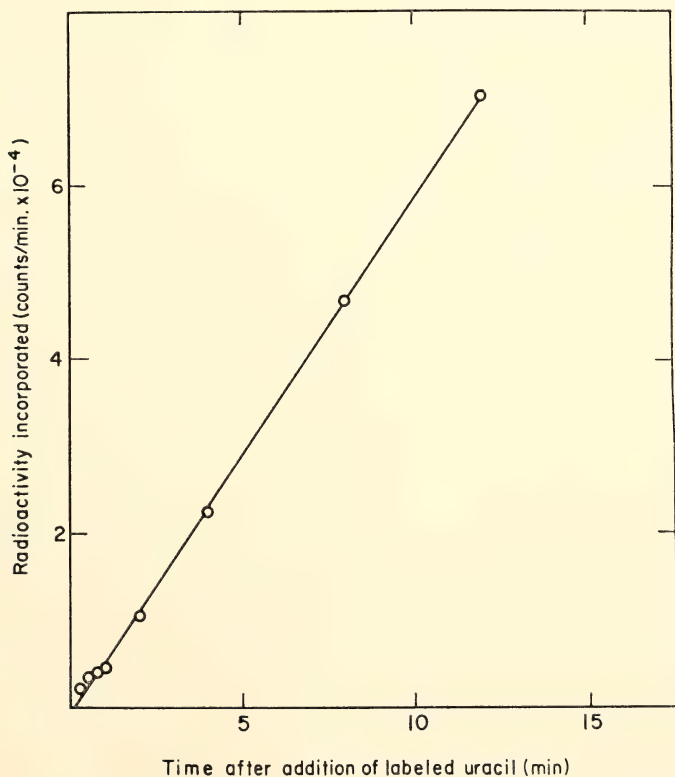


Fig. 108. The time course of incorporation of acid-precipitable radioactivity into an exponentially growing culture of *B. subtilis*.

an estimate of the percentage of messenger RNA in any sample. This decreased from about 15% during the first minute of labeling to 3–4% at 15 minutes' labeling in the 23S peak, with the 16S material showing a similar range (5–12%). After correction of the 23S

RNA peaks for this contamination, it was possible to calculate the rate of RNA chain growth for this RNA species.

In the case of the smaller RNA species a further step was necessary to correct for contamination of 16S RNA peaks by 23S RNA precursors. This was estimated

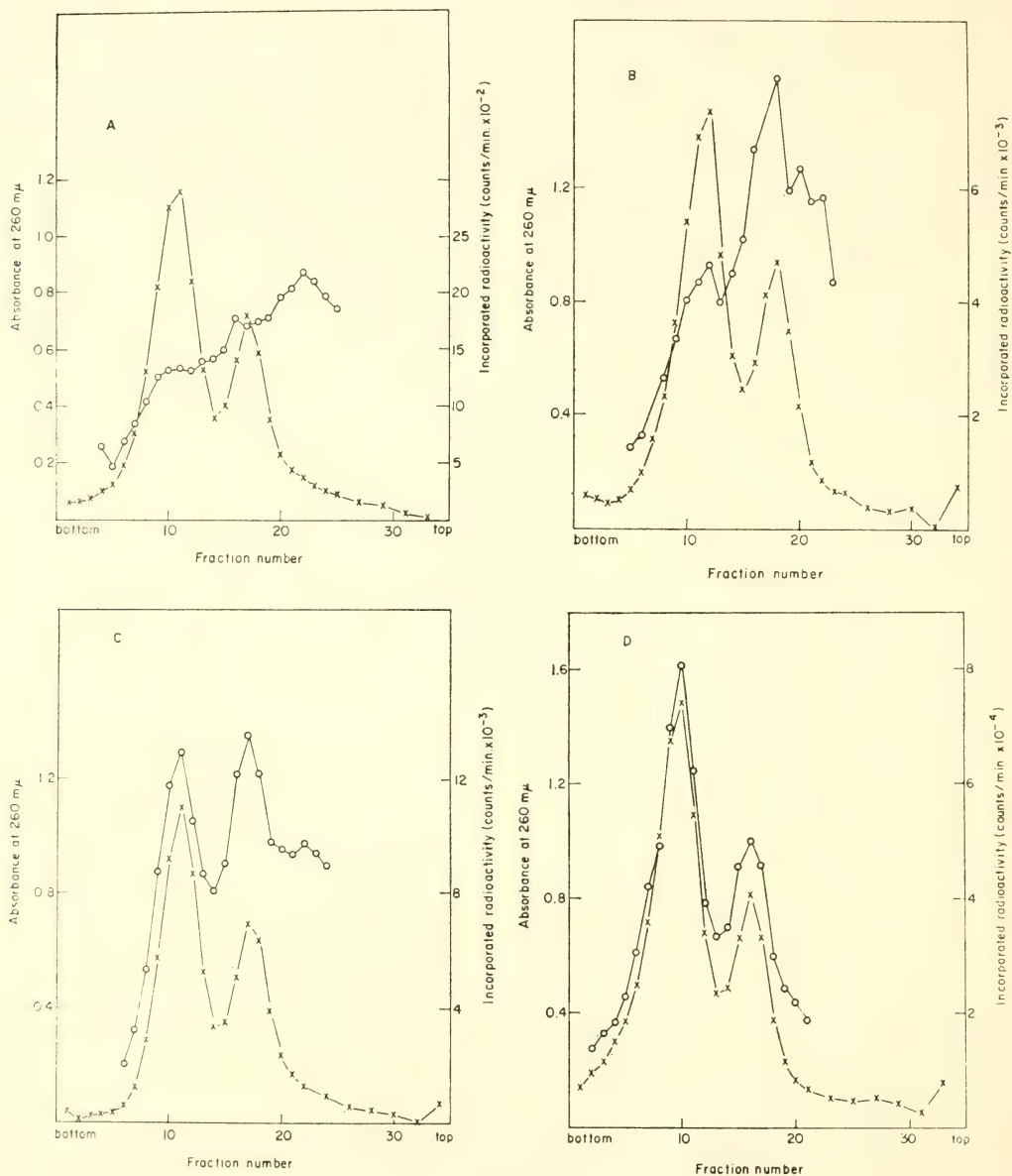


Fig. 109. Sucrose gradient sedimentation analysis of ribosomal RNA extracted from *B. subtilis* cells labeled for various times with tritiated uracil during exponential growth at 37°. Time of incorporation of uracil: 2a—15 sec; 2b—60 sec; 2c—4 min; 2d—15 min. Circles indicate radioactivity, and x's indicate absorbance at 260 mμ.



by hybridization competition experiments, made possible because 23S and 16S RNAs do not compete for each other's binding sites on the DNA in this organism.<sup>192, 193, 194, 195, 196</sup>

Figure 109 shows examples of the profiles obtained in the sucrose gradients of *B. subtilis* RNAs. The resultant curves of incorporation of uracil into finished chains of 23S and 16S RNAs are shown in Figs. 110 and 111. In calculating the results it was assumed that 16S RNA consists of 1600 nucleotides in a linear, unbranched chain.<sup>208, 209</sup> 23S RNA was assumed to be a linear polynucleotide containing 3200 nucleotide residues. The

TABLE 32. Summary of Results for *B. subtilis* Cells Doubling Every 40 Minutes

RNA	Time of Synthesis, min.	Rate of Chain Elongation, nucleotides/sec. at 37°C
16S	1.3	21
23S	2.4	22

kinetic analysis outlined earlier, when applied to Figs. 110 and 111, gave the results presented in Table 32.

The amount of RNA present as unfinished chains of the two ribosomal RNA species can also be calculated from Figs. 110 and 111. A theoretical curve of incorporation into finished plus

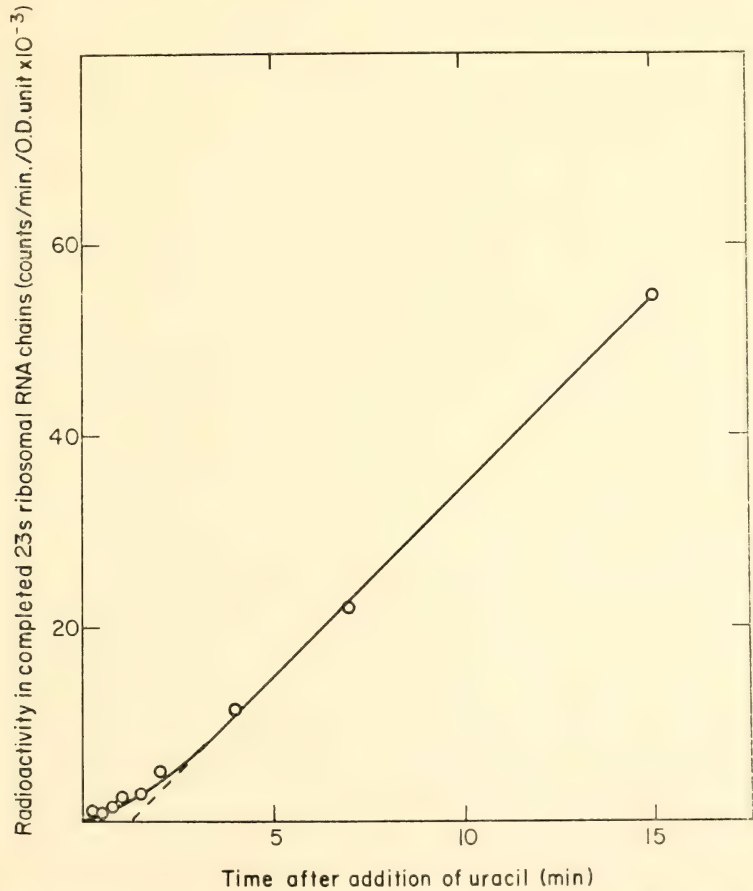


Fig. 110. The time course of incorporation of uracil into completed chains of *B. subtilis* 23S ribosomal RNA. The points represent means of duplicate determinations which for times later than 2 minutes were within 2% of each other. In an identical experiment with the same organism growing under similar conditions a straight line extrapolating to an intercept of 1.1 minutes was obtained.

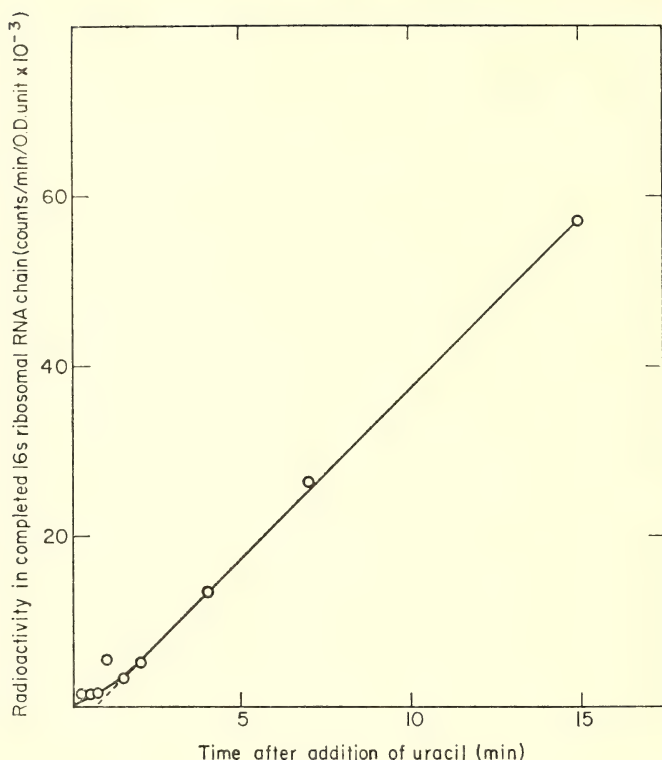


Fig. 111. The time course of incorporation of uracil into completed chains of *B. subtilis* 16S ribosomal RNA. The points represent means of duplicate determinations which for times later than 2 minutes were within 4% of each other. In addition, the straight line portions of Figs. 110 and 111 are virtually parallel as expected.

unfinished chains can be drawn parallel to the curve for finished chains and through the origin. Further, the break point in the kinetics of labeling of finished chains (i.e., the point of saturation of the pool of unfinished chains with label) can be extrapolated to intercept this line. This gives a time in which a quantity of RNA, equivalent to the pool, would be synthesized. This time/doubling time  $\times 100$  then gives the percentage of the total RNA fraction in unfinished chains. If we know the proportion of a given RNA species in total cell RNA, we can relate the percentage of unfinished ribosomal RNA chains to the total RNA in the cell. This works out as 2.2% of the total RNA.

*Discussion.* It is possible to put a limit on the time required for synthesis of a complete ribosomal RNA chain, as a bacterium growing in a defined medium must double its content of ribosomes by the time it is ready for cell division. If in *B. subtilis* doubling about every 40 min. there are approximately 13,000 ribosomes per cell,<sup>198</sup> between 5 and 6 ribosomes must be made each second if the rate of ribosome synthesis does not vary throughout the cell division cycle. If 11 cistrons are responsible for the synthesis of either 16 or 23S RNA,<sup>191</sup> each will produce a molecule every 2 seconds in cells growing under the conditions described.

However, the process may be inter-

mittent and these rates of ribosomal RNA synthesis will thus be considerably underestimated, as they are "averaged out" throughout the whole time period. In addition, of course, it is necessary to distinguish between the rate of output and the rate of polynucleotide chain synthesis of individual ribosomal RNA molecules. There is no reason why a DNA-dependent RNA polymerase molecule producing a ribosomal RNA chain by the transcription of any given cistron has to complete the RNA molecule before a second enzyme can initiate its own RNA synthesis on the same cistron. Thus, it is possible that several ribosomal RNA molecules are being transcribed on the same cistron simultaneously. Indeed, Goldstein, *et al.*,<sup>210</sup> in measurement of the rate of synthesis of total *E. coli* RNA at 0°, determined the number of growing points as  $10^3$  per genome at any given time. This indicates multiple growing points for RNA, certainly on the more active genes. Thus, the rate of *de novo* synthesis of ribosomal RNA in a growing bacterium is a function of two parameters: the number of nascent RNA chains that are being formed at any given time, and the rate at which growth of the nascent RNA chains is propagated. The rate of RNA polynucleotide chain growth is measured as the time needed for one RNA polymerase molecule to transcribe the whole of a cistron. If several polymerases are engaged in transcribing the same cistron, the rate of RNA chain synthesis will be lower than that of RNA output by a factor given by the number of polymerases per cistron, if all are equally active. The results presented here indicate that the time required for an RNA polymerase molecule to synthesize an RNA chain is proportional to the length of that RNA chain. Assuming chain size is a reflection of cistron size, it appears that the rate of movement of polymerase molecules is the same during transcription of all cistrons coding for ribosomal

RNA in *B. subtilis*. Further, as there are equal numbers of cistrons that will hybridize with the 23S and 16S RNA species,<sup>191</sup> it is only necessary to postulate an equal spacing of polymerase molecules on these cistrons to produce the observed 1:1 ratio of 23S and 16S molecules. It is apparent that no such simple explanation is allowed by the results obtained for *E. coli*. The indication given by the hybridization results of a basic difference in ribosomal RNA biosynthesis between the organisms *E. coli* and *B. subtilis* is strengthened by the findings presented here. The results also indicate that the measured delay in appearance of radioactivity in completed ribosomal RNA chains cannot be entirely due to passage through nucleotide pools or recycling of unstable RNAs, as in this case the delay times would be identical for the two ribosomal RNA species.

*Some numerical considerations.* The formation of a chain of *B. subtilis* 23S RNA consisting of about 3200 nucleotide residues in 2.4 minutes at 37° means that the rate of ribosomal RNA propagation in these cultures is about  $3200/144 = 22$  nucleotides/sec. In order to produce the observed amount of RNA from the known number of gene copies, many DNA-dependent RNA polymerase enzymes must function on a DNA cistron at the same moment. With a doubling time of 40 min. at 37°, *B. subtilis* produces 13,150 70S ribosomes (in glucose-salt media)<sup>198</sup> and, therefore, 13,150 RNA chains of molecular weight  $1.1 \times 10^6$  (equivalent to the ribosomal RNA in a 50S ribosomal subunit).<sup>208</sup> Thus, in one minute 13,150/40 or 329 such chains are produced, assuming this is a constant process throughout the time between cell divisions. As there are about 11 cistrons per genome<sup>191</sup> corresponding to the ribosomal RNA (23S) present in each 50S ribosomal subunit, each cistron is responsible for producing about 30 ribosomal RNA molecules per minute. Since it takes 2.4 min. to form a complete



chain of RNA, at least  $2.4 \times 30$  or 72 molecules of DNA-dependent RNA polymerase must be at work at the same time on each cistron that specifies *B. subtilis* 23S ribosomal RNA. Thus, each cistron of 3200 base pairs must have one transcribing enzyme every 44–45 nucleotide residues. As 1 nucleotide residue on the DNA spans 3.4 Å, then the enzyme centers will be about 150 Å apart. This is near the estimated diameter of about 100 Å for *E. coli* DNA-dependent RNA polymerase.<sup>211</sup> Thus it would appear that under these conditions of growth, the bacterial DNA templates specifying the structure of ribosomal RNA are being used close to the limit of their physical capacity for accommodating polymerase enzyme molecules. Furthermore, the nascent RNA product cannot remain in close contact with the DNA template in a way that would impede transcription by a closely succeeding polymerase. The indication appears to be that for even faster growth to occur in *B. subtilis*, the rate of chain growth would have to be a variable factor, although there is still some "slack" that could be taken up by crowding the enzymes even closer together on the DNA.

## BACTERIOPHAGE DNAs

Dean B. Cowie and Roger J. Avery

### Introduction

Bacteriophages have been classified on the basis of their interactions with host bacteria. *Virulent* phages invariably lyse the cells they infect, releasing progeny viruses. *Temperate* phages, on the other hand, have an additional capacity: viral infection often results in the integration of the phage chromosome into the DNA of the host cell. Lysis does not then result and the subsequent nor-

mal replication of host DNA insures the replication of the viral genome.

The DNAs isolated from viruses of these two classes also have characteristic differences.

1. Large-scale intramolecular heterogeneity and an uneven distribution of bases are observed in the DNAs of many temperate phages.<sup>212, 213, 214</sup> DNAs isolated from virulent phages do not show such nucleotide clustering. The distribution of guanine and cytosine (GC) in the DNA molecules isolated from the T phages appears to be unimodal and approximately Gaussian.<sup>212</sup>

2. DNA homologies among virus and host chromosomes occur in a variety of lysogenic systems and the homologous segments appear to be numerous and distributed throughout the viral genome. No evidence for such host-viral DNA homologies has been observed among the virulent phages except with T3, a pseudolysogenic virus.<sup>215</sup> The DNA of temperate phages thus appears to contain certain regions homologous to host DNA, while the DNAs of virulent phages do not. Stimulated by a seminar by Dr. Sewell Champe, who described to us differences among peptides produced after infection with the different T-even phages (T2H, T4D and T6), studies were initiated to examine in detail the DNA of these autonomous virulent phages. Initially it was hoped that specific nucleotide sequences might be identified among the DNAs of these related viruses which could be correlated to portions of the genetic linkage maps extensively described by other investigators.

### *Thermal Denaturation Characteristics of DNAs Isolated from Phages T2H, T4D and T6*

Thermal dissociation profiles have been obtained from studies of the reaction products resulting from the incubation of denatured P<sup>32</sup> labeled T2H DNA

\* This work was carried out in collaboration with Dr. Sewell Champe of Rutgers University.

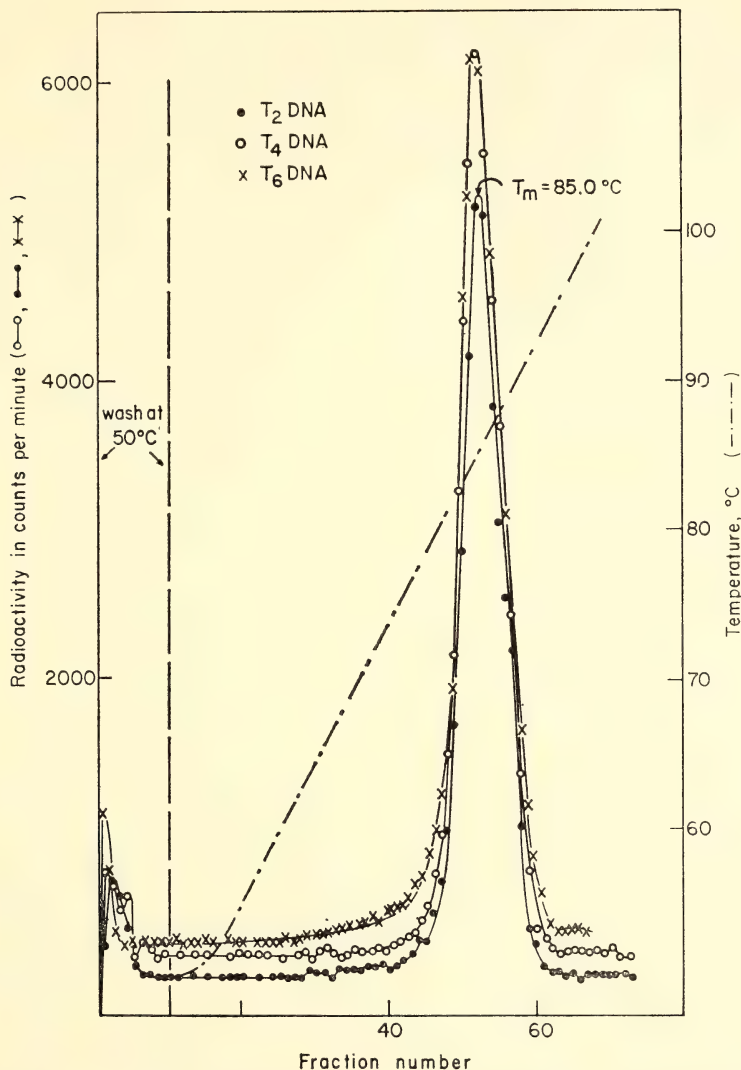


Fig. 112. Thermal elution profiles of the reaction products resulting from the incubation of labeled T2H, T4D, and T6 DNA fragments with excess unlabeled homologous DNAs. Radioactive ( $P^{32}$  labeled) DNAs isolated from the T-even phages and sheared at 50,000 psi were denatured by boiling and immediately incubated at 50°C with similarly treated nonradioactive T-even viral DNAs in 0.14 M phosphate buffer (PB). The concentration of the DNAs employed and the time of incubation were selected to give  $C_{0}t_{0.5}$  of 0.002 and 20.0 for the radioactive DNA and the unlabeled DNAs, respectively. These conditions were selected to provide for greater than 95% reassociation of homologous DNA segments and less than 3% reassociation of the labeled DNA fragments in the absence of other DNAs. A linear temperature gradient, (50 to 100°C) was used to elute DNA fragments.

with excess unlabeled T2H DNA fragments.\*

Figure 112 (lowest curve) shows the elution profile obtained with the reassociated T2 DNA fragments. Similar thermal dissociation profiles resulting from studies of the products of the reaction

\*For such reassociation and thermal denaturation studies, the concentration of the labeled DNA fragments is kept as small as possible in order to minimize its self-reaction. Under the conditions employed less than 3% of the labeled DNA self-reacts and the zero-time binding does not exceed 1%. Other experimental details are described in the legend of Fig. 112.

of T4D and T6 DNA fragments with their homologous DNAs are also shown in Fig. 112. (These additional profiles have been slightly elevated in this figure for clarity in presentation of the data.) In each case more than 95% of the labeled DNA fragments reacted with homologous DNA segments, and temperatures considerably in excess of 50°C were required for their elution with 0.14 *M* phosphate buffer (PB) from the hydroxyapatite columns.

There is no evidence of nucleotide clustering, since the differential plot of the elution data appears almost Gaus-

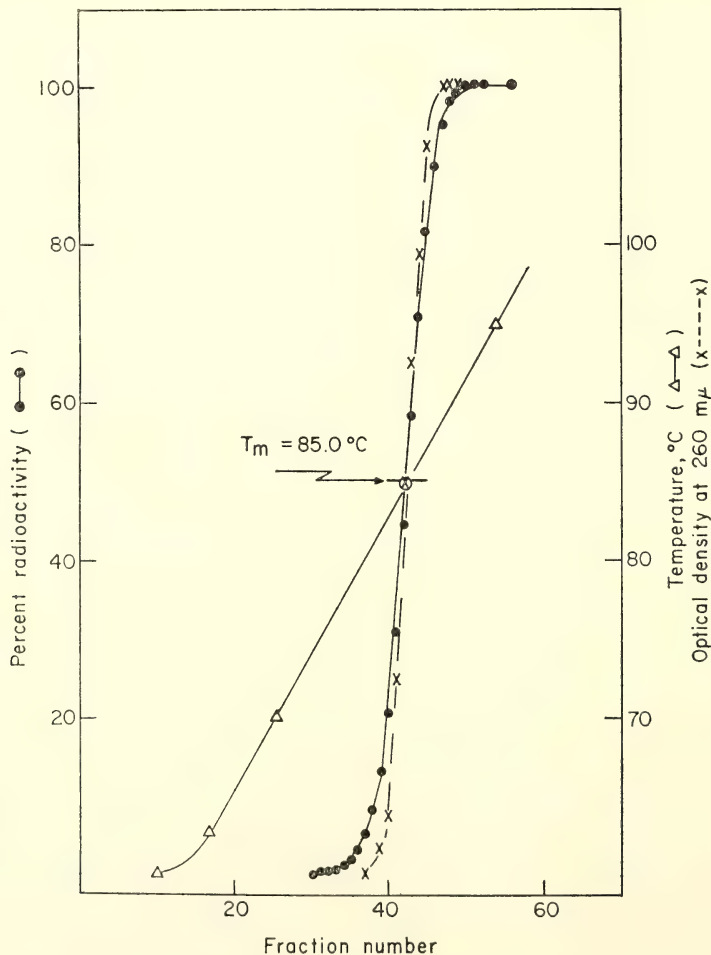


Fig. 113. Reassociation of T4 phage DNA.



sian. Half of the reacted DNA fragments are eluted with only a 6°C increase in temperature (82–88°C).

In these experiments the concentration of the labeled DNA fragments is too low to detect optically. The unlabeled DNA, however, is measurable at 260 m $\mu$  and has been routinely employed to determine by its elution profile the  $T_m$  of this material. The first eight separate determinations of  $T_m$  for each of these T-even phage DNAs were averaged and values of 84.4°C, 84.5°C, and 84.4°C were obtained for the T2, T4, and T6 DNAs, respectively. These optical elution determinations of the  $T_m$ 's serve as internal standards for comparison with the elution profiles of the radioactive materials. For all three of the phage DNAs shown in Fig. 112 the  $T_m$  determined from the optical and radioactivity data was 85°C. A comparison of the  $T_m$ 's obtained from optical and radioactivity measurements of reassociated T4 DNA is shown in Fig. 113.

#### *T-even Viral and Bacterial DNA Studies*

Studies involving DNA-DNA interaction among the bacteriophage DNAs require complete elimination of bacterial host DNA in the purification of phage DNA preparations. Schildkraut and co-workers<sup>216</sup> have reported that no homology could be detected between the DNA of T-even bacteriophages and the DNA of *E. coli*. Furthermore, in this laboratory, by employing an analytic method in which tracer self reaction did not affect the results (DNA-agar method) it was possible to demonstrate that reactions between labeled T4 DNA fragments and *E. coli* DNA had to be less than 1% of the viral genome (Year Book 67, p. 301). In the studies described below, thermal chromatography with hydroxyapatite was exclusively employed to establish both the degree of self reassociation and the purity of the

labeled phage DNA fragments to be used in these investigations. Figure 114 shows the results obtained when labeled T6 DNA fragments were incubated with a large excess of *E. coli* DNA at  $C_0t$ 's of .002 and 61, respectively. The thermal elution profile shown in Fig. 114 shows that no reaction could be detected between labeled T6 fragments and *E. coli*; 98% of the labeled T6 DNA was eluted at 50°C in the 0.14 M PB washes.

The 2% of the radioactive fragments remaining on the hydroxyapatite column required temperatures in excess of 75°C for elution; its denaturation profile is shown (enlarged scale) in Fig. 114. Re-associated *E. coli* DNA, detected optically, eluted with a  $T_m$  of 91°C (Fig. 114), which is significantly higher than the  $T_m$  of the radioactive material at 83.5°C. These  $T_m$  values, measured optically and by radioactivity, are those expected of the *E. coli* (GC 50%) and the T-even phage DNAs (GC 35%), respectively. Furthermore, since from 2% to 3% self reassociation was anticipated for the labeled-phage fragments under these conditions, it was concluded that the elution profile determined by radioactivity represented self-reacting material and that radioactive *E. coli* contaminants were not present. Similar tests carried out with other labeled T-even phage DNA preparations gave comparable results.

The overall similarities observed among the elution profiles of each of the T-even phage DNAs, their essentially Gaussian character, and very similar  $T_m$ 's with most of the DNA fragments eluting over an extremely small temperature range (80–90°C) are all consistent with the close genetic relationships held among these viruses. No large-scale intramolecular heterogeneity in nucleotide composition could be detected. Studies of heterologous DNA-DNA interactions, however, provide additional quantitative information concerning the DNAs of these phages. The major part

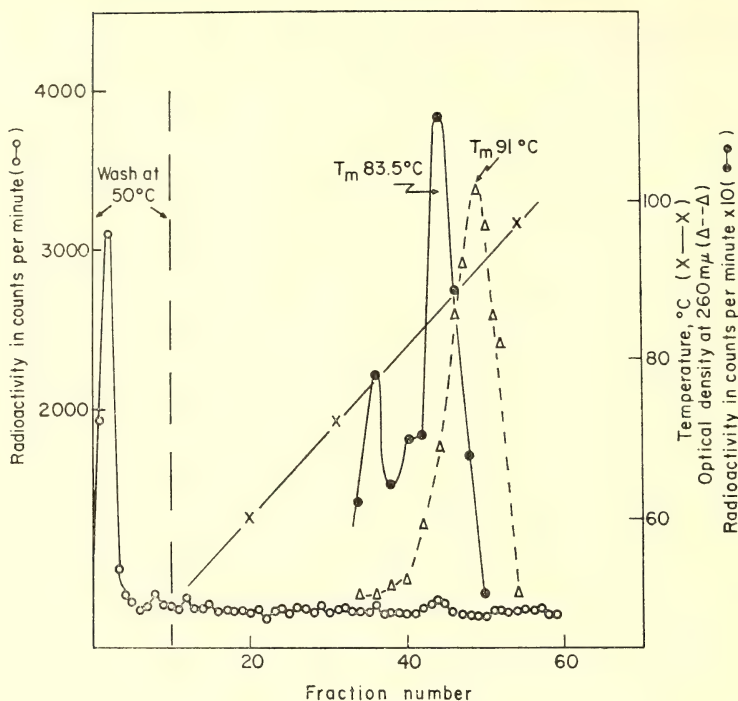


Fig. 114. Thermal elution profiles of the reaction products resulting from the incubation of labeled T6 DNA fragments with excess unlabeled *E. coli* DNA.

of this report describes the results of these investigations.

#### *DNA-DNA Reactions between the Genomes of Bacteriophages T2H and T4D*

When labeled T4 fragments are incubated with a large excess of unlabeled T2 DNA, about 82%\* of the T4 fragments will form nucleotide sequence duplexes with the T2 DNA. Fig. 115 demonstrates that the thermal stability of the T4-T2 reaction products is almost as high as that obtained with studies of the reassociation of homologous T2 or T4 DNA fragments (Fig. 112). The elution profile obtained for the heterologous DNA reaction (solid curve, radioactivity data) has a  $T_m$  about 3° lower than that determined from the

optical elution profile for reassociated T2 DNA (U.V., broken curve). Both elution profiles retain their narrow Gaussian characteristics except for a small amount (about 8%) of the labeled material which elutes at lower temperatures (66–77°C).

The overall lowered thermal stability of the heterologous DNA duplexes can be interpreted in several ways. A major portion of the nucleotide sequences held in common (1) contain short nonhomologous regions, or (2) are richer in adenine+thymine (AT) than intraspecies reassociation products, or (3) are a combination of (1) and (2).

Since such a large part of the T4 DNA fragments react so effectively with the T2 DNA and the overall GC contents of the two DNAs are so similar (equal  $T_m$ 's, Fig. 112), the first possibility above would seem most likely. If this is the

\* All percentages of interspecies homology have been normalized. (See Table 33.)

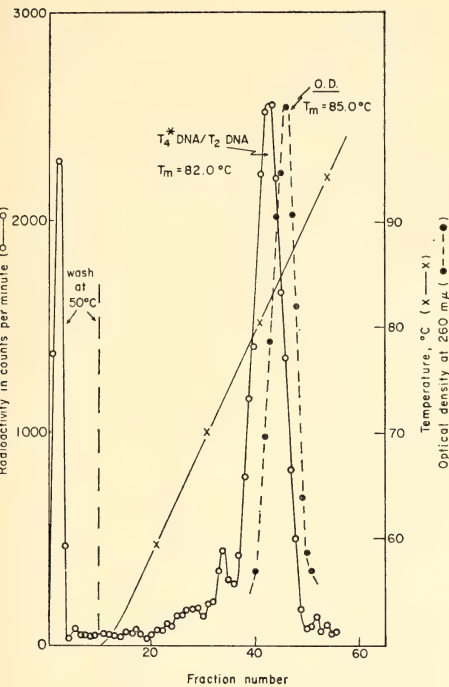


Fig. 115. Thermal elution profiles of the reaction products resulting from the incubation of labeled T4 DNA fragments with excess unlabeled T2 DNA.

case the material represented by the single large elution peak can be estimated to have unmatched base pairs of the order of 4 or 5%. It is surprising,

then, that such a large part of the T4 DNA fragments, about 18%, does not appear to react with the T2 DNA at all, as if in this material no similarities between these two viral DNAs existed.

Reciprocal experiments were carried out as controls by incubating labeled T2 DNA fragments with the excess unlabeled T4 DNA. Again, the results were surprising. Almost 92% of the T2 DNA fragments reacted with the T4 DNA. The elution profiles obtained for this reaction, however, were quite similar to those obtained by reacting labeled T4 DNA with excess T2 DNA. A single major peak was observed with a *T<sub>m</sub>* about 2° lower than that determined from the internal standard. Table 33 summarizes the data obtained from these reciprocal experiments. There can be little doubt that these experiments indicate reciprocal DNA homology values that differ by almost 10%.

The schematic model shown later in this Report illustrates the interpretation of the results presented above.

If it is assumed that the T4 genome is about 10% larger than the T2 genome, the above results can be explained. For the reaction of T2 labeled fragments with T4 DNA 91.4% was observed to react leaving 8.6% unable to react.

In the reciprocal experiment, because

TABLE 33. Reactions between T4D and T2H DNA Fragments

Labeled DNA Frag- ments	Unlabeled DNA Fragments	Percent Homology *			<i>T<sub>m</sub></i> of Labeled Material		$\Delta T_m$ †
		Measured	Normalized				
T4	T4	96.7	100		85.0°C		0
T2	T2	95.2	100		85.0°C		0
T4	T2	78.9	82.2	82.1	81.5	81.7°C	3.3°C
		78.4	82.0		82.0		
T2	T4	87.1	91.9	91.4	83.0	82.7°C	2.3°C
		88.0	91.0		82.5		

\* The homologous DNA reassociation experiments gave 95.2%, 96.7%, and 95.6% reaction for the T2, T4, and T6 DNAs, respectively. The average value of 95.9°C=100% binding was used for normalization of the heterologous reaction data above.

† The  $\Delta T_m$  was determined by comparing the *T<sub>m</sub>* of the radioactive elution profile with its corresponding optical density data (internal standard).



of the longer T4 DNA molecule, the expected homology would be equal to 91.4% of the T2 DNA, which corresponds to  $91.4/110\%$ , about 83% of the T4 DNA. The value obtained experimentally was 82.1%. Furthermore, that portion of the T2 DNA unable to react with the T4 DNA will have an equal portion of the T4 genome unmatched or  $8.6/110\%$  (7.8%) of the T4 genome. To this unreactive portion of the T4 DNA must be added the 10% having no physical counterpart in the T2 molecule. The sum of the unmatched T4 DNA, 17.8%, plus the reacting portion, 82.1%, thus accounts for essentially the whole of the T4 genome.

The model is oversimplified for clarity of discussion. The nonhomologous regions are not necessarily terminal but are probably distributed throughout both of the phage DNAs. The model, however, does suggest experimental tests that could support or reject the conclusions cited above.

*Heterologous DNA-DNA Reactions  
among the DNAs of T4D and T6  
Phages and the DNAs of  
T2H and T6 Phages*

Other comparisons using various labeled phage DNAs to react with excess unlabeled heterologous T-even virus DNAs gave similar results. In no case did reciprocal experiments give equal values. Table 34 summarizes the results

obtained. In each case there was a reduction in the  $T_m$ 's, calculated from the radioactivity elution data and compared to the  $T_m$  measured optically. In most cases the higher the degree of homology between the heterologous DNAs, the higher the  $T_m$  of the heterologous DNA reaction products.

The data contained in Table 34 serve as one test of the model cited above. Since differences in the reciprocal reactions are observed among all of the heterologous DNA-DNA results, and each of the T-even phage DNAs show a great deal of genetic complementation to each other, it is possible to consider the hypothetical increased molecular length of the T4 DNA in terms of the results of other DNA-DNA reciprocal studies.

Ninety-five percent of the T2 DNA reacts with T6 DNA. A comparative study showed that only 87% of the DNA of T6 reacts with the T2 genome (Table 34). On the basis of the model presented earlier, this result indicates that the length of the T6 DNA is about 8% greater than the T2 molecule.

Taken together, these estimates of the comparative lengths of two of the T-even phage DNAs provide data for the calculation of the relative length of the third.

If the lengths of the T4 and T6 DNA molecules are 10% and 8% greater than the T2 DNA molecule, respectively, then the T6 DNA molecule must be 2%

TABLE 34. Summary of Heterologous DNA-DNA Reactions among the T-even Bacteriophages

Labeled DNA Fragments	Un- labeled DNA Frag- ments	Percent Homology *		$T_m$ of Labeled Material * (average)	$\Delta T_m$
		Measured	Normalized		
T2	T6	90.8	94.7	83.7	1.3
T6	T2	83.4	87.0	83.5	1.5
T2	T4	87.6	91.4	82.7	2.3
T4	T2	78.7	82.1	81.7	3.3
T4	T6	79.7	83.2	80.5	4.5
T6	T4	81.1	84.7	80.5	4.5

\* Same normalization procedures as in Table 33.

shorter than that of T4. The comparative studies of the reactions of the T4 and T6 DNAs (Table 34) and the schematic drawing (Figure 117) show that these reactions gave an almost reciprocal result with about a 2% difference favoring a greater length of the T4 molecule.

The molecular weight of the T2 DNA has been measured to be about  $130 \times 10^6$ , corresponding to about  $2.5 \times 10^5$  base pairs. A value greater by 10% for the T4 DNA represents a sizable quantity of material, about 25,000 base pairs ( $mw \sim 1.3 \times 10^7$ ) or about half the quantity of DNA in a T7 phage genome.

One of the objectives of these studies has been to determine the degree (percent homology) and quality (thermal stability) of binding of the nucleotide sequences held in common among the

T-even phage DNAs. The  $T_m$ 's obtained with the heterologous DNA-DNA interactions provided one conclusion: the thermal stability of most of the heterologous DNA reaction products in each case is almost as high as the  $T_m$ 's of the native DNAs. On the other hand, the variations measured in the percentages of homologous sequences make it difficult to establish a simple description of genetic interrelationships. However, the model presented above helps in the interpretation of the data presented. Based on this model, the molecular weight of T2 DNA, and the data presented in Table 34, it is possible to calculate relative values for the molecular weights of T4 and T6 DNAs as follows: (1)  $T_2 = 130 \times 10^6$ , (2)  $T_4 = 143 \times 10^6$ , (3)  $T_6 = 140 \times 10^6$ . Using these molecular weights and the percentages of each labeled DNA which

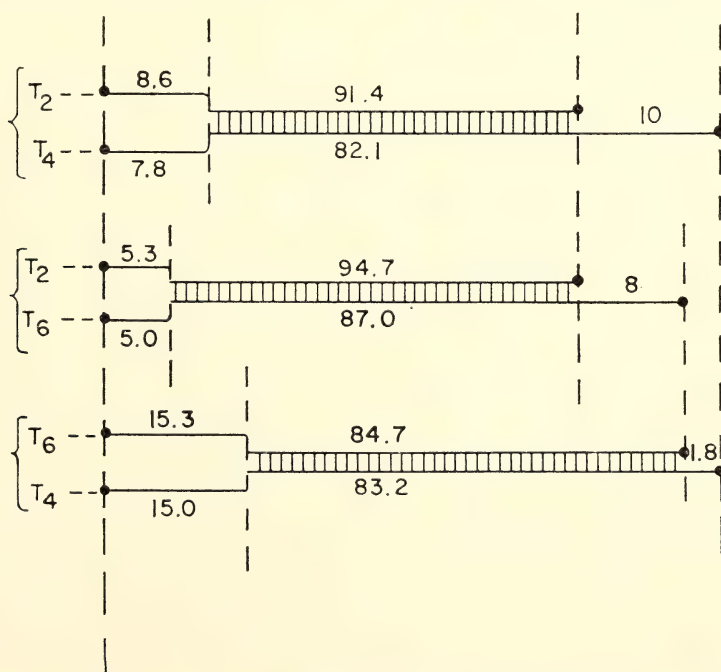


Fig. 116. Comparative reactions among T-even phage DNAs. Solid lines represent T-even phage DNAs. Regions having common nucleotide sequences are cross hatched and the numbers represent percent (normalized) reacting for each labeled genome. For example, 91.4% of T2 reacts with T4 and 82.1% of T4 reacts with T2. The percent of each genome not homologous is shown at the left of the homologous regions and the portions of the DNA molecule having no physical counterpart in the DNA to be compared are shown on the right.

TABLE 35. Molecular Weights of Homologous DNA Segments among the T-Even Phages

Molecular Weight of Phage DNA	Reaction *	Calculated Molecular Weight of Homologous Nucleotide Sequences
T2 $1.3 \times 10^8$	T2*/T6	$1.23 \times 10^8$
	T2*/T4	$1.19 \times 10^8$
T4 $1.43 \times 10^8$	T4*/T6	$1.19 \times 10^8$
	T4*/T2	$1.18 \times 10^8$
T6 $1.40 \times 10^8$	T6*/T4	$1.18 \times 10^8$
	T6*/T2	$1.22 \times 10^8$

\*The symbol T\*/T signifies that labeled T\*DNA fragments reacted with excess T cold DNA.

will react with the other phage genomes it can be seen (Table 35) that the quantity of homologous DNA in each phage DNA is approximately the same.

The thermal stabilities of the reaction products resulting from the interaction of heterologous DNAs show, however, significant qualitative differences among these nucleotide sequences held in common. Tables 33 and 34 show that the thermal stability ( $T_m$ ) of the T2-T6 reaction products is about  $1.5^\circ\text{C}$  lower than that observed for reassocated homologous DNAs. Furthermore, for re-

action involving T4 and T6 DNAs, a difference of  $4.5^\circ\text{C}$  is obtained, and values intermediate between these extremes are observed for the hybridization reaction products of T4 and T2 DNAs. These reduced thermal stabilities are indicative of mismatching of base pairs in the products obtained in heterologous hybridization reactions and have been considered to serve as a measure of the relative evolutionary history of the genomes compared. The data indicate that in evolving from a common ancestor T6 would have diverged from T2 at a later date than T4. Such a family tree is depicted below in Fig. 117.

#### FUNCTIONAL HOMOLOGY BETWEEN PHAGE S13 AND ITS HOSTS

Robert Shleser

Hayashi, Hayashi, and Spiegelman<sup>217</sup> have demonstrated the existence of a species of RNA in uninfected *E. coli* which would hybridize to the single stranded DNA of  $\rho \times 174$ . This finding implied the presence of homologous segments in the phage and host genomes. This homology was later proved in experiments with the closely related virus S13 (Puga, *et al.*, 1970).<sup>218</sup> If there is only one sequence in each *E. coli* genome, which is homologous to a sequence in S13, it would be necessary to have  $1.5 \times 10^9 / 1.2 \times 10^6$  (the single stranded M. W. of the *E. coli* and S13 genomes)  $\mu\text{g}$  of *E. coli* DNA to provide a 1:1 ratio of complementary sequences of S13 segment. The first hybridization experiments were performed with DNA ratios in which it was necessary to estimate the maximum amount of phage DNA that would hybridize to the host DNA.<sup>218</sup> The experiments described below had two purposes: (1) to verify the homology of S13 to *E. coli* under conditions where the host sequences were in such excess that almost all of the complementary DNA of the virus would be hybridized (Year Book 65, pp. 73-88), and (2) to determine if a homologous

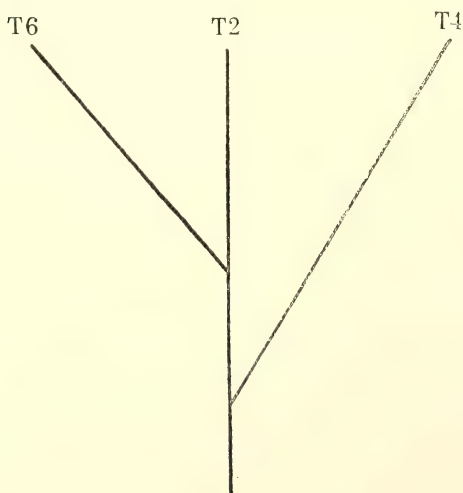


Fig. 117. Family tree for T2, T4, and T6 phages.



TABLE 36. Hybridization Reactions of S13 with Various DNAs

50K Sheared S13 DNA with:	Molar ratio: Host/Virus	<i>C<sub>ot</sub></i>	Percent S13 DNA Hybridized	Percent O.D. in Back Peak
<i>Coli C</i> DNA	100	48	5.4	98
<i>Coli C</i> DNA	200	144	4.9	100
<i>Coli C</i> DNA	500	192	5.2	98
<i>Salmonella typh</i>	200	144	4.9	100
<i>Serratia</i>	200	144	2.1	98
<i>Proteus mirabilis</i>	200	144	0.9	98
<i>Coli B</i>	200	144	4.4	98
Purified RF (MAK)	800	76	82	...
S13 alone	...	0.014	0	...

One hundredth of a microgram of  $^{32}\text{P}$ -labeled 50K sheared S13 DNA (specific activity 250,000 cpm/ $\mu\text{g}$ ) was mixed in 1.0 ml of 0.14 *M* sodium phosphate buffer (PB) with between 2 and 3 mg of 50K sheared unlabeled DNA to be tested for homology. All mixtures were boiled for 3 minutes and incubated at 60°C for from 6 to 16 hours to achieve the number of *C<sub>ots</sub>* as (*Year Book 65*, pp. 73–88) determined from the concentration of the unlabeled species. At the end of the incubation period the samples were diluted with 9.0 ml of 0.14 *M* PB and fractionated into double- and single-stranded DNA on hydroxyapatite columns. Percent S13 DNA hybridized refers to the ratio of  $^{32}\text{P}$  recovered as double-stranded DNA to the total  $^{32}\text{P}$  S13 input. The O.D. in the back peak is the measure of the amount of hybridization achieved in the incubation.

DNA sequence in the host cell is necessary for the reproduction of phage S13 or  $\phi \times 174$ . These virulent viruses are known to infect certain strains of *Salmonella*, *Shigella*, and *E. coli* (Zahler, 1958).<sup>219</sup>

Most varieties of *E. coli* can be converted to phage sensitivity by mutation. However, *E. coli* B has never been successfully converted to S13 sensitivity (Shleser).<sup>220</sup> We speculated that this observation might be explained by the absence of the homologous sequence from the *E. coli* B genome. *Serratia marcescens* and *Proteus mirabilis* have DNA with G:C ratios very different from those observed for *E. coli*. The former DNAs have been shown to contain few sequences in common with *E. coli* in hybridization experiments. DNA extracted from these cells was intended as a control for coincidental or nonfunctional hybridization.

S13 is a single-stranded DNA virus and replicates by the formation of double-stranded or replicative-form DNA in the infected cell. Nonlabeled, replicative-form DNA was hybridized

with  $\text{P}^{32}$  labeled phage DNA to show that the virus DNA could be retained in the double-stranded form by the hydroxyapatite column. The results of these hybridization experiments are shown in Table 36. Table 37 shows the results obtained when the same preparation of  $\text{P}^{32}$  labeled S13 DNA was incubated with preparations of DNA extracted from *Shigella dysenteriae* Y6R and *Shigella flexneri*. Most strains of *Shigella* are

TABLE 37. Hybridization Reactions of S13 with *Shigella dysenteriae* and *Shigella flexneri*, at *C<sub>ot</sub>* 144

50K S13 DNA with:	Molar Ratio	Percent S13 DNA Hybridized
<i>S. Y6R</i> (A)	200	69.3
<i>S. Y6R</i> (B)	20	15.1
<i>S. Y6R</i> (B)	10	7.3
<i>S. flexneri</i>	50	1.0
<i>S. flexneri</i>	10	0.9
<i>S. flexneri</i>	5	0.5

The conditions of hybridization are the same as those described in Table 36. It was necessary to use more phage DNA to obtain significant levels of hybridization due to decay of the  $^{32}\text{P}$ . This resulted in a reduction of the molar ratios.

known to contain episomes. We speculated that the large homologous segment observed in *Shigella dysenteriae* might be contained in episomal DNA. The *Shigella flexneri* was a strain that had been "cured" and demonstrated to be free of episomal DNA. (These cells had been tested and shown to be free of episomes by S. Falkow at Georgetown University, from whom they were obtained.) The lack of homology observed in *flexneri* suggested that the common sequences might be contained in episomes. These experiments were repeated with a new preparation of DNA (preparation B), which was tested and shown to be free of phage contamination. This eliminated the possibility that the high degree of homology was caused by accidental phage contamination.

### Discussion

The generalized homology observed in all the cell strains tested in Table 36 suggests that the presence of these sequences may be coincidental, rather than functional. The piece size of the 50 K sheared phage DNA had been previously measured by sedimentation equilibrium centrifugation.<sup>218</sup> It was estimated to

have molecular weights of between 7 and  $9 \times 10^{-4}$  daltons, or about 5% of the size of the S13 genome. Hybridizations in which less than 5% of the DNA was bound were considered to be nonspecific. This is because 5% of the counts was the minimum that could be hybridized, because of the piece size.

The hybridizations of P<sup>32</sup>-S13 to *Shigella dysenteriae* indicated that 70% of the S13 genome might have complementary sequences in the host cell. When these experiments were repeated with a new preparation of *Shigella* DNA (preparation B, Table 37), this high amount of homology was not seen. On screening the culture from which the DNA was extracted, it was shown to have 3 cell types in almost equal proportions. If only one of these types contained the episome, the lower amount of homology in the second experiments would be explained. *Shigella dysenteriae* is a permissive host for S13 mutants, and it is possible that this permissiveness occurs by complementation between a product of the episome and the functional products of the virus DNA. We plan to isolate episomes from *Shigella* and to determine if the homologous segment is episomal or chromosomal.

### REFERENCES CITED

1. Rubin, Vera C., and W. K. Ford, Jr., *Astrophys. J.*, **159**, 379, 1970.
2. Münch, G., *Astrophys. J.*, **131**, 250, 1960.
3. Sanduleak, N., *Astron. J.*, **74**, 877, 1969.
4. Klose, J. Z., *Phys. Rev.*, **141**, 181, 1966.
5. Klose, J. Z., *Beam-foil spectroscopy*, S. Bashkin, ed., New York: Gordon and Breach Science Publ., p. 285, 1968.
6. Denis, A. J. Desequelles, and M. Duffay, *Comp. Rend. Acad. Sci.*, Paris, **266B**, 1016, 1968.
7. Bennett, W. R., Jr., P. J. Kindlmann, and G. N. Mercer, *Chemical Lasers, Appl. Opt. Suppl.*, **2**, 34, 1965.
8. Bakos, J., J. Szigeti, and L. Varga, *Phys. Lett.*, **20**, 503, 1966.
9. Matilsky, T. A., and J. E. Hesser, *J. Opt. Soc. Amer.*, **59**, 579, 1969.
10. Schnapauff, R., *Z. Astrophys.*, **68**, 431, 1968.
11. Shumaker, J. B., Jr., and C. H. Popenoe, *J. Opt. Soc. Amer.*, **59**, 980, 1969.
12. Garstang, R. H., *Mon. Notic. Roy. Astron. Soc.*, **114**, 118, 1954.
13. Koozekanani, S. H., and G. L. Trusty, *J. Opt. Soc. Amer.*, **59**, 1281, 1969.
14. Assousa, G. E., L. Brown, and W. K. Ford, Jr., *J. Opt. Soc. Amer.*, **60**, 1311-1314, 1970.
15. Brandt, W., and R. Laubert, *Phys. Rev. Lett.*, **24**, 1037, 1970.
16. Dietz, L. A., Ion optics for the V-type surface ionization filament used in mass spectrometry, *Rev. Sci. Instrum.*, **30**, 235-241, 1959.
17. Wasserburg, G. J., D. A. Papanastassiou,

- E. V. Nenow, and C. A. Bauman, A programmable magnetic field mass spectrometer with on-line data processing, *Rev. Sci. Instrum.*, **40**, 288-295, 1969.
18. Cameron, A. E., D. H. Smith, and R. L. Walker, Mass spectrometry of nanogram-size samples of lead, *Anal. Chem.*, **41**, 525-526, 1969.
  19. Compston, W., and V. M. Oversby, Lead isotopic analysis using a double spike, *J. Geophys. Res.*, **74**, 4338-4347, 1969.
  20. Catanzaro, E. J., Absolute isotopic abundance ratios of three common lead reference samples, *Earth Planet. Sci. Lett.*, **3**, 343-346, 1968.
  21. Ozard, J. M., and R. D. Russell, Discrimination in solid source lead isotope abundance measurement, *Earth Planet. Sci. Lett.*, **8**, 331-336, 1970.
  22. Aumento, F., Diorites from the mid-Atlantic Ridge at 45°N, *Science*, **165**, 1112-1113, 1969.
  23. Kay, R., N. J. Hubbard, and P. W. Gast, Chemical characteristics and origin of oceanic ridge volcanic rocks, *J. Geophys. Res.*, **76**, 1585-1613, 1970.
  24. Engel, A. E. J., C. G. Engel, and R. G. Havens, Chemical characteristics of oceanic basalts and the upper mantle, *Bull. Geol. Soc. Amer.*, **76**, 719-734, 1965.
  25. Bryan, W. B., L. W. Finger, and F. Chayes, Estimating proportions in petrographic mixing equations by least-squares approximation, *Science*, **163**, 926-927, 1969.
  26. Philpotts, J. A., and C. C. Schnetzler, Phenocryst-matrix partition coefficients for K, Rb, Sr and Ba, *Geochim. Cosmochim. Acta*, **34**, 307-322, 1970.
  27. Frey, F., M. A. Haskin, J. A. Poetz, and L. A. Haskin, Rare earth abundances in some basic rocks, *J. Geophys. Res.*, **73**, 6085-6098, 1968.
  28. Philpotts, J. A., C. C. Schnetzler, and S. R. Hart, Submarine basalts: Some K, Rb, Sr, Ba and rare-earth data bearing on their alteration, modification by plagioclase, and possible source materials, *Earth Planet. Sci. Lett.*, 1970 (in press).
  29. Miyashiro, A., F. Shido, and M. Ewing, Diversity and origin of abyssal tholeiite from the mid-Atlantic Ridge near 24° and 30° north latitude, *Contr. Mineral. and Petrol.*, **23**, 38-52, 1969.
  30. Gast, P. W., G. R. Tilton, and C. E. Hedge, Isotopic composition of lead and strontium from Ascension and Gough Islands, *Science*, **145**, 1181-1185, 1964.
  31. Tatsumoto, M., Genetic relations of oceanic basalts as indicated by lead isotopes, *Science*, **153**, 1088-1093, 1966.
  32. Griffin, W. L., and V. Rama Murthy, Distribution of K, Rb, Sr, and Ba in some minerals relevant to basalt genesis, *Geochim. Cosmochim. Acta*, **33**, 1389-1414, 1969.
  33. Tatsumoto, M., C. E. Hedge, and A. E. J. Engel, Potassium rubidium, strontium, thorium, uranium and the ratio of strontium-87 to strontium-86 in oceanic tholeiitic basalt, *Science*, **150**, 886-888, 1965.
  34. Gast, P. W., Isotope geochemistry of volcanic rocks, in: *Basalts*, eds. H. H. Hess and A. Poldervart, Interscience Publishers, New York, 325-358, 1967.
  35. Bence, A. E., The differentiation history of the earth by rubidium-strontium isotopic relationships, in *Variations in Isotopic Abundances of Strontium, Calcium, and Argon and Related Topics*, P. M. Hurley, ed., M.I.T. 1381-14, Fourteenth Ann. Program Report, 35-78, 1966.
  36. Gast, P. W., Trace element fractionation and the origin of tholeiitic and alkaline magma types, *Geochim. Cosmochim. Acta*, **32**, 1057-1086, 1968b.
  37. Moorbath, S., and G. P. Walker, Strontium isotope investigation of igneous rocks from Iceland, *Nature*, **207**, 837-840, 1965.
  38. Gast, P. W., Upper mantle chemistry and evolution of the earth's crust, in *The History of the Earth's Crust*, R. A. Phinney, ed., Princeton Univ. Press, Princeton, 1968.
  39. Hart, S. R., and C. Brooks, Rb-Sr mantle evolution models, *Carnegie Institution Year Book* **68**, 426-429, 1969.
  40. Reed, R. D., Geology of California: *Amer. Ass. Petroleum Geol., Bull.*, 355 pp., 1933.
  41. Taliaferro, N. L., Franciscan-Knoxville problem, *Amer. Ass. Petrol. Geol., Bull.*, **27**, 109-219, 1943.
  42. Bailey, E. H., W. P. Irwin, and D. L. Jones, Franciscan and related rocks, and their significance in the geology of western California, *Calif. Div. Mines Geol. Bull.*, **183**, 177 pp., 1964.
  43. Ernst, W. G., Mineral pangenesis in Franciscan metamorphic rocks, Panoche Pasa, California, *Geol. Soc. Amer. Bull.*, **76**, 879-914, 1965.
  44. Hsu, K. J., Mesozoic geology of the California Coast Ranges—A new working hypothesis: Etage Tectoniques, Neuchatel, A la Bacarriere, pp. 279-296, 1966.
  45. Hatherton, T., Geophysical anomalies over the Eu- and Mio-geosynclinal sys-



- tems of California and New Zealand, *Geol. Soc. Amer. Bull.*, 80, 213-230, 1969.
46. Irwin, W. P., and G. D. Bath, Magnetic anomalies and ultramafic rocks in northern California, *U. S. Geol. Survey Prof. Paper* 450 B, B65-B67, 1962.
  47. Ernst, K. G., Tectonic contact between the Franciscan Mélange and the Great Valley Sequence—Crustal expression of a late Mesozoic Benioff zone, *J. Geophys. Res.*, 75, 886-901, 1970.
  48. Page, B. M., Sur-Nacimiento Fault zone of California: Continental Margin tectonics, *Geol. Soc. Amer. Bull.*, 81, 667-690, 1970.
  49. Hart, S. R., G. L. Davis, C. Brooks, and T. E. Krogh, The K, Rb, Cs and Sr geochemistry of Archean metavolcanics, *Carnegie Institution Year Book* 68, 429-433, 1969.
  50. Hart, S. R., and A. J. Nalwalk, K, Rb, Cs and Sr relationships in submarine basalts from the Puerto Rico trench, *Geochim. Cosmochim. Acta*, 34, 145-155, 1970.
  51. Peterman, Z. E., C. E. Hedge, and H. A. Towdelot, Isotopic composition of strontium in sea water through Phanerozoic time, *Geochim. Cosmochim. Acta*, 34, 105-120, 1970.
  52. Tatsumoto, M., and P. D. Snavely, Isotopic composition of lead in rocks of the Coast Range, Oregon and Washington, *J. Geophys. Res.*, 74, 1087-1100, 1969.
  53. Tatsumoto, M., and Roy J. Knight, Isotopic composition of lead in volcanic rocks from central Honshu—with regard to basalt genesis *Geochem. J.*, 3, 53-86, 1969.
  54. Masuda, A., Geochemistry of Lanthanides in basalts of central Japan, *Earth Planet. Sci. Lett.*, 4, 284-292, 1968.
  55. Kuno, H., High-alumina basalt, *J. Petrol.*, 1, 121-145, 1960.
  56. Sugimura, A., Spatial relations of basaltic magmas in Island arcs, in: *Basalts*, eds. H. H. Hess and A. Poldervart, Interscience Publishers, New York, 2, 537-572, 1967.
  57. Dickinson, W. R., and T. Hatherton, Andesitic volcanism and seismicity around the Pacific, *Science*, 157, 801-803, 1967.
  58. Schilling, J. G., and J. W. Winchester, Rare earth contribution to the origin of Hawaiian lavas, *Contrib. Mineral. Petrol.*, 23, 27-37, 1969.
  59. Green, D. H., and A. E. Ringwood, The genesis of basaltic magmas, *Contrib. Mineral. Petrol.*, 15, 103-190, 1967.
  60. Hart, S. R., K, Rb, Cs, Sr and Ba contents and Sr isotope ratios of ocean floor basalts, *Proceedings of the Royal Society meeting on The Petrology of Igneous and Metamorphic Rocks from the Ocean Floor* (in press) 1970.
  61. Taylor, S. R., Trace element chemistry of andesites and associated calc-alkaline rocks, in: *Proceedings of the Andesite Conference*, Bull. 65, Oregon Dept. of Geology and Mineral Industries, 1969.
  62. Green, T. H., and A. E. Ringwood, Origin of the calc-alkaline igneous rock suite, *Earth Planet. Sci. Lett.*, 1, 307-316, 1966.
  63. Armstrong, R. L., A model for the evolution of strontium and lead isotopes in a dynamic earth, *Rev. Geophys.*, 6, 175-199, 1968.
  64. Minear, J. W., and M. Nafi Toksoz, Thermal regime of a downgoing slab and new global tectonics, *J. Geophys. Res.*, 75, 1397-1419, 1970.
  65. McBirney, A. R., Compositional variations in Cenozoic calc-alkaline suites of central America, in: *Proceedings of the Andesite Conference*, Bull. 65, Oregon Dept. of Geology and Mineral Industries, 185-189, 1969.
  66. Green, D. H., A review of experimental evidence on the origin of basaltic and nephelinitic magmas, *Phys. Earth Planet. Interiors*, 13, 221-235, 1970.
  67. Gorskoy, G. S., Geophysics and petrochemistry of andesite volcanism of the Circum-Pacific belt, in: *Proceedings of the Andesite Conference*, Bull. 65, Oregon Dept. of Geology and Mineral Industries, 91-98, 1969.
  68. Anhaeusser, C. R., R. Mason, M. J. Viljoen, and R. P. Viljoen, A reappraisal of some aspects of Precambrian Shield geology, *Bull. Geol. Soc. Amer.*, 80, 2175-2200, 1969.
  69. Martin, H., Problems of age relations and structure in some metamorphic belts of southern Africa, *Geol. Ass. Can. Spec. Pap. No. 5*, 17-26, 1969.
  70. Manson, V., Geochemistry of basaltic rocks: Major elements, in: *Basalts*, eds. H. H. Hess and A. Poldervart, Interscience Publishers, New York, 215-269, 1967.
  71. Prinz, M., Geochemistry of basaltic rocks: Trace elements, in: *Basalts*, eds. H. H. Hess and A. Poldervart, Interscience Publishers, New York, 271-323, 1967.
  72. Gast, P. W., and N. J. Hubbard, Abundance of alkali metals, alkaline and rare earths, and strontium<sup>87</sup>/strontium<sup>86</sup> ratios in lunar samples, *Science*, 167, 485-487, 1970.

73. Turekian, K. K., and K. H. Wedepohl, Distribution of the elements in some major units of the Earth's crust, *Bull. Geol. Soc. Amer.*, **72**, 175-192, 1961.
74. Dasch, E. J., Strontium isotopes in weathering profiles, deep sea sediments, and sedimentary rocks, Ph.D. thesis, Yale University, 1969.
75. Heier, K., and J. A. S. Adams, The geochemistry of the alkali elements, in: *Physics and Chemistry of the Earth*, Pergamon Press, New York, **5**, 255-381, 1963.
76. Kanasawich, E. R., Approximate age of tectonic activity using anomalous lead isotopes, *Geophys. J. Roy. Astron. Soc.*, **7**, 158-168, 1962.
77. Tilton, G. R., and Steiger, R. H., Lead isotopes and the age of the earth, *Science*, **150**, 1805-1808, 1965.
78. Tilton, G. R., and Steiger, R. H., Mineral ages and isotopic composition of primary lead at Manitouwadge, Ontario, *J. Geophys. Res.*, **74**, 2118-2132, 1969a.
79. Chow, T. J., and C. C. Patterson, The occurrence and significance of lead isotopes in pelagic sediments, *Geochim. Cosmochim. Acta*, **26**, 263-308, 1962.
80. Gast, P. W., Isotopic geochemistry of volcanic rocks, in: *Basalts*, eds. H. H. Hess and A. Poldervart, Interscience Publishers, New York, 1967.
81. Sinha, A. K., Model and radiometric ages from the Churchill Province, Canadian Shield, *Geochim. Cosmochim. Acta* **34**, 1089-1106, 1969.
82. Sinha, A. K., The isotopic evolution of common lead and its bearing on the age of the earth, Unpublished Ph.D. thesis, Univ. of Calif., Santa Barbara, 1969.
83. Sinha, A. K., Removal of radiogenic lead from potassium feldspars by volatilization, *Earth Planet. Sci. Lett.*, **7**, 109-115, 1969.
84. Tilton, G. R., and A. K. Sinha, Age of the least radiogenic terrestrial leads (Abstract), *Geol. Soc. Amer. Annual Meeting*, Atlantic City, 1969.
85. Zartman, R. E., and G. J. Wasserburg, The isotopic composition of lead in potassium feldspars from some 1.0 b.y. old North American igneous rocks, *Geochim. Cosmochim. Acta*, **33**, 901-942, 1969.
86. Doe, B. R., G. R. Tilton, and C. A. Hopson, Lead isotopes in feldspars from selected granitic rocks associated with regional metamorphism, *J. Geophys. Res.*, **70**, 1947-1968, 1965.
87. Tatsumoto, M., Isotopic composition of lead in volcanic rocks from Hawaii, Iwo Jima and Japan, *J. Geophys. Res.*, **71**, 1721-1733, 1966.
88. Tatsumoto, M., Genetic relations of oceanic basalts as indicated by lead isotopes, *Science*, **153**, 1094-1101, 1966.
89. Cooper, J. A., and J. R. Richards, Lead isotope measurements on volcanics and associated galenas from Coromandel-Te Aroha Region, New Zealand, *Geochem. J.*, **3**, 1-14, 1968.
90. Catanzaro, E. J., and P. W. Gast, Isotopic composition of lead in pegmatitic feldspars, *Geochim. Cosmochim. Acta*, **19**, 113-126, 1960.
91. Oversby, V. M., and P. W. Gast, Isotopic composition of lead from Oceanic Islands, *J. Geophys. Res.*, **75**, 2097-2114, 1970.
92. Gast, P. W., The isotopic composition of lead from St. Helena and Ascension Islands, *Earth Planet. Sci. Lett.*, **5**, 353-359, 1969.
93. Lee, W. H. K. and S. Uyeda, Review of heat flow data, in: *Terrestrial Heat Flow*, ed. W. H. K. Lee, *Geophys. Monograph No. 8*, Wash., D. C., American Geophysical Union, 1965.
94. Lambert, I. B., and K. S. Heier, The vertical distribution of uranium, thorium and potassium in the continental crust, *Geochim. Cosmochim. Acta*, **31**, pp. 377-390, 1967.
95. Eade, K. E., W. F. Fahrig, and J. A. Maxwell, Composition of crystalline shield rocks and fractionating effects of regional metamorphism, *Nature*, **211**, pp. 1245-1249, 1967.
96. Rickwood, P. C., Possible evidence for regional chemical heterogeneity of the upper mantle, *Contr. Mineral. Petrol.*, **24**, pp. 354-358, 1969.
97. St. Jean, J., Jr., New Cambrian trilobite from the Piedmont of North Carolina (Abstract), *Geol. Soc. Amer. Spec. Pap. No. 82*, 307-308, 1965.
98. White, A. M., Arvid A. Stromquist, T. W. Stern, and Harold Westley, Ordovician age for some rocks of the Carolina slate belt in North Carolina, *U. S. Geol. Survey Prof. Paper 475-C*, pp. C107-C109, 1963.
99. Hills, F. A., and J. R. Butler, Rb-Sr dates for some rhyolites from the Carolina slate belt of the North Carolina Piedmont (Abstract), *Geol. Soc. America, Program 1968 annual meeting Southeastern Section*, Durham, N. C., p. 45, 1968.
100. Tobisch, O. T., and Lynn Glover III, Metamorphic changes across part of the Carolina slate belt-Charlotte belt bound-

- ary, North Carolina and Virginia, *U. S. Geol. Survey Prof. Paper 650-C*, pp. C1-C7, 1969.
101. Wetherill, G. W., Discordant uranium-lead ages, *Trans. Amer. Geophys. Union*, 37, 320-326, 1956.
102. Swartz, F. M., Trenton and sub-Trenton of outcrop areas in New York, Pennsylvania, and Maryland, *Amer. Ass. Petrol. Geol. Bull.*, 32, 1493-1595, 1948.
103. Hopson, C. A., The crystalline rocks of Howard and Montgomery Counties, in, *The Geology of Howard and Montgomery Counties*, Baltimore, Maryland Geol. Survey, pp. 27-215, 1964.
104. Bullen, K. E., in, *An Introduction to the Theory of Seismology*, Cambridge Univ. Press, p. 209, 1959.
105. Engdahl, E. R., Core phases and the earth's core, Ph.D. thesis, St. Louis Univ., 1968.
106. Bolt, B. A., Estimation of PKP travel times, *Bull. Seis. Soc. Amer.*, 58, 1305-1324, 1968.
107. Bolt, B. A., Travel times of PKP up to 145°, *Geophys. J., R. A. S.*, 2, 190, 1959.
108. Bullen, K. E., in *An Introduction to the Theory of Seismology*, Cambridge Univ. Press, eq. 20, p. 128, 1959.
109. Foster, M. R., and N. J. Guinzy, The coefficient of coherence: its estimation and use in geophysical prospecting, *Geophysics*, 32, No. 4, 1967.
110. Haubrich, R. A., Earth noise, 5 to 500 millicycles per second. 1. Spectral stationarity, normality and nonlinearity, *J. Geophys. Res.*, 70, 1415-1427, 1965.
111. Priestley, Joseph, Taut correlation studies of pressure fluctuations on the ground beneath a turbulent boundary layer, M. S. thesis, Univ. of Maryland, 1965.
112. Ozawa, I., Study on elastic strain of the ground in earth tide, *Bull.* 15, Disaster Prevention Research Institute, Kyoto University, Japan, 1957.
113. Bracewell, R. M., *The Fourier transform and its applications*, McGraw-Hill, 1965.
114. Bollinger, G. A., Fault length and fracture velocity for the Kyushu, Japan, earthquake of October 3, 1963, *J. Geophys. Res.*, 75, 955-964, 1970.
115. Ben-Menahem, A., Radiation of seismic surface waves from finite moving sources, *Bull. Seis. Soc. Amer.*, 51, 401-435, 1961.
116. Ben-Menahem, A., Radiation of seismic body waves from a finite moving source in the earth, *J. Geophys. Res.*, 67, 345-350, 1962.
117. Haskell, N. A., Total energy and energy spectral density of elastic wave radiation from propagating faults, *Bull. Seis. Soc. Amer.*, 54, 1811-1841, 1964.
118. Haskell, N. A., Total energy and energy spectral density of elastic wave radiation from propagating faults. Part II, A statistical source model, *Bull. Seis. Soc. Amer.*, 56, 125-140, 1966.
119. Aki, K., Scaling law of seismic spectrum, *J. Geophys. Res.*, 72, 1217-1231, 1967.
120. Savage, J. C., Radiation from a realistic model of faulting, *Bull. Seis. Soc. Amer.*, 56, 577-592, 1966.
121. Maruyama, T., On the force equivalents of dynamical elastic dislocations with reference to the earthquake mechanism, *Bull. Earthquake Res. Inst.*, Tokyo Univ., 41, 467-486, 1963.
122. Archambeau, C. B., General theory of elastodynamic source fields, *Rev. Geophys.*, 6, 241-288, 1968.
123. Ben-Menahem, A., and M. M. Toksöz, Source mechanism from spectra of long period seismic surface waves. 1. The Mongolian earthquake of December 4, 1957, *J. Geophys. Res.*, 67, 1943-1955, 1962.
124. Ben-Menahem, A., and M. N. Toksöz, Source mechanism from spectrums of long period surface waves. 2. The Kamchatka earthquake of November 4, 1952, *J. Geophys. Res.*, 68, 5207-5222, 1963a.
125. Ben-Menahem, A., and M. N. Toksöz, Source mechanism from spectra of long-period seismic surface waves. 3. The Alaska earthquake of July 10, 1958, *Bull. Seis. Soc. Amer.*, 53, 905-919, 1963b.
126. Khattri, K. N., Determination of earthquake fault plane, fault area and rupture velocity from the spectra of long-period *P* waves and the amplitude of *SH* waves, *Bull. Seis. Soc. Amer.*, 59, 615-630, 1969.
127. Aki, K., Generation and propagation of *G* waves from the Niigata earthquake of July 16, 1964. Part 2. Estimation of earthquake moment, released energy, and stress-strain drop from the *G* wave spectrum, *Bull. Earthquake Res. Inst.*, Tokyo Univ., 44, 73-88, 1966.
128. Berckhemer, H., and K. H. Jacob, Investigation of the dynamical processes in earthquake foci by analyzing the pulse shape of body waves, Final Sci. Rept., Contract AF 61(052)-801, 85 pp, Inst. of Meteorology and Geophysics, Univ. of Frankfurt, Germany, 1968.
129. Wyss, M., and J. N. Brune, Seismic moment, stress and source dimensions for



- earthquakes in the California-Nevada region, *J. Geophys. Res.*, **73**, 4681-4694, 1968.
130. Wyss, M., Stress estimates for South American shallow and deep earthquakes, *J. Geophys. Res.*, **75**, 1529-1544, 1970.
  131. Griggs, D. T., and D. W. Baker, The origin of deep-focus earthquakes, in Mark and Fernbeck: Properties of matter under unusual conditions, New York: Wiley-Interscience, 1968.
  132. Woollard, G. P., Seismic crustal studies during the IGY, Part II: Continental Program, *Amer. Geophys. Union Trans., IGY Bull. No. 54*, pp. 351-355, 1960.
  133. Morrison, R. P., The Puna block, from manuscript on geology of South America, in press, 1970.
  134. Dziewonski, A., S. Block, and M. Landisman, A technique for the analysis of transient seismic signals, *Bull. Seis. Soc. Amer.*, **59**, 427-444, 1969.
  135. Block, S., and A. Hales, New techniques for the determination of surface-wave phase velocities, *Bull. Seis. Soc. Amer.*, **58**, 1021-1034, 1968.
  136. Press, F., Seismic velocities, in *Handbook of Physical Constants*, S. P. Clark, Jr., ed., pp. 195-218, 1966.
  137. Birch, F., Density and composition of the upper mantle: First approximation as an olivine layer, in *The Earth's Crust and Upper Mantle*, AGU Monograph 13, P. Hart, ed., pp. 18-36, 1969.
  138. Haskell, N. A., Dispersion of surface waves on multilayered media, *Bull. Seis. Soc. Amer.*, **43**, pp. 17-34, 1953.
  139. Alterman, Z., H. Jarosch, and C. L. Pekeris, Propagation of Rayleigh waves in the earth, *Geophys. J. Roy. Astr.*, **4**, pp. 219-241, 1961.
  140. Knopoff, L., S. Mueller, and W. L. Pilant, Structure of the crust and upper mantle in the Alps from phase velocity of Rayleigh waves, *Bull. Seis. Soc. Amer.*, **56**, pp. 1009-1044, 1966.
  141. Thatcher, W., and J. N. Brune, Higher mode interference and observed anomalous apparent Love wave phase velocities, *J. Geophys. Res.*, **74**, 6603, 1969.
  142. Aki, K., and K. Kaminuma, Phase velocity of Love waves in Japan, 1, Love wave from the Aleutian shock of March 9, 1957, *Bull. Earthquake Res. Inst. Tokyo Univ.*, **41**, 243, 1963.
  143. McEvilly, T. V., Central U. S. crust-upper mantle structure from Love and Rayleigh wave phase velocity inversion, *Bull. Seis. Soc. Amer.*, **54**, 19, 1964.
  144. Takeuchi, H., Y. Hamano, and Y. Hasegawa, Rayleigh- and Love-wave discrepancy and the existence of magma pockets in the upper mantle, *J. Geophys. Res.*, **73**, 3349, 1968.
  145. Aki, K., Seismological evidences for the existence of soft thin layers in the upper mantle under Japan, *J. Geophys. Res.*, **73**, 585, 1968.
  146. Hales, A. L., and S. Block, Upper mantle structure: Are the low velocity layers thin? *Nature*, **221**, 930, 1969.
  147. Boore, D., Effect of higher mode contamination on measured Love wave phase velocities, *J. Geophys. Res.*, **74**, 6612, 1969.
  148. Thomas, P. D., Geodesic arc length on the reference ellipsoid to second-order terms in the flattening, *J. Geophys. Res.*, **70**, 3331-3340, 1965.
  149. Brune, J. N., Surface waves and crustal structure, in *The Earth's Crust and Upper Mantle*, Geophysical Monograph No. 13, 230-242, P. J. Hart, ed., Washington, D.C., American Geophysical Union, 1969.
  150. Johnson, L. R., Array measurement of P velocities in the upper mantle, *J. Geophys. Res.*, **72**, 6309-6325, 1967.
  151. Hales, A. L., J. L. Cleary, and J. L. Roberts, Velocity distribution in the lower mantle, *Bull. Seis. Soc. Amer.*, **58**, 1975-1989, 1968.
  152. Kovack, R. L., and R. Robinson, Upper mantle structure in the Basin and Range Province, Western North America, from the apparent velocities of S waves, *Bull. Seis. Soc. Amer.*, **59**, 1653-1665, 1969.
  153. Herrin, E., The 1968 Seismological Table for P phases, *Bull. Seis. Soc. Amer.*, **58**, 1193-1241, 1968.
  154. Vozoff, K., and C. M. Swift, Jr., *Geophys. Prosp.*, (Netherlands), **16**, No. 4, pp. 454-473, 1968.
  155. Britten, R. J., and D. E. Kohne, *Science*, **161**, 529, 1968.
  156. Laird, C. D., B. L. McConaughy, and B. J. McCarthy, *Nature*, **224**, 149, 1969.
  157. Flamm, W. G., P. M. P. Walker, and M. McCallum, *J. Mol. Biol.*, **40**, 423, 1969.
  158. Hoyer, B. H., and R. B. Roberts, in *Molecular Genetics*, Academic Press, New York.
  159. McClaren, A., and P. Walker, *Genet. Res.*, **6**, 230, 1965.
  160. Sinclair, J. H., and D. D. Brown, *Federation Proc.*, **27**, 335, 1968.
  161. Simons, E., *Scientific American*, **211**, 50, 1964.

162. Simpson, G. G., in *Cold Spring Harbor Symp. Quant. Biol.*, 24, 255, 1959.
163. Romer, A., in *Vertebrate Paleontology*, Chicago: Univ. of Chicago Press.
164. Wilson, A., and V. Sarich, *Proc. Nat. Acad. Sci. U.S.*, 63, 1088, 1969.
165. Bautz, E. K., F. A. Bautz, *Proc. Nat. Acad. Sci. U.S.*, 52, 1476, 1964.
166. Uhlenbeck, O., R. Harrison, and P. Doty, in *Molecular Association in Biology*, New York, Academic Press, p. 107, 1968.
167. Lipsett, M. N., *J. Biol. Chem.*, 239, 1256, 1964.
168. Davidson, E. H., and B. R. Hough, personal communication.
169. Polli, E., G. Correo, E. Ginelli, and P. Bianchi, *Biochim. Biophys. Acta*, 103, 672, 1964.
170. Bernardi, G., Chromatography of nucleic acids on hydroxyapatite. II. Chromatography of denatured DNA, *Biochim. Biophys. Acta*, 174, 435-448, 1969.
171. Becker, W. M., A. Hell, J. Paul, and R. Williamson, Isolation of mammalian RNA-DNA hybrids by hydroxylapatite fractionation and CsCl density centrifugation, *Biochim. Biophys. Acta*, 199, 348-362, 1970.
172. McCarthy, B. J., and E. T. Bolton, An approach to the measurement of genetic relatedness among organisms, *Proc. Nat. Acad. Sci. U. S.*, 50, 156-164, 1963.
173. Brenner, D. J., M. A. Martin, and B. H. Hoyer, Deoxyribonucleic acid homologies among some bacteria, *J. Bacteriol.*, 94, 486-487, 1967.
174. Brenner, D. J., and D. B. Cowie, Thermal stability of *Escherichia coli*-*Salmonella typhimurium* deoxyribonucleic acid duplexes, *J. Bacteriol.*, 95, 2258-2262, 1968.
175. Rogul, M., J. J. Brendle, D. K. Haapla, and A. D. Alexander, Nucleic acid similarities among *Pseudomonas pseudomallei*, *Pseudomonas multivorans*, and *Actinobacillus mallei*, *J. Bacteriol.*, 101, 827-835, 1970.
176. Seiden, L. S., and D. D. Peterson, *J. Pharmacol. Exp. Therap.*, 159, 422, 1968.
177. Schoenfeld, R. I., and L. S. Seiden, *J. Pharmacol. Exp. Therap.* 167, 319, 1969.
178. Flexner, J. B., L. B. Flexner, and E. Stellar, *Science*, 141, 57, 1963.
179. Flexner, L. B., and J. B. Flexner, *Proc. Nat. Acad. Sci. U.S.*, 60, 923, 1966.
180. Flexner, L. B., and J. B. Flexner, *Proc. Nat. Acad. Sci. U.S.*, 55, 369, 1966.
181. Flexner, J. B., and L. B. Flexner, *Proc. Nat. Acad. Sci. U.S.*, 57, 1651, 1967.
182. Flexner, J. B., and L. B. Flexner, *Yale J. Biol. Med.*, 42, 235, 1970.
183. Iversen, L. L., *The Uptake and Storage of Noradrenaline in Sympathetic Nerves*, Cambridge Univ. Press, Cambridge, England, 1967.
184. Schildkraut, J. J., *Amer. J. Psychiat.*, 126:7, 925, 1969.
185. Deutsch, J. A., *Annual Rev. Psychol.*, 20, 91, 1969.
186. Burn, J. H., in *Adrenergic Neurotransmission*, Ciba Foundation Study Group, No. 33, G.E.W. Wolstenholme and M. O'Connor, eds. Little Brown, Boston, 1968.
187. Braun, R., and T. E. Evans, *Biochim. Biophys. Acta*, 182, 511, 1969.
188. Attardi, C., P. C. Huang, and S. Kabat, *Proc. Nat. Acad. Sci. U.S.*, 53, 1490, 1965.
189. Mangiarolti, G., D. Apinoin, D. Schlesinger, and L. Silengo, *Biochemistry*, 7, 456, 1968.
190. Avery, R. J., and J. E. M. Midgley, *Biochem. J.*, 108, 33 pp., 1968.
191. Avery, R. J., J. E. M. Midgley, and G. H. Pigott, *Biochem. J.*, 115, 395, 1969.
192. Oishi, M., and N. Sueoka, *Proc. Nat. Acad. Sci. U.S.*, 54, 483, 1965.
193. Oishi, M., and N. Sueoka, *Proc. Nat. Sci. U.S.*, 55, 1095, 1966.
194. Doi, R. H., and R. T. Igarashi, *J. Bacteriol.*, 92, 88, 1966.
195. Smith, I., D. Duhnan, P. Morell, and I. Marmur, *J. Mol. Biol.*, 33, 123, 1968.
196. Avery, R. J., and J. E. M. Midgley, *Biochem. J.*, 115, 4, 1969.
197. Adesnik, M., and C. Levinthal, *J. Mol. Biol.*, 46, 281, 1969.
198. Avery, R. J., and J. E. M. Midgley, manuscript in preparation.
199. McCarthy, B. J., and R. J. Britten, *Bioophys. J.*, 2, 57, 1962.
200. Buchwald, M., and R. J. Britten, *Biophys. J.*, 3, 155, 1963.
201. Bolton, E. T., and B. J. McCarthy, *Proc. Nat. Acad. Sci. U.S.*, 48, 1390, 1962.
202. Pigott, G. H., and J. E. M. Midgley, *Biochem. J.*, 110, 251, 1968.
203. Midgley, J. E. M., and B. J. McCarthy, *Biochim. Biophys. Acta*, 61, 696, 1962.
204. Midgley, J. E. M., *Biochem. J.*, 115, 171, 1969.
205. Roberts, R. B., D. B. Cowie, P. H. Abelson, E. T. Bolton, and R. J. Britten, in *Studies of Biosynthesis in E. coli*, 1957, Carnegie Inst. Publ. No. 607, Washington, D. C.

206. Pigott, G. H., Ph.D. thesis (1967), University of Leeds, England.
207. Gillespie, D., and S. Spiegelman, *J. Mol. Biol.*, **12**, 829, 1965.
208. Stanley, W. J., Jr., and R. M. Bock, *Biochemistry*, **4**, 302, 1965.
209. Midgley, J. E. M., *Biochim. Biophys. Acta*, **108**, 340, 1965.
210. Goldstein, A., J. B. Kirschbaum, and A. Roman, *Proc. Nat. Acad. Sci. U.S.*, **54**, 1669, 1965.
211. Fuchs, E., W. Zillig, P. H. Hofschneider, and A. Preuss, *J. Mol. Biol.*, **10**, 546, 1964.
212. Falkow, S., and D. B. Cowie, *J. Bacteriol.*, **96**, 777, 1968.
213. Inman, R. B., and G. J. Bertani, *J. Mol. Biol.*, **44**, 533, 1969.
214. Skalka, A., E. Burgi, and A. D. Hershey, *J. Mol. Biol.*, **34**, 1, 1968.
215. Cowie, D. B., and P. Szafranski, *Biophys. J.*, **7**, 567, 1967.
216. Schildkraut, C. L., K. L. Wierchowski, J. Marmur, D. M. Green, and P. Doty, *Virology*, **18**, 43, 1962.
217. Hayashi, M., M. N. Hayashi, and S. Spiegelman, *Proc. Nat. Acad. Sci. U.S.*, **50**, 664-672, 1963.
218. Puga, A., R. Shleser, and D. E. Kohne, *Virology*, 1970 (in press).
219. Zahler, S. A., *J. Bacteriol.*, **75**, 310-312, 1958.
220. Shleser, R., unpublished results.

## BIBLIOGRAPHY

- Aldrich, L. T., Review of book, *Radiometric Dating for Geologists*, E. I. Hamilton and R. M. Farquhar, eds., London, Interscience Publs., 1968, *Tectonophysics*, **7**, 354-355, 1969.
- Aldrich, L. T., S. R. Hart, and T. E. Krogh, Mass spectroscopy and earth science (abstract), International Conference on Mass Spectroscopy, Preprints, Kyoto, Japan, p. 91, Sept. 8-12, 1969.
- Aldrich, L. T., see also Casaverde, M.
- Assousa, G. E., L. Brown, and W. K. Ford, Jr., Mean life measurements of 4p and 4p' levels in argon II using an image tube spectrograph (abstract), Proc. of the Second International Conference on Beam Foil Spectroscopy, Lysekil, Sweden, June 7-12, 1970, *Program*.
- Baum, W. A., J. S. Hall, L. L. Marton, and M. A. Tuve, Annual report of the committee on image tubes for telescopes, *Carnegie Inst. Wash. Year Book* **68**, 493-496, 1968-1969.
- Bertola, F., S. D'Odorico, W. K. Ford, Jr., and Vera C. Rubin, Observations of M82 in the optical infrared, *Astrophys. J.*, **157**, L27-L28, 1969.
- Britten, R. J., Discrete components of the repetitive DNA of higher organisms (abstract), *Publ. Nat. Acad. Sci. U. S.*, **66**, 230-231, 1970.
- Britten, R. J., and E. H. Davidson, Gene regulation for higher cells: A theory, *Science*, **165**, 349-358, 1969.
- Britten, R. J., and D. E. Kohne, Implications of repeated nucleotide sequences, in *Handbook of Molecular Cytology*, pp. 38-51, A. Lima-de-Faria, ed., Amsterdam, North-Holland Publishing Co., 1969.
- Britten, R. J., and D. E. Kohne, Repeated segments of DNA, *Sci. Amer.*, **222**, 24-31, 1970.
- Britten, R. J., and D. E. Kohne, Repetition of nucleotide sequences in chromosomal DNA, in *Handbook of Molecular Cytology*, pp. 22-36, A. Lima-de-Faria, ed., Amsterdam, North-Holland Publishing Co., 1969.
- Brooks, C., S. R. Hart, T. E. Krogh, and G. L. Davis, Sr-isotopic evidence for the heterogeneity and early differentiation of earth's mantle (abstract), Colloquium on the Geochronology of Phanerozoic Orogenic Belts, Switzerland, Aug. 23-Sept. 4, 1969.
- Brown, L., see Assousa, G. E.
- Casaverde, M., A. Giesecke, R. Salgueiro, S. del Pozo, L. Tamayo, and L. T. Aldrich, Conductivity anomaly under the Andes, Proceedings of the Panamerican Symposium on the Upper Mantle (III), Mexico, *Geofisica International* **8**, 55-61, 1968.
- Davidson, E. H., see Britten, R. J.
- Davis, G. L., see Brooks, C.
- Davis, T. E., see Sinha, A. K.
- del Pozo, S., see Casaverde, M.
- D'Odorico, S., Spectroscopic study of the double galaxy NGC 3395-3396, *Astrophys. J.*, **160**, 3-9, 1970.
- D'Odorico, S., see also Bertola, F., and Rubin, Vera C.
- Dorman, L. M., and B. T. R. Lewis, Experimental isostasy. 1. Theory of the determination of the earth's isostatic response to a concentrated load, *J. Geophys. Res.*, **75**, 3357-3365, 1970.
- Dorman, L. M., I. S. Sacks, and D. Evertson, Atmospherically induced vertical and areal



- earth strain noise in borehole strain meters in the period range 20-3000 seconds (abstract), *Trans. Amer. Geophys. Union*, 51, 364, 1970.
- Dorman, L. M., see also Kosalos, J. G., and Lewis, B. T. R.
- Duggal, S. P., S. E. Forbush, and M. A. Pomerantz, The variation with a period of two solar cycles in the cosmic ray diurnal anisotropy of the nucleonic component, *J. Geophys. Res.*, 75, 1150-1156, 1970.
- Erkes, J. W., and K. C. Turner, The neutral hydrogen near HB 21 (abstract), *Bull. Amer. Astron. Soc.*, 2, 191, 1970.
- Evertson, D., see Dorman, L. M., and Sacks, I. S.
- Flexner, J. B., see Roberts, R. B.
- Flexner, L. B., see Roberts, R. B.
- Forbush, S. E., see Duggal, S. P.
- Ford, W. K., Jr., and Vera C. Rubin, Emission lines in the nuclear region of M31 (abstract), *Bull. Amer. Astron. Soc.*, 2, 192, 1970.
- Ford, W. K., Jr., see also Assousa, G. E., Bertola, F., Rubin, Vera C., and Wing, R. F.
- Giesecke, A., see Casaverde, M.
- Hall, J. S., see Baum, W. A.
- Hart, S. R., Isotope geochemistry of crust-mantle processes, in *The Earth's Crust and Upper Mantle*, Geophysical Monograph No. 13, 58-62, P. J. Hart, ed., Washington, D. C., American Geophysical Union, 1969.
- Hart, S. R., K, Rb, Cs contents and K/Rb, K/Cs ratios of fresh and altered submarine basalts, *Earth Planet. Sci. Lett.*, 6, 295-303, 1969.
- Hart, S. R., K, Rb, Cs, Sr, Ba contents and Sr isotope ratios of sea-floor basalts, and the nature of sea-water alteration effects (abstract), The Royal Society, Discussion Meeting on the Petrology of Igneous and Metamorphic Rocks from the Ocean Floor, London, England, *Programme*, p. 13, Nov. 12-14, 1969.
- Hart, S. R., and A. J. Nalwalk, K, Rb, Cs and Sr relationships in submarine basalts from the Puerto Rico Trench, *Geochim. Cosmochim. Acta*, 34, 145-155, 1970.
- Hart, S. R., see also Aldrich, L. T., Brooks, C., and Philpotts, J. A.
- Ishizaka, K., and M. Yamaguchi, U-Th-Pb ages of sphene and zircon from the Hida metamorphic terrain, Japan, *Earth Planet. Sci. Lett.*, 6, 179-185, 1969.
- James, D. E., Andean crustal structure from Rayleigh and Love wave phase velocities (abstract), *Trans. Amer. Geophys. Union*, 51, 355-356, 1970.
- Kohne, D. E., see Britten, R. J.
- Kosalos, J. G., B. T. R. Lewis, L. M. Dorman, and R. P. Meyer, An ocean refraction experiment range 85-1,500 kms (abstract), *Trans. Amer. Geophys. Union*, 51, 356, 1970.
- Krogh, T., see Aldrich, L. T., and Brooks, C.
- Lewis, B. T. R., and L. M. Dorman, Experimental isostasy. 2. An isostatic model for the U.S.A. derived from gravity and topographic data, *J. Geophys. Res.*, 75, 3367-3386, 1970.
- Lewis, B. T. R., see also Dorman, L. M., and Kosalos, J. G.
- Linde, A. T., and I. S. Sacks, Problems in Fourier analysis of long period body waves recorded on standard instruments (abstract), *Trans. Amer. Geophys. Union*, 51, 361, 1970.
- Marton, L. L., see Baum, W. A.
- Meyer, R. P., see Kosalos, J. G.
- Nalwalk, A. J., see Hart, S. R.
- Philpotts, J. A., C. C. Schnetzler, and S. R. Hart, Submarine basalts: some K, Rb, Sr, Ba, rare-earth, H<sub>2</sub>O and CO<sub>2</sub> data bearing on their alteration, modification by plagioclase, and possible source materials, *Earth Planet. Sci. Lett.*, 7, 293-299, 1969.
- Pomerantz, M. A., see Duggal, S. P.
- Roberts, R. B., and L. B. Flexner, The biochemical basis of long-term memory, *Quart. Rev. Biophys.*, 2, 135-173, 1969.
- Roberts, R. B., J. B. Flexner, and L. B. Flexner, Some evidence for the involvement of adrenergic sites in the memory trace, *Proc. Natl. Acad. Sci. U. S.*, 66, 310-313, 1970.
- Rubin, Vera C., and S. D'Odorico, A note on the systemic velocity of M31, *Astron. Astrophys.*, 2, 484-488, 1969.
- Rubin, Vera C., and W. K. Ford, Jr., A comparison of dynamical models of the Andromeda Nebula and the galaxy, in *Intern. Astron. Union Symp. No. 38, The Spiral Structure of Our Galaxy*, pp. 61-68, W. Becker and G. Contopoulos, eds., Dordrecht, Holland, D. Reidel Publ. Co., 1970.
- Rubin, Vera C., and W. K. Ford, Jr., Rotation of the Andromeda Nebula from a spectroscopic survey of emission regions, *Astrophys. J.*, 159, 379-403, 1970.
- Rubin, Vera C., W. K. Ford, Jr., and S. D'Odorico, Emission-line intensities and radial velocities in the interacting galaxies NGC 4038-4039, *Astrophys. J.*, 160, 801-809, 1970.
- Rubin, Vera C., see also Bertola, F., and Ford, W. K., Jr.
- Saa, G., S.J., see Sacks, I. S.
- Sacks, I. S., and D. W. Evertson, A wide range borehole strainmeter, General Scientific Assemblies, IASPEI/IAGA, *Program and Abstracts* (abstract 121), Vol. I, Inter-

- national Association of Seismology and Physics of the Earth's Interior*, Madrid, Spain, Sept. 1-12, 1969.
- Sacks, I. S., and G. Saa, S. J., Core phase and the transition zone of the inner core, General Scientific Assemblies, IASPEI/IAGA, *Program and Abstracts* (abstract 81), Vol. I, *International Association of Seismology and Physics of the Earth's Interior*, Madrid, Spain, Sept. 1-12, 1969.
- Sacks, I. S., see also Dorman, L. M., and Linde, A. T.
- Salgueiro, R., see Casaverde, M.
- Schnetzler, C. C., see Philpotts, J. A.
- Sinha, A. K., and T. E. Davis, Isotopic composition of lead from Franciscan rocks (abstract), *Trans. Amer. Geophys. Union*, 51, 445, 1970.
- Tamayo, L., see Casaverde, M.
- Turner, K. C., Neutral hydrogen and stars in the wing of the Small Magellanic Cloud (abstract), *Bull. Amer. Astron. Soc.*, 2, 222, 1970.
- Turner, K. C., see also Erkes, J. W.
- Tuve, M. A., see Baum, W. A.
- Wing, R. F., and W. K. Ford, Jr., The infrared spectrum of the cool dwarf Wolf 359, *Publ. Astron. Soc. Pac.*, 81, 527-529, 1969.
- Yamaguchi, M., see Ishizaka, K.

### MAJOR PUBLICATION

*Cosmic-Ray Results*. Huancayo, Peru, January 1960-December 1968; Fredericksburg, Virginia, January 1960-December 1968; Christchurch, New Zealand, January 1959-December 1961; Godhavn, Greenland, January 1951-December 1953. By L. Beach and S. E. Forbush. Carnegie Inst. Wash. Publ. 175, vol. 22, 1969. Quarto, vii + 311 pp., 300 tables.

## PERSONNEL

### *Director*

Ellis T. Bolton

### *Associate Director*

L. Thomas Aldrich

### *Staff Members*

Roy J. Britten  
Louis Brown  
Dean B. Cowie  
W. Kent Ford, Jr.  
Stanley R. Hart  
Bill H. Hoyer

David E. James ✓  
David E. Kohne  
Richard B. Roberts  
Vera C. Rubin  
I. Selwyn Sacks  
Kenneth C. Turner

### *Distinguished Service Member of Carnegie Institution*

M. A. Tuve

### *Section Chairmen*

Astrophysics: W. Kent Ford, Jr.

Biophysics: Dean B. Cowie

Geophysics: L. Thomas Aldrich

### *Research Associates*

Mateo Casaverde, Instituto Geofísico del Peru, Lima, Peru

Reynaldo Salgueiro, Instituto Geofísico Boliviano, La Paz, Bolivia

Shigeji Suyehiro, Meteorological Research Institute, Tokyo, Japan

*Fellows*

- George E. Assousa, Florida State University, Tallahassee, Florida
- Roger J. Avery, University of Newcastle Upon Tyne, England <sup>1</sup>
- Willy Z. Barreda R., Universidad Nacional de San Agustín, Arequipa, Peru
- Sandro D'Odorico, Osservatorio Astrofisico, Asiago, Italy <sup>2</sup>
- Le Roy M. Dorman, University of Wisconsin, Madison, Wisconsin <sup>3</sup>
- Joseph W. Erkes, University of Illinois, Urbana, Illinois
- Dale W. Everton, Applied Research Laboratories, University of Texas at Austin, Austin, Texas <sup>4</sup>
- Sandra Moore Faber, Fellow of the National Science Foundation, on study leave from Harvard University, Cambridge, Massachusetts <sup>5</sup>
- Leo J. Grady, Pennsylvania State University, University Park, Pennsylvania <sup>6</sup>
- Alan T. Linde, University of Queensland, Brisbane, Australia
- Nancy Reed Rice, Fellow of the National Institute of General Medical Sciences, Bethesda, Maryland <sup>7</sup>
- Robert Shleser, Fellow of the American Cancer Society, New York, N.Y.
- Akhaury Krishna Sinha, University of California, Santa Barbara, California <sup>8</sup>
- Erich Steiner, University of Basel, Basel, Switzerland.

*Collaborators and Visiting Investigators*

- John Bannister, Universidad de Chile, Santiago, Chile
- Don J. Brenner, Walter Reed Army Institute of Research, Washington, D. C.
- Christopher Brooks, University of Montreal, Montreal, Canada
- Michael Byers, Purdue University, Lafayette, Indiana
- Ramon Cabre, S. J., Observatorio San Calixto, La Paz, Bolivia
- Dorothy Canter, George Washington University, Washington, D. C.
- Heinz-Dieter Carstanjen, New York University, New York, New York
- José Chadwick, Universidad del Norte, Antofagasta, Chile
- Sewell Champe, Rutgers University, New Brunswick, New Jersey
- J. Alfred Chiscon, Purdue University, Lafayette, Indiana
- Stanley J. Czyzak, Ohio State University, Columbus, Ohio
- Erick H. Davidson, Rockefeller University, New York, New York
- Salvador del Pozo, Instituto Geofísico Boliviano, La Paz, Bolivia
- Sisir Dutta, Howard University, Washington, D. C.
- Stanley Falkow, Georgetown University, Washington, D. C.
- Louis B. Flexner, University of Pennsylvania, Philadelphia, Penn.
- Josefa B. Flexner, University of Pennsylvania, Philadelphia, Penn.
- Enrique Gajardo, Centro Regional de Sismología Para America del Sur, Lima, Peru
- Albert Gelderman, National Institutes of Health, Bethesda, Maryland
- Alberto A. Giesecke, Instituto Geofísico del Peru, Lima, Peru
- Lynn Glover III, U. S. Geological Survey, Beltsville, Maryland
- Michael Higgins, U. S. Geological Survey, Beltsville, Maryland
- Edgar Kausel, Universidad de Chile, Santiago, Chile
- William S. Kirk, U. S. Geological Survey, Beltsville, Maryland
- Roman Laubert, New York University, New York, New York
- Jorge Mendiguren, Universidad Nacional de Cuyo, San Juan, Argentina

<sup>1</sup> From September 1, 1969.<sup>2</sup> Through December 31, 1969.<sup>3</sup> From September 1, 1969.<sup>4</sup> May, June 1970.<sup>5</sup> From April 20, 1970.<sup>6</sup> Through September 15, 1969.<sup>7</sup> From September 1, 1969.<sup>8</sup> From September 1, 1969.



- Behzad Mohit, National Institutes of Health,  
Bethesda, Maryland
- Timothy J. O'Brien, University of Southern  
California, Los Angeles, California
- George F. Reed, University of Pennsylvania,  
Philadelphia, Pennsylvania
- Terry P. Roark, Ohio State University, Co-  
lumbus, Ohio
- Anibal Rodriguez, Universidad Nacional de  
San Agustín, Arequipa, Peru
- German Saa, S. J., Universidad del Norte,  
Arica, Chile
- Richard G. Seyler, Ohio State University,  
Columbus, Ohio
- Diglio V. Simoni, Universidad Nacional de  
San Agustín, Arequipa, Peru
- Neil A. Straus, University of Toronto, To-  
ronto, Canada
- Lupe Tamayo, Universidad Nacional de San  
Agustín, Arequipa, Peru
- Carlos Varsavsky, Instituto Argentino de  
Radioastronomía, Villa Elisa, Argentina
- Fernando Volponi, Universidad Nacional de  
Cuyo, San Juan, Argentina
- Robert F. Wing, Ohio State University, Co-  
lumbus, Ohio

*Design Engineer*

Everett T. Ecklund

*Electronic Research Specialists*

Kenneth D. Burrhus  
John B. Doak

Charles A. Little  
Glenn R. Poe

*Research Assistants*

Liselotte Beach  
Lillian K. Prager<sup>9</sup>

Jean F. Smith  
Neltje W. van de Velde

*Office*

Chief, Fiscal Section: Helen E. Russell  
Office Manager: William N. Dove  
Assistant Fiscal Officer: Niels M. Pedersen  
Librarian: Lelah J. Prothro (part time)

Secretary: Claudine C. Ator  
Stenographers: Dorothy B. Dillin, E. Kath-  
leen Hill

*Shop*

Shop manager and Electronics Research Spe-  
cialist: Paul A. Johnson  
Instrumentation Research Specialist: Michael  
Seemann

Instrument Makers: Robert Hoffmaster,<sup>10</sup>  
Carl Rinehart  
Machinist: Francis J. Caherty

*Buildings and Grounds*

Carpenter and Maintenance Foreman: Leo J.  
Haber  
Assistant Maintenance Foreman: Elliott M.  
Quade

Maintenance Assistant: Stanley Gawrys  
Caretakers: Bennie Harris, Willis Kilgore, Jr.

<sup>9</sup> Through December 15, 1969.

<sup>10</sup> Retired June 30, 1970.

*Part Time and Temporary Employees*

Joseph A. Darr

Robert G. Davis

Robert R. De Vroom

Fariborz Ghahremani

Kimberly A. Matthews

Jerome Roddy

Victor A. Scuderi

Carl L. Shears

Robert A. Tapscott

PLATES





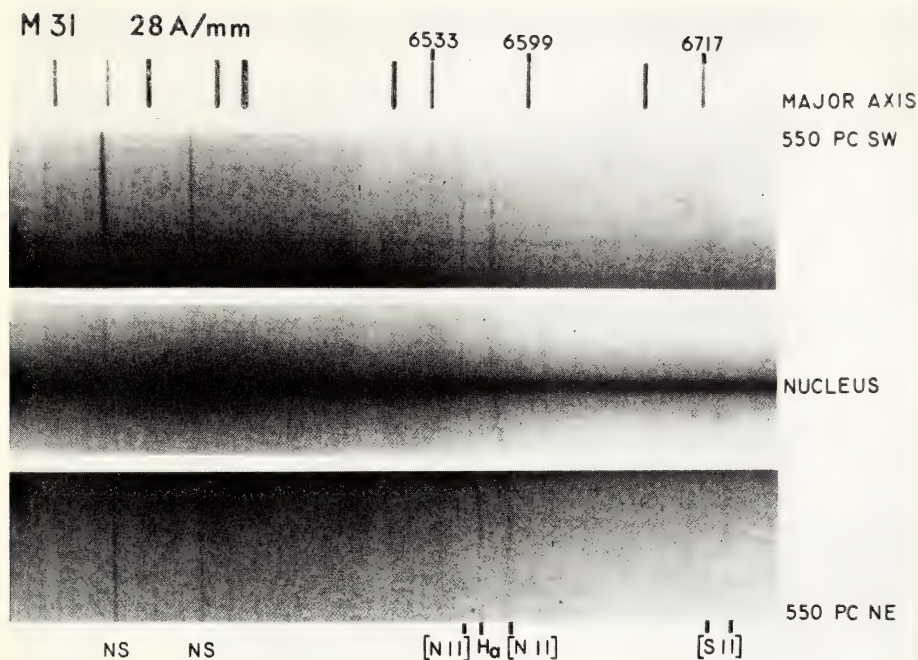


Plate 1. Spectra of the nuclear regions of the Andromeda galaxy M31. These high-dispersion spectrograms were obtained with the DTM image tube spectrograph on the 84-inch telescope at the Kitt Peak National Observatory. The emission lines of H $\alpha$  and SII had not previously been detected. The strikingly asymmetric velocity gradient across the nucleus was unexpected, since much farther out in the galaxy the velocities of the emission regions give a remarkably symmetrical rotation curve.

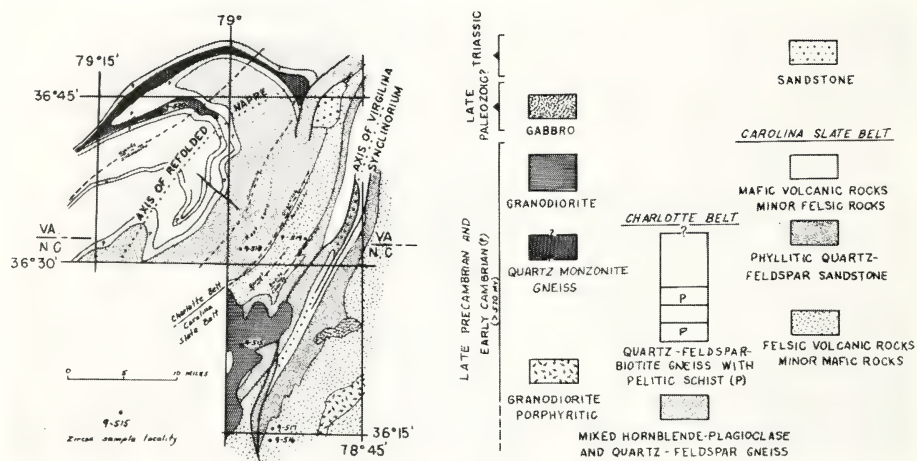


Plate 2. General geology and sample locations of the Carolina slate belt.



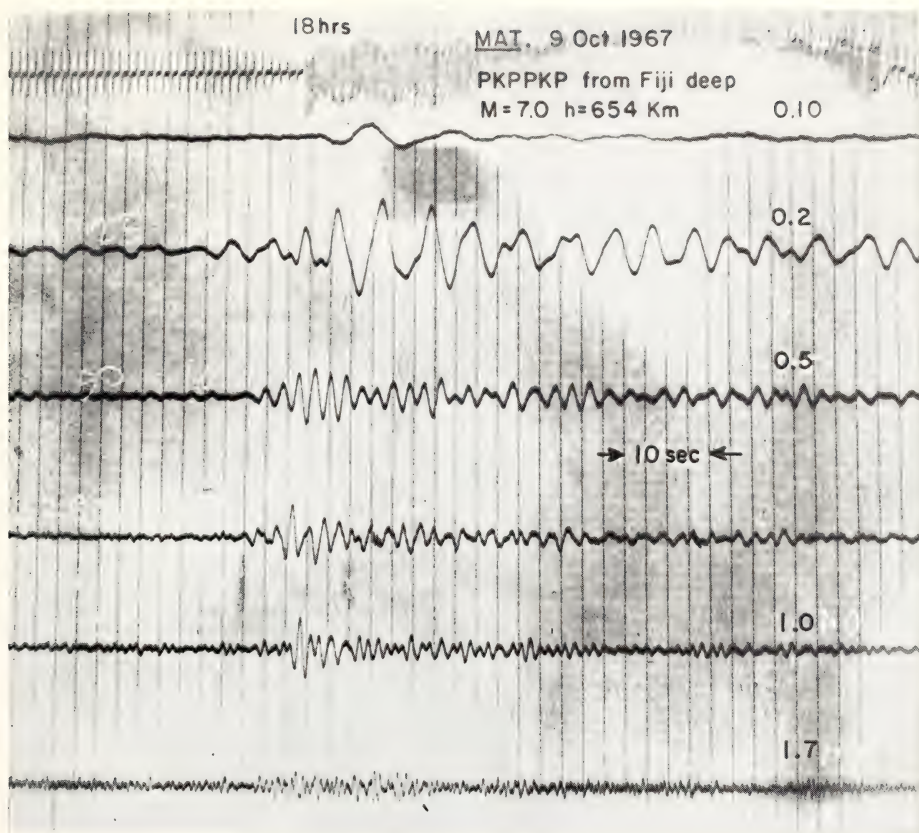


Plate 3. Multiple filtered *PKPPKP* arrival replayed from DTM broad-band tape recording seismograph at Matsushiro, Japan. The numbers on the traces are the filter settings in cycles per second.

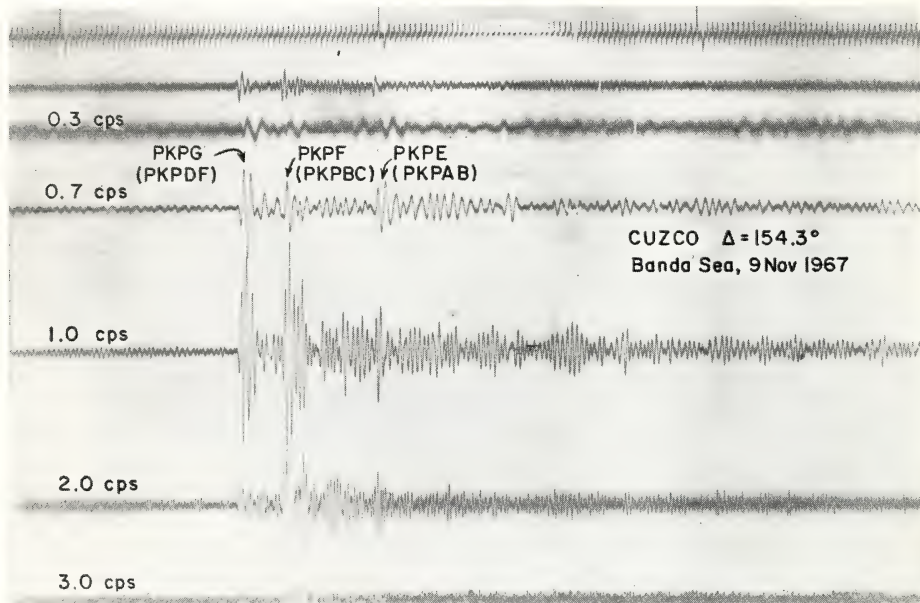
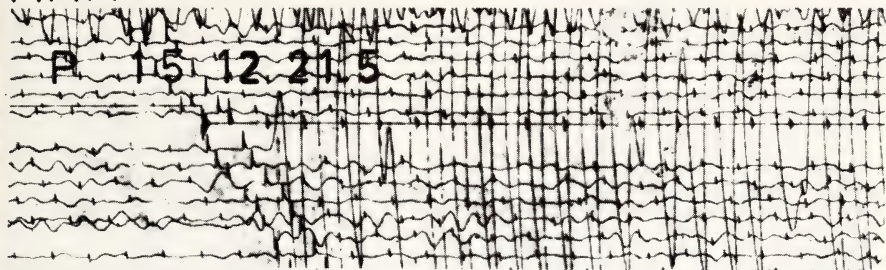


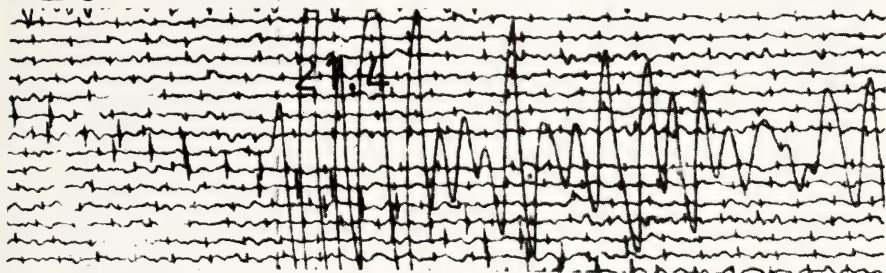
Plate 4. Multiple-filtered core phases showing the effect of anelasticity of the inner core. The first arrival has traveled through the solid inner core, the second through the liquid transition zone, and the third through the liquid outer core. Filter frequencies are marked in the traces.

26 APR 1968

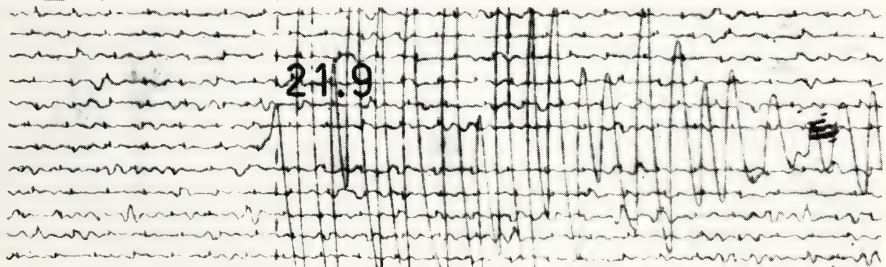
MAA



LEO



CEN



PPA

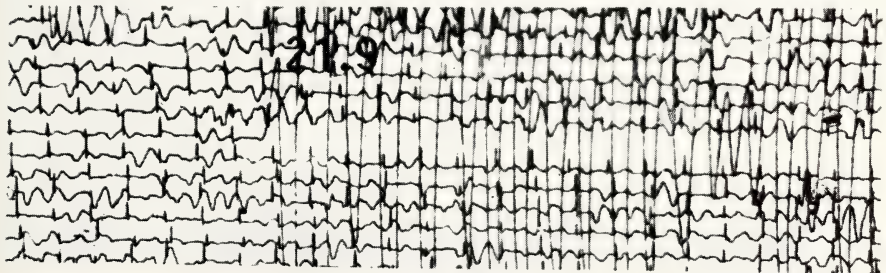
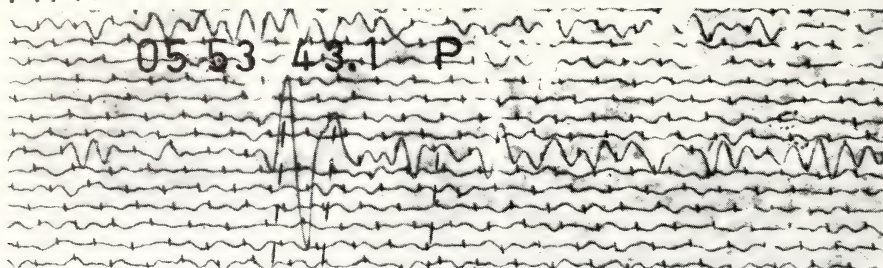


Plate 5. Photograph of the records of BOXCAR artificial explosion of April 26, 1968, phases P.

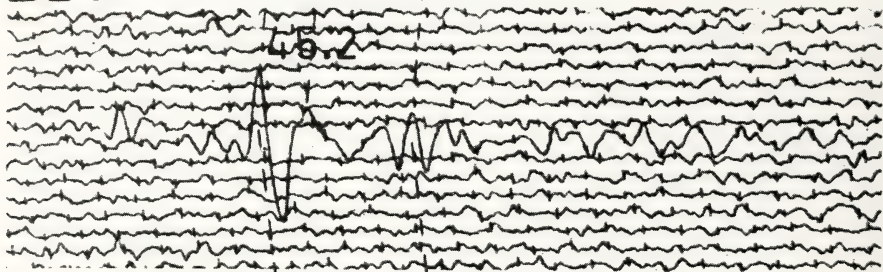


3 MAY 1968

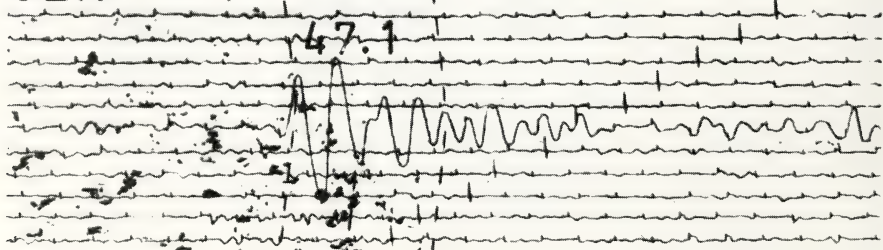
MAA



LEO



CEN



PPA

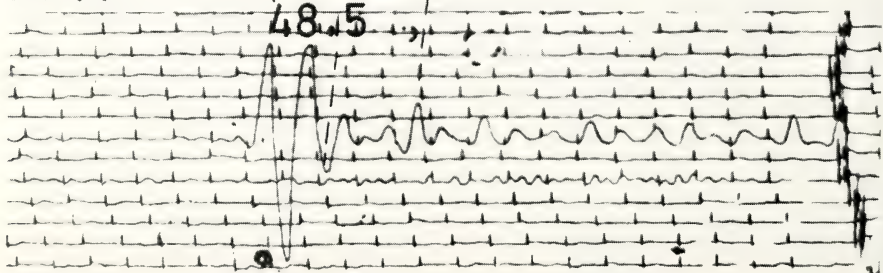


Plate 6. Photograph of the records of the earthquake of May 3, 1968, phases P.

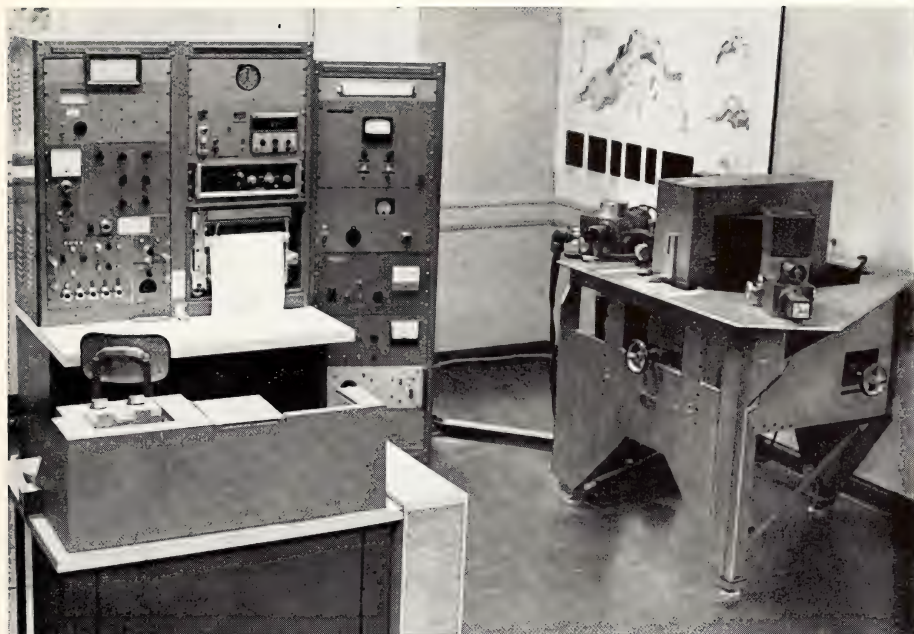


Plate 7. New 9-inch mass spectrometer facility, featuring automatic operation and digital data acquisition system.





# *Committee on Image Tubes for Telescopes*

Cooperative Project of the Hale Observatories, Department of  
Terrestrial Magnetism, Lowell Observatory, National Bureau  
of Standards, and United States Naval Observatory

W. A. Baum  
*Lowell Observatory*

John S. Hall (*Chairman*)  
*Director, Lowell Observatory*  
*Flagstaff, Arizona*

L. L. Marton  
*National Bureau of Standards*

M. A. Tuve  
*Department of Terrestrial Magnetism*  
*Carnegie Institution*



## CASCADED IMAGE INTENSIFIERS

A cascaded image tube provides a method of converting a weak, low light level image of a spectrum or star field into a brighter, intensified image that can be recorded through a relay lens on a conventional photographic plate. The tube has a photocathode which converts photons into photoelectrons, electrodes to provide a uniform electric field by means of which the photoelectrons are accelerated, an efficient electron multiplier consisting of a phosphor-mica-photocathode sandwich, a second set of accelerating electrodes, and, finally, a phosphor screen which converts the electronic image back into an optical one. Focusing is provided by an external magnet, and the acceleration of the electrons is, in currently available tubes, through 10 kv per section. This energy is converted by the phosphor screen to photons. In a cascaded tube with one multiplier, 500 to 1000 photons are typically produced in the focal plane of the relay lens for each primary photoelectron. Each of the primary photoelectrons can then be made to contribute to the recorded image, and the efficiency of detection of a weak image is directly related to the conversion efficiency of photons into photoelectrons by the cathode.

The practical advantage of using a cascaded tube depends on the particular astronomical problem (narrow-band filter photography, low-dispersion spectroscopy, etc.) to which it is applied and on the performance characteristics of the other components of the intensifier system. In general, the presently available tubes in "standard" systems can yield at least a factor of 10 in reduction of exposure time with resolution comparable to unaided photographs. This gain in exposure time can be used either to study more objects or to study fainter objects.

Because these devices have proved to

be efficient, reliable, and well suited for routine observations of faint sources, cascaded intensifier systems are being widely used in astronomical observing programs. The introduction of this new technique has been made possible by a joint National Science Foundation-Carnegie allocations program. Under this program some 34 of these systems have been distributed to observatories in this country and abroad. These devices have been applied to a wide range of astronomical problems.

Most of the tubes allocated through this program have retained their original sensitivity. Of the 45 cascaded tubes with S20 photocathodes that have been tested at the Department of Terrestrial Magnetism since 1964, only six are known to have failed because of loss of cathode sensitivity or intolerable increase in background, and only two are known to have been damaged by accidental mishandling. Thus far, it has usually been possible for us to furnish promptly a replacement tube. The distribution of failures with time indicates that the probability of failure of one of these tubes is less than 5% per year.

One limitation of the present system is the large trade-off in gain for resolution that must be made. With the gain available in a standard tube (C33011) a fast lens is required and the optical performance of such lenses, particularly off-axis, limits the performance of the intensifier system. Specifically, the spherical aberration usually found in the fast lenses causes weak absorption lines in a continuum spectrum to be filled in and lost (washed out). There is also a component of light-induced background in the cascaded tube due to light transmitted through the semi-transparent photocathode being reflected back to the cathode and also to secondary emitted electrons scattered from the phosphor



screens. In the past two years Dr. I. S. Bowen has designed three reflecting-optics transfer systems for phosphor-output image tubes. These systems have

extremely good optical performance, but will probably have limited general use because they are expensive and a bit cumbersome.

## DEVELOPMENT OF IMPROVED TUBES

Advances in the technology of image tube fabrication since the cascaded tubes were developed early in the sixties opened the possibility several years ago of two-stage cascaded tubes that may be operated at higher voltages with no increase in spurious background. The increased radiant energy gain of such high voltage tubes could be used to relax the speed requirements for the transfer optics and thus to achieve an improved modulation transfer function and higher limiting resolution for the overall system. Alternatively, the efficiency requirements on the phosphor screens used in the manufacture of the tubes could be relaxed a bit so that finer-grained screens could be incorporated. With fast transfer optics, such a tube would still be efficient and might permit integration on fine-grain emulsions to provide a better signal-to-noise ratio, and hence the detection of fainter features in the intensified image.

Development contracts initiated by the Carnegie Committee with support from the National Science Foundation have led to the construction by RCA of prototype high-voltage, cascaded tubes

having a rugged ceramic (rather than glass) envelope, a better accelerating electrode system, an improved, cleaner cathode processing scheme, and fewer internal sources of spurious emission. This new design is quite similar in external appearance to the old; it is the same diameter but slightly longer.

Five prototype samples of this improved tube have been delivered to the Department of Terrestrial Magnetism and evaluated during the period of September 1969 through January 1970. These tubes have good S20 cathodes and, as expected, they have higher and more uniform resolution (limiting resolution on axis of 50 plus line pairs per millimeter) and less distortion. The most striking improvement, however, is that these tubes can be operated at voltages up to 30 kv with tolerable background; at this voltage the radiant energy gains range from 10,000 to 20,000 compared with 2500 to 5000 for the standard two-stage tube. This increased gain can be used to improve the performance of the intensifier system for most astronomical problems.

## ACKNOWLEDGMENTS

The development, procurement, and distribution of image tubes have been supported by the National Science Foundation and the Carnegie Institution

of Washington, and the Committee wishes to express its thanks for this continuing support.

# *Department of Embryology*

*Baltimore, Maryland*

James D. Ebert

*Director*





# Contents

Introduction . . . . .	561
Isolation, Characterization and Control of Genes in Development . . . . .	565
Gene purification . . . . .	566
Genes for 28S and 18S rRNAs . . . . .	566
Genes for 5S RNA . . . . .	567
Genes for 4S RNA . . . . .	567
RNA sequence studies . . . . .	567
Multiple forms of RNA polymerase in <i>Xenopus laevis</i> : their relationship to RNA synthesis <i>in vivo</i> and their fidelity of transcription <i>in vitro</i> . . . . .	568
A denaturation map of rDNA . . . . .	571
Differentiation of the silk gland in <i>Bombyx mori</i> . . . . .	571
Cell Determination in <i>Xenopus laevis</i> . . . . .	574
Studies on the Biogenesis of Mitochondria in <i>Xenopus laevis</i> . . . . .	575
Properties and hybridization of mitochondrial RNA . . . . .	576
The mitochondrial ribosome of <i>Xenopus laevis</i> . . . . .	576
Coding properties of polynucleotides in isolated mitochondria . . . . .	577
Mitochondrial RNAs in eggs and embryos of <i>Xenopus</i> . . . . .	578
Biogenesis of mitochondria during development . . . . .	578
Separation of mitochondrial RNA species by preparative electrophoresis . . . . .	579
Cell Differentiation and Viral Susceptibility . . . . .	580
The interaction of Rous sarcoma virus with developing muscle . . . . .	580
Molecular hybridization of RSV-RNA with cellular and viral DNAs . . . . .	583
Characterization of the hybrids . . . . .	583
Hybridization of RSV-RNA with DNA from Chinese hamster chromosomes . . . . .	585
The role of cellular DNA homologous to RSV-RNA . . . . .	586
Isolation of temperature sensitive mutants of Chinese hamster cells, <i>in vitro</i> . . . . .	586
Factors Regulating the Fusion of Myoblasts . . . . .	587
Trophic Effects of Nerve on Muscle . . . . .	587
DNA synthesis and cell division in denervated rat diaphragm . . . . .	588
Pacemaker Development and Intercellular Communication in the Embryonic Heart . . . . .	589
Induction of pacemaker differentiation in the pre-somite embryo . . . . .	589
The potassium-inhibition threshold of isolated embryonic heart cells . . . . .	594
Ultrastructure of myocardial cell contacts . . . . .	597
Comparative Ultrastructure of Cultured Chick Fibroblasts at Early and Late Stages during Their Growth Span . . . . .	600
The Mammalian Embryo in Relation to Its Environment . . . . .	601
Attachment of the rabbit egg to the uterus . . . . .	601
Anatomy and physiology of the placenta . . . . .	603
Baseline studies . . . . .	603
Fetal circulation in the placenta . . . . .	605

Chronically impaired uterine artery blood flow . . . . .	605
Effect of vasoconstrictive drugs on placental circulation . . . . .	606
Morphology of the fetal villus as determined by phase contrast microscopy . . . . .	607
Ovarian tumors in rhesus monkeys . . . . .	608
The monkey colony . . . . .	608
The Collection of Human Embryos . . . . .	609
Developmental stages in human embryos . . . . .	609
Development of the heart . . . . .	609
Development of the larynx . . . . .	610
Staff Activities . . . . .	610
Bibliography . . . . .	611
Personnel . . . . .	613

## INTRODUCTION

In his address, "Hans Spemann and the Organizer Concept," commemorating the hundredth anniversary of Spemann's birth, Viktor Hamburger analyzed the factors contributing to Spemann's success as an experimentalist.

"The strength of both Spemann and Harrison," Hamburger writes, "was in the self-imposed concentration on a few basic themes and problems, and on a single object, the amphibian embryo.... He enjoyed playing with other forms, particularly invertebrates, and he indulged occasionally in this pleasant pursuit.... But he never permitted himself to stray far away from his chosen path." Hamburger goes on to observe, "The strategy of his research was very well expressed in a letter to me: '... to tackle the most immediately solvable question, until, piece by piece, the whole is achieved.'"

To be sure, concentration on a single theme or a single object does not in itself guarantee success. Investigators have followed one track assiduously for a lifetime without performing an experiment of signal importance, while others have captured prizes by quick forays into what was for them uncharted territory. However, most such breakthroughs are possible only because of the existence of a knowledge bank which yields dividends in the form of new insights.

This pattern of discovery, each new finding adding to the existing store of knowledge and permitting the perception of the next "solvable question," is illustrated graphically by the continuing studies of D. D. Brown, I. B. Dawid, and their colleagues on the mechanisms whereby oocytes and embryos of *Xenopus laevis* synthesize ribonucleic acids (RNAs): the ribosomal RNAs (consisting of 28S, 18S and 5S RNAs), 4S RNAs (consisting of multiple transfer RNAs), DNA-like RNAs (including messenger

RNAs and rapidly turning over nuclear RNAs), and the mitochondrial RNAs. These descriptive studies have progressed to the point at which attention must be centered not on the gene products, the RNAs, but on the genes themselves, and on the factors regulating their action.

Brown, Reeder, Roeder, and Wensink are concentrating on the genes that code for the rRNAs and 4S RNAs. It will be recalled that individual 28S and 18S genes are adjacent, about 450 of such pairs alternating with a stretch of "spacer" DNA. Brown and Dawid have called this DNA "ribosomal DNA" or rDNA, although it does not include genes for all rRNA, the genes for 5S RNA being excluded. Each adjacent pair of 28S and 18S genes (but not the spacer DNA) is transcribed as a single polycistronic RNA. The 28S and 18S genes are *linked* and their transcription is *coordinated*.

The genes for 5S RNA are not intermingled with the repeating sequences of rDNA. However, 5S RNA accumulates at the same rate as 28S and 18S RNA during oogenesis and embryogenesis. In anucleolate (0-nu) embryos in which the rDNA is deleted, transcription of 5S genes does not occur even though the 5S genes are present. When rDNA is amplified in oocytes, 5S RNA synthesis increases coordinately with 18S and 28S rRNA synthesis even though the 5S genes are not amplified. Therefore the 5S genes are not linked with 28S and 18S genes but their transcription is *coordinated* with the transcription of 28S and 18S RNA.

The 4S genes are *not linked* to the 28S and 18S genes or the 5S genes and their transcription is *not coordinated* with rRNA synthesis *in vivo*.

The next solvable question—the immediate goal—can now be perceived: to isolate these genes in pure form and



reconstruct their normal controls *in vitro*. The longer range objective is to learn what molecules are involved in coordinating the action of unlinked genes. This is a salient feature of development. In almost all specialized cell types, multiple unlinked genes are coordinated in their action, perhaps the best known example being the genes for the heavy and light chains of antibody molecules.

In the pages to follow, modest advances are described on four fronts: (1) Pieter Wensink is probing the actual structure of rDNAs with the electron microscope; (2) Brown has reported some progress in isolating and characterizing the genes for 5S RNA and has initiated studies of the genes for 4S RNA; (3) Reeder is sequencing the first nucleotides transcribed in RNA polymerase studies; and (4) R. G. Roeder, who joined the Department during the year as a Fellow of the American Cancer Society, is purifying and characterizing the RNA polymerases of *Xenopus laevis* in order to test their ability to transcribe purified genes accurately. His experiments have already established that RNA polymerases I and II from *Xenopus* liver nuclei are similar to their counterparts in other eukaryotes. Thus it becomes possible to examine the relation between the levels of RNA polymerases and the occurrence and rate of RNA synthesis during development. Preliminary experiments reveal that RNA polymerases are detectable in significant quantities in embryos in which no RNA synthesis can be detected *in vivo*. This statement is true both for normal early embryos (stages 2-6) and anucleolate embryos. Thus RNA polymerases I and II cannot themselves account for the changes in amounts and kinds of RNA which characterize embryogenesis in *Xenopus*. These observations set the stage for the identification of control factors that endow the enzymes with the specificity attributed to them *in vivo*.

In an article published in *Proceedings of the National Academy of Sciences*,

66, pp. 117-124 (1970), Dawid and R. F. Swanson, a Fellow of the U. S. Public Health Service (preparing, as this Report is being written, to take up a new appointment as Assistant Professor of Biology at the University of Virginia), have described the isolation and characterization of the mitochondrial ribosome of *Xenopus laevis*. The isolation of these 60S particles from ovarian mitochondria was a logical extension of Swanson's earlier studies (*Year Book* 68, pp. 515-516) on protein synthesis in these mitochondria. The mitochondrial ribosomes contain the 21S and 13S RNAs described earlier in detail by Dawid (*Year Book* 68, pp. 514-515). Thus we know that mitochondria contain a circular DNA molecule (*Year Book* 66, Plate 1), of limited size (16,000 base pairs) and ribosomal particles with specific mitochondrial ribosomal RNAs. The progress thus far makes it reasonable to expect that the entire function of the mitochondrial genome may be understood in the near future.

Douglas M. Fambrough and his colleagues have extended their observations on the control of acetylcholine receptors in muscle fiber membranes by motor neurons. Last year (*Year Book* 68, pp. 531-534) they confirmed that a high concentration of surface receptors develops over the entire surface of each fiber in rat muscle isolated in organ culture. (Normally innervated fibers have a high concentration of receptors only in the area of the neuromuscular junction.) This change in receptor density is prevented by the inhibitors actinomycin D (which blocks nucleic acid synthesis) and puromycin and cycloheximide (which block protein synthesis). Inhibitors that do not block nucleic acid and protein synthesis do not prevent the change. Are new receptor molecules synthesized after denervation? Or are latent receptors activated by newly synthesized molecules? The evidence thus far does not distinguish between the two possibilities. However, which-

ever is correct, the regulation of receptor distribution by motor nerves appears to involve the regulation of gene action in muscle fibers.

Reiji Hirakow, a Carnegie Fellow working with Robert L. DeHaan, has contributed importantly to our understanding of communication between heart cells. One of the features of the hearts of all vertebrates is their ability to conduct electrical stimuli from cell to cell, thereby coordinating contractions into a pumping action. It had been postulated that the low-resistance pathway between heart cells might be the so-called "nexus," or "tight-" or "gap-junction"—a 20 Å gap between apposed membranes. Hirakow has perfected electron microscopic techniques to reveal the existence of these specialized areas in adult and embryonic mice and chickens and in adult *Necturus*. These junctions range from "typical" gap junctions in the mouse at all stages studied and in the adult chicken, to tiny punctate spots in the chick embryo and adult *Necturus*.

In his analysis of Spemann's "personal style," Hamburger quoted from his master's autobiography. "My passion for experimentation," Spemann wrote, "is innermost related to my pedagogic inclinations; with my enjoyment in knowing people, in teaching and education." So it is in our own Department. We enjoy and profit by the participation of students, both postdoctoral and predoctoral, in our programs. Mention has already been made of three postdoctoral fellows, Hirakow, Roeder, and Swanson, and one predoctoral student, Wensink, whose programs are discussed more fully in the body of the Report. The contributions of others are equally impressive.

Yoshiaki Suzuki, a Carnegie Fellow, has continued his studies with Brown, of the genes which function in a very specialized tissue, directing the synthesis of silk fibroin in the posterior silk gland of *Bombyx mori*, the Japanese silkworm. Some of the reasons for this study have been outlined previously (*Year Book 68*,

pp. 509–510). These cell-specific genes may be contrasted with the genes for the rRNAs. The latter genes are not characteristic of any tissue or cell type; they are genes for "housekeeping" functions in all cells and are therefore in direct contrast to genes coding for cell-specific products. Are the two types of genes regulated in the same manner? Brown and Suzuki hope ultimately to apply the kinds of analyses being developed for rRNA genes and 4S RNA genes in *Xenopus* to the genes for fibroin in *Bombyx* to elucidate how a specialized gene functions.

Thus far Suzuki has concentrated on analyzing RNA and protein synthesis in the silk gland. Although he has not yet isolated the message (mRNA) for fibroin, techniques for labeling and isolating RNA have been developed to the point at which a detailed analysis should be possible.

During the year, L. P. Gage, a recent graduate of the Department of Biophysics at the University of Chicago, joined Brown's laboratory as a Fellow of the U. S. Public Health Service. He has begun to examine the factors controlling cell *determination* in *Xenopus*. Determination is the process by which a cell becomes restricted to a given pathway. He has spent most of his time developing an assay system in which early embryonic cells can be maintained *in vitro* during the course of determinative events. His first observations are encouraging. Cleaving embryos can be dissociated, and the cells thus freed continue to divide *in vitro*. In addition, Gage has sought biochemical "signs" of determination. Acetylcholinesterase and collagen may prove to be suitable markers.

Robert J. Hay, Assistant Investigator, who will move to Wright State University as Assistant Professor of Biology during the summer of 1970, has described the fine structure of developing muscle infected with Rous sarcoma virus. In addition, in collaboration with M. A. Brock



of the Gerontology Research Center, he has studied *in vitro* the fine structure of chick fibroblasts at early (rapidly dividing) and late (senescent) stages during their growth span. Another of Ebert's colleagues, Masako Yoshikawa-Fukada, has continued her important studies of the viral oncogenic sequence described in *Year Book* 68, pp. 521-531 and in an article in *Proceedings of the National Academy of Sciences*, 64, 870-877 (1969).

Eijiro Ozawa, trained with Professor S. Ebashi of Tokyo in the biochemistry and physiology of muscle, joined Ebert during the year in an attempt to elucidate the mechanisms of cell fusion. His initial observations are described briefly in the Report.

Elizabeth M. Ramsey and her team, H. R. Misenhimer, M. W. Donner, S. I. Margulies and C. B. Martin, Jr., continued to set an example for us all, not only by their efficiency and productivity, but in the remarkable spirit of cooperation that pervades their collaborative studies. During the spring of 1970 the team was joined by Professor Maurice Panigel of Paris, Professor at the Institut National de la Santé et de la Recherche Médicale, for a week's intensive pilot study of the effects of drugs on the mother and fetus. It is especially noteworthy that while Dr. Ramsey is "rounding out" some aspects of her comprehensive 25-year-long study of uteroplacental and fetoplacental vasculature and circulation, she is at the same time charting new courses.

In June 1970 Dr. Misenhimer left his post at Baltimore City Hospitals to assume a new role at Rush-Presbyterian-St. Luke's Medical Center (Chicago). His three years' association with Ramsey as a Carnegie Fellow have been highly productive ones. With him go not only the Department's best wishes, but some of its better known inhabitants, for the Carnegie monkey colony is moving to Chicago with him.

Thus the principal axis of the placental research team now passes from Los Angeles to Baltimore and Paris *via* Chicago. In the past mere distance has not deterred the group from effective collaboration. There is no reason to believe that the pattern will change. Chicago should prove a friendly haven for placentologists, as Detroit will for embryologists where Bent Böving has moved as Professor of Anatomy and Gynecology-Obstetrics at Wayne State University. In the summer or fall of 1971 he will be joined by Professor Ronan O'Rahilly and the Collection of Human Embryos. During the report year, O'Rahilly laid most of the groundwork for his projected monograph on "Developmental stages in human embryos, being a survey of the Carnegie Collection."

During the year six graduate students elected members of the staff as their major professors: Pieter Wensink and Ralph Stern with Brown; John Chase and Dennis Leister with Dawid; and John Dunning and Criss Hartzell with DeHaan and Fambrough, respectively. The programs of Wensink, Chase, Dunning, and Hartzell are sufficiently advanced to be included in the body of the Report.

Seventeen visiting investigators spent from a few days to several months in the Department; especially notable in this group was Professor Toyooki Fujimoto of Kumamoto University. During his ten months' stay, most of his time was spent in studying slides and reconstructed models of early human embryos in the Collection. Human embryos of the first eight weeks were emphasized, although later stages were also examined. In addition, rhesus monkey material was used to study placentation. Attention was given to implantation, to primordial germ cell migration, and especially to neurulation, including formation, migration, and differentiation of the neural crest. Following in human development



such neural crest derivatives as ganglia and chromaffin tissue was of special interest in view of the author's previous experimental study of that subject and of mechanisms of neurulation in lower vertebrates. More general observation, photography, and note-taking were carried out in preparation for the author's

projected Textbook of Human Embryology.

A short period was spent studying educational systems and curricula for medical science in general and embryology in particular. For these purposes, ten laboratories and universities were visited in New England and the Midwest.

## ISOLATION, CHARACTERIZATION, AND CONTROL OF GENES IN DEVELOPMENT

*D. D. Brown, R. H. Reeder, R. G. Roeder, Y. Suzuki, and P. Wensink*

Several years ago we began descriptive studies on how oocytes and embryos synthesize three classes of ribonucleic acid (RNA): ribosomal RNAs (consisting of 28S, 18S, and 5S RNAs), 4S RNA (consisting of multiple transfer RNAs) and DNA-like RNA (including messenger RNAs and rapidly turning over nuclear RNAs). We found that oocytes and embryos of *Xenopus laevis* synthesize these three general classes of RNA at vastly different rates at different stages of development. Using techniques of molecular hybridization we have centered our attention on the genes which code for the ribosomal RNAs (rRNAs) and 4S RNA.

The following conclusions derived from these studies on RNA and their genes are important for this report:

1. Individual genes for 28S and 18S RNAs are adjacent, about 450 of such gene pairs alternating with a stretch of "spacer" DNA. We call this DNA "ribosomal DNA" or rDNA (Fig. 1). Each adjacent pair of 28S and 18S genes (but not the spacer DNA) is transcribed as a single polycistronic RNA. Therefore the 28S and 18S genes are *linked* and their transcription is *coordinated*.

2. The 5S genes are not linked to the 28S and 18S genes, that is, they are not intermingled with these long repeating sequences of rDNA coding for 28S and 18S RNA. However, 5S RNA accumulates at the same rate as 28S and 18S RNA during oogenesis and embryo-

genesis. In anucleolate (0-nu) embryos that are deleted of their rDNA, transcription of 5S genes does not occur even though the 5S genes are present. When rDNA is amplified in oocytes, 5S RNA synthesis increases coordinately with 18S and 28S rRNA synthesis even though the 5S genes are not amplified. Therefore the 5S genes are not linked with 28S and 18S genes but their transcription is *coordinated* with the transcription of 28S and 18S RNA.

3. The 4S genes are not linked with either the 28S and 18S genes or the 5S genes and their transcription is not coordinated with rRNA synthesis *in vivo*.

Thus we have examples of linked and

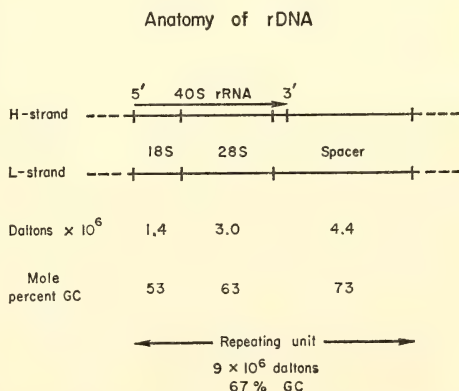


Fig. 1. The model for rDNA. A compilation of information on the arrangement, length, and base composition of the three nucleotide sequences which comprise a repeating unit of rDNA.

coordinated genes (28S and 18S genes), unlinked and coordinated genes (28S and 18S compared with 5S genes), and unlinked and uncoordinated genes (the group of genes for rRNA compared with the genes for 4S RNA).

Our program has evolved gradually to the point where our goals now can be defined very specifically. We wish to isolate these genes in pure form and reconstruct their normal controls *in vitro*. In doing so we should expect to learn what molecules are involved in coordinating the action of unlinked genes. This is a salient feature of development. In almost all specialized cell types, multiple unlinked genes are coordinated in their action, two of the better known examples being the genes directing the synthesis of the heavy and light chains of antibodies and of the hemoglobin proteins.

We recognize that a complete elucidation of the factors regulating the ribosomal and transfer RNA genes may not explain how cell- or tissue-specific genes are controlled in embryogenesis. The genes for these RNAs are not characteristic of any tissue or cell type; they are genes controlling "housekeeping" products found in all cells and may be regulated differently from the hemoglobin and antibody genes. For this reason we have begun to study genes that function in a specialized tissue, the genes for silk fibroin in the posterior silk gland of *Bombyx mori*, the Japanese silkworm. For reasons previously outlined (*Year Book 68*, p. 509), we are attempting to identify these genes by chemical and physical criteria. We hope ultimately to apply the kinds of analyses we are developing for rRNA genes and 4S RNA genes in *Xenopus* to the genes for fibroin in *Bombyx*, so that we can learn how a gene for a specific protein functions.

Many different approaches are being used to contribute to these long term goals. Brown is involved in the isolation of 5S and 4S genes. Reeder is sequencing the first nucleotides transcribed in RNA

polymerase studies. Roeder is purifying and characterizing the RNA polymerases of *Xenopus laevis* in order to test their ability to transcribe purified genes accurately. Wensink is probing the structure of DNAs, using the electron microscope. Suzuki is attempting to isolate the messenger RNA for silk fibroin.

## GENE PURIFICATION

### *Genes for 28S and 18S rRNAs*

*D. D. Brown, I. B. David and R. H. Reeder  
with the assistance of E. Jordan*

The DNA containing the genes for 28S and 18S rRNA has been purified from *Xenopus laevis*. Steps in the isolation and characterization of this DNA have been described in *Year Book 67*, pp. 401-404, and *Year Book 68*, pp. 505-509. The current model for the structure of this DNA (Fig. 1) was derived from our experiments as well as those of Birnstiel and co-workers in Edinburgh, Gall at Yale, and Miller and Beatty at Oak Ridge. It consists of three repeating sequences of DNA of quite different base composition. The repeat length has been estimated at  $8.5-9.0 \times 10^6$  daltons, and it recurs several hundred times within one chromosome of each haploid set in somatic cells. The derivation of each part of this model has been gone into in detail previously and need not be repeated here. It is useful to compare it with electron micrographs of this DNA by Wensink (this Report, p. 571). It should also be noted that each molecule of 40S RNA has its 5' origin at or near one end of each 18S gene sequence. Faithful transcription of this DNA *in vitro* must initiate and terminate at the same site where it occurs *in vivo* (see Reeder, this Report, p. 567). Neither *E. coli* polymerase (*Year Book 68*, pp. 507-508) nor either polymerase I or II of *X. laevis* (see Roeder, this Report, p. 568) transcribes this DNA with absolute fidelity *in vitro*.

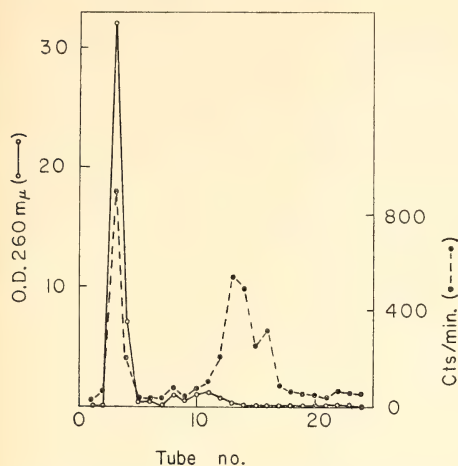


Fig. 2. Hybridization of  $(^3\text{H})$ -5S RNA with *Xenopus* DNA complexed with  $\text{Ag}^+$  and centrifuged in  $\text{Cs}_2\text{SO}_4$ . The DNA was dialyzed against borate buffer,  $\text{Ag}_2\text{SO}_4$  was added as well as  $\text{Cs}_2\text{SO}_4$  and the solution centrifuged at 35,000 rpm in a fixed angle rotor of the Spinco ultracentrifuge for 3 days. The contents of the tube were fractionated and aliquots from each fraction were hybridized with  $(^3\text{H})$ -5S RNA. O.D. 260  $\text{m}\mu$  (open circles); cts/min hybridized (closed circles).

### Genes for 5S RNA

D. D. Brown

with the assistance of E. Jordan

Some progress has been made in the purification of 5S DNA from *Xenopus laevis*. Fortunately these genes are even more redundant than the 28S and 18S genes, since 5S RNA will hybridize with an amount of DNA equivalent to more than 25,000 5S gene sequences. This DNA has a lighter buoyant density than main-band DNA of *X. laevis*. Several techniques have been tried to separate the 5S DNA even further from main-band DNA. The most successful one to date has been to complex the DNA with  $\text{Ag}^+$  and centrifuge it in  $\text{Cs}_2\text{SO}_4$ . The exact mechanism by which silver ions interact with the purine and pyrimidine bases of DNA is unknown. However, it is thought to bind preferentially with GC pairs in native DNA, causing an accentuation of the density differences be-

tween DNAs. The initial purification of 5S DNA using  $\text{Ag}-\text{Cs}_2\text{SO}_4$  centrifugation is shown in Fig. 2. A DNA "satellite" that behaves in many respects like 5S DNA has been isolated from these gradients. However, we are only now in the process of characterizing this DNA.

### Genes for 4S RNA

D. D. Brown

These multiple genes are not as abundant as those for 5S RNA but it should be possible to isolate at least some of them. The buoyant density of 4S DNA is slightly higher than the main band of DNA, and the polylysine precipitation procedure which was used originally for the isolation of rDNA (Year Book 67, p. 404) has been found to enrich this DNA. However, there are two DNA satellites that band close to 4S DNA in  $\text{CsCl}$ ; they have thus far contaminated even our best preparations. By molecular hybridization we judge that we have enriched our best preparations about a hundredfold for the 4S RNA genes.

### RNA SEQUENCE STUDIES

R. H. Reeder with the assistance of D. Prather

When RNA polymerase transcribes a gene in the living cell, it begins transcription at a unique site on that gene and produces RNA transcripts all of which have the same base sequence. The most direct way of determining whether RNA polymerase is acting with similar specificity *in vitro* is by examining the initial sequences of complementary RNA (cRNA) made *in vitro* and determining how many such sequences are made. If our model of rDNA structure is correct (Fig. 1), an RNA polymerase with the proper specificity should always initiate at the same site on the DNA yielding a single kind of RNA with a homogeneous sequence.

The specificity of initiation can be studied by labeling the initial (5') end of cRNA molecules transcribed from



rDNA. First, nucleoside triphosphates are prepared labeled with  $^{32}\text{P}$  only in the  $\gamma$  phosphate. Using a modification of the method of Glynn and Chappell, specific activities of  $5\text{--}8 \times 10^{10}$  CPM/ $\mu\text{mole}$  have been obtained. Hurwitz has shown that when  $\gamma\text{-}^{32}\text{P}$  triphosphates are incorporated internally in an RNA chain, the labeled phosphate is eliminated and does not become part of the chain. Only when the  $\gamma\text{-}^{32}\text{P}$  triphosphate is incorporated as the first nucleotide on the 5' end is the label retained. RNA labeled with  $^{32}\text{P}$  on the 5' end is then digested with a ribonuclease such as pancreatic RNase (which splits the chain only after a pyrimidine residue), and the resulting short oligonucleotides are fractionated according to chain length on a column of DEAE Sephadex. The number of different  $^{32}\text{P}$  labeled oligonucleotides resulting from such a procedure is a direct measure of the number of different initiation sites which the polymerase recognizes on a given template.

In preliminary experiments *E. coli* RNA polymerase was found to initiate RNA chains only with GTP using rDNA as template. However, analysis of the  $\gamma\text{-}^{32}\text{P}$  GTP-labeled oligonucleotides resulting from digestion with pancreatic RNase shows that a number of different sequences starting with GTP are made. This result is not surprising in view of the only moderate fidelity with which *E. coli* polymerase is known to transcribe rDNA (see *Year Book* 68, pp. 507–508). We will continue to apply these methods to RNA transcribed from purified genes *in vitro* to assess the fidelity of initiation of RNA synthesis. We predict that exact transcription of rRNA *in vitro* will result in initiation at a single site and production of a single 5' nucleotide sequence in the cRNA.

MULTIPLE FORMS OF RNA POLYMERASE  
IN *Xenopus laevis*: THEIR RELATIONSHIP  
TO RNA SYNTHESIS *in vivo* AND THEIR  
FIDELITY OF TRANSCRIPTION *in vitro*

R. G. Roeder

There are several mechanisms whereby

the expression of a group of unlinked genes might be coordinated. One possibility is that the genes within a coordinated group might possess identical initiation sites which only one polymerase would recognize; thus, coordinate activation or repression of several genes could be controlled by a single enzyme. The recent discovery in eukaryotic cells of multiple forms of DNA-dependent RNA-polymerase (Roeder and Rutter, *Nature* 224:234, 1969) makes such a scheme plausible. The fact that RNA polymerases I and II are localized in isolated nuclei specifically within the nucleoli and nucleoplasm, respectively, has suggested that they may have specific functions (Roeder and Rutter, *Proc. Nat. Acad. Sci. U. S.* 65:575, 1970). Accordingly, it has been predicted that RNA polymerase I is the enzyme responsible for rRNA synthesis because of its nucleolar localization.

Current experiments with *Xenopus laevis* are directed toward answering several questions related to these observations: (1) Does the presence, abundance, or synthesis of either species of polymerase correlate with the presence, synthesis, or accumulation of any particular kind of RNA? (2) What genes do these enzymes transcribe *in vivo*, and do they retain specificity *in vitro*? (3) Are other factors present within the cell which regulate the activity and/or specificity of these enzymes?

RNA polymerases I and II have been solubilized from adult liver nuclei, separated by DEAE-Sephadex chromatography, and shown to have chromatographic and catalytic properties (activation by  $\text{Mg}^{++}$ ,  $\text{Mn}^{++}$ , and ammonium sulfate) similar to those of other eukaryotic polymerases. In addition, the bicyclic polypeptide  $\alpha$ -amanitin specifically inhibits polymerase II, while it has no effect upon polymerase I activity. Similar results with  $\alpha$ -amanitin have been obtained with polymerases I and II from embryonic tissue (Fig. 3). These observations further establish that polymerases I and II from *Xenopus laevis*

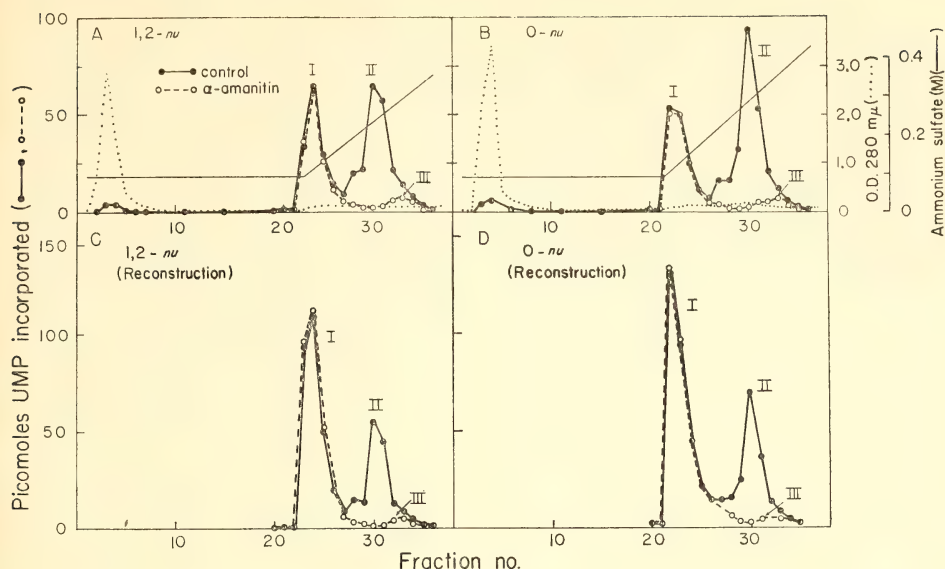


Fig. 3. Resolution of multiple RNA polymerases from normal and anucleolate embryonic tissues. RNA polymerase activity was solubilized from stage 40 anucleolate (0-nu) and normal (2-nu and 1,2-nu) embryos. Samples containing 3.6 and 4.2 mg protein, for the 1,2-nu and 0-nu embryos (C), respectively, were chromatographed on  $0.6 \times 7$  cm columns of DEAE-Sephadex. The activities for the 1,2-nu and the 0-nu enzymes were, respectively, 0.17 and 0.16 picomoles UMP incorporated per 20 minutes per  $\mu\text{g}$  protein at 0.01 mM UTP and were, respectively, 30% and 28% sensitive to  $\alpha$ -amanitin. In experiments A and B aliquots of each fraction were assayed in the presence and absence of  $\alpha$ -amanitin. Fractions 3 and 4 ("breakthrough" protein) were combined in A and in B and were concentrated severalfold. In experiments C and D aliquots of the same fractions assayed in A and B, respectively, were assayed in the presence of 23  $\mu\text{g}$  (C) or 18  $\mu\text{g}$  (D) of the respective concentrated "breakthrough" protein fractions. UMP incorporation represents total picomoles UMP incorporated per fraction (0.50 ml).

liver nuclei are very similar to their counterparts in other eukaryotes.

The extent to which the purified nuclear RNA polymerases transcribe bulk DNA and rDNA, as well as the specificity of transcription of the latter template, have been examined. While these enzymes transcribe several heterologous DNAs to different degrees, each enzyme transcribes limiting amounts of bulk DNA and rDNA to about the same extent in the presence of  $\text{Mn}^{++}$ . In the presence of  $\text{Mg}^{++}$ , polymerases I and II show slight preferences for rDNA and bulk DNA, respectively, although the differences are not striking. Furthermore, polymerase I does not transcribe rDNA with the fidelity that is observed *in vivo*. This has been demonstrated by tran-

scribing rDNA *in vitro* with polymerases I and II (from liver nuclei) under a variety of conditions. The assay system for fidelity of transcription detects RNA transcripts from the 18S and 28S regions of the correct (H) strand of rDNA as well as transcripts from the spacer region of this strand and transcripts of the incorrect (L) strand (see *Year Book 68*, pp. 506–508, and model of rDNA, above). All these regions are transcribed by RNA polymerase I *in vitro* but only the 18S and 28S regions (H strand) are transcribed *in vivo*. The same results are obtained with RNA polymerase II. Thus, proper transcription of rDNA is not achieved with either purified enzyme (with  $\text{Mn}^{++}$  or with  $\text{Mg}^{++}$ ) and indicates

that other factors, which might increase specificity, may have been lost.

Investigations of RNA polymerase in early embryos have also begun. It has been possible to utilize the nuclear polymerase isolation procedures for analysis of homogenates of whole embryos (Table 1). RNA polymerase has been detected in significant quantities as early as stages 2-6, when no RNA synthesis can be detected *in vivo*. In fact, the total polymerase activity per embryo rises only five- to sixfold by stages 40-43, despite the fact that the number of cells has increased many thousandfold. This suggests that some of each polymerase is probably stored in the cytoplasm of early embryos, presumably for use at later developmental stages.

The RNA polymerase activity in anucleolate embryos also has been examined (Table 1). These mutants synthesize neither 18S nor 28S rRNA, nor 5S RNA; the genes for the former have been shown to be absent, although the 5S genes are present and could in theory be transcribed. However, normal and anucleolate embryos were found to have the same levels of total polymerase, and DEAE analysis of solubilized enzyme preparations (Fig. 3A, B) showed that the enzyme patterns were indistinguishable. This holds true even when the assays are conducted in the presence of

$\alpha$ -amanitin (which selectively inhibits polymerase II). Studies with the inhibitor also reveal the presence of a third (minor) component as a shoulder on peak II. This component is insensitive to  $\alpha$ -amanitin and is probably analogous to polymerase III in sea urchin embryos (Roeder and Rutter, *Nature* 224:234, 1969; *Biochemistry*, in press). These observations indicate that neither a true nucleolar structure (which contains the ribosomal genes) nor concomitant rRNA synthesis is required for the increase in polymerase I activity and imply that other control mechanisms must be operative.

Experiments with the polymerases from whole-cell homogenates also have suggested the presence of another factor or factors which affect the activity of the purified RNA polymerase. The activity of embryonic polymerase I from the DEAE columns can be stimulated two- to threefold when assayed in the presence of the bulk of the cellular proteins that do not adhere to the column (Fig. 3C, D). These observations are being pursued in the hope that factors can be isolated which will confer specificity upon purified RNA polymerase.

Thus, preliminary experiments suggest that polymerases I and II as purified on DEAE-Sephadex cannot themselves account for the changes in amounts and

TABLE 1. Levels of RNA Polymerase Activity in *Xenopus laevis* Embryos

Developmental Stage	Cells/Embryo	Activity per mg Embryo Protein	% Inhibition With $\alpha$ -Amanitin
Cleavage (2-6)	2-32	4.8	33
Gastrula (10-12)	50,000	5.2	35
Swimming tadpole (40) (normal)	400,000	21	30
Swimming tadpole (40) (anucleolate)	400,000	23	28

The RNA polymerase activity in whole cell homogenates was measured after solubilization of the enzyme by sonication in the presence of ammonium sulfate. The Nieuwkoop-Faber stages of the embryos are given in parentheses in the first column. Activity represents picomoles UMP incorporated per 20 minutes at 30°C under standard (limiting UTP) assay conditions. Embryo protein represents total embryonic protein.



kinds of RNA which characterize embryogenesis in *Xenopus*. Both enzymes are present at times when no RNA is synthesized *in vivo*. Their relative amounts do not change when large changes in RNA synthesis occur. Polymerase I, always found localized in nucleoli of adult liver is, nevertheless, abundant in the absence of nucleoli and can increase in amount in anucleolate embryos which neither synthesize rRNA nor contain nucleoli. Finally, neither enzyme can transcribe rDNA with greater fidelity than can *E. coli* polymerase. These findings set the stage for the identification of control factors that endow these polymerases with the specificity they are presumed to have *in vivo*.

#### A DENATURATION MAP OF rDNA

Pieter Wensink

Denaturation maps of phage DNAs have been constructed by Inman. In this technique the DNA is partially denatured by high temperature or high pH and the separated strands are reacted with formaldehyde to prevent them from reassociating. The DNA is put on a grid and the location of the single-stranded loops is recorded from photographs taken with the electron microscope. DNA does not denature at random sites: denaturation begins in those regions which have the highest A+T content. Since the model of rDNA (Fig. 1) predicts adjacent regions of DNA which have markedly different base composition, it is ideally suited for this kind of analysis.

Amplified (oocyte) and chromosomal (somatic) rDNA have been denatured by high pH, the DNA being incubated at pH 11.50 in the presence of 10% formaldehyde. Under these conditions the strands separated as a function of time and were 30% separated in about 30 minutes. Samples were neutralized and mixed with native bacteriophage T7 DNA which was used as an internal molecular weight standard. This mixture

was spread according to Westmoreland's variation of the Kleinschmidt monolayer technique, a method that has the advantage of giving a very constant mass per unit length for DNA.

It was found by inspection of partially denatured rDNA that the distribution of single-stranded regions has a very regular repeating pattern. An example of a segment of one molecule of rDNA is given in Plate 1. A tracing of this segment is also provided, with its repeat lengths measured and marked with arrows. The regions, in which strand separation is about 60%, average 2.5  $\mu$  and alternate with long native regions of 1.8  $\mu$ . The combined length of these two sequences is about 4.3  $\mu$  or approximately  $8.0 \times 10^6$  daltons of DNA. This value agrees well with the predicted length of the repeat (Fig. 1). Photographs of many molecules with up to 12 repeats (about  $10^8$  daltons) have been measured. An analysis of the data is now under way.

We expect to answer the following kinds of questions in this study: (1) What is the exact length of the repeating unit in rDNA? (2) Is the repeat length always the same along a single molecule or between two different molecules? (3) Is the pattern of single-stranded regions the same in each repeat? (4) Is there any difference between the somatic and amplified (oocyte) rDNA?

#### DIFFERENTIATION OF THE SILK GLAND IN *Bombyx mori*

Yoshiaki Suzuki

We have undertaken studies of the mechanism of differentiation of the silk gland, our ultimate goal being to isolate the gene(s) for silk fibroin. We decided to isolate the messenger RNA first so that we might be able to use it as a tool for the assay of the gene. As discussed previously (*Year Book 68*, p. 509), the gene for fibroin and its mRNA should have a high GC content of 60–80%, a fact that should aid in their identifica-

tion. During the year the major effort has been concentrated on an analysis of RNA and protein synthesis by the posterior silk gland.

In order to purify the mRNA for fibroin an analysis of polyribosomes (polysomes) was undertaken throughout the fifth instar. Good polysomes can be prepared from a single posterior gland. Radioactive glycine was injected into a silkworm in the late stage of the fifth instar, and the gland was dissected out and homogenized gently in the cold. The homogenate was centrifuged at 10,000 rpm for 10 minutes. The precipitate was resuspended and incubated with deoxycholate and Triton X-100 for 15 minutes at 0°C and then centrifuged again at 10,000 rpm. Both the first and second soluble fractions were analyzed by sucrose density gradient centrifugation (Fig. 4a and b). They contain about 80% of the total ribosomes. The first supernate contains about 20% of the ribosomes, all of which are present as monosomes. These monosomes are not radioactive. The second supernate contains both monosomes and polysomes, and the majority of the acid-insoluble radioactivity is localized in the polysome region. Double labeling experiments reveal that labeled peptides appear in the polysome region first, and then are released and can be detected in a soluble fraction at the top of the gradient (Fig. 5).

Simultaneous injection of  $^3\text{H}$ -leucine and  $^{14}\text{C}$ -glycine demonstrates the synthesis of fibroin on polysomes in the posterior gland. Fibroin is practically devoid of leucine but contains 45% of all its amino acids as glycine. These two amino acids were injected together into animals at different stages of the fifth instar, and the  $^{14}\text{C}$ - to  $^3\text{H}$ -ratios either in the second supernate or in the polysome region of the sucrose density gradient were measured. The ratios in a control gland, such as a fat body or a Malpighian tubule, are 0.5–2 at any stage, whereas those from the posterior

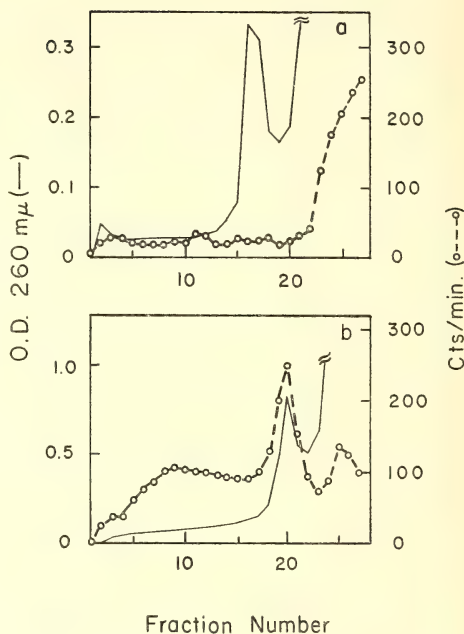


Fig. 4. Sucrose density gradient centrifugation of polyribosomes from the posterior silk gland of *Bombyx mori*.  $^3\text{H}$ -glycine was injected into a silkworm at the late fifth instar. The silk gland was removed in the cold and homogenized with a loose fitting Dounce homogenizer in a buffer containing 0.4 M sucrose, 0.02 M Tris (pH 7.4), 5 mM  $\text{MgCl}_2$ , 50 mM KCl, 5 mM dithiothreitol, 10  $\mu\text{g}/\text{ml}$  of polyvinylsulfate, and 100  $\mu\text{g}/\text{ml}$  of cold glycine. The homogenate was centrifuged at 10,000 rpm for 10 minutes. The pellet was resuspended in the same buffer containing deoxycholate (1%) and Triton X-100 (1%). The suspension was incubated for 15 minutes, and was centrifuged. The first supernate was applied to a 15–30% sucrose gradient (a) and the second to a 15–40% gradient (b). Each gradient contained the same components as the above buffer. The gradients were centrifuged for 3 hours at 25,000 rpm at 2°C in the SW 25.3 rotor. After fractionation TCA insoluble counts of the fractions were measured (open circles). Fig. 4(a) and Fig. 4(b) were obtained from separate experiments: (a) 15  $\mu\text{C}$  of  $^3\text{H}$ -glycine for 10 minutes. (b) 10  $\mu\text{C}$  of  $^3\text{H}$ -glycine for 5 minutes.

part of the silk gland are 0.8, 2.0, and more than 20 at the 2nd, 4th, and 6th day, respectively, of the instar. The cell-free amino acid incorporating system prepared from the posterior gland in the

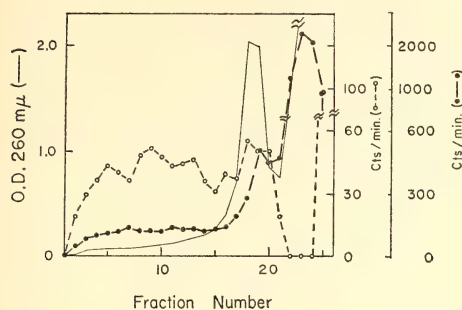


Fig. 5. Double labeling experiment demonstrating the chase of labeled peptides into the supernatant fraction. A silkworm of the late fifth instar was injected with  $1 \mu\text{C}$  of  $^{14}\text{C}$ -glycine and 28 minutes later reinjected with  $10 \mu\text{C}$  of  $^3\text{H}$ -glycine. The gland was dissected out 4 minutes later, and the second supernate was obtained by the same method described in the legend for Fig. 4. The supernate was applied to a 15–40% sucrose gradient and centrifuged for 4 hours at 25,000 rpm at  $2^\circ\text{C}$  in the SW 25.3 rotor. TCA insoluble counts were measured (closed circles,  $^{14}\text{C}$ -, 0–32 min.; open circles,  $^3\text{H}$ -, 28–32 min.).

late fifth instar also showed high glycine and low leucine incorporation into hot TCA-insoluble material, while that from the carcass without silk gland had high leucine and low glycine incorporation. These results confirm earlier findings by Shimura *et al.* that the major peptides synthesized on the isolated polysomes from the gland of the late fifth instar are silk fibroin. The animal is particularly suited for RNA fractionation, since the posterior part of the silk gland incorporates enormous amounts of nucleosides and  $^{32}\text{PO}_4^{---}$  into RNA during the fifth instar. Isolation of mRNA from the polysomes has been unsuccessful to date mainly because the extraction procedures used thus far cause some degradation of RNA. We do not yet know when the mRNA is synthesized and labeled. Therefore labeling experiments with  $^{32}\text{PO}_4^{---}$  at different stages including fourth and fifth instars and direct isolation of total RNA from the gland have been carried out. A cold SDS-phenol method gives essentially undergraded RNA (Fig. 6a

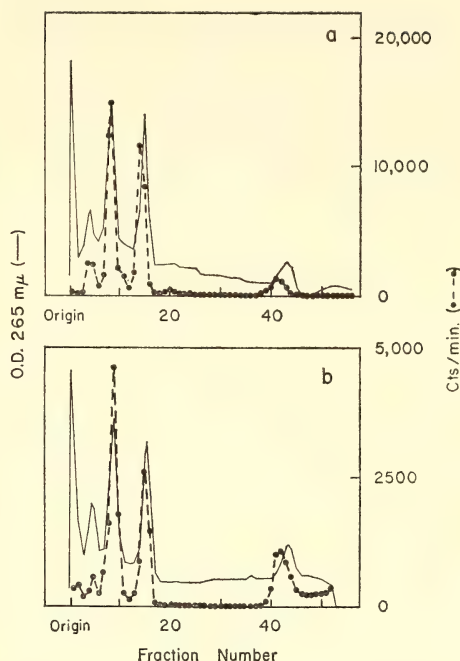


Fig. 6. An analysis of  $^{32}\text{P}$ -RNA synthesized during the fifth instar in the posterior gland of *Bombyx mori*. (a)  $^{32}\text{PO}_4^{---}$  (0.5 mC) was injected into an animal on the second day of the fifth instar, the posterior gland was dissected out 5 days later, and homogenized in 5 ml of buffer containing 0.03 M Tris (pH 7.4), 0.10 M NaCl, 1 mM EDTA, 10  $\mu\text{g}/\text{ml}$  of polyvinylsulfate, and 0.5% SDS recrystallized. The homogenate was shaken vigorously with freshly distilled phenol for 5 minutes in the cold, and was centrifuged. The upper layer was saved. To the phenol layer 2.5 ml of the same buffer was added, shaken again, and centrifuged. The second upper layer was combined with the first and shaking with phenol and centrifugation was repeated twice. RNA was precipitated with ethanol 3 times, and the aliquot (20  $\mu\text{g}$  of nucleic acids of  $1.36 \times 10^4$  cpm/ $\mu\text{g}$ ) was applied to a 2.4% polyacrylamide gel containing 0.5% agarose. Electrophoresis was carried out at 5 mA/tube for 2.0 hours, gel was scanned for absorbancy and sliced into 1.5 mm pieces. Each piece was counted for Tcherenkov radiation. (b)  $^{32}\text{PO}_4^{---}$  (1 mC) was injected into an animal on the sixth day of the fifth instar and RNA from the gland was extracted on the next day. 20  $\mu\text{g}$  of nucleic acids of  $4.54 \times 10^8$  cpm/ $\mu\text{g}$  were applied to the gel.



and b) which is now being analyzed in detail for evidence of fibroin mRNA.

In summary, although the isolation of mRNA for fibroin has not yet been accomplished, techniques for labeling and isolating RNA have been developed

to the point that a detailed analysis can now be carried out.

We express our appreciation to Dr. K. Hayashiya, Kyoto University of Industrial Arts and Textile Fibers, for his kind supply of the artificial diet.

## CELL DETERMINATION IN *Xenopus laevis*

L. Patrick Gage

Cells become committed to their eventual phenotype early in development, and this process is referred to as cell determination. During the past year, an attempt has been made to develop an assay system in which early embryonic cells can be maintained in culture during the course of these determinative events. Cleaving embryos of *Xenopus laevis* can be dissociated, and the cells thus freed will continue to divide *in vitro*. Such cells synthesize DNA and RNA for at least 24 hours after dissociation.

Determined cells are not grossly different from their uncommitted pro-

genitors; therefore a biochemical means of identifying the time of determination is needed. The effect of varying the stage of dissociation at the onset of sRNA and rRNA synthesis, which occurs at specific stages of development *in vivo*, is being analyzed. A determined cell may synthesize small quantities of the gene products that characterize its eventual differentiated stage (e.g., a precursor cell of muscle may synthesize some myosin and actin). With this in mind, the abundance of many of those gene products restricted to specific adult cell types is being measured during early

TABLE 2. Acetylcholinesterase and Creatine Kinase Activities during *Xenopus laevis* Development

Stage	Acetylcholinesterase Activity <sup>1</sup> (nanomoles acetylcholine cleaved/min/embryo)	Creatine Kinase Activity <sup>2</sup> (nanomoles phosphate transferred/min/embryo)
Unfertilized egg		300
Two cell	0.0014	
Blastula		300
Gastrula	0.002	
Neurula	0.006	
Tail bud	0.02	
Early swimming	0.56	
Feeding tadpole		210

1. Assay measures both "true" and "pseudo" cholinesterase activity. Cleavage of (Acetyl-1-<sup>14</sup>C) Choline, 0.018  $\mu$ M/ml and 9.2  $\mu$ Ci/ $\mu$ M, by whole homogenates in 0.05 M phosphate, pH 7.8, was determined by measurement of isotope which did not bind to AG-50W (Na<sup>+</sup>) resin (D. Fambrough, personal communication). Mixing experiments indicated that no inhibitor was present at early stages. Background of assay was  $5 \times 10^{-4}$  units.
2. After homogenization in H<sub>2</sub>O, extracts were freeze-thawed and centrifuged to remove particulates. The supernate was assayed in the firefly extract system described by Strehler and Totter (*Arch. Biochem. Biophys.* 60, 28, 1952). Activity units were determined relative to a creatine kinase standard preparation. Adult leg muscle contains 500 units/mg wet weight. (An egg weighs 1 mg.) Background of assay was about 0.1 units.

frog development. Acetylcholinesterase activity (nervous tissue) is present in small amounts in early cleavage, but increases sharply after gastrulation (Table 2). A substantial level of acetylcholinesterase activity is attained by the early swimming stage, concomitant with the onset of muscular contraction. The early increase in acetylcholinesterase activity may designate the determination of neural cells. Creatine kinase activity, although a thousandfold more abundant in adult muscle than in liver, is inappropriate for such an analysis because of

its high level in unfertilized eggs (Table 2). Collagen synthesis begins at about gastrulation (see *Year Book 66*, pp. 590–592), and a very sensitive assay for this structural protein is being devised.

During the next year, the synthesis of these and other specific proteins will be followed in these embryonic cells *in vitro*. Attempts can then be made to alter determination in some controlled way. Substances in the egg are thought to be responsible for cell determination, and the hope is to isolate and characterize these “determinants.”

## STUDIES ON THE BIOGENESIS OF MITOCHONDRIA IN *Xenopus laevis*

I. B. Dawid, R. F. Swanson, J. W. Chase, and M. Rebbert

Interest in the mechanism of biogenesis of mitochondria has risen in recent years following the demonstration that DNA is present in mitochondria, an observation that gave meaning to earlier suggestions that mitochondria have some degree of autonomy. The extent of this autonomy is limited by the amount and type of information present in mitochondria. Studies of the nature and function of genetic material in the mitochondria of animal cells depend on biochemical and biophysical methods, since no genetic tools are presently available. The total mitochondrial genetic information is contained in a circular DNA molecule with a molecular weight of about 11 million daltons, i.e., 16,000 base pairs. Clearly, this DNA does not contain all the information for the biogenesis of mitochondria; the nucleus controls the formation of most of the mitochondrial components. Nevertheless, mitochondria have retained through evolution their small complement of DNA. Thus it is particularly interesting to determine the function of mitochondrial DNA. Progress on this point has been made during the year.

It has been reported previously (*Year Book 67*, p. 418, and *Year Book 68*,

p. 514) that ovarian mitochondria of *X. laevis* contain two major RNA species of high molecular weight, conventionally termed 21S and 13S RNA. These two RNA molecules are components of a special mitochondrial ribosome that is capable of polypeptide synthesis *in vitro* (see details below). This 60S ribosome appears to be a part of the machinery carrying out protein synthesis inside the mitochondria. The 21S and 13S RNAs are thus mitochondrial ribosomal RNAs. In addition, mitochondria contain a relatively large complement of 4S RNA; the latter almost certainly includes mitochondrial transfer RNA. We show below that 21S and 13S RNA, and some fraction of the 4S RNA hybridize with mitochondrial DNA; approximately one-third of the mitochondrial DNA sequences is represented in these three RNA types.

A large part of the mitochondrial genome therefore functions in the production of the RNA components of a specialized mitochondrial protein synthesizing system. The products of the remaining mitochondrial DNA sequences have not been identified but several minor RNA species have been isolated (see below) which might represent such

products. Mitochondrial DNA is a small part of the entire genome of an animal cell and can be isolated in pure form. The fact that the main products of this DNA have been isolated and their properties studied raises the hope that the entire function of the mitochondrial genome may be understood in the near future.

#### PROPERTIES AND HYBRIDIZATION OF MITOCHONDRIAL RNA

*I. B. Dawid with the assistance of M. Rebbert*

The two major mitochondrial RNA species, 21S and 13S RNA (see *Year Book 67*, p. 418, and *Year Book 68*, p. 514) possess somewhat unusual physical properties. The electrophoretic mobility of 21S RNA relative to RNAs of known size varies depending on the conditions of the experiment, such as the concentration and composition of the gel and the buffer. Because of this behavior the molecular weight of mitochondrial RNA could not be determined by electrophoresis. The sedimentation properties of mitochondrial RNA were studied in several solvents. Under all conditions the mitochondrial "21S" RNA sedimented at the same or at a slightly lower rate than cytoplasmic 18S ribosomal RNA. The term "21S" RNA, based on its electrophoretic mobility in 2.4 to 2.7% polyacrylamide gels, is therefore not really appropriate. However, we will continue to use it as a convenience in identifying this component. These experiments suggest that 21S RNA has an unusual secondary or tertiary structure, different from that of most other known RNA molecules.

Studies on the hybridization of mitochondrial RNA with mitochondrial DNA were continued in the past year. RNA from ovarian mitochondria was labeled chemically by methylation with  $^3\text{H}$ -dimethyl sulfate. Table 3 shows that a mixture of high-molecular-weight RNA, partially purified 21S and 13S RNA, and 4S RNA hybridized well with mito-

TABLE 3. Hybridization of  
Mitochondrial RNA with  
Mitochondrial DNA

RNA fraction	Radioactivity bound, cpm
High molecular weight *	1510
21S RNA †	977
13S RNA †	620
4S RNA	856

All RNA fractions were labeled by reaction with  $^3\text{H}$ -dimethyl sulfate to a specific activity between 4900 and 5500 cpm/ $\mu\text{g}$ . Each RNA fraction at a concentration of 34  $\mu\text{g}/\text{ml}$  was hybridized to 5  $\mu\text{g}$  mitochondrial DNA absorbed to a filter. Only 4S RNA approached saturation at this concentration. The results were corrected for RNA binding to *E. coli* DNA or *X. laevis* nuclear DNA (between 20 and 85 cpm). Cytoplasmic ribosomal and 4S RNAs did not compete in these hybridizations.

\* RNA excluded from a column of Sephadex G-100; this fraction contained mainly 21S and 13S RNA.

† The 21S and 13S RNA fractions were significantly cross-contaminated.

chondrial DNA. Saturation experiments showed that at least 12% of the DNA hybridized effectively with the high-molecular-weight fraction which was composed mainly of 21S and 13S RNA; 3 to 5% of the DNA hybridized with 4S RNA. Since only one strand of DNA codes for RNA at any particular site, these experiments suggest that about one-third of the mitochondrial DNA is complementary to the major mitochondrial RNA components, 21S, 13S, and 4S RNA. The results are also compatible with the hypothesis that each circle of mitochondrial DNA contains one sequence, or gene, for 21S and for 13S RNA, and between 10 and 20 genes for transfer RNAs.

#### THE MITOCHONDRIAL RIBOSOME OF *Xenopus laevis*

*R. F. Swanson*

Continuation of studies on the mechanism of protein synthesis in ovarian mitochondria of *X. laevis* (see *Year Book 68*, p. 515) has led to the isolation of the mitochondrial ribosome from this



material. An extract from ovarian mitochondria was obtained which effected the incorporation of phenylalanine into polypeptides when incubated in the presence of polyuridylic acid (poly U),  $H^3$ -phenylalanine, GTP, magnesium ions, and an energy generating system. The mitochondrial ribosome was isolated from this extract by sedimentation through a sucrose gradient (Fig. 7). The major component is a 60S particle; three other types of particle sedimenting at 30S, 40S, and 87S are also evident. The 87S particles are cytoplasmic ribosomes which contaminate these preparations, while the 30S and 40S particles appear to be subunits of the 60S particle. The 60S particles were isolated from sucrose gradients and shown to be active in polyphenylalanine synthesis in the presence of poly U and a ribosome-free extract (60,000 rpm supernate) of mitochondria. In the absence of either 60S particles or ribosome-free extract no incorporation of phenylalanine was observed. Therefore, the 60S particles have the ability to function as ribosomes in polypeptide synthesis.

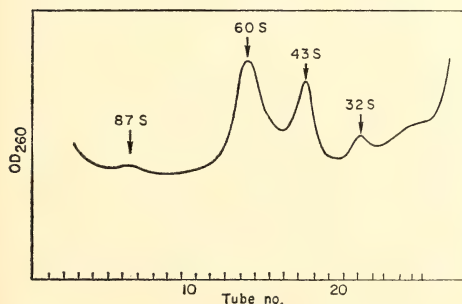


Fig. 7. Sedimentation of mitochondrial extracts. Mitochondria were suspended in a hypotonic medium and sonicated three times for 15 seconds. Debris was removed by centrifugation and the particulate fraction was concentrated by precipitation at pH 5. The resulting precipitate was suspended in neutral buffer and layered on a 15–30% sucrose gradient containing magnesium and potassium ions. After centrifugation the gradient was pumped through a Gilford flow-through cell and the O.D. 260 was monitored.

The origin of the 60S ribosome was established by studying the RNA it contains. RNA was extracted from 60S particles and analyzed by electrophoresis on polyacrylamide gels. The same two high-molecular-weight RNAs (21S and 13S RNA) that had been isolated from whole mitochondria were found in the 60S ribosome; no intact cytoplasmic ribosomal RNA could be detected. The RNA from the 60S ribosome hybridized well with mitochondrial DNA in agreement with experiments using 21S and 13S RNA derived from whole mitochondria (see above). Hybridization-competition experiments furthermore showed that the isolated 60S particles contained less than 1% cytoplasmic ribosomal RNA. This level of contamination is far too low to account for the ability of 60S particles to function in protein synthesis. We therefore conclude that the 60S particle is the mitochondrial ribosome.

#### *Coding Properties of Polynucleotides in Isolated Mitochondria*

Isolated mitochondria incorporate polynucleotides which are then able to code for polypeptide synthesis in these mitochondria. The incorporated polynucleotides, as well as the peptide synthetic activity stimulated by these polynucleotides, are resistant to ribonuclease, provided that the mitochondria are maintained intact. This system makes possible a study of the genetic code used in mitochondrial protein synthesis. Mitochondria were incubated with various polynucleotides and then tested for ability to incorporate the amino acids for which these polynucleotides have been shown to code in other systems (Table 4). It can be seen in Table 4, Experiment 1, that each polynucleotide stimulated the incorporation of the expected amino acid.

In another experiment, mitochondria were incubated with poly U and tested for ability to incorporate various amino acids (Table 4, Experiment 2). Poly U

TABLE 4. Polypeptide Synthesis by Isolated Mitochondria

	Polynucleotide	H <sup>3</sup> -Amino Acid	CPM Incorporated in 40 Minutes
<i>Experiment 1</i>			
	none	phenylalanine	290
	poly U	phenylalanine	16,090
	none	proline	81
	poly C	proline	800
	none	lysine	290
	poly A	lysine	930
	none	leucine *	330
	poly UC	leucine *	4,000
	none	proline †	140
	poly UC	proline †	2,630
<i>Experiment 2</i>			
	none	phenylalanine	120
	poly U	phenylalanine	4,900
	none	leucine	130
	poly U	leucine	500

Mitochondria were incubated in the presence of various polynucleotides for 10 minutes at 22°C. Cofactors and H<sup>3</sup>-amino acids were then added and incorporation of radioactivity into a hot TCA insoluble product was measured after a second incubation period at 30°C. Experiments 1 and 2 were carried out using different preparations of mitochondria.

\* Incorporation was measured in the presence of unlabeled proline, serine and phenylalanine.

† Incorporation was measured in the presence of unlabeled leucine, serine and phenylalanine.

stimulated the rate of phenylalanine and leucine incorporation by about fortyfold and fourfold, respectively. No incorporation of lysine, proline, or methionine was detected in the presence or absence of poly U. Similar results had previously been obtained with other subcellular systems; in all cases reported, poly U codes for both phenylalanine and leucine incorporation. These results give further evidence that the genetic code is truly universal in that it is used not only by all organisms thus far examined but also by different protein synthesizing systems within the same organism.

#### MITOCHONDRIAL RNAs IN EGGS AND EMBRYOS OF *Xenopus*

J. W. Chase

#### *Biogenesis of Mitochondria during Development*

Our study of the biogenesis of mitochondria in *Xenopus laevis* has continued with emphasis on mitochondrial nucleic acid synthesis, particularly the RNAs. We have used <sup>14</sup>CO<sub>2</sub> pulse labeling of

various stages during the development of *X. laevis*, followed by isolation of mitochondria by differential centrifugation and sucrose gradient banding. RNA was then extracted from the mitochondrial pellet and electrophoresed on 2.4% acrylamide-0.5% agarose gels; the gels were then scanned in the UV, sliced, and the radioactivity in each slice determined. Figure 8 shows such an analysis. Contamination by cytoplasmic 28S and 18S RNAs was always observed but the 13S and 21S mitochondrial components represented the major fraction.

Clear evidence for the synthesis of new mitochondrial RNA was first obtained in embryos between stages 17 and 27 of Nieuwkoop and Faber, corresponding in development from neurula to the stage of spontaneous muscular response. The reason for the present uncertainty in the stage at which new synthesis first begins is the relatively long time used for the <sup>14</sup>CO<sub>2</sub> pulse (usually 10-12 hours) and the low levels of radioactivity incorporated in young embryos. The content of mitochondrial

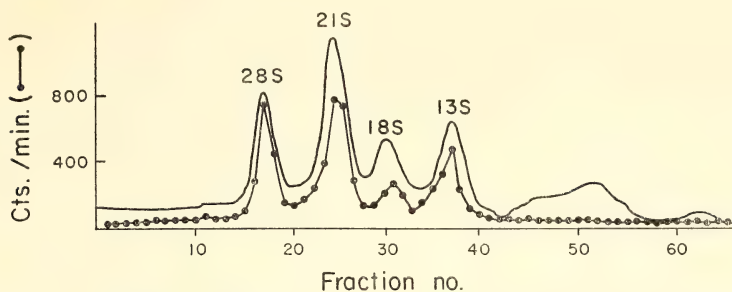


Fig. 8. Mitochondrial RNA prepared from *Xenopus laevis* embryos which had been labeled for 9 hours with  $^{14}\text{CO}_2$ . The embryos were at stage 33 at the beginning of the pulse and had developed to stage 37 at its end. The 21S and 13S RNAs are the mitochondrial components; the 28S and 18S components are cytoplasmic contaminants. Continuous solid line: optical density record; solid line with data points: radioactivity.

21S and 13S RNA per embryo begins increasing at this time from its early constant level and has approximately doubled by stage 43 (swimming tadpole).

The content of mitochondrial DNA per embryo during development has also been measured by a quantitative hybridization technique using labeled complementary RNA (c-RNA) transcribed from mitochondrial DNA with *E. coli* RNA polymerase. The results of this analysis show that there is no detectable net increase in mitochondrial DNA throughout development until stages 40–41. Since earlier attempts to

label mitochondrial DNA with  $^{14}\text{CO}_2$  prior to stage 40 had failed, we now feel that there is no synthesis of mitochondrial DNA until after stage 40. The regulation of the rate of mitochondrial RNA synthesis during embryogenesis that has been observed thus appears to proceed on a constant amount of DNA template.

#### *Separation of Mitochondrial RNA Species by Preparative Electrophoresis*

In order to better characterize mitochondrial RNAs, it is necessary to pre-

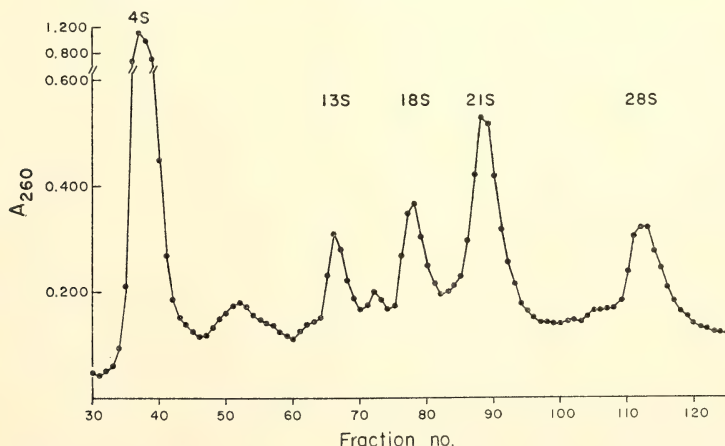


Fig. 9. Continuous flow electrophoresis of *Xenopus laevis* ovarian mitochondrial RNA. RNA separating on an  $85 \times 22$  mm gel column was washed away in a stream of buffer as each component emerged from the gel. Fractions 86–92 (21S) and 65–69 (13S) were pooled and analyzed on analytical acrylamide gels shown in Fig. 10. The region between 4S and 13S contains the minor components described in the text.



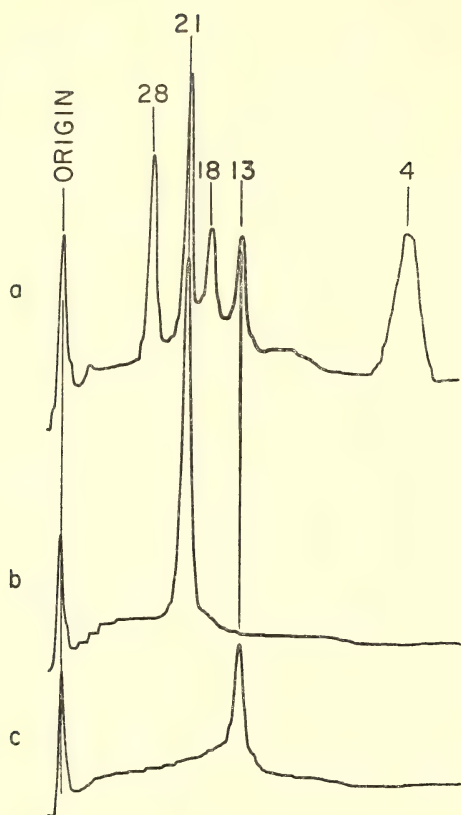


Fig. 10. Pooled fractions from Fig. 9 analyzed on 2.4% analytical acrylamide gels. (a) Unfractionated mitochondrial RNA. (b) Fractions 86-92 (21S). (c) Fractions 65-69 (13S).

pare individual components in relatively large quantities. Sucrose gradient sedimentation is inadequate, as mitochondrial 21S and cytoplasmic 18S RNAs have similar sedimentation properties. On analytical acrylamide gels, however, all of the major cytoplasmic and mito-

chondrial RNAs can be completely separated. We have therefore developed a preparative electrophoresis technique using a gel consisting of a 2.2% to 2.5% inverted gradient which allows us to prepare several hundred micrograms of pure mitochondrial RNAs per run. Figure 9 shows a fractionation of a mitochondrial RNA preparation from total *X. laevis* ovarian mitochondria. Peak fractions were pooled and rerun on analytical acrylamide gels to check for purity and intactness of RNA. Figure 10 shows the results of this analysis. Both mitochondrial RNAs are seen to be completely free of cross contamination within the limits of sensitivity of the analysis. All of the fractionations that we have done using this method have yielded 13S RNA which is completely free of contamination by 18S, 21S, and 28S RNAs, as well as 21S RNA which usually contains a few percent 18S RNA.

We have identified seven minor RNA components that move in the region between 4S and 13S (see Fig. 9). Samples from different preparative runs of independent mitochondrial RNA preparations showed a reproducible pattern of minor RNA species when the corresponding regions were analyzed on 5% analytical acrylamide gels. There may also be a minor fraction in the area between the 13S and 18S RNA peaks. Some or all of these components could be specific degradation products of larger RNA species, or they could represent new *in vivo* components of mitochondrial RNA. The availability of a method for the isolation of these RNA species will allow their further characterization.

## CELL DIFFERENTIATION AND VIRAL SUSCEPTIBILITY

R. J. Hay, M. Yoshikawa-Fukada and J. D. Ebert  
assisted by D. Somerville and B. Smith

### THE INTERACTION OF ROUS SARCOMA VIRUS WITH DEVELOPING MUSCLE

During the course of our studies of the effects of Rous sarcoma virus (RSV)

on DNA synthesis in differentiating muscle (*Year Book 68*, p. 518) we noted the appearance of phase-dense inclusion bodies within mature myotubes in in-

fectured cultures. This was a commonly observed difference between infected and uninfected cultures and often appeared at much higher frequency than did the induction of DNA synthesis. Experiments to determine the nature and origin of these structures have led to several interesting findings. The culture system used is essentially similar to that described earlier (*Year Book* 68, p. 519). Cell suspensions prepared from 11-day embryonic chick leg muscle were infected with RSV type 1 at a multiplicity of infection of 0.1, and the cells were treated the following day by the differential adhesion (DA) method for increasing the ratio of myoblasts to fibroblasts. Cells recovered after DA were seeded to collagen-coated Falcon plates at  $4-6 \times 10^4$  cells per  $\text{cm}^2$  of dish surface area and were examined and used for experiments at intervals thereafter.

The presence of phase-dense bodies was observed, under these conditions, even at early stages during the formation of muscle syncytia, 40 hours after DA seeding (Plate 2E). The number of these bodies in individual myotubes increased with time as did the proportion of myotubes containing the inclusions. A typical example of a myotube from an infected culture at about 96 hours after DA seeding is shown in Plate 2F.

Our next step was to examine such myotubes from infected cultures using the electron microscope. In order to accomplish this cells, treated as usual, were seeded to culture dishes containing coverslips which had been coated with silicone, a thin carbon layer, and collagen. After appropriate incubation periods the coverslips were removed, rinsed in 0.06 *M* phosphate buffer made 0.14 *M* in sucrose (pH 7.4), and were fixed for one hour at 4°C in the same solution containing 3% glutaraldehyde. They were then thoroughly rinsed with the phosphate-buffered sucrose solution and were post-fixed for one hour at 4°C with 1%  $\text{OsO}_4$  in 0.06 *M* phosphate buffer (pH 7.4) containing 0.016 *M* sucrose. The cultures

were dehydrated through an alcohol series and propylene oxide, and were embedded in Epon 812. Myotubes with inclusion bodies were located before final embedding. After polymerization the capsules were snapped off the coverslip at the carbon-silicone interface, and the myotubes were sectioned normal to the culture surface. Sections were mounted on 200-mesh uncoated copper grids, stained with lead citrate, and examined in an Hitachi HU-11E microscope operated at 75 kV.

Plate 3 shows a typical electron micrograph of a muscle syncytium from an infected culture. We assume that the electron-dense bodies observed are the same as the phase-dense structures noted with the light microscope. Interestingly, particles of size and morphology similar to mature RSV particles were found within these inclusions. Two alternate explanations for this result have been considered, and preliminary experiments to determine which is correct have been undertaken.

The first possibility is that the electron-dense bodies represent sites of synthesis or maturation of RSV in myotubes. It is generally agreed that RSV matures at the cell membrane of infected fibroblasts in culture. Haguénau, Beard, and others have observed virus particles within electron-lucent vacuoles unlike the structures found in this study. A novel mode of virus formation might be required in muscle tissue. Our initial approach to this problem has involved fractionation of homogenates of cultured muscle, at intervals after infection, to determine the distribution of infective virus. Cultures were rinsed five times with a cold solution consisting of 0.25 *M* sucrose and 0.001 *M* EDTA. The sixth and final wash was retained for estimation of residual extracellular virus. The cells were removed from the culture vessels by scraping with a rubber policeman and were collected in cold 0.25 *M* sucrose, 0.001 *M* EDTA solution. The tissue was disrupted with a Thomas-Ten

Broeck homogenizer, and the crude homogenate was layered over a solution containing 0.34 *M* sucrose and 0.001 *M* EDTA and was spun at 700 *g* for 10 minutes. The nuclear fraction was retained for assay and the supernatant (1) was spun at 5000 *g* for 10 minutes. The supernatant (2) was then retained for assay and the particulate fraction was washed by two additional centrifugation steps. Results of virus assays on material from this type of fractionation at 68 and 115 hours after infection are presented in Table 5.

It is clear that there was considerable intracellular virus at both sampling times, but the activity was not recovered in the particulate fraction. This could be explained if the electron-dense bodies are unstable during homogenization. Experiments are under way, employing less rigorous homogenization techniques followed by ultrastructural study, to determine whether such is the case. An alternative explanation would be that virus particles become infective only as they are extruded from the dense body. If this occurs at the surface of the myotube we would expect to find aggregates of viral antigen appearing there as has been shown earlier (*Year Book* 65, p. 525).

The second general possibility under consideration is that these structures

TABLE 5. Infective RSV in Fractions Isolated from Cultured Chick Muscle

Sample	Infected Virus (FFU/sample)	
	Time after Infection	
	68 Hours	115 Hours
Final wash		
(extracellular virus)	$8 \times 10^3$	$10^4$
Crude homogenate	$2.5 \times 10^5$	$8.8 \times 10^5$
Supernatant (1)	...	$10^6$
Supernatant (2)	$1.9 \times 10^5$	$10^6$
Nuclear fraction	$3 \times 10^3$	$1.8 \times 10^4$
Particulate fraction	$2.2 \times 10^3$	$3.8 \times 10^4$

could be a part of the vacuolar apparatus and represent sites of breakdown of RSV that has been engulfed during fusion or synthesized elsewhere within the myotube. In this connection, Beard and his associates noted the presence of similar structures, termed "grey bodies," in myeloblasts infected with Avian Myeloblastosis Virus. Studies involving uptake of colloidal gold and other electron-dense markers, as well as ultracytochemical evidence, indicated that the "grey bodies" were lysosome-like digestive organelles.

Estimations of the activities of the lysosomal enzymes acid phosphatase and leucine amino peptidase, present in homogenates of muscle cultures at various stages after infection, are given in Table 6. Although the total activity of

TABLE 6. Activity of Acid Phosphatase and Leucine Amino Peptidase in Homogenates of Cultured Chick Muscle at Intervals after Infection with RSV

Sample	Time after Infection (hours)	Acid Phosphatase			Leucine Amino Peptidase		
		Total Units *	Units per $\mu$ g Protein	Units per $\mu$ g DNA	Total Units †	Units per $\mu$ g Protein	Units per $\mu$ g DNA
Uninfected	44	153;146	3.2;3.4	26;25	18;20	0.36;0.45	3.0;3.3
Infected		151;187	2.2;1.9	26;28	24;44	0.36;0.45	4.1;7.6
Uninfected	66	114;165	2.2;2.4	18;25	14;30	0.27;0.45	2.2;4.7
Infected		232;222	1.8;1.4	31;30	54;72	0.40;0.47	7.1;9.5
Uninfected	90	523;416	2.2;1.6	59;47	74;62	0.31;0.23	8.4;7.0
Infected		710;755	1.7;2.0	56;59	128;153	0.30;0.40	10.0;11.9
Uninfected	115	1100;960	1.7;1.4	83;53	228;211	0.36;0.32	17.3;11.7
Infected		1130;1383	1.3;1.5	67;67	302;420	0.35;0.40	17.9;17.9

\* Expressed as  $m\mu$ moles of p-nitrophenyl phosphate hydrolysed in 30 minutes.

† Expressed as  $m\mu$ moles of L-leucyl- $\beta$ -naphthylamide hydrolysed per hour.



both enzymes was generally higher in infected than in control cultures, this probably reflects an increase in the rate of cell division (*Year Book 66*, p. 599), since the specific activity expressed per unit weight of protein or DNA did not increase significantly. Histochemical staining of representative plates also indicated no clear difference between infected and uninfected cultures. This evidence, however, does not eliminate the hypothesis that the electron-dense bodies arise when extracellular virus is engulfed during myoblast fusion. Studies involving addition of electron-opaque substances to the culture medium during muscle formation as well as ultracytochemical examination will be required to clarify this point.

#### MOLECULAR HYBRIDIZATION OF RSV-RNA WITH CELLULAR AND VIRAL DNAs

##### *Characterization of the Hybrids*

The RNA of Rous sarcoma virus (RSV) hybridizes with DNAs isolated from all eukaryotes tested, with the possible exception of yeast. Bacterial DNAs show no homology to RSV-RNA. DNAs from the oncogenic viruses, adenovirus type 12 and SV 40, show significant homology with RSV-RNA, but those from nononcogenic adenoviruses types 2 and 4 are not homologous. Base ratio analysis of RSV-RNA hybridized with various DNAs suggests that a common base sequence functions in hybridization (see Yoshikawa-Fukada and Ebert, *Proceedings of National Academy of Sciences 64*, pp. 870-877, and *Year Book 68*, pp. 521-527). These studies have been continued during the past year.

Is the base sequence in the several cellular and viral DNAs hybridizing with RSV-RNA the same or closely similar? Another way of approaching the question is through the analysis of the melting temperatures and melting curves of the hybrids. The fact that any two RNA-DNA hybrids have the same melting temperature suggests that they

are formed of similar molecules. A sharp melting curve indicates that hybrids are homogeneous and a broad curve indicates a mixture. Figure 11 shows the melting curve of three different hybrids between RSV-RNA and Adenovirus 12, chick fibroblast-DNA, and HeLa-DNA. Melting proceeds at the same rate in these hybrids, suggesting that RNA molecules with similar base sequences are involved. Melting temperatures of hybrids between RSV-RNA and other DNAs included 74°C for calf thymus DNA, 73°C for chick fibroblast DNA, 75°C for salmon sperm DNA, 72°C for Ad 12 DNA, and 72°C for RSV-transformed chick fibroblast DNA.

Earlier findings from a number of laboratories have suggested that the tumor viruses, RSV among them, contain or have associated with them, in

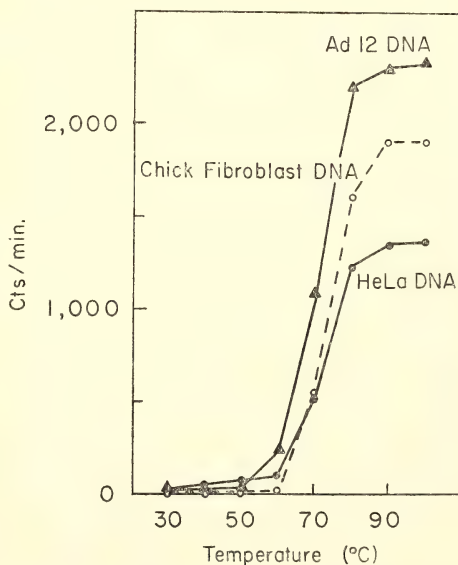


Fig. 11. Melting curve of DNA-RSV-RNA hybrids. RSV-RNA was hybridized with various DNAs in the presence of rRNA, and purified by CsCl centrifugation as previously described (*Year Book 68*, p. 521). Filters containing purified hybrids were incubated in  $2 \times$  SSC for 10 minutes at each temperature from 30°C to 100°C. RNA released at each temperature was precipitated with cold TCA and the radioactivity was counted.

varying degrees of intimacy, molecular constituents of normal cells. We have already shown by competition experiments that the common base sequence involved in the hybridization of RSV-RNA and cellular and viral DNAs is not included in rDNA, the genes coding for ribosomal RNA. However, in a recent article, Carnegie, Deeney, Olson, and Beaudreau (*Biochimica et Biophysica Acta* 190, pp. 274-284, 1969) reported that RNA from Avian Myeloblastosis Virus contains soluble, transfer RNA (sRNA or tRNA). This sRNA will attach amino acids and transfer them to peptide chains under conditions *in vitro* established for cellular tRNA.

It will be recalled, too, that our own earlier findings suggested that the molecular size of the specific segment of RSV-RNA hybridizing with cellular and viral DNAs is about 3S. Moreover, upon heating 71S RSV-RNA, a 4S molecule is released. Thus we were led to inquire whether our "viral oncogenic sequence" reflects, in fact, the interaction of sRNA with its corresponding segment of the genome, sDNA. The answer is clear: it does not. The viral oncogenic sequence is distinct from sRNA and its genome. RNA was extracted from purified RSV and fractionated into 71S and 4S molecules by centrifugation on a sucrose gradient of 5-20%. Competition experiments were performed as previously described (Fig. 12). Only about 10% competition was observed with sRNA, in experiments in which denatured chick fibroblast DNA was incubated with 71S RSV-RNA in the presence of rRNA and different amounts of sRNA and 4S RSV-RNA. Thus we may conclude that the common base sequence involved in the hybridization of RSV-RNA and cellular and viral DNAs is not included in any significant way in sDNA, the genes coding for sRNA. However, since the sRNA-DNA hybrid is detected at almost the same position as the 4S-RSV-RNA-DNA hybrid in CsCl centrifugation, we cannot say

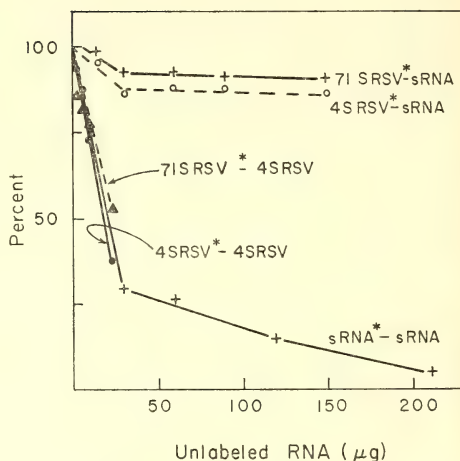


Fig. 12. Competition of sRNA with RSV-RNA in hybridization with cellular DNA. Filters containing 50-100  $\mu$ g of denatured chick fibroblast DNA were incubated with  $P^{32}$  labeled RSV-RNA in the presence of rRNA and different amounts of sRNA and 4S RSV-RNA. After hybridization, filters were washed and treated with RNase, and the radioactivity of hybridized RSV-RNA was counted.

whether 10% competition is nonspecific, or whether cellular sRNA is a component of RSV-RNA.

The same approach permits us to answer another question. Is the 4S segment of RSV-RNA the only part of the 71S RSV-RNA involved in the hybridization with cellular and viral DNAs? Or are the regions of 71S RSV-RNA homologous with cellular DNA different from those of 4S RSV-RNA? It is difficult to get enough 71S RSV-RNA for competition studies; hence all of the experiments have been performed with 4S RSV-RNA as the competitor, with the maximum amount added to the reaction mixture being 25  $\mu$ g. "Homologous competition" is observed; that is, the rate of competition by 4S-RSV-RNA against 71S-RSV-RNA\* is the same as the homologous competition observed with sRNA\*-sRNA or 4S-RSV-RNA\*-4S-RSV-RNA (Fig. 12). The saturation value for 71S-RSV-RNA is the same as that obtained for 4S-RSV-RNA, although the saturation

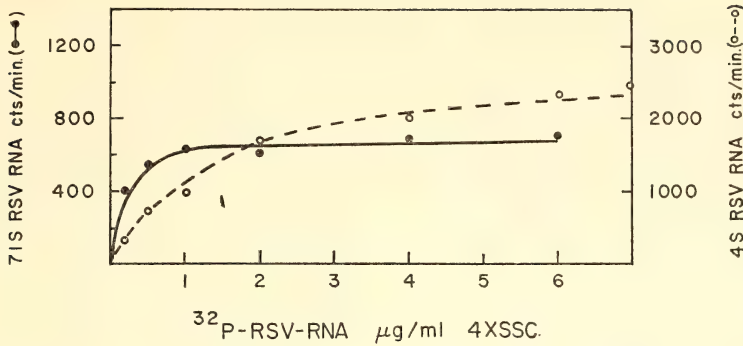


Fig. 13. Saturation curve of  $\text{P}^{32}$  labeled 71S- and 4S-RSV-RNA hybridized with chick embryo DNA. Filters containing from 60 to 100  $\mu\text{g}$  of denatured chick embryo DNA were hybridized with  $\text{P}^{32}$  labeled 17S-RSV-RNA ( $7 \times 10^4 \text{cpm}/\mu\text{g}$ ) or  $\text{P}^{32}$  labeled 4S-RSV-RNA ( $2.2 \times 10^5 \text{cpm}/\mu\text{g}$ ) in the presence of chick cellular rRNA and sRNA. Counts were standardized to 100  $\mu\text{g}$  of DNA.

curve is different (Fig. 13). It is concluded that the same base sequences function in hybridization of both 71S-RSV-RNA and 4S-RSV-RNA with cellular DNA.

HYBRIDIZATION OF RSV-RNA WITH DNA FROM CHINESE HAMSTER CHROMOSOMES

In *Year Book 68*, p. 527, we reported our first attempts to fractionate the isolated chromosomes of a Chinese hamster cell line into different size-groups, in order to determine whether the DNA homologous to RSV-RNA is located in any one size-group. Our preliminary findings suggested that these genes are dispersed among the chromosomes in three size-groups. We have invested substantial effort in attempts to improve the resolution of this approach. Regrettably, we conclude that present methods of chromosome fractionation, including zonal centrifugation, are inadequate for our purpose. Cross-contamination of the groups is simply too great. The quality of our preparations is indicated in Plate 2. Fraction 3 is almost free of the contamination of other size groups, but fraction 1 and especially fraction 2 each contain a considerable number of chromosomes of the other groups. The limits of the method are shown in Figure 14,

in which the measured length of 100 chromosomes in each of the three size classes obtained (broken lines) may be compared with the expected (solid lines). Shrinkage, variation in size, and loss of

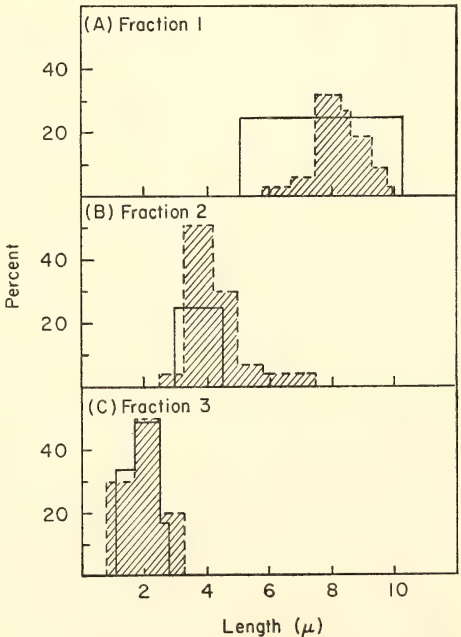


Fig. 14. Distribution of fractionated chromosomes. Measurements of the lengths of 100 chromosomes of each of three size-groups.



TABLE 7. Comparison of Three Classes of Chinese Hamster Chromosomes

Experiment Number (different preparations of chromosomes)	Specific Activity of 71S-RSV-RNA Used	71S-RSV-RNA (cpm/ $\mu$ g DNA) Hybridized with DNA from Chromosomes of 3 Size-Groups		
		1 (large)	2 (medium)	3 (small)
I	$7 \times 10^4$ cpm/ $\mu$ g	91/42	40/22	40/23
II	$1 \times 10^5$ cpm/ $\mu$ g	100/30	70/20	60/18
III	$4.8 \times 10^4$ cpm/ $\mu$ g	65/37	43/23	41/18

chromosomes are observed during preparation. Within the limits of the technique, no significant difference was observed when the DNA of the three size-groups was hybridized with RSV-RNA (Table 7). The method of hybridization *in situ* must be considered. However, specific radioactivity and the amount of RNA hybridized with DNA in a nucleus may be too low to be detected by autoradiography.

#### THE ROLE OF CELLULAR DNA HOMOLOGOUS TO RSV-RNA

What is the role of these genes? As reported last year, DNA extracted from the sediment fraction, prepared by sonication of S-phase nuclei, hybridizes with RSV-RNA to a substantially greater extent than DNA extracted from the supernatant fraction. Moreover, the sediment fraction alone shows DNA synthesizing activity *in vitro*. The kinetics of the reaction suggest that DNA template and DNA polymerase form an active complex in the sediment fraction. These observations, coupled with the related facts that cellular DNA synthesis is indispensable for RSV replication and cellular transformation, and that interaction with the cell membrane is necessary for initiation and synthesis of bacterial DNA replication, encouraged us to suggest that RSV-RNA interacts with the initiating site for cellular DNA synthesis. We have made but little further progress in testing this hypothesis. We are attempting to purify the sediment fraction in relation to the initiation of

DNA synthesis. Sarkasy<sup>1</sup>, which is useful for the purification of the bacterial DNA-membrane complex, was found to inhibit DNA synthesis in this system. Differential precipitation by changing ionic strength is in progress.

#### ISOLATION OF TEMPERATURE SENSITIVE MUTANTS OF CHINESE HAMSTER CELLS, *in vitro*

In relation to our study of the initiation of DNA replication in mammalian cells, we have begun to isolate temperature sensitive (TS) mutants.

Wild type Chinese hamster cells (clone 6) were treated with ethyl methane-sulfonate (EMS) or N-methyl-N'-nitro-N-nitrosoguanadine (MNNG) and cultured at 30°C or 42°C in the presence of BudR. The cells growing at 30°C or 42°C incorporated BudR and were killed by irradiation of visible light. Breakage and disfigurement of chromosomes were observed. Cells surviving these treatments are TS mutants which can grow at 37°C but not at 30°C or 42°C.

Three kinds of mutants have been isolated. TS mutants M(42)16, M(42)20, M(30)12, E(42)10, and E(42)11 synthesize DNA and protein at the same rate as wild type, but not RNA. M(30)11 does not synthesize DNA, RNA, or protein at all at 30°C. E(30)6, -7, -8, and -9 synthesize RNA and protein at the normal rate but do not synthesize DNA at all. The last group may be valuable for the study of regulation and initiation of DNA synthesis. Further characterization of these mutants is in progress.

## FACTORS REGULATING THE FUSION OF MYOBLASTS

*E. Ozawa and J. D. Ebert*

In view of the group's interest in the fusion of mononucleated myoblasts into elongated, multinucleated myotubes, Eijiro Ozawa began his stay in the Department by examining some of the factors influencing the process, and subsequently extended the scope of his investigations into the process of cell fusion more generally. Most of his findings are too preliminary to warrant discussion; however, a brief account of one approach is in order.

In one part of his program, the effect of alkaline earth divalent cations on myotube formation was investigated using primary cultures of 12-day chick embryo muscle cells.

In F12215 medium deprived of calcium ions, the cells did not fuse to form branched myotubes. If the concentration of the ion in the medium was kept below  $10^{-4}M$ , branched myotubes did not appear. In the presence of about  $3 \times 10^{-4}M$

$Ca^{++}$ , cell fusion was observed, but the myotubes did not form so-called ribbons. If the medium contained about  $10^{-3}M$   $Ca^{++}$ , large myotubes were formed. When the concentration of the ion was increased to  $10^{-2}M$ , the myotube, once formed, degenerated within 48 hours. The effect of  $Ca^{++}$  on cell fusion was essentially the same in the presence or absence of magnesium ions.

After myoblasts were prevented from fusing for 120 hours in a low calcium medium, the cells fused promptly and grew up to form large myotubes when an appropriate amount of  $Ca^{++}$  was added. These effects of calcium on cell fusion were not replaced by either strontium or barium.

These observations are compatible with the recent findings of Shainberg, Yagil, and Yaffe using newborn rat skeletal muscle.

## TROPIC EFFECTS OF NERVE ON MUSCLE

*Douglas Fambrough, Criss Hartzell, and Nancy Joseph*

The spatial distribution of acetylcholine receptors in muscle fiber membranes is controlled by motoneurons. Innervated muscle fibers have a high concentration of receptors only in the area of the neuromuscular junction, but, following denervation, a high concentration of receptors develops over the entire surface of each fiber. Last year (*Year Book 68*, pp. 531-534) we confirmed that this change in receptor density would take place in isolated rat muscle maintained in organ culture, and we reported that the inhibitors actinomycin D and puromycin (which block RNA and protein synthesis, respectively) could each prevent this change. We have now extended these observations by demonstrating (1) that a second inhibitor of protein synthesis, cycloheximide, can also prevent the change in receptor dis-

tribution, (2) that concentrations of inhibitors that do not block RNA or protein synthesis do not prevent the change, and (3) that these inhibitors rather specifically block RNA or protein synthesis, and only slowly affect electrical excitability, membrane resting potential, histological appearance, and synthesis of other classes of macromolecules, thus minimally qualifying our conclusions.

We infer from our results that the change in spatial distribution of acetylcholine receptors is dependent upon the synthesis of new RNA and protein molecules by the denervated muscle fibers. At present we cannot distinguish between the two major possibilities: synthesis of new receptor molecules or activation of latent receptors by newly synthesized molecules. In either case, the regulation of receptor distribution by motoneurons

seems to involve regulation of the transcription of specific genes in muscle fibers.

At the time during development when motoneurons and muscle fibers are becoming functionally connected, acetylcholine receptors are present at high concentration along the entire muscle surface. During the next two weeks the extrajunctional receptors mostly disappear, resulting in a receptor distribution typical of the adult. It is not known at what time acetylcholine receptors appear during the formation of muscle. We are examining this question, using cloned myoblasts from embryonic chick and rat. These myoblasts proliferate and fuse to form myotubes that differentiate into striated muscle. So far we know that at the myotube stage acetylcholine receptors are already present. We also suspect that acetylcholine receptors have no important function in the formation of striated muscle in culture, for high concentrations of d-tubocurarine chloride and of acetylcholine maintained in the culture medium do not interfere with muscle development.

Since the nerve restricts the distribution of acetylcholine receptors, it is paradoxical that the highest concentration of receptors is nearest the nerve. Each muscle fiber contains many nuclei spaced rather regularly along the length of the fiber, some close to the neuromuscular junction, others far away. We do not know whether these nuclei migrate, but at any moment those close to the neuromuscular junction should be maximally affected by the nerve. If the regulatory mechanism includes direct neuronal repression of the synthesis of receptors, then the distribution of receptors should be the opposite of that which occurs. An alternative hypothetical control mechanism allows continuous synthesis of receptor molecules in all parts of the muscle, but some neuronal influence causes a concentration of these molecules into the membrane at the neuromuscular junction. This alternative is disfavored

by the effect of actinomycin D on the change in receptor distribution and by the enormous distances involved in the case of long muscle fibers. Probably quite pertinent to the nature of the control mechanism is our observation that the change in receptor density occurs concertedly throughout the length of each fiber, suggesting local synthesis or activation of receptors along the fiber. Thus the expression "spread of acetylcholine sensitivity," which has been repeatedly used to describe this change, is misleading.

Resolution of the paradox and a detailed understanding of receptor control will require some method for the identification and quantification of acetylcholine receptors which is independent of their participation in altering membrane permeability. We have repeatedly but unsuccessfully sought to demonstrate the synthesis of new proteins or glycoproteins in denervated muscle. Currently we are attempting to concentrate the receptors by preparation of highly purified muscle membranes and to test these concentrates for their ability to bind acetylcholine or its agonists and antagonists.

#### DNA SYNTHESIS AND CELL DIVISION IN DENERVATED RAT DIAPHRAGM

The rate of DNA synthesis in rat diaphragm increases about fifteenfold 36 to 48 hours after denervation. We have been interested in the possible relationship of this phenomenon to the trophic interactions of muscle fibers and motoneurons. Thus we have sought to determine whether any of this DNA synthesis and associated mitotic activity involves muscle fibers or their "satellite cells," which are presumably myoblasts. We have found no evidence for the involvement of these cell types and feel that this phenomenon is most probably an injury response and a connective tissue response to passive stretch.

The cells that incorporate  $^3\text{H}$ -thymi-



dine into DNA are mononucleate (as determined by autoradiography). Using vincristine sulfate to halt cells in metaphase, we found that all of the mitoses accumulating between 28 and 52 hours after denervation had incorporated  $^3\text{H}$ -thymidine to which they had been exposed 24 to 48 hours after denervation. Fifty microcuries of  $^3\text{H}$ -thymidine per kilogram of body weight were injected into a rat at 24, 34, and 48 hours after denervation, and 0.15 mg vincristine sulfate per kilogram body weight were injected at 28, 36, and 50 hours. The rat was sacrificed at 52 hours, and the diaphragm was fixed, embedded in araldite and sectioned at  $0.5\ \mu\text{m}$  thickness. Light microscopic examination of these sections revealed about 10–20 mitoses per section.

Sections were obtained from 16 different regions of the diaphragm in three rats. In all but seven cells, the mitoses were confined to mononucleate cells which were located between muscle fibers and which did not resemble satellite cells. In the seven cases, mitoses appeared in cells that at the light microscope level were not unequivocally different from satellite cells. However, electron microscopic study of these cells revealed that each cell was located outside the basement membrane of the muscle fiber and thus was not a satellite cell. Although some of the mitotic cells were very spongy in appearance and were filled with many distended membranous vesicles, they had no fine structural features to enable an unequivocal identification of cell type.

## PACEMAKER DEVELOPMENT AND INTERCELLULAR COMMUNICATION IN THE EMBRYONIC HEART

*R. L. DeHaan, R. Hirakow, J. O. Dunning, and K. A. O'Connell*

During the first day of incubation (stages 3–6) the embryonic chick becomes little more than a three-layered plate of cells. A primitive streak and notochord delineate the future axial structures, but no differentiated organs form. During the ensuing hours, however, paired lateral regions in the mesodermal sheet become folded into channels that swing together into the midline, joining there to form the primitive tubular embryonic heart. By 34–36 hours of incubation (stage 10), this structure begins spontaneously to contract; by the end of the second day (stage 12) it is pumping blood through an intact circulatory system; and at the end of the first week of development, it has molded itself into a complete four-chambered, adult-like heart.

Since our report last year, we have devoted most of our energies to three aspects of cardiac development:

1. Initiation of an analysis by Dunning and DeHaan of the triggering agents—presumably inductive interactions—

which cause undifferentiated lateral mesoderm to begin the differentiative route towards cardiac tissue.

2. Continuation of DeHaan's previous study of the sensitivity of spontaneously active heart cells in culture to suppression by potassium, exploiting the potassium inhibition threshold as an assay for pacemaker development.

3. A comparative ultrastructural study by Hirakow of the contacts between cells in intact cardiac tissues and, in collaboration with DeHaan, an analysis of the formation of specialized contacts between cultured cells in relation to conduction of a contractile stimulus.

### INDUCTION OF PACEMAKER DIFFERENTIATION IN THE PRE-SOMITE EMBRYO

In order to gain further insight into the factors controlling the development of pacemaker activity, it is important to examine how this state of cytodifferentiation comes about. When does proto-

TABLE 8. Beating Cells Differentiated *in vitro* from Dissociated Early Embryos

Embryonic Stages Dissociated and Pooled	Medium	Total Cell Count	IBC *	IBC **	BC + NBC Pair in Contact	Beating Group of Cells
4—, 4, 4+	818A	1200	0	0	0	4
	818B	1500	0	0	0	0
	629A	600	0	0	0	2
	033C	600	0	0	0	0
	0211C	300	0	0	0	0
5—, 5	818A	1200	0	0	0	5
	818B	1000	0	0	0	0
	057Z	500	0	0	0	0
	0211C	300	0	0	0	0
5	818A	600	0	0	0	0
	818AG	600	0	0	0	0
	818B	300	0	0	0	0
	818BG	300	0	0	0	0
5, 5+	818A	1900	0	0	1	2
	818B	1500	0	0	0	2
	057XY	1000	0	0	0	2
5+	818A	1200	0	0	0	1
	818AG	1200	0	0	0	0
	818B	600	0	0	0	0
	818BG	600	0	0	0	0
5+, 6—	818A	1600	0	0	1	1
	818B	1000	0	0	0	1
	057Z	800	0	0	0	1
6—	818A	1800	0	0	1	1
	818AG	1200	0	0	0	4
	818B	600	0	0	0	0
	818BG	600	0	0	0	1
	062A	1200	0	1	0	2
	062AG	1200	0	0	0	0
6—, 6	818A	1600	1	1	0	4
	818B	1400	0	0	1	4
	057XY	1000	0	0	0	1
6	818A	1500	1	1	2	2
	818AG	1000	1	1	0	0
	818B	500	0	0	0	0
	818BG	500	0	1	1	1
	062A	500	0	1	1	1
	062AG	500	1	0	0	2
6, 6+	818A	1000	4	3	1	0
	818B	1000	2	2	1	1
	057Z	800	1	0	0	3
6+	818A	600	0	1	0	3
	062A	800	2	1	0	1
	062AG	500	0	0	1	0
7—, 7, 7+, 8—	818A	3000	8	4	5	13
	818B	1400	3	2	4	13
	062A	1200	4	2	3	7
	062AG	1000	2	2	1	2

IBC \* = Isolated beating cell having no neighboring cell within a radius of 180  $\mu$  about it.

IBC \*\* = Isolated beating cell having one or more neighbors closer than 180  $\mu$  to it.

differentiation of myoblasts occur and through what inductive mechanisms? When does pre-myocyte determination become independent of possible inductive interactions with neighboring cells? Can precardiac mesoderm from pre-somite or early somite embryos be dissociated into single cells that have the capacity to differentiate into isolated pacemaker myocytes? If so, how early in development is this capacity attained?

A modification of DeHaan's techniques designed for the dissociation and culture of heart cells, described in past *Year Books*, was employed by Dunning to obtain cultures of isolated precardiac cells, pooled from carefully staged early embryos. Precardiac regions (with associated endoderm and ectoderm) were cut from explanted blastoderms by trimming off the anterior fifth and posterior two-fifths of the *area pellucida*. Five to ten of these fragments (containing about  $10^5$  cells each) were placed in 1 ml of a disaggregation medium (composed of 0.05% trypsin dissolved in a balanced salt solution) at 37°C with gentle stirring. At three-minute intervals thereafter, the supernatant was transferred to a tube containing 10 ml of trypsin inhibitor and replaced by 1 ml of fresh disaggregation medium. At the end of five of these three-minute intervals the tissue was usually completely dissociated. The entire 15 ml cell suspension in trypsin inhibitor was filtered through bolting silk, pelleted, and resuspended in culture medium. The cells were plated in 35 mm culture dishes, usually at a density of  $5 \times 10^4$  cells/ml.

Plating efficiency in medium 818A was generally between 20% and 40% for cells from embryos between stages 4 and 8; the younger the embryos, the lower the plating efficiency. Cultures were examined at daily intervals for three to five days after plating. Within 48 hours, beating activity was found in isolated cells from stages 6 and 6+ embryos, in less than 1% of cells counted (Table 8). The extent of pacemaker activity in cul-

ture does not appear to be dependent on potassium concentration at this time. Maintenance medium 818A has been found to be superior to growth medium 818B (which contains 4% embryo extract) or other media tested, in terms of both higher plating efficiencies and higher proportion of isolated cells that develop into active pacemakers. Typically, these pacemakers are similar to those isolated from three- to seven-day hearts: rounded, granular, and highly refractile in phase optics (Plate 4). Cultures with beating cells were fixed in alcohol-formol and stained for glycogen. These pacemakers, differentiated *in vitro*, were invariably found to stain strongly with PAS, whereas the majority of cells (presumably those derived from ectoderm, endoderm, and non-cardiac mesoderm) were PAS-negative. In general, the proportion of PAS-positive cells on such plates ranged between 1% and 7% of total cells counted. This proportion was found to be higher in earlier stages (4-, 4, 4+) than in cultures from later stage embryos, perhaps due to the high yolk content of cells from very young embryos. All pacemaker myocytes were found to be PAS-positive when the plates were stained, but only one-third or fewer of the PAS-positive cells were pacemakers.

Experiments to date have included 112 culture plates, containing 11 different media (Table 9), in which a total of 50,200 cells have been counted and scored for spontaneous beating activity. Of these, 46 plates included only cells dissociated from embryos between and including stages 6 and 8-. Among the 19,800 cells examined on these plates, 51 beating heart cells were found, or 0.26% of the total. Optimal conditions for pacemaker development seem to be attained in cultures from embryos dissociated at stage 6 to 6+ grown in medium 818A. In these circumstances 0.7% of the isolated cells counted had differentiated into beating myocytes.

Sixty-two plates contained dissociated



TABLE 9. Components of Media Used (in volume %)

Medium	Balanced Salt Solution	Medium 199	Horse Serum	Fetal Calf Serum	Chick Embryo Extract	Penn.-Strep.
818A 818AG	74 <sup>1</sup>	20	2	4	...	1
818B 818BG	70 <sup>1</sup>	20	2	4	4	1
629A	76	20	4	...	...	1
033C	56	20	20	...	4	1
0211C	60	20	10	...	10	1
057Z	70 <sup>2</sup>	20	2	4	4	1
057XY	74 <sup>3</sup>	20	2	4	...	1
062A	74 <sup>4, 1</sup>	20	2	4	...	1

1. Glucose level in 818A = 5.5 mM and in 818AG = 50 mM.
2. Total ion concentration in 818B (normally, 270-280 mOsm) is raised to 300 mOsm with NaCl.
3. Total ion concentration of 818A (normally, 270-280 mOsm) is raised to 300-340 mOsm with NaCl.
4. Total ion concentration of 818A lowered to 230 mOsm by lowering the NaCl concentration.

cells from embryos younger than stage 6. Of the 28,000 cells counted on these plates only one instance of an isolated beating cell was observed. In this case a neighboring fibroblast was only  $15\mu$  away from the isolated pacemaker. It is conceivable that the two cells may have been in contact at some time prior to observation and that the fibroblast had moved away, breaking this contact. From microcinematographic evidence, DeHaan earlier noted that pacemaker cells, in addition to being rounded and highly refractile in phase optics are non-motile as well. Pacemakers differentiated

*in vitro* were observed to remain in the same position on culture plates over a 50-hour span of time. Fibroblasts, in contrast, were highly motile; however, in the present cultures, in areas distant from cell clusters, random fibroblast movement appeared to result in translocations of no more than about  $60\mu$  over the same period of time. It may be safe to assume that in the 112 cultures examined, an isolated pacemaker observed to have no neighboring cells within a  $180\mu$  radius of it, at the time of observation, had in fact developed independently of contact with another cell over the entire

TABLE 10. Independence of Beating Cell Differentiation with Plating Density

Embryonic Stages Dissociated and Pooled	Medium	Total Cell Count	Observed Density at 2 Days in Cells/mm <sup>2</sup>	IBC	BC + NBC Pair in Contact	Beating Group of Cells
5+, 6-, 6, 6+	818A	600	177	0	0	4
		600	7.8	0	1	3
	818B	600	140	0	0	2
		600	5.7	1	0	2
7-, 7, 7+, 8-	818A	500	101	2	0	1
		500	6.0	2	1	0
	062A	1000	122	4	2	7
		200	4.7	2	1	0
	062AG	500	104	2	1	1
		500	6.8	2	0	1

IBC = Isolated beating cell.

culture period (i.e., had differentiated independently of close-range cell-cell interactions). Over 200 neighbors of isolated beating cells within  $450\mu$  radius were examined for the presence or absence of PAS-staining for glycogen. Only 2.5% of these cells were found to be PAS-positive, suggesting that these cells are representative of the population at large, and that myocytes do not accumulate around isolated pacemakers.

A frequent observation in the cultures was to find a single beating cell attached to a non-beating cell, the latter usually PAS-negative. As such pairs appear in cultures of embryos as early as stage 5 to 5+, they might represent the end-result of an early contact-dependent inductive phase in pacemaker differentiation. The fact that beating groups of two or more conjoint cells are found in cultures of cells dissociated from earlier

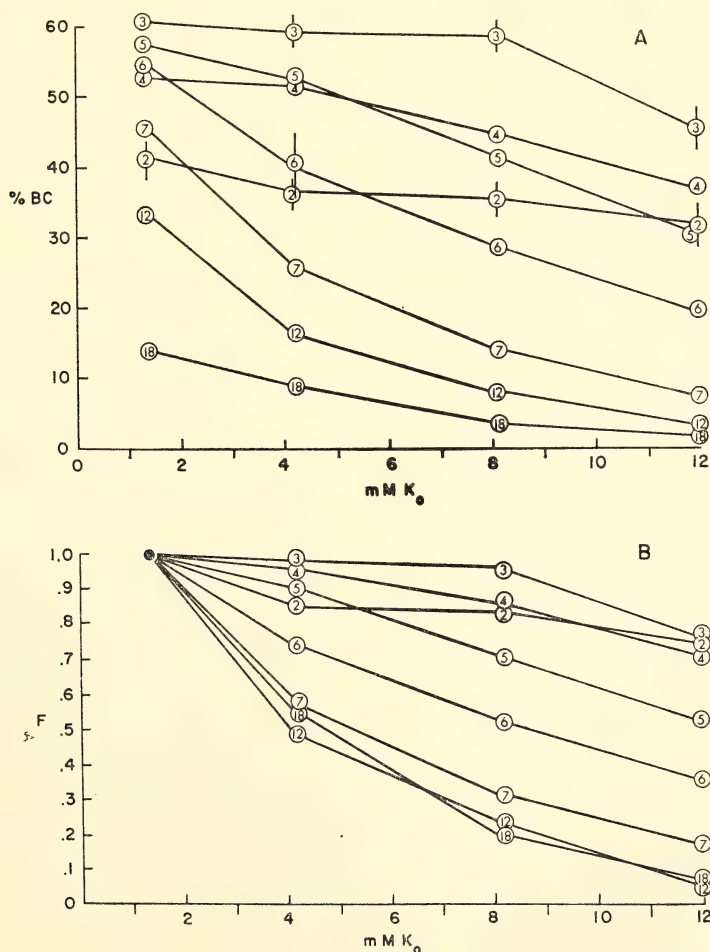


Fig. 15. (A) Percentage of beating cells isolated from hearts aged 2-18 days, as a function of K<sub>0</sub>, counted after 21 hours of culture in medium containing 1.3, 4.2, 8.1, or 12 mM K. Each point represents the mean of 6-18 separate culture plates. One standard error is shown by vertical bars; when not shown the SE was 2% or less. (B) Potassium-inhibition curves. Data shown in Fig. 15(A) has been normalized by expressing each value of %BC at 4, 8 and 12 mM as a fraction (*F*) of the value of 1.3 mM.

stages further supports the idea of a contact-dependent step occurring early in the path of pacemaker differentiation. Preliminary evidence that such a step is likely to occur only before stage 6, so that overall beating activity is not a function of the plating density of cells dissociated from stage 6 and later stages, is recorded in Table 10. If pacemaker differentiation is a result of permanent or temporary cell contacts during the culture period, dense cultures would be expected to have proportionately more beating activity than sparse cell cultures. We have not found this to be true thus far. Cultures of blastoderm fragments *in vitro* and transplantation techniques allowing development of such fragments *in situ* are presently being employed to examine further the possible cell-cell interactions involved in heart myocyte differentiation.

On the basis of the map of the precardiac regions in the stage 6 embryo, determined by Stalsberg and DeHaan, we estimate that these regions represent 9% of the total *area pellucida*, or 17% of the trimmed fragments used in these experiments. Preliminary cell counts made on cross-sections of osmium-fixed stage 6 embryos suggest that mesoderm represents one-third to one-fifth of the total cells contained in the three germ layers included in the fragments. Thus we may predict that precardiac mesoderm could contribute only 3–5% of the dissociated embryonic tissue. Under optimal conditions, the newly differentiated tubular heart of the two-day embryo, when dissociated, yields only 40% beating cells (see Figure 15 and discussion below). Thus if every precardiac mesoderm cell capable of differentiating *in situ* into a spontaneously active myocyte were also able to do so when isolated *in vitro* from stage 6, we would expect that number to be 1.2–2.0%. Thus the observed result of 0.7% represents one-half to one-third of the predicted maximum.

These results may be interpreted to

indicate that no cells in embryos younger than stage 6 have the capacity to differentiate into beating myocytes under the conditions described independent of close-range cell-cell interactions. They suggest strongly, however, that by stage 6, some precardiac cells are stably programmed for pacemaker differentiation, independent of any such interactions, since some of these cells, under the same culture conditions, are able to undergo that differentiation completely isolated from contact with any neighbor. The achievement of such functional differentiation under controllable culture conditions should allow us to examine those factors which regulate that differentiation, and to explore the determinative events which seem to be completed in precardiac cells at stage 6.

#### THE POTASSIUM-INHIBITION THRESHOLD OF ISOLATED EMBRYONIC HEART CELLS

High levels of extracellular potassium tend to depress excitability and spontaneous activity of heart tissue. Embryonic chick myocardium isolated as single cells in culture manifests this sensitivity to extracellular potassium concentration ( $K_o$ ) quantitatively. As demonstrated in past reports, approximately 45% of the cells isolated from seven-day embryonic hearts were found to beat spontaneously in medium containing 1 mM  $K^+$ . Replicate cultures in medium containing 4, 8, or 12 mM  $K^+$  exhibited respectively about 25%, 12%, and 6% beating cells. That is, each increment of  $K_o$  of 4 mM caused the number of cells beating spontaneously to decrease by about one-half. It was reported last year that this K-inhibition is not merely a statistical effect on the cell population as a whole, but results from the fact that each pacemaker cell has a specific and reproducible K-inhibition threshold. Some cells of the seven-day heart were suppressed at levels as low as 2 mM  $K_o$ , while others continued to beat spontaneously at K-concentrations of 12 mM or



even 20 mM. At least some cells from 7- to 15-day chick hearts can beat spontaneously at potassium levels up to 100 mM.

Preliminary experiments indicated that cells isolated from four-day embryonic hearts were less sensitive to inhibition by  $K_0$  than those from older embryos. Therefore DeHaan suggested that the K-inhibition threshold of pacemaker cells is a gradually acquired characteristic resulting from developmental changes taking place in the cell membranes from day 4 to day 7. Experiments performed during the past year were designed to test further the hypothesis that differentiative changes occur in the developing population of cardiac pacemakers and are manifested in a gradual increase in the sensitivity to  $K_0$ .

Hearts were dissected from chick embryos incubated 2 to 18 days and dissociated into their component cells by the multiple-cycle trypsinization method described in previous reports and publications. Potassium-inhibition curves were derived from the 21-hour counts on cultures in medium 818A by expressing each %BC value at 4, 8, or 12 mM  $K^+$  as a fraction of the value at 1.3 mM. The kinetics of the K-inhibition response were measured by seeding replicate plates in 1.3 mM K medium 818A. After the 21-hour count in this medium 0.46 ml of balanced salt solution containing 40 mM  $K^+$  was injected into each of two plates, bringing the final K-concentration to 8.4 mM. Beating cells were counted at 6 minutes, 1 hour, 2.5 hours, 5 hours, and 24 hours after the injection. Control plates into which 0.46 ml of K-free salt solution had been injected were counted at the same times.

The percentage of spontaneously active heart cells derived from embryos incubated 2 to 18 days is shown as a function of  $K_0$  in Figure 15A. From these data, fractional potassium-inhibition curves for each age heart have been calculated (Fig. 15B).

At all ages tested, the %BC was maxi-

mal at 1.3 mM  $K^+$ . In cultures from 7- to 18-day hearts, approximately half of the pacemaker cells stopped beating with each 4 mM increment in  $K_0$ . In contrast, cells from hearts aged two to four days were relatively unaffected by K-levels up to 8 mM. Even at 12 mM  $K_0$ , 70% of the pacemakers of these early hearts continued beating, whereas all but 10-15% were suppressed by that amount of  $K^+$  in cultures derived from 7- to 18-day hearts. Cells from five-day and six-day hearts were intermediate in their response to  $K^+$ .

The curves shown in Figure 15 may be considered to represent cells in a state of equilibrium with their medium, having resided in that environment for the previous 21 hours. To determine (what was assumed would be) the rate of decay of %BC of cells from different age hearts, experiments testing the kinetics of potassium-inhibition were performed by suddenly elevating  $K_0$  from 1.3 mM to 8.4 mM. Counts were made at appropriate intervals thereafter until a new equilibrium level was established (Fig. 16). These results do not show the expected exponential decay curves.

One to two minutes were required for the injected aliquot of KCl to diffuse throughout the 2 ml of culture medium. The first count was made, therefore, two to ten minutes (a mean of six minutes) after injection. At that time, many of the cells that had previously been active had stopped beating in all cultures: about 50% in plates from two- to four-day hearts, close to 70% in six- to seven-day hearts. Within one to two hours, however, some of these cells had recovered, and the %BC was becoming re-established at the 8.4 mM equilibrium level. Instead of a smooth decay from a fraction ( $F$ ) of 1.0 to the new equilibrium level, these data indicate that the activity of most of the pacemaker cells was suppressed by the increment of potassium, and some then recovered (Fig. 16). Control cultures plated initially in cultures containing 1.3 or 8.4 mM  $K^+$

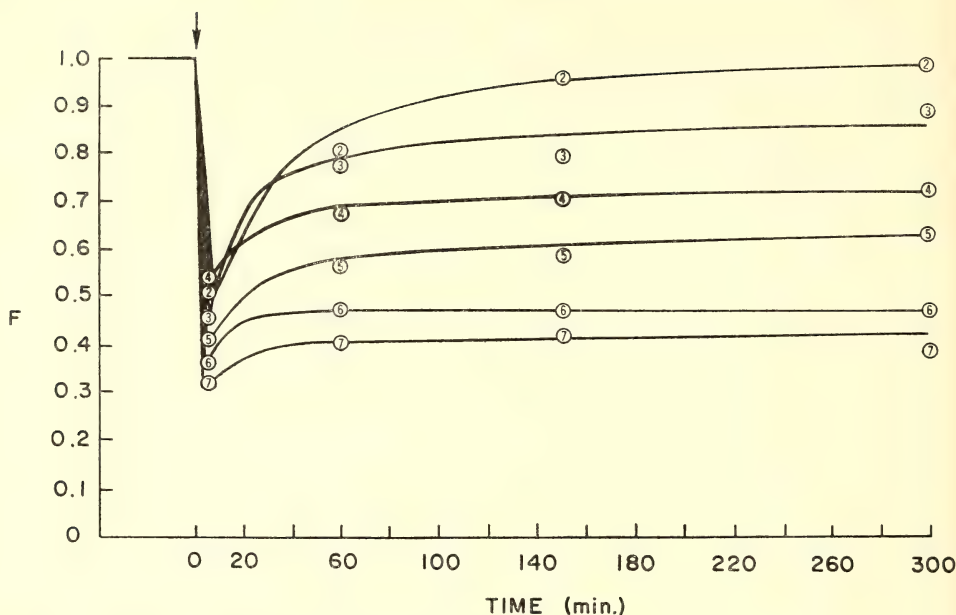


Fig. 16. Kinetics of K-inhibition. After the 21-hour %BC count on cells maintained in medium containing 1.3 mM K,  $K_o$  was rapidly increased to 8.4 mM. The fraction ( $F$ ) of the original pacemaker population (%BC at time 0 in 1.3 mM K) is shown 6 minutes, 1 hour, 2.5 hours, and 5 hours after the injection by the encircled numbers. The hyperbolic line curves were calculated by the equation  $F = \frac{t}{a + bt}$ .

were unaffected by injections of medium containing the same  $K_o$  levels. Such cultures decreased gradually by about 5%BC over the five-hour experimental period.

These results show that during the first three to four days of embryonic development pacemaker cells remain relatively insensitive to the level of extracellular potassium, at least over the range of 1–8 mM, and are only slightly affected by 12 mM  $K^+$ . During the next few days, the percentage of heart cells whose pacemaker activity is suppressed by elevated  $K_o$  increases progressively. The spontaneously active pacemakers of hearts from embryos aged 7, 12, or 18 days are reduced roughly by half with each increment of 4 mM  $K_o$  (Fig. 15A, B). Days 4 to 7 represent, therefore, a period of transition from a state of potassium insensitivity to one of greater sensitivity

of cardiac pacemakers to the level of external  $K^+$ .

Recent experiments by DeHaan and Hirakow, in which atria and ventricles are dissected apart and dissociated separately, indicate that ventricular cells develop this K-sensitivity at an earlier stage than do atrial cells. More than 25% of the pacemakers of the four-day ventricle are suppressed by 8 mM  $K_o$ , but only about 10% of those from the four-day atrium. From the 12-day embryo, however, 80% of ventricular pacemakers but only 30% of atrial ones stop beating in 8 mM  $K_o$ ; that is, the ventricle has approximately the same percentage of K-sensitive pacemakers at four days of development as atrial tissue does at 12 days.

Evidence is now compelling from the works of Noble and others that the electrical activity of mature cardiac cells

conforms to a model similar in many respects to that proposed in 1952 by Hodgkin and Huxley for the squid axon. According to this scheme, at transmembrane voltages near the resting potential ( $-60$  to  $-90$  mv) the cell membrane is substantially more permeable to K outward current ( $i_K$ ) than to an inward current of Na ( $i_{Na}$ ). Thus the membrane potential ( $E_m$ ) lies near the potassium equilibrium potential ( $E_K$ ).

Spontaneous action potentials of cardiac pacemakers arise from a slow diastolic depolarization, called the pacemaker potential. Voltage clamp analyses on adult heart tissue have revealed that this depolarization is caused by an appreciable  $i_{Na}$  during the "rest" interval superimposed on a time-dependent slow decrease in the potassium conductance ( $g_K$ ). Elevated levels of K increase  $g_K$  (despite the diminished transmembrane K-gradient) by affecting directly potassium permeability ( $P_K$ ). Increased K has been shown to increase  $P_K$  in mammalian Purkinje fibers, atrial, and ventricular tissue, and by DeHaan and Gottlieb in embryonic chick heart cells in tissue culture. Thus the potassium inhibition threshold defined above presumably refers to the level of  $K_o$  at which  $g_K$  is too large to permit an adequate net inward current during the rest interval, and thus prevents an effective diastolic depolarization.

On the basis of these considerations, DeHaan suggests several possible explanations for the high threshold to  $K_o$  of early embryonic pacemakers, illustrated in Figure 15. A cell would exhibit a high K-inhibition threshold if it had one or more of the following properties: (1) An abnormally high resting sodium current, resulting either from a large  $P_{Na}$  or a very steep sodium gradient (i.e.,  $Na/Na_i$ ). (2) A relatively small  $g_K$ , or a  $g_K$  which did not increase in response to elevated  $K_o$ . (3) A gradually increasing depolarizing current carried by an ion not regulated by the orthodox sodium-potassium balance (such as  $Ca^{++}$ ).

Distinguishing among these alternative hypotheses will require a conclusive analysis of the properties of developing pacemaker membranes, and the elucidation of their current-voltage relations by voltage clamp techniques.

#### ULTRASTRUCTURE OF MYOCARDIAL CELL CONTACTS

In previous studies Hirakow has investigated the ultrastructure of heart cells in a wide spectrum of vertebrates, comparing the structure and organization of the myofibrils, mitochondria, sarcoplasmic reticulum, transverse tubular system, and intercalated discs. Although seeking common characteristics among the species he examined, on the basis of these features he has distinguished the sauropsidan (reptile and bird) heart from that of the mammal, the former in most respects being more primitive.

One of the common functional features of the hearts of all vertebrates, which must be explained at an ultrastructural level, is their ability to conduct an electrical stimulus from cell to cell throughout the entire myocardial mass, at a conduction rate sufficient to coordinate the contraction of each myocyte into an effective pumping action. Early electron microscopic studies of heart muscle demonstrated that—unlike skeletal muscle in which cells fuse to form a syncytial mass of common cytoplasm—each cardiac myocyte is separated from its neighbors by an intact plasma membrane. Nonetheless, Sylvio Weidmann, in Switzerland, and other electrophysiologists have shown that the electrical resistance between the cells in a cardiac fiber is not much higher than that of the cytoplasm. Moreover, it has recently been shown that the cells of a wide variety of tissues are electrically coupled by similar low-resistance pathways.

When seen in the electron microscope the apposed plasma membranes of neighboring heart cells—or of those of most



other tissues—are generally separated by an electron-lucent space about 200 Å wide, which is continuous with the extracellular space. On closer examination three types of junctional specializations may be seen, designated (1) the “macula adherens” or desmosome, which is the most common binding site between cells, (2) the “fascia adherens,” the dense regions of cell membrane that form the linear perpendicular site of insertion for the myofilaments and represent the major components of the intercalated discs between heart cells, and (3) the “fascia” or “macula ocludens,” or nexus. Only in the nexus is the 200 Å intercellular space occluded as the apposed cell membranes approach true contact. As the interpretation of the ultrastructure of cell contacts has evolved, various investigators have termed the nexal region the pentalaminar junction, tight junction, fused membrane, close junction, and most recently “gap junction” since the discovery of a narrow 20 Å gap between the apposed membranes in the region of closest proximity.

It was first postulated by Lloyd Barr and M. M. Dewey in 1962 that the nexus might be the ultrastructural site of low-resistance communication between heart cells. This idea has now become widely accepted as many examples have been found of tissues which are in electrical communication and which also exhibit nexal junctional complexes between cells. Thus it is now frequently stated that the action potential or electrical contractile stimulus is conducted from cell to cell throughout the heart across the low-resistance nexal junctions.

There are, however, two difficulties in accepting the gap junction—as seen in the electron microscope—as the site of low-resistance communication between cells. (1) Although conduction of the contractile stimulus occurs in cardiac tissue of all vertebrate species, specialized regions of close membrane apposition have been shown only in the adult mammalian heart. Some investigators

have even denied the existence of nexal junctions in avian cardiac tissue, and no one has investigated the question in embryonic heart. (2) The evidence for the hypothesis is purely circumstantial. It has never been demonstrated experimentally that electrical conduction occurs between two cells when and only when nexal junctions exist.

During the past year, Hirakow has extended his comparative electron microscopic studies of heart tissue to include the apposed myocyte membranes. He has perfected techniques (which seem to differ from one species to another) for revealing cell membrane specializations in cardiac tissue of the mouse (adult, embryonic, and neonatal), chicken (adult and embryonic), and *Necturus* (adult), finding that regions of close apposition of cell membranes appear to be universal among the vertebrates as a junctional feature.

In general the method of choice has included fixation of tissues in glutaraldehyde-formaldehyde mixture, post-fixation in  $\text{OsO}_4$ , and treatment with uranyl acetate, prior to dehydration. Lanthanum has been applied as a surface stain for revealing gap junctions. However, in confirmation of the experience of other workers this compound has produced unreliable results. Ruthenium red, in contrast, has been convenient and reproducible in use, and is currently being applied to embryonic, as well as cultured, heart cells (see below).

Gap junctions typical of the adult mammalian heart were found in the 16-day mouse fetus (Plate 5), with a 20–40 Å gap between the apposed membranes, and characterized by a polygonal substructure with a 100 Å center-to-center spacing when viewed tangential to the cell surface. These junctions were generally localized along longitudinal or side-to-side contact areas between fibers.

The heart of the adult chicken also exhibits regions of close membrane apposition, but these are characteristically smaller specializations in the ordinary

myocardium located at transverse regions of cell contact where fibers abut end to end (Plate 6A). Gap junctions in cells of the cardiac conduction system, in contrast, are more similar in size and distribution to those in the mammalian heart (Plate 6B).

In the heart of *Necturus* and the chick embryo junctional structures differ substantially from the typical mammalian "macula ocludens." Areas of close contact may not be visible at all at low EM magnification (Plate 7). At higher magnification, regions of close apposition are seen to be restricted to tiny punctate spots. Moreover, within these junctional points the degree of proximity of the apposed membranes may vary from regions of complete fusion, typical of the "tight junctions" of epithelial cells, to gaps of 20–70 Å interspace (Plate 8). Recent measurements of the total width of the two apposed cell membranes have ranged from 140 to 170 Å. At no point in the 6-day heart have membrane thicknesses less than the 140 Å characteristic of true membrane fusion been measured. This variability in gap width seen in the embryonic heart may represent a primitive or formative stage of nexal junction. However, since it is the only type of close apposition between embryonic myocytes, it is presumed to play the same role in electrical conduction as the definitive nexus.

Techniques described in previous reports for preparing individual isolated heart cells and maintaining them, beating spontaneously for extended periods in culture, seem ideally suited for studying the formation of nexal junctions and for testing the hypothesis that these areas of membrane specialization represent the sites of electrical conduction between cells. DeHaan and Hirakow have initiated experiments with these goals in mind, and have obtained preliminary results.

Seven-day embryonic chick hearts were dissociated into their component cells by techniques described previously

and inoculated into culture plates at a density ( $2 \times 10^5$  cells/plate) designed to yield a high frequency of isolated cells in close proximity. Four to 24 hours after plating each culture dish was transferred to a microscope stage incubator where the temperature, gaseous atmosphere, and humidity could be maintained while observing and photographing the cells. Pairs of rounded myocytes were selected for further observation on the basis of the following criteria: (1) each cell of the pair was beating independently at its own intrinsic rate, which was discernibly different from that of its neighbor; (2) the two cell surfaces at some point were within 3–4 micra of each other; and (3) each member of the pair was at least 10 micra from any other neighbor. These cells were photographed on Polaroid film (Plate 9A) and their respective rates of beating counted. Observations and photographs were repeated periodically (about every 20 minutes), until the cells came into physical contact, as discernible at a magnification of  $200 \times$  (Plate 9B). Observations were then made at shorter intervals until the beats of the two cells synchronized to a common rhythm, at which time the rate was counted, and the plate was quickly rinsed with Ringers solution, flooded with cold formol-glutaraldehyde fixative, and prepared for electron microscopy.

Thus far, 35 cell pairs have been observed, both when beating independently and after synchrony was attained. Of these, the exact time of initial contact and of the establishment of synchrony was observed in 11 pairs, accurate to within a few seconds, as a result of continuous observation. In these pairs that interval ranged from 4 to 38 minutes, with a mean value of 12.3 minutes. In four of these 11 pairs, the cells attained partial synchrony (in which the synchronized rhythm became established in both cells, but one missed occasional beats) a few minutes prior to the recorded time of full synchrony.

We conclude from these data that an interval of approximately 12 minutes (or as short as four minutes in some cases) must intervene after two heart cells come into contact before an electrical stimulus can be conducted from one to the other.

Preliminary electron micrographs of one of these cell pairs, fixed after synchronization (Plates 9C, 10) suggest that the apposed cell membranes have developed regions of nexal-like close contact and other specialized junctional structures. A recent study by Flaxman, Revel, and Hay, of Harvard University,

suggests that such rapid development of specialized contact regions in cell membranes is also feasible in other cell types. They found that mouse L-strain fibroblasts, observed in culture with time-lapse cinematography and fixed within 3–10 minutes after contact had already in some cases formed areas of close apposition with the appearance of tight or gap junctions. However, in their study no assay for functional contact was available. Our experiments with heart cells are consistent with the hypothesis that the nexus may be the site of electrical communication between cells.

## COMPARATIVE ULTRASTRUCTURE OF CULTURED CHICK FIBROBLASTS AT EARLY AND LATE STAGES DURING THEIR GROWTH SPAN

M. A. Brock\* and R. J. Hay

Euploid cells from man and several lower species will survive for only a limited period under the cell culture conditions currently in use. This is an important property distinguishing normal or primary cell lines and permanent lines which often possess karyotypic anomalies and malignant characteristics. The phenomenon of cellular mortality *in vitro* has led to the hypothesis that cultured diploid cells undergo senescent changes analogous to those which occur during cellular aging *in vivo*. Since changes in the gross morphology of chick and human cells have been observed during continued subcultivation, we decided to compare the ultrastructure of early-passage, rapidly dividing cells with that of late-passage cells showing a reduced proliferation rate and degeneration.

Chick fibroblasts were cultured through 4.5 generations (early passage) and 18 generations (late passage). In late-passage cells, the marked lobation of the nucleus, the absence of chromatin adjacent to the nuclear envelope, and ellipsoidal mitochondria, generally bent into

a shallow "U" with longitudinally oriented cristae, contrasted with the nearly oval nuclei containing peripheral chromatin and oval mitochondria with transversely oriented cristae seen in early-passage cells. Highly developed RER and Golgi complexes were observed at both passage levels. The most striking change was the presence of conspicuous secondary lysosomes and residual bodies in over 90% of the late-passage cells. Interestingly, Andrew, Munnell and Getty, Weiss and Lansing, and others have observed similar changes in a variety of cells from old animals.

Our working hypothesis to explain the limited survival of primary strains *in vitro* is essentially that proposed by Orgel to account, at least in part, for cellular aging *in vivo*. He suggested that errors in the synthesis of proteins involved in transcription or translation could be self-propagating to lead ultimately to an "error catastrophe" with degeneration of the cell line. Ample evidence exists indicating that the environment can influence the division potential of cell strains *in vitro*. We reason, there-

\* Gerontology Research Center, Baltimore City Hospitals.



fore, that environmentally induced errors in the synthesis of macromolecules in these cells could cause the degeneration observed, whether or not any link with *in vivo* aging is involved.

The ultrastructure of late-passage chick fibroblasts suggests that active synthesis of macromolecules and break-

down of cellular components are occurring concomitantly. Hruban and his associates provided suggestive evidence that induction of aberrant proteins in mammalian cells may be a stimulus for autolysosome formation. Thus our observations are consistent with the error theory under consideration.

## THE MAMMALIAN EMBRYO IN RELATION TO ITS ENVIRONMENT

### ATTACHMENT OF THE RABBIT EGG TO THE UTERUS

*B. G. Böving*

The attachment of the rabbit egg to the uterus has been analyzed. The attachment has three main phases, each subdivided: a muscular phase of first random transport, then spacing, and finally arrest; an adhesive phase involving first lemmas and then trophoblast; and an invasive phase beginning with penetration and proceeding to spread of trophoblast through uterine epithelium, and finally arrest. However, attachment is a continuous process of progressively intimate association between maternal and conceptual parts achieved through a consistent sequence of mechanisms in which mechanical and chemical agencies of mother and conceptus are in complex and systematically changing interaction. The sequence of major mechanisms and their composition in terms of stimulus, effector, action, and result have been summarized by a table in *Year Book 64*. *Year Book 66* exposed some ideas of how systematic analysis of a natural process, such as implantation, might help bridge the gap between reductionism and holism that troubles the science of functional biology in spite of having no counterpart in nature.

During the past year, thanks to the availability of suitable transducers and recording equipment, studies of rabbit blastocyst propulsion during spacing were extended. It may be recalled that

distribution of rabbit blastocysts along the uterine horn was found to change from random to approximately equidistant between 5 and 7 days after mating (*Year Book 55*), and the achievement of order was traced to mutual repulsion of blastocysts by contraction waves arising from each end of the uterine horn and wherever it is distended by a blastocyst (*Year Book 66* and *Year Book 68*). The mechanics by which a uterine contraction moves a blastocyst have now been examined quantitatively and qualitatively.

A blastocyst may be presumed to be moved by the uterus when the propulsive force of a uterine contraction exceeds the resistance to blastocyst motion. To measure the resistance ( $R$ ) (Fig. 17), spheres of blastocyst size and beyond (1–6 mm) were mounted on stiff wires attached to a force transducer. The transducer was held by hand and the beads were pushed through uterine horns of anesthetized rabbits at 6 days after mating, when spacing occurs. To measure the propulsive force ( $F$ ) that the uterus itself can exert, such wire-mounted spheres of a few selected sizes were allowed to remain in the uterus for a period of time while the force transducer was anchored to the immediately adjacent uterus, the effects of transducer weight and rabbit motion being minimized by suspending the transducer on a long string. Not surprisingly, force occasionally rose to levels exceeding resistance when spheres were used that were of suitable size,

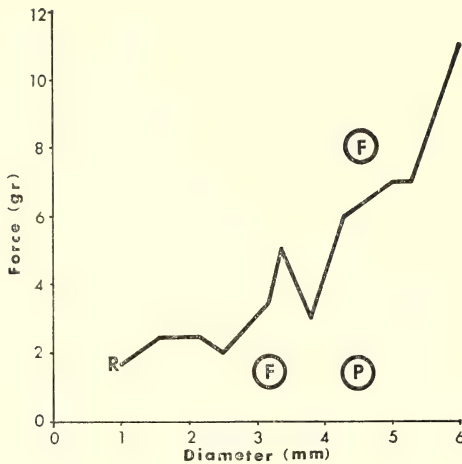


Fig. 17. The graph of *R* represents the resistance of a uterine horn to passage through it of spheres of various diameters. The maximum force that the uterus itself exerted on a 4.5 mm sphere is indicated by *F*. The *F* datum for a 3.2 mm bead is introduced from another but comparable experiment to show how poorly the uterus pushes a small sphere. Propulsive force calculated from measurement of maximum hydraulic pressure difference times the cross-section area of the 4.5 mm spherical piston is shown as *P*. Hydraulic forces are insufficient to overcome uterine resistance or account for the observed force by which the uterus propels its blastocyst-sized contents.

such as 4.5 mm, the diameter of a blastocyst at 6.5 days after mating. More instructively, very little force was exerted on small spheres. No data were collected for spheres too large to be moved. Thus, uterine propulsive force in excess of uterine resistance is exerted on spheres within a relatively narrow size range, and that range corresponds to that of blastocysts during spacing.

Since spermatozoa are far below the minimum size for propulsion by the blastocyst spacing mechanism, it is implied that spermatozoa and blastocysts are propelled by the uterus in mechanically different ways. That makes it somewhat less perplexing that the uterus moves the former up and the latter down. Moreover, if spermatozoa are moved mainly by uterine propulsion of fluid,

as seems likely, then one must doubt that blastocysts are carried along in uterine fluid. One must even hesitate to assume that blastocysts are moved by a contraction wave raising the pressure behind a blastocyst higher than ahead of it; such a hydraulic mechanism presupposes force transfer by fluid, and there is practically no fluid in the uterine lumen at the time of spacing. It is, however, conceivable that the soft lining of the uterus could be pushed along by uterine contraction waves and thereby act as a sort of viscous and anchored pressure-transmitting fluid. Therefore, a hydraulic explanation, while doubted, may not be rejected without test.

Hydraulic pressures during propulsion were measured by transducers linked by thin polyethylene tubes with openings either fore or aft of the bead mounted for force measurement in the manner described in the previous paragraph. Simultaneous recordings were collected of pressure fore and aft of the bead, a summation of those pressures, and the force exerted on the bead by the uterus. In addition, tissue temperature was monitored by a thermistor whose reading was recorded as well as used to regulate a specially devised apparatus that kept the exposed tissues moist and at body temperature during their prolonged exposure. Concurrently recorded were signals indicating time and whether a movie camera was on or off. The movie camera, by field splitting with a mirror, recorded some of the above graphs adjacent to views of the exposed uterus with its contraction waves and enclosed bead. Analysis of the integrated records is far from complete (since efforts were concentrated on collecting as much data as possible before the recording equipment became unavailable), but the essential conclusions are obvious enough to be stated with assurance and have been presented publicly to anatomical colleagues in the form of a motion picture. Waves of uterine contraction at 6 days after mating generate pressure changes

fore and aft of a sphere of blastocyst size, but the peaks of fore and aft pressure difference are not consistently synchronous with the peaks of force, are not even consistently in the direction of the force, and are in no case of magnitude sufficient to account for the simultaneously observed peak of force (Fig. 17). Accordingly, it is concluded that pressure changes in the rabbit uterus during the blastocyst spacing phase are not the essential means of uterine propulsion of its contents; although they occasionally may contribute, they more often appear to be a consequence of such propulsion.

The preceding conclusion discouraged the motivating idea that it might be possible to improve the retention of intrauterine contraceptive devices by providing holes to leak fluid and relieve pressure behind them. There is also an implicit challenge to the considerable clinical literature on intrauterine and intratubal pressure measurement that admits of, or uses, the intuitive assumption that pressure changes imply propulsion of contents. Even if pressures at two points are determined to be different, it is not certain that things will move from the region of high pressure to the region of low pressure. One can just as well reason that movement of contents should relieve pressure difference, and any observation of pressure difference evidences partial or total obstruction. More precisely, a pressure difference between just any two points is not necessarily evidence of a pressure gradient; unless one knows pressures at intervening and adjacent points and knows about patency and the resistance to motion in the segment of uterus to be traversed, there is not sufficient information to reason from pressure to motion. What we need to know is the pressure difference from one end to the other of the item to be moved, the cross sectional area of it, and the resistance to its motion. Measurements of intraluminal pressure, like determinations of barometric pressure,

may vary and may tell whether it is a good day for a blastocyst to go sailing, but they say nothing of the force that moves the ship.

#### ANATOMY AND PHYSIOLOGY OF THE PLACENTA

*E. M. Ramsey, H. R. Misenhimer,  
M. W. Donner, S. I. Margulies,  
and C. B. Martin, Jr.*

##### *Baseline Studies*

The baseline studies commenced in 1967 have in large part been concluded in the experimental season just ended. Building upon the previously accumulated data on blood pressure, pulse rate, and blood gases, and the effect of anesthesia upon these parameters, the attempt was made to define a physiologic steady state for the pregnant rhesus monkey and her fetus. It must be recognized that the administration of anesthesia and the surgical manipulation involved in placing catheters, flow probes, etc. themselves alter the normal state. Until the magnitude of such alterations is established, evaluation of experimental data is impossible.

We have attempted to achieve a "steady state" in our animals by permitting them to recover from anesthesia and surgery in a restraining chair where they remain throughout the study period, eating and drinking *ad lib*. It should be emphasized that, while "steady," this is not a "physiological" state since the animal is restrained and is under the influence of the remote effects of antecedent surgery.

Fifteen experiments carried out at various stages of pregnancy yielded consistent data, exemplified in Figure 18, which is a graph of findings in a typical experiment. The average pattern of change in mean arterial blood pressure for the entire group is shown by the graph in Figure 19.

It will be noted that pentobarbital produced a rapid fall in blood pressure



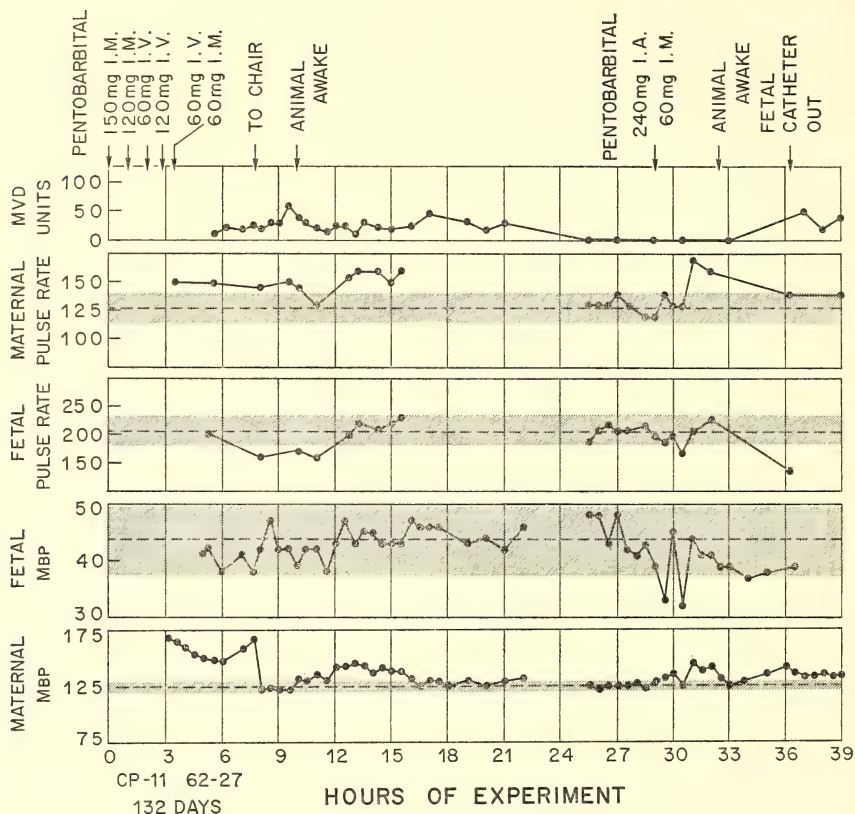


Fig. 18. Graph showing changes in maternal and fetal mean arterial blood pressure ( $M_{BP}$ ) and pulse rate in a typical experiment continued for 39 hours after initial induction of anesthesia. MVD Units: Montevidea units, a measure of myometrial activity. Dotted line: mean; shaded area: 2 sd. Monkey No. 62-27; 132 days pregnant. Experiment No. CP-11.

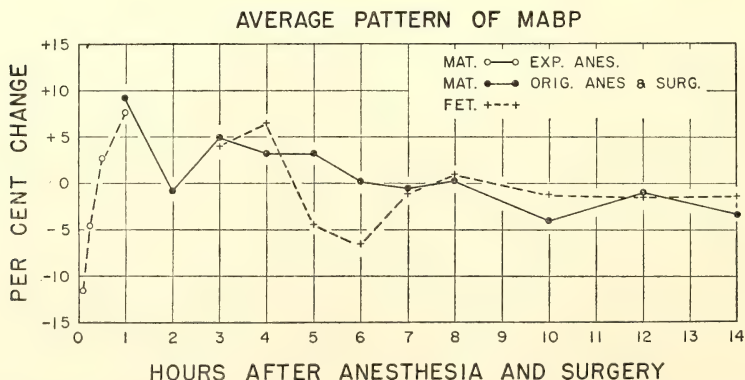


Fig. 19. Graph showing average pattern of change in mean arterial blood pressure (MABP) following anesthesia and surgery.

followed by a rise above the mean, and required an average of 8.3 hours to stabilize at a level within 2 sd of the mean. Pulse rate and blood gases followed a similar pattern.

From these results we must deduce that the effects of the requisite experimental procedures cannot be discounted until at least 8 hours have elapsed.

### *Fetal Circulation in the Placenta*

Previous studies, as reported in *Year Books 59-68* have analyzed the pattern of uteroplacental vasculature in monkey and man and certain aspects of placental circulation. One aspect, the effect of uterine contractions upon circulation of fetal blood through the vessels of the fetal cotyledons, remains in doubt.

On the maternal side such contractions, whether spontaneous or experimentally induced, have a marked effect. Entry of maternal blood from the endometrial spiral arteries into the intervillous space of the placenta is totally abolished in strong contractions and curtailed during weaker ones. As this has important implications for the continuity of fetal nutrition during normal and pathological labor, it appeared desirable to investigate the fetal response to these phenomena.

Employing the technique described in previous *Year Books* as reliable for visualizing the fetal circulation of the placenta, a radiopaque material was injected into the fetal femoral artery in uterine relaxation and during strong, syntocinon-induced uterine contractions followed by rapid serial radiography. To make certain that the contractions exceeded critical strength, maternal injections and radiography were performed immediately subsequent to the fetal injection, while the contraction was still at peak intensity.

When radiograms made following injection in relaxation were compared with those made in the same animal during contractions of sufficient strength to

eliminate all maternal inflow to the intervillous space no difference in pattern or speed of filling of the fetal placental vessels could be demonstrated (Plate 11).

These unvarying findings leave no alternative but to conclude that uterine contractions have no effect upon circulation on the fetal side of the placenta as observed by radioangiography.

This study of fetal placental circulation during uterine contractions rounds out the radioangiographic aspect of the comprehensive study of uteroplacental and fetoplacental vasculature and circulation which has been in progress for the past 25 years in this Laboratory.

### *Chronically Impaired Uterine Artery Blood Flow*

We have previously reported studies of impaired uterine artery blood flow (*Year Book 67*, p. 461, and *Year Book 68*, p. 550). These studies were designed to produce a hypertensive state in the rhesus monkey during pregnancy. Hypertension has not occurred in the six animals initially assigned to this project, and the experimental procedure has produced no changes in the biochemical parameters that were measured, including angiotensin.

Even though the original expectations of this study have not been realized, a new experimental model has emerged: an animal in which there is impairment of uterine artery blood flow that antedates pregnancy. Our studies so far show that uterine artery flow is usually obliterated by the application of non-expandable bands around the arteries. This compromise in uterine perfusion does not reduce fertility. It does, however, appear to have a significantly deleterious effect on reproductive performance, as is shown in Table 11.

The fetal death rate of 33.3% far exceeds the expected midpregnancy loss in rhesus monkeys of the Carnegie colony. During the same three-year period the fetal death rate in normal

TABLE 11. Reproductive Performance of Rhesus Monkeys with Impaired Uteroplacental Circulation

Animal	First Pregnancy after Banding	Second Pregnancy after Banding	Third Pregnancy after Banding
66-88	unexplained death of animal at 118 days		
66-91	livebirth at term	livebirth at term	not pregnant
64-72	livebirth at term	livebirth at term	stillbirth at 128 days, 27 days after radioangiogram
66-87	stillbirth at 117 days	livebirth at term	not pregnant
66-94	stillbirth at 123 days	livebirth at term	living fetus at 115 days *
66-86	not pregnant	stillbirth at 110 days	livebirth at term

\* A stillborn fetus was delivered a few days after the experiment, probably as a direct result of the experimental procedures.

animals after the 100th day of pregnancy was 2.3%. Of further importance is the fact that most of these fetal deaths occurred in the first pregnancy after banding.

Uteroplacental circulation has been studied radioangiographically in some of these banded animals. The results are shown in Table 12.

With the exception of animal 66-91, the postbanding X-rays show a significantly reduced number of spiral artery entries into the intervillous space. It is likely that this impairment of uteroplacental circulation is a major factor in the high incidence of fetal death.

Our future studies are designed to investigate uteroplacental circulation serially in the first pregnancy after banding. We will also evaluate the effect of impaired uteroplacental circulation on the fetus during induced labor at term.

#### *Effect of Vasoconstrictive Drugs on Placental Circulation*

In April 1970 Dr. Maurice Panigel of Paris, Professor at the Institut National de la Santé et de la Recherche Médicale, joined the placental research team. Dr. Panigel, well known for his studies of placental anatomy and physi-

TABLE 12. Results of Pre- and Postbanding Radioangiographic Studies of Uteroplacental Circulation

Animal	Time of X-ray Study	Gest. Age	Placental Discs	Total Spurts	Fetal Outcome
	Prebanding, 1966	138	2	8	livebirth
	Prebanding, 1967	130	2	14	livebirth
64-72	Postbanding, 1968	146	2	4	livebirth
	Postbanding, 1969	147	2	3	livebirth
	Postbanding, 1970	101	2	4	stillbirth
66-87	Prebanding, 1967	138	1	9	livebirth
	Postbanding, 1969	145	2	4	livebirth
66-91	Prebanding, 1967	146	1	15	livebirth
	Postbanding, 1968	153	1	15*	livebirth
66-86	Postbanding, 1970	87	2	5	
	Postbanding, 1970	150	2		livebirth
66-94	Postbanding, 1970	115	2	15†	stillbirth (see Table 11)

\* Uterine arteries occluded bilaterally.

† Uterine arteries patent through the bands bilaterally.



ology in various animals including primates, has been using approaches quite similar to our own; his results and opinions harmonize with ours. Recently he has been investigating the effects of certain drugs upon human and monkey placentas *in vitro*. Our collaborative project carried forward this study into the living animal. A week's intensive work produced pilot studies on the effects of several drugs administered to the monkey under various conditions. These pilot studies have opened up a number of promising avenues for further investigation; during May some of these leads were followed up, and others will be pursued in the next monkey pregnancy season.

Recognizing that even tentative deductions or conclusions are still premature, the nature of the studies to date may be summarized as follows:

*1-Epinephrine.* The drug was administered separately to the fetus or the mother, usually intra-arterially. Blood pressure and uterine activity were monitored continuously and uteroplacental circulation was visualized radiographically. Our data suggest that the administration of 25  $\mu$ gm or more of 1-epinephrine to the mother completely obliterates inflow ("spurts") to the intervillous space. It is of interest that the administration of this drug either to the mother or to the fetus has no visible effect on filling of the fetal placental vascular bed. Regardless of whether the drug is given to the mother or the fetus, all doses in excess of 5  $\mu$ gm have an hypertensive effect on both the mother and the fetus, suggesting transplacental passage. For comparable doses, the effect on maternal hypertension is of the same order whether the drug is given to the fetus or intravenously to the mother. If the drug is given intra-arterially (into the aorta) to the mother, the hypertensive effect is only about 50% of that seen with intravenous injection.

*5 Hydroxytryptamine.* 5 HT has a vasoconstrictive effect which causes an

increase in maternal blood pressure while effectively reducing uteroplacental blood flow. Additional studies suggest that this effect is independent of the drug's effect on uterine activity and thus related to a direct vascular action. The effect of 5 HT on uteroplacental circulation seems to be dose related; our data suggest that this effect is significant when the intra-arterial dose exceeds 2  $\mu$ gm. A single study in which the drug was administered to the fetus shows no decrease in the filling of the fetal placental vascular bed even though increase in fetal and maternal blood pressure occurred.

*Vasopressin.* Our data indicate that vasopressin has a marked vasoconstrictive effect which reduces uteroplacental circulation when the drug is administered intra-arterially to the mother and causes hypertension of essentially the same magnitude regardless of whether the drug is given to the mother or to the fetus. Since the vasopressin used contained small amounts of oxytocin contaminant, additional studies which confirmed no direct uteroplacental vascular effect of the oxytocin were performed.

In summary, each of the three vasoactive drugs effectively reduces blood flow through the placenta. This effect apparently is in direct relationship to the administered dose. All of the drugs seem to cross the placenta in both directions.

#### *Morphology of the Fetal Villus as Determined by Phase Contrast Microscopy*

Phase contrast microscopic examination of the recently delivered placenta has added an important modality to the conventional techniques that have been used to study the placenta. This new technique enables us to study the morphology of the terminal villus, the functional unit of the placenta, in its viable state and without the alterations that are induced by fixation and staining. Using this technique, a number of

abnormalities can be readily identified that would be obscured by standard histologic techniques, e.g., syncytial growth activity in the form of sprouts, varying degrees of villous edema, and a more precise assessment of the relationship of the fetal capillary to the intervillous space, to name but a few. The correlation between some of these abnormalities and the clinical course of the neonate is good. This correlation is good enough, in fact, to have led some investigators to perform percutaneous, transabdominal placental biopsies to obtain placental tissue for phase contrast microscopic examination as another method of assessing the well-being of the fetus.

At present the perfection and application of this technique has surpassed the understanding of the pathogenesis of the lesions that can be described. Until such time as the etiology of these lesions is understood, placental biopsy and phase contrast examination of the fetal placental tissue will have limited usefulness.

We have initiated a program of investigation in the rhesus monkey which is designed to study the pathogenesis of these lesions. The initial problem to be solved is the description of the normal monkey placenta at all stages of pregnancy and simultaneously the determination of the morbidity that accompanies placental biopsy.

Our experience thus far is extremely limited and permits us to state only that the morphology of the monkey fetal villi is similar but not identical to the human and that serial placental biopsies in a few animals between the 70th and 100th days of pregnancy have not resulted in fetal death or abortion.

After these baselines have been established, we will take advantage of the bidiscoid placenta of most rhesus monkeys to study the effect of a variety of agents on the fetal villi of one disc while the remaining disc serves as the control.

### *Ovarian Tumors in Rhesus Monkeys*

Among the 75 rhesus monkeys studied in the Carnegie colony during the five-year period 1964-1968 ovarian tumors were encountered in three animals. In the first case, a large intra-abdominal mass palpated in a newly purchased monkey was found at laparotomy to be a multilocular cystic tumor, histologically a papillary serous cystadenoma of the ovary with evidences of low-grade malignancy. In the second, a large benign cystic teratoma (dermoid cyst) was discovered during laparotomy in a pregnant animal that had lived in the Carnegie colony for two years. This animal had received X-irradiation during previous pregnancies but no ovarian enlargement was detected at laparotomy in preceding years. The third case, also encountered incidentally at laparotomy during pregnancy, was a cavernous hemangioma almost entirely replacing the right ovary.

Only 12 ovarian neoplasms in rhesus monkeys have previously been recorded in the world literature, eight of them benign, four malignant. No hemangioma had been reported until the present case.

### *The Monkey Colony*

The 31 females and three males in the colony have been maintained in excellent health by the skilled and devoted team of Messrs. Abbott, Cleary, and Wilmoth. The pregnancy rate has been one of the highest in the colony's history, 74% up to the 15th of March when vaginal smearing and breeding were discontinued because of the colony's forthcoming removal to Chicago. In previous years several additional pregnancies have occurred between March 15 and July 1, so this year's rate might have reached an even more impressive figure had breeding been continued for the full season.

A total of 32 experiments have been performed on the 23 pregnant animals of

the colony plus an additional one which was already pregnant when purchased. As before, the magnificent facilities of the Radiology Research Laboratory at Johns Hopkins Hospital have been avail-

able to us and have made possible much of the work reported above. The skill of the technical staff, in particular of Mrs. Mary Grove, has been an important factor in the success of the experiments.

## THE COLLECTION OF HUMAN EMBRYOS

*E. M. Ramsey and R. O'Rahilly*

The Collection was enlarged by the accession of six specimens out of the 21 submitted by five physicians in two Maryland cities and two out of state. Both the number submitted and the percentage of them deemed worthy of permanent preservation was low. This is a continuation of the trend of recent years, resulting from our discontinuance of active solicitation of contributions.

Of the specimens saved, two were valuable museum specimens, three were important specimens suitable for histological study and the sixth was an addition to our collection of rubella cases.

During the year, the previously accumulated group of 24 specimens from cases of maternal rubella, which had been sent in 1967 to Dr. Lorenz Zimmerman of the Division of Ophthalmic Pathology of the Armed Forces Institute of Pathology, was returned to the Institution, as Dr. Zimmerman had concluded his work in the field. This material will be of significant assistance in O'Rahilly's ophthalmologic studies.

### DEVELOPMENTAL STAGES IN HUMAN EMBRYOS

In the year under review, Dr. Ronan O'Rahilly has made substantial progress in his survey of the Collection. Attention is being concentrated initially on the serial sections of human embryos. Although a few are still unstaged, some 595 sectioned embryos (up to 32 mm C.-R.) have been staged and are now being tabulated with reference to their measurements, grade, fixative, plane of section, thinness of section, stain, and donor. This tabulation will be incorpo-

rated into a monograph on "Developmental stages in human embryos, being a survey of the Carnegie Collection." The monograph will comprise an account of stages 1 to 9, which have not yet been collated, together with a revision of stage 10 (Heuser and Corner) and stages 11 to 23, as described by Streeter. The term "developmental horizon" is being replaced by "stage," Arabic numerals will be used instead of Roman (thereby conforming to chick and amphibian staging), the timing will no longer be based on the macaque, references to both recent and older literature will be cited, and an index is to be provided. A number of unsatisfactory terms, such as arm bud, leg bud, extremity (in the sense of limb), and anterior and posterior neuropores, are to be replaced.

### *Development of the Heart*

Studies of the development of the human heart, begun by O'Rahilly initially in collaboration with Miss M. H. Cooper, of St. Louis University, have been continued and expanded, and an article is due to appear in *Acta Anatomica*. The principal findings may be summarized as follows:

The human heart at seven postovulatory weeks (chiefly stages 19, 20, and 21), a period largely neglected previously, was studied. Noteworthy changes occur at that time: (1) the septum secundum appears at any stage from 18 to 21; (2) the secondary interventricular foramen becomes obliterated either during stage 18 or during stage 19; (3) the myocardium becomes considerably thickened in both the atria and the ventricles;



and (4) the subepicardial layer of the epimyocardial mantle spreads from the atrioventricular sulcus to the external surface of the ventricles.

Embryonic hearts that have been described in the literature and that are also clearly assignable to one of the recognized embryonic stages from 9 (initial appearance of the cardiac plexus at three postovulatory weeks) to 23 (end of the embryonic period proper at eight postovulatory weeks) are listed in a compre-

hensive table, which serves as a source of reference to early cardiac development in the human.

#### *Development of the Larynx*

A study of the development of the larynx in staged human embryos has been begun by O'Rahilly in collaboration with Dr. John A. Tucker, Department of Bronchology, Esophagology, and Laryngeal Surgery, University of Pennsylvania.

### STAFF ACTIVITIES

Among the symposia and conferences in which various members of the staff participated during the past year were the following:

Ninth International Embryological Conference (Moscow); Workshop on Morphogenetic Tissue Interactions (Helsinki); Third International Congress on Congenital Malformations (The Hague); Lepetit Symposium on RNA Polymerase and Transcription (Florence); Sixth World Congress of Gynaecology and Obstetrics (New York); Symposium on Blastocyst Biology (Lake Wilderness, Washington); Conference on Reproductive Physiology (Chapel Hill, North Carolina); Thirty-Fifth Cold Spring Harbor Symposium (RNA Transcription); and the Brook Lodge Conference on Immunological Surveillance (Kalamazoo, Michigan).

Lectures were presented on a number of campuses including Boston University, California Institute of Technology, Cornell University Medical College, Goucher College, Kansas State University, Morgan State College, Stanford University School of Medicine, State University of New York at Buffalo, State University of New York at Stony Brook, Syracuse University, the Universities of California (Santa Cruz), Colorado, Maryland, Massachusetts, Palermo, Pittsburgh, Rochester, and Vermont, Wright State University, and Yale University.

Special presentations included the G. D. Searle Lecture in Reproductive Biology at the Medical College of Virginia, and a series of lectures at the National University of Mexico.

Members of the staff also spoke at a number of hospitals and research centers, including Beth Israel Medical Center (New York), Columbia Hospital for Women (Washington, D.C.), Marine Biological Laboratory (Woods Hole, Massachusetts), and the New England Primate Center (Southborough, Massachusetts).

Members of the group took part in meetings of a number of learned societies, including, in addition to those already mentioned, the American Association of Anatomists, American Association for the Advancement of Science, American College of Obstetricians and Gynecologists, American Philosophical Society, American Society of Biological Chemists, American Society for Cell Biology, Association of Professors of Gynecology and Obstetrics, Biophysical Society, Cardiac Muscle Society, Federation of American Societies for Experimental Biology, National Academy of Sciences, National Society for Medical Research, Society for Experimental Biology and Medicine, Society for Gynecologic Investigation, and Tissue Culture Association.

Advisory and consultative services

included membership on the editorial boards of *Anales del Desarrollo*, *Developmental Biology*, *In Vitro*, *Journal of Cell Biology*, *Journal of Embryology and Experimental Morphology*, *Excerpta Medica* (section on Human Developmental Biology), *Current Topics in Developmental Biology*, and *Quarterly Review of Biology*.

Members of the staff continued to serve on the University Science Development Advisory Panel, National Science Foundation; and the Visiting Committees of the Departments of Biology of Harvard University, Princeton University, State University of New York (Buffalo), and University of Oregon. In addition, service was rendered on Advisory Committees of the Center for Oral Health Research (University of Pennsylvania) and the International Institute for the Study of Human Reproduction (Columbia University).

Members of the staff also acted in these capacities: Member of the Board of Scientific Overseers, Jackson Laboratory; Trustee and Director-designate, Marine Biological Laboratory; Member of the Board of Scientific Counselors, National Cancer Institute; Member of the Board of Directors, Oak Ridge Associated Universities; and Vice President, Maryland Academy of Sciences.

Other posts occupied by members of the Department include the following: in the American Association for the Advancement of Science, Committee on Science in the Promotion of Human Welfare and Newcomb Cleveland Prize Committee (Chairman); in the Ameri-

can Association of Anatomists, Representative to Division of Medical Sciences of the National Research Council and Representative to the National Society for Medical Research; in the American Institute of Biological Sciences, Chairman of the Committee on Laboratory Animal Care, member, Public Responsibilities Committee and Council of Past Presidents; in the American Society of Zoologists, President; in the National Institutes of Health, member, Cell Biology Study Section; and in the Society for Developmental Biology, Member of Executive Committee.

Formal teaching has been largely confined to the Johns Hopkins Department of Biology, but during the year, lectures were offered in other departments of the University as well, among them Anatomy, Biophysics, Medicine, Obstetrics and Gynecology, and Pediatrics.

*Seminars.* The roster of speakers at the seminars organized by the Department to serve all those working in developmental biology in the region included Michael V. L. Bennett (Albert Einstein School of Medicine); Gary Conrad (University of Chicago); J. Daillie (Université de Lyon); David Epel (Stanford University); Barry Fry (Massachusetts Institute of Technology); Paul Gross (Massachusetts Institute of Technology); Lloyd Guth (National Institutes of Health); Fotis Kafatos (Harvard University); David Luck (Rockefeller University); M. Muramatsu (Japanese Foundation for Cancer Research); G. Stöfler (Max Planck Institut, Berlin).

## BIBLIOGRAPHY

Böving, B. G., *Review of A Survey of Embryology*, by F. G. Gilchrist. *BioScience*, 19, 658-659, 1969.

Böving, B. G., *Review of Traek af Prostatahypertrofien Historie*, by L. Lauridsen. *Bull. Hist. Med.*, 44, 96-97, 1970.

Böving, B. G., Human development. *Encyclopaedia Britannica*. pp. 325-328, 1970.

Böving, B. G., The force and nature of blastocyst propulsion by rabbit uterus. *Anat. Rec.*, 166, 413, 1970.

Böving, B. G., *see also* Tuft, P. H.

Brown, D. D., *Review of Nuclear Physiology and Differentiation*, by R. P. Wagner and E. A. Eakin. *Science*, 168, 566-567, 1970.

- Brown, D. D., and I. B. Dawid, Developmental genetics. *Ann. Rev. Genet.*, **3**, 127-154, 1969.
- Brown, D. D., *see also* Dawid, I. B.; Hallberg, R. L.; Miller, L.; Reeder, R. H.; Roeder, R. G.
- Coon, H. G., and M. C. Weiss, Sendai produced somatic cell hybrids between L cell strains and between liver and L cells. In *Heterospecific Genome Interaction*, V. Defendi, ed., Wistar Institute Press, Philadelphia, pp. 83-96, 1969.
- Dawid, I. B., and D. D. Brown, The mitochondrial and ribosomal DNA components of oocytes of *Urechis caupo*. *Develop. Biol.* **22**, 1-14, 1970.
- Dawid, I. B., *see also* Brown, D. D.; Swanson, R. F.
- DeHaan, R. L., Electrical recording from embryonic heart cells isolated in tissue culture. In *Comparative Physiology of the Heart: Current Trends*, F. V. McCann, ed., Birkhauser Verlag, Basel, pp. 174-175, 1969.
- DeHaan, R. L., The cellular basis of morphogenesis in the embryonic heart. In *Pathophysiology of Congenital Heart Disease*, F. H. Adams, ed., University of California Press, Berkeley, pp. 7-15, 1970.
- DeHaan, R. L., Embryology of the heart. In *The Heart*, J. W. Hurst and R. B. Logue, eds., McGraw-Hill, New York, Second Edition, pp. 7-20, 1970.
- DeHaan, R. L., Cardiac development: A problem in need of synthesis. *Amer. J. Cardiol.*, **25**, 139-140, 1970.
- DeHaan, R. L., guest editor, Symposium issue, Development and ultrastructure of the embryonic heart. Part one. *Amer. J. Cardiol.*, **25**, 139-226, 1970; Part two. *Ibid.*, **25**, 265-310, 1970.
- DeHaan, R. L., and E. W. Schaefer, Jr., The potassium-inhibition threshold of individual pacemaker cells isolated from the embryonic chick heart. *In Vitro*, **6**, A105, 1970.
- Ebert, J. D., Morphogenetic tissue interactions. *Science*, **166**, 1314-1316, 1969.
- Ebert, J. D., Closing Remarks. In *Nucleic Acid Metabolism, Cell Differentiation and Cancer Growth*, E. V. Cowdry and S. Seno, eds., Pergamon Press, Oxford, U. K., p. 469, 1969.
- Ebert, J. D., *Review of Cellular Differentiation* by J. R. Whittaker. *Quart. Rev. Biol.*, **44**, 308-309, 1969.
- Ebert, J. D., Diferenciacion celular y susceptibilidad viral. II Congreso de la Academia Nacional de Medicina. Memorias. Volumen II, Mesas Redondas, pp. 83-98, 1969.
- Ebert, J. D., *Review of Gene Activity in Early Development*, by E. H. Davidson. *Quart. Rev. Biol.*, **45**, 75-76, 1970.
- Ebert, J. D., *Review of Cellular Immunology and Self and Not-Self*, both by MacFarlane Burnet. *Science*, **167**, 1608, 1970.
- Ebert, J. D., Cellular differentiation and viral susceptibility (in Russian). *Ontogenesis*, **1**, 341-361, 1970.
- Ebert, J. D., and I. M. Sussex, *Interacting Systems in Development*, second ed., Holt, Rinehart and Winston, New York, pp. 1-338, 1970.
- Ebert, J. D., *see also* Yoshikawa-Fukada, M.
- Fambrough, D. M., Acetylcholine Sensitivity of Muscle Fiber Membranes: Mechanism of Regulation by Motoneurons. *Science*, **168**, 372-373, 1970.
- Garcia-Bunuel, R., *see* Misenhimer, H. R.
- Hallberg, R. L., and D. D. Brown, Co-ordinated synthesis of some ribosomal proteins and ribosomal RNA in embryos of *Xenopus laevis*. *J. Mol. Biol.*, **46**, 393-411, 1969.
- Hay, R. J., Cell strain senescence *in vitro*: Cell culture anomaly or an expression of a fundamental inability of normal cells to survive and proliferate. In *Aging in Cell and Tissue Culture*, V. J. Cristofalo and E. Holeckova, eds., Plenum Press, New York, pp. 7-24, 1970.
- Hirakow, R., Ultrastructural characteristics of the mammalian and sauropsidan heart. *Amer. J. Cardiol.*, **25**, 195-203, 1970.
- Manasek, F. J., Embryonic development of the heart. II. Formation of the epicardium. *J. Embryol. Exp. Morphol.*, **22**, 233-248, 1969.
- Manasek, F. J., Appearance of granules in the Golgi complex of embryonic cardiac myocytes. *J. Cell Biol.*, **43**, 605-610, 1969.
- Manasek, F. J., Histogenesis of the embryonic myocardium. *Amer. J. Cardiol.*, **25**, 149-168, 1970.
- Miller, L., and D. D. Brown, Variation in the activity of nucleolar organizers and their ribosomal gene content. *Chromosoma (Berl.)*, **28**, 430-444, 1969.
- Misenhimer, H. R., and R. Garcia-Bunuel, Failure of intrauterine contraceptive device and fungal infection in the fetus. *Obstet. Gynecol.*, **34**, 368-372, 1969.
- Ramsey, E. M., New appraisal of an old organ: the placenta. *Proc. Amer. Phil. Soc.*, **113**, 296-304, 1969.
- Reeder, R. H., and D. D. Brown, The fidelity of transcription of *Xenopus* ribosomal RNA



- genes by bacterial RNA polymerase. *J. Cell Biol.*, 43, 114a, 1969.
- Reeder, R. H., and D. D. Brown, The fidelity of transcription of the ribosomal RNA genes from a toad by bacterial RNA polymerase. In *First Lepetit Colloquium on RNA Polymerase and Transcription*, L. Silvestri, ed., North Holland Publishing Co., Amsterdam, pp. 249-259, 1970.
- Schaefer, E. W., Jr., see DeHaan, R. L.
- Stalsberg, H., Regional mitotic activity in the precardiac mesoderm and differentiating heart tube in the chick embryo. *Develop. Biol.*, 20, 18-45, 1969.
- Sussex, I. M., see Ebert, J. D.
- Swanson, R. F., and I. B. Dawid, The mitochondrial ribosome of *Xenopus laevis*. *Proc. Nat. Acad. Sci. U.S.*, 66, 117-124, 1970.
- Tuft, P. H., and B. G. Böving, The forces involved in water uptake by the rabbit blastocyst. *J. Exp. Zool.*, 174, 165-172, 1970.
- Yoshikawa-Fukada, M., and J. D. Ebert, Hybridization of RNA from Rous sarcoma virus with cellular and viral DNAs. *Proc. Nat. Acad. Sci. U.S.*, 64, 870-877, 1969.

## PERSONNEL

*Year Ended June 30, 1970*

(including those whose services began or ended during the year)

*Research Staff*

Bent G. Böving, Physiology  
 Donald D. Brown, Biochemistry  
 Igor B. Dawid, Biochemistry  
 Robert L. DeHaan, Experimental Embryology  
 James D. Ebert, Director  
 Douglas M. Fambrough, Biochemistry  
 Elizabeth M. Ramsey, Placentology and Pathology  
 Ronald H. Reeder, Biochemistry

*Assistant Investigator*

Robert J. Hay

*Research Associates (extramural)*

Louis B. Flexner, Philadelphia  
 Arthur T. Hertig, Boston  
 Irwin R. Konigsberg, Charlottesville

*Fellows*

Masako Fukada, Fellow of Carnegie Institution of Washington  
 Leonard P. Gage, Fellow of U. S. Public Health Service  
 Reiji Hirakow, Fellow of Carnegie Institution of Washington  
 Harold R. Misenhimer, Fellow of Carnegie Institution of Washington  
 Ronan O'Rahilly, Fellow of Carnegie Institution of Washington

Eijiro Ozawa, Fellow of Carnegie Institution of Washington  
 Robert G. Roeder, Fellow of American Cancer Society  
 Yoshiaki Suzuki, Fellow of Carnegie Institution of Washington  
 Ronald F. Swanson, Fellow of U. S. Public Health Service

*Students*

John Chase, Graduate, Johns Hopkins University  
 John O. Dunning, Graduate, Johns Hopkins University  
 H. Criss Hartzell, Jr., Graduate, Johns Hopkins University  
 Mary Kennedy, Graduate, Johns Hopkins University  
 Dennis E. Leister, Graduate, Johns Hopkins University  
 Edward W. Schaefer, Undergraduate, Johns Hopkins University  
 Malcolm M. Smith, Graduate, Johns Hopkins University  
 Ralph Stern, Graduate, Johns Hopkins University  
 Thomas G. Storch, Johns Hopkins University School of Medicine  
 Marjorie A. Tiefert, Graduate, Johns Hopkins University  
 Doreen Ward, Graduate, Johns Hopkins University  
 Pieter C. Wensink, Graduate, Johns Hopkins University

*Visiting Investigators*

J. Daillie, Lyon, France  
 Martin W. Donner, Baltimore, Md.  
 Toyooki Fujimoto, Kumamoto, Japan  
 Raymond F. Gasser, New Orleans, La.  
 Daniel Goor, New York, N. Y.  
 Peter Gruenwald, Philadelphia, Pa.  
 Edward Herbst, Durham, N. H.  
 Takeshi Hoshino, Worcester, Mass.  
 Leslie Iffy, Philadelphia, Pa.  
 Stanley I. Margulies, Baltimore, Md.  
 Chester B. Martin, Jr., Los Angeles, Calif.  
 M. Muramatsu, Tokyo, Japan  
 Maurice Panigel, Paris, France  
 Glenn C. Rosenquist, Baltimore, Md.  
 Bernice F. Stratford, Parkville, Victoria,  
 Australia  
 John A. Tucker, Philadelphia, Pa.  
 Branislav Vidic, St. Louis, Mo.

*Clerical and Technical Staff*

James E. Abbott, Recorder  
 Grace M. Andrews, Secretary-Receptionist  
 Mary N. Barton, Librarian (part time)  
 James Blackwell, Custodian  
 William J. Cleary, Recorder  
 William H. Duncan, Senior Technician  
 Ernestine V. Flemmings, Laboratory  
 Helper  
 Richard D. Grill, Photographer  
 Ernest Harper, Chief Custodian

<sup>1</sup> Died, May 16, 1970.

Virginia Hicks, Laboratory Helper  
 Eddie Jordan, Technician  
 Nancy Joseph, Technician  
 Patricia M. Lamdin, Secretary  
 Edna G. Lichtenstein, Secretary  
 Alice H. Mabin, Laboratory Helper  
 Thomas F. Malooly, Business Manager  
 Juanita Mandy, Laboratory Helper  
 Kathleen A. O'Connell, Technician  
 John Pazdernik, Building Engineer  
 Betty Lou Phebus, Bookkeeper-Clerk  
 Conrad Pott, Custodian <sup>1</sup>  
 Diane M. Prather, Technician  
 Margaret J. Proctor, Secretary  
 Martha Rebbert, Technician  
 Bessie Smith, Laboratory Helper  
 Delores Somerville, Technician  
 Leroy Williams, Custodian  
 David Wilmoth, Assistant Recorder  
 John L. Wiser, Machinist

*Student Assistants*

Paul Fishman, Johns Hopkins University  
 Nancy Kolzak, Smith College  
 Barbara Mann, New Mexico State Uni-  
 versity  
 Donna S. Minor, Morgan State College  
 Lauren E. Pepersack, Towson State Col-  
 lege  
 Jeff Sollins, Drew University  
 Roberta Truitt, Morgan State College

PLATES





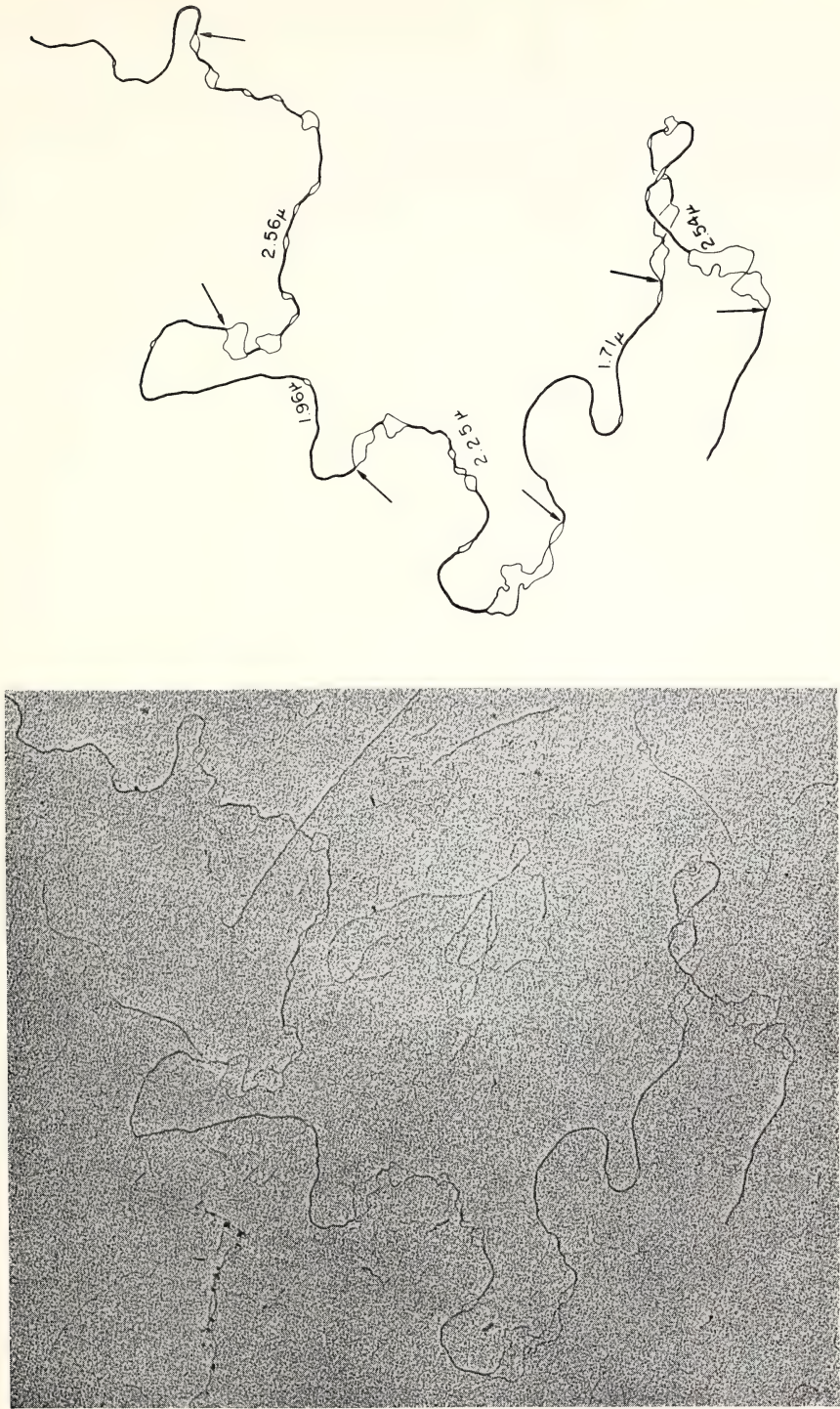


Plate 1. Partially denatured molecule of rDNA. See text for description.



Plate 2. (A) Karyotype of the Chinese hamster, divided into three size-groups. (B), (C), and (D) fractionated chromosomes. Logarithmically growing Chinese hamster cells in suspension culture were treated with  $0.1 \mu\text{g/ml}$  of vinblastine sulfate for 5 hours. Collected cells were washed and incubated in a hypotonic buffer for 10 minutes. Swollen metaphase cells were broken by suspending in  $\text{pH } 3$  buffer containing  $1 \text{ mM}$  of  $\text{Mg}^{++}$  and  $\text{Ca}^{++}$ . Released metaphase chromosomes were purified and fractionated by sucrose density gradient centrifugation. The final preparation was fixed in methanol: acetic acid ( $3=1$ ) and stained in buffered Giemsa. (E) Immature myotube 40 hours after seeding of cells isolated by DA method and 66 hours after infection with RSV. Phase contrast,  $\times 250$ . (F) Large mature myotube 116 hours after seeding and 132 hours after infection. Phase contrast,  $\times 250$ .



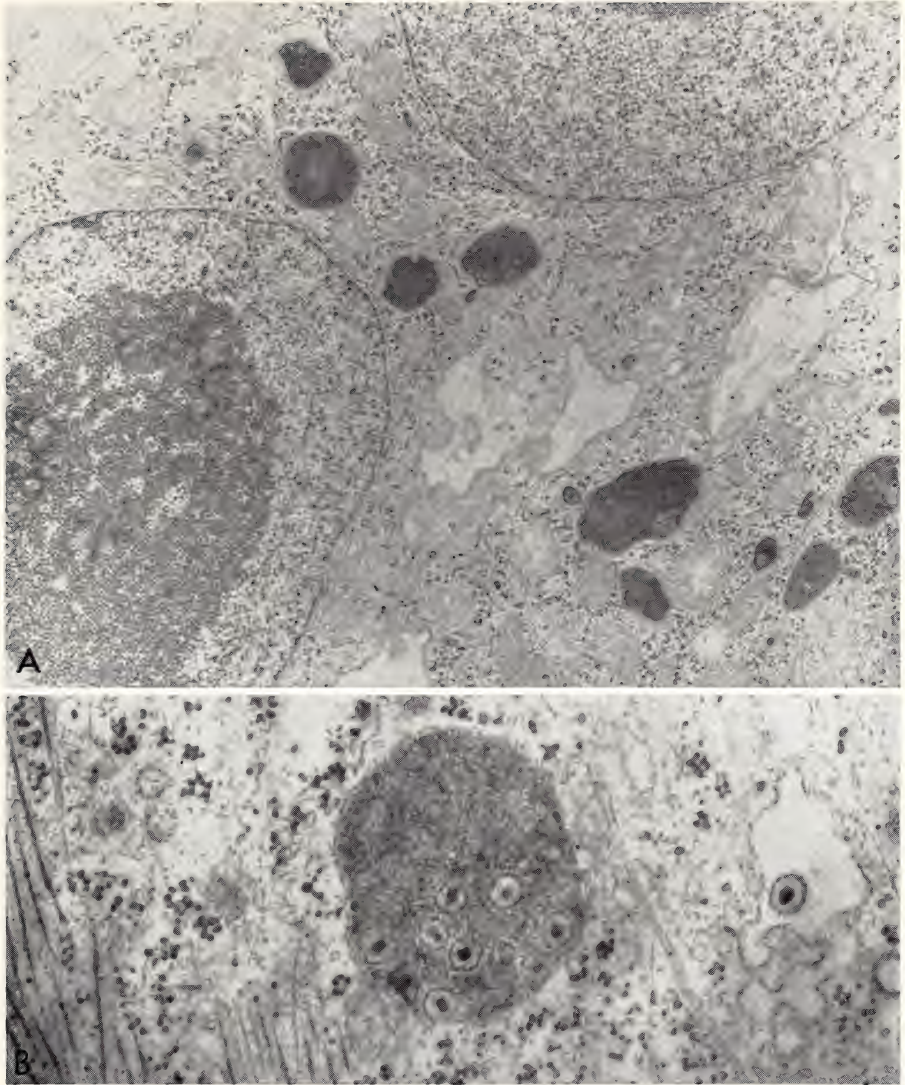


Plate 3. (A) Electron micrograph of myotube from a culture which was infected at time of DA cell seeding and fixed 72 hours later.  $\times 10,580$ . (B) Higher magnification of a myotube from the same preparation as in A, showing a dense body with immature virus particles approximately  $90\text{ m}\mu$  in diameter. Note the presence of a particle of similar size in the electron lucent vesicle.  $\times 32,980$ .

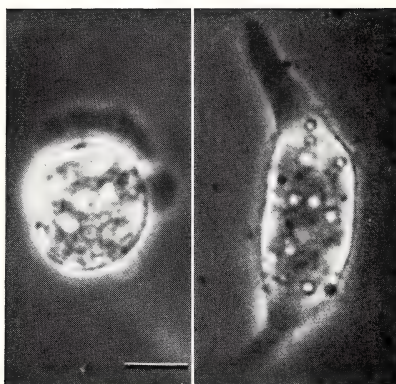


Plate 4. Two examples of isolated beating myocytes which differentiated in culture 48 hours after having been dissociated from a group stage 6-6+ embryos. Scale =  $20\mu$ .

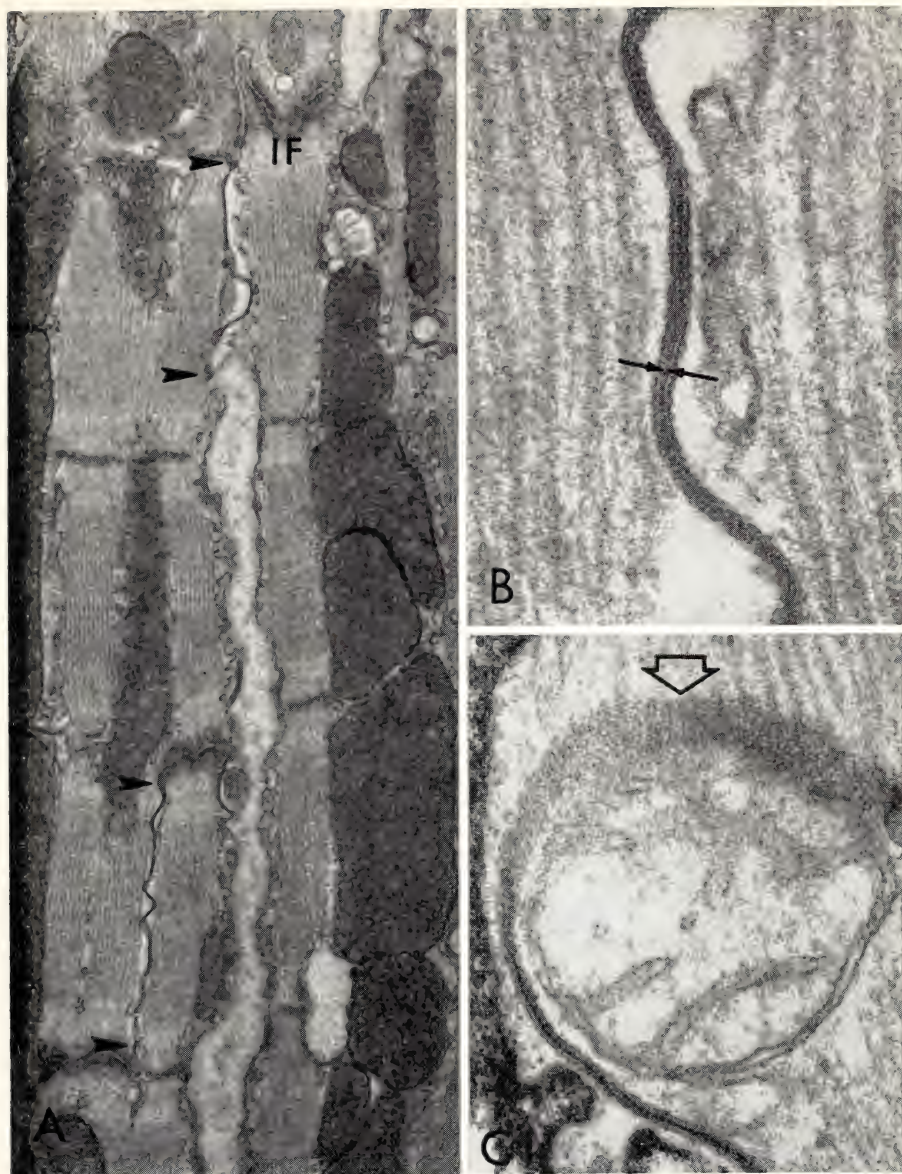


Plate 5. Close cell junction (nexus) between myocardial cells of the adult mouse right ventricle. (A) Low magnification to show the extent and location of nexal regions, seen as dense lines between the arrows. At top of photo, cell boundaries lie perpendicular to the fiber axis as part of an intercalated disc, separating the myofibrils of one cell from another at an interfibrillar (*IF*) region.  $\times 16,800$ . (B) Higher magnification of a nexal junction. A gap of about 20 Å separates the outer leaflets of the apposed plasma membranes (arrows).  $\times 168,000$ . (C) Ventricular tissue treated with ruthenium red to show the hexagonal array of subunits in the gap junction at a site cut tangential to the surface (open arrow). Where the plasma membranes are cut normally (lower left) the junctional gap is seen to be filled with the dense dye.  $\times 120,000$ .



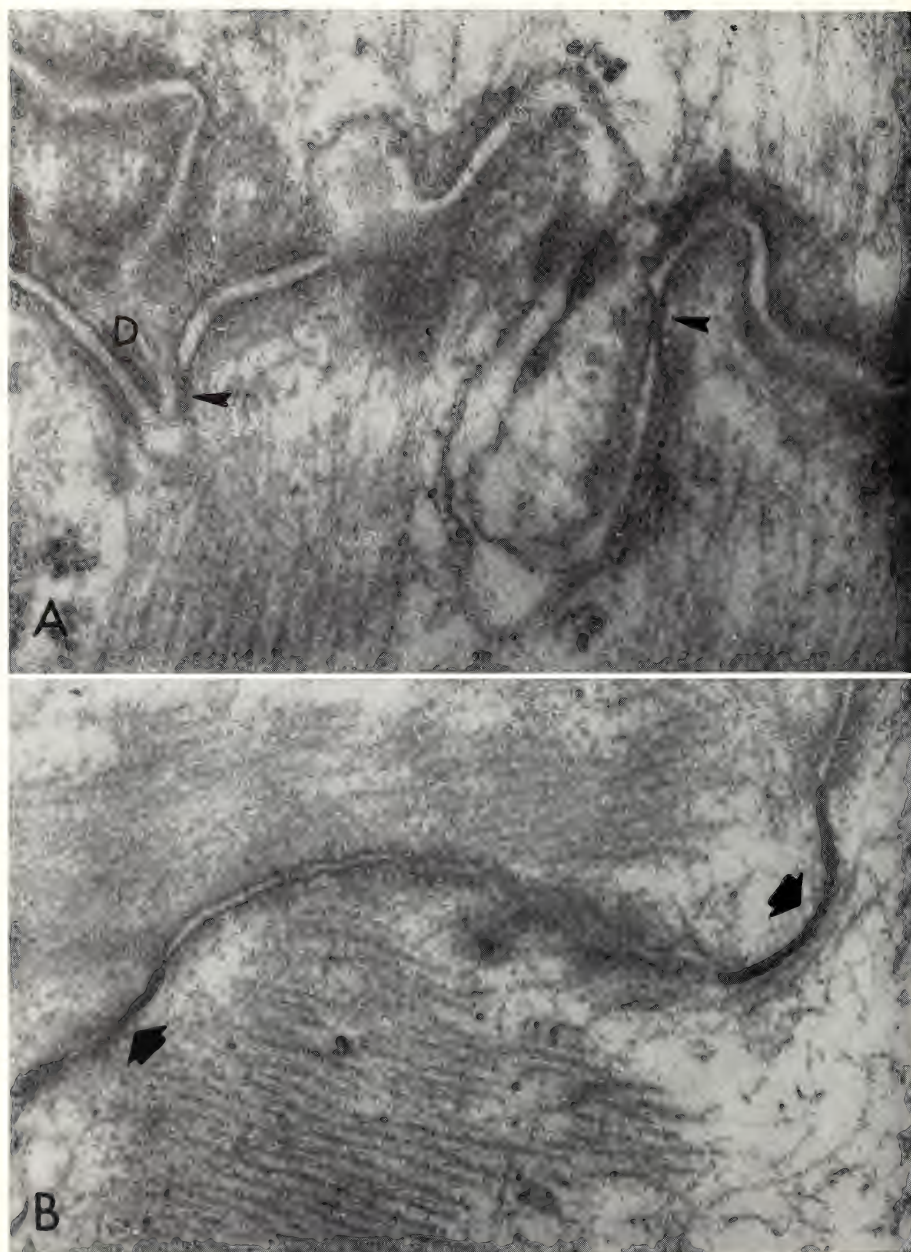


Plate 6. Contact area between cardiac cells of adult chicken right ventricle. (A) Typical intercalated disc crossing the myofibers between two ordinary myocytes. The interspace between the apposed membranes is characteristically 150-250 Å. Small nexal-like areas of close apposition are indicated by arrows.  $\times 91,200$ .

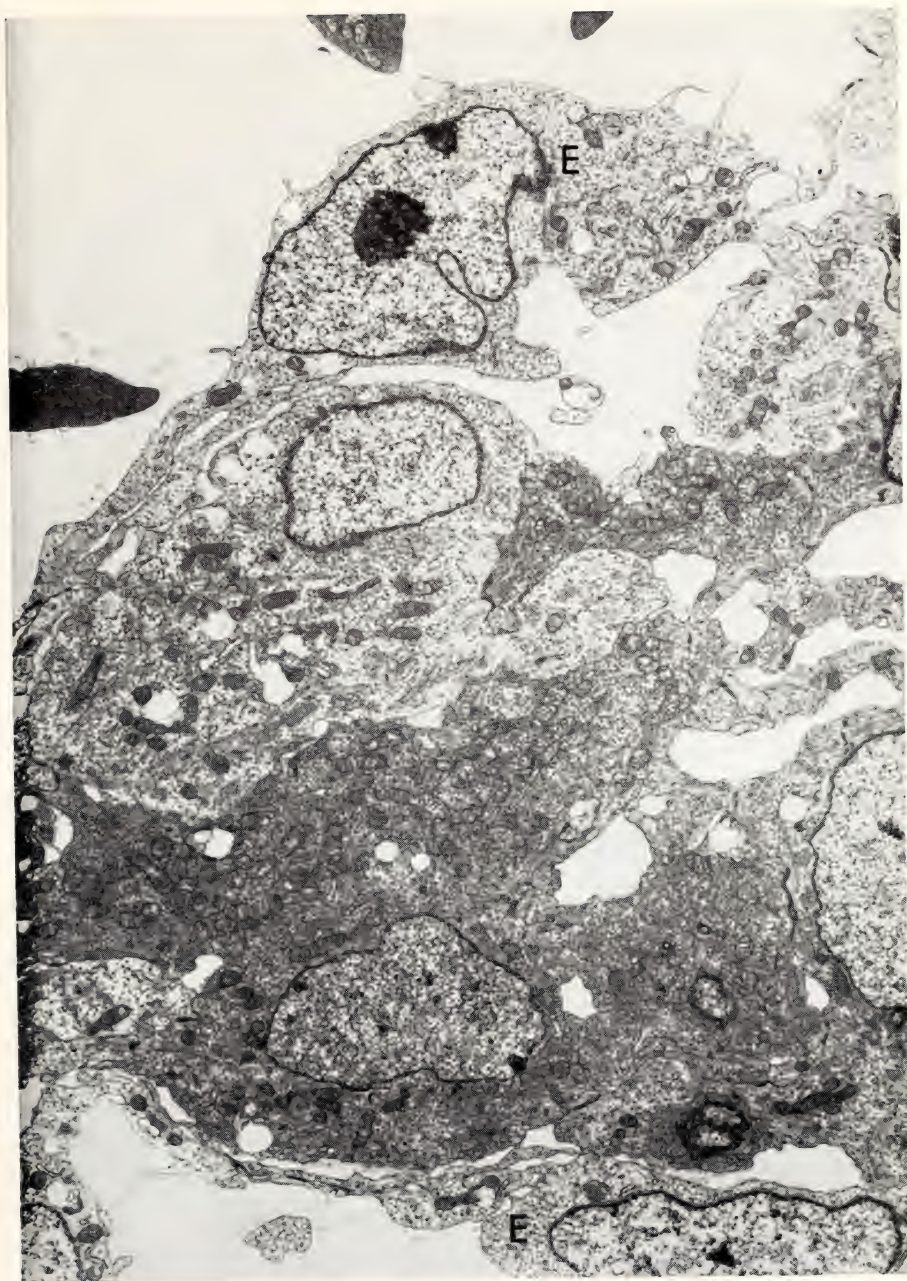


Plate 7. Trabecular tissue of the 6-day embryonic chick ventricle. Endocardial cells (*E*) surround the young muscle cells. Large intercellular spaces are apparent. In this preparation, most of the glycogen has been extracted by treatment with uranylacetate.  $\times 5000$ .



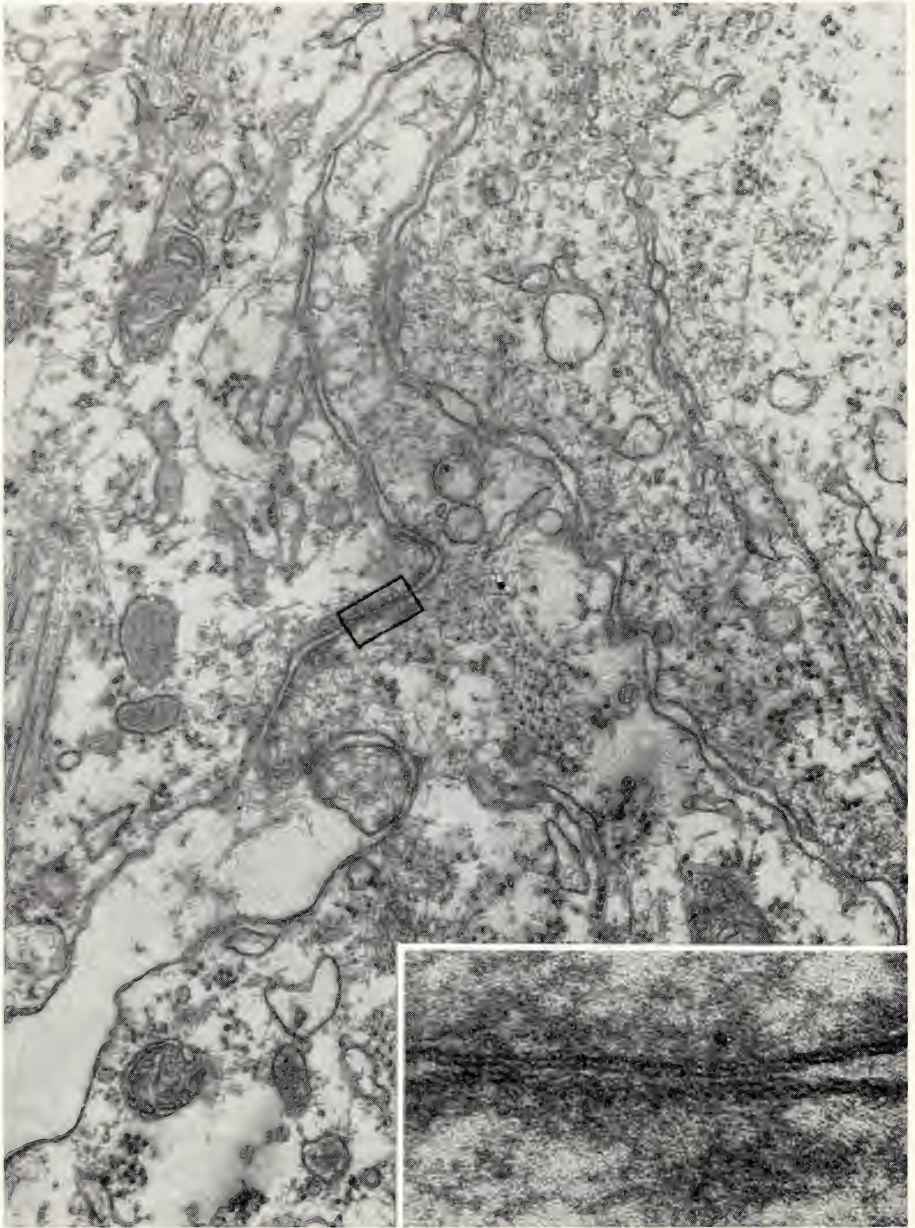


Plate 8. Contact area between cardiac cells of 6-day embryonic chick ventricle. Area of close apposition is circumscribed by a rectangle and enlarged in the inset. The structure of this close junction is not identical either with the typical gap junction in the adult or with "focal tight junctions" seen between mesoderm cells of the early embryo.  $\times 39,200$ . Inset  $\times 240,000$ .



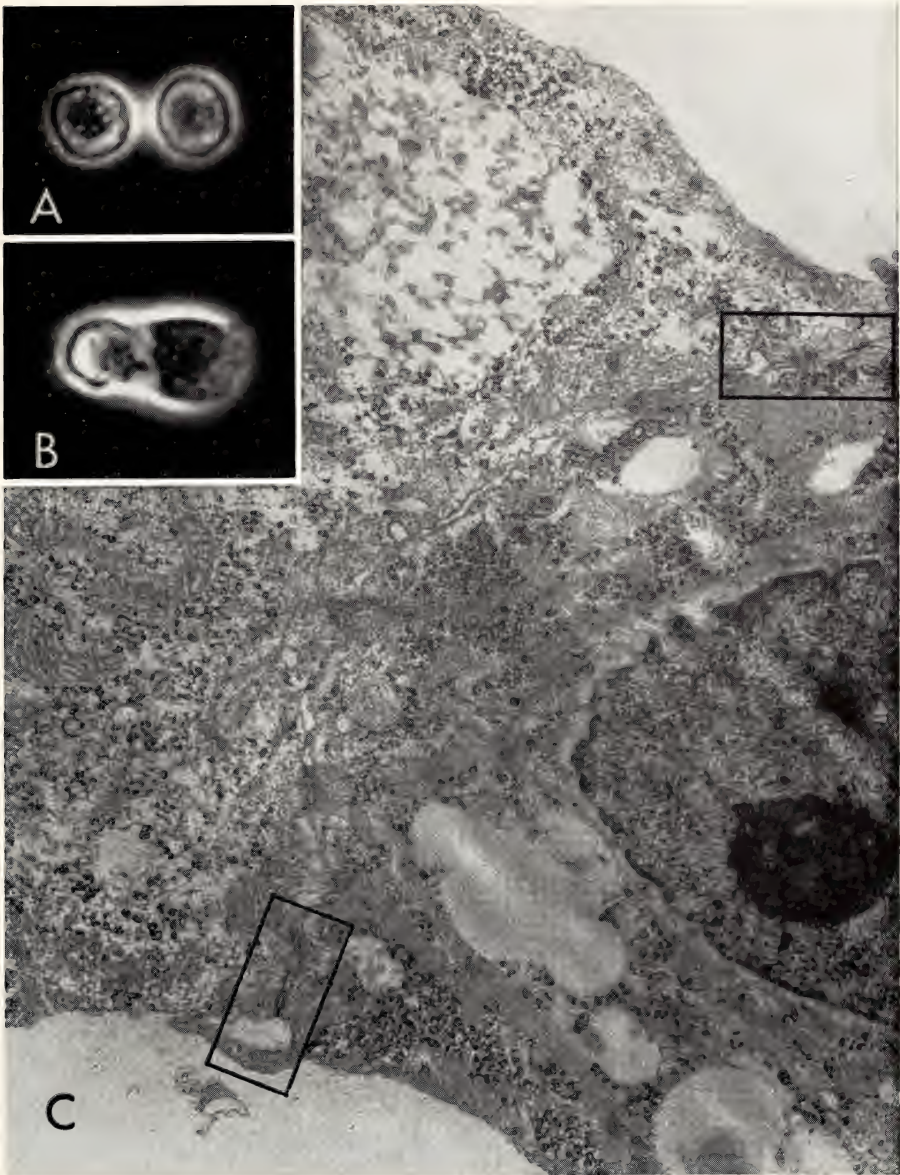


Plate 9. Cultured pair of beating myocytes from 7-day embryonic heart. (A) Photographed live with phase optics about 6 hours after the cells were plated. Cells about 4 micra apart at closest point, each beating at its own rhythm.  $\times 800$ . (B) Same cells after contact has been established and cells have synchronized to a common rhythm.  $\times 800$ . (C) Electron micrograph of contact region between same cells fixed 2 minutes after (B).  $\times 19,300$ .

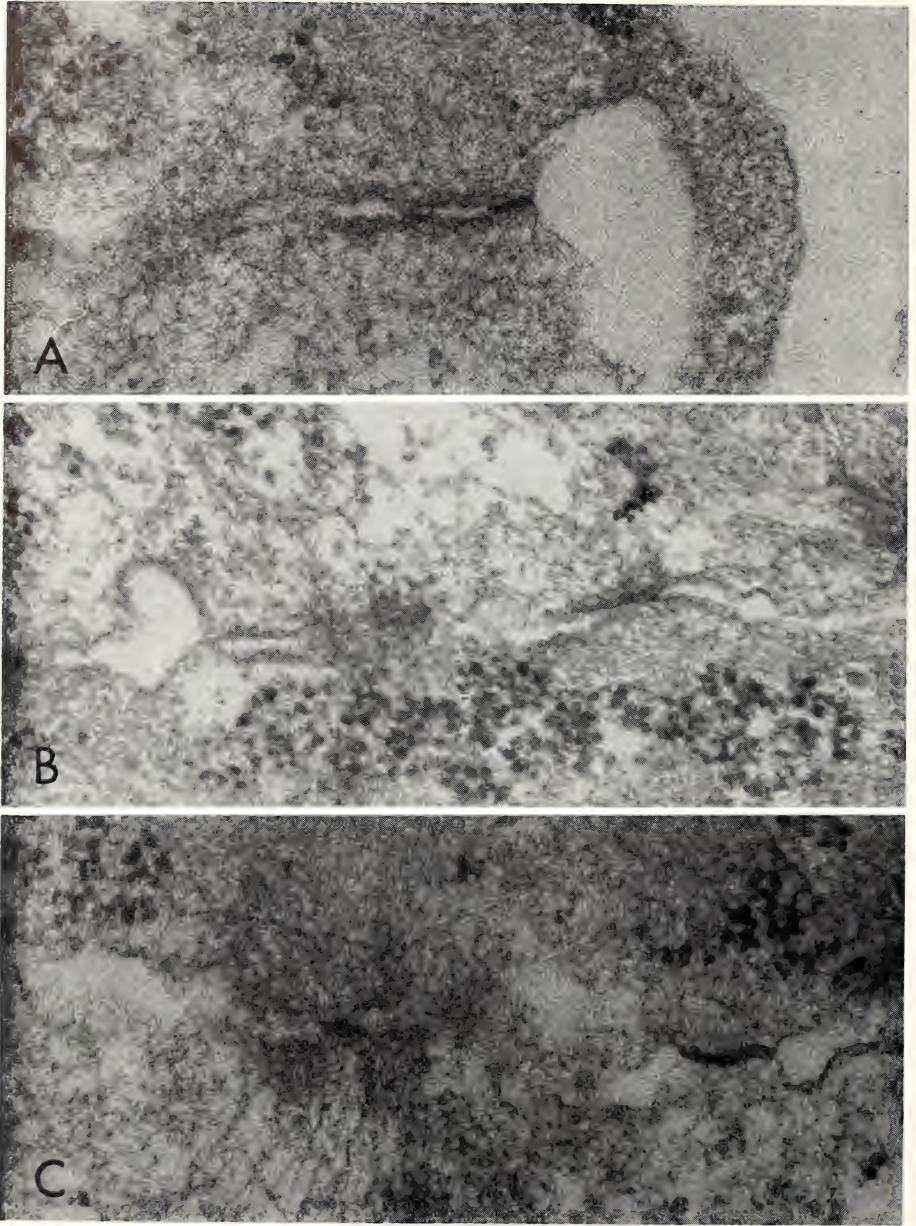


Plate 10. Details of contact area of cells shown in Plate 9 (C). Regions of close apposition surrounded by the small rectangles are enlarged in (A) and (B). (C) Another nexus from next serial section from same cell pair. (A), (B), (C)  $\times 84,000$ .



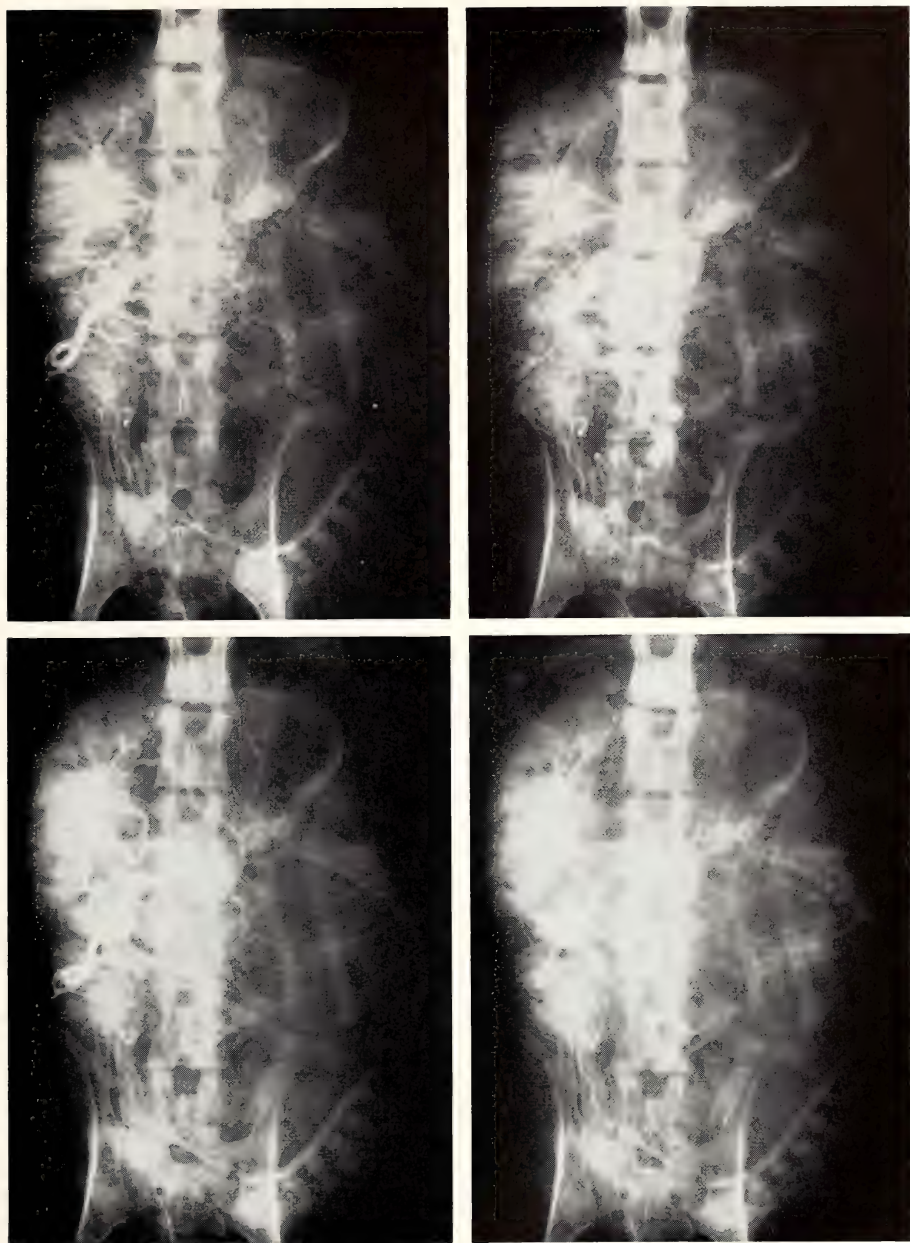


Plate 11. Photographs of X-ray films in which it will be observed that uterine contraction has no effect upon the filling of fetal placental vessels. Top row: Films taken 7 and 9 seconds after injection of a radiopaque medium into the fetal femoral artery during uterine relaxation. Lower row: Films made at comparable times following injection during a strong contraction. Monkey 68-69, 140 days pregnant. SP No. 68.





# *Department of Plant Biology*

*Stanford, California*

C. Stacy French  
*Director*

# Contents

Introduction . . . . .	619
Physiological Ecology Investigations . . . . .	624
Hybrids between <i>Atriplex</i> species with and without $\beta$ -carboxylation photosynthesis . . . . .	624
Cytogenetic and morphological characteristics . . . . .	625
Leaf anatomy and ultrastructure . . . . .	629
Biochemical characteristics . . . . .	632
Photosynthetic characteristics . . . . .	640
The compartmentation of reactions in $\beta$ -carboxylation photosynthesis . . . . .	649
Relationships between nitrogen level, photosynthetic capacity, and carboxydismutase activity in <i>Atriplex patula</i> leaves . . . . .	655
Biochemical Investigations . . . . .	662
Four common forms of chlorophyll <i>a</i> . . . . .	662
Automatic recordings of action spectra for partial reactions of photosynthesis . . . . .	670
Photosystem 1 activity and the long-wavelength forms of chlorophyll . . . . .	678
P700 and cytochrome <i>f</i> oxidation-reduction reactions in fraction 1 particles from spinach . . . . .	682
Photochemical reactions of P700 and cytochrome <i>f</i> and the action of plastocyanin in a grana stack preparation from spinach . . . . .	690
The development of system 2 activity in <i>Chlamydomonas</i> during transition from photo-heterotrophic to autotrophic nutrition . . . . .	695
Effects of monovalent cations on light energy distribution between two pigment systems of photosynthesis . . . . .	699
Separation of spinach chloroplast fractions with the zonal rotor . . . . .	704
Delayed fluorescence emission by fractions of <i>Scenedesmus</i> mutants . . . . .	706
Staff Activities . . . . .	709
Bibliography . . . . .	710
Speeches . . . . .	711
Personnel . . . . .	712



## INTRODUCTION

*Biochemical investigations.* For many years a continuing interest of one group at the Department has been to identify and characterize insofar as possible some of the different complexes of chlorophyll *a* that are found in plants. These chlorophyll complexes are the most obvious colored materials on earth and their key function is to absorb the sunlight that drives photosynthesis in plants. In spite of their abundance and importance their chemical nature and spectroscopic properties are not yet well known.

Two forms of chlorophyll *a* with absorption peaks at wavelengths of approximately 670 and 680 nm, occurring in roughly equal proportions, have been generally considered to constitute the major part of the total combined chlorophyll *a*. This year, however, evidence has accumulated to indicate that each of these apparent chlorophyll *a* complexes is made up of two resolvable components. The present concept considers chlorophyll *a* in plants to consist of four major forms with absorption maxima, as measured at the temperature of liquid nitrogen, at 663, 670, 678, and 684 nm with half-band widths of 8 to 11 nm. The proportions of these different forms of native chlorophyll vary in different species and also differ in the two kinds of particles that may be separated after disruption of chloroplasts. The proportion of the 670 to the 678 nm form ranges from about 0.75 to 1.25 and together these two make up about three-fifths of the total. The 663 and 684 forms each appear to account for approximately one-fifth of all the chlorophyll *a* of many algae and leaves. The proportions of these forms may, however, vary over a wide range in different plants.

These four components, determined by comparative curve analyses of many spectra, now seem to be widely distributed forms in that their peak wavelengths and possibly also their half-widths are essentially the same in many

plant species. To further establish the validity, generality, and limits of this concept we are continuing the measurement and curve analyses of absorption spectra of preparations from a wide variety of selected algal species. The evidence to date suggests that of the two photosystems which may be separated from chloroplasts each contains the same forms of chlorophyll but in different proportions. Whether Ca 684 is a contaminant or a constituent of fraction 2 remains to be decided, since thoroughly pure system 2 fractions cannot yet be prepared. In addition to these four major forms of native chlorophyll, many plants contain, particularly in fraction 1, longer wavelength forms with maxima in the 690- to 710-nm range. The amount of chlorophyll in these long-wavelength complexes is only a few percent of the total and their precise characterization has not yet been satisfactorily accomplished.

The development of the concept of four major, possibly "universal," forms of chlorophyll *a* arose largely from attempts to analyze the spectra of a green alga *Chlamydomonas stellata* when grown under different conditions. This alga is of particular interest because it forms predominantly system 1 pigments if grown in light on acetate, while on CO<sub>2</sub> it also forms system 2 pigments. Dr. Wolfgang Wiessner, a Docent at the University of Göttingen, who has long specialized in the study of this alga, visited the laboratory to investigate further the nature of its pigment complexes. He found that the components needed to match the absorption spectra of this alga grown under different conditions were equally suitable for many other algal preparations.

Past reports have emphasized the need for greatly increased precision and operational simplicity in the measurement of action spectra of the partial reactions of photosynthesis in fractions of chloroplast

particles. During this year progress has been made toward devising improved methods for recording action spectra.

Some years ago at the Department an automatic spectrophotometer was designed for recording action spectra of oxygen evolution from whole cells. Professor Halldal of Umeå University, a former Research Fellow of the Institution, (1955-57), has made a portable machine for this purpose that has been used in work on marine algae. The experiments reported here by Halldal, who this year returned to the Department for six months, concern two different recording procedures for measuring action spectra of any partial reaction of photosynthesis that can be made to cause the color change of an added dye. These methods were used to measure light-induced mammalian cytochrome *c* oxidation by lamella fragments of a blue-green alga *Plectonema*, a system 1 reaction, and for reduction of the dye DCIP by spinach chloroplast particles, a system 2 reaction. The results show some promise of giving a significant improvement over the usual methods for measuring action spectra, and the study is being continued in the hope of devising a simple method for measuring action spectra with a precision approaching that which is routine in absorption spectroscopy.

Methods most frequently used for fragmenting chloroplasts use detergents or sonic treatment. During their visit to the laboratory in 1967-68 Drs. Jean-Marie Michel and Marie-Rose Michel-Wolwertz developed a method whereby chloroplasts, fragmented by extrusion from a pressure cell through a needle valve, were fractionated by centrifugation on a sucrose-density gradient. The procedure yielded three bands of green material. The top and bottom bands were like system 1 and system 2 particles, respectively, prepared by sonic or detergent treatment with regard to their chlorophyll *a* to *b* ratios, P700 contents, and proportion of variable to total

fluorescence. The middle band was rather like system 2 particles. Dr. Norio Murata, a Carnegie Institution Fellow from the University of Tokyo, and Dr. Brown have reinvestigated the photochemical activities of the two kinds of chloroplast particles prepared according to the Michels' procedure. In fraction 1 particles the addition of appropriate cofactors raised the rate of a system 1 reaction, NADP reduction in the presence of an electron donor, by a factor of 8 over the Michels' original value. They found also that, unlike system 1 particles prepared sonically or with detergent, these mechanically prepared particles did not require the addition of plastocyanin for NADP reduction. The particles from the bottom band showed a substantial rate of a system 2 reaction, the Hill reaction with ferrieyanide, and also a weak system 1 activity, whereas particles from the top band gave no evidence of any system 2 activity.

Drs. Fork and Murata studied the electron transport reactions in these fractionated particles by measuring their light-induced absorbance changes. They found that the fraction from the top band (fraction 1 particles) still contained functioning cytochrome *f*. The cytochrome was oxidized within 0.5 msec by strong illumination. The effect is similar to Hildreth's finding in unbroken chloroplasts illuminated with a brief flash from a laser. In addition, Drs. Fork and Murata found that in these fraction 1 particles the addition of plastocyanin had no effect on the light-induced oxidation or dark reduction of either P700 or cytochrome *f*. But when they treated these particles with the detergent Triton X-100, cytochrome *f* was no longer efficiently oxidized by light. Spinach plastocyanin or *c*-type cytochromes from *Euglena* or *Porphyra* accelerated the dark reduction of P700 in detergent-treated particles.

The plastocyanin requirement for NADP reduction in the sonic or detergent-prepared system 1 particles may



thus be a reflection of damage done during preparation. The fraction 1 particles prepared with the pressure cell appear to have an electron-transport system in the native state as it exists in whole chloroplasts.

Professor Günter Jacobi of Göttingen has proposed that the lamellae in spinach chloroplasts which form the connecting links between grana stacks contain only photosystem 1 and that the grana stacks contain photosystems 1 and 2. Prof. Roderic Park and collaborators at the University of California have investigated fractionated particles prepared by the pressure cell and have reached a similar conclusion on the basis of electron microscopy.

Drs. Wiessner and Fork investigated the green alga *Chlamydomonas* that had adapted to growth in the light on acetate. Chloroplasts of acetate-adapted algae contain only separate lamellae and lack grana stacks. Algae in this condition may thus be analogous to fraction 1 particles with regard to their photochemical activities. Investigation revealed, in fact, that the acetate-adapted algae had only system 1 activity. When the cells were transferred out of their acetate medium to a CO<sub>2</sub> medium promoting normal photosynthesis, in which they form grana, then system 2 activity could be detected.

During Professor Jacobi's three-month visit to the laboratory he and Dr. Fork investigated some of the electron-transport reactions occurring in preparations of grana stacks. They found P700 as well as cytochrome *f* to be present in this fraction also. Moreover, the efficient coupling between cytochrome *f* and P700 was disrupted upon addition of the detergent Triton X-100 as it was in fraction 1 particles. In the presence of detergent, added plastocyanin reduced P700 in the dark and restored a slow, but not the fast, light-induced cytochrome *f* oxidation. Drs. Jacobi and Fork therefore suggest that the sequence of transport of electrons from cytochrome *f* to plasto-

cyanin to P700 proposed by Hind was based on the reactivation in detergent-treated chloroplasts of only the slow oxidation of cytochrome *f* by added plastocyanin and so may not reflect the actual *in vivo* pathway.

To identify the particular forms of chlorophyll and other substances constituting the different photochemical systems of photosynthesis it is of the greatest importance to improve the techniques of chloroplast disintegration and fractionation of chloroplast particles. Most of the work on this problem has been done with spinach chloroplasts. However, the far greater variety of pigment systems available in the various species of algae makes it particularly valuable to know more about the possibilities of separating different photosystems from a wide variety of algal species. The blue-green algae lacking chloroplasts have yielded only a system 1-like particle after mechanical disintegration. Dr. Brown's continuing survey of fractions from various plants is at present concentrating on the large green unicellular alga *Eremosphaera viridis* from which it is easier to remove the chloroplasts than from small algae with tough cell walls like *Chlorella*. In collaboration with Mr. O. M. Griffith of the Beckman Instrument Co., Dr. Brown has also tested the fractionation of spinach chloroplasts in a sucrose gradient with a zonal rotor instead of the smaller swinging bucket rotor previously used. This method makes possible a larger scale preparation of chloroplast fractions.

While the pigments connected with each photosystem seem to act primarily by energizing its own reaction center, there is also some transfer of energy from system 2 to system 1. The amount of this transfer is dependent on the state of the reaction center and on the spatial relations between the two pigment systems. Changes in the orientation or spacing of the pigment systems can be caused by environmental influences on the protein pigment carriers. Therefore,



the effects of inorganic salts on inhibition of the energy transfer between system 2 and system 1 have been studied by Dr. Murata. He found the monovalent cations as well as the previously investigated divalent cations to be effective, although only at far higher concentrations. The effect was measured by changes in the fluorescence yields from the two pigment systems as well as by the quantum yields of the two photo-reactions.

Dr. Ronald Ruby, Associate Professor of Physics at the University of California at Santa Cruz, and Dr. Brown have collaborated on a study of the delayed light emission following a brief flash given to two mutants of *Scenedesmus* and their fractions. The results suggest that the short-time delayed fluorescence measured 1 msec after the flash and that measured 30 msec later arise from different processes. The shorter-time light emission is believed to originate from early events in the photosynthetic mechanism.

*Physiological ecology.* Most of the current effort of this group of investigators is directed toward understanding the physiological and biochemical mechanisms of adaptive differentiation in plants that occupy widely diverse ecological habitats. It is necessary that such work be carried out at different levels of organizational complexity ranging from the molecular through the single organ to the population level with the single individual, or genotype, as the unit. Methods from several fields of science including not only plant physiology and biochemistry but also ecology, cytogenetics, and taxonomy are utilized in this work. Since the objective is not to classify plants but to understand the functional basis of speciation and adaptation—and this has been the primary objective for many years—it seems appropriate to change the name of the group from Experimental Taxonomy to Physiological Ecology.

The long-term investigations on *Mim-*

*ulus* were essentially concluded during 1969 and the results have been prepared for publication as an Institution monograph. This is the fifth volume of *Experimental Studies on the Nature of Species: Biosystematics, Genetics and Physiological Ecology of the Erythranthe Section of Mimulus*, under the authorship of William M. Hiesey, Malcolm A. Nobs, and Olle Björkman.

The investigations of ecotypic differentiation of photosynthetic characteristics in *Solanum dulcamara* were also concluded during 1969. These studies, made by Eckard Gaulh during his stay at the Department as a predoctoral Fellow, has resulted in the award of the degree of Doktor Rer. Nat. to him by the University of Frankfurt, Germany.

The experimental work by Drs. Björkman, Nobs, and Pearcey, has been focused on continued comparative studies of *Atriplex* species that possess different pathways for their primary CO<sub>2</sub> fixation. One of these species, *Atriplex rosea*, fixes CO<sub>2</sub> via the  $\beta$ -carboxylation (C<sub>4</sub> dicarboxylic acid) pathway of photosynthesis; it utilizes the enzyme phospho(enol)pyruvate carboxylase for the initial fixation of CO<sub>2</sub>, and the first products of photosynthesis are the C<sub>4</sub> dicarboxylic acids, oxaloacetate, malate, and aspartate. Another species, *Atriplex patula*, fixes CO<sub>2</sub> via the Calvin pathway; it utilizes the enzyme carboxydismutase (ribulose diphosphate carboxylase) for the fixation of CO<sub>2</sub>, and the first products of photosynthesis are 3-phosphoglycerate and sugar phosphates. *Atriplex rosea* and all other species with the  $\beta$ -carboxylation pathway of photosynthesis also possess a specialized leaf anatomy which is absent in *Atriplex patula* and other species lacking this pathway.

The two *Atriplex* species provide material uniquely suited for studies of biochemical differentiation in relation to photosynthetic function and ecological adaptation. *Atriplex rosea*, like many other species with  $\beta$ -carboxylation photosynthesis, occurs predominantly in hot

semi-arid locations. Of particular ecological significance is the fact that the  $\beta$ -carboxylation pathway is associated with a highly efficient utilization of low  $\text{CO}_2$  concentrations for photosynthesis, with high photosynthetic rates at high temperatures, and with the lack of an inhibitory effect of oxygen on photosynthetic  $\text{CO}_2$  uptake. Also, very high light intensities are required to saturate photosynthesis. *Atriplex patula* occurs mostly in cooler areas and is particularly common in coastal salt marshes. It has a lower efficiency for utilizing low  $\text{CO}_2$  concentrations and a lower photosynthetic rate at high temperatures than *Atriplex rosea*. Furthermore its photosynthetic  $\text{CO}_2$  uptake is markedly inhibited by 21% oxygen.

Since information on the necessary genetic divergence between species with and without  $\beta$ -carboxylation photosynthesis can be expected to substantially advance our understanding of the interaction between physiological differentiation and natural selection, much of the group's effort during the year has been devoted to hybridization of the two contrasting *Atriplex* species and to studies of the cytogenetic, leaf anatomical, biochemical, and photosynthetic characteristics of the hybrid derivatives. The first-generation hybrids are diploid with the same chromosome number as the two parental species and are intermediate between these with regard to a number of morphological characteristics. It is also evident that they have inherited the  $\text{CO}_2$  fixation pathways from both of the parental species, since almost half of the initial products of photosynthesis are those of the  $\beta$ -carboxylation pathway and the rest are those of the Calvin pathway. Examination under the light microscope revealed that the leaf anatomy also is intermediate between those of the parents. This was confirmed by electron microscope studies carried out by Dr. John Boynton, a Visiting Investigator at the Department during the summer of 1969. Dr. Boynton's studies

also revealed that the chloroplast structure associated with  $\beta$ -carboxylation photosynthesis is not directly transmitted by the maternal parent.

Despite the intermediate nature of the first-generation hybrids with regard to both biochemical and leaf anatomical characteristics, they are not intermediate in their photosynthetic performance. The intrinsic efficiency for utilizing low  $\text{CO}_2$  concentrations is about one-half of that in the male parent, *Atriplex patula*, and only about one-third to one-fourth of that in the female parent, *Atriplex rosea*. Moreover, the inhibitory effect of oxygen on photosynthesis is as high as in *Atriplex patula*. These result in a much lower light-saturated rate of photosynthesis in the  $F_1$  hybrid than in either parent under normal air.

The second-generation hybrids analyzed to date all possess photosynthetic characteristics very similar to those of the first-generation hybrids despite the fact that they segregate widely in the activity of phospho(enol)pyruvate carboxylase, the enzyme responsible for the initial  $\text{CO}_2$  fixation via the  $\beta$ -carboxylation pathway, as well as in leaf anatomical characteristics. This implies that neither the capacity for  $\text{CO}_2$  fixation via the  $\beta$ -carboxylation of phospho(enol)pyruvate nor the specialized leaf anatomy associated with this pathway is in itself sufficient to provide the high photosynthetic efficiency and the absence of oxygen inhibition found in *Atriplex rosea* and other naturally occurring species with  $\beta$ -carboxylation photosynthesis. Apparently, these desirable characteristics can only be obtained if the component metabolic steps are not only present but are also coordinated in time and space.

In addition to their fundamental value, these results have implications for plant breeding. The hybridization experiments show that the genetic divergence between species possessing and those lacking  $\beta$ -carboxylation photosynthesis need not be great; it may therefore be possible



to introduce desirable photosynthetic traits associated with this pathway from species possessing it to related species that are of agricultural importance but which lack the pathway. However, the results also indicate that even though the inheritance of each one of the component steps specific to the  $\beta$ -carboxylation pathway may be determined by a small number of genes only, they also indicate that efficient operation of the pathway requires that all these components be properly coordinated and spatially compartmented. This makes it highly unlikely that plants with the desirable characteristics of  $\beta$ -carboxylation photosynthesis can be produced by the application of mutagens to plants lacking the pathway.

Dr. Joseph A. Berry from the University of British Columbia, Vancouver, who recently joined the group as a post-doctoral Fellow of the Institution, has continued his studies of compartmentation of photosynthetic reactions in various species with  $\beta$ -carboxylation photosynthesis. He is now extending this work to include the hybrid derivatives of the two *Atriplex* species.

Dr. Ernesto Medina, an Institution Research Fellow, on leave from the University of Caracas, Venezuela, is investigating certain ecological factors influencing photosynthetic capacity in higher plants. A part of this project, currently in progress at the Department, concerns the interaction of light and the level of nitrogen nutrition in the root medium on the properties of the photosynthetic apparatus. In many habitats,

particularly those with high light intensity, available nitrogen often limits plant growth primarily by reducing protein synthesis. In low-light-intensity habitats light is generally the limiting factor and less nitrogen is required for maximum growth. Dr. Björkman has previously shown that the light intensity during growth greatly influences the nature of the photosynthetic apparatus, particularly the level of the enzyme responsible for  $\text{CO}_2$  fixation, carboxydismutase. Since carboxydismutase seems to limit the light-saturated photosynthetic capacity in many higher plants, it is important to understand the environmental factors controlling the level of this enzyme and their interactions.

Dr. Medina has shown that in plants grown under high light intensity, lowering the level of nitrogen in the root medium causes a strong parallel reduction in the levels of carboxydismutase and in the light-saturated photosynthetic rate. Furthermore, the activity of carboxydismutase decreased more than did total protein, indicating that there was a preferential reduction of the synthesis of this enzyme. Addition of nitrogen to the root medium of plants previously grown under low nitrogen resulted in an increase in carboxydismutase activity, indicating that the effects are freely reversible and that there is a rapid turnover of this enzyme. Thus, available nitrogen may limit photosynthetic capacity of higher plants in many natural habitats through its controlling effect on the level of photosynthetic enzymes.

## PHYSIOLOGICAL ECOLOGY INVESTIGATIONS

### HYBRIDS BETWEEN *Atriplex* SPECIES WITH AND WITHOUT $\beta$ -CARBOXYLATION PHOTOSYNTHESIS

The existence of different pathways for photosynthetic  $\text{CO}_2$  fixation within the same genus of higher plants provides an excellent opportunity for studies of bio-

chemical differentiation in relation to photosynthetic function and natural selection. Plants possessing the  $\beta$ -carboxylation ( $\text{C}_4$ -dicarboxylic acid) pathway have different photosynthetic characteristics than plants lacking this pathway, and they occur predominantly in



habitats with high insolation, high temperatures, and often also severe drought. In a recent article in *Annual Review of Plant Physiology*, pp. 141–162, 1970, Hatch and Slack discuss the biochemistry of the pathway and its occurrence in the plant kingdom (also see this *Year Book*, pp. 649–655).

The results of our comparative studies on *Atriplex rosea* L., a species with  $\beta$ -carboxylation photosynthesis, and *Atriplex patula* ssp. *hastata* Hall and Clem., a species lacking this pathway, were reported last year (*Year Book* 68, pp. 620–633). The successful hybridization of the two species with *A. rosea* as the female parent was also reported. During the year we have extended the comparative studies of the parental species to include the first-generation hybrid. Much effort has also been made to produce second-generation hybrids by self-pollinating the  $F_1$  hybrids and to characterize the progeny obtained with regard to cytogenetics, leaf anatomy and ultrastructure, biochemistry, and photosynthetic properties. Since it is necessary that each individual hybrid be analyzed for each one of a number of different characteristics, this work is extraordinarily time consuming. We nevertheless feel that the effort required is worthwhile since such experiments have great potential value in elucidating several important problems:

1. Knowledge of the genetic divergence essential for the functional difference between plants possessing, and those lacking,  $\beta$ -carboxylation photosynthesis is of fundamental biological interest, since it would contribute to understanding the evolutionary interaction between physiological differentiation and natural selection. Such information is also important to the plant breeder in his evaluation of the possibilities of introducing this pathway into species of agricultural importance that lack the  $\beta$ -carboxylation pathway.

2. Plants with and without the  $\beta$ -carboxylation pathway differ with regard

to the leaf anatomy, their photosynthetic capacity and responses to variation in major external parameters, and their productivity. Many of the characteristics associated with  $\beta$ -carboxylation species show absolute correlation with the presence of this  $\text{CO}_2$  fixation pathway in all species thus far investigated. Second-generation hybrids or hybrids of subsequent generations between plants with and without the  $\beta$ -carboxylation pathway may provide a recombination of at least some of the characteristics distinguishing the two types of plants and thus make it possible to determine the functional relationships among the various traits associated with  $\beta$ -carboxylation species.

3. A segregating population would also provide material uniquely suited for experimental studies of the ecological significance of the  $\beta$ -carboxylation pathway and of the other characteristics associated with it. Such studies could substantially advance our understanding of the mechanisms of adaptation and natural selection in plants.

All *Atriplex* materials used in the comparative studies reported below were grown in controlled growth cabinets at the Department under a light intensity of  $1.1 \times 10^5$  erg  $\text{cm}^{-2}$   $\text{sec}^{-1}$  (400–700 nm) for 16 hours alternating with 8 hours of darkness. The temperature during the light and dark periods was 25 and 20°C, respectively. The seedlings were grown in perlite with nutrient solution added daily.

#### *Cytogenetic and Morphological Characteristics*

Malcolm A. Nobs, Olle Björkman, and  
Robert W. Pearcy

The genus *Atriplex* is of worldwide distribution and well over two hundred species have been recognized. Hall and Clements (1923) divide the genus into two major subgenera: *Euatriples* and *Obione*. Their classification was based primarily on embryonic characters. All

species of subgenus *Obione* that have been analyzed thus far possess the  $\beta$ -carboxylation pathway or at least the anatomical or photosynthetic characteristics associated with it. *Atriplex patula* and all other species that have been found to lack the  $\beta$ -carboxylation pathway or associated characteristics are classified as belonging to subgenus *Euatriplex*. Hall and Clements also placed *A. rosea* in this subgenus; moreover, they considered that the species most closely related to the *A. rosea* group belong to the *A. patula* group. This was an important factor in our selecting *A. rosea* and *A. patula* for our comparative studies and hybridization experiments (cf. *Year Book* 68, p. 621). We are not aware of any experimental work concerning genetic relationships within the genus *Atriplex*; neither have we found any reports on attempts to hybridize species with different carboxylation pathways in any other genus or family.

All members of *Atriplex* for which chromosome counts have been reported have  $2n=18$  or  $2n=36$  chromosomes.

As shown in Fig. 1, *A. rosea* and *A. patula* both have  $2n=18$  chromosomes. The chromosomes are small, the largest having a length of approximately  $5\mu$ . It is evident both from the somatic divisions (Fig. 1, top) and from the meiotic divisions (Fig. 1, bottom), that the karyotypes are very similar in the two species. For example, two of the chromosome pairs have satellites both in *A. rosea* and in *A. patula*. The meiotic pairing is perfectly regular, with nine chromosome pairs in both species.

The flowers are unisexual in both species, which would be expected to facilitate controlled crossing experiments. However, in *A. patula* all of the inflorescences contain both staminate and pistillate flowers; since the species is highly self-fertile, controlled pollination would require emasculation, a difficult task, as the flowers are very small (approximately 1 mm at anthesis). The situation in *A. rosea* is similar, but in addition to the capitate bisexual inflorescences this species has axile flowers that are pistillate only. Thus, *A. rosea*

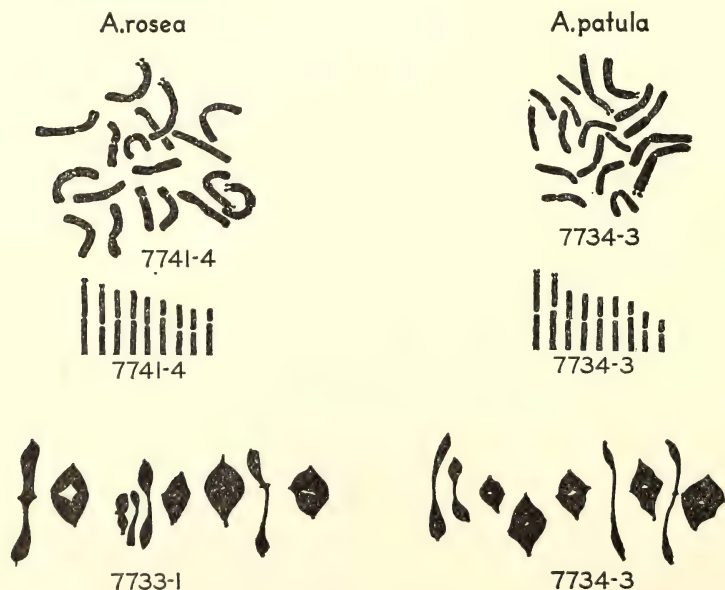


Fig. 1. Somatic and meiotic chromosomes in *Atriplex rosea* and *A. patula* ssp. *hastata*.

can readily be used for controlled pollinations after the capitate inflorescences have been removed.

Approximately 10% of the axile flowers of *A. rosea* that were pollinated repeatedly with *A. patula* pollen yielded seeds. Nearly all seeds were viable, germinated rapidly, and gave rise to strong  $F_1$  seedlings which were highly uniform and morphologically intermediate between the parents. Somatic cells of the  $F_1$  hybrids are diploid with  $2n=18$  chromosomes, and the karyotype is indistinguishable from that of either parent.

Reduction divisions in pollen mother cells of the  $F_1$  hybrids are shown in Fig. 2. The chromosomal pairing is highly irregular and only a maximum of six pairs are formed. Generally there are three to

four pairs but frequently no pairing takes place. In cells where no pairing occurs the chromosomes divide precociously at first metaphase, frequently resulting in the formation of diploid gametes (Fig. 2, center column). In cells where chromosomal pairing does occur a spindle is formed and the paired chromosomes undergo normal separation, whereas the univalents which are not aligned on the spindle may undergo precocious division and those which do not are randomly distributed (Fig. 2, left and right columns). This results in pollen with highly variable chromosome numbers. Presumably a large fraction of this is inviable because only 6-7% of the pollen obtained from the  $F_1$  hybrid is stainable as compared with 95% in the parents. The seed-set is

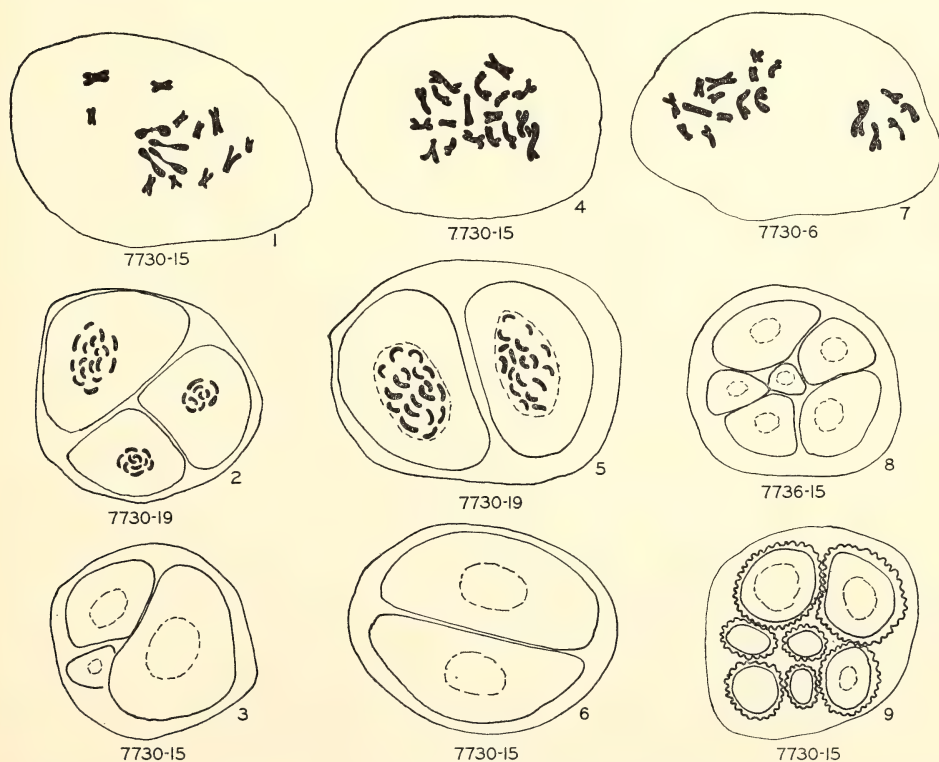


Fig. 2. Microsporogenesis in the first-generation hybrid *Atriplex rosea*  $\times$  *A. patula* ssp. *hastata*. For details see text.



very low in the  $F_1$  and it is therefore likely that the reduction division in the embryo sac is similar to that in the pollen mother cells. We have nevertheless been successful in obtaining sufficient seeds for experimental work. The seed obtained is viable, germinates readily, and generally gives rise to strong plants. As shown in Table 1 the chromosome numbers of our 20  $F_2$  individuals vary from slightly above diploid to more than pentaploid with the median number being around tetraploid. This is a remarkable variation in an  $F_2$  generation. Although most of these  $F_2$  hybrids are essentially sterile, several have very good seed-set and may well prove to be self-perpetuating.

From the polyploid nature of the  $F_2$  hybrids it might be expected that segregation would be strongly limited. Fortunately for our purposes this is not the case (see Plate 1). The growth habit of the  $F_2$  hybrids shows great variation. Hybrid 7735-3, like *A. patula*, has branches that are opposite and horizontal. Hybrid 7740-4 has branches that are alternate and ascending like those of *A. rosea*. In hybrid 7736-1 the branching is intermediate as in the  $F_1$  hybrid. Other recombinations are found as in hybrid 7740-1, which has alternate horizontal branches, while hybrid 7740-5 has opposite ascending branches.

Leaf shapes, diagrammatically shown in Fig. 3, also exhibit great variation, in fact as much as one could expect to ob-

tain in a freely segregating diploid  $F_2$  population. A random sample of as few as twelve  $F_2$  hybrids shows a complete recombination of parental characters. The  $F_2$  hybrid 7744-1 (Fig. 3, center row, extreme left) has an oval blade with a cuneate base like *A. rosea*, while  $F_2$  hybrid 7736-1 has a triangular blade with a hastate base like *A. patula*, and  $F_2$  hybrid 7735-1 has a leaf shape that is intermediate between the parental leaf shapes, as in the  $F_1$ . In other  $F_2$  hybrids the recombinations in leaf shape transcend the basic form found in the parents, as in hybrids 7735-3, 7744-4, and 7735-2 (see Fig. 3 and cf. Plate 1).

Certain other morphological characters do not show recombination in these hybrids, but resemble those of the male parent, *A. patula*. For example, the male and female flowers are evenly distributed in the terminal spicate in-

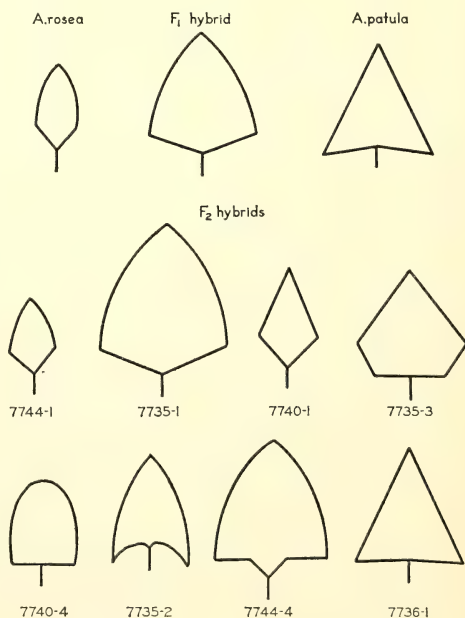


TABLE 1. Chromosome Number of  $F_2$  Hybrids from a Cross between *A. rosea* and *A. patula*

Plant	2n	Plant	2n
7735-1	34	7744-1	34
7735-2	34	7744-4	26
7735-3	37	7745-1	36
7735-4	44	7745-3	38
7735-5	36	7746-1	29
7736-1	21	7746-9	29
7740-1	30	7746-10	28
7740-2	44	7746-12	30
7740-4	46	7746-14	22
7740-5	31	7746-16	28

Fig. 3. Diagrammatic representation of the basic leaf shapes in *Atriplex rosea*, *A. patula* ssp. *hastata*, and recombinations of these leaf shapes in the first- and second-generation hybrids from a cross between these species. Plate 1 also shows these plants.

florescences in all of these hybrids. Similarly, the ripe fruiting-bracts are deep maroon-red to black, are semi-fleshy, and drop from the inflorescence branchlets when ripe, as in *A. patula*. This contrasts strikingly with the female parent, *A. rosea*, whose bracts are light brown, woody, and remain permanently attached to the fragmenting inflorescence branchlets.

### References

Hall, H. M., and F. E. Clements, *The Phylogenetic Method in Taxonomy; The North American Species of Artemisia, Chrysanthamnus, and Atriplex*, Carnegie Inst. Wash. Publ. 326, Washington, D.C., 1923.

### LEAF ANATOMY AND ULTRASTRUCTURE

John E. Boynton, Malcolm A. Nobs, Olle Björkman, and Robert W. Pearcy

Camera lucida drawings of living sections of fully expanded leaves from *Atriplex rosea*, *Atriplex patula*, and their F<sub>1</sub> and F<sub>2</sub> hybrids are shown in Fig. 4. Light and electron micrographs of sections from similar leaves of these plants, fixed in glutaraldehyde, post-fixed in osmium tetroxide, and embedded in epoxy resin, are shown in Plates 2-8.

The leaf anatomy of mature leaves of *A. rosea*, like that of other species with  $\beta$ -carboxylation photosynthesis, is characterized by a well-developed bundle sheath surrounding the vascular bundle (Fig. 4, Plate 2; see also Downton and Tregunna, 1968). A single layer of mesophyll cells radiates outward from this bundle sheath, and the remainder of the mesophyll consists of large, highly vacuolate parenchyma cells. The bundle sheath and radiate mesophyll cells contain numerous chloroplasts, whereas only few and poorly developed plastids are seen in surrounding parenchyma cells (Plate 2). Unlike *Sorghum*, sugar cane, and some other species with  $\beta$ -carboxylation photosynthesis, the bundle sheath chloroplasts of mature *A. rosea* leaves have extremely well-developed grana

compared to those of the radiate mesophyll cells. Bundle sheath cells have peripherally located vacuoles of moderate size and much thicker walls than do the mesophyll cells. The walls between these two cell types are traversed by a great number of plasmodesmata, which are thought to aid the transport of metabolites. At the intracellular level, a similar transport function has been attributed to the well-developed peripheral reticulum observed in chloroplasts of bundle sheath and mesophyll cells of certain species with  $\beta$ -carboxylation photosynthesis including *Atriplex lentiformis* (Laetsch, 1968) and in mesophyll cells of *Atriplex spongiosa* (Osmond *et al.*, 1969). However, no indication of a peripheral reticulum has been observed in chloroplasts of *A. rosea* by us or by Downton *et al.* (1969).

In fully expanded leaves of *A. rosea* the bundle sheath chloroplasts are considerably larger, have more extensive grana, and accumulate much more starch during photosynthesis than do the mesophyll chloroplasts whose lamellar system appears to be in the process of degeneration. The bundle sheath cells contain many large mitochondria tightly oriented in rows between the closely packed chloroplasts. Frequently microbodies with a single bounding membrane, probably peroxisomes (Tolbert and Yamazaki, 1969), can be observed. The presence of high glycolate oxidase activity in the bundle sheath cells of *A. rosea* (Year Book 68, pp. 620-633) is consistent with these observations.

Downton *et al.* (1969) have followed chloroplast development in bundle sheath and mesophyll cells of expanding leaves of *A. rosea*. They have shown that in one-quarter expanded leaves, the chloroplasts are of similar size and structural organization in both cell types, although the bundle sheath cells are already less vacuolate and have thicker walls and denser cytoplasm at this stage than the surrounding mesophyll cells. By the time the leaves are one-half expanded, the

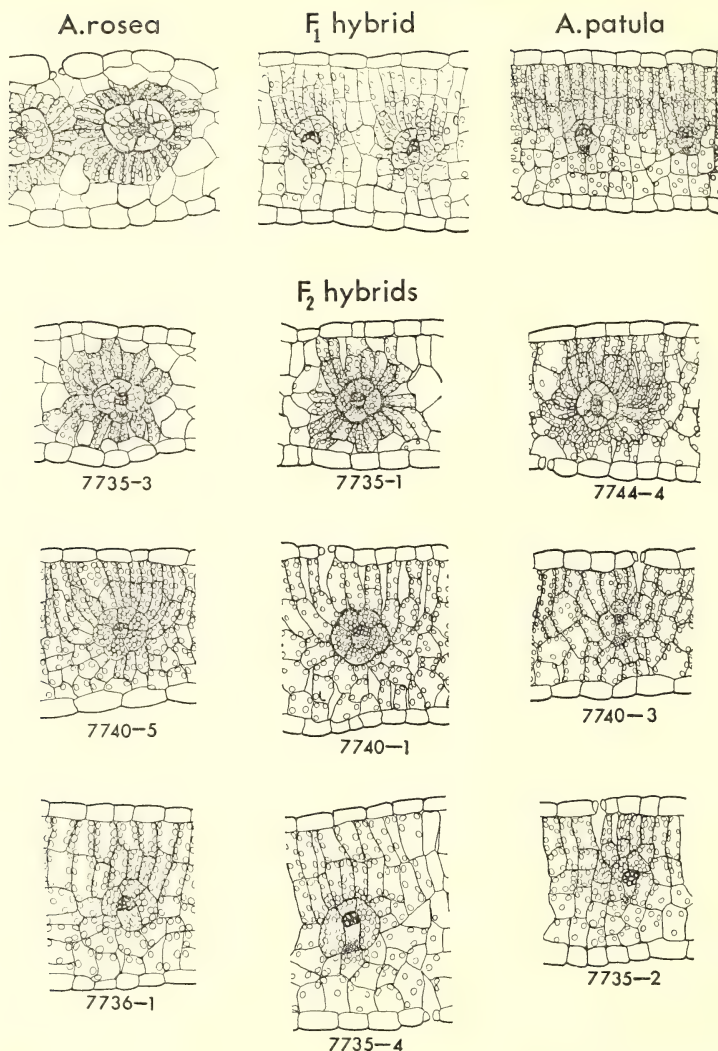


Fig. 4. Camera lucida drawings of living leaf sections of *A. rosea*, *A. patula* ssp. *hastata*, and their first- and second-generation hybrids.

mesophyll chloroplasts have enlarged and developed more extensive lamellar systems than those of the bundle sheath cells. In fully expanded leaves the bundle sheath chloroplasts have become about twice the size of the mesophyll plastids and have formed a highly developed lamellar system, while the mesophyll plastids appear to be senescing.

*A. patula* has a conventional leaf

anatomy (Fig. 4, Plate 3). Mature leaves lack a distinct bundle sheath and cells adjacent to the vascular bundle are identical in size, wall thickness, and structural organization to the palisade and spongy mesophyll cells elsewhere in the leaf. All cells possess numerous plastids of moderate size with a well-developed lamellar system and many starch grains. Microbodies (peroxisomes?) can



be observed in all cells, and the mitochondria are fewer and smaller than in the bundle sheath cells of *A. rosea*. The walls of cells immediately adjacent to the vascular bundle in *A. patula* are considerably thinner than those of the bundle sheath cells of *A. rosea* and are identical with mesophyll cells elsewhere in the leaf.

Fully expanded leaves of the first-generation hybrid are essentially intermediate between the two parents in gross leaf anatomy (Fig. 4, Plate 4). A partially differentiated bundle sheath can be seen in longitudinal section near the terminus of one leaf bundle, whereas undifferentiated layers of meristematic cells surround a larger bundle cut in oblique section elsewhere in the same leaf (Plate 4). Chloroplasts in these cells immediately adjacent to the bundle vary considerably in size, shape, and extent of lamellar development. In some cases they are identical with chloroplasts elsewhere in the mesophyll of the leaf and very similar to those of the palisade and mesophyll cells of the male parent *A. patula*. In other instances (Plate 4) the chloroplasts of the partially differentiated bundle sheath cells of the  $F_1$  hybrids approach the bundle sheath chloroplasts of the female parent *A. rosea* in size and extent of grana development. Starch grains are equally prevalent in plastids of differentiated cells adjacent to and spatially removed from the vascular bundles in the  $F_1$  hybrid. Immature plastids in the layers of undifferentiated cells surrounding some bundles are typical in structural organization to those of meristematic cells.

Partially differentiated bundle sheath cells of the hybrids have somewhat thinner walls and larger, more centrally located vacuoles than do the bundle sheath cells of *A. rosea*. However, their walls are considerably thicker and their vacuoles somewhat smaller than cells similarly juxtaposed to vascular bundles elsewhere in the  $F_1$  hybrid leaf. It is

particularly interesting that those cells surrounding the vascular bundles, which approach *A. rosea* bundle sheath cells in wall thickness and vacuolation, also do so with respect to chloroplast size, shape, and grana formation. Mitochondria of these partially developed bundle sheath cells of the  $F_1$  hybrids are considerably larger and more numerous than those of the mesophyll cells elsewhere in the same leaf and often are lined up in rows between adjacent chloroplasts or between chloroplasts and the cell wall, as in *A. rosea*. The cell walls separating the bundle sheath and mesophyll cells of the hybrids are traversed by plasmodesmata, as in *A. rosea*. No peripheral reticulum has been observed in plastids of the hybrids or in either parent. Both bundle sheath and mesophyll cells of the  $F_1$  hybrids contain single membrane-bound microbodies (peroxisomes?).

Preliminary observations indicate that development of the aforementioned bundle sheath anatomy and cytological organization in the  $F_1$  hybrids is influenced by environmental conditions such as high light intensity to a considerably greater degree than in the maternal parent *A. rosea* (cf. p. 633, this *Year Book*). Leaves of the  $F_1$  hybrids also appear to develop their bundle sheath phenotype at a later age than *A. rosea*. Evidence from the  $F_1$  hybrids alone clearly establishes that the inheritance of chloroplast morphology is not directly transmitted by the maternal parent.

The 20  $F_2$  individuals obtained thus far show great variation in leaf anatomy, and individuals with characteristics approaching both parents have been recovered (Fig. 4). Fully expanded leaves of four selected  $F_2$  hybrids representing the range of gross anatomical types show a somewhat narrower variation in ultrastructural organization in the leaf cells (Plates 5-8). None of these individuals has the characteristic dimorphic bundle sheath and mesophyll chloroplasts of *A. rosea* nor the highly uniform chloroplasts

of *A. patula*; in the four  $F_2$  hybrids examined thus far the cytological organization resembles that in the  $F_1$  hybrids to a greater or lesser degree.

The  $F_2$  hybrids 7735-1 and 7735-3 (Fig. 4, Plates 5 and 7) possess most of the gross anatomical characteristics of *A. rosea*, although the chloroplast development in the bundle sheath and mesophyll cells of 7735-1 most closely resembles that seen in the  $F_1$  hybrids, while that of 7735-3 is somewhere between the  $F_1$  hybrid and *A. rosea*. Although  $F_2$  hybrid 7735-2 approaches the *A. patula* in gross leaf anatomy, its cytological organization is closer to the  $F_1$  hybrid (Plates 5 and 6). The majority of the  $F_2$  hybrids have gross leaf anatomy approaching the  $F_1$  hybrid (e.g., 7735-4 and 7736-1, Fig. 4) and one of these,  $F_2$  hybrid 7735-4, examined in the electron microscope (Plate 8), has cells very similar in ultrastructural organization to the  $F_1$  hybrid (Plate 4).

Observation of the gross leaf anatomy of the various  $F_2$  individuals has revealed many of the possible recombinations of the basic characteristics differentiating the *A. rosea* and *A. patula* parents. For example, hybrid 7744-4 has a well-developed bundle sheath with thick walls like *A. rosea*, but this is surrounded by loosely packed, randomly arranged mesophyll cells which also comprise the remainder of the leaf. Differentiation of a radiating mesophyll and enlarged, highly vacuolate parenchyma with few developed plastids, typical of *A. rosea*, is absent. The  $F_2$  hybrid 7740-5 has a well-developed bundle sheath, but the cell walls are as thin as those of the adjoining mesophyll cells, which are semi-radiate and partially differentiated into palisade and spongy parenchyma. Quantitative characterization of electron micrographs of various  $F_2$  individuals now in progress is expected to reveal similar recombinations of the basic ultrastructural characteristics of the two parents, *A. rosea* and *A. patula*.

## References

- Downton, W. J. S., and E. B. Tregunna, *Can. J. Bot.*, **46**, 207, 1968.  
 Downton, W. J. S., T. Bisalputra, and E. B. Tregunna, *Can. J. Bot.*, **47**, 915, 1969.  
 Laetsch, W. M., *Amer. J. Bot.*, **55**, 875, 1968.  
 Osmond, C. B., J. H. Troughton, and D. J. Goodchild, *Zeit. Pflanzenphysiol.*, **61**, 218, 1969.  
 Tolbert, N. E., and R. K. Yamazaki, *Ann. New York Acad. Sci.*, **168**, 325, 1969.

## Biochemical Characteristics

Robert W. Pearcy, and Olle Björkman

*Carboxylation enzyme activities.* A fundamental difference between plants possessing the  $\beta$ -carboxylation pathway and those lacking it is the presence of high levels of phospho(enol)pyruvate carboxylase (EC 4.1.1.31) in the leaves of the former. This enzyme is responsible for the  $\beta$ -carboxylation of phospho(enol)pyruvate (PEP) to form oxaloacetate as the first product of photosynthesis (Hatch and Slack, 1966). Evidence from this laboratory (Björkman and Gauhl, 1969) and other laboratories (Berry *et al.*, 1970; Slack *et al.*, 1969) shows that in species with  $\beta$ -carboxylation photosynthesis, most, if not all, of this enzyme is located in the radiate mesophyll cells (cf. Table 12, this *Year Book*).

Activities of PEP carboxylase in *A. rosea* and *A. patula* and the  $F_1$  hybrids are summarized in Table 2. Activities in *A. rosea* are about 20 times higher than those in *A. patula*. In the  $F_1$  hybrids, activities are about one-fourth of those in *A. rosea* and about 5 times greater than those in *A. patula*. Thus, although they are not strictly intermediate, the  $F_1$  hybrids have inherited relatively high levels of PEP carboxylase from the female parent, *A. rosea*.

Early experiments indicated that some variation was present in the activities of PEP carboxylase from different leaves of a single  $F_1$  hybrid plant. Such variability could complicate the interpretation

TABLE 2. PEP Carboxylase Activity in Leaf Extracts of Hybrids from a Cross between *A. rosea* and *A. patula* \*

Plant	Activity, $\mu\text{mole CO}_2 \text{ min}^{-1}$	
	Per g Fresh Weight	Per dm <sup>2</sup> Leaf Area
<i>A. rosea</i>	24.42 $\pm$ 1.88	66.5 $\pm$ 3.1
<i>A. patula</i>	1.39 $\pm$ 0.08	3.6 $\pm$ 0.5
F <sub>1</sub> hybrid	6.45 $\pm$ 1.49	14.2 $\pm$ 2.5
F <sub>2</sub> hybrids:		
7735-1	3.21	7.9
7735-2	0.99	1.4
7735-3	5.59	12.7
7735-4	1.59	4.5
7736-1	2.05	4.6
7740-1	12.90	31.0
7740-3	10.53	25.9
7740-4	1.98	4.9
7740-5	8.68	22.0
7744-4	8.48	21.3

\* Assay conditions were as described by Björkman and Gauhl (1969) except that leaf homogenizations were carried out under N<sub>2</sub>.

of other measurements performed on single leaves. Table 4 shows that maximum activity is reached in leaf number 6 (from the top). This corresponds to a leaf of about three-fourths of full expansion. Activities in fully mature leaves were about 50% of the maximum. Leaves 6 and 7 correspond to those used in all other experiments. As an additional precaution, where possible, PEP carboxylase activity was determined on the same leaves used for other experimental purposes.

The activity of PEP carboxylase is also influenced by the light intensity for growth. In the preliminary experiments reported last year (*Year Book* 68, p. 632), when the F<sub>1</sub> hybrids were grown under the same conditions as those used in the present studies, with the exception that the light intensity for growth was only half of that used this year, the PEP carboxylase activity in the F<sub>1</sub> hybrid was only about one-fourth of that reported here. The activities in the parental species were also higher when the plants were grown under the higher light intensity, but the effect of light intensity was considerably less than in the F<sub>1</sub> hybrid. In the present studies, light in-

tensity for growth was the same in all experiments.

Considerable segregation was present in the levels of PEP carboxylase among the F<sub>2</sub> hybrids (Table 2, bottom half). Activities among these hybrids range from slightly less than those found in *A. patula* (F<sub>2</sub> hybrid 7735-2) to about one-half of those found in *A. rosea* (F<sub>2</sub> hybrid 7740-1).

No consistent relationship was found between the level of PEP carboxylase and a leaf anatomy among the F<sub>2</sub> hybrids. For example, F<sub>2</sub> hybrid 7735-3, which is anatomically similar to *A. rosea*, has only average activity of this enzyme (5.6  $\mu\text{mole g}^{-1}$  fresh weight  $\text{min}^{-1}$ ); F<sub>2</sub> hybrid 7740-3 has high activities of PEP carboxylase (10.5  $\mu\text{mole g}^{-1}$  fresh weight  $\text{min}^{-1}$ ), but its leaf anatomy is much closer to *A. patula* than to *A. rosea*.

Activities of carboxydismutase (EC 4.1.1.39) in *Atriplex rosea* are considerably lower than those in *A. patula*. However, the activities in *A. rosea* and other  $\beta$ -carboxylation species are not lower than those found in many species lacking  $\beta$ -carboxylation (Björkman and Gauhl, 1969; cf. p. 649, this *Year Book*). The results presented in Table 3, show that



TABLE 3. Carboxydismutase Activity in Leaf Extracts of Hybrids from a Cross between *A. rosea* and *A. patula* \*

Plant	Activity, $\mu\text{mole CO}_2 \text{ min}^{-1}$		
	Per g Fresh Weight	Per dm <sup>2</sup> Leaf Area	Per mg Soluble Protein
<i>A. rosea</i>	4.09 $\pm$ 0.53	10.7 $\pm$ 1.4	0.29 $\pm$ 0.02
<i>A. patula</i>	12.69 $\pm$ 0.06	26.6 $\pm$ 1.5	0.74 $\pm$ 0.02
F <sub>1</sub> hybrid	11.55 $\pm$ 1.53	27.1 $\pm$ 2.4	0.74 $\pm$ 0.02
F <sub>2</sub> hybrids:			
7735-1	11.62	26.1	0.72
7735-2	12.87	27.1	0.74
7735-3	14.06	30.4	0.59
7735-4	9.25	23.1	0.54
7736-1	13.82	31.1	0.89
7740-1	10.37	31.3	0.50
7740-3	9.00	22.2	0.50
7740-4	8.68	22.0	0.53
7740-5	14.46	37.5	0.60
7744-4	10.21	20.6	0.49
Mean of F <sub>2</sub> hybrids $\pm$ S.D.	11.43 $\pm$ 2.1	27.1 $\pm$ 5.2	0.61 $\pm$ 0.04

\* Assay conditions were as described by Björkman and Gauthl (1969).

the F<sub>1</sub> hybrids have high levels of carboxydismutase similar to those found in *A. patula*. These activities are higher than those reported last year (*Year Book* 68, p. 632) for plants grown at about one-half the light intensity used this year.

Carboxydismutase activities were high in all the second-generation hybrids studied to date (Table 3, bottom half). While some variation was present among different F<sub>2</sub> individuals, the carboxydismutase activities in all the F<sub>2</sub> hybrids are greater than those found in most other higher plants. The mean activity for the F<sub>2</sub> hybrids did not differ statistically from the means for either the F<sub>1</sub> hybrids or the male parent, *A. patula*.

*Carbonic anhydrase activity.* Although the function of carbonic anhydrase (EC 4.2.1.1) in photosynthesis is not yet clear, there is evidence that this enzyme may be necessary for efficient CO<sub>2</sub> fixation by green algae at normal CO<sub>2</sub> concentrations (Reed and Graham, 1968; Nelson *et al.*, 1969). Moreover, specific inhibitors of carbonic anhydrase inhibit photosynthesis by isolated higher plant chloroplasts (Everson, 1970). Studies with artificial membranes show that carbonic anhydrase can facilitate CO<sub>2</sub> transport

across a membrane by as much as a hundredfold (Enns, 1967). A similar effect *in vivo* could influence photosynthetic CO<sub>2</sub> exchange.

Carbonic anhydrase has been reported to be absent in species with  $\beta$ -carboxylation photosynthesis (Hesketh *et al.*, 1965; Waygood *et al.*, 1969), or present in much lower activities than in species lacking this pathway (Everson and Slack, 1968). The results shown in Table 5 indicate that the activities of carbonic anhydrase are as high in *A. rosea* as in *A. patula*. The somewhat lower levels detected in the F<sub>1</sub> hybrid are probably not significant. Experiments I and II were performed with different ratios of tissue to buffer in the extraction proce-

TABLE 4. Effect of Leaf Position on the Activity of PEP Carboxylase in the F<sub>1</sub> Hybrid \*

Leaf No.	Activity, $\mu\text{mole CO}_2 \text{ min}^{-1} \text{ g}^{-1}$ Fresh Weight
5	6.00
6	8.86
7	8.56
8	5.84
10	4.55

\* Counted basipetally from first leaf of at least 2 cm length.

TABLE 5. Carbonic Anhydrase Activity in Leaf Extracts of *A. patula*, *A. rosea*, and Their F<sub>1</sub> Hybrids\*

Plant	Experiment I † Enzyme Units	Experiment II ‡ Enzyme Units
<i>A. rosea</i>	385	821
F <sub>1</sub> hybrid	294	344
<i>A. patula</i>	275	666

\* Enzyme activity expressed according to Rickli *et al.* (1964), where  $E = (T_b/T_c - 1) / g \text{ fr. wt.}$ , and  $T_b$  and  $T_c$  are the times required for completion of the uncatalyzed and catalyzed reaction, respectively. Leaf extracts were prepared according to the procedure used for carboxydismutase and assays were conducted at 2.5°C according to the procedure of Rickli *et al.*

† 957 mg tissue extracted in 10.0 ml buffer.

‡ 200 mg tissue extracted in 10.0 ml buffer.

ture. The increased activities obtained with decreasing ratio of tissue to buffer volume suggest that the procedure employed may greatly influence the results. In addition, previous work in this laboratory has shown that poor breakage of the bundle sheath cells in species with  $\beta$ -carboxylation photosynthesis is often obtained when conventional methods for enzyme extraction are used (Year Book 68, pp. 623-624; and Björkman and Gauhl, 1969). Thus any carbonic anhydrase in the unbroken bundle sheath cells may not have been accounted for in the earlier work.

**Labeling experiments with  $^{14}\text{CO}_2$ .** The most definitive characteristic of plants with  $\beta$ -carboxylation photosynthesis is the formation of C<sub>4</sub>-dicarboxylic acids as the first stable products of photosynthesis. Extensive investigations by Hatch and co-workers (Hatch and Slack, 1966; Hatch, *et al.*, 1967; Johnson and Hatch, 1969) have made use of labeling *in vivo* with  $^{14}\text{CO}_2$  to establish the path of carbon in  $\beta$ -carboxylation plants. Their results, and those of other workers (Berry, *et al.*, 1970) are consistent with the hypothesis that the C<sub>4</sub>-dicarboxylic acids are formed by the  $\beta$ -carboxylation of PEP in the mesophyll cells. These acids are then either transcarboxylated

to an intermediate of the reductive pentose phosphate cycle, or transferred to the bundle sheath where the C<sub>4</sub>-carboxyl may be decarboxylated and the CO<sub>2</sub> re-fixed by carboxydismutase (cf. p. 649, this Year Book).

The early products of photosynthesis in *A. rosea*, *A. patula*, and their F<sub>1</sub> and F<sub>2</sub> hybrids were determined by a  $^{14}\text{CO}_2$  feeding technique similar to that of

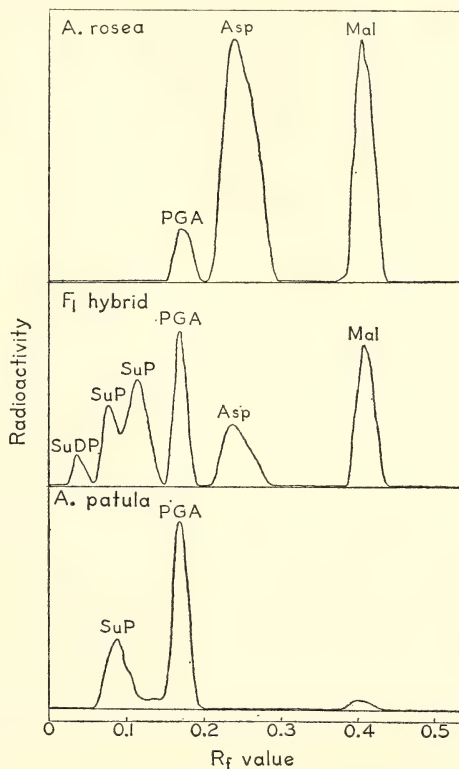


Fig. 5. Radiochromatogram scans showing the products after six seconds of photosynthesis in  $^{14}\text{CO}_2$  by leaves of *Atriplex rosea*, *A. patula*, and their first-generation hybrid. The leaves were dipped into a chamber containing air with  $^{14}\text{CO}_2$  added. After six seconds the leaves were killed in boiling 80% (v/v) ethanol. Extracts were chromatographed on paper with butanol:propionic acid:water (12:8:2 v/v) as the solvent. Light intensity during the pre-illumination and the labeling was  $8.8 \times 10^4 \text{ erg cm}^{-2} \text{ sec}^{-1}$ ; final CO<sub>2</sub> concentration was approximately 400 ppm. Abbreviations are: SuP, sugar phosphates; 3-PGA, 3-phosphoglyceric acid; Mal, malic acid; Asp, aspartic acid.

Hatch and Slack (1966) and of Berry *et al.* (1970). The results of our labeling experiments show that after exposure to  $^{14}\text{CO}_2$  for six seconds, nearly all the  $^{14}\text{C}$  in *A. patula* leaves is in intermediates of the reductive pentose phosphate cycle (Fig. 5 and Table 7, upper half). In *A. rosea* leaves, on the other hand, the radioactivity is almost entirely confined to the  $\text{C}_4$ -dicarboxylic acids, malate and aspartate, with only a very small fraction of label in 3-phosphoglycerate. In similar experiments with the  $\text{F}_1$  hybrids, the radioactivity was found almost equally distributed between  $\text{C}_4$ -acids and 3-phosphoglycerate plus sugar phosphates. The presence of  $^{14}\text{C}$  in the  $\text{C}_4$ -acids is consistent with the finding that the level of PEP carboxylase is relatively high in the  $\text{F}_1$  hybrids.

Further experiments were conducted with the  $\text{F}_1$  hybrids to determine: (1) the initial products of  $\text{CO}_2$  fixation by short-term  $^{14}\text{CO}_2$  feedings; (2) the sequence of  $^{14}\text{C}$  labeling by longer-term  $^{14}\text{CO}_2$  feedings; (3) and precursor-product relationships in the sequence by pulse-chase feedings of  $^{14}\text{CO}_2$  and  $^{12}\text{CO}_2$  (cf. Oaks and Bidwell, 1970). Even in the shortest  $^{14}\text{CO}_2$  feeding intervals (2 and 4 seconds) shown in Fig. 6, both 3-phosphoglycerate and  $\text{C}_4$ -acids are la-

beled. These results provide strong evidence that the initial  $\text{CO}_2$  fixation in the  $\text{F}_1$  hybrids involves direct carboxylation of both PEP and RuDP. With long-term feedings of 32 seconds, the fraction of  $^{14}\text{C}$  in 3-PGA declined but that in the  $\text{C}_4$ -acids remained high (Table 6). In naturally occurring plants with  $\beta$ -carboxylation photosynthesis, the fraction of total label in the  $\text{C}_4$ -acids declines when the labeling of the  $\text{C}_4$ -acids reaches a steady state. This occurs when the rate of  $^{14}\text{CO}_2$  fixation into  $\text{C}_4$ -acids equals the rate of  $^{14}\text{C}$  transferred from  $\text{C}_4$ -acids to subsequent products. The fact that  $^{14}\text{C}$  continues to accumulate in the  $\text{C}_4$ -acids of the  $\text{F}_1$  hybrid indicates a lower rate of transfer of label to these subsequent products. Either the  $\text{C}_4$ -acid pool size is larger in the  $\text{F}_1$  hybrids (thus it saturates more slowly), or the  $\text{C}_4$ -acids do not serve as important precursors to other photosynthetic metabolites. Alternatively, these data could be the result of rapid accumulation of label in  $\text{C}_1$ ,  $\text{C}_2$ , and  $\text{C}_3$  of the  $\text{C}_4$ -acids as well as in the  $\text{C}_4$  position (see Hatch and Slack, 1966). This postulate and the determination of the pool sizes are presently under investigation.

In the pulse-chase experiments, the leaf was exposed briefly to  $^{14}\text{CO}_2$  during

TABLE 6. Effect of Different Treatments on the Distribution of Radioactivity in the Early Products of Photosynthesis in the  $\text{F}_1$  Hybrids

Treatment		Distribution of $^{14}\text{C}$ in Individual Compounds,* percent				
Four Sec with $^{14}\text{CO}_2$ in	Followed by Thirty-two Sec in	SuP	3-PGA	Serine + Glycine	Mal + Asp	Other †
air	...	37.4	37.5	nil	24.4	nil
1% $\text{O}_2$	...	47.4	23.0	nil	22.9	6.4
air	$^{12}\text{CO}_2$ , air	30.8	17.0	18.7	34.5	nil
1% $\text{O}_2$	$^{12}\text{CO}_2$ , 1% $\text{O}_2$	42.9	19.1	2.3	28.9	6.8
1% $\text{O}_2$	$\text{CO}_2$ -free, $\text{N}_2$	34.7	22.7	7.9	25.6	9.1
...	$^{14}\text{CO}_2$ , air	38.7	16.0	16.6	28.6	nil

\* Experimental conditions were the same as those for Fig. 1 except that in 1%  $\text{O}_2$  light intensities were  $1.65 \times 10^6$  erg  $\text{cm}^{-2}$   $\text{sec}^{-1}$  and the leaves were exposed to 1%  $\text{O}_2$  with 350 ppm  $^{12}\text{CO}_2$  for 5 min prior to labeling. Hatch *et al.* (1967) have shown that light intensity does not influence the relative amount of  $\text{CO}_2$  fixed into the  $\text{C}_4$ -acids but that high light increases the speed of turnover of individual compounds.

† Includes radioactivity remaining at the origin and in spots with  $R_f$ -values corresponding to those of sucrose, other free sugars, and alanine.



steady state photosynthesis (pulse), and then killed and extracted after a time of continued photosynthesis in an atmosphere containing unlabeled  $\text{CO}_2$  (chase). The initial products of  $\text{CO}_2$  fixation become labeled during the pulse. During the chase, these labeled compounds serve as precursors for the formation of other photosynthetic metabolites. In such experiments with naturally occurring plants with  $\beta$ -carboxylation (Hatch and Slack, 1966; Johnson and Hatch, 1969; Berry *et al.*, 1970) the proportion of label in  $\text{C}_4$ -acids declines rapidly during the chase. There is a corresponding increase in the proportion of label in 3-PGA and in other intermediates of the

reductive pentose phosphate cycle. These results indicate that the  $\text{C}_4$ -acids are the precursors for the formation of 3-PGA in normal  $\beta$ -carboxylation photosynthesis. In corresponding experiments with the  $\text{F}_1$  hybrids (Fig. 6), the proportion of label in the  $\text{C}_4$ -acids remains constant for at least 32 seconds of chase. This may indicate the absence of a transfer of the  $\text{C}_4$  carbon from the  $\text{C}_4$ -acids to 3-PGA in these plants. In contrast, the rapid decline in label in 3-PGA and the corresponding increases in other compounds indicate that 3-PGA is being rapidly metabolized in the formation of intermediates of the reductive pentose phosphate cycle and of serine and gly-

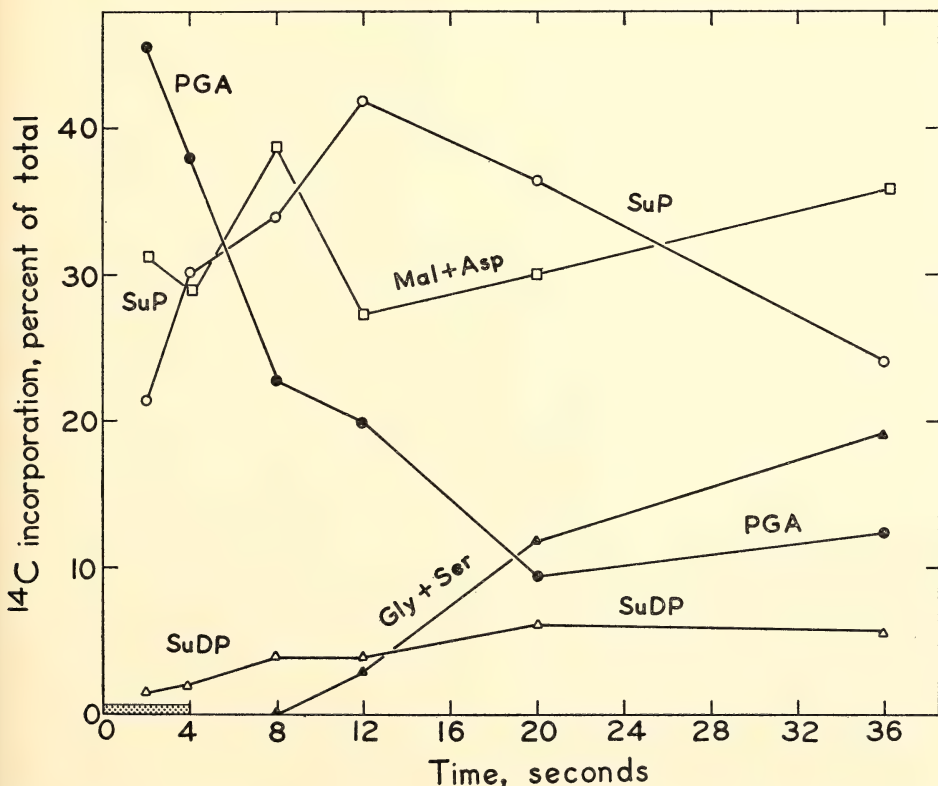


Fig. 6. Distribution of radioactivity after 2 or 4 seconds of photosynthesis in air containing  $^{14}\text{CO}_2$  followed by photosynthesis in air containing  $^{12}\text{CO}_2$  for different lengths of time. Conditions were as given for Fig. 5. Serine and glycine were separated from aspartate by elution of the spots and rechromatography in phenol:water (73:28 v/v). No attempt was made to recover oxaloacetate and glycolate.

cine. The latter compounds are probably derived from intermediates of the reductive pentose phosphate cycle, and are thought to be related to the occurrence of photorespiration (Tolbert and Yamazaki, 1969).

The fraction of label in the  $C_4$ -acids might remain high during the chase if  $^{14}CO_2$  produced by photorespiration were refixed into the  $C_4$ -acids before it could escape from the leaf. To test this hypothesis, labeling experiments were conducted under 1%  $O_2$  where photorespiration does not occur or is at least strongly suppressed. The data given in Table 6 indicate that the fraction of  $^{14}C$  in the  $C_4$ -acids remains high even after 32 seconds' chase in an atmosphere of low oxygen content. Therefore, refixation of photorespired  $^{14}CO_2$  cannot account for the lack of a decrease in the fraction of label in the  $C_4$ -acids during the chase in air. The much lower fraction of radioactivity in serine and glycine formed in 1%  $O_2$  as compared with air confirms that photorespiration was indeed inhibited.

In the previous pulse-chase experiments, removal of  $^{14}C$  from the  $C_4$ -acid pool may be buffered by dilution of the pool with unlabeled  $CO_2$  fixed during the chase. This dilution should be strongly inhibited if any further  $CO_2$  fixation is blocked by placing the leaf in  $CO_2$ -free nitrogen after the initial feeding with  $^{14}CO_2$ . Under these conditions, utilization of the  $C_4$ -acids in photosynthetic reactions should lead to depletion of the  $C_4$ -acid pool (cf. Johnson and Hatch, 1969) and a parallel decline in label in the  $C_4$ -acids. Such an experimental procedure should provide optimum conditions for detecting movement of label out of the  $C_4$ -acid pool. However, as shown in Table 6, no net transfer of  $^{14}C$  from the  $C_4$ -acid pool was observed when this procedure was used with  $F_1$  hybrid leaves. The fraction of label in the  $C_4$ -acid pool remained high even after 32 seconds in  $CO_2$ -free  $N_2$ .

The results presented above suggest

that transfer of carbon (in  $C_4$  position) from the  $C_4$ -acids may be blocked, or at least strongly inhibited in the  $F_1$  hybrids. This might be due to the absence of appropriate enzymes or to inappropriate spatial relationships of the enzymes within the leaf.

Thus, there is conclusive evidence that all reactions necessary for  $CO_2$  fixation via  $\beta$ -carboxylation of PEP and the subsequent conversion of oxaloacetate to malate and aspartate occur in the  $F_1$  hybrids. The evidence, however, indicates that these  $C_4$ -acids may not be important as precursors of 3-PGA formation as they are in normal  $\beta$ -carboxylation photosynthesis. The evidence also indicates that most, if not all, of the 3-PGA formed in the  $F_1$  hybrids is produced by direct fixation of atmospheric  $CO_2$  via the reductive pentose phosphate pathway. It is difficult to estimate the effect of carboxylation via the  $C_4$ -dicarboxylic acids on net photosynthetic  $CO_2$  uptake in the  $F_1$  hybrids. It could be either positive or negative.

As shown in the lower part of Table 7, the results of  $^{14}C$  labeling experiments with the  $F_2$  hybrids were qualitatively similar to those obtained with the  $F_1$  hybrids. The fraction of label found in the  $C_4$ -dicarboxylic acids showed considerable variation among the different  $F_2$  individuals; however, it was significantly higher in all of them than in the *A. patula* parent.

A comparison of the  $^{14}C$  labeling data (Table 7) and the PEP carboxylase activities (Table 2) obtained with the same  $F_2$  individuals indicates that there is an apparent lack of correlation between the fraction of radioactivity incorporated into  $C_4$ -dicarboxylic acids and the PEP carboxylase activity. The discrepancy is particularly striking in  $F_2$  hybrids 7735-2 and 7744-4. In hybrid 7735-2, 26% of the radioactivity was found in the  $C_4$ -dicarboxylic acids, whereas only 14% was found in hybrid 7744-4 in spite of the much higher PEP carboxylase in the latter plant. Since

TABLE 7. Distribution of Radioactivity in Individual Compounds after Photosynthesis in  $^{14}\text{CO}_2$  for Approximately Six Seconds in *A. rosea*, *A. patula*, and Their  $F_1$  and  $F_2$  Hybrids

Plants	Radioactivity, Percent of Total					
	SuP	PGA	Asp	Mal	SuP + PGA	Asp + Mal
<i>A. rosea</i>	1	8	63	28	$\leq 9$	$\geq 91$
<i>A. patula</i>	35	56	4	5	$\geq 91$	$\leq 9$
$F_1$ hybrid	36	20	20	24	56	44
$F_2$ hybrids: 7735-1	38	26	14	22	64	36
7735-2	37	37	13	13	74	26
7735-3	27	36	19	18	63	37
7735-4	34	27	17	22	61	39
7736-1	34	49	9	8	83	17
7740-1 *	48	14	18	20	62	38
7740-3	59	21	9	11	80	20
7740-4 †	46	13	15	26	59	41
7744-4	64	22	10	4	86	14

\* Mean of 3 determinations.

† Mean of 2 determinations.

PEP carboxylase is presumably responsible for the production of  $\text{C}_4$ -dicarboxylic acids, no satisfactory explanation is at hand for the relatively high fraction of label in the  $\text{C}_4$ -dicarboxylic acids in  $F_2$  hybrids with low PEP carboxylase activity. One possibility is that the leaves used for the labeling experiments had lower activity of this enzyme than those used for the determination of enzyme activity. Nevertheless, experiments in which parts of the same  $F_2$  hybrid leaves were used for concomitant  $^{14}\text{CO}_2$  feedings and PEP carboxylase assays also failed to yield a correlation between the fraction of  $^{14}\text{C}$  fixed in  $\text{C}_4$ -dicarboxylic acids and enzyme activity. In plants where high PEP carboxylase was present but which fixed low amounts of  $^{14}\text{C}$  into  $\text{C}_4$ -acids, other steps, such as the regeneration of PEP by pyruvate,  $\text{P}_i$  dikinase, may be limiting, or part of the PEP carboxylase may be localized in places where rates of carboxylation may be limited by supply of substrates, either  $\text{CO}_2$  or PEP, rather than the activity of the enzyme.

A comparison of the  $^{14}\text{C}$  labeling data (Table 7) and leaf anatomy (Fig. 4) among the  $F_2$  hybrids fails to reveal a relationship between the fraction of  $^{14}\text{C}$

fixed in the  $\text{C}_4$ -dicarboxylic acids and the development of the bundle sheath or the radiate mesophyll cells.

### References

- Berry, J. A., W. J. S. Downton, and E. B. Tregunna, *Can. J. Bot.*, **48**, 777, 1970.
- Björkman, O., and E. Gauth, *Planta*, **88**, 197, 1969.
- Enns, T., *Science*, **155**, 44, 1967.
- Everson, R. G., *Phytochem.*, **9**, 25, 1970.
- Everson, R. G., and C. R. Slack, *Phytochem.*, **8**, 581, 1968.
- Hatch, M. D., and C. R. Slack, *Biochem. J.*, **101**, 103, 1966.
- Hatch, M. D., C. R. Slack, and H. S. Johnson, *Biochem. J.*, **102**, 417, 1967.
- Hatch, M. D., C. R. Slack, and T. A. Bull, *Phytochem.*, **8**, 697, 1969.
- Hesketh, J. D., H. Niramoto, and M. A. El-Sharkaway, Rep. No. 2 on Photosynthesis, Dept. of Plant Breeding, Univ. of Arizona, Tucson, 1965.
- Johnson, H. S., and M. D. Hatch, *Phytochem.*, **7**, 375, 1968.
- Nelson, E. B., A. Cendella, and N. E. Tolbert, *Phytochem.*, **8**, 2305, 1969.
- Oaks, A., and R. G. S. Bidwell, *Ann. Rev. Plant Physiol.*, **21**, 43, 1970.



- Reed, M. L., and D. Graham, *Plant Physiol. Supp.*, **43**, S-29, 1968.
- Rickli, E. E., S. A. S. Ghazanfar, B. H. Gibbons, and J. T. Edsall, *J. Biol. Chem.*, **239**, 1065, 1964.
- Slack, C. R., M. D. Hatch, and D. J. Goodchild, *Biochem. J.*, **114**, 489, 1969.
- Tolbert, N. E., and R. K. Yamazaki, *Ann. New York Acad. Sci.*, **168**, 325, 1969.
- Waygood, E. R., R. Mache, and K. C. Tan, *Can. J. Bot.*, **47**, 1455, 1969.

### Photosynthetic Characteristics

Olle Björkman, Robert W. Pearcy, and Malcolm A. Nobs

Photosynthesis in *Atriplex rosea*, as in other species that fix CO<sub>2</sub> via the  $\beta$ -carboxylation pathway, is characterized by a requirement of high light intensity for saturation, an efficient use of low CO<sub>2</sub> concentrations, and a high optimum temperature. Also, the CO<sub>2</sub> compensation point approaches zero at atmospheric oxygen concentration. Another notable photosynthetic characteristic distinguishing this species and other species with  $\beta$ -carboxylation photosynthesis from *A. patula* and other species without  $\beta$ -carboxylation is the absence of an in-

hibition of photosynthetic CO<sub>2</sub> uptake by oxygen, which is commonly attributed to photorespiration. In all species investigated there is an absolute correlation of all these photosynthetic characteristics, a specialized leaf anatomy, high activities of certain enzymes, and the  $\beta$ -carboxylation pathway. As shown in previous sections of this report the F<sub>1</sub> hybrid, *A. rosea*  $\times$  *A. patula* is intermediate between its parents in gross leaf anatomy and has inherited the initial CO<sub>2</sub> fixation reactions characteristic of both its parents. Its photosynthetic characteristics are not intermediate, however.

*Dependence on light intensity.* Figure 7 shows curves for photosynthetic CO<sub>2</sub> uptake in air of normal CO<sub>2</sub> and O<sub>2</sub> content as a function of light intensity. Clearly, the curve for the F<sub>1</sub> hybrid is not intermediate between the parents. Instead, the photosynthetic rate is much lower in the F<sub>1</sub> hybrid than in either of the parents, both at rate-limiting and at rate-saturating light intensities. At light saturation the rate in the F<sub>1</sub> hybrid is slightly more than one-half the rate in *A. patula* and only about one-third the rate in *A. rosea* (Table 8, upper half).

Since the net photosynthetic rate is

TABLE 8. Light-Saturated Rate of CO<sub>2</sub> Uptake at 27° and 300 ppm CO<sub>2</sub> in F<sub>2</sub> Hybrids from a Cross between *A. rosea* and *A. patula* in Comparison with the Parental Species and the F<sub>1</sub> Hybrid

Plant	Net Rate of CO <sub>2</sub> Uptake, $\mu\text{mole min}^{-1} \text{dm}^{-2}$		Ratio, Rate in 21% O <sub>2</sub> Rate in 1.3% O <sub>2</sub>
	21% O <sub>2</sub>	1.3% O <sub>2</sub>	
<i>A. rosea</i>	21.8 $\pm$ 1.0	21.8 $\pm$ 1.0	1.00 $\pm$ 0.00
<i>A. patula</i>	11.8 $\pm$ 0.6	18.5 $\pm$ 1.1	0.63 $\pm$ 0.01
F <sub>1</sub> hybrid	6.5 $\pm$ 0.7	11.3 $\pm$ 1.3	0.57 $\pm$ 0.04
F <sub>2</sub> hybrids: 7735-1	6.2	10.2	0.61
7735-2	6.9	10.7	0.64
7735-3	6.5	9.7	0.64
7735-4	7.6	11.1	0.68
7736-1	7.9	11.9	0.66
7740-1	7.2	11.7	0.61
7740-3	5.7	8.6	0.66
7740-4	5.6	9.6	0.58
7740-5	7.1	10.9	0.65
7744-4	7.0	10.5	0.67
Mean of F <sub>2</sub> hybrids $\pm$ S.D.	6.8 $\pm$ 0.7	10.5 $\pm$ 1.0	0.64 $\pm$ 0.03

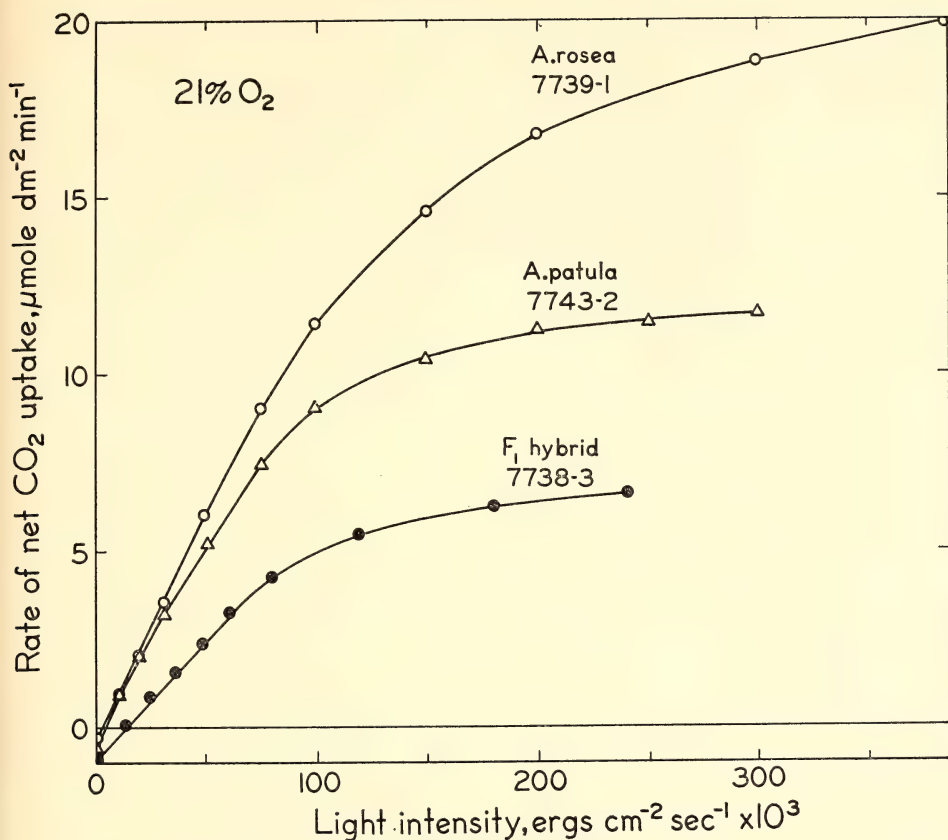


Fig. 7. Photosynthetic CO<sub>2</sub> uptake as a function of light intensity under 21% O<sub>2</sub> with 0.030% CO<sub>2</sub> in the F<sub>1</sub> hybrid *Atriplex rosea* × *A. patula* and the parental species. Leaf temperature was 27°C. Measurements were made with an open system similar to those described by Björkman and Holmgren (1963) and Björkman and Gauhl (1970).

markedly inhibited by 21% O<sub>2</sub> in *A. patula* but not in *A. rosea*, the rates of the two species become much closer when they are measured under 1.5% O<sub>2</sub> (Fig. 8). However, *A. rosea* requires higher light intensities for light-saturation than does *A. patula* even under low O<sub>2</sub> concentration. Under 1.5% O<sub>2</sub> and rate-limiting light intensities the photosynthetic rate of the F<sub>1</sub> hybrid approaches those of its parents, but the light-saturated rate remains considerably lower and saturation occurs at lower light intensities than in either parent. These results indicate that the lower photosynthetic capacity in the F<sub>1</sub> hybrids is not attrib-

utable to a lower intrinsic efficiency of photochemical steps.

**Dependence on temperature.** The temperature dependence of the light-saturated photosynthetic rate in normal air of the two *Atriplex* species and their F<sub>1</sub> hybrid is shown in Fig. 9. Like other species with  $\beta$ -carboxylation photosynthesis, *A. rosea* requires high temperatures for maximum photosynthesis. Also, the rise in photosynthesis with increasing temperature is much steeper in *A. rosea* than in *A. patula* at temperatures beyond 17°C. The temperature dependence in the F<sub>1</sub> hybrid is not at all intermediate. While its photosynthetic rate approaches

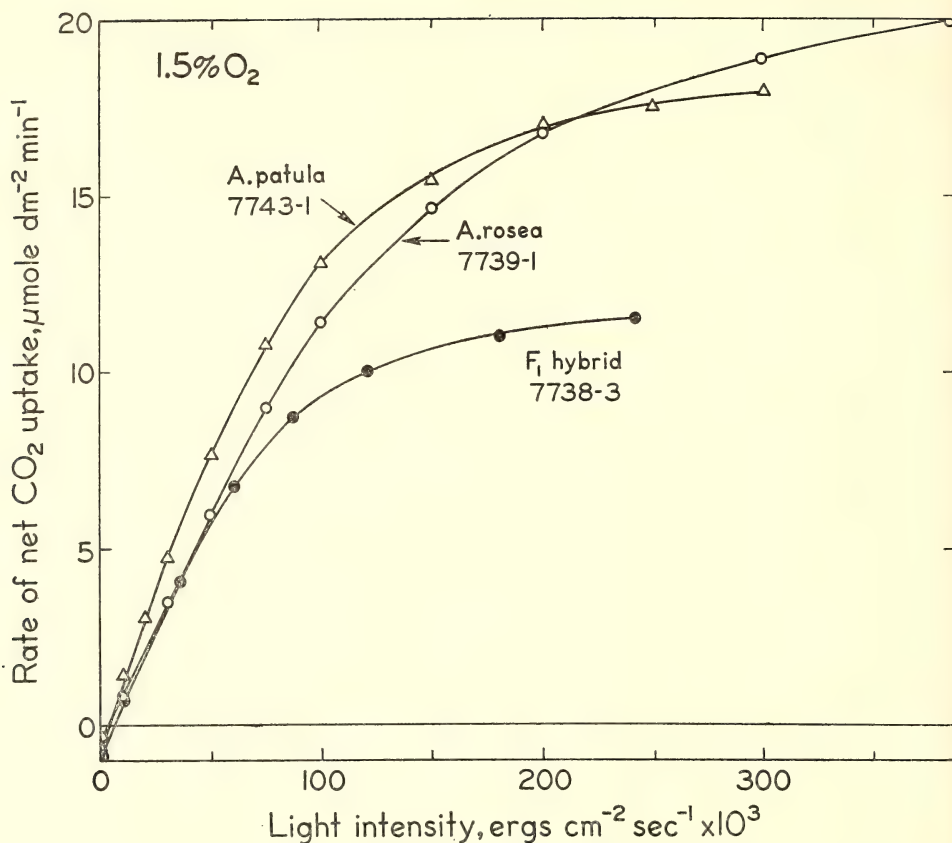


Fig. 8. Photosynthetic CO<sub>2</sub> uptake as a function of light intensity under 1.5% O<sub>2</sub> with 0.030% CO<sub>2</sub> in the F<sub>1</sub> hybrid and the parental species. Leaf temperature was 27°C.

those of the parental species at very low temperatures, the temperature dependence curve is much flatter in the F<sub>1</sub> hybrid.

The temperature dependence of photosynthesis is markedly affected by oxygen concentration in both *A. patula* and the F<sub>1</sub> hybrid but it is unaffected in *A. rosea*. Under low O<sub>2</sub> concentration, the temperature curves are very similar for *A. patula* and *A. rosea* except at temperatures higher than 25°C (Fig. 10). The curve for the F<sub>1</sub> hybrid nearly coincides with those for the parents at low temperatures but it flattens out at much lower temperatures.

The temperature dependence of photo-

synthesis in the F<sub>1</sub> hybrid indicates that the low rates obtained at temperatures beyond 15°C cannot be attributed to a lower capacity of a rate-limiting enzymic step since enzyme activity would be expected to increase with increasing temperatures. *In vitro* determinations of the temperature dependence of the CO<sub>2</sub> fixation reactions, both the reaction catalyzed by PEP carboxylase and that catalyzed by carboxydismutase, reveal high Arrhenius activation energies (Björkman and Gauhl, unpublished, cf. *Year Book* 68, pp. 619 and 627). In addition, the results presented in this *Year Book*, p. 634, show that the activities of carboxydismutase in the F<sub>1</sub> hybrid are as



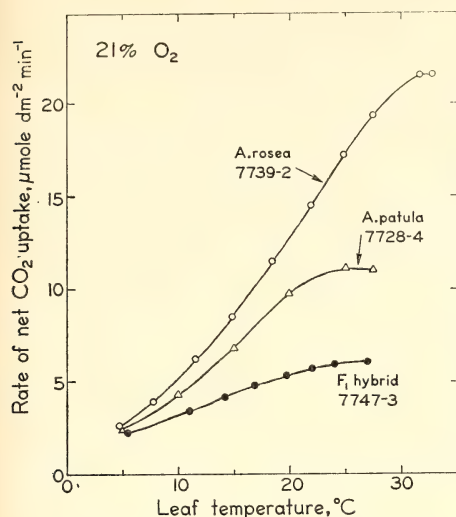


Fig. 9. Photosynthetic CO<sub>2</sub> uptake as a function of leaf temperature under 21% O<sub>2</sub> and 0.030% CO<sub>2</sub> in the F<sub>1</sub> hybrid and the parental species. Saturating light intensities were used for each plant.

high as in the *A. patula* parent and that the activity of PEP carboxylase in the F<sub>1</sub> hybrid is higher than in *A. patula*,

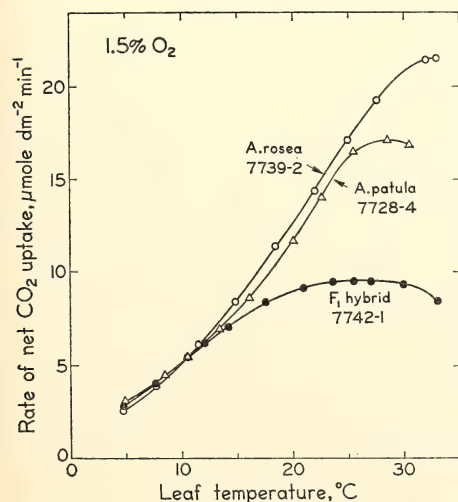


Fig. 10. Photosynthetic CO<sub>2</sub> uptake as a function of leaf temperature under 1.5% O<sub>2</sub> and 0.030% CO<sub>2</sub> in the F<sub>1</sub> hybrid and the parental species. Saturating light intensities were used for each plant.

although it is lower than in *A. rosea*. These lines of evidence give further support to the conclusion, based on the gas exchange measurements in intact leaves, that the low photosynthetic rate in the F<sub>1</sub> hybrid in comparison with its parents is not attributable to a low capacity of the carboxylation step (s).

**Leaf diffusion resistance.** The type of kinetics shown in Figs. 8 and 10 for the F<sub>1</sub> hybrid could be obtained if the resistance to gaseous diffusion of CO<sub>2</sub> from the ambient atmosphere to the mesophyll cell walls were much higher in the F<sub>1</sub> hybrid than in the parents. Since the diffusion of CO<sub>2</sub> from the ambient air to the mesophyll cell walls encounters the same physical barriers (the stomata and the leaf boundary layer) as does the diffusion of water vapor in the opposite direction, the CO<sub>2</sub> diffusion resistance can be calculated from the water vapor diffusion resistance when water vapor exchange is measured simultaneously with that of CO<sub>2</sub>. Such measurements were made using the technique of Slatyer and Bierhuizen (1964). Although some variation was present among individual leaves and experiments, the resistance to the diffusion of water vapor was low in all plants used. The mean values obtained were 1.2, 0.8, and 0.9 for *A. rosea*, *A. patula*, and the F<sub>1</sub> hybrids, respectively. As previously reported (Gauhl and Björkman, 1969; *Year Book* 68, p. 627) changes in oxygen concentration in the range 1–21% had no effect on diffusion resistance in *A. rosea* and *A. patula*; the present studies show that this is also true of the F<sub>1</sub> hybrids. Our values of the diffusion resistances for *A. patula* leaves are very similar to those recently reported by Slatyer (1970) for *A. hastata*, a species very closely related, if not identical, to the subspecies of *A. patula* used by us. Our values for *A. rosea* are also similar to those obtained by Slatyer (*loc. cit.*) for *A. spongiosa*, a perennial Australian species which is not closely related to *A. rosea*.

but which also possesses  $\beta$ -carboxylation photosynthesis.

Since the values for the  $F_1$  hybrids are lower than those for *A. rosea* and as low as for *A. patula*, it is evident that resistance to the gaseous diffusion of  $CO_2$  is not responsible for the comparatively low rate of light-saturated photosynthesis under normal  $CO_2$  concentration in the  $F_1$  hybrids.

*Dependence on  $CO_2$  concentration.* Figure 11 shows the rate of photosynthetic  $O_2$  evolution as a function of  $CO_2$  concentration inside the leaves of *A. rosea*, *A. patula*, and their  $F_1$  hybrid. The measurements were made under saturating light intensity and low  $O_2$  concentration. Water vapor exchange was also simultaneously measured so that any differences in  $CO_2$  concentration inside the leaf due to differences in stomatal aperture, either among the different plants or among the different external

$CO_2$  concentrations used, could be taken into account.

As shown by the steep initial slope of the  $CO_2$  dependence curve for *A. rosea*, this species is considerably more efficient than *A. patula* in utilizing low internal  $CO_2$  concentrations. Consequently, under low ambient  $CO_2$  concentration *A. rosea* is capable of a higher photosynthetic rate than *A. patula* for any given stomatal resistance value. Under normal  $O_2$  concentration the difference between the two species is still greater, since in *A. patula* the initial slope of the curve is then reduced by about one-third and the curve intersects the abscissa at a value corresponding to the  $CO_2$  compensation point, whereas the curve for *A. rosea* is unaffected by  $O_2$  concentration. The difference in initial slope between *A. rosea* and *A. patula* is similar to that recently reported by Osmond, Troughton, and Goodchild (1969) and Slatyer (*loc. cit.*) for *A. spongiosa* and *A. hastata*.

The  $F_1$  hybrids are much less efficient in utilizing low  $CO_2$  concentrations than either parent. Under low  $O_2$  concentration the efficiency in the  $F_1$  hybrids is only about one-half that of *A. patula* and one-third that of *A. rosea* (Fig. 11). Under 21%  $O_2$ , the corresponding values are one-half and one-fifth (not shown). In *A. rosea* photosynthesis saturates at lower  $CO_2$  concentrations than in *A. patula*, but the two species reach about equally high rates at  $CO_2$  saturation. Notably, the  $F_1$  hybrid is also capable of as high a photosynthetic rate at  $CO_2$  saturation but because of its low efficiency it requires much higher  $CO_2$  concentrations to reach saturation than do the parental species.

These results are consistent with the conclusion, based on the responses to light intensity, that the photochemical steps are not responsible for the comparatively low photosynthetic capacity of the  $F_1$  hybrids at normal  $CO_2$  concentration. The results are also consistent with the evidence obtained from the temperature dependence curves that the

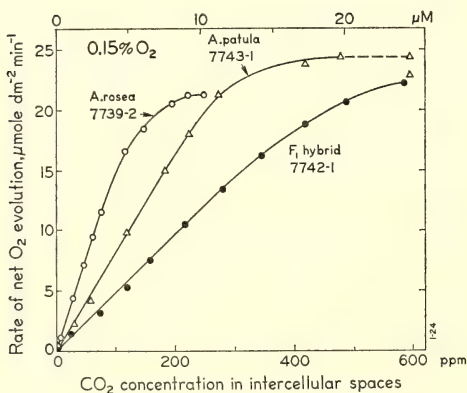


Fig. 11. Photosynthetic oxygen evolution as a function of  $CO_2$  concentration in the intercellular spaces under 0.15%  $O_2$  in the  $F_1$  hybrid and the parental species. Leaf temperature was  $27^\circ C$ . Saturating light intensities were used for each plant and  $CO_2$  concentration. The  $CO_2$  concentration in the intercellular spaces,  $C_i$ , was calculated from the expression  $C_i = C_a - P \times R_w \times D_{CO_2}/D_{H_2O}$  where  $C_a$  is the external and  $C_i$  the internal  $CO_2$  concentration;  $P$ , the measured rate of photosynthesis;  $R_w$ , the measured resistance to water vapor transfer and  $D_{CO_2}/D_{H_2O}$ , the ratio between the diffusion coefficients for  $CO_2$  and water vapor; a value of 1.56 for this ratio was used.

low photosynthetic rate is not attributable to a low activity of the carboxylation enzyme(s); see also Fig. 15, which shows a  $\text{CO}_2$  dependence curve for photosynthesis obtained with *A. patula* leaves with low carboxydismutase activity as a result of nitrogen deficiency. It is also noteworthy that when the  $F_1$  hybrids were grown at one-half the light intensity used in the present work the levels of the two carboxylation enzymes were considerably lower, whereas the photosynthetic rates were not significantly lower (p. 634, this *Year Book*).

The type of  $\text{CO}_2$  dependence exhibited by the  $F_1$  hybrid would usually be interpreted as indicative of a rate limitation by processes concerned with  $\text{CO}_2$  transport inside the leaf. Carbonic anhydrase may serve to facilitate such transport. It has been reported that this enzyme is absent in species with  $\beta$ -carboxylation photosynthesis or that the activity is much lower in these plants than in plants without  $\beta$ -carboxylation photosynthesis. However, the results obtained in this laboratory indicate that carbonic anhydrase is at least as high in *A. rosea* as in *A. patula* and that it is high also in the  $F_1$  hybrids even though it may be somewhat lower than in the parents. It does not seem likely, in view of the present results, that carbonic anhydrase activity is rate limiting in the  $F_1$  hybrid under normal  $\text{CO}_2$  concentration.

Another possible explanation for the comparatively high  $\text{CO}_2$  requirement for  $\text{CO}_2$  saturation in the  $F_1$  hybrid is that its leaf anatomy (pp. 629–632, this *Year Book*) offers a greater physical resistance to  $\text{CO}_2$  transport inside the leaf than the conventional leaf anatomy of *A. patula*. However, this possibility also appears remote. Our results show that the physical component of resistance to  $\text{CO}_2$  transport inside the leaf must be very small in *A. rosea* leaves, and the diffusion path lengths are unlikely to differ substantially between *A. rosea* and *A. patula*; the anatomy of the  $F_1$  hybrids

is intermediate between these. This conclusion is further supported by the results obtained with the  $F_2$  hybrids, reported below. We have therefore not been able to identify any single internal factor or single category of factors that in itself would be sufficient to account for the low photosynthetic capacity in normal air of the  $F_1$  hybrids in comparison with the parental species (pp. 638–639, this *Year Book*).

*Photosynthetic rate in  $F_2$  hybrids.* As reported in previous sections of this report, the  $F_2$  hybrids show great variation in growth habit, leaf shape, and leaf anatomy, as well as in biochemical characteristics. It is surprising to find that despite this variation there is remarkably little variation in their photosynthetic capacity (Table 8). The rates measured at  $27^\circ\text{C}$ , 300 ppm  $\text{CO}_2$ , and 1.3%  $\text{O}_2$  for each of a population of ten different  $F_2$  hybrids show no greater variation than that obtained for a population of  $F_1$  hybrids or for either of the parental species. The mean photosynthetic rate for the  $F_2$  hybrids was  $10.5 \mu\text{mole CO}_2 \text{ min}^{-1} \text{ dm}^{-2}$ , which does not differ statistically from  $11.3 \mu\text{mole CO}_2 \text{ min}^{-1} \text{ dm}^{-2}$  for the  $F_1$  hybrids.

In *A. patula* photosynthetic  $\text{CO}_2$  uptake is inhibited by 21%  $\text{O}_2$ ; at  $27^\circ\text{C}$  and an ambient  $\text{CO}_2$  concentration of 300 ppm the rate under 21%  $\text{O}_2$  is about 63% of that under 1.3%  $\text{O}_2$ , whereas in *A. rosea*  $\text{CO}_2$  uptake is unaffected by oxygen concentration in this range. The hybrids are not intermediate in this respect. The mean photosynthetic rate in 21%  $\text{O}_2$  of four  $F_1$  hybrids was 57% of the rate in 1.3%  $\text{O}_2$ . The corresponding mean for the  $F_2$  hybrids was 64% with essentially no variation among the individual genotypes. Thus the inhibitory effect of oxygen in all hybrids was very close to that in *A. patula* and in other species lacking  $\beta$ -carboxylation photosynthesis.

Stomatal diffusion resistances of the  $F_2$  hybrid leaves were low with values close to those obtained with the *A.*



*patula* and the  $F_1$  hybrid leaves; the values were unaffected by oxygen concentration.

The efficiency of utilization of low  $CO_2$  concentration in the intercellular spaces,  $\Delta P/\Delta C_i$ , is the initial slope of the curve for photosynthesis as a function of  $CO_2$  concentration in the intercellular spaces. Many workers call its reciprocal,  $\Delta C_i/\Delta P$ , the "mesophyll resistance." This was estimated as  $\Delta C_i/\Delta P = (C_a - C_c - P \times R_w)/P$  where:  $C_a$  is the ambient  $CO_2$  concentration;  $C_c$ , the  $CO_2$  compensation point;  $P$ , the measured rate of  $CO_2$  uptake; and  $R_w$ , the resistance of the stomata and leaf boundary layer to  $CO_2$  diffusion.  $\Delta P/\Delta C_i$  has the dimensions  $cm \times sec^{-1}$ , since it is the rate of photosynthesis in  $cm^3 CO_2$  per  $cm^2$  leaf area per sec, ( $cm^3 cm^{-2} sec^{-1}$ ) divided by the concentration of  $CO_2$  in the intracellular spaces expressed as the volume of  $CO_2$  per volume of gas space, ( $cm^3 cm^{-3}$ ). The values obtained for the different plants at  $27^\circ C$  are given in Table 9. Under 1.3%  $O_2$  the mean value for the ten  $F_2$  hybrids is  $0.17 cm sec^{-1}$  as compared with 0.19, 0.36, and 0.67 for the  $F_1$  hybrids, *A. patula*, and *A. rosea*, respectively. Again the mean for the  $F_2$  hybrids and the variation among the different  $F_2$  genotypes are about the same

as for the  $F_1$  hybrids. No single value approaches those of either of the parental species. The inhibitory effect of 21%  $O_2$  on the efficiency of  $CO_2$  conversion ( $\Delta P/\Delta C_i$ ) in the  $F_2$  hybrids does not differ significantly from that in the  $F_1$  hybrids or *A. patula*. No single  $F_2$  hybrid shows any resemblance to *A. rosea* in this respect.

*CO<sub>2</sub> compensation points.* At  $27^\circ C$  and 21%  $O_2$  the  $CO_2$  compensation point in *A. patula* leaves is 44 ppm whereas it is very close to zero in *A. rosea*. The mean value for the  $F_1$  hybrids is 37 ppm, i.e., slightly lower than that for *A. patula*, but this difference is scarcely significant. The temperature dependence of the  $CO_2$  compensation point is the same in *A. patula* and the  $F_1$  hybrids. The  $CO_2$  compensation point, in contrast to the photosynthetic rates, the  $CO_2$  conversion efficiencies, and the inhibitory effect of  $O_2$ , exhibits considerable variation among the  $F_2$  hybrids (Table 10). Some of the  $F_2$  hybrids have as high compensation points as *A. patula*, and one  $F_2$  hybrid has a compensation point as low as 19 ppm, but none of the  $F_2$  hybrids investigated so far approaches *A. rosea* in this respect. No consistent relationship between  $CO_2$  compensation point and leaf anatomy is apparent. The indi-

TABLE 9. The Efficiency of Utilization of  $CO_2$  at Low Concentrations in the Intercellular Spaces,  $\Delta P/\Delta C_i$ , in Parents and Hybrids at  $27^\circ C$

Plant	Efficiency, $\Delta P/\Delta C_i$		Ratio, $\frac{\Delta P/\Delta C_i \text{ in } 21\% O_2}{\Delta P/\Delta C_i \text{ in } 1.3\% O_2}$
	21% $O_2$	1.3% $O_2$	
<i>A. rosea</i>	0.67	0.67	1.00
<i>A. patula</i>	$0.25 \pm 0.02$	$0.36 \pm 0.02$	$0.70 \pm 0.04$
$F_1$ hybrid	$0.11 \pm 0.01$	$0.19 \pm 0.02$	$0.60 \pm 0.05$
$F_2$ hybrids: 7735-1	0.11	0.17	0.64
7735-2	0.13	0.19	0.68
7735-3	0.12	0.18	0.67
7735-4	0.14	0.19	0.74
7736-1	0.14	0.19	0.71
7740-1	0.13	0.20	0.65
7740-3	0.11	0.16	0.71
7740-5	0.13	0.20	0.64
7744-4	0.12	0.18	0.69
Mean of $F_2$ hybrids $\pm$ S.D.	$0.12 \pm 0.01$	$0.17 \pm 0.02$	$0.68 \pm 0.03$

TABLE 10. CO<sub>2</sub> Compensation Point at 27° and 21% O<sub>2</sub> in F<sub>2</sub> Hybrids from a Cross between *A. rosea* and *A. patula* in Comparison with the Parental Species and the F<sub>1</sub> Hybrids

Plant	Compensation Point, ppm CO <sub>2</sub>
<i>A. rosea</i>	≤ 2
<i>A. patula</i>	44.2 ± 1.4
F <sub>1</sub> hybrid	37.0 ± 3.5
F <sub>2</sub> hybrids: 7735-1	37
7735-2	43
7735-3	29
7735-4	34
7736-1	46
7740-3	40
7740-4	35
7740-5	19
7744-4	27

viduals with the lowest compensation points, F<sub>2</sub> hybrids 7740-5, 7744-4, and 7735-3, all have leaf anatomies approaching that of *A. rosea*. However, the resemblance to the leaf anatomy of *A. rosea* is less pronounced in F<sub>2</sub> hybrid 7740-5, which has a compensation point of 19 ppm, than in F<sub>2</sub> hybrid 7735-1, which has a relatively high compensation point of 37 ppm.

With one notable exception (F<sub>2</sub> hybrid 7740-3, which has high PEP carboxylase activity and a high compensation point) there appears to be a fairly good correlation between a high activity of this enzyme and a low compensation point. Such a correlation implies that high PEP carboxylase is necessary for a low CO<sub>2</sub> compensation value. However, one cannot exclude the possibility that this apparent correlation is the result of genetic linkage.

The data do not provide any evidence either for or against the existence of a relationship between CO<sub>2</sub> compensation point and the fraction of CO<sub>2</sub> that is fixed into C<sub>4</sub>-dicarboxylic acids.

It is noteworthy that despite the considerable differences in CO<sub>2</sub> compensation point among the F<sub>2</sub> hybrids there were no corresponding differences in photosynthetic rate under either 21% or 1.3% O<sub>2</sub>.

*General conclusions.* The fact that *A. rosea* and *A. patula* can be hybridized and give rise to strong diploid F<sub>1</sub> hybrids shows that the genetic divergence between species with and without  $\beta$ -carboxylation photosynthesis need not be great. This indicates that it may be possible for the plant breeder (at least in theory) to introduce desirable characteristics associated with  $\beta$ -carboxylation photosynthesis into species that are agriculturally important but which do not possess this pathway.

However, our present results indicate that at least in *Atriplex* the inheritance of the unusually high capacity for photosynthesis associated with  $\beta$ -carboxylation photosynthesis may not be simple even though the inheritance of each single characteristic may be determined by relatively few genes. This is suggested by the remarkably great variation in leaf anatomy, PEP carboxylase activity, and CO<sub>2</sub> compensation point obtained in our small sample of F<sub>2</sub> hybrids. This variation is particularly surprising since the F<sub>2</sub> hybrids were not diploid but had various degrees of polyploidy.

It is clear that the inheritance of the chloroplast morphology associated with  $\beta$ -carboxylation photosynthesis is not directly transmitted by the maternal parent, nor is there any evidence that this is the case with any other factors that underlie the photosynthetic characteristics associated with this pathway.

Even though there is strong evidence that CO<sub>2</sub> fixation in the F<sub>1</sub> hybrids involves both the  $\beta$ -carboxylation of phospho(enol)pyruvate and the direct carboxylation of ribulose-1,5-diphosphate, these plants do not have high photosynthetic capacity in normal air; on the contrary, their capacity is only about one-half that of the male parent and about one-third that of the female parent. This is largely due to the much lower intrinsic efficiency of the F<sub>1</sub> hybrids in utilizing low internal CO<sub>2</sub> concentrations; only at very high CO<sub>2</sub> concentrations do the photosynthetic rates

of the hybrids approach those of the parental species. Moreover, the inhibitory effect of 21% O<sub>2</sub> on photosynthesis is as pronounced in the F<sub>1</sub> hybrids as in the male parent, *A. patula*. The F<sub>1</sub> hybrids thus provide a striking example of "negative heterosis" with regard to photosynthetic capacity.

The gross leaf anatomy shows great variation among the F<sub>2</sub> hybrids, and the anatomical characteristics of both parents have been essentially recovered. PEP carboxylase activity also showed considerable segregation, and activities ranged from as low as those found in *A. patula* to as high as about one-half those in *A. rosea*. There was no consistent relationship between the level of PEP carboxylase and leaf anatomy. However, at least two F<sub>2</sub> individuals possessed characteristics of leaf anatomy closely resembling those of *A. rosea*, and at the same time high levels of PEP carboxylase were present. Nevertheless, their photosynthetic characteristics did not differ from those of the other F<sub>2</sub> hybrids. The photosynthetic efficiency was as low and the inhibitory effect of 21% O<sub>2</sub> was as great as in the F<sub>1</sub> hybrids. These results provide strong evidence that neither the capacity for CO<sub>2</sub> fixation via the  $\beta$ -carboxylation of PEP, nor the specialized leaf anatomy found in species with  $\beta$ -carboxylation photosynthesis is in itself, or even in combination, sufficient for the production of a plant with high photosynthetic efficiency and the absence of the inhibitory effect of O<sub>2</sub>. Evidently, these characteristics can only be obtained if all the component steps are also properly coordinated and/or compartmented. Consequently, it seems likely that the minimum genetic diversity that must be present between species with and species without  $\beta$ -carboxylation photosynthesis, if the desirable photosynthetic characteristics associated with this pathway are to be maintained, involves at least several loci. Unfortunately, if this conclusion is valid for other species, it is unlikely that

mutants possessing the desirable characteristics associated with  $\beta$ -carboxylation photosynthesis are to be found among species that normally lack this pathway and that also lack close relatives possessing it. Neither is it likely that such mutants can be produced artificially. Methods based on intrageneric hybridization between agriculturally valuable species that lack  $\beta$ -carboxylation photosynthesis and species possessing this pathway may have a greater probability of success.

The low fertility of the F<sub>1</sub> hybrid between *A. rosea* and *A. patula* and the polyploid nature of the F<sub>2</sub> hybrids prevent a precise genetic analysis of  $\beta$ -carboxylation photosynthesis. It is therefore of interest that according to Hall and Clements (1923) *A. sabulosa* Rouy (*A. maritima* Hallier in the nomenclature of Hall and Clements) has taxonomic characteristics intermediate between those of the *A. patula* and the *A. rosea* groups. Hence it is possible that *A. sabulosa* may have sufficient genetic compatibility with *A. rosea* or *A. patula* to produce diploid F<sub>2</sub> hybrids with either or with both of them. This possibility is currently being explored.

### References

- Björkman, O., and E. Gauth, *Photosynthetica*, 4, 123, 1970.
- Björkman, O., and P. Holmgren, *Physiol. Plant.*, 16, 889, 1963.
- Gauth, E., and O. Björkman, *Planta*, 88, 187, 1969.
- Hall, H. M., and F. E. Clements, *The Phylogenetic Method in Taxonomy: The North American Species of Artemisia, Chrysothamnus, and Atriplex*, Carnegie Inst. of Wash. Publ. 326, Washington, D.C., 1923.
- Osmond, C. B., J. H. Troughton, and D. J. Goodchild, *Zeit. Pflanzenphysiol.*, 61, 218, 1969.
- Slatyer, R. O., *Planta*, 91, 175, 1970.
- Slatyer, R. O., and J. F. Bierhuizen, *Plant Physiol.*, 39, 1051, 1964.



## PLATES



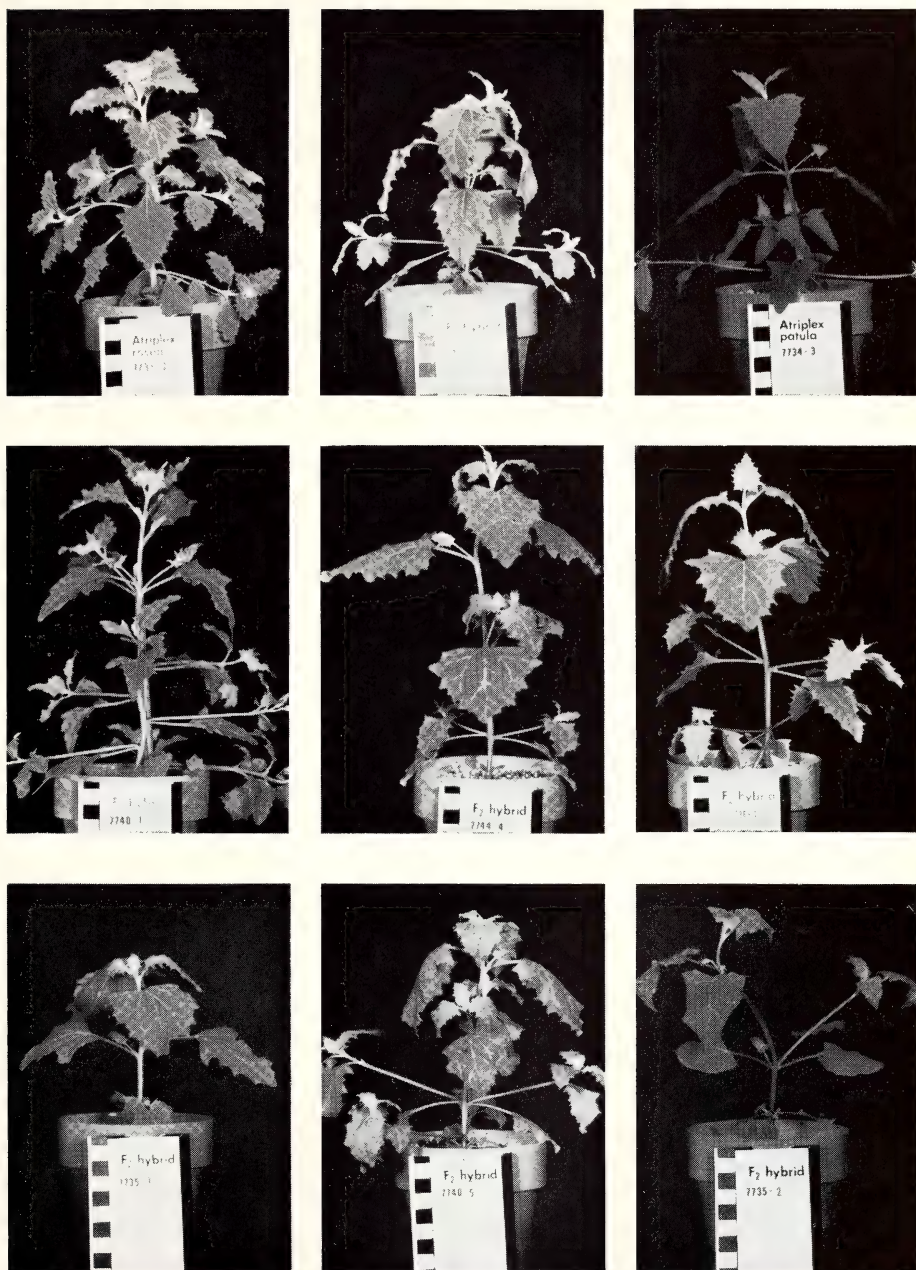


Plate 1. Representative experimental plants of *Atriplex rosea*, *A. patula* ssp. *hastata*, and the first- and second-generation hybrids between the two species. The plants are in a comparable stage of development as grown under uniform conditions in the controlled cabinets. Note the leaf shapes and branching patterns of the parental species in comparison with the recombinations of these characteristics in the hybrids. Also see Fig. 3.



Plates 2-8. Electron micrographs of leaves of *Atriplex rosea*, *A. patula*, their F<sub>1</sub> hybrid, and selected F<sub>2</sub> hybrids. Approximately 1 × 4 mm pieces of fully expanded leaves of *A. rosea*, *A. patula*, their F<sub>1</sub> hybrid, and selected F<sub>2</sub> hybrids were fixed for 1.5 hr with 2.5% glutaraldehyde in 0.067 M phosphate buffer, pH 7.2, at 4°C. After a minimum of 4 changes with phosphate buffer over a period of up to 5 days, the samples were postfixated in 2% OsO<sub>4</sub> in 0.067 M phosphate buffer, pH 7.2, for 1.5 hr at 20°C. Following dehydration in ethyl alcohol, the leaf pieces were infiltrated and embedded in a low viscosity epoxy resin (Spurr, A. R., *J. Ultrastruct. Res.* 26, 31-43, 1969). Silver sections cut on a Cambridge ultramicrotome with a DuPont diamond knife were mounted on uncoated grids and contrasted with uranyl acetate and lead citrate. Micrographs were taken on a Siemens Elmiskop 101 at 60 or 80 Kv.

Plate 2. Sections through a fully expanded leaf of *A. rosea*. A. Light micrograph of a 1 μ-thick section of the leaf area in the electron micrographs B and C below. A well-developed bundle sheath surrounds the xylem vessel seen in longitudinal section near the terminus of the vascular bundle. Mesophyll cells with large vacuoles and thin walls surround the bundle sheath, and extremely large, vacuolate parenchyma cells occupy the remainder of the leaf. Bar = 100 μ. B. Electron micrograph of a thin section through parts of two thick-walled bundle sheath cells (*BS*) and the thin-walled vacuolate mesophyll cells (*MP*) adjacent. Numerous plasmodesmata (*PD*) traverse the wall between these two cell types. Chloroplasts of the mesophyll cells have a highly disordered lamellar system with few grana and starch grains. Bar = 5 μ. C. Electron micrograph of a thin section through part of a xylem vessel element (*XV*) and adjacent well-developed bundle sheath cell (*BS*). Cytoplasm occupies almost the total area of the bundle sheath cells, and the cell walls show conspicuous secondary thickening. Rows of mitochondria are packed between the enlarged chloroplasts which have extremely well-developed lamellar systems. Occasional single membrane-bound bodies thought to be peroxisomes (*P*) are evident. Bar = 5 μ.

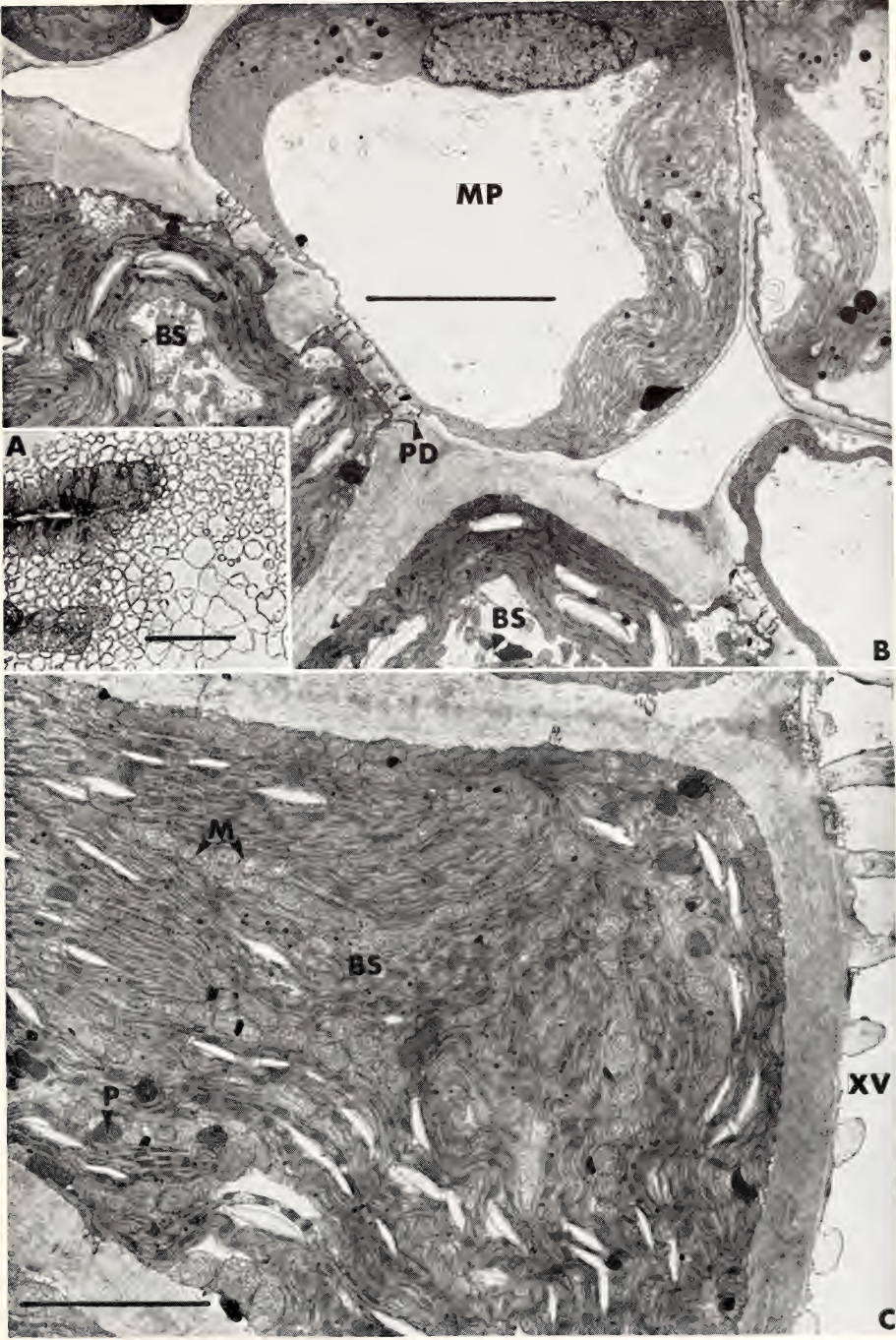


Plate 3. Sections through a fully expanded leaf of *A. patula*. A. Light micrograph of a  $1\mu$ -thick section of the leaf area shown in the electron micrographs B and C below. Bar =  $100\mu$ . B. Electron micrograph of a thin section through parts of three vacuolate, thin-walled mesophyll cells (*MP*). The chloroplasts have a moderately well-developed lamellar system and numerous large starch grains. Bar =  $5\mu$ . C. Electron micrograph of a thin section through parts of two weakly developed bundle sheath cells (*BS*) with thin walls and large vacuoles which surround a vascular bundle. A xylem vessel element (*XV*) is seen in cross section at the right edge of the micrograph. Both mitochondria (*M*) and single membrane-bound peroxisomes (*P*) are recognizable in the thin band of cytoplasm along the cell wall of the bundle sheath cells. Bar =  $5\mu$ .



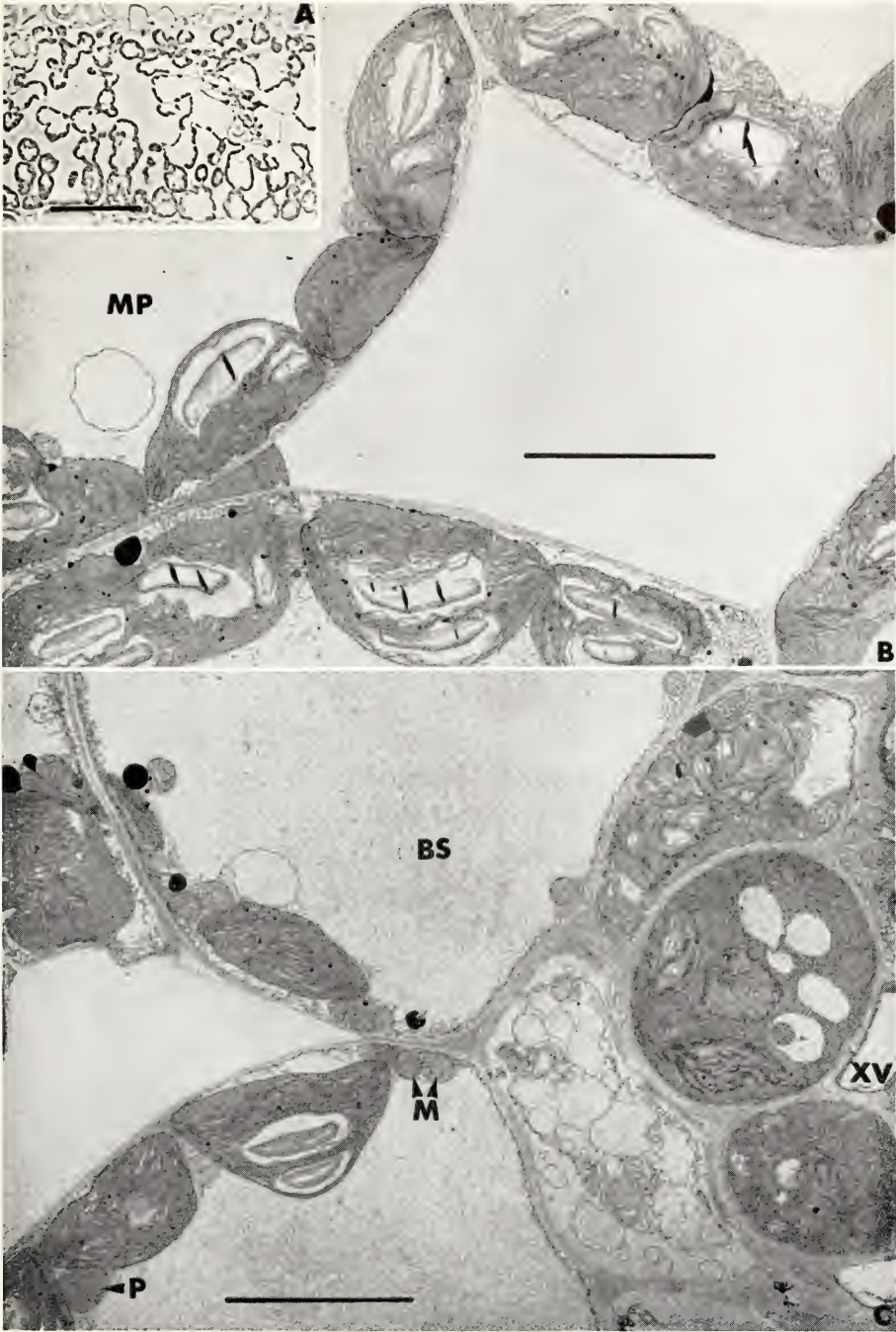


Plate 4. Sections through a fully expanded leaf of the  $F_1$  hybrid no. 7730-4, *A. rosea*  $\times$  *A. patula*. A. Light micrograph of a  $1\mu$ -thick section of the leaf showing a vascular bundle in cross section. The xylem and phloem appear to be mostly surrounded by a mass of small, relatively undifferentiated parenchyma cells. Bar =  $100\mu$ . B. Light micrograph of a  $1\mu$ -thick section of the leaf area depicted in the electron micrographs C and D below, showing a vascular bundle sectioned parallel to the longitudinal axis near its terminus. Bar =  $100\mu$ . C. Electron micrograph of a thin section through parts of 3 mesophyll cells with large vacuoles and thin cell walls. Bar =  $5\mu$ . D. Electron micrograph of a thin section through part of a xylem vessel element (XV) cut parallel to its longitudinal axis and surrounded by bundle sheath cells somewhat intermediate in cytological organization, degree of secondary wall thickening and vacuolation between the *A. rosea* and *A. patula* parents. Mitochondria (*M*) and peroxisomes (*P*) are evident. The chloroplasts show a well-developed lamellar system although they are considerably smaller than those of *A. rosea*. Bar =  $5\mu$ .





Plate 5. Sections through a fully expanded leaf of the  $F_2$  hybrid 7735-1. A. Light micrograph of a  $1\mu$ -thick section of the leaf area depicted in the electron micrograph B showing vascular bundles in cross and longitudinal section, surrounded by a moderately well-developed bundle sheath. Bar =  $100\mu$ . B. Electron micrograph of a thin section through two xylem vessel elements (*XV*) and the adjacent moderately well-developed bundle sheath cells (*BS*). Vacuolate mesophyll cells (*MP*) surround the bundle sheath, and conspicuous plasmodesmata (*PD*) traverse the walls separating the two cell types. Secondary thickening of the wall of the bundle sheath cells is slightly less than in the  $F_1$  and considerably less than in the *A. rosea* maternal parent. The chloroplasts of this  $F_2$  plant are also somewhat smaller, although they show well-developed lamellar systems. Bar =  $5\mu$ .

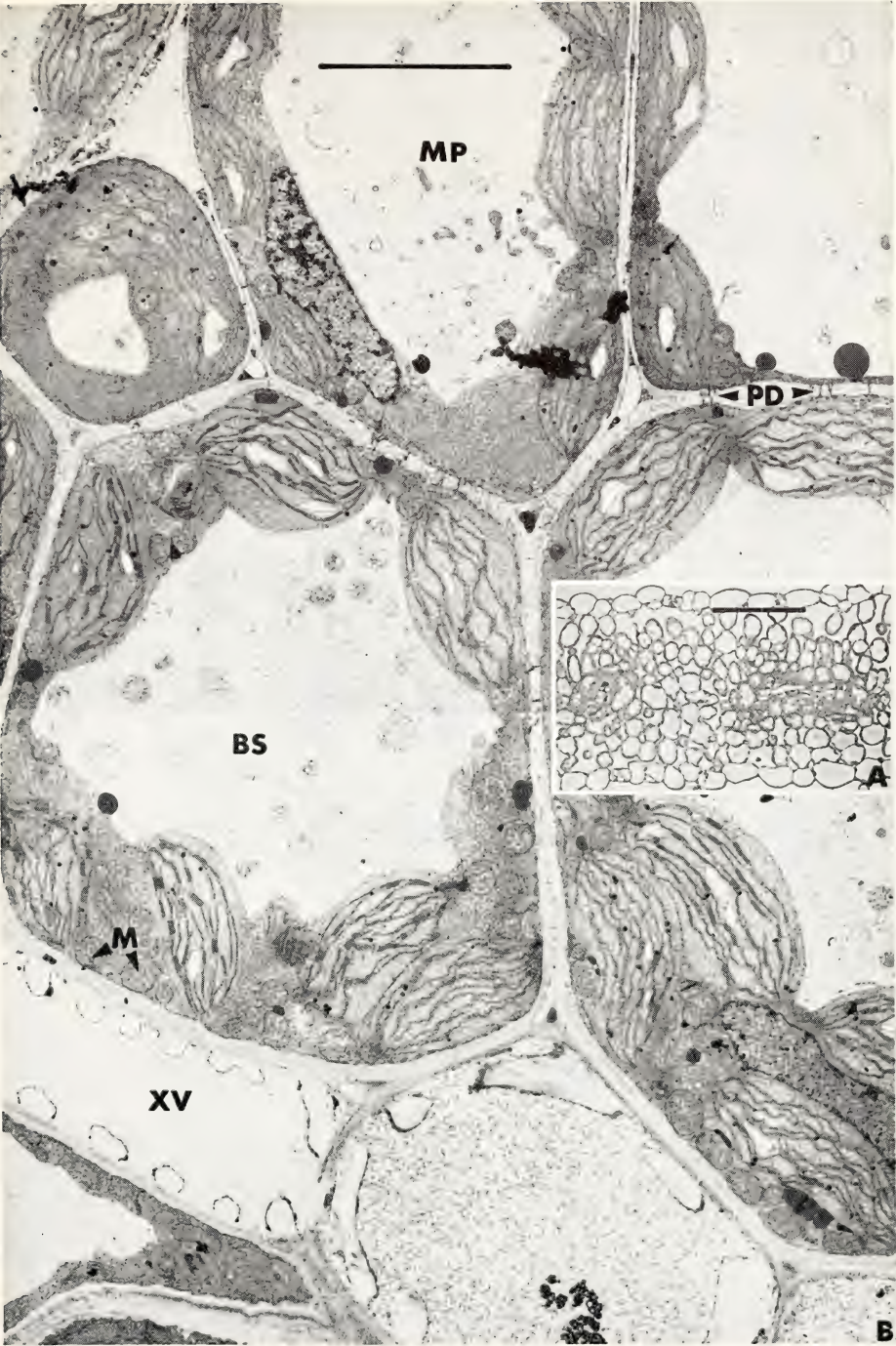


Plate 6. Sections through a fully expanded leaf of the  $F_2$  hybrid 7735-2. A. Light micrograph of a  $1\mu$ -thick section of the leaf area shown in the electron micrograph B. Bar =  $100\mu$ . B. Electron micrograph of a thin section through a xylem vessel element (*XV*), two of the surrounding bundle sheath cells (*BS*), and two of the adjacent mesophyll cells (*MP*). The bundle sheath cells show little secondary wall thickening, although they tend to be less vacuolate than the adjacent mesophyll cells. Plasmodesmata (*PD*) traversing the bundle sheath-mesophyll cell walls are evident. Many large mitochondria are seen in the bundle sheath cells, and both the mitochondria and chloroplasts show a relatively poorly contrasted membrane, suggesting either bad fixation of this sample or premature senescence of the tissue. Bar =  $5\mu$ .



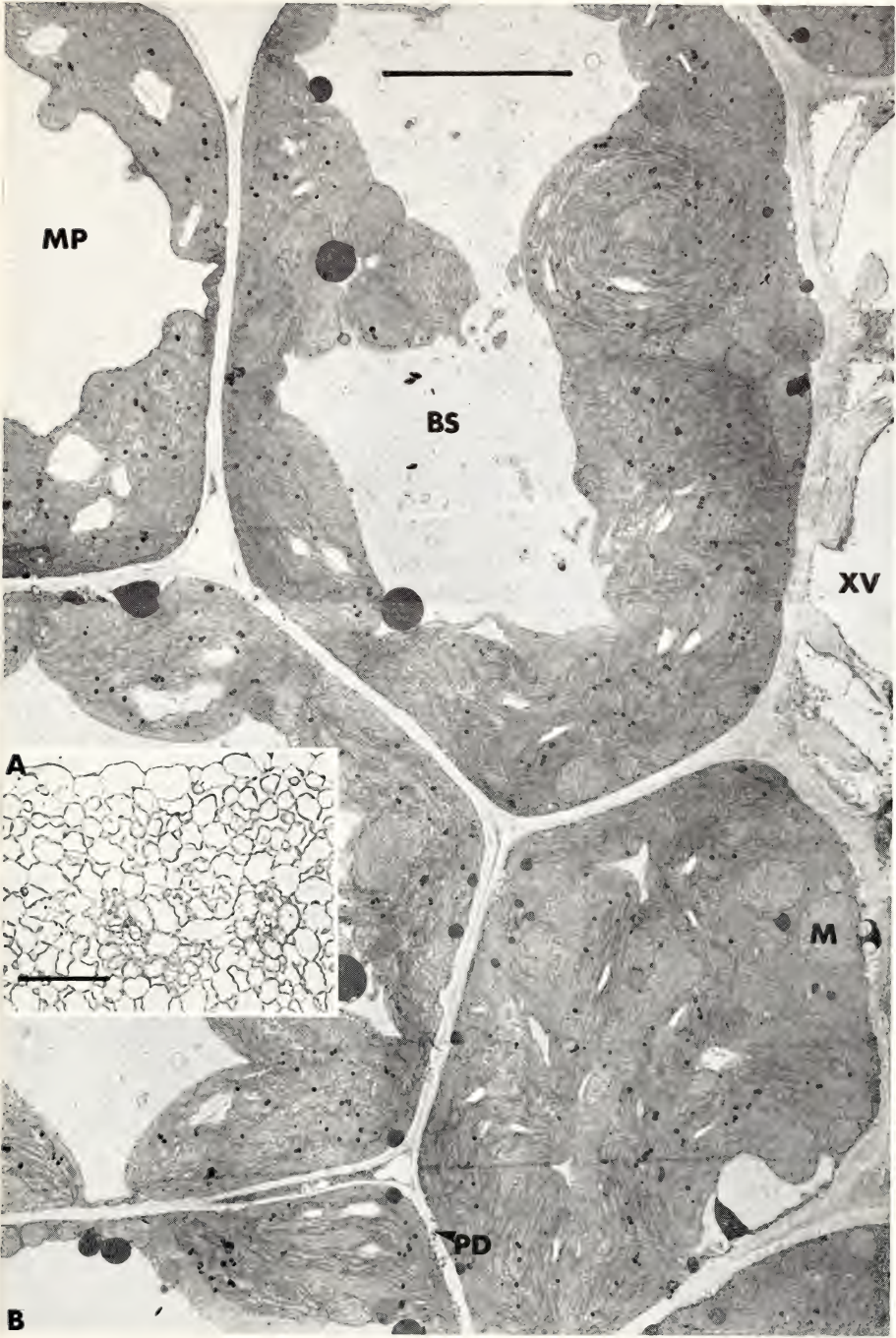


Plate 7. Sections through a fully expanded leaf of  $F_2$  hybrid 7735-3. A. Light micrograph of a  $1\mu$ -thick section of the leaf area of the electron micrograph B showing a moderately well-developed bundle sheath surrounding vascular bundles cut obliquely and parallel to their long axis. Bar =  $100\mu$ . B. Electron micrograph of a thin section cut obliquely through the vascular bundle. A xylem vessel element (XV) can be seen in cross section at the lower right. Two moderately well-developed bundle sheath cells (BS) with rather small vacuoles but with walls having little secondary thickening are connected by their plasmodesmata (PD) to the surrounding highly vacuolate mesophyll cells (MP). Chloroplasts of the bundle sheath cells have better developed lamellar systems and fewer starch grains than those of the mesophyll cells. Bar =  $5\mu$ .

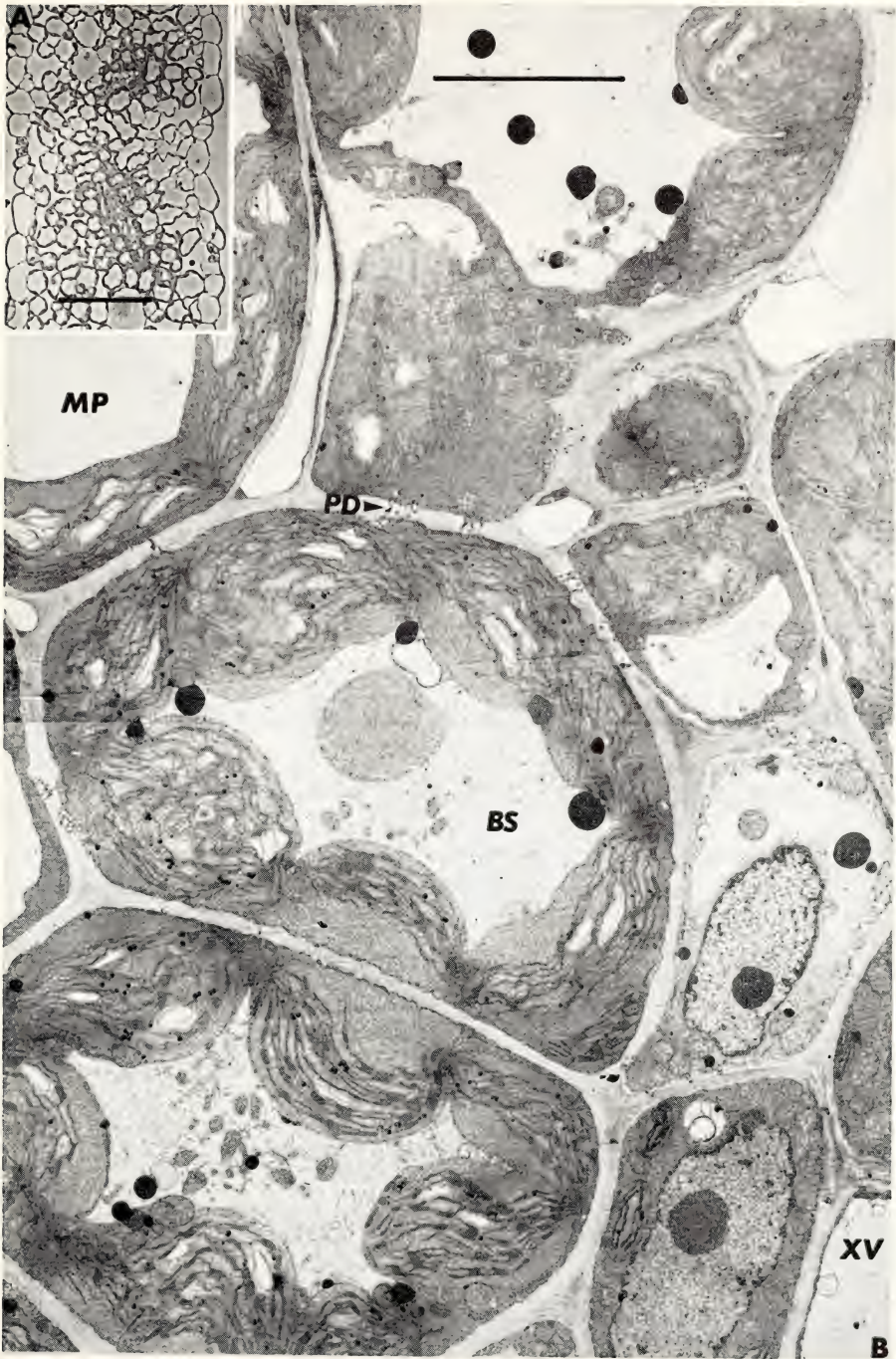




Plate 8. Sections through a fully expanded leaf of  $F_2$  hybrid 7735-4. A. Light micrograph of a  $1\mu$ -thick section of the leaf area of the electron micrograph B depicting a vascular bundle and surrounding bundle sheath and mesophyll cells. Bar =  $100\mu$ . B. Electron micrograph of a thin section through part of the vascular bundle and adjacent bundle sheath (*BS*) and mesophyll (*MP*) cell. Although the bundle sheath cell is almost as highly vacuolate as the surrounding mesophyll cells, it shows considerable secondary thickening of the cell wall. Plasmodesmata (*PD*) traverse the wall between the bundle sheath and mesophyll cell. Numerous small mitochondria (*M*) and occasional peroxisomes (*P*) can be seen in the cytoplasm of the bundle sheath cell. Parts of two xylem vessel elements (*XV*) are shown at the bottom of the micrograph. Bar =  $5\mu$ .

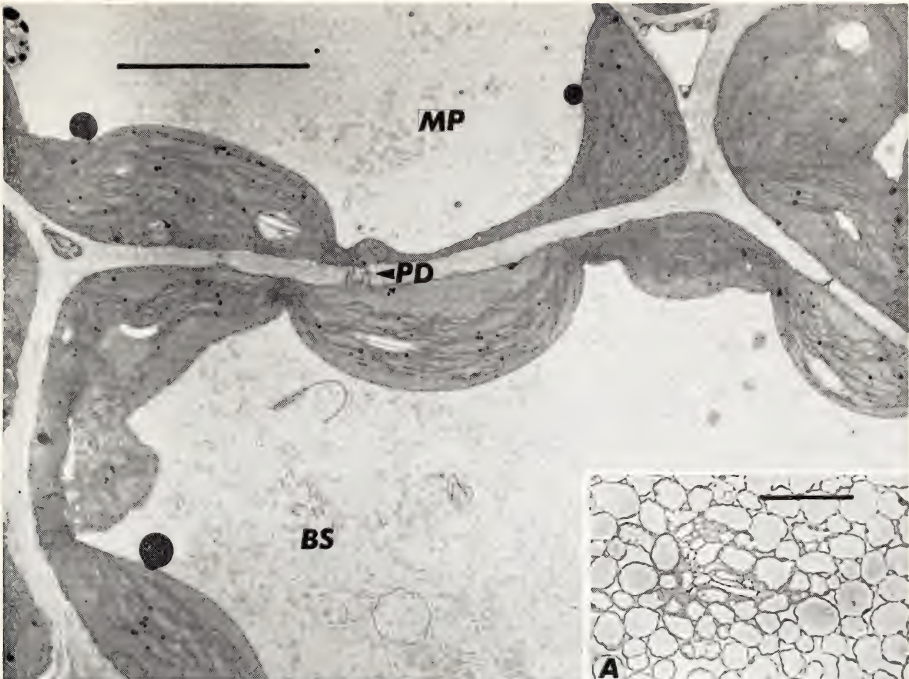
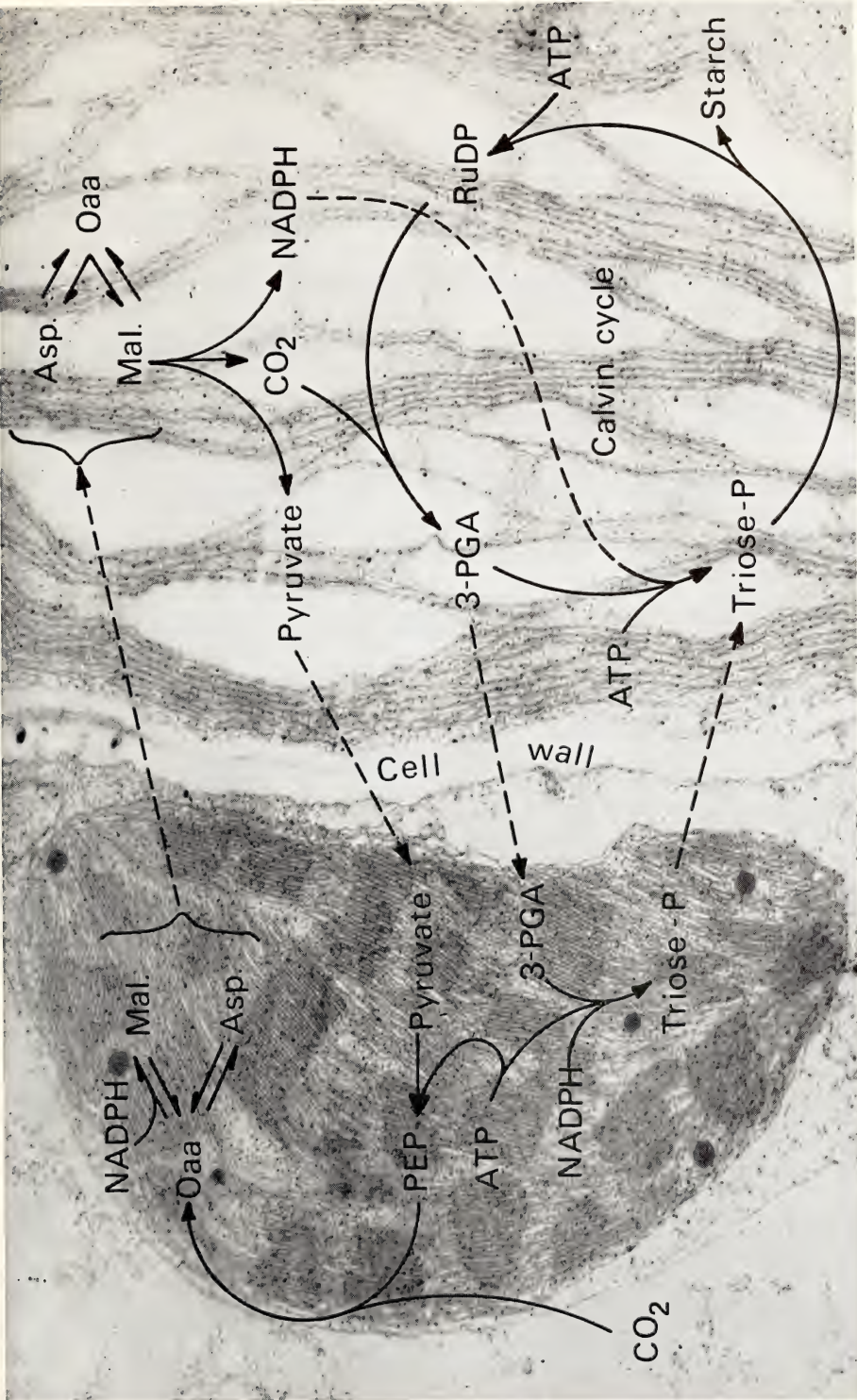


Plate 9. The division of reactions between bundle sheath (right) and mesophyll chloroplasts (left). Solid lines represent chemical transformation; dotted lines represent movement. Abbreviations are the same as those used in the text and in Fig. 12. The background electron micrograph showing adjacent bundle sheath and mesophyll cells of *Sorghum sudanense* was provided courtesy of Dr. Thana Bisalputra. Note the plasmodesmata penetrating the cell wall which separates the two cells.







THE COMPARTMENTATION OF REACTIONS  
IN  $\beta$ -CARBOXYLATION PHOTOSYNTHESIS<sup>1</sup>

J. A. Berry

A number of plants fix  $\text{CO}_2$  in photosynthesis by the  $\beta$ -carboxylation of phospho(enol)pyruvate (PEP). The work of Downton and Tregunna (1968) showed that these plants invariably possessed a specialized leaf anatomy characterized by two chlorophyllous tissues, a bundle sheath of thick-walled cells containing abundant chloroplasts, and a layer of thin-walled palisade, or spongy mesophyll, cells. The two tissues are arranged concentrically around the vascular bundles of the leaf (see also this *Year Book*, pp. 629-632).

The contrasting morphology of these two chlorophyllous tissues has led many workers, notably Rhoades and Carvalho (1946) and Leatsch (1968), to speculate that these tissues are functionally specialized and that this specialization may be required for the operation of the  $\beta$ -carboxylation pathway (*Year Book* 68, p. 622). Evidence indicating that the specialized leaf anatomy is directly involved in the metabolism of carbon in  $\beta$ -carboxylation photosynthesis will be discussed in this article.

*The path of carbon.* Figure 12 illustrates the pathway of carbon metabolism which has been determined from  $^{14}\text{CO}_2$  feeding experiments. The essential feature is that photosynthetic metabolism in these plants occurs by two linked cycles, one involving the  $\text{C}_4$ -acids, malate, aspartate, and oxaloacetate, the other the reductive pentose phosphate (Calvin) cycle. Evidence for this scheme is reviewed elsewhere (Hatch and Slack, 1970). The mechanism linking the two cycles (depicted as the carboxyl transfer) is not definitely established. Hatch and Slack (1966) have proposed that the carboxyl group of oxaloacetate may be

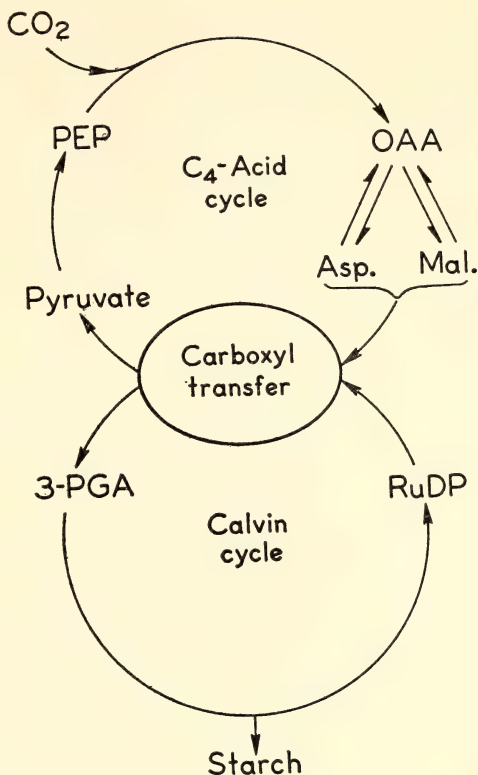


Fig. 12. The pathway of carbon metabolism in  $\beta$ -carboxylation photosynthesis. Abbreviations used: OAA, oxaloacetate; Asp, aspartate; Mal, malate; PEP, phospho(enol)pyruvate; 3-PGA, 3-phosphoglyceric acid; RuDP, ribulose-1,5-diphosphate.

transferred to another molecule (a two- or five-carbon unit) by a transcarboxylase enzyme to form 3-phosphoglycerate (3-PGA). Efforts to detect this enzyme have, however, been unsuccessful thus far. Alternatively it has been proposed (Berry *et al.*, 1970 and *Year Book* 68, p. 624) that this transfer might proceed by decarboxylation of a  $\text{C}_4$ -acid to yield  $\text{CO}_2$  which is re-fixed by carboxylation of ribulose-1,5-diphosphate (RuDP), forming 3-PGA. The latter postulate gains support from studies that indicate the presence of enzymes capable of the decarboxylation and re-fixation steps in extracts of leaves of plants with the  $\beta$ -carboxylation pathway.

<sup>1</sup>These investigations were supported in part by a grant to Dr. E. B. Tregunna, Department of Botany, University of British Columbia, by the National Research Council of Canada.



TABLE 11. Levels of Some Enzymes and the Occurrence of TNBT Reduction in the Bundle Sheath Plastids of Several Plants with  $\beta$ -Carboxylation Photosynthesis \*

Plant	PEP Carboxylase †	Carboxy- dismutase †	"Malic" Enzyme ‡	TNBT Reduction §
<i>Amaranthus edulis</i>	65.8	4.2	0.70	rapid
<i>Atriplex rosea</i>	42.9	4.4	0.1	rapid
<i>Gomphrena globosa</i>	38.9	1.4	9.2	slow
<i>Froelichia gracilis</i>	25.5	0.35	12.8	slow
<i>Panicum texanum</i>	45.1	1.9	0.5	rapid
<i>Panicum maximum</i>	24.8	4.2	0.3	rapid
<i>Sorghum sudanense</i>	60.5	4.2	44.0	absent
<i>Tidestromia oblongifolia</i>	49.4	0.66	15.0	slow
<i>Zea mays</i>	40.6	4.5	21.2	very slow

\* Enzyme activities expressed in  $\mu\text{moles min}^{-1} \text{g}^{-1}$  fresh weight.

† Measured by the method of Björkman and Gauhl, 1969.

‡ Measured by the method of Berry *et al.*, 1970.

§ Determined by the method of Downton *et al.*, 1970.

*Enzyme levels in leaves.* Table 11 presents the activities of some enzymes detected in extracts of several plants possessing the  $\beta$ -carboxylation pathway. The high level of PEP carboxylase is consistent with the proposal that this enzyme functions in initial  $\text{CO}_2$  fixation. The levels of carboxydismutase reported are similar to those reported by Björkman and Gauhl (1969) and Berry *et al.* (1970), and are consistent with the postulate that this enzyme also functions in the photosynthetic sequence of these plants. These values are severalfold greater than those reported by Slack and Hatch (1967), due to more complete extraction of the enzyme in these studies (see *Year Book* 68, pp. 620–633). Levels of "malic" enzyme are also high for several of the plants listed. This enzyme catalyzes the reversible decarboxylation of malic acid. It could serve to produce  $\text{CO}_2$  from malate for re-fixation by carboxydismutase and thus provide a mechanism for the synthesis of 3-PGA in these plants. PEP carboxylase could not operate in this manner, as the reaction proceeds only in the direction of carboxylation (Tchen and Vennesland, 1954). The low levels of "malic" enzyme detected in some of the other plants listed, such as *Atriplex rosea*, indicate that another mechanism may be required to explain the synthesis of 3-PGA from

$\text{C}_4$ -acids in these plants. This may occur via decarboxylation of another  $\text{C}_4$ -acid (aspartate or oxaloacetate) or perhaps by a transcarboxylase. Several plants that have low "malic" enzyme form aspartate as the major product of short-term photosynthesis, while those with high "malic" enzyme form mostly malate (Downton, 1970). In both groups of plants the level of carboxydismutase is normal. Thus,  $\text{CO}_2$  derived from a decarboxylation step could be re-fixed to form 3-PGA.

The sequential carboxylation pathway is a biochemically simple mechanism for which enzymes are available. It does not require new enzymes or alteration of the Calvin cycle. This cycle could operate in these plants much as it does in plants lacking  $\beta$ -carboxylation photosynthesis. Its source of  $\text{CO}_2$  would not, however, be external  $\text{CO}_2$ , but would be internally derived through decarboxylation of a  $\text{C}_4$ -acid. Carbon dioxide fixation by the  $\beta$ -carboxylation reaction and the  $\text{C}_4$ -acid cycle could operate as a shuttle providing  $\text{CO}_2$  to the site of Calvin cycle fixation.

*Other evidence.* Experiments have been reported which may indicate the presence of the Calvin system in plants with  $\beta$ -carboxylation photosynthesis. Johnson and Hatch (1969) present evidence that the carboxyl acceptor in the reaction

leading to the synthesis of 3-PGA in *Sorghum*, a  $\beta$ -carboxylation species, is RuDP. Kortschak and Nickell (1970) report that sugar-cane stalk parenchyma tissue cultured *in vitro* fixes  $\text{CO}_2$  by the Calvin pathway. Edwards *et al.* (1970) report Calvin cycle fixation by isolated cells of *Digitaria sanguinalis*, another species with  $\beta$ -carboxylation photosynthesis. The normal levels of carboxydismutase detected in the plants listed in Table 11 and the high levels of other enzymes of this system detected by Slack and Hatch (1967) also support the proposal that the Calvin system is operative in plants with  $\beta$ -carboxylation.

Light-stimulated decarboxylation reactions have been detected in light-dark and dark-light transients of photosynthetic  $\text{CO}_2$  exchange of plants with  $\beta$ -carboxylation photosynthesis. Radiochemical experiments (Berry *et al.*, 1970) with *Zea mays* indicate that the substrate for decarboxylation is a product of previous  $\text{CO}_2$  fixation and could be a  $\text{C}_4$ -acid. Similar light-activated decarboxylations were detected in many plants with the  $\beta$ -carboxylation pathway of photosynthesis (Downton, 1970) and may be related to the carboxyl transfer process.

Arguments against this mechanism are based on the observations that no detectable  $\text{CO}_2$  is lost from a corn leaf during steady state photosynthesis in the light under low  $\text{CO}_2$  concentration, and that there is no effect of high  $\text{CO}_2$  concentration on the proportion of label incorporated into 3-PGA during photosynthetic  $^{14}\text{CO}_2$  feedings (Hatch and Slack, 1970). If the site of decarboxylation and re-fixation is exposed to external  $\text{CO}_2$ , both should occur. The fact that they do not, of course, could indicate that these reactions do not occur. However, an alternative explanation is that the decarboxylation and re-fixation may be tightly coupled or contained and isolated from external  $\text{CO}_2$ . Containment of these reactions within the bundle sheath cells might provide such isolation.

*The anatomical distribution of en-*

*zymes within the leaf.* Recent work in several laboratories has shown that bundle sheath and mesophyll tissues differ in enzymatic complements. Table 12 indicates the tissue that has the greater activity of some enzymes that have been studied. Some enzymes such as PEP carboxylase, and pyruvate,  $\text{P}_i$  dikinase, which are associated with  $\beta$ -carboxylation  $\text{CO}_2$  fixation, are detected primarily in the mesophyll tissue. In contrast, carboxydismutase, enzymes of the reductive pentose phosphate cycle, and "malic" enzyme, which may be involved in the synthesis of 3-PGA, occur in the bundle sheath. It seems possible that the compartmentation of many of these enzymes is absolute. For example, part or all of the low level of PEP carboxylase detected in bundle sheath tissue may be derived from contaminating mesophyll tissue. High activity of one photosynthetic enzyme, NADP-glyceraldehyde-3-phosphate dehydrogenase, was found in both tissues of *Zea mays*. It is also noteworthy that the activity of nitrite reductase was compartmented in the mesophyll tissues of *Sorghum sudanense* and *Zea mays*, but was found in both the mesophyll and bundle sheath tissues of *Gomphrena globosa*. Further examination may show that the compartmentation of some other photosynthetic enzymes also differs from species to species. However, the dramatic differences that exist between the mesophyll and the bundle sheath tissue are remarkable, even though some photosynthetic enzymes may occur in both tissues.

*The division of reactions between the tissues.* Examination of the location of the enzymes involved in this pathway indicates that no single chloroplast contains all of the required enzymes. Plate 9 provides a summary of how the reactions seem to be arranged in the leaf. Confinement of the decarboxylation of malic acid and the re-fixation of  $\text{CO}_2$  by carboxylation of RuDP to the bundle sheath tissue would serve to minimize

TABLE 12. The Location of Some Photosynthetic Enzymes in Leaves of Plants with the  $\beta$ -Carboxylation Pathway of Photosynthesis

Enzyme	Plant	Location
PEP carboxylase	<i>Zea mays</i> <i>Gomphrena globosa</i> <i>Atriplex rosea</i>	mesophyll <sup>1</sup> mesophyll <sup>1</sup> mesophyll <sup>2</sup>
Pyruvate, P <sub>i</sub> dikinase	<i>Zea mays</i> <i>Amaranthus palmeri</i>	mesophyll <sup>6</sup> mesophyll <sup>5</sup>
NADP-malate dehydrogenase	<i>Sorghum sudanense</i> <i>Zea mays</i> <i>Gomphrena globosa</i>	mesophyll <sup>6</sup> mesophyll <sup>6</sup> both <sup>1</sup>
NADP-glyceraldehyde-3-P dehydrogenase	<i>Zea mays</i> <i>Sorghum sudanense</i>	both <sup>6</sup> both <sup>8</sup>
"Malic" enzyme	<i>Zea mays</i> <i>Gomphrena globosa</i>	bundle sheath <sup>1, 6</sup> bundle sheath <sup>1</sup>
Carboxydismutase	<i>Zea mays</i> <i>Gomphrena globosa</i> <i>Amaranthus palmeri</i> <i>Atriplex rosea</i>	bundle sheath <sup>1, 6</sup> bundle sheath <sup>1</sup> bundle sheath <sup>5</sup> bundle sheath <sup>2</sup>
Phosphoribulo kinase	<i>Zea mays</i>	bundle sheath <sup>6</sup>
Ribose phosphate isomerase	<i>Zea mays</i>	bundle sheath <sup>6</sup>
Fructose diphosphate aldolase	<i>Zea mays</i>	bundle sheath <sup>6</sup>
Fructose diphosphatase	<i>Zea mays</i>	bundle sheath <sup>6</sup>
ADP glucose and UDP glucose pyrophosphorylases	<i>Zea mays</i>	bundle sheath <sup>4</sup>
ADP glucose and UDP glucose transphosphorylases	<i>Zea mays</i>	bundle sheath <sup>4</sup>
Starch phosphorylase	<i>Zea mays</i>	bundle sheath <sup>4</sup>
Glycolic acid oxidase	<i>Zea mays</i> <i>Atriplex rosea</i>	bundle sheath <sup>7</sup> bundle sheath <sup>2</sup>
Nitrate reductase	<i>Gomphrena globosa</i> <i>Sorghum sudanense</i> <i>Zea mays</i>	mesophyll <sup>3</sup> mesophyll <sup>3</sup> mesophyll <sup>3</sup>
Nitrite reductase	<i>Gomphrena globosa</i> <i>Sorghum sudanense</i> <i>Zea mays</i>	both <sup>3</sup> mesophyll <sup>3</sup> mesophyll <sup>3</sup>

<sup>1</sup> Berry *et al.*, 1970.<sup>2</sup> Björkman and Gauhl, 1969.<sup>3</sup> Mellor and Tregunna, 1970.<sup>4</sup> Huber *et al.*, 1969.<sup>5</sup> Slack, 1969.<sup>6</sup> Slack *et al.*, 1969.<sup>7</sup> Tolbert, N. E., 1969.<sup>8</sup> Unpublished observation (J. Berry).

the loss of internally generated CO<sub>2</sub> from the leaf. The thick walls of these cells may block the path of CO<sub>2</sub> exchange with the sub-stomatal cavity. In addition, the bundle sheath is surrounded by the layer of mesophyll cells which fix CO<sub>2</sub> by the  $\beta$ -carboxylation reaction. Most of the CO<sub>2</sub> that might escape from the bundle sheath would very likely be

re-fixed by these cells before it could reach the sub-stomatal cavity. The region contained within the bundle sheath cells might thus be effectively isolated from external CO<sub>2</sub>.

The diagram in Plate 9 is for a specific plant, *Sorghum sudanense*. Other plants may differ in details according to the levels and location of enzymes, and the



extent of grana development in the bundle sheath chloroplasts (see Downton, 1970). Evidence, however, indicates that the mechanism of carboxyl transfer in all plants with  $\beta$ -carboxylation probably involves coupled decarboxylation of a  $C_4$ -acid and carboxylation of RuDP in the bundle sheath chloroplasts.

The high levels of carboxydismutase recently detected indicate that the sequential carboxylation pathway could be the sole route to formation of 3-PGA in these plants. Slack *et al.* (1969) found that labeled RuDP, the probable acceptor molecule in the synthesis of 3-PGA, was confined to the bundle sheath chloroplasts of *Zea mays*. This corresponds to the location of carboxydismutase.

The concerted operation of two kinds of chloroplasts in separate cells would require that some metabolites move from one cell to the other. A study of the location of fixed  $^{14}C$  in the leaves of *Gomphrena globosa* by microradioautography and nonaqueous chloroplast preparation (Berry *et al.*, 1970) showed that labeled  $C_4$ -acids are present in the bundle sheath region. This apparent movement from the site of  $C_4$ -acid formation in the mesophyll cells, precedes the transfer of label to 3-PGA. Most of the  $C_4$ -acids labeled from  $^{14}CO_2$  were found in the nonplastid portion of leaves used in these studies, suggesting that movement of  $C_4$ -acids from cell to cell could occur by plasmodesmata.

Other metabolites must also be transported if the cooperation between the two tissues is to be complete. Pyruvate or a compound related to it must return to the mesophyll to regenerate PEP, the acceptor for the  $CO_2$  fixation process. This return transport has not been investigated. Plate 9 also indicates that 3-PGA and triose phosphates may be transported between the two tissues. Inclusion of this shuttle provides one possible mechanism for balancing NADPH consumption with availability in the two locations.

The separation of photosynthetic reactions may be related to the fact that two simultaneous and sequential carboxylations occur in this pathway. PEP carboxylase is not contained (at least in high activity) in the bundle sheath cells. If it were, it might interfere with the transfer of carbon to 3-PGA by re-fixing  $CO_2$  into the  $C_4$ -acids. Moreover, each carbon unit passed through the  $C_4$ -acid cycle requires the hydrolysis of two ATP molecules. Re-cycling would thus act as an ATPase, resulting in degradation of energy.

The decarboxylation step, if it were present in the mesophyll cells, would also have the potential to interfere with photosynthesis. Decarboxylation of malate or oxaloacetate by "malic" enzyme could reverse the  $CO_2$  fixation process, causing re-cycling of  $CO_2$  or loss of  $CO_2$  from the leaf. Another possible advantage, resulting from location of the decarboxylation of the  $C_4$ -acids in the bundle sheath cells, is that these cells may form a container for  $CO_2$  thus permitting locally a higher  $CO_2$  concentration than the external level to be maintained at the site of  $CO_2$  fixation via the reductive pentose phosphate cycle.

The fact that all plants known to have the  $\beta$ -carboxylation pathway also have a separation of the leaf into mesophyll and bundle sheath tissues, and the fact that the enzymes involved in the two carboxylation reactions are separately located in these tissues appear to be related to the mechanism of operation of the pathway. Disruption of the compartmentation could result in reduced efficiency of operation of the pathway and in impaired photosynthesis (cf. this *Year Book* p. 638).

The hybrid derivatives of the two species of *Atriplex* provide a unique opportunity to study the internal factors underlying the compartmentation of reactions in this pathway. These plants may also allow study of the effects of the absence of appropriate compartmentation and may provide an approach

to study the mechanism of the carboxyl transfer in plants such as *Atriplex rosea*, which has low "malic" enzyme. These studies are in progress.

*The division of energy metabolism between the tissues.* Several plants with  $\beta$ -carboxylation photosynthesis possess bundle sheath plastids with fewer grana than the mesophyll plastids. In extreme examples such as *Sorghum sudanense* (Bisalputra *et al.*, 1969) and sugar cane (Leatsch *et al.*, 1966) the bundle sheath plastids are agranal. The presence of grana seems to be required for noncyclic electron flow from  $H_2O$  to NADPH. In histochemical experiments Downton *et al.* (1970) found that the agranal bundle sheath plastids of *Sorghum sudanense* do not cause light-stimulated reduction of the Hill reagent tetranitro blue tetrazolium chloride (TNBT), while granal chloroplasts (such as those present in the mesophyll tissue of *Sorghum* or in the bundle sheath of *Panicum capillare*) do reduce TNBT. The ability of the bundle sheath plastids of several plants to reduce TNBT is also presented in Table 11. Bundle sheath chloroplasts of *Atriplex rosea*, which are granal (cf. this *Year Book* p. 629) reduce TNBT, as do the bundle sheath plastids of several other plants. In *Gomphrena globosa*, *Froelichia gracilis*, and *Zea mays* the reduction occurs more slowly in the bundle sheath than in the mesophyll plastids. This may indicate a reduced, but not totally absent, capacity for noncyclic electron flow in the bundle sheath plastids of these plants. The bundle sheath plastids of *Zea mays* have been found to contain only rudimentary grana (Wier *et al.*, 1967). In all plants studied, TNBT was reduced by mesophyll chloroplasts and by all plastids of control plants lacking  $\beta$ -carboxylation photosynthesis (e.g., *Atriplex patula*). Artifacts due to the exclusion of TNBT from the site of photochemical activity by permeability barriers are possible in these studies; however, TNBT reduction did occur in all bundle sheath cells when an artificial

electron donor couple of ascorbate and dichlorophenol-indophenol was used in addition to TNBT (Downton *et al.*, 1970). The only effect of this addition should be to compensate for any inability to carry out noncyclic electron flow.

These studies suggest that the bundle sheath chloroplasts of some plants with  $\beta$ -carboxylation photosynthesis may have a lesser capacity to photoreduce NADP *in vivo* but may retain the capacity for cyclic photophosphorylation (a system 1 reaction). An absorption spectrum measured at  $-196^\circ C$  of membrane fragments of bundle sheath chloroplasts of *Sorghum sudanense* resembles that of the system 1 fraction prepared from spinach chloroplasts (*Year Book* 67, p. 510) in having relatively more long-wavelength absorption than do the mesophyll chloroplasts of *Sorghum* or the system 2 fraction of spinach.

Some of the metabolic reactions of the bundle sheath cells require NADPH. The lesser capacity to generate NADPH through photoreduction may correlate with the presence of a compensating mechanism involving "malic" enzyme. The oxidative decarboxylation of malate results in the production of NADPH. Reduction of NADP by malate transported to the bundle sheath may substitute for photochemical reduction. The compartmentation of some reactions also shows some tendency to shift NADPH requiring enzymes to the granal mesophyll chloroplasts (see Table 12). NADP-malate dehydrogenase and nitrite reductase do not occur in the agranal chloroplasts of *Sorghum* bundle sheath tissue. A considerable portion of the NADP-glyceraldehyde-3-phosphate dehydrogenase of leaves of *Zea mays* occurs in the granal chloroplasts of the mesophyll. This may serve to reduce 3-PGA, a product of bundle sheath metabolism. Net movement of 3-PGA to the mesophyll and of triose phosphate back to the bundle sheath, as indicated in Plate 9, could thus compensate for the lower

availability of NADPH in bundle sheath plastids with limited grana formation (as in *Sorghum sudanense* shown in Plate 9). The significance of this compartmentation of energy metabolism is not clear. A detrimental interaction between light reaction 2 ( $O_2$  production) and a reaction of the reductive pentose phosphate cycle might give a selective advantage to such a separation.

**Conclusion.** These studies indicate that the  $\beta$ -carboxylation pathway probably functions by a route involving two consecutive carboxylations. These carboxylations and other reactions occur in separate tissues within the leaf. The possible detrimental interactions between these reactions may have required their separation. Several details of the pathway remain to be worked out, particularly the mechanism of decarboxylation used in plants such as *Atriplex rosea* and the relationship of this pathway to the suppression of photorespiration (cf. *Year Book 68*, pp. 620–633). The development of the two distinctly different tissues within the leaf also presents an interesting problem of developmental differentiation.

### References

- Berry, J. A., W. J. S. Downton, and E. B. Tregunna, *Can. J. Bot.*, **48**, 777, 1970.
- Björkman, O., and E. Gauth, *Planta* **88**, 197, 1969.
- Bisalputra, T., W. J. S. Downton, and E. B. Tregunna, *Can. J. Bot.*, **47**, 15, 1969.
- Downton, W. J. S., *Can. J. Bot.*, **10**, 1795, 1970.
- Downton, W. J. S., and E. B. Tregunna, *Can. J. Bot.*, **46**, 207, 1968.
- Downton, W. J. S., J. A. Berry, and E. B. Tregunna, *Zeit. Pflanzenphysiol.*, **63**, 194, 1970.
- Edwards, G. E., S. S. Lee, T. M. Chen, and C. C. Black, *Biochem. Biophys. Res. Com.*, **39**, 389, 1970.
- Hatch, M. D., and C. R. Slack, *Biochem. J.*, **101**, 103, 1966.
- Hatch, M. D., and C. R. Slack, *Ann. Rev. Plant Physiol.*, **21**, 141, 1970.
- Huber, W., M. A. R. DeFekete, and H. Ziegler, *Planta* **87**, 360, 1969.
- Johnson, H. S., and M. D. Hatch, *Biochem. J.*, **114**, 127, 1969.
- Kortschak, H. P., and L. G. Nickell, *Plant Physiol.*, **45**, 515, 1970.
- Laetsch, W. M., D. A. Stetler, and A. J. Vltos, *Zeit. Pflanzenphysiol.*, **54**, 472, 1966.
- Laetsch, W. M., *Amer. J. Bot.*, **55**, 875, 1968.
- Mellor, G. E., and E. B. Tregunna, *Amer. Soc. Plant Physiol.*, Abstract **58**, 1970.
- Slack, C. R., *Phytochem.*, **8**, 1387, 1969.
- Slack, C. R., and M. D. Hatch, *Biochem. J.*, **103**, 660, 1967.
- Slack, C. R., M. D. Hatch, and D. J. Goodchild, *Biochem. J.*, **114**, 489, 1969.
- Tchen, T. T., and Birgit Vennesland, *J. Biol. Chem.*, **213**, 533, 1954.
- Tolbert, N. E., and R. K. Yamazaki, *Ann. N.Y. Acad. Sci.*, **168**, 325, 1969.
- Wier, T. E., C. R. Stocking, and L. K. Shumway, in *Energy Conversion by the Photosynthetic Apparatus*, Brookhaven National Lab., New York, 353 pp., 1967.

### RELATIONSHIPS BETWEEN NITROGEN LEVEL, PHOTOSYNTHETIC CAPACITY, AND CARBOXYDISMUTASE ACTIVITY IN *Atriplex Patula* LEAVES

Ernesto Medina

Under natural conditions the photosynthetic capacity of higher plants is modified by the light regime and the nutrient level of the habitats in which they are growing. Information on the interaction between these two factors in determining the photosynthetic performance of plants growing under ecologically diverse conditions is important from a physio-ecological point of view.

Light regime and nutrient supply both govern the amount of primary substrates available for protein synthesis and growth. Earlier observations on cultivated plants such as cocoa and coffee show that under low light intensity the



nutrient level required to support normal growth is less than under full sunlight (Murray and Nichols, 1966). It has also been observed by several workers that the ratio of chlorophyll to nitrogen is higher in plants from natural habitats with low light intensity than in plants from habitats with high light intensity, and that the chloroplast structure as well as the proportion between the capacities of photochemical and biochemical steps of photosynthesis differ in plants from shaded and sunny habitats (Björkman and Holmgren, 1963; Björkman, 1966, 1968a; Mousseau, 1967). Björkman (1968b) has demonstrated that the low light saturated photosynthetic rate of plants grown under low light intensities is associated with a low activity of the  $\text{CO}_2$  fixing enzyme, carboxydismutase. Similar results were obtained by Gauhl (Year Book 68, pp. 633–636). Other observations strongly indicate that variations in photosynthetic rate produced during aging or caused by changes in the leaf/root ratio are in correlation with the level of carboxydismutase in the leaves (Woolhouse, 1968; Wareing, Khalifa, and Treharne, 1968).

The objective of the present investigation is to obtain information on the interaction between light intensity and nutrient supply during growth on the structure and function of the photosynthetic apparatus. *Atriplex patula* was chosen as the experimental material primarily because previous studies on this species in this laboratory provide valuable information on its natural habitat, nutrient requirements, and some of its photosynthetic and biochemical characteristics. The species has high photosynthetic capacity and rapid growth rate. Other advantages are that it can be readily grown from seed and a great number of highly uniform seedlings can be obtained.

The present studies include the effect of nitrate nitrogen supply to the roots on leaf nitrogen, protein, and chlorophyll levels, and the relationships between the

photosynthetic capacity and the activity of carboxydismutase, the enzyme responsible for  $\text{CO}_2$  fixation in this species. The results reported here were obtained from plants grown under a constant light intensity.

Seeds of *A. patula* were sown in sand and after 3 weeks the seedlings were transferred to pots with perlite. During the first 4 weeks the plants were watered with complete nutrient solution containing 33 mM nitrate ion (100% nitrogen solution). Nitrate ion was the only nitrogen source. After 4 weeks the plants were subjected to treatments of different nitrate concentrations in the range 3% to 100% of the original solution. The compositions of the solutions are given in Table 13. The nitrate ion was replaced mainly by chloride ion. *A. patula* is very tolerant to this ion but does not require it. The cation concentration was also modified to maintain a constant ratio of  $\text{Ca}^{++}$  to  $\text{Mg}^{++}$ . The plants were grown under a 16-hour photoperiod at an intensity of  $1 \times 10^5$  erg  $\text{cm}^{-2}$   $\text{sec}^{-1}$  (400–700 nm) and a thermoperiod of 25°C during the day and 20°C during the night. Total nitrogen content was determined by the micro-Kjeldahl method and soluble protein by the Lowry-Folin method. Carboxydismutase activity was determined at 30°C as described by Björkman and Gauhl (1969).

Preliminary growth experiments were conducted to establish the nitrogen concentration and time after transfer that

TABLE 13. Composition of Nutrient Solutions

Ions *	Solution		
	100%	12%	3%
(concentration, mM)			
$\text{Ca}^{++}$	11.0	11.0	11.0
$\text{K}^{+}$	23.0	22.9	23.0
$\text{Mg}^{++}$	4.4	4.4	4.4
$\text{H}_2\text{PO}_4^{-}$	2.2	2.2	2.2
$\text{NO}_3^{-}$	32.8	4.1	1.0
$\text{SO}_4^{--}$	4.4	12.7	14.3
$\text{Cl}^{-}$	10.0	22.0	22.0

\* In addition, standard micronutrients and Fe-EDTA were added.

result in desired reductions in the leaf nitrogen level. Table 14 shows the results of one of these experiments. Evidently the nitrate concentration of the nutrient solution must be below 25% of the original nitrate concentration in order to cause a significant decrease in the total nitrogen level of the leaf. In the subsequent experiments the plants were therefore grown with 100%, 12%, and 3% of the nitrate concentration of the original solution. At the time the treatments were started the plants were 28 days old and had 4 pairs of fully developed leaves, with the fifth pair just emerging (about 0.5 cm long). The measurements were initiated when the plants were 35 to 40 days old.

*Leaf development under different nitrogen levels.* The effect of the different treatments on the leaf nitrogen level, chlorophyll content, and the leaf area of the fourth and fifth leaf pair is shown in Table 15. Low nitrate concentration strikingly reduces leaf expansion. The results obtained with the fourth leaf pair clearly show that the reduction in leaf nitrogen levels in both treatments with low nitrate concentration is parallel with a reduction in leaf area and chlorophyll content. With the fifth leaf pair, the development of which took place entirely after transfer of the plants to the

TABLE 14. Total Nitrogen Content in Leaves of *A. patula* as a Function of Nitrogen Concentration in the Nutrient Solution \*

Nitrogen in the Solution (100% = 33 mM NO <sub>3</sub> <sup>-</sup> )	Total Nitrogen in the Leaf (mg g <sup>-1</sup> dry weight)
100%	45.4
50%	45.3
25%	39.3
12%	25.8

\* Measurements were made after the seedlings had been grown under the different treatments for 7 days following 28 days' growth after germination in the 100% solution.

different nutrient solutions, there is a proportionately greater reduction of leaf area than of nitrogen and pigment content. The activity of the carboxylation enzyme, carboxydismutase, was drastically affected by a reduction in nitrate concentration in the nutrient solution (Table 16). Notably, in the fifth leaf pair the relative decrease in activity of this enzyme is greater than the decrease in soluble protein, resulting in a reduction in the specific activity of the enzyme by more than 60%. This indicates that the rate of synthesis of carboxydismutase is preferentially reduced when the nitrogen supply is inadequate. The leaves of plants grown under low nitrogen showed signs of betacyanin accumulation at the edges and the enzyme

TABLE 15. Effect of Nitrogen Concentration in the Nutrient Solution on the Contents of Total Nitrogen and Chlorophyll of the Leaves and on Leaf Area Expansion \*

Nutrient Solution (100% = 33 mM NO <sub>3</sub> <sup>-</sup> )	Nitrogen (mg g <sup>-1</sup> dry weight)	Leaf Area (cm <sup>2</sup> )	Chlorophyll (mg g <sup>-1</sup> fresh weight)
<i>Fourth Leaf Pair</i>			
100%	54.9	30.9	1.6
12%	39.1	23.7	1.0
3%	27.5	17.1	0.7
<i>Fifth Leaf Pair</i>			
100%	53.4	44.5	1.4
12%	35.8	17.4	1.0
3%	26.4	11.2	0.9

\* Plants had been subjected to the different treatments during 10 days (fourth leaf pair) and 14 days (fifth leaf pair). The fourth leaf pair was partially developed at the time the plants were subjected to the different treatments; the fifth leaf pair was just emerging at this time. The plants were 38 to 42 days old.

TABLE 16. Effect of Nitrogen Concentration in the Nutrient Solution on the Soluble Protein Content of the Leaf and on Carboxydismutase Activity \*

Nutrient Solution (100% = 33mM NO <sub>3</sub> <sup>-</sup> )	Soluble Protein (mg g <sup>-1</sup> fresh weight)	Carboxydismutase Activity at 30°C μmole CO <sub>2</sub> min <sup>-1</sup>		
		Per g Fresh Weight	Per dm <sup>2</sup> Area	Per mg Protein
<i>Fourth Leaf Pair</i>				
100%	15.76	12.50	32.72	0.793
12%	11.38	8.72	21.10	0.766
3%	9.90	6.74	15.31	0.681
<i>Fifth Leaf Pair</i>				
100%	17.46	10.86	27.21	0.622
12%	9.08	2.49	5.59	0.274
3%	9.90	2.36	5.16	0.238

\* Experimental conditions were the same as given in Table 15.

extracts obtained from these leaves always had a yellowish color which was absent in the extracts from normal plants. Presumably this color was caused by the presence of flavonoid compounds which might act as enzyme inhibitors. Mixing preparations of leaves grown under high and low nitrate concentrations resulted in a specific activity equal to the mean of the two extracts assayed separately. Thus, the presence of inhibitors of carboxydismutase activity in the plants grown under low nitrate concentration is unlikely to account for the reduction in specific activity of this enzyme.

*Carboxydismutase activity as a function of leaf age.* During the development of a plant there is a continuous transfer of substances from the older to the developing leaves; in general there is an active net protein synthesis in the young leaves, whereas in the old leaves at least some of the protein is broken down and the amino acids translocated to the sites of active growth. Thus it is reasonable to expect that carboxydismutase activity may vary with leaf age. Kannangara and Woolhouse (1968) studying aging in *Perilla* leaves, found that the decrease with age in fraction 1 protein, considered to be the same entity as carboxydismutase, was greater than the decrease in total soluble protein.

In the experiments shown in Fig. 13A the activity of carboxydismutase was followed in leaves at different positions from plants grown under high and low nitrate concentrations. The results shown were obtained with 53-day-old plants. The young leaves, although they have a relatively high protein content, have a lower carboxydismutase activity than the leaves of intermediate age. The specific activity of the enzyme follows the same pattern as the activity expressed on the basis of fresh weight, and is 1.5 to 3 times higher in the plants grown in the 100% than in the plants grown in the 12% nitrogen solutions. The total nitrogen content on the basis of dry weight in normal plants, as well as in nitrogen deficient plants, is highest in young leaves and decreases with increasing age as does the soluble protein.

Aging of leaves at a given leaf position on the plant causes a reduction in carboxydismutase activity similar to that found with leaves of different positions at a given plant age. Figure 13B shows some of the results obtained in these experiments. The data clearly show that the reduction in carboxydismutase as a result of aging is more rapid in leaves from plants grown under low than in plants grown under high nitrate concentration.

*Carboxydismutase activity as affected*



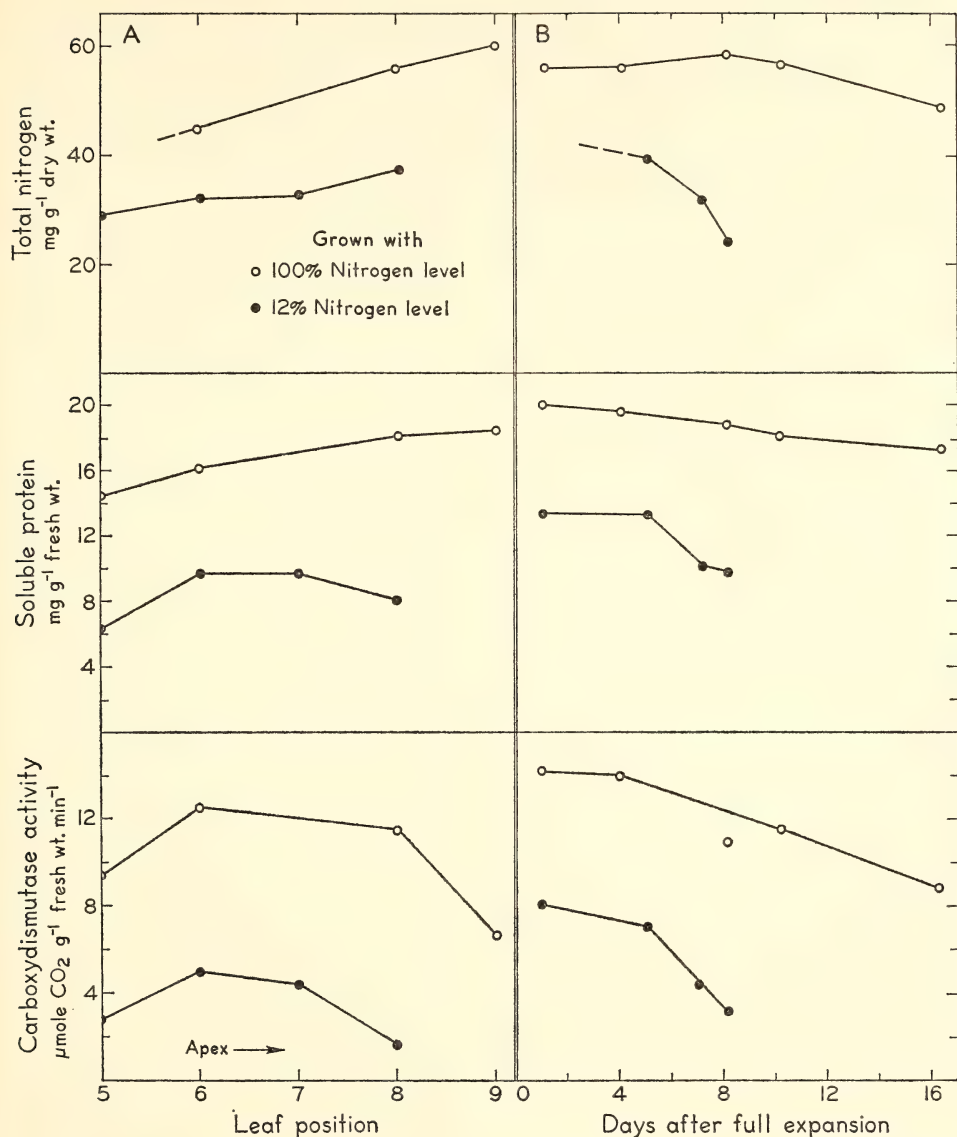


Fig. 13. Contents of total nitrogen, soluble protein, and activity of carboxydismutase in *Atriplex patula* leaves grown under high and low nitrate levels. *A* gives values for leaves at different positions on a 53 day old seedling, *B* for the same leaf position at different seedling ages. The seedling age in *B* was 48 days at the start of the experiments.

by short-term changes in nitrogen supply during growth. Figure 14 shows the results obtained with plants grown for 48 days in high or low nitrogen solutions and then transferred to nitrogen-free and

to 100% solutions, respectively. All determinations were conducted on leaves which were fully developed before the time of transfer. It is clear that changes in the nitrate level in the solution cause

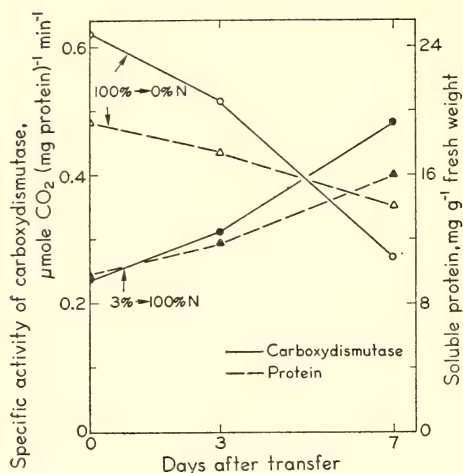


Fig. 14. Effect of transferring *Atriplex patula* seedlings from high to low nitrate levels and *vice versa* on the content of soluble protein and the activity of carboxydismutase. Plants were grown with "100%" and "3%" nitrate solutions for 48 days and were then transferred to nitrate-free and "100%" solutions, respectively. The leaves were fully developed before transfer.

rapid changes in carboxydismutase activity. The specific activity is strongly reduced or increased by changes in the nitrogen supply. The results indicate that there is a rapid enzyme turnover and that the relative rates of synthesis and breakdown depend on age and nitrogen supply. Previous work in this laboratory has shown that light intensity also has a great influence on this turnover rate (Björkman, 1968; *Year Book* 67, pp. 482-487).

Recent reports show that drastic variations in the nitrogen supply during growth of sugar beets and beans have a marked influence on the photosynthetic rate of these plants. Reduction in the nitrogen concentration of the nutrient solution reversibly lowered the photosynthetic rate (Ryle and Hesketh, 1969; Nevins and Loomis, 1970). In view of the present results it seems likely that these changes in photosynthetic rate can be attributed to changes in the carboxydismutase activity of the leaf.

*Relationships between carboxydismutase activity and photosynthetic capacity.* The  $\text{CO}_2$  dependence of photosynthetic  $\text{O}_2$  evolution from *A. patula* grown under 100% and 3% nitrate solutions is shown in Fig. 15. The measurements were carried out at a low  $\text{O}_2$  concentration of 0.15%, using the zirconium oxide ceramic cell (see Björkman and Gauhl, 1970). Transpiration was also simultaneously determined so that any differences in the resistance to diffusion of  $\text{CO}_2$  through the stomata among the different leaves could be taken into account. The  $\text{CO}_2$  concentrations given in Fig. 15 are for the intercellular spaces. No consistent difference in resistance to water vapor transfer was found between plants that had been grown under high and low nitrogen levels.

Light-saturated photosynthesis in leaves grown under 3% solution is only about one-third of that for leaves grown under 100% solution. The  $\text{CO}_2$  dependent rates and the  $\text{CO}_2$  saturated rates of photosynthesis are affected to similar degrees by reduction of the nitrate level. The effect on the  $\text{CO}_2$  limited rate indi-

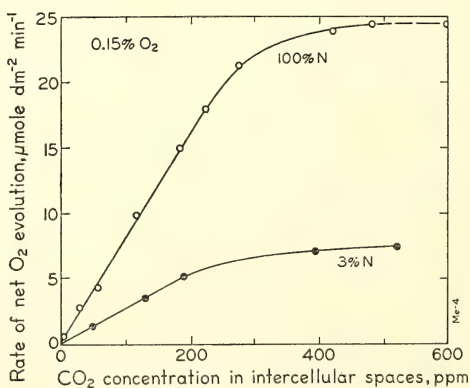


Fig. 15. Photosynthetic oxygen evolution as a function of  $\text{CO}_2$  concentration in the intercellular spaces in leaves from *Atriplex patula* seedlings grown under "100%" and "3%" nitrate solutions. Oxygen evolution was measured at 0.15%  $\text{O}_2$  with the zirconium oxide cell as described by Björkman and Gauhl (1970). Calculations of intercellular space concentration were made as described for Fig. 11, this *Year Book*.

icates that a reduction in the capacity of the carboxylation reaction or in the CO<sub>2</sub> diffusion process is responsible for the reduction in photosynthetic capacity by low nitrate level. The effect on the CO<sub>2</sub> saturated rates indicates that one or several enzymatic steps (including the carboxylation reaction) is responsible for the reduced photosynthetic capacity. As mentioned above, any effects that low nitrate concentration may have on stomatal resistance to diffusion are accounted for. Strong evidence that the decline in photosynthetic capacity as a result of nitrogen deficiency is caused primarily by a reduced capacity of the carboxylation reaction is provided by the data on carboxydismutase activity; this activity was reduced to about the same extent as photosynthesis by growing the plant under low nitrate concentration (Table 17).

In another series of experiments, the rate of light-saturated CO<sub>2</sub> uptake under normal (i.e., rate-limiting) concentrations of CO<sub>2</sub> was measured. The rates were measured both under 21% O<sub>2</sub>, the O<sub>2</sub> concentration of normal air, and under 1.5% O<sub>2</sub>. Under the low O<sub>2</sub> concentration, the inhibitory effect of O<sub>2</sub> ("photorespiration") on net CO<sub>2</sub> uptake is absent and the rates are consequently higher. Carboxydismutase activity was determined on the same leaves immediately after the conclusion of the photosynthesis measurements. Figure 16 shows the rate of photosynthetic CO<sub>2</sub> uptake at CO<sub>2</sub> concentrations corresponding to a constant concentration of 200 ppm CO<sub>2</sub> in

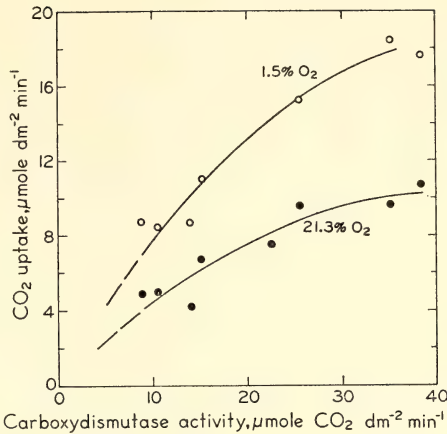


Fig. 16. Relationship between photosynthetic CO<sub>2</sub> uptake and carboxydismutase activity in *Atriplex patula* leaves. Measurements were made under 21% and 1.5% oxygen, saturating light, and 27°C. Photosynthetic rates are for a constant CO<sub>2</sub> concentration of 200 ppm in the intercellular spaces.

the intercellular spaces as a function of carboxydismutase activity for fully developed leaves grown under various levels of nitrate in the nutrient solution. Clearly, photosynthetic CO<sub>2</sub> uptake and carboxydismutase activity show a very high correlation, regardless of whether the photosynthetic rate was determined under low or 21% O<sub>2</sub> ( $r=0.97$  and  $0.94$  in 1.5% and 21% O<sub>2</sub>, respectively). Similar strong correlations between light-saturated photosynthetic rate and carboxydismutase activity was obtained by Björkman (1968a) for plants grown under constant nitrogen level but different light intensities.

TABLE 17. Carboxydismutase Activity in Leaves from Normal and Nitrogen-Deficient Plants\*

Nutrient Solution (100% = 33mM NO <sub>3</sub> <sup>-</sup> )	Carboxydismutase activity at 30°C (μmole CO <sub>2</sub> min <sup>-1</sup> )		
	Per g Fresh Weight	Per dm <sup>2</sup> Area	Per mg Protein
100%	12.50	32.72	0.793
3%	2.91	6.54	0.261

\* These leaves were also used for the experiments on CO<sub>2</sub> dependence of photosynthesis presented in Fig. 15.



Measurements of the level of total nitrogen, soluble protein, and carboxy-dismutase activity were also made on leaves of *A. patula* in its natural habitat in a sunny salt marsh at San Francisco Bay. The wide variation found comprises a good part of the range obtained in the controlled growth experiments. It is likely, therefore, that photosynthetic capacity under natural conditions is often affected by the supply of nitrogen through its effect on the level of the carboxylation enzyme.

The current work is focused on the effect of nitrate concentration on photosynthetic capacity in plants grown under low light intensity, and on the effects of nitrogen level and light intensity on the capacity of other steps of photosynthesis and chloroplast structure.

### References

- Björkman, O., *Brittonia*, 18, 214, 1966.
- Björkman, O., *Physiol. Plant.*, 21, 1, 1968a.
- Björkman, O., *Physiol. Plant.*, 21, 84, 1968b.
- Björkman, O., and E. Gauth, *Planta*, 88, 197, 1969.
- Björkman, O., and E. Gauth, *Photosynthetica*, 4, 123, 1970.
- Björkman, O., and P. Holmgren, *Physiol. Plant.*, 19, 854, 1966.
- Kannangara, C. G., and H. W. Woolhouse, *New Phytol.*, 67, 533, 1968.
- Mousseau, M., *Oecol. Plant.*, 2, 15, 1967.
- Murray, D. B., and R. Nichols, in *Light as an Ecological Factor*, Blackwell Sci. Publ., p. 249, 1966.
- Nevins, D. J., and R. S. Loomis, *Crop Sci.*, 10, 21, 1970.
- Ryle, G. J. A., and J. D. Hesketh, *Crop Sci.*, 9, 451, 1969.
- Wareing, P. R., M. M. Khalifa, and K. J. Treharne, *Nature*, 220, 453, 1968.
- Woolhouse, H. W., *Hilger J.*, 11, 1, 1968.

## BIOCHEMICAL INVESTIGATIONS

### FOUR COMMON FORMS OF CHLOROPHYLL A

C. S. French, J. S. Brown, W. Wiessner,  
and M. C. Lawrence

The wide variations in the shape of the red absorption band of chlorophyll *a* in plants are due to the presence, in various proportions, of a number of forms of chlorophyll *a* having different absorption maxima in the 660–720-nm region.

It is not yet known whether there are specific chlorophyll complexes always having the same absorption peak wavelengths and constant widths or if there are a large number of complexes with variable spectroscopic properties (*Year Book* 68, p. 578). Two forms of chlorophyll *a*, "Ca 670" and "Ca 680," have generally been considered to constitute most of the green color of plants. However, these wavelength designations are considered only approximate, and they refer to classes of pigments rather than

to specific complexes with definite and constant peak positions.

Previously we have made many curve analyses of the absorption spectra of various algae, chloroplasts, and chloroplast fractions to determine the peak position and the half-widths of Ca 670 and Ca 680. This was done by fitting the absorbance spectra with the sums of Gaussian curves. The results always showed that Ca 670 had a greater half-width than Ca 680. In system 1 fractions of chloroplasts Ca 680 always had a greater half-width than in system 2 fractions. Furthermore, the peak positions and the half-widths of both these hypothetical components varied over a wide range of wavelengths when spectra of different preparations were compared. Such a variation in peak wavelength and in half-width would result if each of the two assumed components were in fact composed of two separate chlorophyll forms having fixed peak positions and

widths but occurring in different proportions in the various samples.

An objective has been to see how far it is profitable to go in the interpretation of absorption spectra by fitting the data with Gaussian components. The scope of the work already done has been adequate to define reasonably well the potentialities and limits of this approach to the study of the forms of chlorophyll.

This year's work has made it seem more reasonable to interpret chlorophyll absorption spectra *in vivo* as being composed of four rather than two major forms of chlorophyll *a*. The tentative conclusion is that these four components are widely distributed and maintain essentially constant wavelengths and half-widths.

There are several spectra meeting our criteria for significant curve analyses that clearly indicate a double Ca 670 component. The double nature of the Ca 680 component is also obvious, particularly in the spectra of Ogawa and Vernon (1970), which show 685-nm shoulders.

We report here reasonably close fits to absorption spectra measured at  $-196^{\circ}\text{C}$  in the 660–690-nm region, using bands with the following peak positions: 663, 670, 678, and 684 nm. The results support the constant component hypothesis for these four components in a variety of algae and in several representative higher plants. Furthermore, good fits to less distinct spectra may be obtained by using these same bands. Other longer-wavelength bands in the 690–720 region are present in some but not in all preparations. We will describe several typical spectral types from which these four bands were derived, and the curve analysis methods used for doing so.

### *Procedures*

*Criteria for selection of significant spectra.* Spectra useful for determining the characteristics of their component bands must have distinct enough peaks to establish the peak wavelengths and

widths of several, although not necessarily all, the components in one spectrum. Spectra having the components present in such proportions as to smear out the measured spectrum into a nearly smooth curve may be useful for checking the occurrence of components derived from other spectra, but they are not suitable for finding the peak wavelength and widths of the components themselves.

Spectra of normally green whole chloroplasts or of whole algae are inevitably distorted by the sieve effect, discussed in *Year Book 67*, p. 171, so that they cannot be considered to represent the sums of the spectra of the individual pigments in the preparation. Therefore, we discuss here only spectra of very small particles prepared from finely disintegrated chloroplasts by centrifuging for 10 min at  $3000\times g$  to remove any remaining large particles.

To get a rough estimate as to whether or not there is peak flattening from particles that absorb too much light we compare the peak heights of the 625 and of the 670–680 maxima (*Year Book 66*, p. 174). The height, *H*, of the 625-nm peak, expressed as a fraction of the major peak height, is 0.2 for chlorophyll *a* in 80% acetone. A common range for chloroplast fractions is 0.25 to 0.30. Values much above 0.3 suggest possible complications from the flattening effect.

Since the component bands are appreciably sharper at liquid nitrogen temperature ( $-196^{\circ}\text{C}$ ) than at room temperature, the low temperature spectra are far better for determining the peak positions and widths of the components. Only low temperature spectra are discussed in this article.

For measurements of absorption spectra of scattering samples some arrangement for collecting a representative fraction of the light scattered in all directions is desirable. The opal glass system of Shibata has been used for measurements made in this laboratory with the spectrophotometer described in *Year Book 66*, p. 175. The slit width was 1 nm.

*Digitization of plotted curves.* A curve digitizer was used to tabulate the curve heights at intervals of 1 nm. The least count of this device is 0.00842 inch per unit thus giving a resolution of about 0.1% of full scale for a curve 8 inches high. Visual setting of the cursor facilitates averaging the minor irregularities in the plotted spectra while digitizing.

An automatic readout system depending on a shaft angle encoder connected to the ACME computer has operated successfully on several occasions. At the present time routine use of this automatic feature awaits construction of improved devices for receiving the signals at ACME.

*The RESOLV program.* Some useful capabilities of the curve analysis program obtained through the kindness of Dr. D. D. Tunnicliff of the Shell Development Laboratory, Emeryville, California, have been described (*Year Book* 67, p. 538). For the work summarized here the program is used to transform the wavelength data to wavenumber, to modify estimated Gaussian input bands as necessary to achieve an optimum fit of their sum to the absorbance data, to calculate the error of fit at each point, and to tabulate and plot the results. The program has been modified to permit specifying the allowed variation of the individual input bands. Thus the adjustment of the peak wavelength and the width of each band can be limited either for each iteration or for the final result. For the recent curve analyses we have allowed 12 iterations for each analysis and permitted the major peaks to change in wavelength position or in width by 0.3 nm per iteration. The broader bands 590, 628, 655 nm, and the long wavelength bands, usually 695 and 705 nm, are allowed from 1 to 5 nm similar adjustments per iteration. These program changes make it possible to keep the computer from modifying the estimated input bands so much that they could lose their physical significance.

*Analysis of absorption spectra by*

*Gaussian components.* The fits of Gaussian curves to chlorophyll absorption spectra are far better than those of Lorentzian curves. The tails of Gaussian curves are slightly too low while those of Lorentzian curves are far too high. Addition of Gaussian and Lorentzian curves of the same width and peak wavelength in an adjustable proportion generally gives a better fit in the long wavelength tail region. In the present work, however, only pure Gaussian curves have been used.

It is highly likely that unsymmetrical bands, broader on the short wavelength side, would be more realistic than symmetrical curves. The skew may be introduced by adding a small fixed Gaussian component on one side of a main Gaussian component.

*The shape of chlorophyll spectra in vivo.* The main red absorption band in spectra of chloroplast fractions can be reasonably well matched from 655 to 690 nm by the sums of four Gaussian curves. The red tail beyond about 690 nm sometimes obviously requires one or more extra components. As far as we know, these long wavelength forms may have their peaks anywhere from 690 to beyond 710 nm. It is often difficult to decide whether a small difference between the measured absorbance spectrum and the sum of the long wavelength tails of the 678 and 684 components is due to a real component or to the inadequacy of Gaussian curves for representing the tail of a single absorption band.

A more serious difficulty, however, occurs in the 625-nm region. The side bands, at about 590 and 625 nm, of each chlorophyll form are much wider than that of its main peak. We cannot yet resolve the overlapping bands in the 625-nm region, where there is presumed to be one vibrational band for each of the four main forms of chlorophyll. Because of their width all these bands in the 625-nm region fuse together and appear as a single broad band. The peak position and shape of this composite



625 band vary with the proportions of the various chlorophyll forms. In analyzing the shape of the main peak the 625-nm band must be included because its long wavelength side overlaps the 663 band. Therefore, an estimate of the composite "625-nm" band is used in the present series of curve analyses. Seely (personal communication) has found that this vibrational band may have two components in spectra of pure chlorophyll in some organic solvents.

Between the main peak and the first obvious vibrational band, near 625 *in vivo* and at 615 nm in ether or acetone, there is a hidden band showing clearly only at low temperature (Stensby and Rosenberg, 1961) but its inclusion is necessary for a Gaussian curve analysis even of room temperature spectra (Year Book 67, p. 542, Fig. 47A). In spectra of pure chlorophyll *a* at room temperature measured in 80% acetone this hidden band, detectable only by curve analysis, comes at 652 nm. Therefore, to fit spectra of natural chlorophyll complexes a corresponding composite 655-nm band has usually been included between the main peak and the first obvious vibration band. Like the 625-nm band this one also represents a composite sum of all the chlorophyll forms present. In some spectra adequate fits can, however, be realized without this 655 band. When the 655-nm band is omitted a corresponding increase in height and a minor increase in width of the curves representing all the major components shorter than 684 nm takes place. The resulting analysis may be about as near a true representation of the relative heights and widths of the main peaks as when a 655-nm smear band is used. The error curves in Fig. 17 show that a better fit results from using a 655-nm band in the analyses of fraction 1 from *Scenedesmus*.

Presumably, a complete description of the red spectrum for a single form of chlorophyll *a* would include specifications for this hidden band, which is between the main peak and the first evident

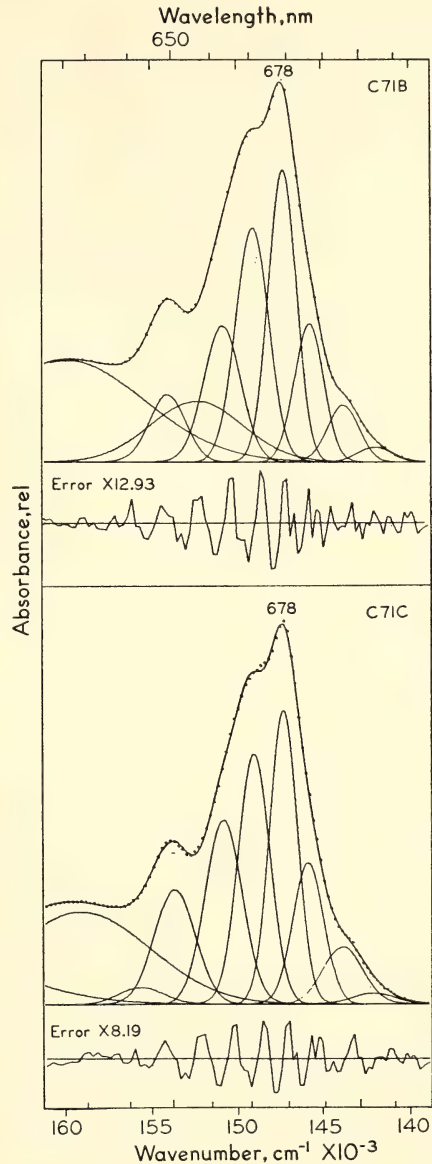


Fig. 17. Curve analyses of *Scenedesmus* fraction 1 with (C71B) and without (C71C) the 655-nm component but with a 641-nm component instead. The bands for C71C are given in Table 18. For C71B with the 656.1 component, 27.2 nm in width, the peaks and widths of the main chlorophyll components are: 649.1, 10.5; 662.7, 11.1; 670.5, 10.2; 678.4, 8.7; 685.6, 9.3; 695.0, 10.4; and 703.9, 11.7 nm.

shorter-wavelength vibrational band. In addition to the main peak and the hidden band, of course, the two obvious shorter-wavelength vibrational components, near 590 and 625 nm, must be specified. Possibly also an extra Gaussian component on the long-wavelength tail of the main peak should be added, not as a real absorption band, but merely to improve the fit of the long-wavelength tail of the main component. Thus the eventual description should be given by listing the wavelength peak, the half-width, and the height in relation to the main peak for all the bands that comprise each form of chlorophyll. However, here we report only peak positions, widths, and relative heights for the main bands.

*Derivation of the peak positions and widths of the components.* About 80 spectra have been studied, and many of them have been repeatedly subjected to curve analysis using various input bands with different program specifications. The spectra fall into groups having characteristic shapes. The most useful curves for explicitly defining the shape and position of the components are the spectra of fractions 1 and 2 from *Stichococcus* (Year Book 67, p. 519, Fig. 31B). The next sharpest group are the *Chlorella*-type spectra illustrated by the fractions 1 and 2 of *Chlamydomonas* and *Scenedesmus* (Year Book 68, p. 568, Fig. 1). Another typical shape is that of the spinach type illustrated by fractions 1 and 2 of *Marchantia* (Year Book 67, p. 519, Fig. 31A), *Oenothera* (Year Book 67, p. 504, Fig. 18), and spinach (Year Book 67, p. 510, Fig. 24). Spectra with large proportions of the long-wavelength components may be called the *Euglena* type, as illustrated in Fig. 31C of Year Book 67 (p. 519) and in Figs. 1–3 of Ogawa and Vernon (1970). The contrasts between these groups of spectra have been illustrated in Year Book 68, p. 585, Fig. 10.

Because the relative size and the distinctness of each band differ in the various spectra, some are more favorable

than others for showing any one band. Table 18 shows the position and width of the major chlorophyll bands in spectra selected as particularly suitable for band characterization. Some curve analyses from which Table 18 was compiled are illustrated in Fig. 18. The largest deviation of the sum curve from the experimental points is about 1% of the peak height.

*Chlorophyll b 640.* In spectra with a large Cb band it is often necessary to use also a 640 component about 10 nm wide. This may be free chlorophyll *b* perhaps dissolved in lipids. Because of its small size, its exact peak position and width are less accurately determined than those of some other bands.

*Chlorophyll b 650.* Fraction 2 spectra contain much more chlorophyll *b* than do those of fraction 1. The peak position of chlorophyll *b* averages 650.3 nm with a half-width of 11.2 nm.

*Chlorophyll a 663.* The peak wavelength of this form suggests that it may be free chlorophyll *a* dissolved in lipid. If, however, it is a protein complex, the chlorophyll must be in monomeric form. This component shows clearly in both fraction 1 and fraction 2 of spinach and of *Stichococcus* (C5, C6, C34 and C35) of Fig. 18. Its inclusion in the analysis of other spectra makes possible a good fit with a single 670-nm form. The presence of a band in this region has also been reported by other workers. It remains to be seen if this form of chlorophyll *a* usually contributes to action spectra. Figures 22, 23, and 24 in another section of this report suggest that Ca 663 may function in system 2. The average peak position is 662.5 nm with an 11.2-nm half-width.

*Chlorophyll a 670.* This form, so obvious in many spectra, is now considered to be about 10 nm wide. Previously a much greater width of Ca 670 was required for curve fitting before the universality of a 663 form was realized. Ca 670 seems to be identical in the two fractions. The average is 670.4 nm with

TABLE 18. The Peak Wavelengths and Half-Widths of Gaussian Curves<sup>1</sup> Representing the Main Peaks of Forms of Chlorophyll *a* as Determined by Curve Analyses of Several Types of Representative Spectra<sup>2</sup>

Curve No.	Species and Fraction	Chlorophyll <i>b</i>			The Major Forms of Chlorophyll <i>a</i>				Long-Wavelength Forms		
		Cb 640	Cb 650	Cb 650	Ca 663	Ca 670	Ca 678	Ca 684	(Ca 693)	(Ca 705)	
Very sharp spectra:											
C34G	<i>Stichococcus</i> , Fract. 1	640.7	8.3	650.3	11.0	670.4	8.9	677.7	8.4	684.2	11.3
C35H	<i>Stichococcus</i> , Fract. 2	641.1	7.3	650.4	10.5	670.6	8.9	677.7	7.6	683.9	8.8
<i>Chlorella</i> -type spectra:											
C76J	<i>Chlorella vulgaris</i> , Homogenate	(640.1	7.0) <sup>3</sup>	649.9	11.8	670.5	9.6	678.6	8.4	685.9	10.6
C62B	<i>Scenedesmus</i> Mutant 8, Homogenate	(643.0	13.1)	650.3	12.1	670.6	9.8	678.4	8.6	684.7	10.1
C27D	<i>Chlorella pyrenoidosa</i> , Fract. 1	642.0	12.1	650.5	12.4	670.1	10.1	678.0	9.8	684.4	10.6
C28E	<i>Chlorella pyrenoidosa</i> , Fract. 2	640.8	11.3	649.2	11.2	670.0	10.2	678.2	9.3	684.0	11.0
C71C	<i>Scenedesmus</i> W.T., Fract. 1	(641.7	12.6)	650.0	11.7	670.2	9.8	678.0	8.8	684.4	9.9
C72A	<i>Scenedesmus</i> W.T., Fract. 2	(640.6	11.3)	649.7	11.2	670.5	10.4	678.5	8.0	685.1	8.2
Spinach-type spectra:											
C5D	spinach, Fract. 1	641.7	10.3	651.4	11.8	670.4	9.7	677.8	10.6	684.5	10.8
C6J	spinach, Fract. 2	640.1	8.5	650.1	11.5	670.4	8.9	677.5	9.0	684.1	8.5
C80C	spinach, like Fract. 1	...	(650.4	13.6))	662.8	11.3	670.4	9.8	678.0	10.2	684.6
C79F	spinach, like Fract. 2	640.2	10.1	649.7	11.2	670.1	9.5	677.5	9.0	684.2	8.9
										Av. 684.5 10.0	
<i>Euglena</i> type spectra: (with 655 band)											
C18B	<i>Euglena</i> , Fract. 1	...	(	*	) <sup>a</sup>	670.5	10.5	678.2	9.0	682.4	9.0
C19B	<i>Euglena</i> , Fract. 2	...	((	*	))	670.5	10.8	678.5	11.0	682.7	11.1
C98E	<i>Euglena</i> , Fract. 1	...	651.6	10.2	662.9	10.8	670.9	10.9	678.3	11.0	683.6
										Av. 682.9 9.8	
Average		640.9	9.7	650.3	11.4	670.4	9.9	678.1	9.2	684.5	10.0
										692.4	15.1
										706.2	17.4
										688.4	17.7
										706.7	22.8
										693.1	15.5
										691.2	12.7
										704.8	17.4
										691.8	10.7
										701.8	13.1
										691.8	9.9
										701.9	10.1
										703.9	13.2
										704.7	16.6

<sup>1</sup> The 655-nm band was used only for the *Euglena* spectra. All had a band about 45 nm in width at about 590 nm and one near 628 nm about 35 nm wide.  
<sup>2</sup> The spectra were measured by the following people: J. S. Brown: C34, C35, C62, C71, C72, C18, C19, C98; G. Jacobi: C79, C80; J. M. Michel and M. R. Michel-Wolwerta: C5, C6, C27, C28; W. Wiessner: C76.  
<sup>3</sup> Components omitted from average: ... Component absent. ( ) Component too small for its parameters to have significance. ( ( ) Inadequate fit of sum curve in this region. ( \* ) Component obscured by 655 band.



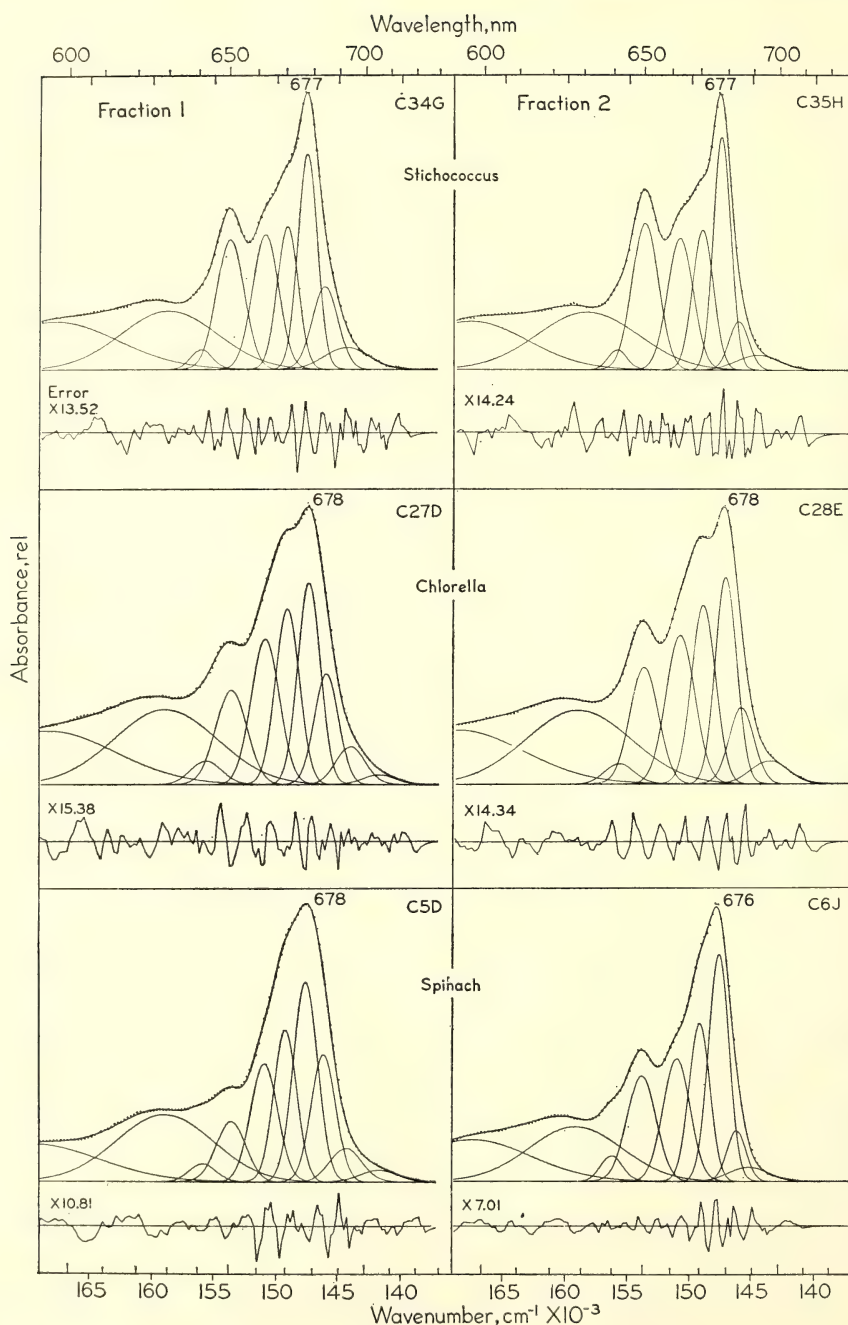


Fig. 18. Absorption spectra of chloroplast fractions fitted with four main chlorophyll *a* bands of Gaussian shape. The parameters of the bands giving these improved fits are listed in Table 18. These spectra were previously analyzed on the basis of two main forms of chlorophyll *a* (for example: C27, C28, in *Year Book 67*, p. 543).

a half-width of 9.9 nm, significantly narrower than *Cb* 650 or *Ca* 663.

*Chlorophyll a* 678. This 678-nm form was previously called "Ca 680." As used now with a 684-nm form, it fits the spectra of both fractions 1 and 2 without significant change of peak wavelength. Whether or not the apparently 10% narrower band-width in fraction 2 than in fraction 1 seen in Table 18 is significant remains a question. There is a possibility that *Ca* 678 may be modified from its true shape by the anomalous dispersion effect of a 670-nm chlorophyll form in solid particles (*Year Book* 67, p. 536). That effect rather than the existence of different *Ca* 678 forms may account for the small differences in half-widths reported in Table 18. The average peak position is 678.1 nm and the half-width is 9.2 nm.

*Chlorophyll a* 684. A 685-nm shoulder is most clearly seen in the low-temperature spectra of Ogawa and Vernon for fractions enriched in P700. This confirms without doubt the reality of the 684 component that we have found to be a necessary though often "hidden" component of all spectra. In fraction 1 preparations the proportion of this form is far greater than in fraction 2 preparations. Its presence in fraction 2 preparations may perhaps be due to incomplete separation of the functional pigment systems. This form of chlorophyll is less specifically defined because it rarely shows as a clear shoulder. Because its apparent peak position is about 2 nm shorter in *Euglena*, those data are averaged separately in Table 18. In the other algae its average position is 684.5 nm with a half-width of 10.0 nm.

### Discussion

With four major forms of chlorophyll and one or two long-wavelength forms all present together, the number of Gaussian curves needed to give a precise description of a single spectrum becomes very large. For each form the main

peak may require one large, narrow Gaussian curve with another smaller and wider Gaussian on the short wave side for the desired asymmetry. Each of the two shorter-wavelength vibration bands needs at least one wide Gaussian, and the fit at the long-wavelength tail can be improved by another very low Gaussian curve in addition to those more obviously necessary. Each recognizable form of chlorophyll therefore may need up to 5 separate Gaussian curves to describe it with high precision. A typical spectrum from 590 to 730 nm could therefore use up to 30 separate Gaussian curves for a complete fit with due consideration of all known aspects of the shape of the spectrum of a single component and the currently recognized number of chlorophyll forms.

To keep the number of component curves down to a small enough total so that a significant analysis can be made we have adopted the expedient discussed above of using broad 590, 628, and 655 smear bands, each of which presumably is the sum of the corresponding band for each of the four major chlorophyll forms. Since there is no reason to expect these composite bands to have a Gaussian shape, minor misfits in the region where these component bands make up a significant part of the curve heights have little significance.

From Table 18 it is evident that *Ca* 663 and *Ca* 670 show no significant variation of peak wavelength either from one alga to another or between the two fractions. *Ca* 678 has a constant peak position but the small difference in width of about 1 nm between fractions 1 and 2 may possibly be significant. The differences between the two fractions lie predominantly and perhaps entirely in the amounts of *Ca* 684 and of longer wavelength pigments.

### Summary

With four major bands at 663, 670, 678, and 684 nm having half-widths of

11.2, 9.9, 9.2, and 10.0 nm it is possible to match spectra of various chloroplast preparations. Bands at longer wavelengths also often occur but with far smaller heights, and they are more common in system 1 than in system 2 fractions. Therefore, it appears that the two pigment systems differ primarily in the amount of Ca 684 and longer wavelength forms rather than in the width or peak positions of the component bands.

We wish to acknowledge Grant GB 8630 of the National Science Foundation which has made this investigation possible.

### References

- Ogura, Teruo, and Leo P. Vernon, *Biochim. Biophys. Acta*, **197**, 332, 1970.  
Stensby, Per S., and Jerome L. Rosenberg, *J. Phys. Chem.*, **65**, 906, 1961.  
Wiessner, W., *Photosynthetica*, **3**, 225, 1969.  
Wiessner, W., and C. S. French, *Planta*, **94**, 78, 1970.

### AUTOMATIC RECORDINGS OF ACTION SPECTRA FOR PARTIAL REACTIONS OF PHOTOSYNTHESIS

*Per Halldal, C. S. French, and Mark Lawrence*

The identification of a pigment as the light absorber for a particular photochemical reaction depends on agreement between the absorption spectrum of the pigment and the action spectrum of the reaction. Our objective is to measure action spectra for each of the two photosystems of photosynthesis with an accuracy approaching that with which absorption spectra are determined. We have attempted to devise easy methods for automatic or semi-automatic recording of action spectra for dye absorption changes that could be used with appropriate modifications of the reaction mixture for studies of various steps in photosynthesis. When this can be done with chloroplast particles small enough to avoid the flattening effect, light scattering distortions, and the shielding effects

of other pigments, it should be possible to make comparisons of action and absorption spectra precisely enough to bring out any small differences that could be caused by the presence of inactive pigments. Such comparisons also might be used, for instance, to give a measure of the purity of isolated fractions believed to be the functional pigment systems for either photoreaction. We report here some progress on improvements in action spectroscopy of photosynthetic pigment systems.

Action spectra for partial reactions of photosynthesis, such as those involving changes in absorption of added substances responding to changes at a specific site in the electron transport chain of photosynthesis, are generally measured point by point. We had previously devised a method for automatic recording of photosynthetic oxygen evolution (*Year Book 58*, p. 323), and a portable apparatus for the purpose has been built (Halldal, 1969). Those instruments used a direct electrical measure of the reaction rate and balanced the back reaction, in that case oxygen consumption, against the production of oxygen by light-induced photosynthesis. An error signal for intensity control was generated by any change in rate from a preset value. Thus as the spectrum was swept the intensity was automatically adjusted to keep the rate constant and the recording of the action spectrum required only the plotting of the reciprocal of that intensity against wavelength.

The presently used measurement of light transmission of a dye that is changed by the reaction gives a signal proportional to the time integral of the reaction rate rather than to its instantaneous value. Furthermore, with dye reaction systems any back reaction may vary in rate with the extent of the forward reaction, thus precluding its utilization for generating an error signal. Consequently, the methods used for automating the action spectrum measurement for oxygen evolution are not



applicable to systems dependent on color changes of dyes. Therefore, two unconventional procedures were used, one based on a single cuvette and the other on two cuvettes both containing the reaction mixture. The two measuring procedures will be described; either of them may be used with reaction systems appropriate for either system 1 or system 2.

### *Apparatus and Principles of the Two Procedures*

**Monochromator.** A monochromator was constructed several years ago from a  $16.4 \times 10$ -cm transmission grating having 7500 lines per inch. This is used with two 20.3-cm diameter amateur telescope mirrors of 1.6 m focal length, mounted so that the exit beam is fixed in a horizontal position. The dispersion is 2.1 nm per mm. The grating, used in the first order, is blazed for blue light.

Massive brass entrance slits cooled by running water are used almost in contact with the lamp. No condenser optics are used in front of the slit. The light source is a 500-w tungsten-iodine lamp with a filament 7.5 cm long. The slit with its attached lamp and the collimator mirror rotate about a horizontal axis to change the wavelength of the exit beam. The half-band width of the actinic beam used for these experiments was 6 nm. A sine mounting enables the wavelength to be swept by means of a selsyn motor similar to one coupling the drive motor to the recorder. The frame of the instrument is made of perforated angle iron to which are added masonite light shields and tin baffles.

**Cuvettes and light measuring systems.** The cuvette holders, transmission-measuring light beams, and other optical parts of the apparatus were built on an extension of the monochromator frame,

#### Single sample method

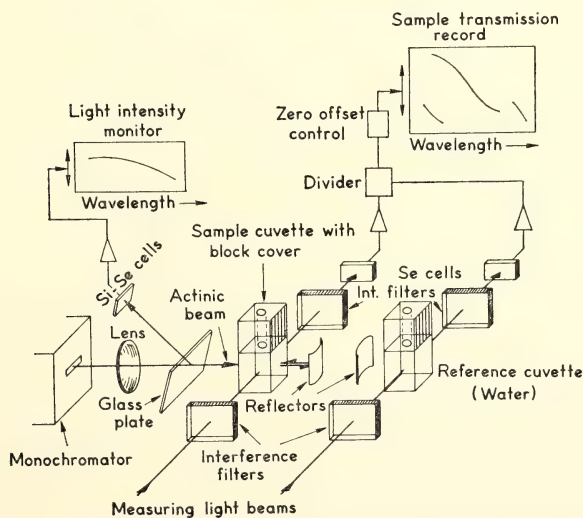


Fig. 19. The system as used to measure action spectra by continuous recording of the transmission of a single sample during a wavelength sweep. The reference cuvette contains water. Ten inches of recorder deflection is equivalent to 10% transmission difference. An exposure to a standard wavelength both precedes and follows each wavelength sweep, thus providing data for correction of rate changes during the experiment. The light intensity monitoring system was calibrated as a function of wavelength as units of absolute intensity at the surface of the sample cell. The records are digitized at 1-nm intervals after the experiment for computation of the action spectrum.

the whole assembly being mounted on casters. Figures 19 and 20 show the light paths and electrical schematics for each procedure.

An image of the grating was focused on the sample in a 1-cm absorption cell with four polished sides. A Plexiglas block with a small center hole to let air bubbles and excess reaction mixture escape is used as a cover. The actinic beam completely covers a 1-cm square face of the reaction vessel. Part of the transmitted actinic light was reflected back to the sample by an aluminum plate. Both the Plexiglas block and the reflecting plate served to equalize the light intensity in all parts of the absorption cell. About 10% of the exciting beam was reflected by a glass plate to a calibrated Se-Si photocell combination. The light level was kept at around  $1800 \text{ erg cm}^{-2} \text{ sec}^{-1}$  during sweeps. The reaction

rate of photosystem 1 was monitored as the increase in transmission due to oxidation of the 549 absorption peak of reduced cytochrome *c*, and that of photosystem 2 as increase in transmission at 593 nm due to reduction of DCIP. Light from the exciting beam was screened out from the monitoring Se photoreceivers by means of baffles. During a normal run the rate was measured before and after the sweep at a standardized wavelength and intensity ( $680 \text{ nm}$ ,  $1940 \text{ erg cm}^{-2} \text{ sec}^{-1}$ ).

**Electronics.** The electrical system was based on an Analog Devices operational amplifier manifold modified by the addition of an Intronics multiplier used for division and a control box giving calibrated offset steps of the recorder's zero. Chopper-stabilized amplifiers were used in low level stages. Plug-in components made the changes of connection easy for

#### Double sample method

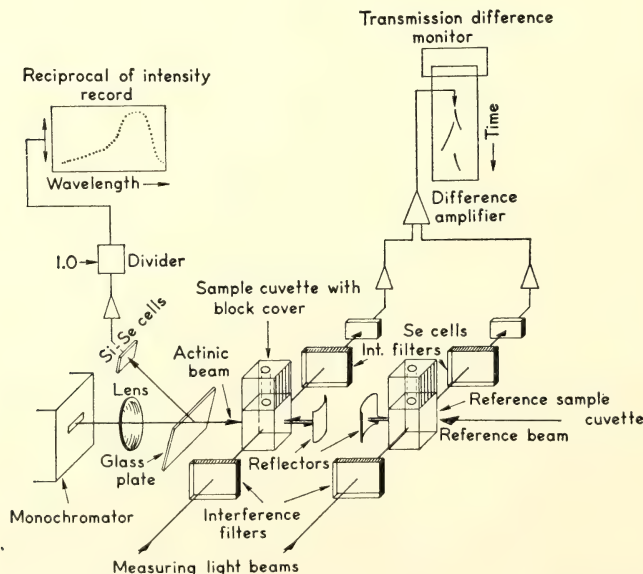


Fig. 20. The double sample system used to measure action spectra with two identical samples, one exposed to a standard beam, the other to a series of actinic wavelengths. The actinic beam is adjusted by the operator at each wavelength to make the transmission of the experimental sample remain equal to that of the reference sample that is exposed to a constant beam. The resulting point-by-point plot needs correction only for the calibration factors of the photocell system used to measure the intensity.

selecting either the single or double sample system of measurement.

*The single sample method.* This procedure illustrated in Fig. 19 simply records on a greatly expanded scale, the transmission of the sample at a fixed wavelength as the actinic beam of recorded intensity is changed in wavelength. These data and the photocell calibration factors are digitized at 1-nm intervals and entered in the computer that plots the corrected action spectrum. Corrections are applied for the small change in rate of reaction of the same cuvette exposed to a standard actinic beam, 680 nm, before and after the wavelength sweep. The computation procedure is: (1) to convert the measured transmission to absorbance, taking into account the large zero shift of the recorder, (2) to compute the derivative of absorbance versus time at each wavelength by fitting an equation to sequential groups of 9 points using Program IV of Jones *et al.* (1968), (3) to apply corrections for intensity of the monitored actinic light at each wavelength using previously determined calibration data, (4) to apply a correction for change of reaction rate at 680 nm (as a linear function of the absorbance change) during the reaction, and (5) to plot the resulting action spectrum.

*The double sample method.* The amount of dye reacting per unit exposure to a standard monochromatic light beam may change appreciably during the course of the experiment. One procedure investigated therefore made use of two identical reaction cuvettes to compensate for this change. The control cuvette was continuously exposed to a constant light source while the experimental cuvette was exposed to a monochromatic beam of varied wavelength and intensity. The intensity of this actinic beam was continuously adjusted to keep the extent of reaction in the experimental cuvette identical to that of the control by monitoring the recorded difference in transmission of the two cuvettes as shown

in Fig. 20. The servo control problems have not yet been solved adequately to make this method useful for automatic recording during wavelength sweeps. There were low-frequency oscillations of large amplitude when complete automation was tried. The double cuvette method has, however, worked very well as a point-by-point procedure with the operator adjusting the intensity at a series of fixed wavelengths. The reciprocal of the monitor photocell response was recorded on a wavelength scale and the intensity calibration data applied later to that rough plot.

### *Plant Material and Reaction Mixtures*

The blue-green alga *Plectonema boryanum* was cultivated and photosystem 1 particles were prepared as described by Brown on p. 678 in this *Year Book*. The composition of the system 1 reaction mixture is: reduced cytochrome *c*, 0.065 *M*; methylviologen, 0.065 *M*; Tricine buffer, pH 7.7, 0.05 *M*; and 1–4  $\mu\text{g}$  chloroplast chlorophyll per ml.

For the system 2 action spectra, spinach chloroplasts are prepared and measured in the following reaction mixture: sucrose, 0.4 *M*; NaCl, 0.01 *M*;  $\text{MgCl}_2$ , 0.005 *M*; Tricine buffer, pH 7.8, 0.05 *M*; methylamine, 0.01 *M*; DCIP, 0.017 mM; and enough chloroplast material to absorb 20–30% at 680 nm in 1 cm.

### *Results and Discussion*

The record of intensity illustrated in Fig. 21 was made with a constant rate of wavelength sweep of 11.2 nm min<sup>-1</sup>. Figure 22 shows the action spectrum calculated from the data of Fig. 21 for a system 2 reaction of whole chloroplasts. Its width and the relative height of the 650 chlorophyll *b* region results from the flattening effect that is inevitable when whole chloroplasts are used. In Fig. 23 the action spectrum for the same DCIP reduction reaction is given for chloro-



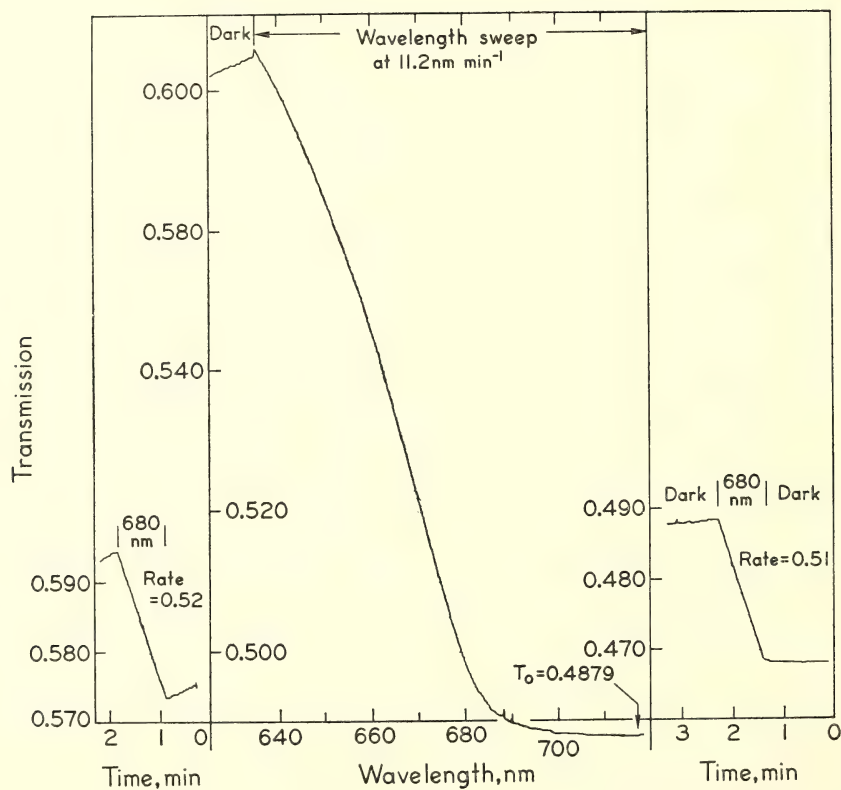


Fig. 21. A recording of a single sample experiment from which the action spectrum of Fig. 22 for DCIP reduction by whole spinach chloroplasts was calculated. The reaction rate was measured before and after the wavelength sweep. The action spectrum is the time derivative of the absorbance calculated, with appropriate corrections for light intensity variation, from this curve of transmittance recorded during the wavelength sweep.

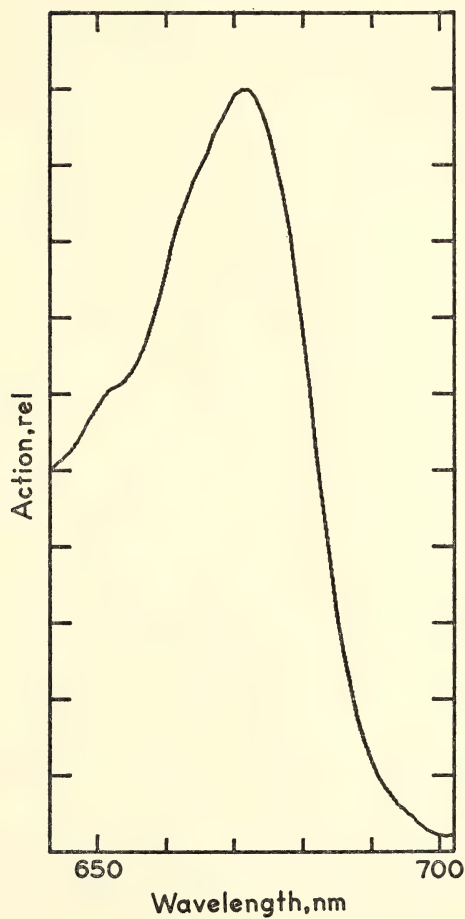


Fig. 22. The action spectrum for DCIP reduction by whole chloroplasts, a system 2 reaction, computed from the data of Fig. 21, an intensity monitoring curve, and photocell calibration factors.

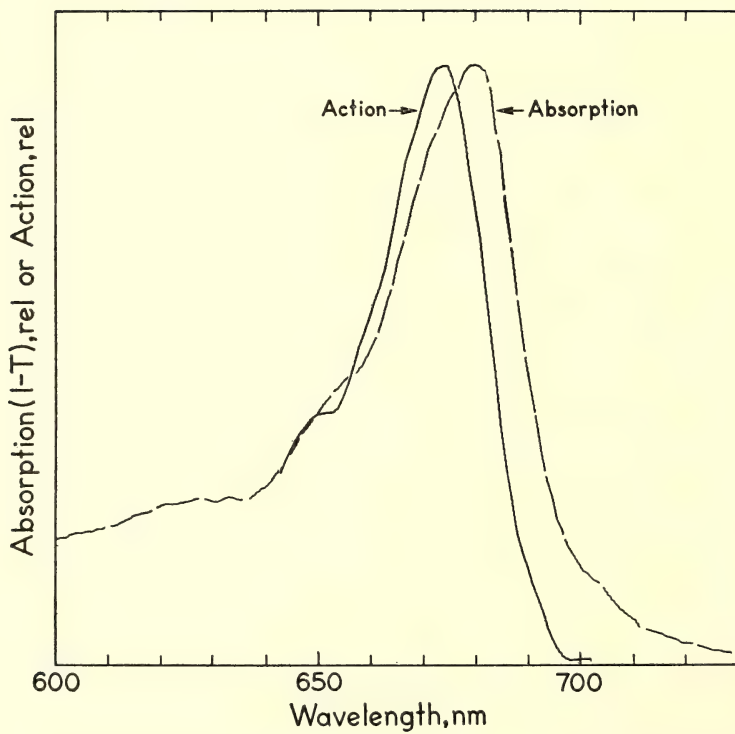


Fig. 23. An action spectrum for DCIP reduction by chloroplast fragments measured by the single sample method and compared with the absorption of the same chloroplast fragments.



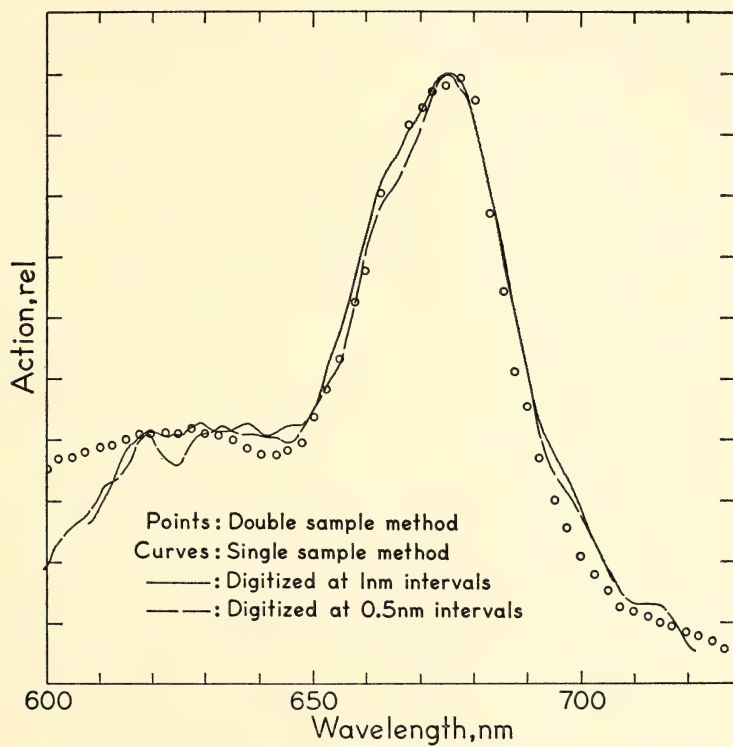


Fig. 24. The action spectrum for mammalian cytochrome *c* oxidation by particles from *Plectonema*, a system 1 reaction measured by the two methods here described. The two curves are from the same transmission curve digitized by two different operators.

plast fragments prepared by Dr. Murata. This action spectrum is narrower than that of Fig. 22 and it peaks at a slightly shorter wavelength. Its most interesting aspect, however, is the discrepancy between the action and the absorption spectra, which clearly shows the presence of absorption of system 1 pigments that are not active in the system 2 reaction.

Figure 24 shows a system 1 reaction, the oxidation of mammalian cytochrome *c*, by particles prepared from *Plectonema* as measured by both methods. The curves of Fig. 24 for the single cuvette method were computed from the same transmission curve digitized by different operators, one at 1.0 the other at 0.5 nm. The reason for the discrepancy between the curve and the points below 620 has not yet been found. However, either method seems to be more reliable than the far more laborious procedure used for Fig. 26 on page 681.

Grant GB 8630 from the National Science Foundation paid for the computer time used in this work.

### References

- French, C. Stacy, Jack Myers, and Guy C. McLeod, in *Comparative Biochemistry of Photoreaction Systems*, M. B. Allen, ed., Academic Press, New York, p. 361, 1960.
- Halldal, Per, *Photochem. Photobiol.*, **10**, 23, 1969.
- Jones, R. N. *et al.*, *Computer Programs for Absorption Spectroscopy*, N.R.C. Bulletin No. 11, National Research Council of Canada, Ottawa, p. 56, 1968.
- PHOTOSYSTEM 1 ACTIVITY AND THE LONG-WAVELENGTH FORMS OF CHLOROPHYLL
- J. S. Brown
- The question whether the chlorophyll *a* that occurs in small long-wavelength absorption bands of various algae is photochemically active has been of interest since these absorption bands were found. It is difficult to answer this question by comparing action spectra of

whole cells with absorption spectra of pigments because of the high concentration of chlorophyll in the chloroplast and because of differential light scattering by the various cell particles and organelles. To avoid some of these difficulties a partial reaction of photosynthesis was measured with a cell free preparation.

Since fragments of the blue-green alga *Plectonema boryanum* showed a distinct small absorption band near 710 nm when measured at  $-196^{\circ}\text{C}$  (*Year Book* 68, p. 569) while fragments of *Anacystis nidulans* did not, a comparison was made of the photochemical activity of preparations from these two algae. The long-wavelength absorbance of *Plectonema* is also somewhat greater than that of *Anacystis* at  $20^{\circ}\text{C}$ .

The photo-oxidation of mammalian cytochrome *c* was chosen for a test system because green particles from blue-green algae will perform this reaction at a relatively high rate without added cofactors. This system has been extensively studied by Kok *et al.* (1964), Fujita and Myers (1965), and Murano and Fujita (1967) and has been shown to be mediated by photosystem 1.

The algae were grown in one liter batches of the Medium C of Kratz and Myers. The flasks were shaken over warm-white (for *Plectonema*) and cool-white (for *Anacystis*) fluorescent lamps. Each received about 5500 lux for 7 days.

The cells were harvested by centrifugation, resuspended in about 35 ml of 0.3 *M* KCl, 0.05 *M* Tricine buffer at pH 7.7, and broken by extrusion through the needle valve. The homogenate was centrifuged at  $3000\times g$  for 10 min to remove unbroken cells. This supernatant was centrifuged at  $60,000\times g$  for 90 min to sediment the green fragments. All of the phycocyanin remained in the supernatant. The green sediment was homogenized in the same buffer without KCl and centrifuged again at  $3000\times g$  for 10 min. The supernatant contained the green particles which remained active

for at least 4 days when stored at 4°C.

A 100  $\mu M$  solution of cytochrome *c*, Type III from Sigma Chemical Co., was reduced with sodium ascorbate and dialysed against water overnight to remove excess ascorbate. An extinction coefficient of 15,000  $M^{-1} \text{ cm}^{-1}$  at 550 nm for reduced minus oxidized cytochrome *c* was used.

One ml of reaction mixture in a cuvette contained approx. 65  $m\mu$  moles cytochrome *c*, 65  $m\mu$  moles methylviologen, and 1 to 4  $\mu g$  chlorophyll *a* in the algal particles, all in 0.05 *M* Tricine buffer, pH 7.7. The methylviologen has been reported to act as a catalyst and did in fact stimulate the oxidation rate by two to three times.

One side of the cuvette was illuminated by a measuring beam from a battery powered tungsten lamp. This beam passed through two 550-nm Balzer interference filters, one on either side of the cuvette, and the change in transmission, detected by a photomultiplier tube, was amplified and measured on a chart recorder.

In preliminary experiments an actinic beam from a 150-w tungsten projection lamp in conjunction with interference and neutral density filters illuminated the cuvette on a side perpendicular to the measuring beam. With this source we determined the light intensity dependence of the oxidation of cytochrome *c* at several wavelengths. The light intensity was measured with a YSI radiometer.

For action spectra measurements, the actinic light source was a 1400-w high pressure capillary PEK Hg lamp giving a continuous spectrum. It was used with a monochromator with slits set to give a half-bandwidth of 3.5 nm. The light intensity was monitored with a silicon cell previously calibrated with a thermopile.

The rate of cytochrome oxidation, *R*, was calculated as:  $R = PK/C$ , where *P* = measured rate of transmission change in percent, *C* = chlorophyll concentration, and *K* converts the rate to  $m\mu$  moles cyt. *c* per hr. At low absorption, 1%  $\Delta T =$

0.00436  $\Delta OD$ . The light path in the cuvette was 0.80 cm. Therefore,  $K = 0.00436 \times 60/15,000 \times 0.8 = 21.8 m\mu$  moles cyt. *c*  $\text{hr}^{-1}$ .

The progressive change in rate as the reaction proceeds is compensated for by referring rates at all wavelengths to the rate at 680 nm which was measured at various times during the course of an experiment.

*Light intensity dependence.* In order to compare the effectiveness of different wavelengths of light, the intensity should be well below that which saturates the reaction. The dependence of cytochrome *c* oxidation upon light intensity was measured at three wavelengths with *Plectonema* particles (Fig. 25). At each wavelength the rate was linear with intensity and extrapolated to zero at zero intensity. The light intensities used in all subsequent experiments were well below the maximum intensities shown in Fig. 25.

*Action spectra.* Action spectra for the photo-oxidation of cytochrome *c* by *Plectonema* and *Anacystis* particles are compared with percent absorption of the same suspensions in Fig. 26. Each action spectrum was made with a single preparation of each alga. With *Plectonema*, 9 sets, and with *Anacystis*, 7 sets of measurements were made with different aliquots of the same cytochrome-algal mixture. Fifty-one reference measurements at 680 nm were made with *Plectonema* and 29 with *Anacystis*. The absorption spectrum of the same sample in the cuvette used for the action spectrum was also measured.

Two problems are evident in both action spectra. First, the action spectra are considerably broader than the absorption spectra. Part of this broadening is caused by the slit width (3.5 nm) used for the action spectrum measurements compared to the 1-nm half-width of the spectrophotometer. However, this cannot account for all of the difference. The possibility of some stray light that might result in a lower relative rate at 680 nm



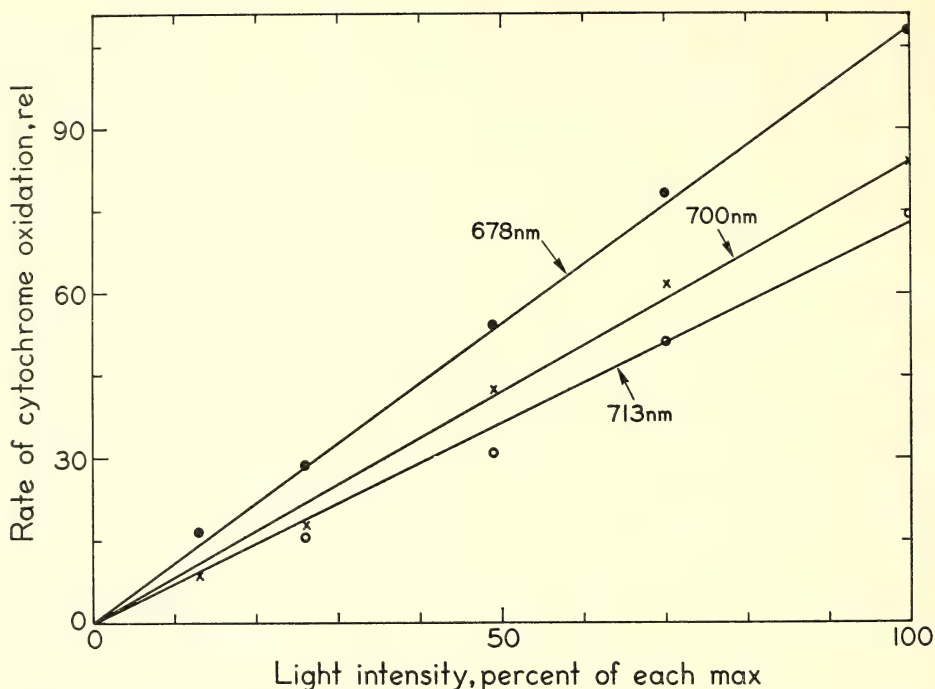


Fig. 25. The light intensity dependence of cytochrome *c* oxidation by *Plectonema* particles. At 678 nm the chlorophyll concentration was  $1.67 \mu\text{g ml}^{-1}$  and the maximum intensity was  $2440 \text{ ergs cm}^{-2} \text{ sec}^{-1}$ . The chlorophyll concentration was  $3.34 \mu\text{g ml}^{-1}$  at 700 nm (max. intensity,  $2380 \text{ ergs cm}^{-2} \text{ sec}^{-1}$ ) and at 713 nm (max. intensity,  $3600 \text{ ergs cm}^{-2} \text{ sec}^{-1}$ ).

has not been ruled out and could account for some of the flattening. Moreover, the large scatter of the action points at each wavelength far exceeds the apparent uncertainty in any of the rate or the intensity determinations. A satisfactory explanation for the scatter is not yet evident. In spite of the poor reproducibility of these measurements it is certain that both algae effectively use light of wavelengths longer than 700 nm for cytochrome oxidation. Any difference be-

tween the two algae is, however, hidden within the range of variation of the data.

*Comparative activity.* Since the action spectra were not accurate enough to show possible differences in activity in the long-wavelength region between *Plectonema* and *Anacystis*, the absorption and activities at three wavelengths were compared for the two algae in a more detailed experiment. The preparation of algal fragments and measurement of cytochrome oxidation were the same as

TABLE 19. The Relative Absorption and Activity of Two Algae at Long Wavelengths as Compared to Their Values at 680 nm \*  
(percent of value at 680 nm)

Wavelength, nm	<i>Plectonema</i>		<i>Anacystis</i>	
	Absorption	Activity	Absorption	Activity
710	18	16	8	16
715	11	14	4	12

\* Each experiment was done with  $2.5 \mu\text{g chl per ml}$ .

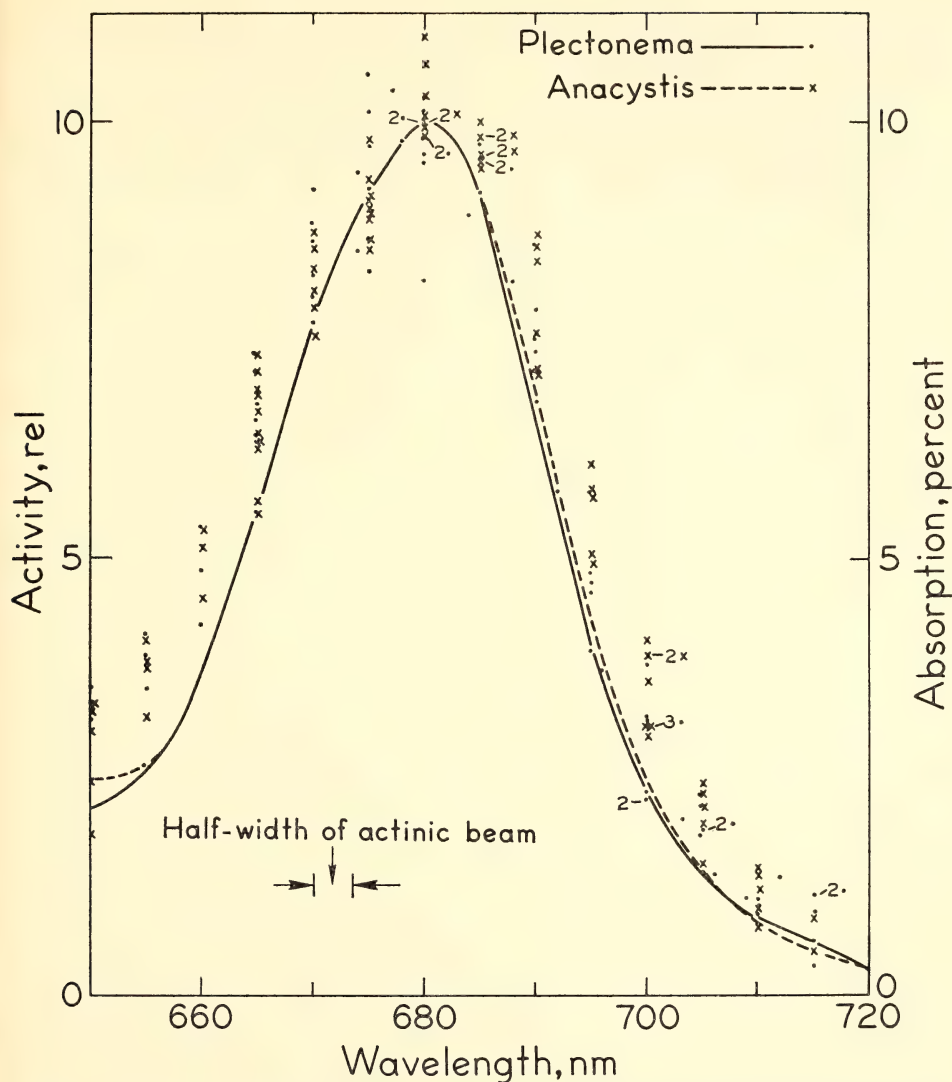


Fig. 26. The rate of cytochrome *c* photo-oxidation as a function of wavelength compared to the percent absorption (solid line) of *Plectonema* (points) and (dashed line) of *Anacystis* (crosses) particles. The optical density at 680 nm was 0.045 (10% absorption) for *Plectonema* and 0.061 (13% absorption) for *Anacystis*. The *Anacystis* data were reduced to the same peak height as those for *Plectonema*. The rate of cytochrome oxidation at 680 nm was  $33.5 \mu\text{moles cyt. } c \text{ mg chl}^{-1} \text{ hr}^{-1}$  with  $1340 \text{ ergs cm}^{-2} \text{ sec}^{-1}$  by *Anacystis*.

for the action spectra. The cytochrome oxidation rate was measured three or four times each at 715, 710, and 680 nm, and this cycle was repeated three times with fresh samples to give 10 measurements at each wavelength. These rates

were averaged and compared in Table 19, setting the rate at 680 nm equal to 100%. The average activities of both algal preparations were nearly the same at 680 nm ( $21 \mu\text{moles cyt. } c \text{ mg chl}^{-1} \text{ hr}^{-1}$  with  $1500 \text{ ergs cm}^{-2} \text{ sec}^{-1}$ ). The percent

absorption of each preparation was similar at 680 nm, but the difference beyond 700 nm was greater than in Fig. 26.

Table 19 shows that although *Plectonema* particles absorbed more than twice as much light at 710 and 715 nm as *Anacystis* particles, their relative effectiveness for oxidizing cytochrome *c* was nearly the same at both wavelengths. In *Plectonema* light absorbed at long wavelengths has about the same effectiveness for oxidizing cytochrome *c* as light absorbed at 680 nm, whereas in *Anacystis* long-wavelength light is 2 to 3 times as effective as light absorbed at 680 nm. These results indicate that the extra light absorbed at long wavelengths by *Plectonema* compared to *Anacystis* does not contribute to an enhanced photosystem 1 activity.

### References

- Fujita, Y., and J. Myers, *Arch. Biochem. Biophys.*, **112**, 519, 1965.
- Kok, B., H. J. Rurainski, and E. A. Harmon, *Plant Physiol.*, **39**, 513, 1964.
- Murano, F., and Y. Fujita, *Plant Cell Physiol.*, **8**, 673, 1967.

### P700 AND CYTOCHROME *f* OXIDATION-REDUCTION REACTIONS IN FRACTION 1 PARTICLES FROM SPINACH

David C. Fork and Norio Murata

A procedure was described by Michel and Michel-Wolwertz (*Year Book* 67, p. 508) by which two kinds of particles could be derived from chloroplasts without the use of detergents. By this method chloroplasts were broken mechanically by passing them three times through the French pressure cell. The resulting fragments were separated by centrifugation on a sucrose density gradient. Fraction 1 particles (light particles remaining near the top of the tube) exhibited system 1 activity and fraction 2 particles (heavy particles) showed system 2 and a little system 1 activity.

Earlier studies (*Year Book* 65, p. 481) on system 1 particles prepared by frag-

menting chloroplasts with the detergent digitonin showed that the chlorophyll/P700 ratio was about 200, based upon measurements of light-induced oxidation of P700. These particles had little functional cytochrome *f*, based upon measurements of light-induced absorbance changes at 420 nm.

Murata and Brown (1970) have found that fraction 1 particles prepared by the pressure cell method did not require added plastocyanin in order to sustain good rates of NADP reduction using is-ascorbate and DCIP (2,6-dichlorophenol indophenol) as the source of electrons. By contrast, particles prepared from chloroplasts by detergent fragmentation have a plastocyanin requirement for NADP reduction (Wessels, 1966; Vernon *et al.*, 1966). It is not known whether this requirement is specific for plastocyanin. It is possible that any substance with properties similar enough to plastocyanin can serve as an electron donor in the detergent-prepared particles.

In this study we have investigated the oxidation-reduction reactions of P700 and cytochrome *f* in fraction 1 particles obtained by breaking chloroplasts mechanically with the French pressure cell.

Time courses for light-induced oxidation of P700 and its dark reduction measured at 703 nm in the presence of ascorbate or ascorbate plus the artificial electron donors DAD (2,3,5,6-tetramethyl-*p*-phenylenediamine), DCIP, and PMS (*N*-methylphenazonium methosulfate) are shown in Fig. 27 before and after treatment with detergent Triton X-100. A downward deflection corresponds to a decrease of absorbance and an oxidation of P700 upon illumination. When the actinic light was turned off, P700 became reduced in the dark. The numbers beside each time course represent the "apparent rate constants" for dark decay in units  $\text{sec}^{-1}$  obtained by dividing the initial rate of absorbance change upon darkening by the steady-state deflection of the absorbance change attained just prior to darkening.



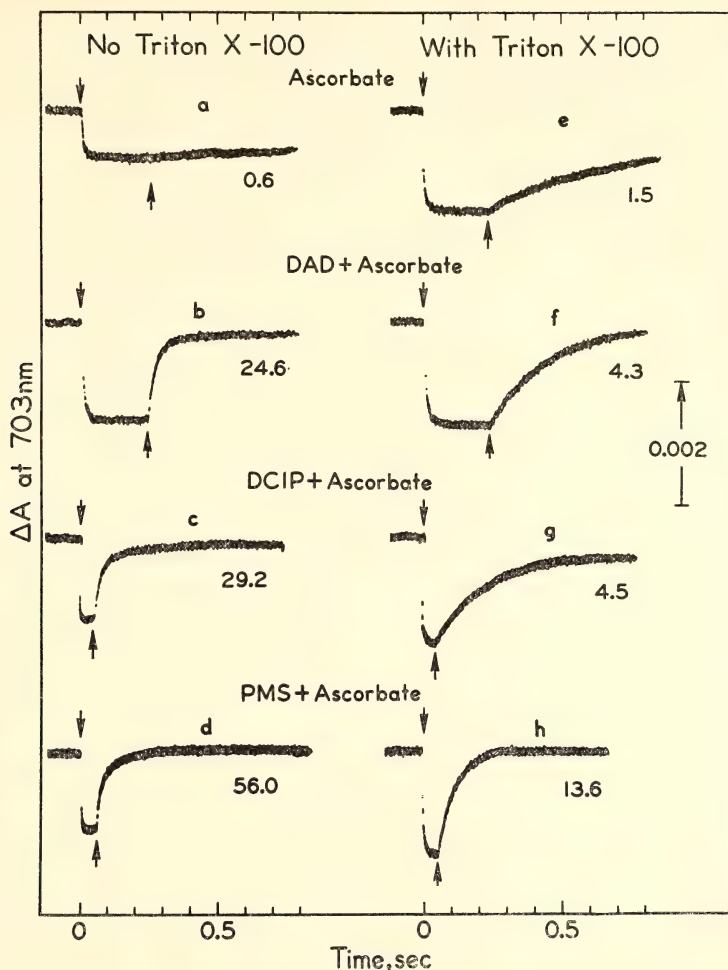


Fig. 27. The effect of artificial electron donors on light-induced changes of absorbance at 703 nm in fraction 1 particles from spinach. The sample was illuminated with a broad band of blue-green actinic light having wavelengths extending from 380 to 590 nm obtained as described in the text. The intensity of this actinic light was  $1.4 \times 10^6$  ergs  $\text{cm}^{-2} \text{sec}^{-1}$ . The measuring beam had a half-band width of 4 nm. The final concentrations of substances in the reaction mixture were: DCMU,  $10 \mu\text{M}$ ; methyl viologen,  $10 \mu\text{M}$ ; sodium ascorbate,  $1 \text{ mM}$ ; KCl,  $60 \text{ mM}$ ; Tricine buffer ( $\text{pH } 7.7$ ),  $20 \text{ mM}$ ; chlorophyll concentration,  $12.8 \text{ g/ml}$ ; and, when added, DAD,  $58 \mu\text{M}$ ; DCIP,  $9.7 \mu\text{M}$ ; PMS,  $9.7 \mu\text{M}$ ; Triton X-100,  $0.08\%$ . The numbers beside each time course represent the apparent "rate constants" for the decay (described in the text). Arrows pointing downward and upward mark when the actinic light was turned on and off, respectively.

It can be seen that before addition of Triton X-100 the dark decay was extremely slow in the presence of ascorbate alone, and a relatively small steady-state P700 change was produced. With DAD, DCIP, or PMS in addition to ascorbate, dark reduction of P700 was

rapid and the maximum change was observed.

After treatment of these particles with Triton X-100 there was, in the presence of ascorbate alone, an increase of the steady-state deflection and an acceleration of dark decay by about 3 times.

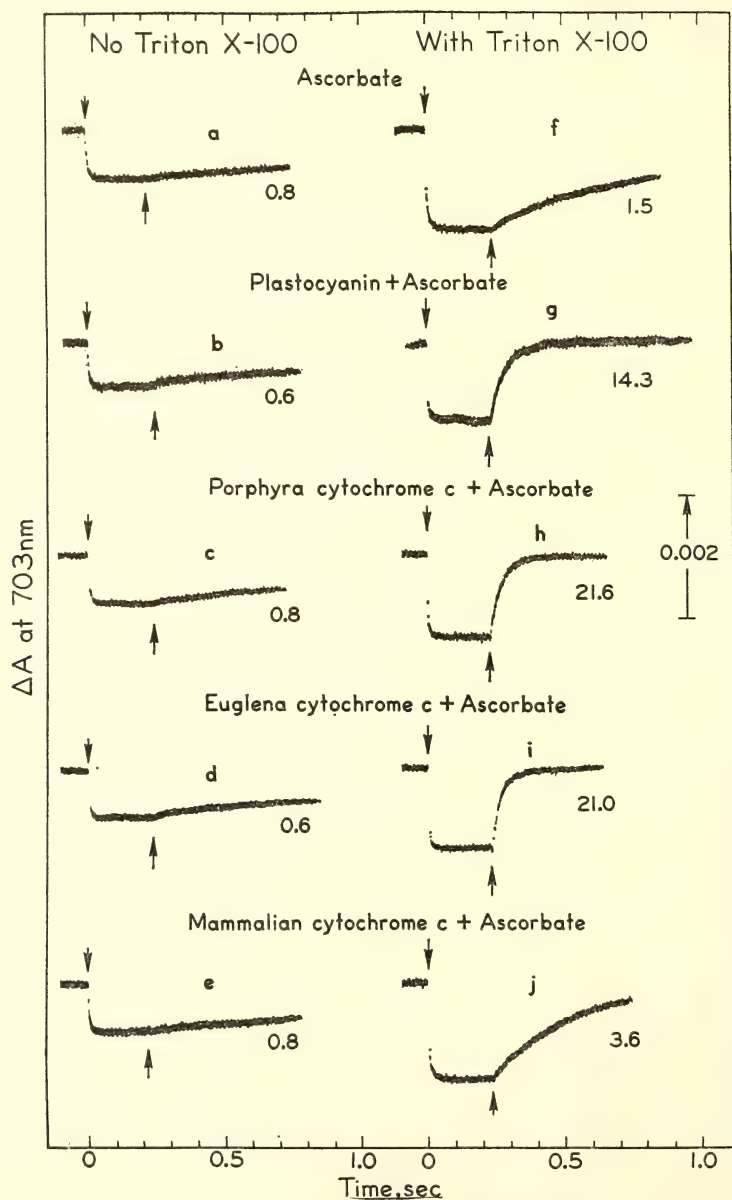


Fig. 28. The effect of natural electron donors on the light-induced changes of absorbance at 703 nm in fraction 1 particles measured as described for Fig. 27. The reaction mixture was illuminated with the same actinic light and contained the same additions and chlorophyll concentration as described for Fig. 27. Those for spinach plastocyanin and *Porphyra* cytochrome 553, *Euglena* cytochrome 552, and horse heart cytochrome *c* were 0.35, 1.1, 1.6, and 1.8  $\mu M$ , respectively. The numbers by each time course are the "rate constants" for decay as described in the text.

However, the dark decay was only slightly accelerated after addition of the artificial electron donors. The treatment with Triton X-100 markedly decreased the dark reduction of P700 when artificial electron donors and ascorbate were present. With DAD or DCIP the decay was decreased about 6 to 7 times and about 4 times with PMS.

An opposite effect of detergent upon the dark reduction of P700 was seen when natural electron carriers such as plastocyanin or cytochromes were used instead of DAD, DCIP, or PMS. Figure 28 shows that the addition of reduced spinach plastocyanin, *Porphyra* cytochrome-553, or *Euglena* cytochrome-552\* did not accelerate the reduction of P700 until after these particles had been treated with Triton X-100. After Triton treatment these electron carriers (with the exception of mammalian cytochrome *c*) strongly stimulated the dark reduction (compare traces *a* and *f*, *b* and *g*, *c* and *h*, *d* and *i*, with *e* and *j*).

The concentration dependence of natural and artificial electron donors to P700 was investigated in the particles treated with Triton X-100. Reduced plastocyanin was most active in reducing P700 in these detergent-treated particles. Cytochromes from *Porphyra* and *Euglena* were about equally active but about 4 times less so than plastocyanin. Mammalian cytochrome *c* was about 14 times less active than *Euglena* or *Porphyra* cytochromes. Compared to plastocyanin, PMS is about 100 times less active in reducing P700 in the presence of Triton X-100. DAD is less active than PMS in reducing P700 in the presence and absence of Triton X-100.

Figure 29 shows a difference spectrum in the region from 670 to 725 nm for absorbance changes induced by blue-green actinic light. Two peaks occur at 682.5 and 701 nm similar to those seen

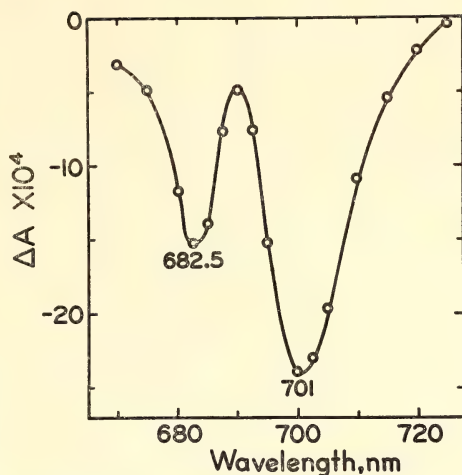


Fig. 29. Light-induced difference spectrum for absorbance changes produced in the red region upon illumination with blue-green light of fraction 1 particles from spinach. The half-band width of the measuring beam was 2.5 nm. The intensity of the actinic light was the same as described in Fig. 27. The final concentration of the substances in the reaction mixture were: DCMU, 7  $\mu M$ ; methyl viologen, 7  $\mu M$ ; sodium ascorbate, 0.7 mM; DAD, 3.5  $\mu M$ ; KCl, 75 mM; Tricine buffer (pH 7.7), 25 mM. Chlorophyll concentration was 14.5  $\mu g/ml$ . No detergent was added.

by Murata and Takamiya (1969) and Vernon *et al.* (1969). The absorbance changes at these peak wavelengths had similar kinetics.

Figure 30 shows the difference spectra measured with DAD and ascorbate, using high and low actinic light intensities. The spectrum measured with low actinic intensity had a maximum near 403 nm and minima at 420 and 552 nm. A shoulder was seen around 430–435 nm. The spectrum measured using higher actinic intensity had a slightly broader maximum around 403 nm as well as a maximum at 450 nm. Minima were found at 420 and 553 nm. A pronounced shoulder occurred around 430 nm in this spectrum. The difference between these curves (dashed line) had a minimum at 430 and maxima at 450 and about 400 nm.

It is well known that the negative

\* Crystalline cytochrome-553 from *Porphyra tenera* and cytochrome-552 from *Euglena gracilis* were kindly supplied by Dr. A. Mitsui (Mitsui and Tsushima, 1968).



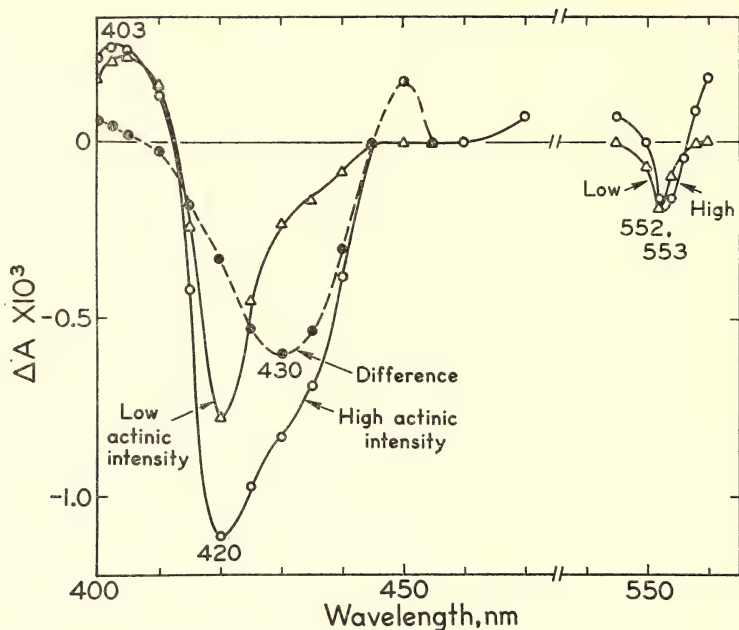


Fig. 30. Light-minus-dark difference spectra for fraction 1 particles from spinach obtained using 1-sec exposures to a broad band of red actinic light having wavelengths extending from 640 to about 800 nm. The spectrum measured at low intensity was done using  $1.6 \times 10^3$  ergs  $\text{cm}^{-2} \text{sec}^{-1}$  and at high intensity with  $1.6 \times 10^5$  ergs  $\text{cm}^{-2} \text{sec}^{-1}$ . The final concentrations of the substances in the reaction mixture were: sodium ascorbate, 978  $\mu\text{M}$ ; DAD, 4.9  $\mu\text{M}$ ; DCMU, 9.8  $\mu\text{M}$ ; KCl, 75 mM; Tricine buffer (pH 7.7), 25 mM. Chlorophyll concentration, 8.5  $\mu\text{g}/\text{ml}$ . No detergent was added.

changes at 420 and 553 nm and the positive change at 403 nm are characteristic of the oxidized-minus-reduced difference spectrum of cytochrome *f*. The negative changes at 430 and 700 nm are produced by P700. The results also indicate that the oxidized-minus-reduced difference spectrum for P700 has maxima near 400 and 450 nm.

The difference spectra of Fig. 30 indicate that at low light intensities cytochrome *f* is mostly oxidized and at high light intensities both cytochrome *f* and P700 are oxidized. If it is assumed that cytochrome *f* is oxidized by P700 in a dark reaction, these results suggest that the reaction between P700 and cytochrome *f* is rapid in fraction 1.

The light intensity dependence of the 420- and 435-nm absorbance changes are shown in Fig. 31. We examined the

contribution of cytochrome *f* and P700 to the changes observed at 420 and

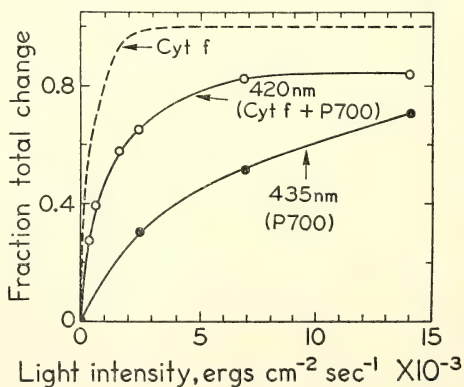


Fig. 31. The dependence of the 420- and 435-nm absorbance changes upon light intensity in fraction 1 particles. The red actinic light used was described in Fig. 30. The sample and the additions are the same as used for Fig. 30.

435 nm by measuring light-induced difference spectra at various light intensities. With a high intensity light sufficient to cause full oxidation of cytochrome *f* and P700 the change at 435 nm was produced almost entirely by P700. Both cytochrome *f* and P700 contribute to the absorbance change observed at 420 nm. The contribution of each at this wavelength was estimated to be 50% ( $\pm 5\%$ ). The light intensity dependence of cytochrome *f* (dashed line in Fig. 31) was calculated by using the light intensity curve of P700 oxidation and subtracting its contribution from the absorbance change at 420 nm. It can be seen that cytochrome *f* saturates at much weaker light intensity than does the P700 change. Oxidation of 50% of the P700 required a light intensity about 20 times higher than that needed to produce 50% oxidation of cytochrome *f*.

The effect of detergent upon the kinetics of light-induced absorbance changes at 420 and 430 nm in the pres-

ence of DAD and ascorbate is shown in Fig. 32. Before Triton treatment the decay at 430 nm was faster than at 420 nm. The steady state deflection was reached in a fraction of a second in both cases (traces *a* and *c*). As mentioned previously, the 430-nm change is estimated to be produced almost entirely by P700. Cytochrome *f* and P700 contribute about equally to the absorption change seen at 420 nm.

It was possible to reconstruct the portion of the absorbance change at 420 nm that was produced by cytochrome *f* alone. To do this the absorption change produced by P700 at 420 nm was subtracted from the change measured at 420 nm. Trace *b* of Fig. 32 shows that cytochrome *f* remains almost completely oxidized until P700 becomes almost reduced. After Triton treatment the decays at 420 and 430 nm upon darkening became slower and were about the same in both cases. The rapid decrease produced at 420 nm upon illumination was

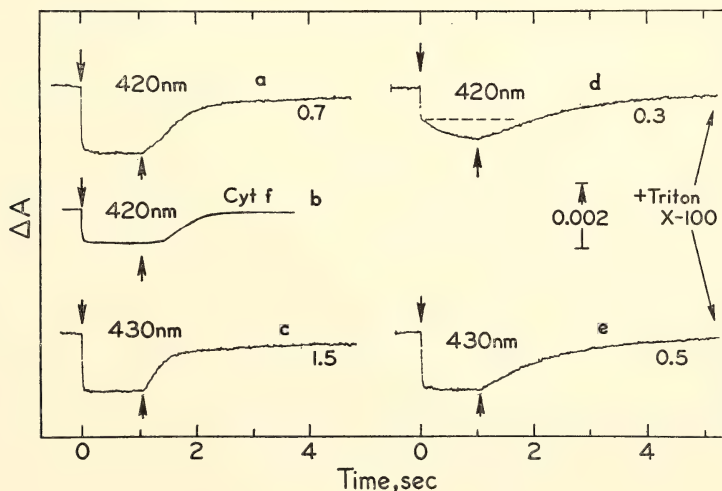


Fig. 32. A comparison of time courses of light-induced absorbance changes at 420 and 430 nm in fraction 1 particles from spinach before and after addition of detergent. Trace *b* was constructed as described in the text. The same red actinic light as described in Fig. 30 was used and had an intensity of about  $2.5 \times 10^5$  ergs  $\text{cm}^{-2} \text{sec}^{-1}$ . Half-band width of measuring beam, 2 nm. The final concentrations of the substances in the reaction mixture were: sodium ascorbate, 972  $\mu\text{M}$ ; DAD, 4.9  $\mu\text{M}$ ; methyl viologen, 9.7  $\mu\text{M}$ ; DCMU, 9.7  $\mu\text{M}$ ; KCl, 75 mM; Tricine buffer (pH 7.7), 25 mM; Triton X-100 (when used), 0.08%; chlorophyll concentration, 20  $\mu\text{g}/\text{ml}$ . The numbers by each time course represent the apparent "rate constant" of the decay as described in the text.

reduced about one-half. This rapid deflection is the portion of the 420-nm change produced by P700. A second, slower decrease of absorbance was seen at 420 nm during the illumination period. This second, slow oxidation was almost absent at 430 nm.

Difference spectra for the initial rapid deflection occurring upon illumination (see Fig. 32) were measured before and after the addition of Triton X-100. It can be seen in Fig. 33 that the spectrum measured before Triton treatment had maxima at about 403 and 450 nm and minima at 420 and 554 nm. A pronounced shoulder occurred around 430 nm. After detergent treatment maxima were found at 405 and 450 nm and a single minimum occurred at 430 nm characteristic of P700. Subtraction of these two difference spectra produces a curve characteristic of the oxidized-minus-reduced difference spectrum of cytochrome *f*. When the difference spectrum was measured for the second, slow absorbance change (such as seen in Fig. 32 for the 420-nm change in the presence of Triton) a minimum

was found at 420 and maxima around 404 and 450 nm, and the spectrum was also very similar to the difference spectrum of cytochrome *f*. These findings suggest that Triton treatment breaks the linkage of electron transport between P700 and cytochrome *f*. After treatment only the slow oxidation of cytochrome *f* occurs.

Figure 34 shows that a 1-msec red actinic flash produces a change of absorbance at 418 nm within 0.5 msec.

The behavior of cytochrome *f* in the fraction 1 particles is similar to that observed in whole chloroplasts. Hildreth (1968) found half-times for cytochrome *f* oxidation from 0.3 to 9 msec when spinach chloroplasts were excited with a 30-nsec flash from a Q-switched ruby laser. As mentioned above, the oxidation of cytochrome *f* took place within 0.5 msec in the fraction 1 particles. The fraction 1 particles are also similar to whole chloroplasts because the latter are effectively reduced by low concentrations of artificial electron donors such as DAD, DCIP, and PMS probably via

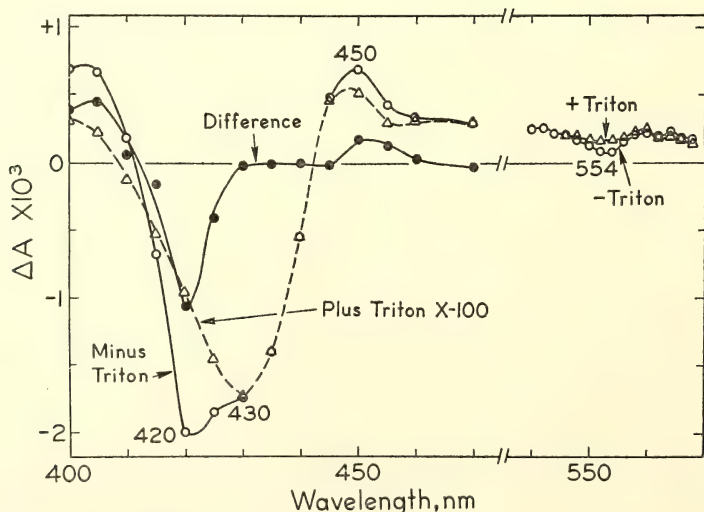


Fig. 33. Light-induced difference spectra for fraction 1 particles before and after treatment with Triton X-100. The half-band width of the measuring beam was 2 nm. The rapid deflection upon turning on the actinic light was taken from time courses as shown in Fig. 32. The actinic light and the sample mixture were the same as described for Fig. 32. Triton X-100 (when added), 0.08%.



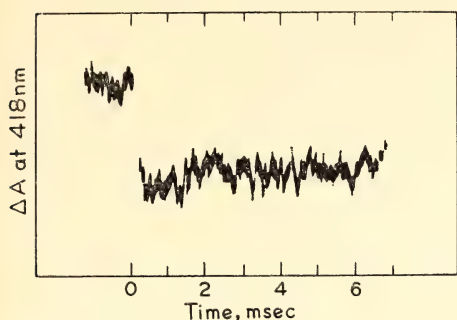


Fig. 34. The time course of the 418-nm change produced by a flash of red actinic light lasting 1 msec. The wavelength distribution of this light was as described in Fig. 30. The reaction mixture contained the same additions and concentrations as described for Fig. 30, except that the Triton X-100 concentration (when used) was 0.18%. Chlorophyll concentration, 20  $\mu\text{g/ml}$ .

cytochrome *f* or another electron carrier but not by added plastocyanin.

Treatment of the fraction 1 particles with Triton X-100 altered them because after treatment, DAD, DCIP, or PMS were no longer effective donors to P700; but plastocyanin and algal *c*-type cytochromes were able to donate electrons to P700, probably directly. The behavior of these donors is characteristic of system 1 particles prepared from chloroplasts by detergent fragmentation. The P700 in system 1 particles prepared by sonic oscillation is likewise effectively reduced by plastocyanin but not by DCIP. It thus appears that particles prepared by using the pressure cell have most of the electron transport carriers of system 1 in their native state.

In the Triton-treated fraction 1 particles, plastocyanin, as well as the *c*-type cytochromes from *Euglena* or *Porphyra*, are effective donors to P700. Plastocyanin is a well-known electron donor to P700 in detergent or sonic-treated particles (Wessels, 1966; Vernon *et al.*, 1966; Jacobi, 1969). Mammalian cytochrome *c* is quite inactive, however. It appears that the electric charge on the proteins rather than the redox potential

is of most importance in relation to their reactivity with P700. Spinach plastocyanin, *Porphyra*, and *Euglena c*-type cytochromes are acidic proteins and have  $\text{pK}$ 's of about 3.5, 3.5, and 5.5, respectively (Kato *et al.*, 1962; Kato, 1960; Perini *et al.*, 1964). Mammalian cytochrome *c* has a  $\text{pK}$  around 10.5. Therefore, around neutrality the above-mentioned proteins, with the exception of mammalian cytochrome *c*, would have a negative charge. If we assume that P700 or the moiety around P700 has positive charges, then plastocyanin and the algal cytochromes can easily approach P700, but mammalian cytochrome *c* cannot. The redox potentials of these substances at neutral  $\text{pH}$  are 370 mV for spinach plastocyanin, 330 mV for *Porphyra* cytochrome-553 and 370 mV for *Euglena* cytochrome-552 (Kato *et al.*, 1962; Kato, 1960; Perini *et al.*, 1964). Mammalian cytochrome *c* has a redox potential of 260 mV at this  $\text{pH}$ . Thus the oxidation-reduction potential does not seem to be the essential factor in the ability of a compound to reduce P700 because mammalian cytochrome *c* showed much less activity in reducing P700 in spite of the fact that its potential is lower than those of plastocyanin or the algal cytochromes.

The effectiveness of plastocyanin in restoring NADP reduction in detergent-treated particles in the presence of DCIP and ascorbate, for example, may be due to the ability of plastocyanin to reduce P700 directly. But restoration of NADP reduction in detergent-prepared particles appears not to have a specific plastocyanin requirement because appropriate algal cytochromes can reduce P700 almost as effectively as plastocyanin and, therefore, would be expected to restore photoreduction of NADP in these particles also.

The inability of reduced plastocyanin to accelerate the reduction of P700 (or cytochrome *f*) until after the fraction 1 particles have been treated with detergent raises the question of whether

plastocyanin is present in these particles which have functional P700 and cytochrome *f*. Experiments of Murata and Brown (1970) have shown that plastocyanin was not required by these particles for the reduction of NADP supported by DCIP and isoascorbate. It is possible that a certain amount of plastocyanin is tightly bound to these particles and does not leach out after breakage in the pressure cell. It will be necessary to examine these particles to determine if any bound plastocyanin still remains in them.

This work was supported in part by a grant from the National Science Foundation (GB 8630) to David C. Fork.

### References

- Hildreth, W. W., *Biochim. Biophys. Acta*, **153**, 197, 1968.
- Jacobi, G., *Z. Pflanzenphysiol.*, **61**, 203, 1969.
- Kato, S., *Plant Cell Physiol.*, **1**, 91, 1960.
- Kato, S., I. Shiratori, and A. Takamiya, *J. Biochem.*, **51**, 32, 1962.
- Mitsui, A., and K. Tsushima, in *Structure and Function of Cytochromes*, K. Okunuki, M. D. Kamen, and I. Sekuzu, eds., Univ. Tokyo Press, Tokyo, p. 459, 1968.
- Murata, N., and J. S. Brown, *Plant Physiol.*, **45**, 360, 1970.
- Murata, N., and A. Takamiya, *Plant Cell Physiol.*, **10**, 193, 1969.
- Perini, F., M. D. Kamen, and J. A. Schiff, *Biochim. Biophys. Acta*, **88**, 74, 1964.
- Vernon, L. P., E. R. Shaw, and B. Ke, *J. Biol. Chem.*, **241**, 4101, 1966.
- Vernon, L. P., H. Y. Yamamoto, and T. Ogawa, *Proc. Nat. Acad. Sci. U.S.*, **63**, 911, 1969.
- Wessels, J. S. C., *Biochim. Biophys. Acta*, **126**, 581, 1966.

### PHOTOCHEMICAL REACTIONS OF P700 AND CYTOCHROME *f* AND THE ACTION OF PLASTOCYANIN IN A GRANA STACK PREPARATION FROM SPINACH

David C. Fork and Günter Jacobi

It is possible to obtain different types of particles from spinach chloroplasts,

depending upon the conditions and methods used for fragmentation. In this study we used a preparation of intact grana stacks and investigated the reactions of P700 and cytochrome *f* and the effect of detergent treatment and plastocyanin addition.

The results have shown that both P700 and cytochrome *f* are present in the grana stack preparation and that the cytochrome can be rapidly oxidized, probably by P700. Detergent treatment destroys the rapid cytochrome oxidation which cannot be reestablished by subsequent plastocyanin addition.

Chloroplasts from spinach were isolated in a medium containing 300 mM sucrose, 1 mM pyrophosphate, pH 7.5, 1 mM MgCl<sub>2</sub> as described before (Jacobi, 1963). The pellet from once-washed chloroplasts was suspended in a solution containing 343 mM NaCl, 1 mM MgCl<sub>2</sub>, 1 mM Tricine buffer, pH 7.5, and 0.1% bovine serum albumin and adjusted to 1 mg chlorophyll ml<sup>-1</sup> (Jacobi and Lehmann, 1969).

Fragmentation was accomplished by passing the suspension of chloroplasts through the French pressure cell at 2000 lb in<sup>-2</sup> (128 kg cm<sup>-2</sup>) or by sonicating in a Branson Sonifier (Step VI) for 15 sec. Starch and unbroken material were removed by centrifugation at 2000×*g* for 5 min. The fraction containing heavier fragments used in these experiments was isolated by further centrifugation at 12,000×*g* for 15 min. This fraction was shown by electron microscopy to contain intact grana stacks (Jacobi and Lehmann, 1969).

Plastocyanin was isolated from an acetone powder of isolated chloroplasts essentially according to the method of Kato *et al.* (1962) but included some other steps (Jacobi, 1967).

Figure 35 shows the kinetics of light-induced absorbance changes produced at 420 and 430 nm upon illumination of the grana stack preparation with red light. In addition, Fig. 35 illustrates the effects produced at these wavelengths

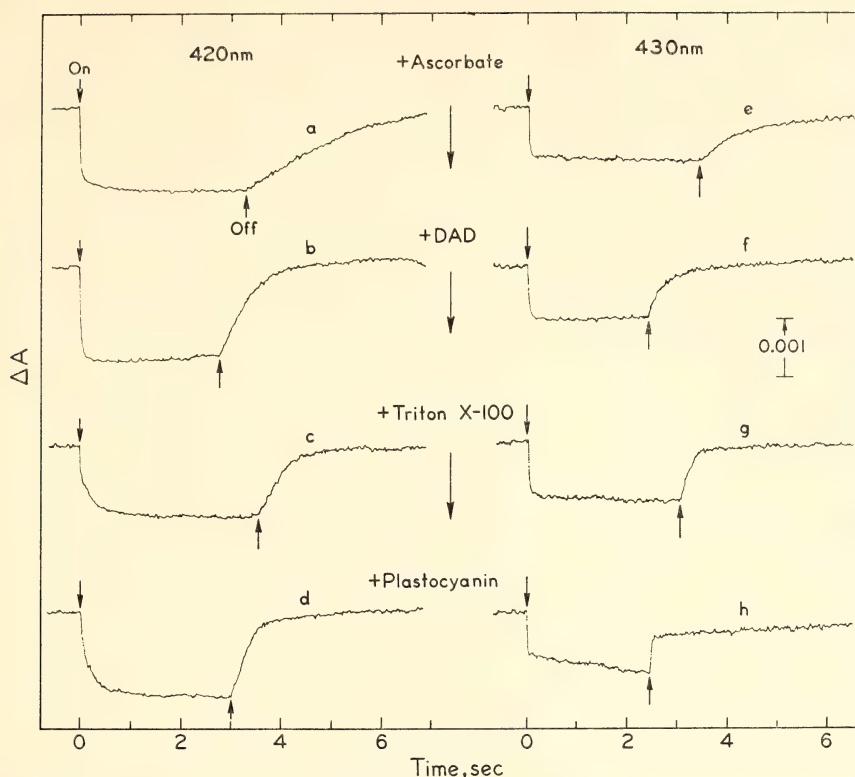


Fig. 35. Light-induced changes of absorbance at 420 and 430 nm in a grana stack preparation prepared by sonication from spinach chloroplasts. The sample was illuminated with monochromatic red light having a peak at 668 nm, a half-width of 11 nm, and an intensity of  $4.1 \times 10^4$  ergs  $\text{cm}^{-2}$   $\text{sec}^{-1}$ . The half-width of the measuring beam was 2 nm. All the traces shown were obtained from one sample and the additions shown were made sequentially. The final concentrations of substances in the reaction mixture were: DCMU, 5  $\mu\text{M}$ ; MES buffer (pH 6.3), 25 mM; NADP, 0.5 mM;  $\text{MgCl}_2$ , 5 mM; sodium ascorbate, 10.0 mM; DAD (when added), 66  $\mu\text{M}$ ; Triton X-100 (when added), 0.1%; chlorophyll concentration, 30  $\mu\text{g ml}^{-1}$ , plastocyanin (when added), 2.2  $\mu\text{M}$ . A saturating amount of ferredoxin and ferredoxin-NADP-reductase was also used. Downward and upward arrows mark the beginning and end of illumination, respectively. A downward deflection of the trace corresponds to a decrease of absorbance.

upon the sequential addition of ascorbate, DAD, Triton X-100, and plastocyanin. Traces *a* and *e* of Fig. 35 show that, in the presence of ascorbate alone, illumination produces rapid decreases of absorbance both at 420 and 430 nm. A steady deflection is attained in the light after about a second of illumination.

Traces *b* and *f* of Fig. 35 show the effects on the 420- and 430-nm absorbance changes of adding DAD to the fragments containing ascorbate. The steady-state 420-nm change was attained

more rapidly in the presence of DAD and the dark decay was strongly accelerated. Dark decay of the 430-nm change was also accelerated by DAD. The difference spectrum in the presence of DAD and ascorbate for the rapid absorbance decrease occurring within 50 msec upon illumination is shown in Fig. 36. This spectrum has a large minimum at 420 and a shoulder near 430 nm, suggesting accumulation of oxidized cytochrome *f* and some P700. The effect of DCIP was



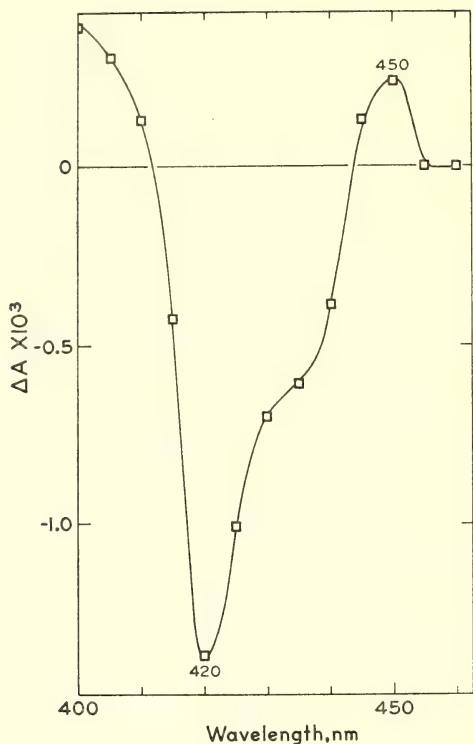


Fig. 36. Light-minus-dark difference spectra for absorbance changes produced within 50 msec upon illumination of a grana stack preparation with red actinic light described in Fig. 35. The reaction mixture contained DAD and ascorbate and other additions as described in Fig. 35.

found to be the same as DAD in this preparation.

The occurrence of P700 changes under these conditions was confirmed by measuring a difference spectrum in the red region. In this spectrum the minimum occurred around 701 nm and the half-band of the negative peak was about 12 nm.

Addition of Triton X-100 altered the kinetics of the absorbance changes at 420 but did not produce much effect on the kinetics at 430 nm (traces *c* and *g* of Fig. 35). The rapid negative absorbance change at 420 nm produced upon illumination was noticeably decreased by Triton treatment. But at 420 nm a

slow decrease requiring about 3 sec for completion persisted. Addition of plastocyanin to chloroplasts treated with Triton did not influence the rapid light-induced absorbance decrease at 420 nm but this slowly decreasing change was enhanced by plastocyanin (trace *d*, Fig. 35). In the presence of plastocyanin the dark decay at 430 nm was accelerated (trace *h*, Fig. 35).

Difference spectra for the rapid changes occurring within 50 msec were measured after the addition of Triton and subsequent addition of plastocyanin. Figure 37 shows that both these spectra have a single maximum centered at 430 nm and positive maxima at 450 and around 400 nm, suggesting P700 participation only. The peak at 420 nm, produced by cytochrome *f* was eliminated by the Triton treatment and was not restored by plastocyanin addition. Figure 38 shows difference spectra for the slow

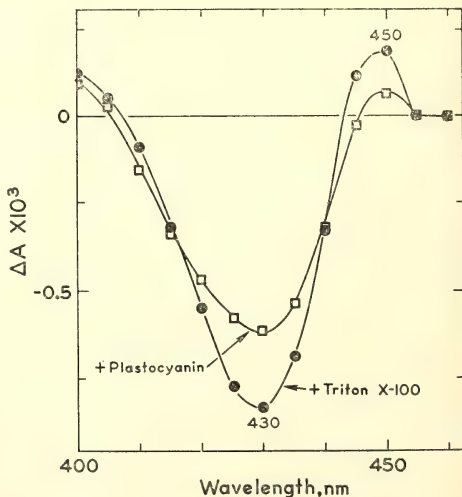


Fig. 37. The effect of Triton X-100 and plastocyanin on light-induced difference spectra for absorbance changes produced within 50 msec upon illumination of a grana stack preparation with red actinic light described in Fig. 35. The spectrum labeled Triton X-100 contained the substances described for Fig. 35, including DAD and ascorbate. Subsequent addition of plastocyanin to this preparation yielded the difference spectrum as shown.

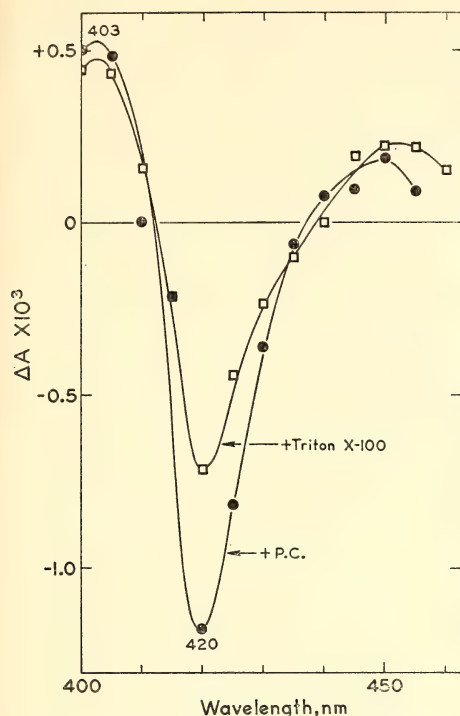


Fig. 38. Light-induced difference spectra for slow absorbance changes (occurring within several seconds) produced upon illumination with red light as described for Fig. 35. The same sample was used as described in Fig. 37.

absorbance changes that took several seconds for completion. The spectra for these slow changes seen with Triton as well as with plastocyanin have minima at 420 and maxima at about 403 and 450 nm.

Since the contribution of cytochrome *f* to the difference spectrum at 430 nm is almost zero (Kato, 1960; Fork and Murata, 1971; see also another section of this report) the change at 430 nm is most likely produced only by P700. Under the conditions of these experiments no evidence was found for the production of absorbance changes in this region by other substances such as the *b*-type cytochromes. The contribution of P700 to absorbance changes at 420 can be estimated to be about 66% from the

difference spectrum obtained after adding Triton (Fig. 37). A comparison was made of the dark reduction of P700 and cytochrome *f* in the presence of DAD and ascorbate by measuring traces similar to *b* and *f* of Fig. 35. To do this the absorbance change at 430 nm was reduced to 66% and subtracted from the change measured at 420 nm. The result shown in Fig. 39 compares the decay of P700 and cytochrome *f* alone. It can be seen when half of the P700 is in the reduced state that cytochrome *f* is still almost 90% oxidized.

The results of these experiments show that grana stack preparations, as well as the fraction 1 particles (described in another section), contain cytochrome *f* and P700. As with the fraction 1 particles, the cytochrome *f* in the presence of ascorbate or DAD and ascorbate is rapidly oxidized in the light. Addition of the detergent Triton X-100 abolished the rapid light-induced oxidation of cytochrome *f* but not the oxidation of P700 because the difference spectrum for the rapid change after treatment showed only a minimum at 430 nm and did not have the minimum previously seen at 420 nm. Subsequent addition of plastocyanin to the Triton-treated grana stack preparation did not reestablish the rapid oxidation of cytochrome *f*. After the addition of plastocyanin the difference spectrum still had a single minimum centered at 430 nm. The magnitude of the P700 change is somewhat smaller probably because reduced plastocyanin competes with accumulation of the photo-oxidized P700. A slow accumulation of photo-oxidized cytochrome *f*, taking several seconds to reach steady state, still occurs after Triton treatment and is stimulated by added plastocyanin. It appears from this study and the one on fraction 1 particles (described in another section) that Triton treatment breaks the linkage between P700 and cytochrome *f*. Slow oxidation of cytochrome *f* probably represents an *in vitro* reaction. Perhaps plastocyanin mediates the light-

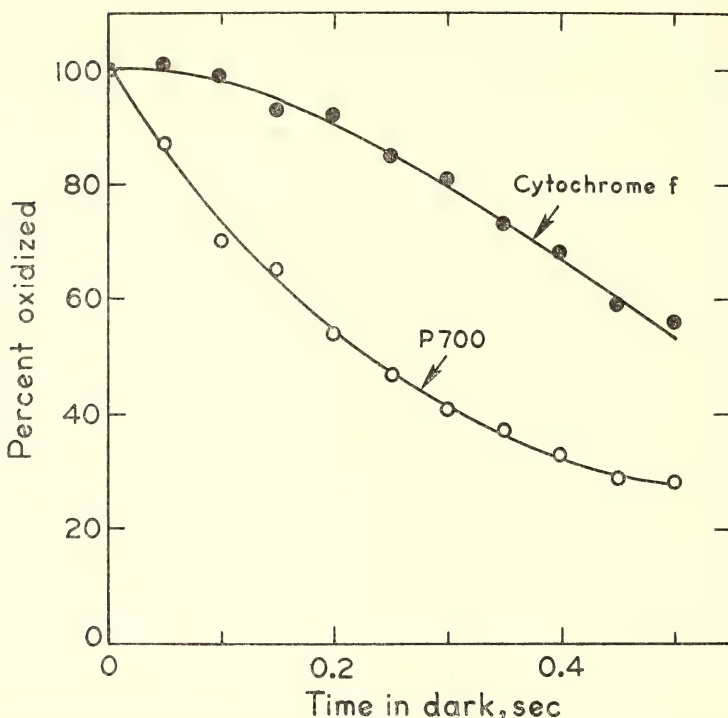


Fig. 39. The dark reduction of P700 and cytochrome *f* after a period of illumination with red actinic light as described in Fig. 35. The additions included DAD and ascorbate and other substances as indicated for Fig. 35.

induced photo-oxidation of cytochrome *f* disrupted by detergent treatment. Hind (1968) has concluded that the electron transport sequence in chloroplasts treated with detergent is cytochrome *f*, plastocyanin, P700. The data were obtained with a double-beam spectrophotometer that could only measure slow changes. Those occurring sooner than about several tenths of a second are not detected with this apparatus. Therefore, only slow changes such as those shown in traces *c* and *d* of Fig. 35 could be investigated. The results of Fig. 38 agree with those reported by Hind in that a slow oxidation of cytochrome *f* is stimulated by added plastocyanin. But Fig. 37 shows that added plastocyanin does not restore rapid photo-oxidation of cytochrome *f*. Thus the sequence proposed by Hind may not be the electron transport sequence operating *in vivo*.

The simplest hypothesis to explain the results obtained in this study is that cytochrome *f* is oxidized rapidly, but not necessarily directly, by P700. In Fig. 39 it was seen that after a period of illumination cytochrome *f* tended to remain oxidized until P700 became reduced. A similar behavior of P700 and cytochrome *f* was also found in fraction 1 particles isolated from spinach.

This work was supported in part by a grant from the National Science Foundation (GB 8630) to David C. Fork.

#### References

- Fork, D. C., and N. Murata, *Photochem. Photobiol.*, in press, 1971.
- Hind, G., *Biochim. Biophys. Acta*, 153, 235, 1968.
- Jacobi, G., *Z. Naturforsch.*, 19b, 312, 1963.
- Jacobi, G., *Z. Pflanzenphysiol.*, 57, 255, 1967.



Jacobi, G., and H. Lehmann, in *Progress in Photosynthesis Research*, H. Metzner, ed., Intern. Union Biol. Sci., p. 159, 1969.

Katoh, S., *Nature*, 186, 138, 1960.

Katoh, S., I. Shiratori, and A. Takamiya, *J. Biochem.* (Tokyo), 51, 32, 1962.

THE DEVELOPMENT OF SYSTEM 2  
ACTIVITY IN *Chlamydomobrys*  
DURING TRANSITION FROM PHOTO-  
HETEROTROPHIC TO AUTOTROPHIC  
NUTRITION

Wolfgang Wiessner and David C. Fork

When the green alga *Chlamydomobrys stellata* is grown photo-heterotrophically

on acetate, it has a very low capacity for photosynthetic CO<sub>2</sub> fixation and for the Hill reaction with dichlorophenol indophenol (Merrett, 1969; Wiessner, 1969). The thylakoids of its chloroplasts are almost all separated from each other by stroma. Only a few membranes of neighboring thylakoids can be seen to form connections (Wiessner and Amelunxen, 1969a, 1969b). However, autotrophically grown cells photosynthesize normally and their chloroplasts contain a large number of grana. On the basis of these results, Wiessner and Amelunxen (1969a, 1969b) speculated that chloro-

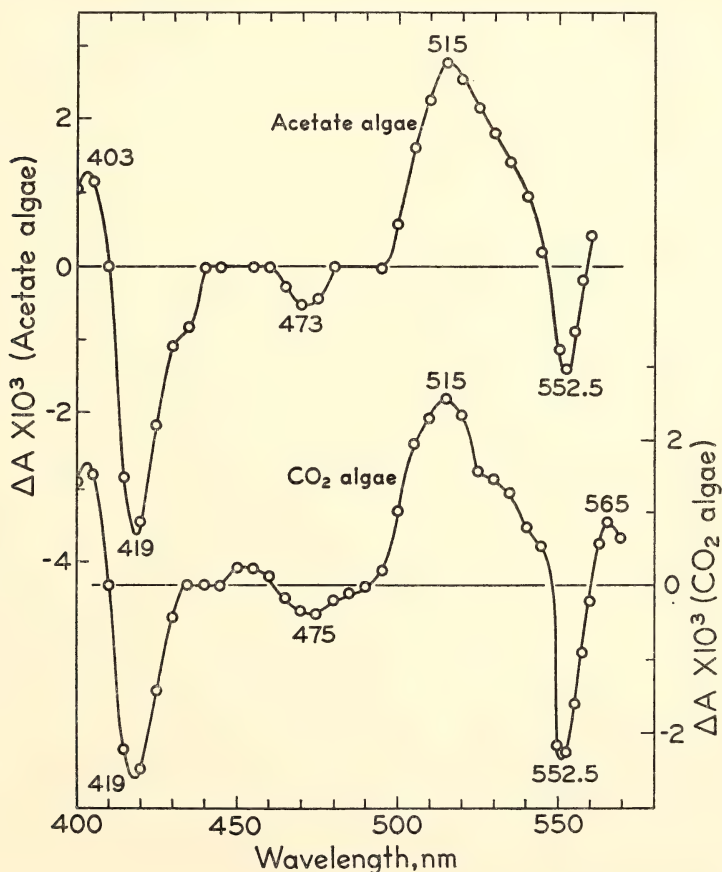


Fig. 40. Light-minus-dark difference spectra for absorbance changes produced upon illumination of *Chlamydomobrys stellata* adapted to photo-heterotrophic (light + acetate) or autotrophic growth (with CO<sub>2</sub>). The red actinic light had an intensity of  $3.1 \times 10^5$  ergs cm<sup>-2</sup> sec<sup>-1</sup> in a broad band extending from about 640 to 800 nm. Half-band of the measuring beam was 2 nm.

plasts lacking grana are devoid of a functional light reaction 2 and may, in addition, lack components needed to transport electrons derived from water to photoreaction 1.

We have investigated the activity of systems 1 and 2 in photo-heterotrophically and in autotrophically grown cells and have also studied the changes that occur during the transition from one form of nutrition to another.

*Chlamydomobryx stellata*, strain 10-1e from the culture collection of algae of the Pflanzenphysiologisches Institut der Universität Göttingen, was grown at 30°C with a light intensity of 9000 lux either autotrophically or photo-heterotrophically in the medium described by Wiessner (1968). In the case of the changeover experiments from photo-heterotrophic to autotrophic nutrition the acetate-grown algae were freed of the acetate-containing medium by

centrifugation and resuspended in autotrophic growth medium.

The absorbance changes were measured with algae collected during the exponential phase of growth after they were centrifuged and resuspended in nutrient solution lacking acetate and ammonium chloride.

Figure 40 shows light-induced difference spectra for both photo-heterotrophically and autotrophically grown cells in the region from 400 to 570 nm. A maximum was found at 403 nm and minima at 419 and 552.5 nm, demonstrating light-induced oxidation of the *f*-type cytochrome in algae cultured either with acetate or CO<sub>2</sub>. The 419-nm band is too small in relation to the 552.5-nm band largely because of the so-called flattening or sieve effect (Duysens, 1956). In addition, both spectra show minima at 475 and maxima at 515 nm produced in part by chlorophyll *b* (Fork and Ames, 1956).

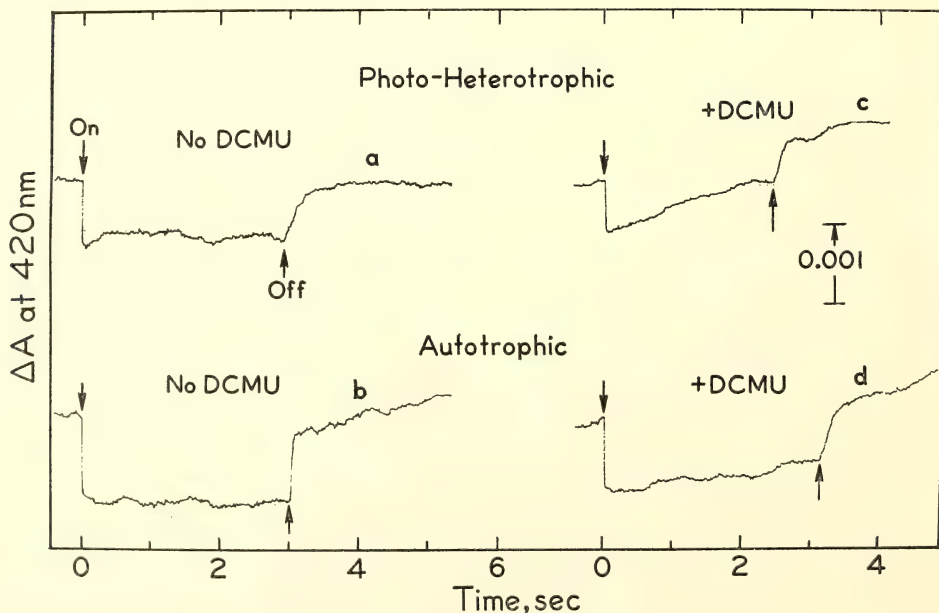


Fig. 41. Light-induced changes of absorbance produced at 420 nm upon illumination of *Chlamydomobryx stellata* adapted to photo-heterotrophic or autotrophic growth. Other conditions as described for Fig. 40. DCMU (when used) 50  $\mu$ M. The instability of the traces is produced by increased mobility of the cells when illuminated with blue measuring wavelengths. Downward- and upward-pointing arrows mark the beginning and end of the illumination period, respectively. A downward deflection of the trace corresponds to a decrease of absorbance (oxidation).

1969). The spectrum for the  $\text{CO}_2$  algae shows a band at 565 nm probably produced by reduction of a  $b_6$ -type cytochrome.

Figure 41 shows time courses of the cytochrome  $f$  change in photo-heterotrophic and in autotrophic organisms in the presence and absence of  $5 \times 10^{-5} M$  DCMU [3-(3,4-dichlorophenyl)-1,1-dimethylurea]. The dark reduction of cytochrome proceeded about 10 times faster in autotrophic cells than in photo-heterotrophic cells (traces  $a$  and  $b$ ). DCMU had very little effect on the endogenous dark reduction of cytochrome  $f$  in the acetate-grown algae. In

autotrophic organisms, on the other hand, it retarded the speed of the reduction rate significantly.

The rate of dark reduction of cytochrome  $f$  that was oxidized previously during a period of illumination is shown in Fig. 42 as a function of the time that cells have had to adapt from nutrition with acetate to photosynthetic growth with  $\text{CO}_2$ . Measurements were also made with cells treated with DCMU in order to block system 2 reduction of this cytochrome. It can be seen that the cells adapted to growth with acetate have no system 2 activity. The same rate of cytochrome  $f$  reduction occurred in the pres-

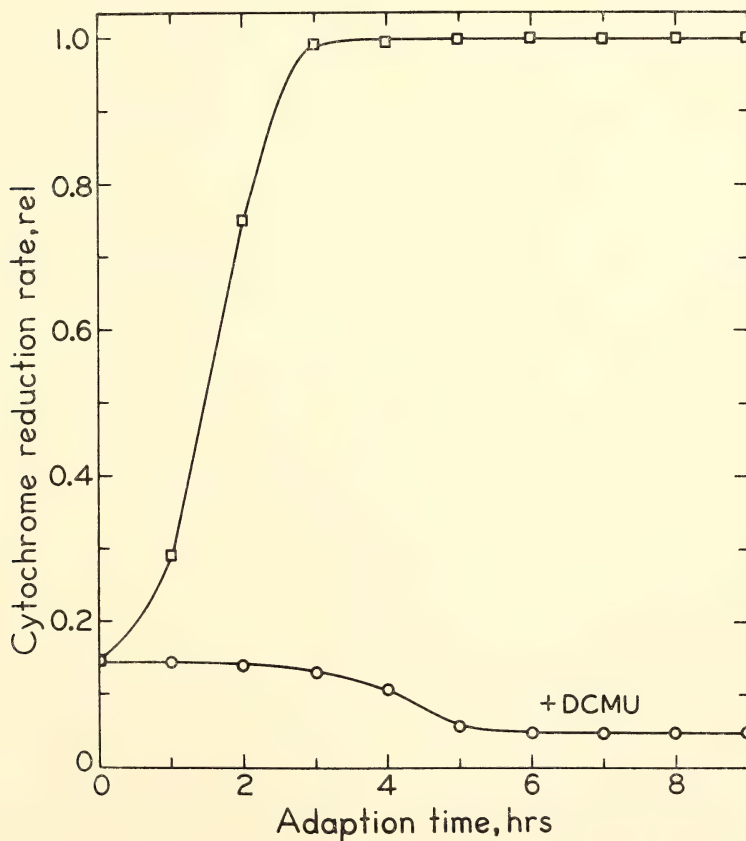


Fig. 42. Dark reduction of the  $f$ -type cytochrome in *Chlamydomonas stellata* as a function of the time after transfer of acetate-grown cells to a medium containing  $\text{CO}_2$  and devoid of acetate. Cytochrome  $f$  reduction was measured as the rate of absorbance increase at 420 nm following a period of illumination with red actinic light as described in Fig. 40.



ence and absence of DCMU. But after two hours of adaptation from nutrition with acetate to photosynthetic growth with  $\text{CO}_2$  the rate of cytochrome reduction was increased fivefold. It is clear from these results that electron transport from water mediated by system 2 does not exist in *Chlamydomobotrys* grown in the light with acetate.

We were also able to obtain information about the functioning of systems 1 and 2 by following the absorbance change at 515 nm in these organisms. This absorbance change has been shown to be produced in green algae and higher plants by both system 1 and system 2. The change is only partly inhibited by DCMU and the action spectrum for the change remaining after poisoning is produced by system 1. A second, slower 515-nm change appears at higher intensities and is activated by system 2. This

slower phase is sensitive to DCMU (Fork and Ames, 1969).

Time courses for the 515-nm absorbance change in *Chlamydomobotrys* grown photo-heterotrophically with acetate, as well as the changes that occur during transition to autotrophic growth, are shown in Fig. 43. Trace *a* shows that the 515-nm change in cells grown in acetate is almost the same as that produced by cells poisoned with DCMU (compare traces *a* and *g*). Although not shown in this figure, the addition of DCMU had very little effect on the change produced by photo-heterotrophically grown cells. Sometimes DCMU produced a slight decrease of the steady state change and of the dark-decay rate. Two hours after transfer of the cells out of the acetate-containing medium some slow phase of the 515-nm change could be seen. Addition of DCMU inhibited this phase and

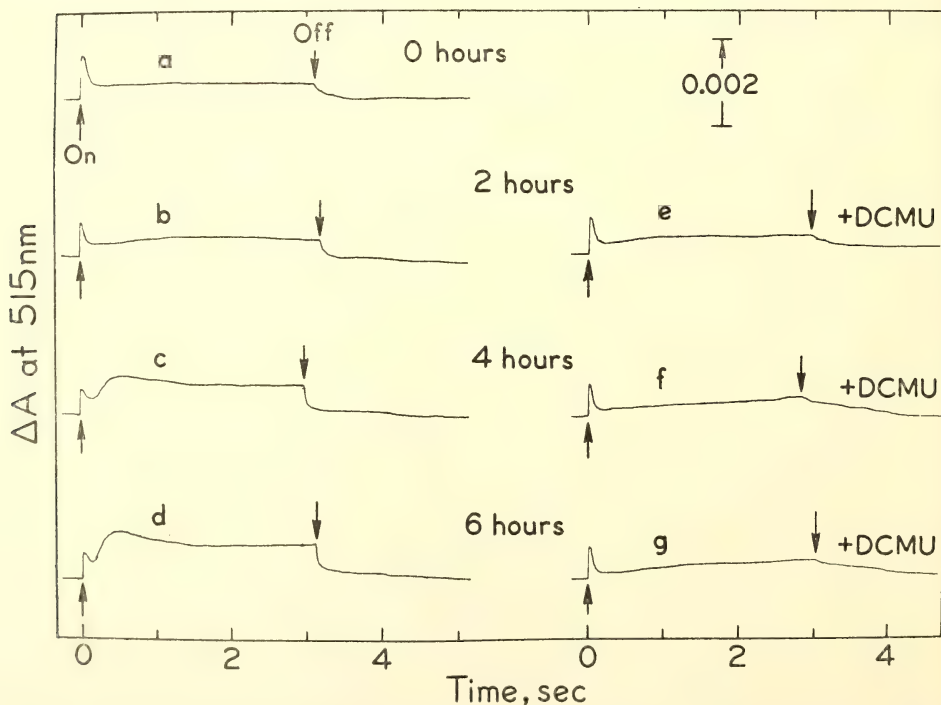


Fig. 43. Kinetics of the light-induced absorbance change at 515 nm in *Chlamydomobotrys stellata* in the presence and absence of DCMU as a function of the time after transfer of cells grown in acetate to a medium lacking acetate but containing  $\text{CO}_2$ .

decreased the dark decay (traces *b* and *e*). The progressive development of the 515-nm change can be seen in the traces obtained 4 and 6 hours after transfer.

It can clearly be seen that photo-heterotrophic nutrition in *Chlamydomobry*s depends only on the functioning of system 1. Thus the cytochrome oxidized by system 1 in these cells is not reduced by system 2 because the change is almost identical to that seen in cells grown under normal, autotrophic conditions and poisoned with DCMU. Similarly, the 515-nm change in cells grown in acetate is like normally grown cells poisoned with DCMU.

Photosystem 2 activity is lacking in *Chlamydomobry*s grown photo-heterotrophically, and in this condition the thylakoids in the chloroplasts of these cells are almost all separated from each other and not stacked to form grana. Grana stacks are formed during the transition to normal autotrophic growth with CO<sub>2</sub>. Since the appearance of system 2 activity parallels the elaboration of the grana, it would appear that they are required for normal photosynthesis. A similar conclusion was reached by Ohad *et al.* (1967) who examined mutants of *Chlamydomonas reinhardtii* and by Homann and Schmid (1967) who studied *Nicotiana tabacum*.

This work was supported in part by a grant from the National Science Foundation (GB 8630) to David C. Fork.

### References

- Duysens, L. N. M., *Biochim. Biophys. Acta*, **19**, 1, 1956.
- Fork, D. C., and J. Ames, *Ann. Rev. Plant Physiol.*, **20**, 305, 1969.
- Homann, P. H., and G. H. Schmid, *Plant Physiol.*, **42**, 1619, 1967.
- Merrett, M., *Arch. Mikrobiol.*, **65**, 1, 1969.
- Ohad, I., P. Siekevitz, and G. E. Palade, *J. Cell Biol.*, **35**, 553, 1967.
- Wiessner, W., *Planta*, **79**, 92, 1968.
- Wiessner, W., *Photosynthetica*, **3**, 225, 1969.
- Wiessner, W., and F. Amelunxen, *Arch. Mikrobiol.*, **66**, 14, 1969a.
- Wiessner, W., and F. Amelunxen, *Arch. Mikrobiol.*, **67**, 357, 1969b.

### EFFECTS OF MONOVALENT CATIONS ON LIGHT ENERGY DISTRIBUTION BETWEEN TWO PIGMENT SYSTEMS OF PHOTOSYNTHESIS

Norio Murata

Divalent metal cations such as Mg<sup>2+</sup>, Ca<sup>2+</sup>, Sr<sup>2+</sup>, Ba<sup>2+</sup>, and Mn<sup>2+</sup> change the light energy distribution between two pigment systems of photosynthesis in isolated chloroplasts (Murata, 1969; Murata, Tashiro, and Takamiya, 1970). Since these ions increase the light energy in pigment system 2 and decrease it in pigment system 1, it is suggested that this control of light energy distribution results from the suppression by the divalent cations of the excitation transfer from bulk chlorophyll *a* of pigment system 2 to that of pigment system 1.

Homann (1969) first discovered an increase in yield of chlorophyll *a* fluorescence produced by monovalent cations in isolated chloroplasts. The present study shows that monovalent cations induce a rearrangement of light energy distribution between the two pigment systems, as divalent metal cations do, by suppressing the excitation transfer from pigment system 2 to pigment system 1.

Spinach chloroplasts were used as test materials. Market spinach leaves were ruptured in a Waring Blender with 400 mM sucrose, 10 mM NaCl, and 50 mM phosphate buffer pH 7.8. The chloroplast suspension was filtered through cheese cloth and centrifuged at 1,000×*g* for 5 min. The sedimented chloroplasts were suspended in 300 mM KCl and 50 mM Tricine buffer, pH 7.8, and centrifuged again at 1,000×*g* for 5 min. The pellet was resuspended in the same solution, and the aggregated chloroplasts and cell wall fragments were removed by centrifugation at 200×*g* for 1 min.

For the measurement of fluorescence and of photochemical reactions, a 0.1-ml chloroplast suspension was diluted with 2.9 ml distilled water. The resulting concentrations of KCl and Tricine buffer were 10 mM and 1.7 mM. Effects of salts were examined by adding a small amount of highly concentrated salt solution to the diluted chloroplast suspension. The change in volume of the sample was so small that its effect upon the fluorescence yield was negligible compared to the fluorescence change due to the effects of salts.

NADP reduction and the Hill reaction with DCIP were measured by following the absorption changes at 340 and 590 nm, respectively, produced by the illumination of chloroplasts.

The addition of a highly concentrated solution of NaCl to the chloroplast suspension of low salt concentration increased the yield of chlorophyll *a* fluorescence by 40–70%. The maximum steady level was attained about 5 min after the addition.  $\text{MgCl}_2$  showed the same effect upon the fluorescence yield. As shown in Fig. 44, 100 mM NaCl was required to saturate the increase of fluorescence yield while only 2 mM  $\text{MgCl}_2$  gave the same effect. These findings confirmed Homann's (1969) observation about the cation effects upon the fluorescence yield.

DCMU, which inhibits the photosynthetic electron transport, was added to avoid a quenching effect of photoreaction 2. Therefore, the possibility that NaCl may have increased the fluorescence yield by inhibiting or stimulating the electron transport reactions is excluded. The change in fluorescence yield by NaCl suggests the presence of a control mechanism regulating the excitation transfer between pigment molecules in the chloroplasts. Since the chlorophyll *a* fluorescence in the chloroplasts at room temperature is emitted from pigment system 2, the increase in fluorescence yield upon the addition of NaCl indicates an

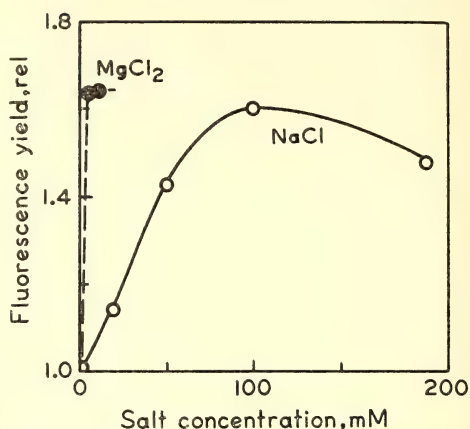


Fig. 44. Relationship between fluorescence yield and concentrations of NaCl and  $\text{MgCl}_2$ . The sample contained 10 mM KCl, 1.7 mM Tricine buffer (pH 7.8), 10  $\mu\text{M}$  DCMU and the chloroplasts at 1  $\mu\text{g ml}^{-1}$  chlorophyll concentration. Small amounts of concentrated salt solutions (3 M NaCl and 60 mM  $\text{MgCl}_2$ ) were added to 3.0 ml of the sample, to obtain the final concentrations described in the figure. Excitation light was 480 nm. Fluorescence was measured at 684 nm 5 min after the addition of salt solution.

increase by the salt of light energy in pigment system 2.

At liquid nitrogen temperature, there are three emission bands of chlorophyll fluorescence in spinach chloroplasts, two from pigment system 2 and one from pigment system 1 (Murata, Nishimura and Takamiya, 1966). In order to see the effects of NaCl on the fluorescence yield of pigment system 1, the fluorescence spectra were measured at liquid nitrogen temperature in the presence and absence of NaCl. Figure 45 shows that NaCl decreased the yield of the fluorescence band at 735 nm, which is emitted from pigment system 1, while it increased the yields of fluorescence bands at 684 and 695 nm, which are emitted from pigment system 2.

It is concluded here that the addition of NaCl changes the distribution of light quanta between the two pigment systems, increasing the amount of light energy in pigment system 2 and decreasing that in pigment system 1.



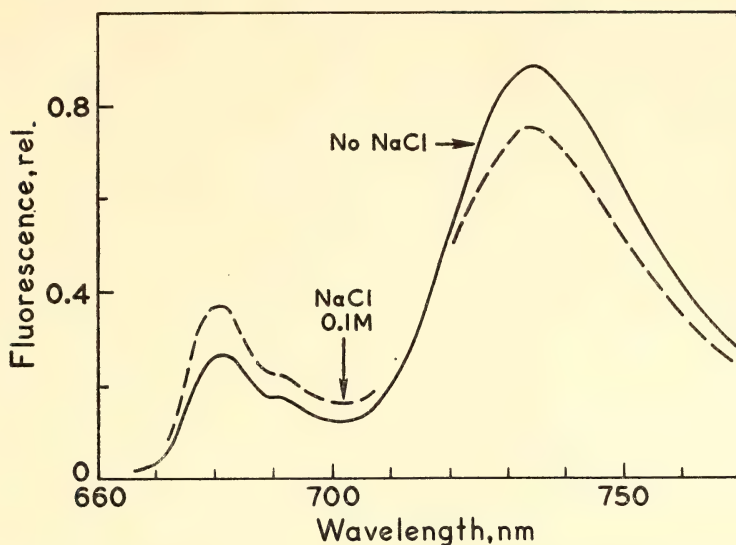


Fig. 45. Fluorescence spectra at liquid nitrogen temperature with and without NaCl. NaCl was added 5 min before cooling the sample. Excitation light, 475 nm.

The effects of other sodium salts such as NaBr, NaNO<sub>3</sub>, and Na<sub>2</sub>SO<sub>4</sub> on fluorescence yields were examined at room and at liquid nitrogen temperatures. These salts had effects similar to NaCl on chlorophyll *a* fluorescence in the chloroplasts. Their addition increased the fluorescence yield of system 2 but decreased that of system 1. Time courses of fluorescence change after the addition, and the maximum levels of fluorescence increase were the same as those with the addition of NaCl. The same concentration dependences were observed in NaCl, NaBr, and NaNO<sub>3</sub>. The increase saturated at 100 mM. In the case of Na<sub>2</sub>SO<sub>4</sub> the fluorescence yield reached its maximum level at 50 mM.

There is a question whether the effects of the salts upon the light energy distribution depend on the concentration of Na<sup>+</sup> or on the ionic strength in the suspension medium of the chloroplasts. The curves of the fluorescence yield measured for various concentrations of NaCl and Na<sub>2</sub>SO<sub>4</sub> show that Na<sub>2</sub>SO<sub>4</sub> was exactly twice as effective as NaCl on the basis of molar concentration. This is the

expected result if the effects depend on the concentration of Na<sup>+</sup>. However, if the effect were due to the ionic strength, then Na<sub>2</sub>SO<sub>4</sub> should be three times as effective as NaCl. These findings indicate that the Na<sup>+</sup> concentration rather than the ionic strength controls the light energy distribution between pigment systems in isolated chloroplasts.

Chloride salts of other monovalent cations including Li<sup>+</sup>, K<sup>+</sup>, Rb<sup>+</sup>, Cs<sup>+</sup>, and NH<sub>4</sub><sup>+</sup> were also investigated. Table 20 shows the effects of their chloride salts as well as of MgCl<sub>2</sub> upon the fluorescence yield at room temperature. The increase in fluorescence yield was almost the same in all the salts tested. The concentration dependence curves showed the effect to saturate around 100 mM with each monovalent cation. Low-temperature fluorescence spectra showed that all the monovalent cations enhanced the fluorescence yield of pigment system 2 but suppressed that of pigment system 1. Therefore, it is concluded that all the monovalent ions tested have the same effect upon the chloroplasts in changing the

TABLE 20. Effects of salts on yield of chlorophyll *a* fluorescence in spinach chloroplasts\*

Salts †	Relative Fluorescence Yield ‡
No addition	1.00
LiCl	1.69
NaCl	1.63
KCl	1.64
RbCl	1.60
CsCl	1.59
NH <sub>4</sub> Cl	1.57
MgCl <sub>2</sub> (2 mM)	1.75

\* Experimental conditions were the same as for Fig. 44.

† Concentrated salt solutions were added to obtain the final concentrations of 100 mM, except in MgCl<sub>2</sub>, which was 2 mM.

‡ Fluorescence yield was measured 5 min after the addition of salts.

light energy distribution between the two pigment systems.

The effects of NaCl on quantum efficiencies of two photoreactions were investigated to confirm the control by the monovalent cations of light energy distribution between the two pigment systems. The efficiency of photoreaction 1 was measured by the NADP reduction sup-

ported by ascorbate and DCIP in the presence of DCMU. The efficiency of photoreaction 2 was measured by the Hill reaction with DCIP. The intensities of actinic light used were so low that the primary photoreactions were the rate-limiting steps. Under this condition the quantum efficiencies of the reactions correspond to the amount of light quanta delivered to each photoreaction. Figure 46 shows that NaCl suppressed the quantum efficiency of the NADP reduction by about 35% and that NaCl slightly stimulated the Hill reaction with DCIP.

It can be seen in Fig. 45 that NaCl increased the fluorescence yield of pigment system 2 but decreased that of pigment system 1. The quantum efficiency of photoreaction 1 measured by NADP reduction with ascorbate and DCIP was suppressed by the addition of NaCl. This result is consistent with the decrease in fluorescence yield in pigment system 1 measured at liquid nitrogen temperature.

On the other hand, the quantum effi-

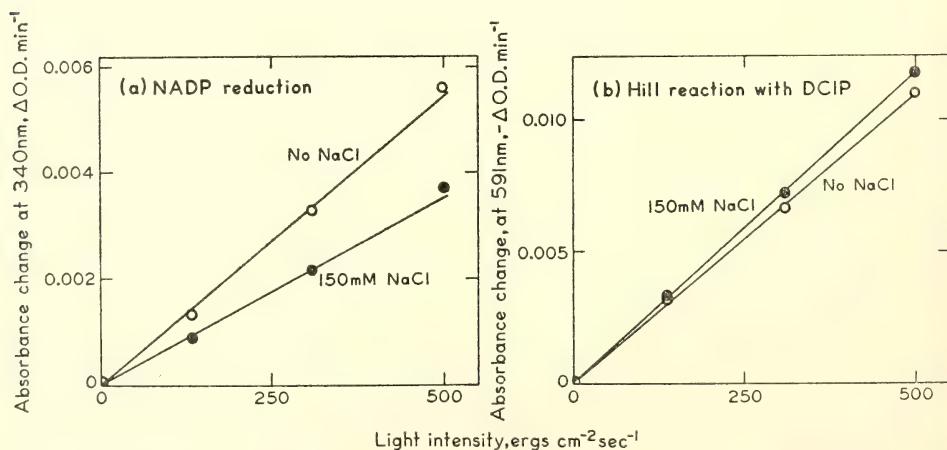


Fig. 46. (a) Effects of NaCl on NADP reduction supported by ascorbate and DCIP in the presence of DCMU. NADP reduction was measured by its absorption change at 340 nm produced by 650 nm actinic light. The reaction medium contained 0.5 mM NADP, 0.5 mM Na-ascorbate, 0.03 mM DCIP, 0.02 mM DCMU, 10 mM KCl, 1.7 mM Tricine buffer (pH 7.8), and a sufficient amount of ferredoxin. (b) Effect of NaCl on the Hill reaction with DCIP. Reduction of DCIP was measured by the absorption change at 591 nm produced by 650 nm actinic light. The reaction medium contained 0.017 mM DCIP, 10 mM KCl, and 1.7 mM Tricine buffer (pH 7.8).

ciency of photoreaction 2 measured by the Hill reaction with DCIP was only slightly stimulated by  $\text{Na}^+$ , while the fluorescence yield of pigment system 2 measured at room temperature in the presence of DCMU was increased by 60%. The finding that  $\text{Na}^+$  has different effects on the quantum efficiency of photoreaction 2 and on the fluorescence yield of pigment system 2 suggests a mechanism for the mode of action of  $\text{Na}^+$  given in Fig. 47.

It should be noted that the effects of  $\text{Na}^+$  upon the quantum efficiency and fluorescence yield were measured under different conditions with respect to the state of reaction center of system 2. In the measurement of quantum efficiency of the Hill reaction, almost all of the primary electron acceptor, Q, according to Duysens and Sweers (1963), must be oxidized in the presence of an electron acceptor under very weak light intensities (lower than  $500 \text{ ergs cm}^{-2} \text{ sec}^{-1}$ ). The primary photochemical reaction captures the excitation energy in the pigment system so fast that it pre-

dominates over other degradation processes such as heat production, fluorescence emission, and transfer of excitation to other pigment molecules. Thus almost all the excitation in pigment system 2 is trapped by photoreaction 2. The experimental data show that under this condition  $\text{Na}^+$  only slightly stimulates the quantum efficiency of photoreaction 2.

In the presence of DCMU, which was added for the measurement of fluorescence yield, Q is fully reduced in the light. Therefore, photoreaction 2 cannot quench the excited state, so the excitation energy is dissipated by fluorescence emission, heat production, and transfer of excitation to other pigment molecules. The experimental results show that  $\text{Na}^+$  increases the fluorescence yield of pigment system 2 under this condition.

In summary, when Q is in the oxidized state and the quenching effect of photoreaction 2 is at the maximum,  $\text{Na}^+$  only slightly enhances the excitation energy in system 2. When Q is in the reduced state and there is no quenching effect of photoreaction 2,  $\text{Na}^+$  increases the fluorescence yield in system 2. These findings lead us to consider the mechanism shown in Fig. 47.

In this scheme,  $\text{Na}^+$  suppresses the excitation transfer from chlorophyll *a* of pigment system 2 to that of pigment system 1. The rate constant of the heat-producing process is estimated to be about  $10^9 \text{ sec}^{-1}$  from the lifetime of chlorophyll *a* fluorescence in isolated chloroplasts (Müller and Lumry, 1965). The rate constant of fluorescence emission is estimated to be about  $10^8 \text{ sec}^{-1}$  (Brody and Rabinowitch, 1957) and can be neglected in the estimation of the fate of excitation energy. The rate of photoreaction 2 must be much faster than the heat-producing process, because almost all the light quanta are captured by the photoreaction when all of the Q is in the oxidized state. Therefore, the apparent rate constant of photoreaction 2 can be

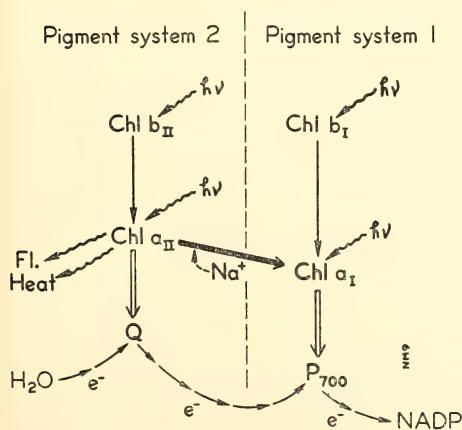


Fig. 47. Scheme for excitation transfer between pigments in spinach chloroplasts. Arrows indicate the excitation transfer steps. Chl  $a_1$  and Chl  $a_2$  are chlorophyll *a* in pigment systems 1 and 2, respectively. The thick closed arrow is the step that is suppressed by  $\text{Na}^+$  and other monovalent cations. Thick open arrows are photoreactions.



estimated to be equal to or faster than  $10^{10} \text{ sec}^{-1}$  when all of the Q is oxidized.

When photoreaction 2 does not quench the excitation in the presence of DCMU, the fluorescence yield is increased by 40–70%. This indicates that the rate constant of excitation transfer from pigment system 2 to 1 is comparable to that of the heat-producing process and is therefore estimated to be about  $10^9 \text{ sec}^{-1}$ . The apparent rate constant of photoreaction 2 with fully oxidized Q capturing the excitation energy is still much faster than the sum of the heat-producing process and the excitation transfer from system 2 to 1. Under this condition, a suppression of excitation transfer between the pigment systems cannot be expected to stimulate strongly photoreaction 2.

In the above consideration, we assume that  $\text{Na}^+$  controls the excitation transfer from pigment system 1. The possibility that  $\text{Na}^+$  controls the excitation transfer from the light collecting pigments, such as chlorophyll *b* or carotenoids, to chlorophyll *a* is excluded because if  $\text{Na}^+$  increased the transfer efficiency from the light collecting pigments to chlorophyll molecules in pigment system 2 which emit fluorescence, the Hill reaction with DCIP should be enhanced with the addition of  $\text{Na}^+$  in parallel to the increase in fluorescence yield of pigment system 2.

### References

- Brody, S. S., and E. Rabinowitch, *Science*, **125**, 555, 1957.
- Duysens, L. N. M., and H. E. Sweers, in *Studies on Microalgae and Photosynthetic Bacteria*, Japan Soc. of Plant Physiologists, The Univ. of Tokyo Press, p. 353, 1963.
- Homann, P. H., *Plant Physiol.*, **44**, 932, 1969.
- Müller, A., and R. Lumry, *Proc. Nat. Acad. Sci. U.S.*, **54**, 1479, 1965.
- Murata, N., M. Nishimura, and A. Takamiya, *Biochim. Biophys. Acta*, **126**, 234, 1966.
- Murata, N., H. Tashiro, and A. Takamiya, *Biochim. Biophys. Acta*, **197**, 250, 1970.

### SEPARATION OF SPINACH CHLOROPLAST FRACTIONS WITH THE ZONAL ROTOR

J. S. Brown and O. M. Griffith \*

Since chloroplasts were successfully fractionated by Michel and Michel-Wolwertz (*Year Book* 67, p. 508) by breaking in the needle-valve press and separating by centrifugation in a sucrose density-gradient into particle fractions enriched in photosystems 1 and 2, various aspects of the procedure have been improved and extended (*Year Book* 68, p. 566). Although sucrose density-gradient centrifugation in the Spinco SW-25.1 swinging bucket rotor provides adequate separation of the fractions, the volume of each fraction recovered from a centrifuge run is limited to 5 ml per tube. This amount is sufficient for the measurement of photochemical activity and for spectroscopic measurements, but not for a chemical analysis of the fractions.

The use of the zonal rotor, originally designed and developed by Dr. Norman Anderson at Oak Ridge, Tenn., was suggested as a means to obtain larger volumes of the separated fractions than is possible in the swinging bucket rotor. We, therefore, separated the fractions in a Spinco zonal rotor, as described below, and monitored the absorbance at 680 nm during the unloading of the rotor after centrifugation. We were thus able to estimate the amount of chlorophyll in each fraction in a manner similar to, but more refined than, that used by Sesták (*Year Book* 68, p. 572).

### Methods and Results

About 100 g of market spinach leaves were deveined and blended for 15 sec with 100 ml of 0.4 M sucrose, 0.05 M Tricine buffer at pH 7.4. The brei was filtered through cheesecloth, and the filtrate centrifuged for 10 min at  $3000 \times g$ . The pellet was resuspended in 20 to 30 ml of 0.3 M KCl, 0.05 M Tricine, pH 7.7,

\* Spinco Division, Beckman Instruments, Inc., Palo Alto.

and pressed through the needle-valve 3 times at 12,500 psi.\* The resulting homogenate was centrifuged at  $3000\times g$  for 10 min to remove the larger cell fragments. It was then diluted with 50% sucrose to make 25 ml homogenate containing about 0.6 mg chlorophyll per ml in 5% sucrose buffer.

The Spinco Ti XIV zonal rotor was loaded with a step-wise sucrose gradient while spinning at 5000 rpm. The sucrose solutions were made up in 0.15 M KCl, 0.05 M Tris buffer at pH 7.7 and pumped into the rotor from center to edge as follows: 100 ml 10% w/w sucrose, 400 ml 30% w/w sucrose, and 100 ml 50% w/w sucrose. The 25 ml of homogenate was loaded into the center followed by 25 ml

\*Sane *et al.* (1970) have prepared a similar homogenate by using much lower pressure on their Aminco-French Pressure Cell. They separated the fractions by differential centrifugation.

of water for the overlay. The rotor was accelerated to give  $60,000\times g$  for 45 min ( $\int \omega^2 dt = 3588 \times 10^7 \text{ rad}^2 \text{ sec}^{-1}$ ) while the temperature was maintained at 5°C.

At the end of the 45-min run the rotor speed was decreased to 5000 rpm, and the rotor was unloaded from the center while spinning. The entire rotor contents flowed through a cuvette placed in a Beckman DB spectrophotometer set to monitor the effluent at 680 nm. Figure 48 shows the absorbance on a logarithmic scale plotted against the volume of liquid displaced from the rotor. Fractions 1 and 2 were collected near the two absorption peaks, 180 to 220 and 500 to 520 ml. The sucrose concentration was measured in a refractometer. Table 21 shows the sucrose concentrations in which the two fractions were banded.

Fraction 2 was further purified by dialysing against water to remove the

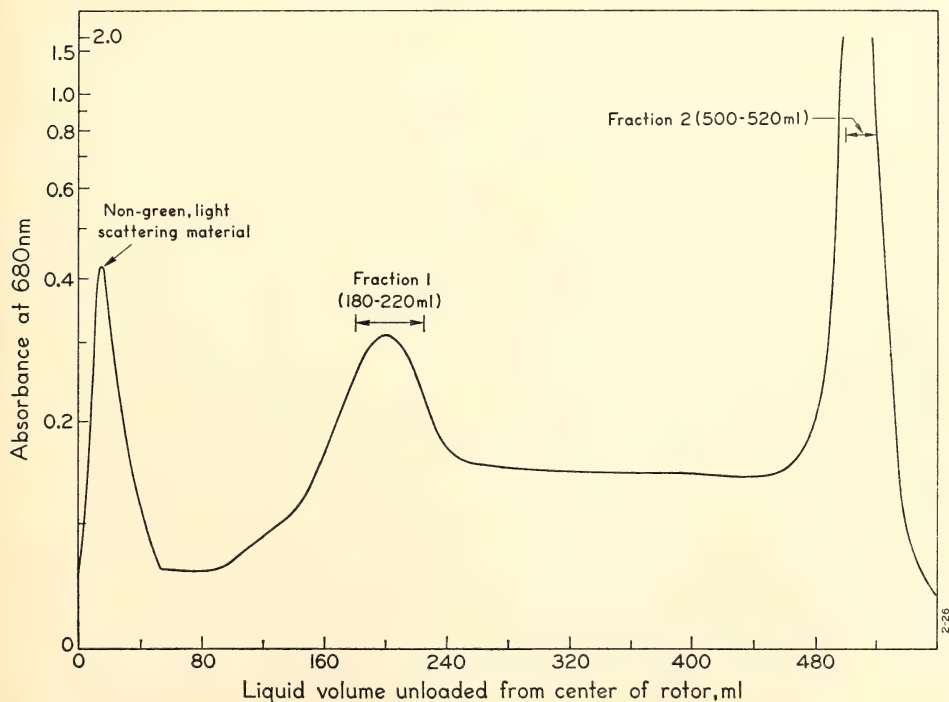


Fig. 48. The absorbance at 680 nm of the separated fractions of spinach particles plotted against the volume of liquid unloaded from the center of the rotor.

TABLE 21. Chlorophyll Distribution in the Zonal Rotor Fractions

Sample	Volume (ml)	Chl. conc. ( $\mu\text{g ml}^{-1}$ )	Chl. amount ( $\mu\text{g}$ )	Sucrose conc. (percent)	Ratio Chl. <i>a</i> /Chl. <i>b</i>
Homogenate	25	627	15,600	5	3.97
Fraction 1	40	28	1,120	27	8.31
Fraction 2	20	263	5,260	38	3.20
Purified fraction 2	...	...	...	...	2.62

sucrose, then spinning at  $10,000 \times g$  for 30 min. The chlorophyll *a* to *b* ratios of the resulting purified sediment and the original fractions are compared in Table 21.

Since the separation described above and those previously made in the swinging bucket rotor depended upon the different sizes of particles in the fractions sedimenting at different rates, we performed two experiments in which a homogenate was placed on a linear sucrose gradient and centrifuged for 17 hrs at  $60,000 \times g$ . In each case only one major green band was observed when the rotor was unloaded. A measurement of the sucrose concentration of this band revealed that both fractions were isopycnicly banded in 39% w/w sucrose.

### Conclusions

The results presented in Fig. 48 and Table 21 show that a good separation of the fractions was accomplished with the zonal rotor, and that a substantial amount of each fraction could be collected in one operation. It is apparently easy to determine the relative amounts of chlorophyll in each fraction with a spectrophotometer. However, since the particles in fraction 2 are visibly larger than those in fraction 1, probably a part of the apparent absorption of the fraction 2 band is due to light scattering rather than chlorophyll absorption.

### Reference

- Sane, P. V., D. J. Goodechild, and R. B. Park, *Biochim. Biophys. Acta*, 216, 162, 1970.

### DELAYED FLUORESCENCE EMISSION BY FRACTIONS OF *Scenedesmus* MUTANTS

R. H. Ruby\* and J. S. Brown

Two mutants of *Scenedesmus* have essentially the same pigment systems as the wild-type; one of them lacks photosystem 1 activity and the other lacks photosystem 2 activity. These three strains of *Scenedesmus* therefore provide an opportunity to study the effects of an inactive photosystem 1 or 2 on delayed light emission from algae with similar pigments.

We compared the delayed fluorescence of intact cells and of particulate fractions from the green alga, *Scenedesmus obliquus* D<sub>3</sub> and Mutants nos. 8 and 11 derived from it (kindly supplied by Dr. Norman I. Bishop). Last year (Year Book 68, p. 566) green particles exhibiting absorption and fluorescence characteristics of systems 1 and 2 were separated by sucrose density-gradient centrifugation from wild-type *Scenedesmus* broken with the Braun "MSK" mechanical cell homogenizer. This year fractionation of the mutants also yielded particles with absorption and fluorescence spectra characteristic of system 1 or 2, although mutant no. 8 showed relatively less absorption near 700 nm in both fractions. Thus the pigment systems of the mutants appear to be normal even though Mutant no. 8 lacks system 1

\* Physics Department, University of California at Santa Cruz. Work supported in part by funds received during the tenure of an Alfred P. Sloan Research Fellowship (1966-1968).



activity and Mutant no. 11, system 2 activity.

The delayed fluorescence of whole cells of the wild-type and mutants of *Scenedesmus* has been studied by Bertsch *et al.* (1967) and by Azzi (1966). Bertsch *et al.* reported a very low intensity of emission from Mutant no. 11 from several ms to 100 ms which is consistent with the lack of photosystem 2 in this mutant. Azzi found that the prompt and delayed fluorescence emission spectra of the wild-type and Mutant no. 8 were essentially the same.

### Methods

The wild-type algae were grown in one-liter batches in shake flasks on minimal medium in the light or on glucose-yeast extract medium in darkness. The mutants were grown on the latter. The cells suspended in 0.3 *M* KCl, 0.05 *M* Tricine at pH 7.8 were broken by shaking with glass beads in the "MSK" homogenizer. The resulting homogenate was layered on a step gradient composed of 10–30–50% (w/v) sucrose and spun in a swinging bucket rotor for 1 hr at 60,000  $\times g$ . Two green layers near the top and bottom of the tubes were called fraction 1 and 2, respectively. Fraction 1 had a higher chlorophyll *a* to *b* ratio and more long-wavelength fluorescence at low temperature relative to the fluorescence

emitted at 680 nm than the homogenate or fraction 2.

The delayed fluorescence was measured in the apparatus described by Ruby (1970). The flash from a xenon lamp (General Radio Type 1539A) had an intensity corresponding to approximately 0.5 photon per flash absorbed per 1000 chlorophyll molecules (about  $2 \times 10^7$  photons  $\text{sec}^{-1} \text{ cm}^{-2}$  incident during the peak of the flash) and a width of 2  $\mu\text{s}$ . The delayed fluorescence intensity was measured in a broad band of wavelengths above 680 nm at 0.5 ms ( $D_b^1$ ) and 30 ms ( $D_b^{30}$ ) after the exciting flash.

### Results

The observations of  $D_b^1$  and  $D_b^{30}$  are summarized in Table 22. The measurements have been normalized to a total chlorophyll concentration of 1.4  $\mu\text{g}/\text{ml}$ , which was also within 20% of the concentration actually used. The numbers in the table are ratios of the delayed fluorescence intensity to that observed in dark-grown wild-type cells. Most of the entries in the table represent 3 or more separate experiments. For comparison, the delayed fluorescence in spinach chloroplasts measured at 0.5 ms is: chloroplasts, 0.1; homogenate, 0.5; fraction 1, 0.1; and fraction 2, 0.5. These numbers are normalized in the same manner as those in Table 22. Due to

TABLE 22. The Relative Intensity of Delayed Fluorescence from Normal and Mutant *Scenedesmus* at Two Times after Exposure

	Wild-Type, Light Grown	Wild-Type, Dark Grown	Mutant No. 11	Mutant No. 8
At 0.5 ms, $D_b^1$				
Whole cells	0.7	$\equiv 1$	0.2	1.0
Homogenate	1.2	1.0	0.1	3.2
Fraction 1	1.5	0.2	0.1	0.9
Fraction 2	4.3	0.5	0.1	4.4
At 30 ms, $D_b^{30}$				
Whole cells	0.5	$\equiv 1$	0.02	1.1
Homogenate	0.3	0.08	0.01	0.2
Fraction 1	0.06	0.02	0.01	0.06
Fraction 2	0.2	0.04	0.01	0.2

variabilities either in the material itself or in the preparative process, the limit of confidence in the table entries is about  $\pm 50\%$ . The reproducibility in the homogenate samples was poor.

It was noted earlier (Ruby, 1971) that if, prior to the time of the flash, the sample received a background illumination of approximately  $10 \text{ photons sec}^{-1}$  absorbed per 1000 chlorophyll molecules (about  $5 \times 10^{13} \text{ photons sec}^{-1} \text{ cm}^{-2}$ ) at 675 nm, there was a significant enhancement of  $D_b^1$  from wild-type cells. This effect of background light was found to be almost twice as large in cells of Mutant no. 8. The effect was absent, within experimental error, in whole cells of Mutant no. 11 and in the homogenates and fractions of all cells.

### Discussion

Evidence is accumulating (Ruby, 1971) that the delayed fluorescence observed in whole cells at times of about 1 ms and after-times of the order of tens of ms and longer may represent different processes. A comparison of the effect of breaking the cells on  $D_b^1$  and  $D_b^{30}$  in Table 22 is consistent with this notion. An unpublished investigation shows that the change is not in the shape of the decay but is better described as a change in the relative amounts of two components. Apparently the delayed fluorescence observed at the longer time is more dependent on the structural integrity of the cells. The observation that delayed fluorescence at 1 ms is produced by the fractions suggests that the shorter component of delayed fluorescence may be related to early events in the photosynthetic mechanism.

The results in  $D_b^{30}$  with whole cells are consistent with the interpretation by Bertsch *et al.* (1967) that delayed fluorescence is a photosystem 2 phenomenon. The enhancement of  $D_b^1$  by background illumination is also a system 2 phenomenon, as suggested earlier (Ruby, 1971).

The observations on  $D_b^1$ , however, are in part inconsistent with those of Bertsch *et al.* The results in Mutant no. 11 cells suggest that while the bulk of delayed fluorescence at 1 ms comes from system 2, there is participation of system 1. The reason for the difference in observations is not clear. It may be due to differences in experimental approach (flash versus phosphorescope), differences in operating conditions (low light intensity versus saturating light), or sample conditions. The difference between results from light-grown and dark-grown wild-type cells demonstrates the importance of the physiological conditions. The interpretation that system 1 participates in producing  $D_b^1$  is reinforced by the observation of  $D_b^1$  from fraction 1 chloroplast fragments of the wild-type. The observation of  $D_b^1$  from fraction 1 of spinach, where a clear separation of system 1 had been shown (Murata and Brown, 1970), also supports this interpretation.

Unfortunately, the ratios in Table 22 are not all consistent with each other. It is not clear why the homogenate and fractions of Mutant no. 8 show higher values than the dark-grown wild-type, nor why fraction 1 of Mutant no. 11 shows a small value.

However, the data do suggest that the lesions in Mutant no. 8 may not be in the early steps in photosynthesis but rather in the electron transport chain, which is consistent with the recent work of Gee *et al.* (1969). This would also explain why two pigment fractions can be obtained from Mutant no. 8 even though it is missing a functional photosystem.

### References

- Azzi, J. R., Oak Ridge National Laboratory, Technical Memo No. 1534, 1966.
- Bertsch, W., J. R. Azzi, and J. B. Davidson, *Biochim. Biophys. Acta*, **143**, 129, 1967.
- Gee, R., P. Saltman, and E. Weaver, *Biochim. Biophys. Acta*, **189**, 106, 1969.

Murata, N., and J. Brown, *Plant Physiol.*, 45, 360, 1970.

Ruby, R. H., *Photochem. Photobiol.*, in press, 1971.

## STAFF ACTIVITIES

During the year two retired Staff Members died and the leader of the Experimental Taxonomy group retired. Dr. James H. C. Smith who joined the group in 1927 died on January 8, 1970, at the age of 74. He had been active in the laboratory for several years following his retirement in 1961 although he was in ill health for the past four years. Dr. Jens C. Clausen joined the laboratory in 1931, retired in 1956, and continued his active career until he died on November 22, 1969. Dr. William M. Hiesey continued for six months after his June 30, 1969, retirement to complete an Institution monograph with Drs. Nobs and Björkman. He has since moved to Camino, in the Sierra foothills, where he plans to prepare for publication a book on the Department's investigations on apomixis in the genus *Poa*.

The leadership of the Experimental Taxonomy group has been taken up by Dr. Olle Björkman and the descriptive title of Physiological Ecology has been adopted to conform more closely with the nature of the group's work in recent years. Dr. Björkman participated in two Symposia on "Photosynthesis and Productivity" organized by the International Biological Programme. The first meeting was held in Třeboň, Czechoslovakia in September, the second in Moscow in October 1970.

On a joint expedition, Drs. Björkman, Percy, and Medina of this Department and Mr. Tyrone Harrison and Prof. Harold Mooney of the Department of Biological Sciences at Stanford University visited the floor of Death Valley, California, with a mobile laboratory unit during late June and early July 1970. The objective of this research trip was to determine if the few plants that grow in this, one of the earth's most extreme

environments, can successfully photosynthesize during the height of the summer heat or if, rather, they go dormant during this period. The results of these studies will appear in next year's report.

Drs. Björkman, Boynton, Brown, Clausen, Fork, French, N. Murata, and Percy attended the XI International Botanical Congress at Seattle in August-September 1969. Dr. Clausen was one of 11 American Honorary Vice-Presidents of the Congress. Members of the Department hosted two field trips for the participants in the Congress during their visits to the Institution's transplant stations at Timberline, Mather, and Stanford. The first was a general botanical field trip which included 40 members from 11 different nations. The second consisted of 31 specialists interested in experimental ecology from 10 countries. During both of these excursions Dr. Jens Clausen lectured on the origin of the different components of the regional flora. Dr. William Hiesey presented the basic philosophy and history of the transplant studies and Dr. Malcolm Nobs summarized the current studies on the genus *Mimulus*.

Two classes from Stanford University used the Mather transplant station during the year. Prof. Harold Mooney's class on field research techniques in biology visited on May 18-21 with the Physiological Ecology group. In addition to discussions concerning the transplant gardens, the class conducted field research projects in the area. During May 22-24 Prof. John Thomas and his systematics class visited the Mather Station with Dr. Nobs to study the floristics of the area.

Dr. Brown attended a "Microsymposium and Workshop in Particle Sepa-



ration from Plant Materials" at Oak Ridge, Tennessee, in January 1970. This was primarily to learn about the use of zonal centrifuge rotors developed by Dr. Norman Anderson. Drs. Brown, Halldal, Fork, French, and Murata attended the third Gatlinburg Symposium on the Photosynthetic Unit in May 1970. On that occasion Drs. Lawrence R. Blinks, C. Stacy French, Hans Gaffron, and Eugene I. Rabinowitch were invited

to share in the honors initially planned to mark the retirement of Dr. William Arnold of the Oak Ridge National Laboratory. Dr. French spent two weeks in November 1969 as Regents Lecturer at the University of California at Riverside.

At the close of the report year the Bush Cabin at Inverness, a gift of Dr. Vannevar Bush for recreation of the laboratory staff, was completed under the direction of Mr. Richard W. Hart.

## BIBLIOGRAPHY

- 457\* Ames, J., see Fork, D.  
 Björkman, Olle, see Hiesey, William M.
- 455 Briggs, Winslow R., and David C. Fork, Long-lived intermediates in phytochrome transformation I: In vitro studies. *Plant Physiol.*, 44, 1080-1088, 1969.
- 456 Briggs, Winslow R., and David C. Fork, Long-lived intermediates in phytochrome transformation II: In vitro and in vivo studies. *Plant Physiol.*, 44, 1089-1094, 1969.
- 450 Brown, Jeanette S., Absorption and fluorescence of chlorophyll *a* in particle fractions from different plants, *Biophys. J.*, 9, 1542-1552, 1969.
- Brown, Jeanette, see Murata, Norio.
- 459 Clausen, Jens, The Harvey Monroe Hall Natural Area. C.I.W.-D.P.B. Publication, 48 pp., Carnegie Institution, 1530 P Street, Northwest, Washington, D.C. 20005.
- 443 Fork, David C., Evidence for the participation of carotenoids in the photosynthesis of algae and in a higher plant. *Progress in Photosynthesis Research*, II, Helmut Metzner, ed., Internat. Union Biol. Sci., Tübingen, pp. 800-810, 1969.
- Fork, David C., see Briggs, Winslow R.
- 457 Fork, David C., and J. Ames, Spectrophotometric studies of the mechanism of photosynthesis. *Photophysiology*, V, Arthur C. Giese, ed., Academic Press, New York, pp. 97-126, 1970.
- 445 French, C. S., Biophysics of plastid pigments. Closing Session Summary, International Congress of Photosynthesis Research, Freudenstadt, June 4-8, 1969, *Progress in Photosynthesis Research*, II, Helmut Metzner, ed., Internat. Union Biol. Sci. Tübingen, pp. 880-887, 1969.
- 444 French, C. S., and Lillian Prager, Absorption spectra for different forms of chlorophyll. *Progress in Photosynthesis Research*, II, Helmut Metzner, ed., Internat. Union Biol. Sci., Tübingen, pp. 555-564, 1969.
- French, C. S., see Wiessner, W.
- Hiesey, William M., Review of *Principles and Methods of Plant Biosystematics*, by Otto T. Solbrig, Collier-Macmillan Canada, Ltd., Toronto, xiii + 266 pp., *Science*, 170, 525-526, 1970.
- 467 Hiesey, W. M., and M. A. Nobs, Genetic and transplant studies on contrasting species and ecological races of the *Achillea millefolium* complex. *Bot. Gaz.*, 131, 245, 1970.
- Hiesey, William M., Malcolm A. Nobs, and Olle Björkman, Experimental studies on the nature of species. V. Biosystematics, genetics, and physiological ecology of the *Erythranthe* section of *Mimulus*. Carnegie Institution of Washington Pub. no. 628, vi + 210 pp., 1971.
- 464 Mantai, Kenneth E., Carbonylcyanide *m*-chlorophenylhydrazone as an inhibitor of coupled electron transport in trypsin treated spinach chloroplasts. *Biochim. Biophys. Acta*, 189, 449-451, 1969.
- 452 Mantai, Kenneth E., Some effects of hydrolytic enzymes on coupled and uncoupled electron flow in chloroplasts. *Plant Physiol.*, 45, 563-566, 1970.
- 451 Michel, J.-M., and M.-R. Michel-Wolwertz, On the fractionation of the photosynthetic apparatus of spinach chloroplasts. *Progress in Photosynthesis Research*, I,

\* Department of Plant Biology publication numbers.

- Helmut Metzner, ed., Internat. Union Biol. Sci., Tübingen, pp. 115-127, 1969.
- 470 Michel, J.-M., and Marie-Rose Michel-Wolwertz, Fractionation and photochemical activities of photosystems isolated from broken spinach chloroplasts by sucrose-density gradient centrifugation. *Photosynthetica*, 4, 146-155, 1970.
- Michel-Wolwertz, M.-R., see Michel, J.-M.
- 465 Murata, Norio, and Jeanette Brown, Photochemical activities of spinach chloroplast particles fractionated after French press treatment. *Plant Physiol.*, 45, 360-361, 1970.
- Murata, Norio, see Fork, David C.
- Nobs, Malcolm A., see Hiesey, William M.
- Prager, Lillian, see French, C. S.
- 448 Šesták, Z., Ratio of photosystem 1 and 2 particles in young and old leaves of spinach and radish. *Photosynthetica*, 3, 285-287, 1969.
- 466 Wiessner, W., and C. S. French, The forms of native chlorophyll in *Chlamydomonas stellata* and their changes during adaptation from photoheterotrophic to autotrophic growth. *Planta*, 94, 78-90, 1970.

## SPEECHES

- Björkman, Olle, Characteristics of the photosynthetic apparatus as revealed by laboratory measurements. International Symposium on Photosynthesis and Productivity I: Models and Methods. Organized by the International Biological Programme, Czechoslovak Academy of Sciences, Tréboň, Czechoslovakia, September 18, 1969.
- Björkman, Olle, Effect of oxygen concentration on growth in relation to photosynthesis and photorespiration. International Symposium on Photosynthesis and Productivity II: Theoretical Foundations of Optimization of the Photosynthetic Productivity. Organized by the International Biological Programme, Academy of Sciences of the USSR, Moscow, September 26, 1969.
- Björkman, Olle, Comparative studies of photosynthetic characteristics of two species of *Atriplex*. Institute of Plant Physiology, University of Uppsala, October 2, 1969.
- Björkman, Olle, Photosynthetic characteristics of species with different pathways for carbon dioxide fixation. Department of Botanical Sciences, University of Stockholm, October 3, 1969.
- Björkman, Olle, Characteristics of hybrids between *Atriplex* species with and without  $\beta$ -carboxylation photosynthesis. Division of Natural Sciences, University of California at Santa Cruz, May 27, 1970.
- Björn, Lars, The thylakoid as a unit for energy storage in photosynthesis. Meeting of Swedish Biochemists and Biophysicists, Gothenburg, Sweden, June 9, 1970.
- Brown, Jeanette S., A study of spectroscopically different chloroplast particles. XI International Botanical Congress, Seattle, Washington, August 25, 1969.
- Brown, Jeanette S., Centrifugation and zonal rotors. Stanford-Carnegie Plant Physiology Graduate Seminar, Department of Plant Biology, Carnegie Institution, February 11, 1970.
- Brown, Jeanette S., Photosystem 1 particles prepared by an improved method. Pacific Division, AAAS, Berkeley, California, June 24, 1970.
- Fork, David C., The effect of detergent on the activity of natural and artificial electron donors to P700 and cytochrome *f* in fraction-1 particles from spinach. International Conference on the Photosynthetic Unit, Gatlinburg, Tennessee, May 20, 1970.
- French, C. S., Analysis of absorption spectra of chloroplast fractions. XI International Botanical Congress, Seattle, Washington, August 25, 1969.
- French, C. S., Forms of chlorophyll in plants, October 21, 1969, History of photosynthesis research, October 27, 1969, Kinetics and action spectra for oxygen evolution, October 29, 1969, Department of Life Sciences, University of California at Riverside.
- French, C. S., The forms of chlorophyll in plants. Biology Department, Harvard University, November 18, 1969, Department of Biology, Brandeis University, November 19, 1969, Department of Biology, Simon Fraser University, British Columbia, November 21, 1969.
- French, C. S., Forms of chlorophyll. Stanford-Carnegie Plant Physiology Seminar, University of California at Santa Cruz, April 15, 1969.
- French, C. S., Reminiscences of photosynthesis. International Conference on the Photosynthetic Unit, Gatlinburg, Tennessee, May 19, 1970.

- French, C. S., Four forms of native chlorophyll and a discussion of Halldal's new procedure for recording action spectra. International Conference on the Photosynthetic Unit, Gatlinburg, Tennessee, May 20, 1970.
- Halldal, Per, Photosynthetic adaption to impoverished light conditions by algae in nature. Stanford-Carnegie Plant Physiology Graduate Seminar, Department of Plant Biology, Carnegie Institution, January 21, 1970.
- Halldal, Per, Algal photosynthesis under extreme light conditions in massive corals. Department of Biology, University of California at Santa Barbara, February 13, 1970.
- Halldal, Per, Algal photosynthesis under extreme light conditions in massive corals. Department of Botany, University of Hawaii, March 12, 1970.
- Jacobi, Günter, Fragmentation of chloroplasts. Stanford-Carnegie Plant Physiology Graduate Seminar, Department of Plant Biology, Carnegie Institution, October 29, 1969.
- Loos, Eckhard, Photosystem 1 reactions. Stanford-Carnegie Plant Physiology Graduate Seminar, Department of Plant Biology, Carnegie Institution, October 22, 1969.
- Medina, Ernesto, Ecology of the black water regions of the high Orinoco. Stanford-Carnegie Plant Physiology Graduate Seminar, Department of Plant Biology, Carnegie Institution, June 3, 1970.
- Murata, Norio, Effects of metal ions on distribution of light energy between two pigment systems in photosynthesis. Department of Physiology, University of California at Berkeley, March 4, 1970.
- Murata, Norio, Control mechanisms of light energy distribution between two pigment systems of photosynthesis. Department of Botany, University of Illinois, Urbana, May 28, 1970.
- Murata, Norio, Relationship between change in excitation transfer and membrane structure of chloroplasts. International Conference on the Photosynthetic Unit, Gatlinburg, Tennessee, May 18, 1970.
- Nobs, Malcolm A., Genetics of ecotypic adaptation. Stanford-Carnegie Plant Physiology Graduate Seminar, Department of Plant Biology, Carnegie Institution, December 10, 1969.
- Pearcy, Robert, Adaptations in hot spring and snow algae. Stanford-Carnegie Plant Physiology Graduate Seminar, Department of Plant Biology, Carnegie Institution, November 5, 1969.
- Wiessner, Wolfgang, Photometabolism of *Chlamydomonas*. Stanford-Carnegie Plant Physiology Graduate Seminar, Department of Plant Biology, Carnegie Institution, November 5, 1969.

## PERSONNEL

### *Biochemical Investigations*

*Staff:* C. Stacy French, *Director*; Jeanette S. Brown, David C. Fork, James H. C. Smith, *Emeritus*<sup>1</sup>

*Senior Fellows:* Per Halldal,<sup>2</sup> Günter Jacobi,<sup>3</sup> Wolfgang Wiessner<sup>4</sup>

*Carnegie Corporation Fellow:* Kenneth E. Mantai<sup>5</sup>

<sup>1</sup> Died January 8, 1970.

<sup>2</sup> From December 30, 1969. From Umeå University, Sweden.

<sup>3</sup> From September 2, 1969, through November 12, 1969. From Bot. Inst., Tierärztlichen Hochschule, Hannover. (Now at Pflanzenphysiologisches Institut, Göttingen.)

<sup>4</sup> From September 2, 1969, through November 9, 1969. From Pflanzenphysiologisches Institut, Göttingen.

<sup>5</sup> From September 5, 1968, through September 9, 1969. From Oregon State University, Corvallis, to Brookhaven National Laboratory, Upton, New York.



*Carnegie Institution Research Fellows:* Norio Murata,<sup>6</sup> Teruyo Murata,<sup>7</sup> Lars-Olof Björn,<sup>8</sup> Eckhard E. Loos,<sup>9</sup> Colin A. Wraight<sup>10</sup>

*Technical Assistants:* Mary L. Hegedus,<sup>11</sup> Helen Kennedy<sup>12</sup>

*Physiological Ecology Investigations*

*Staff:* Olle Björkman, Malcolm A. Nobs, Jens C. Clausen, *Emeritus*,<sup>13</sup> William M. Hiesey, *Emeritus*

*Carnegie Institution Research Fellows:* Robert W. Pearcy,<sup>14</sup> Joseph A. Berry,<sup>15</sup> Ernesto Medina,<sup>16</sup> John E. Boynton<sup>17</sup>

*Technical Assistants:* Frank Nicholson, Gregory S. Martinelli<sup>18</sup>

*Gardener:* Archibald H. Lawrence

*Summer Research Assistant:* Peter G. Mika<sup>19</sup>

*Part-Time Garden Helpers:* Charles J. Wright II,<sup>20</sup> Lance S. Parker<sup>21</sup>

*Administrative Secretary-Accountant:* Clara K. Baker

*General Department Secretary:* Karen D. Roberts

*Mechanical Engineer:* Richard W. Hart

*Electrical Engineer:* Mark C. Lawrence

*Custodian:* Jan Kowalik

<sup>6</sup> From June 3, 1969. From University of Tokyo.

<sup>7</sup> From June 10, 1970. From Toho University, Chiba, Japan. (Guest Investigator from June 3, 1969 through September 1, 1969.)

<sup>8</sup> From January 3, 1969, through August 30, 1969. From University of Lund.

<sup>9</sup> From January 6, 1968, through October 30, 1969. From Institut für Angewandte Botanik, Technische Hochschule, Munich.

<sup>10</sup> From June 23, 1969, through September 26, 1969. From University of Bristol, England.

<sup>11</sup> From May 11, 1970.

<sup>12</sup> From February 3, 1969, through June 1, 1970.

<sup>13</sup> Died November 22, 1969.

<sup>14</sup> From July 1, 1969. From Colorado State University, Fort Collins.

<sup>15</sup> From April 23, 1970. From University of British Columbia, Vancouver.

<sup>16</sup> From March 8, 1970. From Universidad Central de Venezuela, Caracas.

<sup>17</sup> From June 9, 1969, through September 12, 1969. From Duke University, Durham, North Carolina.

<sup>18</sup> From June 19, 1969.

<sup>19</sup> From June 16 to September 15, 1969, and from May 3, 1970.

<sup>20</sup> From May 13, 1969, through September 30, 1969.

<sup>21</sup> From June 22, 1969.



# *Genetics Research Unit*

*Cold Spring Harbor, New York*

Alfred D. Hershey

*Director*



*Contents*

Persistent Heterozygotes in Phage T4 . . . . . 717

Bibliography . . . . . 722

Personnel . . . . . 722

## PERSISTENT HETEROZYGOTES IN PHAGE T4

Parma and Ingraham are studying the genetic structure of phage lines that carry chromosomal duplications. The point of interest in their work, as in much of phage biology, lies in the possibility of understanding at the molecular level phenomena known to have their counterparts in higher organisms. Before summarizing the experimental results, it is necessary to recall some peculiarities of phage T4. They are interesting in their own right.

The *rII* gene of T4 is known from the work of Benzer (1955), who used it in experiments that bridged the gap between the structure of DNA and the structure of genes. The *rII* gene consists of two adjacent DNA segments, A and B, that together comprise about one percent of the DNA of the phage. Except for their cooperative function, A and B behave like separate genes, each subject to mutation from the active (+) to the inactive (-) form. Thus Benzer recognized four genotypic classes:  $A^+B^+$ ,  $A^+B^-$ ,  $A^-B^+$ , and  $A^-B^-$ . Only  $A^+B^+$  can perform *rII* function. The three inactive classes are distinguishable both by breeding analysis and by the fact that only the chromosome pair  $A^+B^-$  and  $A^-B^+$  can cooperate, when present in the same bacterial cell, to carry out *rII* function. This fact, together with evidence that  $A^-$  and  $B^-$  mutations occur in adjacent, nonoverlapping segments of the DNA, reveals the bipartite structure of the gene.

The function of the gene is superfluous to phage growth in ordinary bacterial strains but is essential for growth in bacterial strains lysogenic for phage  $\lambda$ . The critical function in phage  $\lambda$  has been traced to a gene called *rex*. Neither *rII* nor *rex* function is known in chemical terms. The technical importance of the *rII* gene resides in its bipartite structure and in the ease of recognition of its partial functions.

If two phages of genotypes  $A^+B^-$  and  $A^-B^+$  are crossed, one gets among the progeny a few percent of  $A^+B^+$  recombinants, and about one percent of  $A^+B^-/A^-B^+$  heterozygotes. Among the heterozygotes some are "internal hets" (two DNA strands of different parental origin) and some are "terminal hets" (repetitions at the ends of the DNA molecule marked by genes of different parental origin). If the particular mutants *rJ101* and *r1589* are crossed, one gets no internal hets (because the mutants contain mismatching deletions) and no  $A^+B^+$  recombinants (because the two deletions correspond to overlapping nucleotide sequences). Nevertheless, owing to their exceptional structure, the respective mutants are functionally  $A^+B^-$  and  $A^-B^+$ , and the cross does generate  $A^+B^-/A^-B^+$  terminal hets. The mutants *rJ101* and *r1589* are especially useful in genetic experiments, including those described below, that require detection of exceptional events. In principle, though, any functionally equivalent mutants would serve, and for clarity I shall stick to the more descriptive generalized notation.

F. W. Stahl and his colleagues (*Proceedings of the National Academy of Sciences*, 1965) first prepared  $A^+B^-/A^-B^+$  terminal hets and proved their structure. Among other things they found that such phage particles could carry out *rII* function in a lysogenic host cell, but yielded progeny that were exclusively of the original mutant types. The prompt segregation identified the particles as heterozygotes rather than recombinants, and the functional complementation was consistent with the expected structure of terminal hets, but not with that of internal hets. (Internal hets would contain part of their genetic information in the unreadable DNA strand, information that could be expressed only after replication.)

At the time of Stahl's work, interest in T4 genetics was focused on terminal repetition and circular permutation of nucleotide sequences, and much effort was devoted to the search for mutants lacking one or both of these features. No such mutants were found, but the purposes of the search are being accomplished in other ways.

Mosig (*Year Book 64*, p. 521) described exceptional particles of phage T4 that contain single DNA fragments of only two-thirds the normal molecular length. Such DNA fragments represent a random, continuous segment of the genome. They lack terminal repetitions but also lack about one-third of the normal set of genes. The doubly defective particles are of course noninfective. Mosig (now at Vanderbilt University) and Werner (now at the University of Miami School of Medicine) sought to determine what sort of lesion the absence of a terminal repetition entails.

Mosig and Werner (*Proceedings of the National Academy of Sciences*, 1969) obtained physical evidence that many of the DNA fragments start to reproduce, but on the average duplicate only half their length. Mosig and her students subsequently showed that replication starts at a point between genes 41 and 42, proceeds in the direction of gene 43, and presumably stops when it reaches the end of the fragment. Terminal repetitions in DNA molecules therefore represent "joining sequences" that are essential for ring formation, on which replication ultimately depends (*Year Book 67*, p. 562). Botstein has more direct evidence that in phage P22 replication depends on ring closure and that ring closure is brought about by intramolecular crossing over between repetitious molecular ends. In view of these facts, mutants of T4 lacking repetitions could hardly exist. Independently of replication mechanisms, the only model we have for packaging of DNA into T4 phage particles leads to the same inference. It too requires terminal repetition and generates

circular permutation (Streisinger, Emrich, and M. M. Stahl, *Proceedings of the National Academy of Sciences*, 1967). Nevertheless, the search for phage lines with a nonpermuted gene sequence has proved fruitful in unexpected ways.

Weil, Terzaghi, and Crasemann (*Genetics*, 1965) reported that  $rII$  crosses of the type  $A^+B^- \times A^-B^+$  yielded about one phage particle in 10 million of a special type that could form a plaque on plates seeded with the lysogenic bacterial host. The resulting clones contained physiologically  $A^+B^+$  phage, but proved to segregate with relatively high frequency particles of the ancestral genotypes  $A^+B^-$  and  $A^-B^+$ . Such particles could be recognized as heterozygotes of the genotype  $A^+B^-/A^-B^+$ , and Weil *et al.* concluded that they were stabilized terminal hets, or else carried duplications of another sort.

Duplications of another sort have in fact been revealed by the work of Weil and Terzaghi and of Parma and Ingraham. The experimental results can be appreciated best if the applicable genetic principles are first brought to mind.

The local event that gives rise to recombinant chromosomes is called crossing over. Typically, crossing over is observed between homologous partners and produces no persistent local lesions: parental and recombinant chromosomes differ only with respect to content of genetic markers. The overall process therefore consists, in effect, of interchange of exactly corresponding segments of homologous chromatids. Since crossing over can occur at practically any chromosomal site, one is forced to think of a matching principle based on complementary nucleotide sequences.

In T4, a single crossover involves pairing restricted to the appropriate short segment of DNA (Drake, *Proceedings of the National Academy of Sciences*, 1967). It is therefore plausible to imagine occasional local mispairing accompanied by "illegitimate" crossing over. The hypothetical products of single illegiti-



mate crossovers between homologous chromatids are deletions and tandem duplications, as illustrated in Fig. 1. Note that the tandem duplication (II) is not a cyclic permutation or a biological equivalent of the corresponding terminal repetition (IV), because IV does not contain the sequence  $\cdots mk \cdots$  and cannot generate it except by something equivalent to illegitimate crossing over. Thus a tandem duplication can be exactly defined as one product of a single illegitimate crossover. In terms of DNA structure it is characterized by a single repeat in a nucleotide sequence containing just one joint of novel origin.

Illegitimate crossing over, like typical crossing over, is known by its products. Neither process is understood in mechanical or chemical terms.

Illegitimate crossing over is unequal in the sense that the reciprocal products are not homologous with respect to each other or their parents. Nevertheless, in chromosomes containing tandem duplications the ancestral genome is not lost and is, in fact, spontaneously regenerated with rather high frequency. The reasons for this were made clear by Sturtevant

in experiments with the Bar eye mutant of *Drosophila*. His experiments also provided the criteria for recognizing tandem duplications.

Figure 2 shows the results of unequal crossing over between homologous chromosomes containing a duplication. Here the parental type represents Bar and the products are normal eye and "double Bar." The crossover is "legitimate" in that it involves local homology just as ordinary crossing over does. The main point is that the reduced product of unequal crossing over will be homologous with the ancestral type only if the original duplications are tandem. The genetic results obtained by Sturtevant were further clarified by Bridges, who ascertained by examination of salivary gland chromosomes that the Bar mutant carries a tandem duplication of a set of bands that occurs once in the normal segregant and three times in the double Bar segregant. The interpretation in terms of a duplication, originating by illegitimate crossing over and erased by unequal crossing over according to Figs. 1 and 2, was thus verified in the most satisfactory manner possible.

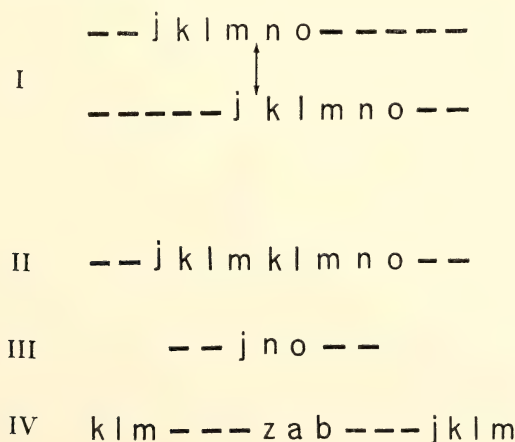


Fig. 1. Illegitimate crossing over. Nucleotide sequences corresponding to parts of the genome are represented by alphabetical sequences in which each letter stands for many nucleotides. In I, two molecules are mispaired. An illegitimate crossover at the double arrow generates a tandem duplication (II) and the corresponding deletion (III). Structure IV is the terminal repetition analogous to II.

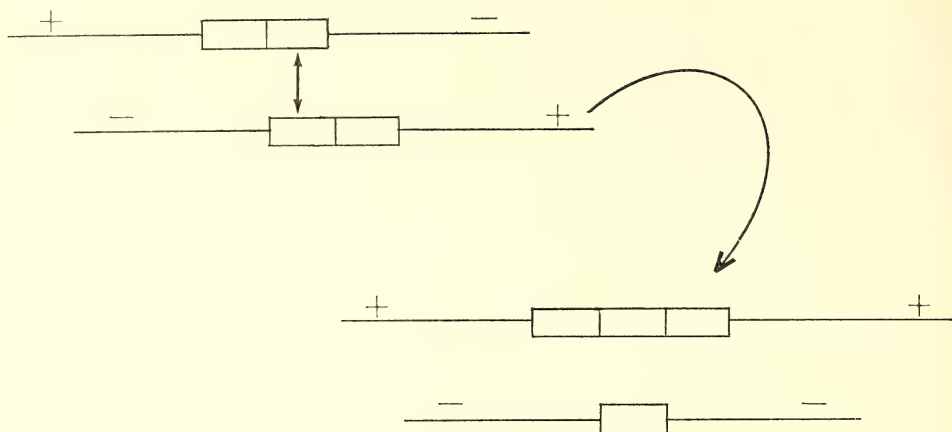


Fig. 2. Unequal crossing over between DNA molecules containing a duplication. Each unit of the repeated sequence is indicated by a rectangle. The plus and minus signs signify genetic markers bracketing the repeats.

The foregoing line of thought carries over from *Drosophila* to T4 with just one complication. In genetic experiments with T4, recombinant DNA molecules are detected only if they can be put into phage particles, a requirement that prohibits lengthening. Thus a DNA molecule containing a duplicated DNA segment must usually suffer deletion of another, dispensable, DNA segment if it is to be recovered in viable form. Matvienko (*Molekulyarnaya Biologiya*, 1969) verified by density analysis that persistent hets of one line contained only the normal length of DNA per particle.

According to the ideas outlined above, Weil's persistent hets might be expected to contain tandem duplications of a DNA segment including the *rII* gene, and to have suffered deletions of non-essential DNA elsewhere in the chromosome. This is the hypothesis that Parma and Ingraham have investigated. Their conclusions are summarized below.

1. Persistent hets produce three types of progeny besides particles like themselves:  $A^+B^-$  segregants,  $A^-B^+$  segregants, and inviable particles. The segregants comprise 15% to 45% of the viable particles, their proportion being char-

acteristic for each line of hets, depending, most likely, on the length of the particular duplication. The number of inviable particles is about equal to the number of segregants. The inviable particles therefore can be interpreted as triplications generating a gene set too large to go into a phage particle without loss. Then the segregants and triplications are just reciprocal products of unequal crossing over according to Fig. 2.

2. The *r* segregants from persistent hets marked by revertible *rII* mutants are themselves revertible to  $r^+$ , showing that the revertants are haploid rather than homozygous diploid in structure (Weil *et al.*, 1965). The same inference follows from the fact that crosses between pairs of segregants do not regenerate persistent hets at very high frequency (*cf.* item 4 below). These facts support the interpretation in terms of tandem duplications as opposed to duplications of other kinds.

3. Crosses of the type  $A^+B^- \times A^-B^+$ , in which the phages are segregants from persistent hets, generate terminal (non-persistent) hets at higher than normal frequency, the actual frequency being characteristic of the particular line of

persistent hets from which the segregants were derived. This Parma and Ingraham interpret as evidence that the duplications are often accompanied by deletions, the net effect being to lengthen terminal repetitions. Weil and Terzaghi have evidence for deletions of known genes in some of their persistent hets.

4. In crosses of the type last mentioned, segregants from persistent hets also regenerate new persistent hets with appreciably higher frequency than do the corresponding ancestral lines. This too may be an indication that the segregants contain deletions, since lengthened terminal repetitions might be expected to favor viability of newly formed duplications.

5. Parma and Ingraham prepared their persistent hets from stocks containing multiple genetic markers. The distribution of these markers in the hets clearly shows that the duplications arise by a single crossover in the vicinity of the *rII* gene, and that the resulting duplication is usually not more than a dozen or so recombination units in length.

6. The markers recovered in the persistent hets, as well as other genetic tests, show that the duplications usually have the genetic structure  $\cdots B^+A^-B^+A^-\cdots$  rather than  $\cdots B^-A^+B^+A^-\cdots$ . This result is expected if short duplications are more likely to survive than long ones. Persistent hets can be recognized only if they contain intact  $A^+$  and  $B^+$  segments. In the first structure this requirement can be met without duplicating the entire *rII* gene, whereas in the second it cannot.

These results are evidently consistent with the hypothesis that persistent hets contain tandem duplications accompanied by compensating deletions. The alternative hypotheses that seem to be excluded are: stabilized terminal repetitions, inverted duplications, and non-tandem duplications in general. None of the alternatives can account for the fact that persistent hets sport haploid segre-

gants and inviable particles at similar high frequencies.

The origin of the tandem duplications seems to be accounted for satisfactorily by the hypothesis of illegitimate crossing over. It is not so easy to account for the accompanying deletions. If the two aberrations arise independently, crosses between appropriately marked stocks already carrying deletions should generate persistent hets with much higher frequency than they do. The alternative, that generation of a repeat during phage growth favors a concomitant deletion in the same chromosome, is not an intelligible hypothesis at present.

Apart from questions about detailed genetic mechanisms, what do these findings signify? The mere fact that species exist tells us that genetic replication and genetic recombination are conservative processes. The mere fact that species evolve should tell us that both processes are likely to exhibit limited fidelity. Replication errors (mutations) are better known than recombination errors (illegitimate crossing over), but apparently only because errors of the first kind are easier to detect. Heretofore, tandem duplications were known chiefly from Sturtevant's analysis of Bar in *Drosophila*. The work of Weil and Parma and their colleagues translates Sturtevant's findings into molecular terms and goes further in showing that illegitimate crossing over occurs with surprisingly high frequency. No numerical frequency can be given except to say that duplications of a specific region in T4 DNA reveal themselves in one out of 10 million progeny of the appropriate cross in spite of the fact that the great majority of similar aberrations must go undetected unless accompanied by a viable deletion. In short, gross aberrations, both additions and subtractions, are now part of the molecular chemistry made visible by genetic analysis.



## BIBLIOGRAPHY

- Hershey, A. D., Genes and hereditary characteristics, *Nature*, 226, 697-700, 1970.
- Hershey, A. D., Idiosyncrasies of DNA structure, Nobel Lecture published in *Science*, 168, 1425-1427, 1970.
- Yamagishi, Hideo, Nucleotide distribution in the DNA of *Escherichia coli*, *J. Mol. Biol.*, 49, 603-608, 1970.

## PERSONNEL

*Year ended June 30, 1970*

- |   |   |
|---|---|
| Elizabeth M. Bocskay, Chief Clerk                   | David H. Parma, National Science Foundation Postdoctoral Fellow                     |
| Elizabeth Burgi, Associate in Microbiology          | Jennie B. Pope, Curator of <i>Drosophila</i> Stocks                                 |
| Agnes C. Fisher, Secretary to Director;<br>Editor   | Irwin Rubenstein, Special Fellow, National<br>Institute of General Medical Sciences |
| Alfred D. Hershey, Director                         | Anna Marie Skalka, Carnegie Corporation<br>Fellow                                   |
| Laura J. Ingraham, Research Assistant               | Carole E. Thomason, Technical Assistant   |
| Barbara McClintock, Distinguished Service<br>Member | Hideo Yamagishi, Carnegie Institution Fellow  |
| Shraga Makover, Carnegie Institution Fellow         |   |

# Bibliography

July 1, 1969–June 30, 1970

## PUBLICATIONS OF THE INSTITUTION

*Carnegie Institution of Washington Year Book* 68. Octavo, xi + 716 pages, 24 plates, 233 figures, Washington, D.C., February 1970.

*The Harvey Monroe Hall Natural Area*. Jens C. Clausen. (Department of Plant Biology publication number 459). Octavo, 48 pages, frontispiece, July 1969.

175. *Cosmic Ray Results, Researches of the Department of Terrestrial Magnetism, Vol. XXII*. Liselotte Beach and Scott E. Forbush. Quarto, vii + 311 pages, 300 tables, December 1969.

*Carnegie Institution of Washington Catalogue for 1970–1971*. Octavo, 96 pages, 14 plates, February 1970.

87. *California Earthquake of April 18, 1906*. Reprint. Quarto, Vol. I, xviii + 451 pages, 146 plates; Vol. II, vii + 192 pages, 2 plates; Atlas, 25 maps, 15 seismograms. March 1970.

## PUBLICATIONS BY THE PRESIDENT OF THE INSTITUTION

Caryl P. Haskins

A message of our times. Review of *So Human An Animal*, by René Dubos. In *The Virginia Quarterly Review*, Vol. 45, No. 1, Winter 1969, pp. 128–135.

*The Scientific Revolution and World Politics* (see *Year Book* 63, p. 615), Burmese edition, Maung Maung Kyaw, Rangoon, January 1969; Spanish edition, Editorial Troquel, Buenos Aires, June 1969.

The humanities and natural sciences. *American Scientist*, Vol. 58, No. 1, January–February 1970, pp. 23–33.

Report of the President. Reprinted from *Carnegie Institution of Washington Year Book* 68, 94 pages, 4 plates, 12 figures, February 1970.

A participant in great events. Review of *My Several Lives*, by James B. Conant. In *Science*, Vol. 168, No. 3932, May 8, 1970, pp. 688–690.

Advances and challenges in science in 1969. Excerpts from Report of the President, *Carnegie Institution of Washington Year Book* 68, reprinted in *American Scientist*, Vol. 58, No. 4, July–August 1970, pp. 365–377.





# *Administrative Reports*



# *Report of the Executive Committee*

## *To the Trustees of the Carnegie Institution of Washington*

Gentlemen:

In accordance with the provisions of the By-Laws, the Executive Committee submits this report to the Annual Meeting of the Board of Trustees.

During the fiscal year ending June 30, 1970, the Executive Committee held four meetings. Printed accounts of these meetings have been or will be mailed to each Trustee.

The estimate of expenditures for the fiscal year beginning July 1, 1970, has been reviewed by the Executive Committee.

The terms of office of the Chairmen of all Committees of the Board expire on May 1, 1970. The terms of the following members of Committees also expire on May 1, 1970:

*Finance Committee*

Alfred L. Loomis  
Henry S. Morgan  
Keith S. McHugh

*Auditing Committee*

Keith S. McHugh  
Alfred L. Loomis  
Juan T. Trippe

*Retirement Committee*

Garrison Norton

*Nominating Committee*

Crawford H. Greenewalt  
Keith S. McHugh

HENRY S. MORGAN, *Chairman*

*May 1, 1970*





# *Report of Auditors*

LYBRAND, ROSS BROS. & MONTGOMERY

## REPORT OF INDEPENDENT CERTIFIED PUBLIC ACCOUNTANTS

To the Auditing Committee of  
Carnegie Institution of Washington:

We have examined the statement of assets and funds of Carnegie Institution of Washington as of June 30, 1970, and the related summary statement of changes in funds for the year then ended and the supporting exhibits and schedules. Our examination was made in accordance with generally accepted auditing standards, and accordingly included confirmation from the custodian of investments held at June 30, 1970, and such tests of the accounting records and such other auditing procedures as we considered necessary in the circumstances. We previously examined and reported upon the financial statements of the Institution for the year ended June 30, 1969.

These statements have been prepared on the general basis of cash receipts and disbursements and accordingly, they do not purport to present financial position or results of operations as they would appear had generally accepted accrual basis accounting principles been applied in their preparation.

In our opinion, the aforementioned financial statements and supporting exhibits and schedules (Pages 730 to 742) present fairly the assets and funds of Carnegie Institution of Washington at June 30, 1970 and 1969, and the changes in funds for the year ended June 30, 1970, on the basis indicated above consistently applied, except for the change, in which we concur, in accounting for the cost of equipment acquisitions as described in note (b) to the statement of assets and funds.

*Lybrand, Ross Bros. & Montgomery*

Washington, D. C.  
August 25, 1970

## STATEMENT A

## ASSETS AND FUNDS

JUNE 30, 1970 and 1969

## ASSETS

	1970	1969
Cash .....	\$ 312,294.95	\$ 688,866.39
Advances .....	93,398.65	38,410.02
Investments (cost) (a), Schedule 2:		
Governmental obligations .....	1,099,625.00	1,892,625.00
Nongovernmental bonds .....	38,329,221.79	39,123,254.31
Common stocks .....	38,530,069.74	37,711,702.61
Mortgage .....	11,432.64	13,983.06
Land (cost) .....	434,806.42	389,306.96
Buildings (cost) .....	2,868,732.64	2,543,209.03
Equipment (cost) (b) .....	<u>.....</u>	<u>4,205,580.26</u>
Total assets .....	<u>\$81,679,581.83</u>	<u>\$86,606,937.64</u>

## FUNDS

Operating Fund, Exhibit 1 .....	\$ 1,815,968.69	\$ 2,318,156.83
Restricted Grants, Exhibit 2 .....	26,443.43	105,817.51
Endowment and Special Funds, Exhibit 3 .....	76,533,630.65	77,044,867.05
Land and buildings .....	<u>3,303,539.06</u>	<u>7,138,096.25</u>
Total funds .....	<u>\$81,679,581.83</u>	<u>\$86,606,937.64</u>

(a) Approximate market value on June 30, 1970: \$89,417,789.00.

(b) Effective July 1, 1969, the Institution adopted the practice of excluding the cost of equipment acquisitions from assets and fund balance. In effecting the change in accounting method, the accumulated cost of equipment at that date (\$4,205,580.26) was eliminated against the Equipment Fund Balance.



## STATEMENT B

## SUMMARY STATEMENT OF CHANGES IN FUNDS

FOR THE YEAR ENDED JUNE 30, 1970

	<i>Operating Fund (Exhibit 1)</i>	<i>Restricted Grants (Exhibit 2)</i>	<i>Endowment and Special Funds (Exhibit 3)</i>	<i>Land and Buildings</i>	<i>Total</i>
Balance, July 1, 1969 .....	\$2,318,156.83	\$105,817.51	\$77,044,867.05	\$7,138,096.25	\$86,606,937.64
<i>Additions:</i>					
Realized capital loss, net .....	.....	.....	(116,769.18)	.....	(116,769.18)
Investment income					
Interest .....	.....	.....	1,926,969.52	.....	1,926,969.52
Dividends .....	.....	.....	2,150,829.49	.....	2,150,829.49
Restricted grants .....	.....	437,657.75	.....	.....	437,657.75
Gifts .....	.....	.....	5,410.00	.....	5,410.00
Other income .....	.....	.....	45,053.77	.....	45,053.77
Land and buildings .....	.....	.....	.....	371,023.07	371,023.07
Appropriations					
Budget .....	4,518,330.00	.....	(4,518,330.00)	.....	.....
Employee benefits, Bush Gift .....	4,400.00	.....	(4,400.00)	.....	.....
	<u>4,522,730.00</u>	<u>437,657.75</u>	<u>(511,236.40)</u>	<u>371,023.07</u>	<u>4,820,174.42</u>
<i>Deductions:</i>					
Expenditures .....	5,024,918.14	517,031.83	.....	.....	5,541,949.97
Equipment Write-Off (a) .....	.....	.....	.....	4,205,580.26	4,205,580.26
	<u>5,024,918.14</u>	<u>517,031.83</u>	<u>.....</u>	<u>4,205,580.26</u>	<u>9,747,530.23</u>
Net change during year .....	(502,188.14)	(79,374.08)	(511,236.40)	(3,834,557.19)	(4,927,355.81)
Balance, June 30, 1970 .....	\$1,815,968.69	\$ 26,443.43	\$76,533,630.65	\$3,303,539.06	\$81,679,581.83

(a) See note (b) on Statement A.

## EXHIBIT 1

CHANGES IN OPERATING FUND  
FOR THE YEAR ENDED JUNE 30, 1970

Balance, July 1, 1969 .....	\$2,318,156.83
-----------------------------	----------------

*Appropriations, Statement B:*

Budget, July 1, 1969 to June 30, 1970—Exhibit 3 .....	\$4,518,330.00	
Employee benefits, special, Bush Gift .....	4,400.00	4,522,730.00

Total available for expenditures .....	6,840,886.83
--	--------------

*Expenditures:*

Salaries .....	2,337,957.89
Laboratory .....	606,050.94
Land and buildings .....	340,039.34
Employee benefits, retirement contributions .....	298,327.68
Building .....	247,375.82
Equipment .....	218,625.81
Operating .....	149,183.34
Publications .....	142,569.51
Fellowships .....	125,318.32
Employee benefits, other .....	120,245.70
Travel .....	94,488.40
Taxes .....	91,366.51
Consulting fees and insurance .....	85,263.69
Financial advisory services .....	69,559.82
Rent .....	27,408.27
Awards .....	26,929.64
Dormitory .....	18,583.99
Shop .....	17,407.51
Entertainment .....	8,215.96

Total expenditures .....	5,024,918.14

Balance, June 30, 1970 .....	\$1,815,968.69

## EXHIBIT 2

## CHANGES IN RESTRICTED GRANTS

FOR THE YEAR ENDED JUNE 30, 1970

	<i>Balance July 1, 1969</i>	<i>Grants</i>	<i>Expenditures</i>		<i>Balance June 30, 1970</i>
			<i>Salaries</i>	<i>Other</i>	
American Cancer Society . . . . .	...	\$ 500.00	..	...	\$ 500.00
American Chemical Society . . . . .	...	10,000.00	..	\$ 9,400.00	600.00
Armin J. Deutsch Memorial . . . . .	...	1,000.00	..	1,000.00	...
Carnegie Corporation of New York . . . . .	\$ 25,087.01	80,000.00	..	104,756.91	330.10
Helen Hay Whitney Foundation . . . . .	625.00	9,500.00	\$10,125.00	...	...
Jet Propulsion Laboratory . . . . .	302.98	...	..	60.60	242.38
Lalor Foundation . . . . .	...	3,000.00	..	...	3,000.00
National Aeronautics & Space Administration . . . . .	(14,847.74)	87,343.75	592.15	58,699.92	13,203.94
National Science Foundation . . . . .	96,448.80	186,500.00	23,006.30	243,133.98	16,808.52
Office of Naval Research . . . . .	(830.00)	18,164.00	8,396.00	16,974.36	(8,036.36)
Public Health Service . . . . .	(968.54)	41,650.00	19,881.68	21,004.93	(205.15)
Total . . . . .	<u>\$105,817.51</u>	<u>\$437,657.75</u>	<u>\$62,001.13</u>	<u>\$455,030.70</u>	<u>\$26,443.43*</u>

\*Does not include grants to be received as follows:

American Chemical Society . . . . .	\$ 5,000.00
National Aeronautics & Space Administration . . . . .	159,517.25
National Science Foundation . . . . .	169,723.05
Office of Naval Research . . . . .	13,000.00
Public Health Service . . . . .	6,860.00
	<u>\$354,100.30</u>



## EXHIBIT 3

## CHANGES IN ENDOWMENT AND SPECIAL FUNDS

FOR THE YEAR ENDED JUNE 30, 1970

	Balance July 1, 1969	Investment Income	Gifts and Other Income	Realized Capital Loss, net	Appropriations	Transfers	Balance June 30, 1970
<i>Endowment Fund</i>							
Gifts							
Andrew Carnegie	\$22,000,000.00	.....	.....	.....	.....	.....	\$22,000,000.00
Carnegie Corporation of New York	10,000,000.00	.....	.....	.....	.....	.....	10,000,000.00
Realized capital gain, net	31,678,942.63	.....	.....	\$ 98,327.12	.....	.....	31,580,615.51
Unrestricted Capital Fund							
Gifts	107,143.99	.....	.....	.....	.....	.....	107,143.99
Realized capital gain, net	5,350,691.31	.....	.....	17,258.20	.....	.....	5,333,433.11
Income							
Andrew Carnegie, reserve	2,500,000.00	.....	.....	.....	.....	.....	2,500,000.00
Other	538,829.29	.....	.....	.....	.....	.....	538,829.29
Working Capital Fund							
Income	3,980,954.98	\$4,039,038.07	.....	.....	\$4,484,130.00	\$45,053.77	3,580,916.82
Sales							
Assets			\$ 781.61	.....	.....	(781.61)	.....
Drosophila cultures	.....	.....	3,810.85	.....	.....	(3,810.85)	.....
Optical services	.....	.....	9,901.95	.....	.....	(9,901.95)	.....
Publications	.....	.....	21,646.76	.....	.....	(21,646.76)	.....
Refunds	.....	.....	959.74	.....	.....	(959.74)	.....
Publication royalties	.....	.....	6,162.10	.....	.....	(6,162.10)	.....
Rent	.....	.....	1,061.00	.....	.....	(1,061.00)	.....
Miscellaneous	.....	.....	729.76	.....	.....	(729.76)	.....
<i>Special Funds</i>							
Astronomy	.....	1.80	60.00	.09	.....	.....	61.71
Bush Gift	16,305.10	1,539.43	.....	42.83	4,400.00	.....	13,401.70
Colburn	191,384.60	10,125.84	.....	308.31	10,110.00	.....	191,090.13
Hale Relief	7,046.48	357.27	.....	10.89	370.00	.....	7,022.86
Harkavy	9,519.81	441.91	.....	13.45	450.00	.....	9,498.27
Morgenroth	34,067.02	1,227.09	.....	37.37	290.00	.....	34,966.74
Special Instrumentation	65,311.39	2,490.63	5,350.00	83.30	.....	.....	73,068.72
Teple	19,471.65	988.27	.....	30.10	985.00	.....	19,444.82
Wood	545,198.80	21,590.70	.....	657.52	21,995.00	.....	544,136.98
<b>Total</b>	<b>\$77,044,867.05</b>	<b>\$4,077,799.01</b>	<b>\$50,463.77</b>	<b>\$116,769.18</b>	<b>\$4,522,730.00</b>	<b>.....</b>	<b>\$76,533,630.65</b>

SCHEDULE 1

BUDGET SUMMARY OF OPERATING FUND

FOR THE YEAR ENDED JUNE 30, 1970

	<i>Unexpended Appropriations July 1, 1969</i>	<i>Appropriations</i>	<i>Transfers and Allotments</i>	<i>Total Expenditures</i>	<i>Unexpended Appropriations June 30, 1970</i>
Plant Biology . . . . .	\$ 4,783.99	\$ 257,778.04	(\$ 11,005.08)	\$ 244,473.08	\$ 7,083.87
Geophysical Laboratory . . . . .	44,558.72	755,557.54	(4,401.85)	768,349.69	27,364.72
Mount Wilson Observatory . . . . .	939,154.52	811,369.74	712,871.62	1,619,812.45	843,583.43
Terrestrial Magnetism . . . . .	45,312.41	812,571.84	(242.12)	801,147.49	56,494.64
Embryology . . . . .	47,766.48	649,473.04	(30,854.09)	612,650.52	53,734.91
Genetics Research Units . . . . .	7,013.71	168,929.80	(20,272.35)	150,749.16	4,922.00
Research Projects, etc. . . . .	50,770.56	70,395.00	(35,417.54)	63,540.00	22,208.02
Office of Administration . . . . .	2,760.90	468,055.00	12,081.34	468,788.01	14,109.23
Consulting fees, insurance, taxes . . . . .	1,416.66	50,000.00	37,382.39	44,273.05	44,526.00
Contingent operating fund . . . . .	26,500.00	225,000.00	(237,000.00)	. . . . .	14,500.00
Financial advisory services . . . . .	16,000.00	80,000.00	(13,315.18)	69,559.82	13,125.00
General publications . . . . .	7,430.00	104,100.00	24,234.36	110,631.36	25,133.00
Employee benefits, retirees . . . . .	347,141.28	60,500.00	8,402.82	65,430.21	350,613.89
Employee benefits, special . . . . .	957.08	9,000.00	(3,397.48)	5,513.30	1,046.30
Unallocated Appropriations . . . . .	776,590.52	. . . . .	(439,066.84)	. . . . .	337,523.68
Total . . . . .	<u>\$2,318,156.83</u>	<u>\$4,522,730.00</u>	<u>. . . . .</u>	<u>\$5,024,918.14</u>	<u>\$1,815,968.69</u>

<i>Description</i>	<i>Par</i>	<i>Cost</i>	<i>Approximate Market</i>
<b>Federal Agency Bonds</b>			
Federal National Mortgage Association, 5½ s, 1972 .....	\$ 100,000	\$ 99,625.00	\$ 94,750
Federal National Mortgage Association, Part. Certificates, 5½ s, 1973 .....	1,000,000	1,000,000.00	930,000
Total .....	<u>\$ 1,100,000</u>	<u>\$ 1,099,625.00</u>	<u>\$ 1,024,750</u>
<b>International Bank and Foreign Bonds</b>			
Alberta Government Telephone Commission, Deb., 4¾ s, 1989 .....	\$ 700,000	\$ 700,000.00	\$ 374,500
Alcan Aluminum Corporation, Prom. Note, 4¾ s, 1984 .....	750,000	750,000.00	515,625
Aluminum Co. of Canada, Ltd., S. F. Deb., 4½ s, 1980 .....	489,000	493,512.04	352,080
Aluminum Co. of Canada, Ltd., S. F. Deb., 9½ s, 1995 .....	500,000	518,750.00	501,250
Australia (Commonwealth of), 5½ s, 1982 .....	466,000	467,682.92	363,480
Bell Telephone Co. of Canada, 1st Mtg. Series X, 4¾ s, 1988 .....	750,000	747,300.00	418,125
Churchill Falls (Labrador) Corp. Ltd., 1st Mtg. Series A, 7¾ s, 2007 .....	800,000	800,000.00	594,000
Industrial Acceptance Corp. Ltd., Sec. Note Series Z, 5¼ s, 1982 .....	750,000	750,000.00	455,625
Intl. Bank for Reconstruction & Development, 3 s, 1976 .....	125,000	125,000.00	98,125
Intl. Bank for Reconstruction & Development, 3¾ s, 1975 .....	125,000	123,125.00	98,750
Intl. Bank for Reconstruction & Development, 4½ s, 1977 .....	250,000	250,000.00	197,500
Quebec Hydro-Electric Commission, S. F. Deb., 5s, 1988 .....	736,000	723,120.00	471,040
Quebec Hydro-Electric Commission, Deb. Series BN, 9¾ s, 1995 .....	500,000	504,375.00	478,750
Shawinigan Water & Power Co., 1st Mtg. & Collat. Tr. S. F. Series M, 3s, 1971 .....	200,000	200,360.00	190,000
Shell Funding Corp., Collat. Tr. Series B, 4¾ s, 1985 .....	968,000	968,000.00	713,900
Toronto (Municipality of Metropolitan), S. F. Deb., 5s, 1979 .....	500,000	498,637.50	372,500
Total .....	<u>\$ 8,609,000</u>	<u>\$ 8,619,862.46</u>	<u>\$ 6,195,250</u>



INVESTMENTS—Continued

<i>Description</i>	<i>Par</i>	<i>Cost</i>	<i>Approximate Market</i>
Public Utility Bonds			
Colonial Pipeline Co., Sec. Note Series A, 4.829s, 1990 . . . . .	\$ 750,000	\$ 750,000.00	\$ 485,625
Consolidated Edison Co. of N. Y., 1st & Ref. Mtg. Series N, 5s, 1987 . . . . .	300,000	301,326.14	204,750
Consumers Power Co., 1st Mtg., 4½ s, 1987 . . . . .	4,000	4,014.64	2,695
Minnesota Power & Light Co., 1st Mtg., 3½ s, 1975 . . . . .	200,000	200,765.61	157,500
Niagara Mohawk Power Corp., Gen. Mtg., 3½s, 1986 . . . . .	250,000	251,721.06	147,188
Niagara Mohawk Power Corp., Gen. Mtg., 4½ s, 1987 . . . . .	400,000	401,978.85	274,500
Pacific Gas & Electric Co., 1st & Ref. Mtg. Series BB, 5s, 1989 . . . . .	250,000	251,145.62	175,938
Pacific Power & Light Co., 1st Mtg., 4½ s, 1986 . . . . .	250,000	251,711.11	148,125
Potomac Electric Power Co., Deb., 4½ s, 1982 . . . . .	236,000	238,875.78	157,825
Public Service Co. of Indiana, 1st Mtg. Series F, 3½ s, 1975 . . . . .	200,000	200,904.53	158,000
Public Service Co. of Indiana, 1st Mtg. Series L, 4½ s, 1987 . . . . .	400,000	400,000.00	233,000
Southern California Edison Co., 1st & Ref. Mtg. Series H, 4½ s, 1982 . . . . .	250,000	250,859.44	155,625
Southern California Edison Co., 1st & Ref. Mtg. Series J, 4½ s, 1982 . . . . .	200,000	201,039.75	137,000
Washington Water Power Co., 1st Mtg., 4½ s, 1987 . . . . .	300,000	300,000.00	204,000
Total . . . . .	<u>\$ 3,990,000</u>	<u>\$ 4,004,342.53</u>	<u>\$ 2,641,771</u>
Communication Bonds			
Mountain States Telephone & Telegraph Co., Deb. 3½ s, 1978 . . . . .	\$ 200,000	\$ 200,210.00	\$ 134,000
New York Telephone Co., Ref. Mtg. Series E, 3½ s, 1978 . . . . .	100,000	100,345.17	70,125
Pacific Telephone & Telegraph Co., Deb., 3½ s, 1978 . . . . .	200,000	200,662.12	138,000
Southwestern Bell Telephone Co., Deb., 3½ s, 1983 . . . . .	300,000	302,000.00	178,125
Total . . . . .	<u>\$ 800,000</u>	<u>\$ 803,217.29</u>	<u>\$ 520,250</u>

*INVESTMENTS—Continued*

<i>Description</i>	<i>Par</i>	<i>Cost</i>	<i>Approximate Market</i>
<b>Railroad Bonds</b>			
Chesapeake & Ohio Railway Co., Gen. Mtg., 4½ s, 1992 .....	\$ 100,000	\$ 99,500.00	\$ 56,250
Fort Worth & Denver Railway Co., 1st Mtg., 4½ s Guar., 1982 .....	267,000	268,015.87	144,180
Total .....	<u>\$ 367,000</u>	<u>\$ 367,515.87</u>	<u>\$ 200,430</u>

**Industrial and Miscellaneous Bonds**

Boeing Co., Notes, 6½ s, 1986 .....	\$ 1,000,000	\$ 1,000,000.00	\$ 765,000
Columbia Broadcasting System, Inc., Prom. Note, 5½ s, 1991 .....	920,000	920,000.00	657,800
Commercial Credit Co., Note, 3½ s, 1976 .....	400,000	402,208.90	296,000
Commercial Credit Co., Note, 4½ s, 1982 .....	700,000	700,000.00	439,250
Crown Zellerbach Corp., Prom. Note, 4½ s, 1981 .....	300,000	300,000.00	232,500
Crown Zellerbach Corp., S. F. Deb., 8½ s, 2000 .....	1,000,000	1,028,625.00	995,000
Erie Mining Company, 1st Mtg. Series B, 4½ s, 1983 .....	451,000	437,866.88	258,198
First National City Bank, Capital Conv. Notes, 4s, 1990 .....	1,000,000	1,075,715.00	930,000
FMC Corp., S. F. Deb., 3.8s, 1981 .....	500,000	500,000.00	355,000
Four Corners Pipe Line Co. Sec. Note, 5s, 1982 .....	169,000	169,000.00	132,243
General Electric Credit Corp. (N. Y.), Sub. Note, 4¼ s, 1987 .....	500,000	500,000.00	260,000
General Electric Credit Corp. (N. Y.), Prom. Note, 5s, 1975 .....	500,000	500,000.00	400,000
General Motors Acceptance Corp., Deb., 3½ s, 1972 .....	200,000	200,000.00	185,250
General Motors Acceptance Corp., Deb., 4s, 1979 .....	480,000	435,037.50	331,800
General Motors Acceptance Corp., Deb., 4¼ s, 1987 .....	1,000,000	990,000.00	670,000
General Motors Acceptance Corp., Deb., 5s, 1977 .....	200,000	195,000.00	161,000
General Motors Acceptance Corp., Deb., 5s, 1981 .....	200,000	199,000.00	143,500

*INVESTMENTS—Continued*

<i>Description</i>	<i>Par</i>	<i>Cost</i>	<i>Approximate Market</i>
<b>Industrial and Miscellaneous Bonds</b>			
<i>—Continued</i>			
General Portland Cement Co.			
Conv. Sub. Deb., 5s, 1977 .....	\$ 150,000	\$ 154,500.00	\$ 113,625
Household Finance Corp.,			
Deb., 4% s, 1993 .....	750,000	746,250.00	436,875
Hyston Fibers, Inc.,			
Notes, 5% s, 1986 .....	1,000,000	1,000,000.00	750,000
Instlcorp, Inc.,			
Collat. Tr. Note, A-16, 1991 .....	330,069.29	319,043.82	261,580
Instlcorp, Inc.,			
Collat. Tr. Note, A-19, 1991 .....	276,596.99	267,444.86	218,511
Instlcorp, Inc.,			
Collat. Tr. Note, A-21, 1991 .....	149,021.87	143,806.12	117,354
Instlcorp, Inc.,			
Collat. Tr. Note, A-23, 1991 .....	187,274.30	184,240.54	147,946
Instlcorp, Inc.,			
Collat. Tr. Note, A-36, 1992 .....	602,417.35	577,814.37	456,331
Intl. Harvester Credit Corp.,			
Deb., 4% s, 1979 .....	400,000	398,000.00	275,500
Kaiser Aluminum & Chemical Corp.,			
1st Mtg., 5½ s, 1987 .....	223,000	223,000.00	152,198
Kresge (S. S.) Company,			
Prom. Note, 4% s, 1983 .....	653,333.34	653,333.34	450,800
Montgomery Ward Credit Corp.,			
Deb., 4% s, 1980 .....	200,000	199,000.00	137,000
National Dairy Products Corp.,			
Deb., 2¼ s, 1970 .....	95,000	94,617.50	92,625
Owens-Illinois, Inc.,			
Notes, 5s, 1991 .....	700,000	700,000.00	451,500
Penney (J. C.) Company, Inc.,			
Conv. Sub. Deb., 4¼ s, 1993 .....	2,000,000	2,248,083.75	1,880,000
Sears Roebuck Acceptance Corp.,			
Sub. Deb., 4% s, 1977 .....	525,000	511,505.00	397,688
Shell Oil Company,			
Deb., 5s, 1991 .....	1,000,000	1,000,000.00	690,000
Spiegel, Inc.,			
Deb., 5s, 1987 .....	250,000	250,000.00	157,500
Statewide Stations Inc.,			
Sec. Note, 4% s, 1994 .....	446,000	446,000.00	254,220
Sylvania Electric Products Inc.,			
Demand Note .....	1,035,000	1,035,000.00	1,035,000
Talcott (James) Inc.,			
Senior Note, 5½ s, 1980 .....	215,000	212,850.00	174,150
Texas Gulf Sulphur Co.,			
Prom. Note, 4.7s, 1989 .....	665,000	665,000.00	462,175
Trailer Train Co.,			
4¼ s, 1976 .....	388,254.01	388,254.01	321,280



INVESTMENTS—Continued

<i>Description</i>	<i>Par</i>	<i>Cost</i>	<i>Approximate Market</i>
Industrial and Miscellaneous Bonds —Continued			
Tremarco Corporation, 1st Mtg. Series E, 5s, 1983 .....	\$ 262,000	\$ 262,000.00	\$ 201,740
United Air Lines, Inc., Notes, 5s, 1984 .....	700,000	700,000.00	455,000
United Shoe Machinery Corporation, S. F. Deb., 5¼ s, 1992 .....	680,000	678,300.00	487,050
U. S. Steel, S. F. Sub. Deb., 4¼ s, 1996 .....	542,500	443,873.50	325,500
Woolworth (F. W.) Company, Prom. Note, 5s, 1982 .....	479,913.55	479,913.55	304,745
Total .....	<u>\$24,425,380.70</u>	<u>\$24,534,283.64</u>	<u>\$18,420,434</u>
 Bonds, funds invested .....	 <u>\$39,291,380.70</u>	 <u>\$39,428,846.79</u>	 <u>\$29,002,885</u>
Mortgage			
Alfred D. Hershey and Harriet D. Hershey, 5½ s, 1974 .....	\$ 11,432.64	\$ 11,432.64	\$ 11,433

INVESTMENTS—Continued

<i>Description</i>	<i>Shares</i>	<i>Cost</i>	<i>Approximate Market</i>
<b>Common Stocks</b>			
American Electric Power Co., Inc. . . . .	23,110	\$ 162,703.74	\$ 508,420
American Telephone & Telegraph Company . . .	45,352	1,322,061.49	1,870,770
Armstrong Cork Company . . . . .	32,000	131,908.39	764,000
Avon Products, Inc. . . . .	24,000	1,111,961.35	1,689,000
Caterpillar Tractor Co. . . . .	34,800	601,472.84	1,204,950
Chesebrough-Pond's Inc. . . . .	28,000	911,861.03	997,500
Chicago Pneumatic Tool Co. . . . .	25,500	928,574.31	717,188
Coca-Cola Company (The) . . . . .	39,200	628,984.09	2,719,500
Continental Oil Company (Del.) . . . . .	36,000	146,960.65	765,000
Disney (Walt) Productions . . . . .	7,000	1,060,511.84	821,625
E. I. du Pont de Nemours & Co. . . . .	7,500	874,270.56	854,063
Eastman Kodak Company . . . . .	43,972	443,434.12	2,792,222
Federated Department Stores, Inc. . . . .	24,000	582,805.81	702,000
First National City Corp. . . . .	15,104	348,278.77	944,000
General Electric Company . . . . .	30,627	767,899.37	2,067,323
General Foods Corp. . . . .	13,800	1,210,911.44	1,019,475
General Motors Corporation . . . . .	35,419	1,143,847.99	2,200,405
Gillette Company . . . . .	36,200	1,239,112.08	1,366,550
Goodyear Tire & Rubber Company . . . . .	83,424	1,702,971.74	2,054,316
Gulf Oil Corporation . . . . .	40,012	154,333.51	920,276
Heinz (H. J.) Co. . . . .	33,000	1,144,051.04	1,072,500
International Business Machines Corp. . . . .	31,668	851,095.87	7,917,000
International Nickel Co. of Canada Ltd. . . . .	61,175	1,296,074.87	2,324,650
International Paper Company . . . . .	57,000	2,112,936.24	1,738,500
Johnson & Johnson . . . . .	38,700	750,762.93	1,804,388
Kennecott Copper Corporation . . . . .	53,030	1,550,424.92	2,293,548
Merck & Co., Inc. . . . .	15,000	107,286.55	1,306,875
Minnesota Mining & Manufacturing Co. . . . .	19,000	1,916,654.93	1,434,500
Mobil Oil Corporation . . . . .	30,700	1,099,916.18	1,343,125
National Cash Register Company . . . . .	32,000	2,110,474.17	1,332,000
Polaroid Corporation . . . . .	5,500	694,336.65	291,500
Schlumberger Ltd. . . . .	10,000	954,850.00	638,750
Sears, Roebuck and Co. . . . .	4,600	207,078.03	255,875
Southern Co. . . . .	32,800	878,283.72	631,400
Standard Oil Co. (New Jersey) . . . . .	23,561	671,594.17	1,289,965
TRW Inc. . . . .	44,000	2,214,408.91	1,210,000
Texaco Inc. . . . .	48,380	249,172.89	1,257,880
Texas Utilities Co. . . . .	7,600	104,621.78	388,550
U. S. Plywood-Champion Papers Inc. . . . .	56,800	697,928.16	1,356,100
Virginia Electric Power Co. . . . .	35,999	636,133.86	652,482
Whirlpool Corporation . . . . .	20,000	943,953.26	980,000
Xerox Corp. . . . .	26,100	1,863,165.49	1,905,300
Common stocks, funds invested . . . . .		<u>\$38,530,069.74</u>	<u>\$60,403,471</u>
Aggregate investments . . . . .		<u><u>\$77,970,349.17</u></u>	<u><u>\$89,417,789</u></u>

## SCHEDULE 3

## SUMMARY OF INVESTMENT TRANSACTIONS

FOR THE YEAR ENDED JUNE 30, 1970

Cash, July 1, 1969 ..... \$ 124,491.11

## Sales and Redemptions

	<i>Capital</i>		<i>Book Value</i>
	<i>Gain</i>	<i>Loss</i>	
Bonds .....	\$ 6,232.79	\$ 726,021.30	\$ 7,640,460.53
Mortgage .....	.....	.....	2,550.42
Common stocks .....	1,693,675.46	1,090,656.13	6,574,201.22
	<u>1,699,908.25</u>	<u>1,816,677.43</u>	<u>14,217,212.17</u>
Realized capital loss, net— Statement B .....	116,769.18	.....	(116,769.18)
	<u>\$1,816,677.43</u>	<u>\$1,816,677.43</u>	
Total sales and redemptions .....			14,100,442.99
Income applied to amortization of bond premium .....			4,444.49
Cash transferred to drawing account .....			<u>(770,369.33)</u>
Total .....			13,459,009.26

## Acquisitions

Bonds .....	\$6,057,872.50
Common stocks .....	<u>7,392,568.35</u>
Total acquisitions .....	<u>13,450,440.85</u>

Cash, June 30, 1970 ..... \$ 8,568.41



# *Abstract of Minutes*

## *of the Seventy-Second Meeting of the Board of Trustees*

The annual meeting of the Board of Trustees was held in the Board Room of the Administration Building on Friday, May 1, 1970. Chairman James N. White called the meeting to order.

The following Trustees were present: Sir Eric Ashby, Amory H. Bradford, Vannevar Bush, Michael Ference, Jr., William T. Golden, Crawford H. Greenewalt, Caryl P. Haskins, Alfred L. Loomis, Keith S. McHugh, William McChesney Martin, Jr., Henry S. Morgan, William I. Myers, Garrison Norton, Robert M. Pennoyer, William M. Roth, William W. Rubey, Charles H. Townes, Juan T. Trippe, and James N. White.

The minutes of the Seventy-First Meeting were approved.

Positions as officers of the Board of Trustees, with terms ending in 1973, were filled as follows: Garrison Norton as Vice Chairman, and William McChesney Martin, Jr., as Secretary.

The following were elected for one-year terms: Garrison Norton as Chairman of the Executive Committee, Richard S. Perkins as Chairman of the Finance Committee, Henry S. Morgan as Chairman of the Nominating Committee, Keith S. McHugh as Chairman of the Auditing Committee, and Frank Stanton as Chairman of the Retirement Committee.

Vacancies in standing committees, with terms as indicated in parentheses, were filled as follows: Henry S. Morgan (1973) and Michael Ference, Jr. (1972) were elected members of the Executive Committee; Henry S. Morgan (1971) and Charles H. Townes (1973) were elected members of the Nominating Committee; Alfred L. Loomis (1973), Keith S. McHugh (1973), and Henry S. Morgan (1973) were elected members of the Finance Committee; Keith S. McHugh (1973), Alfred L. Loomis (1973), and Juan T. Trippe (1973) were elected members of the Auditing Committee; and William M. Roth (1971), was elected a member of the Retirement Committee.

The reports of the Executive Committee, the Finance Committee, the Retirement Committee, and the Auditing Committee were accepted. On the recommendation of the latter it was resolved that Lybrand, Ross Bros. and Montgomery be appointed as public accountants for the fiscal year beginning July 1, 1970.

The annual report of the President was accepted.

To provide for the operation of the Institution for the fiscal year beginning July 1, 1970, and upon recommendation of the Executive Committee, the sum of \$5,227,564 was appropriated.



# Articles of Incorporation

Fifty-eighth Congress of the United States of America;

At the Second Session,

Begun and held at the City of Washington on Monday, the seventh day of December, one thousand nine hundred and three.

---

## AN ACT

To incorporate the Carnegie Institution of Washington.

---

*Be it enacted by the Senate and House of Representatives of the United States of America in Congress assembled,* That the persons following, being persons who are now trustees of the Carnegie Institution, namely, Alexander Agassiz, John S. Billings, John L. Cadwalader, Cleveland H. Dodge, William N. Frew, Lyman J. Gage, Daniel C. Gilman, John Hay, Henry L. Higginson, William Wirt Howe, Charles L. Hutchinson, Samuel P. Langley, William Lindsay, Seth Low, Wayne MacVeagh, Darius O. Mills, S. Weir Mitchell, William W. Morrow, Ethan A. Hitchcock, Elihu Root, John C. Spooner, Andrew D. White, Charles D. Walcott, Carroll D. Wright, their associates and successors, duly chosen, are hereby incorporated and declared to be a body corporate by the name of the Carnegie Institution of Washington and by that name shall be known and have perpetual succession, with the powers, limitations, and restrictions herein contained.

SEC. 2. That the objects of the corporation shall be to encourage, in the broadest and most liberal manner, investigation, research, and discovery, and the application of knowledge to the improvement of mankind; and in particular—

(a) To conduct, endow, and assist investigation in any department of science, literature, or art, and to this end to cooperate with governments, universities, colleges, technical schools, learned societies, and individuals.

(b) To appoint committees of experts to direct special lines of research.

(c) To publish and distribute documents.

(d) To conduct lectures, hold meetings, and acquire and maintain a library.

(e) To purchase such property, real or personal, and construct such building or buildings as may be necessary to carry on the work of the corporation.



(f) In general, to do and perform all things necessary to promote the objects of the institution, with full power, however, to the trustees hereinafter appointed and their successors from time to time to modify the conditions and regulations under which the work shall be carried on, so as to secure the application of the funds in the manner best adapted to the conditions of the time, provided that the objects of the corporation shall at all times be among the foregoing or kindred thereto.

SEC. 3. That the direction and management of the affairs of the corporation and the control and disposal of its property and funds shall be vested in a board of trustees, twenty-two in number, to be composed of the following individuals: Alexander Agassiz, John S. Billings, John L. Cadwalader, Cleveland H. Dodge, William N. Frew, Lyman J. Gage, Daniel C. Gilman, John Hay, Henry L. Higginson, William Wirt Howe, Charles L. Hutchinson, Samuel P. Langley, William Lindsay, Seth Low, Wayne MacVeagh, Darius O. Mills, S. Weir Mitchell, William W. Morrow, Ethan A. Hitchcock, Elihu Root, John C. Spooner, Andrew D. White, Charles D. Walcott, Carroll D. Wright, who shall constitute the first board of trustees. The board of trustees shall have power from time to time to increase its membership to not more than twenty-seven members. Vacancies occasioned by death, resignation, or otherwise shall be filled by the remaining trustees in such manner as the by-laws shall prescribe; and the persons so elected shall thereupon become trustees and also members of the said corporation. The principal place of business of the said corporation shall be the city of Washington, in the District of Columbia.

SEC. 4. That such board of trustees shall be entitled to take, hold and administer the securities, funds, and property so transferred by said Andrew Carnegie to the trustees of the Carnegie Institution and such other funds or property as may at any time be given, devised, or bequeathed to them, or to such corporation, for the purposes of the trust; and with full power from time to time to adopt a common seal, to appoint such officers, members of the board of trustees or otherwise, and such employees as may be deemed necessary in carrying on the business of the corporation, at such salaries or with such remuneration as they may deem proper; and with full power to adopt by-laws from time to time and such rules or regulations as may be necessary to secure the safe and convenient transaction of the business of the corporation; and with full power and discretion to deal with and expend the income of the corporation in such manner as in their judgment will best promote the objects herein set forth and in general to have and use all powers and authority necessary to promote such objects and carry out the purposes of the donor. The said trustees shall have further power from time

to time to hold as investments the securities hereinabove referred to so transferred by Andrew Carnegie, and any property which has been or may be transferred to them or such corporation by Andrew Carnegie or by any other person, persons, or corporation, and to invest any sums or amounts from time to time in such securities and in such form and manner as are permitted to trustees or to charitable or literary corporations for investment, according to the laws of the States of New York, Pennsylvania, or Massachusetts, or in such securities as are authorized for investment by the said deed of trust so executed by Andrew Carnegie, or by any deed of gift or last will and testament to be hereafter made or executed.

SEC. 5. That the said corporation may take and hold any additional donations, grants, devises, or bequests which may be made in further support of the purposes of the said corporation, and may include in the expenses thereof the personal expenses which the trustees may incur in attending meetings or otherwise in carrying out the business of the trust, but the services of the trustees as such shall be gratuitous.

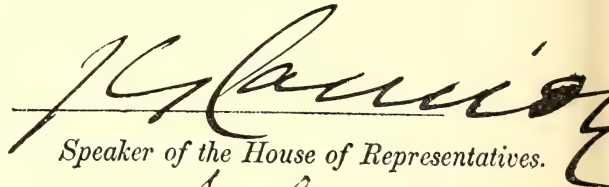
SEC. 6. That as soon as may be possible after the passage of this Act a meeting of the trustees hereinbefore named shall be called by Daniel C. Gilman, John S. Billings, Charles D. Walcott, S. Weir Mitchell, John Hay, Elihu Root, and Carroll D. Wright, or any four of them, at the city of Washington, in the District of Columbia, by notice served in person or by mail addressed to each trustee at his place of residence; and the said trustees, or a majority thereof, being assembled, shall organize and proceed to adopt by-laws, to elect officers and appoint committees, and generally to organize the said corporation; and said trustees herein named, on behalf of the corporation hereby incorporated, shall thereupon receive, take over, and enter into possession, custody, and management of all property, real or personal, of the corporation heretofore known as the Carnegie Institution, incorporated, as hereinbefore set forth under "An Act to establish a Code of Law for the District of Columbia, January fourth, nineteen hundred and two," and to all its rights, contracts, claims, and property of any kind or nature; and the several officers of such corporation, or any other person having charge of any of the securities, funds, real or personal, books or property thereof, shall, on demand, deliver the same to the said trustees appointed by this Act or to the persons appointed by them to receive the same; and the trustees of the existing corporation and the trustees herein named shall and may take such other steps as shall be necessary to carry out the purposes of this Act.

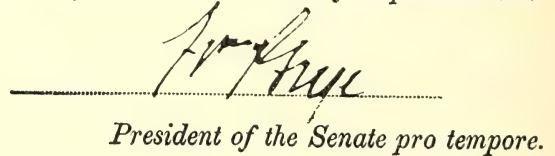
SEC. 7. That the rights of the creditors of the said existing corporation known as the Carnegie Institution shall not in any manner be impaired by the

passage of this Act, or the transfer of the property hereinbefore mentioned, nor shall any liability or obligation for the payment of any sums due or to become due, or any claim or demand, in any manner or for any cause existing against the said existing corporation, be released or impaired; but such corporation hereby incorporated is declared to succeed to the obligations and liabilities and to be held liable to pay and discharge all of the debts, liabilities, and contracts of the said corporation so existing to the same effect as if such new corporation had itself incurred the obligation or liability to pay such debt or damages, and no such action or proceeding before any court or tribunal shall be deemed to have abated or been discontinued by reason of the passage of this Act.

SEC. 8. That Congress may from time to time alter, repeal, or modify this Act of incorporation, but no contract or individual right made or acquired shall thereby be divested or impaired.

SEC. 9. That this Act shall take effect immediately.

  
Speaker of the House of Representatives.

  
President of the Senate pro tempore.

Approved.

April 28, 1904.

Theodore Roosevelt



# By-Laws of the Institution

*Adopted December 13, 1904. Amended December 13, 1910, December 13, 1912, December 10 1937, December 15, 1939, December 13, 1940, December 18, 1942, December 12, 1947, December 10, 1954, October 24, 1957, May 8, 1959, May 13, 1960, May 10, 1963, May 15, 1964, March 6, 1967, and May 3, 1968.*

## ARTICLE I

### *The Trustees*

1. The Board of Trustees shall consist of twenty-four members with power to increase its membership to not more than twenty-seven members. The Trustees shall hold office continuously and not for a stated term.

2. In case any Trustee shall fail to attend three successive annual meetings of the Board he shall thereupon cease to be a Trustee.

3. No Trustee shall receive any compensation for his services as such.

4. All vacancies in the Board of Trustees shall be filled by the Trustees by ballot at an annual meeting, but no person shall be declared elected unless he receives the votes of two-thirds of the Trustees present.

5. If, at any time during an emergency period, there be no surviving Trustee capable of acting, the President, the Director of each existing Department, and the Executive Officer, or such of them as shall then be surviving and capable of acting, shall constitute a Board of Trustees *pro tem*, with full powers under the provisions of the Articles of Incorporation and these By-Laws. Should neither the President, nor any such Director, nor the Executive Officer be capable of acting, the senior surviving Staff Member of each existing Department shall be a Trustee *pro tem* with full powers of a Trustee under the Articles of Incorporation and these By-Laws. It shall be incumbent on the Trustees *pro tem* to reconstitute the Board with permanent members within a reasonable time after the emergency has passed, at which time the Trustees *pro tem* shall cease to hold office. A list of Staff Member seniority, as designated annually by the President, shall be kept in the Institution's records.

## ARTICLE II

### *Officers of the Board*

1. The officers of the Board shall be a Chairman of the Board, a Vice-Chairman, and a Secretary, who shall be elected by the Trustees, from the members of the Board, by ballot to serve for a term of three years. All vacancies shall be filled by the Board for the unexpired term; provided, however, that the Executive Committee shall have power to fill a vacancy in the office of Secretary to serve until the next meeting of the Board of Trustees.

2. The Chairman shall preside at all meetings and shall have the usual powers of a presiding officer.

3. The Vice-Chairman, in the absence or disability of the Chairman, shall perform the duties of the Chairman.

4. The Secretary shall issue notices of meetings of the Board, record its transactions, and conduct that part of the correspondence relating to the Board and to his duties.

#### ARTICLE III

##### *Executive Administration*

##### *The President*

1. There shall be a President who shall be elected by ballot by, and hold office during the pleasure of, the Board, who shall be the chief executive officer of the Institution. The President, subject to the control of the Board and the Executive Committee, shall have general charge of all matters of administration and supervision of all arrangements for research and other work undertaken by the Institution or with its funds. He shall prepare and submit to the Board of Trustees and to the Executive Committee plans and suggestions for the work of the Institution, shall conduct its general correspondence and the correspondence with applicants for grants and with the special advisers of the Committee, and shall present his recommendations in each case to the Executive Committee for decision. All proposals and requests for grants shall be referred to the President for consideration and report. He shall have power to remove, appoint, and, within the scope of funds made available by the Trustees, provide for compensation of subordinate employees and to fix the compensation of such employees within the limits of a maximum rate of compensation to be established from time to time by the Executive Committee. He shall be *ex officio* a member of the Executive Committee.

2. He shall be the legal custodian of the seal and of all property of the Institution whose custody is not otherwise provided for. He shall sign and execute on behalf of the corporation all contracts and instruments necessary in authorized administrative and research matters and affix the corporate seal thereto when necessary, and may delegate the performance of such acts and other administrative duties in his absence to the Executive Officer. He may execute all other contracts, deeds, and instruments on behalf of the corporation and affix the seal thereto when expressly authorized by the Board of Trustees or Executive Committee. He may, within the limits of his own authorization, delegate to the Executive Officer authority to act as custodian of and affix the corporate seal. He shall be responsible for the expenditure and disbursement of all funds of the Institution in accordance with the directions of the Board and of the Executive Committee, and shall keep accurate accounts of all receipts and disbursements. Following approval by the Executive Committee he shall transmit to the Board of Trustees before its annual meeting a written report of the operations and business of the Institution for the preceding fiscal year with his recommendations for work and appropriations for the succeeding fiscal year.

3. He shall attend all meetings of the Board of Trustees.

4. There shall be an officer designated Executive Officer who shall be appointed by and hold office at the pleasure of the President, subject to the approval of the Executive Committee. His duties shall be to assist and act for the President as the latter may duly authorize and direct.

5. The President shall retire from office at the end of the fiscal year in which he becomes sixty-five years of age.

#### ARTICLE IV

##### *Meetings and Voting*

1. The annual meeting of the Board of Trustees shall be held in the City of Washington, in the District of Columbia, in May of each year on a date fixed by the Executive

Committee, or at such other time or such other place as may be designated by the Executive Committee, or if not so designated prior to May 1 of such year, by the Chairman of the Board of Trustees, or if he is absent or is unable or refuses to act, by any Trustee with the written consent of the majority of the Trustees then holding office.

2. Special meetings of the Board of Trustees may be called, and the time and place of meeting designated, by the Chairman, or by the Executive Committee, or by any Trustee with the written consent of the majority of the Trustees then holding office. Upon the written request of seven members of the Board, the Chairman shall call a special meeting.

3. Notices of meetings shall be given ten days prior to the date thereof. Notice may be given to any Trustee personally, or by mail or by telegram sent to the usual address of such Trustee. Notices of adjourned meetings need not be given except when the adjournment is for ten days or more.

4. The presence of a majority of the Trustees holding office shall constitute a quorum for the transaction of business at any meeting. An act of the majority of the Trustees present at a meeting at which a quorum is present shall be the act of the Board except as otherwise provided in these By-Laws. If, at a duly called meeting, less than a quorum is present, a majority of those present may adjourn the meeting from time to time until a quorum is present. Trustees present at a duly called or held meeting at which a quorum is present may continue to do business until adjournment notwithstanding the withdrawal of enough Trustees to leave less than a quorum.

5. The transactions of any meeting, however called and noticed, shall be as valid as though carried out at a meeting duly held after regular call and notice, if a quorum is present and if, either before or after the meeting, each of the Trustees not present in person signs a written waiver of notice, or consent to the holding of such meeting, or approval of the minutes thereof. All such waivers, consents, or approvals shall be filed with the corporate records or made a part of the minutes of the meeting.

6. Any action which, under law or these By-Laws, is authorized to be taken at a meeting of the Board of Trustees may be taken without a meeting if authorized in a document or documents in writing signed by all the Trustees then holding office and filed with the Secretary.

7. During an emergency period the term "Trustees holding office" shall, for purposes of this Article, mean the surviving members of the Board who have not been rendered incapable of acting for any reason including difficulty of transportation to a place of meeting or of communication with other surviving members of the Board.

## ARTICLE V

### *Committees*

1. There shall be the following Standing Committees, *viz.* an Executive Committee, a Finance Committee, an Auditing Committee, a Nominating Committee, and a Retirement Committee.

2. All vacancies in the Standing Committees shall be filled by the Board of Trustees at the next annual meeting of the Board and may be filled at a special meeting of the Board. A vacancy in the Executive Committee and, upon request of the remaining members of any other Standing Committee, a vacancy in such other Committee may be filled by the Executive Committee by temporary appointment to serve until the next meeting of the Board.

3. The terms of all officers and of all members of Committees, as provided for herein, shall continue until their successors are elected or appointed.

### *Executive Committee*

4. The Executive Committee shall consist of the Chairman, Vice-Chairman, and Secretary of the Board of Trustees, the President of the Institution *ex officio*, and, in



addition, not less than five or more than eight Trustees to be elected by the Board by ballot for a term of three years, who shall be eligible for re-election. Any member elected to fill a vacancy shall serve for the remainder of his predecessor's term.

5. The Executive Committee shall, when the Board is not in session and has not given specific directions, have general control of the administration of the affairs of the corporation and general supervision of all arrangements for administration, research, and other matters undertaken or promoted by the Institution. It shall also submit to the Board of Trustees a printed or typewritten report of each of its meetings, and at the annual meeting shall submit to the Board a report for publication.

6. The Executive Committee shall have power to authorize the purchase, sale, exchange, or transfer of real estate.

#### *Finance Committee*

7. The Finance Committee shall consist of not less than five and not more than six members to be elected by the Board of Trustees by ballot for a term of three years, who shall be eligible for re-election.

8. The Finance Committee shall have custody of the securities of the corporation and general charge of its investments and invested funds, including its investments and invested funds as trustee of any retirement plan for the Institution's staff members and employees, and shall care for and dispose of the same subject to the directions of the Board of Trustees. It shall have power to authorize the purchase, sale, exchange, or transfer of securities and to delegate this power. It shall consider and recommend to the Board from time to time such measures as in its opinion will promote the financial interests of the Institution and of the trust fund under any retirement plan for the Institution's staff members and employees, and shall make a report at each meeting of the Board.

#### *Auditing Committee*

9. The Auditing Committee shall consist of three members to be elected by the Board of Trustees by ballot for a term of three years.

10. Before each annual meeting of the Board of Trustees, the Auditing Committee shall cause the accounts of the Institution for the preceding fiscal year to be audited by public accountants. The accountants shall report to the Committee, and the Committee shall present said report at the ensuing annual meeting of the Board with such recommendations as the Committee may deem appropriate.

#### *Nominating Committee*

11. The Nominating Committee shall consist of the Chairman of the Board of Trustees *ex officio* and, in addition, three Trustees to be elected by the Board by ballot for a term of three years, who shall not be eligible for re-election until after the lapse of one year. Any member elected to fill a vacancy shall serve for the remainder of his predecessor's term, provided that of the Nominating Committee first elected after adoption of this By-Law one member shall serve for one year, one member shall serve for two years, and one member shall serve for three years, the Committee to determine the respective terms by lot.

12. Sixty days prior to an annual meeting of the Board the Nominating Committee shall notify the Trustees by mail of the vacancies to be filled in membership of the Board. Each Trustee may submit nominations for such vacancies. Nominations so submitted shall be considered by the Nominating Committee, and ten days prior to the annual meeting the Nominating Committee shall submit to members of the Board by mail a list of the persons so nominated, with its recommendations for filling existing vacancies on the Board and its Standing Committees. No other nominations shall be received by the Board at the annual meeting except with the unanimous consent of the Trustees present.

*Retirement Committee*

13. The Retirement Committee shall consist of three members to be elected by the Board of Trustees by ballot for a term of three years, who shall be eligible for re-election and the Chairman of the Finance Committee *ex officio*. Any member elected to fill a vacancy shall serve for the remainder of his predecessor's term.

14. The Retirement Committee shall, subject to the directions of the Board of Trustees, be responsible for the maintenance of a retirement plan for staff members and employees of the Institution and act for the Institution in its capacity as trustee under any such plan, except that any matter relating to investments under any such plan shall be the responsibility of the Finance Committee subject to the directions of the Board of Trustees. The Committee shall submit a report to the Board at the annual meeting of the Board.

## ARTICLE VI

*Financial Administration*

1. No expenditure shall be authorized or made except in pursuance of a previous appropriation by the Board of Trustees, or as provided in Article V, paragraph 8, hereof.

2. The fiscal year of the Institution shall commence on the first day of July in each year.

3. The Executive Committee shall submit to the annual meeting of the Board a full statement of the finances and work of the Institution for the preceding fiscal year and a detailed estimate of the expenditures of the succeeding fiscal year.

4. The Board of Trustees, at the annual meeting in each year, shall make general appropriations for the ensuing fiscal year; but nothing contained herein shall prevent the Board of Trustees from making special appropriations at any meeting.

5. The Executive Committee shall have general charge and control of all appropriations made by the Board. Following the annual meeting, the Executive Committee may allocate these appropriations for the succeeding fiscal year. The Committee shall have full authority to reallocate available funds, as needed, and to transfer balances.

6. The securities of the Institution and evidences of property, and funds invested and to be invested, shall be deposited in such safe depository or in the custody of such trust company and under such safeguards as the Finance Committee shall designate, subject to directions of the Board of Trustees. Income of the Institution available for expenditure shall be deposited in such banks or depositories as may from time to time be designated by the Executive Committee.

7. Any trust company entrusted with the custody of securities by the Finance Committee may, by resolution of the Board of Trustees, be made Fiscal Agent of the Institution, upon an agreed compensation, for the transaction of the business coming within the authority of the Finance Committee.

8. The property of the Institution is irrevocably dedicated to charitable purposes, and in the event of dissolution its property shall be used for and distributed to those charitable purposes as are specified by the Congress of the United States in the Articles of Incorporation, Public Law No. 260, approved April 28, 1904, as the same may be amended from time to time.

## ARTICLE VII

*Amendment of By-Laws*

1. These By-Laws may be amended at any annual or special meeting of the Board of Trustees by a two-thirds vote of the members present, provided written notice of the proposed amendment shall have been served personally upon, or mailed to the usual address of, each member of the Board twenty days prior to the meeting.





# Index of Names

- Abbott, J. E., 608, 614  
 Abbott, M. J., 189, 348  
 Abelson, P. H., vii, 43, 44, 140, 141, 344, 359  
   report of Director of Geophysical Laboratory,  
     129-360  
   studies, 327-334  
 Ackerman, Edward A., ix  
 Adams, L. H., 143, 348  
 Ade-Hall, J. M., 259, 348  
 Adelman, Saul J., 65, 89  
   publications, 128  
 Adesnik, M., 544  
 Adkins, John, 128  
 Adkison, Bruce, 121, 122, 130  
 Agassiz, Alexander, x, 745, 746  
 Agrell, S. O., 348  
 Aki, K., 439, 440, 460, 542, 543  
 Akimoto, S., 177, 202, 206, 243, 283, 348  
 Albee, A. L., 282, 290, 292, 348  
 Aldrich, L. T., vii, 363, 383, 547  
   publications, 545  
   studies, 384-385, 470-471  
 Allen, P., 301, 348  
 Aller, Lawrence J., 110  
 Allmann, R., 344, 346  
 Alterman, Z., 452, 543  
 Althaus, E., 193, 348  
 Altschuler, Martin, 78  
 Amelunxen, F., 695, 699  
 Ames, J., 696, 698, 699  
   publications, 710  
 Anderson, A. T., Jr., 152, 348  
   publications, 346  
 Anderson, Christopher M., 122  
 Anderson, Norman, 704, 710  
 Anhaeusser, C. R., 405, 540  
 Archambeau, C. B., 439, 440, 442, 542  
 Armstrong, R. L., 403, 540  
 Arnold, William, 710  
 Arp, Halton, vii, 64, 97, 101, 108, 110  
   publications, 123  
 Ashby, Eric S., v, vi, 2, 743  
 Assousa, G. E., 367, 383, 538, 548  
   publications, 545  
   studies, 377-382  
 Attardi, C., 544  
 Aumento, F., 260, 262, 348, 539  
 Avery, R. J., 471, 544, 548  
   studies, 521-528, 528-536  
 Azzi, J. R., 707, 708  
  
 Baade, Walter, 7, 31, 75, 93, 95  
 Babcock, Horace W., vii, 31, 61, 64, 121, 127  
   report of Director of Hale Observatories,  
     71-130  
 Bagnuolo, W. G., 65, 128  
  
 Bahcall, John N., 65, 108, 128  
   publications, 122  
 Bailey, D. K., 145, 160, 171, 172, 348  
 Bailey, E. H., 394, 539  
 Bailey, J. C., 217, 267, 348  
 Baker, P. E., 254, 256, 348  
 Bakos, J., 538  
 Baldwin, George J., x  
 Bancroft, G. M., 190, 348  
 Banerjee, S. K., 283, 356  
 Bannister, J., 383, 548  
   studies, 470-471  
 Barr, L., 598  
 Barreda R., Willy Z., 548  
 Barron, L. M., 302, 348  
 Barton, P. B., Jr., 326, 358  
 Bashkin, Stanley, 377  
 Baski, A. K., 260, 359  
 Bassett, W. A., 326, 348  
 Baum, W. A., 553  
   publications, 545  
 Bautz, E. K., 489, 544  
 Beach, L., 547, 549  
 Beatty, L. B., 350  
 Becker, W. M., 508, 544  
 Becklin, E. E., 110  
   publications, 122  
 Bell, James F., x  
 Bell, P. M., vii, 43, 45, 55, 57, 136, 139, 140,  
   169, 170, 172, 208, 209, 323, 325, 326, 345,  
   348, 349, 359  
   publications, 346  
   studies, 168-170, 193-194, 194-195, 207-216,  
     228-229  
 Bell, R. A., 86, 87  
 Bence, A. E., 217, 225, 227, 272, 349, 393, 539  
 Ben-Menahem, A., 439, 440, 542  
 Bennett, W. R., Jr., 538  
 Berckhemer, H., 440, 542  
 Bergh, Sidney van den, 115, 116  
   publications, 122  
 Bernardi, G., 508, 544  
 Berner, R. A., 318, 319, 349  
 Bertola, F., 97, 110, 545  
   publications, 123  
 Berry, J. A., 49, 624, 632, 635, 636, 637, 639,  
   650, 651, 652, 653, 655, 713  
   studies, 649-655  
 Bertsch, W., 707, 708  
 Bhatnagar, A., 65, 78, 79, 128  
   publications, 123  
 Bidwell, R. G. S., 636, 639  
 Bieging, J. H., 65, 128  
 Bierhuizen, J. F., 643, 648  
 Biggar, G. M., 245, 356  
 Billings, John S., x, 745, 746, 747

- Billings, M. P., 290, 291, 349  
 Birch, F., 208, 349, 452, 543  
 Bird, M., 360  
 Birle, J. D., 302, 303, 349  
 Bisalputra, T., 632, 654, 655  
 Bishop, Norman I., 706  
 Björkman, Olle, viii, 46, 47, 48, 49, 622, 624, 629, 632, 633, 635, 639, 641, 642, 643, 648, 650, 651, 655, 656, 660, 661, 662, 709, 711, 713  
     publications, 710  
     studies, 625-629, 632-639, 640-648  
 Björn, Lars, 711, 713  
 Blasse, G., 283, 349  
 Blinks, Lawrence R., 710  
 Bliss, Robert Woods, x  
 Block, S., 450, 451, 452, 460, 463, 543  
 Boettcher, A. L., 169, 349  
 Bohlin, J. David, 65, 78, 128  
     publications, 123  
 Boise, James W., ix  
 Bolfa, J., 283, 350  
 Bollinger, G. A., 438, 542  
 Bolt, B. A., 419, 421, 424, 425, 467, 542  
 Bolton, E. T., vii, 59, 471, 509, 544, 547  
     report of Director of Department of Terrestrial Magnetism, 363-550  
 Bonnichsen, Bill, 288, 349  
 Boore, D., 462, 464, 543  
 Böving, B. G., viii, 564, 613  
     publications, 611  
     studies, 601-603  
 Bowen, Ira S., 65, 119, 120, 128, 556  
     publications, 123  
 Bowen, N. L., 142, 143, 148, 150, 156, 158, 171, 182, 276, 288, 349  
 Bowie, S. H. V., 242, 357  
 Bown, M. G., 288, 349  
 Boyd, F. R., vii, 43, 44, 55, 136, 148, 149, 150, 152, 156, 171, 172, 174, 187, 195, 208, 225, 250, 289, 290, 324, 326, 345, 348, 349, 359  
     publications, 346, 347  
     studies, 216-228, 294  
 Boyden, J. E., 128  
 Boynton, John, 623, 629, 709, 713  
 Bracewell, R. M., 431, 432, 542  
 Bradford, Amory H., v, vi, 743  
 Bradford, Lindsay, x  
 Bradley, Montgomery, ix  
 Bradley, Omar N., x  
 Braly, Kenneth A., 65, 128  
 Branch, David R., 65, 86, 87, 128  
 Brandt, Werner, 382, 538  
 Braxton, H., 344  
 Braun, R., 518, 544  
 Breger, M., 111  
 Brenner, D. J., 509, 544, 548  
 Brett, P. R., 346  
 Brežný, B., 197, 349  
 Bridgman, P. W., 208, 349  
 Briggs, Winslow R., 710  
 Bright, N. F. H., 200, 203, 207, 358  
 Britten, R. J., vii, 32, 33, 35, 36, 471, 472, 477, 482, 484, 543, 547  
     publications, 545  
     studies, 501-503, 503-506, 506-507, 520-521  
 Brock, M. A., 563  
     studies, 600-601  
 Brockway, L. O., 308, 356  
 Brody, S. S., 703, 704  
 Brookings, Robert S., x  
 Brooks, C., 383, 548  
     publications, 545  
     studies, 400-405  
 Brown, D. D., viii, 36, 37, 38, 39, 561, 562, 563, 564, 566, 613  
     publications, 611, 612  
     studies, 565-566, 566, 567  
 Brown, G. M., 225, 269, 283, 289, 290, 305, 349  
     publications, 346  
 Brown, J. S., viii, 58, 620, 621, 622, 667, 673, 682, 690, 708, 709, 710, 711, 712  
     publications, 710  
     studies, 662-670, 704-706, 706-708  
 Brown, L., vii, 367, 383, 538, 547  
     publications, 545  
     studies, 370-371, 377-382, 382-383  
 Brueckel, F. J., 128  
 Brune, J. N., 454, 455, 460, 461, 462, 463, 543  
 Bryan, R. F., 344  
 Bryan, W. B., 43, 45, 136, 138, 218, 229, 252, 253, 255, 257, 285, 302, 345, 349, 359, 390, 539  
     studies, 238-243, 245-249, 258-259  
 Buchwald, M., 544  
 Buddington, A. F., 148, 198, 202, 231, 278, 281, 349  
 Buhl, David, 14  
 Bull, T. A., 639  
 Bullen, K. E., 413, 422, 542  
 Bumba, V., 79  
 Bunch, T. E., 248, 346, 348, 349  
 Bunsen, R. W., 349  
 Burbidge, G. R., 123  
 Burd, S., 128  
 Burdick, C. L., 315  
 Burges, N. A., 336, 349  
 Burgi, Elizabeth, viii, 722  
 Burn, J. H., 518, 544  
 Burnham, C. W., 191, 192, 193, 303, 307, 319, 324, 350  
     publications, 347  
 Burns, R. G., 190, 302, 305, 348, 350  
 Burrhus, K., 549  
     studies, 384-385, 385-386  
 Buseck, P. R., 231, 350  
 Bush, Vannevar, v, x, 710, 743  
 Butcher, Harvey, 65, 128  
 Butler, P., 288, 331, 350  
 Byers, Michael, 548  
 Cabre, R., 383, 548  
 Cadwalader, John L., x, 745, 746  
 Cameron, A. E., 350, 386, 539

- Cameron, E. N., 156, 225, 230, 231, 342, 348, 350  
     publications, 346  
 Cameron, K. L., 349, 360  
 Cameron, Maryellen, 360  
 Campbell, William W., x  
 Canter, Dorothy, 548  
 Carmichael, C. M., 189, 190, 198, 203, 204, 263,  
     280, 281, 283, 285, 350  
 Carmichael, I. S. E., 350  
 Carnegie, Andrew, 584, 747  
 Caron, L. G., 304, 350  
 Carr, J. M., 224, 350  
 Carruthers, Lucy M., 79, 128  
 Carstanjen, Heinz-Dieter, 382, 548  
 Carty, John J., x  
 Casaverde, M., 383, 547  
     publications, 545  
     studies, 470-471  
 Cassie, R. M., 45, 138, 359  
     studies, 170-175  
 Catanzaro, E. J., 386, 387, 406, 539, 541  
 Cendella, A., 639  
 Chadwick, José, 548  
 Champe, Sewell, 528, 548  
 Champness, P. E., 348  
 Chapman, D. R., 255, 256, 350  
 Chase, J., 564, 613  
     studies, 575-576, 578-580  
 Chase, S., Jr., 123  
 Chayes, F., vii, 45, 137, 145, 250, 290, 294, 299,  
     300, 301, 345, 350, 359  
     publications, 347  
     studies, 295-301  
 Chevalier, R. A., 123  
 Chevallier, R., 283, 350  
 Chinner, G. A., 177, 178, 187, 188, 290, 292, 350  
 Chiscon, J. A., 33, 35, 548  
     studies, 488-501  
 Chisholm, J. E., 188, 189, 358  
 Chow, T. J., 406, 541  
 Christensen, C. G., 65, 128  
 Clardy, K. D., 128  
 Clark, A. H., 318, 350  
 Clark, J. R., 164, 227, 350  
 Clausen, Jens C., 60, 709, 713  
     publications, 710  
 Clayton, R. N., 261, 355  
 Cleary, W. J., 608  
 Clements, F. E., 625, 626, 629, 648  
 Coes, L., Jr., 156, 157, 350  
 Cohen, G. H., 344  
 Cohen, Judith G., 65, 84, 87, 128  
     publications, 123  
 Cole, Whiteford R., x  
 Coleman, R. G., 164, 171, 350  
 Compston W., 386, 387, 539  
 Coombs, D. S., 259, 350  
 Coon, H. G., 612  
 Cooper, J. A., 406, 541  
 Corner, George, 609  
 Courtes, G., 111  
 Cowie, D. B., vii, 35, 471, 509, 545, 547  
     studies, 528-536  
 Cowley, J. P., 128  
 Cragg, T. A., 128  
 Craig, J. R., 246, 347, 350  
 Crewe, A. V., 348  
 Cromer, D. T., 303, 319, 350  
 Cronin, J., 66, 128  
 Cruickshank, D. W. J., 344  
 Cuzzi, A. P., 82  
 Czyzak, S. J., 548  
 Daillie, J., 614  
 Dallwitz, M. J., 386  
 Damon, P. E., 148, 350  
 Dasch, E. J., 541  
 Davidon, W. C., 191, 351  
 Davidson, E. H., 32, 506, 544, 548  
     publications, 545  
 Davies, D. R., 309, 344  
 Davis, B. T. C., 348  
 Davis, G. L., vii, 140, 149, 172, 174, 359, 383  
     publications, 545  
     studies, 337-339, 339-341, 386-388, 394-400,  
     400-405, 408-412, 412-413  
 Davis, T. E., 545  
 Dawid, I. B., viii, 36, 37, 38, 561, 562, 564, 613  
     publications, 612  
     studies, 566, 575-576, 576  
 Deer, W. A., 223, 231, 236, 241, 351  
 Defay, R., 200, 356  
 Defouw, Richard J., 65, 128  
     publications, 123  
 DeHaan, R. L., viii, 563, 564, 589, 591, 592, 594,  
     595, 596, 597, 599, 613  
     publications, 612  
     studies, 589-600  
 Deharveng, J. M., 111  
 Delano, Frederic A., x  
 Dence, M. R., 348  
 Denis, A. J. Desequelles, 538  
 Dennison, Edwin W., vii, 64, 127  
     publications, 123  
 Deutsch, Armin J., 60, 111, 113, 518, 544  
     publications, 123  
 Dewey, M. M., 598  
 Dickey, J. S., 346  
 Dickinson, W. R., 402, 540  
 Dietz, L. A., 384, 538  
 Doak, John B., 549  
 Dodd, R. T., 159, 351  
 Dodge, Cleveland H., x, 745, 746  
 Dodge, William E., x  
 D'Odorico, S., 370, 548  
     publications, 545  
     studies, 367-370  
 Doe, B. R., 541  
 Doi, R. H., 544  
 Donnay, G., vii, 61, 139, 310, 313, 344, 345, 351,  
     359  
     publications, 347  
     studies, 306-309, 309-311, 311, 313, 314



- Donnay, J. D. H., 308, 310, 360  
 Donner, M. W., 546, 614  
   studies, 603-609  
 Dorman, L. M., 54, 383, 548  
   publications, 545, 546  
   studies, 426-430  
 Douglas, J. A. V., 348  
 Downton, W. J. S., 629, 632, 639, 649, 650, 651,  
   654, 655  
 Dowty, Eric, 360  
   studies, 190-193  
 Duggal, S. P., 546  
 Duncumb, P., 294, 351  
 Dunham, A. C., 348  
 Dunning, J. O., 564, 589, 591, 613  
   studies, 589-600  
 Dutta, S., 548  
 Duysens, L. N. M., 696, 699, 703, 704  
 Dziewonski, A., 450, 463, 543
- Eade, K. E., 408, 541  
 Eakin, E. A., 611  
 Ebert, J. D., viii, 36, 38, 564, 583, 613  
   publications, 612  
   report of Director of Department of Embry-  
     ology, 557-614  
   studies, 580-586, 587  
 Eckermann, H. von, 152, 351  
 Ecklund, E. T., 549  
   studies, 371-377  
 Edgar, A. D., 173, 174, 175, 355  
 Edsall, J. T., 640  
 Edwards, G. E., 651, 655  
 Eggen, Olin J., 83  
   publications, 123  
 Elftmann, A. H., 152, 351  
 El Goresy, A., 230, 242, 311, 351  
   publications, 346  
 Eliseev, E. N., 303, 351  
 Ellis, J. H., 315  
 Elmore, P. L. D., 284  
 El-Sharkaway, M. A., 639  
 Emerson, M. E., 156, 350  
 Emslie, R. F., 148, 151, 154, 155, 351, 360  
   studies, 148-155  
 Engdahl, E. R., 414, 419, 542  
 Engel, A. E. J., 388, 393, 401, 539  
 England, J. L., vii, 55, 148, 149, 152, 160, 171,  
   172, 174, 187, 195, 208, 209, 323, 324, 325,  
   326, 348, 349, 359  
 Enns, T., 634, 639  
 Erkes, J. W., 367, 383, 548  
   publications, 546  
   studies, 371-377  
 Ernst, K. G., 398, 540  
 Ernst, W. G., 189, 351, 394, 539  
 Espenshade, G. H., 290, 351  
 Essene, E., 245, 356  
 Esson, J., 348  
 Evans, B. W., 351  
 Evans, H. T., Jr., 216, 222, 225, 232, 265, 274,  
   275, 318, 344, 351
- Evans, T. E., 518, 521  
 Everson, R. G., 634, 639  
 Everton, D., 54, 383, 438, 548  
   publications, 546  
   studies, 426-430  
 Ewart, A., 256, 257, 349, 351  
   studies, 249-258
- Faber, Sandra M., 548, 578  
 Fairall, A. P., 111  
   publications, 123  
 Fairbairn, H. W., 351  
 Falkow, S., 538, 545, 548  
 Fambrough, D. M., viii, 562, 564, 613  
   publications, 612  
   studies, 587-589  
 Fawcett, J. J., 177, 180, 351  
 Felten, James E., 123  
 Fenner, Charles P., x  
 Ference, Michael, Jr., v, vi, 743  
 Ferguson, Homer L., x  
 Finger, L. W., vii, 136, 139, 193, 202, 204, 206,  
   250, 283, 290, 303, 344, 351, 359  
   publications, 347  
   studies, 294, 302-305, 305-306, 318-322  
 Fisher, G. W., 302, 351  
 Flamm, W. G., 475, 478, 543  
 Flexner, J. B., 515, 516, 544, 548  
   publications, 546  
 Flexner, L. B., 515, 516, 544, 548, 613  
   publications, 546  
 Flexner, Simon, x  
 Forbes, W. Cameron, x  
 Forbush, S. E., 383  
   publications, 546, 547  
 Ford, W. K., Jr., vii, 61, 368, 383, 538, 547  
   publications, 546  
   studies, 367-370, 370-371, 377-382  
 Fork, David C., 620, 621, 690, 693, 694, 696,  
   698, 709, 710, 711, 712  
   publications, 710  
   studies, 682-690, 690-694, 695-699  
 Forrestal, James, x  
 Foster, D. M., 156, 356  
 Foster, M. R., 427, 542  
 Foukal, Peter, 65, 80, 128  
 Frankel, J. J., 231, 351  
 Frarey, M. J., 351  
   studies, 337-339  
 Frazier, Edward N., 123  
 Freeman, Kenneth C., 123  
 French, C. S., viii, 58, 670, 678, 709, 710, 711, 712  
   publications, 710  
   report of Director of Department of Plant  
     Biology, 617-713  
   studies, 662-670, 670-678  
 Freud, P. J., 208, 351  
 Frew, William N., x, 745, 746  
 Frey, F., 392, 539  
 Frey, M., 290, 352  
 Friedman, G., 327

- Frogel, J. A., 66, 90, 128  
     publications, 122  
 Frondel, C., 156, 159, 352  
 Fuchs, E., 545  
 Fuchs, L., 159, 352  
 Fujimoto, T., 564, 614  
 Fujita, Y., 678, 682  
 Fuller, R. E., 266, 352  
 Fyfe, W. S., 348
- Gaffron, Hans, 710  
 Gage, Lyman J., x, 745, 746  
 Gage, L. P., 563, 613  
     studies, 574-575  
 Gajardo, E., 383, 548  
 Ganguly, J., 290, 352  
 Garcia-Bunuel, R., 612  
 Garrison, Robert F., 111  
     publications, 123  
 Garstang, R. H., 538  
 Gasser, R. F., 614  
 Gast, P. W., 388, 392, 393, 394, 401, 403, 406,  
     539, 540, 541  
 Gauth, Eckhard, 46, 622, 632, 633, 635, 639, 641,  
     642, 643, 648, 650, 652, 655, 656, 660, 662  
 Gay, Helen, viii  
 Gee, R., 708  
 Gelderman, A., 548  
 Gerling, E. K., 146, 352  
 Getting, I. C., 163, 172, 208, 210, 213, 352  
 Ghazanfar, S. A. S., 640  
 Ghose, S., 190, 332, 346, 352  
 Gibbons, B. H., 640  
 Gibbons, G. S., 325, 352  
 Gibbs, G. V., 349  
 Gibson, I. L., 352  
 Gibson, R. E., 143, 348  
 Giesecke, A. A., Jr., 383, 548  
     publications, 546  
 Gifford, Walter S., x  
 Gilbert, Carl J., v  
 Gilbert, Cass, x  
 Gilbert, M. C., 169, 172, 174, 281, 282, 352, 360  
 Gilchrist, F. G., 611  
 Giles, Sol, 66, 128  
 Gillespie, D., 545  
 Gillett, Frederick H., x  
 Gilman, Daniel C., x, 745, 746, 747  
 Ginsberg, A. S., 143, 352  
 Glasser, F. P., 160, 163  
 Glover, E. D., 294  
 Glover, L., III, 383, 409, 548  
     studies, 408-412  
 Goldberg, M., 312  
 Golden, William T., v, vi  
 Goldreich, Peter, 123  
 Goldsmith, J. R., 348  
 Goldstein, A., 527, 545  
 Goodchild, D. J., 632, 640, 644, 648, 655, 706  
 Goor, D., 614  
 Gorshkov, G. S., 540  
 Gott, J. Richard, III, 123
- Grady, Leo M., 548  
 Grahm, D., 640  
 Green, D. H., 151, 258, 352, 540  
 Green, T. H., 148, 149, 154, 169, 352, 540  
 Greenewalt, Crawford H., v, vi, 727, 743  
 Greenstein, Jesse L., vii, 64, 76, 82, 83, 84, 91,  
     108, 120, 127  
     publications, 123  
 Greenwood, H. J., 179, 352  
 Griffith, O. M., 621  
     studies, 704-706  
 Griffin, W. L., 392, 539  
 Griggs, D. T., 442, 543  
 Grove, M., 609  
 Grout, F. F., 152, 352  
 Gruenwald, P., 614  
 Grygar, J., 123  
 Gunn, J. E., vii, 64, 96, 108, 109, 127  
     publications, 123  
 Gunning, B. E. S., 352  
 Güven, N., 192
- Hadidiacos, C. G., 294  
 Hafner, S. S., 190, 191, 193, 352  
 Hägg, G., 319, 352  
 Haggerty, S. E., 43, 135, 137, 189, 190, 227, 229,  
     230, 231, 232, 242, 243, 262, 265, 280, 303,  
     305, 345, 352, 359  
     publications, 347  
     studies, 229-238, 259-264, 264-269, 278-284  
 Hales, A. L., 460, 463, 464, 543  
 Halferdahl, L. B., 290, 352  
 Hall, J. S., 546, 553  
 Hall, Harvey Monroe, 625, 626, 629, 648  
 Hallberg, R. L., 612  
 Halldal, Per, 58, 620, 678, 710, 712  
     studies, 670-678  
 Hamburger, V., 561, 563  
 Hamilton, W. C., 304, 352  
 Hannaford, W. L. W., 259, 357  
 Hanneman, R. E., 208, 352  
 Hansen, Olav, L., 66, 128  
 Haraburda, Joseph M. S., ix  
 Haramura, H., 245, 354  
 Hardorp, Johannes, 114  
     publications, 123  
 Hardy, Eduardo, 65, 128  
 Hare, P. E., vii, 140, 141, 313, 345, 359  
     studies, 327-334  
 Hargraves, R. B., 225, 227, 272, 353  
 Harker, A., 250, 353  
 Harris, R. L., 350  
 Harrison, Tyrone, 709  
 Hart, Richard W., 710  
 Hart, S. R., vii, 383, 394, 395, 401, 539, 540, 547  
     publications, 546  
     studies, 384-385, 385-386, 386-388, 388-394,  
     400-405, 408-412, 412-413  
 Hartzell, H. C., Jr., 564, 613  
     studies, 587-589  
 Harvey, J., 79  
     publications, 123

- Harvey, P. H., 91  
 Harvey, P. M., 66, 128  
 Haskell, N. A., 439, 452, 542, 543  
 Haskins, Caryl P., v, vi, ix, 743  
   publications, 723  
   Report of the President, 1-68  
 Hatch, M. D., 625, 632, 635, 636, 637, 638, 639,  
   640, 649, 650, 651, 655  
 Hatherton, T., 394, 402, 539  
 Hatzenbeler, H., 123  
 Haubrich, R. A., 427, 542  
 Hay, John, x, 745, 746  
 Hay, R. J., 563, 600, 613  
   publications, 612  
   studies, 580-586, 600-601  
 Hayashi, M., 536, 545  
 Hayashiya, K., 574  
 Haynes, V., 327  
 Hays, J. F., 164, 187, 352  
 Heatfield, B. M., 314  
 Heath, S. A., 353  
 Heier, K., 541  
 Heintze, J. R. W., 124  
 Hekinian, R., 259, 356  
 Henard, Kenneth R., ix  
 Henderson, E. P., 246  
 Henrickson, W., 344  
 Henry, Barklie McKee, x  
 Herbst, E., 614  
 Herk, G. van, 116  
 Herrick, Myron T., x  
 Herrin, E., 467, 543  
 Hershey, Alfred D., viii, 39, 40, 41, 42, 61  
   publications, 722  
   report of Director of Genetics Research Unit,  
   715-722  
 Hertig, A. T., 613  
 Hesketh, J. D., 634, 639, 660, 662  
 Hess, H. H., 151, 353  
 Hewitt, Abram S., x  
 Hiesey, William M., viii, 60, 622, 709, 713  
   publications, 710  
 Higgins, M. W., 383, 548  
   studies, 408-412, 412-413  
 Higginson, Henry L., x, 745, 746  
 Hildreth, W. W., 620, 690  
 Hills, F. A., 409, 541  
 Hiltner, W. A., 124  
 Hind, G., 621, 694  
 Hirakow, R., 563, 589, 596, 597, 598, 599, 613  
   publications, 612  
   studies, 589-600  
 Hitchcock, Ethan A., x, 745, 746  
 Hitchcock, Henry, x  
 Hoag, Arthur A., 124  
 Hoering, Thomas C., vii, 140, 327, 332, 359  
   studies, 334-337  
 Hoffmeister, J. E., 250, 353  
 Hofmann, A. W., 359  
 Hoggan, H. W., 121, 129  
 Holmgren, P., 641, 648, 656, 662  
 Hollister, L. S., 225, 227, 272, 292, 346  
 Homan, P. H., 699, 700, 704  
 Hoover, Gordon, 66, 128  
 Hoover, Herbert, x  
 Hopson, C. A., 412, 413, 542  
 Hornblower, Marshall, ix  
 Horning, G., 157, 355  
 Hoschek, G., 353  
 Hoshino, T., 614  
 Howard, Robert, vii, 64, 77, 78, 79, 119, 127  
   publications, 124  
 Howe, William Wirt, x, 745, 746  
 Howie, R. A., 223, 231, 236, 241, 351  
 Hoyer, B. H., vii, 33, 35, 471, 486, 487, 543, 547  
   studies, 488-501 507-515  
 Hsu, K. J., 394, 539  
 Hsu, L. C., 187, 353  
 Hubble, E. P., 367  
 Huber, W., 652, 655  
 Huckenholz, H. G., 138, 174, 182, 188, 346, 359  
   studies, 182-188  
 Hudson, Hugh, 124  
 Hughes, H., 159, 353  
 Hunt, J., 327  
 Hurst, H. M., 336, 349  
 Hutchinson, Charles L., x, 745, 746  
 Hyland, A. R., 65, 85, 87, 90, 123  
   publications, 124  
 Iffy, L., 614  
 Ingamells, C. O., 244, 353  
 Ingersoll, A. P., 65, 82, 128  
 Ingham, William, 124  
 Ingraham, Laura J., 40, 42, 717, 718, 721  
 Inman, R. B., 545  
 Irving E., 262, 263, 353  
   studies, 259-264  
 Irwin, W. P., 394, 540  
 Ishizaka, K., 546  
 Ito, J., 292, 353  
 Iversen, L. L., 544  
 Jacobi, Günter, 621, 667, 689, 690, 694, 695,  
   712  
   studies, 690-694  
 Jackson, Robert, 66, 128  
 Jaeger, J. C., 266, 353  
 Jahns, R. H., 142, 355  
 Jakes, P., 254, 353  
 Jambor, J. L., 302, 353  
 James, D. E., vii, 51, 383, 547  
   publications, 546  
   studies, 447-460, 460-464  
 James, O. B., 346, 348  
 Jarosewich, E., 250, 252, 253, 255, 256, 355  
 Jessup, Walter A., x  
 Jewett, Frank B., x  
 Johannes, W., 169  
 Johnson, H. M., 111  
 Johnson, H. S., 635, 637, 638, 639, 650, 655  
 Johnson, L. R., 464, 543  
 Johnson, R. W., 283, 355  
 Jones, R. N., 673, 678



- Jordan, E., 566, 567, 614  
 Joseph, N., 587, 614  
 Joy, Alfred H., 65, 128  
 Julian, William H., 65, 109, 110, 128  
   publications, 124
- Kanasawich, E. R., 406, 541  
 Kang, K., 360  
 Kannangara, C. G., 658, 662  
 Kano, H., 275, 353  
 Karig, D. E., 250, 353  
 Katem, Basil, 95, 128  
 Katoh, S., 689, 690, 693, 695  
 Katsura, T., 202, 206, 282, 284, 302, 348  
 Kausel, E., 383, 548  
 Kawai N., 207, 353  
 Kay, B. D., 255  
 Kay, R., 388, 390, 392, 403, 539  
 Keck, D. D., 60  
 Keenan, P. C., 111  
   publications, 124  
 Keil, K., 231, 240, 242, 246, 247, 248, 353  
 Kelsey, C. H., 188, 189, 353  
 Kennedy, M., 613  
 Kennedy, W. Q., 163, 169, 170, 171, 172, 208,  
   210, 211, 213, 295  
 Kerrick, D. M., 193, 194, 353  
 Khalifa, M., 656, 662  
 Khattri, K. N., 440, 542  
 Kindström, A. L., 319, 353  
 Kintner, P. L., 311, 358  
 Kirk, W. S., 383, 548  
   studies, 408–412, 412–413  
 Kitayama, K., 282, 302, 353  
 Klein, C., 156, 159, 352  
 Klose, J. Z., 538  
 Knopoff, L., 453, 543  
 Kodaira, Keiichi, 65, 87, 89  
   publications, 124  
 Köhler, A., 275, 353  
 Kohne, D. E., vii, 33, 35, 471, 472, 477, 482,  
   496, 498, 512, 547  
   publications, 546  
   studies, 485–488, 488–501  
 Kok, B., 678, 682  
 Königsberg, I. R., 613  
 Koozekanani, S. H., 538  
 Kortschak, H. P., 651, 655  
 Kosalos, J. G., 546  
 Kotov, N. V., 146, 352  
 Kouvo, O., 318, 319, 353  
 Kovack, R. L., 464, 543  
 Kowal, Charles T., 102, 103, 128  
   publications, 124  
 Kracek, F. C., 160, 162, 353  
 Kraft, Robert P., 124  
 Kranck, S. H., 288, 354  
 Krogh, T. E., vii, 140, 345, 359, 383  
   studies, 337–339, 339–341, 341–344, 384–385,  
   385–386, 386–388, 400–405
- Kristian, Jerome, vii, 64, 96, 101, 102, 103, 104,  
   105, 107, 116, 127  
   publications, 124  
 Krumbein, W. C., 301, 354  
 Kruskal, W., 300, 350  
 Krzeminski, W., 124  
 Kuiper, G. P., 111  
 Kullerud, G., vii, 43, 136, 138, 139, 229, 249,  
   307, 323, 325, 326, 345, 350, 354, 359  
   publications, 347  
   studies, 155–157, 238–243, 245–249, 306–309,  
   315–318, 322–325  
 Kuno, H., 269, 354, 401, 402, 540  
 Kushiro, I., 144, 148, 150, 152, 153, 154, 155,  
   164, 168, 177, 178, 183, 216, 224, 227, 243,  
   245, 299, 354  
   publications, 347
- Lacroix, A., 255, 354  
 Laetsch, W. M., 629, 632, 649, 654, 655  
 Laird, C. D., 474, 489, 493, 497, 498, 500, 543  
 Lambert, D. L., 65, 80, 128  
   publications, 124  
 Lambert, I. B., 408, 541  
 La Mori, P. N., 208, 351  
 Landis, C. A., 259, 350  
 Langley, Samuel P., x, 745, 746  
 Larson, E. E., 263, 354  
 Larson, Richard B., 124  
 Lasker, Barry M., 125  
 Laspeyres, H., 156, 157, 354  
 Laubert, Roman, 382, 548  
 Laughlin, A. W., 140, 145, 146, 148, 354  
   studies, 145–148  
 Lauridsen, L., 611  
 Law, Sai Kit, 66, 128  
 Lawrence, Ernest O., x  
 Lawrence, M. C., 662, 670  
 Le Bas, M. J., 152, 354  
 Lee, D. E., 350  
 Lee, W. H. K., 408, 541,  
 Legg, C. A., 231, 232, 354  
 Lehmann, H., 690, 695  
 Leighton, R. B., vii, 64, 127  
 Leister, D. E., 564, 613  
 Lewis, B. T. R., 546  
 Lindbergh, Charles A., x  
 Linde, A. T., 383, 548  
   publications, 546  
   studies, 430–439, 439–442  
 Lindsay, William, x, 745, 746  
 Lindsley, D. H., vii, 44, 136, 137, 148, 151, 155,  
   174, 189, 190, 191, 198, 199, 200, 201, 202,  
   203, 204, 205, 206, 207, 217, 231, 265, 266,  
   268, 269, 270, 275, 281, 282, 283, 284, 285,  
   288, 290, 294, 305, 345, 354, 359  
   publications, 347  
   studies, 188–190, 190–193, 264–269, 269–274,  
   274–278, 278–284, 284–285  
 Lipsett, M. N., 503, 544  
 Little, C. A., 549  
   studies, 371–377

- Livingston, D. E., 145, 354  
 Locanthi, D. D., 128  
 Lodge, Henry Cabot, x  
 Lombard, R. H., 306, 355  
 Long, A., 318, 360  
 Lonsdale, K., 310, 311, 344  
 Loomis, Alfred L., v, vi, 727, 743  
 Loos, Eckhard, 712, 713  
 Louisnathan, S. J., 302, 354  
 Love, W. E., 344  
 Lovett, Robert, A., v  
 Low, Seth, x, 745, 746  
 Lowen, A. L., 128  
 Lumry, R., 703, 704  
 Lundquist, C. A., 250, 252, 253, 255, 256  
 Luth, W. C., 142, 355  
 Luyten, William J., 76, 106, 112  
 Lynden-Bell, Donald, 112  
 Lynds, Beverly T., 112  
 Lynds, C. R., 125  
  
 Macdonald, G. A., 284, 355  
 MacGregor, I. D., 157, 174, 354  
 Mache, R., 640  
 MacKenzie, W. S., 348  
 MacRae, N. D., 360  
 MacVeagh, Wayne, x, 745, 746  
 Maeda, Y., 191, 355  
 Maio, J. J., 512  
 Makover, Shraga, 722  
 Major, A., 169, 352  
 Mallia, E. A., 125  
 Manasek, F. J., 612  
 Mangiarolti, G., 544  
 Mann, J. B., 303, 319, 350  
 Manson, V., 401, 540  
 Mantai, Kenneth E., 712  
   publications, 710  
 Mao, Ho Kwang, 45, 55, 138, 139, 140, 359  
   studies, 163-168, 168-170, 207-216, 325-326  
 Margulies, S. I., 564, 614  
   studies, 603-609  
 Martin, C. B., Jr., 564, 614  
   studies, 603-609  
 Martin, H., 540  
 Martin, William McC., Jr., v, vi, 743  
 Marton, L. L., 546, 553  
 Maruyama, T., 439, 542  
 Marvin, V. B., 159, 351  
 Masuda, A., 540  
 Mathieu, S., 283, 350  
 Matilsky, T. A., 538  
 Matson, Dennis, 66, 82, 128  
 Matsui, Y., 190, 355  
 Matthews, A., 5, 95  
 May, I., 342, 355  
 Mayall, N. U., 367  
 McBirney, A. R., 540  
 McCarthy, B. J., 509, 544  
 McClaren, A., 486, 543  
 McClintock, Barbara, viii, 722  
 McCord, T. B., 112  
  
 McEvilly, T. V., 460, 464, 543  
 McGough, Sheila A., ix  
 McHugh, Keith S., v, vi, 727, 743  
 McKenzie, David, 125  
 McKie, D., 189, 353  
 McQueary, G. L., 128  
 Medaris, L. G., Jr., 286, 302, 355  
 Medina, Ernesto, 624, 709, 712, 713  
   studies, 655-662  
 Mellon, Andrew W., x  
 Mellor, G. E., 652, 655  
 Melson, W. G., 250, 251, 255, 256, 355  
 Menard, H. W., 249, 357  
 Mendez, J., 336, 355  
 Mendiguren, J., 383, 548  
 Merrett, M., 695, 699  
 Merwin, H. E., 306, 355  
 Meyer, H. O. A., 43, 157, 229, 232, 242, 243, 345,  
   355, 359, 360  
   publications, 347  
   studies, 229-238  
 Meyer, R. P., 546  
 Michaud, Georges, 125  
 Michel, Jean-Marie, 58, 620, 667, 682  
   publications, 710, 711  
 Michel-Wolwertz, Marie-Rose, 620, 667, 682  
   publications, 710, 711  
 Midgley, J. E. M., 522, 544  
 Miesch, A. T., 300, 355  
 Miley, G. K., 107  
 Miller, Margaret Carnegie, x  
 Miller, L., 566, 612  
 Miller, Roswell, x  
 Miller, William C., 102, 128  
   publications, 125  
 Mills, Darius O., x, 745, 746  
 Milton, C., 318, 355  
 Milton, D. J., 318, 355  
 Minear, J. W., 540  
 Miner, E., 125  
 Minkowski, Rudolph, 7  
 Misenhimer, H. R., 564, 613  
   publications, 612  
   studies, 603-609  
 Mitchell, S. Weir, x, 745, 746, 747  
 Mitchell, W. E., 112  
 Mitsui, A., 685, 690  
 Miyashiro, A., 392, 539  
 Moh, G. H., 347  
 Mohit, Behzad, 549  
 Montague, Andrew J., x  
 Mooney, Harold, 709  
 Moorbatch, S., 539  
 Moore, J. G., 216, 222, 225, 232, 265, 274, 275,  
   276, 355  
 Moore, J. M., 292  
 Moore, P. B., 348, 349  
 Morey, G. W., 158, 160, 324, 355  
 Morgan, Henry S., v, vi, 727, 743  
 Morimoto, N., 192, 355  
 Morrison, R. P., 450, 459, 543  
 Morrow, William W., x, 745, 746

- Morse, S. A., 234, 355  
 Mosig, G., 718  
 Mousseau, M., 656, 662  
 Muan, A., 43, 45, 139, 182, 195, 196, 197, 282, 302, 355, 360  
   studies, 194–195, 195–197, 243–245  
 Muehlenbachs, K., 261, 355  
 Mudd, Seeley G., x  
 Muir, I. D., 216, 223, 269, 283, 289, 297, 355  
   publications, 347  
 Müller, A., 703, 704  
 Mumford, George S., 125  
 Münch, Guido, vii, 64, 81, 82, 83, 89, 92, 120, 368, 538  
   publications, 125  
 Munoz, J. L., 191, 290, 347  
 Munson, R. A., 323, 324, 355  
 Muramatsu, M., 614  
 Murano, F., 678, 682  
 Murata, Norio, 620, 622, 678, 685, 690, 693, 694, 700, 708, 709, 710, 712, 713  
   publications, 711  
   studies, 682–690, 699–704  
 Murata, Teruyo, 713  
 Murray, D. B., 656, 662  
 Myers, A. T., 156, 356  
 Myers, J., 678, 682  
 Myers, William I., v, vi, 743  
  
 Nafziger, R. H., 282, 302, 355  
 Nakamura, Y., 243, 245, 354  
 Naldrett, A. J., 347  
 Nalwalk, A. J., 546  
 Náray-Szabó, I., 292, 355  
 Nash, W. P., 283, 355  
 Navrotsky, A., 196, 355  
 Néel, L., 283, 355  
 Nelson, E. B., 639  
 Neugebauer, G., 65, 81, 82, 90, 91, 96, 99, 102, 105, 107, 108, 110, 128  
   publications, 125  
 Neuhaus, A., 156, 355  
 Newell, E. B., 125  
 Newkirk, Gordon, 78  
 Newnham, R. E., 304, 350  
 Newton, M. S., 169, 170, 355  
 Newton, R. C., 180, 355  
 Nevins, D. J., 660, 662  
 Nicholls, J., 189, 190, 280, 281, 285, 355  
 Nichols, R., 656, 662  
 Nickell, L. G., 651, 655  
 Nikogosyan, C. S., 143, 352  
 Nixon, P. H., 157, 355  
 Nobs, Malcolm A., 46, 49, 622, 629, 709, 712, 713  
   publications, 711  
   studies, 625–629, 640–648  
 Nolan, J., 173, 174, 175, 355  
 Norton, Garrison, v, vi, 727, 743  
 Norton, S. A., 291, 357  
 Nuramoto, H., 639  
 Oaks, A., 636, 639  
 O'Brien, T. J., 549  
 O'Connell, K. A., 589, 614  
 Oemler, August, Jr., 66, 128  
 Ogura, Teruo, 670  
 Ohad, I., 699  
 O'Hara, M. J., 171, 177, 178, 245, 356  
 Oinas, Valdar, 66, 128  
 Oishi, M., 544  
 Oke, J. B., vii, 64, 75, 82, 85, 92, 96, 98, 100, 102, 105, 108, 114, 121, 127  
   publications, 125  
 Olsen, E. J., 348  
 Onken, H., 304, 356  
 Onuma, K., 227, 359  
 Opdyke, N. D., 259, 355  
 O'Rahilly, R., 564, 609, 610, 613  
   studies, 609–610  
 O'Reilly, W., 283, 356  
 Orville, P. M., 346  
 Osborn, E. F., 182, 356  
 Osborn, William Church, x  
 Osmer, P. S., 96  
 Osmond, C. B., 629, 632, 644, 648  
 Ostriker, Jeremiah P., 109  
   publications, 125  
 Otalora, G., 225, 227, 272, 353  
 Oversby, V. M., 386, 387, 406, 539, 541  
 Owen, Tobias, 82, 113  
 Ozard, J. M., 387, 539  
 Ozawa, E., 564, 587, 613  
   studies, 587  
 Ozawa, I., 428, 542  
  
 Page, B. M., 540  
 Panigel, M., 564, 606, 614  
 Papike, J. L., 217, 225, 227, 349  
 Park, J. K., 263, 353  
 Park, Roderic, 621, 706  
 Parker, P. L., 327  
 Parma, David H., 40, 42, 717, 718, 721, 722  
 Parmelee, James, x  
 Parsons, William Barclay, x  
 Paton, Stewart, x  
 Pauling, L., 308, 315, 356  
 Pawson, D. L., 312, 347  
 Peach, John V., 125  
 Pearcy, Robert W., 46, 47, 48, 49, 622, 629, 709, 712, 713  
   studies, 625–629, 632–639, 640–648  
 Pearson, K., 299  
 Peckett, A., 348  
 Peery, B. F., Jr., 86, 113  
 Pellet, A., 111  
 Pennoyer, Robert M., v, vi, 743  
 Penrose, Bruce, 66, 128  
 Penston, M. V., 65, 87, 93, 97, 113, 128  
 Pepper, George W., x  
 Percious, J. K., 148, 350  
 Perini, F., 689, 690  
 Perkins, Richard S., v, vi, 743  
 Pershing, John J., x



- Persson, S. Eric, 66, 92, 128  
 Peterman, Z. E., 397, 540  
 Peterson, D. M., 65, 84, 85, 114, 128  
 Philip, A. G. D., 113  
 Philpotts, J. A., 390, 391, 392, 401, 539, 546  
 Pinsker, Z. G., 193, 359  
 Pigott, G. H., 523, 544, 545  
 Plant, A. G., 348  
 Poe, G. R., 368, 549  
 Poldervaart, A., 223, 356  
 Polli, E., 506, 544  
 Pollock, Harry E. D., ix  
 Pomerantz, M. A., 546  
 Potter, D. B., 290, 351  
 Pozo, S. del, 383, 548  
     publications, 545  
     studies, 470-471  
 Prager, L. K., 549  
     publications, 711  
 Prata, Stephen W., 65, 78, 128  
 Prather, D., 567, 614  
 Prentis, Henning W., Jr., x  
 Presnall, D. C., 145, 347, 356  
 Press, F., 452, 543  
 Preston, George W., III, vii, 64, 87, 88, 89, 127  
     publications, 125  
 Preston, H., 309, 344, 347  
 Prewitt, C. T., 217, 225, 227, 277, 356  
 Priestley, Joseph, 427, 542  
 Prigogine, I., 200, 356  
 Prinz, M., 346, 348, 401, 540  
 Pritchett, Henry S., x  
 Proskouriakoff, Tatiana, ix  
 Pruss, Gail J., 128  
 Puchelt, H., 347, 359  
 Puga, A., 536, 545  
 Pushkarev, Y. D., 146, 352  
  
 Rabinowitch, E., 703, 704, 710  
 Racine, René, 114  
     publications, 125  
 Rake, Adrian, 515  
 Ramdohr, P., 156, 230, 231, 242, 249, 307, 318, 356  
     publications, 346  
 Ramsey, E. M., viii, 61, 564, 613  
     publications, 612  
     studies, 603-609, 609-610  
 Rebbert, M., 575, 576, 614  
 Reed, George, 377, 549  
 Reed, M. L., 640  
 Reed, R. D., 394, 539  
 Reeder, R. H., viii, 38, 39, 561, 562, 566, 613  
     publications, 612, 613  
     studies, 565-566, 566, 567-568  
 Reed, S. J. B., 294, 356  
 Rees, Martin, 109  
 Reid, A. M., 233, 241, 356  
 Rentschler, Gordon S., x  
 Rice, N., 32, 34, 471, 472, 486, 548  
     studies, 472-479, 479-482, 482-485  
 Richards, A. F., 259, 350  
  
 Richardson, J., 344  
 Richardson, S. W., 169, 172, 245, 290, 292, 356  
 Rickard, James L., 65, 92, 128  
 Rickli, E. E., 640  
 Rickwood, P. C., 408, 541  
 Riley, M. S., 128  
 Ringwood, A. E., 169, 245, 258, 356  
 Roark, T. P., 549  
 Roberts, Morton, 369  
 Roberts, R. B., vii, 471, 486, 487, 544, 547  
     publications, 546  
     studies, 501-503  
 Robertson, W. A., 262, 353  
 Robie, R. A., 193, 201, 207, 325, 356  
 Robinson, P. W., 179, 356  
 Robinson, R., 464  
 Rockefeller, David, x  
 Rodgers, A. W., 125  
 Rodriguez, A., 383, 447, 549  
     studies, 470-471  
 Roedder, E. W., 158, 159, 302, 356  
 Roeder, R. G., 38, 561, 562, 563, 566, 568, 570  
     publications, 613  
     studies, 565-566, 568-571  
 Rogul, M., 509, 544  
 Romer, A., 544  
 Root, Elihu, x, 745, 746, 747  
 Root, Elihu, Jr., x  
 Roseboom, E. H., Jr., 170, 346, 349  
 Rosenberg, Jerome, 665, 670  
 Rosenwald, Julius, x  
 Rosenquist, G. C., 614  
 Ross, C. S., 355  
 Ross, M., 156, 217, 227, 356  
 Roth, William M., v, vi, 743  
 Rowe, J. J., 342, 355  
 Rubenstein, Irwin, 722  
 Rubey, William W., v, 743  
 Rubin, Vera C., vii, 368, 383, 538, 547  
     publications, 546  
     studies, 367-370  
 Ruby, Ronald, 622, 707, 708  
     studies, 706-708  
 Rule, Bruce H., vii, 64, 119, 121, 128  
 Rumble, Douglas, III, 139, 207, 291, 346, 359  
     studies, 198-207, 290-294  
 Ryerson, Martin A., x  
 Ryle, G. J. A., 660, 662  
  
 Saa, G., 383, 464, 549  
     publications, 546  
     studies, 419-426  
 Sacks, I. S., vii, 54, 59, 383, 438, 442, 460, 464, 547  
     publications, 546, 547  
     studies, 413-414, 414-416, 416-419, 419-426, 426-430, 430-439, 439-442  
 Sahama, T. G., 302, 359  
 Saleuddin, A. S. M., 313, 356  
 Salgueiro, R., 383, 547  
     publications, 547  
     studies, 470-471  
 Salomons, W., 360

- Sandage, Allan, vii, 5, 31, 32, 36, 64, 75, 91, 93,  
94, 95, 96, 100, 101, 102, 103, 105, 106, 107,  
112, 116, 117, 121, 122, 123, 127  
publications, 125, 126
- Sanduleak, N., 373, 538
- Sane, P. V., 706
- Santoro, R. P., 304, 350
- Sargent, Anneila I., 83, 128  
publications, 126
- Sargent, Wallace L. W., vii, 64, 89, 96, 97, 98, 99,  
100, 101, 102, 109, 128  
publications, 126
- Sasvári, K., 292, 355
- Sato, M., 262, 278, 356
- Savage, J. C., 439, 542
- Saxena, S. K., 190, 356
- Scatchard, G., 206, 356
- Schaefer, E. W., Jr., 612, 613
- Schaeffer, R. M., 263, 357
- Schairer, J. F., vii, 43, 45, 138, 149, 153, 156, 157,  
159, 160, 161, 162, 171, 174, 177, 178, 182,  
227, 299, 346, 357, 359  
studies, 157-160, 160-163, 197-198, 243-248
- Schatten, Kenneth, 79
- Scheiber, L. C., 255, 256, 350
- Schild, Rudolph E., 85, 114, 115  
publications, 126
- Schildkraut, C. L., 545
- Schildkraut, J. J., 517, 531, 544
- Schilling, J. G., 357, 540
- Schmidt, Maarten, vii, 5, 65, 76, 103, 106, 107,  
108, 128  
publications, 126
- Schmincke, H.-U., 357
- Schnapauff, R., 538
- Schnetzler, C. C., 547
- Schoenfeld, R. I., 515, 544
- Schofield, D., 126
- Scholz, M. T., 65, 84, 87, 114, 126, 128  
publications, 126
- Schreyer, W., 159, 177, 179, 180, 187, 290, 292,  
357
- Schwarz, E. J., 263, 357
- Slater, J. G., 249, 357
- Scott, A., 272, 357
- Searle, L. T., vii, 64, 98, 99, 100, 101  
publications, 126
- Segal, D., 344
- Seiden, L. S., 515, 544
- Seifert, F., 179, 187, 357
- Serson, P. H., 259, 357
- Severs, Judy, 360
- Seyler, Richard G., 549
- Šesták, Z., 704  
publications, 711
- Shaffer, D. B., 66, 128
- Shand, S. J., 296, 357
- Shannon, R. D., 227, 277, 357
- Shepley, Henry R., x
- Shleser, R., 36, 471, 537, 545, 548  
studies, 536-538
- Shinyayev, A., 360
- Shumaker, J. B., Jr., 538
- Silverton, E. W., 344
- Simon, Michal, 65, 128  
publications, 126
- Simoni, D., 383, 447, 549
- Simons, E., 494, 543
- Simpson, G. G., 497, 544
- Simpson, P. R., 242, 357
- Sinclair, J. H., 490, 543
- Sinha, A. K., 383, 406, 407, 541, 548  
publications, 547  
studies, 386-388, 394-400, 405-408, 408-412,  
412-413
- Skalka, A., 545, 722
- Skinner, B. J., 240, 357
- Slack, C. R., 625, 632, 634, 635, 636, 637, 639,  
640, 649, 650, 651, 652, 653, 655
- Slatyer, R. O., 643, 644, 648
- Smith, B., 580, 614
- Smith, Douglas, 137, 138, 189, 190, 217, 223, 264,  
265, 270, 292, 294, 302, 308, 342, 346, 357, 359  
studies, 264-269, 269-274, 274-278, 284-285,  
285-290
- Smith, I., 482, 484, 544
- Smith, J. V., 357
- Smith, James H. C., 60, 61, 709, 712
- Smith, Jean F., 35, 549  
studies, 506-507, 520-521
- Smith, M. M., 613
- Smith, P. J., 357
- Smith, Sara F., 77
- Smith, Theobald, x
- Snetsinger, K. G., 248, 349
- Snyder, Lewis E., 14
- Soderblom, L., 66, 128
- Somerville, D., 580, 614
- Southwick, D. L., 357
- Speidel, D. H., 281, 357
- Speman, H., 561, 563
- Spooner, John C., x, 745, 746
- Stahl, F. W., 40, 717
- Stalsberg, H., 594  
publications, 613
- Stanford, G., 327
- Stanley, W. J., Jr., 545
- Stanton, Frank, v, vi, 743
- Steiner, E., 367, 383, 548  
studies, 382-383
- Stensby, Per S., 665, 670
- Stephenson, A., 283, 306, 357
- Stern, R., 564, 613
- Stevenson, F. J., 331, 336, 357
- Stewart, J. M., 347
- Stice, G. D., 349
- St. Jean, J., Jr., 408, 541
- Stokes, N. R., 126
- Stook, P. W., 326, 348
- Storeh, T. G., 613
- Storey, William Benson, x
- Strange, D. L. P., 126

- Stratford, B. F., 614  
 Straus, Neil A., 549  
 Strom, K. M., 126  
 Strom, S. E., 126  
 Strong, D. F., 208, 272, 357  
 Strong, John, 126  
 Strong, Richard P., x  
 Stumpf, E. F., 348  
 Swope, H., 65, 93, 128  
 Sugimura, A., 402, 540  
 Sussex, I. M., 612, 613  
 Suyehiro, S., 383, 447, 547  
   studies, 442-447  
 Suzuki, Y., 38, 39, 61, 563, 566, 613  
   studies, 565-566, 571-574  
 Swanson, R. F., 38, 562, 563, 612, 613  
   publications, 613  
   studies, 575-576, 576-578  
 Swartz, F. M., 412, 542  
 Sweers, H. E., 703, 704  
 Sykes, L. R., 249, 357  
 Syono, Y., 177, 191, 355
- Taft, Charles P., v, vi  
 Taft, William H., x  
 Takahashi, T., 326, 348  
 Takamiya, A., 685, 690, 695, 699, 700, 704  
 Takeuchi, H., 460, 543  
 Taliaferro, N. L., 394, 539  
 Tamayo, L., 383, 549  
   publications, 547  
   studies, 470-471  
 Tammann Gustav A., 32, 65, 75, 93, 94, 95, 115, 128  
   publications, 126  
 Tan, K. C., 640  
 Tanenbaum, Andrew W., 79  
   publications, 126  
 Tatsumoto, M., 392, 393, 394, 397, 398, 403, 404, 406, 539, 540, 541  
 Taylor, L. A., 43, 45, 136, 139, 140, 200, 203, 207, 229, 257, 357, 359  
   publications, 347, 348  
   studies, 193-194, 194-195, 238-243, 315-318, 318-322, 322-325, 325-326  
 Taylor, R. W., 357  
 Taylor, S. R., 540  
 Tchen, T. T., 650, 655  
 Thackeray, A. D., 126  
 Thatcher, W., 455, 460, 461, 462, 463, 464, 543  
 Thayer, T. P., 156, 357  
 Thayer, William S., x  
 Thomas, John, 709  
 Thomas, P. D., 449, 463, 543  
 Thomas, Pamela W., ix  
 Thompson, A. Gerald, ix  
 Thompson, J. B., Jr., 188, 189, 200, 202, 203, 204, 283, 290, 291, 292, 293, 305, 306, 357, 358  
 Thompson, R. N., 358  
 Tiefert, M. A., 613  
 Tilley, C. E., 142, 149, 187, 188, 269, 284, 295, 296, 297, 299, 358
- Tilton, G. R., 406, 541  
 Tobisch, O. T., 409, 541  
 Tolbert, N. E., 629, 632, 639, 640, 652, 655  
 Toulmin, P., III, 326, 358  
 Townes, Charles H., v, vi, 14, 743  
 Trafton, Laurence M., 81  
   publications, 126  
 Trail, R. J., 348  
 Tregunna, E. B., 629, 632, 639, 649, 652, 655  
 Treharne, K. J., 656, 662  
 Troughton, J. H., 632, 644, 648  
 Trippe, Juan T., v, vi, 727, 743  
 Tsushima, K., 685, 690  
 Tucker, J. A., 610, 614  
 Tuft, P. H., 611, 613  
 Tukey, J., 298  
 Tunell, G., 309  
 Tunnichiff, D. D., 664  
 Turekian, K. K., 541  
 Turner, K. C., vii, 367, 547  
   publications, 547  
   studies, 371-377  
 Turnock, A. C., 360  
 Tuve, M. A., 50, 59, 367, 383, 449, 547, 553  
   publications, 547  
   studies, 371-377  
 Tuttle, O. F., 142, 276, 358  
 Tye, Henry, 66, 128  
 Tyrrell, G. W., 267, 358
- Uhlenbeck, O., 544  
 Unno, W., 126
- Van der Kaaden, G., 275, 358  
 Van Schmus, W. R., 159, 246, 247, 249, 358  
 Varsavsky, C. M., 367, 549  
 Vaughan, Arthur H., Jr., vii, 65, 89, 120, 128  
 Vdovykin, G. P., 311, 358  
 Veeder, Glenn J., 66, 80, 112, 128  
   publications, 126  
 Velde, N. W. van de, 549  
   studies, 507-515  
 Vennesland, Birgit, 650, 655  
 Verhoogen, J., 227, 358  
 Vernon, Leo P., 663, 666, 669, 670, 682, 685, 689, 690  
 Vess, Grace, 128  
 Viaene, W., 359  
 Vidie, B., 614  
 Vincent, E. A., 201, 207, 358  
 Virgo, D., 190, 191, 193, 358  
 Visvanathan, N., 116  
   publications, 126  
 Volponi, F., 51, 52, 383, 549  
   studies, 464-470  
 Vorpahl, J., 79  
   publications, 126  
 Vozoff, K., 471, 543  
 Vuorelainen, Y., 318, 353
- Wadsworth, James W., x  
 Wager, L. R., 270, 358



- Wagner, R. P., 611  
 Walburn, Marjorie H., ix  
 Walcott, Charles D., x, 745, 746, 747  
 Walcott, Frederic C., x  
 Walcott, Henry P., x  
 Waldbaum, D. R., 200, 201, 202, 204, 207, 325, 358  
 Walkden, B., 336, 349  
 Walker, G. P. L., 143, 285, 358  
 Walker, J. C., 372, 377  
 Walker, R. L., 342, 350  
 Wallerstein, George, 117  
   publications, 126  
 Wanless, R. K., 260, 358  
 Ward, D., 613  
 Wareing, P. R., 656, 662  
 Warner, G., 229  
 Wasserburg, G. J., 384, 538  
 Waters, A. C., 264, 358  
 Watkins, N. D., 231, 262, 278, 280, 358  
 Waygood, E. R., 634, 640  
 Weart, Spencer R., 80  
   publications, 126  
 Webster, A. H., 200, 203, 207, 358  
 Weed, Lewis H., x  
 Wehmiller, J. H., 359  
 Weidmann, S., 597  
 Weill, D. F., 216, 222, 223, 358  
 Weiss, M., 600, 612  
 Welch, William H., x  
 Wells, A. F., 344  
 Wensink, P. C., 38, 561, 562, 563, 564, 566, 613  
   studies, 565–566, 571  
 Wessels, J. S. C., 682, 689, 690  
 Westphal, J. A., 65, 82, 103, 105, 116, 117, 128  
   publications, 127  
 Wetherill, G. W., 410, 542  
 Wheeler, E. P., 223, 285, 286, 288, 289, 358  
 White, A. J. R., 254, 353  
 White, A. M., 408, 541  
 White, Andrew D., x, 745, 746  
 White, Edward D., x  
 White, Henry, x  
 White, James N., v, vi, 743  
 Whittaker, A. G., 311, 358  
 Wier, T. E., 654, 655  
 Wiessner, Wolfgang, 619, 621, 667, 670, 696, 699, 712  
   publications, 711  
   studies, 662–670, 695–699  
 Wilbur, K. M., 313  
 Wilcox, John M., 79  
   publications, 127  
 Williams, D. W., 171, 211, 358  
 Williams, R. J., 282, 358  
 Williamson, J., 160, 163, 324, 358  
 Wilson, A., 499, 500, 544  
 Wilson, Olin C., vii, 65, 85, 86, 128  
 Wilson, R. L., 262, 358  
 Wilson, Robert E., x  
 Wing, R. F., 547, 549  
 Wolff, Sidney C., 88  
   publications, 127  
 Wones, D. R., 280, 281, 282, 358  
 Wood, J. A., 148, 152, 246, 249, 359  
 Woodward, Robert S., x  
 Woollard, G. P., 449, 450, 543  
 Woolley, Sir Richard, 85  
   publications, 127  
 Woolhouse, H. W., 656, 658, 662  
 Wraight, Colin, 713  
 Wright, Carroll D., x, 745, 746, 747  
 Wright, T. L., 262, 267, 278  
 Wyckoff, R. W. G., 309  
 Wyllie, P. J., 169, 348, 349  
 Wyss, M., 440, 542, 543  
 Yagi, K., 171, 172, 227, 359  
 Yamagishi, Hideo, 722  
 Yamaguchi, M., 547  
 Yamazaki, R. K., 629, 632, 640, 655  
 Yoder, H. S., Jr., vii, 45, 138, 140, 141, 142, 145, 148, 149, 152, 154, 155, 156, 157, 158, 161, 171, 172, 174, 175, 177, 178, 180, 182, 187, 188, 257, 284, 296, 299, 302, 346, 359  
   publications, 348  
   studies, 141–145, 145–148, 155–157, 157–160, 160–163, 176–181, 182–188, 197–198  
 York, D., 260, 359  
 Yoshida, M., 202, 206, 348  
 Yoshikawa-Fukada, M., 564, 583, 612  
   publications, 613  
   studies, 580–586  
 Yund, R. A., 306, 307, 315, 359  
   publications, 347  
 Zaartman, R. E., 406, 541  
 Zachariasen, W. H., 303, 319, 359  
 Zahler, S. A., 537, 545  
 Zen, E-an, 193, 359  
 Zies, E. G., 359  
 Zirin, Harold, vii, 65, 77, 79, 80, 89, 119, 121, 128  
   publications, 127  
 Zussman, J., 223, 231, 236, 241, 348, 351  
 Zvyagin, B. B., 193, 359  
 Zwicky, Fritz, 65, 96, 98, 99, 100, 101, 102, 108, 128  
   publications, 127













